WOODHEAD PUBLISHING SERIES IN BIOMATERIALS

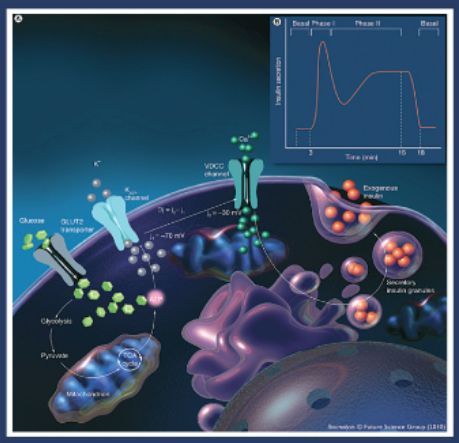

Microfluidic devices for biomedical applications

Edited by Xiujun (James) Li and Yu Zhou

WP
WOODHEAD PUBLISHING

Microfluidic devices for biomedical applications

Related titles:

MEMS for biomedical applications
(ISBN 978-0-85709-129-1)

Implantable sensor systems for biomedical applications
(ISBN 978-1-84569-987-1)

Biosensors for medical applications
(ISBN 978-1-84569-935-2)

Details of these books and a complete list of titles from Woodhead Publishing can be obtained by:

- visiting our web site at www.woodheadpublishing.com
- contacting Customer Services (e-mail: sales@woodheadpublishing.com; fax: +44 (0) 1223 832819; tel.: +44 (0) 1223 499140 ext. 130; address: Woodhead Publishing Limited, 80 High Street, Sawston, Cambridge CB22 3HJ, UK)
- in North America, contacting our US office (e-mail: usmarketing@woodheadpublishing.com; tel.: (215) 928 9112; address: Woodhead Publishing, 1518 Walnut Street, Suite 1100, Philadelphia, PA 19102–3406, USA

If you would like e-versions of our content, please visit our online platform: www.woodheadpublishingonline.com. Please recommend it to your librarian so that everyone in your institution can benefit from the wealth of content on the site.

We are always happy to receive suggestions for new books from potential editors. To enquire about contributing to our Biomaterials series, please send your name, contact address and details of the topic/s you are interested in to laura.overend@woodheadpublishing.com. We look forward to hearing from you.

The team responsible for publishing this book:

Commissioning Editor: Laura Overend
Publications Coordinator: Emily Cole
Project Editor: Elizabeth Moss
Editorial and Production Manager: Mary Campbell
Production Editor: Richard Fairclough
Project Manager: Newgen Knowledge Works Pvt. Ltd.
Copyeditor: Newgen Knowledge Works Pvt. Ltd.
Proofreader: Newgen Knowledge Works Pvt. Ltd.
Cover Designer: Terry Callanan

Woodhead Publishing Series in Biomaterials: Number 61

Microfluidic devices for biomedical applications

Edited by
Xiujun (James) Li
and Yu Zhou

Oxford Cambridge Philadelphia New Delhi

Published by Woodhead Publishing Limited,
80 High Street, Sawston, Cambridge CB22 3HJ, UK
www.woodheadpublishing.com
www.woodheadpublishingonline.com

Woodhead Publishing, 1518 Walnut Street, Suite 1100, Philadelphia,
PA 19102-3406, USA

Woodhead Publishing India Private Limited, 303 Vardaan House, 7/28 Ansari Road,
Daryaganj, New Delhi – 110002, India
www.woodheadpublishingindia.com

First published 2013, Woodhead Publishing Limited

British Library Cataloguing in Publication Data
A catalogue record for this book is available from the British Library.

Library of Congress Control Number: 2013948043

ISBN 978-0-85709-697-5 (print)
ISBN 978-0-85709-704-0 (online)
ISSN 2049-9485 Woodhead Publishing Series in Biomaterials (print)
ISSN 2049-9493 Woodhead Publishing Series in Biomaterials (online)

The publisher's policy is to use permanent paper from mills that operate a sustainable forestry policy, and which has been manufactured from pulp which is processed using acid-free and elemental chlorine-free practices. Furthermore, the publisher ensures that the text paper and cover board used have met acceptable environmental accreditation standards.

Cover image is reprinted with permission from Future Science Ltd, taken from *Bioanalysis* (2010), 2(10), Chapter 19, 1729–1744, Future Science Ltd

Typeset by Newgen Knowledge Works Pvt Ltd, India
Printed by Lightning Source

Contents

Contributor contact details

(* = main contact)

Editors

XiuJun (James) Li
University of Texas at El Paso
USA
E-mail: Xli4@utep.edu
Yu Zhou
ABS Global
USA

E-mail: zhouyu9917@gmail.com

Chapter 1

Wen-I Wu, Pouya Rezai, Huan-Hsuan Hsu, P. Ravi Selvaganapathy*
JHE 316, Department of Mechanical Engineering
McMaster University
1280 Main St W
Hamilton, Ontario
Canada L8S 4L7

E-mail: selvaga@mcmaster.ca

Chapter 2

Bahige G. Abdallah and Alexandra Ros*
Department of Chemistry and Biochemistry
Arizona State University
PO Box 871604
Tempe, AZ 85287
USA

E-mail: Alexandra.Ros@asu.edu

Chapter 3

Amgad Rezk, James Friend and Leslie Yeo*
RMIT University
Melbourne VIC 3000
Australia

E-mail: leslie.yeo@rmit.edu.au

Chapter 4

Christopher M. Collier, Jacqueline Nichols and Jonathan F. Holzman*
The University of British Columbia
3333 University Way
Kelowna, BC
Canada V1V1V7

E-mail: jonathan.holzman@ubc.ca

Chapter 5

Ning Gao*
Department of Chemistry and Chemical Biology
Harvard University M-003
12 Oxford Street
Cambridge, MA 02138
USA

E-mail: ngao@cmliris.harvard.edu

XiuJun (James) Li
Department of Chemistry
University of Texas at El Paso
El Paso, TX 79968
USA

E-mail: Xli4@utep.edu

Chapter 6

Thakur Raghu Raj Singh, Hannah McMillan, Karen Mooney, Ahlam Zaid Alkilani and Ryan F Donnelly*
School of Pharmacy
Queens University Belfast
Medical Biology Centre
97 Lisburn Road
Belfast BT9 7BL
Northern Ireland
UK

E-mail: r.donnelly@qub.ac.uk

Chapter 7

Jaspreet Singh Kochhar, Sui Yung Chan, Pei Shi Ong and Lifeng Kang*
Department of Pharmacy
National University of Singapore
18 Science Drive 4
Singapore 117543

E-mail: lkang@nus.edu.sg

Won Gu Lee
Department of Mechanical Engineering
College of Engineering
Kyung Hee University
1 Seochon, Giheung, Yongin, Gyeonggi 446–701
Republic of Korea

Chapter 8

Henry Fatoyinbo
University of Surrey
Faculty of Engineering and Physical Sciences
Centre for Biomedical Engineering
Guildford, Surre GU2 7XH, UK

E-mail: h.fatoyinbo@surrey.ac.uk

Chapter 9

Xinyu Liu*
Department of Mechanical Engineering
McGill University
Montreal, Quebec
Canada H3A 0C3

E-mail: xinyu.liu@mcgill.ca

Yu Sun
Department of Mechanical and Industrial Engineering
University of Toronto
Toronto, Ont.
Canada M5S3G8

E-mail: sun@mie.utoronto.ca

Chapter 10

Lien T. Chau, Jessica E. Frith, Richard J. Mills, Donna J. Menzies, Drew M. Titmarsh, Justin J. Cooper-White*
Australian Institute for Bioengineering & Nanotechnology
The University of Queensland
St. Lucia QLD 4072
Australia

E-mail: j.cooperwhite@uq.edu.au

Chapter 11

Dong-Ku Kang, Jente Lu, Wenwen Zhang, Elizabeth Chang, Mark A. Eckert, Md Monsur Ali and Weian Zhao*
Department of Pharmaceutical Sciences
Department of Biomedical Engineering
Sue and Bill Gross Stem Cell Research Center
Chao Family Comprehensive Cancer Center
Department of Biomedical Engineering
University of California
Irvine, CA 92697
USA

E-mail: weianz@uci.edu
weianzhao.uci@gmail.com

Chapter 12

Jonathan Lee and Paul C. H. Li*
Department of Chemistry
Simon Fraser University
8888 University Drive
Burnaby, BC
Canada V5A 1S6

E-mail: paulli@sfu.ca

Chapter 13

Bin Zhuang, Wupeng Gan and Peng Liu*
Department of Biomedical Engineering
Tsinghua University
School of Medicine
Haidian District
Beijing 100084
China

E-mail: pliu@tsinghua.edu.cn

Chapter 14

Merwan Benhabib*
785 Golden Gate Ave Apt#201
San Francisco, CA 94102
USA

E-mail: merwanbenhabib@gmail.com

XiuJun (James) Li
Department of Chemistry
University of Texas at El Paso
El Paso, TX 79968
USA

E-mail: Xli4@utep.edu

Chapter 15

Jiashu Sun and Xingyu Jiang*
National Center for Nanoscience and Technology
No. 11 Beiyitiao, Zhongguancun,
Beijing 100190
China

Email: xingyujiang@nanoctr.cn

Chapter 16

Yong Wang* and Joshua E. Mendoza-Elias
Department of Surgery/Transplant
University of Illinois at Chicago College of Medicine
840 South Wood Street
Clinical Sciences Building (MC 958), Suite 502
Chicago, IL 60612
USA

E-mail: wangy@uic.edu and jmendo27@uic.edu

Chapter 17

Artem Y. Lebedev
University of California Los Angeles
UCLA Ahmanson Biomedical Cyclotron
780 Westwood Plaza
mailroom CHS B2–096
Los Angeles, CA 90095
USA

E-mail: lebedevfedora@gmail.com

Woodhead Publishing Series in Biomaterials

1 **Sterilisation of tissues using ionising radiations**
Edited by J. F. Kennedy, G. O. Phillips and P. A. Williams
2 **Surfaces and interfaces for biomaterials**
Edited by P. Vadgama
3 **Molecular interfacial phenomena of polymers and biopolymers**
Edited by C. Chen
4 **Biomaterials, artificial organs and tissue engineering**
Edited by L. Hench and J. Jones
5 **Medical modelling**
R. Bibb
6 **Artificial cells, cell engineering and therapy**
Edited by S. Prakash
7 **Biomedical polymers**
Edited by M. Jenkins
8 **Tissue engineering using ceramics and polymers**
Edited by A. R. Boccaccini and J. Gough
9 **Bioceramics and their clinical applications**
Edited by T. Kokubo
10 **Dental biomaterials**
Edited by R. V. Curtis and T. F. Watson
11 **Joint replacement technology**
Edited by P. A. Revell
12 **Natural-based polymers for biomedical applications**
Edited by R. L. Reiss et al
13 **Degradation rate of bioresorbable materials**
Edited by F. J. Buchanan
14 **Orthopaedic bone cements**
Edited by S. Deb
15 **Shape memory alloys for biomedical applications**
Edited by T. Yoneyama and S. Miyazaki
16 **Cellular response to biomaterials**
Edited by L. Di Silvio

17 **Biomaterials for treating skin loss**
Edited by D. P. Orgill and C. Blanco
18 **Biomaterials and tissue engineering in urology**
Edited by J. Denstedt and A. Atala
19 **Materials science for dentistry**
B. W. Darvell
20 **Bone repair biomaterials**
Edited by J. A. Planell, S. M. Best, D. Lacroix and A. Merolli
21 **Biomedical composites**
Edited by L. Ambrosio
22 **Drug–device combination products**
Edited by A. Lewis
23 **Biomaterials and regenerative medicine in ophthalmology**
Edited by T. V. Chirila
24 **Regenerative medicine and biomaterials for the repair of connective tissues**
Edited by C. Archer and J. Ralphs
25 **Metals for biomedical devices**
Edited by M. Ninomi
26 **Biointegration of medical implant materials: science and design**
Edited by C. P. Sharma
27 **Biomaterials and devices for the circulatory system**
Edited by T. Gourlay and R. Black
28 **Surface modification of biomaterials: methods analysis and applications**
Edited by R. Williams
29 **Biomaterials for artificial organs**
Edited by M. Lysaght and T. Webster
30 **Injectable biomaterials: Science and applications**
Edited by B. Vernon
31 **Biomedical hydrogels: Biochemistry, manufacture and medical applications**
Edited by S. Rimmer
32 **Preprosthetic and maxillofacial surgery: Biomaterials, bone grafting and tissue engineering**
Edited by J. Ferri and E. Hunziker
33 **Bioactive materials in medicine: Design and applications**
Edited by X. Zhao, J. M. Courtney and H. Qian
34 **Advanced wound repair therapies**
Edited by D. Farrar
35 **Electrospinning for tissue regeneration**
Edited by L. Bosworth and S. Downes
36 **Bioactive glasses: Materials, properties and applications**
Edited by H. O. Ylänen

37 **Coatings for biomedical applications**
Edited by M. Driver
38 **Progenitor and stem cell technologies and therapies**
Edited by A. Atala
39 **Biomaterials for spinal surgery**
Edited by L. Ambrosio and E. Tanner
40 **Minimized cardiopulmonary bypass techniques and technologies**
Edited by T. Gourlay and S. Gunaydin
41 **Wear of orthopaedic implants and artificial joints**
Edited by S. Affatato
42 **Biomaterials in plastic surgery: Breast implants**
Edited by W. Peters, H. Brandon, K. L. Jerina, C. Wolf and V. L. Young
43 **MEMS for biomedical applications**
Edited by S. Bhansali and A. Vasudev
44 **Durability and reliability of medical polymers**
Edited by M. Jenkins and A. Stamboulis
45 **Biosensors for medical applications**
Edited by S. Higson
46 **Sterilisation of biomaterials and medical devices**
Edited by S. Lerouge and A. Simmons
47 **The hip resurfacing handbook: A practical guide to the use and management of modern hip resurfacings**
Edited by K. De Smet, P. Campbell and C. Van Der Straeten
48 **Developments in tissue engineered and regenerative medicine products**
J. Basu and J. W. Ludlow
49 **Nanomedicine: technologies and applications**
Edited by T. J. Webster
50 **Biocompatibility and performance of medical devices**
Edited by J-P. Boutrand
51 **Medical robotics: minimally invasive surgery**
Edited by P. Gomes
52 **Implantable sensor systems for medical applications**
Edited by A. Inmann and D. Hodgins
53 **Non-metallic biomaterials for tooth repair and replacement**
Edited by P. Vallittu
54 **Joining and assembly of medical materials and devices**
Edited by Y. (Norman) Zhou and M. D. Breyen
55 **Diamond-based materials for biomedical applications**
Edited by R.Narayan
56 **Nanomaterials in tissue engineering: Fabrication and applications**
Edited by A. K. Gaharwar, S. Sant, M. J. Hancock and S. A. Hacking
57 **Biomimetic biomaterials: Structure and applications**
Edited by A. Ruys

58 **Standardisation in cell and tissue engineering: Methods and protocols**
Edited by V. Salih
59 **Inhaler devices: Fundamentals, design and drug delivery**
Edited by P. Prokopovich
60 **Bio-tribocorrosion in biomaterials and medical implants**
Edited by Yu Yan
61 **Microfluidic devices for biomedical applications**
Edited by X-J. James Li and Y. Zhou
62 **Decontamination in hospitals and healthcare**
Edited by J. T. Walker
63 **Biomedical imaging: Applications and advances**
Edited by P. Morris
64 **Characterization of biomaterials**
Edited by M. Jaffe, W. Hammond, P. Tolias and T. Arinzeh
65 **Biomaterials and medical tribology**
Edited by J. Paolo Davim

About the editors

XiuJun (James) Li, PhD, is a tenure-track assistant Professor in the Department of Chemistry, Border Biomedical Research Center, and Materials Science & Engineering at University of Texas at El Paso (UTEP). After he obtained his PhD degree in microfluidic single-cell analysis with Prof. Paul Li from Simon Fraser University (SFU) in Canada in 2008, he pursued his postdoctoral research in integrated microfluidic devices for genetic analysis with Professor Richard Mathies at UC Berkeley, and low-cost diagnosis with Professor George Whitesides at Harvard University, while holding an Postdoctoral Fellowship from Natural Sciences and Engineering Research Council (NSERC) of Canada. He has gained extensive experiences in bioanalysis using microfluidic systems, such as single-cell analysis, genetic analysis, low-cost diagnosis, pathogen detection, 3D cell culture, and so on. Dr Li's research interest is centered on the development of innovative microfluidic technologies and nanotechnologies for bioanalysis and bioengineering. He has authored about 30 publications, including 2 book chapters. His research has been funded by National Institute of Health (NIH), UT System, UTEP, State Key Laboratory of Bioreactor Engineering of China and other agencies. He is the recipient of Dean of Graduate Studies Convocation Medal (SFU) in 2009 and UT STARS award in 2012.

Yu Zhou, PhD, is a Research Scientist in the Department of Research and Development at ABS Global Inc., USA. Dr Zhou received his PhD degree in mechanical engineering from University of Illinois at Chicago in 2010. After graduation, he joined ABS Global, the world-leading genetics provider company as a key researcher and has been working on the development of a high-throughput microfluidic flow cytometry for biological cell detection and manipulation. He obtained extensive experience in design and fabrication of silicon-based microsystems and disposal plastic microfluidic chips, precision fluid delivery, and microfluidics-based single cell separation and analysis. He is a member of ASME and serves on the advisory editorial board for several technical journals including *Microsystem Technologies* and *Journal of Mechanical Engineering Research* (Canada) since 2011.

Note: The order of editors' names does not denote their importance in producing this book.

Preface

Biomedical applications ranging from drug discovery and delivery and disease diagnosis to point of care (POC) devices and tissue engineering have attracted increasing attention since the last few decades. Biomedical engineering, closely related to biomedical applications, has only recently emerged as its own discipline. Conventional biomedical techniques however often face increasing challenges in different biomedical applications, such as high cost, slow diagnosis, expensive instrumentation, low drug delivery efficiency, and high failure rates in drug discovery due to the discrepancy between 2D cell-based assays and living tissues. Additionally, many cases of global diseases (e.g. malaria, tuberculosis, or TB, meningitis and hepatitis B) happen in high-poverty areas, such as rural areas and developing nations which often cannot afford expensive and high-precision instruments. For instance, according to World Health Organization (WHO) data in 2012, 'one million cases of bacterial meningitis are estimated to occur and 200 000 of these die annually'. All these pose great challenges to conventional biomedical techniques.

Microfluidic or lab-on-a-chip (LOC) devices emerged in the 1990s and have grown explosively in the last two decades due to their inherent advantages associated with miniaturization, integration, parallelization, as well as portability and automation, including low consumption of reagents and samples, rapid analysis, cost-effectiveness, high efficiency and less human interference during operation. Microfluidics offers great potential in addressing those challenges in biomedical applications. Countless microfluidic systems have been developed for high-throughput genetic analysis, single-cell analysis, proteomics, low-cost diagnosis, pathogen detection, controlled-drug release, and tissue engineering. After a concise introduction of the fundamentals of microfluidic technologies, this book highlights current cutting-edge research of microfluidic devices or LOC platforms in biomedical applications.

Part I mainly aims to introduce the fundamentals of microfluidic technologies. Suitability of device construction materials and methods is highly critical to the success of different biomedical applications. Chapter 1 is dedicated to introduce a variety of widely used materials in microfluidic devices and their corresponding fabrication methods. Because stable and well-characterized surfaces are essential to achieve desired performance in some

biomedical applications, Chapter 2 provides an overview of strategies used to accomplish surface coating. Covalent and adsorptive coating strategies are included. Actuators are responsible for sophisticated manipulation of fluids and particles in microfluidic systems and have been proved to be of significant importance in the successful implement of microfluidic operations. Chapter 3 summarizes major actuation principles used in medical devices, and concentrates on two mechanisms, namely, electrokinetics and acoustics. Digital microfluidics has recently emerged as a popular approach to transport individual droplets on an array of patterned electrodes. Therefore, Chapter 4 discusses the most recent development of this technology with particular attention to actuation and sensing scalability.

Part II focuses on applications of microfluidic devices for drug delivery and discovery. The applications of microfluidics technology in drug delivery and discovery have experienced a sustainable growth in the past two decades. Microfluidic devices have become an increasingly important tool to improve the efficiency of drug delivery and reduce side effects of treatment. Chapter 5 provides an overview of controlled drug delivery with various microfluidic devices and triggering mechanisms. In particular, Chapter 6 is dedicated to the study of the transdermal delivery of drug molecules and monitoring biological fluids using microfabricated needles and provides an overview of recent progress on the microneedle technology. The last chapter in Part II, Chapter 7, presents the roles of microfluidic chips in current drug discovery and in high-throughput screening, identification of drug targets and preclinical testing. Potential applications of microfluidic devices in chemical analysis as well as analysis of metabolites in blood for studying pathology are also discussed herein.

The cell is the basic organization unit of living organisms, capable of many basic life processes. Part III is dedicated to applications of microfluidic devices related to cellular analysis and tissue engineering. The behaviors of particles or cells in microfluidic channels have been found important to understand the motion of particles or cells of interest. Chapter 8 describes the fundamentals of microscale fluid dynamics and key issues relating to biological cell behaviors within microfluidic chips. Different mechanisms available to manipulate cells and recent development in these areas are presented in detail. Chapter 9 describes an application of a glass-based microfluidic device in trapping and automated injection of single mouse embryos for large scale biomolecule testing. Many efforts have also been dedicated to the study of cells and the surrounding culture microenvironments, which is the key to understand the complex cell biology and tissue genesis. Chapter 10 is more relative to current advances of microfluidic platforms for tissue engineering and regenerative medicine applications. Stem cells, special types of biological cells that can divide and differentiate into diverse specialized cell types, are the basic building blocks of the human body, and

the research on stem cells is one of the most fascinating areas. Chapter 11 focuses on the applications of microfluidics technology for molecular and cellular analysis of stem cells.

Part IV focuses on applications of microfluidic devices in diagnostic sensing. Miniaturization helps investigators get rid of the restrictions of low concentration, low volume of samples in protein detection and clinical diagnostics. The focus of Chapter 12 is on the development of immunoassays for antibodies and cytokines analysis on nano-bioarray chips. The impact of fully integrated microfluidic systems on high performance genetic analysis is described in Chapter 13. Recent development in DNA sequencing, gene expression analysis, infectious disease detection and forensic short tandem repeat (STR) typing with integrated microfluidic platforms has been reviewed. Many conventional diagnostic methods require bulky and expensive instruments, limiting their applications in resource-poor settings, especially in developing nations. Paper-based analytical devices have been developed for low cost and easy-to-use diagnostic applications. The ability to fabricate microfluidic channels in paper to perform parallel analysis of various biochemical analysts has been demonstrated. Chapter 14 summarizes recent advances in paper-based microfluidic devices. In addition, rapid and multiplexed detection of viral infection is highly desired in many diagnostic applications. Thus, attention has been given to microfluidic POC devices for sensitive viral detection with high specificity based on immunoassays and nucleic acid-based testing in Chapter 15. Furthermore, microfluidic devices have been applied in the field of pancreatic islet transplantation as a clinical therapy for diabetes and radiochemical synthesis for medical imaging in clinical practices, as discussed in Chapters 16 and 17, respectively. In Chapter 16, microfluidic devices are used for the study of pancreatic islet and β-cell physiology and disease pathophysiology. Chapter 17 focuses on the topic of microfluidic devices for radiochemical synthesis in production of radioactively labeled tracers for Positron Emission Tomography and Single Photon Emission Computed Tomography, which are commonly used to quantify biochemical processes in live organisms.

Xiujun James Li and Yu Zhou
August, 2013

1

Materials and methods for the microfabrication of microfluidic biomedical devices

W. I. WU, P. REZAI, H. H. HSU and
P. R. SELVAGANAPATHY, McMaster University, Canada

DOI: 10.1533/9780857097040.1.3

Abstract: The materials that have been employed for the construction of microfluidic devices have been diverse, ranging from traditional materials, such as silicon and glass, to newer polymeric materials. Similarly, the methods for microfabrication have included lithography, casting, injection molding and hot embossing, to name a few. In this chapter, we provide an overview of the various materials and methods that have been used in a diverse range of microfluidic applications. Details on the physical and chemical properties of the materials, as well as the performance characteristics of the microfabrication methods, are provided.

Key words: microfabrication, soft lithography, injection molding, hot embossing stereo lithography, parylene, PDMS, Su-8, paper, glass, silicon, polycarbonate, polyimide, PMMA, CoC/CoP, polyurethane.

1.1 Introduction

Advanced microfluidic and lab-on-a-chip devices have been extensively studied and developed over the last two decades, due to their inherent advantages such as low consumption of chemicals, rapid analysis, biocompatibility, low cost and automation in biological, biomedical and analytical chemistry studies. Since the technology for developing these devices was initially adapted from the conventional semiconductor microelectronic industry, initial devices were primarily made from silicon and glass. Many commercially available microfluidic devices are made using this technology. However, these materials are expensive, require high cost fabrication methods; newer polymeric materials have been investigated and fabrication processes have developed, especially in the context of rapid prototyping and disposable applications. Polymers are macromolecules polymerized from smaller molecules called monomers through a series of chemical reactions. They can be categorized on the basis of their structures and behaviors (Nicholson, 1997), but are mostly classified in accordance with their response to thermal treatment. They have a low cost (suited for disposable devices), can be easily

mass-produced by various rapid prototyping techniques, have a wide range of material properties (chemical inertness, low electrical, thermal conductivity, etc.), can also be tailored (using surface modification techniques) appropriately for the analyte under consideration and, more importantly, have been already used in tools and laboratory equipment where conventional biological and chemical assays have been conducted. The devices made of polymers are very amenable to automation and high throughput screening. This chapter describes some of the materials widely used in biomicrofluidic and manufacture of microelectromechanical systems (MEMS), their properties, and their fabrication methods.

1.2 Microfabrication methods

The microfabrication techniques used in construction of microfluidic devices can be broadly classified into two types. These are (1) photolithography-based, and (2) replication based. In photolithographic microfabrication, light is used to define patterns on a photosensitive material, and its wavelength determines the resolution that can be achieved. The final resolution of the pattern also depends on the limitation of optical components, and material properties such as numerical aperture and the polarity of photoresist. The photosensitive material itself can be used as a structural feature of the device, or this pattern can be transferred onto another structural material. In the replication method, a master mold is made using either the photolithographic process or traditional machining processes. This mold, which could be of any material, can withstand the operating conditions of the process, and is used to replicate the pattern or feature onto another softer material through direct physical contact. The choice of the fabrication method in any application depends on various factors such as the desired substrate, cost, speed, feature size, and profile. The following sections will briefly describe existing microfabrication technologies and materials used in microfluidic applications, along with their advantages and limitations.

1.2.1 Photolithography-based microfabrication

Photolithography is the technique of using light to define features on a photo-definable material. This technique, along with the established semiconductor manufacturing process of thin film deposition and etching, was initially adapted to produce the first microfluidic devices on silicon (Manz *et al.*, 1991; Terry *et al.*, 1979) and glass (Fan *et al.*, 1992; Jacobson *et al.*, 1994) substrates. New methods to fabricate high-aspect-ratio open microchannel structures in silicon or glass substrate using various etching techniques such as reactive ion etching, HF wet etching, or KOH wet etching, were simultaneously developed. Subsequently, the microchannels were

enclosed using bonding techniques such as electromagnetic induction heating (Thompson *et al*., 2002), hydrophobic silicon bonding (Tong *et al*., 1994), fusion bonding (Harendt *et al*., 1992), and anodic bonding (Kutchoukov *et al*., 2003). Although these processes are well developed, the cost of the substrates and of microfabrication in a clean room facility makes them unsuitable for disposable microfluidic devices. These microfabrication techniques have been extensively reviewed in review articles (Bustillo *et al*., 1998; Gad-El-Hak, 2002; Hoffmann and Voges, 2002; Judy, 2001a, 2001b; Lang, 1996; Maluf, 2002; Miki, 2005; Petersen, 1982; Rai-Choudhury, 1997; Stokes and Palmer, 2006).

The cost consideration led to the investigation and use of photo-definable polymers such as conventional photoresists that have been used for patterning in the microelectronics industry as structural elements in microfluidic devices. For instance, these photoresists were applied to create manifolds for microfluidic devices (Burns *et al*., 1998), though channel height is limited to <3 μm due to their physical parameters. Even earlier, X-rays were used to define features in photoresist using a process known as *lithographie, galvanoformung, abformung* (LIGA) to obtain >350 μm microstructures with an aspect ratio of >100:1 (Becker *et al*., 1986). Later, the photoresist SU-8, which requires no complex X-ray facility, was developed for high microstructures using the standard photolithography process (Lin *et al*., 2002; Sikanen *et al*., 2005; Yang, 2004). A channel height of 100 μm and aspect ratio of >10:1 is achievable, according its manufacturer (MICROCHEM, 2012).

Various methods have been adopted for fabrication of photoresist-based microfluidic devices. The first method shown in Fig. 1.1c begins with a spin-coating of photoresist onto a substrate, and patterning with a photomask (Metz *et al*., 2004; Tay *et al*., 2001). Once the open microchannels are created, a sacrificial material is filled into the space of the microchannel. Subsequently, a second layer of photoresist is spin-coated and patterned on top to define the access holes for inlet and outlet. Finally, the sacrificial layer is dissolved to create the closed microchannels. The major disadvantage in this process is the slow dissolution, therefore only short microchannels are applicable. The second method shown in Fig. 1.1b laminates a dry SU-8 or Kapton film on top of the open microchannels (Agirregabiria *et al*., 2005). Although this process is relatively simple, the alignment and the bonding strength of lamination could be challenging. The third method shown in Fig. 1.1a uses two exposures at different wavelengths to create the embedded microchannels in SU-8 (Dykes *et al*., 2007). The first exposure (365 nm) defines the sidewalls of the microchannels, while the second exposure (254 nm) creates the encapsulation layer for the microchannels, due to its shallower absorption depth. The exposure with two wavelengths could be inconvenient in certain circumstances and a slow dissolution problem similar to that in the first method could happen here.

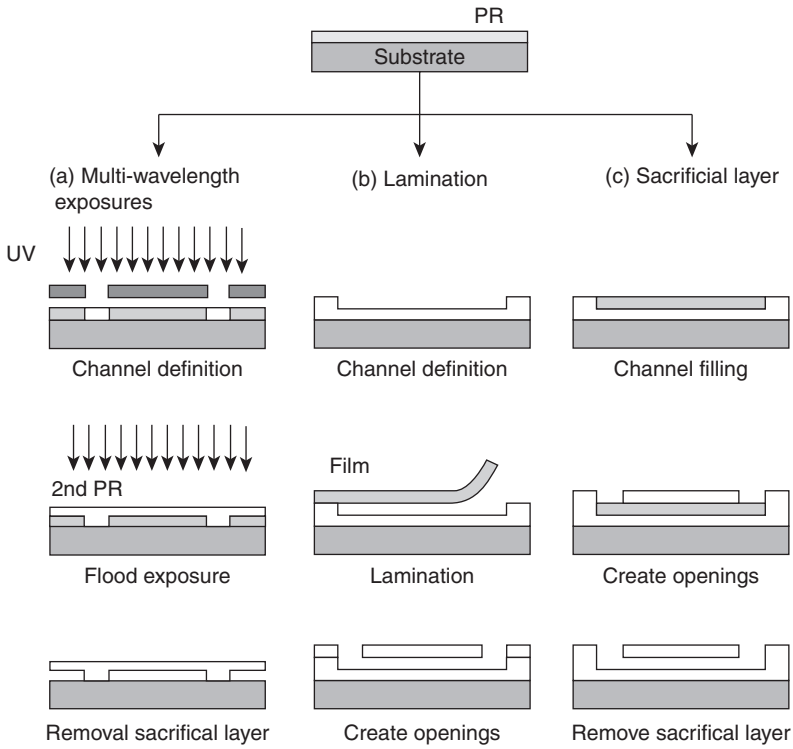

1.1 Microfabrication processes for (a) multi-wavelength exposures, (b) lamination and (c) sacrificial layer.

Alternatively, stereolithography (Morimoto *et al.*, 2009; Tse *et al.*, 2003) and laser ablation are also used for the microfabrication for microfluidic devices. The former method is an additive manufacturing process that employs liquid resins and high intensity light beams to build 3D microstructures. The photo-induced cross-linking happens upon the exposure of the liquid resin. The process time depends on the complexity of the 3D microstructures; therefore, it is commonly used for prototyping. An extensive review on stereolithography can be found in (Arnaud Bertsch *et al.*, 2002; Melchels *et al.*, 2010). The latter method is a subtractive manufacturing process that uses a focused high intensity laser beam to evaporate the material from the surface (Jensen *et al.*, 2004; Khan Malek, 2006). Laser ablation is mostly used to fabricate microchannels in thermosetting polymers such as polyimide due to its physical properties (Metz *et al.*, 2001, 2004; Yin *et al.*, 2005). Microstructures of nanometer scale have been demonstrated (Kim *et al.*, 2005); however, the surface roughness and properties using laser ablation are difficult to control and highly dependent on the manufacturing parameters. An extensive review on laser micromachining can be found in Rizvi (2003), Shiu *et al.* (2008), Dubey and Yadava (2008) and Gattass and Mazur (2008).

1.2.2 Replication based methods

One of the major advantages of using polymers in microfabrication owes largely to low cost, high volume replication methods such as soft lithography, hot embossing, and injection molding. A master (also called a mold) is an essential tool for all replication methods, and it can be fabricated through conventional photolithography, silicon etching, LIGA, laser ablation, and micro-electrode discharge machining (micro-EDM). The selection of mold fabrication method depends on the available material, resolution, aspect ratio, and processing conditions. In the following sections, brief descriptions of various replication methods and their performance characteristics are given.

Soft lithography

Due to its simple process, excellent material properties, low manufacturing cost, and high replicating accuracy, the soft lithography process has become one of the main rapid prototyping methods (Xia and Whitesides, 1998) used in microfluidics. Commonly used materials, such as Sylgard 184 by Dow Corning and RTV 615 by Elastosil, contain two components, a base elastomer and a curing agent. The mixture is degased to prevent the formation of air bubbles and then cast on the mold as shown in Fig. 1.2. After curing, the elastomer is peeled from the mold and bonded to a glass slide or other polymer sheets to create closed microchannels. Various methods have been developed to increase the bonding strength for each polymer. For example, a treatment with oxygen or air plasma can lead to a permanent bond between two PDMS layers. A replication accuracy of ~ 10 nm feature has been demonstrated using this method (Hua *et al*., 2006). In addition to elastomers, other polymers, such as polyurethane and polyester, can also be used in casting microfluidic structures since they can be cured through temperature or UV exposure (Fiorini

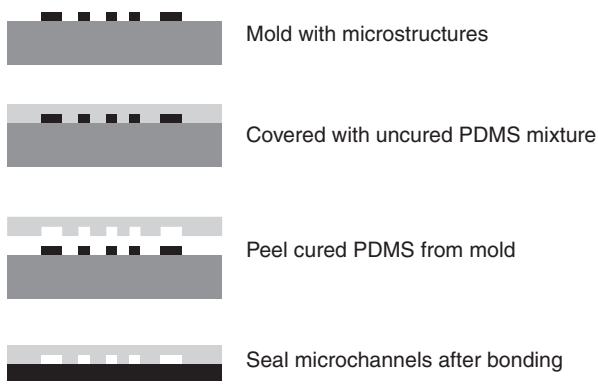

1.2 Process flow for soft lithography.

et al., 2007; Wu *et al*., 2012). An extensive review on soft lithography can be found here (Rogers and Nuzzo, 2005; Qin *et al*., 2010).

Hot embossing

Hot embossing had been commonly used for the microstructuring of polymers in industry before it was adapted for microfluidic applications due to its relatively simple process, wide selection of materials, and availability of facility. As shown in Fig. 1.3, the microstructures are transferred from the master to the polymer by stamping the master into the polymer, softened by heating above its glass transition temperature. This method is limited to thermoplastic polymers, and a variety of polymers have been successfully hot embossed with microstructures, including polycarbonate (Klintberg *et al*., 2003), polyimide (Youn *et al*., 2008), cyclic olefin copolymer (COC) (Jeon *et al*., 2011), and PMMA (Becker, 2000). The surface quality, temperature uniformity, and chemical compatibility of the master determine the success of the hot embossing. A replication accuracy of a few tens of nanometers has been achieved using this method (Kolew *et al*., 2010; Roos *et al*., 2002; Schift *et al*., 2000). A variation of this method is known as 'nano imprinting', where the feature size is from a few tens to hundreds of nanometers. An extensive review of hot embossing and nano-imprint lithography can be found in Guo (2007), Matthias Worgull (2009) and Worgull *et al*. (2005).

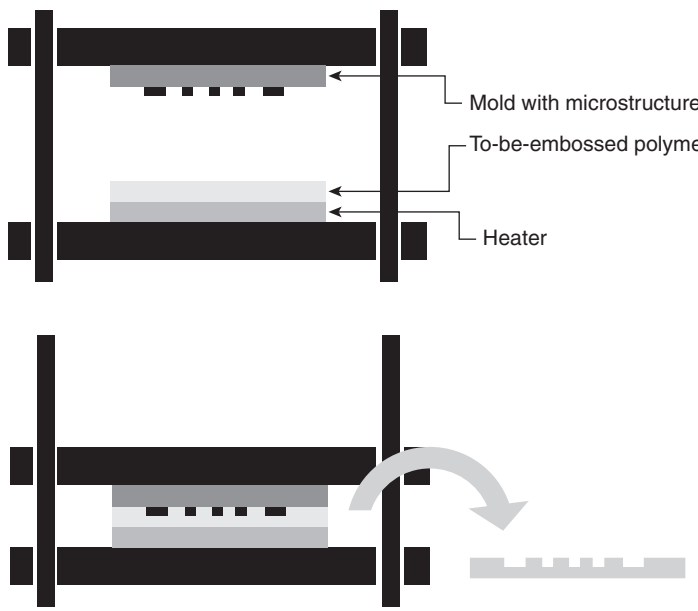

1.3 Process flow for hot embossing.

Injection molding

Similar to hot embossing, injection molding is well established as the most suitable fabrication process for polymers in high volume production, due to its fast process time and high replication accuracy. As shown in Fig. 1.4, the polymer is fed into a chamber and melted through heating (200–350°C depending on the melting temperature of polymer). It is then injected into the mold cavity and cooled to form a replica. In the microfluidic application, a good filling without trapping air bubbles is one of the key requirements for successful molding. Although the cycle times for injection molding can be as fast as several seconds, insufficient cooling time for polymers can lead to thermal stress and defect formation. The process control over various parameters such as injection pressure, molding temperatures and their duration, and cycle times etc. increases its complexity. Moreover, the relatively high cost of the mold material to ensure it is capable of withstanding a high temperature process is also one of its disadvantages. However, the major advantage of injection molding over other replication methods is its ability to form 3D microstructures without geometrical constraints, using both thermosetting and thermoplastic polymers. Additional fluidic components, such as interconnections and connectors, can also be integrated together (Gartner *et al*., 2007; Mair *et al*., 2006). An extensive review on injection molding can be found in (Attia *et al*., 2009a; Attia and Alcock, 2011; Heckele and Schomburg, 2004).

The fabrication techniques that have been briefly described in this section represent commonly used methods for fabrication of microfluidic devices.

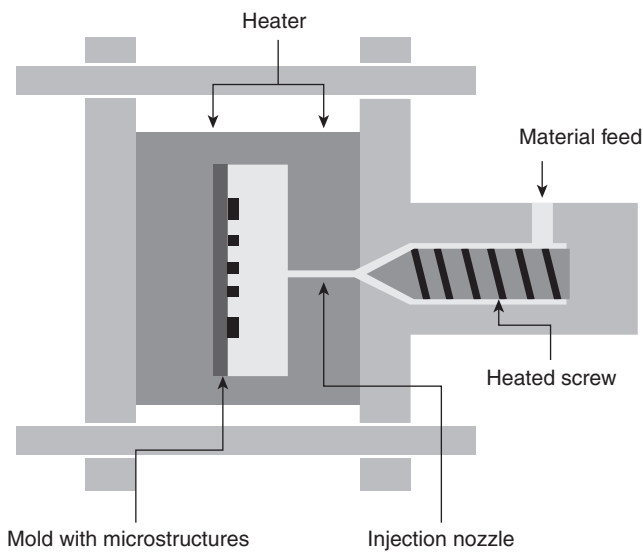

1.4 Set-up for injection molding.

In addition, there is a wide range of other methods, such as micro-thermoforming, micro-electrodischarge machining, LIGA machining, micro-milling, and precision machining, that have been used, though less frequently, for microfluidic device fabrication. These methods are reviewed in (Giselbrecht *et al*., 2004; Hupert *et al*., 2006; Malek and Saile, 2004; Nikumb *et al*., 2005; Truckenmuller *et al*., 2002; Wolfgang Ehrfeld *et al*., 1996).

1.3 Materials for biomedical devices

Although there have been several advances in the processing of microstructured materials for use in medical diagnosis and treatment such as the functional biomaterials that provide unique interactions with proteins and other biological specimens, this section will cover the common materials used for biomedical devices.

1.3.1 Glass

Glass is an amorphous, solid, silicon compound that can be also applied in fabricating microfluidic devices. This material has number of favorable features, e.g. chemically inert, insulated, transparent, and low fluorescence emission, that make it suitable for microfluidic devices used in biological or optical applications. The most commonly used glass for microfluidic device manufacturing is Corning Pyrex 7740, due to its compatibility in thermal expansion with silicon (Grétillat *et al.*, 1997). Fused silica (quartz) is another attractive material in certain applications that require UV-transparency; however, it is expensive. Also, quartz has a crystalline structure that makes anisotropic etching possible. Apart from these, there are two other kinds of glasses that have been used to fabricate microfluidic devices, namely soda lime glass and FOTURAN glass, which will be introduced in following sections.

Fabrication

The fabrication techniques for glass-based microfluidic devices have not been extensively investigated, and are not as well developed as those for silicon. Due to the amorphous nature of most glass substrates, etching using wet chemicals is usually isotropic and hence the aspect ratios obtainable are typically lower than with silicon. Despite this factor, glass has been used for fabrication of microfluidic devices, as many biochemical reactions have been characterized and standardized in these substrates. Various methods, including wet chemical etching (Zhang *et al*., 2001), plasma etching (Xinghua Li *et al*., 2001), powder machining (Schlautmann *et al*., 2001), laser micromachining (Ke *et al*., 2005), and ultrasonic drilling (Egashira *et al*., 2002) have been used to microstructure glass.

Wet chemical etching

Wet chemical etching is the most common strategy for glass microfabrication. In most cases, hydrofluoric acid (HF) is used as the main etchant for any type of silicate glass. Some other components, such as HCl, HNO_3, and NH_4F-buffer may also be added to control the etch rate (Spierings, 1993). The chemical reaction for etching is shown below:

$$SiO_2 + 6HF \rightarrow H_2SiF_6 + 2H_2O \qquad [1.1]$$

Wet chemical etching is isotropic and produces rounded side wall microchannels. The shape and angle of the side wall may be adjusted by applying

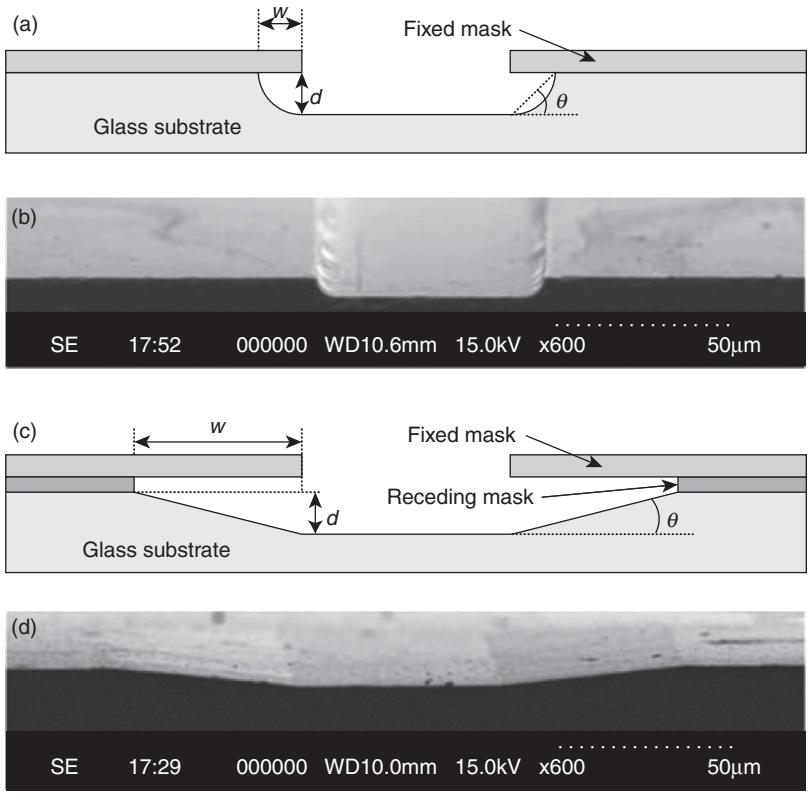

1.5 Schematic representation of etching of glass using (a) Si passive etch mask and (b) SEM image of the cross-section of a isotropic glass etching using a fixed a-Si as the etch mask. (c) Schematic representation of etching of glass with a bilayer mask made of a fixed mask and a receding mask. (d) SEM image of the cross-section of a channel etched in glass using a 10-nm layer of Ti as a receding mask. (*Source*: Reprint from Pekas *et al.* (2010) with permission.)

titanium as a receding mask during wet etching (Fig. 1.5) (Pekas *et al.*, 2010). The depth of the channel is controlled by the etch rate and etch duration. Furthermore, the width of the channel can be estimated by the mask opening plus twice the channel depth. Gold (Au) is a suitable masking material for HF etching because of its inert nature. Usually, a patterned chromium (Cr)/Au thin film is used as a mask for glass wet etching, where Cr provides the adhesion between glass and Au Poly-Si layer patterned by plasma dry etching, and photolithography is another popular masking method. In the case of some shallow etches, a thick layer of negative photoresists (i.e. SU-8) may be a simple, low cost but suitable masking material. Anisotropic wet etching of glass is possible if crystalline quartz is used as the substrate material. Z-cut wafers are typically used, as the etch rate in this direction is significantly greater than any other direction. With proper design and tuning of etch conditions (i.e. etchant concentration and temperature) (Rangsten and Hedlund, 1998), appropriate shapes required for microfluidic structures can be obtained.

Plasma etching

The fundamental principle of reactive ion etching (RIE) of glass is similar to that for silicon. During RIE etching, gas phase etchants such as CHF, CHF_3, CF_4, or their combination, are introduced in plasma to produce fluorine radicals that directionally bombard and etch the glass substrate. The chemical reaction for etching is presented below:

$$SiO_2 + CF_4 \rightarrow CO_2 + SiF_4 \qquad [1.2]$$

The etching rate decreases strongly with increasing proportion of non-volatile oxides produced during etching, resulting in a low etch rate (10 nm/min) (Ronggui, 1991). High speed directional etching of glass was achieved by applying high-density inductively coupled plasma (ICP) and a strong permanent magnet to stabilize the plasma. By doing so, the etching rates of 0.3 μm/min glass and 1 μm/min for quartz can be obtained (Xinghua Li *et al.*, 2001) (See Fig. 1.6).

Other methods

A simple method of micromachining glass has been devised through the use of the dicing process. Diamond blades (blade widths can be very thin (below 100 μm) depending on the diameter of the blade) are used in this process, with low depth of cuts to precisely define microchannels. Photoresist coating on the dicing substrate is used to prevent redeposition of debris from the dicing process onto the substrate (Ngoi and Sreejith, 2000). However, this method is usually limited to fabricating simple,

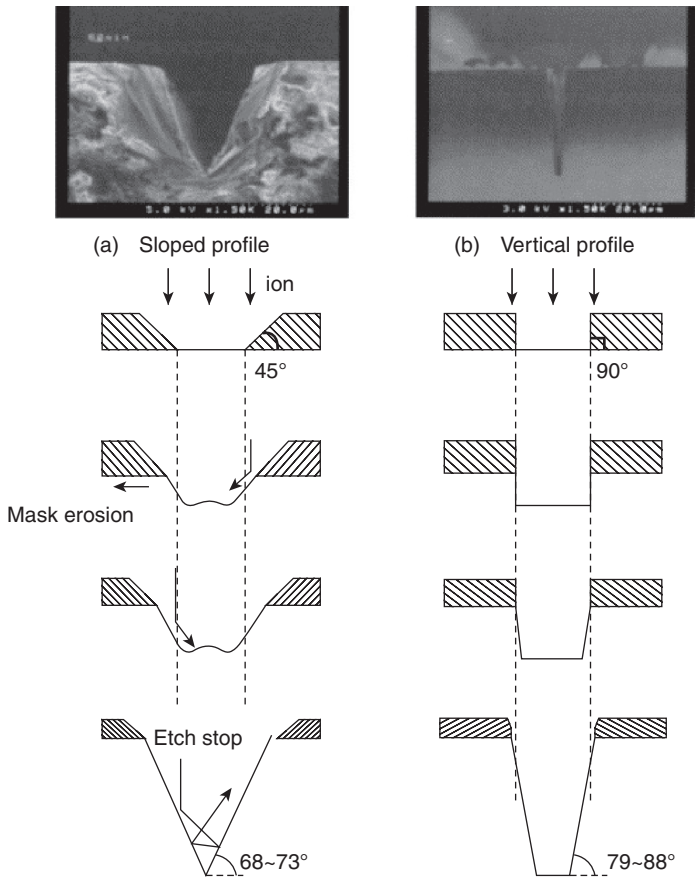

1.6 SEM images and schematic illustrations of the observed etched profiles of ICP-RIE etching (pressure 0.2 Pa, self-bias voltage 390 V, etching time 1 h). (*Source*: Reprint from Xinghua Li *et al.* (2001) with permission.)

straight microchannel structures. The aspect ratio of structures produced by dicing can be further improved by introducing ultrasonic vibration during cutting, since it can reduce cutting force thus avoiding breakage of the glass (Egashira *et al.*, 2002).

Conventional laser micromachining has been used for making a number of through-holes in glass. In this method, glass is removed by targeted ablation with a pulsed laser. The removed materials usually form debris that redeposit on the substrate, which limits its application in fabrication channel shape features (Bu *et al.*, 2004). However, Ke *et al.* performed laser micromachining under fluid where the debris could be carried away from the machining site, avoiding redeposition. By this approach, the microchannel features

were successfully synthesized in glass without any post-processing (Ke *et al.*, 2005). Recently, the femtosecond laser has been applied for nanofabrication glass with a resolution down to several hundred nanometers (100–500 nm) (Korte *et al.*, 2003). In this process, the debris formed per pulse is small and it solidifies before redeposition. By applying this technique, micro- and nanochannels with high aspect ratios and good wall-surface quality are made successfully (Hwang *et al.*, 2004; Kudryashov *et al.*, 2007).

Powder machining is another technique that is used for making interconnect through-holes in glass. In this process, sharp indenting particle jets are shot at high speed on to the substrate protected by a thick layer of masking material (Ordyl BF410 resist foil). The impingement of these sharp particles generates micro-cracks, which erode the exposed regions (defined by polymer mask) of the glass substrates (Belloy *et al.*, 2000). This procedure is able to provide fast etching rate (25 μm/min), but requires special facilities and produces features with high surface roughness (Schlautmann *et al.*, 2001).

Soda lime glass is a multi-component mixture consisting of small amounts of Na_2O, CaO, MgO, and Al_2O_3, as well as SiO_2. This material is also employed in glass microfluidic device fabrication for facilitating the glass-to-glass fusion bonding procedures (for enclosing the microfluidic channel), as well as reducing the fabrication cost (Lin *et al.*, 2001). FOTURAN glass is another special glass that made by special components that contained CeO_2, Ag_2O, and Sb_2O_3. This material would crystallize after exposure under UV light and the etch rate of the crystallized regions is increased significantly. Thus, high-aspect-ratio (20) glass microfluidic features can be obtained by using this material. More details on FOTURAN microfabrication and mechanism can be obtained in (Dietricha *et al.*, 1996).

Bonding

Glass, glass and glass-silicon wafer bonding are usually employed for sealing the fabricated glass microfluidic features. The wafer bonding can also be used to assemble several wafers with different micro-features on them to construct a complex, tall microfluidic design. Other materials, such as GaAs and SiC, can also bond on wafer to create versatile devices, e.g. electrodes, heaters, sensors, and detectors. Bonding techniques used for glass include fusion bonding, anodic bonding, and adhesive bonding. The details of these wafer bonding approaches can be found in the review paper (Gösele and Tong, 1998; Schmidt, 1998).

Applications and future trends

Since glass is one of the most widely used substrate material in biology, biomedical microfluidic devices such as those used for the DNA stretch and capture device (Sidorova *et al.*, 2009), DNA mass spectrometry (Erickson

and Li, 2004), and micro-DNA amplification (polymer chain reaction (PCR)) devices (Lagally *et al*., 2000) have typically been microfabricated in glass. Many components such as monolithic membrane valves/diaphragm pumps for high throughput assays, micro-pumps, micro-flow, and pressure sensors (Grover *et al*., 2003) have also been integrated with glass microfluidic devices. Moreover, because glass is transparent under a wide wavelength range (glass: vis–near IR transparent; quartz: UV–near IR transparent), it is widely used in making micro-optical bioanalytical devices (Xudong Fan and White, 2011).

With its unique properties, glass is the most suitable substrate for microfluidic devices for biological and biomedical application. The surface properties of glass have been well characterized for surface functionalization, as well as for electrophoretic and electrokinetic assays. Additionally, by applying the laser microfabrication, the glass-based microfluidic device can be made by signal step. However, the amorphous nature of glass, cost of the substrate, and lack of a simple bonding method have prevented widespread use of glass as a substrate in many microfluidic applications, especially in research. However, it will remain the material of choice for biological and medical applications in the commercial domain.

1.3.2 Silicon

Silicon is the second most abundant element in the Earth's crust, after oxygen. Highly pure silicon is usually extracted directly from silica (SiO_2) or other silicon compounds by molten salt electrolysis and refined by the Czochralski process into ultra-high purity single crystals that are used in the semiconductor industry and for MEMS and microfluidic devices (Lang, 1996). The widespread availability of single crystal silicon wafers, and the techniques developed for their processing in the semiconductor industry, facilitated the development of some of the first microfluidic devices, such as inkjet print heads (Kim *et al*., 2008), and gas chromatograph columns (Terry *et al*., 1979) on this substrate. Subsequently, numerous silicon-based microfluidic devices with applications in chemical and biochemical assays (Lion *et al*., 2003), disease diagnostics (Lee *et al*., 2010), drug delivery (Zafar Razzacki *et al*., 2004), and environmental monitoring (Jang *et al*., 2011) have been developed.

Fabrication

Microfabrication of silicon-based devices can be broadly classified as bulk micromachining and surface micromachining. In bulk micromachining, single crystal silicon is used as a substrate and various etching processes (wet and dry etching) are used to etch into the substrate to create the microchannel

structure. In surface micromachining, the substrate provides a stable and flat base, upon which the microchannel structure is constructed by depositing various materials in thin film form.

Bulk micromachining

In this process (Fig. 1.7a), photolithography is used to define patterns on a silicon wafer. Subsequently, the microscale features thus patterned, such as microfluidic channels and chambers, are constructed by etching into the exposed regions in the silicon substrates. Finally, another silicon or glass wafer is bonded to the micro-structured wafer to form closed microfluidic structures. The etching process used in bulk micromachining can be classified as wet (liquid) and dry (gas) etching, based on the phase of the reactants used. Depending on the etchants used, isotropic or anisotropic etching is possible (Fig. 1.8) (Petersen, 1982).

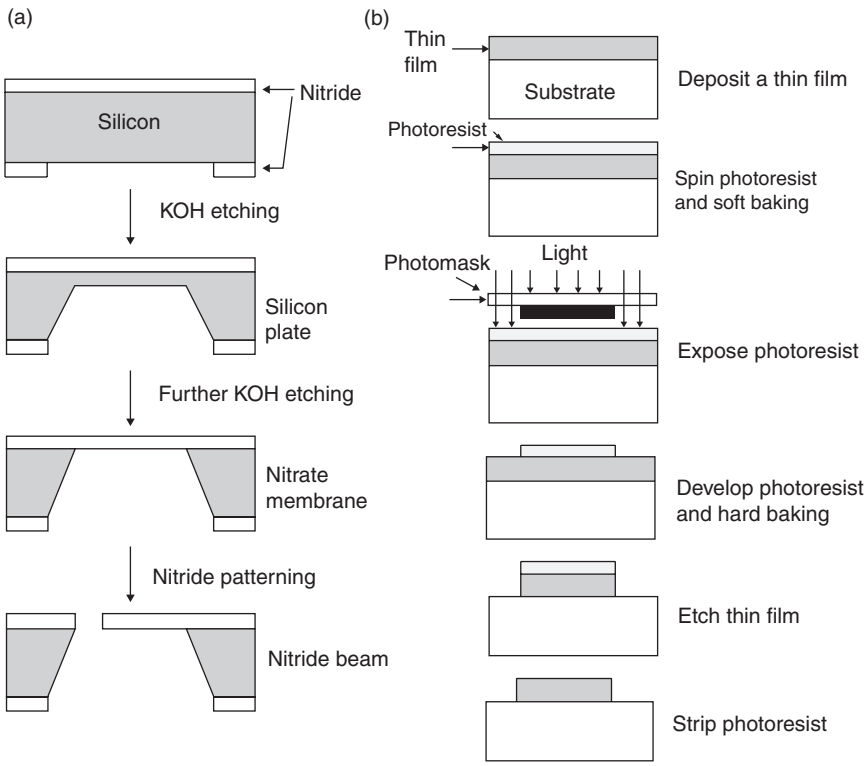

1.7 (a) Bulk micromachining and (b) surface micromachining. (*Source*: Reprint from Ziaie (2004) with permission.)

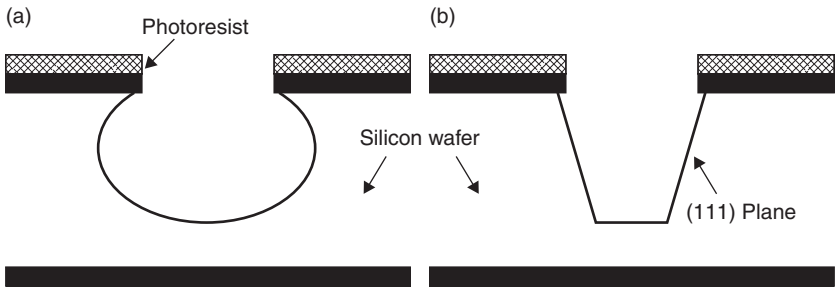

1.8 (a) Isotropic and (b) anisotropic etching. (*Source*: Reprint from Ziaie (2004) with permission.)

For instance, the combination of hydrofluoric acid (HF), nitric acid (HNO_3), and acetic acid (CH_3COOH) etches silicon without any directional dependence (isotropic). The HNO_3 oxidizes the exposed silicon surface into SiO_2, which is then subsequently etched by HF, and the reaction products dissolve into the etchant solution. The etch rate can be controlled from 0.1 to over 100 μm/min by varying the ratio of acid mixture in HNA (Maluf, 2002). Alternatively, potassium hydroxide (KOH), sodium hydroxide (NaOH), ammonium hydroxide (NH_4OH), and ethylenediamine pyrocatechol (EDP) produce anisotropic etching. The etch rate is related to the surface density of silicon atoms, which are different along various crystallographic directions in single crystal silicon. In general, the etching rate in <111> direction is two to three orders of magnitude slower than in <110> and <100> directions. The <111> planes serve as etch stop, and 3D structures with submicrometer resolution can be obtained using these etches. Microfluidic channels with sloping sidewalls (54.74°) made of (111) planes have been made using <100> wafers, while <110> wafers are used for vertical sidewalls (90°).

Dry etching of silicon is typically carried out by using reactants (etchants) in gaseous form to the wafer and using plasma to energize and direct them toward the wafer. This process is known as RIE. This process can be either isotropic or anisotropic, depending on the pressure in the plasma chamber and the electric field that provides directionality to the ionic species in the plasma (Verpoorte and De Rooij, 2003). One of the most popular RIE processes is the Bosch process, which involves the alternative plasma etching and protection layer deposition step. Deep reactive ion etching (DRIE) using the Bosch process can obtain very high-aspect-ratio structures with anisotropies in the order of 30:1 and sidewall angles of 90±2 degrees with typical etch rates of 2–3 μm/min (Kovacs *et al*., 1998). An extensive review of bulk micromachining processes are detailed in Fu *et al*. (2009).

Surface micromachining

In this process (Fig. 1.7b), silicon-based materials are deposited in thin film form using chemical vapor deposition processes to produce structural features on a substrate. Two kinds of materials are deposited alternately till the entire structure is built. Poly-silicon (Poly-Si) is generally used as a structural material while silicon dioxide (SiO_2) and silicon nitride (Si_3N_4) is used as the sacrificial material. First, the sacrificial material (SiO_2) is deposited and patterned using photolithography to produce the features of the microfluidic channels or networks. Then, poly-Si is deposited over it and patterned, again using photolithography, to expose the structural material only in the reservoir or interconnect regions. Several layers of microchannels or microscale features can be built by alternately depositing and patterning the structural and sacrificial materials. Finally, the fabricated devices are exposed to HF, which etches all of the patterned SiO_2, leaving behind the poly-Si structure that forms the microfluidic network. The process requires highly compatible materials and chemical etchants with high etch selectivity so that the etching of one will not affect the other. An extensive review of various surface micromachining methods and process is detailed in (Bustillo *et al*., 1998).

Applications and future trends

Many essential components of microfluidic devices have been fabricated in silicon, such as (1) micro-valves (Oh and Ahn, 2006); (2) micro-pumps (Laser and Santiago, 2004); and (3) channels (Verpoorte and De Rooij, 2003), using a combination of the various micromachining methods. Silicon-based microfluidic devices have found application in inkjet printing (Petersen, 1979), liquid chromatography (LC) (Manz *et al*., 1990), gas chromatography (GC) (Terry *et al*., 1979), mass spectroscopy (MS) (Schultz *et al*., 2000), cell detection (Verpoorte *et al*., 1992), disease diagnostics (Vo-Dinh and Cullum, 2000), DNA extraction (Tian *et al*., 2000), drug delivery (Chung *et al*., 2008), and miniaturized flow injection analysis (FIA) (1994).

Silicon is one of the first materials used for fabricating microfluidic devices. There are several advantages that make silicon suitable: (1) the micromachining technology for silicon is well developed; (2) oxidation of silicon surface produces SiO_2, which is an ideal surface that is suitable for biochemical analysis; and (3) various surface modification chemistries are available for silicon and SiO_2 that make it suitable for functionalization of biomolecules. However, the cost associated with cleanroom processing and the time involved with micromachining, along with the cost of the substrate itself, make devices made of silicon expensive. Still, the advantages that silicon possesses make it an ideal material of choice for microfluidic components and some devices in the commercial domain.

1.4 Polymers

Polymers are macromolecules polymerized from smaller molecules called monomers through a series of chemical reactions. They can be categorized on the basis of their structures and behaviors but are mostly classified according to their response to thermal treatment.

1.4.1 Polydimethyl siloxane (PDMS)

PDMS exists in various forms such as fluid, gel, elastomer, resin, and rubber (Brook, 2000) and has been used extensively in microfluidic applications for analytical chemistry (Seethapathy and Górecki, 2012), biology (Sia and Whitesides, 2003; Kartalov *et al*., 2006), biomedical devices, and medicine. PDMS consists of repeating Si-O backbones with two CH_3 organic side-arms linked in the polymeric chain. PDMS can be made into its elastomeric form by a process of cross-linking long chain siloxane oligomers containing vinyl-terminated end groups (base) with short chain cross linkers. The reaction mixture also contains platinum-based catalyst, inhibitors, and silica filler (Fu *et al*., 2003). The process of cross-linking and polymerization is accelerated by heat treatment and increasing the volumetric ratio of cross-linker to base, which also increases the rigidity of the final elastomer (Campbell *et al*., 1999).

Fabrication of microfluidic devices using PDMS

The process used to fabricate microdevices in PDMS material is termed soft lithography (Xia and Whitesides, 1998; McDonald *et al*., 2000). In this process, a master mold is created where the microchannel geometry is defined on photoresists photo-lithographically on a silicon wafer as protruded features (Qin *et al*., 1996; Duffy *et al*., 1998; Xia and Whitesides, 1998). Master molds have also been fabricated using silicon bulk micromachining methods (Effenhauser *et al*., 1997). Then, components of commercially available PDMS base and agent (Sylgard 184 Kit, Dow Corning, USA) are mixed in an appropriate volumetric ratio and cast over the master mold. Cross-linking and polymerization are achieved through the application of heat (65–90°C for 2–4 h), after which the PDMS elastomer formed is peeled off the master mold, forming a negative replica. Fluid access ports are punctured and the micro-structured substrate is bonded to a second PDMS layer for enclosure. Chemical surface treatment (i.e. silanized in 3% v/v dimethyloctadecylchlorosilane in toluene for 2 h) of the master mold before casting can serve as a mold release layer and improve the reliability of the casting process. The process flow is depicted in Fig. 1.2. Fabricated PDMS microchannels are shown in Fig. 1.9.

A replication accuracy of ~10 nm has been demonstrated for PDMS material itself (Hua *et al*., 2006). Therefore, the feature size that can be obtained largely depends on the resolution and capability of the process creating

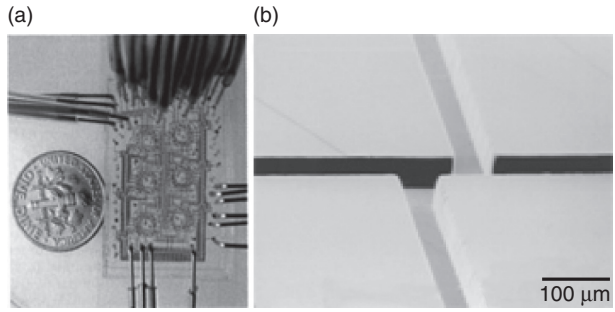

1.9 (a) A bioreactor fabricated from PDMS with multiple side input/output interconnects. (*Source*: Reprinted with permission from Balagadde *et al*. (2005).) (b) Scanning electron microscopy view of the microchannels of another capillary electrophoresis device made of PDMS. (*Source*: Reprinted with permission from Duffy *et al*. (1998), Copyright (1998) American Chemical Society.)

Table 1.1 Minimum feature sizes (MFS) and maximum aspect ratios (AR) fabricated in PDMS

Fabrication method	MFS (μm)	AR	Ref.
Multi-spinning of SU8 for photolithography and soft lithography	20	17	Natarajan *et al.*, 2008
LIGA and PDMS casting	20	15	Kim *et al.*, 2002
Laser and electron discharge micromachining followed by PDMS casting	<20	4	Shiu *et al.*, 2010
Proton Beam Writing for Ni masters and PDMS casting	2.5	5.2	van Kan *et al.*, 2007

master molds. Table 1.1 summarizes the minimum feature sizes and maximum aspect ratios achieved in PDMS replication using various processes that are commonly used to make master molds.

Interconnection and bonding

One of the contributing factors toward the popularity of PDMS as a rapid prototyping material is the ease with which strong bonding to various substrates can be obtained as well as the variety of methods for interconnection.

Interconnection is used to connect microfluidic networks in chips to macroscale devices, ports, and fittings. Various methods have been developed for interconnection to PDMS devices, including manual or machine-based coring and insertion of needles or tubing such as low density polyethylene (LDPE) tube, as well as the usage of more standardized world-to-chip interface sockets. These have yielded interconnects that withstand pressure of 100–700 kPa without leakage (Fredrickson and Fan, 2004; Christensen *et al*., 2005b; Bhagat *et al*., 2007; Quaglio *et al*., 2008; Westwood *et al*., 2008). The strength of the interconnect has also been enhanced through plasma oxidization prior to interconnection, intermediate adhesive layers, and usage of fastening O-rings (Li and Chen, 2003; Fredrickson and Fan, 2004; Christensen *et al*., 2005a; Saarela *et al*., 2006; Bhagat *et al*., 2007; Quaglio *et al*., 2008).

Reversible and irreversible bonding of PDMS to itself as well as a variety of other materials has been realized. Some of the widely used methods of bonding PDMS include:

Plasma treatment: after peeling off the master mold, the surface of the PDMS is inertly hydrophobic due to the presence of the surface methyl groups. Exposure to oxygen plasma opens up hydrophilic hydroxyl radicals on the surface, which upon conformal contact with another oxidized PDMS surface will form irreversible Si-O-Si bonds (Duffy *et al*., 1998). The plasma exposed surfaces have to be brought into contact immediately to ensure strong bonding. Delay after exposure leads to diffusion of PDMS chains from the bulk onto the surface, which reduces the surface density of hydroxyl groups responsible for bonding (Hillborg *et al*., 2000). In addition to PDMS (Duffy *et al*., 1998; Eddings *et al*., 2008), bonding to glass, Si (Bhattacharya *et al*., 2005) and passivated layers on Si (i.e. phosphosilicate glass (PSG), undoped silicate glass (USG), Si_3N_4, and SiO_2 (Tang *et al*., 2006) have also been achieved by this method. Plasma treatment with other gases (1:2 argon:oxygen) has also been employed to investigate the bond between polyethylene terephthalate glycol (PETG), COC, and polystyrene (PS) with PDMS and polyurethane (PU) layers (Mehta *et al*., 2009). PDMS and parylene have been bonded using exposure to SF_6:N_2 plasma (Rezai *et al*., 2011). In addition to surface oxidization for making the PDMS surface hydrophilic, methods involving treatment of PDMS surface with sodium silicate (low temperature adhesive for glass bonding applications) (Wang *et al*., 1997; Ito *et al*., 2002), sol-gel techniques (Roman *et al*., 2005), silanization (Papra *et al*., 2001), chemical vapor deposition (Lahann *et al*., 2003), atom transfer radical polymerization (Xiao *et al*., 2002), and polyelectrolyte multilayers (Liu *et al*., 2000) have also been investigated.

Chemical treatment: Eddings *et al*. (2008) used other chemical-based methods such as partial PDMS curing, varying base:agent mixing ratio and uncured PDMS adhesive to bond two PDMS layers. Fabrication of multilayer microfluidic 3D networks has been achieved by the 'multilayer soft

Table 1.2 PDMS bonding to various materials

PDMS bonded to	Bond quality	Bonding method	Parameters	Description	Ref.
Glass	74 psi	Oxygen plasma	Time: 5–60 s, power: 5–150 W, pressure: 20–1000 mTorr	Optimum: time 20 s, pressure >700 mTorr, power 20 W	Bhattacharya *et al.*, 2005
PSG USG Si3N4	100% bonded area	Oxygen plasma	Power: 20–140 W, Pressure: 30–500 mTorr, time: 10–40 s, Temperature ineffective	Optimum: Pressure 30 mTorr, Power 60 W for PSG, USG, Si3N4.	Tang *et al.*, 2006
SiO2	0% bonded area				
LTCC [a]	No leakage	Oxygen plasma	1.5 mL/min flow (1 kPa) into PDMS/LTCC channel		Malecha *et al.*, 2009
PDMS	300 kPa 290 kPa 650 kPa 470 kPa 670 kPa	oxygen plasma corona discharge partial PDMS curing PDMS base:agent ratio uncured PDMS adhesive	with optimum ratio of 15:1 base:agent		Eddings *et al.*, 2008
PETG [b], COC [c], PS [d]	120 kPa for PETG–PU bonds	Plasma	1:2 argon:oxygen Plasma and overnight 60°C heat and 1 lb pressure	PDMS bonding to these materials was stable over several months	Mehta *et al.*, 2009
PDMS PMMA	400 kpa 1100 kPa	Chemical + Plasma	5% APTES [e] in water		Vlachopoulou *et al.*, 2009
PC PET U-PET	178 kPa and 579 kPa 579 kPa 607 kPa	Chemical gluing + Plasma	APTES [d] and GPTES [f]	U-PET is PET with a urethane functionality on the surface	Tang and Lee, 2010
Parylene	1.7 MPa	SF_6 and N_2 plasma		Parts fabricated, then bonded	Rezai *et al.*, 2011

Source: Rezai (2011).

[a] Low temperature co-fired ceramics

[b] Polyethylene terephthalate glycol

[c] COC

[d] polystyrene

[e] 3-aminopropyltriethoxysilane

[f] 3-glycidoxypropyltriethoxysilane

lithography' method (Unger *et al*., 2000). Each layer containing an excess amount of PDMS base or cross-linker chemical is cast over its mold, peeled off, and bonded to the other layer with an opposite chemical composition. Migration of excess molecules toward the interface forms a bond, resulting in a monolithic elastomeric device.

PDMS-PDMS and PDMS—PMMA bonds were realized by immersing or spin-coating the surfaces with a thin layer of diluted silane solution (5% 3-aminopropyltriethoxysilane (APTES) in water), plasma oxidizing, and physically attaching together (Vlachopoulou *et al*., 2009). An extension of this technique was used to bond PDMS to PMMA, PC, PET, U-PET and PI (Tang and Lee, 2010).

Mechanical: PDMS-PMMA and PDMS-parylene bonding have been achieved by low temperature and applied mechanical pressures on the assembly (Ko *et al*., 2003; Kim and Najafi, 2005; Chow *et al*., 2006).

A comprehensive view of the various bonding methods used, methodology and the bond strengths obtained is summarized in Table 1.2.

Applications and future trends

PDMS is considerably cheaper compared to traditional MEMS substrates such as silicon or glass; it can be easily replicated and bonded to a diverse range of substrates; it has been used to develop various fluidic components (Ng *et al*., 2002); and it has satisfactory optical transparency, mechanical stability (Armani and Liu, 2000), gas permeability, and biocompatibility (Chang *et al*., 2007). These characteristics make PDMS the material of choice for rapid prototyping of microfluidic devices. The evidence of this is its extensive use in prototyping of microfluidic devices for chemistry, biology, and medicine-based applications (Sia and Whitesides, 2003; Kartalov *et al*., 2006; Seethapathy and Górecki, 2012). PDMS will continue to be used as a popular rapid prototyping material for microfluidic devices in a variety of academic and industrial setting.

1.4.2 Parylene

Parylene is another widely used polymer in microfluidic applications. It has a *para*-xylylene backbone and is commercially available in the forms of basic N (poly-*para*-xylylene) and C and D that have 1 and 2 chlorine atom replaced in their benzene backbone, respectively. Parylene has been widely used in fabrication of microchannels (Man *et al*., 1997; Webster and Mastrangelo, 1997), micro-valves (Rich and Wise, 1999; Wang *et al*., 1999; Carlen and Mastrangelo, 2002; Chen, 2007), membrane filters (Yang *et al*., 1998), peel-off masks for protein and cell micro-patterning (Ilic and Craighead, 2000; Jinno *et al*., 2008; Wright *et al*., 2007, 2008; Delivopoulos *et al*., 2009; Tan *et al*.,

2010), functionalized coated surfaces for 3D patterning of proteins (Chen and Lahann, 2005), spatially selective coating of microchannels for surface functionalizing (Chen *et al*., 2006a; Chen and Lahann, 2007), microelectronic circuits (Olson, 1989; Lin and Wong, 1992), biological sample encapsulations (Nosal *et al*., 2009), dielectric interlayers (Selbrede and Zucker, 1997), and wire bond enforcement (Flaherty, 1995) in microchip packaging. Readers are referred to a recent article by Tan and co-workers (Tan and Craighead, 2010) for more elaborate review of parylene applications.

Fabrication of microfluidic devices using parylene

Parylene has a high molecular weight and its structure is linear and highly crystalline, therefore it cannot be molded (high T_g) in a process similar to PDMS. As a result, it can only be vapor deposited in the form of thin conformal layers (Gorham, 1966) with an inherent hydrophobic property (surface free energy of 19.6 mN/m). Deposition is done through thermal sublimation of dimers at 140–160°C (in furnace), vapor phase splitting into monomers at 680°C (in pyrolysis chamber), and conformal deposition (Lee *et al*., 1995) and polymerization on the surfaces under vacuum at room temperature (in deposition chamber).

Complex structures can be microfabricated after parylene deposition using surface (Fig. 1.10a) (Webster *et al*., 1998) and bulk (Tacito and Steinbruchel, 1996) micromachining as well as micro-molding (Fig. 1.10b) (Noh *et al*., 2004) techniques. Since it is resistant to solvents, it can be used

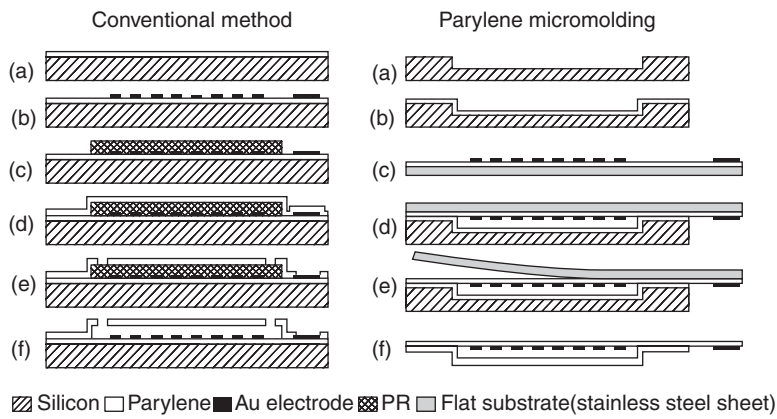

1.10 Parylene microfabrication. (a) Surface micromachining: parylene deposition, electrode patterning, photolithography, 2nd parylene deposition and photoresist etch away and (b) micro-molding: substrate etching, parylene deposition, electrode patterning, 2nd parylene lamination and base peel-off. (*Source*: With permission Noh *et al*., 2004.)

Table 1.3 Minimum feature sizes (MFS) and maximum AR fabricated in parylene

Fabrication method	MFS (μm)	AR	Ref.
O_2 and Ar ICP [a]	6	9	Selvarasah *et al.*, 2008
DRIE-based Si molds, parylene deposition and release by Si wet etching	10	10–30	Suzuki and Tai, 2003, 2006
DRIE Si etching, parylene deposition and back plasma realease etching	20	10	Zoumpoulidis *et al.*, 2009

[a] ICP: inductively coupled plasma.

in lithographic processes as the main structural layer (using patterned photoresist as sacrificial layers, Fig. 1.10a) or can be dry etched in oxygen- and/or fluorine-based plasmas.

Similar to many other materials, various applications require high-aspect-ratio and microscopic structures fabricated in parylene (a few examples are listed in Table 1.3).

Interconnection and bonding

Interconnection to parylene-based micro- and nano-fluidic channels has been achieved using a variety of methods. Peeled-off parylene channels were punched by needles and polyimide-coated silica micro-tubes were attached and epoxy glued to them, withstanding up to 0.2 SCCM water flow (Noh *et al.*, 2004). Photocurable adhesives have also been used for interfacing parylene micro-tubes to microfluidic reservoirs (Ilic *et al.*, 2002). In order to interface surface micromachined parylene channels, SU-8 anchors housing multiple PDMS sockets at the end of the parylene channel were used, each receiving a syringe needle horizontally as the interconnects (Lo and Meng, 2011). Most of these methods tend to fail at high flow or high pressure conditions, making interconnection to parylene devices a more difficult task compared with PDMS.

Bonding of parylene to other materials is somewhat more challenging, due to the strong chemical backbone structure of this material; however, a number of bonding methods have been introduced (Rezai *et al.*, 2011) that are listed in Table 1.4. Here are the most popular methods used for parylene bonding to other materials:

Silanization: Parylene adhesion to silicon oxide and nitride layers, as well as metals such as Au, Cr, and Ti, was enhanced by using a surface silanization pretreatment step. However, this method was not as effective in bonding parylene to silicon and Al.

Plasma treatment: Similar to the PDMS-based bonding methods discussed above, surface plasma treatment (using Ar, CH_4, O_2. SF_6, and N_2 gases) of

Table 1.4 Parylene bonding to various materials

Parylene bonded to	Bond quality	Evaluation method	Bonding method	Parameters	Description	Ref.
PTFE [a], PP [b], PE [c], PMMA, glass	4–5	Qualitative 0–5 scale, 5 being best bonding	Argon and methane plasma	Plasma treatment was followed by direct parylene layer deposition	Thin hydrocarbon formed after exposure	Sharma and Yasuda, 1982
Parylene	3.6 MPa	Tensile	Thermo-compressive	Heat + 0.1 MPa Pressure	For bonding Si wafers	Kim and Najafi, 2005
PDMS	1.7 MPa	Tensile	SF_6 and N_2 plasma		Parts fabricated, then bonded, interface bond stronger than PDMS itself	Rezai *et al.*, 2011
Au, PI	Weak	Peel test: Bond strength (mN/cm)=peel force/sample width	Oxygen plasma and dispersion in the silane A-174 before deposition	Effect of annealing, deposition pressure and steam sterilization after deposition was studied		Hassler *et al.*, 2010
Si_3N_4, Pt	1000 mN/cm				Enhanced three magnitude orders just by Silane	
Parylene C	2000 mN/cm				Generally strong, PO distracting bond	
Parylene	Strong	Qualitative	Thermo-compressive	545 K Heat + 1.1 kPa Pressure	Reactive multilayer Ni/Al foils	Qiu *et al.*, 2009
SiO_2	10 MPa	Tensile	O_2 Plasma + Thermo-compression	200W, 15 s + 280°C–100 kPa, 40 min	Should start bonding with 1 h after plasma	Ciftlik and Gijs, 2011
Si_3N_4	23 MPa	Tensile	O_2 Plasma + Thermo-compression	200W, 15 s + 280°C–100 kPa, 40 min	Should start bonding with 1 h after plasma	Ciftlik and Gijs, 2012

Source: Rezai *et al.*, 2011 with permission.

[a] Polytetra fluoroethylene

[b] polypropylene

[c] polyethylene

various surfaces (parylene, PTFE, PP, PE, PMMA, glass, SiO_2, Si_3N_4, PDMS, Au, and Pt as the most widely used materials), followed by an immediate parylene deposition process, has been extensively studied and used for bonding purposes (Sharma and Yasuda, 1982; Hassler *et al*., 2010; Ciftlik and Gijs, 2011, 2012; Rezai *et al*., 2011). Plasma treatment of parylene results in etching a thin layer off the surface and subsequent exposure of active nucleation sites that can enhance bonding. Hessler *et al*. (2010) used oxygen plasma treatment to successfully bond parylene to itself, Si_3N_4, and Pt as an encapsulation material for neural prostheses. In this study, oxygen plasma exposure alone was ineffective in bonding parylene to Si_3N_4 and Pt and a pretreatment with silane A-174 before deposition was required. In the study by Sharma *et al*. (Sharma and Yasuda, 1982), it has been reported that Ar and CH_4 plasma treatments are more effective in bonding parylene to several other materials (Table 1.4) than that of O_2 plasma, due to generation of more radical species on the surfaces for covalent bonding to parylene.

Most of the plasma-based methods introduced above are followed immediately by parylene deposition without breaking the vacuum pressure conditions of the chamber. With this, it is not possible to perform post-parylene-deposition processes such as patterning of the surfaces. Rezai *et al*. (2011) introduced a method to bond already-cured PDMS and parylene surfaces together using a plasma enhanced method. With this, fabrication of dual-material PDMS-parylene microchannels in an easy way without a need for sacrificial layers was made possible.

Thermo-mechanical: Another method that has been widely used for parylene bonding is the application of heat and compressive forces, mostly in order to bond already deposited parylene layers to other surfaces such as nitrides and oxides. This is useful when patterning of the parylene layer is required before bonding, such as for fabrication of microfluidic channels (Ciftlik and Gijs, 2011, 2012). The heat can be generated externally or internally on the chip by using reactive multilayer Ni/Al foils for exothermic reaction-based heat generation (Qiu *et al*., 2009). This method has been widely applied to bonding silicon wafers to each other by the application of a parylene interfacial layer (Kim and Najafi, 2005).

Applications and future trends

Parylene is inherently hydrophobic. The hydrophobicity can be enhanced by buffered hydrofluoric acid (BHF) and hydrofluoric acid (HF) exposure, or changed to hydrophilicity by chromium etchant or oxygen plasma (Hwang *et al*., 2004) exposure. Due to vacuum-based fabrication process and lack of initiators and catalysts in parylene polymerization, chemically pure parylene layers can be deposited. Room-temperature deposition process leads to formation of mechanical stress-free layers with no pin-holes

(useful for PDMS coating for long gas permeability (Lei *et al*., 2011)) and good dielectric breakdown properties, especially below 1 μm. As opposed to other porous polymers such as PDMS, parylene has a low gas permeability (moisture vapor permeability of 1.7×10^{-16} kg-m/N.s) and good stability against organic solvents. Parylene is also optically transparent (low optical absorption above 280 nm wavelengths) with a low auto-fluorescence behavior (Sasaki *et al*., 2010), as well as chemically and biologically inert (Tooker *et al*., 2005; Chang *et al*., 2007), which make it an ideal material for biomicrofluidic and biomedical applications. Using these fabrication processes, parylene-based devices have been used for DNA separation (Webster *et al*., 1998), PCR (Man *et al*., 1997), cochlear implants (Bell *et al*., 1997), biochemical reactions (Brahmasandra *et al*., 1998), biological materials surfaces protection (Nosal *et al*., 2009), micro-valves for drug delivery (Rich and Wise, 1999; Carlen and Mastrangelo, 2002), electro-osmotic pumping (Freire *et al*., 2011), micro-needles, micro-tubes (Ilic *et al*., 2002), microchannels (Chen *et al*., 2006b), 3D micro-fluidic mixers (Liu *et al*., 2008), and neurocages (Fig. 1.11) (Erickson *et al*., 2008). Although the properties of parylene make it suitable for some applications, especially those requiring chemical inertness, minimal adsorption, or electrical insulation, the lack of a simple yet strong bonding and interconnection method has prevented its continued widespread use in rapid prototyping of a wide variety of microfluidic devices.

1.4.3 Polycarbonate

Polycarbonates (PC) are one of the thermoplastic polymers which can be easily molded using thermoforming processes. The major advantages of PC over other plastics are its ultimate strength (~2.0 GPa) and transparency

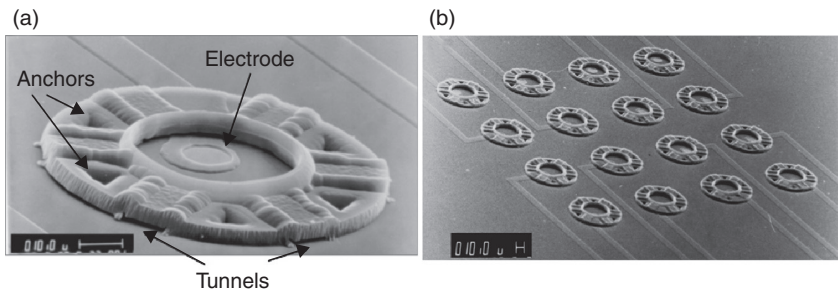

1.11 SEM pictures of (a) a single and (b) an array of microfabricated neurocages made out of 4 μm of parylene integrated with electrodes. Cages were used to study neuronal signaling actuated by electrical stimuli. Scale bars = 10 μm. (*Source*: With permission Erickson *et al.,* 2008.)

throughout the visible spectrum down to 400 nm. It is not as chemically inert as plastics. For instance, organic solvents such as acetone and ammonia are not compatible with PC. Its high refractive index ($n = 1.58$) make it attractive for optical applications. PC has a glass transition temperature of 145°C, which is usually sufficient for most biological microfluidic applications such as PCR thermal cycling.

Microfabrication methods for PC can be categorized as direct structuring such as laser ablation (Lin *et al.*, 1999; Waddell, 2002; Suriyage *et al.*, 2004) with a width over 50 μm and an aspect ratio up to 10, and micro-milling (Ogonczyk *et al.*, 2010) with a diameter over 30 μm and an aspect ratio up to 1, or replication methods such as injection molding (Ruprecht *et al.*, 1995; Holger Becker and Locascio, 2002; Gottschlich, 2004; Chen *et al.*, 2005; Griffiths *et al.*, 2007; Attia *et al.*, 2009b), and hot embossing (Liu *et al.*, 2001; Ye *et al.*, 2005) with a width over 40 μm and an aspect ratio up to 2. An extensive review of microfabrication methods for PC can be found elsewhere (Holger Becker and Locascio, 2002; Jensen *et al.*, 2004; Holger Becker and Gärtner, 2008; Attia *et al.*, 2009b).

Various bonding methods have been used in the fabrication of PC microfluidic devices and they can be classified into thermal, chemical and adhesive methods. Thermal processes (Yang *et al.*, 2002; Chen *et al.*, 2005; Park *et al.*, 2008; Ogonczyk *et al.*, 2010) use compression at a temperature around its glass transition temperature for bonding slabs or thin foils, and results in an average bonding strength of 0.55 MPa. Chemical bonding induced by the modification of surface chemistry can be achieved by the plasma treatment (Klintberg *et al.*, 2003; Wang *et al.*, 2008) or the introduction of active surface groups (Lee and Ram, 2009), and shows a highest bonding strength of over 6.8 MPa. Alternatively, there are some commercial glues or adhesives that can be used to create a strong bonding as well.

Due to its higher glass transition temperature and low manufacturing cost, PC is an ideal material for fabrication of disposal devices and has been used in several biomedical and bioanalytical applications such as PCR (Fig. 1.12) (Liu *et al.*, 2001; Yang *et al.*, 2002; Hashimoto *et al.*, 2004; Chan *et al.*, 2008; Cooney *et al.*, 2012; Peham *et al.*, 2012).

1.4.4 Polyimide

Polyimide (PI) is a thermosetting plastic and exhibits very low creep and high tensile strength compared to other thermoplastics. PI also has excellent thermal stability ($T_g > 400$°C) and chemical resistance, thus it has been used as an insulation film in flexible printed circuit boards (PCB) for the electronics industry, and adhesive and photoresist in the semiconductor industry.

Due to PI's photosensitivity, structural features can be fabricated in it using conventional photolithography processes, which is a significant

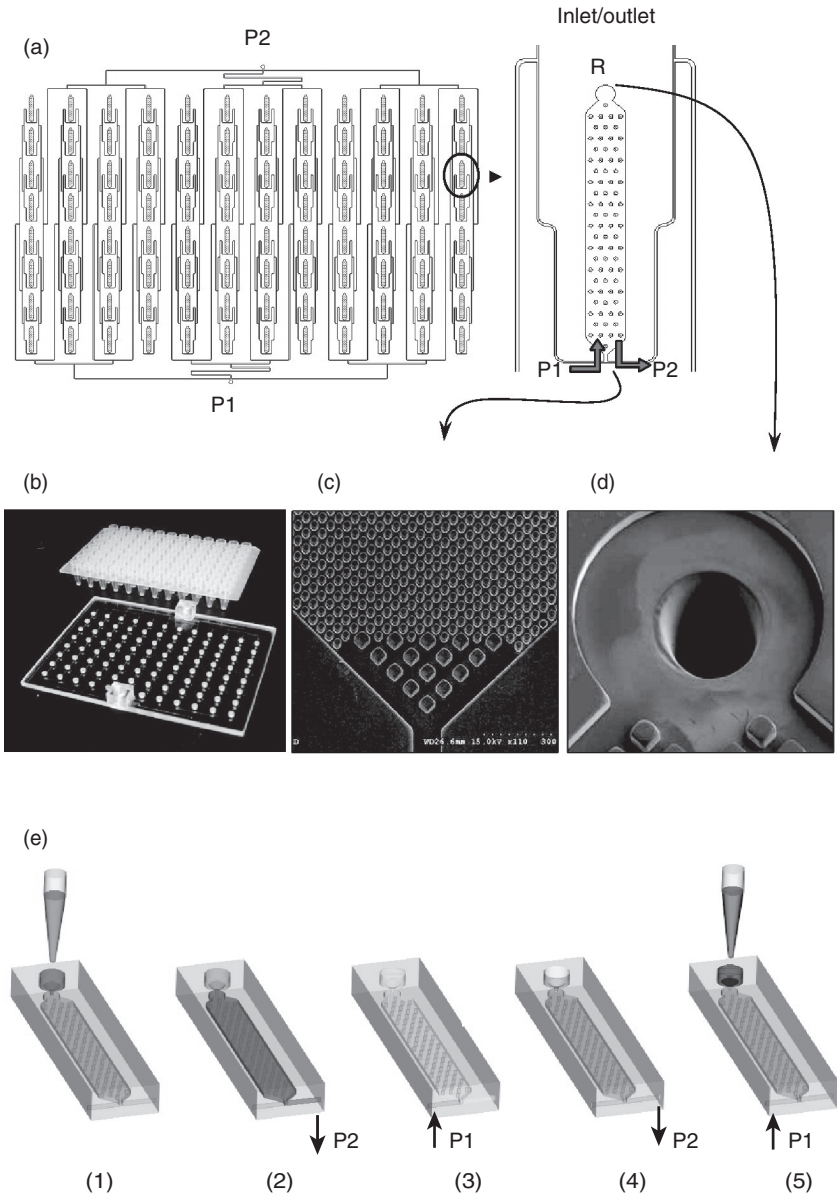

1.12 Layout of the polycarbonate plate-based microfluidic platform. (a) Schematics of the microfluidic device, P1 and P2 are the control ports and R is the sample inlet/outlet reservoirs. (b) Photography of the polycarbonate microfluidic plate and a commercial 96-well titer plate. (c–d) SEM images at the entrance and exit section with a 150 μm bed entrance hole drilled using laser. (*Source*: M. A Witek *et al.*, 2008) – Reproduced by permission of *Journal of Analytical Chemistry*.)

advantage. Open microfluidic channel structures using PI can be micromachined by direct structuring techniques laser ablation (Yin *et al*., 2004; Khan Malek, 2006), hot embossing (Youn *et al*., 2008), dry etching (Nguyen and Lee, 2007), and photolithography (Stefan Metz *et al*., 2001; Metz *et al*., 2004; Lake *et al*., 2011), and subsequently closed by laminating a cover layer (Fig. 1.13). Various lamination techniques have been developed to fabricate PI-based microfluidic devices. For instance, solvent bonding (Glasgow *et al*., 1999) was used to laminate a PI microstructured layer between two wafers. Similarly, a thin layer of polyimide precursor as adhesive can be used for PI bonding (Mangriotis *et al*., 1999; Stefan Metz *et al*., 2001).

Alternatively, microfluidic channels can be made by applying surface micromachining techniques that use sacrificial resist layers embedded in PI to form microchannels. The sacrificial layer is then removed by solvent dissolution (Man *et al*., 1997), dry etching (Bagolini *et al*., 2002), or heating (Suh *et al*., 2000; Metz *et al*., 2004) to reveal the microchannel structure. Materials such as silicon oxide, metals, and photoresists have been used as sacrificial layers for the construction of PI microchannels, although this method is usually a time-consuming process, especially when fabricating submicron channels where dissolution is limited by diffusion.

Due to its mechanical flexibility and good adhesion to metal layers, PI has been already widely used in flexible PCBs such as DuPont™ Kapton®. In a similar vein, PI has been used to make flexible microfluidic devices with embedded electronic circuits, such as neural electrodes (Kato *et al*., 2012), microfluidic mass spectrometers (Spectrometry *et al*., 2010), bioelectric activity monitors (Metz *et al*., 2004), liquid flow sensors (Kuoni *et al*., 2003), and impedance spectroscopy flow cytometers (Gawad *et al*., 2001).

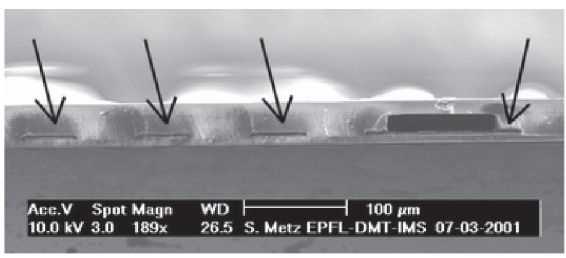

1.13 Cross-section of a polyimide device with three adjacent interconnection lines (left side) and a microchannel (width 100 µm, height 20 µm) with an electrode inside the channel (right side). (*Source*: Stefan Metz *et al.*, 2001). Reproduced by permission of The Royal Society of Chemistry.)

1.4.5 Poly methyl methacrylate (PMMA)

Poly(methyl methacrylate) (PMMA) is a rigid transparent thermoplastic material that undergoes phase transition to a viscoelastic state above T_g = 105°C (Ucar *et al*., 2012). Accordingly, it is well suited for mass industrial production and, due to its excellent chemical, mechanical, and optical properties (Table 1.5), it has recently attracted considerable attention in medical (orthopedics (Jaeblon, 2010)) and biological (Chen *et al*., 2008) applications for analysis of: DNA (Chen and Chen, 2000; Sassi *et al*., 2000); amino acids, peptides and proteins (Xue *et al*., 2001; Wainright *et al*., 2002); saccharine (Dang *et al*., 2006); pollutants and explosives (Wang *et al*., 2002b); and ions and organic acids (Pumera *et al*., 2002). Some review papers (Becker and Gartner, 2000; Fiorini *et al*., 2005; Chen *et al*., 2008; Jaeblon, 2010) have been published with more detailed information on PMMA fabrication methods, bonding and applications.

Fabrication of microfluidic devices using PMMA

The cost of manufacturing PMMA-based products is relatively low as compared to silicon and glass. Various methods described in the microfabrication methods section have been used to develop single-layer PMMA parts bonded to other materials, or to PMMA itself, for the purpose of forming microfluidic devices. These methods include hot embossing (Martynova *et al*., 1997), room-temperature imprinting (Xu *et al*., 2000), injection molding (McCormick *et al*., 1997; Piotter *et al*., 1997), laser ablation (Sun *et al*., 2006), *in situ* polymerization (Chen *et al*., 2003), and solvent etching (Chen *et al*., 2007) as thoroughly reviewed by Chen *et al*. (2008). In the hot embossing method, a substrate containing the microfluidic network design as protruded features is used, and a PMMA plate is embossed against it at elevated temperatures ($>T_g$ = 105ºC) and pressures. Figure 1.14 illustrates a high surface area PMMA-based microfluidic device fabricated by X-ray lithography and used for extraction of DNA by testing various post features in a microchannel (Reedy *et al*., 2011).

Some of the smallest feature sizes and highest aspect ratios achieved in fabrication of PMMA microdevices are listed in Table 1.6.

Interconnection and bonding

In addition to conventional interconnection methods described in other sections, world-to-chip interfacing into PMMA microfluidic devices has been achieved through an adhesive-free in-plane interconnection method (Sabourin *et al*., 2010). The connection is made by press-fit interconnection of oversized deformable tubes with PMMA and subsequent UV-assisted bonding. Capillaries and optical fibers have also been interconnected with

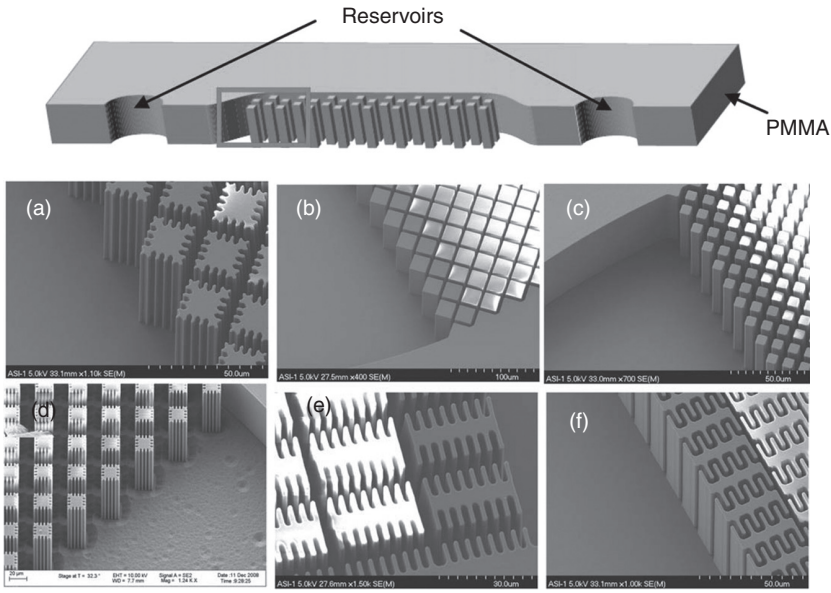

1.14 Schematic of the PMMA microchannel for DNA extraction (Dimensions: 1 cm long channel, 800 μm wide and 50 μm deep) with various post designs shown (SEM images of the red box) in (a)–(f). (a) 14 μm square posts with ~3 μm extensions with 4 μm distance between posts. (b) 22 μm square posts with 4 μm distance between posts. (c) 8 μm square posts with 4 μm distance between posts. (d) Similar to design A but with 17 μm between each post. (e) 6 μm × 30 μm posts with 8 μm extensions. (f) 6 μm × 30 μm posts with 5 μm extensions. (*Source*: With permission Reedy *et al.,* 2011.)

PMMA channels (Hartmann *et al*., 2008) by in-plane insertion into the channel and usage of UV-curable glues to fix them on the device.

Direct and indirect bonding methods have been used for fabricating enclosed PMMA microdevices. Direct bonding includes thermal fusion bonding (Martynova *et al*., 1997), local welding by ultrasonic (Truckenmuller *et al*., 2006) or microwave energy (Lei *et al*., 2004) and solvent bonding (Wang *et al*., 2002a; Shah *et al*., 2006). Bond strength as high as 23.5 MPa has been reported for PMMA using the solvent bonding method (Hsu and Chen, 2007). In the indirect bonding method, which is simpler, an additional glue or epoxy layer is required to facilitate bonding of PMMA to itself or to other materials (Becker and Gartner, 2000; Chen *et al*., 2005). However, the challenge is not to clog the microchannels with the gluing material, which has been avoided by techniques such as control of wetting tension between the UV-curable adhesive and the surface of substrate (Pocius, 2002), screen printing (Han, 2003), and micro-contact printing (Dang, 2005). PMMA bonding to PDMS and parylene have already been discussed in the PDMS

Table 1.5 Physical properties of various materials commonly used in microfabrication

	Silicon	Glass	PDMS	Parylene C	PC	PMMA	PI	PU	COC/COP	Paper
T_m (°C)	1414	700 (Soda lime) 1750 (Quartz) 820 (Pyrex) 465 (Foturan)	-40	290 [8]	260 [12]	250–260 [16]	none	unavailable	190–320[28]	N/A
T_g (°C)	3265	2239 (SiO_2)	-125[1]	90[9]	150 [12]	100–122 [16]	>400[19]	unavailable	70–155[28]	N/A
CTE ($10^{-6}°C^{-1}$)	2.49	9.2 (Soda lime) 0.54 (Quartz) 3.3 (Pyrex) 8.6 (Foturan)	310 µm/(m °C)[2]	35 [10]	60–70 [12]	70–150 [16]	20[19]	150[23]	60–80[29]	111 (cellulose) [32]
Moisture absorption (%)	N/A	N/A	0.03	0.06	0.12–0.34	0.3–0.6 [16]	0.32	<0.2	<0.01	70% (whatman no. 1) [33]
Solvent resistance	Good	Good	Soluble in toluene, swell in nonpolar organic solvent	Insoluble in all organic solvents up to 150°C, can be dissolved in chloronaphthalene at 175°C	Good [13]	Good [16]	Good[20]	Good[24,25]	Excellent[30]	Good
UV transmission	Moderate	Poor below 300 nm (Quartz is excellent) (Foturan absorb UV for curing)	Transparent; UV cutoff 240 nm. Optical detection from 240 to 1100 nm [3]	Transparent, strong absorption below 280 nm	Poor [14]	Good [16]	Good >425 nm[21]	Poor[26]	Excellent	N/A

Hardness	12–13 (Gpa)	585 kg/mm^2 (Soda lime) 522 kg/mm^2 (Quartz) 418 Kg/mm^2 (Pyrex) 469 kg/mm^2 (Foturan)			M70-M75	RM92	E53–99, R129, M95	Shore 85A	130–180 N/mm^2	39.1 (N/15mm) [34]
Thermal conductivity (10^{-4} g cal-cm s^{-1} cm–2°C)	150 (W/mK)	1.12 (Soda lime) 1.4 (Quartz) 1.1 (Pyrex) 1.35 (Foturan)	0.15–0.2 W/mK [4]	0.082 W/mK [11]	4.7 [12]	0.167–0.25 [17]	2.3–4.2[19]	0.209 W/mK[24]	0.12–0.15 W/mK[31]	0.05 (W/mK) [34]
Dielectric strength (MV m^{-1})	N/A	10 (Soda lime) 8 (Quartz) 14 (Pyrex) 1.2 (Foturan)	2.3–2.8 [5]		15–16 [15]	25	16–22[22]	12–20[27]	unavailable	16[35]
Young's modulus (MPa)	160(Gpa)	70 (Soda lime) 107 (Quartz) 64 (Pyrex) 78 (Foturan)	0.360–0.870 [6]	69	2200 [12]	1800–3100	2550[19]	55[23]	3000[31]	3600–3800[36]
Tensile or fracture strength (MPa)	2000	20 (Soda lime) 48 (Quartz) 20.7 (Pyrex) 60 (Foturan)	2.24 [7]	3200 [8]	65 [12]	48–76 [18]	90[19]	50[23]	60[31]	Wet: 0.179 Dry: 7.17[37]

(*Continued*)

Table 1.5 Continued

	Silicon	Glass	PDMS	Parylene C	PC	PMMA	PI	PU	COC/COP	Paper
Ref.	Kohlmann and Vogel, 1979	Kohlmann and Vogel, 1979	[1]Clarson and Semlyen, 1993; [2]Kunnavakkam *et al.*, 2003; [3] McDonald and Whitesides, 2002; [4]Chuang and Wereley, 2009; [5]McDonald *et al.*, 2001; [6]Armani *et al.*, 1999; [7]Mata *et al.*, 2005	[8]Tan and Craighead, 2010; [9]Noh *et al.*, 2004a; [10]Noh *et al.*, 2004b; [11]Shin *et al.*, 2003	[12]J. E. Mark, 2007; [13]Utracki, 2002; [14]Rabek, 1995; [15]Minges, 1989	[16]Tsao and DeVoe, 2009; [17]Assael *et al.*, 2005; [18]Boger *et al.*, 2008	[19]J. E. Mark, 2007; [20]Utracki, 2002; [21]Rabek, 1995; [22]Minges, 1989	[23]J. E. Mark, 2007; [24]Utracki, 2002; [25]Wu *et al.*, 2012; [26]Rabek, 1995; [27]Minges, 1989	[28]Todo and Kashiwa, 1996; [29]Sastri, 2010; [30] Biron, 2007; [31] Shin, 2005	[32]Hori *et al.*, 2005; [33]Pelton, 2009; [34]Mark and Borch, 2001; [35]Rigden, 1996; [36]Schröder *et al.*, 2002; [37]Bishop *et al.*, 1965

Table 1.6 Minimum feature sizes (MFS) and maximum AR fabricated in PMMA

Fabrication method	MFS (μm)	AR	Ref.
E-beam lithography	0.16	7	Gorelick *et al.*, 2010
LIGA	5	10	Reedy *et al.*, 2011
LIGA	8	19	Becker and Heim, 2000

and parylene sections. Other bonding methods for PMMA have been summarized in two review articles (Chen *et al.*, 2008; Tsao and DeVoe, 2009).

PMMA is low cost and easy to form for developing microfluidic devices with exceptional mechanical, optical, and chemical properties (Table 1.5). Extreme hydrophobicity, due to the lack of ionizable functional groups in PMMA, has limited its application and led to the development of various surface modification processes. They have been categorized (Chen *et al.*, 2008) into covalent modifications for the formation of amine-terminated surfaces (Henry *et al.*, 2000), dynamic coating with charged surfactants or hydrophilic neutral polymers (Dang *et al.*, 2003), and bulk modification (Wang *et al.*, 2005) of the polymer during the fabrication process by copolymerization of monomers.

1.4.6 Cyclic olefin copolymers (COC) and cyclic olefin polymers (COP)

Both COC and cyclic olefin polymers (COP) are amorphous polymers produced by chain copolymerization of cyclic monomers. Typically, COC and COP have glass-like transparency (>90%) in near-UV, high tensile strength (46–63 MPa), high moisture resistance (<0.01%), good chemical resistance to acids, bases and polar solvents (Topas Advanced Polymers, 2012), and high dielectric constant (30 kV/mm) (Lamonte and Mcnally, 2000). They are commercially available in pellet, solution, and sheet form from various manufacturers.

Similar to other polymers, fabrication methods for COC/COP can be categorized as direct structuring methods, such as laser ablation (Sabbert *et al.*, 1999; Jensen *et al.*, 2004; Bundgaard *et al.*, 2006) and micro-milling (Bundgaard *et al.*, 2006; Grumann *et al.*, 2006), and replication methods, such as injection molding (Kim and Kwon, 2009; Pakkanen *et al.*, 2002; Appasamy *et al.*, 2005; Lee *et al.*, 2005; Ito *et al.*, 2007; Kalima *et al.*, 2007; Steigert *et al.*, 2007; Angelov and Coulter, 2008; Schütte *et al.*, 2010), hot embossing (Fig. 1.15) (Kameoka *et al.*, 2001; Yang *et al.*, 2005; Bhattacharyya

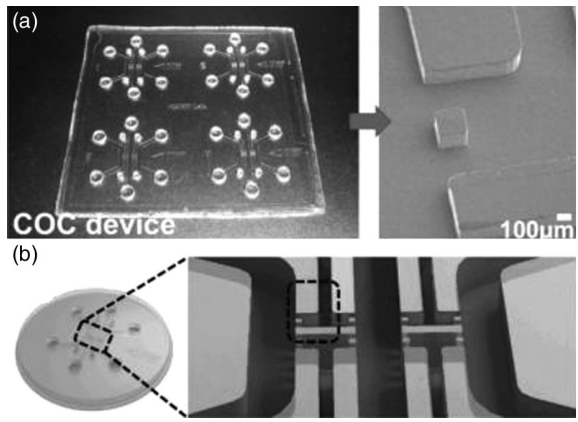

1.15 (a) Photograph of 4 COC device array and SEM of the post (left) and channel structure of a device (right). (b) A single device schematic with the gel area expanded shows the SEM image area outlined. (*Source*: Jeon *et al.* (2011) – Reproduced by permission of *Journal of Biomedical Microdevices*.)

and Klapperich, 2006; Fredrickson *et al.*, 2006; Liu *et al.*, 2007; Faure *et al.*, 2008; Park *et al.* 2008; Illa *et al.*, 2009), and nano-imprint lithography (Bilenberg *et al.*, 2005; Gourgon *et al.*, 2005; Nilsson *et al.*, 2005; Gustafsson *et al.*, 2008).

A bonding step is essential for the fabrication of microfluidic systems, which usually requires sealed microchannels to prevent sample contamination and evaporation. Use of adhesives or glues is one of the most common bonding techniques for polymers. UV adhesives (Do and Ahn, 2008) have been demonstrated to bond COP parts together at room temperature to form a microfluidic chip with a bonding strength of 2 MPa. Thermal bonding is also commonly used for thermoplastic polymers such as COP (Kim and Kwon, 2009; Kameoka *et al.*, 2001; Daniel Nilsson *et al.*, 2005; Yang *et al.*, 2005; Bedair and Oleschuk, 2006; Bhattacharyya and Klapperich, 2006; Kim *et al.*, 2006; Mair *et al.*, 2006; Wallow *et al.*, 2007; Choi *et al.*, 2008; Gustafsson *et al.*, 2008), which is heated above its glass transition temperature to allow the polymer chains to diffuse between the mating surfaces thus promoting adhesion. No quantitative study of the bonding strength had been undertaken due to the low surface energy of thermoplastics. Oxygen plasma (Kettner *et al.*, 2006) and UV/ozone (Tsao *et al.*, 2007) treatments were then used to activate surfaces and improve the bonding strength of COP substrates up to 0.8 mJ/cm^2 under specific bonding conditions (Tsao *et al.*, 2007). Solvent bonding, also known as solvent welding, can also be used to temporarily dissolve the surfaces of COP, enabling the mobility of polymer chains across the bonding interface, and thus results in the highest bonding

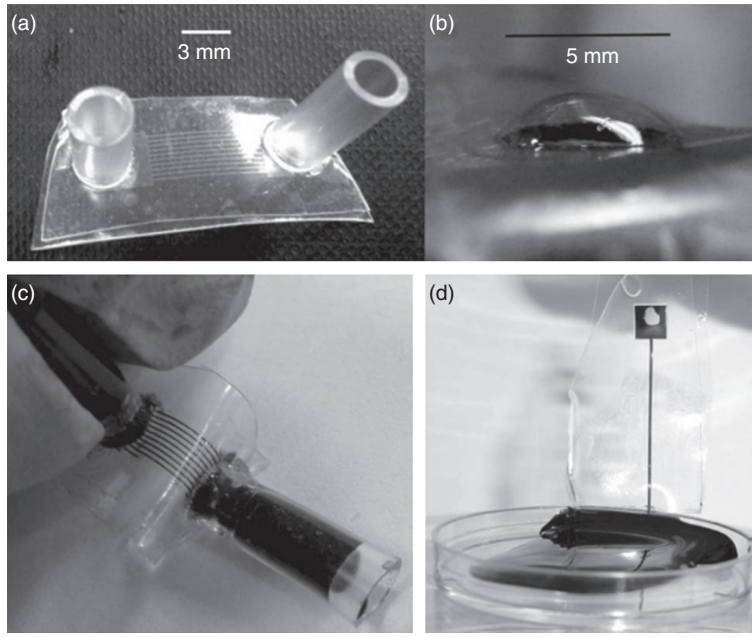

1.16 Photos of PU-based microfluidic devices. (a) Sealed device with integrated interconnect, (b) a deflected PU membrane under a pressure of 200 kPa (diameter 5 mm and membrane thickness = 25 μm), (c) a flexible and bendable device with colored microchannels for visualization, (d) self-priming microchannel (4 cm x 500 mm x 80 mm) filled with DI water (dyed with methylene blue) due to its hydrophilicity. (*Source*: W.-I. Wu *et al.* (2012) – Reproduced by permission of The Royal Society of Chemistry.)

strength of 10 MPa (Kettner *et al.*, 2006; Ro *et al.*, 2006; Liu *et al.*, 2007; Tsao *et al.*, 2007, 2008; Wallow *et al.*, 2007; Chen *et al.*, 2008; Faure *et al.*, 2008).

Due to its surface properties and optical transparency, COP-based microchip electrophoresis provides faster separation and easier integration of sample preparation (Blas *et al.*, 2008; Sueyoshi *et al.*, 2008) and optical detection (Mogensen *et al.*, 2001; Bliss *et al.*, 2007; Hurth *et al.*, 2008) than traditional capillary electrophoresis. Compared to other polymers, COP-based microchips usually have lower background fluorescence, and higher electrophoretic efficiency (Yi *et al.*, 2008). COP-based microchannels have also been used in solid phase extraction where either the interested analytes or the undesired impurities are retained by the stationary phase (Gustafsson *et al.*, 2008; Illa *et al.*, 2009). Moreover, COP-based electrospray emitters have been used for mass spectrometry where the ionized analytes are separated depending on their interaction with external electric and/or magnetic fields (Jun Kameoka *et al.*, 2002; Yang *et al.*, 2004, 2005; Park *et al.*, 2008;

Shinohara *et al*., 2008). Since COP is relatively transparent compared to other polymers at shorter wavelengths (240–360 nm), it can be used as optical components such as micro lenses (Appasamy *et al*., 2005), photonic crystals (Bilenberg *et al*., 2004), and optical waveguides (Okagbare *et al*., 2010). Because of its moisture resistance and adhesion to metallic films, COP can be applied as substrate for blood contacting (Grumann *et al*., 2006; Jang *et al*., 2006; Kim *et al*., 2006; Choi *et al*., 2008) and DNA analysis applications (Gulliksen *et al*., 2005; Bhattacharyya and Klapperich, 2006; Castaño-Alvarez *et al*., 2007; Hurth *et al*., 2008; Larsen *et al*., 2008).

1.4.7 Polyurethane (PU)

Polyurethane (PU) is a polymer composed of a chain of organic units joined by urethane links. Because urethane is available in a broad hardness range, PU can be synthesized to offer the specific elasticity combined with toughness and durability. Therefore, its mechanical properties, namely higher tensile strength (62 MPa), Young's modulus (55 MPa), and hardness (94 Shore A), are superior. Its density (1.15 g/cc) and melting point (215.5°C) are similar to PDMS. Its dielectric constant is similar to that of PDMS, and it performs well as an insulator. PU is commercially available, either in pellet or sheet, as raw material from various manufacturers.

Traditionally, solvent molding techniques such as vertical dipping, rotating mandrel, and rotating plate are used to fabricate PU parts such as sheets, membranes, and tubing. The rotating plate method is used for fabricating PU films and sheets, while vertical dipping and rotating mandrel are used for fabricating cylindrical parts, such as tubing. However, these fabrication techniques are not suitable for replicating the intricate and detailed microscale features present in microfluidics devices. PU-based microfabrication typically involves injection molding (Folch *et al*., 2000; Kuo *et al*., 2009), hot embossing (Shen *et al*., 2006), imprinting (Xu *et al*., 2000), plasma etching (Rossier *et al*., 2002), sacrificial material (Haraldsson *et al*., 2006), and reaction polymerization (Thorsen *et al*., 2001; Kim *et al*., 2003; Haraldsson *et al*., 2006; Piccin *et al*., 2007; Kuo *et al*., 2009). These methods are not suited for rapid prototyping as they use high cost intermediate molds and expensive fabrication equipment. Furthermore, the substrates produced are rigid and not transparent. Solvent casting is more suitable, since intermediate molds can be fabricated using photolithography and the fabrication equipment is low cost (Wu *et al*., 2012).

To achieve irreversible bonding, semi-cured parts of PU have been placed in contact and heated above the glass transition temperature, causing fusion of the two parts (Piccin *et al*., 2007; Kuo *et al*., 2009). However, this method is not suitable for retaining the fine structural features needed in microchannels. Recently, dry and wet bonding methods using plasma treatment

and solvent welding have been developed to overcome this issue. A highest bonding strength of 326.4 kPa using wet bonding was reported (Wu *et al.*, 2012) (Fig. 1.16).

PU, since its development in the 1930s (Boretos and Pierce, 1968; Lyman *et al.*, 1971), has been widely used in various blood-contact applications such as the artificial heart (Lyman *et al.*, 1971), intra-aortic balloons (Brash *et al.*, 1973), pacemaker leads (Devanathan *et al.*, 1980), heart valves (Tsutsui *et al.*, 1981), and hemodialysis membranes (Lyman *et al.*, 1977). Hydrophobic surfaces are essentially water repellent and provoke adverse reactions in blood contact. Many studies have shown that the blood compatibility of polyurethanes can be improved by making the surface more hydrophilic (Takahara *et al.*, 1985). A number of *in vivo* and *in vitro* studies have been carried out to assess the cellular and tissue responses of PU subcutaneously, intramuscularly, or intraperitoneally (Han *et al.*, 1992; Okoshi *et al.*, 1992; Marois *et al.*, 1989, 1993, 1996, Bakker *et al.*, 1990; Bruin *et al.*, 1993; Watkinson *et al.*, 1995; van der Giessen *et al.*, 1996; Akiyama *et al.*, 1997; Wu *et al.*, 2012). PU-based microchip electrophoresis has also been tested with various analytes to evaluate its separation performance (Piccin *et al.*, 2007). Due to its excellent hardness, high-aspect-ratio (~3.5) microstructure made from PU can be easily fabricated and bonded, whereas microstructures made from PDMS are too soft to stand their own weight. These microstructures were then used as microfluidic filters to separate or concentrate the targeted particles or cells (Kuo *et al.*, 2009). The other main advantage of PU over other polymers is in its feasibility to be chemically tailored for specific applications; thus, it has been widely used in applications such as cell culture and tissue scaffolds (Folch *et al.*, 2000; Vermette *et al.*, 2001; Shen *et al.*, 2006; Moraes *et al.*, 2009).

1.4.8 Paper

Paper, usually as a cellulose fiber network, can spontaneously generate the capillary flow to transport aqueous liquids, due to its porosity and hydrophilicity. This self-pumping/priming mechanism makes it an attractive substrate for use in low cost microfluidic devices for diagnostic applications, if a method to direct and control the flow of fluid can be devised. The velocity of motions in the paper-based microfluidic channels is determined by many factors, such as the pore size, porosity, surface energy of paper, as well as the viscosity of the liquid, and can be estimated by the well-known Lucas-Washburn equation (Anbuhi *et al.*, 2012). The first paper-based microfluidic device was presented by Muller and co-workers, who patterned paraffin boundary on paper to speed up the elution of a pigment mixture (Müller and Clegg, 1949). Recently, with the advancement of micromachining technologies, Whitesides Group of Harvard University has developed many

Table 1.7 The performance parameters of paper micro-patterning technologies

Methods	Channel size (μm)	Barrier size (μm)	Reagents
Photolithography	186 ± 13	248 ± 13	SU-8
Ink jet etching	420 ± 50	N/A	Polystyrene
Plotting	1000	1000	Polydimethylsiloxane
Wax printing	561 ± 45	850 ± 50	Wax
Surface treatments	1500	N/A	Alkyl ketene dimer
Paper cutting	400[a]	N/A	N/A

[a]laser cutting; resolution depended on the type of paper (Nie *et al.,* 2012).

novel patterning strategies with more delicate control of flowing path and flow rate (Martinez *et al*., 2007). Following these early works, many other channel patterning technologies have been investigated, which can be categorized as follows: (i) photolithography (Martinez *et al*., 2008); (ii) ink jet etching (Abe *et al*., 2008); (iii) plotting (Bruzewicz *et al*., 2008); (iv) wax printing (Lu *et al*., 2009); (v) surface treatments (Xu Li *et al*., 2008); and (vi) paper cutting (Wang *et al*., 2010).

Except for cutting, where the individual regions on the substrate are physically separated from each other, the fundamental mechanism for directing flow in paper has been through the creation of difference of hydrophobicity between channels (hydrophilic) and boundaries (hydrophobic) by patterning. Generally, the patterning can be accomplished by three different principles: (i) printing the hydrophobic materials (Wax and PDMS) on paper as boundaries (photolithography and plotting); (ii) uniformly coating paper with hydrophobic materials (SU-8 and Polystyrene) then using solvents to dissolve those materials and making channels; and (iii) applying chemicals to modify the surface hydroxide group on the designed area of the paper to make the hydrophobic boundaries. Table 1.7 lists some important performance parameters of each of the patterning technologies.

Most applications of paper-based microfluidic devices have been on developing low cost diagnostic devices. The ability to use patterning to fabricate microfluidic channels in paper to perform parallel analysis of various analytes was first demonstrated Whitesides and co-workers (Martinez *et al*., 2007). Here, wax printing was used to pattern a microfluidic channel network that enabled a urine sample at the inlet reservoir to be split into three segments for simultaneous analysis of glucose and proteins. Other reactants were patterned at the end of the respective microchannel, which produced a colorimetric assay when the sample arrived at that location due to capillary flow. The colorimetric paper-based analytical devices have been extensively reviewed by Chao in 2008 (Zhao and Van der Berg, 2008) and Whitesides in 2010 (Martinez *et al*., 2009). Other than colorimetric detection, electrochemical (EC) (Dungchai *et al*., 2009) or electrochemiluminescence (ECL)

(Delaney *et al*., 2011) principles have been used for detection in paper-based microfluidic devices. EC and ECL sensing methods provide lower detecting limits (down to the nM range), higher accuracy, and a shorter detection time than colorimetric methods. Recent developments in EC and ECL detection in paper-based microfluidic devices were reviewed by Li *et al*. in 2012 (Xu Li *et al*., 2012). Various unit operations, such as hydrodynamic focusing (Fu *et al*., 2010), mixing (Rezk *et al*., 2012), dilution (Osborn *et al*., 2010), and separation (Osborn *et al*., 2010) have also been demonstrated in paper-based microfluidic devices. In addition, power sources on-chip that could power the unit operation have been developed (Thom *et al*., 2012). Recently, paper-based devices have also been shown to be usable for 3D cell culture (Li *et al*., 2012).

Paper is superior to other materials for making analytical microfluidic devices because of its unique properties: (1) low cost; (2) porous structure (for both self-driven capillary flow and reagent immobilization); (3) flexibility (easy to pack and carry). However, the non-uniform nature of this cellulose fiber network, and the time it takes to transport the sample in the microfluidic network, may make it unsuitable for accurate liquid handling.

1.5 Conclusion and future trends

Materials and manufacturing techniques used in the microelectronic semiconductor industry were adapted to develop the first MEMS and microfluidic devices. Silicon and glass were initially utilized because their fabrication techniques already existed and were highly developed. Some properties of these materials, such as their solvent resistance, stiffness, and durability still make them the material of choice in many microfluidic applications. However, to lower the cost and enhance the functionality of these devices, materials other than silicon and glass have been investigated extensively in the past two decades. Polymers are among the materials that have attracted a widespread attention, among academic researchers as well as commercial companies. Polymers are macromolecules, composed of repeating monomer units, with an extraordinary range of mechanical, chemical, and optical properties. They exist in highly elastic or stiff forms (highly dependent on their polymer chain size and length) with chemical inertness and biocompatibility. Their surface properties can be modified physically (plasma, corona, mechanical roughening, etc.) or chemically (monolayer deposition, grafting, etc.). More importantly, the conventional optical (photolithography) or micromechanical (micro-injection molding, hot embossing, laser micromachining, micromilling, casting, stereolithography, and inkjet printing) fabrication methods have been applied in mass producing the polymeric materials. This lowers the cost of the devices significantly, and suits the technology for the development of disposable devices, which is highly important in biomedical applications. Most of the microfabrication techniques in polymers take advantage of the

temperature-dependent phase transition behavior of polymers and the ability to form them into any shape afterwards. Using these techniques, a wide range of microfluidic devices composed of silicon, glass, PDMS, parylene, polycarbonate, polyimide, PMMA, COC/COP, polyurethane, and paper have been developed. These devices have been used in a wide range of applications, such as biology, medical diagnostics, drug delivery, drug discovery, analytical chemistry, and molecular diagnosis. The major challenges for many polymers are that reliable and strong bonding and interconnection methods need to be developed. Also, methods of integrating various polymeric materials need to be developed. Although it is still not clear which of the materials introduced above will be the dominant one in the development of lab-on-a-chip devices, from the point of view of cost, ease of fabrication, and accessibility, paper seems to demonstrate extraordinary potential to be adapted in the near future. Glass and silicon devices will continue to dominate in commercial production of microfluidic components and in biochemical applications. The existence of the extensive level of research and development on PDMS, and its suitability for rapid prototyping has made it the material of choice for research and development. Polymeric materials will continue to lead progress of lab-on-a-chip devices as the field advances and demands more biological and chemical compatibilities.

1.6 References

Abe, K., Suzuki, K. and Citterio, D. (2008). Inkjet-printed microfluidic multianalyte chemical sensing paper. *Analytical Chemistry*, **80**(18), pp. 6928–34.

Agirregabiria, M. *et al*. (2005). Fabrication of SU-8 multilayer microstructures based on successive CMOS compatible adhesive bonding and releasing steps. *Lab on a Chip*, **5**(5), pp. 545–52. Available at: http://dx.doi.org/10.1039/B500519A.

Akiyama, N. *et al*. (1997). A comparison of CORVITA and expanded polytetrafluoroethylene vascular grafts implanted in the abdominal aortas of dogs. *Surgery today*, **27**(9), pp. 840–5. Available at: http://www.ncbi.nlm.nih.gov/pubmed/9306607 [Accessed 11 October 2011].

Anbuhi, S. *et al*. (2012). Creating fast flow channels in paper fluidic devices to control timing of sequential reactions. *Lab on a Chip*, **12**, pp. 5079–85.

Angelov, A. and Coulter, J. (2008). The development and characterization of polymer microinjection molded gratings. *Polymer Engineering & Science*, **48**(11), pp. 2169–4346. Available at: http://dx.doi.org/10.1002/pen.21162.

Appasamy, S. *et al*. (2005). High-throughput plastic microlenses fabricated using microinjection molding techniques. *Optical Engineering*, **44**, p. 123401. Available at: http://link.aip.org/link/opegar/v44/i12/p123401/s1/html.

Armani, D., Liu, C. and Aluru, N. (1999). Re-configurable fluid circuits by PDMS elastomer micromachining. In: Twelfth IEEE International Conference on Micro Electro Mechanical Systems, MEMS '99, 1999, 222–227.

Assael, M.J., Botsios, S., Gialou, K. and Metaxa, I.N. (2005). Thermal Conductivity of Polymethyl Methacrylate (PMMA) and Borosilicate Crown Glass BK7. *International Journal of Thermophysics*, **26**, pp. 1595–605.

Attia, U.M. and Alcock, J.R. (2011). A review of micro-powder injection moulding as a microfabrication technique. *Journal of Micromechanics and Microengineering*, **21**(4), p. 043001. Available at: http://stacks.iop.org/0960–1317/21/i=4/a=043001 [Accessed 27 September 2012].

Attia, U.M., Marson, S. and Alcock, J.R. (2009). Micro-injection moulding of polymer microfluidic devices. *Microfluidics and Nanofluidics*, **7**(1), pp. 1–28. Available at: http://www.springerlink.com/content/942q72w1g938816x/ [Accessed 20 August 2012].

Bagolini, A. *et al*. (2002). Polyimide sacrificial layer and novel materials for post-processing surface micromachining. *Journal of Micromechanics and Microengineering*, **12**(4), p. 385. Available at: http://stacks.iop.org/0960–1317/12/i=4/a=306.

Bakker, D. *et al*. (1990). Biocompatibility of a polyether urethane, polypropylene oxide, and a polyether polyester copolymer. A qualitative and quantitative study of three alloplastic tympanic membrane materials in the rat middle ear. *Journal of Biomedical Materials Research*, **24**(4), pp. 489–515. Available at: http://www.ncbi.nlm.nih.gov/pubmed/2347874 [Accessed 11 October 2011].

Becker, E.W. *et al*. (1986). Fabrication of microstructures with high aspect ratios and great structural heights by synchrotron radiation lithography, galvanoforming, and plastic moulding (LIGA process). *Microelectronic Engineering*, **4**(1), pp. 35–56. Available at: http://dx.doi.org/10.1016/0167–9317(86)90004–3.

Becker, H. (2000). Hot embossing as a method for the fabrication of polymer high aspect ratio structures. *Sensors and Actuators A: Physical*, **83**(1–3), pp. 130–5. Available at: http://dx.doi.org/10.1016/S0924–4247(00)00296-X [Accessed 11 October 2011].

Becker, H. and Gärtner, C. (2008). Polymer microfabrication technologies for microfluidic systems. *Analytical and Bioanalytical Chemistry*, **390**(1), pp. 89–111. Available at: http://www.ncbi.nlm.nih.gov/pubmed/17989961.

Becker, H. and Locascio, L.E. (2002). Polymer microfluidic devices. *Talanta*, **56**(2), pp. 267–87. Available at: http://www.ncbi.nlm.nih.gov/pubmed/18968500.

Bedair, M. and Oleschuk, R. (2006). Fabrication of porous polymer monoliths in polymeric microfluidic chips as an electrospray emitter for direct coupling to mass spectrometry. *Analytical Chemistry*, **78**(4), pp. 1130–8. Available at: http://dx.doi.org/10.1021/ac0514570.

Belloy, E. *et al*. (2000). The introduction of powder blasting for sensor and microsystem applications. *Sensors and Actuators A: Physical*, **84**(3), pp. 330–7.

Bertsch, A. *et al*. (2002). Microstereolithography: a review. *MRS Proceedings*, **758**(-1). Available at: http://journals.cambridge.org/abstract_S1946427400153357 [Accessed 27 September 2012].

Bhattacharyya, A. and Klapperich, C. (2006). Thermoplastic microfluidic device for on-chip purification of nucleic acids for disposable diagnostics. *Analytical Chemistry*, **78**(3), pp. 788–880. Available at: http://dx.doi.org/10.1021/ac051449j.

Bilenberg, B. *et al*. (2004). PMMA to SU-8 bonding for polymer based lab-on-a-chip systems with integrated optics. *Journal of Micromechanics and Microengineering*, **14**, p. 814. Available at: http://iopscience.iop.org/0960–1317/14/6/008.

Bilenberg, B. *et al*. (2005). Topas-based lab-on-a-chip microsystems fabricated by thermal nanoimprint lithography. *Journal of Vacuum Science & Technology B: Microelectronics and Nanometer Structures*, **23**, p. 2944. Available at: http://d.wanfangdata.com.cn/NSTLQK_NSTL_QKJJ028349443.aspx.

Biron, M. (2007). *Thermoplastics and Thermoplastic Composites: Technical Information for Plastics Users* (Google eBook) (p. 944). Elsevier. Available at: http://books.google.com/books?id=g_11KTQ-RjYC&pgis=1

Bishop, Henkel, D.J. (1965). *Laboratory Shear Testing of Soils*, ASTM.

Blas, M., Delaunay, N. and Rocca, J.-L. (2008). Electrokinetic-based injection modes for separative microsystems. *Electrophoresis*, **29**(1), pp. 20–52. Available at: http://dx.doi.org/10.1002/elps.200700389.

Bliss, C.L., McMullin, J.N. and Backhouse, C.J. (2007). Rapid fabrication of a microfluidic device with integrated optical waveguides for DNA fragment analysis. *Lab on a Chip*, **7**(10), pp. 1280–7. Available at: http://pubs.rsc.org/en/content/articlehtml/2007/lc/b708485d [Accessed 2 July 2012].

Boger, A., Bisig, A., Bohner, M., Heini, P. and Schneider, E. (2008). Variation of the mechanical properties of PMMA to suit osteoporotic cancellous bone. *Journal of Biomaterials Science, Polymer Edition*, **19**, pp. 1125–42.

Boretos, J.W. and Pierce, W.S. (1968). Segmented polyurethane: a polyether polymer. An initial evaluation for biomedical applications. *Journal of Biomedical Materials Research*, **2**(1), pp. 121–30. Available at: http://www.ncbi.nlm.nih.gov/pubmed/5708000 [Accessed 11 October 2011].

Brash, J.L., Fritzinger, B.K. and Bruck, S.D. (1973). Development of block copolyether-urethane intra-aortic balloons and other medical devices. *Journal of Biomedical Materials Research*, **7**(4), pp. 313–34. Available at: http://www.ncbi.nlm.nih.gov/pubmed/4725705 [Accessed 11 October 2011].

Bruin, P. *et al*. (1993). Autoclavable highly cross-linked polyurethane networks in ophthalmology. *Biomaterials*, **14**(14), pp. 1089–97. Available at: http://www.ncbi.nlm.nih.gov/pubmed/7508760 [Accessed 11 October 2011].

Bruzewicz, D. A, Reches, M. and Whitesides, G.M. (2008). Low-cost printing of poly(dimethylsiloxane) barriers to define microchannels in paper. *Analytical Chemistry*, **80**(9), pp. 3387–92.

Bu, M. *et al*. (2004). A new masking technology for deep glass etching and its microfluidic application. *Sensors and Actuators A: Physical*, **115**(2–3), pp. 476–82.

Bundgaard, F., Perozziello, G. and Geschke, O. (2006). Rapid prototyping tools and methods for all-Topas® cyclic olefin copolymer fluidic microsystems. *Proceedings of the Institution of Mechanical Engineers, Part C: Journal of Mechanical Engineering Science*, **220**(11), pp. 1625–32. Available at: http://pic.sagepub.com/lookup/doi/10.1243/09544062JMES295 [Accessed 6 April 2012].

Burns, M.A. *et al*. (1998). An integrated nanoliter DNA analysis device. *Science*, **282**(5388), pp. 484–7. Available at: http://www.sciencemag.org/cgi/doi/10.1126/science.282.5388.484.

Bustillo, J.M., Howe, R.T. and Muller, R.S. (1998). Surface micromachining for microelectromechanical systems. *Proceedings of the IEEE*, **86**(8), pp. 1552, 1574. DOI: 10.1109/5.704260.

Castaño-Alvarez, M., Fernández-Abedul, M. and Costa-García, A. (2007). Electroactive intercalators for DNA analysis on microchip electrophoresis. *Electrophoresis*, **28**(24), pp. 4679–768. Available at: http://dx.doi.org/10.1002/elps.200700160.

Chan, C.-H., Chen, J.-K. and Chang, F.-C. (2008). Specific DNA extraction through fluid channels with immobilization of layered double hydroxides on polycarbonate surface. *Sensors and Actuators B: Chemical*, **133**(1), pp. 327–32. Available at: http://www.sciencedirect.com/science/article/pii/S0925400508001548.

Chen, G., Svec, F. and Knapp, D. (2008). Light-actuated high pressure-resisting microvalve for on-chip flow control based on thermo-responsive nanostructured polymer. *Lab on a Chip*, **8**(7), pp. 1198–402. Available at: http://dx.doi.org/10.1039/b803293a.

Chen, J. *et al*. (2005). Electrokinetically synchronized polymerase chain reaction microchip fabricated in polycarbonate. *Analytical Chemistry*, **77**(2), pp. 658–66. Available at: http://pubs.acs.org/doi/abs/10.1021/ac048758e.

Chen, S.C., Chang, J.A., Chang, Y.J. and Chau, S.W. (2005). Micro injection molding of micro fluidic platform. Proceedings of the Annual Technical Conference - ANTEC, pp. 1–5.

Choi, S.H., Kim, D.S. and Kwon, T.H. (2008). Microinjection molded disposable microfluidic lab-on-a-chip for efficient detection of agglutination. *Microsystem Technologies*, **15**(2), pp. 309–16. Available at: http://www.springerlink.com/content/y7k28g1043q71x0p/ [Accessed 14 March 2012].

Chung, A.J., Kim, D. and Erickson, D. (2008). Electrokinetic microfluidic devices for rapid, low power drug delivery in autonomous microsystems. *Lab on a Chip*, **8**(2), pp. 330–8.

Chuang, H.S. and Wereley, S. (2009). Design, fabrication and characterization of a conducting PDMS for microheaters and temperature sensors. *Journal of Micromechanics and Microengineering*, **19**, p. 045010.

Clarson, S.J. and Semlyen, J.A. (1993). *Siloxane Polymers*. Englewood Cliffs, NJ: Prentice-Hall.

Cooney, C. *et al*. (2012). A plastic, disposable microfluidic flow cell for coupled on-chip PCR and microarray detection of infectious agents. *Biomedical Microdevices*, **14**(1), pp. 45–53. Available at: http://dx.doi.org/10.1007/s10544–011–9584–9.

Delaney, J.L. *et al*. (2011). Electrogenerated chemiluminescence detection in paper-based microfluidic sensors. *Analytical Chemistry*, **83**(4), pp. 1300–6.

Devanathan, T., Sluetz, J.E. and Young, K.A. (1980). In vivo thrombogenicity of implantable cardiac pacing leads. *Biomaterials, Medical Devices, and Artificial Organs*, **8**(4), pp. 369–79. Available at: http://www.ncbi.nlm.nih.gov/pubmed/7272410 [Accessed 11 October 2011].

Dietricha, T.R. *et al*. (1996). Fabrication technologies for microsystems utilizing photoetchable glass. *Microelectronic Engineering*, **30**(1–4), pp. 497–504.

Do, J. and Ahn, C. (2008). A polymer lab-on-a-chip for magnetic immunoassay with on-chip sampling and detection capabilities. *Lab on a Chip*, **8**(4), pp. 542–51. Available at: http://dx.doi.org/10.1039/b715569g.

Dubey, A.K. and Yadava, V. (2008). Laser beam machining – a review. *International Journal of Machine Tools and Manufacture*, **48**(6), pp. 609–28. Available at: http://dx.doi.org/10.1016/j.ijmachtools.2007.10.017 [Accessed 10 August 2012].

Dungchai, W., Chailapakul, O. and Henry, C.S. (2009). Electrochemical detection for paper-based microfluidics. *Analytical Chemistry*, **81**(14), pp. 5821–6.

Dykes, J.M. *et al*. (2007). Creation of embedded structures in SU-8. *Proceedings of SPIE*, **6465**, pp. 64650N–64650N–12. Available at: http://link.aip.org/link/PSISDG/v6465/i1/p64650N/s1&Agg=doi [Accessed 13 August 2012].

Egashira, K., Mizutani, K. and Nagao, T. (2002). Ultrasonic vibration drilling of microholes in glass. *CIRP Annals – Manufacturing Technology*, **51**(1), pp. 339–42.

Ehrfeld, W. *et al*. (1996). Microelectro discharge machining as a technology in micromachining. In S. W. Pang *et al*., eds. *Micromachining and Microfabrication '96*.

pp. 332–337. Available at: http://proceedings.spiedigitallibrary.org/proceeding.aspx?articleid=1023907 [Accessed 3 October 2012].

Erickson, D. and Li, D. (2004). Integrated microfluidic devices. *Analytica Chimica Acta*, **507**(1), pp. 11–26.

Fan, X. and White, I.M. (2011). Optofluidic microsystems for chemical and biological analysis. *Nature Photonics*, **5**(10), pp. 591–7.

Fan, Z., Ludi, H. and Widmers, H.M. (1992). Capillary electrophoresis and sample injection systems integrated on a planar glass chip. *Analytical Chemistry*, **64**(17), pp. 1926–32. Available at: http://pubs.acs.org/doi/abs/10.1021/ac00041a030.

Faure, K. *et al*. (2008). Development of an acrylate monolith in a cyclo-olefin copolymer microfluidic device for chip electrochromatography separation. *Electrophoresis*, **29**(24), pp. 4948–5003. Available at: http://dx.doi.org/10.1002/elps.200800235.

Fiorini, G.S. *et al*. (2007). Fabrication improvements for thermoset polyester (TPE) microfluidic devices. *Lab on a Chip*, **7**(7), pp. 923–26. Available at: http://www.ncbi.nlm.nih.gov/pubmed/17594014.

Folch, A., Mezzour, S. and Du, M. (2000). Stacks of microfabricated structures as scaffolds for cell culture and tissue engineering. *Tissue Engineering*, **2**(3), pp 207–14.

Fredrickson, C.K., Xia, Z., Das, C., Ferguson, R., Tavares, F.T. and Fan, Z.H. (2006). Effects of fabrication process parameters on the properties of cyclic olefin copolymer microfluidic devices. *Journal of Microelectromechanical Systems*, **15**(5), pp. 1060, 1068. DOI: 10.1109/JMEMS.2006.880352.

Fu, E. *et al*. (2010). Controlled reagent transport in disposable 2D paper networks. *Lab on a Chip*, **10**(7), pp. 918–20.

Fu, Y.Q. *et al*. (2009). Deep reactive ion etching as a tool for nanostructure fabrication. *Journal of Vacuum Science & Technology B: Microelectronics and Nanometer Structures*, **27**(3), pp. 1520–6.

Gad-El-Hak, M. (2002). *The Mems Handbook (Google eBook)*, CRC Press. Available at: http://books.google.com/books?id=g0v3r6WNaBkC&pgis=1 [Accessed 27 September 2012].

Gartner, C., Klemm, R. and Becker, H. (2007). Methods and instruments for continuous-flow PCR on a chip. *Polymer*, **6465**, pp. 646502–646502–8. Available at: http://link.aip.org/link/PSISDG/v6465/i1/p646502/s1&Agg=doi.

Gattass, R.R. and Mazur, E. (2008). Femtosecond laser micromachining in transparent materials. *Nature Photonics*, **2**(4), pp. 219–25. Available at: http://dx.doi.org/10.1038/nphoton.2008.47 [Accessed 29 July 2012].

Gawad, S., Schild, L. and Renaud, Ph. (2001). Micromachined impedance spectroscopy flow cytometer for cell analysis and particle sizing. *Lab on a Chip*, **1**(1), pp. 76–82. Available at: http://dx.doi.org/10.1039/B103933B.

Van der Giessen, W.J. *et al*. (1996). Marked inflammatory sequelae to implantation of biodegradable and nonbiodegradable polymers in porcine coronary arteries. *Circulation*, **94**(7), pp. 1690–7. Available at: http://www.ncbi.nlm.nih.gov/pubmed/8840862 [Accessed 11 October 2011].

Giselbrecht, S. *et al*. (2004). Microthermoforming as a novel technique for manufacturing scaffolds in tissue engineering (CellChips). *IEE Proceedings. Nanobiotechnology*, **151**(4), pp. 151–7. Available at: http://ieeexplore.ieee.org/xpls/abs_all.jsp?arnumber=1352836 [Accessed 3 October 2012].

Glasgow, I.K., Beebe, D.J. and White, V.E. (1999). Design rules for polyimide solvent bonding. *Sensors and Materials*, **11**(5), pp. 269–78.

Gottschlich, N. (2004). Production of plastic components for microfluidic applications. *Business Briefing: Future Drug Discovery*, pp. 1–4. Available at: http://www.touchbriefings.com/pdf/855/fdd041_greiner_tech.pdf [Accessed 11 July 2012].

Gourgon, C. *et al*. (2005). Uniformity across 200 mm silicon wafers printed by nanoimprint lithography. *Journal of Physics D: Applied Physics*, **38**, p. 70. Available at: http://iopscience.iop.org/0022–3727/38/1/012.

Grétillat, M.-A, Paoletti, F., Thiébaud, P., Roth, S., Koudelka-Hep, M., de Rooij, N.F. (1997). A new fabrication method for borosilicate glass capillary tubes with lateral inlets and outlets. *Sensors and Actuators A: Physical*, **60**(1–3), pp. 219–22. ISSN 0924-4247, http://dx.doi.org/10.1016/S0924-4247(97)01360-5.

Griffiths, C.A. *et al*. (2007). The effects of tool surface quality in micro-injection moulding. *Journal of Materials Processing Technology*, **189**(1), pp. 418–27.

Grover, W.H. *et al*. (2003). Monolithic membrane valves and diaphragm pumps for practical large-scale integration into glass microfluidic devices. *Sensors and Actuators B: Chemical*, **89**(3), pp. 315–23.

Grumann, M. *et al*. (2006). Sensitivity enhancement for colorimetric glucose assays on whole blood by on-chip beam-guidance. *Biomedical Microdevices*, **8**(3), pp. 209–14. Available at: http://www.ncbi.nlm.nih.gov/pubmed/16732473 [Accessed 30 April 2012].

Gulliksen, A. *et al*. (2005). Parallel nanoliter detection of cancer markers using polymer microchips. *Lab on a Chip*, **5**(4), pp. 416–36. Available at: http://dx.doi.org/10.1039/b415525d.

Guo, L.J. (2007). Nanoimprint Lithography: methods and material requirements. *Advanced Materials*, **19**(4), pp. 495–513. Available at: http://doi.wiley.com/10.1002/adma.200600882 [Accessed 16 July 2012].

Gustafsson, O., Mogensen, K. and Kutter, J. (2008). Underivatized cyclic olefin copolymer as substrate material and stationary phase for capillary and microchip electrochromatography. *Electrophoresis*, **29**(15), pp. 3145–97. Available at: http://dx.doi.org/10.1002/elps.200800131.

Gösele, U. and Tong, Q.-Y. (1998). Semiconductor wafer bonding. *Annual Review of Materials Science*, **28**(1), pp. 215–41.

Han, D.K. *et al*. (1992). In vivo canine studies of a Sinkhole valve and vascular graft coated with biocompatible PU-PEO-SO3. *ASAIO Journal (American Society for Artificial Internal Organs : 1992)*, **39**(3), pp. M537–41. Available at: http://www.ncbi.nlm.nih.gov/pubmed/8268593 [Accessed 11 October 2011].

Haraldsson, K.T. *et al*. (2006). 3D polymeric microfluidic device fabrication via contact liquid photolithographic polymerization (CLiPP). *Sensors and Actuators B: Chemical*, **113**(1), pp. 454–60. Available at: http://linkinghub.elsevier.com/retrieve/pii/S0925400505003370 [Accessed 18 September 2011].

Harendt, C. *et al*. (1992). Silicon fusion bonding and its characterization. *Journal of Micromechanics and Microengineering*, **2**(3), pp. 113–16. Available at: http://www.iop.org/EJ/abstract/0960–1317/2/3/001.

Hashimoto, M. *et al*. (2004). Rapid PCR in a continuous flow device. *Lab on a Chip*, **4**(6), pp. 638–45. Available at: http://dx.doi.org/10.1039/B406860B.

Heckele, M. and Schomburg, W.K. (2004). Review on micro molding of thermoplastic polymers. *Journal of Micromechanics and Microengineering*, **14**(3), pp. R1–R14. Available at: http://stacks.iop.org/0960–1317/14/i=3/a=R01 [Accessed 27 September 2012].

Hoffmann, M. and Voges, E. (2002). Bulk silicon micromachining for MEMS in optical communication systems. *Journal of Micromechanics and Microengineering*,

12(4), pp. 349–60. Available at: http://stacks.iop.org/0960–1317/12/i=4/a=301 [Accessed 27 September 2012].

Hori, R. and Wada, M. (2005). The thermal expansion of wood cellulose crystals. *Cellulose*, **12**(5), pp. 479–84.

Hua, F. *et al*. (2006). Processing dependent behavior of soft imprint lithography on the 1–10-nm scale. *Nanotechnology, IEEE Transactions on*, **5**(3), pp. 301–8.

Hupert, M.L. *et al*. (2006). Evaluation of micromilled metal mold masters for the replication of microchip electrophoresis devices. *Microfluidics and Nanofluidics*, **3**(1), pp. 1–11. Available at: http://www.springerlink.com/content/b26186631385p394/ [Accessed 20 August 2012].

Hurth, C., Lenigk, R. and Zenhausern, F. (2008). A compact LED-based module for DNA capillary electrophoresis. *Applied Physics B*, **93**(2–3), pp. 693–9. Available at: http://www.springerlink.com/content/606h2j7n43763613/ [Accessed 2 July 2012].

Hwang, D.J., Choi, T.Y. and Grigoropoulos, C.P. (2004). Liquid-assisted femtosecond laser drilling of straight and three-dimensional microchannels in glass. *Applied Physics A: Materials Science & Processing*, **79**(3), pp. 605–12.

Illa, X. *et al*. (2009). An array of ordered pillars with retentive properties for pressure-driven liquid chromatography fabricated directly from an unmodified cyclo olefin polymer. *Lab on a Chip*, **9**(11), pp. 1511–17. Available at: http://dx.doi.org/10.1039/b818918h.

Ito, H., Kazama, K. and Kikutani, T. (2007). Effects of process conditions on surface replication and higher order structure formation in micromolding. *Macromolecular Symposia*, **249**(1), pp. 628–1262. Available at: http://dx.doi.org/10.1002/masy.200750447.

Jacobson, S.C. *et al*. (1994). High-speed separations on a microchip. *Analytical Chemistry*, **66**(7), pp. 1114–18. Available at: http://dx.doi.org/10.1021/ac00079a029.

Jang, A. *et al*. (2011). State-of-the-art lab chip sensors for environmental water monitoring. *Measurement Science and Technology*, **22**(3), p. 032001.

Jang, W.I. *et al*. (2006). Self-operated blood plasma separation using micropump in polymer-based microfluidic device. *Proceedings of SPIE*, **6415**, p.641511. Available at: http://cat.inist.fr/?aModele=afficheN&cpsidt=18866544.

Jensen, M.F. *et al*. (2004). Rapid prototyping of polymer microsystems via excimer laser ablation of polymeric moulds. *Lab on a Chip*, **4**(4), pp. 391–5. Available at: http://www.ncbi.nlm.nih.gov/pubmed/15269810.

Jeon, J.S. *et al*. (2011). Hot embossing for fabrication of a microfluidic 3D cell culture platform. *Biomedical Microdevices*, **13**(2), pp. 325–33. Available at: http://www.pubmedcentral.nih.gov/articlerender.fcgi?artid=3117225&tool=pmcentrez&rendertype=abstract [Accessed 15 March 2012].

Judy, J.W. (2001). Microelectromechanical systems (MEMS): fabrication, design and applications. *Smart Materials and Structures*, **10**(6), pp. 1115–34. Available at: http://stacks.iop.org/0964–1726/10/i=6/a=301 [Accessed 27 September 2012].

Kalima, V. *et al*. (2007). Transparent thermoplastics: Replication of diffractive optical elements using micro-injection molding. *Optical Materials*, **30**(2), pp. 285–91. Available at: http://www.sciencedirect.com/science/article/pii/S092534670600437X.

Kameoka, J. *et al*. (2001). A polymeric microfluidic chip for CE/MS determination of small molecules. *Analytical Chemistry*, **73**(9), pp. 1935–76. Available at: http://toxnet.nlm.nih.gov/cgi-bin/sis/search/r?dbs+hsdb:@term+@rn+541–15–1.

Kameoka, J. *et al*. (2002). An electrospray ionization source for integration with microfluidics. *Analytical Chemistry*, **74**(22), pp. 5897–6798. Available at: http://toxnet.nlm.nih.gov/cgi-bin/sis/search/r?dbs+hsdb:@term+@rn+50–49–7.

Kato, Y.X. *et al*. (2012). Photosensitive-polyimide based method for fabricating various neural electrode architectures. *Frontiers in Neuroengineering*, **5**(June), p. 11. Available at: http://www.pubmedcentral.nih.gov/articlerender.fcgi?artid=3376501&tool=pmcentrez&rendertype=abstract [Accessed 18 July 2012].

Ke, K., Hasselbrink, E.F. and Hunt, A.J. (2005). Rapidly prototyped three-dimensional nanofluidic channel networks in glass substrates. *Analytical Chemistry*, **77**(16), pp. 5083–8.

Kettner, P. *et al*. (2006). New results on plasma activated bonding of imprinted polymer features for bio MEMS applications. *Journal of Physics: Conference Series*, **34**, p. 65. Available at: http://iopscience.iop.org/1742–6596/34/1/011.

Khan M.C. (2006). Laser processing for bio-microfluidics applications (part I). *Analytical and Bioanalytical Chemistry*, **385**(8), pp. 1362–9. Available at: http://dx.doi.org.libaccess.lib.mcmaster.ca/10.1007/s00216–006–0517-z [Accessed 10 September 2009].

Kim, D. and Kwon, T. (2009). Microinjection molded disposable microfluidic lab-on-a-chip for efficient detection of agglutination. *Microsystem Technologies*, **15**, pp. 309–16. Available at: http://www.springerlink.com/index/Y7K28G1043Q71X0P.pdf.

Kim, D.S. *et al*. (2006). Disposable integrated microfluidic biochip for blood typing by plastic microinjection moulding. *Lab on a Chip*, **6**(6), pp. 794–802, 15, pp. 309–16. Available at: http://www.ncbi.nlm.nih.gov/pubmed/16738733.

Kim, T.N. *et al*. (2005). Femtosecond laser-drilled capillary integrated into a microfluidic device. *Applied Physics Letters*, **86**(20), p. 201106. Available at: http://link.aip.org/link/APPLAB/v86/i20/p201106/s1&Agg=doi.

Kim, Y.-M. *et al*. (2008). Design and fabrication of electrostatic inkjet head using silicon micromachining technology. *JSTS: Journal of Semiconductor Technology and Science*, **8**(2), pp. 121–7.

Kim, Y.S., Lee, H.H. and Hammond, P.T. (2003). High density nanostructure transfer in soft molding using polyurethane acrylate molds and polyelectrolyte multilayers. *Nanotechnology*, **14**(10), pp. 1140–4. Available at: http://stacks.iop.org/0957–4484/14/i=10/a=312?key=crossref.255e51eab33e6bb6c94003fc84adee1e.

Kirby, A., Jebrail, M., Yang, H. and Wheeler, A. (2010). Low-cost microfluidic emitters for nano-electrospray ionization. Mass Spectrometry. pp. 605–607. Available at: http://www.rsc.org/binaries/LOC/2010/PDFs/Papers/209_0589.pdf.

Klintberg, L. *et al*. (2003). Fabrication of a paraffin actuator using hot embossing of polycarbonate. *Sensors and Actuators A: Physical*, **103**(3), pp. 307–16. Available at: http://www.sciencedirect.com/science/article/pii/S092442470200403X.

Kohlmann, M. and Vogel, W. (1979). Stochastic control theory and stochastic differential systems: Proceedings of a Workshop of the 'Sonderforschungsbereich 72 Der Deutschen Forschungsgemeinschaft an Der Universit{ä}t Bonn' which Took Place January 1979 at Bad Honnef, Springer-Verlag.

Kolew, A. *et al*. (2010). Hot embossing of micro and sub-micro structured inserts for polymer replication. *Microsystem Technologies*, **17**(4), pp. 609–18. Available at: http://www.springerlink.com/index/10.1007/s00542–010–1182-x.

Korte, F. *et al*. (2003). Towards nanostructuring with femtosecond laser pulses. *Applied Physics A: Materials Science & Processing*, **77**(2), pp. 229–35.

Kovacs, G.T.A., Maluf, N.I. and Petersen, K.E. (1998). Bulk micromachining of silicon. *Proceedings of the IEEE*, **86**(8), pp. 1536–51.

Kudryashov, S.I. *et al*. (2007). Nanochannels fabricated by high-intensity femtosecond laser pulses on dielectric surfaces. *Applied Physics Letters*, **91**(14), p. 141111.

Kunnavakkam, M.V., Houlihan, F.M., Schlax, M., Liddle, J.A., Kolodner, P., Nalamasu, O. and Rogers, J.A. (2003). Low-cost, low loss microlens arrays fabricated by soft-lithography replication process. *Applied Physics Letters*, **82**, pp. 1152–4.

Kuo, J.S. *et al*. (2009). Microfabricating high-aspect-ratio structures in polyurethane-methacrylate (PUMA) disposable microfluidic devices. *Lab on a Chip*, **9**(13), pp. 1951–6. Available at: http://www.ncbi.nlm.nih.gov/pubmed/19532971 [Accessed 25 July 2010].

Kuoni, A. *et al*. (2003). Polyimide membrane with ZnO piezoelectric thin film pressure transducers as a differential pressure liquid flow sensor. *Journal of Micromechanics and Microengineering*, **13**(4), p. S103. Available at: http://stacks.iop.org/0960–1317/13/i=4/a=317.

Kutchoukov, V.G. *et al*. (2003). Fabrication of nanofluidic devices using glass-to-glass anodic bonding. *Sensors and Actuators. A, Physical*, **114**, pp. 521–7.

Lagally, E.T., Simpson, P.C. and Mathies, R.A. (2000). Monolithic integrated microfluidic DNA amplification and capillary electrophoresis analysis system. *Sensors and Actuators B: Chemical*, **63**(3), pp. 138–46.

Lake, J.H. *et al*. (2011). Maskless grayscale lithography using a positive-tone photodefinable polyimide for MEMS applications. *Microelectromechanical Systems, Journal of*, **20**(6), pp. 1483–8.

Lamonte, R.R. and Mcnally, D. (2000). Uses and processing of cyclic olefin copolymers. *Plastics Engineering*, **56**, pp. 51–5.

Lang, W. (1996). Silicon microstructuring technology. *Materials Science and Engineering: R: Reports*, **17**(1), pp. 1–55.

Larsen, A. *et al*. (2008). Pinched flow fractionation devices for detection of single nucleotide polymorphisms. *Lab on a Chip*, **8**(5), pp. 818–39. Available at: http://dx.doi.org/10.1039/b802268b.

Laser, D.J. and Santiago, J.G. (2004). A review of micropumps. *Journal of Micromechanics and Microengineering*, **14**(6), pp. R35–64.

Lee, D.-S. *et al*. (2005). Wafer-scale fabrication of polymer-based microdevices via injection molding and photolithographic micropatterning protocols. *Analytical Chemistry*, **77**(16), pp. 5414–34. Available at: http://dx.doi.org/10.1021/ac050286w.

Lee, K.S. and Ram, R.J. (2009). Plastic-PDMS bonding for high pressure hydrolytically stable active microfluidics. *Lab on a Chip*, **9**(11), pp. 1618–24. Available at: http://www.rsc.org/Publishing/Journals/article.asp?doi=b820924c.

Lee, W.G. *et al*. (2010). Nano/Microfluidics for diagnosis of infectious diseases in developing countries. *Advanced Drug Delivery Reviews*, **62**(4–5), pp. 449–57.

Li, X., Abe, T. and Esashi, M. (2001). Deep reactive ion etching of Pyrex glass using SF 6 plasma. *Sensors and Actuators A: Physical*, **87**(3), pp. 139–45, ISSN 0924-4247, http://dx.doi.org/10.1016/S0924-4247(00)00482-9.

Li, X., Tian, J., Nguyen, T. and Shen, W. (2008). Paper-based microfluidic devices by plasma treatment. *Analytical Chemistry*, **80**(23), pp. 9131–4.

Li, X., Ballerini, D.R. and Shen, W. (2012). A perspective on paper-based microfluidics: Current status and future trends. *Biomicrofluidics*, **6**(1), pp. 11301–113.

Lin, C.-H. *et al*. (2001). A fast prototyping process for fabrication of microfluidic systems on soda-lime glass. *Journal of Micromechanics and Microengineering*, **11**(6), pp. 726–32.

Lin, C.-H. *et al*. (2002). A new fabrication process for ultra-thick microfluidic microstructures utilizing SU-8 photoresist. *Journal of Micromechanics and Microengineering*, **12**(5), pp. 590–7. Available at: http://stacks.iop.org/0960–1317/12/i=5/a=312?key=crossref.de8cb11e0784181e5f3f73a6204debc4.

Lin, Y. *et al*. (1999). Laser micromachined isoelectric focusing devices on polymer substrate for electrospray mass spectrometry. In *Proceedings of SPIE*. The International Society for Optical Engineering. **3877**, pp. 28–35.

Lion, N. *et al*. (2003). Microfluidic systems in proteomics. *Electrophoresis*, **24**(21), pp. 3533–62.

Liu, J. *et al*. (2007). Monolithic column plastic microfluidic device for peptide analysis using electrospray from a channel opening on the edge of the device. *International Journal of Mass Spectrometry*, **259**(1), pp. 65–137. Available at: http://www.sciencedirect.com/science/article/pii/S1387380606004143.

Liu, Y. *et al*. (2001). Microfabricated polycarbonate CE devices for DNA analysis. *Analytical Chemistry*, **73**(17), pp. 4196–201. Available at: http://pubs.acs.org/doi/abs/10.1021/ac010343v.

Lu, Y. *et al*. (2009). Rapid prototyping of paper-based microfluidics with wax for low-cost, portable bioassay. *Electrophoresis*, **30**(9), pp. 1497–500.

Lyman, D., Seare, W. and Albo, D. (1977). Polyurethane elastomers in surgery. *International Journal of Polymeric Materials*, **5**, pp. 211–29.

Lyman, D.J. *et al*. (1971). The development and implantation of a polyurethane hemispherical artificial heart. *Transactions – American Society for Artificial Internal Organs*, **17**, pp. 456–63. Available at: http://www.ncbi.nlm.nih.gov/pubmed/5158130 [Accessed 11 October 2011].

Mair, D. *et al*. (2006). Injection molded microfluidic chips featuring integrated interconnects. *Lab on a Chip*, **6**(10), pp. 1346–400. Available at: http://dx.doi.org/10.1039/b605911b.

Malek, C.K. and Saile, V. (2004). Applications of LIGA technology to precision manufacturing of high-aspect-ratio micro-components and -systems: a review. *Microelectronics Journal*, **35**(2), pp. 131–143. Available at: http://dx.doi.org/10.1016/j.mejo.2003.10.003 [Accessed 20 July 2012].

Maluf, N. (2002). An introduction to microelectromechanical systems engineering. *Measurement Science and Technology*, **13**(2), p. 229.

Man, P.F., Jones, D.K. and Mastrangelo, C.H. (1997). Microfluidic plastic interconnects for multibioanalysis chip modules. In K.H. Chau and P.J. French, eds. *Micromachined Devices and Components III*. SPIE, pp. 196–200. Available at: http://link.aip.org/link/?PSI/3224/196/1.

Mangriotis, M.D. *et al*. (1999). Flexible microfluidic polyimide channels. In *The 10th International Conference on Solid-State Sensors and Actuators*. Sendai, Japan, pp. 772–5.

Manz, A. *et al*. (1990). Design of an open-tubular column liquid chromatograph using silicon chip technology. *Sensors and Actuators B: Chemical*, **1**(1–6), pp. 249–55.

Manz, A. *et al*. (1991). Miniaturization of chemical-analysis systems – a look into next century technology or just a fashionable craze. *Chimia*, **45**(4), pp. 103–5.

Mark, J.E. (2007). *Physical Properties of Polymers Handbook (Google eBook)* (p. 1076). Springer. Available at: http://books.google.com/books?id=fZl7q7UgEXkC&pgis=1

Mark, R.E. *et al*. (2001). *Handbook of Physical Testing of Paper* 2nd ed. Burien, Washington, USA and International Paper: CRC Press.

Marois, Y. *et al*. (1989). In vivo evaluation of hydrophobic and fibrillar microporous polyetherurethane urea graft. *Biomaterials*, **10**(8), pp. 521–31. Available at: http://www.ncbi.nlm.nih.gov/pubmed/2605286 [Accessed 11 October 2011].

Marois, Y. *et al*. (1993). A novel microporous polyurethane vascular graft: in vivo evaluation of the UTA prosthesis implanted as infra-renal aortic substitute in dogs. *Journal of Investigative Surgery: The Official Journal of the Academy of Surgical Research*, **6**(3), pp. 273–88. Available at: http://www.ncbi.nlm.nih.gov/pubmed/8398999 [Accessed 11 October 2011].

Marois, Y. *et al*. (1996). Vascugraft microporous polyesterurethane arterial prosthesis as a thoraco-abdominal bypass in dogs. *Biomaterials*, **17**(13), pp. 1289–300. Available at: http://www.ncbi.nlm.nih.gov/pubmed/8805976 [Accessed 11 October 2011].

Martinez, A.W. *et al*. (2009). Diagnostics for the developing world: microfluidic paper-based analytical devices. *Analytical Chemistry*, **82**(1), pp. 3–10.

Martinez, A.W. *et al*. (2007). Patterned paper as a platform for inexpensive, low-volume, portable bioassays. *Angewandte Chemie (International ed. in English)*, **46**(8), pp. 1318–20.

Martinez, A.W., Phillips, S.T. and Whitesides, G.M. (2008). Three-dimensional microfluidic devices fabricated in layered paper and tape. *Proceedings of the National Academy of Sciences of the United States of America*, **105**(50), pp. 19606–11.

Mata, A., Fleischman, A. J. and Roy, S. (2005). Characterization of polydimethylsiloxane (PDMS) properties for biomedical micro/nanosystems. *Biomedical Microdevices*, **7**, pp. 281–93.

McDonald, J.C., Metallo, S.J. and Whitesides, G.M. (2001). Fabrication of a configurable, single-use microfluidic device. *Analytical Chemistry*, **73**, pp. 5645–50.

McDonald, J.C. and Whitesides, G.M. (2002). Poly(dimethylsiloxane) as a material for fabricating microfluidic devices. *Accounts of Chemical Research*, **35**, pp. 491–9.

Melchels, F.P.W., Feijen, J. and Grijpma, D.W. (2010). A review on stereolithography and its applications in biomedical engineering. *Biomaterials*, **31**(24), pp. 6121–30. Available at: http://dx.doi.org/10.1016/j.biomaterials.2010.04.050 [Accessed 12 July 2012].

Metz, S., Bertsch, A. *et al*. (2004). Flexible polyimide probes with microelectrodes and embedded microfluidic channels for simultaneous drug delivery and multichannel monitoring of bioelectric activity. *Biosensors and Bioelectronics*, **19**(10), pp. 1309–18. Available at: http://www.ncbi.nlm.nih.gov/pubmed/15046764.

Metz, S., Jiguet, S., Bertsch, A. and Renaud, Ph. (2004). Polyimide and SU-8 microfluidic devices manufactured by heat-depolymerizable sacrificial material technique. *Lab on a Chip*, **4**(2), pp. 114–20. Available at: http://dx.doi.org/10.1039/B310866J.

Metz, S., Trautmann, C., *et al*. (2004). Polyimide microfluidic devices with integrated nanoporous filtration areas manufactured by micromachining and ion track technology. *Journal of Micromechanics and Microengineering*, **14**(3), pp. 324–31. Available at: http://stacks.iop.org/0960–1317/14/i=3/a=002 [Accessed 31 July 2012].

Metz, S., Holzer, R. and Renaud, P. (2001). Polyimide-based microfluidic devices. *Lab on a Chip*, **1**(1), pp. 29–34. Available at: http://www.ncbi.nlm.nih.gov/pubmed/15100886.

MICROCHEM (2012). SU-8 Negative Epoxy Series Resists. Available at: http://www.microchem.com/Prod-SU8_KMPR.htm.

Miki, N. (2005). Wafer bonding techniques for MEMS. *Sensor Letters*, **3**(4), p. 11. Available at: http://www.ingentaconnect.com/content/asp/senlet/2005/00000003/00000004/art00001 [Accessed 27 September 2012].

Minges, M.L. (1989). *Electronic Materials Handbook: Packaging* (p. 1224). ASM International. Available at: http://books.google.com/books?id=c2YxCCaM9RIC&pgis=1

Mogensen, K.B. *et al*. (2001). Monolithic integration of optical waveguides for absorbance detection in microfabricated electrophoresis devices. *Electrophoresis*, **22**(18), pp. 3930–8. Available at: http://www.ncbi.nlm.nih.gov/pubmed/11700723 [Accessed 2 July 2012].

Moraes, C. *et al*. (2009). Integrating polyurethane culture substrates into poly(dimethylsiloxane) microdevices. *Biomaterials*, **30**(28), pp. 5241–50. Available at: http://www.ncbi.nlm.nih.gov/pubmed/19545891.

Morimoto, Y., Tan, W.-H. and Takeuchi, S. (2009). Three-dimensional axisymmetric flow-focusing device using stereolithography. *Biomedical Microdevices*, **11**(2), pp. 369–77. Available at: http://www.ncbi.nlm.nih.gov/pubmed/19009352.

Müller, R.H. and Clegg, D.L. (1949). Automatic paper chromatography. *Analytical Chemistry*, **21**(9), pp. 1123–5.

Ngoi, B.K.A. and Sreejith, P.S. (2000). Ductile regime finish machining – a review. *The International Journal of Advanced Manufacturing Technology*, **16**(8), pp. 547–50.

Nguyen, T.N.T. and Lee, N.-E. (2007). Deep reactive ion etching of polyimide for microfluidic applications. *Journal of the Korean Physical Society*, **51**(3), p. 984. Available at: http://www.kps.or.kr/jkps/abstract_view.asp?articleuid=A8A3FF79–647E-4A84-AA25–48C2D0B0BF1B.

Nikumb, S. *et al*. (2005). Precision glass machining, drilling and profile cutting by short pulse lasers. *Thin Solid Films*, **477**(1–2), pp. 216–21. Available at: http://dx.doi.org/10.1016/j.tsf.2004.08.136 [Accessed 6 August 2012].

Nilsson, D., Balslev, S. and Kristensen, A. (2005). A microfluidic dye laser fabricated by nanoimprint lithography in a highly transparent and chemically resistant cycloolefin copolymer (COC). *Journal of Micromechanics and Microengineering*, **15**, p. 296. Available at: http://iopscience.iop.org/0960–1317/15/2/008.

Noh, H.-S., Huang, Y.S. and Hesketh, P.J. (2004a). Parylene micromolding, a rapid and low-cost fabrication method for parylene microchannel. *Sensors and Actuators B: Chemical*, **102**, pp. 78–85.

Noh, H.-S., Moon, K.S., Cannon, A., Hesketh, P.J. and Wong, C.P. (2004b). Wafer bonding using microwave heating of parylene intermediate layers. *Journal of Micromechanics and Microengineering*, **14**, pp. 625–31.

Ogonczyk, D. *et al*. (2010). Bonding of microfluidic devices fabricated in polycarbonate. *Lab on a Chip*, **10**(10), pp. 1324–27. Available at: http://www.rsc.org/Publishing/Journals/article.asp?doi=b924439e.

Oh, K.W. and Ahn, C.H. (2006). A review of microvalves. *Journal of Micromechanics and Microengineering*, **16**(5), pp. R13–39.

Okagbare, P. *et al*. (2010). Fabrication of a cyclic olefin copolymer planar waveguide embedded in a multi-channel poly(methyl methacrylate) fluidic chip for evanescence excitation. *Lab on a Chip*, **10**(1), pp. 66–139. Available at: http://dx.doi.org/10.1039/b908759a.

Okoshi, T. *et al*. (1992). Penetrating micropores increase patency and achieve extensive endothelialization in small diameter polymer skin coated vascular grafts. *ASAIO Journal (American Society for Artificial Internal Organs : 1992)*, **42**(5), pp. M398–401. Available at: http://www.ncbi.nlm.nih.gov/pubmed/8944915 [Accessed 11 October 2011].

Olson, R.E., & Kiefer, M.L. (1963). Effect of Lateral Filter-Paper Drains on the Triaxial Shear Characteristics of Soils. *Laboratory Shear Testing of Soils* (p. 482). Ottawa, Canada: American society for testing and materials.

Osborn, J.L. *et al*. (2010). Microfluidics without pumps: reinventing the T-sensor and H-filter in paper networks. *Lab on a Chip*, **10**(20), pp. 2659–65.

Pakkanen, T.T. *et al*. (2002). Replication of sub micron features using amorphous thermoplastics. *Polymer Engineering & Science*, **42**(7), pp. 1600–3208. Available at: http://dx.doi.org/10.1002/pen.11055.

Park, D. *et al*. (2008). A titer plate-based polymer microfluidic platform for high throughput nucleic acid purification. *Biomedical Microdevices*, **10**(1), pp. 21–33. Available at: http://dx.doi.org/10.1007/s10544–007–9106-y.

Park, S. *et al*. (2008). Fabrication and testing of a PDMS multi-stacked hand-operated LOC for use in portable immunosensing systems. *Biomedical Microdevices*, **10**(6), pp. 859–927. Available at: http://dx.doi.org/10.1007/s10544–008–9200–9.

Park, S.-M., Lee, K. and Craighead, H. (2008). On-chip coupling of electrochemical pumps and an SU-8 tip for electrospray ionization mass spectrometry. *Biomedical Microdevices*, **10**(6), pp. 891–898. Available at: http://dx.doi.org/10.1007/s10544–008–9203–6.

Peham, J. *et al*. (2012). Disposable microfluidic chip for rapid pathogen identification with DNA microarrays. *Microsystem Technologies*, **18**(3), pp. 311–18. Available at: http://dx.doi.org/10.1007/s00542–011–1401–0.

Pekas, N. *et al*. (2010). Wet-etching of structures with straight facets and adjustable taper into glass substrates. *Lab on a Chip*, **10**(4), pp. 494–8.

Pelton, R. (2009). Bioactive paper provides a low-cost platform for diagnostics. *Trends in Analytical Chemistry*, **28**(8), pp. 925–42.

Petersen, K.E. (1979). Fabrication of an integrated, planar silicon ink-jet structure. *Electron Devices, IEEE Transactions on*, **26**(12), pp. 1918–20.

Petersen, K.E. (1982). Silicon as a mechanical material. *Proceedings of the IEEE*, **70**(5), pp. 420–57.

Piccin, E. *et al*. (2007). Polyurethane from biosource as a new material for fabrication of microfluidic devices by rapid prototyping. *Journal of Chromatography. A*, **1173**(1–2), pp. 151–8. Available at: http://www.ncbi.nlm.nih.gov/pubmed/17964580.

Qin, D., Xia, Y. and Whitesides, G.M. (2010). Soft lithography for micro- and nanoscale patterning. *Nature Protocols*, **5**(3), pp. 491–502. Available at: http://dx.doi.org/10.1038/nprot.2009.234 [Accessed 24 July 2012].

Rabek, J.F. (1995). *Polymer Photodegradation: Mechanisms and Experimental Methods (Google eBook)* (p. 664). Springer. Available at: http://books.google.com/books?id=dXwbS128lXoC&pgis=1

Rai-Choudhury, P. (1997). *Handbook of Microlithography, Micromachining, and Microfabrication, Volume 1*, IET. Available at: http://books.google.com/books?hl=en&lr=&id=-kbT328H1XQC&pgis=1 [Accessed 27 September 2012].

Rangsten, P. and Hedlund, C. (1998). Etch rates of crystallographic planes in Z -cut quartz – experiments and simulation. *Journal of Micromechanics and*

Microengineering, **8**(1), pp. 1–6. Retrieved from http://iopscience.iop.org/0960-1317/8/1/001.

Rezk, A.R. *et al*. (2012). Uniform mixing in paper-based microfluidic systems using surface acoustic waves. *Lab on a Chip*, **12**(4), pp. 773–9.

Rigden, J.S. (1996). *Macmillan Encyclopedia of Physics*, New York: Simon & Schuster Macmillan.

Rizvi, N. (2003). Femtosecond laser micromachining: current status and applications. *Riken Review*, **50**(50), pp. 107–12.

Ro, K., Liu, J. and Knapp, D. (2006). Plastic microchip liquid chromatography-matrix-assisted laser desorption/ionization mass spectrometry using monolithic columns. *Journal of Chromatography. A*, **1111**(1), pp. 40–7. Available at: http://dx.doi.org/10.1016/j.chroma.2006.01.105.

Rogers, J.A. and Nuzzo, R.G. (2005). Recent progress in soft lithography. *Materials Today*, **8**(2), pp. 50–6. Available at: http://dx.doi.org/10.1016/S1369–7021(05)00702–9 [Accessed 27 September 2012].

Ronggui, S. (1991). Characterization of reactive ion etching of glass and its applications in integrated optics. *Journal of Vacuum Science & Technology A: Vacuum, Surfaces, and Films*, **9**(5), p. 2709.

Roos, N. *et al*. (2002). First and second generation purely thermoset stamps for hot embossing. *Engineering Conference*, **62**(1–3), pp. 399–405. Available at: http://linkinghub.elsevier.com/retrieve/pii/S0167931702005129.

Rossier, J.S. *et al*. (2002). Plasma etched polymer microelectrochemical systems. *Lab on a Chip*, **2**(3), pp. 145–50. Available at: http://pubs.rsc.org/en/content/articlehtml/2002/lc/b204063h [Accessed 19 October 2011].

Ruprecht, R., Bacher, W., Hausselt, J. H., Piotter, V. (1995). Injection molding of LIGA and LIGA-similar microstructures using filled and unfilled thermoplastics. *Proc. SPIE* 2639, Micromachining and Microfabrication Process Technology, 146 (September 19, 1995); doi:10.1117/12.221272.

Sabbert, D., Landsiedel, J., Bauer, H.-D., Ehrfeld, W. (1999). ArF-excimer laser ablation experiments on Cycloolefin Copolymer (COC). *Applied Surface Science*, **150**(1–4), pp. 185–9, ISSN 0169-4332, http://dx.doi.org/10.1016/S0169-4332(98)00334-1.

Sastri, V.R. (2010). *Plastics in Medical Devices: Properties, Requirements and Applications (Google eBook)* (p. 352). Elsevier. Available at: http://books.google.com/books?id=WX4MW1GU3bMC&pgis=1.

Schift, H. *et al*. (2000). Nanoreplication in polymers using hot embossing and injection molding. *Microelectronic Engineering*, **53**(1–4), pp. 171–4. Available at: http://linkinghub.elsevier.com/retrieve/pii/S0167931700002896.

Schlautmann, S. *et al*. (2001). Powder-blasting technology as an alternative tool for microfabrication of capillary electrophoresis chips with integrated conductivity sensors. *Journal of Micromechanics and Microengineering*, **11**(4), pp. 386–9.

Schmidt, M.A. (1998). Wafer-to-wafer bonding for microstructure formation. *Proceedings of the IEEE*, **86**(8), pp. 1575–85.

Schröder, A. and Bensarsa, D. (2002). The Young's modulus of wet paper. *Journal of Pulp and Paper Science*, **28**(12), pp. 410–15.

Schultz, G., Corso, T., Prosser, S. and Zhang, S. (2000). A fully integrated monolithic microchip electrospray device for mass spectrometry. *Analytical Chemistry*, **72**(17), pp. 4058–63.

Schütte, J. *et al*. (2010). A method for patterned in situ biofunctionalization in injection-molded microfluidic devices. *Lab on a Chip*, **10**(19), pp. 2551–9. Available at: http://dx.doi.org/10.1039/c005307d.

Search, H. *et al*. (1994). Three-dimensional micro flow manifolds for miniaturized chemical analysis systems. 246.

Shen, J.-Y. *et al*. (2006). UV-embossed microchannel in biocompatible polymeric film: application to control of cell shape and orientation of muscle cells. *Journal of Biomedical Materials Research. Part B, Applied Biomaterials*, **77**(2), pp. 423–30. Available at: http://www.ncbi.nlm.nih.gov/pubmed/16292762 [Accessed 29 October 2010].

Shin, Y.S., Cho, K., Lim, S.H., Chung, S., Park, S., Chung, C., Han, D. and Chang, J.K. (2003). PDMS-based micro PCR chip with Parylene coating. *Journal of Micromechanics and Microengineering*, **13**, p. 768.

Shin, J.Y. (2005). Chemical Structure and Physical Properties of Cyclic Olefin Copolymers: IUPAC Technical Report (p. 14). International Union of Pure and Applied Chemistry. Available at: http://books.google.com/books?id=9gTnPgAACAAJ&pgis=1

Shinohara, H. *et al*. (2008). Polymer microchip integrated with nano-electrospray tip for electrophoresis-mass spectrometry. *Sensors and Actuators B: Chemical*, **132**(2), pp. 368–741. Available at: http://www.sciencedirect.com/science/article/pii/S0925400507007927.

Shiu, P.P. *et al*. (2008). Rapid fabrication of tooling for microfluidic devices via laser micromachining and hot embossing. *Journal of Micromechanics and Microengineering*, **18**(2), p. 025012. Available at: http://stacks.iop.org/0960–1317/18/i=2/a=025012 [Accessed 27 September 2012].

Sidorova, J.M. *et al*. (2009). Microfluidic-assisted analysis of replicating DNA molecules. *Nature Protocols*, **4**(6), pp. 849–61.

Sikanen, T. *et al*. (2005). Characterization of SU-8 for electrokinetic microfluidic applications. *Lab on a Chip*, **5**(8), pp. 888–96. Available at: http://www.ncbi.nlm.nih.gov/pubmed/16027941.

Spierings, G.A.C.M. (1993). Wet chemical etching of silicate glasses in hydrofluoric acid based solutions. *Journal of Materials Science*, **28**(23), pp. 6261–73.

Steigert, J. *et al*. (2007). Rapid prototyping of microfluidic chips in COC. *Journal of Micromechanics and Microengineering*, **17**, p. 333. Available at: http://iopscience.iop.org/0960–1317/17/2/020.

Stokes, C. and Palmer, P.J. (2006). 3D micro-fabrication processes: a review. Proceedings of the Seminar on MEMS Sensors and Actuators, 2006. The Institution of Engineering and Technology, pp. 289, 298, 28 April 2006.

Sueyoshi, K., Kitagawa, F. and Otsuka, K. (2008). Recent progress of online sample preconcentration techniques in microchip electrophoresis. *Journal of Separation Science*, **31**(14), pp. 2650–716. Available at: http://dx.doi.org/10.1002/jssc.200800272.

Suh, H.-J. *et al*. (2000). Dendritic material as a dry-release sacrificial layer. *Microelectromechanical Systems, Journal of*, **9**(2), pp. 198–205.

Suriyage, N.U. *et al*. (2004). Fabrication, measurement, and modeling of electroosmotic flow in micromachined polymer microchannels. In *Proceedings of SPIE*. The International Society for Optical Engineering, **5275**, pp. 149–60.

Takahara, A., Tashita, J.I. and Kajiyama, T. (1985). Microphase separated structure, surface composition and blood compatibility of segmented poly(urethaneureas) with various soft segment components. *Polymer*, **26**, pp. 987–96.

Tan, C.P. and Craighead, H.G. (2010). Surface engineering and patterning using parylene for biological applications. *Materials*, **3**, pp. 1803–2.

Tay, F.E.H. *et al*. (2001). A novel micro-machining method for the fabrication of thick-film SU-8 embedded microchannels. *Journal of Micromechanics and Microengineering*, **11**(1), pp. 27–32. Available at: http://iopscience.iop.org/0960–1317/11/1/305.

Terry, S.C., Jerman, J.H. and Angell, J.B. (1979). A gas chromatographic air analyzer fabricated on a silicon wafer. *IEEE Transactions on Electron Devices*, **26**(12), pp. 1880–6. DOI:10.1109/T-ED.1979.19791.

Thom, N.K. *et al*. (2012). 'Fluidic batteries' as low-cost sources of power in paper-based microfluidic devices. *Lab on a Chip*, **12**(10), pp. 1768–70.

Thompson, K. *et al*. (2002). *Direct silicon-silicon bonding by electromagnetic induction heating*, Available at: http://ieeexplore.ieee.org/lpdocs/epic03/wrapper.htm?arnumber=1022838.

Thorsen, T. *et al*. (2001). Dynamic pattern formation in a vesicle-generating microfluidic device. *Physical Review Letters*, **86**(18), pp. 4163–6. Available at: http://prl.aps.org/abstract/PRL/v86/i18/p4163_1 [Accessed 13 June 2011].

Tian, H., Hühmer, A.F. and Landers, J.P. (2000). Evaluation of silica resins for direct and efficient extraction of DNA from complex biological matrices in a miniaturized format. *Analytical Biochemistry*, **283**(2), pp. 175–91.

Tong, Q.Y. *et al*. (1994). Hydrophobic silicon wafer bonding. *Applied Physics Letters*, **64**(5), p. 625. Available at: http://link.aip.org/link/APPLAB/v64/i5/p625/s1&Agg=doi.

Topas Advanced Polymers (2012). *Topas Advanced Polymers*, Available at: http://www.topas.com/products-topas_coc [Accessed 2 July 2012].

Truckenmuller, R. *et al*. (2002). Low-cost thermoforming of micro fluidic analysis chips. *Journal of Micromechanics and Microengineering*, **12**(4), pp. 375–9. Available at: http://stacks.iop.org/0960–1317/12/i=4/a=304 [Accessed 3 October 2012].

Tsao, C. *et al*. (2007). Low temperature bonding of PMMA and COC microfluidic substrates using UV/ozone surface treatment. *Lab on a Chip*, **7**(4), pp. 499–1004. Available at: http://dx.doi.org/10.1039/b618901f.

Tsao, C.W., Liu, J and DeVoe, D.L. (2008). Droplet formation from hydrodynamically coupled capillaries for parallel microfluidic contact spotting. *Journal of Micromechanics and Microengineering*, **18**, p. 25013. Available at: http://iopscience.iop.org/0960–1317/18/2/025013.

Tsao, C.W. and Devoe, D.L. (2009). Bonding of thermoplastic polymer microfluidics. *Microfluidics and Nanofluidics*, **6**, pp. 1–16.

Tse, L.A. *et al*. (2003). Stereolithography on silicon for microfluidics and microsensor packaging. *Microsystem Technologies*, **9**(5), pp. 319–23. Available at: http://www.springerlink.com/Index/10.1007/s00542–002–0254-y.

Tsutsui, T., Imamura, E. and Kayanagi, H. (1981). The development of nonstended trileaflet valve prosthesis. *Artif Organs (Japan)*, **10**, pp. 590–3.

Utracki, L.A. (2002). *Polymer Blends Handbook (Google eBook)* (p. 1442). Springer. Available at: http://books.google.com/books?id=VSmgMoUNBV4C&pgis=1.

Vermette, P. *et al*. (2001). *Biomedical Applications of Polyurethanes*, Landes Bioscience Austin, TX. Available at: http://asterix.msp.univie.ac.at/.Chemistry eBooks Collection/Polymers/Biomedical applications of polyurethanes 2001 – Vermette.pdf [Accessed 30 November 2010].

Verpoorte, E. *et al*. (1992). A silicon flow cell for optical detection in miniaturized total chemical analysis systems. *Sensors and Actuators B: Chemical*, **6**(1–3), pp. 66–70.

Verpoorte, E.M.J. *et al.* (1994). Three-dimensional micro flow manifolds for miniaturized chemical analysis systems. *Journal of Micromechanics and Microengineering*, **4**, pp. 246–56.

Verpoorte, E. and De Rooij, N.F. (2003). Microfluidics meets MEMS. *Proceedings of the IEEE*, **91**(6), pp. 930–53.

Vo-Dinh, T. and Cullum, B. (2000). Biosensors and biochips: advances in biological and medical diagnostics. *Fresenius' Journal of Analytical Chemistry*, **366**(6), pp. 540–51.

Waddell, E. (2002). UV laser micromachining of polymers for microfluidic applications. *Journal of the Association for Laboratory Automation*, **7**(1), pp. 78–82. Available at: http://www.sciencedirect.com/science/article/B75DF-4BRJG7V-5W/1/7a2f18fd5d4dd6c64b149cebd74e0838.

Wallow, T. *et al*. (2007). Low-distortion, high-strength bonding of thermoplastic microfluidic devices employing case-II diffusion-mediated permeant activation. *Lab on a Chip*, **7**(12), pp. 1825–56. Available at: http://dx.doi.org/10.1039/b710175a.

Wang, W., Wu, W.-Y. and Zhu, J.-J. (2010). Tree-shaped paper strip for semiquantitative colorimetric detection of protein with self-calibration. *Journal of Chromatography. A*, **1217**(24), pp. 3896–9.

Wang, Y. *et al*. (2008). A high-performance polycarbonate electrophoresis microchip with integrated three-electrode system for end-channel amperometric detection. *Electrophoresis*, **29**(9), pp. 1881–8. Available at: http://www.ncbi.nlm.nih.gov/pubmed/18393335 [Accessed 29 March 2012].

Watkinson, A.F. *et al*. (1995). Esophageal carcinoma: initial results of palliative treatment with covered self-expanding endoprostheses. *Radiology*, **195**(3), pp. 821–7. Available at: http://www.ncbi.nlm.nih.gov/pubmed/7538682 [Accessed 11 October 2011].

Witek, M.A. *et al*. (2008). 96-well polycarbonate-based microfluidic titer plate for high-throughput purification of DNA and RNA. *Analytical Chemistry*, **80**(9), pp. 3483–91. Available at: http://www.pubmedcentral.nih.gov/articlerender.fcgi?artid=2584777&tool=pmcentrez&rendertype=abstract.

Worgull, M., Heckele, M. and Schomburg, W.K. (2005). Large-scale hot embossing. *Microsystem Technologies*, **12**(1–2), pp. 110–15. Available at: http://www.springerlink.com/content/b3252203l4227j11/ [Accessed 27 September 2012].

Worgull, M. (2009). *Hot Embossing: Theory and Technology of Microreplication (Google eBook)*, William Andrew. Available at: http://books.google.com/books?hl=en&lr=&id=Ycg-fKKf_s4C&pgis=1 [Accessed 27 September 2012].

Wu, W.-I. *et al*. (2012). Polyurethane-based microfluidic devices for blood contacting applications. *Lab on a Chip*, **12**(5), pp. 960–70. Available at: http://www.ncbi.nlm.nih.gov/pubmed/22273592 [Accessed 12 March 2012].

Xia, Y. and Whitesides, G.M. (1998). Soft Lithography. *Angewandte Chemie International Edition*, **37**(5), pp. 550–75. Available at: http://dx.doi.org.libaccess.lib.mcmaster.ca/10.1002/(SICI)1521–3773(19980316)37:5<550::AID-ANIE550>3.0.CO;2-G [Accessed 10 September 2009].

Xu, J. *et al*. (2000). Room-temperature imprinting method for plastic microchannel fabrication. *Analytical Chemistry*, **72**(8), pp. 1930–3. Available at: http://dx.doi.org/10.1021/ac991216q [Accessed 11 October 2011].

Yang, J. *et al*. (2002). High sensitivity PCR assay in plastic micro reactors. *Lab on a Chip*, **2**(4), pp. 179–87. Available at: http://dx.doi.org/10.1039/B208405H.

Yang, L. (2004). Fabrication of SU-8 embedded microchannels with circular cross-section. *International Journal of Machine Tools and Manufacture*, **44**(10), pp. 1109–14. Available at: http://linkinghub.elsevier.com/retrieve/pii/S0890695504000525.

Yang, Y., Li, C., Kameoka, J. *et al*. (2005a). A polymeric microchip with integrated tips and in situ polymerized monolith for electrospray mass spectrometry. *Lab on a Chip*, **5**(8), pp. 869–945. Available at: http://dx.doi.org/10.1039/b503025k.

Yang, Y., Li, C., Lee, K., *et al*. (2005b). Coupling on-chip solid-phase extraction to electrospray mass spectrometry through an integrated electrospray tip. *Electrophoresis*, **26**(19), pp. 3622–52. Available at: http://dx.doi.org/10.1002/elps.200500121.

Yang, Y. *et al*. (2004). Quantitative mass spectrometric determination of methylphenidate concentration in urine using an electrospray ionization source integrated with a polymer microchip. *Analytical Chemistry*, **76**(9), pp. 2568–642. Available at: http://dx.doi.org/10.1021/ac0303618.

Ye, M.-Y., Yin, X.-F. and Fang, Z.-L. (2005). DNA separation with low-viscosity sieving matrix on microfabricated polycarbonate microfluidic chips. *Analytical and Bioanalytical Chemistry*, **381**(4), pp. 820–7. Available at: http://www.springerlink.com/content/efbcc1hqn7b70g13.

Yi, L., Xiaodong, W. and Fan, Y. (2008). Microfluidic chip made of COP (cyclo-olefin polymer) and comparison to PMMA (polymethylmethacrylate) microfluidic chip. *Journal of Materials Processing Technology*, **208**(1–3), pp. 63–9. Available at: http://dx.doi.org/10.1016/j.jmatprotec.2007.12.146 [Accessed 7 March 2012].

Yin, H. *et al*. (2004). Microfluidic chip for peptide analysis with an integrated HPLC column, sample enrichment column, and nanoelectrospray tip. *Analytical Chemistry*, **77**(2), pp. 527–33. Available at: http://dx.doi.org/10.1021/ac049068d.

Yin, H. *et al*. (2005). Microfluidic chip for peptide analysis with an integrated HPLC column, sample enrichment column, and nanoelectrospray tip. *Analytical Chemistry*, **77**(2), pp. 527–33. Available at: http://www.ncbi.nlm.nih.gov/pubmed/15649049.

Youn, S.-W. *et al*. (2008). Dynamic mechanical thermal analysis, forming and mold fabrication studies for hot-embossing of a polyimide microfluidic platform. *Journal of Micromechanics and Microengineering*, **18**(4), p. 45025. Available at: http://stacks.iop.org/0960–1317/18/i=4/a=045025.

Zafar Razzacki, S. *et al*. (2004). Integrated microsystems for controlled drug delivery. *Advanced Drug Delivery Reviews*, **56**(2), pp. 185–98.

Zhang, J. *et al*. (2001). Polymerization optimization of SU-8 photoresist and its applications in microfluidic systems and MEMS. *Journal of Micromechanics and Microengineering*, **11**(1), pp. 20–6.

Zhao, W. and Van der Berg, A. (2008). Lab on paper. *Lab on a Chip*, **8**(12), pp. 1988–91.

Ziaie, B. (2004). Hard and soft micromachining for BioMEMS: review of techniques and examples of applications in microfluidics and drug delivery. *Advanced Drug Delivery Reviews*, **56**(2), pp. 145–72. Available at: http://dx.doi.org/10.1016/j.addr.2003.09.001 [Accessed 12 July 2012].

1.7 Appendix: acronyms

APTES	3-aminopropyltriethoxysilan
COC	Cyclic Olefin Copolymers
COC	Cyclic Olefin Copolymer
COP	Cyclic Olefin Polymers
DNA	Deoxyribonucleic acid
DRIE	Deep Reactive Ion Etching
EC	electrochemical
ECL	electrochemiluminescence
EDM	electrode discharge machining
GPTES	3-glycidoxypropyltriethoxysilane
HF	Hydrofluoric Acid
ICP	Inductively Coupled Plasma
LDPE	Low Density Polyethylene
LIGA	Lithographie, Galvanoformung, Abformung
MEMS	Microelectromechanical systems
MFS	Minimum Feature Size
PC	Polycarbonate
PCB	Printed Circuit Board
PCR	Polymerase Chain Reaction
PDMS	Polydimethylsiloxane
PETG	Polyethylene Terephthalate Glycol
PI	Polyimide
PMMA	Poly(methyl methacrylate)
PP	Polypropylene
PR	Photoresist
PS	Polystyrene
PSG	Phosphosilicate Glass
PTFE	Polytetrafluoroethylene
PU	Polyurethane
RIE	Reactive Ion Etching
SCCM	Standard Cubic Centimeters per Minute
USG	Undoped Silicate Glass
UV	Ultraviolet

2

Surface coatings for microfluidic-based biomedical devices

B.G. ABDALLAH and A. ROS,
Arizona State University, USA

DOI: 10.1533/9780857097040.1.63

Abstract: Stable and well-characterized surfaces are essential for medical and diagnostic applications using microfluidic devices. Surface coating strategies can be classified into two major categories: covalent and adsorptive coatings. For covalent coating methods, the most common strategies are discussed based on the chemical characteristics of the device material. Furthermore, major classes of adsorptive coating strategies are presented, compared to their covalent counterparts, and discussed in relation to their respective importance in medical and diagnostic applications.

Key words: covalent, adsorption, polymer, coating, microfluidic.

2.1 Introduction

Microfluidic devices have attracted interest in the medical and diagnostic fields as they have the potential to perform many current large scale applications at a much smaller scale so as to reduce sample consumption and instrument size. Some applications, especially electrophoretic separations, have demonstrated excellent performance, such as rapid separations on the order of seconds and efficient separations of diagnostically relevant species (Li and Kricka, 2006; Reyes *et al.,* 2002; Verpoorte, 2002). For example, rapid DNA sequencing has been demonstrated in a high throughput format (Paegel *et al.,* 2002), and microfluidic-based protein and DNA separations, similar in working principle to gel electrophoresis techniques, have now been commercialized for over a decade (Panaro *et al.,* 2000). A further advantage of swift analysis is also appreciated in time-critical situations, such as during surgery or for analytes that change composition over time. Another intriguing advantage of microfluidic devices is their portability and potential for point-of-care diagnostics (Yager *et al.,* 2006), which has been demonstrated via a variety of marketed applications (Chin *et al.,* 2012). Additionally, as most microfluidic

devices only require sample volumes in the nanoliter range or below for analyses, they are further suited for situations when sample amount is limited, such as in minimally invasive diagnosis. As medical and diagnostic applications of microfluidic devices focus on qualitative or quantitative determination of biomolecules, the biocompatibility of these devices becomes critical.

The latter refers to several requirements for microfluidic devices. First, microchannel surfaces should resist non-specific adsorption of biomolecules (see Fig. 2.1) and provide a stable and non-altering composition over the course of an analysis. Due to the high surface-to-volume ratio apparent in microchannels, there is a high potential for surface adsorption and deterioration, especially in combination with diagnostic samples such as body fluids. Consequently, microfluidic applications strongly depend on the tailoring and control of surface properties in such devices. Second, for cell-based assays, the microfluidic environment has to be adapted so that cells can adhere to surfaces if required, and that intra- and inter-cellular processes proceed regularly, which poses an important requirement for the matrices used to embed or hold specific cells. Third, several other specific surface conditions arising from the particular application at hand have to be considered, such as temperature compatibility, stability under flow and applied electric fields, and solvent compatibility. Considering these guidelines and requirements, most microfluidic applications require some sort of surface pretreatment prior to analysis. Treatments can involve passivation strategies to prevent non-specific adsorption or unwanted changes in surface properties during the course of an analysis. Furthermore, if the sensing element in a microfluidic application is a biomolecule, immobilization strategies rendering a high yield of active biomolecules on a surface are required. The control of specific biomolecule immobilization is thus another important requirement in many microfluidic applications.

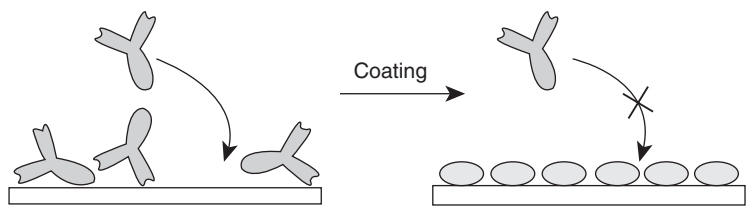

2.1 Schematic representing the prevention of non-specific adsorption to surfaces via adequate coating strategies. Left: proteins (here an IgG molecule is shown schematically) can adsorb to the untreated surface. Right: Due to coating with a blocking agent (i.e. another protein as specified in Section 2.4.1) the IgG molecules are hindered from non-specific adsorption. Coatings can be of other non-covalent type or covalently bound to the surface.

Microfluidic devices can be created with a variety of materials, thus surface treatment strategies strongly depend on the properties of the material. Covalent immobilization schemes require specific active surface groups, which vary from material to material deeming such strategies specific for a given microfluidic device. Bifunctional linker molecules may also be used, which allow for specific linkage to a surface reactive group but also react specifically with functional groups on biomolecules. In contrast to covalent immobilization schemes, adsorptive coatings may present an alternative, less complex route to coat microfluidic surfaces for various purposes. Knowledge of the non-covalent interactions driving an adsorptive coating is important for the quality of the coating. In general, such interactions are determined by electrostatic, van der Waals, and/or hydrophobic interactions. The functionality of the coating can be tuned similarly to covalent strategies, and non-specific adsorption can be suppressed in most cases. Functional groups of the adsorptive coating material can also be used for further specific biomolecule immobilization. The ease of use of adsorptive strategies, and often diverse applicability to various materials, has led to their widespread recognition in microfluidics.

The objective of this chapter is to provide an overview of the various strategies used to accomplish surface coating procedures for medically related microfluidic devices. First, covalent strategies are described in sections based on various substrate material properties and thus surface functional groups. Next, adsorptive coatings are discussed based on the specific class of coating materials. Finally, selected microfluidic applications for medical research are detailed and future perspectives on coating procedures are discussed.

2.2 Covalent immobilization strategies: polymer devices

Covalent strategies are characterized by a chemical bond formed between a functional group of the substrate surface, i.e. the microfluidic channel walls, and a functional group of the coating agent (see Fig. 2.2). The chemical reactivity of the functional group of the coating agent is specifically chosen based on the functional group on the substrate. Covalent coatings are usually characterized by their excellent stability during microfluidic manipulations; however, they have to be adapted to the available surface functionality of the microfluidic material. This makes universal strategies between different microfluidic device materials difficult compared to other surface treatment methods. Covalent strategies for the most popular microfluidic device materials are outlined in this section, separated into subsections based on compatible substrates.

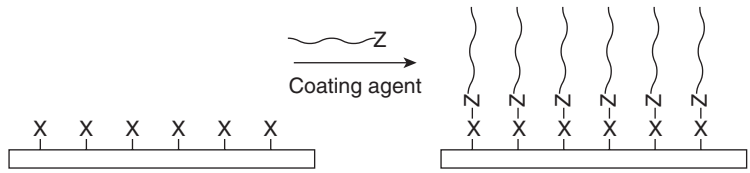

2.2 General scheme of covalent coating strategies. (X= reactive functional group of substrate surface, Z = reactive functional group of coating agent).

2.2.1 Polydimethylsiloxane (PDMS) devices

Microfluidic systems fabricated with polydimethylsiloxane (PDMS) represent a significant portion of microfluidic devices, especially those used for important bioanalytical and medical applications (Gross *et al.,* 2007; Ni *et al.,* 2009; Nisar *et al.,* 2008; Sung and Shuler, 2010; Wu *et al.,* 2010). A major advantage of this material arises due to its widely ranging optical transparency in the visible and ultraviolet light regions, which makes it amenable for many fluorescence-based applications. Additionally, PDMS is gas-permeable, which accommodates cell culturing within microfluidic devices fabricated with this material – a considerable advantage for cell-based studies. Moreover, PDMS devices can be fabricated from a pre-structured master exhibiting the negative relief of a desired microdevice. The pre-structured master can be obtained via standard photolithography techniques, and minimal clean room infrastructure is further required for PDMS chip assembly. PDMS devices thus provide a suitable route for prototyping techniques, which has led to their widespread adoption in microfluidics research.

One issue with PDMS devices – as for many other microfluidic devices – is an inconsistent surface composition over the time course of an analytical measurement. Due to its polymeric character and long chain polymer reorientation effects on the surface, strategies need to be developed in order to maintain a given surface composition. The various strategies reported for bioanalytical and biomedical applications are described in the following sections, as well as suitable techniques for stable surface functionalization.

Silanization strategies

One of the most commonly used covalent attachment strategies involves the linkage of alkoxysilane derivatives via hydroxyl group bearing surfaces resulting in siloxane linkages (see Fig. 2.3a). This method has been extensively used with glass and silica surfaces (see Section 2.3.1), but has also found widespread use for its application in PDMS-based microfluidic devices. A considerable advantage of this technique is the fact that

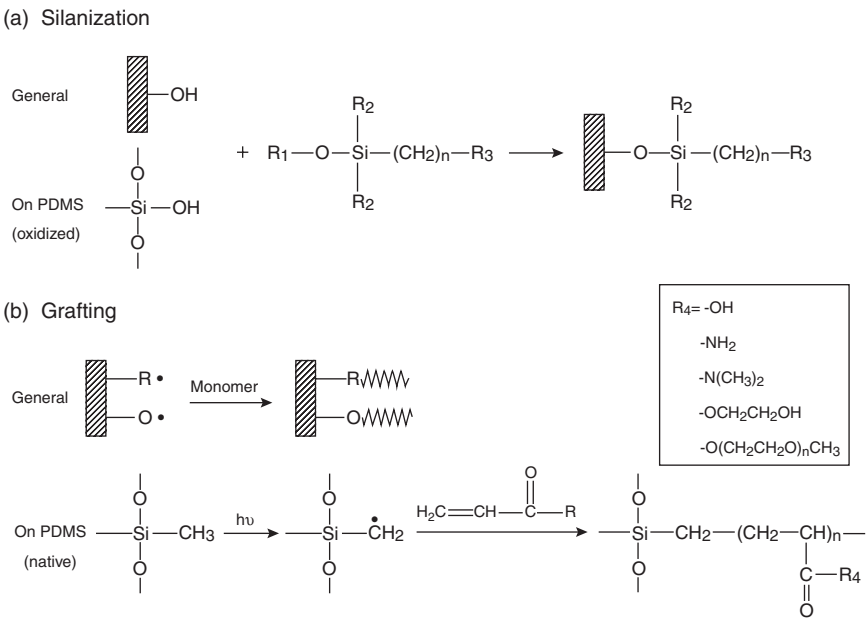

2.3 Schematics for selected covalent immobilization schemes: (a) Silanization refers to the condensation reaction of alkoxysilanes with hydroxyl groups on surfaces. This reaction can generally be used on hydroxylated surfaces, but has also found application on oxidized PDMS. (R_2= alkyl or alkoxy, R_3=functional end-group such as -NH_2 or -COOH). (b) Grafting is a widespread method for immobilizing a variety of polymers. After activation and radical formation on the surface, reaction with monomers results in covalent polymer immobilization on a surface. Also shown is the activation scheme for UV activated grafting of acrylamides on native PDMS surfaces.

the linkage can be mediated via one to three alkoxy groups of the reacting silane, providing a means for proper orientation and stable cross-linking to the surface. Furthermore, the functionality of the silane can be adjusted to obtain a desired chemical reactivity. As a result, hydrophobic or hydrophilic side-chains can be introduced, but also various chemical functionalities become accessible for further cross-linking if desired. This is a key benefit of PDMS, as a variety of chemical functionalities can be established on PDMS microchannel surfaces in contrast to other polymers that are more limited towards generalized surface functionalization. It is important to understand that silanization strategies are only successful with a considerable quantity of hydroxide groups on the surface. Hydroxyl groups can be created on microchannel walls vi oxidative treatments, including oxygen plasma, air plasma (McDonald *et al.*, 2000), and UV irradiation (Efimenko *et al.*, 2002) in an oxygen rich atmosphere (this pretreatment step is not a covalent

immobilization strategy but merely provides necessary functional groups on the substrate surface. See Section 2.5 for more details). PDMS surfaces treated with these techniques are hydrophilic and exhibit contact angles on the order of < 20°, in contrast to native PDMS that exhibits a contact angle on the order of ~120° (Hellmich *et al.,* 2005). Although the mentioned treatments are very effective, PDMS devices need to be stored in aqueous solutions or used immediately after oxidative treatment due to the hydrophobic recovery phenomenon (Fritz and Owen, 1995) – an effect that renders a hydrophilic PDMS surface hydrophobic with a half-life of one day, due to the reorganization of surface polymer chains when exposed to air.

Probably the most utilized silane molecules are amino derivatives usually in the triethoxy- or trimethoxy-silane form. The amino group serves as the linker molecule for well-known amide bond formations with carboxylic groups mediated by carbodiimide (Miyaki *et al.,* 2007). For example, aminopropyltriethoxysilane (APTES) has been used for antibody attachment and cell adhesion to PDMS (Misiakos *et al.,* 2004; Zhang *et al.,* 2005). Furthermore, Yu *et al.* (2009) reported improved covalent immobilization of proteins due to increased hydrophilicity after APTES treatment. This was achieved by binding an aldehyde modified dextran to APTES immobilized on a PDMS surface. With this covalent strategy, a PDMS-based device could be used to detect various biomarkers via an enzyme-linked immunosorbent assay (ELISA). Other silanization examples consist of the use of trimethoxymethylsilane to suppress non-specific protein adsorption and attach biomolecules to microchannel walls after a silanization procedure (Sui *et al.,* 2006). Silane-based coatings have also been demonstrated that significantly reduce non-specific protein adsorption and improve cell adhesion to PDMS surfaces (Jon *et al.,* 2003). This silanization process was applied via a patterning procedure consisting of a silane-copolymer anchor bound to a functional polyethylene glycol (PEG). Control of electroosmotic flow (EOF) in a microchannel is also critical in many types of experiments to improve reproducibility between trials and substrate types and to increase analysis times. In addition to its use for immobilization purposes, a methoxysilane can be used to link a highly ionizable carboxyl-polymer to PDMS to introduce a high EOF (Miyaki *et al.,* 2007).

Another strategy for attaching silanes has been demonstrated via the self-assembly of thiolated silanes on gold surfaces. After coating PDMS microfluidic devices with a thin gold layer, attachment of the thiolated silanes is accomplished via the self-assembly and stable linkage of thiols to gold. This approach is very popular in surface derivatization applications and has been applied to render surfaces hydrophilic via PEGylated thiols in microfluidic networks (Papra *et al.,* 2001), as well as in microcontact printing applications (Delamarche *et al.,* 2003). Furthermore, 3-mercaptopropyl trimethoxysilane has been employed as a coating procedure in a PDMS device to

detect CD4+ T cells using an ester-based coupling agent functionalized to the surface followed by the immobilization of avidin and a biotinylated CD4 antibody to the surface (Cheng *et al.,* 2009). CD4 cells could then be isolated from whole blood and counted, which is necessary when monitoring the stages of a disease such as HIV in positively tested patients. Similarly, an optical real-time affinity biosensor developed using a PDMS-based channel for multi-analyte detection was also reported using thiolated silanes and biotin/avidin immobilization (Misiakos *et al.,* 2004).

Derivatized silanes can also be exploited to covalently attach a wider variety of molecules to PDMS surfaces. A combination of UV activation with silanization to covalently pattern polyacrylamide to the surface of PDMS has been explored by Xiao *et al.* (2002, 2004). An initial UV exposure oxidizes the PDMS, which allows silanes to self-assemble on the surface. In this case, a trichlorosilane was adhered to the surface due to its capability of initiating atom-transfer radical polymerization of polyacrylamide. The resulting formation of a polyacrylamide layer on the PDMS surface reduces non-specific adsorption and maintains hydrophilicity, two important improvements critical for efficient and highly sensitive biomolecule separation and diagnostics.

Other immobilization schemes on PDMS

An effective and commonly used alternative method to silanization is photoinitiated UV grafting to facilitate the covalent linkage of polymers to PDMS surfaces (Hu *et al.,* 2002) (see Fig. 2.3b). A major motivation for this approach is its ability to increase surface hydrophilicity while reducing protein adsorption on the substrate. Additionally, stabilization of EOF can be achieved using this surface treatment, which results in a significant increase in the resolution of electrophoretic separations. In the follow-up work, the dynamics of this approach were studied by examining the ability to differentially pattern various regions on a PDMS surface using UV initiated grafting, which proved to be feasible (Hu *et al.,* 2004). In terms of biomedical applications, UV grafting can be used to selectively micropattern PDMS in specific regions to direct cell attachment and growth as well as to immobilize antibodies for immunoassays (Hu *et al.,* 2005).

Another alternative to silanization is to coat PDMS with poly-xylylenes via a chemical vapor deposition method (Lahann *et al.,* 2003). Such polymer coatings can be employed to immobilize molecules, facilitate antibody/biotin binding assays, and improve cell adhesion assays for pharmacology studies. Follow-up studies of this approach also employed chemical vapor deposition to discontinuously pattern bio-inert species and reduce non-specific protein adsorption (Chen *et al.,* 2005, 2008). Another polymerization strategy utilizing cerium-catalyzed polymerization of various monomeric compounds

can be employed for polymer coatings. The exploited Ce-catalytic action originates from the formation of siloxane radicals, which further react with selected monomers resulting in their immobilization. When applied to electrochromatography studies, an increased separation efficiency and selectivity can be realized (Slentz *et al.,* 2002).

2.2.2 Polymethylmethacrylate (PMMA) devices

Polymethylmethacrylate (PMMA) is also a very popular material for microfluidic applications. A variety of different surface activation and coupling procedures addressing a broad range of functionalities have been reported for PMMA. Several of these methods are aimed at introducing amine functionalities on PMMA surfaces (see Fig. 2.4). One example of this is a poly(ethyleneimine) (PEI) coating, which is an amine-bearing polymer that can enhance antibody binding to the surface of PMMA (Bai *et al.,* 2006). An improved antibody surface coverage with up to a ten-fold increase in overall binding was demonstrated with this immobilization strategy, leading to significant improvements in immunoassay performance.

Another example surface treatment of PMMA with amine functionalities is based on an activation procedure with lithiated diamines to link alkylcyanates to PMMA (Henry *et al.,* 2000). This method was further employed by Hashimoto *et al.* (2005, 2006) for improved detection of single DNA base mutations. Similar activation strategies can be used to detect low abundance mutations in DNA using a microarray (Wang *et al.,* 2003). Primers are linked to a PMMA surface functionalized with amines, followed by a ligase detection reaction with immobilized primers to induce hybridization detection. Additionally, PMMA can be silanized to incorporate a larger variety of functional groups on the surface such as specialized amines for the immobilization of biomolecules. A procedure using lithium aluminum hydride

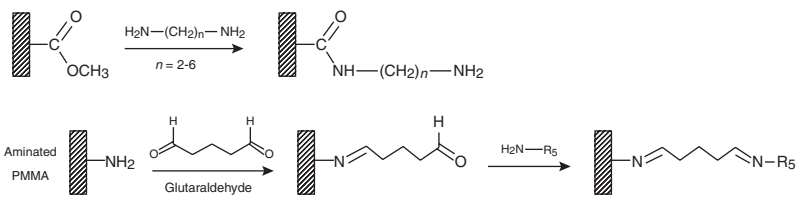

2.4 Amination on PMMA is shown via activation of a short bifunctional amine. Other methods exist to create aminated PMMA, as discussed in the text. Amine groups can further be used to link other functional molecules, such as that shown in the reaction with the bifunctional glutaraldehyde and subsequent immobilization of amine-bearing molecules, such as proteins.

(LAH) to expose hydroxyl groups on the PMMA surface can be applied for further functionalization with organosilanes that facilitate the immobilization of DNA oligos for DNA microarray analysis (Cheng *et al.,* 2004).

Oxidation for carboxylic acid functionality has also been reported as a suitable covalent immobilization strategy for PMMA. For example, McCarley *et al.* (2005) discussed a device to capture and concentrate cells and proteins using treatments for patterning polymers to substrate surfaces. For this purpose, carboxylic acid groups can be patterned on a PMMA surface with UV treatment in an oxygen rich environment, onto which antibodies are immobilized for the detection of cells (for example MCF-7 breast cancer cells) and other proteins in solution. Antibody linkage for immunoassays has also been reported via a sol-gel immobilization strategy (Wang *et al.,* 2008). Sol-gel films are first adsorbed to substrate surfaces in which biomolecules can be immobilized within the gel networks. The mildness of this procedure is beneficial in that bioreactivity is preserved, non-specific adsorption is reduced, and effective immobilization of target analytes can be achieved for immunosensing with low detection limits. For example, this method has been applied in a microreactor for proteolysis via trypsin immobilization on a sol-gel coated PMMA microchannel surface (Huang *et al.,* 2006).

An indirect approach to immobilize antibodies within a PMMA/polycarbonate microfluidic device to perform ELISA is also possible using functionalized carbon nanotubes (CNT) (Sun *et al.,* 2010). In this example, a pressure-driven device was used and antibody immobilization was achieved via linkage onto carbon nanotubes functionalized with poly(diallyldimethylammonium chloride). This functionalization step renders a positive charge on the coated CNTs, therefore immobilization is achieved via electrostatic interactions with a negatively charged antibody. The developed ELISA was used to detect bacterial toxins such as staphylococcal enterotoxin B (SEB) with detection limits comparable to conventional ELISA, leading to a point-of-care device that could perform with high sensitivity.

Various other coating procedures based on commercial coating agents have been reported including the chemical SurModics (a company specializing in surface coatings for medical applications) and Reacti-Bind™ procedures (Liu and Rauch, 2003). These methods and the cetrimonium bromide (CTAB) surfactant were tested in the development of microfluidic hybridization array (MHAC) devices in which DNA probe attachment is a crucial step. It was shown that the Reacti-Bind™ method is the least effective of the three, whereas the CTAB method provides improved immobilization of amine modified DNA oligos and the SurModics procedure is the most effective in producing high quality spots along the array with the least amount of surface pretreatment. As a whole, all of these methods can improve DNA-oligomer immobilization and consequently chip efficiencies, hybridization kinetics, and detection limits.

2.2.3 Polycarbonate devices

A successful approach to covalent linkage on polycarbonate involves the creation of carboxylic groups on the surface. Accordingly, several of the previously described reaction schemes can be employed. For example, UV/ozone treatment can be used to create COOH groups for the linkage of amino groups via carbodiimide activation (Li *et al.,* 2007). Subsequently, DNA probes can be attached within a polycarbonate DNA microarray coupled to PDMS microchannels for hybridization assays. Complementary DNA fluorescence assays carried out in such a device show great selectivity against mismatched pairs, giving them great potential to be used for portable plastic biochips. For the attachment of antibodies and other proteins, carboxylic groups can be patterned as described previously for PMMA. This approach is applicable for mammalian cell capture, such as capturing MCF-7 breast cancer cells, in addition to protein capture by immobilizing various amide polymers (McCarley *et al.,* 2005). Another approach that has been successful on PMMA can also be exploited for polycarbonate (Hashimoto *et al.,* 2005, 2006). Surface activation with lithiated diamines can also be used with polycarbonate for the coupling of DNA on microfluidic surfaces to detect single base pair mutations in addition to improving polymerase chain reaction (PCR) applications. Furthermore, spraying a photosensitive polymer ('3D' link blocking solution of SurModics brand 'CodeLink™') as a thin film, followed by UV polymerization, can also successfully derivatize polycarbonate surfaces. Codelink™ coatings utilize a hydrophilic polymer containing *N*-hydroxysuccinimide ester reactive groups, which promotes binding of amine modified DNA while suppressing non-specific adsorption (SurModics, 2012). This approach can also be used to treat DNA microarrays coupled to PCR experiments (Lenigk *et al.,* 2002). An improvement of hybridization kinetics (efficiency of the process increasing hybridization velocity) was reported with this approach for the purpose of studying single nucleotide polymorphisms using a patterned Codelink™ coated array.

2.2.4 Polystyrene devices

Although it is the least common polymer used in medical microfluidics, polystyrene can also be used as a microfluidic device material. One well received example utilizes a gold coating and thiol–linker with a carboxylic acid head group for self-assembly on polystyrene surfaces (Darain *et al.,* 2009). In this example, carbodiimide activation was employed to covalently bind to the amino groups of immunoglobulin G (IgG) molecules, and the device was tested with a surface coated antibody/antigen assay to detect IgG via fluorescence microscopy. Detection limits were in the range of typical microfluidics detection assays with a wide linear response for the immunosensor. In

comparison to conventional immunoassay-based detection methods such as ELISA, this method provided a significantly lower time requirement on the order of 25 min (compared to several hours for competing methods) and had a more conservative sample volume requirement.

2.3 Covalent immobilization strategies: glass devices

Silicon dioxide (SiO_2) surfaces are likely the most studied surfaces for microfluidic applications. Their surface properties are suitable for a variety of applications, not only in microfluidics but also in capillary chromatography and capillary electrophoresis. Glass, fused silica, and quartz materials can all be derivatized via the same coupling chemistry. By far the most used derivatization strategy is silanization via silanol groups generated on SiO_2 surfaces. Activation schemes involve reactive oxygen treatment, pre-activation with acids such as piranha acid or other strong acids, and treatment with strong bases such as NaOH.

2.3.1 Silanization

As discussed in Section 2.2.1, silanol groups on SiO_2 surfaces react with alkoxysilanes forming a stable covalent bond. Silanes similar to those used with PDMS are employed for SiO_2 and subsequent covalent reactions to bind other entities occur depending on the employed silane head group. The applications of silanization on glass are multifarious, and several examples are given in the following paragraphs.

Proteins such as antibodies can be immobilized to glass microchannel substrates for the detection of bacteria via a biosensor using APTES. APTES is used to create an amine reactive surface to bind carboxyl-groups for antibody attachment. A device of this type operates with a continuous flow of a bacterial suspension through a microchannel to facilitate specific immobilization of bacteria to an antibody derivatized channel wall for sensitive detection (Boehm *et al.,* 2007). Silanization can also be employed for bilayer lipid membrane (BLM) attachment on glass surfaces to reconstitute membrane proteins for electrophysiological and single molecule studies. For example, perfluorooctyl-trichlorosilane (PF-TCS) can be used to render glass hydrophobic followed by an injection of a lipid-based solution to facilitate the formation of BLMs. The incorporation of a spark-assisted chemical engraving method to develop the glass microstructures makes the complete device fabrication process simple and quick for easy integration (Sandison *et al.,* 2007).

A slightly different application of silanization can be used to immobilize antibodies on glass beads to detect pathogens within a microchannel

(Lee *et al.,* 2006). Initially, the glass beads are coated with an aminosilane (APTMS) and functionalized with aldehydes to form a carboxy terminus for covalent immobilization with the primary amines of various antibodies. The channel is then packed with the functionalized beads and, in this example, was used to specifically bind with IgG as well as *E. coli*, using their respective antibodies. Highly specific binding to the target analyte can be achieved with this method, and the use of glass beads provides a greater functionalized surface area and thus a higher antibody concentration, resulting in improved detection sensitivity compared to devices where only channel walls are treated. Application of this method in a glass microfluidic channel is also possible to covalently attach enzymes for biocatalysis studies (Lee *et al.,* 2003a). Another antibody immobilization technique via silanization in a glass microchannel involves a protein A surface coating following a necessary pre-silanization step for IgG attachment (Dodge *et al.,* 2001). Coating channels with protein A for antibody binding reduces antibody denaturation and provides a higher binding affinity compared to direct glass immobilization resulting in increased antibody pre-concentration and assay sensitivity. Additionally, protein A bound antibodies are oriented correctly for efficient antigen binding, resulting in an even greater increase in immunoassay efficiency.

Bifunctional silanization of a glass substrate can also be applied to microfluidic PCR (Shoffner *et al.,* 1996) or capillary electrophoresis (Hjertén, 1985) coupled with a secondary treatment using various polymers. Untreated or not properly treated devices have the potential to inhibit PCR, making it important to develop devices with optimal surface chemistries. Possible PCR compatible silanes include SurfaSil™ and SigmaCote™ coated with the polymers polyglycine and polyadenylic acid. It has been shown that higher yields of amplified product are obtained from channels coated with SurfaSil™ and a polymer, namely polyglycine, with results comparable, and in some cases exceeding, those obtained from a conventional PCR experiment. In terms of capillary electrophoresis, polydimethylacrylamide can be immobilized to glass capillary walls with trimethoxysilane via a well-known coating procedure to reduce EOF (high EOF reduces resolution by causing the sample plug to broaden) and non-specific adsorption of analytes (which leads to a heterogeneous spatial distribution of the analyte and thus poor separation). This method has been applied extensively for the aforementioned benefits, namely in lab-on-a-chip devices that incorporate cell lysis, DNA amplification by PCR, and analysis by CE (Waters *et al.,* 1998).

Silanization strategies are also used for flow-through DNA microarray devices (Wei *et al.,* 2005). One distinct example is a glass/PMMA hybrid device, in which a PMMA microfluidic channel is used to deliver sample to a microarray patterned on glass via 'shuttle hybridization.' As mentioned

previously, PMMA can be silanized and functionalized with organosilanes for DNA immobilization (Cheng *et al.,* 2004). To immobilize DNA on the glass portion of the device, the surface is silanized with triethoxysilane and then functionalized with an aldehyde derivative for immobilization of amine-functionalized DNA oligo probes. Overall, the continuous flow mechanism within the device significantly reduces DNA hybridization time. Similar silanization methods are employed within three-dimensional DNA microarray devices that connect glass microfluidic channels perpendicular to a 2D glass surface. In these devices, channel walls are silanized and functionalized to immobilize amine-derivatized DNA oligos on the glass channel surface onto which injected analyte can be hybridized. Using this surface treatment method, high-density immobilization is successfully attained compared to traditional two-dimensional array patterning methods (Benoit *et al.,* 2001; Cheek *et al.,* 2001).

2.3.2 Polymer immobilization

Immobilization of the polymer polyvinylalcohol (PVA) has been used extensively for applications related to electrophoresis. Generally, PVA-based coatings increase device efficiency by reducing non-specific adsorption which improves separations due to reduced analyte-wall interactions. PVA coatings are further stable in a broad pH range and facilitate the suppression of EOF while concomitantly increasing the resolution of the applied separation. To demonstrate PVA-based coatings and illustrate its advantages, several groups have coated glass microfluidic devices for electrophoresis (Belder *et al.,* 2002; Ludwig and Belder, 2003). The PVA-coating procedure is very simple and non-complex, as a 1% aqueous solution of PVA is simply flushed through microchannels to coat them. Thermal bonding is then used to covalently attach the polymer to channel walls. PVA coated devices vs non-coated devices exhibit controllable and suppressed EOF, reduced non-specific adsorption of analyte fluorophores, and a three-fold increase in separation efficiency. Furthermore, sensitivity is increased, and the need to wash or etch devices for reuse is unnecessary, thus improving robustness. To potentially increase separation efficiency even further, PVA coatings coupled with an organic background electrolyte solution can be used (Varjo *et al.,* 2004). The use of a lower conductivity buffer solution allows for stronger electric fields to be applied, thus increasing sensitivity. Under these conditions, a similar comparison of PVA vs non-PVA coated channels showed that PVA coated channels improved the resolution of a complex separation, while non-coated channels could not even achieve baseline resolution. The same PVA-coating procedure can also be applied to a PDMS-based device to achieve similar improvements in overall electrophoretic separation (Wu *et al.,* 2005).

2.4 Adsorption strategies

In contrast to covalent attachment techniques, adsorption strategies rely on intramolecular interactions between the coating material and the substrate surface. They can be mediated via electrostatic interactions, van der Waals forces, and/or hydrophobic interactions. A major characteristic of these coatings is their ease of use, since microchannels generally have to be incubated with a solution containing the coating agent for a certain length of time. Subsequent use for biomedical applications is straightforward and advantageous, as minimal washing procedures are required. In some cases, the coating agent can even be added to the solution during specific analyses, which is referred to as dynamic coating. In contrast, coating of the substrate prior to the actual analyses is termed static coating.

Adsorptive coatings have been widely adopted and can perform similarly to covalent strategies in terms of preventing biofouling and non-specific adsorption as well as to serve as linker molecules for further biomolecular attachment. Due to their non-covalent nature, strategies for adsorptive coatings vary from material to material and are also based on previous surface treatment steps. Adsorptive coating agents can be classified into four major groups, which are characterized by multivalent interactions with the substrate surface, strong electrostatic interactions, or a combination of the two. In the following sections, polymer, polyelectrolyte, surfactant, and protein adsorptive coatings are described, which constitute the majority of non-covalent coating strategies for microfluidic applications as schematically depicted in Fig. 2.5.

2.4.1 Proteins

Protein coatings represent a very popular approach to coating microfluidic channel surfaces. For example, coating with the protein bovine serum albumin (BSA) has been used in molecular biology for several decades to block surface sites from non-specific adsorption. BSA is a soluble protein with a high tendency to adsorb to hydrophobic surfaces such as wax-coated, paper-based microfluidic immunoassay devices, where it can be used as a surface coating to reduce non-specific adsorption (Lu *et al.,* 2010). Despite this characteristic, BSA surface treatments are not limited only to hydrophobic surfaces, but can also be applied to hydrophilic surfaces, a contributing factor to their widespread use. A representative application of BSA coating applied to PDMS has been described by Eteshola *et al.* (2001), who reported background reduction by reducing the non-specific adsorption of analytes in a sensor detecting IgG molecules for immunohistochemical analysis. BSA was not only employed to directly suppress non-specific adsorption, but also

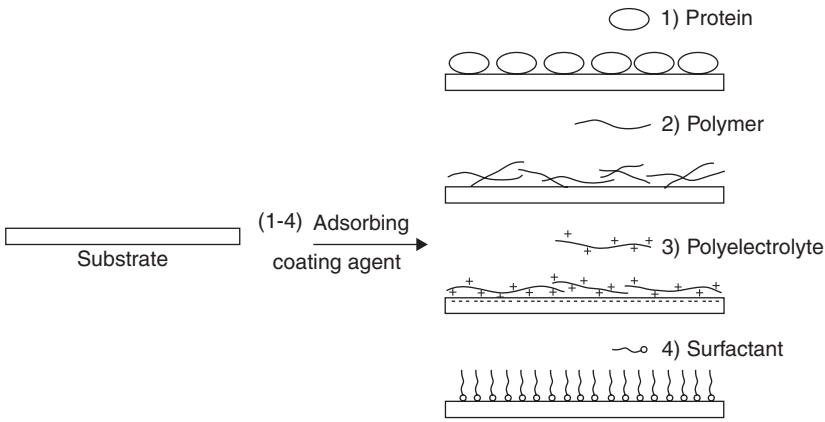

2.5 Schematic of adsorptive coatings discussed in Sections 2.4.1–2.4.4.

as a linker to covalently bind protein A for subsequent directed immobilization of IgG. A detection limit in the nanomolar range was reported in the employed sensor performing an ELISA. Further discussion of BSA as an advantageous medical device surface coating can be found in Section 2.6.2.

The tetrameric protein streptavidin has also been employed extensively as a linker molecule by taking advantage of its very high binding affinity to biotin. Biotin–streptavidin binding is nearly covalent in strength and the small molecule biotin can be readily derivatized with other linker molecules or proteins. As a result, this binding pair has found widespread application in the physical and life sciences, and can also be employed in adsorptive strategies for microfluidic surface coatings. Utilizing multilayers of biotin and NeutrAvidin, a derivative of streptavidin with similar binding characteristics to biotin, is one method to accomplish this on PDMS (Linder *et al.,* 2001). The multilayer approach consists of sandwiched layers of biotinylated IgG, followed by NeutrAvidin and biotinylated dextran. This three-layer sandwich has the ability to reduce non-specific protein adsorption and maintain stable EOF for electrophoresis applications. The same strategy can also be used to immobilize other biomolecular probes to biotinylated surfaces. There are other less complex protein-based dynamic coatings to reduce non-specific adsorption and control EOF, as demonstrated in PMMA-based microfluidic devices, but likely compatible with a variety of substrates (Naruishi *et al.,* 2006). Protein blocking agents commonly found in ELISA procedures, such as Block Ace and UltraBlock as well as lysozyme, can be used for this purpose. Depending on the protein coating employed, EOF can be enhanced or reduced, and its direction can be changed depending on buffer pH and charge on the protein.

For cell-based assays, other strategies mimicking extracellular matrices are commonly pursued. The matrices can be applied with an adsorptive strategy that allows for embedding biological cells for subsequent *in vitro* studies. A key point is to provide biocompatible surfaces in which cell studies can be performed in optimized and non-hazardous environments. An example for a cell-based assay with potential in tissue engineering, cell-matrix interactions, and cellular communication studies within a patterned microfluidic PDMS device has been demonstrated by Hou *et al.* (2008). PDMS in its native state resists cell adhesion and growth, which are necessary in cell-based assays, thus motivating the need for an appropriate surface coating procedure. An extracellular matrix mixture consisting of collagen, fibronectin, and hyaluronic acid can be coated onto PDMS to facilitate cell adhesion and growth with sufficient biocompatibility. Furthermore, a technique for layer-by-layer deposition of extracellular matrix has also been developed to micropattern cell co-cultures as a future tissue engineering tool to study cell–cell communication and cell–matrix interactions (Fukuda *et al.,* 2006). Others have also suggested complete fabrication processes using alternate substrates such as polystyrene to overcome some of the potential disadvantages of PDMS in cell-based assays such as gas permeability, substrate deterioration, small molecule adsorption, and hydrophobic recovery (Young *et al.,* 2011). Cell assays including cell culture and blood neutrophil migration detection have been successfully performed with a polystyrene device surface coated using similar extracellular matrix proteins to promote cell adhesion.

2.4.2 Adsorptive polymer coatings

Adsorptive polymer coatings have proven to be a versatile method for a variety of adsorptive coating strategies; however, the choice of the coating polymer depends strongly on the microfluidic surface due to variations in surface interactions among materials. Because glass, silica, and PDMS exhibit a similar surface chemistry, similar polymer-based coating strategies can be applied.

In Section 2.3.2, polyvinylalcohol immobilization was discussed; however, dynamic coating of this polymer is also possible and advantageous for electrophoretic applications. The dynamic coating method can be more stable than static immobilization, due to constantly replenishing the substrate surface with coating material. Furthermore, a variety of polymer microfluidic materials have been subjected to dynamic coating procedures. On PMMA, dynamic adsorptive coating of cellulose was reported to enable long term use (100+ runs) of a single microfluidic device for DNA electrophoresis. Devices with this type of coating can last on the order of one month and only require replenishment of the coating agent daily. The application of

gel electrophoresis was performed multiple times in which consistently high and reproducible separation efficiencies were realized for the duration of the device's lifetime (Du and Fang, 2005). An added benefit in this case is that the same medium containing the coating agent also contains the sieving medium that drives the separation, which simplifies their integration.

An additional dynamic coating of PDMS with poly(dimethylacrylamide) (PDMA) can be applied to electrophoresis applications. The coating procedure is simple, in that 0.01% PDMA is added to the normal running buffer solution, which is then injected into a microchannel in the same manner as conventional capillary electrophoresis. In a study of this procedure, PDMA surface adsorption was confirmed with contact angle measurements and infrared spectroscopy indicating a successful and stable surface coating when applied (Chen *et al.,* 2004). PDMA-coated channels show a reversal in EOF to a negative polarity, which allows for improved injection of negatively charged samples. Additionally, a suppression of EOF occurs, which improves sensitivity, and a hydrophilic surface is maintained within the microchannel, which increases substrate robustness and reproducibility.

2.4.3 Polyelectrolyte multilayers

Polyelectrolyte multilayers (PEM) represent another adsorptive approach that has been widely used for a variety of applications. The interaction forces between the coating and substrate surface are mediated via electrostatic interactions, which contributes to the stability of such coatings. Compared to the short lifetime of many physical adsorption strategies, PEMs can offer a more robust solution. Additionally, in electrophoretic applications, PEMs have the potential to control EOF in that they can reduce or even reverse EOF according to the polyelectrolyte charge characteristics of the exposed layer. This resulting EOF stabilization is a key player in increasing separation efficiency and resolution. For example, capillary electrophoresis coupled to electrospray ionization – mass spectrometry (ESI–MS) benefits from the use of PEMs such as polyamine-coated glass surfaces in which ESI-MS can be performed without an external pressure source or spray tip (Mellors *et al.,* 2008). The reduction of non-specific adsorption and control of EOF contributed to this efficient, stable, and sensitive microfluidic mass spectrometric approach for protein detection. On glass and silica as well as polymers, PEM coatings are able to change the direction of, and control, EOF due to differing surface charges in the employed polyelectrolyte solution (Katayama *et al.,* 1998a, 1998b).

PEM-coating procedures, called successive multiple ionic-polymer layer (SMIL) coatings can also be applied by placing a cationic polybrene solution between the anionic polymer dextran sulfate and the channel wall. These

types of coatings maintain stability across a wide pH range, show robustness against strong acids and bases, and improve device reproducibility. Another PEM example of the many available utilizes a positively charged poly(allylamine hydrochloride) layer electrostatically self-assembled to a negatively charged silicon surface (Hau *et al.,* 2003). A similar approach can be applied to a PDMS microfluidic electrophoresis device to attain EOF control and improve overall stability (Liu *et al.,* 2000).

It becomes apparent that the large variety of polyelectrolytes and their simple administration as a surface treatment makes this method versatile for a diverse set of applications and microfluidic substrates. More extensive methods for further fine tuning can be employed as well. To further study the stabilization PEMs provide, devices made of various substrates have been compared for consistency in separation performance (Currie *et al.,* 2009). In this study, PMMA and glass microchannels were coated with poly(diallyldimethylammonium chloride) and polystyrene sulfonate (PSS) and compared to non-coated glass channels to show that PEM-coated glass had a stable EOF that was independent of solution pH. Additionally, PMMA coated with PEMs provides comparable, and in some cases better, separation efficiency than glass devices, which is generally not the case due to fabrication inconsistencies with polymer-based substrates. Polystyrene and poly(ethylene terephthalate) glycol (PETG) substrates have also been studied due to their significantly different polymer surface chemistries and EOF mobilities in relation to more popular polymers. With these polymers, similar results can be realized with alternating layers of cationic poly(allylamine hydrochloride) and anionic PSS that give either negative or positive surface charges, respectively, for directional control of EOF (Barker *et al.,* 2000a, 2000b). EOF mobilities of this system in both polymers were measured, and demonstrated the ability to bring the dissimilar EOF characteristics of the untreated polymers into close proximity with one another with a uniform PEM coating. This overall increase in performance and reduced variation between substrate materials as a result of PEM surface coatings opens up the possibility to confidently use cheaper and easier to fabricate polymeric-based substrates to improve many biomedical microfluidic applications.

PEMs can also be employed as a stable surface coating procedure that can be combined with subsequent immobilization of analytes. The polyelectrolytes poly(ethyleneimine) and poly(acrylic acid) can improve specific protein binding as well as long term stability and bioreactivity due to an increase in the hydrophilicity of a coated PDMS substrate (Sung *et al.,* 2008). A slightly more complex multistep protein modification of PDMS can also be accomplished with PEM coating, gold nanoparticle patterning, and protein patterning. An example application of such a device illustrated the ability to separate a group of neurotransmitters as well as environmental

pollutants with high separation efficiency, reproducibility, and stability (Wang *et al.,* 2006).

Cell immobilization can also be undertaken using PEM coatings. Poly(diallyldimethylammonium chloride) and PSS have been shown to improve cell adhesion due to increasing the wettability of PDMS (Kidambi *et al.,* 2007). Using this method to treat PDMS, the degree of adhesion of various cell types with dissimilar cellular morphologies has been examined, in which an overall improvement in cell culturing capability was realized regardless of cell type. The importance of this PEM method becomes apparent in tissue engineering applications, where cell proliferation and adhesion are imperative and require a cell-friendly substrate material.

2.4.4 Surfactants

Surfactant molecules are generally amphiphilic, consisting of a hydrophobic tail and hydrophilic head moiety, and have the potential to combine these two unique properties into an effective surface coating. First, the hydrophilic, often charged, moiety can be employed for electrostatic attachment. Second, the hydrophobic moiety can be employed to further control surface properties, such as reducing non-specific protein adsorption, or to control EOF velocity and direction. It has to be noted that depending on substrate surface properties, these two properties of the surfactant can be interchanged, such that the more hydrophobic entity interacts with the surface more strongly.

A commonly employed surfactant in traditional protein analyses is sodium dodecyl sulfate (SDS), which has also been adapted and employed as an adsorptive coating agent in a variety of microfluidic applications. For example, the influence of SDS on the separation of hydrophobic species by micellar electrokinetic chromatography in PDMS devices has been studied (Roman *et al.,* 2006). Notably, SDS forms a pseudo-chromatographic phase, eliminating protein adsorption and increasing EOF, consequently resulting in a rapid, highly resolved, and efficient separation. Mixed coatings with other polymers can also be employed with SDS to tune the degree of adsorption to PDMS surfaces based on the concentration of SDS in solution (Berglund *et al.,* 2003).

The non-ionic polyoxyethylene Brij®-35 and cetyltrimethylammonium bromide (CTAB) surfactants are also candidates for the reduction of non-specific binding and EOF control in electrophoretic separations. Usually these surfactants are employed as dynamic coating agents and are added to an electrophoresis running buffer; however, cross-linked PDMS layers on silica capillaries and glass devices in conjunction with a Brij®-35 adsorptive surface treatment can also decrease EOF in addition to reducing buffer pH dependence (Youssouf Badal *et al.,* 2002). Furthermore, CTAB and SDS were

shown to work as alternative adsorptive surface coating agents for additional control of EOF. An even simpler Brij®-35 coating, involving only the incubation of PDMS channels with the surfactant, can be used to improve separation efficiency by increasing wettability and significantly reducing non-specific adsorption and EOF for a wide solution pH range (Dou *et al.,* 2004).

The majority of non-ionic surfactants are block-copolymers consisting of long chains of ethylene oxide (or PEGs) and propylene oxide, commercialized under the trademark 'Pluronic®'. Good resistance to protein adsorption on PDMS surfaces was demonstrated with Pluronic® F108 under dynamic coating conditions (Viefhues *et al.,* 2011). Triton X-100™, another amphiphilic Pluronic® polyethylene oxide, can also be used as a coating agent that yields an acceptable reduction in protein adsorption as well as improved performance in capillary-based electrophoretic applications in PDMS/glass devices (Kang *et al.,* 2005). In addition to dynamic coating, non-ionic surfactants can also be successfully applied as surface coating agents statically. Various Pluronics® on PDMS surfaces have been reported to reduce EOF as well as maintain long term stability when statically coated (Hellmich *et al.,* 2005).

A final and slightly different surfactant that has gained popularity is the phospholipid bilayer system, which forms by spontaneous fusion of lipid vesicles with microchannel walls made of substrates such as PDMS or glass (Yang *et al.,* 2003). These systems can be employed for ligand binding assays, in which ligand–receptor binding can be measured under simulated membrane conditions along a microchannel, for example with dinitrophenyl conjugated lipids and corresponding antibodies. Additionally, fluorescence assays can be used to rapidly construct complete binding curves in one experiment, thus using less protein sample compared to traditional methods (Yang *et al.,* 2001). Controlled bilayer environments also open up new possibilities for biosensors in cell signaling studies in which key cellular functionalities stem from cell membrane ligand–receptor mechanisms.

2.5 Other strategies utilizing surface treatments

The coating strategies discussed thus far function either by covalently binding suitable molecules to various substrates or by an adsorptive coating to form surface layers, mostly based on organic molecules. Although these two categories encompass many of the surface treatments available for microfluidic devices, there remain other approaches that can be used to change the surface properties of biomedical microfluidic devices. For instance, exposure to reactive plasma gases can produce radicals that change the chemical composition of a surface, and physical sputtering techniques can be used to deposit thin layers on surfaces. One common example of this involves the use of reactive oxygen species to alter PDMS and glass surfaces via UV or

plasma treatment in oxygen or ozone atmospheres. While these treatments may be required as a precursor to subsequent covalent strategies, such as silanization (discussed in Section 2.2), they can also be used as a standalone method to alter surface properties as desired.

UV and UV/ozone exposure have been shown to increase surface wettability with UV/ozone treatment being more effective based on greater observed changes in surface chemistry (Efimenko *et al.,* 2002). Polycarbonate that has been irradiated with UV light shows a similar increase in wettability, in addition to EOF changes that are pH independent after treatment, unlike with glass substrates (Liu *et al.,* 2001). Increasing the wettability of substrates such as PDMS improves performance in bioanalytical applications, a possible example being DNA electrophoresis in a UV treated device yielding high resolution and reproducibility. UV/ozone treatment can be taken a step further to form porous polymer monoliths by adsorbing a UV activated photoinitiator and monomers to channel walls, followed by polymerization to non-covalently adhere the polymer to the surface. The durability and robustness of this attachment has been shown to withstand high pressures, despite its adsorptive nature (Burke and Smela, 2012).

Oxygen plasma treatment is a considerably widespread surface modification method for microfluidic devices, mainly PDMS-based, but can also be used with other substrates. A short treatment on the order of 1 min produces hydroxyl groups on the PDMS surface allowing for the formation of covalent siloxane bonds (Si–O–Si) with other substrates including itself, glass, silicon, polystyrene, and others. This adhesion is irreversible and bond strengths between PDMS and other substrates have been shown to increase linearly with the degree of plasma exposure (Bhattacharya *et al.,* 2005). This high correlation between bond strength and plasma exposure can be used to develop optimized plasma treatment parameters based on the degree of bonding needed. Concomitantly, an increase in surface wettability occurs due to the creation of silanol groups (Si–OH), rendering negatively charged channel walls for electroosmosis (Duffy *et al.,* 1998). Changes in PDMS wettability after plasma treatment, and after exposure to several chemicals, have also been studied (Mata *et al.,* 2005). While plasma treatment increases the wettability of PDMS, treatment with several different acids and bases, including strong acids such as H_2SO_4, revert the contact angle of plasma treated PDMS to a more native hydrophobic and less wettable state. This opens up the possibility of differentially patterning hydrophobic and hydrophilic regions on the same substrate in a lab-on-a-chip microfluidic device depending on the surface properties needed at each zone.

Metal sputtering methods can also be utilized in surface treatment schemes, for example sputtering and evaporation of gold on microchannel surfaces. The gold-coated surfaces serve as templates for self-assembled monolayers (SAM), to which a variety of coupling schemes can be applied

with an adequate choice of thiol head groups (see also Section 2.2.1). One example of this involves binding collagen to SAMs using Schiff base chemistry for the development of cell analysis arrays with improved cell adhesion and attraction to treated channel walls (Leong *et al.,* 2009). Other metals can also be coated on microfluidic devices, for example aluminum sputtering coupled with plasma treatment to create a biocompatible surface for increased cell adhesion and proliferation (Patrito *et al.,* 2007). The metal is etched in areas designated by a mask to expose a hydrophilic and reactive PDMS surface that favors cell adhesion. The novelty of this inexpensive and simple method over others discussed is that only a single-component substrate is used, without the need for surfactants or extracellular matrix protein adsorption methods previously described.

2.6 Examples of applications

The majority of the microfluidic surface modifications mentioned in this chapter have a specific focus in terms of application. While popular surface modifications were discussed, the applications they are tuned for were only briefly mentioned. In this section, three diagnostic applications are examined in further detail to demonstrate the great potential of microfluidics in the medical sciences, as well as to further emphasize the necessity of adequate surface coatings for successful analyses. The applications selected are those that are highly regarded in their respective fields and take proof-of-concept surface treatment studies and apply them to biological and medically focused applications. The microfluidic devices discussed herein are considered to be complete lab-on-a-chip devices, in that they are fully integrated analysis systems capable of complete diagnostics-based studies.

2.6.1 Lab-on-a-chip drug analysis of blood serum

Throughout this chapter, a significant number of the surface treatments discussed were applied to bioanalysis assays using microfluidic capillary electrophoresis. Two major issues with capillary electrophoresis in a microfluidic device are sample adsorption to capillary walls and unstable, high EOF. Both of these effects reduce resolution and efficiency, and therefore need to be addressed to attain a high quality separation. As presented in many of the previous sections, a variety of channel wall surface treatments have been shown to significantly reduce EOF as well as non-specific adsorption. There are benefits and drawbacks of different surface coatings based on invasiveness, difficulty, and durability, in which an ideal coating would be easy to apply, not interfere with sample analytes, and be robust throughout multiple trials over time using the same device.

(a)

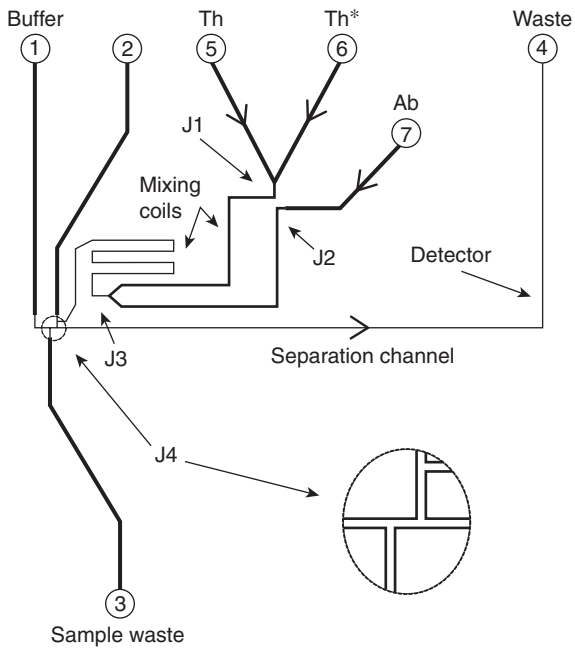

(b)

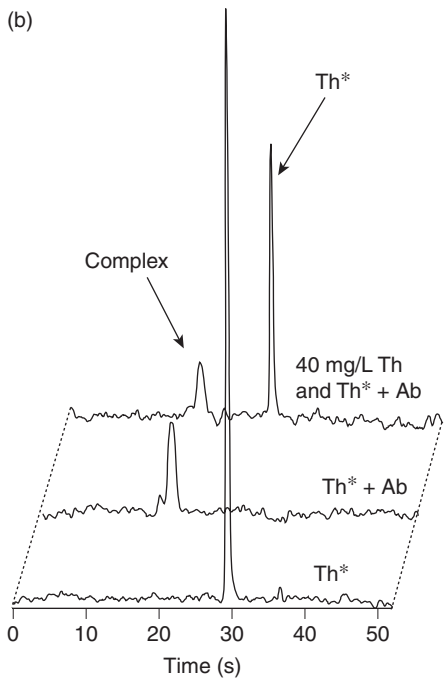

(*Continued on page 86*)

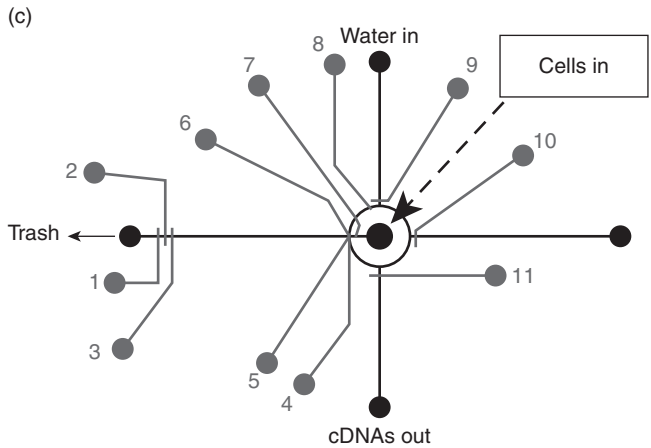

2.6 (a) Drug detection device (Section 2.6.1) schematic showing the various operating regions. Mixing of the antigen (Th) with the tracer (Th*) is performed between J1 and J3. Antibody (Ab) is then mixed with antigen and tracer in the J3-J4 immunoassay region. J4 shows the injection point into the electrophoresis region followed by detection. (*Source*: Reproduced from Chiem and Harrison (1998) with permission.) (b) A representative electropherogram showing actual results from a complete experiment. The bottom-most plot represents a control containing only tracer in buffer. The middle plot represents a mixture of antibody and tracer and the top plot represents a sample immunoassay with tracer and antibody. The Ab-Th* complex shows a distinct peak that is high when only tracer is present (middle) but decreases when Th is added due to competitive binding to Ab. A comparison of the two is used to quantify Th concentration. (*Source*: Reproduced from Chiem and Harrison (1998) with permission.) (c) Schematic of the single cell transcriptome device (Section 2.6.2). Numbers 1–11 represent independently controlled valves and the center 'cells in' region is used for sample injection. Initially, valves 1–3 are used to pump sample and cell trapping occurred at closed valves 4–7. Valves 8 and 10 were used to add cell lysis reagents and reverse transcriptase for PCR. (*Source*: Reproduced from Bontoux *et al.* (2008) with permission.)

A lab-on-a-chip device with complete drug analysis capabilities, including sample mixing, immunoreaction, separation using capillary electrophoresis, and analysis, has been realized using a glass microfluidic device (Chiem and Harrison, 1998) (see Fig. 2.6a). The automatability and positive results achieved with this device have opened new possibilities to further develop such devices for clinical use. Specifically in this study, the detection and analysis of the asthma drug theophyllin (Th) from a blood serum sample was demonstrated. The mixing portion involved the labeling of diluted blood serum with a tracer and immunoreaction with a specific antibody, anti-Th. The free Th was then separated from antibody-bound Th for quantitative analysis

(see Fig. 2.6b). The performance of the device was comparable to traditional, non-integrated methods with great detection limits and analysis times were significantly shortened due to the microscale nature of the device.

Because surface treatments are the focus of this chapter, it is important to mention the contribution of a surface treatment to the success of this integrated device. Similar devices without surface treatment showed low efficiency, tailing of analytes, and background fluorescence due to adsorption (Nielsen *et al.,* 1991). Dynamic coating using the non-ionic surfactant Tween® 20 was utilized to reduce non-specific adsorption for a variety of reasons, including ease of application compared to covalent methods and biocompatibility (Tween® 20 is a common immunoassay washing agent that prevents non-specific antibody binding). Additionally, this surface coating contributed to stable sample migration times due to a stabilization of EOF (Chiem and Harrison, 1997). In this specific experiment, Tween® 20 was shown to be beneficial; however, as mentioned throughout this chapter, a multitude of different surface coatings have been utilized for capillary electrophoresis. When selecting a surface coating for your application, it is important to consider all aspects of the experiment and choose one that meets the requirements of the experiment (substrate, analyte, etc.).

2.6.2 Single cell transcriptome analysis with microfluidic polymerase chain reaction (PCR)

Gene expression is a highly studied area to improve our understanding of organisms including their regulatory pathways, growth, etc. To investigate complete genetic expression or the transcriptome, single cell analysis is appropriate. Due to small sample volume availability in these types of studies, microfluidics is an excellent platform to employ, especially since there is the potential for complete lab-on-a-chip development. Similar to the analysis of proteins examined in Section 2.6.1, DNA analysis poses similar obstacles in terms of substrate/analyte interactions that can impede successful analysis, exemplifying the need for surface treatments. Advancements in microfluidics have led to the development of a PDMS device that can capture and lyse cells followed by reverse transcriptase polymerase chain reaction (RT-PCR) amplification and analysis to study gene expression in mouse brain (Bontoux *et al.,* 2008). The layout of this device is schematically depicted in Fig. 2.6c. Injection of individual neuronal cells into the device and subsequent processing and analysis allowed for an average detection of 5000 genes per cell, the expected number in a single cell of this type. This exceptional sensitivity and ability to study a cell's transcriptome is a significant clinical advancement towards rapid and more complete genetic analysis to understand the pathology and physiology of an organism.

A necessary and common surface treatment was used in this device: dynamic channel coating with the protein BSA. Due to its biocompatibility and ease of use, BSA surface passivation has been commonly used in microfluidic PCR to reduce adsorption (Zhang *et al.,* 2006) in addition to other applications discussed in Section 2.4.1. It has been reported that *Taq* polymerase adsorption is significant and contributes the most to poor PCR performance compared to DNA adsorption, which still occurs but to a lesser extent (Erill *et al.,* 2003). BSA has found widespread use due to its competitive adsorption to substrate walls with *Taq* and DNA, effectively reducing unwanted analyte adsorption. A potential explanation of this phenomenon is that BSA has similar charge characteristics as DNA under microfluidic PCR conditions and therefore has similar attraction to substrate channel walls (Nagai *et al.,* 2001). An added benefit of BSA is that it acts as a stabilizing agent of polymerase enzymes in solution. Similar to the Tween® 20 capillary electrophoresis surface coating, an appropriate surface coating for DNA PCR was applied with multiple benefits to ensure increased performance while remaining simple to apply without introducing detrimental side effects to the sample. Following a common theme, a vast number of surface treatments have been developed for microfluidic PCR in addition to the selected example so it is recommended to review Section 2.8 for more resources and other potential surface treatments applicable for PCR.

2.6.3 Immunosensor to detect pathogenic bacteria

Immunoassays such as ELISA are very common diagnostic tools in the health sciences, due to their high specificity, sensitivity, and versatility in detecting a wide range of target analytes. Traditional immunoassays involve an antibody coated on a substrate such as a standard titer plate to which a sample is applied. If target antigens are present, they bind to the immobilized antibodies and can be detected by a variety of readout methods. One can imagine that bound antibodies required in immunoassays could also be coated to the surface of a microfluidic device as discussed in Section 2.2 for a variety of substrate materials.

An important real world health application for immunoassays is the detection of pathogens such as *E. coli* in the food industry due to the health risks associated with foodborne pathogens. Consequently, rapid analysis of low sample volumes is needed, which makes microfluidics favorable over complex, labor intensive immunoassays such as conventional ELISA. This has led to the development of simpler detection methods using impedance measurements, classified as immunosensors. One such example based on immunosensing is a PDMS micro-immunosensor that can detect dangerous foodborne pathogens such as *E. coli* and *S. aureus*. The device utilizes

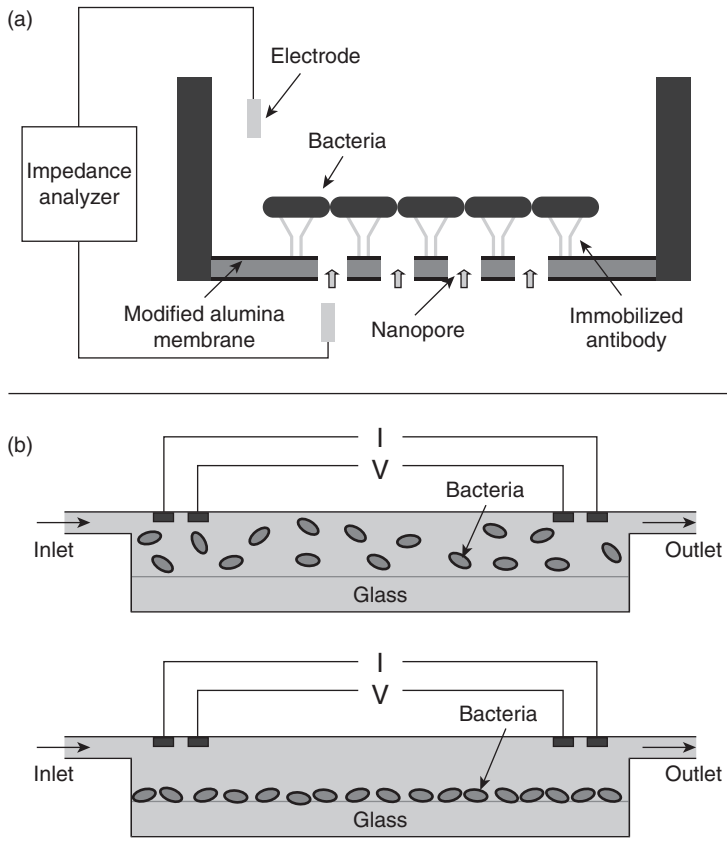

2.7 (a) Immunosensor schematic showing the capture of bacteria as it passes through a nanopore membrane. Antibodies immobilized to the surface trap bacteria which block the pores leading to an increase in impedance through the system. (*Source*: Reproduced from Tan *et al.* (2011) with permission.) (b) Another example of an impedance based immunosensor using a simpler two chamber design in which glass is silanized to immobilize antibodies. As bacteria flow from the inlet into the large chamber (top), they are captured by the antibodies (bottom) which alters the electrical properties of the chamber. Bacterial sensing is accomplished by observing a change in impedance. (*Source*: Reproduced from Boehm *et al.* (2007) with permission.)

an integrated nanoporous alumina membrane to which bacterial antibodies are covalently immobilized to a self-assembled, epoxy-functionalized trimethoxysilane monolayer (Tan *et al.*, 2011). As described in other silanization procedures, reactive hydroxyl groups on the substrate surface are needed (in this case formed with H_2O_2 treatment) to react with silane methoxy groups to silanize the surface. Amino groups on the antibodies then react with an open epoxy group functionalized to the silane, which provides

a covalent linkage between the antibody and the substrate surface. When a sample flows into the membrane, sensing is accomplished when bacteria attach to the antibodies and begin to block a nanopore, effectively increasing the impedance through the device (see Fig. 2.7a).

Similar surface chemistry has also been applied to a glass microfluidic bacterial immunosensor (Boehm *et al.*, 2007). Instead of an integrated membrane, the immunoassay takes place in a chamber within the glass chip silanized to immobilize antibodies (Fig. 2.7b). As sample flows into the chamber, bacteria bind to antibodies and act as insulators by replacing equal volumes of conducting solution, thus altering the impedance of the system. In both of the aforementioned examples, analysis times are very rapid and high sensitivity is attained, illustrating the capability of microfluidics as a platform for immunosensing. Furthermore, the versatility of silanization and covalent immobilization of antibodies is illustrated with the ability to apply this surface treatment to multiple substrates and device designs. Despite these differences, the treatment remains effective in driving the immunoassay and maintaining high sensitivity. Further versatility can be realized by considering the ability to immobilize a variety of antibodies to various surfaces to detect complex bacterial samples or other biological analytes.

2.7 Conclusion and future trends

It is apparent that surface coatings are essential for the success of many medical microfluidic devices for a variety of applications, whether applied to sensitive diagnosis or as research tools in the field of medicinal biology and chemistry. As was demonstrated throughout this chapter, the variety of materials and coating strategies for microfluidic materials is enormous. Among those, silicon dioxide-based devices are the best characterized and their covalent surface chemistry can be well adapted to a specific problem. It is therefore not astonishing that glass devices are used in many commercial microfluidic devices, such as in the cartridges used for the Bioanalyzer instrument from Agilent, for example. On the other hand, most polymer devices are flexible; a property that could become advantageous for point-of-care devices, implantation, and continuous monitoring. Additionally, most polymer devices can be fabricated with mass replication tools such as injection molding, which allows for economical and mass production. Nowadays, such replication tools can even be generated with nanometer-sized features allowing for versatile integration and parallelization.

Despite advancements in microfluidics, the surface chemistry of polymer devices strongly depends on the chemical composition of the polymer employed making general surface treatment schemes, such as that provided by the silanization of glass, not available. Consequently, the application of

polymer devices greatly depends on the choice of the polymer material, thus available immobilization strategies will have to be adapted to novel polymer materials. A large variety of successful usages of polymer devices have been demonstrated and discussed throughout this chapter, illustrating that adequate surface coatings can be developed for polymers to compete with glass devices in various applications. A specific advantage of polymer materials over glass devices arises from their gas permeability, which becomes important for cell-based studies and diagnosis. PDMS, for example, has shown excellent gas permeability and cell culturing capability in tandem with appropriate surface treatments. In summary, one can expect the continuation of silicon dioxide-based devices for high sensitivity applications and where reproducibility is greatly influenced by covalent and stable coatings. Polymer devices have great potential for point-of-care and single use applications where within-chip reproducibility is not a stringent requirement but cost effectiveness is essential.

2.8 Sources of further information and advice

In this chapter, a general overview of covalent and adsorptive surface coatings for microfluidic applications was given for the most common strategies used. For other materials and detailed protocols, the reader is referred to the literature cited in this chapter. Moreover, review articles provide useful information on coating strategies and their applications. For example, one of the most common materials used in the field is PDMS (Section 2.2.1) and the properties and general handling procedures of PDMS are described by Mata *et al.* (2005) and Lee *et al.* (2003b). Moreover, various common surface modifications for PDMS are summarized in references Makamba *et al.* (2003), Wong and Ho (2009), Zhou *et al.* (2010, 2012) and surface modifications of other polymers, specifically PMMA and polycarbonate, were reviewed by Soper *et al.* (2002).

The interested reader is further referred to reviews in the clinically important field of tissue engineering and PCR analysis. Surface treatments and procedures regarding tissue engineering were outlined by Park *et al.* (2007). In relation to miniaturized PCR analysis, various substrates were discussed by Zhang *et al.* (2006) including PDMS, PMMA, and polycarbonate. Static and dynamic passivation with separate and coupled surface chemistries were outlined including protein coatings, surfactants, silanization, polymer coatings, etc. This review covers a vast majority of papers published covering on-chip PCR as well as methods to develop such devices including aspects of fabrication, surface chemistry, implementation, etc., and specific applications such as microbial detection and disease diagnosis. Finally, surface treatments for microchip electrophoresis have also been extensively reviewed in Doherty *et al.* (2003) and Dolnik (2004).

2.9 References

Bai, Y., Koh, C.G., Boreman, M., Juang, Y.J., Tang, I.C., Lee, L.J. and Yang, S.T. (2006) 'Surface modification for enhancing antibody binding on polymer-based microfluidic device for enzyme-linked immunosorbent assay', *Langmuir,* **22**, 9458–9467.

Barker, S.L., Ross, D., Tarlov, M.J., Gaitan, M. and Locascio, L.E. (2000a) 'Control of flow direction in microfluidic devices with polyelectrolyte multilayers', *Analytical Chemistry,* **72**, 5925–5929.

Barker, S.L., Tarlov, M.J., Canavan, H., Hickman, J.J. and Locascio, L.E. (2000b) 'Plastic microfluidic devices modified with polyelectrolyte multilayers', *Analytical Chemistry,* **72**, 4899–4903.

Belder, D., Deege, A., Kohler, F. and Ludwig, M. (2002) 'Poly(vinyl alcohol)-coated microfluidic devices for high-performance microchip electrophoresis', *Electrophoresis,* **23**, 3567–3573.

Benoit, V., Steel, A., Torres, M., Yu, Y., Yang, H. and Cooper, J. (2001) 'Evaluation of three-dimensional microchannel glass biochips for bultiplexed nucleic acid fluorescence hybridization assays', *Analytical Chemistry,* **73**, 2412–2420.

Berglund, K.D., Przybycien, T.M. and Tilton, R.D. (2003) 'Coadsorption of sodium dodecyl sulfate with hydrophobically modified nonionic cellulose polymers. 1. Role of polymer hydrophobic modification', *Langmuir,* **19**, 2705–2713.

Bhattacharya, S., Datta, A., Berg, J. and Gangopadhyay, S. (2005) 'Studies on surface wettability of poly(dimethyl) siloxane (PDMS) and glass under oxygen-plasma treatment and correlation with bond strength', *Journal of Microelectromechanical Systems,* **14**, 590–597.

Boehm, D.A., Gottlieb, P.A. and Hua, S.Z. (2007) 'On-chip microfluidic biosensor for bacterial detection and identification', *Sensors and Actuators B: Chemical,* **126**, 508–514.

Bontoux, N., Dauphinot, L., Vitalis, T., Studer, V., Chen, Y., Rossier, J. and Potier, M.C. (2008) 'Integrating whole transcriptome assays on a lab-on-a-chip for single cell gene profiling', *Lab on a Chip,* **8**, 443–450.

Burke, J.M. and Smela, E. (2012) 'A novel surface modification technique for forming porous polymer monoliths in poly(dimethylsiloxane)', *Biomicrofluidics,* **6**, 016506.

Cheek, B.J., Steel, A.B., Torres, M.P., Yu, Y. and Yang, H. (2001) 'Chemiluminescence detection for hybridization assays on the Flow-Thru Chip, a three-dimensional microchannel biochip', *Analytical Chemistry,* **73**, 5777–5783.

Chen, H.Y., McClelland, A.A., Chen, Z. and Lahann, J. (2008) 'Solventless adhesive bonding using reactive polymer coatings', *Analytical Chemistry,* **80**, 4119–4124.

Chen, H. and Lahann, J. (2005) 'Fabrication of discontinuous surface patterns within microfluidic channels using photodefinable vapor-based polymer coatings', *Analytical Chemistry,* **77**, 6909–6914.

Chen, L., Ren, J., Bi, R. and Chen, D. (2004) 'Ultraviolet sealing and poly(dimethylacrylamide) modification for poly(dimethylsiloxane)/glass microchips', *Electrophoresis,* **25**, 914–921.

Cheng, J., Wei, C., Hsu, K. and Young, T. (2004) 'Direct-write laser micromachining and universal surface modification of PMMA for device development', *Sensors and Actuators B: Chemical,* **99**, 186–196.

Cheng, X., Gupta, A., Chen, C., Tompkins, R.G., Rodriguez, W. and Toner, M. (2009) 'Enhancing the performance of a point-of-care CD4+ T-cell counting microchip

through monocyte depletion for HIV/AIDS diagnostics', *Lab on a Chip,* **9**, 1357–1364.

Chiem, N. and Harrison, D.J. (1997) 'Microchip-based capillary electrophoresis for immunoassays: analysis of monoclonal antibodies and theophylline', *Analytical Chemistry,* **69**, 373–378.

Chiem, N.H. and Harrison, D.J. (1998) 'Microchip systems for immunoassay: an integrated immunoreactor with electrophoretic separation for serum theophylline determination', *Clinical Chemistry,* **44**, 591–598.

Chin, C.D., Linder, V. and Sia, S.K. (2012) 'Commercialization of microfluidic point-of-care diagnostic devices', *Lab on a Chip,* **12**, 2118–2134.

Currie, C.A., Shim, J.S., Lee, S.H., Ahn, C., Limbach, P.A., Halsall, H.B. and Heineman, W.R. (2009) 'Comparing polyelectrolyte multilayer-coated PMMA microfluidic devices and glass microchips for electrophoretic separations', *Electrophoresis,* **30**, 4245–4250.

Darain, F., Gan, K.L. and Tjin, S.C. (2009) 'Antibody immobilization on to polystyrene substrate – on-chip immunoassay for horse IgG based on fluorescence', *Biomedical Microdevices,* **11**, 653–661.

Delamarche, E., Donzel, C., Kamounah, F.S., Wolf, H., Geissler, M., Stutz, R., Schmidt-Winkel, P., Michel, B., Mathieu, H.J. and Schaumburg, K. (2003) 'Microcontact printing using poly(dimethylsiloxane) stamps hydrophilized by poly(ethylene oxide) silanes', *Langmuir,* **19**, 8749–8758.

Dodge, A., Fluri, K., Verpoorte, E. and de Rooij, N.F. (2001) 'Electrokinetically driven microfluidic chips with surface-modified chambers for heterogeneous immunoassays', *Analytical Chemistry,* **73**, 3400–3409.

Doherty, E.A., Meagher, R.J., Albarghouthi, M.N. and Barron, A.E. (2003) 'Microchannel wall coatings for protein separations by capillary and chip electrophoresis', *Electrophoresis,* **24**, 34–54.

Dolnik, V. (2004) 'Wall coating for capillary electrophoresis on microchips', *Electrophoresis,* **25**, 3589–3601.

Dou, Y., Bao, N., Xu, J., Meng, F. and Chen, H. (2004) 'Separation of proteins on surface-modified poly(dimethylsiloxane) microfluidic devices', *Electrophoresis,* **25**, 3024–3031.

Du, X.G. and Fang, Z.L. (2005) 'Static adsorptive coating of poly(methyl methacrylate) microfluidic chips for extended usage in DNA separations', *Electrophoresis,* **26**, 4625–4631.

Duffy, D.C., McDonald, J.C., Schueller, O.J.A. and Whitesides, G.M. (1998) 'Rapid prototyping of microfluidic systems in poly(dimethylsiloxane)', *Analytical Chemistry,* **70**, 4974–4984.

Efimenko, K., Wallace, W.E. and Genzer, J. (2002) 'Surface modification of Sylgard-184 poly(dimethyl siloxane) networks by ultraviolet and ultraviolet/ozone treatment', *Journal of Colloid and Interface Science,* **254**, 306–315.

Erill, I., Campoy, S., Erill, N., Barbé, J. and Aguiló, J. (2003) 'Biochemical analysis and optimization of inhibition and adsorption phenomena in glass–silicon PCR-chips', *Sensors and Actuators B: Chemical,* **96**, 685–692.

Eteshola, E. and Leckband, D. (2001) 'Development and characterization of an ELISA assay in PDMS microfluidic channels', *Sensors and Actuators B: Chemical,* **72**, 129–133.

Fritz, J.L. and Owen, M.J. (1995) 'Hydrophobic recovery of plasma-treated polydimethylsiloxane', *The Journal of Adhesion,* **54**, 33–45.

Fukuda, J., Khademhosseini, A., Yeh, J., Eng, G., Cheng, J., Farokhzad, O.C. and Langer, R. (2006) 'Micropatterned cell co-cultures using layer-by-layer deposition of extracellular matrix components', *Biomaterials,* **27**, 1479–1486.

Gross, P.G., Kartalov, E.P., Scherer, A. and Weiner, L.P. (2007) 'Applications of microfluidics for neuronal studies', *Journal of the Neurological Sciences,* **252**, 135–143.

Hashimoto, M., Hupert, M.L., Murphy, M.C., Soper, S.A., Cheng, Y.W. and Barany, F. (2005) 'Ligase detection reaction/hybridization assays using three-dimensional microfluidic networks for the detection of low-abundant DNA point mutations', *Analytical Chemistry,* **77**, 3243–3255.

Hashimoto, M., Barany, F. and Soper, S.A. (2006) 'Polymerase chain reaction/ligase detection reaction/hybridization assays using flow-through microfluidic devices for the detection of low-abundant DNA point mutations', *Biosensors & Bioelectronics,* **21**, 1915–1923.

Hau, W.L.W., Trau, D.W., Sucher, N.K., Wong, M. and Zohar, Y. (2003) 'Surface-chemistry technology for microfluidics', *Journal of Micromechanics and Microengineering,* **13**, 272.

Hellmich, W., Regtmeier, J., Duong, T.T., Ros, R., Anselmetti, D. and Ros, A. (2005) 'Poly(oxyethylene) based surface coatings for poly(dimethylsiloxane) microchannels', *Langmuir : the ACS Journal of Surfaces and Colloids,* **21**, 7551–7557.

Henry, A.C., Tutt, T.J., Galloway, M., Davidson, Y.Y., McWhorter, C.S., Soper, S.A. and McCarley, R.L. (2000) 'Surface modification of poly(methyl methacrylate) used in the fabrication of microanalytical devices', *Analytical Chemistry,* **72**, 5331–5337.

Hjertén, S. (1985) 'High-performance electrophoresis : Elimination of electroendosmosis and solute adsorption', *Journal of Chromatography A,* **347**, 191–198.

Hou, S., Yang, K., Qin, M., Feng, X., Guan, L., Yang, Y. and Wang, C. (2008) 'Patterning of cells on functionalized poly(dimethylsiloxane) surface prepared by hydrophobin and collagen modification', *Biosensors and Bioelectronics,* **24**, 912–916.

Hu, S., Ren, X., Bachman, M., Sims, C.E., Li, G.P. and Allbritton, N. (2002) 'Surface modification of poly(dimethylsiloxane) microfluidic devices by ultraviolet polymer grafting', *Analytical Chemistry,* **74**, 4117–4123.

Hu, S., Ren, X., Bachman, M., Sims, C.E., Li, G.P. and Allbritton, N.L. (2004) 'Surface-directed, graft polymerization within microfluidic channels', *Analytical Chemistry,* 7**6**, 1865–1870.

Huang, Y., Shan, W., Liu, B., Liu, Y., Zhang, Y., Zhao, Y., Lu, H., Tang, Y. and Yang, P. (2006) 'Zeolite nanoparticle modified microchip reactor for efficient protein digestion', *Lab on a Chip,* **6**, 534–539.

Jon, S., Seong, J., Khademhosseini, A., Tran, T.T., Laibinis, P.E. and Langer, R. (2003) 'Construction of nonbiofouling surfaces by polymeric self-assembled monolayers', *Langmuir,* **19**, 9989–9993.

Kang, J., Yan, J., Liu, J., Qiu, H., Yin, X., Yang, X. and Wang, E. (2005) 'Dynamic coating for resolving rhodamine B adsorption to poly(dimethylsiloxane)/glass hybrid chip with laser-induced fluorescence detection', *Talanta,* **66**, 1018–1024.

Katayama, H., Ishihama, Y. and Asakawa, N. (1998a) 'Stable cationic capillary coating with successive multiple ionic polymer layers for capillary electrophoresis', *Analytical Chemistry,* **70**, 5272–5277.

Katayama, H., Ishihama, Y. and Asakawa, N. (1998b) 'Stable capillary coating with successive multiple ionic polymer layers', *Analytical Chemistry,* **70**, 2254–2260.

Kidambi, S., Udpa, N., Schroeder, S.A., Findlan, R., Lee, I. and Chan, C. (2007) 'Cell adhesion on polyelectrolyte multilayer coated polydimethylsiloxane surfaces with varying topographies', *Tissue Engineering,* **13**, 2105–2117.

Lahann, J., Balcells, M., Lu, H., Rodon, T., Jensen, K.F. and Langer, R. (2003) 'Reactive polymer coatings: a first step toward surface engineering of microfluidic devices', *Analytical Chemistry,* **75**, 2117–2122.

Lee, M., Srinivasan, A., Ku, B. and Dordick, J.S. (2003a) 'Multienzyme catalysis in microfluidic biochips', *Biotechnology and Bioengineering,* **83**, 20–28.

Lee, J.N., Park, C. and Whitesides, G.M. (2003b) 'Solvent compatibility of poly(dimethylsiloxane)-based microfluidic devices', *Analytical Chemistry,* **75**, 6544–6554.

Lee, N.Y., Yang, Y., Kim, Y.S. and Park, S. (2006) 'Microfluidic immunoassay platform using antibody-immobilized glass beads and its application for detection of *Escherichia coli O157:H7*', *Bulletin of the Korean Chemical Society,* **27**, 479–483.

Lenigk, R., Liu, R.H., Athavale, M., Chen, Z., Ganser, D., Yang, J., Rauch, C., Liu, Y., Chan, B., Yu, H., Ray, M., Marrero, R. and Grodzinski, P. (2002) 'Plastic biochannel hybridization devices: a new concept for microfluidic DNA arrays', *Analytical Biochemistry,* **311**, 40–49.

Leong, K., Boardman, A.K., Ma, H. and Jen, A.K.-Y. (2009) 'Single-cell patterning and adhesion on chemically engineered poly(dimethylsiloxane) surface', *Langmuir,* **25**, 4615–4620.

Li, S.F.Y. and Kricka, L.J. (2006) 'Clinical analysis by microchip capillary electrophoresis', *Clinical Chemistry,* **52**, 37–45.

Li, Y., Wang, Z., Ou, L.M.L. and Yu, H. (2007) 'DNA detection on plastic: surface activation protocol to convert polycarbonate substrates to biochip platforms', *Analytical Chemistry,* **79**, 426–433.

Linder, V., Verpoorte, E., Thormann, W., de Rooij, N.F. and Sigrist, H. (2001) 'Surface biopassivation of replicated poly(dimethylsiloxane) microfluidic channels and application to heterogeneous immunoreaction with on-chip fluorescence detection', *Analytical Chemistry,* **73**, 4181–4189.

Liu, Y. and Rauch, C.B. (2003) 'DNA probe attachment on plastic surfaces and microfluidic hybridization array channel devices with sample oscillation', *Analytical Biochemistry,* **317**, 76–84.

Liu, Y., Fanguy, J.C., Bledsoe, J.M. and Henry, C.S. (2000) 'Dynamic coating using polyelectrolyte multilayers for chemical control of electroosmotic flow in capillary electrophoresis microchips', *Analytical Chemistry,* 72, 5939–5944.

Liu, Y., Ganser, D., Schneider, A., Liu, R., Grodzinski, P. and Kroutchinina, N. (2001) 'Microfabricated polycarbonate CE devices for DNA analysis', *Analytical Chemistry,* **73**, 4196–4201.

Lu, Y., Shi, W., Qin, J. and Lin, B. (2010) 'Fabrication and characterization of paper-based microfluidics prepared in nitrocellulose membrane by wax printing', *Analytical Chemistry,* **82**, 329–335.

Ludwig, M. and Belder, D. (2003) 'Coated microfluidic devices for improved chiral separations in microchip electrophoresis', *Electrophoresis,* **24**, 2481–2486.

Makamba, H., Kim, J.H., Lim, K., Park, N. and Hahn, J.H. (2003) 'Surface modification of poly(dimethylsiloxane) microchannels', *Electrophoresis,* **24**, 3607–3619.

Mata, A., Fleischman, A. and Roy, S. (2005) 'Characterization of polydimethylsiloxane (PDMS) properties for biomedical micro/nanosystems', *Biomedical Microdevices,* **7**, 281–293.

McCarley, R.L., Vaidya, B., Wei, S., Smith, A.F., Patel, A.B., Feng, J., Murphy, M.C. and Soper, S.A. (2005) 'Resist-free patterning of surface architectures in polymer-based microanalytical devices', *Journal of the American Chemical Society,* **127**, 842–843.

McDonald, J.C., Duffy, D.C., Anderson, J.R., Chiu, D.T., Wu, H., Schueller, O.J. and Whitesides, G.M. (2000) 'Fabrication of microfluidic systems in poly(dimethylsiloxane)', *Electrophoresis,* **21**, 27–40.

Mellors, J.S., Gorbounov, V., Ramsey, R.S. and Ramsey, J.M. (2008) 'Fully integrated glass microfluidic device for performing high-efficiency capillary electrophoresis and electrospray ionization mass spectrometry', *Analytical Chemistry,* **80**, 6881–6887.

Misiakos, K., Kakabakos, S.E., Petrou, P.S. and Ruf, H.H. (2004) 'A monolithic silicon optoelectronic transducer as a real-time affinity biosensor', *Analytical Chemistry,* **76**, 1366–1373.

Miyaki, K., Zeng, H., Nakagama, T. and Uchiyama, K. (2007) 'Steady surface modification of polydimethylsiloxane microchannel and its application in simultaneous analysis of homocysteine and glutathione in human serum', *Journal of Chromatography A,* **1166**, 201–206.

Nagai, H., Murakami, Y., Morita, Y., Yokoyama, K. and Tamiya, E. (2001) 'Development of a microchamber array for picoliter PCR', *Analytical Chemistry,* **73**, 1043–1047.

Naruishi, N., Tanaka, Y., Higashi, T. and Wakida, S. (2006) 'Highly efficient dynamic modification of plastic microfluidic devices using proteins in microchip capillary electrophoresis', *Journal of Chromatography A,* **1130**, 169–174.

Ni, M., Tong, W.H., Choudhury, D., Rahim, N.A., Iliescu, C. and Yu, H. (2009) 'Cell culture on MEMS platforms: A review', *International Journal of Molecular Sciences,* **10**, 5411–5441.

Nielsen, R.G., Rickard, E.C., Santa, P.F., Sharknas, D.A. and Sittampalam, G.S. (1991) 'Separation of antibody—antigen complexes by capillary zone electrophoresis, isoelectric focusing and high-performance size-exclusion chromatography', *Journal of Chromatography A,* **539**, 177–185.

Nisar, A., Afzulpurkar, N., Mahaisavariya, B. and Tuantranont, A. (2008) 'MEMS-based micropumps in drug delivery and biomedical applications', *Sensors and Actuators B: Chemical,* **130**, 917–942.

Paegel, B.M., Emrich, C.A., Wedemayer, G.J., Scherer, J.R. and Mathies, R.A. (2002) 'High throughput DNA sequencing with a microfabricated 96-lane capillary array electrophoresis bioprocessor', *Proceedings of the National Academy of Sciences of the United States of America,* **99**, 574–579.

Panaro, N.J., Yuen, P.K., Sakazume, T., Fortina, P., Kricka, L.J. and Wilding, P. (2000) 'Evaluation of DNA fragment sizing and quantification by the Agilent 2100 Bioanalyzer', *Clinical Chemistry,* **46**, 1851–1853.

Papra, A., Bernard, A., Juncker, D., Larsen, N.B., Michel, B. and Delamarche, E. (2001) 'Microfluidic networks made of poly(dimethylsiloxane), Si, and Au coated with polyethylene glycol for patterning proteins onto surfaces', *Langmuir,* **17**, 4090–4095.

Park, H., Cannizzaro, C., Vunjak-Novakovic, G., Langer, R., Vacanti, C.A. and Farokhzad, O.C. (2007) 'Nanofabrication and microfabrication of functional materials for tissue engineering', *Tissue Engineering,* **13**, 1867–1877.

Patrito, N., McCague, C., Norton, P.R. and Petersen, N.O. (2007) 'Spatially controlled cell adhesion via micropatterned surface modification of poly(dimethylsiloxane)', *Langmuir,* **23**, 715–719.

Reyes, D.R., Iossifidis, D., Auroux, P.A. and Manz, A. (2002) 'Micro total analysis systems. 1. Introduction, theory, and technology', *Analytical Chemistry,* **74**, 2623–2636.

Roman, G.T., McDaniel, K. and Culbertson, C.T. (2006) 'High efficiency micellar electrokinetic chromatography of hydrophobic analytes on poly(dimethylsiloxane) microchips', *Analyst,* **131**, 194–201.

Sandison, M.E., Zagnoni, M., Abu-Hantash, M. and Morgan, H. (2007) 'Micromachined glass apertures for artificial lipid bilayer formation in a microfluidic system', *Journal of Micromechanics and Microengineering,* **17**, S189–S196.

Shoffner, M.A., Cheng, J., Hvichia, G.E., Kricka, L.J. and Wilding, P. (1996) 'Chip PCR. I. Surface passivation of microfabricated silicon-glass chips for PCR', *Nucleic Acids Research,* **24**, 375–379.

Slentz, B.E., Penner, N.A. and Regnier, F.E. (2002) 'Capillary electrochromatography of peptides on microfabricated poly(dimethylsiloxane) chips modified by cerium(IV)-catalyzed polymerization', *Journal of Chromatography A,* **948**, 225–233.

Soper, S.A., Henry, A.C., Vaidya, B., Galloway, M., Wabuyele, M. and McCarley, R.L. (2002) 'Surface modification of polymer-based microfluidic devices', *Analytica Chimica Acta,* **470**, 87–99.

Sui, G., Wang, J., Lee, C., Lu, W., Lee, S.P., Leyton, J.V., Wu, A.M. and Tseng, H. (2006) 'Solution-phase surface modification in intact poly(dimethylsiloxane) microfluidic channels', *Analytical Chemistry,* **78**, 5543–5551.

Sun, S., Yang, M., Kostov, Y. and Rasooly, A. (2010) 'ELISA-LOC: lab-on-a-chip for enzyme-linked immunodetection', *Lab on a Chip,* **10**, 2093–2100.

Sung, J.H. and Shuler, M.L. (2010) 'In vitro microscale systems for systematic drug toxicity study', *Bioprocess and Biosystems Engineering,* **33**, 5–19.

Sung, W., Chang, C., Makamba, H. and Chen, S. (2008) 'Long-term affinity modification on poly(dimethylsiloxane) substrate and its application for ELISA analysis', *Analytical Chemistry,* **80**, 1529–1535.

SurModics (2012) 'Codelink™ Activated Slides', www.surmodics.com (online).

Tan, F., Leung, P.H.M., Liu, Z., Zhang, Y., Xiao, L., Ye, W., Zhang, X., Yi, L. and Yang, M. (2011) 'A PDMS microfluidic impedance immunosensor for *E. coli O157:H7* and *Staphylococcus aureus* detection via antibody-immobilized nanoporous membrane', *Sensors and Actuators B: Chemical*, **159**, 328–335.

Varjo, S.J., Ludwig, M., Belder, D. and Riekkola, M.L. (2004) 'Separation of fluorescein isothiocyanate-labeled amines by microchip electrophoresis in uncoated and polyvinyl alcohol-coated glass chips using water and dimethyl sulfoxide as solvents of background electrolyte', *Electrophoresis,* **25**, 1901–1906.

Verpoorte, E. (2002) 'Microfluidic chips for clinical and forensic analysis', *Electrophoresis,* **23**, 677–712.

Viefhues, M., Manchanda, S., Chao, T.C., Anselmetti, D., Regtmeier, J. and Ros, A. (2011) 'Physisorbed surface coatings for poly(dimethylsiloxane) and quartz microfluidic devices', *Analytical and Bioanalytical Chemistry,* **401**, 2113–2122.

Wang, A., Xu, J. and Chen, H. (2006) 'Proteins modification of poly(dimethylsiloxane) microfluidic channels for the enhanced microchip electrophoresis', *Journal of Chromatography A,* **1107**, 257–264.

Wang, H., Meng, S., Guo, K., Liu, Y., Yang, P., Zhong, W. and Liu, B. (2008) 'Microfluidic immunosensor based on stable antibody-patterned surface in PMMA microchip', *Electrochemistry Communications,* **10**, 447–450.

Wang, Y., Vaidya, B., Farquar, H.D., Stryjewski, W., Hammer, R.P., McCarley, R.L., Soper, S.A., Cheng, Y.W. and Barany, F. (2003) 'Microarrays assembled in microfluidic chips fabricated from poly(methyl methacrylate) for the detection of low-abundant DNA mutations', *Analytical Chemistry,* **75**, 1130–1140.

Wang, Y., Lai, H.H., Bachman, M., Sims, C.E., Li, G.P. and Allbritton, N.L. (2005) 'Covalent micropatterning of poly(dimethylsiloxane) by photografting through a mask', *Analytical Chemistry,* **77**, 7539–7546.

Waters, L.C., Jacobson, S.C., Kroutchinina, N., Khandurina, J., Foote, R.S. and Ramsey, J.M. (1998) 'Microchip device for cell lysis, multiplex PCR amplification, and electrophoretic sizing', *Analytical Chemistry,* **70**, 158–162.

Wei, C.W., Cheng, J.Y., Huang, C.T., Yen, M.H. and Young, T.H. (2005) 'Using a microfluidic device for 1 microl DNA microarray hybridization in 500 s', *Nucleic Acids Research,* **33**, e78.

Wong, I. and Ho, C.M. (2009) 'Surface molecular property modifications for poly(dimethylsiloxane) (PDMS) based microfluidic devices', *Microfluidics and Nanofluidics,* **7**, 291–306.

Wu, D., Luo, Y., Zhou, X., Dai, Z. and Lin, B. (2005) 'Multilayer poly(vinyl alcohol)-adsorbed coating on poly(dimethylsiloxane) microfluidic chips for biopolymer separation', *Electrophoresis,* **26**, 211–218.

Wu, M.H., Huang, S.B. and Lee, G.B. (2010) 'Microfluidic cell culture systems for drug research', *Lab on a Chip,* **10**, 939–956.

Xiao, D., Le, T.V. and Wirth, M.J. (2004) 'Surface modification of the channels of poly(dimethylsiloxane) microfluidic chips with polyacrylamide for fast electrophoretic separations of proteins', *Analytical Chemistry,* **76**, 2055–2061.

Xiao, D., Zhang, H. and Wirth, M. (2002) 'Chemical modification of the surface of poly(dimethylsiloxane) by atom-transfer radical polymerization of acrylamide', *Langmuir,* **18**, 9971–9976.

Yager, P., Edwards, T., Fu, E., Helton, K., Nelson, K., Tam, M.R. and Weigl, B.H. (2006) 'Microfluidic diagnostic technologies for global public health', *Nature,* **442**, 412–418.

Yang, T., Jung, S., Mao, H. and Cremer, P.S. (2001) 'Fabrication of phospholipid bilayer-coated microchannels for on-chip immunoassays', *Analytical Chemistry,* **73**, 165–169.

Yang, T., Baryshnikova, O.K., Mao, H., Holden, M.A. and Cremer, P.S. (2003) 'Investigations of bivalent antibody binding on fluid-supported phospholipid membranes: the effect of hapten density', *Journal of the American Chemical Society,* **125**, 4779–4784.

Young, E.W., Berthier, E., Guckenberger, D.J., Sackmann, E., Lamers, C., Meyvantsson, I., Huttenlocher, A. and Beebe, D.J. (2011) 'Rapid prototyping of arrayed microfluidic systems in polystyrene for cell-based assays', *Analytical Chemistry,* **83**, 1408–1417.

Youssouf Badal, M., Wong, M., Chiem, N., Salimi-Moosavi, H. and Harrison, D.J. (2002) 'Protein separation and surfactant control of electroosmotic flow in poly(dimethylsiloxane)-coated capillaries and microchips', *Journal of Chromatography A,* **947**, 277–286.

Yu, L., Li, C.M., Liu, Y., Gao, J., Wang, W. and Gan, Y. (2009) 'Flow-through functionalized PDMS microfluidic channels with dextran derivative for ELISAs', *Lab on a Chip,* **9**, 1243–1247.

Zhang, C., Xu, J., Ma, W. and Zheng, W. (2006) 'PCR microfluidic devices for DNA amplification', *Biotechnology Advances,* **24**, 243–284.

Zhang, Z.L., Crozatier, C., Le Berre, M. and Chen, Y. (2005) 'In situ bio-functionalization and cell adhesion in microfluidic devices', *Microelectronic Engineering,* **78–79**, 556–562.

Zhou, J., Ellis, A.V. and Voelcker, N.H. (2010) 'Recent developments in PDMS surface modification for microfluidic devices', *Electrophoresis,* **31**, 2–16.

Zhou, J., Khodakov, D.A., Ellis, A.V. and Voelcker, N.H. (2012) 'Surface modification for PDMS-based microfluidic devices', *Electrophoresis,* **33**, 89–104.

3

Actuation mechanisms for microfluidic biomedical devices

A. REZK, J. FRIEND and
L. YEO, RMIT University, Australia

DOI: 10.1533/9780857097040.1.100

Abstract: The dominance of surface and viscous forces at small scales, in particular, render the actuation and manipulation of fluids and particles in microfluidic systems a significant challenge, especially if integration into a portable handheld platform is desired, for example, in miniaturized devices for point-of-care diagnostics and biosensing. We provide a summary of the main actuation techniques that underpin a broad spectrum of microfluidic operations, and, in particular, briefly overview the role of electric and acoustic fields for this purpose. The former are currently mechanisms of choice that are already widely used, whereas the latter, especially surface acoustic waves, comprise an emerging technique that has gained considerable attention of late.

Key words: fluid and particle manipulation, microfluidics, mechanical and non-mechanical actuation, electrokinetics, surface acoustic waves (SAW).

3.1 Introduction

Actuating and manipulating fluids and particles at microscale dimensions poses a considerable challenge, primarily due to the surface area to volume ratio as the characteristic system dimension is reduced, which reflects the increasing dominance of surface and viscous forces in retarding fluid flow. This is captured by the characteristically small Reynolds numbers ($\mathrm{Re} \equiv \rho UL/\mu \lesssim 1$) in microfluidic systems, wherein ρ and μ are the density and viscosity of the fluid, and U and L are the characteristic velocity and length scales, respectively. Laminarity of the flow is also inherent in these low Re systems, thereby highlighting further challenges with regards to fluid mixing, especially in diffusion-limited systems.

To date, external syringe pumps have been widely utilized to induce flow and mixing in microfluidic systems. Although these are precise and reliable, they are fairly large and hence confined to laboratory benchtops, thereby proving difficult to integrate with other operations on the microfluidic device comprising a miniaturized handheld platform for portable

operations, for example, for use at the point of need (Yeo *et al.*, 2011). This is further complicated by the inlet and outlet tubing and ancillary connections required for fluid transfer between the pump and the chip, which requires careful handling by a skilled user, therefore making their use considerably challenging for adoption by patients, for example, in diagnostic testing. The majority of medical testing also involves molecular and bioparticle manipulation, which require additional microfluidic capability for fast and sensitive preconcentration, sorting and detection.

In this chapter, we summarize the various mechanisms for microfluidic actuation within two subcategories: mechanical and non-mechanical actuation mechanisms (Table 3.1). This is followed by a brief overview of two mechanisms, namely electrokinetics and acoustics, which we believe constitute the most promising and practical methods for driving fluid and particle motion in microfluidic devices, as reflected by recent growing interest and popularity in their use.

3.2 Electrokinetics

To date, electrokinetics, which concerns the use of electric fields to manipulate fluid flow, is one of the most preferred and widely used methods for microfluidic actuation. This is because electrodes are cheaply and easily fabricated, and can be integrated without much difficulty in microfluidic devices, and have the ability to provide high electroosmotic flow rates, efficient electrophoretic separation, and precise dielectrophoretic particle positioning. Here, we provide an overview of the basic principles underlying these flows and a brief summary of their use for microfluidic actuation. The reader is referred to a more comprehensive treatise on the subject in Chang and Yeo (2010).

3.2.1 The electric double layer

A channel surface in contact with an electrolyte solution tends to acquire a net charge through various surface-charging mechanisms (Hunter, 1987). Consequently, free ions in the bulk with opposite charge to that on the surface (counter-ions) are attracted to the channel surface, while ions with like charge (co-ions) are repelled. A thin polarized layer rich in counter-ions, known as the Debye double layer, therefore arises adjacent to the channel surface, as depicted in Fig. 3.1a and 3.1b.

The electric potential field φ in the double layer can be described via a solution of Gauss' Law $\nabla^2\varphi = -\rho_e/\varepsilon$ governing charge conservation. For planar systems of symmetrical binary electrolytes, the volume charge density ρ_e can be specified by the Poisson-Boltzmann distribution; in the limit of small

Table 3.1 Summary of the main *mechanical* and *non-mechanical* actuation mechanisms for microfluidic actuation

Mechanical	Principal/Notes	References
Piezoelectric	A diaphragm comprising a piezoelectric disc, or a stack, that deforms when subject to an electric field to induce fluid motion by peristaltic (i.e., sequential contraction and relaxation) action along the length of the channel.	Koch *et al.*, 1998; Schabmueller *et al.*, 2002; Jang *et al.*, 2007; Yang *et al.*, 2008
Pneumatic/ Thermopneumatic	Air is employed to actuate and relax a diaphragm to create a pressure difference that pumps the fluid; often combined with diffusers. Heated and cooled air are used in thermopneumatic versions.	Pol *et al.*, 1990; Jeong and Yang, 2000; Kim *et al.*, 2005; Grover *et al.*, 2006
Rotary/Centrifugal (e.g., rotary gears, Lab-on-a-CD)	Reservoirs, valves and channels are patterned on a compact disc (CD). Fluid actuation within these structures arising from centrifugal forces is achieved upon rotation using a laboratory micromotor. A thermopneumatic addition combines this with heating of the reservoir to allow bidirectional pumping.	Gorkin *et al.*, 2010; Abi-Samra *et al.*, 2011
Shape-memory alloys (SMAs)	SMAs are thin films, and more recently wires, used as valves, pumps, latches and multiplexers due to their ability to exert large strains on soft elastomers such as PDMS under an electric field.	Benard *et al.*, 1998; Xu *et al.*, 2001; Vyawahare *et al.*, 2008
Electromagnetic	Fluid actuation is achieved by applying an oscillating magnetic field with the use of magnetic elements strategically embedded in a soft polymeric structure, resulting in its vibration. This is combined with diffuser and nozzle elements close to the inlets and outlets to achieve net flow direction.	Khoo and Liu, 2000; Al-Halhoulia *et al.*, 2010; Zhou and Amirouche, 2011
Electrostatic	Coulombic attraction force between oppositely charged plates drives the deflection of a soft membrane when an appropriate voltage is applied. The deflected membrane returns to its initial position upon relaxation of the field. The alternating deflection results in a pressure difference that, in turn, pumps the fluid.	Zengerle *et al.*,1992; Machauf *et al.*, 2005; Bae *et al.*, 2007

Acoustic (e.g., flexural waves, bubble streaming and SAWs)	Flexural Waves: Bulk vibration of a thin piezoelectric film that generates an acoustic field, which, in turn, causes fluid to flow (acoustic streaming). Bubble streaming: Acoustic streaming driven via excitation of bubbles attached at strategic positions on a channel using a piezoelectric transducer. Typically used for fluid mixing and recently for particle sorting and trapping. SAW: MHz order frequency electromechanical surface waves that generate a direct acoustic force on particles or a momentum that generates fluid flow (acoustic streaming) for fluidic actuation and micro/nano particle and biomolecule manipulation.	Moroney *et al.*, 1991; Luginbuhl *et al.*, 1997; Meng *et al.*, 2000 Ahmed *et al.*, 2009a, 2009b; Wang *et al.*, 2012; Hashmia *et al.*, 2012 Friend and Yeo, 2011; Yeo *et al.*, 2011

Non-Mechanical	Principal/Notes	References
Capillary (e.g., pressure and surface tension gradients)	Pressure gradient: Flow induced by a pressure difference across an interface that drives wetting of fluids in channels or in paper-based substrates. Attractive because it offers a passive actuation mechanism without requiring active pumping. Surface tension gradient: Generation of interfacial flow due to chemical (e.g., surfactant) concentration, thermal (thermocapillary), electrical (electrocapillary), or optical (optocapillary) gradients.	Ichikawa *et al.*, 2004; Gervais and Delamarche 2009; Martinez *et al.*, 2010 Darhuber and Troian, 2005; Basu and Gianchandani, 2008
Electrokinetics (e.g., electroosmosis, electrophoresis, dielectrophoresis and electrowetting) – Chang and Yeo (2010)	Electroosmosis: Bulk motion of aqueous solution along a fixed solid boundary due to an external electric field. Electrophoresis: Use of an applied electric field to move charged particles or ions in a stationary fluid. Dielectrophoresis: Motion of dielectric particles suspended in a medium due to the application of a *non-uniform* electric field.	Lazar and Karger, 2002; Takamura *et al.*, 2003; Wang *et al.*, 2009 Wu *et al.*, 2008; Kenyon *et al.*, 2011 Pethig, 2010; Menachery *et al.*, 2010

(*Continued*)

Table 3.1 Continued

Non-Mechanical	Principal/Notes	References
	Electrowetting: Control of the wettability of a drop or film through an applied electric field by the generation of a Maxwell force at the contact line or a Maxwell pressure along the interface (depending on electrode configuration).	Yeo and Chang, 2005; Mugele and Baret, 2005; Wheeler, 2008
Optics (optofluidics) (e.g., laser microfluidic actuation, optical tweezing and, optical chromatography) – Fainman *et al.* (2010)	Laser microfluidic actuation: The momentum carried by incident propagating light gives rise to a radiation pressure at the fluid interface due to the difference in refractive index, resulting in interfacial deformation or even jetting. In addition, localization of the laser beam induces thermocapillary forces leading to fluid flow (see also *Capillary* entry).	Grigoriev, 2005; Baroud *et al.*, 2007; Delville *et al.*, 2009; Dixit *et al.*, 2010
	Optical tweezers: Dielectric particles can be trapped and moved due to the optical gradient within the tightly focused laser beam. Alternatively, birefringence can be exploited in which a particle can be rotated in a standard optical trap simply by manipulating the polarization of the light beam.	Grier, 1997; Dholakia *et al.*, 2002; Chiou *et al.*, 2005; Neale *et al.*, 2005
	Optical chromatography: Use of a focused laser beam to trap particles along its axis of propagation, where the beam is positioned against the fluid flow and the particles' trapped location is a balance between fluid drag and optical pressure.	Imasaka, 1998; Hart and Terray, 2003; Hart *et al.*, 2007
Magnetohydrodynamic	Use of a Lorentz force to pump conducting fluids, perpendicular to both the electric and the magnetic field.	Lemoff and Lee, 2000; Jang and Lee 2000; Bau *et al.*, 2001; Eijel *et al.*, 2003
Microbubbles	Generated either electrochemically (e.g., via electrolysis) or thermally (e.g., cavitation). The bubble oscillation is used to drive pumping in microchannels, often by pushing on diaphragms.	Suzuki and Yoneyama, 2002; Yoshimi *et al.*, 2004; Kabata and Suzuki, 2005; Yin and Prosperetti, 2005

surface potentials $\varphi_s << RT/zF \sim 25.7$ mV (298 K), linearization of the resultant Poisson equation together with boundary conditions prescribed by the surface potential $\varphi = \varphi_s = \lambda_D E_s$ ($y = 0$) and a potential and electric field $E = -\mathrm{d}\varphi/\mathrm{d}y$ that decays away from the surface to the bulk ($y \to \infty$) permit an approximate analytical solution in the form

$$\varphi = \varphi_s e^{-y/\lambda_D}, \qquad [3.1]$$

where

$$\lambda_D = \sqrt{\frac{\varepsilon RT}{2F^2 z^2 C_\infty}} \qquad [3.2]$$

is the Debye screening length or double layer thickness. The above is known as the *Debye–Hückel approximation* (Debye and Hückel, 1923), wherein y is the coordinate normal to the surface, ε the permittivity, R the molar gas constant, T the absolute temperature, z' the ionic valency, F the Faraday constant and C_∞ the bulk ion concentration. We note the inverse relationship between the Debye length and the ion concentration (and hence conductivity) in Equation [3.2]: strong electrolytes lead to thin double layers (~0.1–10 nm), whereas weaker electrolytes give rise to thicker double layers (~10 nm–1 μm).

The Debye–Hückel approximation, which assumes that the counter-ions are mobile point charges distributed by rapid and random thermal motion in the *diffuse* double layer, nevertheless fails to account for hydration or solvation effects due to the finite ion size. These effects were later taken into account by allowing for a *Stern* layer comprising hydrated counter-ions that are bound by water molecules, whose local screening effect permits their adsorption onto the surface (Fig. 3.1c) (Stern, 1924). A slip plane therefore must exist between the rigid and stationary Stern layer and the mobile diffuse layer, along which the potential, more specifically known as the zeta potential ζ, can be experimentally measured (in contrast to the difficulty in characterizing the actual potential on the surface). For weak to moderate electrolytes, in keeping with the small potential limit in the Debye–Hückel approximation, $\zeta \sim \lambda_D E_s \sim \lambda_D \sigma_s/\varepsilon$.

Electrokinetic phenomena therefore arise as a consequence of slippage of the diffuse double layer over the charged surface upon the application of an applied electric field to generate bulk flow (*electroosmosis* in the case of stationary charged surfaces) or particle motion (*electrophoresis* in the case of a stationary medium), or an applied external force to produce an electric potential (*streaming potential* in the case of flow over a stationary surface or *sedimentation potential* in the case of charged particles moving in

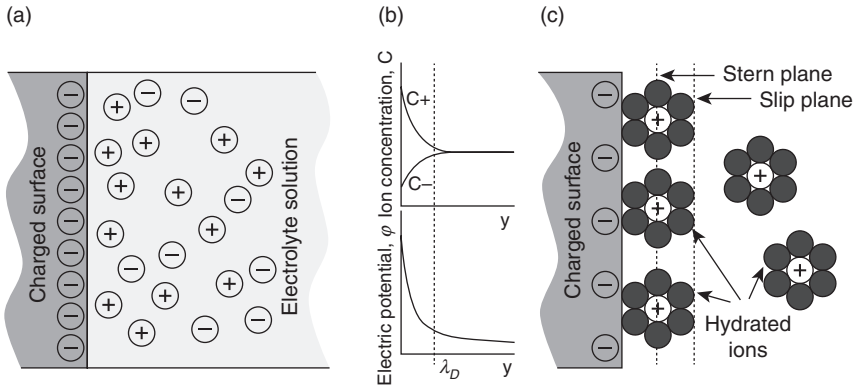

3.1 (a) Schematic depiction of, and (b) concentration profile (top) and electric potential variation (bottom) in the Debye double layer of thickness λ_D that arises as a consequence of an electrolyte solution in contact with charged surface, showing the enrichment in counter-ions and depletion in co-ions. (c) Stern layer that comprises hydrated counter-ions bound by water molecules.

a stationary medium). Given their relevance to microfluidic actuation, we briefly highlight the first two cases in the discussion to follow.

3.2.2 Electroosmosis

Electroosmotic slip

In its most general case, electroosmosis comprises the bulk motion of electrolyte that arises when a tangential electric field is applied across the *equilibrium* double layer that forms when the electrolyte is in contact with a solid boundary that acquires surface charge as a consequence. As depicted in Fig. 3.2, counter-ions in the diffuse layer are attracted to the electrode with opposite polarity, their net charge giving rise to a Maxwell (Lorentz) force $\rho_e E$ and hence momentum transfer on the liquid, which drives an electrokinetic slip at the slip plane. This slip can be derived from a balance between the hydrodynamic viscous and Maxwell stresses, assuming that the double layer is sufficiently thin compared to the channel radius/width such that the flow is unidirectional along the channel and that the pressure gradient only arises as a consequence of the tangential gradient in the normal surface field. Details of the derivation can be found in Chang and Yeo (2010); here, it suffices to quote the result, known as the *Smoluchowski slip velocity*:

$$u_s = -\frac{\varepsilon \zeta E_x}{\mu}, \qquad [3.3]$$

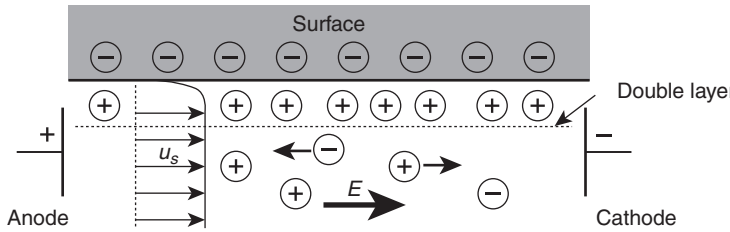

3.2 Counter-ions within the diffuse double layer are attracted towards the electrode with the opposite polarity upon application of a tangential electric field, giving rise to a net Maxwell force and hence bulk motion of the fluid known as electroosmosis. Given the double layer is thin relative to most microchannel dimensions, the flow velocity profile is essentially flat across the channel.

where E_x is the applied tangential field and μ is the viscosity. Typically, ζ ~10–100 mV and hence slip velocities up to around 1 mm/s can be generated with fields of approximately 100 V/cm.

Electroosmotic pumping

The velocity therefore increases from its zero value (i.e., no-slip) at the channel wall to the maximum value given in Equation [3.3] at the slip plane. Consequently, the slip drags the rest of the liquid in the channel along, giving rise to bulk electroosmotic flow. Given the asymptotically small Debye length, the bulk flow can be considered to arise from slip at the channel walls, and hence the velocity profile is essentially flat across the channel. This plug flow is convenient and particularly advantageous over pressure-driven flow from many perspectives, especially for microfluidic applications, since it minimizes hydrodynamic dispersion that leads to sample band broadening. Moreover, the independence of the slip velocity on the channel dimension then suggests that the volumetric flow rate, which is proportional to the channel cross-sectional area, scales as the square of the characteristic channel dimension H^2. This is a considerable advantage over the H^4 scaling of the volumetric flow rate arising from pressure-driven flows, which sharply diminishes with miniaturization of the channel dimension as H decreases. Together with the benefits of on-chip electrode integration – therefore removing the need for cumbersome fluid transfer from large mechanical or syringe pumps onto the microfluidic device, the elimination of mechanically moving parts, the ease of changing the flow direction upon reversal of the electrode polarity and the constant pulse-free fluid motion – electroosmotic pumps thus constitute a very attractive mechanism for microfluidic actuation.

It can further be shown from simple scaling arguments that a channel dimension H close to λ_D optimizes the power efficiency of the electroosmotic

pump (Chang and Yeo, 2010) – in larger channels, power is wasted in the large electroneutral bulk region outside the double layer where there is no net momentum transfer due to the absence of net charge, whereas in smaller channels, the flow is suppressed by increased viscous dissipation. As such, and given that the volumetric flow rate scales with cross-sectional area, it is expedient to employ a parallel bundle of thin channels (e.g., nanopores) whose dimensions are comparable to the double layer thickness – an example being that in packed capillaries or porous silica monoliths (Chen *et al.*, 2005; Wang *et al.*, 2006). For cylindrical pore geometries, and neglecting the tortuosity of the pore networks, the maximum pressure that can be developed in such pumps, taking into account the hydrodynamic load that imposes a back pressure within a channel, can be expressed by

$$\Delta p_{\max} = \frac{8\mu Q_{\text{eo}}}{\left(A_p R_p^2 / L_p\right) + \left(A_l R_l^2 / L_l\right)}, \qquad [3.4]$$

where $Q_{\text{eo}} = u_s A_p = n\pi R_p^2 u_s$ is the electroosmotic flow rate of the pump comprising n cylindrical pores of radius R_p and length L_p, i.e., the maximum flow rate when there is no pressure-driven flow ($\Delta p = 0$), and $A_l = \pi R_l^2$ the effective cross-sectional area of the hydrodynamic load section with radius R_l and length L_l, whose flow rate is specified by the Hagen-Poiseuille equation:

$$Q = \frac{A_l R_l^2}{8\mu} \frac{\Delta p_{\max}}{L_l}. \qquad [3.5]$$

Substituting Equation [3.4] into Equation [3.5],

$$Q = Q_{\text{eo}} \left(1 - \frac{\Delta p}{\Delta p_{\max}}\right), \qquad [3.6]$$

indicating the linear relationship between the back pressure and flow rate, and from which the efficiency of the pump can be obtained:

$$\eta = \frac{Q}{Q_{\text{eo}}} = 1 - \frac{\Delta p}{\Delta p_{\max}}. \qquad [3.7]$$

The pump becomes more efficient therefore as $\Delta p_{\max}$ increases, which, from Equation [3.4], can be obtained by reducing R_p/R_l such that Q approaches

Q_{eo}. This is however constrained, since decreasing R_p below λ_D results in overlapping double layers and hence diminishing slip velocities. The pump operation is therefore optimal when $R_p \sim \lambda_D$, as suggested above, noting from Equation [3.4] that Q_{eo}, and hence Q, can be compensated by increasing the applied field strength, although this, on the other hand, is limited by undesirable effects of bubble generation as a consequence of the increased current, which can cause blockage of the channel and whose large capillary pressures could cancel out any increase in the flow rate.

The theory above, nevertheless, breaks down for nanochannels when the channel dimension becomes comparable to the Debye length, such that an electroneutral ohmic region in the bulk no longer exists and the entire channel consists of a polarized region due to double layer overlap. In addition, entrance, resistive, pore neck charge storage, and electroviscous effects may also become important in these cases (Chang and Yeo, 2010). There are several analytical models as well as molecular simulations dedicated to nanochannel electroosmosis (see, for example, Petsev (2010) and Qiao and Aluru (2003)); we refer the reader to these, as the subject is beyond the scope of the present overview.

Electroosmotic mixing

Given the irrotationality of the electric field, the similarity between the hydrodynamic streamlines and the electric field – i.e., both velocity and electric fields are governed by the same divergence-free conditions – renders the electroosmotic flow an irrotational potential flow (hence the flat velocity profiles observed in Fig. 3.2) in the absence of an externally applied pressure gradient (Chang and Yeo, 2010). An unfortunate consequence of this result, which is quite unexpected for microfluidic flows where viscous stresses are usually dominant, is the absence of flow vortices to induce mixing in the microfluidic device, which, although advantageous in minimizing sample dispersion as discussed earlier, can be problematic given the typically low biomolecular diffusivities that result in long reaction times in transport-limited cases. Various strategies have therefore been adopted to increase mixing efficiency in electroosmotic flows. For example, it is possible to revoke the field and streamline similarity by generating a back pressure gradient in the channel through the introduction of surface charge, or bulk pH or electrolyte concentration (and hence ζ-potential) gradients along the channel (Ajdari, 1995; Herr *et al.*, 2000; Minerick *et al.*, 2002). Alternatively, interfacial instabilities can be introduced in the case of two co-flowing electrolytes with differences in their conductivities (Lin *et al.*, 2004; Pan *et al.*, 2007), as illustrated in Fig. 3.3, although the electric fields required to drive such transverse electrokinetic instabilities are often fairly large.

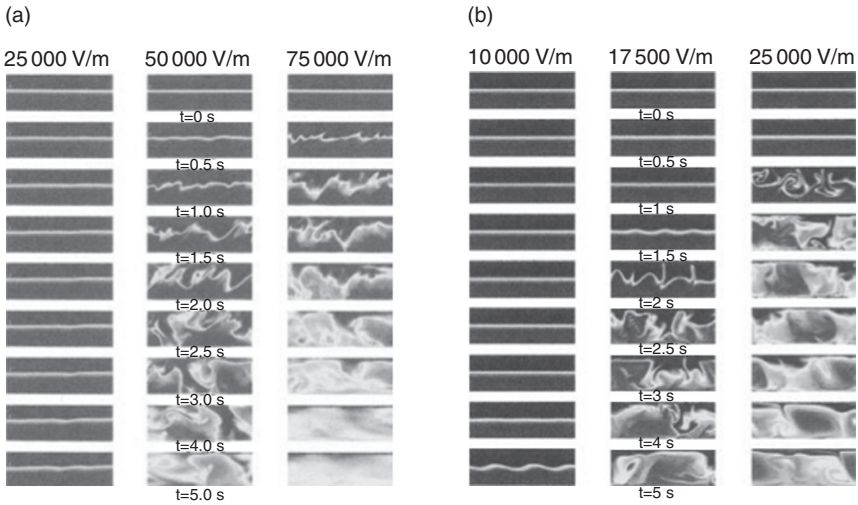

3.3 Transient electrokinetic instability driven by the gradient in the conductivity of two co-flowing electrolyte solutions under an applied longitudinal electric field. (a) Experimental results and (b) numerical simulation. (*Source*: Reprinted with permission from Lin *et al.* (2004). Copyright 2004, American Institute of Physics.)

3.2.3 Electrophoresis

Electrophoresis refers to the application of electric fields to move charged particles or ions in a stationary fluid. Two asymptotic limits for the particle size a can be considered (Chang and Yeo, 2010). In the small particle size limit (Fig. 3.4a), i.e., $a << \lambda_D$, the particle can be assumed to be a point charge and hence double layer screening effects can be neglected. In this case, the presence of the point charge does not influence and hence distort the field lines, and simply translates under electromigration effects in the absence of electrokinetic slip in the double layer around the particle. A balance between the Coulomb force exerted by the point charge q and the viscous drag force then leads to the Hückel equation for the electrophoretic mobility of the particle:

$$v_{\text{ep}} = \frac{2\varepsilon\zeta}{3\mu}, \qquad [3.8]$$

which is related to the electrophoretic velocity through $u_{\text{ep}} = v_{\text{ep}}E$.

In the large particle size limit (Fig. 3.4b), i.e., $a >> \lambda_D$, the double layer screens the external field, and hence the Maxwell force only acts in the double layer to drive an electrokinetic slip flow and not on the particle itself.

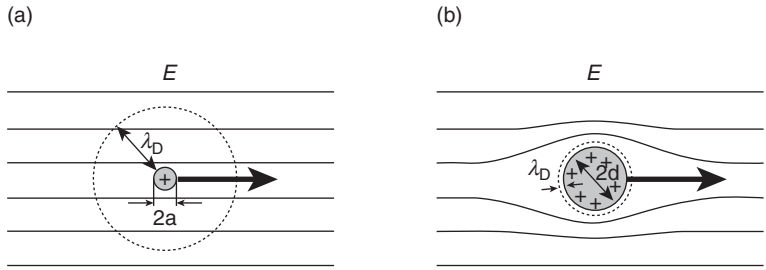

3.4 (a) The electric field lines around a particle remain undistorted around a charged particle if its size *a* is small compared to the Debye double layer thickness ($a << \lambda_D$). (b) On the other hand, the double layer screens the external field when the particle size is large compared to the double layer thickness ($a >> \lambda_D$).

In this case, the Smoluchowski slip velocity in Equation [3.3] can be used along the particle surface such that the electrophoretic velocity has the same dependency as the electroosmotic slip velocity but with opposite sign:

$$u_s = \frac{\varepsilon \zeta E_x}{\mu}. \qquad [3.9]$$

The discrimination in the electrophoretic mobility and hence migration velocity based on charge (more specifically, the surface charge density and hence the ζ-potential) in Equations [3.8] and [3.9] provides the underlying basis for electrophoretic separation technology. We note, however, the absence of the dependence on particle size or shape (although the former is implicit in the ζ-potential in the point charge theory). More common, however, is the use of gels or polymer (i.e., gel electrophoresis), which provides a medium that acts as a molecular sieve to facilitate steric and reptation effects, thus permitting size-based discrimination (i.e., smaller molecules migrate more quickly in the gel compared to larger molecules with the same electrophoretic mobility under the same electric field). More recently, a powerful technique has been proposed as an alternative to gel electrophoresis, in which the ends of polyelectrolyte molecules are tagged with a large uncharged monodispersed protein or polymer that exerts a large drag on the molecule whilst leaving its net charge intact. This technique, known as end-labelled free-solution electrophoresis (Meagher *et al.*, 2005), has been demonstrated as a fast and efficient method for the separation of gene fragments in DNA sequencing. Other methods for multiplex DNA sequencing using capillary array electrophoresis in microfluidic platforms (Paegel *et al.*, 2002), as well as electrophoretic detection of DNA sequence variations in microfluidic devices, have also been proposed – for the latter see, for example, the

work on single nucleotide polymorphism detection using restriction fragment length polymorphism (Footz *et al*., 2004) and single-strand conformation polymorphism (Szántai and Guttman, 2006). The reader is also referred to the review by Wu *et al*. (2008) and Yeo *et al*. (2011).

We note that the buffer solution also moves due to electroosmosis, and hence the electroosmotic velocity must be taken into account. Defining an electroosmotic mobility $v_{eo} = u_s/E$, the apparent mobility and hence the apparent velocity of the charged particle moving through the buffer solution under combined electrophoresis and electroosmosis is simply the sum of the electrophoretic and electroosmotic mobilities. When the charged particles have the same polarity as that of the ions in the buffer solution, the apparent mobility therefore exceeds the electrophoretic mobility, whereas the converse is true if the charged species has the opposite polarity to the ions in solution. Interestingly then, the charged particles can be trapped when the electrophoretic and electroosmotic mobilities are equal, which can be exploited to reduce the length required for electrophoretic separation.

To date, several extensions to the above electrophoretic theories have been proposed with more sophisticated theories to account for electroviscous effects – including that for non-spherical (Chen and Koch, 1996) and porous particles (Natraj and Chen, 2002), tangential surface conduction (Camp and Capitano, 2005), counter-ion condensation (Chang and Yeo, 2010), as well as conducting Stern layer and convective currents effects (Shubin *et al*., 1993).

3.2.4 AC electrokinetics

The use of DC electric fields is not without inherent disadvantages. High DC field intensities can sustain large currents that cause molecular and cellular degradation, and particle aggregation, as well as bubble and ion contamination generation. These problems can, however, be circumvented with the use of high frequency (>10 kHz) AC fields. The polarization mechanism and hence flow dynamics associated with AC electrokinetics are, however, fundamentally different from its DC or low frequency AC counterpart. Above frequencies associated with time scales that are below the double layer charge relaxation time scale $\lambda_D^2/D = \varepsilon/\sigma$, wherein D is the ionic diffusivity and σ the conductivity, there is insufficient time to polarize the double layer. As such, AC electrokinetics utilizes the electric field itself to induce polarization on the electrode surface in place of polarization due to the natural surface charges on the channel surface, as in DC electrokinetics (Chang and Yeo, 2010). Correspondingly, the induced polarization is non-uniform, given the double layer is no longer in equilibrium; as a result, the ζ-potential is now field-dependent, and thus it can be seen, for example, from the slip velocity given by Equation [3.3], that AC electrokinetic phenomena are

non-linear. Moreover, at these high frequencies, electrochemical reactions at the electrodes are usually absent at the RMS voltages typically employed, and hence problems associated with bubble and ion generation are non-existent. Further, the AC current is localized in the double layer, therefore minimizing penetration and thus damage in molecular and cellular structures. Below, we provide only a very brief summary of this subject in the context of AC electroosmosis; for a more in-depth discourse on non-linear and non-equilibrium electrokinetics, the reader may wish to consult the text by Chang and Yeo (2010). It is worth noting that it is possible to drive similar field-induced double layer polarization using DC fields (alternatively known as induced-charge electrokinetic phenomena (Squires and Quake, 2005), also discussed further in Chang and Yeo (2010)).

The simplest case of AC electroosmotic flow occurs due to capacitive charging over symmetric coplanar electrodes, as illustrated in Fig. 3.5; it is also possible that AC electroosmotic flows can be generated due to Faradaic charging (Lastochkin *et al.*, 2004; Ng *et al.*, 2009), although we will refrain from discussing this mechanism here. In one half of the AC cycle, ions in the bulk are driven by the field towards electrodes of opposite polarity to form a double layer whose total charge balances that on the electrodes. In the next half cycle, the electrode polarity reverses and so does that of the double layer on each electrode. In both cases, however, an outward tangential Maxwell force arises, which does not reverse in direction upon reversal of the field. This therefore gives rise to a net non-zero time-average Maxwell stress and hence an electroosmotic slip to result in a pair of recirculating vortices with length scales comparable to the electrode dimension. This symmetric vortex pair, however, cancels and hence no net flow is produced. In order to create a net global flow, it is therefore necessary to break the vortex symmetry with the use of asymmetric electrodes or an asymmetric field (e.g., a travelling wave) (Ajdari, 2000; Brown *et al.*, 2000; Ramos *et al.*,

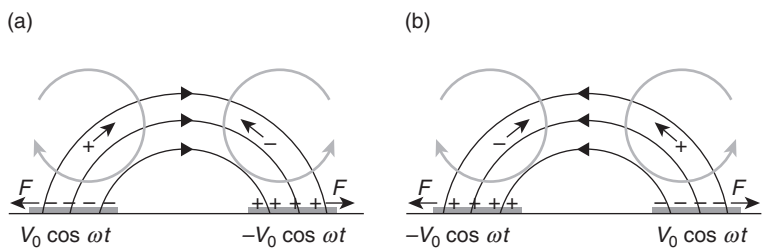

3.5 Schematic of AC electroosmotic flow on symmetric coplanar electrodes that is due to the capacitive charging mechanism. (a) and (b) show the electric field directions, the resultant time-averaged Maxwell force, and the corresponding flow profiles in successive AC half-cycles. (*Source*: After Ben and Chang (2005).)

2003); practical devices also include an upper surface to suppress the back flow associated with the larger vortex. In fact, the most efficient flow can therefore be produced with maximum asymmetry through an orthogonal (T) electrode design given the near singular field at the tip of the vertical section of the 'T' (Lastochkin *et al*., 2004). First derived by González *et al*. (2000), the time-averaged AC electroosmotic slip on the electrode can be shown to assume the form

$$u_s = -\frac{\varepsilon_l}{4\mu}\nabla_s \left|\Phi \mp \frac{V_0}{2}\right|^2, \qquad [3.10]$$

where Φ is the potential in the bulk immediately adjacent to the double layer and $|V_0|$ the RMS amplitude of the applied voltage signal; ∇_s is a surface gradient operator across each electrode. It is then apparent from this, together with a charge balance across the double layer,

$$\sigma\frac{\partial\varphi}{\partial n} = i\omega C\left(\Phi - \frac{V_0}{2}\right) \qquad [3.11]$$

(where ω is the applied AC frequency, C the total capacitance in the double layer, and n the coordinate normal to the electrode surface) that the slip velocity reaches a maximum at an optimum frequency ω_0 associated with the RC or double layer charging time (R being the electrolyte resistance) $D/\lambda_D d$, where d is the electrode separation. Away from this optimum frequency, the slip velocity decays monotonically to zero. At low frequencies $\omega \to 0$, the double layer is completely polarized and completely screens the field such that the electrode resembles a perfect insulator; consequently, the potential drop occurs mainly across the double layer. At high frequencies $\omega \to \infty$, there is insufficient time to charge the double layer, and hence the electrode resembles a constant potential surface (i.e., a perfect conductor) and the potential drop occurs mainly across the bulk (Chang and Yeo, 2010).

Squires and Bazant (2004) later extended the analysis of AC electroosmotic flows to allow for charging on ideally polarizable surfaces other than electrodes. In particular, they examined a conducting cylinder (e.g., a metal wire) immersed in an electrolyte, which when subjected to a uniform field, attracted the normal field lines, thus facilitating normal field penetration into the double layer and giving rise to an electroosmotic slip (Fig. 3.6). Again, the time-averaged slip velocity exhibits a maximum due to complete screening in the low frequency limit and incomplete charging in the high frequency limit. In any case, the resulting flow is quadrupolar as shown in

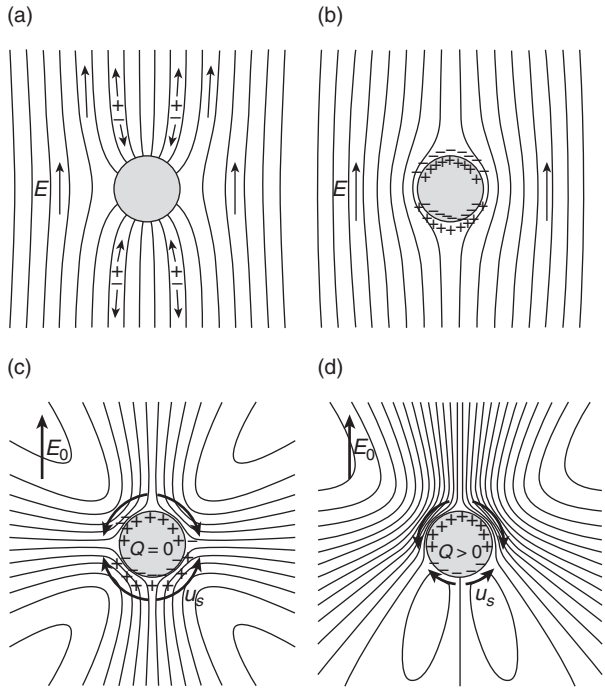

3.6 Double layer charging mechanisms of a polarizable conducting cylinder immersed in an electrolyte solution. Field lines (a) before and (b) after charging of the double layer. (c) Resulting electroosmotic flow streamlines, and (d) the corresponding streamlines obtained if the net charge on the cylinder surface is non-zero. (*Source*: Reprinted with permission from Squires and Bazant (2004). Copyright 2004, American Physical Society.)

Fig. 3.6c, wherein fluid is drawn along the field lines at the poles and ejected radially at the equator.

In addition to micropumping applications, the planar converging stagnation flow associated with the recirculating vortex pair in AC electroosmosis above symmetric coplanar electrodes has also been exploited for linear particle assembly (Ben and Chang, 2005). A similar system was later used to convect single DNA molecules in a bulk suspension and immobilize them onto the electrode surface for subsequent stretching (Lin *et al.*, 2005). Long-range convective trapping of DNA has also been demonstrated using the T-electrode design – the horizontal section of the 'T' being used to sweep particles in the bulk toward the vertical section of the 'T' which then funnels the concentrated particles into a conical region (Du *et al.*, 2008). Whilst such long-range convective mechanisms are not extremely effective at local trapping, since flow conservation renders a true stagnation point impossible, it is possible to combine the AC electroosmotic flow with short-range forces to

provide enhanced particle localization. Dielectrophoresis is one such short-range mechanism, which we shall discuss next.

3.2.5 Dielectrophoresis

Upon application of an electric field, a dielectric particle suspended in a dielectric medium acquires an interfacial charge due to the discontinuity in the permittivity across the phases. The interfacial polarization, however, is dependent on the orientation of the field due to the alignment of the individual dipoles within the particle and medium with the field, which can collectively be described by a single particle dipole that produces an effective dipole moment. For a spherical particle of radius a under an external AC field $\mathbf{E}$, upon solving for the potential of the particle and the medium through an expansion in spherical harmonics, this takes the form (Chang and Yeo, 2010)

$$\mathbf{p} = 3\varepsilon_m f_{\mathrm{CM}} V \mathbf{E}, \qquad [3.12]$$

where

$$f_{\mathrm{CM}} = \frac{\widetilde{\varepsilon_p} - \widetilde{\varepsilon_m}}{\widetilde{\varepsilon_p} + 2\widetilde{\varepsilon_m}} \qquad [3.13]$$

is the Clausius–Mossotti factor that describes the polarizability of the particle. In the above, V is the particle volume and

$$\widetilde{\varepsilon_i} = \varepsilon_i - i\frac{\sigma_i}{\omega} \qquad [3.14]$$

is a complex permittivity in which the subscripts p and m denote particle and medium properties, respectively. When subject to an applied AC electric field with constant phase, this induced effective particle dipole then results in a time-averaged force on the particle, which reads (Green and Morgan, 1999):

$$\langle \mathbf{F} \rangle = \frac{1}{T}\int_0^T (\mathbf{p}\cdot\nabla)\widetilde{\mathbf{E}}\,\mathrm{d}t = \pi\varepsilon_m a^3\,\mathrm{Re}\left[f_{\mathrm{CM}}\right]\nabla|\mathbf{E}|^2, \qquad [3.15]$$

where T denotes the period of AC forcing.

We note that the force is short range, depending on the particle dimension cubed as well as the electric field gradient. This non-uniform field is

necessary since the net interfacial charge on both ends of the particle are of opposite polarities but equal magnitudes; the force therefore cancels out in a uniform field since there is no effective dipole moment. The resulting particle motion that arises from this interaction between the non-uniform field with the induced dipole moment is therefore known as dielectrophoresis (DEP).

The versatility of DEP manipulation arises from the reversal in the polarizability specified by the real part of the Clausius–Mossotti factor $\mathrm{Re}[f_{\mathrm{CM}}]$ about a crossover frequency

$$\omega_c = \frac{1}{2\pi}\sqrt{\frac{(\sigma_m - \sigma_p)(\sigma_m + 2\sigma_p)}{(\varepsilon_p - \varepsilon_m)(\varepsilon_p + \varepsilon_m)}}. \qquad [3.16]$$

For frequencies at which $\mathrm{Re}[f_{\mathrm{CM}}] > 0$, particles are thus drawn toward regions of high field intensity (positive DEP), whereas for frequencies at which $\mathrm{Re}[f_{\mathrm{CM}}] < 0$, particles are drawn toward regions of low field intensity (negative DEP). The dependence of f_{CM} on the particle and medium conductivities and permittivities also allows the design of a DEP sorter that endows one particle species with a positive DEP force and another with a negative DEP force through judicious choice of a specific applied frequency (Gagnon and Chang, 2005). Multiple species, for example, can also be sorted by different DEP mobilities, which can be estimated from a balance between the DEP force in Equation [3.15] and the Stokes drag on the particle:

$$v_{\mathrm{DEP}} = \frac{\varepsilon_m a^2 \,\mathrm{Re}\left[f_{\mathrm{CM}}\right]}{6\mu}. \qquad [3.17]$$

An integrated multiplex continuous flow microfluidic platform for filtering debris and for sorting and trapping of colloidal beads or pathogens at a rate of 100 particles/s is shown in Fig. 3.7 (Cheng *et al.*, 2007). Whilst this sorting rate is still two orders of magnitude smaller than conventional flow cytometry, the technology offers the possibility for carrying out cell sorting and identification with costs and portability that are not afforded by laboratory-based cell sorters.

Consequently, DEP has emerged as a powerful tool for size-based discrimination for microfluidic detection and sorting. Numerous applications for DEP cell (blood cells, stem cells, neuronal cells, pathogens) sorting and characterization, pathogen (bacterial and viral) detection, and DNA, protein and chromosomal manipulation are summarized in the excellent review by Pethig (2010). Given the emergence of bead-based assays to enhance

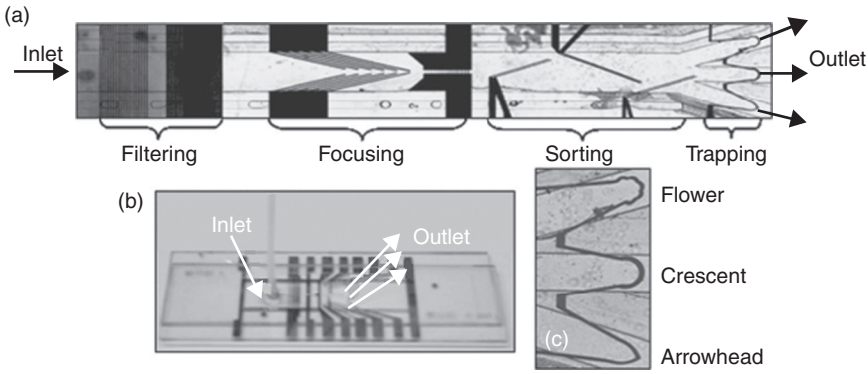

3.7 Bioparticle filtering, focusing, sorting, trapping and detection using an integrated dielectrophoretic chip. (a) Image of the setup comprising different bioparticle manipulation stages. (b) Image showing the electrodes fabricated on two glass slides, giving rise to three-dimensional effects. (c) A top view of the three different trapping electrode configuration, comprising a flower – multiple curved electrode, crescent – a semicircle electrode, and an arrowhead – a pointed electrode. (*Source*: Reprinted with permission from Cheng *et al.* (2007). Copyright 2007, American Institute of Physics.)

detection, for example, in DNA hybridization and sequencing assays (Yeo *et al.*, 2011), we anticipate DEP will play a major role in facilitating rapid and precise bead identification and sorting in microfluidic devices. Already, it has been shown that DNA concentration and the hybridized DNA conformation has a strong influence on the crossover frequency and the effective bead hydrodynamic radius (Gagnon *et al.*, 2009). This was exploited for trapping silica nanocolloids functionalized with oligonucleotides complementary to specific target DNA sequences for rapid microfluidic DNA identification in under 10 min. Beyond diagnostics and biosensing applications, DEP has also been used for isolating and positioning single cells in a similar manner to optical tweezers but with the advantage of design simplicity and significantly lower costs, primarily given that an expensive and complex laser is not required (Menachery *et al.*, 2011).

3.3 Acoustics

Despite its many advantages, electrokinetic actuation technology is hampered by the necessity for external ancillary equipment such as signal generators and amplifiers, which render complete miniaturization and integration with the microfluidic chip difficult. This is further compounded by the limitation of electrolyte solutions, which may be prohibitive in certain cases, and the requirement for high voltages in some other cases. An

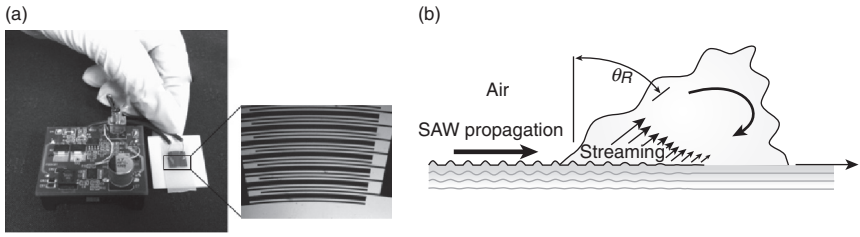

3.8 (a) A typical SAW device comprising a piezoelectric substrate on which IDT electrodes are patterned (as shown in the enlarged inset) and a portable battery-operated electronic circuit and power supply. (b) Schematic depiction of the Eckart streaming generated when energy leaks into a drop at the Rayleigh angle θ_R when it is irradiated by SAWs propagating along the underlying substrate.

alternative mechanism that has demonstrated significant promise is the use of acoustic fields to drive microfluidic actuation, which has the ability to generate relatively large throughput and high pressures. Whilst fairly low voltages are required, this is however compromised by the large sizes of the piezoelectric transducers often required to generate bulk ultrasonic manipulation that do not facilitate easy integration and miniaturization. Further, the large stresses that arise from the vibration, with frequencies typically of the order of 10–100 kHz and up to 1 MHz, and, in many cases, the accompanying cavitation that ensues, inflict considerable biomolecular and cellular damage.

These limitations, however, can be circumvented with a technology that has attracted considerable traction of late – the use of SAWs (Yeo and Friend, 2009; Friend and Yeo, 2011). Since the piezoelectric substrate required could comprise the microfluidic chip itself and as the interdigital transducer (IDT) electrodes required to generate the SAW can be integrated on the substrate, there is no need for the large transducers typically used in conventional ultrasonic microfluidics. Moreover, it has been shown that the ability to access high (MHz order and above) frequencies significantly limits the amount of molecular damage caused. One further advantage is the typically low powers ($\lesssim$1 W) required to drive fluid and particle actuation with SAWs, even to the point of fluid atomization, thereby allowing the entire operation to be driven using a portable driver circuit powered by camera batteries, which, together with the chip-scale substrate (Fig. 3.8a), potentially allows for complete miniaturization and integration into a truly handheld and portable microfluidic device (Yeo and Friend, 2009). Here, we briefly discuss the basic principles underlying acoustic fluid and particle actuation, and review developments in the field to date, particularly focusing on the SAW technology.

3.3.1 Basic principles of acoustic fluid and particle manipulation

A sound wave is the result of pressure or velocity oscillations that propagate through a compressible medium, and can be generated through bulk or surface vibration of solid materials. A convenient way to produce such vibration, especially at small scales in microfluidic systems, is with the use of oscillating electric fields by exploiting the electromechanical coupling afforded by piezoelectric transducers or substrates. There are primarily two broad strategies employed for acoustic particle and fluid actuation, which we describe next.

The first, generally known as *acoustophoresis*, exploits standing acoustic waves set up in a resonator configuration to spatially trap and move cells. The fundamental basis of the particle localization at pressure nodes/antinodes of the standing wave, and hence the ability to carry out particle separation, arises from a competition between the dominant forces acting on the particle (assuming that sedimentation and buoyancy forces are negligible), namely, the primary acoustic radiation force

$$F_a = -kE_aV_p\phi(\beta,\rho)\sin(2kx), \qquad [3.18]$$

assuming a one-dimensional planar standing wave, and the drag force

$$F_d = -6\pi\mu ua \qquad [3.19]$$

acting on the particle of dimension a and volume V_p, in which x is the distance from a pressure node along the wave propagation axis. In the above, $k = 2\pi f/c_l$ is the wave number, with f denoting the applied frequency and c_l the sound speed in the fluid medium, $E_a = p_0^2\beta_l/4 = p_0^2/4K_l = p_0^2/4\rho_l c_l^2$ the acoustic energy density of the standing wave, with p_0 being the pressure amplitude of the standing wave, β_l the liquid compressibility, K_l the bulk modulus, ρ_l the liquid density, and

$$\phi = \frac{5\rho_p - 2\rho_l}{2\rho_p + \rho_l} - \frac{\beta_p}{\beta_l}, \qquad [3.20]$$

is an acoustic contrast factor in which ρ_p and β_p are the particle density and compressibility, respectively. Particles therefore aggregate at the pressure nodes for $\phi > 0$ and at the antinodes for $\phi < 0$.

The second exploits the fluid flow that results as the acoustic wave propagates through a fluid, known as *acoustic streaming* (Friend and Yeo, 2011).

Different acoustic streaming phenomena are observed to occur over a variety of length scales imposed by the system geometry. In a thin boundary layer of fluid immediately adjacent to the vibrating surface with a characteristic thickness defined by the viscous penetration depth $(2\nu/\omega)^{1/2}$, strong viscous dissipation of the acoustic wave gives rise to flow known as *Schlichting streaming* (Schlichting, 1932), which is vortical in nature due to the no-slip condition at the oscillating solid boundary; ν is the kinematic viscosity and ω the frequency. At the edge of the boundary layer (also known as the Stokes layer) over a length scale on the order of the sound wavelength in the liquid λ_L (which, in turn, is related to the excitation frequency), a steady irrotational drift flow, known as *Rayleigh streaming*, occurs as a consequence of the periodic recirculation in the boundary layer (Rayleigh, 1884; Manor *et al*., 2012). Over longer length scales $>> \lambda_L$, the viscous dissipation of the acoustic radiation due to absorption in the fluid, whose pressure and velocity fluctuations gives rise to a time-averaged particle displacement and hence steady momentum flux (i.e., Reynolds stress), which is non-zero despite the harmonic oscillation due to the non-linear effects arising from viscous attenuation of the wave (Lighthill, 1978); the resultant flow being known as *Eckart streaming* (Eckart, 1948). It is not uncommon for a combination or all of the various streaming phenomena to exist together in a system, although one particular mechanism typically dominates, contingent on the system geometry. This is reflected in the flow phenomena observed, which can be remarkably distinct depending on the particular streaming mechanism that gives rise to them (Rezk *et al*., 2012a).

3.3.2 Bulk ultrasonic vibration

The majority of the early work on acoustically-driven microfluidic actuation was focused on the use of bulk ultrasonic transducers. These typically consisted of thin plates or membranes comprising a piezoelectric ceramic along which flexural waves (i.e., asymmetric Lamb waves) were generated, the plate/membrane thickness being a fraction of the wavelength of the flexural wave. For example, Moroney *et al*. (1991) and Meng *et al*. (2000) coated silicon nitride onto a ground plate, followed by the deposition of a thin zinc oxide layer and subsequently the aluminium interdigital electrodes. The bulk vibration that ensued then drove acoustic streaming, which due to the large attenuation length for the 1 MHz order employed, extended over a long range, typically a few centimetres from the membrane (Luginbuhl *et al*., 1997); as such, the device can also be used for mixing applications (Yaralioglu *et al*., 2004). Nevertheless, these flexural wave pumps are not as efficient compared to the SAW fluid actuation which we discuss in the next section, with larger powers required, and one to two orders of magnitude

lower in the velocity (typically up to 100 μm/s) that can be produced, even when focusing electrodes are employed (Meng *et al*., 2000).

In a similar manner, it is also possible to exploit substrate vibration to depin contact lines, and to drive droplet motion in open microfluidic platforms. In the former, a contact line hysteresis condition for a drop subject to vibration was derived in which the depinning was dependent on the vibrational acceleration (Noblin *et al*., 2004); in other work, the drop could be shown to spread under 1 MHz order piston-like thickness mode vibration of the underlying substrate, which induced a boundary layer streaming flow that endowed an additional surface force at the contact line (Manor *et al*., 2011). In the latter, a flexurally vibrating beam was employed by Alzuaga *et al*. (2005) on which different modes were excited in order to translate the drop between nodal locations.

Ultrasound-induced bubble oscillation can also be exploited to induce oscillatory flows, particularly useful for micromixing, or to facilitate nucleic acid transfection across cell membranes (i.e., sonoporation), even to the point of cell lysis (Ohl *et al*., 2006). In these cases, the bubbles are sonicated at resonance (typically kHz order) to induce a strong flow known as *cavitational microstreaming* that arises as the sound energy is dissipated due to the fluid viscosity in a boundary layer surrounding the bubble (Nyborg, 1958). Pumping flows of around several mm/s can be achieved, for example, with multiple bubbles housed in a cavity array, and can be used to drive micromixing (Tovar and Lee 2009) or even cell sorting (Patel *et al*., 2012). More examples of the use of bubble oscillation in microfluidics can be found in the review by Hashmi *et al*. (2012). Whilst relatively fast flows with reasonable throughput on the order of 100 μL/min and efficient mixing can be generated using bubble-based microfluidic actuators, difficulties associated with generating, trapping and maintaining the stability of bubbles is a common problem that has yet to be adequately resolved, in addition to limitations arising from molecular/cell lysis due to cavitational damage that can be undesirable in bioapplications other than gene transfection.

Much more progress has been observed on the acoustophoretic front, on the other hand, in which ultrasonic standing waves are employed to focus particles onto nodal lines for cell sorting (Harris *et al*., 2005), colloidal filtering (Hawkes and Coakley, 2001) or particle switching (Manneberg *et al*., 2009) applications. Particles can also be separated based on size by exploiting the discrepancy in the size scaling between Equations [3.18] and [3.19] and hence the dependence of the particle migration time on the particle dimension (larger particles aggregate more quickly compared to smaller ones); such fractionation is more specifically known as free-flow acoustophoresis when conducted in a continuous flow system with the particles being driven orthogonally to the flow. Other design variations have also been investigated, for example flow splitting (Johnson and Feke, 1995) and frequency

switching (Liu and Lim, 2011). Two vastly different particle species can also be separated given that the acoustic radiation force switches directions between positive and negative contrast factors in Equation [3.20] – a property that was exploited for separating lipids from red blood cells (Petersson *et al.*, 2004). The reader is referred to Laurell *et al.* (2007) for a more detailed discussion on acoustophoresis and its applications.

3.3.3 Surface acoustic waves (SAW)

Nanometre amplitude surface vibrations on a substrate in the form of Rayleigh waves offer an attractive and arguably superior alternative for microfluidic actuation compared to bulk ultrasound. The energy localization of these SAWs on the substrate and their efficient coupling into the fluid allows fluid actuation to be carried out with significantly lower dispersive losses, and hence the power requirement to drive comparable fluid actuation to that generated by bulk acoustics is significantly less, by one to two orders of magnitude, therefore offering the possibility for battery-powered operation, which, together with the chip-scale SAW device in Fig. 3.8a, enables attractive miniaturization possibilities (Yeo and Friend, 2009). Further, the low powers, together with the higher frequencies accessible with the SAWs, 10 MHz and above, have been found to suppress shear or cavitation damage on molecules (Qi *et al.*, 2010), thus making them attractive for bioapplications.

The SAW can be generated on a piezoelectric substrate by applying a sinusoidal electrical signal to IDT electrodes patterned on the substrate, whose finger width d determines the frequency f of the SAW and hence its wavelength λ_{SAW}, i.e., $f = c_s/4d = c_s/\lambda_{SAW}$. As illustrated in Fig. 3.8b, the coupling of acoustic energy into the fluid to drive Eckart streaming (Section 3.3.1) then arises from the diffraction of the SAW front in the presence of the fluid, which leads to leakage of the energy into the fluid at the Rayleigh angle, defined as the ratio between the sound speed of the Rayleigh wave on the substrate c_s to the speed of sound in the fluid c_l, i.e., $\theta_R = \sin^{-1}(c_s/c_l)$. In addition to the recirculation within the fluid, the acoustic radiation pressure also imparts a force at the interface, that together with the momentum transfer to the interface due to Eckart streaming, imparts a body force on the drop whose horizontal component causes it to translate in the direction of the SAW. Similarly, the elliptical retrograde motion of solid elements on the substrate as the SAW traverses underneath the drop also induces Schlichting and Rayleigh streaming, which has been shown to pull out a thin front-running wetting film in the opposite direction to that of the SAW propagation (Manor *et al.*, 2012; Rezk *et al.*, 2012a). In the same way that ultrasonic standing waves and acoustic streaming can be exploited to drive microscale fluid actuation and particle manipulation, we provide a short

discussion of the use of SAWs for this purpose and their associated applications. For a more detailed discussion on SAW microfluidics, see, for example, Friend and Yeo (2011).

SAW particle manipulation

Acoustophoretic manipulation can also be carried out using standing SAWs in a similar manner to bulk ultrasonic standing waves (Section 3.3.2). The standing wave, in the SAW devices, however, arises when diffraction of the SAW from the substrate into the liquid (Fig. 3.8b) generates sound waves in the liquid bulk that reflects off the walls of the microchannel (often fabricated from polydimethylsiloxane (PDMS) and placed on top of the SAW substrate). Depending on the channel dimension and the sound wavelength in the fluid, the particles then aggregate along one or more pressure nodal (or antinodal) lines along the channel. Conventionally, the IDTs are placed perpendicular to the channel and hence flow direction (Shi *et al*., 2008) to achieve linear focusing and subsequent separation/sorting, for example, by size, compressibility or density (Nam *et al*., 2012). In addition, the IDTs can also be arranged orthogonally at two lateral sides of a square chamber to obtain two-dimensional patterning (Shi *et al*., 2009). A discussion on the use of these devices as 'acoustic tweezers' for cell manipulation is given by Lin *et al*. (2012).

In addition, the nodal and hence particle positions can also be shifted along the axis of the standing wave by shifting the relative phase between the input IDT signal (Meng *et al*., 2011; Orloff *et al*., 2011). Particle alignment and sorting can also be carried out using IDTs placed at the ends of the channel such that the SAW propagates along the channel axis (Tan *et al*., 2009a). One advantage of this configuration is the ability to alter between fluid pumping and particle focusing simply by switching the frequency from the fundamental mode to a higher harmonic (Tan *et al*., 2010).

SAW fluid actuation and manipulation

SAW particle aggregation, trapping, patterning and separation is typically carried out at low input powers, considerably below 1 W, where the SAW displacement amplitude and velocity are relatively small, on the order of 0.1 nm and 0.01 m/s, respectively, such that the streaming is weak in order to avoid dispersion of the particles. At these low powers, other particle patterning phenomena are also observed, for example, those that form on the nodes or antinodes of capillary waves induced on the free surface of drops vibrated by the SAW excitation (Li *et al*., 2008).

At moderate power levels (approximately up to 1 W), it is possible to dispense and transport drops (Renaudin *et al*., 2006). For example, sessile drops

can be translated on the substrate when the acoustic radiation pressure and acoustic streaming results are sufficient to impart momentum transfer to the interface to overcome the pinning of the contact line (Brunet *et al*., 2010). This was shown for a variety of applications in open microfluidic systems such as polymerase chain reactions (Wixforth *et al*., 2004), bioparticle sampling, collection and concentration (Tan *et al*., 2007), scaffold cell seeding (Li *et al*., 2007a), and protein unfolding (Schneider *et al*., 2007). In addition, SAW droplet manipulation, such as mixing and particle concentration as well as sensing, has also been combined with electrowetting to enhance drop manipulation operations such as drop positioning and splitting (Li *et al*., 2012).

At these powers, the SAW can also be used to drive strong convective flows both within the drop and in channels. For example, it is possible to break the planar symmetry of the SAW to drive azimuthal recirculation in a drop or a microfluidic chamber to generate a rapid microcentrifugation effect (Li *et al*., 2007b; Shilton *et al*., 2008). This was used for example for inducing rapid and chaotic mixing (Shilton *et al*., 2011) (Fig. 3.9a), which can be used to enhance chemical and biochemical reactions (Kulkarni *et al*., 2009, 2010), or for particle concentration/separation (Fig. 3.9b). It is also possible to sort two particle species based on size in this microcentrifugation flow by exploiting the discrepancy in the scaling between the acoustic radiation force and the drag force exerted on the particle (Equations [3.18] and [3.20]): from a balance between these two forces, it is then possible to derive a frequency-dependent crossover particle size (which, in certain respects, is an analogue to the dielectrophoretic crossover frequency in Equation [3.15]) below which the drag force dominates to drive smaller particles to the centre of the drop and above which the acoustic force dominates to drive larger particles to the periphery (Fig. 3.9c) (Rogers *et al*., 2010). Finally, the drop rotation can also be used to spin 100 μm–10 mm thin SU-8 discs on which microfluidic channels and chambers can be patterned, as a miniaturized counterpart to the Lab-on-a-CD (Madou *et al*., 2006) for centrifugal microfluidic operations; unlike the Lab-on-a-CD, however, the SAW miniaturized Lab-on-a-Disc (miniLOAD) platform does not require a laboratory bench-scale motor, as the SAW can be driven using a portable driver circuit (Fig. 3.8a), therefore constituting a completely handheld microfluidic platform (Fig. 3.10) (Glass *et al*., 2012).

SAW streaming has been demonstrated for fluid actuation in PDMS channels placed atop the substrate (Masini *et al*., 2010), in channels ablated into the SAW substrate (Tan *et al*., 2009a), and even on paper (Rezk *et al*., 2012b). In addition, it was also shown that the SAW can be used to deflect the interfaces of co-flowing streams for directing emulsion droplets (Franke *et al*., 2009) and sorting cells (Franke *et al*., 2010). Whilst the body of earlier work was carried out in open microchannels, which have severe limitations

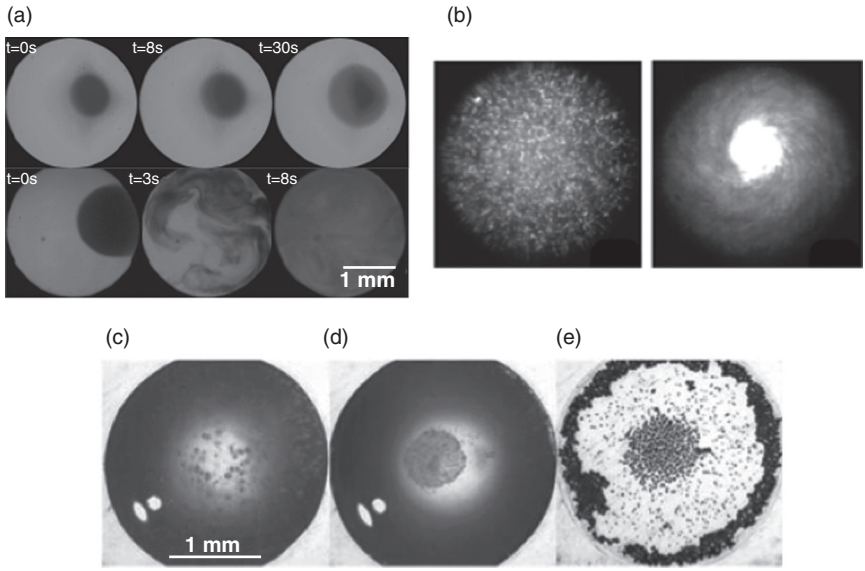

3.9 (a) The images in the top row show mixing of a dye due to pure diffusion without the action of the SAW, whereas the images in the bottom row show effective mixing under chaotic flow conditions driven by the SAW with an input power of ~1 W. (*Source*: After Shilton *et al*. (2011).) (b) Concentration of particles in a 0.5 μL drop via drop rotation induced by acoustic radiation due to the SAW. (*Source*: After Shilton *et al*. (2008).) (c)–(e) Separation of pollen and synthetic particles. (*Source*: After Rogers *et al*. (2010).) (c) Prior to the application of the SAW, the pollen and synthetic particles were suspended homogeneously throughout the entire quiescent drop. (d) After 3 s of applying the SAW, the pollen particles appear to concentrate in the centre of the drop and are hence separated from the synthetic particles, which tend to concentrate along the periphery of the drop. (e) The two species remain separated even after removal of the SAW and when the drop is fully evaporated after 1 min.

due to evaporation and possible contamination, recent work has focused on fluid actuation in a closed PDMS microchannel loop (Schmid *et al*., 2012) although the efficiency of the pump remained modest as a consequence of the strong absorption of the acoustic energy by the PDMS channel placed atop the SAW substrate. A way to circumvent this limitation was proposed by Langelier *et al*. (2012), in which a glass superstrate housing the microchannel was directly bonded to the SAW substrate using UV epoxy; alternatively, an SU-8 glue layer can also be used (Johanssen *et al*., 2012). Importantly, it was shown that the SAW is retained at the interface between the substrate and superstrate. This is in contrast to previous uses of a superstrate, first proposed by Hodgson *et al*. (2009), in which a fluid layer between the SAW substrate and the superstrate was employed to couple the

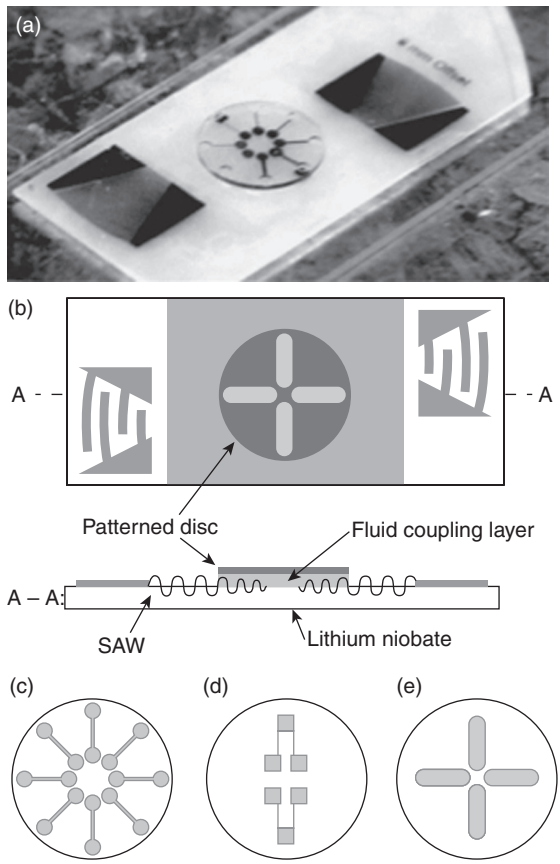

3.10 (a) Image and (b) schematic depiction of the miniLOAD platform comprising a 10 mm diameter SU-8 disc on which microchannels with a variety of designs ((c)–(e)) are fabricated to demonstrate capillary valving, micromixing and particle concentration/separation on a miniaturized centrifugal platform. The disc rotation is driven by coupling an asymmetric pair of SAWs into the fluid underneath the disc. (*Source*: Reprinted with permission from Glass *et al.* (2012). Copyright 2012, Wiley.)

acoustic energy into the latter, resulting in a Lamb wave on the superstrate. Nevertheless, it was shown, that it is possible to achieve similar fluid actuation and particle manipulation on the superstrate through Lamb wave excitation, albeit at a cost of considerably lower efficiency. Regardless, the use of a superstrate remains attractive since the microfluidic operations can be carried out in conventional silicon-based materials, which are considerably cheaper, thus allowing the option of disposability. Bourquin *et al.* (2010) later showed that it was possible to pattern periodic arrays of holes or posts in the superstrate to form a phononic crystal lattice that acted as a bandgap

to drive similar azimuthal recirculation to that discussed for a drop above, or to filter, scatter, reflect or focus the Lamb wave. This was employed for the development of a biosensor platform for the concentration of beads labelled with antibodies onto surface sites for subsequent binding and fluorescent detection (Bourquin *et al*., 2011).

At higher power, above 1 W, it is possible to drive sufficient interfacial deformation of a film or a drop to extrude fluid jets (Tan *et al*., 2009b; Bhattacharjee *et al*., 2011) or to drive atomization (Qi *et al*., 2008). Given that a monodispersed distribution of 1–10 μm aerosol droplets can be formed in the latter without requiring nozzles or orifices, the latter is particularly useful for pulmonary drug delivery (Qi *et al*., 2009), especially the next generation of therapeutic agents such as DNA, peptides and proteins, in a miniaturized portable platform for point-of-care therapeutics and personalized medicine. A significant advantage of the SAW pulmonary delivery platform over conventional nebulizers is the ability to preserve the viability of the drug, particularly shear-sensitive molecules such as DNA and peptides. In addition to drug delivery, the SAW atomization platform has been shown to be an efficient ionization source for microfluidic mass spectrometry interfacing (Heron *et al*., 2010; Ho *et al*., 2011). The atomization of polymer solutions using the SAW is also a rapid technique for template-free polymer patterning for microarray applications (Alvarez *et al*., 2008a) as well as for synthesizing 100 nm dimension protein and polymer nanoparticles (Alvarez *et al*., 2008b; Friend *et al*., 2008) within which drugs can be encapsulated (Alvarez *et al*., 2009). This was more recently extended to synthesize nanocapsules of complementary polyelectrolyte layers for DNA encapsulation, as an example of tunable controlled release delivery (Qi *et al*., 2011).

3.4 Limitations and future trends

Microscale and nanoscale fluid actuation and particle manipulation comprises the underpinning technology which enables a revolutionary field that could potentially provide innovative solutions for chemical and biological applications by performing tasks much faster, cheaper, with considerably less reagent volume, and ideally more easily – tasks that include DNA amplification by polymerase chain reaction, chemical synthesis, proteomics, and point-of-care diagnostics, among others (Robinson and Dittrich, 2013). Yet, the primary limitation that besets this enabling technology is at present posing a severe bottleneck in the development of true integrated and miniaturized devices for these applications: the inability to scale down and incorporate compact and efficient fluid actuation and particle manipulation with the rest of the microfluidic operations on the chip device. Whilst bench-scale capillary pumps and ancillary equipment such as amplifiers, signal generators, lasers, transducers and motors are adequate in driving reasonably

fast and efficient fluid actuation in a microfluidic chip for demonstrative purposes, such large and cumbersome components, and the difficulties of incorporating them on the chip, are impracticable when true portable functionality – the underlying motivation for adopting microfluidics in many applications – is desired.

Beyond miniaturization, another considerable challenge that has yet to be overcome is actuation efficiency. At present, the best fluidic actuation technologies that can be incorporated onto a chip, although not without their own challenges, are not comparable with their macroscopic counterparts in terms of efficiency. Electrokinetic and acoustic pumps, for example, have the ability to generate fast flow rates, but cannot match capillary pumps as far as the pressures that can be generated are concerned. Particle and cell manipulation schemes have sorting efficiencies and throughputs that are well below those achievable with conventional fluorescent activated cell sorting (FACS) technology, often by over two to three orders of magnitude. Further, long term reliability of microfluidic actuation technology has yet to be demonstrated. Another challenge that has yet to be widely addressed is chip automation and control – without which the device would be inoperable by an untrained user, thus defeating the goal of the 'Lab on a Chip' for point-of-care use and rendering the device closer in concept to a 'Chip-in-a-Lab'.

With continued advances in the research and development in microscale fluid actuation, we nevertheless believe that these challenges can be overcome. It is our opinion, however, that the solution may not necessarily lie with a single technology, but rather by combining several complementary technologies such that the limitations of a particular technology may be overcome with the strengths of another. An example of such that has already been demonstrated is the combination of fast, long-range electroosmotic convection and precise, short-range trapping offered by DEP. We anticipate further technology combinations in the future, especially cross-platform technologies such as the integration of acoustofluidics and electrokinetics.

Nanoscale actuation is another exciting area in which we foresee further growth given the promise for nanofluidic platforms (Mukhopadhyay, 2006; Napoli *et al*., 2010; Piruska *et al*., 2010), in particular for single molecule manipulation and sensing. Considerable work has been undertaken to date to elucidate mechanisms that govern nanoscale transport (Rauscher and Dietrich, 2008; Schoch *et al*., 2008; Chang and Yossifon, 2009; Sparreboom *et al*., 2009; Zhou *et al*., 2011) and we anticipate their widespread translation into practical technology in the near future. Nanofluidic actuation, nevertheless, faces similar, if not more challenging, hurdles to those encountered by its microfluidic counterpart, most importantly in practical device integration, given the additional complication of dealing with the micro/nano interface.

3.5 References

Abi-Samra, K., Clime, L. Kong, L., Gorkin III, R., Kim, T. H., Cho, Y. K. and Madou, M. (2011) 'Thermo-pneumatic pumping in centrifugal microfluidic' *Microfluid. Nanofluid*., **11**, 643–652.

Ahmed, D., Mao, X., Juluri, B. K. and Huang, T. J. (2009a) 'A fast microfluidic mixer based on acoustically driven sidewall-trapped microbubble' *Microfluid. Nanofluid*., **7**, 727–731.

Ahmed, D., Mao, X., Shi, J, Juluria, B. K. and Huang, T. J. (2009b) 'A millisecond micromixer via single-bubble-based acoustic streaming' *Lab Chip*, **9**, 2738–2741.

Ajdari, A. (1995) 'Electro-osmosis on inhomogeneously charged surfaces' *Phys. Rev. Lett*., **75**, 755–758.

Ajdari, A. (2000) 'Pumping liquids using asymmetric electrode arrays' *Phys. Rev. E*, **61**, R45–R48.

Al-Halhoulia, A. T., Kilanib, M. I. and S. Büttgenb, S. (2010) 'Development of a novel electromagnetic pump for biomedical applications' *Sens. Actuat. A: Phys.*, **162**, 172–176.

Alvarez, M., Friend, J. R. and Yeo, L. Y. (2008a) 'Surface vibration induced spatial ordering of periodic polymer patterns on a substrate' *Langmuir*, **24**, 10629–10632.

Alvarez, M., Friend, J. R. and Yeo, L. Y. (2008b) 'Rapid generation of protein aerosols and nanoparticles via SAW atomisation' *Nanotechnology*, **19**, 455103.

Alvarez, M., Friend, J. R. and Yeo, L. Y. (2009) 'Rapid production of protein loaded biodegradable microparticles using surface acoustic waves' *Biomicrofluidics*, **3**, 014102.

Alzuaga, S., Manceau, J.-F. and Bastien, F. (2005) 'Motion of droplets on solid surface using acoustic radiation pressure' *J. Sound Vib*., **282**,151–162.

Bae, B., Han, J., Masel, R. I. and Shannon, M. A. (2007) 'A bidirectional electrostatic microvalve with microsecond switching performance' *J. Microelectromech. Sys*.,**16**, 1461–1471.

Baroud, C. N., Vincent, M. R. S. and Delville, J.-P. (2007) 'An optical toolbox for total control of droplet microfluidics' *Lab Chip*, **7**, 1029–1033.

Basu, A. S. and Gianchandani, Y. B. (2008) 'Virtual microfluidic traps, filters, channels and pumps using Marangoni flows' *J. Micromech. Microeng*,, **18**, 115031.

Bau, H. H., Zhong, J. and Yi, M. (2001), 'A minute magneto hydro dynamic (MHD) mixer' *Sens. Actuat. B: Chem.*, **79**, 205–213.

Ben, Y. and Chang, H. C. (2005) 'Nonlinear electrokinetic devices', in *The MEMS Handbook*, ed. M. Gad-el-Hak (CRC Press, Boca Raton).

Benard, W. L., Kahn, H., Heuer, A. H. and Huff, M. A. (1998) 'Thin-film shape-memory alloy actuated micropumps' *J. Microelectromech. Sys*., **7**, 245–251.

Bhattacharjee, P. K., McDonnell, A. G., Prabhakar, R., Yeo, L. Y. and Friend, J. R. (2011) 'Extensional flow of low-viscosity fluids in capillary bridges formed by pulsed surface acoustic wave jetting' *N. J. Phys*., **13**, 023005.

Bourquin, Y., Reboud, J., Wilson, R. and Cooper, J. M. (2010) 'Tuneable surface acoustic waves for fluid and particle manipulations on disposable chips' *Lab Chip*, **10**, 1898–1901.

Bourquin, Y., Reboud, J., Wilson, R., Zhang, Y. and Cooper, J. M. (2011) 'Integrated immunoassay using tuneable surface acoustic waves and lensfree detection' *Lab Chip*, **11**, 2725–2730.

Brown, A. B. D., Smith, C. G. and Rennie, A. R. (2000) 'Pumping of water with ac electric fields applied to asymmetric pairs of microelectrodes' *Phys. Rev. E*, **63**, 016305

Brunet, P., Baudoin, M., Matar, O. B. and Zoueshtiagh, F. (2010) 'Droplets displacement and oscillations induced by ultrasonic surface acoustic waves: a quantitative study' *Phys. Rev. E*, **81**, 036315.

Camp, J. P. and Capitano, A. T. (2005) 'Size-dependent mobile surface charge model of cell electrophoresis' *Biophys. J*., **113**, 115–122.

Chang, H.-C. and Yossifon, G. (2009) 'Understanding electrokinetics at the nanoscale: a perspective' *Biomicrofluidics*, **3**, 012001.

Chang, H.-C. and Yeo, L. Y. (2010) *Electrokinetically Driven Microfluidics and Nanofluidics* (Cambridge University, New York).

Chen, S. B. and Koch, D. L. (1996) 'Rheology of dilute suspensions of charged fibres' *Phys. Fluids*, **8**, 2792–2807.

Chen, Z., Wang, P. and Chang, H.-C. (2005)' An electro-osmotic micro-pump based on monolithic silica for micro-flow analyses and electro-sprays' *Anal. Bioanal. Chem*., **382**, 817–824.

Cheng, I.-F., Chang, H.-C., Hou, D. and Chang, H.-C. (2007) 'An integrated dielectrophoretic chip for continuous bioparticle filtering, focusing, sorting, trapping, and detecting' *Biomicrofluidics*, **1**, 021503.

Chiou, P. Y., Ohta, A. T. and Wu, M. C. (2005) 'Massively parallel manipulation of single cells and microparticles using optical images'*Nature*, **436**, 370–372.

Darhuber, A. A. and Troian, S. M. (2005) 'Principles of microfluidic actuation by modulation of surface stresses' *Annu. Rev. Fluid Mech*., **37**, 425–455.

Debye, P. and Hückel, E. (1923) 'Zut Theorie der Electrolyte. II. Das Grenzgesetz für die elektrishe Leitfähigkeit' *Phys. Z*., **24**, 305–325.

Delville, J.P., de Saint Vincent, M. R., Schroll, R. D., Chraibi, H., Issenmann, B., Wunenburger, R., Lasseux, D., Zhang, W. W. and Brasselet, E. (2009) 'Laser microfluidics: fluid actuation by light' *J. Opt. A*, **11**, 034015.

Dholakia, K., MacDonald, M. and Spalding, G. (2002) 'Optical tweezers: the next generation' *Phys. World*, **15**, 31–35.

Dixit, S. S., Kim, H., Vasilyev, A., Eid, A. and Faris, G. W. (2010) 'Light driven formation and rupture of droplet bilayers' *Langmuir*, **26**, 6193–6200.

Du, J.-R., Juang, Y.-J., Wu, J.-T. and Wei, H.-H. (2008) 'Long-range and superfast trapping of DNA molecules in an ac electrokinetic funnel' *Biomicrofluidics*, **2**, 044103.

Eckart, C. (1948) 'Vortices and streams caused by sound waves' *Phys. Rev*., **73**, 68–76.

Eijel, J. C. T., Dalton, C., Hayden, C. J., Burt, J. P. H. and Manz, A. (2003) 'A circular AC magnetohydrodynamic micropump for chromatographic applications' *Sens. Actuat. B:Chem.*, **92**, 215–221.

Fainman, Y., Lee, L., Psaltis, D. and Yang, C. (2010) *Optofluidics: Fundamentals, Devices, and Applications* (McGraw-Hill, New York).

Footz, T., Somerville, M. J., Tomaszewski, R., Elyas, B. and Backhouse. C. J. (2004) 'Integration of combined heteroduplex/restriction fragment length polymorphism analysis on an electrophoresis microchip for the detection of hereditary haemochromatosis' *Analyst*, **129**, 25–31.

Franke, T., Abate, A. R., Weitz, D. A. and Wixforth, A. (2009) 'Surface acoustic wave (SAW) directed droplet flow in microfluidics for PDMS devices' *Lab Chip*, **9**, 2625–2627.

Franke, T., Braunmüller, S., Schmid, L., Wixforth, A. and Weitz, D.A. (2010) 'Surface acoustic wave actuated cell sorting (SAWACS)' *Lab Chip*, **10**, 789–794.

Friend, J. R. and Yeo, L. Y. (2011) 'Microscale acoustofluidics: microfluidics driven via acoustics and ultrasonics' *Rev. Mod. Phys*., **83**, 647–704.

Friend, J. R., Yeo, L. Y., Arifin, D. R. and Mechler, A. (2008) 'Evaporative self-assembly assisted synthesis of polymer nanoparticles by surface acoustic wave atomization' *Nanotechnology*, **19**, 145301.

Gagnon, Z. and Chang, H.-C. (2005) 'Aligning fast alternating current electroosmotic flow fields and characteristic frequencies with dielectrophoretic traps to achieve rapid bacteria detection' *Electrophoresis*, **26**, 3725–3737.

Gagnon, Z., Senapati, S., Gordon, J. and Chang H.-C. (2009) 'Dielectrophoretic detection and quantification of hybridized DNA molecules on nano-genetic particles' *Electrophoresis* **29**, 4808–4812.

Gervais, L. and Delamarche, E. (2009) 'Toward one-step point-of-care immunodiagnostics using capillary-driven microfluidics and PDMS substrates' *Lab Chip*, **9**, 3330–3337.

Glass, N. R., Shilton, R. J., Chan, P. P. Y., Friend, J. R. and Yeo, L. Y. (2012) 'Miniaturized Lab-on-a-Disc (miniLOAD)' *Small*, **8**, 1881–1888.

González, A., Ramos, A., Green, N. G., Castellanos, A. and Morgan H. (2000) 'Fluid flow induced by nonuniform ac electric fields in electrolytes on microelectrodes. II. A linear double-layer analysis' *Phys. Rev. E*, **61**, 4019–4028.

Gorkin, III R. Clime, L. Madou, M. and Kido, H. (2010) 'Pneumatic pumping in centrifugal microfluidic platforms' *Microfluid. Nanofluid*., **9**, 541–549.

Green, N. G. and Morgan, H. (1999) 'Dielectrophoresis of submicrometer latex spheres. 1. Experimental results' *J. Phys. Chem. B*, **103**, 41–50.

Grier, D. G. (1997) 'Optical tweezers in colloid and interface science' *Curr. Op. Colloid Interface Sci*., **2**, 264–270.

Grigoriev, R. O. (2005) 'Optical tweezers in colloid and interface science' *Phys. Fluids*, **17**, 033601.

Grover, W. H., Ivester, R. H. C., Jensen, E. C. and Mathies, R. A. (2006) 'Development and multiplexed control of latching pneumatic valves using microfluidic logical structures' *Lab Chip*, **6**, 623–631.

Harris, N. R, Hill, M., Townsend, R., White, N. M. and. Beeby S. P. (2005) 'Performance of a micro-engineered ultrasonic particle manipulator' *Sens. Actuators B: Chemical*, **111**, 481–486.

Hart, S. J. and Terray, A. V. (2003) 'Refractive-index-driven separation of colloidal polymer particles using optical chromatography' *Appl. Phys. Lett*., **83**, 5316–5318.

Hart, S. J., Terray, A., Arnold, J. and Leski, T. A. (2007) 'Sample concentration using optical chromatography' *Opt. Express*, **15**, 2724–2731.

Hashmi, A., Yua, G., Reilly-Collette, M., Heiman, G. and Xu, J. (2012) 'Oscillating bubbles: a versatile tool for lab on a chip applications' *Lab Chip*, **12**, 4216–4227, DOI: 10.1039/C2LC40424A.

Hawkes, J. J. and Coakley, W. T. (2001) 'Force field particle filter, combining ultrasound standing waves and laminar flow' *Sens. Actuat. B: Chem.*, **75**, 213–222.

Heron, S. R., Wilson, R., Shaffer, S. A., Goodlett, D. R. and Cooper, J. M. (2010) 'Surface acoustic wave nebulization of peptides as a microfluidic interface for mass spectrometry' *Anal. Chem*., **82**, 3985–3989.

Herr, A. E., Molho, J. I., Santiago, J. G., Mungal, M. G., Kenny, T. W. and Garguilo, M. G. (2000) 'Electroosmotic capillary flow with nonuniform zeta potential' *Anal. Chem*., **72**, 1053–1057.

Ho, J., Tan, M. K., Go, D., Yeo, L. Y., Friend, J. R. and Chang, H.-C. (2011) 'A paper-based microfluidic surface acoustic wave sample delivery and ionization source for rapid and sensitive ambient mass spectrometry' *Anal. Chem*., **83**, 3260–3266.

Hodgson, R. P., Tan, M., Yeo, L. Y. and Friend, J. R. (2009) 'Transmitting high power RF acoustic radiation via fluid couplants into superstrates for microfluidics' *Appl. Phys. Lett*., **94**, 024102.

Hunter, R. J. (1987) *Foundations of Colloid Science*, Vol. 1 (Oxford University, Oxford).

Ichikawa, N., Hosokawa, K. and Maeda, R. (2004) 'Interface motion of capillary-driven flow in rectangular microchannel' *J. Colloid Interface Sci*., **280**, 155–164.

Jang, J. and Lee, S. S. (2000) 'Theoretical and experimental study of MHD (magneto-hydrodynamic) micropump' *Sens. Actuators A: Phys*., **80**, 84–85.

Jang, L. S., Li Y. J., Lin S. J., Hsu, Y. C., Yao, W. S., Tsai, M. C. and Hou, C. C. (2007) 'A stand-alone peristaltic micropump based on piezoelectric actuation' *Biomed. Microdev*., **9**, 185–194.

Jeong, O. K. and Yang, S. S. (2000) 'Fabrication and test of a thermopneumatic micropump with a corrugated *p*+ diaphragm' *Sens. Actuators A: Physical*, **83**, 249–255.

Johansson, L., Enlund, J., Johansson, S., Katardjiev, I., Wiklund, M. and Yantchev, V. (2012) 'Surface acoustic wave-induced precise particle manipulation in a trapezoidal glass microfluidic channel' *J. Micromech. Microeng*., **22**, 025018.

Johnson, D. A. and Feke D. L. (1995) 'Methodology for fractionating suspended particles using ultrasonic standing wave and divided flow fields' *Sep. Tech*., **5**, 251–258.

Kenyon, S. M., Meighan, M. M. and Haye, M. A., (2011) 'Recent developments in electrophoretic separations on microfluidic devices' *Electrophoresis*, **32**, 482–93.

Kim, J.-H, Na, K.-H., Kang, C. J. and Kim, Y.-S. (2005) 'A disposable thermopneumatic-actuated micropump stacked with PDMS layers and ITO-coated glass' *Sens Actuators A: Physical*, **120**, 365–369.

Koch, M., Harris, N., Evans, A. G. R., White, N. M. and Brunnschweiler, A. (1998) 'A novel micromachined pump based on thick-film piezoelectric actuation' *Sens. Actuators A*, **70**, 98–103.

Kulkarni, K. P., Friend, J. R., Yeo, L. Y. and Perlmutter, P. (2009) 'Surface acoustic waves as an energy source for drop scale synthetic chemistry' *Lab Chip*, **9**, 754–755.

Kulkarni, K. P., Ramarathinam, S. H., Friend, J. R., Yeo, L. Y., Purcell, A. W. and Perlmutter, P. (2010) 'Rapid microscale in-gel processing and digestion of proteins using surface acoustic waves' *Lab Chip*, **10**, 1518–1520.

Langelier, S. M., Yeo, L. Y. and Friend, J. R. (2012) 'UV epoxy bonding for enhanced SAW transmission and microscale acoustofluidic integration' *Lab Chip*, **12**, 2970–2976.

Lastochkin, D., Zhou, R., Wang, P., Ben, Y. and Chang, H.-C. (2004) 'Electrokinetic micropump and micromixer design based on ac Faradaic polarisation' *J. Appl. Phys*., **96**, 1730–1733.

Laurell, T., Petersson, F. and Nilsson A. (2007) 'Chip integrated strategies for acoustic separation and manipulation of cells and particles' *Chem. Soc. Rev*., **36**, 492–506.

Lazar, I. M. and Karger, B. L. (2002) 'Multiple open-channel electroosmotic pumping system for microfluidic sample handling' *Anal. Chem*., **74**, 6259–6268.

Lemoff, A. V. and Lee, A. P. (2000) 'An AC magnetohydrodynamic micropump' *Sens. Actuators B: Chemical*, **63**,178–185.

Li, H., Friend, J. R. and Yeo, L. Y. (2007b) 'Surface acoustic wave concentration of particle and bioparticle suspensions' *Biomed. Microdev*., **9**, 647–656.

Li, H., Friend, J. R. and Yeo, L. Y. (2008) 'Microfluidic colloidal island formation and erasure induced by surface acoustic wave radiation' *Phys. Rev. Lett*., **101**, 084502.

Li, H., Friend, J. R. and Yeo, L. Y. (2007a) 'A scaffold cell seeding method driven by surface acoustic waves' *Biomaterials*, **28**, 4098–4104.

Li, Y., Fu, Y. Q., Brodie, S. D., Alghane, M. and Walton A. J. (2012) 'Integrated microfluidics system using surface acoustic wave and electrowetting on dielectrics technology' *Biomicrofluidics*, **6**, 012812.

Lighthill, J. (1978) 'Acoustic streaming' *J. Sound Vib*., **61**, 391–418.

Lin, H.-Y., Tsai, L.-C., Chi, P.-Y. and Chen, C.-D. (2005) 'Positioning of extended individual DNA molecules on electrodes by non-uniform AC electric fields' *Nanotechnology*, **16**, 2738–2742.

Lin, H., Storey, B. D., Oddy, M. H., Chen, C.-H. and Santiago, J. G. (2004) 'Instability of electrokinetic microchannel flows with conductivity gradients' *Phys. Fluids*, **16**, 1922–1935.

Lin, S. C., Mao, X. and Huang T. J. (2012) 'Surface acoustic wave (SAW) acoustophoresis: now and beyond' *Lab Chip*, **12**, 2766–2770.

Liu, Y. and Lim, K. M. (2011) 'Particle separation in microfluidics using a switching ultrasonic field' *Lab Chip*, **11**, 3167–3173.

Luginbuhl, P., Collins, S. D., Racine, G., Gretillat, M. A., Rooij, N. F. D., Brooks, K. G. and Setter, N. (1997) 'Microfabricated lamb wave device based on PZT Sol–gel thin film for mechanical transport of solid particles and liquids' *J. Microelectromech. Sys*., **6**, 337–345.

Machauf, A., Nemirovsky, Y. and Dinnar, U. (2005) 'A membrane micropump electrostatically actuated across the working fluid' *J. Micromech. Microeng*., **15**, 2309–2316.

Madou, M., Zoval, J., Jia, G., Kido, H., Kim, J. and Kim, N. (2006) 'Lab on a CD' *Annu. Rev. Biomed. Eng*., **8**, 601–628.

Manneberg, O., Hagsäter, M. S., Svennebring, J., Hertz H. M., Kutter J. P., Bruus, H. and Wiklund, M. (2009) 'Spatial confinement of ultrasonic force fields in microfluidic channels' *Ultrasonics*, **49**, 112–119.

Manor, O., Dentry, M., Friend, J. R. and Yeo, L. Y. (2011) 'Substrate dependent drop deformation and wetting under high frequency vibration' *Soft Matter*, **7**, 7976–7979.

Manor, Yeo, L. Y. and Friend, J. R. (2012) 'The appearance of boundary layers and drift flows due to high-frequency surface waves' *J. Fluid Mech*., **707**, 482–495.

Martinez, A. W., Phillips, S. T. and Whitesides, G. M. (2010) 'Diagnostics for the developing world: microfluidic paper-based analytical devices' *Anal. Chem*., **82**, 3–10.

Masini, L., Cecchini, M., Girardo, S., Cingolani, R., Pisignano, D. and Beltram, F. (2010) 'Surface-acoustic-wave counterflow micropumps for on-chip liquid motion control in two-dimensional microchannel arrays' *Lab Chip*, **10**, 1997–2000.

Meagher, R. J., Won, J. I., McCormick, L. C., Nedelcu, S., Bertrand, M. M., Bertram, J. L., Drouin, G., Barron, A. E. and Slater, G. W. (2005) 'End-labeled free-solution electrophoresis of DNA' *Electrophoresis*, **26**, 331–50.

Menachery, A., Graham D., Messerli, S. M., and Pethig, R. and Smith, P. J. S. (2011) 'Dielectrophoretic tweezer for isolating and manipulating target cells' *IET Nanobiotechnol*., **5**,1–7.

Meng, A. H., Nguyen, N.-T. and White, R. M. (2000) 'Focused flow micropump using ultrasonic flexural plate waves' *Biomed. Microdev*., **2**, 169–174.

Meng, L., Cai, F., Zhang, Z., Niu, L., Jin, Q., Yan, F., Wu, J., Wang, Z. and Zheng, H. (2011) 'Transportation of single cell and microbubbles by phase-shift introduced to standing leaky surface acoustic waves' *Biomicrofluidics*, **5**, 044104.

Minerick, A. R., Ostafin A. E. and Chang, H.-C. (2002) 'Electrokinetic transport of red blood cells in microcapillaries' *Electrophoresis*, **23**, 2165–2173.

Moroney, R. M., White, R. M. and Howe R. T. (1991) 'Microtransport induced by ultrasonic Lamb waves' *Appl. Phys. Lett*., **59**, 774–776.

Mugele, F. and Baret, J.-C. (2005) 'Electrowetting: from basics to applications' *J. Phys.: Condens. Matter*, **17**, R705–R774.

Mukhopadhyay, R. (2006) 'What does nanofluidics have to offer?' *Anal. Chem*., **78**, 7379–7382.

Nam, J., Lim, H., Kim, C., Kang, J. Y. and Shin, S. (2012) 'Density-dependent separation of encapsulated cells in a microfluidic channel by using a standing surface acoustic wave' *Biomicrofluidics*, **6**, 024120.

Napoli, M., Eijkel, J. C. and Pennathur, S. (2010) 'Nanofluidic technology for biomolecule applications: a critical review' *Lab Chip*, **10**, 957–85.

Natraj, V. and Chen, S. B. (2002) 'Primary electroviscous effect in a suspension of charged porous spheres' *J. Colloid Interface Sci*., **251**, 200–207.

Neale, S. L., Macdonald, M. P., Dholakia, K., and Krauss, T. F. (2005) 'All-optical control of microfluidic components using form birefringence' *Nat. Mater*., **4**, 53–533.

Ng, W. Y., Lam, Y. C. and Rodríguez, I. (2009) 'Experimental verification of Faradaic charging in ac electrokinetics' *Biomicrofluidics*, **3**, 022405.

Noblin, X., Buguin, A. and Brochard-Wyart, F. (2004) 'Vibrated sessile drops: transition between pinned and mobile contact line oscillations' *Eur. Phys. J. E*, **14**, 395–404.

Nyborg, W. L. (1958) 'Acoustic streaming near a boundary' *J. Acoust. Soc. Am*., **30**, 329–339.

Ohl, C.-D., Arora, M., Ikink, R., Jong, N. D. Versluis, M., Delius, M. and Lohse, D. (2006) 'Sonoporation from jetting cavitation bubbles' *Biophys. J*., **91**, 4285–4295.

Orloff, N. D., Dennis, J. R., Cecchini, M., Schonbrun, E., Rocas, E., Wang, Y., Novotny, D., Simmonds, R. W., Moreland, J., Takeuchi, I. and Booth, J. C. (2011) 'Manipulating particle trajectories with phase-control in surface acoustic wave microfluidics' *Biomicrofluidics*, **5**, 044107.

Paegel B. M., Emrich, C. A., Wedemayer, G. J., Scherer, J. R. and Mathies, R. A. (2002) 'High throughput DNA sequencing with a microfabricated 96-lane capillary array electrophoresis bioprocessor' *Proc. Natl. Acad. Sci. USA*, **99**, 574–579.

Pan, Y.-J., Ren, C.-M. and Yang, R.-J. (2007) 'Electrokinetic flow focusing and valveless switching integrated with electrokinetic instability for mixing enhancement' *J. Micromech. Microeng*., **17**, 820–827.

Patel, M. V.,Tovar, A. R. and Lee, A. P. (2012) 'Lateral cavity acoustic transducer as an on-chip cell/particle microfluidic switch' *Lab Chip*, **12**, 139–145.

Petersson, F., Nilsson, A., Holm, C., Jönsson, H. and Laurell, T. (2004) 'Separation of lipids from blood utilizing ultrasonic standing waves in microfluidic channels' *Analyst*, **129**, 938–943.

Pethig, R. (2010) 'Dielectrophoresis: status of the theory, technology, and applications' *Biomicrofluidics*, **4**, 022811.

Petsev, D. N. (2010) 'Transport in fluidic nanochannels' *Surfactant Sci. Ser*., **147**, 221–247.

Piruska, A., Gong, M., Sweedler, J. V. and Bohn, P. W. (2010) 'Nanofluidics in chemical analysis' *Chem. Soc. Rev*., **39**, 1060–1072.

Pol, F. C. M., Lintel, H. T. G., Elwenspoek, M. and Fluitman, J. H. J. (1990) 'A thermopneumatic micropump based on micro-engineering techniques' *Sens. Actuators A: Physical*, **21**, 198–202.

Qi, A., Chan, P., Ho, J., Rajapaksa, A., Friend, J. R. and Yeo, L. Y. (2011) 'Template-free synthesis and encapsulation technique for layer-by-layer polymer nanocarrier fabrication' *ACS Nano*, **5**, 9583–9591.

Qi, A., Friend, J.R., Yeo, L. Y., Morton, D.A., McIntosh, M. P. and Spiccia, L. (2009) 'Miniature inhalation therapy platform using surface acoustic wave microfluidic atomization' *Lab Chip*, **9**, 2184–2193.

Qi, A., Yeo, L. Y. and Friend J. R. (2008) 'Interfacial destabilization and atomization driven by surface acoustic waves' *Phys. Fluids*, **20**, 074103.

Qi, A., Yeo. L.Y., Friend, J. R. and Ho, J. (2010) 'The extraction of liquid, protein molecules and yeast cells from paper through surface acoustic wave atomization' *Lab Chip*, **10**, 470–476.

Qiao, R. and Aluru, N. R. (2003) 'Ion concentrations and velocity profiles in nanochannel electroosmotic flows' *J. Chem. Phys*., **118**, 4692–4701.

Ramos, A., González, A., Castellanos, A., Green, N. G. and Morgan, H. (2003) 'Pumping of liquids with ac voltages applied to asymmetric pairs of microelectrodes' *Phys. Rev. E*, **67**, 0563.

Rauscher, M. and Dietrich, S. (2008) 'Wetting phenomena in nanofluidics' *Annu. Rev. Mater. Res*., **38**, 143–172.

Rayleigh, L. (1884) 'On the circulation of air observed in Kundt's tubes and on some allied acoustical problems' *Phil. Trans. R. Soc. Lond*., **175**, 1–21.

Renaudin, A., Tabourier, P., Zhang, V., Camart, J. C. and Druon, C. (2006) 'SAW nanopump for handling droplets in view of biological applications' *Sens. Actuators B: Chemical*, **113**, 389–397.

Rezk, A. R., Manor, O., Friend, J. R. and Yeo, L. Y. (2012a) 'Acoustowetting: film spreading, fingering instabilities and soliton-like wave propagation', *Nat. Commun*., **3**, 1167.

Rezk, A. R., Qi, A., Friend, J. R., Li, W. H. and Yeo, L. Y. (2012b) 'Uniform mixing in paper-based microfluidic systems using surface acoustic waves' *Lab Chip*, 12, 773–779.

Robinson, T. and Dittrich, P. S. (2013) 'Microfluidic technology for molecular diagnostics' *Adv. Biochem. Eng. Biotechnol*., **133**, 89–114, DOI: 10.1007/10_2012_139.

Rogers, P. R., Friend, J. R. and Yeo, L. Y. (2010) 'Exploitation of surface acoustic waves to drive size-dependent microparticle concentration within a droplet' *Lab Chip*, **10**, 2979–2985.

Schabmueller, C. G. J., Koch, M., Mokhtari, M. E., Evans, A. G. R., Brunnschweiler, A. and Sehr, H. (2002) 'Self-aligning gas/liquid micropump' *J. Micromech. Microeng.*, **12**, 420–424.

Schlichting, H. (1932) 'Calculation of even periodic barrier currents' *Physik. Z.*, **33**, 327–335.

Schmid, L., Wixforth, A., Weitz, D. A. and Franke, T. (2012) 'Novel surface acoustic wave (SAW)-driven closed PDMS flow chamber' *Microfluid. Nanofluid.*, **12**, 229–235.

Schneider, S. W., Nuschele, S., Wixforth, A., Gorzelanny, C., Alexander-Katz, A., Netz, R. R. and Schneider, M. F. (2007) 'Shear-induced unfolding triggers adhesion of von Willebrand factor fibers' *Proc. Natl. Acad. Sci. USA*, **104**, 7899–7903.

Schoch, R. B., Han, J. and Renaud, P. (2008) 'Transport phenomena in nanofluidics' *Rev. Mod. Phys.*, **80**, 839–883.

Shi, J., Ahmed, D., Mao, X., Lin, S. C. S., Lawit, A. and Huang, T. J. (2009) 'Acoustic tweezers: patterning cells and microparticles using standing surface acoustic waves (SSAW)' *Lab. Chip*, ***9***, 2890–2895.

Shi, J., Mao, X., Ahmed, D., Colletti, A. and Huang, T. J. (2008) 'Focusing microparticles in a microfluidic channel with standing surface acoustic waves (SSAW)' *Lab Chip*, **8**, 221–223.

Shilton, R. J., Yeo, L. Y. and Friend, J. R. (2011) 'Quantification of surface acoustic wave induced chaotic mixing-flows in microfluidic wells' *Sens. Actuators B: Chemical*, **160**, 1565–1572.

Shilton, R., Tan M. K., Yeo, L. Y. and Friend, J. R. (2008) 'Particle concentration and mixing in microdrops driven by focused surface acoustic waves' *J. Appl. Phys.*, **104**, 014910.

Shubin, V. E., Hunter, R. J. and O'Brien, R. W. (1993) 'Electroacoustic and dielectric study of surface conduction' *J. Colloid Interface Sci.*, **159**, 174–183.

Sparreboom, W., van den Berg, A. and. Eijkel, J. C. T. (2009) 'Principles and applications of nanofluidic transport' *Nat. Nanotechnol.*, **4**, 713–720.

Squires, T. M. and Bazant, M. A. (2004) 'Induced-charge electro-osmosis' *J. Fluid Mech.*, **509**, 217–252.

Squires, T. M. and Quake, S. R. (2005) 'Microfluidics: fluid physics at the nanoliter scale' *Rev. Mod. Phys.*, **77**, 977–1026.

Stern, O. (1924) 'The theory of electrical double layer' *Z. Elektrochem.*, **30**, 508–516.

Suzuki, H. and Yoneyama, R. (2002) 'A reversible electrochemical nanosyringe pump and some considerations to realize low power consumption' *Sens. Actuators B*, **86**, 242–250.

Szántai, E. and Guttman, A. (2006) 'Genotyping with microfluidic devices' *Electrophoresis*, **27**, 4896–4903.

Takamura, Y., Onoda, H., Inokuchi, H., Adachi, S., Oki, A. and Horiike, Y. (2003) 'Low-voltage electroosmosis pump for stand-alone microfluidics devices' *Electrophoresis*, **24**, 185–192.

Tan, M. K., Friend, J. R. and Yeo, L. Y. (2007) 'Microparticle collection and concentration via a miniature surface acoustic wave device' *Lab Chip*, **7**, 618–625.

Tan, M. K., Yeo, L. Y. and Friend, J. R. (2009b) 'Interfacial jetting phenomena induced by focused surface vibrations' *Phys. Rev. Lett.*, **103**, 024501.

Tan, M. K., Yeo, L. Y. and Friend, J. R. (2010) 'Unique flow transitions and particle collection switching phenomena in a microchannel induced by surface acoustic waves' *Appl. Phys. Lett*., **97**, 234106.

Tan, M. K., Yeo, L. Y. and Friend, J. R. (2009a) 'Rapid fluid flow and mixing induced in microchannels using surface acoustic waves' *Europhys. Lett*., **87**, 47003.

Tovar, A. R. and Lee, A. P. (2009) 'Lateral cavity acoustic transducer' *Lab Chip*, **9**, 41–43.

Vyawahare, S., Sitaula, S., Martin, S., Adalianb, D. and Scherer, A. (2008) 'Electronic control of elastomeric microfluidic circuits with shape memory actuators' *Lab Chip*, **8**, 1530–1535.

Wang, C., Jalikop, S. V. and Hilgenfeldt, S. (2012) 'Efficient manipulation of microparticles in bubble streaming flows' *Biomicrofluidics*, **6**, 012801.

Wang, P., Chen, Z. and Chang, H.-C. (2006) 'A new electro-osmotic pump based on silica monoliths' *Sens. Actuators B: Chemical*, **113**, 500–509.

Wang, X., Wang, S., Gendhar, B., Cheng, C., Byun, C. K., Li, G, Zhao, M. and Liu, S. (2009) 'Electroosmotic pumps for microflow analysis' *Trends Anal. Chem*., **28**, 64–74.

Wheeler, A. R. (2008) 'Putting electrowetting to work' *Science*, **322**, 539–540.

Wixforth, A., Strobl, C., Gauer, C. H., Toegl, A., Scriba, J. and Guttenberg, Z. V. (2004) 'Acoustic manipulation of small droplets' *Anal. Bioanal. Chem*., **379**, 982–991.

Wu, D., Qin, J. and Lin, B. (2008) 'Electrophoretic separations on microfluidic chips' *J. Chromatogr. A*, **1184**, 542–559.

Xu, D., Wang, L., Ding, G., Zhou, Y., Yu, A. and Cai, B. (2001) 'Characteristics and fabrication of NiTi/Si diaphragm micropump' *Sens. Actuators A: Physical*, **93**, 87–92.

Yaralioglu, G. G., Wygant, I. O., Marentis, T. C. and Khuri-Yakub, B. T. (2004) 'Ultrasonic mixing in microfluidic channels using integrated transducers' *Anal. Chem*., **76**, 3694–3698.

Yeo, L. Y. and Chang, H.-C. (2005) 'Static and spontaneous electrowetting' *Mod. Phys. Lett. B*, **19**, 549–569.

Yeo, L. Y., Chang, H.-C., Chan, P. P. Y. and Friend, J. R. (2011) 'Microfluidic devices for bioapplications' *Small*, **7**, 12–48.

Yeo, L.Y. and Friend, J. R. (2009). 'Ultrafast microfluidics using surface acoustic waves', *Biomicrofluidics* **3**, 012002.

Yin, Z. and Prosperetti, A. (2005) 'A microfluidic 'blinking bubble' pump' *J. Micromech. Microeng*., **15**, 643–651.

Yoshimi, Y., Shinoda, K., Mishima, M., Nakao, K. and Munekane, K. (2004) 'Development of an artificial synapse using an electrochemical micropump' *J. Artif. Organs*, **7**, 210–215.

Zhou, Y. and Amirouche, F. (2011) 'An electromagnetically-actuated all-PDMS valveless micropump for drug delivery' *Micromachines*, **2**, 345–355.

Zhou, K., Perry, J. M. and Jacobson, S. C. (2011). 'Transport and sensing in nanofluidic devices' *Annu. Rev. Anal. Chem*., **4**, 321–341.

4

Digital microfluidics technologies for biomedical devices

C. M. COLLIER, J. NICHOLS and
J. F. HOLZMAN, The University of British Columbia, Canada

DOI: 10.1533/9780857097040.1.139

Abstract: Droplet-based digital microfluidics is a topic with growing relevance to biological, chemical, and health-science fields. The high precision and excellent reagent economy of such systems are unparalleled. There are, however, fundamental challenges related to actuation and sensing in terms of system scalability, and these challenges are addressed within this chapter. In particular, a new digital microfluidics multiplexer is shown to overcome contemporary on-chip microdrop motion addressability issues and eliminate droplet interference challenges. At the same time, an integrated folded-cavity optical sensor provides highly localized and sensitive probing of internal fluid refractive indices. The complete system offers improved microdrop motion and sensing capabilities for future lab-on-a-chip technologies.

Key words: biomedical applications, digital microfluidics, lab-on-a-chip, optical sensing.

4.1 Introduction

Microfluidic devices have received much attention in recent years (Au *et al*., 2011) and offer important practical advantages for laboratory analyses. Enhanced portability, improved sensitivity, high throughput, and significantly reduced power consumption are some of the many advantages of these microfluidic devices when controlling fluids down to a picoliter volumetric level. This intricate microfluidic control has supported general biotechnological processing in pharmaceutical (Welch *et al*., 2006) and clinical (Li *et al*., 2010) settings. The demand for such microfluidic systems has been even greater, however, in biomedical research settings, with numerous technologies now benefiting from the superior analytical capabilities of microfluidics – including, for example, enzymatic analyses (Miyazaki *et al*., 2008), DNA analyses (Humphreys *et al*., 2009), proteomics (Lee *et al*., 2009), and even bio-analytical mass spectrometry (Figeys *et al*., 1998). At the core of all of these applications lie two fundamental microfluidic operations, microdrop

motion and sensing, and the further development of microfluidic systems must carefully consider the scalability of these important microdrop motion and sensing processes.

The contemporary approach for microfluidic microdrop motion makes use of continuous-flow architectures with in-line, one-dimensional (1-D) flow channels. The simplicity of these 1-D fluid flow systems supports standard device fabrication through wet-etching and micromilling processes (Becker and Locascio, 2002). The capabilities of these 1-D microfluidic devices have been tremendous, and perhaps the greatest results have been witnessed for fluid control applications demanding filtering (Zhu *et al.*, 2004) and/or mixing (Wiggins and Ottino, 2004). A fundamental challenge does become apparent, however, from the practical use of 1-D flow channels. Fluid flow through the constrained 1-D flow channels is prone to clogs and blockages, and such failures can be catastrophic to operation. Permanent 1-D flow architectures offer few opportunities to reroute or adapt by way of reconfigurability or fault control.

If one wishes to introduce increased fluid control, a natural extension would involve the use of a two-dimensional (2-D) microfluidic architecture. Microdrop motion in a 2-D plane offers greater possibilities for adaptations via a real-time fault control, as well as increased opportunities for parallel on-chip microdrop mixing/splitting algorithms in bio/chemical reactors. It is with this 2-D vision in mind that the field of digital microfluidics has emerged (Fair, 2007). A digital microfluidic architecture employs a generalized microdrop motion platform with the potential for microdrop motion in a 2-D plane. (This digital microfluidics technology should not be confused with continuous-flow microfluidic systems with submerged microdrops being carried in a 1-D flow channel (Huebner *et al.*, 2008; Song *et al.*, 2006).) In digital microfluidics, microdrop motion is not pressure-based, thus it is not necessary to restrict motion to 1-D flow channels. Instead, microdrop motion is achieved by localized voltage signals throughout the 2-D plane. User-controlled voltage distributions are applied to carry out fluid processing tasks with adaptations provided by way of voltage signals. Real-time adaptations can therefore come about for path planning and fault control (in stark contrast to the 1-D constraints of continuous-flow microfluidic systems). Such reconfigurable operation can be carried out with especially low fluid volumes and high sensitivities. Moreover, the 2-D format of this generalized digital architecture can be adapted via voltage-control software for highly-parallel operation, with reaction-based microdrop mixing, splitting, routing, etc. being carried out simultaneously at multiple on-chip locations. Such digital microfluidic implementations are now being applied to immunoassays (Alphonsus *et al.*, 2010), DNA ligations (which are very sensitive to reagent economy) (Liu *et al.*, 2008), and DNA pyrosequencing (Fair *et al.*, 2007). The low fluid volumes, high sensitivities, and parallel operation of

2-D digital microfluidic systems can together meet growing demands for high throughput on-chip analyses. At the same time, the need to work with larger fluid volumes can be met with digital microfluidic microdrop generation/extraction from adjacent on-chip reservoirs. Details for such splitting algorithms can be found in Cho *et al*. (2003), Elvira *et al*. (2012), and Ren *et al*. (2004).

A primary issue in any 2-D digital microfluidics design is microdrop motion scalability. Microdrop motion is dynamic and demands appropriate time synchronization and voltage localization from many system inputs to induce interfacial surface tension changes and microdrop motion (Dolatabadi *et al*., 2006). This is especially challenging in devices that are being scaled for use with increasing numbers of system inputs and finer and finer spatial resolutions. The contemporary approach for digital microfluidic microdrop motion has used a voltage-activated 2-D square electrode grid with M rows and N columns, but such a structure becomes grossly impractical for highly-parallel operation (requiring a tremendous number, $M \times N$, of independent input electrical address lines to control all $M \times N$ square electrode grid locations). For this reason, such structures have been restricted to grid sizes on the order of 5×5 grid (Davids *et al*., 2006). With these electrical addressability issues in mind, our work on digital microfluidic multiplexing has eased these electrical addressability and control constraints (Collier *et al*., 2011) and is introduced in this work as a bi-layered electrode structure with upper row and lower column electrodes. Differential voltages, with values biased about the microdrop motion threshold voltage, are shown to establish microdrop motion at all $M \times N$ gridpoints with only $M + N$ electrical inputs. This technique overcomes the ubiquitous microdrop interference effect (Xu and Chakrabarty, 2008) and operates at an input voltage, 0.64 V_{rms} (root-mean-squared volts) (Nichols *et al*., 2012), that is well within the 5 V maximum for future CMOS/TTL lab-on-a-chip systems (Li *et al*., 2008).

A second issue in 2-D digital microfluidics relates to fluid sensing scalability. Fluid sampling sensitivity is diminished when devices trend toward smaller scales with lower reagent volumes. Signal levels associated with standard optical imaging (Madou and Cubicciotti, 2003) and capacitance sensing (Ahmadi *et al*., 2010) scale down proportionally with the sampling area, and the associated on-chip analyses can have unacceptably low signal levels. With this in mind, it is desired to improve the sensing abilities of the localized sampling elements being integrated on the smaller and smaller dimensions of emerging digital microfluidics devices. A new concept for on-chip sensing is demonstrated in this work by way of a folded-cavity optical refractometry. An overhead microlens is integrated into the aforementioned digital microfluidic multiplexer to form a folded cavity with an especially sensitive relationship to internal fluid refractive indices. It is shown that the microoptical architecture can be tailored for on-chip optical sensing over

wide refractive index ranges with user-controlled sensitivities. The on-chip sensing technique is ultimately shown to facilitate effective fluid sensing for integration with future generations of digital microfluidic devices.

4.2 On-chip microdrop motion techniques

Digital microfluidic devices are often implemented as microdrop-based systems. Such systems use applied voltages to draw microdrops to prescribed locations across the chip. There are multiple implementations to bring about this microdrop motion and the generalized architectures are introduced here. The digital microfluidic multiplexer architecture is shown to be advantageous for microdrop motion scalability, and its relevant theory, fabrication, and results are presented in the following subsections.

4.2.1 Architectures

The greatest degree of freedom for on-chip microdrop motion can be achieved by implementing microdrop motion with a 2-D square electrode grid (Davids *et al.*, 2006). A voltage applied to an activated electrode in the $M \times N$ grid creates a localized electric field that attracts neighboring microdrops through an energy minimization process. The advantage of this 2-D square electrode grid is its simplicity – the $M \times N$ grid electrodes are activated by $M \times N$ independent voltage inputs for complete control of microdrops across the 2-D plane. The use of independent inputs for each grid location can, however, become a practical limitation. Large-scale $M \times N$ gridpoints, beyond roughly a 5×5 grid (Davids *et al.*, 2006), are difficult to implement in the on-chip 2-D plane without resorting to complex via-holes for out-of-plane access points. Each square electrode requires an individual electrical address line to be patterned onto the plane of the chip, without it crossing other electrodes or lines. The scalability challenges in such highly-parallel $M \times N$ gridpoints, with increasingly small electrode dimensions, can become unwieldy or even impossible.

The generalized square electrode grid architecture is shown in Fig. 4.1a, with two microdrops present on the 16×16 grid. If a user desires to move microdrop 1, but not microdrop 2, a sufficiently high voltage, V_0, can be applied to the address line for the electrode adjacent to microdrop 1. In Fig. 4.1a, this is shown with the darkened electrode. The voltage creates a strong electric field at this location to modify the local solid–liquid surface tension (Dolatabadi *et al.*, 2006) and ultimately pull the microdrop over the activated electrode. By carrying out this voltage-activation process through sequence of steps, multiple microdrops can be moved to various locations across the chip without interfering with adjacent and stationary microdrops. For the structure shown, 256 input signals must be routed throughout the

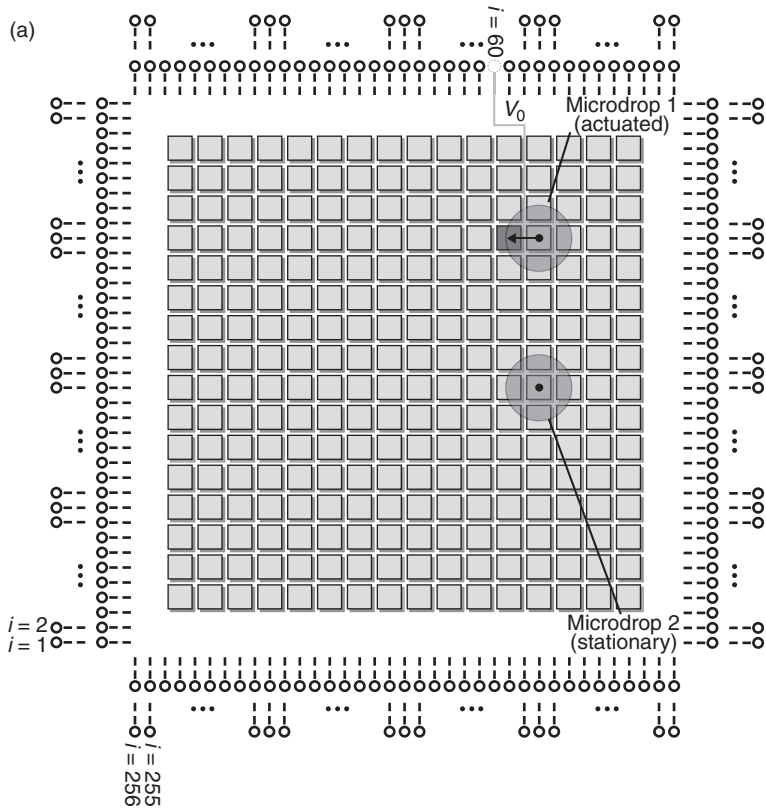

4.1 Digital microfluidic architectures are shown. In (a), the square electrode grid has a voltage applied to the left of microdrop1 ($i = 60$ electrode), and microdrop 1 is actuated while microdrop 2 is stationary. In (b), the cross-referenced grid has an above-threshold voltage ($V_0 >> V_{th}$) applied to the left of microdrops 1 and 2, and both microdrops actuate to the left. In (c), the multiplexer uses a voltage that is both smaller than the threshold voltage and larger than half the threshold voltage ($V_{th}/2 < V_0 < V_{th}$), and only microdrop 1 actuates to the left.

(Continued)

square electrode grid, and the required address lines for this can make the system design particularly challenging.

Given the above 2-D square electrode grid challenges, an interesting addressing solution has been demonstrated by way of the cross-referenced grid (Xu and Chakrabarty, 2008). The cross-referenced grid uses a bi-layered structure with voltages applied to perpendicular upper row and lower column linear electrodes. The beauty of such an implementation lies in the fact that each linear electrode acts as both the actuating electrode and its own address line. This dual-purpose allows the number of electrode inputs to be

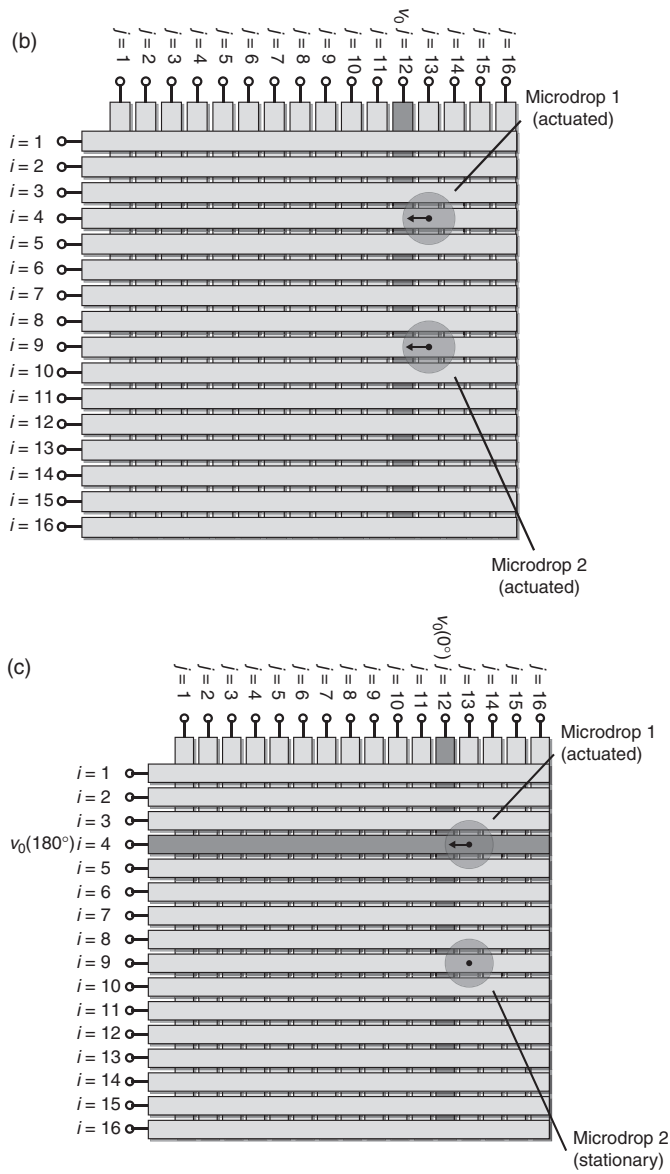

4.1 Continued

greatly reduced: only $M + N$ inputs are needed for actuating microdrops across the $M \times N$ grid. The cross-referenced grid does have a fundamental challenge, however, when used with multiple microdrops. When the desired actuating microdrop shares a row or column with neighboring microdrops, electrical activation of the row or column results in motion of

all the microdrops. This challenge is known as microdrop interference (Xu and Chakrabarty, 2008). Xiao *et al*. have proposed interesting solutions to this challenge by way of a microdrop router (Xiao and Young, 2010a) and Integer Linear Programming (Xiao and Young, 2010b). In addition, Xu and Chakrabarty (2008) have presented a microdrop mapping scheme according to the clique-partitioning graph theory problem. However, such techniques offer only algorithmic solutions to microdrop interference and undoubtedly increase the complexity of microdrop motion sequences of large-scale $M \times N$ grids with many microdrops being present.

The generalized cross-referenced structure is shown in Fig. 4.1b. Horizontal upper row electrodes are indexed with i, while vertical column electrodes are indexed with j. These electrodes are patterned onto the chip as upper and lower planes. In Fig. .1b, microdrop 1 is situated at $i = 4, j = 13$, while microdrop 2 is situated at $i = 8, j = 13$. Voltage activation is applied to the $j = 12$ column electrode, pulling both microdrop 1 *and* microdrop 2 to the left. Note that it is not possible to actuate microdrop 1 while keeping microdrop 2 stationary because of microdrop interference. Clearly, an alternative microdrop motion architecture is needed for systems operating with multiple microdrops.

Given the successes and challenges of the aforementioned microdrop motion techniques, the following work introduces a digital microfluidic multiplexer. Our previous work (Collier *et al*., 2011) has shown that the digital microfluidic multiplexer can provide complete and independent microdrop motion across a $M \times N$ grid along with the reduced $M + N$ input complexity of the cross-referenced structure. The multiplexer makes use of the nonlinear relationship between microdrop motion and the applied voltage, by way of a well-defined microdrop motion threshold voltage (Renaudot *et al*., 2011). The desired microdrop motion is brought about by the doubling of a differential voltage that appears between overlapped upper row and lower column electrodes having opposite voltage polarities. The system is biased such that only the doubled voltage in the overlapping region overcomes the microdrop motion threshold voltage to initiate microdrop motion. Neighboring microdrops experience voltages that are lower than the threshold voltage and do not undergo microdrop motion – thereby eliminating the microdrop interference challenge. Given a practical limit of 10 μm microdrop diameters and similarly sized electrode widths, one would expect that such a multiplexing technique can ultimately be scaled for use with 1000 + 1000 input lines controlling motion at 1000 × 1000 gridpoints in a 1 cm^2 chip.

The digital microfluidic multiplexer uses the same physical structure as the cross-referenced grid, but there are two important design differences in its operation: (i) the multiplexer operates in a nonlinear microdrop motion regime biased about a threshold voltage, and (ii) the multiplexer is driven by a bipolar voltage AC waveform having both positive and negative polarities.

Such a structure is shown in Fig. 4.1c. The microdrop motion is achieved using two voltage waveforms. A voltage of $+V_0$ is applied on the $i = 4$ upper row electrode while $-V_0$ is applied on the $j = 12$ lower column electrode, where the positive value V_0 is defined as the actuating voltage amplitude. A voltage difference of V_0 is created between upper and lower plates in all regions along the row and column electrodes *except* for the overlapped region, where the voltage difference is $2V_0$. By noting the threshold voltage, V_{th}, needed for microdrop motion, this localized $2V_0$ can be leveraged by selecting V_0 to be within the range $V_{th}/2 < V_0 < V_{th}$. Thus, microdrop motion only occurs within the overlapped region. Figure 4.1c shows that only microdrop 1 moves to the left while microdrop 2 remains stationary. Such a digital microfluidic multiplexer has only $M + N$ inputs but ultimately allows complete $M \times N$ microdrop control.

4.2.2 Multiplexer theory

To gain a thorough understanding on the digital microfluidic multiplexer implementation, it is necessary to establish the relationship between row and column input applied voltages and the desired 2-D microdrop motion. In this work, the *i*th upper row electrode receives an actuating voltage amplitude of V_0 and the state is represented by the row voltage matrix $[V_{row,i}]$. The spatial voltage distribution (normalized to V_0) is

$$\frac{[V_{row,i}]}{V_0} = \begin{bmatrix} 0 & 0 & 0 & 0 & 0 & \cdots & 0 \\ \vdots & \vdots & \vdots & \vdots & \vdots & \cdots & 0 \\ 0 & 0 & 0 & 0 & 0 & \cdots & 0 \\ 1 & 1 & 1 & 1 & 1 & \cdots & 1 \\ 0 & 0 & 0 & 0 & 0 & \cdots & 0 \\ \vdots & \vdots & \vdots & \vdots & \vdots & \cdots & \vdots \\ 0 & 0 & 0 & 0 & 0 & \cdots & 0 \end{bmatrix}. \quad [4.1]$$

The shown values of '1' along the *i*th row signify positive voltage activation. Similarly, the *j*th lower column electrode receives an actuating voltage amplitude of $-V_0$ and its state is represented by the column voltage matrix $[V_{column,j}]$. The spatial voltage distribution (normalized to $-V_0$) is

$$\frac{[V_{column,j}]}{-V_0} = \begin{bmatrix} 0 & \cdots & 0 & 1 & 0 & \cdots & 0 \\ 0 & \cdots & 0 & 1 & 0 & \cdots & 0 \\ 0 & \cdots & 0 & 1 & 0 & \cdots & 0 \\ 0 & \cdots & 0 & 1 & 0 & \cdots & 0 \\ 0 & \cdots & 0 & 1 & 0 & \cdots & 0 \\ \vdots & \cdots & \vdots & \vdots & \vdots & \cdots & \vdots \\ 0 & \cdots & 0 & 1 & 0 & \cdots & 0 \end{bmatrix}. \quad [4.2]$$

The shown values of '1' along the *j*th column signify negative voltage activation.

The motion that results from the input states of Equations [4.1] and [4.2] manifests itself through a surface-tension change – denoted here as the matrix $[\Delta\gamma_{ij}]$. There are two distinct forms for the surface-tension change in relation to input voltages. The first form for the surface-tension change and microdrop motion corresponds to a linear system, without a microdrop motion threshold. Surface-tension changes result from the existence of a nonzero value for either $[V_{\text{row}},i]/V_0$ or $[V_{\text{column}},j]/V_0$. This 'or' condition is critical to the device input–output characteristic and is represented here by the Boolean operator $\vee$ in the resulting surface-tension change:

$$\left[\Delta\gamma_{ij}\right] = \frac{\left[V_{\text{row},i}\right]}{V_0} \vee \frac{\left[V_{\text{column},j}\right]}{-V_0} = \begin{bmatrix} 0 & 0 & 0 & 0 & 0 & \cdot\cdot & 0 \\ \vdots & \vdots & \vdots & \vdots & \vdots & \cdot\cdot & 0 \\ 0 & 0 & 0 & \mathbf{0} & 0 & \cdot\cdot & 0 \\ 1 & 1 & 1 & 1 & 1 & \cdot\cdot & 1 \\ 0 & 0 & 0 & 0 & 0 & \cdot\cdot & 0 \\ \vdots & \vdots & \vdots & \vdots & \vdots & \cdot\cdot & \vdots \\ 0 & 0 & 0 & 0 & 0 & \cdot\cdot & 0 \end{bmatrix} \vee \begin{bmatrix} 0 & \cdot\cdot & \mathbf{0} & 1 & 0 & \cdot\cdot & 0 \\ 0 & \cdot\cdot & 0 & 1 & 0 & \cdot\cdot & 0 \\ 0 & \cdot\cdot & 0 & 1 & 0 & \cdot\cdot & 0 \\ 0 & \cdot\cdot & 0 & 1 & 0 & \cdot\cdot & 0 \\ 0 & \cdot\cdot & 0 & 1 & 0 & \cdot\cdot & 0 \\ \vdots & \cdot\cdot & \vdots & \vdots & \vdots & \cdot\cdot & \vdots \\ 0 & \cdot\cdot & 0 & 1 & 0 & \cdot\cdot & 0 \end{bmatrix}$$

$$= \begin{bmatrix} 0 & \cdot\cdot & 0 & 1 & 0 & \cdot\cdot & 0 \\ \vdots & \cdot\cdot & \vdots & \vdots & \vdots & \cdot\cdot & \vdots \\ 0 & \cdot\cdot & 0 & 1 & 0 & \cdot\cdot & 0 \\ 1 & \cdot\cdot & 1 & 1 & 1 & \cdot\cdot & 1 \\ 0 & \cdot\cdot & 0 & 1 & 0 & \cdot\cdot & 0 \\ \vdots & \cdot\cdot & \vdots & \vdots & \vdots & \cdot\cdot & \vdots \\ 0 & \cdot\cdot & 0 & 1 & 0 & \cdot\cdot & 0 \end{bmatrix}. \qquad [4.3]$$

Unfortunately, such a system shows potential for surface-tension changes over the full length of the *i* and *j* electrodes. This linear dependency and propensity for microdrop interference is a manifestation of the large applied voltages ($V_0 >> V_{\text{th}}$) that are typically used in cross-referenced architectures. When multiple microdrops are present, thoughtful path planning, routing, and scheduling (Ricketts *et al*., 2006; Yuh *et al*., 2008) must be used to prevent inadvertent motion of neighboring microdrops and to avoid microdrop interference.

The second manifestation for surface-tension changes and microdrop motion comes about through a nonlinear relationship between microdrop motion and applied inputs. In such a system, surface-tension changes are initiated from the simultaneous existence of nonzero values for both $[V_{\text{row}},i]/V_0$ and $[V_{\text{column}},j]/V_0$. This 'and' condition is critical to this response and is represented here by the Boolean operator ^ in the resulting surface-tension change for this nonlinear distribution:

$$\left[\Delta\gamma_{ij}\right] = \frac{\left[V_{\text{row},i}\right]}{V_0} \wedge \frac{\left[V_{\text{column},j}\right]}{-V_0} = \begin{bmatrix} 0 & 0 & 0 & 0 & 0 & \cdot\cdot & 0 \\ \vdots & \vdots & \vdots & \vdots & \vdots & \cdot\cdot & 0 \\ 0 & 0 & 0 & \mathbf{0} & 0 & \cdot\cdot & 0 \\ 1 & 1 & 1 & 1 & 1 & \cdot\cdot & 1 \\ 0 & 0 & 0 & 0 & 0 & \cdot\cdot & 0 \\ \vdots & \vdots & \vdots & \vdots & \vdots & \cdot\cdot & \vdots \\ 0 & 0 & 0 & 0 & 0 & \cdot\cdot & 0 \end{bmatrix} \wedge \begin{bmatrix} 0 & \cdot\cdot & \mathbf{0} & 1 & 0 & \cdot\cdot & 0 \\ 0 & \cdot\cdot & 0 & 1 & 0 & \cdot\cdot & 0 \\ 0 & \cdot\cdot & 0 & 1 & 0 & \cdot\cdot & 0 \\ 0 & \cdot\cdot & 0 & 1 & 0 & \cdot\cdot & 0 \\ 0 & \cdot\cdot & 0 & 1 & 0 & \cdot\cdot & 0 \\ \vdots & \cdot\cdot & \vdots & \vdots & \vdots & \cdot\cdot & \vdots \\ 0 & \cdot\cdot & 0 & 1 & 0 & \cdot\cdot & 0 \end{bmatrix}$$

$$= \begin{bmatrix} 0 & \cdot\cdot & 0 & 0 & 0 & \cdot\cdot & 0 \\ \vdots & \cdot\cdot & \vdots & \vdots & \vdots & \cdot\cdot & \vdots \\ 0 & \cdot\cdot & 0 & 0 & 0 & \cdot\cdot & 0 \\ 0 & \cdot\cdot & 0 & 1 & 0 & \cdot\cdot & 0 \\ 0 & \cdot\cdot & 0 & 0 & 0 & \cdot\cdot & 0 \\ \vdots & \cdot\cdot & \vdots & \vdots & \vdots & \cdot\cdot & \vdots \\ 0 & \cdot\cdot & 0 & 0 & 0 & \cdot\cdot & 0 \end{bmatrix}. \qquad [4.4]$$

The response in Equation [4.4] signifies the operation of the digital microfluidic multiplexer and its ability to offer complete $M \times N$ microdrop motion (one location at a time) with only $M + N$ inputs.

The condition for localized motion only in the overlapped region requires adherence to the $V_{th}/2 < V_0 < V_{th}$ relation – which sets the actuating voltage amplitude V_0 between upper and lower limits defined by the threshold voltage V_{th}. One can therefore design the system to have an appropriate operating voltage range by noting material dependencies for the threshold voltage by way of (Berthier, 2008; Ahmadi *et al.*, 2009)

$$V_{th} \approx 2\sqrt{\frac{\gamma\alpha\sin\theta_0}{c}}, \qquad [4.5]$$

where α is the hysteresis angle, γ is the microdrop liquid surface tension, θ_0 is the resting contact angle, and c is the capacitance per unit area (Berthier, 2008). If small threshold/operating voltages are desired, it is advantageous to minimize static friction forces and maximize capacitance per unit area. If rapid microdrop motion is desired, larger threshold/operating voltages can be used by maximizing static friction forces and minimizing capacitance per unit area. The following section will elaborate on these practical issues through digital microfluidic multiplexer design, fabrication, and implementation.

4.2.3 Multiplexer fabrication and results

A bipolar AC voltage waveform biasing scheme is ideal to facilitate operation of the digital microfluidic multiplexer. A positive-polarity voltage

waveform is applied to an upper row electrode with an opposite-polarity voltage waveform applied to a lower column electrode. Such a scheme has the lower-voltage benefits of AC biasing (compared to DC). Moreover, AC operation lends itself to implementations with voltage transformers. It is therefore possible to have a sufficiently high V_0 applied on-chip, while the device input voltages can be made low enough for operation with digital and CMOS/TTL integration below 5 V. (This voltage step-up advantage comes about from the highly-insulating dielectric layers on the chip, which minimize the current draw and power consumption.) For the digital microfluidic multiplexer, a center-tapped transformer is selected because it gives a large voltage increase (having a voltage gain that is equal to the turns ratio) with two opposite-polarity AC voltage waveform outputs (having equal amplitudes and a 180° phase difference).

A Hammond 117E4 center-tapped transformer is chosen for testing and demonstration of the device. This transformer receives a sinusoidal AC voltage waveform input, V_{in}, at a frequency of 470 Hz. At this frequency, the transformer has a voltage gain of 75. Two AC voltage waveforms of opposite polarity are extracted at the three-output center-tapped transformer and applied to the multiplexer with an electrode switching scheme. The device setup is shown in Fig. 4.2. The AC voltage waveform $V_0(0°)$ is applied by the *j*-phase electrode switch onto lower column electrodes, while the out-of-phase AC voltage waveform $V_0(180°)$ is applied by the *i*-phase electrode switch onto upper row electrodes. An overhead LEICA APOZ6 microscope and camera (not shown) capture the on-chip microdrop motion.

Testing is performed on a 16 × 16 digital microfluidic multiplexer with upper and lower plates separated by 1 mm. The plates initially consist of 1 mm thick silica with 50 nm thick copper films (layers of metal can be added to a silica substrate using sputtering processes) patterned as electrodes via ultraviolet (UV) photolithography – with spin-coating of positive photoresist (PHOTOPOSIT SP 24D) at 5000 RPM, a 60 min hard bake, 250 nm UV exposure, development, and a $FeCl_3$ isotropic wet-etch. The resulting multiplexer has electrodes with 600 μm center-to-center pitch and 550 μm width. The plates are then spin-coated at 5000 RPM with a 10 μm thick polydimethylsiloxane (PDMS) layer with a silicone elastomer curing-to-base ratio of 1:10. Finally, a thin Teflon layer is applied by way of a 2000 RPM spin-coat. The multiplexer grid is left with uniform and homogeneous layers of PDMS and Teflon. The inset of Fig. 4.2 shows the final orthogonal and overlapped electrode plates. All testing of the multiplexer microdrop motion presented in this section is performed with deionized water microdrops.

To successfully operate the digital microfluidic multiplexer, it is necessary to determine the threshold voltage of the system. To do this, a 1600 μm diameter microdrop is placed at the $i = 12.8, j = 13.4$ point on the multiplexer, as shown in Fig. 4.3a. (Note that row *i* and column *j* fractions indicate

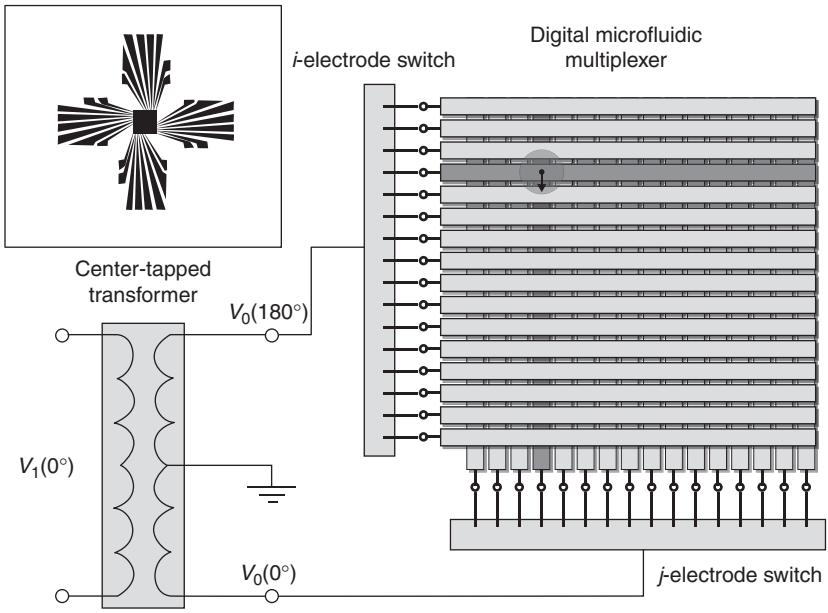

4.2 The digital microfluidic multiplexer is shown. The center-tapped transformer has V_{in} coupled to its input. The outputs of the transformer, $V_0(0°)$ and $V_0(180°)$, are applied to the multiplexer electrodes. The inset shows the orthogonal and overlapped upper row and lower column electrode plates.

intermediate locations between grid positions.) In general, the microdrop diameters can be reduced to the center-to-center pitch (in this case 600 μm) to provide effective addressability and control. The structural dimensions can be reduced if smaller microdrops are desired. The microdrop is tested for motion to the intermediate position between the $i = 11$ and 12 electrode pair and the $j = 13$ and 14 electrode pair. The voltage AC waveform $V_0(0°)$ is applied to the $j = 13$ and 14 electrode pair, while the out-of-phase voltage AC waveform $V_0(180°)$ is applied to the $i = 11$ and 12 electrode pair. The input AC voltage is initially set at $V_{in} = 0\ V_{rms}$ then increased. The microdrop first moves at $V_{in} = 8.3\ V_{rms}$, and this voltage is recorded to give the corresponding on-chip threshold voltage $V_{th} = 620\ V_{rms}$. The post-motion-induction microdrop position is shown in Fig. 4.3b. The established threshold voltage range for multiplexing, $V_{th}/2 < V_0 < V_{th}$, will therefore be $310\ V_{rms} < V_0 < 620\ V_{rms}$ for this device, with a corresponding input range of $8.3\ V_{rms} < V_{in} < 16.6\ V_{rms}$.

On a fundamental level, the multiplexer is able to move a single microdrop without disturbing neighboring microdrops. This important aspect is tested with the two-microdrop experiment shown in Fig. 4.4. Two microdrops of

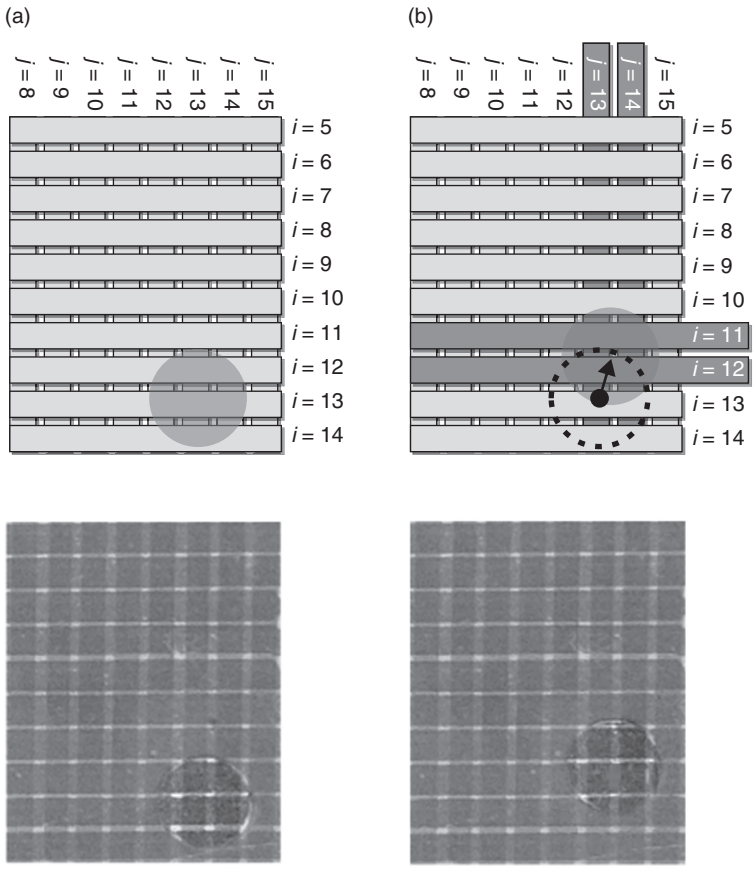

4.3 The configuration for determining the minimum required threshold voltage V_{th} is shown. The (a) initial and (b) final locations of a tested 2.06 nL microdrop are displayed. This threshold voltage is found by slowly increasing the applied voltage up to the point of microdrop motion. The electrode pair of $i = 11$ and 12 is activated with $V_0(180°)$ while the $j = 13$ and 14 electrode pair is activated with $V_0(0°)$.

1700 μm diameter are initially placed at $i = 9$, $j = 6$ and $i = 9$, $j = 11.3$, as shown in Fig. 4.4a. Note that both microdrops share the same horizontal i upper row electrode. The end result is shown in Fig. 4.4b. By applying an input voltage $V_{in} = 10.0\ V_{rms}$, one can successfully actuate microdrop 2 with a velocity of 1.0 mm/s to a new position of $i = 4.8$ and $j = 12.1$, while microdrop 1 is unperturbed.

In order to accommodate practical applications as a biofluidic device (Ho *et al.*, 2005; Chandrakasan *et al.*, 2008; Lam *et al.*, 2009), the multiplexer should be adapted to operate with a lower threshold voltage. The previous input voltage of 10 V_{rms} is larger than what is allowed for TTL/CMOS

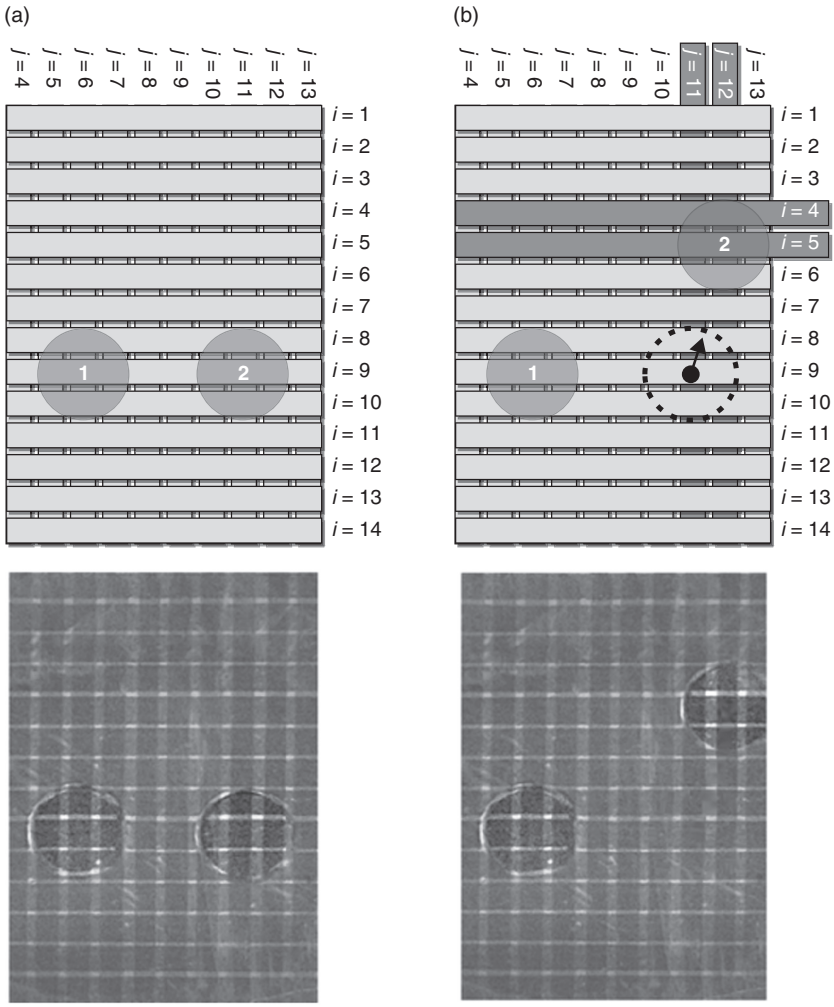

4.4 The independent actuation abilities of the multiplexer are shown. The microdrops are 2.14 nL in volume and the (a) initial and (b) final locations are displayed. The device input is V_{in} = 10.0 V_{rms}. The waveforms $V_0(180°)$ = 375 V_{rms} and $V_0(0°)$ = 375 V_{rms} are directed to the i = 4, i = 5 electrodes and j = 11, j = 12 electrodes, respectively. Microdrop 2 is moved from i = 9, j = 11.3 to a new position of i = 4.8, j = 12.3 and microdrop 2 is stationary.

integration (Moon *et al.*, 2002; Li *et al.*, 2008). With this in mind, the multiplexer is redesigned to have a thinner PDMS layer of 1 μm (Renaudot *et al.*, 2011). This will allow the same localized electric field to be formed across the insulating layers with a reduced voltage level. The revised digital microfluidic multiplexer is tested and found to have V_{th} = 48 V_{rms}, corresponding

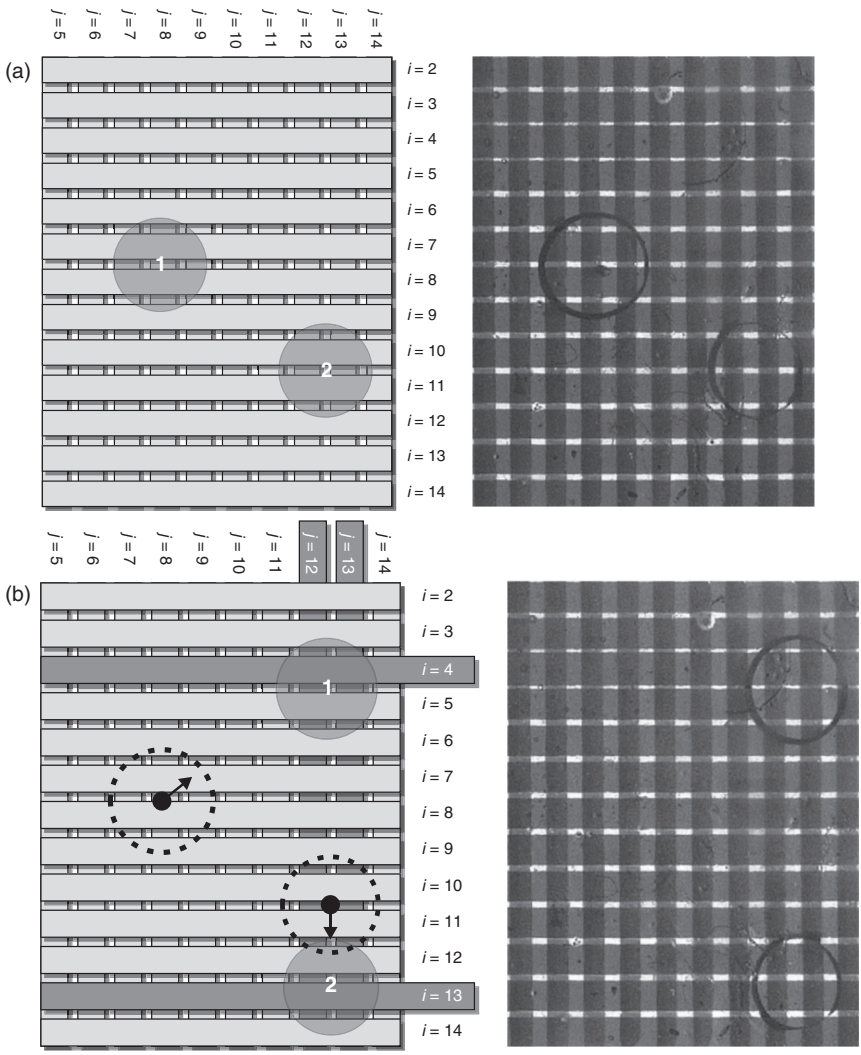

4.5 Shown here is the complex motion and merging process for two microdrops. Two microdrops are moved in sequence and ultimately mixed. The microdrops are (a) initially at rest, (b) separated from each other, (c) moved towards each other, and (d) finally merged together.

(Continued)

to an input voltage within the range $0.64\ V_{rms} < V_{in} < 1.28\ V_{rms}$. An input voltage of $V_{in} = 0.64\ V_{rms}$ is selected for use with the device.

The new low-voltage multiplexer operation is shown in Fig. 4.5. Two microdrops are used, with microdrop 1 having a 1800 μm diameter and 2.54 nL volume and microdrop 2 having a 1600 μm diameter and 2.01 nL volume.

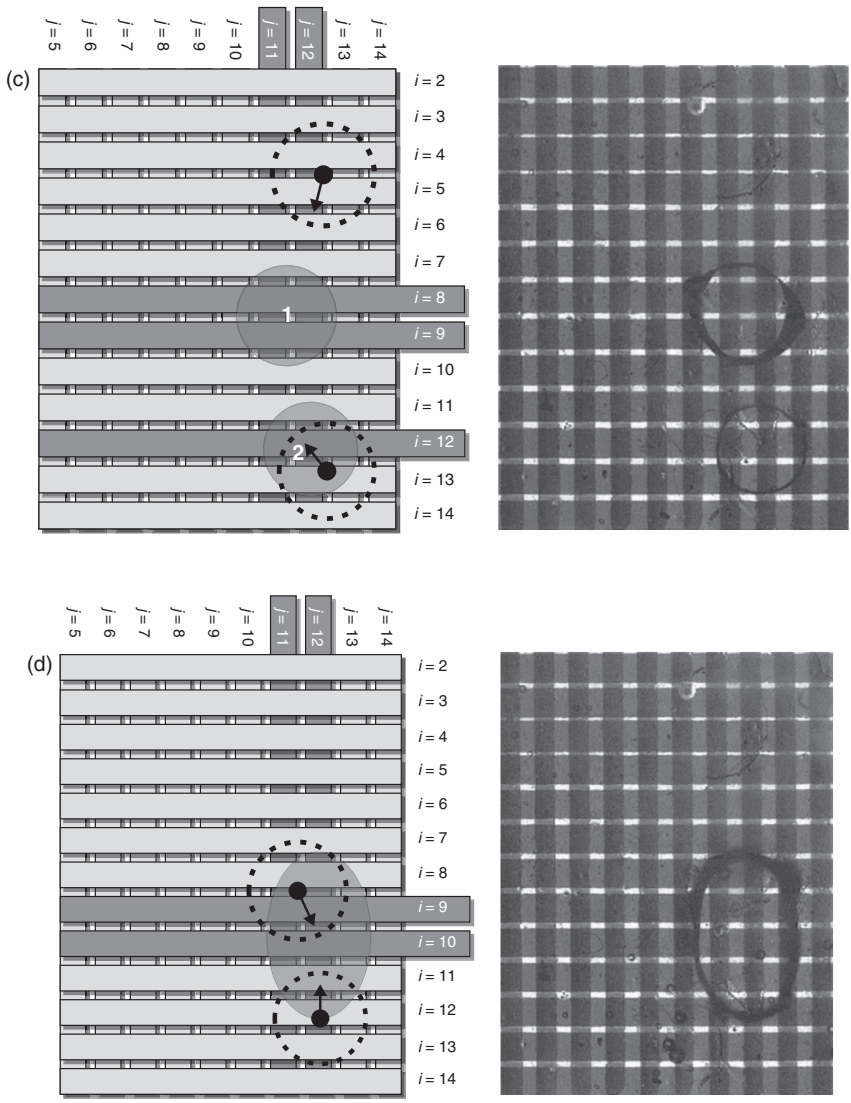

4.5 Continued

As shown in Fig. 4.5a, the two microdrops are initially at rest on the chip, with microdrop 1 positioned at $i = 7.5$, $j = 8$ and microdrop 2 positioned at $i = 10.5$, $j = 12.5$. The microdrops are then moved in the sequence shown in Fig. 4.5b. Rows $i = 4$ and 13 and columns $j = 12$ and 13 are activated to move microdrop 1 to the $i = 4.5$, $j = 12.5$ position and microdrop 2 to the $i = 12.5$, $j = 12.5$ position. To facilitate microdrop mixing, these microdrops are moved into closer proximity, as shown in Fig. 4.5c. Rows $i = 8, 9$ and 12, and columns

$j = 11$ and 12 are activated to move microdrop 1 to the $i = 8.5, j = 11.5$ position and microdrop 2 to the $i = 12, j = 12$ position. Finally, rows $i = 9$ and 10 and columns $j = 9$ and 10 are activated to merge the microdrops at the $i = 10, j = 12$ position.

4.3 Sensing techniques

The previous section highlighted the scalability challenges for microdrop motion. It became difficult to provide localized microdrop motion given increasingly small device dimensions and a correspondingly high number of inputs. The same holds true for scalability in fluid sensing. When on-chip structures are scaled to small dimensions, the resulting signal levels can become unacceptably low. This is because contemporary on-chip sensing techniques, with for example capacitance or optical sensing, have signals that scale down with the reducing sampling area. Clearly, one needs to develop systems with higher sampling sensitivity when small on-chip structures are considered. The generalized implementations for bringing about on-chip sensing are introduced in Section 4.3.1, followed by an analysis of theory, fabrication, and results for our folded-cavity architecture in Sections 4.3.2 and 4.3.3.

4.3.1 Architectures

On-chip sensing is fundamental to lab-on-a-chip operation. The ability to probe fluid states is at the core of many on-chip analytical processes, but such probing can become difficult when scalability is sought with diminishing device dimensions.

Capacitance sampling is a well-established method for sampling on-chip fluid characteristics (Ahmadi *et al*., 2010). Low-frequency dielectric properties are probed through localized capacitance measurements – as a linear relationship exists between the capacitance and internal fluid dielectric constant. However, such dielectric constant values have limited ability to provide broad-range (e.g., spectroscopic) information, as the measurements are fundamentally low-frequency/DC in nature. With this in mind, sampling technologies with higher-frequency optical analyses have been pursued.

Standard optical sensing makes use of fluid detection with an overhead or integrated camera/sensor. Real-time fluid motion tracking has proven to be highly successful for such implementations (e.g., those displayed by the photographs in Figs. 4.3–4.5). Moreover, optical sensing allows for material quantification by way of spectroscopic analyses across the high-frequency UV/visible/IR spectra. Numerous on-chip optical sensing systems exist with structures such as optical waveguides, ring resonators, and even optofluidic lasers (Gai *et al*., 2011). The remaining challenge for standard optical sensing relates to its scalability, however, and is particularly relevant to on-chip

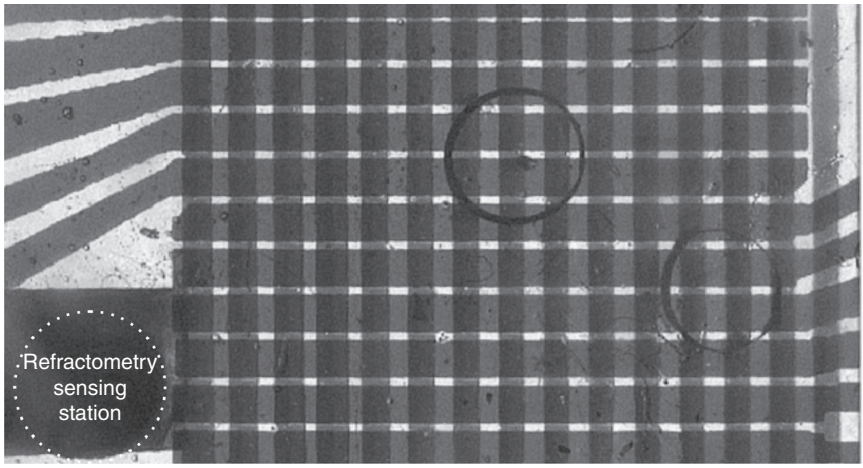

4.6 The multiplexer with integrated refractometry sensing station.

applications seeking operation with increasingly small device dimensions. The returned optical signal level typically scales with the sampling area, and this can make micron-scale sampling particularly challenging.

Given the advantages of optical sensing for material quantification, the work presented here makes use of optical sensing in a folded-cavity scheme. Such an arrangement is ideally suited for use with small device dimensions, as appreciable signal levels can be produced for especially small sampling areas. For the ongoing study, the folded-cavity optical sensor will be integrated for use as a fluid refractive index probe with the aforementioned digital microfluidic multiplexer being used for microdrop motion.

4.3.2 Folded-cavity theory

A folded-cavity sensor can be implemented for on-chip probing of refractive indices, and integrated directly onto the multiplexer, shown in Fig. 4.6 as the refractometry sensing station. A cross-section generalized schematic is shown in Fig. 4.7. The cross-section shows a profile of the upper and lower digital microfluidic multiplexer plates with an internal fluid (Fig. 4.7a) and without an internal fluid (Fig. 4.7b). The ray paths displayed in Figs 4.7a and 4.7b are calculated with ray-tracing analyses for fluid refractive indices $n_f = 1.52$ and $n_f = 1.00$, respectively, with a microlens contact angle of $\theta = 42.5°$ and a radius of 900 μm. The optical system is thoroughly analyzed, and the microlens on the superstrate is tuned to provide intense back-reflection onto the overhead image sensor. When a high refractive index fluid is present in the system, the image sensor records a high-intensity focal point. When fluid is absent (or a lower refractive index fluid is present), the

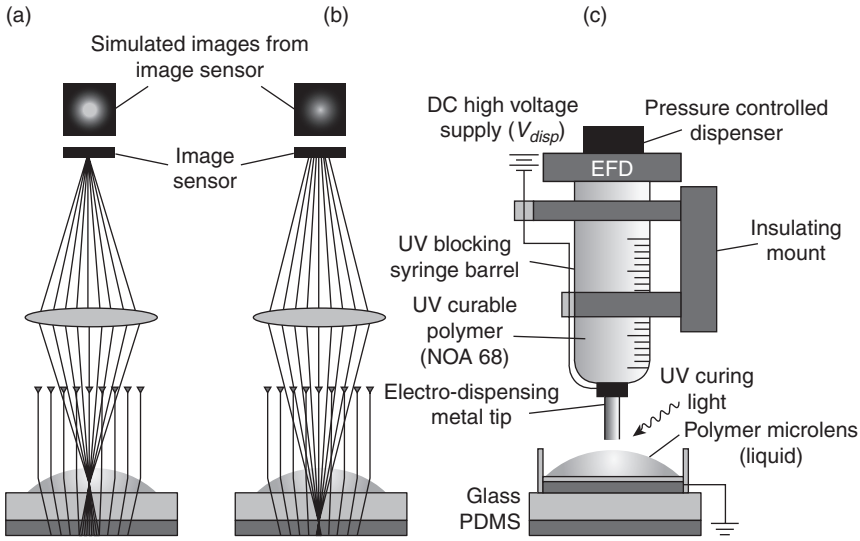

4.7 The folded-cavity optical arrangement is shown as the sampling station on the digital microfluidic multiplexer. Ray-traced back-reflected beams and simulated images on the image sensor are shown for (a) a high refractive index fluid being present, and (b) no fluid being present. The electro-dispensing apparatus is shown in (c) with the dispensed polymer microlens on the sampling station's superstrate.

focal image becomes diffuse and the central beam intensity diminishes. The folded-cavity sensor uses this especially sensitive relationship between the internal fluid refractive index and central beam intensity to optically probe the state of internal fluids.

It is important to note that the relationship between the back-reflected beam's optical axis intensity, I_{OA}, and the internal fluid refractive index, n_f, is precisely set by the microlens contact angle. Figure 4.8 shows I_{OA} vs n_f as triangles for this $\theta = 42.5°$ case. The linear trend line is found to be $I_{OA}(n_f) = 0.8145n_f - 0.2396$ ($R^2 = 0.9999$), with a linear operational range of $n_f = 1.28$–1.52. This refractive index operational range is particularly wide, although it comes at the cost of a coarse resolution ($\Delta n_f = 0.0024$). The resolution can be improved, however, by using sharper focusing with a higher microlens contact angle. This modified relationship between I_{OA} and n_f can be seen for the case of a $\theta = 52.5°$ microlens, whose results are shown by diamonds in Fig. 4.8. Note the increased slope, and its resulting improvement to the refractive index resolution ($\Delta n_f = 0.0007$) for this $I_{OA}(n_f) = 2.9398n_f - 3.4741$ ($R^2 = 0.9973$) trend. Even higher microlens contact angles can be used if one wishes to further improve the refractive index resolution. This can be seen for the case of a $\theta = 72.5°$ microlens, denoted by squares in Fig. 4.8. The I_{OA} vs n_f trend is now $I_{OA}(n_f) = 24.13n_f - 35.202$ ($R^2 = 0.9965$), and the

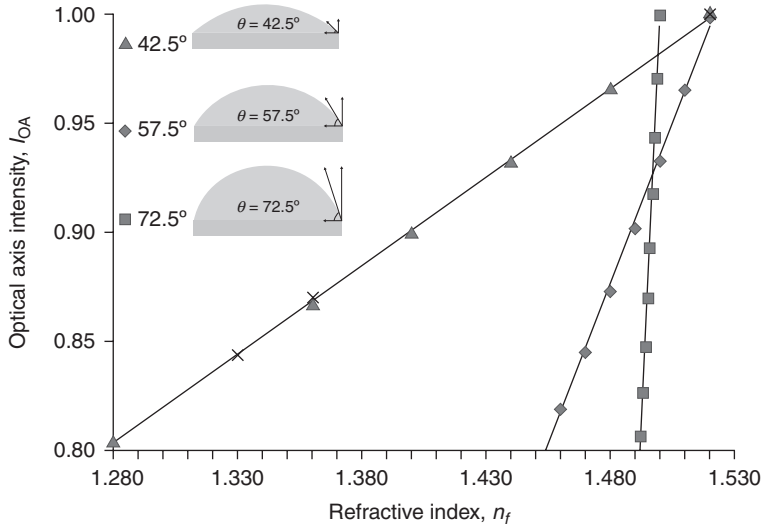

4.8 The linear relationship between the back-reflected optical axis intensity, I_{OA}, and the refractive index, *nf*, is shown for three different microlens contact angles. Curves with triangles, diamonds, and squares show theoretical I_{OA} values for $\theta = 42.5°$, $\theta = 57.5°$, and $\theta = 72.5°$ respectively. Experimental results are shown as crosses for $\theta = 42.5°$.

resulting increased slope dramatically improves the refractive index resolution ($\Delta n_f = 0.0001$). The improved resolution can be particularly useful for sensitive measurements of chemical kinetics (Ladam *et al.*, 2001) and temperature characteristics where refractive index perturbations of 0.0005 must be resolved (Li *et al.*, 1994).

The overall relationship between the refractive index range/resolution and microlens contact angle is summarized by Fig. 4.9. The refractive index range is shown on the left vertical axis and the refractive index resolution is shown on the right vertical axis. Note how an increased contact angle offers a finer refractive index resolution, and this comes at the cost of a lower refractive index range. For practical high-sensitivity measurements of refractive indices, contact angles above $\theta = 65°$ can provide the required fine resolution. For wide-range measurements of refractive indices, contact angles below $\theta = 50°$ can provide the required broad measurement range. Fabrication details and measurements for the wide-range refractive index probe are presented in the following section.

4.3.3 Folded-cavity fabrication and results

The aforementioned folded-cavity refractive index probing technique will be integrated with the digital microfluidic multiplexer. The combined system

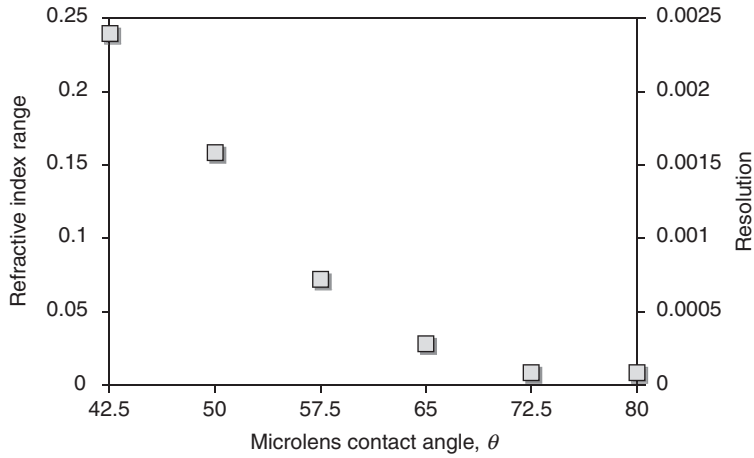

4.9 The relationship between the refractive index range (left vertical axis) and its corresponding resolution Δn_f (right vertical axis, being one-hundredth the range) are shown as a function of the microlens contact angle θ.

offers a scalable design for microdrop motion and sensing. Given that the multiplexer dimensions have been fixed for optimal microdrop motion, it is necessary to accomplish the optimized refractive index probing given only modifications to the folded-cavity microlens. Such modifications come about through microlens contact angle tuning and resulting modifications to the relationship between the internal fluid refractive index and image sensor's optical axis intensity.

The desire for contact-angle tuning can be met with our established electro-dispensing technique (Born *et al.*, 2010). Electro-dispensing is an *in situ* polymer deposition process in which a dispensing tip voltage is used during the dispensing to create the desired microlens form. The structure can then be solidified with UV-curing (~5 min with a 400 nm wavelength 10 mW laser). The complete setup is shown in Fig. 4.6c. A localized electric field is formed between the grounded copper plate and metal dispensing tip. The dispensing tip voltage, V_{disp}, and nominal polymer surface tensions define the dispensed droplet profile and contact angle $\theta(V_{\text{disp}})$ according to the Lippmann–Young equation:

$$\cos\theta\left(V_{\text{disp}}\right) = \cos\theta_0 + \frac{cV_{\text{disp}}^2}{2\gamma_{\text{lf}}} = \frac{\gamma_{\text{sf}} - \gamma_{\text{sl}}}{\gamma_{\text{lf}}} + \frac{cV_{\text{disp}}^2}{2\gamma_{\text{lf}}} \qquad [3.3.1]$$

where c is the capacitance per unit area. Initial conditions are defined for $V_{\text{disp}} = 0$, with solid–filler (γ_{sf}), solid–liquid (γ_{sl}), and liquid–filler (γ_{lf}) surface

tensions being defined for the initial contact angle of θ_0. User-controlled modifications to the contact angle occur when $V_{disp} > 0$. To start, an appropriate substrate and a surrounding filler fluid are chosen to establish a sufficiently high initial contact angle θ_0. This contact angle can then be lowered according to Equation [3.3.1] to tune the focusing conditions for UV-curing and use in the desired application.

For the present analysis, with wide-range refractive index measurements being desired, a microlens profile with a contact angle of $\theta = 42.5°$ is chosen. A UV-curable polymer (NOA 68) is dispensed with an air filler onto a PTFE-coated glass substrate to form the microlens. A pressure-controlled dispenser (Nordson Ultimus V) is used to deposit the desired volume, with a microlens radius of 900 μm, then the dispensing tip voltage is tuned over the range $V_{disp} = 300–1500\ V_{DC}$ to form the desired microlens contact angle. UV-curing is then applied. A 100 pL volume yields a microlens with radius of 900 μm and contact angle of 42.5°.

The fabricated microlens facilitates folded-cavity sensing and is incorporated as a sampling station adjacent to the digital microfluidic multiplexer. This element provides the desired localized optical sensing of fluid refractive indices between the two plates. To determine the fluid refractive index, a collimated white LED illuminates the structure. The back-reflected optical beam is then sampled by a beamsplitter and overhead image sensor. An appropriate sequence of multiplexer electrode activations is used to pull the fluid samples into the sampling station where images are then captured and refractive indices are determined.

The folded-cavity sensing system is calibrated with well-known refractive indices. The optical axis intensities are recorded for water ($n_f = 1.33$), ethanol ($n_f = 1.36$), and silicone oil ($n_f = 1.52$). Results are displayed as crosses in Fig. 4.8 and are seen to follow the theoretical linear trend for the $\theta = 42.5°$ microlens. Ultimately, the folded-cavity sensing system is found to be successful in characterizing a wide variety of fluids within the on-chip microdrop motion/sensing system.

The system introduced here addresses some of the fundamental challenges in contemporary on-chip biomedical devices. Operation on small dimensions with highly-parallel formats is typically desired. The scalable nature of the presented multiplexer makes it especially useful for these micron-scale parallel systems. Biomedical operations incorporating bioassays and clinical diagnostics on human urine, saliva, tears, and sweat can therefore be carried out concurrently with small sample volumes (Srinivasan *et al.*, 2003, 2004). The work presented here, with the combined multiplexer and refractometry system, can be used as a complete control/sensing analytical tool for *in sit*u diagnostics. Examples include the monitoring of hemoglobin concentrations in red blood cells (Park *et al.*, 2009), protein and lipid concentrations (Barer, 1955), and distilled/saturated solution concentrations (Yunus and Rahman, 1988).

4.4 Future trends

Droplet-based digital microfluidic technologies are growing rapidly. The precise control and reagent economy made available by the systems have allowed these technologies to excel in a growing number of biomedical fields. Processes based upon immunoassays (Alphonsus *et al*., 2010), DNA ligations (Liu *et al*., 2008), DNA pyrosequencing (Fair, 2007), enzymatic analyses (Miyazaki *et al*., 2008), proteomics (Lee *et al*., 2009), and bio-analytical mass spectrometry (Figeys *et al*., 1998) have all benefited from these technologies. These fields have sought improved control and sensing capabilities, and droplet-based digital microfluidics can provide these capabilities.

Future research trends will likely focus on the applied challenges for the aforementioned digital microfluidic implementations, with particular attention paid to four contemporary challenges of a practical nature. The first practical challenge relates to evaporation – an especially important issue when reagent economy is sought. On-chip systems are being developed to address this practical concern through techniques based upon environmental control (Barbulovic-Nad *et al*., 2008), seals (Gong *et al*., 2004), and ambient fillers (Pollack *et al*., 2000). The second practical challenge relates to contamination. External contamination can be controlled by way of the same ambient filler solutions that minimize droplet evaporation (Pollack *et al*., 2000). At the same time, cross-contamination between internal fluid samples is a practical concern – especially when biomolecular adsorption effects are pronounced. Appropriate thin-film layers and wash operations (Zhao and Chakrabarty, 2009) can be applied to control these contaminations. The third practical challenge relates to packaging. Droplet-based systems for bioreactors, etc., typically require a reservoir from which fluids can be drawn, and such systems must provide reliable seals, overcome strong capillary forces, and mitigate the formation of bubbles. Srinivasan *et al*. have demonstrated numerous advances in overcoming these practical constraints (Srinivasan, 2005). The fourth and final practical challenge for droplet-based digital microfluidics relates to routing constraints. Microdrop control becomes an issue of increased importance when fine resolutions and large numbers of droplets/inputs are required. And such considerations are of particular concern when applications are sought with droplets in close proximity – with processes such as mixing, sorting, and splitting (Yuh *et al*., 2008).

4.5 Conclusion

The fundamental issue of scalability has been addressed to a large extent by the work presented here. The digital microfluidic multiplexer was shown to provide complete 2-D microdrop motion in a system with decreased input

complexity (and input voltages compatible with TTL/CMOS technologies). At the same time, an optical sampling station with a folded-cavity arrangement was fabricated and demonstrated for improved sensitivity in sampling internal fluid refractive indices. Such technologies can become cornerstones for emerging biotechnological and biomedical applications that benefit from microsystem integration.

4.6 References

Ahmadi A, Najjaran H, Holzman J F and Hoorfar M (2009), 'Two-dimensional flow dynamics in digital microfluidic systems', *J. Micromech. Microeng*., **19**, 065003.

Ahmadi A, Devlin K D, Najjaran H, Holzman J F and Hoorfar M (2010), 'In situ characterization of microdroplet interfacial properties in digital microfluidic systems', *Lab Chip*, **10**(11), 1429–1435.

Alphonsus H C N, Uddayasankar U and Wheeler A R (2010), 'Immunoassays in microfluidic systems', *Anal. Bioanal. Chem*., **397**, 991–1007.

Au A K, Lai H, Utela B R and Folch A (2011), 'Microvalves and micropumps for biomems', *Micromachines*, **2**(2), 179–220.

Barbulovic-Nad I, Yang H, Park P S and Wheeler A R (2008), 'Digital microfluidics for cell-based assays', *Lab Chip*, **8**, 519–526.

Becker H and Locascio L E (2002), 'Polymer microfluidic devices', *Elsevier Science*, **56**, 267–287.

Berthier J (2008), *Microdrops and Digital Microfluidics*, 1st ed, William Andrew: Norwich, NY, USA, 196–201.

Born B, Landry E L and Holzman J F (2010), 'Electro-dispensing of micro-spheroids for lateral refractive and reflective photonic elements', *IEEE Photon. J*., **2**(6), 873–883.

Chandrakasan A P, Verma N and Daly D C (2008), 'Ultralow-power electronics for biomedical applications', *Annu. Rev. Biomed. Eng*., **10**(1), 247–274.

Cho S K, Moon H, and Kim C-J (2003), 'Creating, transporting, cutting, and merging liquid droplets by electrowetting-based actuation for digital microfluidic circuits', *J. MEMS*, **12**(1), 70–80.

Collier C M, Wiltshire M, Nichols J, Born B, Landry E L and Holzman J F (2011), 'Nonlinear dual-phase multiplexing in digital microfluidic architectures', *Micromachines*, **2**, 369–384.

Davids D, Datta S, Mukherjee A, Joshi B and Ravindran A (2006), 'Multiple fault diagnosis in digital microfluidic biochips', *ACM J. Emerg. Technol*., **2**(4), 262–276.

Dolatabadi A, Mohseni K and Arzpeyma A (2006), 'Behaviour of a moving droplet under electrowetting actuation: numerical simulation', *Can. J. Chem. Eng*., **84**, 17–21.

Elvira K S, Leatherbarrow R, Edel J and deMello A (2012), 'Droplet dispensing in digital microfluidic devices: assessment of long-term reproducibility', *Biomicrofluidics*, **6**, 022003.

Fair R B (2007) 'Digital microfluidics: is a true lab-on-a-chip possible?', *Microfluid. Nanofluid*., **3**, 245–281.

Fair R B, Khlystov A, Tailor T D, Ivanov V, Evans R D, Griffin P B, Srinivasan V, Pamula V K, Pollack M G and Zhou J (2007) 'Chemical and biological applications of digital-microfluidic devices', *IEEE Design Test Comp*., **24**, 10–24.

Figeys D, Gygi S P, McKinnon G and Aebersold R (1998), 'An integrated microfluidics-tandem mass spectrometry system for automated protein analysis', *Anal. Chem*., **70**, 3738–3734.

Gai H, Li Y and Yeung E S (2011), 'Optical detection systems on microfluidic chips', *Top Curr Chem*, **304**, 171–201.

Gong J, Fan S-K and Kim C-J (2004), 'Portable digital microfluidics platform with active but disposable lab-on-chip', *Proc. 17th IEEE International Conference on Micro Electro Mechanical Systems*, Masstricht, Netherlands, 355–358.

Ho C-T, Lin R -Z, Chang H-Y and Liu C-H (2005), 'Micromachined electrochemical T-switches for cell sorting applications', *Lab Chip*, **5**(11), 1248–1258.

Huebner A, Sharma S, Srisa-Art M, Hollfelder F, Edel J B and deMello A J (2008), 'Microdroplets: a sea of applications?', *Lab Chip*, **8**, 1244–1254.

Humphreys T, Andersson J, Södervall U and Melvin T (2009), 'World-to-chip interconnects for efficient loading of genomic DNA into microfluidic channels', *J. Micromech. Microeng*., **19**, 105024.

Ladam G, Schaaf P, Cuisinier F J G, Decher G and Voegel J-C (2001), 'Protein adsorption onto auto-assembled polyelectrolyte films', *Langmuir*, **17**(2–6), 878–882.

Lam R H W, Kim M-C and Thorsen T (2009), 'Culturing aerobic and anaerobic bacteria and mammalian cells with a microfluidic differential oxygenator', *Anal. Chem*., **81**(14), 5918–5924.

Lee J, Soper S A and Murray K K (2009), 'Microfluidics with MALDI analysis for proteomics – a review', *Anal. Chim. Acta*., **649**, 180–190.

Li T, Zhang L, Leung K M and Yang J (2010), 'Out-of-plane microvalves for whole blood separation on lab-on-a-CD', *J. Micromech. Microeng*., **20**, 105024.

Li W B, Segré P N, Gammon R W, Sengers J V and Lamvik M (1994), 'Determination of the temperature and concentration dependence of the refractive index of a liquid mixture', *J. Chem. Phys*., **101**(6), 5058–5069.

Li Y, Parkes W, Haworth L I, Stokes A A, Muir K R, Li P, Collin A J, Hutcheon N G, Henderson R, Rae B and Walton A J (2008), 'Anodic Ta_2O_5 for CMOS compatible low voltage electrowetting-on-dielectric device fabrication', *Solid-State Electron*., **52**(9), 1382–1387.

Liu Y-J, Yao D-J, Lin H-C, Chang W-Y and Chang H-Y (2008), 'DNA ligation of ultramicro volume using an EWOD microfluidic system with coplanar electrodes', *J. Micromech. Microeng*., **18**, 045017.

Madou M J and Cubicciotti R (2003), 'Scaling issues in chemical and biological sensors', *Proc. IEEE*, **91**(6), 830–838.

Miyazaki M, Honda T, Yamaguchi H, Briones M P P and Maeda H (2008), 'Enzymatic processing in microfluidic reactors', *Biotechnol. Genet. Eng*., **25**, 405–428.

Moon H, Cho S-K, Garrell R L and Kim C-J (2002), 'Low voltage electrowetting-on-dielectric', *J. Appl. Phys*., **92**(7), 4080–4087.

Nichols J, Collier C M, Landry E L, Wiltshire M, Born B and Holzman J F (2012), 'On-chip digital microfluidic architectures for enhanced actuation and sensing', *J. Biomed. Opt*., **17**(6), 067005.

Park Y, Yamauchi T, Choi W, Dasari R and Feld M S (2009), 'Spectroscopic phase microscopy for quantifying hemoglobin concentrations in intact red blood cells', *Opt. Lett*., **34**(23), 3668–3670.

Pollack M G, Shenderov A D and Fair R B (2000), 'Electro-wetting based actuation of liquid droplets for microfluidic applications', *Appl. Phys. Lett*., **77**(11), 1725–1726.

Ren H, Fair R B and Pollack M G (2004), 'Automated on-chip droplet dispensing with volume control by electro-wetting actuation and capacitance metering', *Sensor. Actuat. B*, **98**, 319–327.

Renaudot R, Agache V, Daunay B, Lambert P, Kumemura M, Fouillet Y, Collard D and Fujita H (2011), 'Optimization of liquid dielectrophoresis (LDEP) digital microfluidic transduction for biomedical applications', *Micromachines*, **2**(2), 258–273.

Ricketts A J, Irick K, Vijaykrishnan N and Irwin M J (2006), 'Priority scheduling in digital microfluidics-based biochips', *Proc. Design, Automation and Test in Europe*, Munich, Germany, 6–10 March, 329–334.

Song H, Chen D L and Ismagilov R F (2006), 'Reactions in droplets in microfluidic channels', *Angew. Chem. Int. Ed*., **45**, 7336–7356.

Srinivasan V (2005) 'A digital microfluidic lab-on-a-chip for clinical applications', Ph.D. thesis, Duke University.

Srinivasan V, Pamula V K, Pollack M G and Fair R B (2003), 'Clinical diagnostics on human whole blood, plasma, serum, urine, saliva, sweat, and tears on a digital microfluidic platform', *Proc. MicroTAS*, **2003**, 1287–1290.

Srinivasan V, Pamula V K and Fair R B (2004), 'An integrated digital microfluidic lab-on-a-chip for clinical diagnostics on human physiological fluids', *Lab Chip*, **4**(4), 310–315.

Welch C J, Sajonz P, Biba M, Gouker J and Fairchild J (2006), 'Comparison of multiparallel microfluidic HPLC instruments for high throughput analyses in support of pharmaceutical process research', *J. Liq. Chrom. Rel. Technol*., **29**(15), 2185–2200.

Wiggins S and Ottino J M (2004), 'Foundations of chaotic mixing', *Phil. Trans. R. Soc. Lond. A*, **362**, 937–970.

Xiao Z and Young E F Y (2010a), 'CrossRouter: a droplet router for cross-referencing digital microfluidic biochips', *Proc. 15th Asia South Pacific Design Automation Conference*, Hong Kong, China, 18–21 January, 269–274.

Xiao Z and Young E F Y (2010b), 'Droplet-routing-aware module placement for cross-referencing biochips', *Proc. 19th International Symposium on Physical Design*, San Francisco, USA, 14–17 March, 193–199.

Xu T and Chakrabarty K (2008), 'A droplet-manipulation method for achieving high-throughput in cross-referencing-based digital microfluidic biochips', *IEEE Trans. Computer-Aided Design Integr. Circuits Syst*., **27**(11), 1905–1917.

Yuh P-H, Yang C-L and Chang Y-W (2008), 'BioRoute: a network-flow-based routing algorithm for the synthesis of digital microfluidic biochips', *IEEE Trans. Computer-Aided Design Integr. Circuits Syst*., **27**(11), 1928–1941.

Yunus W M bin M and Rahman A bin A (1988), 'Refractive index of solutions at high concentrations', *Appl. Opt*., **27**(16), 3341–3343.

Zhao Y and Chakrabarty K (2009), 'Cross-contamination avoidance for droplet routing in digital microfluidic biochips', *Proc. DATE*, Nice, France, 20–24 April, 1290–1295.

Zhu L, Zhang Q, Feng H, Ang S, Chau F S and Liu W T (2004), 'Filter-based microfluidic device as a platform for immunofluorescent assay of microbial cells', *Royal Soc. Chem*., **4**, 337–341.

5

Controlled drug delivery using microfluidic devices

N. GAO, Harvard University, USA and X.J. LI, University of Texas at El Paso, USA

DOI: 10.1533/9780857097040.2.167

Abstract: Efficient drug delivery plays a crucial role in disease treatment and remains an important challenge in medicine. Recent advances in the field of microfabrication have offered the possibility to develop controlled release systems for drug delivery. Herein, we will mainly address two kinds of delivery devices: microreservoir and micro/nanofluidic devices. For each type of drug delivery device, we start with working principles and the fabrication process, and then summarize the recent applications of each type of drug delivery system, with a focus on how to control drug delivery with different triggered systems. At the end of this chapter, challenges and the future prospect of chip-based controlled drug delivery will be discussed.

Key words: microfluidic, controlled drug release, drug delivery, fabrication, triggered system.

5.1 Introduction

Drug delivery is the method or process of administering a pharmaceutical compound to achieve a therapeutic effect on disease. Conventional dosages mean oral delivery and injection are the predominant routes for drug administration. The main drawbacks of these types of dosage are non-local treatment and toxicity to healthy tissues.[1] An ideal drug delivery would be controlled for high efficiency treatment and local drug release to minimize toxicity. With the development of micro/nano electromechanical system (MEMS/NEMS) technology and material science, a variety of devices have been developed to achieve drug delivery for disease treatment over the years. The devices with micro/nanostructures, as powerful platforms, can provide better drug therapy because they allow precise, local, and controlled dosing with lower toxicity. These devices can offer opportunities to address unmet medical needs related to disease therapy.

An ideally controlled drug delivery system requires simultaneous consideration of several factors, such as the mechanism of drug release, the route of

administration, and capability of targeting. The approach of drug release has a significant effect on therapeutic efficacy. An ideal approach should maintain drug levels within the therapeutic window to avoid potential health hazards, maximize therapeutic efficiency, and provide a well-controlled drug release triggered by stimuli. Drug concentration above the therapeutic window is toxic, and below the therapeutic window will lose therapeutic efficacy. Conventional drug delivery systems, such as oral and injection, generally have a high initial level of the drug after the first administration, followed by sharp decrease in blood concentration (Fig. 5.1a). Controlled drug release helps to address this issue. Figure 5.1b shows two profiles of most common time dependent release, sustained release, and pulsatile release. Sustained release can offer a constant drug concentration within the therapeutic window. However, pulsatile release provides a consecutive burst drug delivery. To improve treatment efficiency of the disease, controlled drug delivery can be achieved in different approaches based on different compounds or different therapeutic needs. Most treatments request a sustained release of drug at a constant rate over long periods of time. For some specific drugs, such as insulin and hormones,

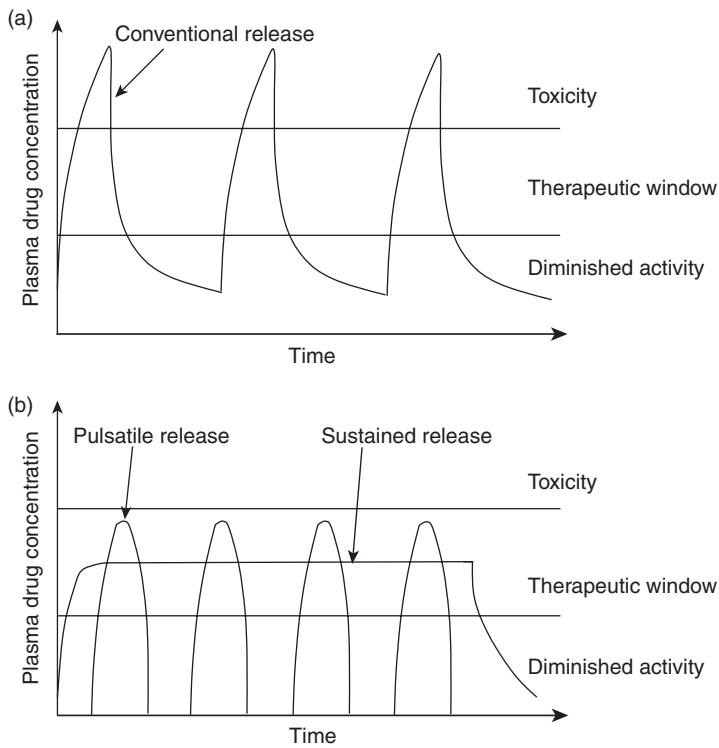

5.1 Profile of conventional, sustained, and pulsatile drug release. (a) Plasma concentration versus time curve for conventional drug administration. (b) Plasma concentration versus time curve for pulsatile and sustained drug release.

the drug release should mimic the body's natural pulsatile. A variety of controlled drug delivery devices have been developed to achieve a good therapeutic effect over the years. Controlled drug release can be triggered by different stimuli, such as temperature, pH, magnetic and electric field, etc. These devices use different routes of administration, and different methods and materials for device fabrication, typically including polymer- and silicon-based micropumps, microneedles, microreservoirs, and microfluidic systems. In this chapter, to avoid duplication with other chapters, we will focus on two kinds of delivery devices: microreservoir and micro/nanofluidic devices.

5.2 Microreservoir-based drug delivery systems

Compared to traditional approaches, microreservoir devices allow more precise control over the drug delivery rate and limit side effects with local implantation. As one of next generation target delivery systems, the microreservoir system offers the possibility for self-managed and high effectient patient therapy.

5.2.1 Working principle

The controlled release microreservoir device typically consists of reservoirs containing drugs, release control systems, and biodegradable polymers or metallic layers as membranes. Individual or multiple drugs are sealed in the reservoirs, isolating them from the environment. The metallic or polymer layer covering on the reservoir is opened, or degraded on command, to expose their contents to the body. The structure of microreservoir-based devices includes single and multi-reservoir systems. The covers can be trigged with different approaches, including temperature, pH, and magnetic and electric field.

5.2.2 Microreservoir fabrication

Devices of microreservoir-based drug release are mainly of silicon structure and polymer structure. Fabrication of silicon-based devices is commonly achieved by photolithography, etching, and deposition steps in order to produce the desired configuration of features such as reservoirs, valves, and membranes or trigger systems. The fabrication can proceed according to the standard processes of MEMS techniques, such as bulk micromachining and surface micromachining. Figure 5.2 is a schematic of the typical fabrication process of bulk micromachining.[2] It starts with an anisotropic silicon etch using an oxide mask (Fig. 5.2a and 5.2b). This is followed by a conformal plasma-enhanced chemical vapor deposition (PECVD) oxide deposition (Fig. 5.2c). Subsequently, an anisotropic oxide etch is used to remove the oxide at the bottom of the trenches, leaving the sidewall oxide intact

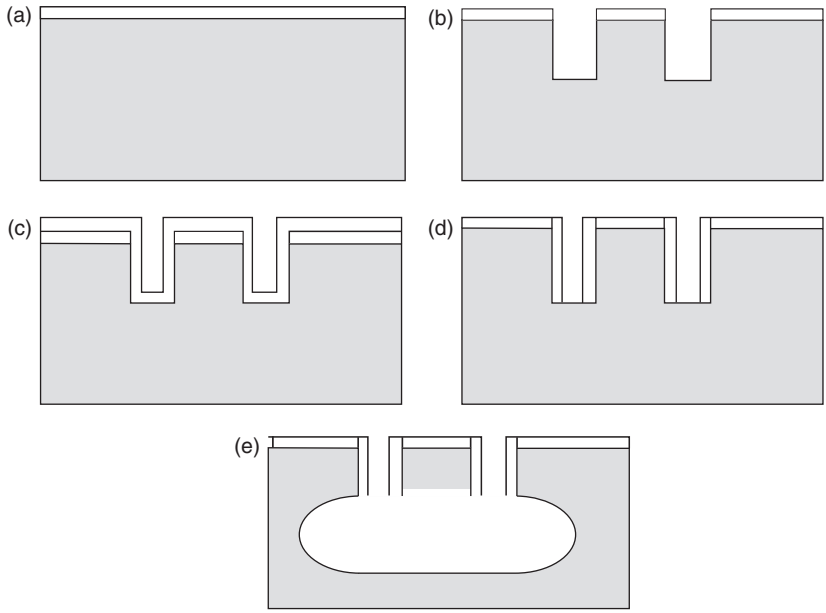

5.2 Cross-section of bulk micromachining process. (a) Wafer with oxide layer. (b) Anisotropic oxide etch. (c) Deposition. (d) Anisotropic oxide etch. (e) Undercut. (*Source*: Copyright permission from Elsevier.[2])

(Fig. 5.2d). At this stage, an isotropic silicon etch (SF_6) is performed, which results in undercut and finalization of the silicon structures (Fig. 5.2e).

The fabrication of surface micromachining usually starts to construct a sacrificially patterned layer on top of a silicon substrate. The structural material is then deposited and patterned. Finally, the sacrificial layer is removed, leaving the desired microstructure.

Recently, fabrication of polymer-based devices has also been well developed. Three techniques can be used to fabricate polymer-based structures for microreservoir-based devices: photolithography, replica molding, and surface machining.[3] Photolithograph is usually used to construct devices with thin membranes. SU-8 and PMMA are commonly used polymers. A fabrication process of the SU-8 photolithograph is illustrated in Fig. 5.3. Polymeric structures are also formed by molding and embossing techniques. In this technique, a master mold is generally created with a hard material, such as silicon wafer, using the standard MEMS fabrication process. A pre-polymer is deposited in the mold and solidified after surface treatment to reduce adhesion of the mold to the polymeric materials. The polymeric structure is then removed. The advantage of molding is that the mold can be repeatedly used. This method is normally used to obtain micro-size structures.

Another important technique that can be used to build polymeric structures on a silicon substrate is surface machining. Surface machining can be

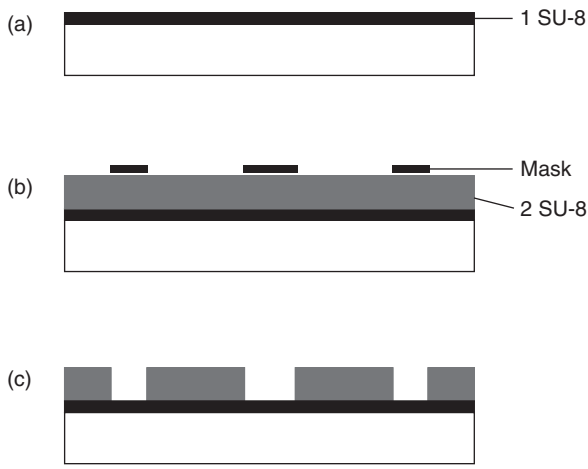

5.3 Schematic of the photolithographic steps with a SU-8 photoresist. (a) Spin-coating and flood-exposure of SU-8 photoresist on silicon. (b) Coating and exposure of a second SU-8 for generation of structure using the mask. (c) SU-8 development.

used to create small sized structure. However, due to the increased surface nonplanarity with the additional layer, there are limitations when creating a multi-layer structure. The basic surface micromachining process is described in the fabrication of silicon structure-based devices.

5.2.3 Examples of applications

Silicon-based devices

Microreservoir-based devices have been developed over years.[4] A number of silicon-based drug delivery devices have been reported. These devices can achieve drug release by different triggers, such as electrochemical dissolution,[5,8] telemetry,[6] temperature/thermal,[7] polymer degradation,[9] and magnetic force.[10] Silicon-based microreservoirs typically have an array of cavity shape, with metallic walls on a lateral surface. The top and bottom basis can be sealed by metallic or polymeric layers. Drugs can be released from microreservoirs if the sealed layer is opened. Figure 5.4a is a multi-pulse drug delivery system fabricated on a silicon substrate using electrochemical dissolution to control the drug release.[5] Each reservoir can be filled with a 20 nL volume drug. Gold membranes with excellent biocompatible properties as anodes are on top of the reservoirs, preventing drug exposure before the trigger. Gold anodes are dissolved in the presence of chloride ions when anodic voltage is applied to the membrane. The drug is released when the thin gold membrane disappears after the application of a voltage for several seconds. This profile of drug release presents

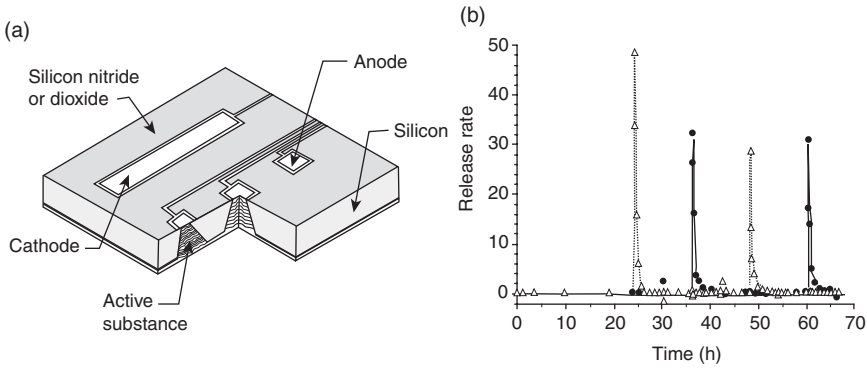

5.4 (a) A prototype microchip for controlled release showing the shape of a single reservoir. (b) Pulsatile release of multiple substances from a single microchip device. (*Source*: Copyright permission from Nature publishing group.[5])

a burst drug delivery. Figure 5.4b shows the result of a prototype device filled with two model chemicals. The results demonstrated that the activation of each reservoir could be controlled individually with separated circuit. Varying amounts of drugs in solid, liquid, or gel could be released into solution in a pulsatile manner, a continuous manner, or a combination of both. In addition, the applied potential of the device was just 1.04 V vs. SCE with low power consumption.

More recently, Microchips Inc. presented a controlled pulsatile release of the polypeptide leuprolide from microchip implants over 6 months in dogs, which demonstrated an excellent biocompatibility of the device.[6] In this design, each microchip contains an array of discrete 300 nL reservoirs, from which dose delivery can be individually controlled by telemetry (Fig. 5.5). The filled and titanium hermetically sealed chip was electrically connected to wireless communication hardware, power supply, and circuit boards on the *in vivo* implant (Fig. 5.5c). The devices were remotely programmed to open selected reservoirs, initiating drug release. The profile of the maximum drug concentration (C_{max}) in Fig. 5.5d showed the release kinetics of the drug over a period of 25 weeks.

Electrothermal induction, as a traditional technique, has been applied in controlled drug delivery.[7] In this study, an electrothermally induced single reservoir is sealed by a silicon nitride membrane. Activation causes thermal shock to the suspended membrane allowing the drugs inside the reservoir to diffuse into the region of interest. Also, the size of reservoirs can be engineered for offering on-demand drug release. This work explored a fuse activation mechanism that operates controlled release electrothermally for low energy consumption. The reason for low consumption is that the fuse for opening the membranes is geometrically laid out on the weakest point of

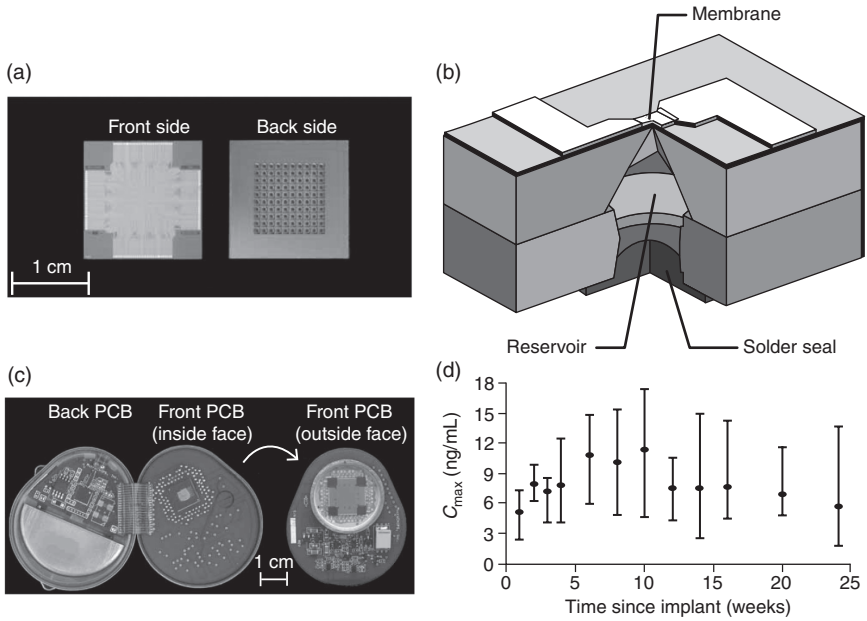

5.5 Reservoir-based implantable drug delivery system. (a) Front and back of the 100-reservoir microchip. (b) Representation of a single reservoir. (c) Electronic components on the printed circuit board (PCB) in the device package. (d) Average C_{max} for each release event throughout the 6-month study. (*Source*: Copyright permission from Nature publishing group.[6])

the membranes. The energy consumption for the *in vitro* release is approximately 134 μJ, which reduced four orders of magnitude over the previous devices made with a full gold membrane. The reported device could provide a sustained drug release for more than 200 h.

Polymer-based device

Polymer devices, as low-cost drug delivery systems, have been successfully fabricated for administration of biopharmaceuticals. Figure 5.6a is a multi-pulse drug delivery device with 1.2 cm in diameter and 480–560 μm thick consisting of 36 poly (L-lactic acid) reservoirs and poly (D, L-lactic-*co*-glycolic acid) (PLGA) membranes.[9] The timing of drug release can be controlled with the different biodegradable rates of the materials used, the molecular mass, and the composition and thickness of membranes. In this work, drug release from reservoirs was maintained over a period of months. Figure 5.6b shows the percentage of initial loading released from a representative device, in which both heparin and dextran were loaded into reservoirs sealed with molecular mass PLGA. The *in vivo* drug release was studied

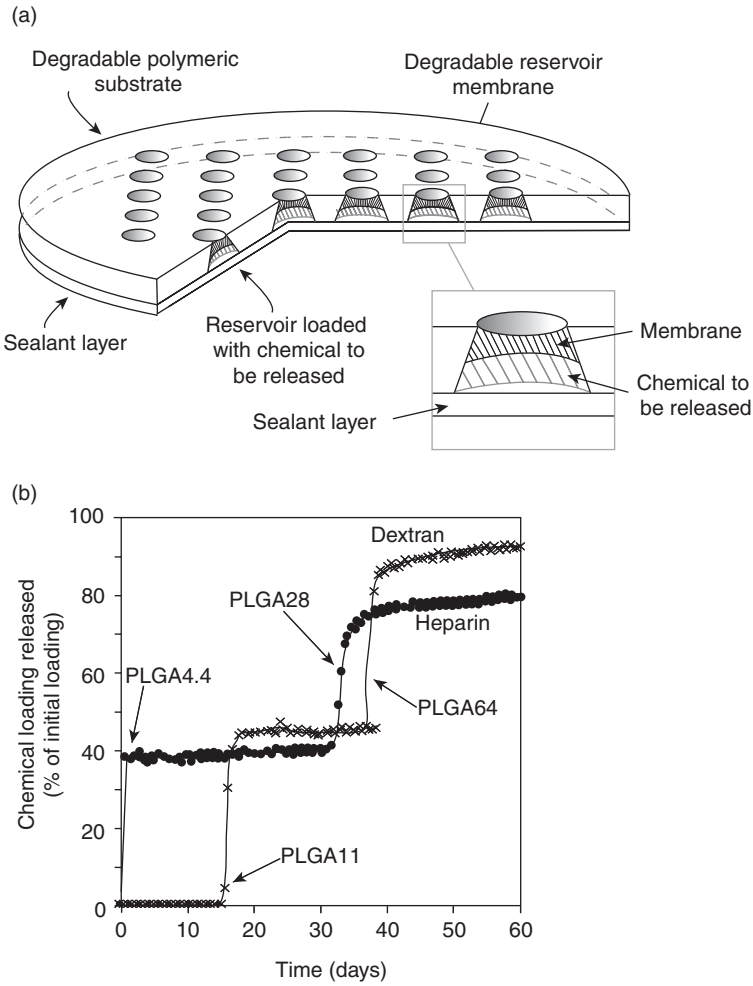

5.6 (a) Diagram of polymeric microchip device. The main body of the device is composed of a reservoir-containing substrate that is fabricated from a degradable polymer. Truncated conical reservoirs in the substrate are loaded with the chemical to be released, and sealed with polymeric degradable reservoir membranes on one end and a sealant layer (polyester tape) on the opposite end. Inset, close-up of a reservoir, reservoir membrane, sealant layer and chemical to be released. (b) Cumulative percentage of initial loading released from microchip device *in vitro*. Release results are shown for a representative device that was loaded with both 14C-dextran (crosses) and 3H-heparin (circles). (*Source*: Copyright permission from Nature publishing group.[9])

and it was revealed that pulsatile release was analogous to that observed in other *in vitro* studies.

Differently from the sturcture above, a magnetically controlled device capable of on-demand release of defined quantities of an antiproliferative drug, docetaxel (DTX), was reported in 2011.[10] This device consists of a single reservoir which was created by molding polydimethylsiloxane (PDMS) on SU-8 pattern using photolithography. A PDMS membrane coated with magnetic iron oxide nanoparticles is used to seal the reservoir. This magnetic PDMS membrane deforms and the drug solution is released from the device under a magnetic field. A sustained leakage release of docetaxel, an antiproliferative drug, was achieved for 35 days at a rate of 171 ± 16.7 ng per actuation interval. In the cell viability experiment, released docetaxel caused cell viability in HUVEC and PC3 cells decreasing to 24% and 58% after one actuation, and to 21% and 34% after ten actuations, respectively. This device, made with biocompatible PDMS, presents a promising prospect on *in vivo* implantation.

In other reports,[11,12] researchers built poly (methyl methacrylate) (PMMA) microdevices using photolithography and reactive ion etching (RIE). RIE can easily create reservoirs with varying depths by controlling the etch time and the ion flow rate, which provides a simple approach to adjust the drug loading volume. The different individual model drugs were loaded into each reservoir on the device. (See Plate I in the colour section between pages 328 and 329.) The use of different hydrogel systems in each reservoir shows difference in the controlled release of the respective drugs over the same release period and offers independent release of multiple drugs. In addition, the PMMA surface was functionalized with lectin to improve bioadhesion of the device and epithelium, enhancing drug retention time. Plate I shows the fabrication processes for both single drug and multi-drug loaded devices. The independent drug releases are performed independently from each other.

5.3 Micro/nanofluidics-based drug delivery systems

With smaller delivery channels and exits, micro/nanofluidic devices could easily penetrate health issue to reach relatively inaccessible locations. Simultaneously, they offer opportunities to integrate multi-techniques to perform drug release, sensing and feedback in the local organ.

5.3.1 Working principle

Micro/nanofluidics is the science of manipulating, controlling, and studying fluids at micro/nanodimensions. This unique characteristic allows

micro/nanofluidic devices as controllable platforms to precisely perform drug delivery. In general, reservoirs, channels, pumps, and valves are primary components of micro/nanofluidic devices for precise drug delivery by implanted or transdermal techniques. Drugs stored in reservoirs are precisely moved to desired locations by control parts, such as micropumps and valves. The advantage of the micro/nanochannel-based drug delivery system is that it can provide a stable drug concentration in bodies. The device, with a long and narrow channel, can minimize drug degradation as compared to a device that directly exposes the whole reservoirs to the environment. It is more useful for delivering sensitive, unstable, and easily-contaminated drug. The rate of drug delivery is mostly manipulated through flow diffusion. More new control systems have been reported recently, such as systems using electrokinetic force[13] and pH tunable nanofluidic diode.[14] Mostly, micro- and nano-channel-based devices provide a sustained drug release.

5.3.2 Fabrication of microfluidic drug delivery systems

Microfluidic-based devices for drug delivery are mostly constructed with polymers. Similarly to microreservoir-based devices, microfluidic devices are fabricated by standard photolithography, etching, deposition, and molding techniques.

For nanofluidic devices, due to their tiny dimensions, fabrication of nanochannels needs to be done in a clean room to minimize the contamination of particles. Standard semiconductor processing techniques are utilized to construct nanofluidic devices. Generally, four highly effective and reproducible methods are used: (1) bulk nanomachining, (2) surface nanomachining, (3) buried channel technology, and (4) nanoimprinted lithography (NIL).

In the bulk nanomachining process (Fig. 5.7), the wafer is lithographically patterned, and the oxide mask is etched with an HF solution. The silicon is then anisotropically etched with a developer solution, tetramethylammonium hydroxide (TMAH). Finally, the oxide mask is stripped and bonded to a borofloat glass wafer. For surface nanomachining, the fabrication of nanofluidic devices is similar to that used in microreservoir devices. Buried channel technology can also be used to fabricate nanofluidic devices, especially reservoir-based nanofluidic devices. The detailed fabrication process is shown in Fig. 5.8 (left).[15] The process can be implemented with several steps: deep reactive ion etching to from trench, trench coating with protective material, etch coating at bottom of trench, second isotropic etching to round out bottom, strip coating and channel closing by trench filling. On the right of Fig. 5.8 are SEM images of the device.

Nanoprinting lithography with a two-step process is an alternative fabrication method. The first process is the imprint step, which duplicates the nanostructures on the mold in the polymer. The polymer is heated to become

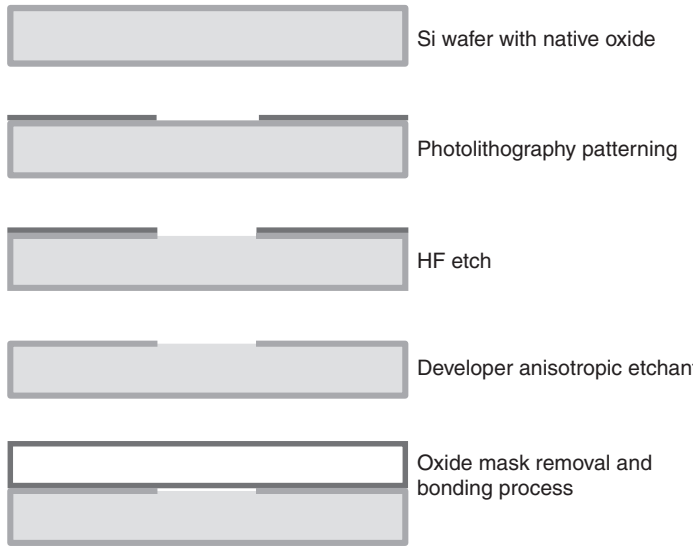

5.7 A fabrication process for bulk nanomachining with wafer bonding.

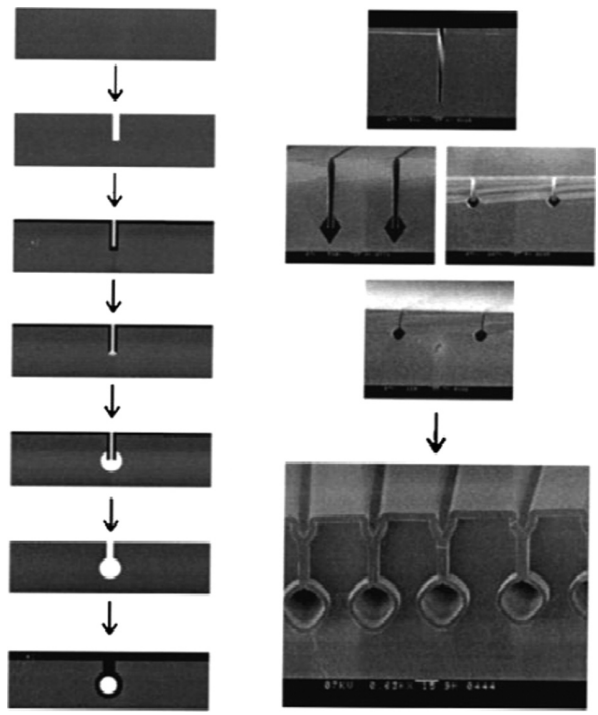

5.8 Process sequence (left) and SEM micrographs (right) of buried channels. (*Source*: Copyright permission from Elsevier.[15])

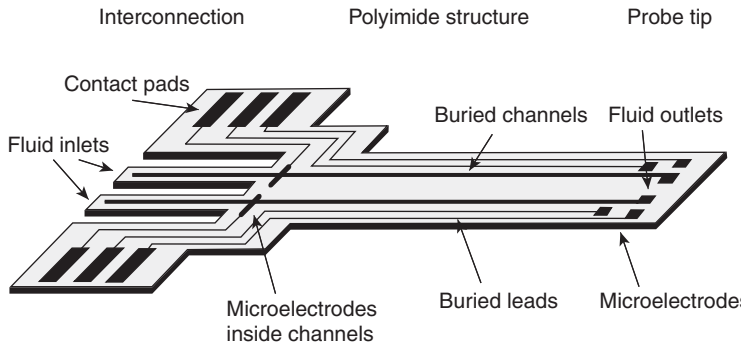

5.9 Illustration of implantable, flexible polyimide probe with microelectrodes and microfluidic channels. (*Source*: Copyright permission from Elsevier.[19])

a viscous liquid, which allows it to deform into the shape of the mold. The second step is the pattern transfer where an etching anisotropic process, such as RIE, is used to remove the residual polymer in the compressed area. PMMA with a small thermal expansion and pressure shrinkage coefficient is a common polymer used in NIL.

5.3.3 Examples of applications

Before 2000, the applications of microfluidic and nanofluidic devices were concentrated on diagnosis, microchemical reactors, protein and DNA separation, and cellular analysis. Since then, more efforts have been devoted to developing micro/nanofluidic drug delivery and disease therapy. Here, a few drug delivery systems of micro/nanofluidics, as examples of applications, will be introduced, including diffusion delivery, pressure injection, and electrokinetic force.

Diffusion drug release is one of the simplest drug delivery microfluidic methods[16–18]. Using this method, the storage cavity or reservoir, embedded in the microchannel, is filled with the reagent. These devices exhibited a sustained drug release. In one work, the microchip was fabricated with PMMA, embedded with one or more microwells and microchannels with different lengths[16]. The well and the channel filled with biocompatible polymer serve as the drug reservoir and diffusion barrier, respectively. When the matrix is exposed to flowing liquid, the reagent dissolves and is released from the cavity. With increasing length of channels, the onset time and duration of drug release increase. Multiple microwells on the microchip can perform differently prolonged periods of time by designing different lengths of micorchannels. Though fabrication of diffusion delivery

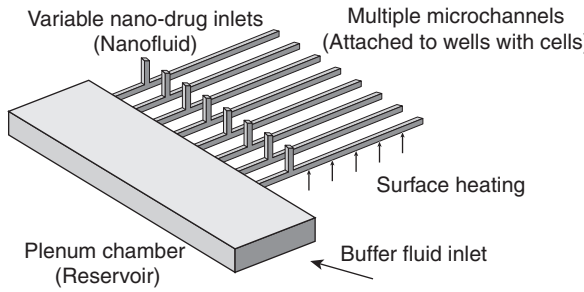

5.10 Nanomedicine delivery system with eight microchannels. (*Source*: Copyright permission from Elsevier.[20])

devices is simple, in some cases it may not be able to perform the drug delivery precisely.

Figure 5.9 shows a polymer-based implantable device with embedded microelectrodes and microfluidic channels.[19] This implanted device combines electric with fluidic technique, which allows simultaneous, selective chemical delivery/probing and performs multi-channel recording/simulation of bioelectric activity. In this device, microelectrodes were characterized by impedance spectroscopy, and drug delivery was achieved with pressure injection techniques. This device enables the monitoring of chemical and electrical information exchange among cells. The devices combine for the first time simultaneous electric and fluidic interfacing to tissue with a flexible micro-implant. This design can be used to study the chemical and electrical information exchange and communication of cells both *in vivo* and *in vitro* experiments.

Another device is a combination of nanofluidics and microfluidics (Fig. 5.10).[20] The plenum chamber as a reservoir provides the nutrient supply and/or purging fluid. Nano-drugs can be supplied by setting the supply pressure of the nano-drug solution higher than that of the fluid supply side. Except a positive influence on drug-concentration uniformity, a heat flux beneath the microchannels ensures that the drug-fluid mixture is delivered to the living cells at an optimal temperature. An ideal nano-drug delivery system is an integration of drug preparation, feeding, sensing and feedback functions. It requests the well-controlled fluid to reach different function parts. The microchannels can alter the fluid to the requested function sections by adjusting the individual inlet pressure. With independent controlled microchannels, the microfluidic device offers a possibility to perform all those functions in a single device.

Electrokinetic actuation is another example of common approaches used to control drug delivery.[12,21–23] In one of the papers,[21] an implantable and mechanically robust nanofluidic membrane was manufactured with precise silicon nanofabrication techniques. Two integrated platinum electrodes at the inlet and outlet play the roles of reversing the nanoflow by applying opposite

voltages as well as controlling the rate of nanoflow. This electrokinetically actuated nanofluidic membrane can provide a sustained drug release at a low applied voltage. The delivery performance of the nanochannel membrane was measured and monitored with a fluorescence microscope over a period of 33 days. Compared with the active release, the passive leakage is less than ~10% and 20% for FITC-BSA and lysozyme after 33 days and 10 day release, respectively. This nanofluidic membrane can achieve rhythmic delivery by electrokinetic actuation and control the range of release rates by the mechanical dimension of the fluidic network, the voltage, and the electrophoretic mobility of the molecules.

In some cases, combining other techniques with microfluidics can produce some interesting designs. In an exemplar study, the researchers present a device that combines the porous supraparticle with microfluidic channels, providing a sustained drug release.[24] In this work, porous supraparticles are fabricated via dry self-assembly method using droplet templates dispensed in superhydrophobic substrates inside a microfluidic channel. The porous supraparticle as a reservoir stores drugs. The device is fabricated with PDMS. A stable rate of drug release can be achieved by controlling porosity, size, and chemistry properties of particles and drugs. Although this device provides just a ~10 min drug delivery, the microfluidic combination with functional particles presents a new horizon for microfluidic-based controlled drug delivery.

In addition, microfluidics can be integrated with the needle structure for controlled drug release.[25,26] For example, in a nanoneedle drug release device, a microfluidic channel as an interconnector and reservoir provides fluidic interconnection of external devices and drug storage room.[25] A microfluidic interconnector assembly was designed and fabricated using SU-8 and conventionally machined PMMA in a way that it has a male interconnector that directly fits into the fluidic reservoir of the microneedle array at one end, and another male interconnector that provides fluidic interconnection to external devices at the other end.

In a different report, microfluidics are integrated with convection enhanced drug delivery (CED), which is a promising therapeutic method for treating diseases of the brain (Fig. 5.11).[27] By increasing the rate of infusion at positive pressure, CED can enhance the drug penetration distance and overcome limitations of traditional treatment for brain tumors caused by the large tumor size and the difficulty of delivering drugs into their dense tissue. Compared to the CED using needles and cannulas delivering drugs, this integrated microfluidic system for CED shows several advantages, including small size to minimize tissue damage, low backflow, the rigid tip to penetrate deep into tissue, and the fluidic outlet located away from the penetrating edge to avoid occlusion of the channel. Moreover, it offers the possibility of

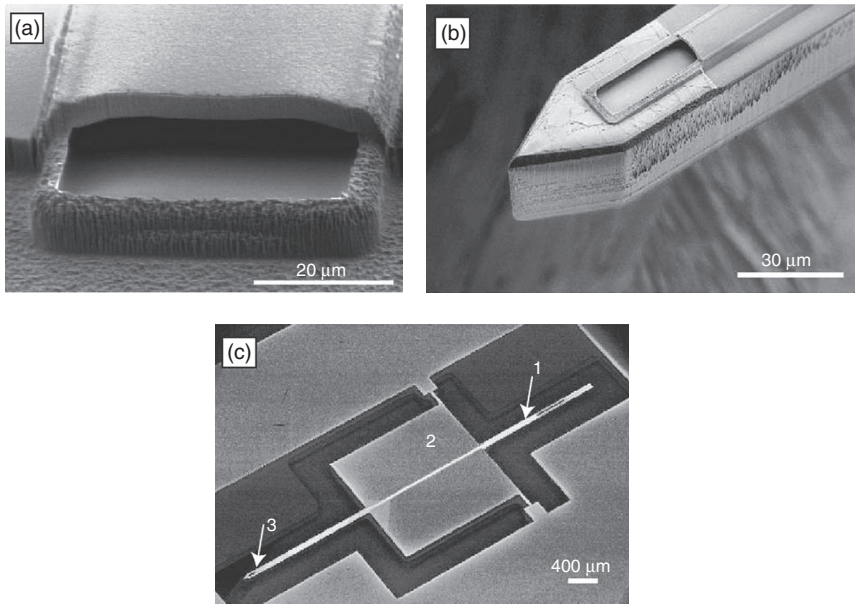

5.11 Electron micrographs of microfluidic probe. (a) Parylene microfluidic channel with dimension of 50 × 10 μm. (b) Pointed tip of insertable portion of probe. (c) Entire probe with protrusion for fluidic connection (1), base for handling (2) and tissue penetrating insert (3). (*Source*: Copyright permission from Elsevier.[27])

integrating electrical, mechanical, and chemical sensors to record the local environment and further control drug concentration.

5.4 Conclusion

MEMS/NEMS technology, combined with new materials and data management, opens revolutionary opportunities to develop low-cost, biocompatible, and controlled drug delivery devices. Both sustained and pulsatile drug delivery in the therapeutic window have been achieved. The multiple reservoir-based device allows people to perform multiple drug delivery simultaneously. Also, different controlling approaches provide more options to selectively deliver drug in local tissues according to different physiological environment and needs. Nowadays, microreservoir devices have become commercial products of drug delivery. With the development of compatible materials, new controllers and delivery methods, and microfluidic-based drug delivery devices will also be ultimately applied in clinic.

5.5 Future trends

In addition to providing well-controlled drug release, highly efficient treatment for diseases, and low toxicity for health tissues, an ideal drug delivery system should include a monitored or triggered feedback to manage the drug release in response to a therapeutic marker or patient's body. However, the drug delivery devices on the market usually need to control drug release under patients and experts' administration according to the result of the outer monitor. How to obtain low-cost drug delivery devices with combination of monitored sensors of therapeutic marker and drug release network is a challenge for controlled drug devices. Advances in micro/nanofabrication, material science, communication technique, and biology will contribute to the design of ideal devices that can integrate biomonitoring with drug delivery in a closed-loop system on a single chip, without expert administration.

To date, pH and temperature controlled drug releases are two approaches that can be directly used in clinic without a complicated control system. pH sensitive materials have been used in clinic to perform controlled drug release according to different pHs of healthy and unhealthy tissues or physiological environments. In addition, temperature triggered drug release also can build the simple triggered drug delivery device.

Besides, new biodegradable materials with low toxicity and high degradable rate are essential to improve the qualification of the implanted device, especially those that can be used to create biocompatible and flexible micro- even nano-sized structure with MEMS/NEMS. Developing more 'smart' materials with unique properties (such as temperature sensitive and memory materials) will offer more opportunities to design customized delivery and feedback loop devices.

Also, local drug release can minimize the drug toxicity to healthy tissues, which is critical for long-term drug delivery. Surface modification with receptors can be utilized to specifically target unhealthy tissues and fix the devices at the target location during a long period of drug release.

As a multidisciplinary field, the combination of new technology and new materials guidance promises to foster further innovation of drug delivery.

5.6 References

1. Sharma, S., Nijdam, A. J., Sinha, P. M., Walczak, R. J., Liu, X., Cheng, M. M. and Ferrari, M. (2006) 'Controlled-release microchips', *Expert Opin Drug Deliv*., **3**(3):379–94.
2. Ziaie, B., Baldi, A., Lei, M., Gu, Y. and Siegel, R.A. (2004) 'Hard and soft micromachining for BioMEMS review of techniques and examples of applications in microfluidics and drug delivery', *Adv Drug Deliv Rev*., **56**(2):145–72.
3. Hand, B. and Gärtner, C. (2008) 'Polymer microfabrication technologies for microfluidic systems', *Anal Bioanal Chem*., **390**:89–111.

4. Staples, M. (2010) 'Microchips and controlled- release drug reservoirs', *Wiley Interdiscip Rev Nanomed Nanobiotechnol.*, **2**(4):400–17.
5. John, T., Santini, Jr, Cima, M. J. and Langer, R. (1999) 'A controlled-release microchip', *Nature*, **397**(6717):335–8.
6. Prescott, J. H., Lipka, S., Baldwin, S., Sheppard, N. F. Jr, Maloney, J. M., Coppeta, J., Yomtov, B., Staples, M. A. and Santini, J. T. Jr. (2006) 'Chronic programmed polypeptide delivery from an implanted multireservoir microchip device', *Nat Biotechnol.*, **24**(4):437–8.
7. Elman, N. M., Masi, B. C., Cima, M. J. and Langer, R. (2010) 'Electro-thermally induced structural failure actuator (ETISFA) for implantable controlled drug delivery devices based on Micro-Electro-Mechanical-Systems', *Lab Chip*, **10**(20):2796–804.
8. Voskerician, G., Shawgo, R. S., Hiltner, P. A., Anderson, J. M., Cima, M. J. and Langer, R. (2004) 'In vivo inflammatory and wound healing effects of gold electrode voltammetry for MEMS micro-reservoir drug delivery device', *IEEE Trans Biomed Eng.*, **51**(4):627–35.
9. Richards Grayson, A. C., Choi, I. S., Tyler, B. M., Wang, P. P., Brem, H., Cima, M. J. and Langer, R. (2003) 'Multi-pulse drug delivery from a resorbable polymeric microchip device', *Nat Mater.*, **2**(11):767–72.
10. Pirmoradi, F. N., Jackson, J. K., Burt, H. M. and Chiao, M. (2011) 'On-demand controlled release of docetaxel from a battery-less MEMS drug delivery device', *Lab Chip*, **11**(16):2744–52.
11. Chirra, H. D. and Desai, T. A. (2012) 'Multi-reservoir bioadhesive microdevices for independent rate-controlled delivery of multiple drugs', *Small*, 2012, **8**(24): 01367.
12. Tao, S. L., Lubeley, M. W., and Desai, T. A. (2003) 'Bioadhesive poly(methyl methacrylate) microdevices for controlled drug delivery', *J Control Release*, **88**(2):215–28.
13. Fine, D., Grattoni, A., Zabre, E., Hussein, F., Ferrari, M. and Liu, X. (2011) 'A low-voltage electrokinetic nanochannel drug delivery system', *Lab Chip*, **11**(15):2526–34.
14. Ali, M., Ramirez, P., Mafé, S., Neumann, R. and Ensinger, W. (2009) 'A pH-tunable nanofluidic diode with a broad range of rectifying properties', *ACS Nano*. **3**(3):603–8.
15. Fintshenko, Y. and van den Berg, A. (1998) 'Silicon microtechnology and microstructures in separation science', *J Chromtograph A*, **819**:3–12.
16. Lee, S. H., Park, M., Park, C. G., Lee, J. E., Prausnitz, M. R. and Choy, Y. B. (2012) 'Microchip for sustained drug delivery by diffusion through microchannels', *AAPS PharmSciTech.*, **13**(1):211–17.
17. Garcia, E., Kirkham, J. R., Hatch, A. V., Hawkins, K. R. and Yager, P. (2004) 'Controlled microfluidic reconstitution of functional protein from an anhydrous storage depot', *Lab Chip*, **4**(1):78–82.
18. Su, Y. and Lin, L., (2004) 'A water-powered micro drug delivery system', *J. Microelectromechan. Syst.*, **13**:175–82.
19. Metz, S., Bertsch, A., Bertrand, D. and Renaud, P. (2004) 'Flexible polyimide probes with microelectrodes and embedded microfluidic channels for simultaneous drug delivery and multi-channel monitoring of bioelectric activity', *Biosens Bioelectron.*, **19**(10):1309–18.

20. Kleinstreuer, C., Li, J. and Koo, J. (2008) 'Microfluidics of nano-drug delivery', *Int. J. Heat Mass Trans*., **51**:5590–7.
21. Fine, D., Grattoni, A., Zabre, E., Hussein, F., Ferrari, M. and Liu, X. (2011) 'A low-voltage electrokinetic nanochannel drug delivery system', *Lab Chip*, **11**(15):2526–34.
22. Fine, D., Grattoni, A., Hosali, S., Ziemys, A., De Rosa, E., Gill, J., Medema, R., Hudson, L., Kojic, M., Milosevic, M., Brousseau, LiiL, Goodall, R., Ferrari, M. and Liu, X. (2010) 'A robust nanofluidic membrane with tunable zero-order release for implantable dose specific drug delivery', *Lab Chip*, **10**(22):3074–83.
23. Grattoni, A., De Rosa, E., Ferrati, S., Wang, Z., Gianesini, A., Liu, X., Hussain, F., Goodall, R. and Ferrari, M. (2009) 'Analysis of a nanochanneled membrane structure through convective gas flow', *J. Micromech. Microeng*., **19**:115018.
24. Rastogi, V., Velikov, K. P. and Velev, O. D. (2010) 'Microfluidic characterization of sustained solute release from porous supraparticles', *Phys Chem Chem Phys*., **12**(38):11975–83.
25. Kim, K. and Lee, J. B. (2007) 'High aspect ratio tapered hollow metallic microneedle arrays with microfluidic interconnector', *Microsyst. Technol*., **13**:231–5.
26. Bodhale, D. W., Nisar, A. and Afzulpurkar, N. (2010) 'Structural and microfluidic analysis of hollow side-open polymeric microneedles for transdermal drug delivery applications', *Microfluid. Nanofluid*., **8**:373–92.
27. Neeves, K. B., Lo, C. T., Foley, C. P., Saltzman, W. M. and Olbricht, W. L. (2006) 'Fabrication and characterization of microfluidic probes for convection enhanced drug delivery', *J. Control Release*, **111**(3):252–62.

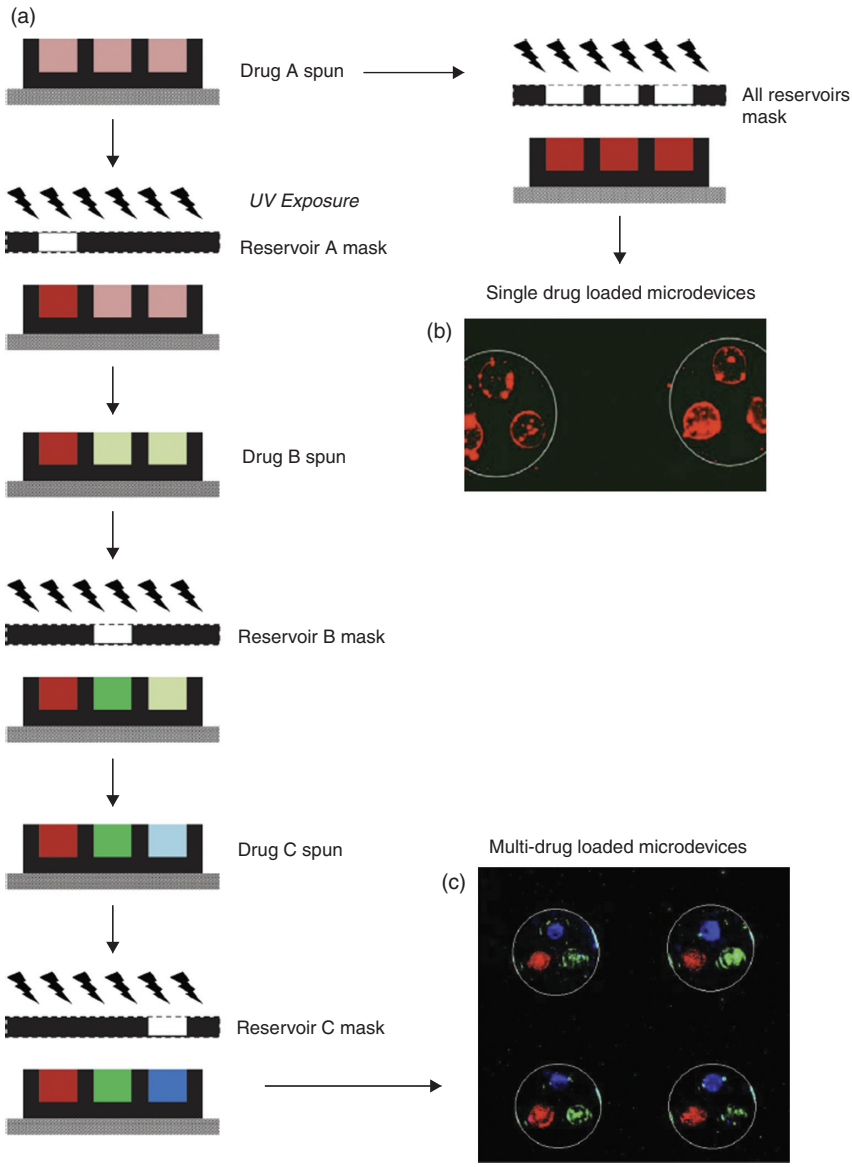

Plate I (Chapter 5) (a) Schematic process overview for fabricating single or multi-drug loaded microdevices using photolithography. (b) A fluorescent micrograph showing the presence of a single model drug (Texas red-BSA) loaded in all three reservoirs of the same microdevice. (c) A fluorescent micrograph composite of a multi-drug (Texas red-BSA, red; FITC-BSA, green; DNP-BSA, blue) loaded microdevice as individual drug in separate reservoirs. The white circle highlights the microdevice area. (*Source*: Copyright permission from John Wiley & Sons Inc. Chirra, H. D. and Desai, T. A. (2012) 'Multi-reservoir bioadhesive microdevices for independent rate-controlled delivery of multiple drugs', *Small*, 8(24): 01367.)

6

Microneedles for drug delivery and monitoring

T. R. R. SINGH, H. MCMILLAN, K. MOONEY, A. Z. ALKILANI and R. F. DONNELLY,
Queens University Belfast, UK

DOI: 10.1533/9780857097040.2.185

Abstract: Microneedles (MN) are micron-sized needles, ranging from 25 to 2000 μm in height, made of a variety of materials and shapes. Application of MNs to the skin can create micron-sized transport pathways that allow enhanced delivery of a wide range of drug molecules. The concept of MNs was first conceived in 1976; however, it was not possible to make them until the first exploitation of microelectromechanical systems (MEMS) in 1998. Therefore, this chapter will focus on the fabrication techniques of MNs using MEMS, the design and material consideration of MNs, and the application of MNs in drug delivery and monitoring biological fluids.

Key words: microneedles, microelectromechanical systems, transdermal drug delivery, skin, drug delivery, biological fluid monitoring.

6.1 Introduction

Transdermal delivery is currently restricted to around 20 drug molecules that are approved by the US Food and Drug Administration for delivery by transdermal patches; for example, fentanyl for pain management, and nicotine for smoking cessation (Prausnitz *et al*., 2004). These approved molecules are all of low molecular weight (<500 Da), have adequate solubility in both water and oil, and require a low daily dose to be administered (Chu and Prausnitz, 2011; Teo *et al*., 2006). Other properties required for good skin permeation include high but balanced octanol:water partition coefficient and a low melting point, which correlates with good solubility (Potts, 1990; Teo *et al*., 2006). The limited permeability of molecules that do not possess the above properties is due to the outermost layer of the skin, the *stratum corneum* (*SC*). This 'dead' layer of tissue has the ability to prevent the permeation of foreign compounds, including drug molecules, and therefore acts as a very effective barrier (Naik *et al*., 2000).

In order to enhance drug permeation of the skin, a number of chemical and physical methods have been investigated. Chemical penetration enhancers, such as azone and l-α-lecithin have shown inconsistent results in terms of drug permeation and inflammatory reactions (Fang *et al*., 2003). The peptide magainin is a natural pore former and it can be used to increase skin permeability (Kim *et al*., 2007). Physical methods, such as ultrasound, iontophoresis and electro poration, have been investigated but these methods require additional equipment to generate the physical disruption (Conjeevaram *et al*., 2002; Joshi and Raje, 2002; Vanbever *et al*., 1996).

The concept of MNs for use in drug delivery was initially considered a number of decades ago, with the first patent being filed by Gerstel and Place in 1976 (Gerstel and Place, 1976), but it was not until late into the 1990s that papers were published detailing a viable technique, due to previous limitations in fabrication. Since that time, interest in this method of drug delivery has expanded significantly. According to Kim *et al*., the current count of papers detailing the use of MN for drug delivery stands at over 350 (Kim *et al*., 2012a). These papers describe the delivery of a range of drug molecules via a number of methods, including vaccines. The main body of work has involved the investigation of the use of MNs to aid the delivery of drugs via the transdermal route. MNs, as previously described, are micron-sized projections that can be produced in a range of conformations and materials, offering a new way to deliver drug molecules. In order to facilitate this, Kim *et al*. stated 'a MN should be large enough to deliver almost any drug but still be small enough to avoid pain, fear and the need for expert training to administer' (Kim *et al*., 2012b). As the *SC* is only 15–50 μm thick in the dry state, the MNs have been developed so they bypass the *SC* but avoid the deeper tissues, which contain nerve endings and blood vessels, and so overcome the drawbacks associated with hypodermic needles (Shawgo *et al*., 2002; Xie *et al*., 2005).

In the last few decades, the development of new therapeutics has seen the emergence of a large number of biotherapeutics. Due to the nature of these molecules, I.V via hypodermic needle is the most commonly employed method of delivery. This allows the gastrointestinal tract and first-pass metabolism to be avoided; however, the disadvantages noted above are cause for concern. Previously the transdermal route was not a feasible route to use to deliver these drugs, but through the utilisation of MN, the skin has become a target for delivering these molecules. Using MN to circumvent the *SC*, the range of drugs that can be delivered across the skin has been considerably increased to include biotherapeutics and vaccines as well as low molecular weight drugs. In addition to improving transdermal delivery, MN has been shown to facilitate delivery to the eye, cell nucleus, and localised tissue delivery.

6.2 Fabrication of microneedles (MNs)

Microelectromechanical systems (MEMS) technology is the most promising method to fabricate the optimal design of MNs for specific application, as it allows for accurate replication of MNs to produce extremely precise devices. It was the microelectronics industry that allowed the production of these very small structures through microfabrication. The earliest MNs were manufactured using standard microfabrication techniques to etch arrays of micron-size needles into silicon (Henry *et al.*, 1998). Since then, they have been produced using a range of materials, such as ceramic, glass, polydimethylsiloxane (PDMS), dextrin and polymers, as well as metal such as stainless steel and titanium. They have also been produced in numerous geometries, sizes, and shapes, with or without a bore, allowing use for different applications. Use of MEMS techniques has led to potential applications in biomedical fields (called BioMEMS), such as in drug delivery, DNA sequencing devices, biosensors and chemical analysis systems (Ashraf *et al.*, 2011; Donnelly *et al.*, 2012). The most common substrate material for micromachining is silicon. It has been successful in the microelectronics industry and will continue to be in areas of miniaturisation for several reasons, such as it is abundant, inexpensive compared to metal and ceramic, and can be processed to unparalleled purity. Silicon's ability to be deposited in thin films is also very amenable to MEMS (Donnelly *et al.*, 2010b; Garland *et al.*, 2011; Kim *et al.*, 2012b).

Most MN fabrication methods are based on the conventional microfabrication techniques of adding, removing, and copying microstructures utilising photolithographic processes, laser cutting, metal electroplating, silicon etching, metal electropolishing and micromoulding (Kim *et al.*, 2012b). The three basic techniques in MEMS technology are the deposition of thin films of material on a substrate, applying a patterned mask on top of a film by photolithographic imaging, and etching the films selectively to the mask.

6.2.1 Thin film deposition

Thin film deposition involves processing above the substrate surface (typically a silicon wafer with a thickness of 300–700 μm). Material is added to the substrate in the form of thin film layers, which can be either structural layers or act as spacers later to be removed. MEMS deposition techniques fall into two categories, depending on whether the process is primarily chemical or physical (Madou Marc, 1997). In chemical deposition, films are deposited via a chemical reaction between the hot substrate and inert gases in the chamber at low or atmospheric pressure. Depending on the phase of the precursor, chemical deposition is further classified into plating, spin coating, chemical vapour deposition (CVD) (e.g. low pressure CVD, plasma-enhanced CVD,

Table 6.1 Different MEMS deposition techniques

Physical vapour deposition (PVD) techniques	CVD techniques	Others deposition techniques
• Thermal evaporation • Sputtering • Molecule-beam epitaxy • Ion plating • Laser ablation deposition • Cluster-beam deposition	• Plasma-enhanced CVD (PECVD) • Atmospheric pressure CVD • Low pressure CVD (LPCVD) • Very low pressure CVD (VLPCVD) • Metallorganic CVD • Spray pyrolysis	• Epitaxy • Casting • Electrochemical deposition • Silk-screen printing • Plasma spraying • Casting

and very low pressure CVD), and atomic layer deposition. In physical deposition, the raw materials (solid, liquid or vapour) are released and physically moved to the substrate surface, e.g. thermal evaporation, sputtering and ion plating. The choice of deposition process is dependent upon several factors, e.g. substrate structure, operating temperature, rate of deposition and source. These film layers are deposited and subsequently patterned using photolithographic techniques, then etched away to release the final structure (Banks, 2006; Madou Marc, 1997). A summary of MEMS deposition techniques can be found in Table 6.1.

6.2.2 Photolithography

Photolithography is a technique used to transfer copies of a master pattern onto the surface of a substrate of some material (usually a silicon wafer). The substrate is covered with a thin film of some material, e.g. silicon dioxide (SiO_2), on which a pattern of holes will be formed, as seen in Fig. 6.1. There are different types of lithography, including photolithography, electron beam lithography, ion beam lithography and X-ray lithography. Diamond patterning is also an option for lithography. A thin layer of an organic polymer, known as photosensitive or photoresist, which is sensitive to ultraviolet (UV) radiation, is then deposited on the oxide layer (Fig. 6.1a). A photomask, consisting of a glass plate (transparent) coated with a chromium pattern (opaque), is then placed in contact with the photoresist-coated surface (Madou Marc, 1997). The wafer is exposed to the illumination; the simplest form is via the use of UV, transferring the pattern on the mask to the photoresist, which is then developed (Fig. 6.1c). The radiation causes a chemical reaction in the exposed areas of the photoresist, of which there are two types: positive and negative. During the development processes, the rinsing solution removes either the exposed areas or the unexposed areas

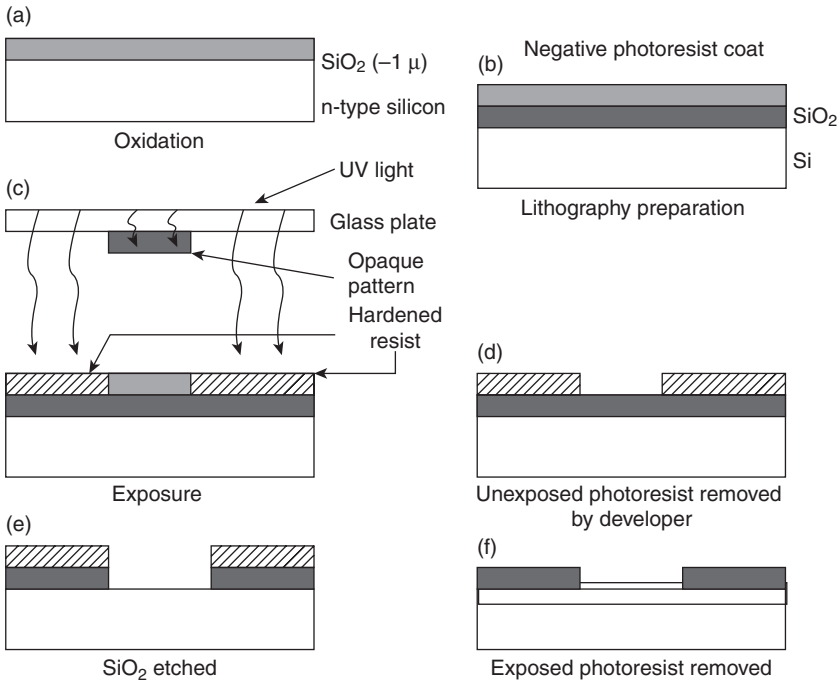

6.1 Sequential processes in the transfer of a pattern to the substrate surface.

of photoresist, either by wet (using solvent) or dry (using vapour phase or plasma) and leaving a pattern of bare and photoresist-coated oxides on the wafer surface (Fig. 6.1d). After that, the unwanted photoresist left after the development process is removed by oxygen plasma treatment (Banks, 2006; Donnelly *et al.*, 2012; Madou Marc, 1997). The final oxide pattern is then either a positive or negative copy of the photomask pattern and used as a mask in subsequent processing steps (Fig. 6.1f). In MEMS, the oxide is used as a subsequent mask for either further additional chemical etching creating deeper 3D holes, or new layers on which to build further layers, resulting in an overall 3D structure or device (Banks, 2006; Madou Marc, 1997).

6.2.3 Etching

Etching is a technique to cut the unprotected parts of a material's surface by using strong acid or a physical process to create a design in it, and can be divided into two categories: wet etching and dry etching. The selection of any of the abovementioned methods largely depends on the material of construction and the type of MNs (Donnelly *et al.*, 2012). It is used to etch

the thin films previously deposited and/or the substrate itself. In wet etching the material is removed by immersion of a material (typically a silicon wafer) in a liquid bath of a chemical etchant. These etchants are classified into isotropic and anisotropic. Isotropic etchants attack the material at the same rate in all directions. Anisotropic etchants etch material at different rates in different directions, so they are faster in a preferred direction. Potassium hydroxide (KOH) and tetramethyl ammonium hydroxide (TMAH) are the most common anisotropic etchants. Structures formed in the substrate are dependent on the crystal orientation of the substrate or wafer. The dry etching technology can be divided into three classes: reactive ion etching (RIE), sputter etching, and vapour phase etching. Deep reactive ion etching (DRIE) is a higher-aspect-ratio, up to 50:1, etching method involving an alternating process of high-density plasma etching and CVD. This process, called BOSCH, was patented by Laermer and Schilp at Robert Bosch GmbH in 1994 (Laermer and Schilp, 1996). For silicon, DRIE is one of the most important promising technologies for high volume production. The BOSCH process provides a tool to optimise fabrication parameters to achieve high etch rate, high aspect ratio, straight sidewalls and small sidewall scalloping. The probability of getting non-vertical, tapered sidewalls is limited (Roxhed *et al.*, 2007).

6.3 MN design parameters and structure

The shape and geometry of MN is critical during design and fabrication. The needles must be capable of inserting into skin without breaking and the needles should be of suitable length, width and shape to avoid nerve contact (McAllister *et al.*, 2003; Park *et al.*, 2005; Yung *et al.*, 2012). The elastic properties of human skin can prevent MN from penetrating by twisting around the needles during MN application, particularly in the case of blunt and short MNs (McAllister *et al.*, 2003). Metals are typically strong enough, whereas polymers must be selected in order to ensure they have sufficient mechanical strength. Typical MN geometries vary from 25 to 2500 μm in length, 50 to 250 μm in base width and 1 to 25 μm in tip diameter (McAllister *et al.*, 2003; Yung *et al.*, 2012).

Based on the fabrication process, the MNs are classified as in-plane MNs, out-of-plane MNs, or a combination as seen in Fig. 6.2. Considering the in-plane designs (Fig. 6.2a), the MNs are parallel to the machined surface of the substrate (e.g. Si wafer). The major advantage of in-plane MNs is easily and accurately controlled production of MNs with various lengths during fabrication process. In out-of-plane designs (Fig. 6.2b), the MNs are perpendicular to the fabrication surface of Si wafer and are easier to produce in arrays than in-plane (Ashraf *et al.*, 2011; Donnelly *et al.*, 2012). MNs can also be classified as solid, coated, dissolving, and hollow, according to the structure.

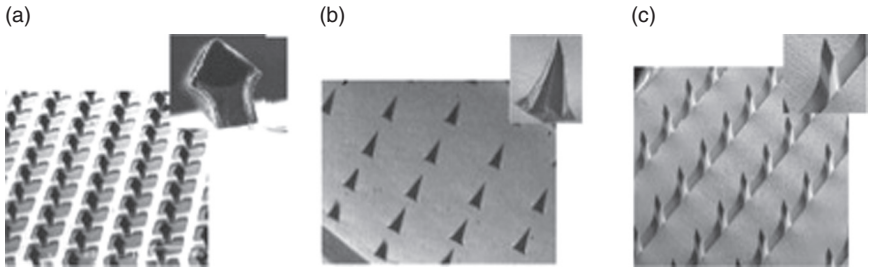

6.2 Scanning electron microscope (SEM) images of (a) in-plane MNs (Daddona, 2002), (b) out-of-plane MNs (Donnelly *et al.*, 2009b), and (c) combined in-plane and out-of-plane MNs (Jae-Ho *et al.*, 2008).

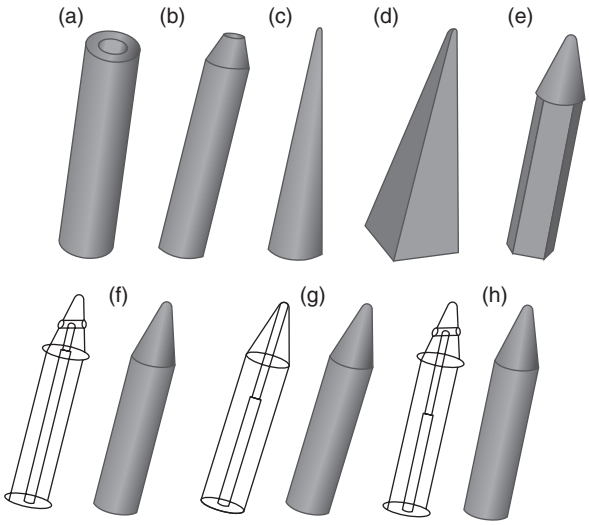

6.3 Shapes of MN (a) Cylindrical; (b) Tapered tip; (c) Canonical; (d) Square base; (e) Pentagonal-base canonical tip; (f) Side-open single lumen; (g) Double lumen; (h) Side-open double lumen. (*Source*: Adapted from Ashraf *et al.*, 2011.)

MNs can be classified on the basis of overall shape and tip, ranging from cylindrical, rectangular, pyramidal, conical, octagonal, to quadrangular, with different needle lengths and widths. The tip shape of MNs is important for skin penetration, because sharper MNs have higher potential for penetrating the skin, but larger tip diameters require higher insertion forces, which may lead to bending or breaking of the needles in the skin (Arora *et al.*, 2008; Banga, 2009; Teo *et al.*, 2006). In addition, the shape of the tips of hollow MNs is essential for the flow rate; the flow from a blunt-tip MN is lower than a bevel-tip MN, because a blunt-tip MN compacts the skin and thus

has higher risk of clogging (Bodhale *et al.*, 2010; Luttge *et al.*, 2007). To overcome this problem, it should have very sharp tip, with the bore of the MN off-centred or on the side of the MN. Increasing the number of bores in hollow MNs will increase the flow rate; nevertheless, this results in decreased MN strength and a reduction in sharpness (Stoeber and Liepmann, 2002). Figure 6.3 summarises the multiple geometries of MN available.

6.3.1 Solid MNs

As the name suggests, these MNs are solid with no openings in the structure. In order to utilise these MNs for drug delivery, a variety of materials have been used for manufacture, including metals (Gill and Prausnitz, 2007a; Matriano *et al.*, 2002), silicon (Gardeniers *et al.*, 2003), glass (McAllister *et al.*, 2003), non-biodegradable polymers (Jin *et al.*, 2009; Moon *et al.*, 2005) and biodegradable polymers (Park *et al.*, 2005) (Table 6.2). The most common materials are discussed below.

Silicon MN

Prausitz's research group from Georgia Institute of Technology, Atlanta, USA fabricated the first MN, which was made up of silicon. The Si wafer was etched by an oxygen/fluorine plasma mixture in a RIE (a dry etching process), with a chromium mask. The dimensions of needles were approximately 80 μm at the base, 150 μm in length, and approximately 1 μm radius of curvature at the tip. These needles were able to increase skin permeability of calcein, insulin and bovine serum albumin (Henry *et al.*, 1998; McAllister

Table 6.2 Lists of the most common materials used for fabrication of MN

Metals	Synthetic polymer		Natural polymer
	Biodegradable	Non-biodegradable	
Silicon	Poly lactic acid (PLA)	Poly vinyl acetate	Carboxy methyl cellulose (CMC)
Stainless steel	Poly glycolic acid (PGA)	Alginic acid	Amylopectin
Titanium	Polycarbonate	Gantrez AN139	Dextran
Palladium	Poly vinyl pyrrolidone (PVP)	Carbopol 971 P-NF	Galactose
Nickel	Polylactide-co-glycolic acid (PLGA)	Polyetherimide	Maltose

et al., 2000). Wilke *et al*. (2005) fabricated silicon MN by a dry etching technique (a modified RIE), using a standard wafer of 525μm thickness, and a conical-shaped solid MN with an aspect ratio of 4.5:1 (height: base diameter). As usual, undercut etch rate to vertical etch (using SF_6/O_2) was utilised with the BOSCH-DIRE process (Wilke *et al*., 2005).

Another type of solid silicon MNs, called microenhancer arrays, were etched from silicon wafers using lithography and potassium hydroxide etching, were able to deliver naked plasmid DNA into mice skin. These needles measured 50–200 μm in length over a $1cm^2$ area and had a blunt tip (Mikszta *et al*., 2002). The significance of this study was the feasibility of using blunt-tipped MNs to scrape the skin for increased the delivery of DNA vaccine to generate an immune response.

Roxhed *et al*. (2008a) fabricated sharp hollow silicon MN tips with side-openings. In addition, the tips were sealed with a layer of gold coating, to yield a closed-package system. The MNs were made on a 600 μm thick, monocrystalline silicon wafers using a two-mask process, an anisotropic DRIE etch through the BOSCH process, and an isotropic SF_6 plasma etching. There were two designs of MN: a 310 μm long cross-shaped, and 400 μm long circular-shaped. Three different methods to open the gold seals are burst opening, opening upon insertion into the skin, and electrochemical opening (Roxhed *et al*., 2008a). Moreover, Roxhed *et al*. (2008b) integrated the 400 μm long circular-shaped HMN with an electrically controlled liquid dispensing unit to form a patch-like drug delivery system. This liquid dispenser was made up of three different layers: a 500 μm thick printed circuit board (PCB) heater layer, a 500 μm thick expandable layer (a mixture of silicone elastomers), and a liquid reservoir (total volume of 12 μL). This integrated device was used for delivery of insulin in diabetic rats and showed consistent control over blood glucose levels (Roxhed *et al*., 2008b).

Metal MNs

Metal MN have good mechanical strength, are easy to fabricate, relatively inexpensive, and the metals used, such as stainless steel, titanium, and nickel, have established safety records in FDA medical approved devices (Gill and Prausnitz, 2007a). They have been fabricated by laser cutting (e.g. stainless steel), wet etching (e.g. titanium), laser ablation, and metal electroplating methods (Kim *et al*., 2012b). The smallest used hypodermic needles (30/31 G) were translated into arrays of MNs. A research group at Alza Corp reported titanium MN arrays (commercially called Macroflux®) fabricated by applying a thin layer of photoresist onto a titanium or stainless steel sheet, contact-exposing and developing the resist with the desired pattern, and bending the arrays to a 90° angle (relative to horizontal sheet plane), which ranged from 175–430 μm in length, 190–320 arrays/cm^2 over an area of

2 cm^2, base width 170 μm and thickness 35 μm. These microprojection arrays were able to deliver oligodeoxynucleotides, ovalbumin, synthetic peptide, and human growth hormone across hairless guinea pigs' skin (Cormier and Daddona, 2003).

Omatsu *et al*. (2010) fabricated MNs on a metal surface based on laser ablation using circularly polarised optical vortices having non-zero total angular momentum, known as twisted light with spin, for the first time. The needle showed a height of at least 10 μm above the target surface and a tip diameter of less than 0.5 μm. They also demonstrated the fabrication of a two-dimensional 5 × 6 MN array. This technique forms a metal MN by deposition of a few laser pulses onto a metal target, significantly improving the time and cost of fabrication of two-dimensional metal MN arrays (Omatsu *et al*., 2010).

Bai *et al*. (2012) fabricated micro-nickel needle arrays by Lithographie, Galvanoformung, Aboformung (LGIA) process, which is a high aspect ratio fabrication technique based on polydimethylsiloxane (PDMS) mould and nickel transfer technology. The density of the array was 900 MN/cm^2 and the height was 150 μm; the advantages of this fabrication method are in forming complex 3D micro metal structures, low cost, and high throughput.

Ceramic MN

The use of ceramic materials raised the possibility to fabricate solid and porous MNs, which could be loaded with liquid for drug delivery or diagnostic sampling (Bystrova and Luttge, 2011). Solid ceramic MNs were fabricated by micromolding alumina slurry using a (PDMS) MN mould and ceramic sintering (Donnelly *et al*., 2012; Kim *et al*., 2012b). Bystrova and Luttge (2011) from University of Twente, the Netherlands, fabricated ceramic MNs by the micromachining of the SU-8/Si master, which allowed a variety of needle geometries, such as disc shape. The multiple replication of the PDMS mould gives a low cost production mould that can be reused for ceramic (Bystrova and Luttge, 2011).

Ceramic MNs have also been lithographically fabricated using a two-photon-induced polymerisation approach. An intense laser was scanned within a photosensitive polymer–ceramic hybrid resin using a galvano-scanner and a micropositioning system to induce polymerisation locally in the shape of the MN (Bystrova and Luttge, 2011; Kim *et al*., 2012b).

Coated MNs

The micron lengths of needles enforce special coating formulation to obtain uniform coatings and spatial control over the region of the MN to be coated, because the effects of surface tension, capillarity and viscous forces become more prominent at these small length scales. Therefore, for coating drug

formulation, solid MNs should be composed of surfactants to facilitate wetting and spreading of the drug solution on the MN surface during the coating process, viscosity enhancers to increase coating thickness, and stabilising agent to protect and stabilise biomolecules during drying and storage (Choi *et al*., 2012; Gill and Prausnitz, 2007b). In addition, coating solution excipients and solvent should be safe for human use, and the coating method should be compatible with manufacturing processes and not damage coated drugs.

In 2012, Peters and colleagues from Zosano Pharma, Inc., California, USA, demonstrated for the first time that erythropoietin Alfa (EPO) can be formulated at high concentration and coated onto an MN patch without loss of efficacy or formation of insoluble aggregates. In this study, titanium MN arrays were made by photo/chemical etching, and the drug formulation which was 15% w/w EPO, 15% w/w sucrose and 0.2% w/w polysorbate 20 coated on the MN array, was spun at 50 rpm, in a drug formulation reservoir (2 mL in volume) to produce a thin film of drug with controlled thickness of ~100 μm. The tips of the needles were dipped into the thin film, and the coating per area adjusted by the number of dips. The time between each dip coating was less than 5 s, which was enough to allow the coating to dry. The dose per patch was also optimised by the MN array area (from 0.3 to 3 cm^2) (Peters *et al*., 2012). DeMuth *et al*. (2010) fabricated multilayer-coated MN, which achieved transcutaneous delivery of plasmid DNA to the epidermis. Plasmid DNA was delivered to the skin by MN application to achieve co-localisation with Langerhans dendritic cells (DeMuth *et al*., 2010).

6.3.2 Hollow MNs

Hollow MNs (HMN) are of interest for pharmaceutical application because they enable transfer of a wide range of molecules transdermally with the advantages of hypodermic injection, such as rapid onset action without the drawbacks (e.g. pain, skin reaction). The flow rate can be modulated for a rapid bolus injection, a slow infusion, or a time varying delivery rate. HMNs can be integrated into a smart biomedical device consisting of a biosensor, and blood sampling and drug delivery systems (Donnelly *et al*., 2012; Kim *et al*., 2012b; van der Maaden *et al*., 2012).

HMNs were made of glass; polymer and metal have been prepared from substrates by conventional fabrication methods. These needles have been produced either from material substrate of MEMS directly, or from multiple substrates with different physicochemical properties to be utilised as sacrificial layer and fabricated by different techniques including laser micromachining, DRIE of silicon, an integrated lithographic moulding technique, deep X-ray photolithography, and wet chemical etching and microfabrication (Kim *et al*., 2012b).

McAllister *et al.* (1999) demonstrated the first out-of-plane HMNs The fabrication process combined a solid silicon MN with the BOSCH process to form a needle bore, 150 μm long HMN and microtubes. The paper also presented the fabrication of metal HMNs which were fabricated by electroplating the needles (lost-mould technique), had bore openings of 10 μm in diameter, and penetrated epidermal tissue *in vitro*. Kim *et al.* (2004) demonstrated later in the same way the fabrication of metal HMNs by electroplating needles on solid MN arrays made of SU-8. The silicon HMNs were fabricated by the BOSCH process to create hollow shell structures with high aspect ratio, after which isotropic and wet etching processes were used to obtain sharper tips. To obtain a polymer HMN, a drilling process, to make the bore hole, and milling, to create the bevelled tip shape out of polyphenylsulfone polymer, were utilised (Daugimont *et al.*, 2010).

6.4 Strategies for MN-based drug delivery

MNs manufactured using a variety of materials such as metals (Gill and Prausnitz, 2007a; Matriano *et al.*, 2002), silicon (Gardeniers *et al.*, 2003), glass (McAllister *et al.*, 2003), non-biodegradable polymers (Jin *et al.*, 2009; Moon *et al.*, 2005) and biodegradable polymers (Park *et al.*, 2005) have been used for enhancing TDD. Four main approaches, one using hollow MNs and the other three utilising solid MNs, have been utilised, as shown in Fig. 6.4.

6.4.1 Skin pretreatment: 'poke and patch'

Skin pretreatment produces microconduits through which molecules are able to travel (Banga, 2009; Singh *et al.*, 2010) (Fig. 6.4a). Drugs are contained within a patch or a semi-solid topical formulation that is applied over the area where the MNs were applied (Williams, 2003). This method is suitable for both localised delivery to the target tissue but also systemic delivery. The delivery of drugs via this method initially investigated the feasibility of delivering molecules such as calcein (623 Da), across the skin with and without using MNs. An increase in permeability of around 10 000-fold was observed when MNs were applied for 10 s, while application of the MNs for 1 h prior to removal resulted in a 25 000-fold increase in calcein permeability (Henry *et al.*, 1998). Naltrexone delivery was investigated across both guinea pig and human skin by the delivery of drugs to human skin by this method. After application of the MNs, elevated levels of naltrexone in the plasma were observed for 3 days following, compared to non-treated MN skin. Permeability of the guinea pig skin to the hydrophilic naltrexone hydrochloride was augmented 10-fold with similar results observed for human skin (Banks *et al.*, 2008, 2010).

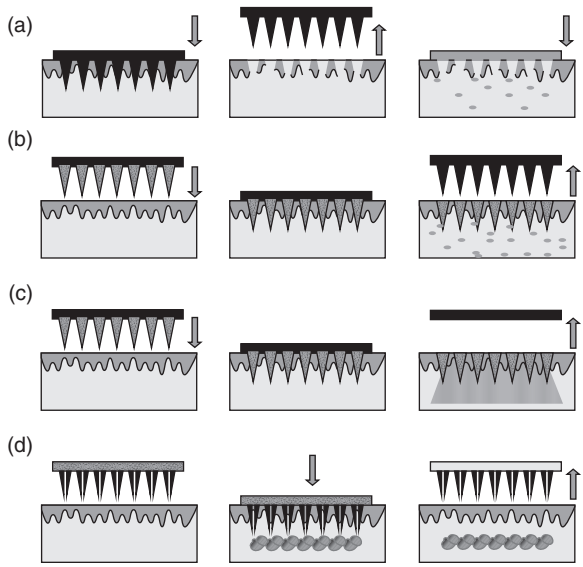

6.4 (a) Solid MNs applied and removed to create micropores followed by the application of a traditional transdermal patch. (b) Solid MNs coated with drug molecules applied for instant delivery. (c) Polymeric MNs which remain in skin and dissolve over time to deliver the drug within the MNs. (d) Hollow MNs for continuous drug delivery or body fluid sampling. (*Source*: Adapted from Arora *et al.*, 2008.)

More recent work has produced data relating to the localised delivery of phenylephrine (PE) to the anal sphincter muscle using MN for the treatment of faecal incontinence. Pretreating human cadaver skin with an array of 50 MN resulted in a 6-fold increase in the amount of PE delivered, with a 100 MN array increasing the amount delivered by 10-fold compared to without MN treatment (Baek *et al.*, 2011). A further application of this approach has been in the delivery of 5-aminolevulinic acid (ALA) used in photodynamic therapy, which involves the combination of photosensitisers and light to kill target cells (Dai *et al.*, 2009; Donnelly *et al.*, 2008). Topical delivery of ALA has shown good clearance rates and is not associated with cutaneous photosensitivity, and therefore can treat superficial lesions successfully. Deeper lesions, however, are resistant to this method of delivery as ALA is hydrophilic and therefore can only penetrate the top layers of tissue. Pretreatment of murine skin with silicone MN for 30 s and then the application of ALA-containing patches saw no significant change in ALA levels in deeper tissues, but there was a reduction in application time and the ALA dose necessary to produce high levels of the photosensitiser protoporphyrin IX in skin (Donnelly *et al.*, 2008).

6.4.2 Dissolving, swelling or porous MN: 'poke and release'

This method of delivery involves application of the MNs, which either can dissolve/swell, or can contain pores, through which drug will diffuse into systemic circulation (Fig. 6.4c). The materials from which the MNs are produced act as drug depots holding the drugs until the trigger for release occurs, i.e. dissolution or swelling (Van der Maaden *et al.*, 2012).

Dissolving MNs upon insertion into tissue is the trigger for drug release that is encapsulated within the needles. Both sugars and polymers have been utilised to produce these MNs with the degradation of the structures over time resulting in no fragments being left in the skin or hazardous waste (Migalska *et al.*, 2011; Sullivan *et al.*, 2008). Initial studies involving dissolving MNs employed organic solvents and elevated temperatures for production, which caused concern in relation to the stability of drugs, especially those of a proteinaceous nature (Park *et al.*, 2006; Sullivan *et al.*, 2008). Sugars such as maltose and galactose were used to fabricate these MNs but elevated temperatures of over 100°C were required to produce molten forms of these sugars, known as caramels (Donnelly *et al.*, 2009a; Miyano *et al.*, 2005). Alternatively, Lee *et al.* in 2008 used polylactic acid (PLA), carboxymethyl cellulose (CMC), amylopectin and bovine serum albumin (BSA) as dissolving materials for the delivery of a range of molecules to the skin. Those MN formulations with drug only in the needle shaft were hypothesised to be useful for bolus dosing due to rapid dissolution, confirmed by the study of sulforhodamine in the porcine skin 5 min after insertion of the MN. Prolonged release from these systems is not possible due to the small loading capacity of the MN. In order to extend the delivery life of the system, drugs were also incorporated into the backing layer, or only into the backing layer and not the needles, meaning a reservoir of drug was available. Prolonged release of over 1 day was observed with CMC MNs containing sulforhodamine. Encapsulation of the protein, lysozyme, inside the MN matrix for dissolution was also shown to have no adverse effects on the secondary structure (Lee *et al.*, 2008). The encapsulation of other drugs such as erythropoietin and enzymes within dissolving MNs has been shown to retain the activity of the drugs even after 2 months of storage, which is encouraging (Ito *et al.*, 2006; Lee *et al.*, 2008; Sullivan *et al.*, 2008). In a study by Li *et al.*, the maltose MN dissolved within 1 min, with the microconduits formed remaining open for 24 h, allowing the rapid delivery of monoclonal antibodies (Li *et al.*, 2009).

Hydrogels are macromolecular polymeric materials that are crosslinked to form a 3-D network that permits the retention of relatively large volumes of water, while avoiding solubilisation in an aqueous environment (Kim *et al.*, 1992; Peppas *et al.*, 2000). Therefore, this swelling property of hydrogel

MNs allows fluid uptake that in turn allows dissolution of drug within the MN to provide continuous drug diffusion from the MNs into surrounding tissue. Release from these structures can be controlled by alteration of the polymer or polymer content that in turn affects the swelling behaviour (Hennink and van Nostrum, 2002; Hoffman, 2002; Kim *et al*., 1992). In a recent study conducted by Kim *et al*., hydrogel microparticles were incorporated into the hydrophobic polymer, poly(lactic-co-glycolic) acid. Insertion into porcine cadaver skin resulted in the microparticles swelling, resulting in rhodamine release. This design can also serve as a method to deliver hydrophobic drugs as well as hydrophilic (Kim *et al*., 2012a). Similarly, we have showed, for the first time, hydrogel-forming MNs prepared from crosslinked polymers, which contain no drug themselves. Instead, they rapidly take up skin ISF upon skin insertion to form continuous, unblockable, hydrogel conduits from attached patch-type drug reservoirs to the dermal microcirculation. This technology has the potential to overcome the limitations of conventional MN designs, and greatly increase the range of drug deliverable transdermally. Using these novel MNs we have shown sustained delivery of molecules of different molecular weights, such as BSA (67 000 Da), insulin (6000 Da), theophylline (180 Da), metronidazole (171 Da), caffeine (194 Da) and methylene blue (320 Da) (Donnelly *et al*., 2012).

Porous MNs have been manufactured from both non-biodegradable and biodegradable materials, with biodegradable materials being favoured due to the inherent weakness of these structures compared to solid MNs (Park *et al*., 2007). The structural weakness may result in fracturing of the needles, therefore if non-biodegradable materials are used fragments of the material may be left in the skin once drug delivery has ceased and the needles are removed. A progression on this technology incorporates a solid silicone MN with a macroporous silicone tip. Macroporous silicone is biodegradable, and therefore this overcomes the problem non-biodegradable tip fragments being left in tissue, and therefore offers an alternative method of drug loading (Ji *et al*., 2006).

6.4.3 Coated MN: 'coat and poke'

Coated MNs can provide extremely quick drug delivery, in some cases within one minute. The most common method for producing these MNs is to dip-coat the needles in the drug solution once or repeatedly (Bariya *et al*., 2012) (Fig. 6.4b). Drug delivery is limited, due to the small dimensions of the MN shaft and tip, and therefore the area for coating is typically low (i.e. up to 1 mg) due to smaller MN arrays (Gill and Prausnitz, 2007b); this method, therefore, is normally reserved for potent drug molecules such as vaccines (Bal *et al*., 2010; Banga, 2009). Thick layers of drug coating are not feasible, as low skin delivery efficiency has been shown resulting from a blunting of

the MN and therefore poor penetration (Chen *et al*., 2009; Cormier *et al*., 2004; Matriano *et al*., 2002; Xie *et al*., 2005). Both hydrophilic and hydrophobic drugs, along with microparticles, proteins, DNA and RNA, have been delivered in this manner (Bal *et al*., 2010; Cormier *et al*., 2004; Gill *et al*., 2010; Gill and Prausnitz, 2007a, 2007b; Xie *et al*., 2005). A variation of this delivery method uses the 'dip and scrape' method, which involves the scraping of previously coated solid MN across the skin (Mikszta *et al*., 2002). This action produces very small abrasions that provide access to the lower layers of tissue. However, some difficulties have arisen due to potential skin irritation and lack of control over drug delivery (van der Maaden *et al*., 2012).

6.4.4 Continuous drug delivery using hollow MNs: 'poke and flow'

Hollow MNs are used to deliver drug solutions via the 'poke and flow' method, which involves insertion of the MN into tissue and then a drug solution can be transported through the bore of the MN in similar fashion to a hypodermic needle (Gardeniers *et al*., 2003; Wang *et al*., 2006) (Fig. 6.4d). Due to the limited amounts of drug that could be administered by the other conformations of MNs, hollow MNs were developed (Bariya *et al*., 2012). Passive diffusion of the drug solution may occur through the MN, with active delivery allowing more rapid rates. Active delivery requires a driving force, which may be produced by a number of methods that have been detailed in literature. Commonly, a syringe is used to drive the solution through the MN into the tissue, but some studies have combined the MN systems with a pump or pressurised gas (Amirouche *et al*., 2009; Bal *et al*., 2010; Gupta *et al*., 2009; McAllister *et al*., 2003). This method of delivery, however, does have distinct shortcomings in that flow rates are normally less than 300 nL min^{-1} (Martanto *et al*., 2006; Roxhed *et al*., 2008b; Wang *et al*., 2006), with higher rates of administration in the order of μL min^{-1} requiring the incorporation of hyaluronidase into the formulation to degrade the skin collagen fibres (Martanto *et al*., 2006). Also, as the bore of the MN is small, there is a risk of blockage, which would prevent further delivery of drug solution (Jiang *et al*., 2009).

A study conducted by Gupta *et al* utilised a single hollow MN to deliver local anaesthesia, lidocaine. This method of delivery was compared to the conventional mode of using a hypodermic needle to deliver the lidocaine intradermally. Results showed that the subsequent levels of local anaesthesia were the same for each method but patient satisfaction with the MN technique was much greater due to a reduction in pain observed determined by VAS pain scores. Consequently, 77% of the participants favoured MNs, and 80% indicated that they did not deem the MNs to be painful (Gupta *et al*., 2012). Insulin delivery through hollow MNs has been investigated by

a number of research groups. A study conducted by McAllister *et al*. in 2003 involved the microinfusion of insulin through hollow MNs to diabetic, hairless rats. A drop in blood glucose levels of over 70% from was observed in comparison to preinfusion levels and also compared to control rats infused saline, and those with insulin solution applied topically (McAllister *et al*., 2003). In a similar experiment carried out in male Sprague Dawley hairless rats using metal MNs, the post-infusion blood glucose level was reduced by 47% in comparison with the preinfusion levels. Negative control investigations showed that topical insulin without MNs produced undetectable levels of plasma insulin (Davis *et al*., 2005).

6.4.5 Challenges relating to microneedles and drug delivery

MN development is a vast and ever-expanding area of research and this is demonstrated by a large number of patent applications that have been filed. Many of these patents focus on the design of MN and not the final development of a viable drug delivery device. Each of the systems mentioned previously that utilise MN to deliver a range of drugs would still be considered to be in the developmental stage. The challenge with this technology lies in the production of a viable and useable complete system that would allow effective amounts of drug to be delivered across the skin. Decades of research have yet to yield a single product, due to difficulties in development.

First in terms of MN design, as has been alluded to, hollow MNs carry a risk of blockage and they are structurally weaker than the other conformations. When considering coated MNs, only a thin coating layer of drug solution is possible, to avoid blunting of the tip and poor penetration. The tips of solid MNs have also been shown to fracture once inserted into skin, which could result in immune reactions to foreign bodies (Chen *et al*., 2008). The 'coat and poke' method of drug application has an inherent disadvantage; this is a two-step process, which may limit its ease of use compared to other methods (Garland *et al*., 2011). The material used to manufacture the MN can result in a number of issues in relation to the use in drug delivery. Solid MNs produced from metals can leave metallic traces in the skin, which in turn may result in irritation, erythema and swelling among other effects (Donnelly *et al*., 2011). The 'ideal' MN has not been identified, due to the vast number of variables in design and manufacture. This area is therefore an ongoing topic of research worldwide. Attention must also be paid to the potential site of MN application when delivery of drugs is an aim. As is widely known, the thickness of our skin varies across our bodies and also between individuals. This factor poses an issue in relation to bioavailability variation, and needs to be considered when developing delivery systems (Godin and Touitou, 2007).

Even without considering the challenges that the development of MN devices poses, there is also an issue regarding the attitude that healthcare professionals and the public have concerning MN. If a delivery device is to succeed in the market, those individuals that would potentially prescribe or use the device must have a positive attitude towards the device. Birchall and colleagues undertook a study to identify the attitudes of both the public and healthcare professionals towards MN. The advantages, such as reduced pain and tissue damage, as well as the potential for self-administration, were identified. Disadvantages, including cost, delayed onset of action and dosing reliability, were stressed as concerns. The healthcare professionals raised issues relating to inter-patient variation, inadvertent self-administration and the ability to deliver an accurate dosage. Both the public and professionals highlighted the problem regarding the inability to determine whether the dose had been successfully administered, therefore a visual aid would be integral to the finished product. This study identified issues that the research community needs seriously to consider throughout their development processes in order to facilitate the transfer this technology into the healthcare market. However, overall the attitude of both the public and those healthcare professionals was positive (Birchall *et al.*, 2011).

6.5 MN-mediated monitoring using skin interstitial fluid (ISF) and blood samples

Monitoring of analytes in biological fluids represents an important aspect of modern day healthcare. This may be in the form of drug level measurements, as in therapeutic drug monitoring, or could involve the monitoring of key biomarkers for diagnostic purposes or in the management of disease states. Little true progress, however, has been realised within clinical practice with regards to the methods used to extract these analytes and, for most measurements, conventional blood sampling remains routine, despite the renowned drawbacks associated with this invasive method. For example, hypodermic needles are associated with risk of needle-stick injuries, and cross-contamination, such as 37.6% of Hepatitis B infections, 39% of Hepatitis C infections and 4.4% HIV/AIDs infections among world healthcare workers (Rapiti *et al.*, 2005). In addition to the health implications, needle-stick injuries also represent a significant economic burden, with one study estimating an annual cost of £500 000 per NHS trust (Ball, Pike, 2009). Premature neonates, in particular, can exhibit blood volumes as low as 80 mL/kg, making blood sampling to any degree far from ideal and frequent sampling increasing the risk of anaemia (Koren, 1997). From the patient's perspective, minimally invasive sampling offers less discomfort and could offer significant benefits for those with needle-phobia and low sample volumes.

Minimally invasive monitoring methods include the use of reverse iontophoresis (Bouissou *et al.*, 2009; Ching *et al.*, 2011; Ebah *et al.*, 2012; Leboulanger *et al.*, 2004), reverse iontophoresis combined with electroporation (Lee *et al.*, 2010), low frequency ultrasound (Paliwal *et al.*, 2010), capillary microdialysis (Kim *et al.*, 2008; Nielsen *et al.*, 2009), and by pore creation using a near infrared laser (Venugopal *et al.*, 2008), to name just a few. ISF monitoring is common practice and an alternative technique to blood extraction (Ching *et al.*, 2010; Liu *et al.*, 2005, 2007; Sun *et al.*, 2010; Wang *et al.*, 2005). While the majority of minimally invasive extraction methods remove ISF, MNs have been explored for both blood and ISF sampling, with some claiming an adaptation to either matrix possible. For ISF, MN penetration depths of 50–150 μm have been reported satisfactory, whereas arrays designed for blood extraction should offer much larger penetration depths, with values of around 400 μm (Khanna *et al.*, 2008). Others report penetration values as large as 1 mm (Gardeniers *et al.*, 2003) or 1500 μm (Chaudhri *et al.*, 2010) as necessary for successful blood withdrawal. A penetration depth of 325 μm (Mukerjee *et al.*, 2003) is unlikely to guarantee successful blood access however, considering penetration into the dermis is required for blood capillary targeting, with investigations recording that the epidermis possibly extends as far as 400 μm below the skin (Donnelly *et al.*, 2012). Various different approaches to monitoring using MN have been proposed, including the use of HMN arrays for fluid collection and analysis, solid arrays for pretreatment and subsequent fluid collection, as well as integrated options which negate the need for fluid removal entirely. Regardless of the approach, to represent a valuable alternative to current practice, the MN device must be capable of successful and reproducible penetration without fracture, and enable accurate measurements of the target analyte.

6.5.1 Fluid flow

Irrespective of the fluid to be accessed, consideration must be given to the force which will drive fluid flow and ensure adequate fluid collection, with some quoting flow rates between 1 and 100 $\mu L\ h^{-1}$ as necessary (Gardeniers *et al.*, 2003). Many designs rely on passive extraction alone, depending solely on capillary action to generate fluid flow. One such design proposed uses a bi-mask process to achieve sharp tips, a cylindrical body and side ports to minimise blockage of the HMN, and is suggested for use in either drug delivery or microbiological sampling (Zhang and Jullien, 2003). The authors recommend this design as easily fabricated to provide a high needle density and offering a low flow resistance and good structural strength. In a paper that follows, they describe this design further and investigate performance (Zhang and Jullien, 2005). The needles, fabricated using silicon dioxide, were capable of human skin penetration without breakage but passive liquid

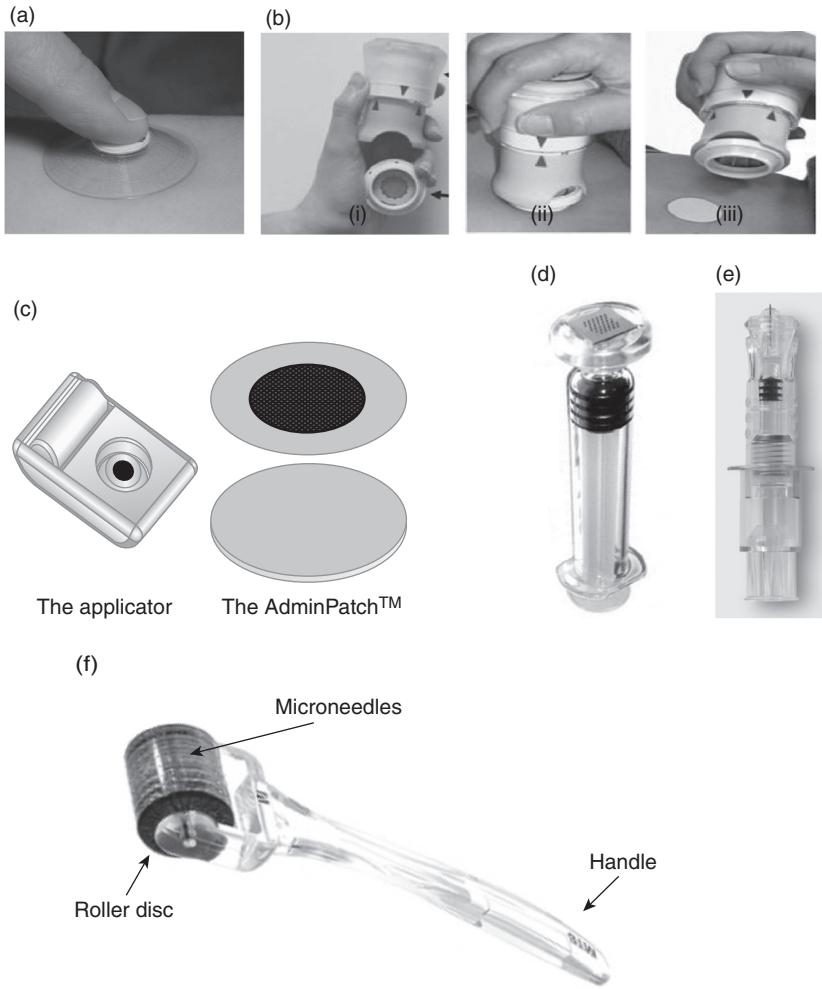

6.5 MN applicators from different companies. (a) MicroCor™ applicator. (*Source*: Adapted from Cleary, 2009.) (b) Zosano's Macroflux® (i) applicator loaded with patch, (ii) applicator activated, (iii) patch delivered to the site. (*Source*: Adapted from Zosanopharma®, 2009.) (c) AdminPatch® MN array applicator. (*Source*: Adapted from Nanobiosciences®, 2009.) (d) MicronJet® MN device. (*Source*: Adapted from Nanopass®, 2009.) (e) BD Soluvia™ applicator. (*Source*: Adapted from BD, 2009.) (f) MTS-Rollers™ applicator. (*Source*: Adapted from Microneedle®, 2009.)

extraction was only demonstrated on potato. Another early study, describing a system amenable to both ISF and whole blood, used an HMN array with integrated fluidic microchannels, fabricated using silicon and glass, and conducted preliminary tests on the ear lobe of one human volunteer

(Mukerjee *et al.*, 2004). The authors outline three needle tip designs including a 'volcano-like design', a 'micro-hypodermic' design and a 'snake-fang' design shown in Fig. 6.5. A common issue with hollow designs is the potential for blockage and the first two listed here exhibited this issue. The third, 'snake-fang', design was reported as superior since it was found to be less susceptible to this difficulty, with the bore here placed 25 μm off-centre. The fluid capture from the ear lobe by capillary action was described, but penetration testing conducted on the first knuckle of the thumb concluded that a 1.5 ± 0.25 N force was required for penetration. The risk of glass becoming embedded within the skin represented a major drawback with this design.

Other work has focused more on the theoretical considerations behind fluid flow, driven by capillary action, in HMN and the development of models and calculations to aid in the determination of optimal MN design for optimum fluid flow. Work by one group developed a theoretical fluid model to enable interpretation of microfluidic properties of Newtonian fluids within silicon MN, and concluded a faster fluid filling when the length width ratio of the microchannel was $\sqrt{2}+1$ (Liu *et al.*, 2006).

The employment of arrays with a high needle density has been suggested as a possible means to enable sufficient rates of flow, with the use of out-of-plane arrays recommended as most appropriate for achieving such specifications (Gardeniers *et al.*, 2003). In contrasting with this, others discuss the need for more active extraction methods to ensure adequate fluid collection rather than reliance of capillary force alone. The use of vacuum force to assist with fluid withdrawal has been described (Tsuchiya *et al.*, 2010), as well as more novel approaches such as exploitation of the phase transition of a gel to power sample extraction. The latter approach was first documented in the literature using poly (*N*-isopropylacrylamide) integration within a microsystem intended for glucose sensing (Kobayashi and Suzuki, 2001). The volume change exhibited by the gel in response to a variation in temperature was utilised in this study to power a micropump for fluid extraction, with the ultimate aim of achieving spontaneous sampling in response to the temperature of human skin. While successful sampling of a glucose solution was achieved through a 50 μm diameter MN using this concept, flow was only unidirectional and in response to temperature shifts between 30°C and 40°C and, thus, not relevant for human body temperature. Work to instigate sampling at more relevant temperatures (30–37°C) was subsequently carried out (Suzuki *et al.*, 2002). The improved design incorporated a silicon membrane to enable repeated gel use as a result of its elastic force. By shifting the system between hotplates maintained at 30°C and 37°C, volume changes were found to occur within less than 1 min and 90% response time of the sensor reported to range between 30 and 40 s. This modified system could also successfully achieve bi-directional flow; however, the use of non-ideal materials, such as silicon, for MN fabrication is again declared

a challenge by the authors. Further work by this group then explored the possibility of continuous monitoring adopting this approach. Adjustment of pH, in addition to temperature, to induce the volume change was used. This study also explored the use of an enzyme-loaded gel to extend the time for volume reduction even further (Suzuki *et al*., 2004). Using this combined approach of pH and temperature-induced changes the time for sampling was prolonged, while the use of the enzyme-loaded gel provided opportunity for further adjustment. The work also demonstrated continuous glucose sampling using an external glucose sample solution.

6.5.2 The 'female mosquito' paradigm

Many within the field have used the female mosquito as an inspiration for their designs. The proboscis of the female mosquito has been recognised as an ideal model for achieving painless penetration of the skin, given their approach to feeding and, thus, have been examined by those wishing to exploit natural design (Kong and Wu, 2010; Ramasubramanian *et al*., 2008). Painless skin penetration by the mosquito has been noted to be achieved at an extremely low force, estimated around 16.5 μN, with the efficient design remaining resistant to buckling or fracture (Kong and Wu, 2010). Such properties have been recognised as critical in MN design and close imitation of the female mosquito's feeding mechanism was recognised a means towards optimisation (Ramasubramanian *et al*., 2008). One blood collection system proposed to mimic the mosquito focused on achieving a jagged shape to the HMN, through use of wet etching, to form a jagged groove on the silicon (Oka *et al*., 2002). Successful penetration without breakage was demonstrated in this work through hard silicon rubber and the system was claimed to be impervious to leakage after testing using a commercial pump and liquid ink. However, the fabrication process suggested failed to result in an accurate jagged shape across the entire MN length. Another mosquito-inspired system for the purposes of blood extraction, as well as for drug delivery, used SU-8 to produce cylindrical HMNs with a height of 1540 μm, wall thickness of 15 μm and inner diameter of 100 μm (Chaudhri *et al*., 2010). The authors noted lower wall thickness and heights larger than 800 μm of insufficient strength to endure the development process. Based on theoretical calculations derived from fundamental mechanical engineering principles, the MNs proposed are claimed unlikely to succumb to buckling upon skin penetration. A desire to emulate the high aspect ratio possessed by the target species (~400) was discussed and a value of 103 was achieved. While fabrication is outlined in detail, tests on mechanical strength and functionality were not presented. A further study attempting to emulate the female mosquito instead demonstrated the use of titanium alloys for MN fabrication via a thin film deposition process (Tsuchiya *et al*., 2010). To allow

close imitation of the labium, MN inner diameters of 100 μm or less were selected, while MN height was fixed at 4 mm. The design also incorporated a vacuum to facilitate blood extraction, aiming for an extraction speed of 5 μL/s. The use of titanium was found to alter the surface properties of the MN, resulting in an accelerated extraction time in comparison to stainless steel, but both materials fell short of the aim when the inner diameter was 50 μm. MN inner diameter was thus proven to be a critical determinant of blood extraction speeds, and an inner diameter of 100 μm for titanium MN was deemed sufficient for blood glucose determination with a commercial glucose monitor. This study also found MN length and shape to be pivotal to flow rate.

6.5.3 Differential strategies for fluid extraction

While much work in the area of MN-mediated monitoring has focused on the development of HMN for fluid collection, alternative approaches have also been explored. One group suggested a novel array to remove the use of conventional holes altogether, instead developing MNs with quadruped grooves for blood storage following capillary force extraction (Khumpuang *et al.*, 2004). This interesting suggestion used a biocompatible material, polymethacrylate (PMMA), for MN fabrication by a novel technique, plain-pattern to cross-section. Penetration of this array into chicken meat was confirmed using a liquid with similar viscosity to blood (aniline blue); however, they failed to successfully demonstrate fluid flow along the grooves with this approach.

Another approach described used a combination design based on both hollow and solid silicon MN for ISF extraction (Mukerjee *et al.*, 2003). This strategy used HMNs for fluid flow in the centre only, and designed with a bevelled tip to impede pore blockage. The incorporation of an outer border of solid needles functioned to stretch the skin to facilitate successful penetration. Human skin penetration of this device was demonstrated using an *in vivo* confocal microscope, with some MN tip breakage identified. Such events are clearly not ideal, particularly when dealing with materials with poor biocompatibility. Application to the human ear lobe resulted in flow through the 80 μm wide channels, which was assumed to be ISF.

A two-stage approach to sample extraction has also been explored, using solid MN for skin pretreatment with subsequent fluid extraction, using vacuum force (Wang *et al.*, 2005). This study used glass MNs for ISF extraction for subsequent glucose analysis, with insertion achieved using a vibration technique and involved both animal (rats) and human subjects. The vacuum was applied for 2–10 min and 5–10 min on rats and humans, respectively. In human volunteers, volumes of 1–10 μL were extracted from a 1 cm^{-2} area with 7–10 MN-created conduits. The vacuum procedure was reported to

cause erythema in human subjects, but the overall procedure defined as relatively painless. ISF glucose measurements obtained using this design were found proportional to that of the blood. However the need for a calibration factor using blood was an obvious flaw for this system. Importantly, these authors showed detection of rapidly changing blood glucose levels without any associated time-lag using this technique; an issue previously alluded to for other minimally invasive monitoring work (Potts *et al*., 2002; Sieg *et al*., 2004). In work that followed this group attempted to examine the accuracy of electrochemical monitors for glucose measurement by comparison with a gas chromatography-mass spectrometry method for the different matrices, blood and ISF, with the conclusion that use of ISF results in a bias which must be accounted for (Vesper *et al*., 2006).

Sato *et al*. (2011) adopted a similar approach by using polycarbonate MN arrays (305 MN arrays per 50 mm^2 area), with a length of 300 μm. In contrast to the vacuum approach outlined by Wang *et al*. (2005), a reservoir was used for ISF collection by passive diffusion and osmotic pressure only, allowing for sodium to be used as an internal standard. Two reservoir designs were proposed; the first was a plastic chamber containing 1.2% KCL solution, the second a hydrogel patch consisting of polyvinyl alcohol with 2% KCL solvent and adhesive tape. Interstitial glucose measurements were found to be in close correlation with blood measurements, but this was based only on data from healthy volunteers, thus exhibiting minimal glucose fluctuations, rather than for a more representative diabetic population. Furthermore, a recent patent has also outlined the possible use of this two-stage approach for extraction in a design which claims flexibility to, not only blood and ISF collection, but also other bodily fluids, including saliva, tears, lymph and urine, for analytical evaluation (Brancazio, 2012). Again, the designs outlined here incorporated vacuums or chambers to ensure pressures lower than atmospheric to facilitate fluid flow rather than placing sole reliance on passive mechanisms.

6.5.4 Integrated designs

The development of integrated systems that negate the formal extraction of fluid and instead rely on the use of integrated sensors has also been explored. Analyte detection for MN-mediated monitoring can therefore be on-site, with the incorporation of integrated sensors, as well as off-site, using fluid extracted for subsequent analysis. In the case of the former, sensor development and optimisation have been critical aspects of design progressions to date towards a complete, optimised, integrated system. One system to allow easy integration with a polymethylsiloxane (PDMS) biochip involved the first single-crystal-silicon MN array fabricated in the plane of the substrate (Paik *et al*., 2003). The extraction fluid of interest in this design was blood,

using MNs with lengths around 2 mm and microchannel diameters around 20 μm. Fluid flow *in vitro* and *in vivo*, with successful penetration into the tail vein of a mouse, was demonstrated. In a paper that followed, penetration was tested using agarose gel, chicken breast, rat-tail vein and rabbit ear, and fluid flow confirmed using agarose gel and chicken breast (Paik *et al*., 2004). The authors outline optimisation of the design, highlighting the need to balance sharpness with mechanical strength, and propose a tip taper angle of 30°C to be superior, producing a 6.28 N buckling load enabling penetration without breakage. However, the actual functioning of the integrated biochip was not addressed.

A group in the Netherlands proposed a combination of anisotropic wet etching and the BOSCH-DIRE process to produce an out-of-plane silicon HMN array, with flow channels positioned off-centre to avoid blockage (Gardeniers *et al*., 2003). Subsequent works have also adopted this strategy in an attempt to avert this issue (Bodhale *et al*., 2010; Luttge *et al*., 2007). The triangular-tipped MNs produced had height of only 350 μm and maximum channel width of 70 μm. As already discussed, such heights seem insufficient for successful blood withdrawal, thus possibly indicating the fabrication approach as unfit for purpose. The diagnostic capabilities of the device were therefore examined using blood collected with a 1.8 mm lancet. Compatibility of the array with a capillary electrophoresis chip was demonstrated using 30 μL of the collected blood, but inaccuracies compared to expected blood concentrations were evident. In work that followed, water was used to fill the volume between the chip and the sampler, resulting in the successful demonstration of potassium, sodium, magnesium and lithium measurement (Vrouwe and Luttge, 2005). However, this again was based only on a model for the MN system, composed of CE chip and sample collector, and failed to demonstrate actual MN blood extraction. The same group later suggested the use of SU-8 as a material for HMN fabrication, improving biocompatibility, and outlined novel fabrication methods to produce this polymeric MN patch, achieving needle heights $\geq$ 500 μm (Luttge *et al*., 2007). They suggest this device enables blood collection for analysis off-site, as well as again describing integration with a CE chip. Only preliminary results were presented to show the capabilities of the device in blood diagnostics, proving the device suitable for sample transfer, such as to a CE chip, so facilitating the analysis of inorganic ions in blood.

Another integrated system for sampling and glucose sensing was suggested, using in-plane silicon HMN and gold microelectrodes (Liu *et al*., 2005). Here a unique approach was taken to glucose sensing, using electrochemical detection as well as a novel technique for enzyme immobilisation, relying on capillary force to immobilise the enzymes on the microelectrode surface. The sensor showed good linearity for glucose in the concentration range 0–500 mg/dL when tested using standard solutions. Enzyme

immobilisation was also a key component in the system described by Goud *et al.* (2007), consisting of a novel biosensor integrated with microfluidic channels and MNs fabricated using Ormocer®, an organically modified ceramic material for glucose monitoring (Goud *et al.*, 2007). This design, unlike that proposed by Liu *et al.* (2005), offered the advantage of MNs fabricated using a material described as biologically inert and non-toxic, i.e. Ormocer®. The biosensor used here incorporates electrodes, developed from carbon nanotubes and glassy carbon, alongside the enzyme, glucose oxidase, encapsulated within a zirconia/Nafion matrix to offer improved sensitivity and specificity. This system displayed prompt glucose detection, using standard glucose solutions, signifying its potential value in glucose monitoring applications. In both instances, however, extensive evaluation of the integrated functioning of the entire system failed to be conducted.

The exploitation of enzyme-mediated bioluminescent reactions for detection has also been outlined as part of an autonomous MN system. This system consisted of an MN array with an associated reaction chamber and photodetector (Chandrasekaran *et al.*, 2003). With this approach, metabolite concentrations were determined by coupling reactions with other enzyme-linked reactions that emitted light. Light emitted could then be subsequently measured. In this study, the production of ATP during glucose consumption was exploited, since the enzyme-catalysed process of luciferin oxidation uses ATP and results in bioluminescence. Subsequent measurement of light intensity was thus related to glucose concentration. The use of ATP in many biochemical reactions broadens the potential applications of this design. The hollow metal MNs integrated within the system demonstrated successful fluid flow (1000–4000 $\mu L\ h^{-1}$) without leakage, with a 1500 μm shaft length and 4.1 mm lumen length. The novel photodetection approach was illustrated as feasible with the sensor characterised within the range relevant to glucose detection (2.0–7.0 mM of ATP). However, the performance of this device was limited by a decreased light intensity.

A different integrated design focused on arrays composed of gold-coated silicon with a hetero-bifunctional poly(ethylene glycol) coated to its surface for protein biomarker capture (Corrie *et al.*, 2010). The surface modifications were designed to enable selective detection of AF-IgG, which was tested using a 10% mouse serum. Application to mouse ear skin in this study illustrated the device to be capable of selective biomarker capture, and the ease of removal for subsequent analysis. As with many of the designs suggested, various modifications are essential prior to optimal human targeting, such as ensuring an adequate penetration depth and biocompatibility considerations, to name but a few.

A similar approach has also been outlined for hydrogen peroxide and lactate detection using an array of HMNs with integrated carbon-paste electrodes (Windmiller *et al.*, 2011a). In this case, a biocompatible polymer was

used to produce MNs with a height of 1500 μm and a vertical central bore of 425 μm. *In vitro* studies performed indicated the selectivity and sensitivity of this sensor, which demonstrated stability over the time period (2 h). This group have also proposed a different design to remove the need for fluid extraction for glutamate oxidase and glucose detection, with a view towards their continuous monitoring (Windmiller *et al.*, 2011b). This design incorporates both hollow and solid MNs, using the same polymer during fabrication, to form a single array with multiple microcavities, in which the detection enzymes, glutamate oxidase and glucose oxidase, are entrapped within a thin film of poly(*o*-phenylenediamine) (PPD) to minimise interference. High sensitivity and fast detection within clinically relevant ranges was shown for this biosensor using both a buffer matrix and human serum. A different paper also focuses on the use of an integrated design incorporating solid MNs, which themselves act as the sensor surface for glucose and lactate detection (Trzebinski *et al.*, 2012). These were developed using SU-8 coated with gold and then an enzyme layer, before being surrounded in a protective epoxy-PU membrane. Stability of this device was claimed for the 48 h period. Again, glucose detection within the clinically relevant ranges was demonstrated for this device, and the concurrent detection of both glucose and lactate are suggested as a possibility.

With an aim of cost reduction, other researchers have proposed a microvalve for fluid extraction, which is intended for integration within an MN array and biosensing system (Miguel Moreno *et al.*, 2009; Moreno *et al.*, 2008). By removing the standard high energy need for valve operation, and through use of low cost polymers, which are easily fabricated, a cost reduction for this approach was intended. The valve design employs two chambers with varied pressures separated by a SU-8 wall and undergoes both thermal and mechanical activation. A gold wire, bonded to a copper line on a PCB substrate, crosses the wall and functions to collapse the wall via thermal destruction upon current flow. Different pressures between the chambers will also facilitate this destruction. Miniaturisation of this system has yet to be demonstrated, however, as well as the actual sensing functionalities for biomedical monitoring purposes.

With biosensors clearly at the forefront of monitoring using an MN array-based approach, consideration has also been given to prolonging sensor lifetime. The destruction proteins can impart on enzyme-based sensors has been addressed with suggestions made to exclude large molecular weight compounds and, thus, prolong enzyme-based biosensor lifetime. One approach in an attempt to achieve this aim involved the integration of a dialysis membrane within the monitoring device (Zahn *et al.*, 2000). Two designs based on silicon MN for ISF extraction were suggested. First, the use of a diffusion membrane of layered polysilicon either side of a thin thermally grown oxide of approximately 10–50 μm with etch holes was described. The second

design was based on a permeable polysilicon. It is concluded within this work that the latter design should offer superiority, in terms of mass transfer rates as well as filtration capabilities. In work that follows, this group go further with this concept in the design of an MN-based glucose monitoring system, with the addition of an integrated glucose sensor (Zimmermann *et al.*, 2003). In this design, ISF flows through the out-of-plane MN (200 μm length) before passing through a porous polysilicon dialysis membrane, thus excluding larger proteins before coming into contact with the sensor for detection. This in-device glucose sensor had a suggested optimum flow rate of 25 μL/min and response linearity was illustrated for glucose concentrations in the region of 0–160 mg/dL. While the capabilities for ISF sampling and glucose sensing with the integrated device are demonstrated, the use of only eight MNs proved insufficient for a significant sensor response, relying on capillary action and evaporation alone for fluid extraction. An increased array density was, however, proposed as a solution. Work with this design is further explained within a later paper; however, results remain preliminary and are largely based upon models and estimations (Zahn *et al.*, 2005).

A recently published patent also cites the prevention of protein entry into the collection chamber as a crucial element of sensor design (Mischler and Werner, 2012), suggesting the incorporation of a filter membrane which prevents entry of molecules greater than 10 TDa, such as that previously outlined (Zahn *et al.*, 2005). The invention functions to continuously monitor analytes in ISF using optical detection methods, negating the need for reagents and relying on the correlation between analyte concentration and absorbed radiation. A miniaturised system is described consisting of an array of HMNs that enable fluid flow to a chamber. The chamber has a window allowing radiation entry and transmission. Diamond coating is a suggestion to further minimise protein disruption by preventing protein attachment to the window surface. A detector on the other side of the window enables radiation detection, and is coupled to a unit functioning to quantify analyte concentrations. Possible analytes outlined by the authors include glucose, cholesterol, creatinine, urea and triglycerides. Importantly, this integrated design's on-site approach to sample analysis also eliminates the need for additional regents to be used for analyte quantification. The inventors here also suggest a watch-type design for this device, with needles attached to the portion of the watch face in contact with the arm, with the face displaying the calculated concentration. Such considerations regarding ease of use and convenience for the user are critical for the advancement of these alternative strategies from novel ideas into useful and applicable approaches to patient monitoring.

The amalgamation of drug delivery, alongside the processes of blood extraction, filtration and insertion, has also been described for a device targeted for patients with renal disease (Tayyaba *et al.*, 2011). The electronic

components of this system include a microcontroller, which controls transport according to pressure, as determined by the flow sensors. Blood extraction with this system is achieved using 1700 μm polyglycolic-acid (PGA) MN with a double-radius structure, creating a pressure difference to prevent clogging. Following extraction, blood enters a heparin-containing mixing chamber before passing through the filtration membrane to remove molecules such as urea and vancomycin, with high molecular weight molecules. One such molecule, beta2-microglobulin (β2m), requires filtration, however, necessitating the inclusion of a β2m absorbent material to ensure its removal. The dual lumens were constructed to have lengths of 800 and 900 μm with corresponding diameters of 60 and 100 μm. The authors highlight viscosity as an important determinant of flow rate and, based on a 5 × 5 array, flow rates for acetone, water and blood for the system were defined at 1182, 971, and 845 μL min^{-1}, respectively. While the proposed system is outlined in terms of fabrication and theoretically analysed, progress towards the demonstration of the integrated system's actual functionality is needed. Furthermore, the advantage of using biocompatible PGA for MNs within the blood extraction component of this device seems degraded by the use of silicon for MNs within the drug delivery element of the design (Tayyaba *et al.*, 2011).

6.6 Future trends

There has been a substantial increase in the attention that MN technology has received over the last 5 years, with number of publications concerning MN evaluation more than tripling since 2005. It is envisaged that this will be a continuing trend, with MN-focused academic research groups increasing in number and size, and an increased attention from industry. It is likely that MN technology will be useful for delivering not only the growing number of biopharmaceuticals available, but also for small water soluble molecules not normally amenable to transdermal delivery and active cosmaceutical ingredients. There are currently a number of companies working towards commercialisation of their respective MN technologies, including Zosano Pharma, Corium, Nanopass, 3M, and Beckton-Dickinson. Zosano Pharma are currently preparing to enter a pivotal Phase III clinical trial using the Macroflux® technology developed by Alza. A solid drug-coated MN patch system (MN height 190 μm) for the delivery of parathyroid hormone in the treatment of severe post-menopausal osteoporosis will be used. There appears to be a high likelihood of positive outcomes, based upon extremely encouraging and relatively large-scale Phase II results. Importantly, Zosano Pharma have incorporated an applicator system as an essential component of this delivery system. This applicator applies a consistent, pain-free force, and has been optimised for easy use by elderly patients. Furthermore,

focus study groups (288 post-menopausal women with osteoporosis aged 60–85 years) were conducted to evaluate patient perception of this technology, with positive outcomes noted. It was highlighted that 93% of patients liked the patch concept 'extremely well', while 90% rated it as easy to use, as exemplified by the fact that 82% of patients were capable of applying the patch correctly the first time without any help. Indeed, it appears that incorporation of the applicator device lead to enhanced patient acceptability and faith in the device as a drug delivery system. NanoPass technologies Ltd have conducted a number of clinical trials demonstrating effective, safe, and painless intradermal delivery of local anaesthetics, insulin, and influenza vaccine via their MicronJet® technology (hollow MN device). Similarly, 3M's microstructured transdermal system (MTS), having either solid or hollow MNs, has shown promising results in several pre-clinical studies investigating delivery of proteins, peptides and vaccines. While the above-mentioned MN devices have been based upon solid or hollow MN systems, it is envisaged that devices based upon FDA-approved, biodegradable/dissolving polymeric MN formulations will receive increased attention from pharma companies moving forwards. This is due to a number of inherent advantages associated with such polymeric systems. In particular, the self-disabling nature of these devices may aid in their regulatory approval. Once inserted into skin, polymeric systems will either rapidly dissolve, or undergo such morphological changes that disable effective skin penetration if used on another individual. Post-removal of this is particularly advantageous if polymeric microneedle devices were to be used as part of large-scale vaccination programmes, eliminating the need for sterilisation of a needle that may be reused between individuals, and avoiding the potential for cross-contamination to occur in countries that may not have access to sterilisation equipment, as well as reducing the potential for needle-stick injuries occurring. Specialised means of disposal would not be required.

The Donnelly's Group in Belfast is working on MN arrays prepared from hydrogel-forming polymeric systems (Donnelly *et al*., 2012). Such arrays are hard in the dry state but, upon insertion into skin, take up interstitial fluid and undergo a transition to form discrete *in situ* hydrogel bulbs. The MNs themselves contain no drug, but instead are connected to a conventional matrix-type transdermal patch. Drug can thus diffuse through the swollen MNs, which act as a continuous unblockable conduit between drug reservoir and dermal microcirculation (Fig. 6.4). Importantly, drug delivery is no longer limited by how much drug can be loaded into the MNs themselves, so delivery of greater doses over longer time periods is now possible. In an alternative application, the MNs can be used to extract skin interstitial fluid for diagnostic or therapeutic monitoring purposes (Fig. 6.6).

The Group have obtained substantial funding from the UK Biotechnology and Biological Sciences Research Council (BB/E020534/1, Donnelly

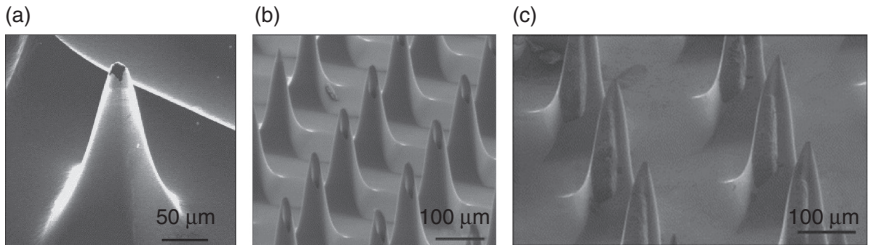

6.6 SEM micrographs of (a) 'Volcano' MN design, (b) 'Hypodermic' MN design, and (c)'Snake Fang' MN design. (*Source*: Adapted from Mukerjee *et al.*, 2004.)

RF 'Transdermal delivery of macromolecules mediated by microneedle arrays' and BB/FOF/287, Donnelly RF, Woolfson AD '*In vitro* and *in vivo* safety investigations to support the commercialisation of novel microneedle arrays for transdermal drug delivery'), the Engineering and Physical Sciences Research Council (EP/H021647/1, Donnelly RF *et al.* 'Microneedle-mediated enhanced Raman therapeutic drug monitoring'), The Royal Society ('Microneedle delivery of bio-inspired nanoparticles for psoriasis treatment') and Invest Northern Ireland (PoC21A 'Polymeric microprojection arrays for Transdermal delivery of active pharmaceutical ingredients') and are now pursuing commercialisation of a range of different applications of the technology with several major industry players.

6.6.1 Moving forwards

Given the ever-increasing evidence available within the academic and patent literature that MNs of a wide variety of designs are capable of achieving successful intradermal and transdermal delivery of conventional drugs, biopharmaceuticals, vaccines and active cosmaceutical ingredients, it is envisaged that the already concerted industrial effort into development of microneedle devices will now intensify. Furthermore, novel applications of microneedle technology are likely to come to the forefront. The ability of microneedle arrays to extract bodily fluids for drug and/or endogenous analyte monitoring is particularly interesting. The ability of MN-based devices to both deliver and extract molecules across the skin in a minimally invasive manner opens up the possibility for the development of a closed-loop responsive device, with an MN-based delivery component delivering a therapeutic molecule in response to information provided by an MN-based monitoring component. As technological advances continue, MN arrays may well become the pharmaceutical dosage forms and monitoring devices of the near future. However, there are a number of barriers that will firstly need to be addressed in order for MN technology to progress.

The ultimate commercial success of MN-based delivery and monitoring devices will depend upon not only the ability of the devices to perform their intended function, but also their overall acceptability by both health care professionals (e.g. doctors, nurses and pharmacists) and patients. Accordingly, efforts to ascertain the views of these end-users will be essential in moving forwards. The seminal study by the Birchall Group in this regard was highly-informative (Birchall *et al*., 2011). The majority of healthcare professionals and members of the public recruited into this focus-group-centred study were able to appreciate the potential advantage of using MNs, including reduced pain, tissue damage, risk of transmitting infections and needle-stick injuries, feasibility for self-administration and use in children, needlephobes and/or diabetics. However, some concerns regarding effectiveness, means to confirm successful drug delivery (such as a visual dose indicator), delayed onset of action, cost of the delivery system, possible accidental use, misuse and abuse were also raised. Healthcare professionals were also concerned about inter-individual variation in skin thickness, problems associated with injecting small volumes and risk of infection. Several other possible issues (accidental or errors based) and interesting doubts regarding microneedle use were discussed in this study. Overall, the Group reported that 100% of the public participants and 74% of the health care professional participants were optimistic about the future of microneedle technology. Such studies, when appropriately planned to capture the necessary demographics, will undoubtedly aid industry in taking necessary action to address concerns and develop informative labelling and patient counselling strategies to ensure safe and effective use of microneedle-based devices. Marketing strategies will, obviously, also be vitally important in achieving maximum market shares relative to existing and widely used conventional delivery systems.

In order to gain acceptance from healthcare professionals, patients and, importantly, regulatory authorities (e.g. the US FDA and the MHRA in the UK), it appears a strong possibility that an applicator aid and a 'dosing indicator' will be included within the overall MN 'package', with the MN array itself being disposable and the applicator/dosing indicator reusable. While a wide variety of applicator designs have been disclosed within the patient literature, only a few, relatively crude, designs based upon high impact/velocity insertion, or rotary devices have been described. Our own previous work has shown that application force has a significant role to play in MN insertion depth (Donnelly *et al*., 2010a). Clearly, patients cannot 'calibrate' their hands and, so, will apply MNs with different forces. Unless a large-scale study can be done showing consistent rates and extents of MN-mediated drug delivery when the MNs have been inserted by hand, then, for consistent dosing across the population, applicator devices will need to be supplied. Moreover, patients will need a level of assurance that the MN device has actually been inserted properly into their skin. This would be

especially-true in cases of global pandemics or bioterrorism incidents where self-administration of MN-based vaccines becomes a necessity. Accordingly, a suitable means of confirming that skin puncture has taken place may need to be included within an applicator device or the MN product itself.

From a regulatory point of view, currently little is known about the safety aspects that would be involved with long term usage of microneedle devices. In particular, studies will need to be conducted to assess the effect that repeated microporation has upon recovery of skin barrier function. However, given the minimally invasive nature of the micropores created within the skin following MN application, especially in comparison to the use of a hypodermic needle, and the fact that statistically it is highly unlikely that MNs would be inserted at exactly the same sites more than once in a patient's lifetime, it is envisaged that MN technology will be shown to have a favourable safety profile. Indeed, skin barrier function is known to completely recover within a few hours of MN removal, regardless of how long the MNs were in place. Local irritation or erythema (reddening) of the skin may be an issue for some patients. Since the skin is a potent immunostimulatory organ, it would be interesting to know whether repeated MN use would ever cause an immune reaction to the drug or excipients of MN materials, and whether such an effect would be so significant as to cause problems for patients.

Infection is an issue that has long been discussed in relation to use of MN-based systems, since MNs, by necessity, puncture the skin's protective *SC* barrier. However, as we and others have shown (Donnelly *et al*., 2009b), microbial penetration through MN-induced holes is minimal. Indeed, there have never been any reports of MNs causing skin or systemic infections. This may be because of the abovementioned immune component of the skin, or the skin's inherent non-immune, enzyme-based, defences. Alternatively, since the micropores are aqueous in nature, microorganisms may be more inclined to remain on the more hydrophobic *SC*. Whether skin cleansing before MN application is necessary remains to be seen and is a vital question. Ideally, this would not have to be done, so as to avoid unnecessarily inconveniencing patients and making the use of the product in the domiciliary setting appear more akin to a self-administered injection than application of a conventional transdermal patch. Regulators will ultimately make the key decisions based on the weight of available evidence. Depending upon the application (e.g. drug/vaccine/active cosmaceutical ingredient delivery or minimally invasive monitoring), MN-based devices may be classed as drug delivery stems, consumer products or medical devices. From a delivery perspective, it will be important if MNs are considered as injections rather than topical/transdermal/intradermal delivery systems, since this will determine whether the final product will need to be sterilised, prepared under aseptic conditions, or simply host a low bioburden. Any contained microorganisms may

need to be identified and quantified, as may the pyrogen content. Should sterilisation be required, then the method chosen will be crucial, since the most commonly employed approaches (moist heat, gamma or microwave radiation, ethylene oxide) may adversely affect the MNs themselves and/or any contained active ingredient (e.g. biomolecules).

Sterilisation and/or aseptic production will add considerably to costs for manufacturers. Indeed, the practicalities involved in the large-scale production of MN devices for commercial applications will need to be carefully considered. Currently, MNs are made by a wide variety of techniques, often in processes that are completely different from those used in the production of conventional dosage forms. Often, multiple manufacturing steps are required, particularly for coated MNs and those micromoulded from silicon or metal masters. Silicon MNs typically require clean room processing. As such, it would appear that any pharmaceutical or medical devices firm wishing to commercialise MN technology would need to a make a significant capital investment in order to design, develop and optimise a cost effective, reproducible, method for mass MN production. Adaptation of standard quality control procedures will also be required. Ultimately, the regulatory specifications applied to the first generation of MN products that reach the market may set the bar for all those that follow. Packaging of MN-based devices will be important, especially during transport and storage. Patient handling may only be controlled to a limited extent by effective product labelling and pharmacist-led counselling. Packaging should be sufficiently robust to prevent damage, contamination or accidental release of active ingredients during storage.

6.7 Conclusion

A wide variety of MN types and designs have been shown to be effective for the transdermal delivery of a diverse range of molecules, both *in vitro* and *in vivo*. The potential now exists to greatly expand the range of types of drugs that can be delivered effectively across the skin. This will significantly enhance the value of the transdermal delivery market and will be increasingly-important over the coming years as the number of new drugs of biological origin continues to increase. Small-scale clinical trials have highlighted the minimally invasive nature of MN-based systems, causing no pain, minimal irritation if any, and complete skin recovery within a few hours. Vaccine-loaded MN arrays have been shown to elicit a greater immune response in comparison to conventional injections and have a number of key advantages over the use of hypodermic needles. The ability of microorganisms to traverse MN-induced skin pores within the skin has been found to be minimal and with a lower incidence for occurrence when compared to the skin damage caused through hypodermic needle

skin puncture. MN devices also have the potential for use in non-invasive therapeutic drug/analyte monitoring and the possibility for closed-loop delivery systems may become important moving forwards. Focus group studies have identified key areas that need to be addressed by the MN community in order for the technology to progress. These include a means to ensure reproducible MN application in every patient every time and confirmation of successful device insertion. A significant number of small and large industry players are presently engaged in clinical trials, with the aim of commercialisation of their respective MN-based devices. Future studies will be needed to address potential regulatory concerns over the use of microneedle devices, as well as focusing on the design and development of processes to enable a low cost, efficient means for microneedle mass production.

Overall, the future for the MN sector appears to be very bright, with rapid expansion in fundamental new knowledge feeding industrial development. In due course, it is hoped that MN-based technological advancements will lead to enhanced disease prevention, diagnosis and control, with concomitant improvement in health-related quality of life for patients worldwide.

6.8 References

Amirouche, F., Zhou, Y. and Johnson, T. (2009), 'Current micropump technologies and their biomedical applications', *Microsystem Technologies*, vol. **15**, no. 5, pp. 647–666.

Arora, A., Prausnitz, M.R. and Mitragotri, S. (2008). 'Micro-scale devices for transdermal drug delivery', *International Journal of Pharmaceutics*, vol. **364**, pp. 227–36.

Ashraf, M.W., Tayyaba, S. and Afzulpurkar, N. (2011), 'Micro electromechanical systems (MEMS) based microfluidic devices for biomedical applications', *International Journal of Molecular Sciences*, vol. **12**, no. 6, pp. 3648–3704.

Baek, C., Han, M., Min, J., Prausnitz, M. and Park, J.H. (2011), 'Local transdermal delivery of phenylephrine to the anal sphincter muscle using microneedles', *Journal of Controlled Release: Official Journal of the Controlled Release Society*, vol. **154**, no. 2, pp. 138–147.

Bai, W., Li, Y., Yang, C., Liu, J., He, D. and Sugiyama, S. (2012), 'Fabrication of metal micro needle array by LIGA process', *Advanced Materials Research*, vol. **418**, pp. 1911–1914.

Bal, S., Ding, Z., van Riet, E., Jiskoot, W. and Bouwstra, J. (2010), 'Advances in transcutaneous vaccine delivery: do all ways lead to Rome?' *Journal of Controlled Release*, vol. **148**, no. 3, pp. 266–282.

Ball, J. and Pike, G. (2009), *Needlestick Injury in 2008*, Royal College of Nursing, 20 Cavendish Square, London, WIG ORN.

Banga, A. (2009), 'Microporation applications for enhancing drug delivery', *Expert Opinion on Drug Delivery*, vol. **6**, no. 4, pp. 343–354.

Banks, D. (2006), Microengineering, MEMS, and Interfacing: A Practical Guide, CRC, Boca Raton, Taylor and Francis, 21–72.

Banks, S.L., Pinninti, R.R., Gill, H.S., Crooks, P.A., Prausnitz, M.R. and Stinchcomb, A.L. (2008), 'Flux across of microneedle-treated skin is increased by increasing charge of naltrexone and naltrexol in vitro', *Pharmaceutical Research*, vol. **25**, pp. 1677–1685.

Banks, S.L., Pinninti, R.R., Gill, H.S., Paudel K.S., Crooks, P.A., Brogden, N.K., Prausnitz, M.R. and Stinchcomb, A.L. (2010), 'Transdermal delivery of naltrexol and skin permeability lifetime after microneedle treatment in hairless guinea pigs', *Journal of Pharmaceutical Research*, vol. **99**, pp. 3072–3080.

Bariya, S., Gohel, M., Mehta, T. and Sharma, O. (2012), 'Microneedles: an emerging transdermal drug delivery system', *Journal of Pharmacy and Pharmacology*, vol. **64**, no. 1, pp. 11–29.

BD. Available online at: http://www.bd.com/pharmaceuticals/prod- ucts/microinjection.asp, accessed 1 October 2009.

Birchall, J., Clemo, R., Anstey, A. and John, D. (2011), 'Microneedles in clinical practice – an exploratory study into the opinions of Healthcare professionals and the Public', *Pharmaceutical Research*, vol. **28**, pp. 95–106.

Bodhale, D.W., Nisar, A. and Afzulpurkar, N. (2010), 'Structural and microfluidic analysis of hollow side-open polymeric microneedles for transdermal drug delivery applications', *Microfluidics and Nanofluidics*, vol. **8**, no. 3, pp. 373–392.

Bouissou, C., Sylvestre, J., Guy, R. and Delgado-Charro, M. (2009), 'Reverse iontophoresis of amino acids: identification and separation of stratum corneum and subdermal sources in vitro', *Pharmaceutical Research*, vol. **26**, no. 12, pp. 2630–2638.

Brancazio, D. (2012), *Systems and Interfaces for Blood Sampling*, 600/576 edn, A61B 5/15, US.

Bystrova, S. and Luttge, R. (2011), 'Micromolding for ceramic microneedle arrays', *Microelectronic Engineering*, vol. **88**, no. 8, pp. 1681–1684.

Chandrasekaran, S., Mohanty, S. and Frazier, A. (2003), *'Surface micromachined metallic microneedles', Journal of MEMS.* vol. **12**, pp. 281–288.

Chaudhri, B., Ceyssens, F., De Moor, P., Van Hoof, C. and Puers, R. (2010), 'A high aspect ratio SU-8 fabrication technique for hollow microneedles for transdermal drug delivery and blood extraction', *Journal of Micromechanics and Microengineering*, vol. **20**, no. 6, pp. 064006.

Chen, B., Wei, J., Tay, F., Wong, Y. and Iliescu, C. (2008), 'Silicon microneedle array with biodegradable tips for transdermal drug delivery', *Microsystem Technologies*, vol. **14**, no. 17, pp. 1015–1019.

Chen, X., Prow, T., Crichton, M., Jenkins, D., Roberts, M.S., Frazer, I.H., Fernando, G.J. and Kendall, M.A. (2009), 'Dry-coated microprojection array patches for targeted delivery of immunotherapeutics to the skin', *Journal of Controlled Release*, vol. **139**, no. 3, pp. 212–220.

Ching, C., Chou, T., Sun, T., Huang, S. and Shieh, H. (2011), 'Simultaneous, noninvasive, and transdermal extraction of urea and homocysteine by reverse iontophoresis', *International Journal of Nanomedicine*, vol. **6**, pp. 417–423.

Ching, C., Sun, T., Huang, S., Shieh, H. and Chen, C. (2010), 'A mediated glucose biosensor incorporated with reverse iontophoresis function for noninvasive glucose monitoring', *Annals of Biomedical Engineering*, vol. **38**, no. 4, pp. 1548–1555.

Choi, H., Yoo, D., Bondy, B., Quan, F., Compans, R., Kang, S. and Prausnitz, M. (2012), 'Stability of influenza vaccine coated onto microneedles', *Biomaterials*, vol. **33**, no. 14, pp. 3756–3769.

Chu, L. and Prausnitz, M. (2011), 'Separable arrowhead microneedles', *Journal of Controlled Release*, vol. **149**, no. 3, pp. 242–249.

Cleary, G.W. (2009), 'The emergence of active transdermal drug delivery', *Control Release Society Presentation*, 18–22 July, Copenhagen, Denmark.

Conjeevaram, R., Banga, A. K. and Zhang, L. (2002), 'Electrically modulated transdermal delivery of fentanyl', *Pharmaceutical Research* vol. **19**, pp. 440–444.

Cormier, M. and Daddona, P.E. (2003), 'Macroflux technology for transdermal delivery of therapeutic proteins and vaccines', *Drugs and the Pharmaceutical Sciences*, vol. **126**, pp. 589–598.

Cormier, M., Johnson, B., Ameri, M., Nyam, K., Libiran, L., Zhang, D. and Daddona, P. (2004), Transdermal delivery of desmopressin using a coated microneedle array patch system. *Journal of Controlled Release*, vol. **97**, pp.503–511.

Corrie, S., Fernando, G., Crichton, M., Brunck, M., Anderson, C. and Kendall, M. (2010), 'Surface-modified microprojection arrays for intradermal biomarker capture, with low non-specific protein binding', *Lab on a Chip*, vol. **10**, no. 20, pp. 2655–2658.

Daddona, P. (2002), 'Macroflux® transdermal technology development for the delivery of therapeutic peptides and proteins', *Drug Delivery Technology*, vol. **2**.

Dai, T., Huang, Y. and Hamblin, M. (2009), 'Photodynamic therapy for localized infections-state of the art', *Photodiagnosis and Photodynamic Therapy*, vol. **6**, no. 3–4, pp. 170–188.

Daugimont, L., Baron, N., Vandermeulen, G., Pavselj, N., Miklavcic, D., Jullien, M.-C., Cabodevila, G., Mir, L. and Préat, V. (2010), 'Hollow microneedle arrays from intradermal drug delivery and DNA electroporation', *Journal of Membrane Biology*, vol. **236**, pp. 117–125.

Davis, S., Martanto, W., Allen, M. and Prausnitz, M. (2005), 'Hollow metal microneedles for insulin delivery to diabetic rats', *IEEE Transactions on Bio-medical Engineering*, vol. **52**, no. 5, pp. 909–915.

DeMuth, P., Su, X., Samuel, R., Hammond, P. and Irvine, D. (2010), 'Nano-layered microneedles for transcutaneous delivery of polymer nanoparticles and plasmid DNA', *Advanced Materials*, vol. **22**, no. 43, pp. 4851–4856.

Ding, Z., Verbaan, F., Bivas-Benita, M., Bungener, L., Huckriede, A., van den Berg, D.J., Kersten, G. and Bouwstra, J.A. (2009), 'Microneedle arrays for the transcutaneous immunization of diphtheria and influenza in BALB/c mice', *Journal of Controlled Release*, vol. **136**, no. 1, pp. 71–78.

Donnelly, R.F., McCarron, P. and Tunney, M. (2008), 'Antifungal photodynamic therapy.' *Microbiological Research*, vol. **163**, no. 1, pp. 1–12.

Donnelly, R.F., Majithiya, R., Singh, T.R., Morrow, D.I., Garland, M.J., Demir, Y.K., Migalska, K., Ryan, E., Gillen, D., Scott, C.J. and Woolfson, A.D. (2011), 'Design, optimization and characterisation of polymeric microneedle arrays prepared by a novel laser-based micromoulding technique', *Pharmaceutical Research*, vol. **28**, no. 1, pp. 41–57.

Donnelly, R.F., Morrow, D., McCarron, P., Woolfson, A., Morrissey, A., Juzenas, P., Juzeniene, A., Iani, V., McCarthy, H.O. and Moan, J. (2008), 'Microneedle-mediated intradermal delivery of 5-aminolevulinic acid: potential for enhanced

topical photodynamic therapy', *Journal of Controlled Release*, vol. **129**, no. 3, pp. 154–162.

Donnelly, R.F., Morrow, D., Singh, T., Migalska, K., McCarron, P.A., O'Mahony, C. and Woolfson, A.D. (2009a), 'Processing difficulties and instability of carbohydrate microneedle arrays', *Drug Development and Industrial Pharmacy*, vol. **39**, no. 10, pp. 1242–1254.

Donnelly, R.F., Singh, T., Morrow, D. and Woolfson, A. (2012), *Microneedle-Mediated Transdermal and Intradermal Drug Delivery*, John Wiley & Sons, Ltd, Chichester, UK. doi: 10.1002/9781119959687.index

Donnelly, R.F., Singh, T., Tunney, M., Morrow, D., McCarron, P., O'Mahony, C. and Woolfson, A. (2009b), 'Microneedle arrays allow lower microbial penetration than hypo-dermic needles in vitro', *Pharmaceutical Research*, vol. **26**, pp. 2513–2522.

Donnelly, R.F., Garland, M.J., Morrow, D.I., Migalska, K., Singh, T.R., Majithiya, R. and Woolfson, A.D. (2010a), 'Optical coherence tomography is a valuable tool in the study of the effects of microneedle geometry on skin penetration characteristics and in-skin dissolution', *Journal of Control Release*, vol. **147**, no. 3, pp. 333–341.

Donnelly, R.F., Singh, T. and Woolfson, A.D. (2010b), 'Microneedle-based drug delivery systems: microfabrication, drug delivery, and safety', *Drug Delivery*, vol. **17**, no. 4, pp. 187–207.

Donnelly, R.F., Singh, T., Garland M., Migalska, K., Majithiya, R., McCrudden, C., Kole, P., Tuan-Mahmood, T., McCarthy, H. and Woolfson, A. (2012), 'Hydrogel-forming microneedle arrays for enhanced transdermal drug delivery', *Adv Funct Mat*, vol. **22**, no. 23, pp. 4879–4890.

Ebah, L.M., Read, I., Sayce, A., Morgan, J., Chaloner, C., Brenchley, P. and Mitra, S. (2012), 'Reverse iontophoresis of urea in health and chronic kidney disease: a potential diagnostic and monitoring tool?', *European Journal of Clinical Investigation*, vol. **42**, no. 8, pp. 840–847.

Ehrenpreis, E.D., Chang, D. and Eichenwald, E. (2007), 'Pharmacotherapy for fecal incontinence: a review', *Diseases of the Colon and Rectum*, vol. **50**, no. 5, pp. 641–649.

Erdos, G., Donahue, C., Zhang, J., Gambotto, A., Ozdoganlar, B.O. and Falo, L.D. (2012), 'Dissolvable microneedle arrays enable delivery of live adenovectors to the skin for cutaneous transduction and genetic immunization', *Journal of Investigative Dermatology*, vol. **132**, pp. S105–S105.

Fang, J-Y, Hwang, T-L, Fang, C-L and Chiu, H-C (2003), 'In vitro and in vivo evaluations of the efficacy and safety of skin permeation enhancers using flurbiprofen as a model drug', *International Journal of Pharmaceutics*, vol. **255**, no. 1–2, pp. 153–166.

Gardeniers, H.J.G.E., Luttge, R., Berenschot, E.J.W., de Boer, M.J. (2003), 'Silicon micromachined hollow microneedles for transdermal liquid transport', *Journal of Microelectromechanical Systems*, vol. **12**, no. 6, pp. 855–862.

Garland, M.J., Migalska, K., Mazlelaa, T., Mahmood, T.,Singh, T.R.R., Woolfson, A.D. and Donnelly, R.F. (2011), 'Microneedle arrays as medical devices for enhanced transdermal drug delivery', *Expert Review of Medical Devices*, vol. **8**, no. 4, pp. 459–482.

Gary, C. (2009), 'The emergence of active transdermal drug delivery', *Controlled Release Society Annual Meeting*, 18–22 July, Copenhagen, Denmark.

Gerstel, M and Place, V. (1976), 'Drug Delivery Device.' US Patent Number 3, 964, 482.

Gill, H.S. and Prausnitz, M.R. (2007a), 'Coated microneedles for transdermal delivery', *Journal of Controlled Release*, vol. **117**, no. 2, pp. 227–237.

Gill, H.S. and Prausnitz, M.R. (2007b), 'Coating formulations for microneedles', *Pharmaceutical Research*, vol. **24**, no. 7, pp. 1369–1380.

Gill, H.S., Söderholm, J., Prausnitz, M.R. and Sällberg, M. (2010), 'Cutaneous vaccination using microneedles coated with hepatitis C DNA vaccine', *Gene Therapy*, vol. **17**, no. 6, pp. 811–814.

Godin, B. and Touitou, E. (2007), 'Transdermal skin delivery: predictions for humans from in vivo, ex vivo and animal models', *Advanced Drug Delivery Reviews*, vol. **59**, no. 11, pp. 1152–1161.

Goud, J., Raj, P.M., Liu, J., Narayan, R. and Iyer, M. (2007), *Electrochemical Biosensors and Microfluidics in Organic System-on-package Technology*, Institute of Electrical and Electronics Engineers [etc.], New York [etc.].

Gupta, J., Felner, E.I. and Prausnitz, M.R. (2009), 'Minimally invasive insulin delivery in subjects with type 1 diabetes using hollow microneedles', *Diabetes Technology & Therapeutics*, vol. **11**, no. 6, pp. 329–337.

Gupta, J., Denson, D.D., Felner, E.I. and Prausnitz, M.R. (2012), 'Rapid local anesthesia in humans using minimally invasive microneedles', *The Clinical Journal of Pain*, vol. **28**, no. 2, pp. 129–135.

Hennink, W. and van Nostrum, C. (2002), 'Novel crosslinking methods to design hydrogels', *Advanced Drug Delivery Reviews*, vol. **54**, no. 1, pp. 13–36.

Henry, S., McAllister, D.V., Allen, M.G. and Prausnitz, M.R. (1998), 'Microfabricated microneedles: a novel approach to transdermal drug delivery', *Journal of Pharmaceutical Sciences*, vol. **87**, no. 8, pp. 922–925.

Hoffman, A.S. (2002), 'Hydrogels for biomedical applications', *Advanced Drug Delivery Reviews*, vol. **54**, no. 1, pp. 3–12.

Ito, Y., Hagiwara, E., Saeki, A., Sugioka, N. and Takada, K. (2006), 'Feasibility of microneedles for percutaneous absorption of insulin', *European Journal of Pharmaceutical Sciences*, vol. **29**, no. 1, pp. 82–88.

Jae-Ho, O., Park, H., Ki-Young, D., Han, M., Hyun, D., Kim, C., Kim, C., Lee, S., Sung-Joo, H., Shin, S. and Cho, C. (2008), 'Influence of the delivery systems using a microneedle array on the permeation of a hydrophilic molecule, calcein', *European Journal of Pharmaceutics and Biopharmaceutics*, vol. **69**, pp. 1040–1045.

Ji, J., Tay, F.E., Miao, J. and Iliescu, C. (2006), 'Microfabricated silicon microneedle array for transdermal drug delivery', *Journal of Physics: Conference Series*, vol. **34**, no. 1, pp. 1127–1131.

Jiang, J., Moore, J.S., Edelhauser, H.F. and Prausnitz, M.R. (2009), 'Intrascleral drug delivery to the eye using hollow microneedles', *Pharmaceutical Research*, vol. **26**, no. 2, pp. 395–403.

Jin, C.Y., Han, M.H., Lee, S.S. and Choi, Y.H. (2009), 'Mass producible and biocompatible microneedle patch and functional verification of its usefulness for transdermal drug delivery', *Biomedical Microdevices*, vol. **11**, no. 6, pp. 1195–1203.

Joshi, A. and Raje, J. (2002), 'Sonicated transdermal drug transport', *Journal of Controlled Release*, vol. **83**, no. 1, pp. 13–22.

Khanna, P., Strom, J., Malone, J. and Bhansali, S. (2008), 'Microneedle-based automated therapy for diabetes mellitus', *Journal of Diabetes Science and Technology*, vol. **2**, no. 6, pp. 1122–1129.

Khumpuang, S., Kawaguchi, G. and Sugiyama, S. (2004), *Quadruplets-microneedle Array for Blood Extraction*, Nano Science Technology Inst, Cambridge.

Kim, A., Suecof, L., Sutherland, C., Gao, L., Kuti, J. and Nicolau, D. (2008), 'In vivo microdialysis study of the penetration of daptomycin into soft tissues in diabetic versus healthy volunteers', *Antimicrobial Agents and Chemotherapy*, vol. **52**, no. 11, pp. 3941–3946.

Kim, K., Park, D.S., Lu, H.M., Che, W., Kim, K., Lee, J.B. and Ahn, C.H. (2004), 'A tapered hollow metallic microneedle array using backside exposure of SU-8', *Journal of Micromechanics and Microengineering*, vol. **14**, pp. 597.

Kim, M., Jung, B. and Park, J-H. (2012a), 'Hydrogel swelling as a trigger to release biodegradable polymer microneedles in skin', *Biomaterials*, vol. **33**, no. 2, pp. 668–678.

Kim, S.W., Bae, Y.H. and Okano, T. (1992), 'Hydrogels: swelling, drug loading, and release', *Pharmaceutical Research*, vol. **9**, no. 3, pp. 283–290.

Kim, Y-C, Ludovice, P.J. and Prausnitz, M.R. (2007), 'Transdermal delivery enhanced by magainin pore-forming peptide', *Journal of Controlled Release*, vol. **122**, no. 3, pp. 375–383.

Kim, Y.C., Park, J.H. and Prausnitz, M.R. (2012b), 'Microneedles for drug and vaccine delivery', *Advanced Drug Delivery Reviews*, vol. **64**, no. 14, pp. 1547–1568.

Kim, Y., Jarrahian, C., Zehrung, D., Mitragotri, S. and Prausnitz, M. (2012), 'Delivery systems for intradermal vaccination', *Intradermal Immunization*, vol. **351**, pp. 77–112.

Kobayashi, K. and Suzuki, H. (2001), 'A sampling mechanism employing the phase transition of a gel and its application to a micro analysis system imitating a mosquito', *Sensors and Actuators B, Chemical*, vol. **80**, no. 1, pp. 1–8.

Kong, X.Q. and Wu, C.W. (2010), 'Mosquito proboscis: an elegant biomicroelectromechanical system', *Physical Review E*, vol. **82**, no. 1, pp. 011910.

Koren, G. (1997), 'Therapeutic drug monitoring principles in the neonate. National Academy of Clinical Biochemistry', *Clinical Chemistry*, vol. **43**, no. 1, pp. 222–227.

Laermer, F. and Schilp, A. (1996), Method of Anisotropically Etching Silicon. US Patent Number 5,501,893.

Leboulanger, B., Aubry, J., Bondolfi, G., Guy, R. and Delgado-Charro, M. (2004), 'Lithium monitoring by reverse iontophoresis in vivo', *Clinical Chemistry*, vol. **50**, no. 11, pp. 2091–2100.

Lee, C., Ching, C.T., Sun, T., Tsai, C., Huang, W., Huang, H., Kuo, J., Lai, L., Chien, M., Tseng, H., Pan, H., Huang, S., Shieh, H., Liu, W., Liu, C. and Huang, H. (2010), 'Non-invasive and transdermal measurement of blood uric acid level in human by electroporation and reverse iontophoresis', *International Journal of Nanomedicine*, vol. **5**, pp. 991–997.

Lee, J.W., Park, J.H. and Prausnitz, M.R. (2008), 'Dissolving microneedles for transdermal drug delivery', *Biomaterials*, vol. **29**, no. 13, pp. 2113–2124.

Li, G., Badkar, A., Nema, S., Kolli, C.S. and Banga, A.K. (2009), 'In vitro transdermal delivery of therapeutic antibodies using maltose microneedles', *International Journal of Pharmaceutics*, vol. **368**, no. 1–2, pp. 109–15.

Liu, J., Liu, C., Liu, H., Jiang, L., Yang, Q. and Cai, X. (2007), 'Study of noninvasive sampling of subcutaneous glucose by reverse iontophoresis', IEEE Service Center, 445 Hoes Lane, PO Box 1331, Piscataway, NJ 08855–1331 USA.

Liu, R., Wang, X., Tang, F., Feng, Y. and Zhou, Z. (2005), 'An in-plane microneedles used for sampling and glucose analysis', *Proceedings of 13th International on Solid-State Sensors, Actuators and Microsystems*, vol. **2**, pp. 1517–1520.

Liu, R., Wang, X., Feng, Y., Wang, G. and Liu, J. (2006), 'Theoretical analytical flow model in hollow microneedles for non-forced fluid extraction', *Proceedings of 1st IEEE International Conference on Nano/Micro Engineered and Molecular Systems*, pp. 1039–1042.

Luttge, R., Berenschot, E.J.W., de Boer, M.J., Altpeter, D.M., Vrouwe, E.X., van den Berg, A. and Elwenspoek, M. (2007), 'Integrated lithographic molding for microneedle-based devices', *Journal of Microelectromechanical Systems*, vol. **16**, no. 4, pp. 872–884.

van der Maaden, K., Jiskoot, W. and Bouwstra, J. (2012), 'Microneedle technologies for (trans)dermal drug and vaccine delivery', *Journal of Controlled Release*. vol. **161**, no. 2, pp. 645–55.

Madou Marc, J. (1997), *Fundamentals of Microfabrication*, 2nd edition, CRC Press, Boca Raton, pp. 1–71.

Matriano, J.A., Cormier, M., Johnson, J., Young, W.A., Buttery, M., Nyam, K. and Daddona, P.E. (2002), 'Macroflux microprojection array patch technology: a new and efficient approach for intracutaneous immunization', *Pharmaceutical Research*, vol. **19**, no. 1, pp. 63–70.

Martanto, W., Moore, J.S., Kashlan, O., Kamath, R., Wang, P.M., O'Neal, J.M. and Prausnitz, M.R. (2006), 'Microinfusion using hollow microneedles', *Pharmaceutical Research*, vol. **23**, no. 1, pp. 104–113.

McAllister, D.V., Cros, F., Davis, S.P., Matta, L.M., Prausnitz, M.R. and Allen, M.G. (1999). 'Three dimensional hollow microneedle and microtube arrays', *Proceedings of 10th International Conference on Solid-State Sensor and Actuators Transducers*, pp. 1098–1101.

McAllister, D.V., Allen, M.G. and Prausnitz, M.R. (2000), 'Microfabricated microneedles for gene and drug delivery', *Annual Review of Biomedical Engineering*, vol. **2**, no. 1, pp. 289–313.

McAllister, D.V., Wang, P.M., Davis, S.P., Park, J-H., Canatella, P.J., Allen, M.G. and Prausnitz, M.R. (2003), 'Microfabricated needles for transdermal delivery of macromolecules and nanoparticles: fabrication methods and transport studies', *Proceedings of the National Academy of Sciences of the United States of America*, vol. **100**, no. 24, pp. 13755–13760.

Microneedle. (2009). Available online at : http://www.microneedle. com/main/index. html, accessed 1 October 2009.

Migalska, K., Morrow, Desmond I.J., Garland, M.J., Thakur, R., Woolfson, A.D. and Donnelly, R.F. (2011), 'Laser-engineered dissolving microneedle arrays for transdermal macromolecular drug delivery', *Pharmaceutical Research*, vol. **28**, no. 8, pp. 1919–1930.

Mikszta, J.A., Alarcon, J.B., Brittingham, J.M., Sutter, D.E., Pettis, R.J. and Harvey, N.G. (2002), 'Improved genetic immunization via micromechanical disruption of skin-barrier function and targeted epidermal delivery', *Nature Medicine*, vol. **8**, no. 4, pp. 415–419.

Mikszta, J.A., Dekker, J.P., Harvey, N.G., Dean, C.H., *et al*. (2006), 'Microneedle-based intradermal delivery of the anthrax recombinant protective antigen vaccine', *Infection and Immunity*, vol. **74**, no. 12, pp. 6806–6810.

Mischler, R. and Werner, G. (2012), *Microneedle Arrays with ATR Sensor*, 600/310 edn, A61B 5/1455, US.

Miyano, T., Tobinaga, Y., Kanno, T., Matsuzaki, Y., Takeda, H., Wakui, M. and Hanada, K. (2005), 'Sugar micro needles as transdermic drug delivery system', *Biomedical Microdevices*, vol. **7**, no. 3, pp. 185–188.

Moon, S.J., Lee, S.S., Lee, H.S. and Kwon, T.H. (2005), 'Fabrication of microneedle array using LIGA and hot embossing process', *Microsystem Technologies*, vol. **11**, no. 4–5, pp. 311–318.

Moreno, M., Aracil, C. and Quero, J. (2008), 'High-integrated microvalve for Lab-on-chip biomedical applications', *Proceedings of Biomedical Circuits and Systems Conference*, pp. 313–316.

Moreno, M., Aracil, J.C. and Quero, J. (2009), 'Low cost fluid microextractor for lab-on-chip', *Proceedings of Spanish Conference on Electron Devices*, pp. 274–277.

Mukerjee, E., Collins, S., Isseroff, R. and Smith, R. (2004), 'Microneedle array for transdermal biological fluid extraction and in situ analysis', *Sensors and Actuators A, Physical*, vol. **114**, no. 2–3, pp. 267–275.

Mukerjee, E., Issseroff, R., Collins, S. and Smith, R. (2003), Microneedle array with integrated microchannels for transdermal sample extraction and in situ analysis. In proceeding of: Transducers, Solid-State Sensors, Actuators and Microsystems, 12th International Conference on. Vol **2**. 1440–1441.

Naik, A., Kalia, Y.N. and Guy, R.H. (2000), 'Transdermal drug delivery: overcoming the skin's barrier function', *Pharmaceutical Science & Technology Today*, vol. **3**, no. 9, pp. 318–326.

Nanopass. (2009), Available online at: http://www.nanopass.com/content-d.asp?tcid=19&cid=24, accessed 1 October 2009.

Nielsen, J.K., Freckmann, G., Kapitza, C., Ocvirk, G., Koelker, K.H., Kamecke, U., Gillen, R., Amann-Zalan, I., Jendrike, N., Christiansen, J.S., Koschinsky, T. and Heinemann, L. (2009), 'Glucose monitoring by microdialysis: performance in a multicentre study', *Diabetic Medicine*, vol. **26**, no. 7, pp. 714–721.

Oka, K., Aoyagi, S., Arai, Y., Isono, Y., Hashiguchi, G. and Fujita, H. (2002), 'Fabrication of a micro needle for a trace blood test', *Sensors and Actuators A: Physical*, vol. **97–98**, pp. 478–485.

Omatsu, T., Chujo, K., Miyamoto, K., Okida, M., Nakamura, K., Aoki, N. and Morita, R. (2010), 'Metal microneedle fabrication using twisted light with spin', *Optics Express*, vol. **18**, no. 17, pp. 17967–17973.

Paik, S., Byun, A., Lim, J., Park, Y., Lee, A. and Chung, S. (2004), 'In-plane single-crystal-silicon microneedles for minimally invasive microfluid systems', *Sensors and Actuators A, Physical*, vol. **114**, no. 2–3, pp. 276–284.

Paik, S., Lim, J., Jung, I., Park, Y. and Byun, S. (2003), A novel microneedle array integrated with a PDMS biochip for microfluid systems, Transducers – Conference, pp. 1446–1449.

Paliwal, S., Ogura, M. and Mitragotri, S. (2010), 'Rapid sampling of molecules via skin for diagnostic and forensic applications', *Pharmaceutical Research*, vol. **27**, no. 7, pp. 1255–1263.

Park, J.H., Allen, M.G. and Prausnitz, M.R. (2005), 'Biodegradable polymer microneedles: fabrication, mechanics and transdermal drug delivery', *Journal of Controlled Release*, vol. **104**, no. 1, pp. 51–66.

Park, J.H., Allen, M.G. and Prausnitz, M.R. (2006), 'Polymer microneedles for controlled-release drug delivery', *Pharmaceutical Research*, vol. **23**, no. 5, pp. 1008–1019.

Park, J.H., Choi, S.O., Kamath, R., Yoon, Y-K., Allen, M.G. and Prausnitz, M.R. (2007), 'Polymer particle-based micromolding to fabricate novel microstructures', *Biomedical Microdevices*, vol. **9**, no. 2, pp. 223–234.

Park, J.S., Kang, S.B., Kim, D-W., Namgung, H-W. and Kim, H-L. (2007), 'The efficacy and adverse effects of topical phenylephrine for anal incontinence after low anterior resection in patients with rectal cancer', *International Journal of Colorectal Disease*, vol. **22**, no. 11, pp. 1319–1324.

Peppas, N., Bures, P., Leobandung, W. and Ichikawa, H. (2000), 'Hydrogels in pharmaceutical formulations', *European Journal of Pharmaceutics and Biopharmaceutics*, vol. **50**, no. 1, pp. 27–46.

Peters, E.E., Ameri, M., Wang, X., Maa, Y.F. and Daddona, P.E. (2012), 'Erythropoietin-coated ZP-microneedle transdermal system: preclinical formulation, stability, and delivery', *Pharmaceutical Research*, vol. **29**, no. 6, pp. 1–9.

Potts, R.O. (1990), 'Lipid biophysics of water loss through the skin', *Proceedings of the National Academy of Sciences*, vol. **87**, no. 10, pp. 3871–3873.

Potts, R., Tamada, J. and Tierney, M. (2002), 'Glucose monitoring by reverse iontophoresis', *Diabetes/metabolism Research and Reviews*, vol. **18**, no. S1, pp. S49–S53.

Prausnitz, M.R., Mitragotri, S. and Langer, R. (2004), 'Current status and future potential of transdermal drug delivery', *Nature Reviews Drug Discovery*, vol. **3**, no. 2, pp. 115–124.

Ramasubramanian, M.K., Barham, O.M. and Swaminathan, V. (2008), 'Mechanics of a mosquito bite with applications to microneedle design', *Bioinspiration & Biomimetics*, vol. **3**, no. 4, pp. 046001.

Rapiti, E., Prüss-Üstün, A. and Hutin, Y. (2005), 'Sharps injuries: assessing the burden of disease from sharps injuries to health-care at national and local levels', *WHO Environmental Burden of Disease Series*, no. 11.

Roxhed, N., Griss, P. and Stemme, G. (2008a), 'Membrane-sealed hollow microneedles and related administration schemes for transdermal drug delivery', *Biomedical Microdevices*, vol. **10**, no. 2, pp. 271–279.

Roxhed, N., Samel, B., Nordquist, L., Griss, P. and Stemme, G. (2008b), 'Painless drug delivery through microneedle-based transdermal patches featuring active infusion', *Biomedical Engineering, IEEE Transactions on*, vol. **55**, no. 3, pp. 1063–1071.

Roxhed, N., Griss, P. and Stemme, G. (2007), 'A method for tapered deep reactive ion etching using a modified Bosch process', *Journal of Micromechanics and Microengineering*, vol. **17**, no. 5, pp. 1087–1092.

Sato, T., Okada, S., Hagino, K., Asakura, Y., Kikkawa, Y., Kojima, J., Watanabe, T., Maekawa, Y., Isobe, K., Koike, R., Nakajima, H. and Asano, K. (2011), 'Measurement of glucose area under the curve using minimally invasive interstitial fluid extraction technology: evaluation of glucose monitoring concepts

without blood sampling', *Diabetes Technology & Therapeutics*, vol. **13**, no. 12, pp. 1194–1200.

Shawgo, R.S., Richards Grayson, A.C., Li, Y. and Cima, M.J. (2002), 'BioMEMS for drug delivery', *Current Opinion in Solid State and Materials Science*, vol. **6**, no. 4, pp. 329–334.

Sieg, A., Guy, R. and Delgado-Charro, M. (2004), 'Electroosmosis in transdermal iontophoresis: implications for noninvasive and calibration-free glucose monitoring', *Biophysical Journal*, vol. **87**, no. 5, pp. 3344–3350.

Singh, R., Singh, S. and Lillard, J.W. (2008), 'Past, present, and future technologies for oral delivery of therapeutic proteins', *Journal of Pharmaceutical Sciences*, vol. **97**, no. 7, pp. 2497–2523.

Singh, T.R.R., Garland, M.J., Cassidy, C.M., Migalska, K., Demir, Y.K., Abdelghany, S., Ryan, E., Woolfson, A.D. and Donnelly, R.F. (2010), 'Microporation techniques for enhanced delivery of therapeutic agents', *Recent Patents on Drug Delivery & Formulation*, vol. **4**, no. 1, p. 17.

Stoeber, B. and Liepmann, D. (2002), 'Design, fabrication and testing of a MEMS syringe.' Presented at the Solid-State Sensor, Actuator and Microsystems Workshop, Hilton Head, SC.

Sullivan, S.P., Murthy, N. and Prausnitz, M.R. (2008), 'Minimally invasive protein delivery with rapidly dissolving polymer microneedles', *Advanced Materials*, vol. **20**, no. 5, pp. 933–938.

Sun, T., Shieh, H., Ching, C., Yao, Y., Huang, S. and Liu, C. (2010), 'Carbon nanotube composites for glucose biosensor incorporated with reverse iontophoresis function for noninvasive glucose monitoring', *International Journal of Nanomedicine*, vol. **5**, pp. 343–349.

Suzuki, H., Tokuda, T. and Kobayashi, K. (2002), 'A disposable "intelligent mosquito" with a reversible sampling mechanism using the volume-phase transition of a gel', *Sensors and Actuators B, Chemical*, vol. **83**, no. 1–3, pp. 53–59.

Suzuki, H., Tokuda, T., Miyagishi, T., Yoshida, H. and Honda, N. (2004), 'A disposable on-line microsystem for continuous sampling and monitoring of glucose', *Sensors and Actuators B, Chemical*, vol. **97**, no. 1, pp. 90–97.

Tayyaba, S., Ashraf, M. and Afzulpurkar, N. (2011), 'Blood filtration system for patients with kidney diseases', *IET Communications*, Manuscript ID COM-2011–0176.

Teo, A.L., Shearwood, C., Nga, K.C., Lu, J. and Moochhala, S. (2006), 'Transdermal microneedles for drug delivery applications', *Materials Science and Engineering: B*, vol. **132**, no. 1–2, pp. 151–154.

Trzebinski, J., Sharma, S., Moniz, A., Michelakis, K. and Zhang, Y. (2012), 'Microfluidic device to investigate factors affecting performance in biosensors designed for transdermal applications', *Lab on a Chip*, vol. **12**, no. 2, pp. 348–352.

Tsuchiya, K., Jinnin, S., Yamamoto, H., Uetsuji, Y. and Nakamachi, E. (2010), 'Design and development of a biocompatible painless microneedle by the ion sputtering deposition method', *Precision Engineering*, vol. **34**, no. 3, pp. 461–466.

Vanbever, R., LeBoulengé, E. and Préat, V. (1996), 'Transdermal delivery of fentanyl by electroporation. I. Influence of electrical factors', *Pharmaceutical Research*, vol. **13**, no. 4, pp. 559–565.

Venugopal, M., Feuvrel, K., Mongin, D., Bambot, S., Faupel, M. and Panangadan, A. (2008), 'Clinical evaluation of a novel interstitial fluid sensor system for remote continuous alcohol monitoring', *IEEE Sensors Journal*, vol. **8**, no. 1, pp. 71–80.

Vesper, H., Wang, P., Archibold, E., Prausnitz, M. and Myers, G. (2006), 'Assessment of trueness of a glucose monitor using interstitial fluid and whole blood as specimen matrix', *Diabetes Technology Therapeutics*, vol. **8**, no. 1, pp. 76–80.

Vrouwe, E. and Luttge, R. (2005), *Sampling for Point-of-care Analysis of Lithium in Whole Blood with Chip Based CE*, Springer, New York.

Wang, P., Cornwell, M. and Prausnitz, M. (2005), 'Minimally invasive extraction of dermal interstitial fluid for glucose monitoring using microneedles', *Diabetes Technology Therapeutics*, vol. **7**, no. 1, pp. 131–141.

Wang, P.M., Cornwell, M., Hill, J. and Prausnitz, M.R. (2006), 'Precise microinjection into skin using hollow microneedles', *The Journal of Investigative Dermatology*, vol. **126**, no. 5, pp. 1080–1087.

Wilke, N., Mulcahy, A., Ye, S.R. and Morrissey, A. (2005), 'Process optimization and characterization of silicon microneedles fabricated by wet etch technology', *Microelectronics Journal*, vol. **36**, no. 7, pp. 650–656.

Williams, A. (2003), *Transdermal and Topical Drug Delivery from Theory to Clinical Practice*, Pharmaceutical Press, London, UK.

Windmiller, J., Zhou, N., Chuang, M., Valdes Ramirez, G., Santhosh, P. and Miller, P. (2011a), 'Microneedle array-based carbon paste amperometric sensors and biosensors', *Analyst*, vol. **136**, no. 9, pp. 1846–1851.

Windmiller, J., Valdes Ramirez, G., Zhou, N., Zhou, M. and Miller, P. (2011b), 'Bicomponent microneedle array biosensor for minimally-invasive glutamate monitoring', *Electroanalysis*, vol. **23**, no. 10, pp. 2302–2309.

Xie, Y., Xu, B. and Gao, Y. (2005), 'Controlled transdermal delivery of model drug compounds by MEMS microneedle array', *Nanomedicine : Nanotechnology, Biology, and Medicine*, vol. **1**, no. 2, pp. 184–190.

Yung, K., Xu, Y., Kang, C., Liu, H., Tam, K., Ko, S., Kwan, F. and Lee, T.M.H. (2012), 'Sharp tipped plastic hollow microneedle array by microinjection moulding', *Journal of Micromechanics and Microengineering*, vol. **22**, pp. 015016.

Zahn, J., Trebotich, D. and Liepmann, D. (2000), 'Microfabricated microdialysis microneedles for continuous medical monitoring', *Proceedings of 1st Annual International Conference on Microtechnologies in Medicine and Biology*, pp. 375–380, October 12–14, 2000, Lyon, FRANCE.

Zahn, J., Trebotich, D., Liepmann, D., Trebotich, D. and Liepmann, D. (2005), 'Microdialysis microneedles for continuous medical monitoring', *Biomedical Microdevices*, vol. **7**, no. 1, pp. 59–69.

Zhang, P. and Jullien, G. (2003), 'Micromachined needles for microbiological sample and drug delivery system', *Proceedings of International Conference on MEMS, NANO and Smart Systems*, pp. 247–250, July 20–23, 2003 in Banff, Alberta–Canada.

Zhang, P. and Jullien, G. (2005), 'Microneedle arrays for drug delivery and fluid extraction', *Proceedings of International Conference on MEMS, NANO and Smart Systems*, pp. 392–395, October 12–14, Washington, DC, USA.

Zimmermann, S., Fienbork, D., Stoeber, B., Flounders, A. and Liepmann, D. (2003), A microneedle-based glucose monitor: fabricated on a wafer-level

using in-device enzyme immobilization, Transducers, Solid-State Sensors, Actuators and Microsystems, 12th International Conference on, vol. **1**, pp. 99–102.

Zosanopharma. (2009), 'Zosano's Macroflux.' Available online at: http://www.zosanopharma.com/, accessed 1 October 2009.

Zosanopharma. 'ZP Technology Platform.' Available online at: http://www.zosanopharma.com/index.php/20091103117/Research/Research-General/Technology-Platform.html, accessed 26 April 2012.

7

Microfluidic devices for drug discovery and analysis

J. S. KOCHHAR, S. Y. CHAN and P. S. ONG, National University of Singapore, Singapore, W. G. LEE, Kyung Hee University, Republic of Korea and L. KANG, National University of Singapore, Singapore

DOI: 10.1533/9780857097040.2.231

Abstract: Microdevices, since their inception in the last decade of the twentieth century, have changed our view of science, due to their potential applications in fields ranging from optics, semiconductors and the microelectronics industry to drug discovery and development, point-of-care clinical diagnostics, sensitive bioanalytical systems and other areas of the biological sphere. In this chapter we review the potential applications of microfluidic platforms for drug discovery applications comprising high-throughput screening in target selection, lead identification/optimization and preclinical testing. Application of microfluidics in chemical analysis, as well as analysis of metabolites in blood for studying pathology, is also discussed.

Key words: microfluidics, drug discovery, high-throughput screening, drug analysis, point-of-care diagnostics.

7.1 Introduction

The ascent of microfabrication research and development at the turn of the century has opened several avenues for the biomedical sector. Micron-scale chips, with micrometre dimension channels, can be used to manipulate fluid flow at the micron/submicron scale. The spatial control offered by this technology, known as 'microfluidics', has potential applications in handling, processing and analysis of fluids (Whitesides, 2006). The miniaturized scale of these devices requires lower sample volumes (in nanolitres) than conventional microplate assays (requiring hundreds of microlitres), hence making them economical alternatives. The minute dimensions of the devices offer shorter diffusion path lengths, allowing faster analysis and precise control of fluid flow, and leading to specificity in chemical microreactors. Design manipulation, easily achievable by conventional lithographical and novel

nanotechnology techniques, provides versatility in mixing fluids that can be controlled by external physical forces such as magnetic and electric fields. These microdevices may either be integrated into existing macrodevices, or constitute comprehensive analytical systems by themselves. The miniaturization provided by these high-throughput devices allows for a large number of replicates on a small chip, enabling massive parallelization and thereby increasing efficiency and lowering costs (Lombardi and Dittrich, 2010). The fluid flow properties at microscale are very different from those at macroscale, and this can be exploited using microfluidic devices (Beebe *et al.*, 2002). These advantages make them an ideal choice in disciplines spanning across molecular analysis, biodefence programmes, and the discovery and development of new drugs in the pharmaceutical and biotechnological industries.

Initially, the concept of microfluidics was applied to the field of analytical chemistry. Lithographic patterning/etching, used to produce chemical sensors and analytical techniques on glass/silicon substrates, provided proof of concept for their applicability (Harrison *et al.*, 1993; Manz *et al.*, 1990). Afterwards, chemical and biological sensors that could thwart the threats of bioterrorism, and aid in biodefence sample testing (Liszewski, 2003), were developed. With the surge in biotechnological methods, proteomics, genomics, and the discovery of protein-based therapeutics, microfluidics offers brighter prospects in DNA sequencing and genotyping as well as in protein separation and analysis (Chen *et al.*, 2010; Gomez, 2011). Microfluidic devices have also provided valuable opportunities for drug discovery and development processes, with their benefits at each stage from target identification (Malmstadt *et al.*, 2006) to lead identification/optimization (Jones *et al.*, 2005), and further to preclinical studies (Matsui *et al.*, 2006), clinical trials (Herr *et al.*, 2007), formulation development (Alsenz and Kansy, 2007) and the manufacturing stage (Szita *et al.*, 2005). Additionally, these devices have been used for improved confinement of cells in three-dimensional (3D) scaffolds, cell-based testing and cell component analysis. The cellular and molecular interactions at a scale proportional to their dimensions (Whitesides, 2003) are very different from those observed at macroscale volumes. An interesting application has been in the field of tissue engineering, whereby microfluidic platforms provide 3D scaffolds mimicking the natural environment for growth and mutual interaction between cells (Li *et al.*, 2012; Yamada *et al.*, 2012). They have also been investigated for transdermal and pulmonary delivery of drugs (Ashraf *et al.*, 2011; Yeo *et al.*, 2010), as well as for personalized diagnostic kits (Yager *et al.*, 2006).

In this chapter we will present an overview of the microfluidic devices that have been researched for drug discovery and drug analysis. First, we discuss the role played by microfluidics in the current paradigm for drug discovery, in identifying druggable targets, and in the progress achieved by high throughput screening (which has allowed thousands of molecules to be

screened on a chip), followed by optimizing few lead molecules and assessing their pharmacokinetic and pharmacodynamic properties in preclinical systems. Later, we discuss the application of microfluidic devices in chemical analysis.

7.2 Microfluidics for drug discovery

Discovering new therapeutics for a pathophysiological condition involves identifying a specific target (Kang *et al.*, 2008). With the help of computational biology and/or experimental methods, such targets can be identified. This is followed by validating the target by a series of complicated cell-based or animal experiments. Once validated, screening of drug libraries, produced by combinatorial chemistry, composed of millions (usually $>10^6$ compounds) of drug molecules to find a few lead molecules for clinical trials, is carried out. This is aimed at getting the safest, most reliable and efficacious pharmaceutical compound, which is then filed as a new drug application for approval by regulatory agents such as the United States Food and Drug Administration (FDA). The complex and lengthy procedure of discovering a suitable drug candidate is exemplified by the fact that it takes 10–15 years for a drug to go from bench to bedside, and it has been estimated to cost approximately 1 billion USD (Wu *et al.*, 2010). The attrition, from thousands of new chemical structures in the drug library, to a few lead compounds, to a single successful therapeutic agent, is a result of the inefficient procedures used in the conventional/current drug discovery and development process.

Progress in the use of microscale platforms aids the process of drug discovery through efficient and expeditious design of therapeutics and provision of information on biological targets (Lal and Arnsdorf, 2010). High-throughput microfluidic devices have shown considerable promise over the conventional methods, which required long processing times and expensive equipment, thereby delaying the whole drug discovery process. In the following sections, we describe the contribution of microfluidics to various segments of drug discovery.

7.2.1 Identification of druggable targets

The process of drug discovery begins with the identification of the function of a potential drug target and comprehending its role in the disease process. Discovering pharmacological activities was conventionally carried out by testing various substances (usually plant extracts) in living organisms to observe the changes caused in a particular phenotype. However, towards the end of the twentieth century, this process of phenotype-based target identification was largely replaced by a target-based approach. With progressive acquisition of knowledge in the field of molecular biology and

improvement in isolation techniques, identification of complex systems that are responsible for a drug's pharmacological response has evolved to be the new approach in identification of drug targets and it has reduced the use of living organisms and living tissues (Terstappen *et al*., 2007).

Drug targets, which may be a cellular receptor, an ion channel, nucleic acids, DNA or RNA, enzymes, polysaccharides and lipids, are chemically well-defined molecular structures capable of interacting with therapeutic drug moieties (Imming *et al*., 2006). This interaction leads to downstream clinical effects. Common drug targets belong to the classes of kinases, proteases, phosphatases and G protein coupled receptors. Ion channel proteins represent another attractive target in the drug discovery paradigm, as they have been implicated in several cardiovascular and neuronal disorders (Dunlop *et al*., 2008). Around 40% of targets in drug discovery belong to the class of ligand-gated ion channels (Yin *et al*., 2008).They act as the main targets for the currently available pharmaceutical agents, as well as majority of those agents in the drug development phase, and hence have been the focus of intense research resulting in dedicated conferences and numerous publications (Perrin *et al*., 2006; Zagnoni, 2012).

As most of these targets are a part of the cell membrane lipid bilayer structure, their functionality depends on the membrane integrity. The proteins may be denatured once dissociated from the membrane, and hence are required to be integrated into the membrane throughout the analytical procedure (Suzuki *et al*., 2004). Target validation employing isolated membrane proteins and ion channels offers many technological challenges, as reproducing these nano-scale systems is very complex (2007). However, incorporating these drug targets in artificially synthesized lipid bilayer membranes, and by specifically controlling the membrane architecture and surface characteristics, simulating the natural environment of a drug target is envisaged as an option for target identification (Zagnoni, 2012).

Microfluidic technology has played a key role in the fabrication of bilayer lipid membranes (BLM) (Mayer *et al*., 2003). Micron-sized BLMs with integrated membrane proteins and ion channels are advantageous over macro-systems, providing economical and time saving analysis platforms. These BLMs bear remarkable electric sealing, and hence are amenable to recording electrical signals across single membrane protein. On-chip planar bilayer structures were first introduced in 2004 by Suzuki *et al*. (2004). They fabricated a bilayer membrane chip using a silicon wafer having flow channels on both sides that are connected to apertures (Fig. 7.1a). Lipid solution and buffer, injected alternatively, resulted in the formation of the lipid bilayer. The proteins were incorporated in the bilayer using protein laden liposomes. Integrated microelectrodes could be used for determining the membrane potential, and thus could serve as a tool for ligand-binding

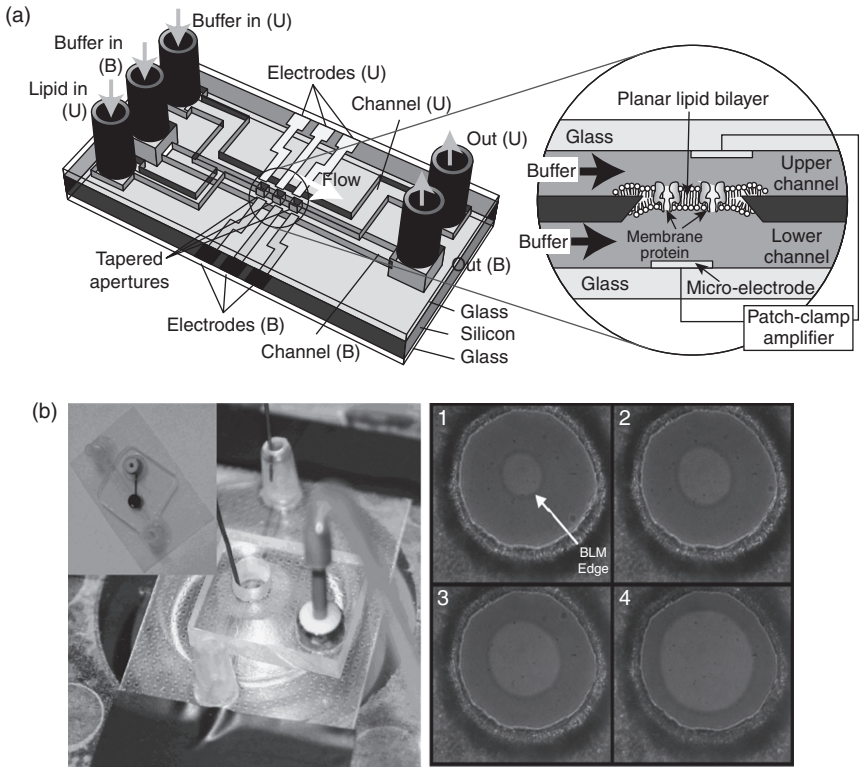

7.1 Formation of bilayer lipid membranes (BLM) on microfluidic chips. (a) Conceptual diagram of a membrane fluid chip having fluid channels and apertures. Alternate flow of lipid and buffer solutions leads to formation of BLMs. (Suzuki *et al.*, 2004). (b) A microfluidic device with a channel extending from a trench, where electrodes are inserted in both the upper well (containing lipid) and the lower channel (containing buffer). The bilayer is formed within an aperture upon exposure to air (left), the growth of which is monitored over 20 s (right). The setup was placed over a microscope to observe BLM formation that appeared as a bright region in the centre (Sandison *et al.*, 2007).

studies. However, silicon-based devices suffer from many disadvantages, including high dielectric loss of silicon leading to high electrical noise. Apart from that, the manufacture of silicon-based devices is time consuming, and the reproducibility of the BLMs is questionable. Other materials used for fabrication include epoxy photoresist (Cheng *et al.*, 2001), glass (Fertig *et al.*, 2002) and Teflon (Mayer *et al.*, 2003), but the resultant BLMs were fragile and unstable.

Polymeric microfluidic devices have the potential to overcome these drawbacks, offering advantages of economy and ease of fabrication. Poly (methyl methacrylate) (PMMA) has been seen as viable alternative, due

to its good optical and dielectric properties, low glass transition temperature, ease of processing, and ability to bond other materials, unlike Teflon (Sandison *et al*., 2007). Suzuki *et al*. modified their previous silicon-based design, to make a PMMA-based device providing a tapered aperture for lipid flow, and hence achieve a constant amount of lipid solution at the aperture. Further application of a static pressure to control film thickness yielded a more reproducible (90%) bilayer. With further optimization, embedding of four lipid bilayers on a single chip and gramicidin peptide, a monovalent cation channel, incorporated into the bilayer, was achieved (Suzuki *et al*., 2006). One of the unique advantages of this microfluidic device is that it facilitates easy microscopic observation of the bilayer (Suzuki *et al*., 2007). Sandison *et al*. created microfluidic channels on PMMA-coated glass substrates by using hot embossing and laser micromachining (Fig. 7.1b). PMMA surface was chemically treated to render it hydrophobic. Lower channel was filled with buffer, and lipid solution was applied to the upper well, which was later filled with the buffer. Lipid bilayers could be achieved by exposure of the top surface to air (Sandison *et al*., 2007).

Malmstadt *et al*. suggested that the air required in triphasic PMMA-based BLMs can be problematic, and automation is limited as continuous operator vigilance is needed during device fabrication. Also, an annulus was formed around the membrane due to the solvent, limiting the miniaturization capability (Malmstadt *et al*., 2006). They developed a novel method based on hydrophobic properties of poly (dimethylsiloxane) (PDMS). A non-aqueous solution of the lipid was suspended in an aqueous flow stream through a microfluidic channel in PDMS. Solvent, being hydrophobic, partitions into PDMS, shrinking the lipid membranes together and forming a bilayer (Fig. 7.2a). Ide and Ichikawa developed a microfluidic device based on successive stacking of a glass slide, plastic sheet, PDMS spacer and agarose-coated coverslip (Fig. 7.2b). Lipid solution is first applied to the plastic aperture and sucked by vacuum to form a thin layer over the coverslip. Electrolyte was then added to the well and the aperture was moved towards the coverslip, compressing the spacer. Before applying a thin layer of lipid, excess electrolyte was removed. Another layer of electrolyte was applied over this and excess lipid drained by the means of lateral diffusion, leaving behind central lipid bilayer. The area of the bilayer could be controlled by modulating the aperture movement (Ide and Ichikawa, 2005). This method offers the advantage of specific control of bilayer thickness due to application of vacuum and provision for aperture adjustment.

Kreier *et al*. developed a solvent-free method for creating lipid bilayers, using giant unilamellar vesicles that were made to burst by suction through a micron-sized glass orifice. Ion channel proteins were integrated in the bilayer by incubation of giant unilamellar vesicles to obtain proteoliposomes in a simpler and less time consuming manner than with previous

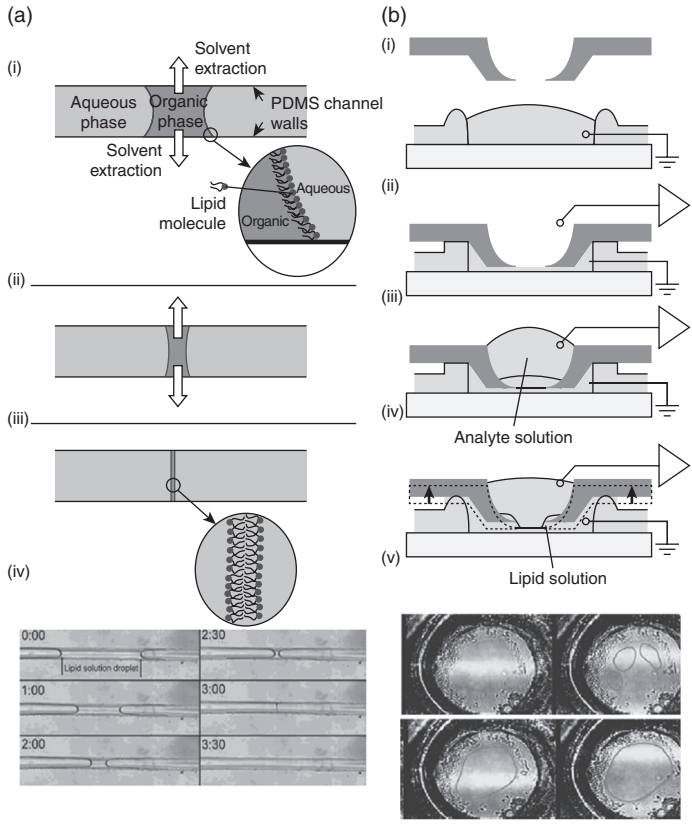

7.2 Formation of bilayer lipid membranes (BLM). (a) By microfluidic solvent extraction, (i) droplet of organic solvent with dissolved lipid is formed in an aqueous stream of fluid. Lipids are organized on the hydrophobic–hydrophilic interface (inset). (ii) As solvent enters the PDMS, the two interfaces approach one another. (iii) Finally, only the lipid layers are left behind, forming a bilayer membrane. (iv) Images showing solvent extraction from a lipid solution droplet in a microfluidic channel, over a period of time (minutes:seconds), the BLM, although not visible in the last image, was formed and confirmed by electrical measurements (Malmstadt *et al.*, 2006). (b) By microfluidic bilayer chamber method, (i) A drop of electrolyte was applied to the well of spacer. (ii) A plastic sheet was placed on the spacer and moved downward until the aperture hit the bottom. Then excess electrolyte was removed with a pipette. (iii) Small amount of lipid solution and a sample solution were added sequentially. Alternatively, lipid solution was sprayed through a fine pipette to the edge of the aperture with bubbling without removing the electrolyte in (ii). (iv) After formation of a thick membrane across the aperture, the plastic sheet was moved upwards. The membrane expanded, reached the agarose layer and thinned to form a bilayer. (v) Successive bright-field images of BLM formation (Ide and Ichikawa, 2005).

techniques. Typical gating phenomena were observed by changes in pH and membrane voltage in the outer membrane protein OmpF obtained from *Escherichia coli* (Kreir *et al*., 2008). Chip-based bilayers have been used for bacterial toxin binding studies. Using total internal reflection fluorescence microscopy, cholera toxin B subunit and tetanus toxin C fragment could be detected as low as 100 pM (Moran-Mirabal *et al*., 2005). It was suggested that this method is adaptable for proteins and nucleic acids as well.

These techniques to fabricate BLMs *in vitro* provide a good platform to identify ion channel proteins as drug targets. Also, once identified, these targets can then be used to screen new therapeutic agents and identify lead compounds for preclinical studies. They can also be used for determination of membrane properties under non-physiological conditions and gain access to ion channels in intracellular membranes (Kreir *et al*., 2008).

Cellular receptors and the downstream signal transduction pathways are being increasingly recognized to play a critical role in drug action and astounding progress has been made in characterizing their behaviour. Signal transduction has also been enormously researched with many companies having dedicated programmes for signal transduction based drug discovery (Anonymous, 2000). Enzymes such as tyrosine kinase play an important role in phosphorylating proteins, forming the essential links in signal transduction pathways (Wang *et al*., 2008). Wang *et al*. recently developed a novel microfluidic device combining the function of electroporation and flow cytometry to measure the translocation of fluorescently tagged tyrosine kinase to the cell membrane, at a single cell level. It was demonstrated that cells stimulated through antigen receptor retained more kinase than their non-stimulated counterparts. These results could have a marked impact on target-based drug discovery, as kinases are frequently involved in common diseases such as cancer (Wang *et al*., 2008).

Analysis of protein molecules from a single cell has been envisaged as a potential tool to identify specific targets. Recently, single cell analysis has gained considerable importance in microfluidics-based drug discovery, as these devices are able to perform manipulation, lysis, labelling, separation and quantification of the protein contents in a single cell (Huang *et al*., 2007). Although this technique is not amenable to live cell monitoring, it provides for simultaneous detection of multiple targets, combining higher sensitivity with higher throughput. Using a single cell analysis chip, the number of β_2 adrenergic receptors was determined. The integrated microfluidic chip facilitated cell and chemical handling, cell lysis, electrophoretic separation, and detection of lysate using laser-induced fluorescence (Gao *et al*., 2004; Wu *et al*., 2004). Separation of proteins and peptides has also been achieved on miniaturized electrophoretic cells (Schulze and Belder, 2012; Sikanen *et al*., 2012). Some of these techniques have been dealt with in greater detail in the subsequent section on analysis.

Understanding of the interactions between receptors and their ligands provide insightful information on disease progression, and exploration of such drug–receptor pairs provides us an opportunity to discover drugs selectively targeting a particular receptor (Goldberg *et al*., 2009). Modulation of physiological events, such as cell differentiation and death, release of neurotransmitters and hormones, is a result of activation/suppression of signal transduction pathways, which are often coupled to cellular receptors. This activation/suppression is in turn due to binding of specific ligands to these receptors. Much of the research work in discovering new receptor ligands has been focused on binding studies of low molecular weight molecules to macromolecular receptors, followed by screening of biochemical changes. However, it has been reported that lack of a particular biochemical event does not necessarily translate into lack of receptor activation. Other cellular components and events, such as second messengers, downstream processes, gene transcription and change in receptor configuration, have to be looked into. This, however, is not possible with the conventional assay procedures (Gurwitz and Haring, 2003). High-throughput ligand-binding assays provide a suitable alternative to perform multiple tasks on a small chip. Moreover, the discovery of many new 'orphan' receptors, for which no ligands are currently known, offers a promising avenue for drug discovery.

Microfluidic devices are beneficial for ligand-binding studies, as they reduce interaction times, enhance sensitivity and throughput (Kang *et al*., 2008), and aid in separation of complexed and uncomplexed molecules (Bange *et al*., 2005). For these binding studies, receptor or ligand molecules can be immobilized on a PDMS substrate by adsorption (Makamba *et al*., 2005), or covalent bonding (Sui *et al*., 2006), or by microcontact printing as achieved for solution hybridized oligonucleotides (Razumovitch *et al*., 2009). These binding interactions are usually quantified by the measurement of equilibrium dissociation constant (K_d) of the ligand–receptor complex.

Goldberg *et al*. demonstrated the interaction of glycopeptide antibiotics, teicoplanin and vancomycin, immobilized on a PDMS microchannel with 5-carboxyfluorescein-D-Ala-D-Ala-D-Ala (5-FAM-$(DA)_3$). The K_d was reported to be similar to previously reported values as measured by commercial systems, even though it utilized a smaller amount of reagents (Goldberg *et al*., 2009). Centrifugal microfluidic platforms, which are disc-shaped microfluidic devices, have also been developed whereby the fluid flows by simple rotation of the disc. Interaction between phenothiazine antidepressants and calmodulin, attached to a green fluorescent protein, was studied. Drug binding affected the fluorescence properties, and hence concentration of the drug bound to the protein receptor could be determined (Puckett *et al*., 2004). The BLMs described earlier have been used extensively for ligand-binding studies over the past two decades. Recently, phospholipid bilayers were patterned with bovine serum albumin by lithography.

Following repeated cycles of patterning, ganglioside GM1 was coated along the microfluidic channels in different concentrations, and its interaction with varying concentrations of cholera toxin B was studied (Shi *et al*., 2008). Javanmard *et al*. demonstrated a novel method of coupling a microfluidic device with shear force spectroscopy to study the interaction between protein molecules and DNA base pairs. The method could be used to measure the affinity of bonding between the interacting molecules by measuring the drag force required to detach the ligand bound to the microfluidic channel when the receptor attached to the surface of microbeads is pressure driven through these channels (Javanmard *et al*., 2010).

7.2.2 Hit identification and lead optimization

After the identification of a particular druggable target, the next step in the drug discovery process is to identify a 'hit', which involves the phases of hit identification (HI), lead identification (LI), and lead optimization (LO). A 'hit' is a particular chemical or biological moiety that binds to a specific target which has been implicated in an ailment. Screening and optimization of millions of 'hits' results in several 'lead' compounds. This whole multiphase process, in which 'leads' are optimized by an initial screening involving multiple 'hits', is described as a 'hit-to-lead' process (Goodnow, 2006). Synthesizing and screening the right drugs which can potentially be used, carried forward through a drug development programme, and enter a clinic, starts from correct identification of hits and leads. These steps are imperative, since drug discovery is an expensive process. An error at this stage may lead to an expensive failure at a later stage.

Drug candidates may either be derived from combinatorial libraries or be of natural origin. Drug libraries have been estimated to be in the order of 10^{63} (Bohacek *et al*., 1996). Microfluidic chip-based combinatorial chemistry and high-throughput screening, together aim to result in a paradigm shift, leading to the development of methods of sequential synthesis and testing of thousands of compounds in parallel (Knight, 2000).

Synthesis of drug libraries

Recognition of drug targets has kept pace with the fast progress in genomic and proteomic tools. Pharmaceutical companies on the other hand are facing challenges to generate drug compounds at the fastest possible rate, in an inexpensive manner. Synthesis of drug libraries has been described as the biggest impediment in the drug discovery process (Jones *et al*., 2005). Improved methods in combinatorial chemistry have resulted in rapid synthesis of large number of chemical compounds, and have produced enormous drug libraries. This has been further accelerated by the improvement

in the design of the microfluidic reactors. These microfluidic reactors can be classified into three types, based on the flow pattern, namely (i) flow-through type, (ii) droplet or slug type, and (iii) batch type. The most common flow-through type enables multiple reagents to be maintained at a temperature, and be pressure driven through the channels. These reactors have been used widely in extraction procedures as well as in multiple chemical syntheses (Keng *et al*., 2012).

Parallel combinatorial synthesis in multiple microfluidic reactors has also been demonstrated utilizing the continuous flow of reagents in microfluidic channels. A multiple microfluidic reactor assembly was fabricated to synthesize carbamates in a multistep procedure (Sahoo *et al*., 2007). However, this method sacrifices the advantages of an integrated system for several reactions to be carried out on a single chip. Researchers then looked to fabricate a consolidated device with multiple layers of parallel chips. A multilayer glass chip was developed for a 2×2 series synthesis in parallel (Kikutani *et al*., 2002). The complexity and expense of fabrication of this multi-layered device was a concern. Recently, Dexter and Parker exhibited parallel combinatorial synthesis of compounds on a single-layered microfluidic chip (Fig. 7.3a). They fabricated a single layer PDMS chip for synthesizing a 2×2 series of amide formation products (Dexter and Parker, 2009).

However, continuous flow reactors are not suitable for multistep reactions, especially those involving sequential synthesis. A modified technique, termed batch microfluidics, in which specific microvalves control the delivery of reagents in batches, has been developed. These isolated batches can be delivered to the microfluidic reactor chamber at specific time points in a reaction cycle, exercising greater control over the reaction (Lee *et al*., 2005). A fluoride radiolabelled imaging probe, in nano/microgram scale, was synthesized in five sequential processes involving fluoride concentration, water evaporation, radiofluorination, solvent exchange, and hydrolytic deprotection (Fig. 7.3b).

A newer technology, known as droplet microfluidics, has recently come to the fore. It is based on compartmentalization of each assay in a small droplet, usually in the range of 1 pL–10 nL, surrounded by an immiscible oil, which can be manipulated and processed in a high-throughput manner (Brouzes, 2012). Each of these droplets can act as a tiny microfluidic reactor, notably reducing the reagent volumes required. A mesh-grid design microwell array was fabricated by Um *et al*., which allows for continuous addition and trapping of picolitre single cell droplets in the microwells (Fig. 7.3c). Due to miniaturization, the device provides high-throughput screening of the droplets (Um *et al*., 2012), but multistep reactions using these devices are still a big challenge.

In addition, these microfluidic reactors have also been used for synthesis of biological molecules, such as DNA. Short synthetic oligonucleotides

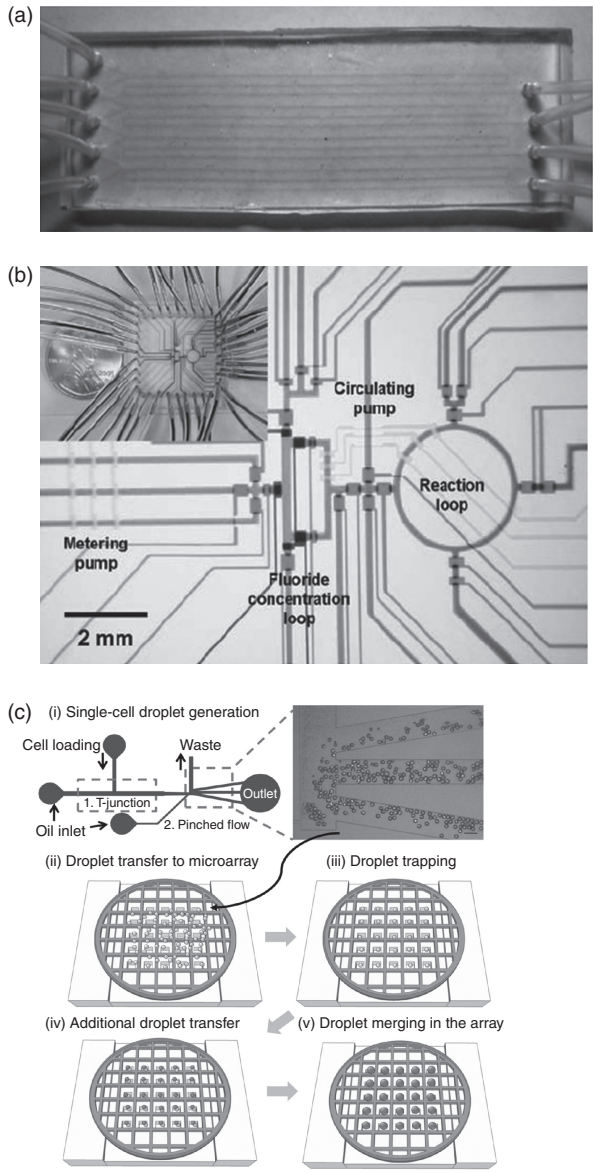

7.3 Different types of microfluidic reactors. (a) A continuous PDMS-based microfluidic flow reactor for 2 × 2 parallel combinatorial synthesis. The tubing has been inserted at each inlet and outlet port (Dexter and Parker, 2009). (b) Optical micrograph of a batch type microfluidic reactor with actual dimension (inset) (Lee *et al.*, 2005). (c) Schematic of a microdroplet manipulator, including functions for (i) droplet generation, (ii) transfer of droplets to a microwell array, (iii) migration of droplets into the wells, (iv) trapping of second droplets and (v) oil change to induce droplet merging (Um *et al.*, 2012).

were joined under thermal cycling in a microfluidic picoArray device to form DNA constructs up to 10 kb instantaneously. The fabricated DNA construct was shown to express relevant proteins and may be used for cell free protein expression on a large scale (Zhou *et al*., 2004). Mei *et al*. developed a microfluidic array device for synthesis of chloramphenicol acetyl-transferase and luciferase, and reported the yield to be 13–22 times higher than that achieved in microcentrifuge tube, with a 5–10 times longer lasting protein expression. The device is composed of an array of units that allowed for fabrication of different proteins, protein expression and nutrient supply. The device is also capable of synthesis and analysis of proteins on a single chip, potentially eliminating the need to harvest proteins, thereby reducing wastage and increasing process efficiency (Mei *et al*., 2007). A droplet-based microfluidic method was recently developed for on-chip protein synthesis. Production of a water-in-oil-in-water (W/O/W) emulsion was accomplished by formation of a water-in-oil emulsion on a poly (methyl methacrylate) chip, up first, followed by complete emulsion formation on a PDMS/glass microchip. Synthesis and expression of a green fluorescent protein from a DNA template was successfully demonstrated using a microfluidic platform (Wu *et al*., 2011).

Most of the devices developed use PDMS as the substrate material due to its excellent optical properties as well as its mouldability. However, PDMS is incompatible with many organic solvents and adsorbs many hydrophobic compounds due to its surface properties. Keng *et al*. fabricated a microfluidic platform that is operated by electrowetting-on-dielectric (EWOD). The device was made from inorganic materials coated with perfluoropolymer, and offers flexibility in use with organic and hydrophobic reagents (Keng *et al*., 2012). The device was shown to be suitable for diverse chemical reactions with minimal consumption of reagents, with suitability for multistep procedures requiring several solvent exchange rounds.

These devices have been put to efficient use to generate drug libraries, which provide a powerful source that needs to be screened to explore new drugs. To screen these large combinatorial libraries of compounds, the pharmaceutical industry has looked at high-throughput screening (HTS) methodologies over the past two decades. Conventional screening methods were able to screen 5000–20 000 compounds over a few years, resulting in inefficient screening of only 2–20% of the compounds on the whole library. However, HTS, or newly termed ultra-high throughput screening (uHTS), methodologies aim to screen 10 000–100 000 compounds over a period of 24 h, resulting in generation of 2–18 million screening results per year (Beggs, 2001). This logarithmic increase in screening capability has given a boost to the hit-to-lead discovery process.

High-throughput screening

Traditionally, high density microplates including 96, 384, 1536 and those with >1536 wells have been used extensively for HTS (Battersby and Trau, 2002; Brandish *et al*., 2006). However, liquid handling on a microlitre scale in these microplates was found to be difficult due to their inability to be integrated with robotic liquid handling technologies as well as suitable detection platforms. Microfluidic platforms can further miniaturize the HTS platforms, lowering the assay volume required. Also, these platforms can be easily modelled for convenient liquid handling and integrated with analytical devices. Microfluidic HTS platforms for confining reagents have been studied in both serial and parallel configurations. Using the serial method, compounds are screened successively with only one detector unit. However, in this approach, the throughput is largely dependent on flow rate and concentration of the sample, as well as acquisition speed of the detector. In contrast, parallel screening offers faster analysis, segregating multiple samples into miniaturized compartments of a high density microplate, and analysing by a single detector. Parallel analysis is, however, limited by the miniaturization capacity and hence the extent of parallelization (Thorsen, 2004). Nevertheless, both methods have been extensively used in microfluidic HTS.

Microfluidic microwell arrays are versatile tools for cell culture and high-throughput experimentation through cell-based assays, particularly important in drug screening and offering a potential alternative to animal-based testing. Nearly 50% of all drug discovery processes rely on cell-based assays (Fox *et al*., 2006). Seeding many cell types on a single chip offers the advantages of testing the effect of drugs on different cells types. It also offers the potential of testing many compounds on a single cell type in high throughput. A multiwell microelectrode array was fabricated using PDMS by conventional soft lithographic process. The array was then coated with a cell-adhesive layer of poly-D-lysine followed by patterning a non-conducting agarose gel layer to isolate the individual neuronal micro-circuits and record individual action potentials of drugs such as bicuculline and *N*-methyl-D-aspartic acid (Kang *et al*., 2009) (Fig. 7.4a). Chen *et al*. developed a complementary microwell and microcolumn system for screening of drugs (Fig. 7.4b). They used microelectro-mechanical systems (MEMS) to first fabricate a microwell array on a glass substrate to culture the cells. Employing a similar process, they fabricated complementary microcolumns that would carry the drugs to be topically applied onto the cells. The system was found to be suitable for delivering high-throughput identification of epidermal growth factor receptor inhibitors (Chen *et al*., 2011c). An integrated multilayer microdevice incorporating a drug/medium concentration gradient generator, flow controlling microvalves, and microchambers for

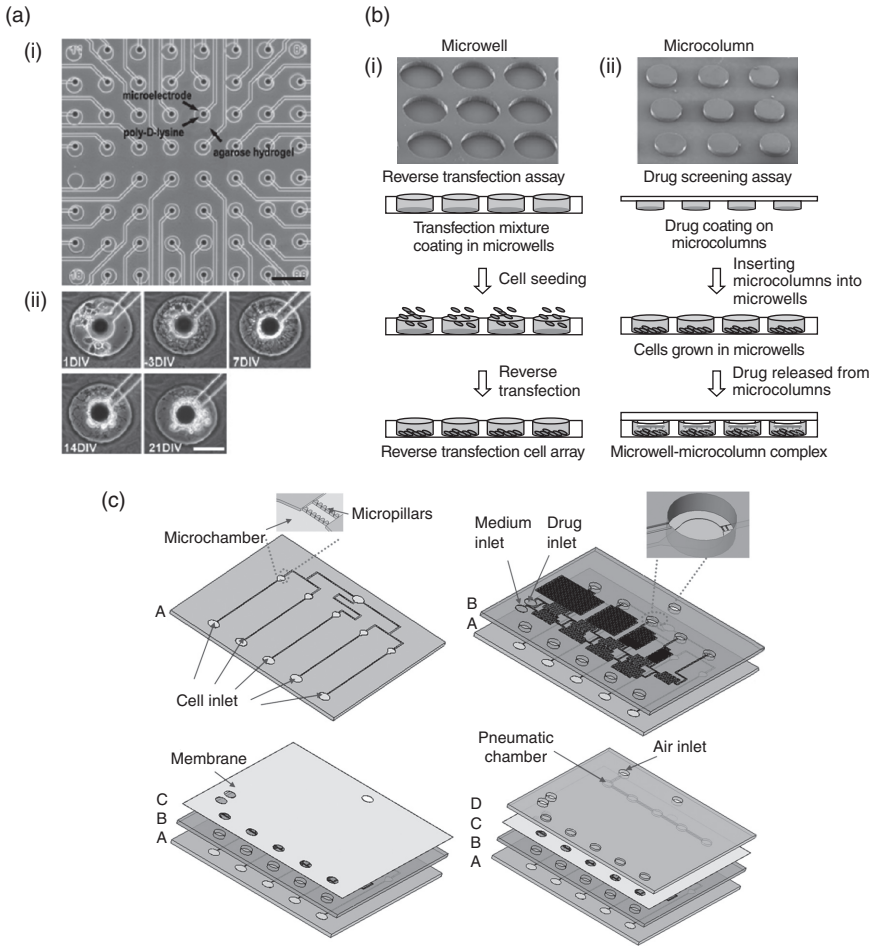

7.4 Microfluidic microarrays for cell based high-throughput screening. (a) A multiwell microelectrode array, (i) phase contrast image of agarose microwells on a micro-electrode array. Each microwell is composed of a microelectrode, poly-D-lysine coated surface, and agarose hydrogel wall, scale – 200 μm. (ii) The growth of neuronal conduits in microwells over a period of 3 weeks, scale – 50 μm (DIV – days *in vitro*) (Kang *et al.*, 2009). (b) Schematic illustration of the microwell and microcolumn cell based assays, (i) workflow for reverse transcription, and (ii) drug screening assay (Chen *et al.*, 2011b). (c) Schematic of a multilayered microfluidic device for drug screening. Layer A consists of pear shaped microchambers for cell culture. The microchambers were surrounded by micropillars to confine the cells inside. Layer B was used to generate concentrations of drug solutions. Layer C was made of PDMS and had microvalves for controlling the drug/medium volume dispensed below. Layer D had an air inlet for distribution of air to pneumatic chambers (Liu *et al.*, 2012).

cell culture was recently fabricated by Liu *et al*. for testing the apoptosis behaviour in a cisplatin-resistant cancer cell line (Liu *et al*., 2012). A vertical perfusion mode was adopted in this device, as shear stress due to horizontal fluid flow can adversely impact the cells. Using the set-up, sequential loading of cells, medium, drugs and air was achieved in successive layers of the device (Fig. 7.4c).

Despite a lot of progress in developing microscale arrays for cell culture, cell seeding in these arrays is a challenge. Kang *et al*. addressed this issue by developing a simple wiping method to seed cells in microwells (Fig. 7.5). A coverslip was used to slowly wipe the cells suspended in the growth medium across the surface of the microwell array. Cell concentration, microwell geometry and wiping speed controlled the cell seeding density (Kang *et al*., 2010). They also developed an algorithm and software for automatic counting of cells in a microwell array. The software, named Arraycount, detects the cell count from the fluorescent cell images in high throughput. The results were in close correlation with cell counts from the manual methods (Kachouie *et al*., 2009).

Studying single cell characteristics offers an advantage over observing the behaviour of a group of cells, as single cell characteristics might be hugely different from the entire population of cells. Microwell arrays have been developed to confine single cells, for observation of these and their progeny over a period of time. One of the first studies pertaining to single cell confinement in microwell arrays for drug screening was reported by Rettig and Folch (2005). PDMS microwells were fabricated by conventional soft lithography, and controlled seeding of single cells into microwells could be achieved by optimizing the geometry of the microwells. It was observed that microwells with an aspect ratio (diameter: depth) close to 1 had more than 85% wells with single cell occupancy for both adherent and non-adherent cells (Rettig and Folch, 2005). An interesting round bottom microwell array was recently developed by Liu *et al*. by creating PDMS microwell arrays by reverse moulding using polystyrene microspheres melted on a glass substrate (Liu *et al*., 2010). The size of these microwells could be tuned to 10–20 μm, which is difficult to achieve with conventional soft lithography. The PDMS microwells were then used to confine single cells by pouring excess cell suspension over the microwells, which allowed the cells to settle in. The enzymatic activity of the cells was studied by carrying out the carboxylesterase assay using calcein AM. Fluorescence intensities from single cells could be captured to reveal different kinetic behaviour of entrapped cells, which was related to cell viability (Fig. 7.6). Another novel way of constraining single cells in microwells was demonstrated by Wang *et al*. (2012). The flexibility of PDMS was exploited by stretching the patterned PDMS array using a tube that delivered the cells onto the array. After loading, the tube was withdrawn and cells settled in the microwells, which were then

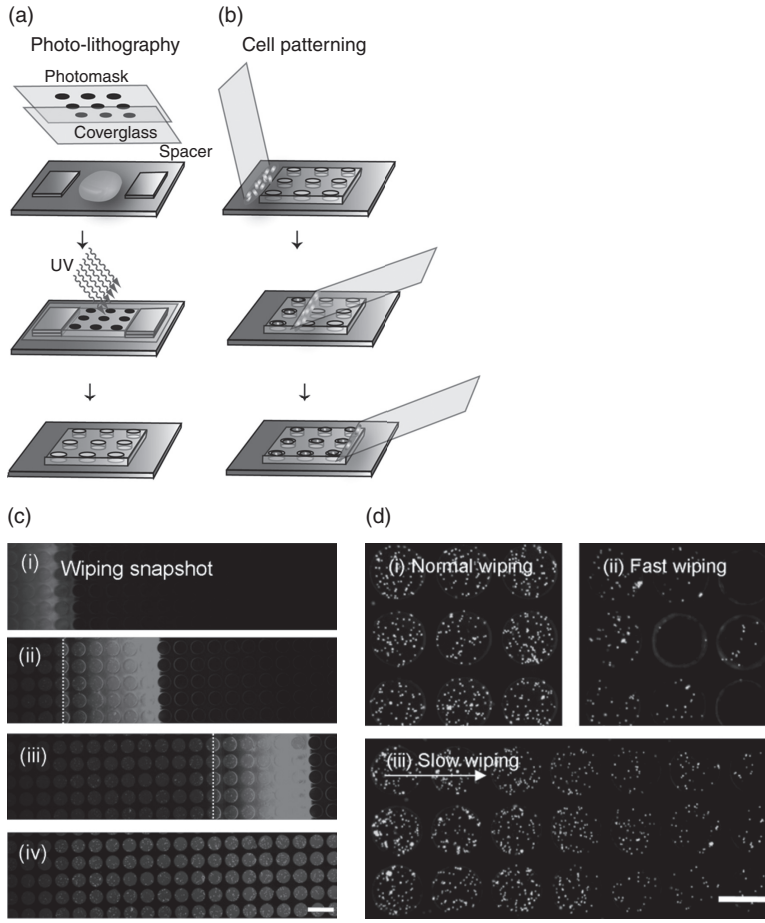

7.5 Microwell fabrication by photolithography and cell confinement using wiping method. (a) Photolithography: Poly(ethylene glycol) diacrylate was patterned into microwells using a photomask. (b) Cell patterning; a drop of cell solution was pipetted onto a thin glass slide and placed in contact at an obtuse angle with the microwell slide adjacent to the array. The cover glass was rotated to an angle of 45° and moved across the array, spreading the cell solution into the microwells and removing excess solution from the surface. This process localized cells and isolated liquid in the microwells. (c) (i)–(iv) shows the time lapse images of wiping a wedge of rhodamine/cell solution, leaving behind cells in the microwells with no excess liquid on array surface. The dotted line indicates the actual contact of the glass slide on the array surface. (d) (i)–(iii) Effect of wiping speed on cell distribution in microwells, where fast (>10 mm/s) and slow (<0.1 mm/s) wiping resulted in non-uniform distribution of cells, while normal (1.0 mm/s) resulted in uniform distribution (Scale – 400 μm) (Kang *et al.*, 2010).

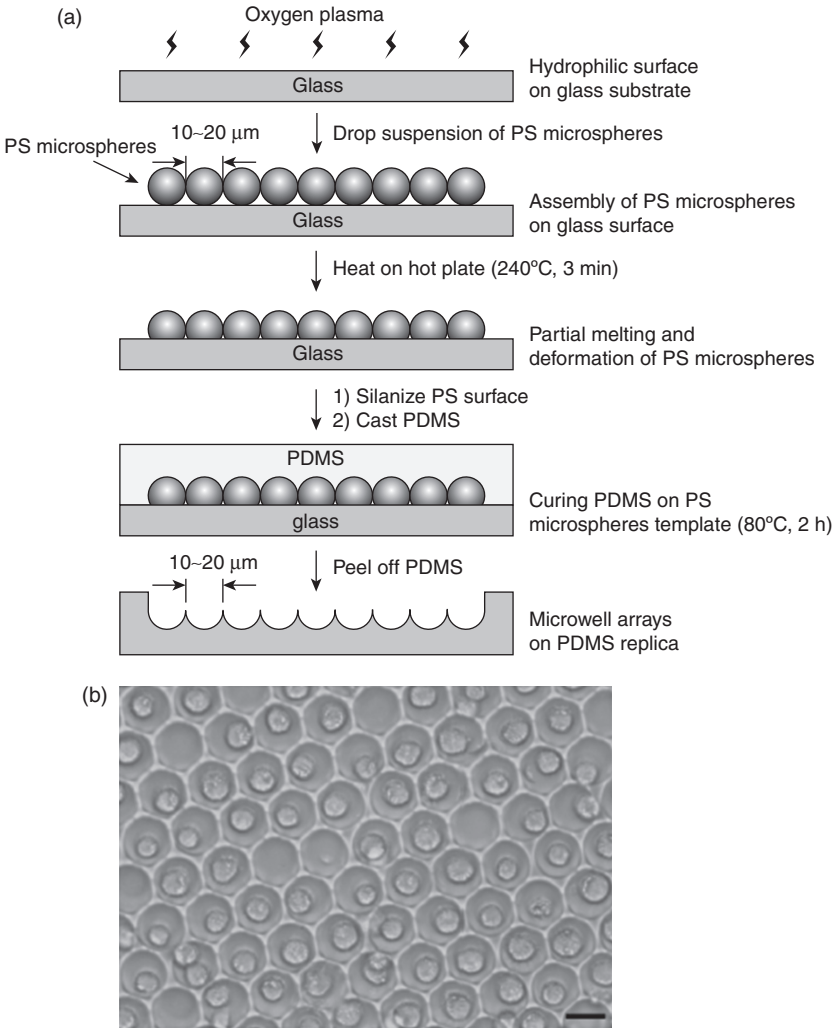

7.6 Microwell arrays for single cell analysis. (a) Fabrication of PDMS-based microwell arrays using polystyrene microbeads, and (b) micrograph image of Ramos cells in each microwell (Scale 20 μm) (Liu *et al.,* 2010).

amenable to further analytical treatment. They also demonstrated that cells within the microwells could be isolated by deforming the PDMS substrate using a microneedle (Wang *et al.*, 2012). A further example was illustrated by Lew and co-workers, who devised a plastic microwell array by using economical materials such as shrink wrap film and tape. A carbon dioxide laser was used to cut holes in the tape, which acted as a mask to etch wells in the shrink wrap by oxygen plasma (Lew *et al.*, 2011).

Apart from multiwell arrays, multiplexed screening platforms have also been developed to screen multiple samples in one run. The ability to analyse multiple proteins, nucleic acids as well as small molecules, reduces assay time, reagent volume and cost. Multiplexed measurements provide the ability to increase the throughput without a simultaneous increase in the density of the microfluidic array. Multiplexing technology has been applied to two different types of microfluidic platforms: planar arrays and suspension (particle based) arrays. For protein and DNA analysis, planar arrays have been used, whereby protein molecules have been patterned as microarrays onto substrates using lithography (MacBeath and Schreiber, 2000). Such systems offer application specific advantages, ranging from study of protein–protein interactions to establishing proteins as targets for small molecules and specific functions of enzymes. Suspension arrays, on the other hand, offer the advantages of studying the properties of compounds in solution, thereby providing ease of sample modification, higher throughput and increased batch-to-batch uniformity (Nolan and Sklar, 2002).

A multiplexed system could be used to screen a compound against multiple kinases, or study protein–protein interaction and detect changes in enzyme conformation (Xue *et al*., 2001). In this report, four kinases were screened against a substrate. The reaction products/substrates could be separated by electrophoretic separation on a chip and analysed. Multiplexed screening of picolitre-sized droplets that could be manipulated using an array of electrodes has also been reported. For example, caspase-3, a marker of apoptosis, which is an important tool in cancer drug discovery, was measured after human cervical adenocarcinoma HeLa cells were treated with different concentrations of staurosporine. The technique termed as digital microfluidics was compared with conventional techniques involving 96-well plate. It resulted in a 33-fold reduction in sample volume together with a lower detection limit for caspase-3 analysis compared with conventional techniques. This can be attributed to the lack of delamination in apoptotic cells in the digital microfluidics platform that uses the droplet manipulation system instead of pipetting or aspiration of liquids with conventional techniques (Bogojevic *et al*., 2012).

Analysing multiple samples by multiplexing, however, poses a challenge in sample recognition. Hence, it is necessary to have an encoding scheme integrated into the system to allow for rapid and precise analyte identification. Encoding schemes based on spectrometric (Han *et al*., 2001), graphical (Evans *et al*., 2003), electronic (Service, 1995) and physical techniques (Vaino and Janda, 2000) have been developed. An exhaustive review of various encoding techniques has been published by Braeckmans *et al*. (2002). Spectrometric techniques utilize specific wavelengths to analyse a

compound. In contrast, graphical methods use certain optical elements that are chemically patterned onto the microarray. These techniques require much sophistication, and are expensive and may require a considerable amount of time for fabrication and integration.

Pregibon *et al.* recently developed a novel encoding scheme for multiplexed platforms (Pregibon *et al.*, 2007). In this system, two poly(ethylene glycol)-based monomer solutions, one being a fluorescent dye and the other being an acrylated probe, were made to flow through microfluidic channels. The solutions during flow were exposed to ultraviolet light using conventional techniques of continuous flow lithography to develop a patterned particle (Pregibon *et al.*, 2007). The morphological properties of the particles were determined by a photomask, inserted into a fluorescence microscope (Pregibon *et al.*, 2007). A simple dot coding scheme was used on the photomask that could generate over two million particles, with each having a unique code. Although the particle size achieved in this method was larger than in previous methods, the authors demonstrated that the sample volume required was manageable, together with providing higher sensitivity and reproducibility. The system was able to detect DNA at very low concentrations, without signal amplification, proving it to be a completely integrated encoding device, with advantages of low cost, high efficiency with virtually unlimited number of codes possible, and all this achievable with the services of a simple fluorescence microscope.

Inkjet printing technology has been purported as a highly efficient screening alternative, providing efficiencies greater than 200 000 compounds per day, currently achievable with the microfluidic platforms described earlier. The technology offers capabilities to simultaneously deposit cells and drugs to be tested in a small picolitre volume. Post-processing, the cell characteristics can be studied to evaluate the drug effects. Such a novel platform was developed by Rodríguez-Dévora *et al.* (2012). They developed an inkjet printer-based method to pattern green fluorescent protein expressing *Escherichia coli* cells grown on a soy agar medium, on a coverslip. Live/Dead™ assay, used to assess bacterial cell viability, demonstrated high rate of cell survival after imprinting. Fast screening utilizing low volumes to assess the effect of three antibiotics patterned together with the bacterial cells could be carried out. This bioprinting approach was compared to the standard micro-pipetting approach and was found to yield similar results at much lower volumes (Rodríguez-Dévora *et al.*, 2012).

These microfluidic platforms have significantly enhanced the profile of HTS, leading to optimization of hits and leads, before the leads are put through preclinical testing for evaluation of their preliminary pharmacokinetic and toxicological properties.

7.2.3 Preclinical evaluation

Interaction with the molecular targets begins the journey of the drug in the human body. When a drug is administered, it has to be absorbed across mucous membranes, followed by its distribution to its target site and metabolism to an inactive metabolite to be eliminated from the body. It should also be devoid of any toxic effects. These characteristics, respectively known as absorption, distribution, metabolism, elimination and toxicology (ADMET) are essential factors in determining the path of the drug in the later stages of the drug discovery process. A fine balance between these pharmacokinetic characteristics is needed for the development of a drug from a chemical entity (Muster *et al*., 2008). Unsatisfactory ADMET profiles account for attrition of 50–60% drug candidates at the preclinical development stage (Smith, 2007), with lack of efficacy and undesirable toxicity being the major causes (Kramer *et al*., 2007). It has been reported that the lack of efficacy accounts for 30% of failures of new drug entities and toxicity further accounts for another 30%. If these are detected at later stages in the drug development process, the overall cost of the programme will be increased, as cost escalates with each stage (Kola and Landis, 2004). This is why pharmaceutical companies are nowadays adopting the '*fail early; fail cheap*' approach to identifying the toxicological properties of drug compounds. This is done in lieu of savings in the event that toxicological properties are identified at a much later stage or even after the launch of the product, necessitating an inevitable and highly expensive market recall. It has been reported that market recalls, as a percentage of approvals, in the United States has fallen from 27.2% in 1980s to 5.2% in 2000s (Qureshi *et al*., 2011). This has, in part, been the contribution of more novel and efficient toxicity screening platforms that have been developed in the past two decades. It also underlines the importance of proficient preclinical programmes, and the role played by them in drug development.

In vitro toxicological testing in cell models provides useful information about the drug candidates, much before the expensive animal experiments and first-in-human clinical trials are conducted. *In vitro* experiments have been long touted to replace animal testing, especially due to the ethical concerns surrounding animal experimentation (Wen *et al*., 2012). Moreover, *in vitro* toxicity in excised animal organs may not be extrapolated to correctly reflect human toxicities. On the other hand, *in vivo* preclinical testing in live animals requires a large amount of compound under investigation, which is usually available in limited quantities and may be prohibitively expensive (Muster *et al*., 2008).

In vitro *evaluation*

Three-dimensional (3D) cell culture mimics the natural environment of the cells, including cell–cell and cell–extracellular matrix interactions, as opposed to planar two-dimensional (2D) cultures that are used to maintain cells (Pampaloni *et al*., 2007). An excellent collation of advantages of 3D cell culture over the 2D format has been provided by Zhang and van Noort (2011). Also, these 3D cultures offer an *ex vivo* alternative to live animal testing, and potentially reduce the cost of toxicity screening during drug development. Nonetheless, 3D cell cultures present a few shortcomings, especially with sample handling and imaging. Since these cultures are thicker than conventional 'petri-dish' cultures, they are difficult to adapt to conventional microscopic techniques. Liquid handling in patterned microstructures requires sophisticated micro/nanolitre scale devices. However, the advantages of studying the cells in an environment outweigh the technological shortcomings, which, too, are being addressed simultaneously.

As hepatotoxicity has been the leading cause of failure at the clinical trial stages and post launch market withdrawals, many researchers have looked at developing *in vitro* cell-based hepatotoxicity assays. It is important to notice here that most of these agents went through preclinical animal testing and were assumed to be safe (Kaplowitz, 2005). Microfluidic 3D cell culture platforms aim to address this problem, and have been designed to provide deeper insights into cell behaviour when exposed to cytotoxic agents. A multiwell 3D cell culture platform was designed using soft lithography to co-culture primary hepatocytes with mouse 3T3-J2 fibroblasts (Fig. 7.7a). A PDMS stencil containing through-holes in a 24-well format was first applied to a polystyrene plate, followed by application of collagen-I through the holes. After removal of the PDMS stencil and application of a 24-well PDMS blank, hepatocytes were cultured on the 24 wells, which attached to the collagen, surrounded by fibroblasts. The hepatocyte morphology was maintained in the wells for 4–6 weeks. Albumin and urea synthesis, measured as markers of protein synthesis and nitrogen metabolism and typically considered as a measure of liver function, were reported to be normal. On the other hand, pure cultures were reported to be morphologically unstable and there was a loss of albumin and urea synthesis (Khetani and Bhatia, 2008).

Kane *et al*. designed a microfluidic 8 × 8 array, composed of PDMS. Each well in the array had two chambers. The primary chamber's bottom was made of glass coated with collagen, for co-culturing rat hepatocytes and 3T3-J2 fibroblasts; the collagen aided selective adhesion of hepatocytes, while continuous perfusion of medium and removal of waste products was achieved by microfluidic tubing connected to the chamber. The secondary chamber, which was separated from the primary chamber by a thin PDMS

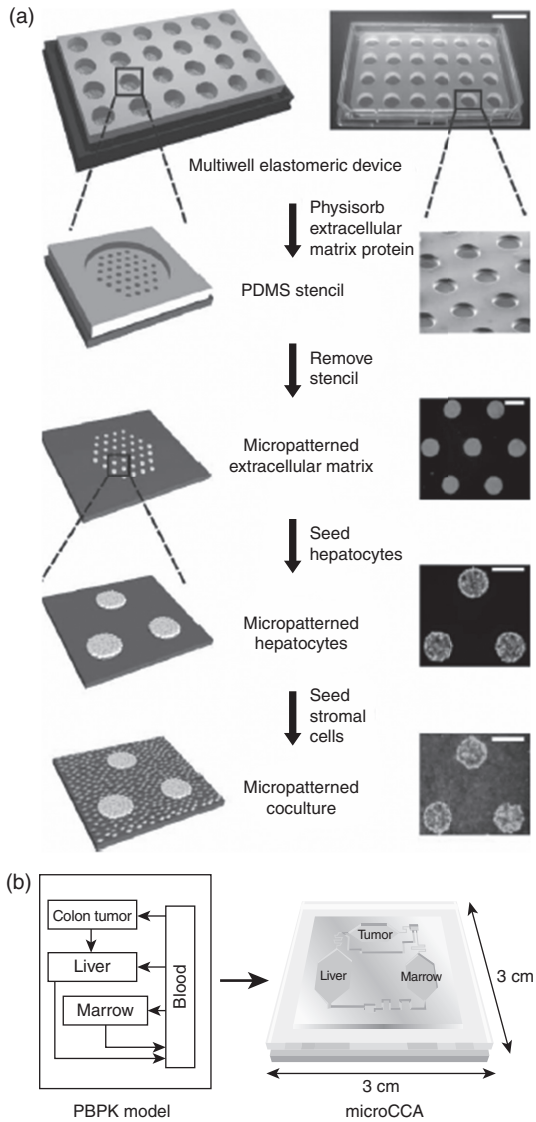

7.7 Multiwell culture for *in vitro* toxicity testing. (a) Schematic of the fabrication process (left panel) with photomicrographs of each step (right panel). A PDMS stencil in a 24-well format with through holes at the bottom of each well is sealed to a polystyrene plate, with collagen-I adsorbed on exposed polystyrene. The stencil is then peeled off followed by be application of blank PDMS stencil before cell seeding. Hepatocytes are then seeded which selectively attach to collagen-I, allowing fibroblasts to be seeded in other bare areas (Khetani and Bhatia, 2008). (b) A mathematical PBPK model and a corresponding physical μCCA based on the human body. A μCCA consists of liver, tumour and marrow chambers, interconnected with channels mimicking the blood flow pattern in the human body (Sung and Shuler, 2009).

membrane, was linked to microfluidic channels supplying humidified air with 10% carbon dioxide at 37°C. They also reported similar results, with increased albumin and urea production (Kane *et al*., 2006). Such microfluidic platforms have also been used to assess cardiotoxicity, neurotoxicity, embryotoxicity and cytolysis, a summary of which has been provided in a review by Wen *et al*. (2012). These microfluidic devices, which can emulate a particular organ *in vitro*, are referred to as organ-on-a-chip devices.

Although the above listed cell-based assays provide information about a compound's therapeutic and toxic properties on the tissue under consideration, they do not tell anything about the effect on the whole body or interactions with other organs and related dose dynamics. As a drug in the body goes through the complex process of ADME, collectively called as pharmacokinetics (PK), with contributions from different organs, cell culture using cells-on-a-chip or organ-on-a-chip technology, fails to capture these responses. Of late, scientists have developed miniaturized multi-compartment cell culture platforms better known as body-on-a-chip devices. These can promote tissue–tissue interactions by creation of environment and flow conditions scaled down to *in vivo* tissue sizes. They can also aid in studying interactions between organs in a high-throughput manner, enabling the study of multiorgan metabolic and toxicity profiles of a compound. Microscale systems designed for physiologically based pharmacokinetic modelling (PBPK), having different compartments for different tissues, can assist in understanding parameters such as tissue-to-blood perfusion, enzyme kinetics, liquid-to-cell ratio and physiological stress on a particular tissue/organ (Esch *et al*., 2011).

A novel microfluidic system, microscale cell culture analogue (μCCA), has been developed for multiorgan toxicity analysis. A multiorgan culture system, the integrated discrete multiple organ culture or 'wells-within-a-well' system, was designed by Li *et al*. Cells from different organs were cultured in small wells in their respective media in a bigger well. They cultured primary cells from liver, kidney, lungs, central nervous system, blood vessels as well as human breast adenocarcinoma cancer cell line, MCF-7. For testing the toxicity of a model drug, the bigger wells were flushed with a medium containing the drug, tamoxifen. The effect of tamoxifen was evaluated and its comparative toxicity towards various organs was also examined. Apart from this, the system offers another advantage in enabling the analysis of the anticancer activity of a drug with respect to its effect on normal tissues. Although the authors did not delve into multiorgan interactions, this in principle can be adapted for this purpose and its capabilities should be further investigated (Li *et al*., 2004).

In a model based on PBPK to emulate the dynamics of the human body, different compartments hosting different cell types were connected through microfluidic channels to mimic blood circulation. Four different cells were

cultured on a μCCA, including hepatocytes (HepG2/C3A), bone marrow cells (MEG-01), uterine cancer cells (MES-SA), and a multidrug resistant (MDR) uterine cancer cell line (MES-SA/DX-5). In a combination drug therapy of chemotherapeutic doxorubicin, with MDR modulators cyclosporine and nicardipine, treated for 24 h or 72 h, a selective toxicity towards MES-SA/DX-5 was detected, a synergy not observed in conventional 96-well plate assays. This device could thus be used in drug screening and selection of potential MDR modulators, as well as gather dose required and dose response curves for subsequent *in vivo* animal experiments or clinical trials (Tatosian and Shuler, 2009). 3D hydrogel cultures in μCCA format were developed by Sung and Shuler (Fig. 7.7b). Three types of cells, hepatocytes (HepG3/C3A), myeloblasts (Kasumi-1) and colon cancer cells (HCT-116), were embedded in different chambers in 3D hydrogels, representing different organs. The cytotoxic effect of tegafur, a prodrug of active anticancer drug, 5-fluorouracil, commonly used in colon cancer was tested using this device. An interesting revelation, as compared to conventional 96-well plate assay was that, although, the liver cells in μCCA showed metabolism of tegafur similar to 96-well plate, the metabolism led to the death of hepatocytes, an effect which was unnoticeable in well plate assays (Sung and Shuler, 2009). The literature is replete with tegafur toxicity data, particularly its hepatotoxicity (Maruyama *et al*., 1995). In such a scenario, development of microfluidic systems providing critical toxicity information in *in vitro* models bodes well for preclinical drug testing.

Ex vivo *evaluation*

Apart from *in vitro* microfluidic cell culture platforms, some researchers have also looked at *ex vivo* microfluidic platforms by isolating animal tissues, particularly liver, and culturing excised explants to analyse the toxicity of various compounds. It has been reported that precision cut liver slices fare better than hepatocytes alone with respect to metabolic activity (Graaf *et al*., 2007). Continuous perfusion of nutrient medium can further reduce the loss of metabolic activity and prolong protein expression in these slices. Microfluidic devices have been designed to continuously replenish the spent medium and remove waste material from these slices. van Midwoud *et al*. designed a PDMS-based 'perifusion' device, with liver slices supported on polycarbonate membranes (Fig. 7.8a). The term 'perifusion' was used instead of perfusion, as the medium flowed around the slices. PDMS membranes were purposely kept thin so as to allow for efficient gaseous exchange. Metabolic activity of 7-ethoxycoumarin observed was comparable to the well plate-based method was observed in this device (van Midwoud *et al*., 2010). Another PDMS-based device was developed to analyse ethanol toxicity in liver explants. Using this device, concentrations as low as 20 mM produced a decrease in mitochondrial

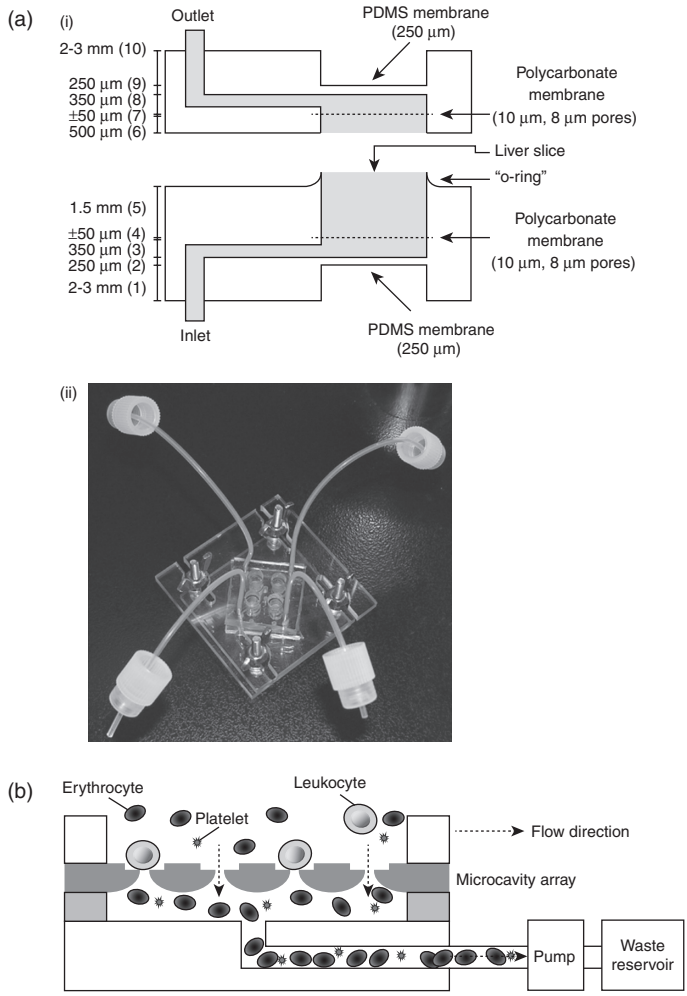

7.8 Microfluidic platforms for *ex vivo* experiments. (a) For culturing liver slices. (i) Cross-sectional view of a PDMS-based biochip for culturing liver slices that were supported on a polycarbonate membrane. The device was termed as a 'perifusion' device as culture medium flowed around the slices. Thin PDMS membranes allowed for efficient gaseous exchange. (ii) A photograph of the device mentioned in (i) (van Midwoud *et al.*, 2010). (b) For leukocyte counting and assessment of haematotoxicity. A microcavity array was created by PDMS to form a sieve like structure that retained the leukocytes, while allowing other blood cells to pass through. The cells can then be separately analysed for toxicity due to various drugs (Hosokawa *et al.*, 2012).

metabolic activity as well increased lactate dehydrogenase activity, a marker of cell death. These effects were observed in a concentration dependent manner, together with a decrease in albumin and urea synthesis (Hattersley *et al*., 2011). Such devices utilizing excised tissues represent clinically more relevant models to replace animal experimentation.

In vivo *evaluation*

Microfluidic platforms have also been used to assist *in vivo* animal experiments, for blood sampling, sample preparation and analysis (Kang *et al*., 2008). An automatic blood collection microfluidic chip-based on PDMS was developed by Wu *et al*. for withdrawal of blood from mice without the need of trained personnel. The device consisted of two layers, holding channels for blood inlet, outlet, heparin block, blood reservoir and sample wells. A microfluidic device was used for processing blood samples from mice for determining haematotoxicity (Fig. 7.8b). In this device, a microcavity array was created by master-moulding PDMS structures to form a sieve-like structure that separated leukocytes from other blood cells. Benzene toxicity was assessed by staining the leukocytes and counting them over a period of 2 weeks (Hosokawa *et al*., 2012). Microfluidic platforms have been designed to be integrated with novel analytical techniques such as matrix assisted laser/desorption ionization–mass spectrometry (MALDI-MS), which can facilitate fast sample analysis with high precision and resolution of many metabolites in biological samples (Lee *et al*., 2008; Xu *et al*., 2006).

These microfluidic systems have thus played a critical role in various stages of the drug development process. Beginning with the identification of targets, to synthesis of compounds for generation big compound libraries, to HTS and preclinical development, microfluidics has been effectively adapted to reduce the consumption of reagents and make the drug discovery process more efficient and cost effective. In the subsequent section, we will discuss about the application of microfluidics in analysis of chemical and biological drugs. We also discuss the role played by these devices in detection of diseases and routine diagnostic purposes, which may reduce the healthcare costs.

7.3 Microfluidics for drug analysis and diagnostic applications

Miniaturization of analytical tools has been propelled by the recent surge in the development and maturation of microfabrication techniques. The better control of physical processes at the micron-scale has further fuelled the interest in micro-analytical systems as new paradigms for pharmaceutical analysis. These systems are aimed at reducing both the sample volume

and time of analysis, besides being amenable to integration with the other platforms and potential for high throughput. High parallelization, thus now possible, had made analysis of multiple compounds fast and easy (Lee *et al.*, 2009). Design modification can provide integrated facilities for handling fluids, and thermal and spatial control for targeting specific detection components to enhance selectivity (DeMello, 2006). With the mass fabrication of micron-sized platforms now made possible through sophisticated instruments, the cost of production of these devices has come down, providing an opportunity to develop single use analytical devices, thereby reducing the possibility of cross contamination (Lion *et al.*, 2004).

7.3.1 Microfluidics for drug analysis

Although there have been many mechanistic and experimental advancements in analysis of drugs, the basic analytical equipment and components have not changed much over the past few decades. Recently, with the application of microscale techniques adopted from the semiconductor industry, scientists are now poised for choice to carry out analytical assessments at an order 5–9 times lower than conventional counterparts (DeMello, 2006). Microscale analytical devices, also termed as micro-total analytical systems (μTAS), comprise microchannel networks that aim to replicate the analysis procedures on physically shrunk platforms, without compromising the analytical efficiency or sensitivity. Apart from this, μTAS can be designed to attain a high level of automation, thereby making multiplexed assays possible and providing a system that reduces manual errors, helping to increase the assay accuracy. These devices have been more popular in the analysis of biological molecules such as proteins and nucleic acids (Guo *et al.*, 2012; Meagher and Thaitrong, 2012), and have been the subject of other chapters in this book. Here, we would limit our focus to discussion about the application of microfluidics in the analysis of drug entities.

Analysis of pharmaceutical compounds has been carried out using high performance liquid chromatography (HPLC), linked to various detection modules including ultraviolet and fluorescence spectrophotometers as well as mass spectrometry, electrophoresis, potentiometry, colorimetry, radioisotopic assay, microbiological methods, enzymatic methods, surface plasmon resonance based biosensor assays and chemiluminescence, among many others. Microfluidic platforms, due to the flexibility in their design, are docile to integration with most of the above listed analytical methods. With the increasing demand for highly sensitive and minuscule working volume microfluidic platforms, it is imperative that the chosen method is able to detect low amounts of the analyte. Chemiluminescence (CL) was reported to be a highly sensitive technique, with vitamin B_{12} concentrations as low as 5 pg/mL being detected easily (Kumar *et al.*, 2009). CL-based methods have

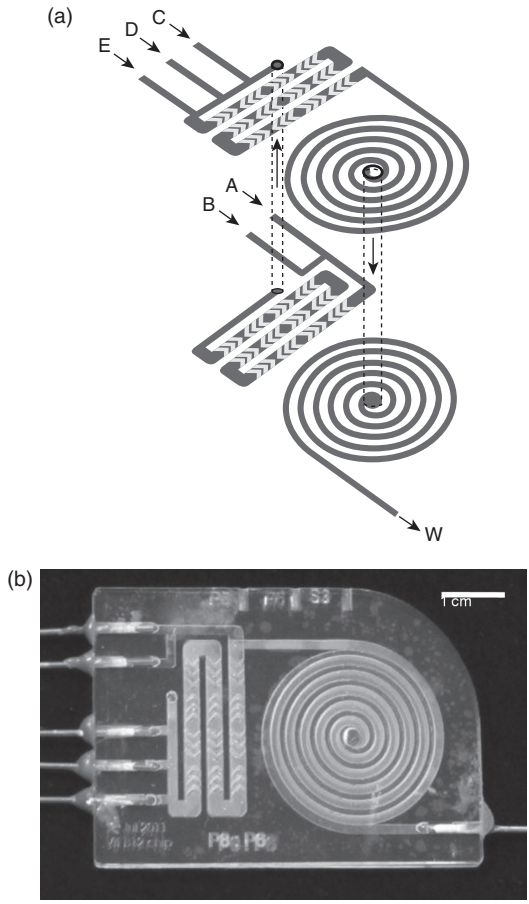

7.9 Microfluidic chip for chemiluminescence based detection of vitamin B_{12}. (a) Schematic of the chip with five inlets, two mixing chambers and two spiral detection units, and the fabricated chip (b) (Lok *et al.*, 2012).

been used for microfluidic detection of vitamin B_{12} and L-phenylalanine. Luminol oxidation by hydrogen peroxide in the presence of externals catalyst ions, such as cobalt (II) and copper (II) and amino acids such as L-phenylalanine under alkaline conditions, is the basis of this test. The resultant product is a blue compound (3-aminopthalate ion) that can be detected at a wavelength of 425 nm (Chen *et al.*, 2007; Wang *et al.*, 2007).

Lok *et al.* developed a microfluidic chip to detect the concentration of vitamin B_{12} using a continuous flow microfluidic chip (Fig. 7.9). The device consisted of a two passive mixing reaction chambers and a double spirally wound microchannel network as an optical detection unit, spanning the three sequentially fabricated layers. Microchannels in the second layer were

covered by the first layer. The second consisted of a mixing chamber and a clockwise spiral detection unit. The third layer had the other mixing chamber and an anticlockwise spiral detection set. The mixing chambers were designed in layers to counter the problem of mixing in the laminar flow. The spirally designed detection channels presented a better CL signal to the optical detector as compared to a single loop unit. The microchip also had a chamber for acidification of vitamin B_{12}, as cobalt present in vitamin B_{12} complex is not released passively to catalyse the reaction. Using the device, up to 0.3 pg/mL of vitamin B_{12} could be detected (Lok *et al.*, 2012). In another CL-based microfluidic chip, using the same principle of oxidation of luminol catalysed by copper sulphate, was used to detect L-phenylalanine, as the CL signal increased in the presence of L-phenylalanine in alkaline medium. PDMS was used to fabricate the device by soft lithography. The device was provided with four sample inlets and one outlet, and was able to detect around 39 picogramme/ml of L-phenylalanine in commercial soft drinks as well as pharmaceutical injections (Kamruzzaman *et al.*, 2012).

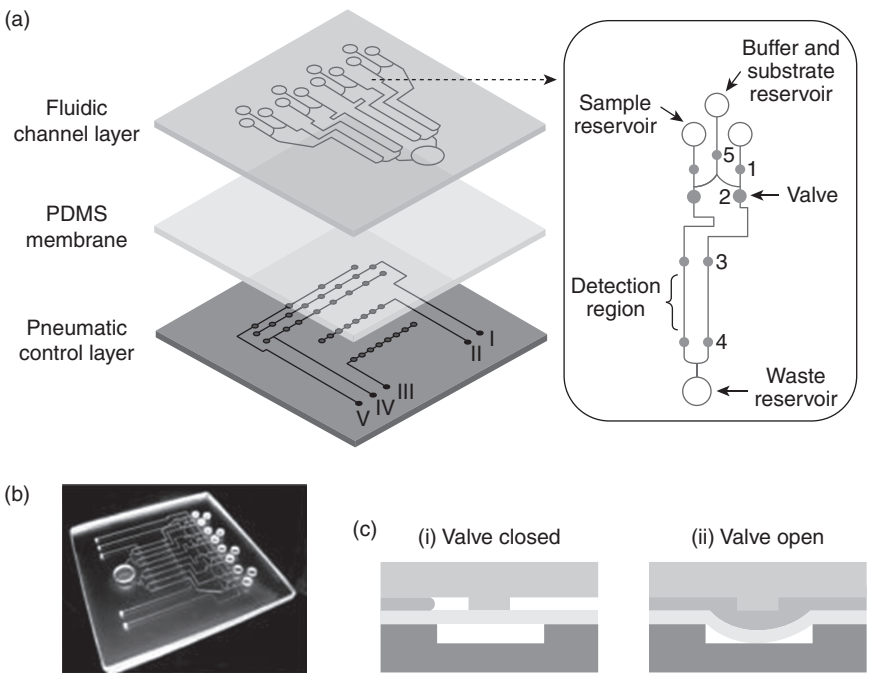

7.10 Schematic of a multilayered microfluidic device for analysis of drugs. (a) The device comprised three layers; the top and bottom layer were made of glass and a PDMS membrane was sandwiched between the two layers. (b) Photograph of the device. (c) Cross-sectional view of the microvalves showing closed and open position (Kong *et al.*, 2009).

Won *et al*. developed a microfluidic device on glass slides for simultaneous detection of five sulphonamide drugs (Won *et al*., 2012). The device was provided with modules for pre-concentration and electrokinetic separation of drugs using the field amplified sample stacking (FASS) and field amplified sample injection (FASI) techniques in two parallel channels (Shiddiky and Shim, 2007). Subsequent electrochemical detection of sulphonamides was carried out at the end of the separation channel, which consisted of a silver/silver chloride, platinum wire and aluminium-gold nanoparticles modified carbon paste electrode. The device was able to detect femto-molar level concentrations of these drugs and provide an opportunity to simultaneously detect these drugs in clinical samples. A microfluidic chip integrated to a laser-induced fluorescence scanner was developed for the detection of β_2 agonist drugs such as clenbuterol (Fig. 7.10). These drugs increase muscle mass and have been often misused in farm animals (Martinez-Navarro, 1990), as well as in power sports by athletes (Delbeke *et al*., 1995; Hesketh *et al*., 1992), making it vital to analyse them in a rapid and accurate manner. The three layers of the device consisted of a fluidic channel, a PDMS membrane, and a pneumatic control layer interspersed with many pneumatic microvalves and micropumps to enable the delivery of reagents. Glass was used to fabricate the fluidic channel and pneumatic control layer by standard lithography and etching to create microchannels. The PDMS membrane was then sandwiched between the two layers and generated pneumatic valve and pump effect due to deflection by compressed air. The drugs could be detected within 30 min and at a concentration as low as 0.088 ng/mL (Kong *et al*., 2009). Thus, microfluidic devices can play a crucial role in detection drugs and pharmaceuticals, and can be routinely used in chemical, pharmaceutical and clinical settings with high precision in an economical way.

7.3.2 Microfluidics for diagnostic purposes

The conventional diagnostic techniques based on sophisticated macroscopic equipment such as gas chromatography–mass spectrometry are only feasible in big air-conditioned laboratories, which are equipped with trained workforces and devices for sample handling, together with ample ancillary resources needed for efficient diagnosis. But this is not attainable outside the realm of these laboratories, especially in the developing world, particularly in rural areas (Lee *et al*., 2010; Yager *et al*., 2006). Miniaturized versions of analytical platforms have been recently conceptualized, primarily based on microfluidic technology, to perform diagnostic analysis, consuming minimal amounts of reagents with high efficiency and speed, making the device a portable point-of-care, self-usable system. This not only reduces the logistical issues with sample handling and transfer, but also provides patients

with the luxury of testing for various markers, such as blood glucose, in the comfort of their homes, which is particularly suitable for geriatric patients. These microfluidic diagnostic devices may reduce the healthcare costs associated with diagnosis.

Microfluidic biosensors, as they are commonly known, have been fabricated for a variety of purposes. Particularly important among these are on-chip enzymatic assays. As enzymes have the potential of converting a large number of substrate molecules into product in a fraction of a second, in a highly selective manner, they offer an exciting avenue for chemical analysis. Enzyme assay on a chip may be either homogenous or heterogeneous. In the former, all the reactants are in solution phase (Hadd *et al*., 1997), while in the latter either of the enzyme/substrate/inhibitor needs to be immobilized on a solid surface (Mao *et al*., 2002; Krenkova and Foret, 2004). Mostly, enzyme immobilization is carried out on microchannel walls or onto some support inside the channels. This provides the advantages of enzyme recycling, placement of enzyme at specific locations on microchannels, and analysis in a continuous flow environment, making immobilized assays a preferable choice (Kim *et al*., 2009).

Enzyme immobilization has been mostly carried out on microspheres, also known as microbeads, due to their similar size properties to microchannels, as well as large surface area for enzyme support (Peterson, 2005). They offer the advantage of being contained at appropriate locations by using mechanical barriers or magnetic devices. Kim *et al*. developed a microfluidic device for glucose detection. The device consisted of two separate chambers, for reaction and detection, respectively. In the reaction chamber, microbeads were covalently bound to an enzyme, glucose oxidase, and were supported by microfilters. A poly (ethylene glycol)-based microarray (fabricated by photolithography) encapsulating a horseradish peroxidize, formed the detection chamber. The bienzymatic reaction was used to detect the conversion of non-fluorescent substrate (Amplex Red fluorescence indicator) to a fluorescent resorufin, with glucose concentrations in the range of 1–10 mM detected successfully by fluorescence microscopy and quantified by software (Kim *et al*., 2009). In a modified version, Sheng *et al*. used glucose oxidase modified magnetic nanoparticles, constrained in the microchannel with the aid of external magnetic field, for the amperometric analysis of glucose. The device offered a simple alternative to other such devices, as no mixing was needed, achieving higher sensitivity. Detection was linear with a range between 25 μM and 15 mM. The device also possessed a separation channel that avoided the entry of macromolecules, thereby eliminating the need to pre-process the sample. This allowed the serum samples to be directly used for glucose analysis (Sheng *et al*., 2012). Other devices integrating enzyme and immunoassays have been fabricated for simultaneous detection of glucose and insulin (Wang *et al*., 2003).

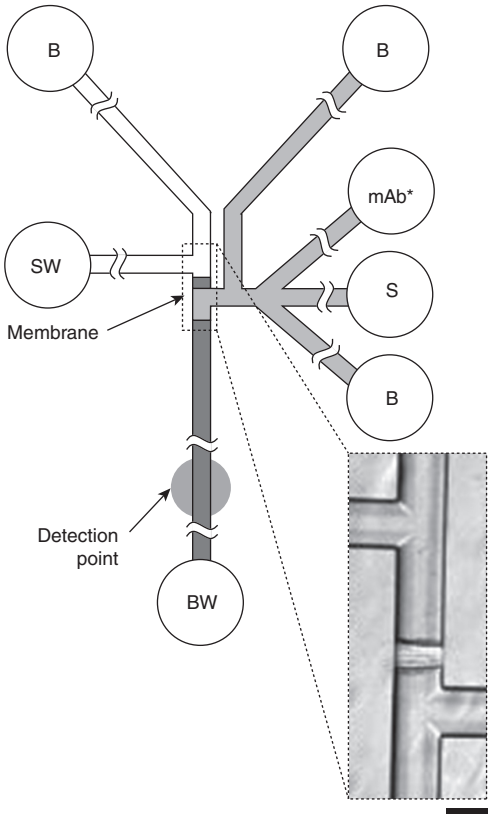

7.11 Microchip electrophoretic immunoassay (μCEI) chip. The device had fluid wells for: S, sample; B, buffer; SW, sample waste; BW, buffer waste; mAb*, fluorescently labelled monoclonal antibody. The device possessed molecular sieves to enrich the sample and electrophoretically separate the molecular antibody that is bound to an enzyme (Herr *et al.*, 2007).

Herr *et al.* designed a microchip-based device for the detection of disease biomarkers in periodontal disease (Fig. 7.11). The multifaceted device had integrated capabilities for sample pretreatment, including filtering, mixing and enrichment of the saliva, which could be withdrawn in a hands-free manner. The device, a microchip electrophoretic immunoassay (μCEI), was provided with molecular sieves fabricated using hydrogel, to enrich the sample, followed by electrophoretic separation to resolve a fluorescent antibody bound to an enzyme, responsible for tissue decay. Using the method, they could dispense with the need for using matched antibody pairs as well as to immobilize the antibody (Herr *et al.*, 2007).

Enzyme-linked immunosorbent assay (ELISA) has been the mainstay of clinical diagnostics for detection of antigens and antibodies. However, the

conventional macroscale ELISA protocols are laborious, sluggish, require multiple reagent addition and washing steps, and often result in inconsistent results due to manual glitches. Furthermore, commercially available ELISA kits, as well as the instruments used, are costly (Lai *et al.*, 2004). Chip-based ELISA methods offer the advantage of faster antigen–antibody reaction with the consumption of significantly less reagent (Cesaro-Tadic *et al.*, 2004; Murakami *et al.*, 2004). Microfluidic ELISA platforms have been researched in great detail in the past few years (Herrmann *et al.*, 2006; Holmes *et al.*, 2007). Lee *et al.* developed a fully automatic ELISA platform for detecting antigen and antibody for hepatitis B virus, on a disposable plastic disc, made of poly (methyl methacrylate), having arrangements for conducting immunoassays from whole blood. The device had facilities for plasma separation and chambers for storage of buffers, reagents, substrates, collection of waste,

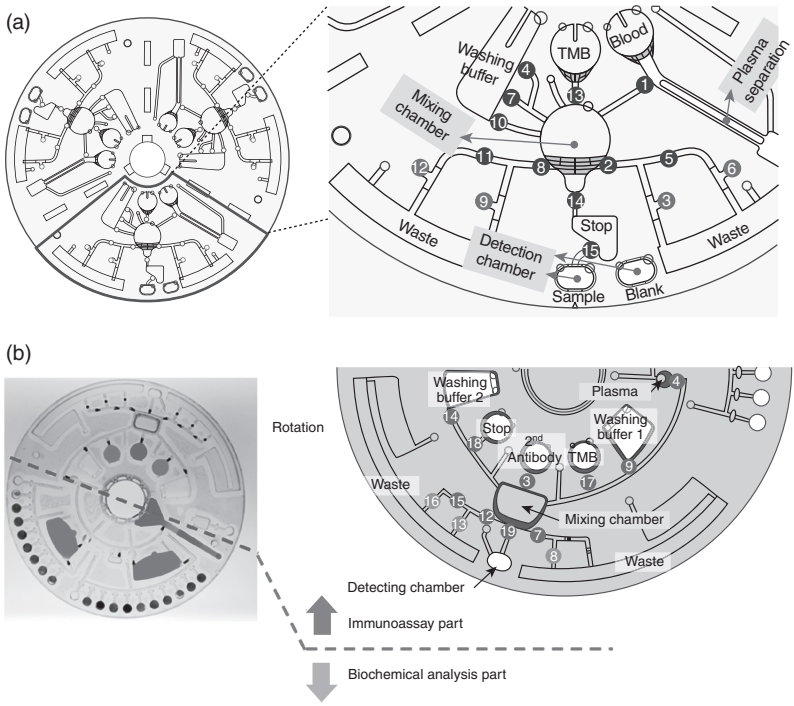

7.12 Microfluidic lab-on-a-disc platforms. (a) Schematic of a fully automatic disposable ELISA platform, with facilities for plasma separation, storage of buffers, reagents, mixing the reactants and collection of waste. ELISA assay could be performed in half as volume and less than 30 min. The numbers indicate the sequence of reaction (Lee *et al.*, 2009). (b) Schematic of an improvised platform with facilities for assessing both immunoassay and clinical chemistry of blood, provided on a single disc. The detection chamber could be used at 10 different wavelengths to accommodate a range of reactions (Lee *et al.*, 2011).

mixing the reagents, and detection of the product. Using just 150 μL of blood, the assay could be performed as opposed to double this volume with conventional methods; the whole assay could be carried out in 30 min, whereas conventional well plate-based ELISA yields results in a minimum of 2 h (Lee *et al*., 2009). Miniaturization did not compromise the sensitivity of the device, and a similar detection limit could be achieved (Fig. 7.12a). Recently, they developed an advanced chip to carry out the immunoassay as well as biochemical assessment of whole blood (Fig. 7.12b). The chip had an automated arrangement for plasma separation, mixing, incubation and detection. The freeze-dried reagents for both assays were stored in dedicated compartments, and the detection was carried out by optical measurements at ten different wavelengths to accommodate various reactions (Lee *et al*., 2011). Their group has also developed a multiplexed immunoassay, based on three different biomarkers to improve detection efficiency (Park *et al*., 2012).

Droplet-based microfluidic approaches have been used for analysis of human physiological fluids such as blood, serum, plasma, sweat and tears. These might be very useful in a point-of-care setting, whereby a patient can use a microdroplet of his/her sample, with minimal training, without much inconvenience, and read the results in real time. A monolithic electrowetting platform consisting of a photolithographically patterned metal electrode array on a glass substrate was designed and the sample was sandwiched between this array and another plate of glass. The sample droplet was encapsulated in silicone oil to prevent evaporation and ensure smooth transport, at frequencies of 20 Hz and voltage less than 65 V. Glucose concentration was determined by a colorimetric assay in various physiological samples and results were found to be comparable to reference values (Srinivasan *et al*., 2004).

Electrochemical methods of detection are recognized to be among the most sensitive, as they do not involve any label tagging for studying the fate of biological compounds. Electrodes serving as sensors have found their niche in medical diagnostics, due to their relative ease of fabrication and integration with analytical devices. With several markers being pliable for electrochemical analysis, many methods of electrode fabrication have been pursued (Wartelle *et al*., 2005; Quinton *et al*., 2011). Screen printed electrodes (SPE) based on carbon are another form of electrochemical analytical device that has been studied for the detection of chemicals, such as nitric oxide (Miserere *et al*., 2006), and biomarkers for cancer (Wan *et al*., 2011). They are useful for electrochemical immunosensor assays, as they offer the advantages of low background current, ease of chemical modification on carbon surface and relative inertness of carbon-based materials. A variety of materials such as nylon, glass, alumina, and organic films have been used for electrode fabrication and present an interesting alternative for point-of-care testing (Miserere *et al*., 2006; Schuler *et al*., 2009).

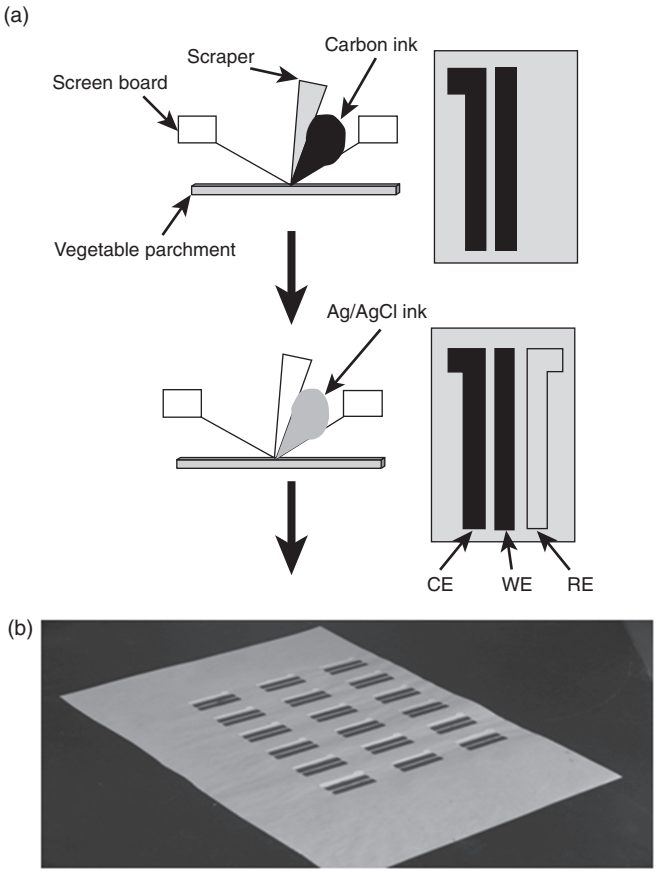

7.13 Screen printed electrodes as microfluidic platforms for immunosensor applications. (a) Carbon and silver/silver chloride electrodes were printed on a sheet of vegetable parchment, with WE, working electrode; RE, reference electrode; CE, counter electrode. (b) A sheet of vegetable parchment with 18 electrodes (Yan *et al.*, 2012).

Recently, Yan *et al.* fabricated SPEs on vegetable parchment as a substrate for disposable immunosensor fabrication in detection of prostate specific antigen (PSA) (Fig. 7.13). Electrodes were printed from carbon and silver/silver chloride ink. The device was then integrated to a paper-based microfluidic device, to absorb detection solution and immersing the electrodes in electrolyte. The immunosensor was fabricated by coating the SPEs with a sheet of functionalized graphenes, containing the enzyme-linked antibody on gold nanoparticles. The assay could detect PSA as low as 2 pg/mL, and offers a suitable method for detecting potential disease specific biomarkers, allowing for early diagnosis in a disease (Yan *et al.*, 2012).

A microfluidic magnetic disc has been used to separate rare, circulating endothelial cells (CEC) from peripheral blood mononuclear cells (Chen *et al*., 2011b). These CECs have been associated with many diseases, and their low concentration in blood impedes their detection. A magnetic disc was used to trap the cells attached to immunomagnetic beads. Human umbilical vein endothelial cells (HUVEC) were used as a model for CECs and stained with anti-CD146-phycoerythrin antibody, which was tagged to anti-phycoerythrin magnetic beads that attracted these cells to the magnetic disc. This magnetic disc had an inlet channel, connecting channels and a waste reservoir. When the disc was rotated, the centrifugal force propelled away the non-magnetic cells through the connecting channels to the waste reservoir, effectively retaining target cells (HUVECs) in the inlet reservoir, which had a multistage magnet over it.

As a basic criterion, the point-of-care diagnostic devices meant for the developing world must be inexpensive and integrated, dispensing the services of ancillary equipments (Mabey *et al*., 2004; Martinez *et al*., 2008a). In the wake of this cost consideration, paper-based microfluidic devices offer a potential alternative to glass/polymer-based open channel microsystems. These devices can also enable a multitude of sample outlets from a single inlet, ensuring simultaneous analytical assays, without the need for an external pumping device. Being light in weight and easy to stack makes their shipment logistically much easier than glass/polymer-based devices. Paper-based microfluidic devices have been researched in detail by the laboratory of George Whitesides at Harvard, called 3D microfluidic paper analytical devices (μPAD) (Bruzewicz *et al*., 2008; Martinez *et al*., 2007, 2008b, 2008c).

Microfluidic devices have also been developed for diagnosis of lysosomal storage disorders (Shen *et al*., 2012), cancer (Lien *et al*., 2010; Chen *et al*., 2011a; Tang *et al*., 2012), H1N1 influenza (Lee *et al*., 2012) and herpes simplex virus (Zubair *et al*., 2011), sickle cell disease (Hersher, 2012) and Johne's disease in cattle (Wadhwa *et al*., 2012). In principle, all microfluidic diagnostic devices consist of a molecular sensing unit coupled to a signal converter (transducer) that reads out the results quantitatively. An elaborate review of different mechanistic approaches of biosensors is provided by (Mohanty and Kougianos, 2006). Since the biosensors vary greatly in their design, and hence their sensitivity and efficiency, the reader is referred to a few state-of-the-art reviews for more detailed information (Choi *et al*., 2011; Mohammed and Desmulliez, 2011).

It is expected that microfluidic technology will play a crucial role in medical diagnostics in the coming years, essentially with the development of disposable, sample-to-result devices, making routine diagnosis a more personalized approach (Eicher and Merten, 2011; Foudeh *et al*., 2012).

7.4 Conclusion and future trends

Conclusively, microfluidic devices have shown initial promise in all areas of drug discovery and development, as well as in the domains of miniaturized diagnostic devices. The future of microfluidic devices for application in drug discovery appears bright with a lot of research activity being focused on the development of miniaturized chips. However, the concern remains about the integration of these devices with ancillary equipment, including electrical accessories, pressure pumps and platforms for analysis of samples. Due to their increased acceptance and potential benefits as economical alternatives to conventional bench-top macroscale equipments, it is important to develop integrated 'everything-on-a-chip' systems that are widely accepted in all stages of drug discovery and development. This may entail an inter-disciplinary effort from engineers and researchers working on fluid dynamics to design micropumps, analytical equipment manufacturers to scale down analysis systems to commensurate with the chip size, and finally researchers working on microfabrication to further miniaturize the platforms and making them adaptable to these ancillary systems.

Industry has played a crucial role in this respect so far. Fluidigm Corporation (http://www.fluidigm.com/), a venture by Dr Stephen Quake from Caltech, has developed various platforms for microfluidic device integration. Based on the technology known as multilayer soft lithography, 3D structures can be created from elastomers to form integrated valves (NanoFlex™), pumps and channels. Besides this, Caliper Life Sciences (http://www.caliperls.com/) have also developed several automated/semi-automated robotics controlled liquid handling systems (Zephyr®) that can be potentially integrated with microfluidic devices. These microfluidic integration tools are expected to aid microfluidic-based drug discovery by improving efficiency and scalability.

With the rate of approval of new drugs declining in the past few years and the pharmaceutical industry still lacking effective tools in discovering new drugs, microfluidic platforms come with a ray of hope, chaperoning routine assays in a more efficient manner and hopefully allowing more highly efficacious and safe drugs to be discovered.

On the other hand, miniaturized devices as diagnostic kits have made inroads into the households of many diabetic patients as blood glucose monitors. Miniaturized devices for other applications not only face fabrication and technical issues of being an integrated and comprehensive system, but they also face the challenge of patient acceptance, having a direct interface with the end user. Although their acceptance is propelled by the convenience of use, the future of such devices for routine practice in other pathological conditions would rely on how the users perceive them. A sizeable population, particularly in remote villages and tribal areas in developing world, lack good education, and training to use such devices might prove to be a

daunting task. Moreover, it would require sincere effort on the part of clinicians and marketing professionals, to persuade the patients in developed world, who have been so used to visiting a clinic to get their routine biochemical check-ups, to adopt such self-usable devices. In addition, it has to be ensured that such devices are safe to use and dispose, without causing any serious environmental hazards.

7.5 Sources of further information and advice

Although we have tried to encompass the major developments on the drug discovery and analysis front in this chapter, the reader is referred to the following for further details. A review reflecting on the origins and the current status of microfluidics by George Whitesides is highly recommended (Whitesides, 2006). Another comprehensive review, by Yeo *et al*., that describes the role of microfluidics in various biological applications is also recommended (Yeo *et al*., 2011). Other important works that appear in literature and circumscribe the two areas of interest in this chapter include (Imming *et al*., 2006; Yager *et al*., 2006; Kang *et al*., 2008; Wen and Yang, 2008; Lombardi and Dittrich, 2010; Livak-Dahl *et al*., 2011).

7.6 References

Alsenz, J. and Kansy, M. (2007). High throughput solubility measurement in drug discovery and development. *Adv Drug Deliv Rev*, **59**, 546–67. DOI 10.1016/j.addr.2007.05.007

Anonymous (2000). Signal transduction as a drug-discovery platform. *Nat Biotechnol*, **18**, 37–9.

Ashraf, M. W., Tayyaba, S. and Afzulpurkar, N. (2011). Micro electromechanical systems (mems) based microfluidic devices for biomedical applications. *Int J Mol Sci*, **12**, 3648–704. DOI 10.3390/ijms12063648

Bange, A., Halsall, H. B. and Heineman, W. R. (2005). Microfluidic immunosensor systems. *Biosens Bioelectron*, **20**, 2488–503. DOI 10.1016/j.bios.2004.10.016

Battersby, B. J. and Trau, M. (2002). Novel miniaturized systems in high-throughput screening. *Trends Biotechnol*, **20**, 167–73.

Beebe, D. J., Mensing, G. A. and Walker, G. M. (2002). Physics and applications of microfluidics in biology. *Annu Rev Biomed Eng*, **4**, 261–86. DOI 10.1146/annurev.bioeng.4.112601.125916

Beggs, M. (2001). HTS – where next? *Drug Discov World*, **2**, 125–34.

Bogojevic, D., Chamberlain, M. D., Barbulovic-Nad, I. and Wheeler, A. R. (2012). A digital microfluidic method for multiplexed cell-based apoptosis assays. *Lab Chip*, **12**, 627–34. DOI 10.1039/c2lc20893h

Bohacek, R. S., Mcmartin, C. and Guida, W. C. (1996). The art and practice of structure-based drug design: a molecular modeling perspective. *Med Res Rev*, **16**, 3–50. DOI 10.1002/(SICI)1098–1128(199601)16:1<3::AID-MED1>3.0.CO;2–6

Braeckmans, K., De Smedt, S. C., Leblans, M., Pauwels, R. and Demeester, J. (2002). Encoding microcarriers: present and future technologies. *Nat Rev Drug Discov*, **1**, 447–56. DOI 10.1038/nrd817

Brandish, P. E., Chiu, C. S., Schneeweis, J., Brandon, N. J., Leech, C. L., Kornienko, O., Scolnick, E. M., Strulovici, B. and Zheng, W. (2006). A cell-based ultra-high-throughput screening assay for identifying inhibitors of D-amino acid oxidase. *J Biomol Screen*, **11**, 481–7. DOI 10.1177/1087057106288181

Brouzes, E. (2012). Droplet microfluidics for single-cell analysis. *Methods Mol Biol*, **853**, 105–39. DOI 10.1007/978–1–61779–567–1_10

Bruzewicz, D. A., Reches, M. and Whitesides, G. M. (2008). Low-cost printing of poly(dimethylsiloxane) barriers to define microchannels in paper. *Anal Chem*, **80**, 3387–92. DOI 10.1021/Ac702605a

Cesaro-Tadic, S., Dernick, G., Juncker, D., Buurman, G., Kropshofer, H., Michel, B., Fattinger, C. and Delamarche, E. (2004). High-sensitivity miniaturized immunoassays for tumor necrosis factor a using microfluidic systems. *Lab Chip*, **4**, 563–9. DOI 10.1039/B408964b

Chen, H., Gao, F., He, R. and Cui, D. (2007). Chemiluminescence of luminol catalyzed by silver nanoparticles. *J Colloid Interface Sci*, **315**, 158–63. OI 10.1016/j.jcis.2007.06.052

Chen, J. K., Bai, B. J. and Chang, F. C. (2011a). Diagnosis of breast cancer recurrence using a microfluidic device featuring tethered cationic polymers. *Appl Phys Lett*, **99**, 1–3. DOI 10.1063/1.3608239

Chen, K. C., Lee, T. P., Pan, Y. C., Chiang, C. L., Chen, C. L., Yang, Y. H., Chiang, B. L., Lee, H. and Wo, A. M. (2011b). Detection of circulating endothelial cells via a microfluidic disk. *Clin Chem*, **57**, 586–92. DOI 10.1373/clinchem.2010.157404

Chen, P. C., Huang, Y. Y. and Juang, J. L. (2011c). MEMS microwell and microcolumn arrays: novel methods for high-throughput cell-based assays. *Lab Chip*, **11**, 3619–25. DOI 10.1039/c0lc00696c

Chen, Y. J., Roller, E. E. and Huang, X. (2010). DNA sequencing by denaturation: experimental proof of concept with an integrated fluidic device. *Lab Chip*, **10**, 1153–9. DOI 10.1039/b921417h

Cheng, Y. L., Bushby, R. J., Evans, S. D., Knowles, P. F., Miles, R. E. and Ogier, S. D. (2001). Single ion channel sensitivity in suspended bilayers on micromachined supports. *Langmuir*, **17**, 1240–42.

Choi, S., Goryll, M., Sin, L. Y. M., Wong, P. K. and Chae, J. (2011). Microfluidic-based biosensors toward point-of-care detection of nucleic acids and proteins. *Microfluid Nanofluidics*, **10**, 231–47.

Delbeke, F. T., Desmet, N. and Debackere, M. (1995). The abuse of doping agents in competing body builders in Flanders (1988–1993). *Int J Sports Med*, **16**, 66–70. DOI 10.1055/s-2007–972966

Demello, A. J. (2006). Control and detection of chemical reactions in microfluidic systems. *Nature*, **442**, 394–402. DOI 10.1038/nature05062

Dexter, J. P. and Parker, W. (2009). Parallel combinatorial chemical synthesis using single-layer poly(dimethylsiloxane) microfluidic devices. *Biomicrofluidics*, **3**, 34106. DOI 10.1063/1.3230501

Dunlop, J., Bowlby, M., Peri, R., Vasilyev, D. and Arias, R. (2008). High-throughput electrophysiology: an emerging paradigm for ion-channel screening and physiology. *Nat Rev Drug Discov*, **7**, 358–68. DOI 10.1038/nrd2552

Eicher, D. and Merten, C. A. (2011). Microfluidic devices for diagnostic applications. *Expert Rev Mol Diagn*, **11**, 505–19.DOI 10.1586/ERM.11.25

Esch, M. B., King, T. L. and Shuler, M. L. (2011). The role of body-on-a-chip devices in drug and toxicity studies. *Annu Rev Biomed Eng*, **13**, 55–72. DOI 10.1146/annurev-bioeng-071910–124629

Evans, M., Sewter, C. and Hill, E. (2003). An encoded particle array tool for multiplex bioassays. *Assay Drug Dev Technol*, **1**, 199–207. DOI 10.1089/154065803321537926

Fertig, N., Blick, R. H. and Behrends, J. C. (2002). Whole cell patch clamp recording performed on a planar glass chip. *Biophys J*, **82**, 3056–62.

Foudeh, A. M., Fatanat Didar, T., Veres, T. and Tabrizian, M. (2012). Microfluidic designs and techniques using lab-on-a-chip devices for pathogen detection for point-of-care diagnostics. *Lab Chip*, **12**, 3249–66.

Fox, S., Farr-Jones, S., Sopchak, L., Boggs, A., Nicely, H. W., Khoury, R. and Biros, M. (2006). High-throughput screening: update on practices and success. *J Biomol Screen*, **11**, 864–9. DOI 10.1177/1087057106292473

Gao, J., Yin, X. F. and Fang, Z. L. (2004). Integration of single cell injection, cell lysis, separation and detection of intracellular constituents on a microfluidic chip. *Lab Chip*, **4**, 47–52. DOI 10.1039/b310552k

Goldberg, M. D., Lo, R. C., Abele, S., Macka, M. and Gomez, F. A. (2009). Development of microfluidic chips for heterogeneous receptor-ligand interaction studies. *Anal Chem*, **81**, 5095–8. DOI 10.1021/ac9006649

Gomez, F. A. (2011). Microfluidics in protein chromatography. *Methods Mol Biol*, **681**, 137–50. DOI 10.1007/978–1–60761–913–0_8

Goodnow, R.A. (2006). Hit and lead identification: integrated technology based approaches. *Drug Discovery Today*, **3**, 367–75.

Graaf, I. a. M., Groothuis, G. M. M. and Olinga, P. (2007). Precision-cut tissue slices as a tool to predict metabolism of novel drugs. *Exp Opin Drug Metab Toxicol*, **3**, 879–98. DOI 10.1517/17425255.3.6.879

Guo, M. T., Rotem, A., Heyman, J. A. and Weitz, D. A. (2012). Droplet microfluidics for high-throughput biological assays. *Lab Chip*, **12**, 2146–55. DOI 10.1039/c2lc21147e

Gurwitz, D. and Haring, R. (2003). Ligand-selective signaling and high-content screening for GPCR drugs. *Drug Discov Today*, **8**, 1108–9.

Hadd, A. G., Raymond, D. E., Halliwell, J. W., Jacobson, S. C. and Ramsey, J. M. (1997). Microchip device for performing enzyme assays. *Analy Chem*, **69**, 3407–12.

Han, M., Gao, X., Su, J. Z. and Nie, S. (2001). Quantum-dot-tagged microbeads for multiplexed optical coding of biomolecules. *Nat Biotechnol*, **19**, 631–5. DOI 10.1038/90228

Harrison, D. J., Fluri, K., Seiler, K., Fan, Z., Effenhauser, C. S. and Manz, A. (1993). Micromachining a miniaturized capillary electrophoresis-based chemical analysis system on a chip. *Science*, **261**, 895–7. DOI 10.1126/science.261.5123.895

Hattersley, S. M., Greenman, J. and Haswell, S. J. (2011). Study of ethanol induced toxicity in liver explants using microfluidic devices. *Biomed Microdevices*, **13**, 1005–14. DOI 10.1007/s10544–011–9570–2

Herr, A. E., Hatch, A. V., Throckmorton, D. J., Tran, H. M., Brennan, J. S., Giannobile, W. V. and Singh, A. K. (2007). Microfluidic immunoassays as rapid saliva-based clinical diagnostics. *Proc Natl Acad Sci U S A*, **104**, 5268–73. DOI 10.1073/pnas.0607254104

Herrmann, M., Veres, T. and Tabrizian, M. (2006). Enzymatically-generated fluorescent detection in micro-channels with internal magnetic mixing for the development of parallel microfluidic ELISA. *Lab Chip*, **6**, 555–60. DOI 10.1039/b516031f

Hersher, R. (2012). Microfluidic chips promise better diagnosis for sickle cell disease. *Nat Med*, **18**, 475. DOI 10.1038/nm0412–475

Hesketh, J. E., Campbell, G. P., Lobley, G. E., Maltin, C. A., Acamovic, F. and Palmer, R. M. (1992). Stimulation of actin and myosin synthesis in rat gastrocnemius muscle by clenbuterol; evidence for translational control. *Comp Biochem Physiol C*, **102**, 23–7.

Holmes, D., She, J. K., Roach, P. L. and Morgan, H. (2007). Bead-based immunoassays using a micro-chip flow cytometer. *Lab Chip*, **7**, 1048–56. DOI 10.1039/B707507n

Hosokawa, M., Asami, M., Yoshino, T., Tsujimura, N., Takahashi, M., Nakasono, S., Tanaka, T. and Matsunaga, T. (2012). Monitoring of benzene-induced hematotoxicity in mice by serial leukocyte counting using a microcavity array. *Biosens Bioelectron*, **40**, 110–14.

Huang, B., Wu, H., Bhaya, D., Grossman, A., Granier, S., Kobilka, B. K. and Zare, R. N. (2007). Counting low-copy number proteins in a single cell. *Science*, **315**, 81–4. DOI 10.1126/science.1133992

Ide, T. and Ichikawa, T. (2005). A novel method for artificial lipid-bilayer formation. *Biosens Bioelectron*, **21**, 672–7. DOI 10.1016/j.bios.2004.12.018

Imming, P., Sinning, C. and Meyer, A. (2006). Drugs, their targets and the nature and number of drug targets. *Nat Rev Drug Discov*, **5**, 821–34. DOI 10.1038/nrd2132

Javanmard, M., Babrzadeh, F. and Davis, R. W. (2010). Microfluidic force spectroscopy for characterization of biomolecular interactions with piconewton resolution. *Appl Phys Lett*, **97**, 173704. DOI 10.1063/1.3491547

Jones, R., Godorhazy, L., Szalay, D., Gerencser, J., Dorman, G., Urge, L. and Darvas, F. (2005). A novel method for high-throughput reduction of compounds through automated sequential injection into a continuous-flow microfluidic reactor. *QSAR Comb Sci*, **24**, 722–27. DOI 10.1002/qsar.200540006

Kachouie, N., Kang, L. and Khademhosseini, A. (2009). Arraycount, an algorithm for automatic cell counting in microwell arrays. *Biotechniques*, **47**, 10–16. DOI 10.2144/000113202

Kamruzzaman, M., Alam, A. M., Kim, K. M., Lee, S. H., Kim, Y. H., Kim, G. M. and Dang, T. D. (2012). Microfluidic chip based chemiluminescence detection of L-phenylalanine in pharmaceutical and soft drinks. *Food Chem*, **135**, 57–62. DOI 10.1016/j.foodchem.2012.04.062

Kane, B. J., Zinner, M. J., Yarmush, M. L. and Toner, M. (2006). Liver-specific functional studies in a microfluidic array of primary mammalian hepatocytes. *Anal Chem*, **78**, 4291–8. DOI 10.1021/ac051856v

Kang, G., Lee, J. H., Lee, C. S. and Nam, Y. (2009). Agarose microwell based neuronal micro-circuit arrays on microelectrode arrays for high throughput drug testing. *Lab Chip*, **9**, 3236–42. DOI 10.1039/b910738j

Kang, L., Chung, B. G., Langer, R. and Khademhosseini, A. (2008). Microfluidics for drug discovery and development: from target selection to product lifecycle management. *Drug Discov Today*, **13**, 1–13. DOI 10.1016/j.drudis.2007.10.003

Kang, L., Hancock, M. J., Brigham, M. D. and Khademhosseini, A. (2010). Cell confinement in patterned nanoliter droplets in a microwell array by wiping. *J Biomed Mater Res A*, **93**, 547–7. DOI 10.1002/jbm.a.32557

Kaplowitz, N. (2005). Idiosyncratic drug hepatotoxicity. *Nat Rev Drug Discov*, **4**, 489–99. DOI 10.1038/nrd1750

Keng, P. Y., Chen, S., Ding, H., Sadeghi, S., Shah, G. J., Dooraghi, A., Phelps, M. E., Satyamurthy, N., Chatziioannou, A. F., Kim, C. J. and Van Dam, R. M. (2012). Micro-chemical synthesis of molecular probes on an electronic microfluidic device. *Proc Natl Acad Sci U S A*, **109**, 690–5. DOI 10.1073/pnas.1117566109

Khetani, S. R. and Bhatia, S. N. (2008). Microscale culture of human liver cells for drug development. *Nat Biotechnol*, **26**, 120–6. DOI 10.1038/nbt1361

Kikutani, Y., Horiuchi, T., Uchiyama, K., Hisamoto, H., Tokeshi, M. and Kitamori, T. (2002). Glass microchip with three-dimensional microchannel network for 2 x 2 parallel synthesis. *Lab Chip*, **2**, 188–92. DOI 10.1039/b208382p

Kim, D. N., Lee, Y. and Koh, W. G. (2009). Fabrication of microfluidic devices incorporating bead-based reaction and microarray-based detection system for enzymatic assay. *Sens Actuators B Chem*, **137**, 305–12. DOI 10.1016/j.snb.2008.12.042

Knight, A. R. (2000). HTS – A strategy for drug discovery. *Drug Disov World*, **1**, 32–8.

Kola, I. and Landis, J. (2004). Can the pharmaceutical industry reduce attrition rates? *Nat Rev Drug Discov*, **3**, 711–15. DOI 10.1038/Nrd1470

Kong, J., Jiang, L., Su, X., Qin, J., Du, Y. and Lin, B. (2009). Integrated microfluidic immunoassay for the rapid determination of clenbuterol. *Lab Chip*, **9**, 1541–7. DOI 10.1039/b818430e

Kramer, J. A., Sagartz, J. E. and Morris, D. L. (2007). The application of discovery toxicology and pathology towards the design of safer pharmaceutical lead candidates. *Nat Rev Drug Discov*, **6**, 636–49. DOI 10.1038/nrd2378

Kreir, M., Farre, C., Beckler, M., George, M. and Fertig, N. (2008). Rapid screening of membrane protein activity: electrophysiological analysis of OmpF reconstituted in proteoliposomes. *Lab Chip*, **8**, 587–95. DOI 10.1039/b713982a

Krenkova, J. and Foret, F. (2004). Immobilized microfluidic enzymatic reactors. *Electrophoresis*, **25**, 3550–63. DOI 10.1002/elps.200406096

Kumar, S. S., Chouhan, R. S. and Thakur, M. S. (2009). Enhancement of chemiluminescence for vitamin B12 analysis. *Anal Biochem*, **388**, 312–6. DOI 10.1016/j.ab.2009.02.029

Lai, S., Wang, S., Luo, J., Lee, L. J., Yang, S. T. and Madou, M. J. (2004). Design of a compact disk-like microfluidic platform for enzyme-linked immunosorbent assay. *Anal Chem*, **76**, 1832–7. DOI 10.1021/ac0348322

Lal, R. and Arnsdorf, M. F. (2010). Multidimensional atomic force microscopy for drug discovery: a versatile tool for defining targets, designing therapeutics and monitoring their efficacy. *Life Sci*, **86**, 545–62. DOI 10.1016/j.lfs.2009.02.030

Lee, B. S., Lee, J. N., Park, J. M., Lee, J. G., Kim, S., Cho, Y. K. and Ko, C. (2009). A fully automated immunoassay from whole blood on a disc. *Lab Chip*, **9**, 1548–55. DOI 10.1039/b820321k

Lee, B. S., Lee, Y. U., Kim, H. S., Kim, T. H., Park, J., Lee, J. G., Kim, J., Kim, H., Lee, W. G. and Cho, Y. K. (2011). Fully integrated lab-on-a-disc for simultaneous analysis of biochemistry and immunoassay from whole blood. *Lab Chip*, **11**, 70–8. DOI 10.1039/c0lc00205d

Lee, C. C., Sui, G. D., Elizarov, A., Shu, C. Y. J., Shin, Y. S., Dooley, A. N., Huang, J., Daridon, A., Wyatt, P., Stout, D., Kolb, H. C., Witte, O. N., Satyamurthy, N., Heath, J. R., Phelps, M. E., Quake, S. R. and Tseng, H. R. (2005). Multistep synthesis of a radiolabeled imaging probe using integrated microfluidics. *Science*, **310**, 1793–6. DOI 10.1126/science.1118919

Lee, K. G., Lee, T. J., Jeong, S. W., Choi, H. W., Heo, N. S., Park, J. Y., Park, T. J. and Lee, S. J. (2012). Development of a plastic-based microfluidic immunosensor chip for detection of H1N1 influenza. *Sensors*, **12**, 10810–19.

Lee, S. H., Lee, C. S., Kim, B. G. and Kim, Y. K. (2008). An integrated microfluidic chip for the analysis of biochemical reactions by MALDI mass spectrometry. *Biomed Microdevices*, **10**, 1–9. DOI 10.1007/s10544–007–9104–0

Lee, W. G., Kim, Y. G., Chung, B. G., Demirci, U. and Khademhosseini, A. (2010). Nano/Microfluidics for diagnosis of infectious diseases in developing countries. *Adv Drug Deliv Rev*, **62**, 449–57. DOI 10.1016/j.addr.2009.11.016

Lew, V., Nguyen, D. and Khine, M. (2011). Shrink-induced single-cell plastic microwell array. *J Lab Autom*, **16**, 450–6. DOI 10.1016/j.jala.2011.06.003

Li, A. P., Bode, C. and Sakai, Y. (2004). A novel in vitro system, the integrated discrete multiple organ cell culture (IdMOC) system, for the evaluation of human drug toxicity: comparative cytotoxicity of tamoxifen towards normal human cells from five major organs and MCF-7 adenocarcinoma breast cancer cells. *Chem Biol Interact*, **150**, 129–36. DOI 10.1016/j.cbi.2004.09.010

Li, X. J., Valadez, A. V., Zuo, P. and Nie, Z. (2012). Microfluidic 3D cell culture: potential application for tissue-based bioassays. *Bioanalysis*, **4**, 1509–25. DOI 10.1063/1.3687398

Lien, K. Y., Chuang, Y. H., Hung, L. Y., Hsu, K. F., Lai, W. W., Ho, C. L., Chou, C. Y. and Lee, G. B. (2010). Rapid isolation and detection of cancer cells by utilizing integrated microfluidic systems. *Lab Chip*, **10**, 2875–86. DOI 10.1039/c005178k

Lion, N., Reymond, F., Girault, H. H. and Rossier, J. S. (2004). Why the move to microfluidics for protein analysis? *Curr Opin Biotechnol*, **15**, 31–7. DOI 10.1016/j.copbio.2004.01.001

Liszewski, K. (2003). Broader uses for microfluidics technologies – Applications expand from drug discovery to battlefield. *Gen Eng News*, **23**, 66–7.

Liu, C., Liu, J., Gao, D., Ding, M. and Lin, J. M. (2010). Fabrication of microwell arrays based on two-dimensional ordered polystyrene microspheres for high-throughput single-cell analysis. *Anal Chem*, **82**, 9418–24. DOI 10.1021/ac102094r

Liu, C., Wang, L., Xu, Z., Li, J. M., Ding, X. P., Wang, Q. and Li, C. Y. (2012). A multilayer microdevice for cell-based high-throughput drug screening. *J Micromech Microeng*, **22**, 1–7. DOI 10.1088/0960–1317/22/6/065008

Livak-Dahl, E., Sinn, I. and Burns, M. (2011). Microfluidic chemical analysis systems. *Annu Rev Chem Biomol Eng*, **2**, 325–53. DOI 10.1146/annurev-chembioeng-061010–114215

Lok, K. S., Abdul Muttalib, S. Z., Lee, P. P., Kwok, Y. C. and Nguyen, N. T. (2012). Rapid determination of vitamin B12 concentration with a chemiluminescence lab on a chip. *Lab Chip*, **12**, 2353–61. DOI 10.1039/c2lc00037g

Lombardi, D. and Dittrich, P. S. (2010). Advances in microfluidics for drug discovery. *Exp Opin Drug Discov*, **5**, 1081–94. DOI 10.1517/17460441.2010.521149

Mabey, D., Peeling, R. W., Ustianowski, A. and Perkins, M. D. (2004). Diagnostics for the developing world. *Nat Rev Microbiol*, **2**, 231–40. DOI 10.1038/Nrmicro841

Macbeath, G. and Schreiber, S. L. (2000). Printing proteins as microarrays for high-throughput function determination. *Science*, **289**, 1760–63.

Makamba, H., Hsieh, Y. Y., Sung, W. C. and Chen, S. H. (2005). Stable permanently hydrophilic protein-resistant thin-film coatings on poly(dimethylsiloxane) substrates by electrostatic self-assembly and chemical cross-linking. *Anal Chem*, **77**, 3971–8. DOI 10.1021/ac0502706

Malmstadt, N., Nash, M. A., Purnell, R. F. and Schmidt, J. J. (2006). Automated formation of lipid-bilayer membranes in a microfluidic device. *Nano Lett*, **6**, 1961–5. DOI 10.1021/nl0611034

Manz, A., Graber, N. and Widmer, H. M. (1990). Miniaturized total chemical-analysis systems – a novel concept for chemical sensing. *Sens Actuators B Chem*, **1**, 244–48.

Mao, H., Yang, T. and Cremer, P. S. (2002). Design and characterization of immobilized enzymes in microfluidic systems. *Anal Chem*, **74**, 379–85.

Martinez-Navarro, J. F. (1990). Food poisoning related to consumption of illicit beta-agonist in liver. *Lancet*, **336**, 1311.

Martinez, A. W., Phillips, S. T., Butte, M. J. and Whitesides, G. M. (2007). Patterned paper as a platform for inexpensive, low-volume, portable bioassays. *Angew Chem Int Ed*, **46**, 1318–20. DOI 10.1002/anie.200603817

Martinez, A. W., Phillips, S. T., Carrilho, E., Thomas, S. W., 3rd, Sindi, H. and Whitesides, G. M. (2008a). Simple telemedicine for developing regions: camera phones and paper-based microfluidic devices for real-time, off-site diagnosis. *Anal Chem*, **80**, 3699–707. DOI 10.1021/ac800112r

Martinez, A. W., Phillips, S. T. and Whitesides, G. M. (2008b). Three-dimensional microfluidic devices fabricated in layered paper and tape. *Proc Natl Acad Sci U S A*, **105**, 19606–11. DOI 10.1073/pnas.0810903105

Martinez, A. W., Phillips, S. T., Wiley, B. J., Gupta, M. and Whitesides, G. M. (2008c). FLASH: a rapid method for prototyping paper-based microfluidic devices. *Lab Chip*, **8**, 2146–50. DOI 10.1039/b811135a

Maruyama, S., Hirayama, C., Abe, J., Tanaka, J. and Matsui, K. (1995). Chronic active hepatitis and liver cirrhosis in association with combined tamoxifen/tegafur adjuvant therapy. *Dig Dis Sci*, **40**, 2602–7.

Matsui, N., Kaya, T., Nagamine, K., Yasukawa, T., Shiku, H. and Matsue, T. (2006). Electrochemical mutagen screening using microbial chip. *Biosens Bioelectron*, **21**, 1202–9. DOI 10.1016/j.bios.2005.05.004

Mayer, M., Kriebel, J. K., Tosteson, M. T. and Whitesides, G. M. (2003). Microfabricated teflon membranes for low-noise recordings of ion channels in planar lipid bilayers. *Biophys J*, **85**, 2684–95.

Meagher, R. J. and Thaitrong, N. (2012). Microchip electrophoresis of DNA following preconcentration at photopatterned gel membranes. *Electrophoresis*, **33**, 1236–46. DOI 10.1002/elps.201100675

Mei, Q., Fredrickson, C. K., Simon, A., Khnouf, R. and Fan, Z. H. (2007). Cell-free protein synthesis in microfluidic array devices. *Biotechnol Prog*, **23**, 1305–11. DOI 10.1021/bp070133p

Miserere, S., Ledru, S., Ruille, N., Griveau, S., Boujtita, M. and Bedioui, F. (2006). Biocompatible carbon-based screen-printed electrodes for the electrochemical detection of nitric oxide. *Electrochem Commun*, **8**, 238–44. DOI 10.1016/j.elecom.2005.11.016

Mohammed, M. I. and Desmulliez, M. P. (2011). Lab-on-a-chip based immunosensor principles and technologies for the detection of cardiac biomarkers: a review. *Lab Chip*, **11**, 569–95. DOI 10.1039/c0lc00204f

Mohanty, S. P. and Kougianos, E. (2006). Biosensors: a tutorial review. *Potentials, IEEE*, **25**, 35–40. DOI 10.1109/mp.2006.1649009

Moran-Mirabal, J. M., Edel, J. B., Meyer, G. D., Throckmorton, D., Singh, A. K. and Craighead, H. G. (2005). Micrometer-sized supported lipid bilayer arrays for

bacterial toxin binding studies through total internal reflection fluorescence microscopy. *Biophys J*, **89**, 296–305. DOI 10.1529/biophysj.104.054346

Murakami, Y., Endo, T., Yamamura, S., Nagatani, N., Takamura, Y. and Tamiya, E. (2004). On-chip micro-flow polystyrene bead-based immunoassay for quantitative detection of tacrolimus (FK506). *Anal Biochem*, **334**, 111–6. DOI 10.1016/j.ab.2004.07.029

Muster, W., Breidenbach, A., Fischer, H., Kirchner, S., Muller, L. and Pahler, A. (2008). Computational toxicology in drug development. *Drug Discov Today*, **13**, 303–10. DOI 10.1016/j.drudis.2007.12.007

Nolan, J. P. and Sklar, L. A. (2002). Suspension array technology: evolution of the flat-array paradigm. *Trends Biotechnol*, **20**, 9–12.

Pampaloni, F., Reynaud, E. G. and Stelzer, E. H. K. (2007). The third dimension bridges the gap between cell culture and live tissue. *Nat Rev Mol Cell Biol*, **8**, 839–45. DOI 10.1038/Nrm2236

Park, J., Sunkara, V., Kim, T. H., Hwang, H. and Cho, Y. K. (2012). Lab-on-a-disc for fully integrated multiplex immunoassays. *Anal Chem*, **84**, 2133–40. DOI 10.1021/ac203163u

Perrin, D., Fremaux, C. and Scheer, A. (2006). Assay development and screening of a serine/threonine kinase in an on-chip mode using caliper nanofluidics technology. *J Biomol Screen*, **11**, 359–68. DOI 10.1177/1087057106286653

Peterson, D. S. (2005). Solid supports for micro analytical systems. *Lab Chip*, **5**, 132–9. DOI 10.1039/b405311g

Pregibon, D. C., Toner, M. and Doyle, P. S. (2007). Multifunctional encoded particles for high-throughput biomolecule analysis. *Science*, **315**, 1393–6. DOI 10.1126/science.1134929

Puckett, L. G., Dikici, E., Lai, S., Madou, M., Bachas, L. G. and Daunert, S. (2004). Investigation into the applicability of the centrifugal microfluidics development of protein-platform for the ligand binding assays incorporating enhanced green fluorescent protein as a fluorescent reporter. *Anal Chem*, **76**, 7263–8. DOI 10.1021/Ac049758h

Quinton, D., Girard, A., Thi Kim, L. T., Raimbault, V., Griscom, L., Razan, F., Griveau, S. and Bedioui, F. (2011). On-chip multi-electrochemical sensor array platform for simultaneous screening of nitric oxide and peroxynitrite. *Lab Chip*, **11**, 1342–50. DOI 10.1039/c0lc00585a

Qureshi, Z. P., Seoane-Vazquez, E., Rodriguez-Monguio, R., Stevenson, K. B. and Szeinbach, S. L. (2011). Market withdrawal of new molecular entities approved in the United States from 1980 to 2009. *Pharmacoepidemiol Drug Saf*, **20**, 772–7. DOI 10.1002/pds.2155

Razumovitch, J., Meier, W. and Vebert, C. (2009). A microcontact printing approach to the immobilization of oligonucleotide brushes. *Biophys Chem*, **139**, 70–4. DOI 10.1016/j.bpc.2008.10.005

Rettig, J. R. and Folch, A. (2005). Large-scale single-cell trapping and imaging using microwell arrays. *Anal Chem*, **77**, 5628–34. DOI 10.1021/Ac0505977

Rodríguez-Dévora, J. I., Zhang, B., Reyna, D., Shi, Z. D. and Xu, T. (2012). High throughput miniature drug-screening platform using bioprinting technology. *Biofabrication*, 1–8.

Sahoo, H. R., Kralj, J. G. and Jensen, K. F. (2007). Multistep Continuous-Flow Microchemical Synthesis Involving Multiple Reactions and Separations. *Angew Chem Int Ed*, **46**, 5704–8. DOI 10.1002/anie.200701434

Sandison, M. E., Zagnoni, M. and Morgan, H. (2007). Air-exposure technique for the formation of artificial lipid bilayers in microsystems. *Langmuir*, **23**, 8277–84. DOI 10.1021/la7007528

Schuler, T., Asmus, T., Fritzsche, W. and Moller, R. (2009). Screen printing as cost-efficient fabrication method for DNA-chips with electrical readout for detection of viral DNA. *Biosens Bioelectron*, **24**, 2077–84. DOI 10.1016/j.bios.2008.10.028

Schulze, M. and Belder, D. (2012). Poly(ethylene glycol)-coated microfluidic devices for chip electrophoresis. *Electrophoresis*, **33**, 370–8. DOI 10.1002/elps.201100401

Service, R. F. (1995). Chemistry – radio tags speed compound synthesis. *Science*, **270**, 577.

Shen, J., Zhou, Y., Lu, T., Peng, J., Lin, Z., Huang, L., Pang, Y., Yu, L. and Huang, Y. (2012). An integrated chip for immunofluorescence and its application to analyze lysosomal storage disorders. *Lab Chip*, **12**, 317–24. DOI 10.1039/c1lc20845d

Sheng, J., Zhang, L., Lei, J. and Ju, H. (2012). Fabrication of tunable microreactor with enzyme modified magnetic nanoparticles for microfluidic electrochemical detection of glucose. *Anal Chim Acta*, **709**, 41–6. DOI 10.1016/j.aca.2011.10.008

Shi, J., Yang, T. and Cremer, P. S. (2008). Multiplexing ligand-receptor binding measurements by chemically patterning microfluidic channels. *Anal Chem*, **80**, 6078–84. DOI 10.1021/ac800912f

Shiddiky, M. J. A. and Shim, Y. B. (2007). Trace analysis of DNA: Preconcentration, separation, and electrochemical detection in microchip electrophoresis using Au nanoparticles. *Anal Chem*, **79**, 3724–33. DOI 10.1021/Ac0701177

Sikanen, T., Aura, S., Franssila, S., Kotiaho, T. and Kostiainen, R. (2012). Microchip capillary electrophoresis-electrospray ionization-mass spectrometry of intact proteins using uncoated Ormocomp microchips. *Anal Chim Acta*, **711**, 69–76. DOI 10.1016/j.aca.2011.10.059

Smith, C. (2007). Tools for drug discovery: tools of the trade. *Nature*, **446**, 219–22. DOI 10.1038/446219a

Srinivasan, V., Pamula, V. K. and Fair, R. B. (2004). An integrated digital microfluidic lab-on-a-chip for clinical diagnostics on human physiological fluids. *Lab Chip*, **4**, 310–15. DOI 10.1039/b403341h

Sui, G., Wang, J., Lee, C. C., Lu, W., Lee, S. P., Leyton, J. V., Wu, A. M. and Tseng, H. R. (2006). Solution-phase surface modification in intact poly(dimethylsiloxane) microfluidic channels. *Anal Chem*, **78**, 5543–51. DOI 10.1021/ac060605z

Sung, J. H. and Shuler, M. L. (2009). A micro cell culture analog (microCCA) with 3-D hydrogel culture of multiple cell lines to assess metabolism-dependent cytotoxicity of anti-cancer drugs. *Lab Chip*, **9**, 1385–94. DOI 10.1039/b901377f

Suzuki, H., Tabata, K., Kato-Yamada, Y., Noji, H. and Takeuchi, S. (2004). Planar lipid bilayer reconstitution with a micro-fluidic system. *Lab Chip*, **4**, 502–5. DOI 10.1039/b405967k

Suzuki, H., Tabata, K. V., Noji, H. and Takeuchi, S. (2006). Highly reproducible method of planar lipid bilayer reconstitution in polymethyl methacrylate microfluidic chip. *Langmuir*, **22**, 1937–42. DOI 10.1021/La052534p

Suzuki, H., Tabata, K. V., Noji, H. and Takeuchi, S. (2007). Electrophysiological recordings of single ion channels in planar lipid bilayers using a polymethyl methacrylate microfluidic chip. *Biosens Bioelectron*, **22**, 1111–15. DOI 10.1016/j.bios.2006.04.013

Szita, N., Boccazzi, P., Zhang, Z. Y., Boyle, P., Sinskey, A. J. and Jensen, K. F. (2005). Development of a multiplexed microbioreactor system for high-throughput bioprocessing. *Lab Chip*, **5**, 819–26. DOI 10.1039/B504243g

Tang, C. K., Vaze, A. and Rusling, J. F. (2012). Fabrication of immunosensor microwell arrays from gold compact discs for detection of cancer biomarker proteins. *Lab Chip*, **12**, 281–6. DOI 10.1039/c1lc20833k

Tatosian, D. A. and Shuler, M. L. (2009). A novel system for evaluation of drug mixtures for potential efficacy in treating multidrug resistant cancers. *Biotechnol Bioeng*, **103**, 187–98. DOI 10.1002/bit.22219

Terstappen, G. C., Schlupen, C., Raggiaschi, R. and Gaviraghi, G. (2007). Target deconvolution strategies in drug discovery. *Nat Rev Drug Discov*, **6**, 891–903. DOI 10.1038/nrd2410

Thorsen, T. A. (2004). Microfluidic tools for high-throughput screening. *Biotechniques*, **36**, 197–9.

Um, E., Rha, E., Choi, S. L., Lee, S. G. and Park, J. K. (2012). Mesh-integrated microdroplet array for simultaneous merging and storage of single-cell droplets. *Lab Chip*, **12**, 1594–7. DOI 10.1039/c2lc21266h

Vaino, A. R. and Janda, K. D. (2000). Euclidean shape-encoded combinatorial chemical libraries. *Proc Natl Acad Sci U S A*, **97**, 7692–6.

Van Midwoud, P. M., Groothuis, G. M. M., Merema, M. T. and Verpoorte, E. (2010). Microfluidic biochip for the perifusion of precision-cut rat liver slices for metabolism and toxicology studies. *Biotechnol Bioeng*, **105**, 184–94. DOI 10.1002/Bit.22516

Wadhwa, A., Foote, R. S., Shaw, R. W. and Eda, S. (2012). Bead-based microfluidic immunoassay for diagnosis of Johne's disease. *J Immunol Methods*, **382**, 196–202. DOI 10.1016/j.jim.2012.06.006

Wan, Y., Deng, W., Su, Y., Zhu, X., Peng, C., Hu, H., Peng, H., Song, S. and Fan, C. (2011). Carbon nanotube-based ultrasensitive multiplexing electrochemical immunosensor for cancer biomarkers. *Biosens Bioelectron*, **30**, 93–9. DOI 10.1016/j.bios.2011.08.033

Wang, J., Bao, N., Paris, L. L., Wang, H. Y., Geahlen, R. L. and Lu, C. (2008). Detection of kinase translocation using microfluidic electroporative flow cytometry. *Anal Chem*, **80**, 1087–93. DOI 10.1021/Ac702065e

Wang, J., Ibanez, A. and Chatrathi, M. P. (2003). On-chip integration of enzyme and immunoassays: simultaneous measurements of insulin and glucose. *J Am Chem Soc*, **125**, 8444–5. DOI 10.1021/ja036067e

Wang, L., Yang, P., Li, Y. X., Chen, H. Q., Li, M. G. and Luo, F. B. (2007). A flow injection chemiluminescence method for the determination of fluoroquinolone derivative using the reaction of luminol and hydrogen peroxide catalyzed by gold nanoparticles. *Talanta*, **72**, 1066–72. DOI 10.1016/j.talanta.2006.12.050

Wang, Y., Shah, P., Phillips, C., Sims, C. E. and Allbritton, N. L. (2012). Trapping cells on a stretchable microwell array for single-cell analysis. *Anal Bioanal Chem*, **402**, 1065–72. DOI 10.1007/s00216–011–5535–9

Wartelle, C., Schuhmann, W., Blochl, A. and Bedioui, F. (2005). Integrated compact biocompatible hydrogel-based amperometric sensing device for easy screening of drugs involved in nitric oxide production by adherent cultured cells. *Electrochim Acta*, **50**, 4988–4994. DOI 10.1016/j.electacta.2004.12.048

Wen, Y. and Yang, S. T. (2008). The future of microfluidic assays in drug development. *Exp Opin Drug Discov*, **3**, 1237–53. DOI 10.1517/17460440802434510

Wen, Y., Zhang, X. and Yang, S. T. (2012). Medium to high throughput screening: microfabrication and chip-based technology. *Adv Exp Med Biol*, **745**, 181–209. DOI 10.1007/978–1–4614–3055–1_11

Whitesides, G. M. (2003). The 'right' size in nanobiotechnology. *Nat Biotechnol*, **21**, 1161–5. DOI 10.1038/nbt872

Whitesides, G. M. (2006). The origins and the future of microfluidics. *Nature*, **442**, 368–73. DOI 10.1038/nature05058

Won, S. Y., Chandra, P., Hee, T. S. and Shim, Y. B. (2012). Simultaneous detection of antibacterial sulfonamides in a microfluidic device with amperometry. *Biosens Bioelectron*, **39**, 204–9. DOI 10.1016/j.bios.2012.07.043

Wu, H., Wheeler, A. and Zare, R. N. (2004). Chemical cytometry on a picoliter-scale integrated microfluidic chip. *Proc Natl Acad Sci U S A*, **101**, 12809–13. DOI 10.1073/pnas.0405299101

Wu, M. H., Huang, S. B. and Lee, G. B. (2010). Microfluidic cell culture systems for drug research. *Lab Chip*, **10**, 939–56. DOI 10.1039/b921695b

Wu, N., Oakeshott, J. G., Easton, C. J., Peat, T. S., Surjadi, R. and Zhu, Y. (2011). A double-emulsion microfluidic platform for in vitro green fluorescent protein expression. *J Micromech Microeng*, **21**, 1–7. DOI 10.1088/0960–1317/21/5/054032

Xu, Y., Little, M. W. and Murray, K. K. (2006). Interfacing capillary gel microfluidic chips with infrared laser desorption mass spectrometry. *J Am Soc Mass Spectrom*, **17**, 469–74. DOI 10.1016/j.jasms.2005.12.003

Xue, Q., Wainright, A., Gangakhedkar, S. and Gibbons, I. (2001). Multiplexed enzyme assays in capillary electrophoretic single-use microfluidic devices. *Electrophoresis*, **22**, 4000–7.

Yager, P., Edwards, T., Fu, E., Helton, K., Nelson, K., Tam, M. R. and Weigl, B. H. (2006). Microfluidic diagnostic technologies for global public health. *Nature*, **442**, 412–8. DOI 10.1038/Nature05064

Yamada, M., Sugaya, S., Naganuma, Y. and Seki, M. (2012). Microfluidic synthesis of chemically and physically anisotropic hydrogel microfibers for guided cell growth and networking. *Soft Matter*, **8**, 3122–30. DOI 10.1039/C2sm07263g

Yan, M., Zang, D., Ge, S., Ge, L. and Yu, J. (2012). A disposable electrochemical immunosensor based on carbon screen-printed electrodes for the detection of prostate specific antigen. *Biosens Bioelectron*, **38**, 355–61. DOI 10.1016/j.bios.2012.06.019

Yeo, L. Y., Chang, H. C., Chan, P. P. and Friend, J. R. (2011). Microfluidic devices for bioapplications. *Small*, **7**, 12–48. DOI 10.1002/smll.201000946

Yeo, L. Y., Friend, J. R., Mcintosh, M. P., Meeusen, E. N. T. and Morton, D. a. V. (2010). Ultrasonic nebulization platforms for pulmonary drug delivery. *Exp Opin Drug Deliv*, **7**, 663–79. DOI 10.1517/17425247.2010.485608

Yin, H. B., Pattrick, N., Zhang, X. L., Klauke, N., Cordingley, H. C., Haswell, S. J. and Cooper, J. M. (2008). Quantitative comparison between microfluidic and microtiter plate formats for cell-based assays. *Anal Chem*, **80**, 179–85.

Zagnoni, M. (2012). Miniaturised technologies for the development of artificial lipid bilayer systems. *Lab Chip*, **12**, 1026–39. DOI 10.1039/c2lc20991h

Zhang, C. and Van Noort, D. (2011). Cells in microfluidics. *Top Curr Chem*, **304**, 295–321. DOI 10.1007/128_2011_147

Zhou, X., Cai, S., Hong, A., You, Q., Yu, P., Sheng, N., Srivannavit, O., Muranjan, S., Rouillard, J. M., Xia, Y., Zhang, X., Xiang, Q., Ganesh, R., Zhu, Q., Matejko, A., Gulari, E. and Gao, X. (2004). Microfluidic PicoArray synthesis of oligodeoxynucleotides and simultaneous assembling of multiple DNA sequences. *Nucleic Acids Res*, **32**, 5409–17. DOI 10.1093/nar/gkh879

Zubair, A., Burbelo, P. D., Vincent, L. G., Iadarola, M. J., Smith, P. D. and Morgan, N. Y. (2011). Microfluidic LIPS for serum antibody detection: demonstration of a rapid test for HSV-2 infection. *Biomed Microdevices*, **13**, 1053–62. DOI 10.1007/s10544–011–9575-x

8

Microfluidic devices for cell manipulation

H. O. FATOYINBO, University of Surrey, UK

DOI: 10.1533/9780857097040.3.283

Abstract: This chapter discusses issues relating to the processing of biological cells in microfluidic channels and the different techniques available to manipulate cells in microfluidic systems. Broadly classified into electrical, hydrodynamic, optical, magnetic and acoustic mechanisms, the forces acting on micrometre-sized particles and current technological developments as applied to cells will be presented. Recent technological advances in cancer research, based on microfluidic devices, will be addressed to illustrate the potential of these new microsystems as powerful diagnostic tools, particularly when multiple technologies are combined to complement each other in engineering the next generation of miniaturised medical diagnostic devices.

Key words: micromanipulation, cancer, microfluidics, microenvironment, lab on a chip.

8.1 Introduction

Since the concept of microfluidic systems in the late 1970s (Terry *et al.*, 1979), a range of microfluidic systems incorporating physical, electrical and bio/chemical elements performing μ-processes on biological cells have been engineered, and are generally referred to as laboratories-on-a-chip (LOC) or bio-microelectromechanical (BioMEMS) systems (Manz *et al.*, 1990; Reyes *et al.*, 2002).

In this chapter some key issues relating to cell behaviour within microfluidic systems, including the *in vitro* cellular microenvironment, flow regimes and considerations of channel networks will be discussed. Within these systems, microscale technologies engineered to act on particles dispersed in microflows can be classified in to electrical, hydrodynamic, optical, magnetic and acoustic mechanisms. These forces acting on particles and current technological developments for processes such as separation, characterisation, focusing and trapping will be addressed. Finally, there is an overview of these technologies applied in cancer research, i.e., flow through operations and detection, with a general outlook for future trends in applications and system development will be explored.

8.1.1 Key issues

The significant reduction in system dimensions has a positive effect on performance, as characterised by various dimensionless numbers (Table 8.1), offering increased throughput and mass parallelisation of on-chip processes such as cell culturing and cellular bioassays. To tackle various issues such as system designs for biocompatibility, efficiency and cost effectiveness, enhanced understanding of biological processes by engineers, and approaches for standardisation and system integration of modular

Table 8.1 Dimensionless numbers commonly encountered in analysis of microfluidic systems

Name	Notation	Ratio	Description	Equation
Reynolds	Re	$\frac{\rho u D_h}{\mu}$	$\frac{\text{Inertial}}{\text{viscous}}$	[8.1]
Péclet	Pe	$\frac{D_h u}{D}$	$\frac{\text{convection}}{\text{diffusion}}$	[8.2]
Weissenberg	Wi	$\tau_p \dot{\gamma}$	shear rate × relax.time	[8.3]
Deborah	De	$\frac{\tau_p}{\tau_{\text{flow}}}$	$\frac{\text{relax.time}}{\text{flow time}}$	[8.4]
Dean	Dn	$\text{Re}\left(\frac{D_h}{2r}\right)^{1/2}$	$\frac{\text{transverse flow}}{\text{longitudinal flow}}$	[8.5]
Elasticity	El	$\frac{\tau_p \mu}{\rho r^2}$	$\frac{\text{elastic effects}}{\text{inertial effects}}$	[8.6]
Knudsen	Kn	$\frac{L_p}{L}$	$\frac{\text{mean free path}}{\text{length}}$	[8.7]
Raleigh	Ra	$\frac{u_b D_h}{D}$	Pe for buoyant flow	[8.8]
Grashof	Gr	$\frac{\rho u_b D_h}{\mu}$	Re for buoyant flow	[8.9]
Capillary	Ca	$\frac{\mu u}{\gamma}$	$\frac{\text{viscous}}{\text{interfacial}}$	[8.10]
Weber	We	$\frac{\rho u^2 r}{\gamma}$	$\frac{\text{inertial}}{\text{surface tension}}$	[8.11]
Stokes	N_{St}	$\frac{\mu u}{\rho g D_h^2}$	$\frac{\text{viscous}}{\text{gravitational}}$	[8.12]
Poiseuille	Po	$\frac{r^2 \Delta P}{\mu L u}$	$\frac{\text{pressure}}{\text{viscous}}$	[8.13]

components, an interdisciplinary approach is required amongst physicians, scientists and engineers.

8.2 Microenvironment on cell integrity

The ability for biological cells to maintain their functionality in vitro is critical for accurate cell based processes. A good understanding of cell properties and factors which can contribute to cellular damage in microfluidic systems is needed in order to fabricate systems for long-term cell survival.

8.2.1 Cell structure and function

Biological cells are the functional unit of all living organisms classified as either prokaryotic or eukaryotic (Alberts *et al.*, 1994). Structurally, they typically consist of an internal fluidic compartment (i.e., cytoplasm) dispersed with microscopic organs – organelles (e.g., cytoskeleton, mitochondria, ribosomes, etc.) of varying functional roles that maintain both internal and external microenvironments through a range of biological activities (e.g., cellular respiration, DNA replication, biochemical signalling and protein synthesis). A semi-permeable membrane surrounding the cytoplasm consists primarily of adjacent phospholipids – a hydrophilic phosphate head and two hydrophobic glyceride tails. Phospholipid heads are in contact with either the cytoplasm or the extracellular matrix (ECM), while the diglyceride tails are repelled from the cytoplasm and ECM forming the main hydrophobic region of the two-layered structure commonly referred to as the lipid bilayer. Other biological constituents of a cell membrane include ion channels, surface receptors, aquaporins, enzymes and hormones, which all play vital roles in regulating cellular activity and structural integrity.

8.2.2 External stresses on cells

In some cell types (e.g., bacteria, fungi), a cell wall is present representing an additional structural boundary on the outer side of the cell membrane, offering rigidity and protection to mechanical stresses. For example, the cell wall of bacteria is made of peptidoglycans of varying thicknesses (10–80 nm) essential to their survival with a high (90%) or low (10%) presence of peptidoglycan signifying its' positive or negative Gram strain, respectively. Yeast cells (e.g., *S. cerevisiae*) by comparison are the most common cell model for biologists in life science research, and have been extensively studied down to the molecular level revealing the cell wall as a highly adaptable organelle (Klis *et al.*, 2006). It has four major functions: (1) stabilisation of internal osmotic conditions, (2) physical stress protection, (3) maintaining cell shape, a pre-condition of morphogenesis, and (4) scaffold for proteins, limiting the permeability of the cell

wall to macromolecules. Physiological adaptation to changes in environmental conditions have been attributed to membrane-spanning mechanosensors detecting perturbations in the cell wall and/or plasma membrane, initiating a *cell wall integrity* (CWI) signal transduction pathway to induce gene expression for products involved in cell wall structure and remodelling (Jendretzki *et al.*, 2011). Similar transduction pathways feature in all cells, with any mutation in their component frequently associated with a type of cancer (Kim and Choi, 2010). In general, all ECMs, including fungal and bacterial cell walls, consist of proteins and polysaccharides, highly variable between taxonomic groups, providing signalling cues to cells to adjust their biophysical properties based on the external stresses placed upon them.

Mammalian cells bathed in various iso-osmotic solutions, possess a selectively permeable plasma membrane (~10 nm in thickness) as their outer barrier, with a resting voltage potential ranging between –100 and +5 mV. This membrane potential arises due to the fact that the cytoplasm of most cells is more negative with respect to the ECM or its external microenvironment (Jackson, 2006). Concentration of potassium ions along with negatively charged proteins and phosphate ions is higher inside the cell than outside, while sodium and chloride ions are more abundant outside the cell than inside. This microenvironment condition creates an electrochemical gradient across the cell membrane which is constantly regulated by ion channels to restore homeostasis. Changes in external salinity or osmolality, detected by osmosensors have been found to initiate signalling pathways to alter the rate of protein synthesis, cell volume and intracellular electrolyte concentrations in response (Kultz and Chakravarty, 2001). It was shown that excessive osmotic stresses on mammalian kidney cells also caused cell cycle interference and genomic damage.

Red blood cells (RBC) are *specialised* anucleated biconcave cells, ~8 μm in diameter and ~2 μm in thickness at rest (Guido and Tomaiuolo, 2009); when transported under pressure in microfluidic channels smaller in size than the cells themselves, they are physiologically suited to a high degree of mechanical stresses and the protein spectrin makes it flexible, allowing it to deform so as to exit capillaries and enter the ECM (Barshtein *et al.*, 2007). Osmotic deviations to normal physiological saline conditions (~0.9% NaCl) cause RBCs to swell (haemolysis) in hypotonic solutions, or shrink (crenate) in hypertonic solutions. This situation, 'osmotic shock', can arise with all mammalian cell types when removed from their normal environment and placed within microfluidic systems of inadequate media formulations. Phenotypic change in an endothelial cell line was found to be a result of shifts in osmolarity due to water evaporation in a microfluidic cell culture platform, while it has been reported that microsystems in which a fluid–air interface exists (e.g., electrowetting on dielectric (EWOD), nanovial arrays or passive pumping) have significant evaporation and loss of fluid volume issues (Heo *et al.*, 2006; Berthier *et al.*, 2008).

8.3 Microscale fluid dynamics

Many classical macroscale fluid dynamic relationships can be scaled down accurately describing flow properties of solids at the microscale. Furthermore, a range of physical phenomena present themselves which are either more influential at the microscale or absent at the macroscale. In this section a brief overview of some important hydrodynamic theory in microchannels for biological fluids is given. For a more comprehensive analysis refer to (Gad-el-Hak, 2001; Beebe *et al.*, 2002; Stone *et al.*, 2004; Squires and Quake, 2005).

8.3.1 Dimensionless numbers

Dimensionless numbers reduce the number of variables that describe a system, thereby reducing the amount of experimental data required to make correlations of physical phenomena to scalable systems. The most common dimensionless group in fluid dynamics is the *Reynolds number* (Re), named after Osborne Reynolds who published a series of papers describing flow in pipes (Reynolds, 1883). It represents the ratio of inertial forces to viscous forces (Equation [8.1]), where ρ is the fluid density, u is average fluid velocity, D_h is cross-sectional length of the system, and μ is the dynamic fluid viscosity.

Gravesen *et al.* (1993) indicated that flow regimes within 32 different microfluidic devices analysed were not simply laminar or turbulent but had a transitional Reynolds number, $\mathrm{Re}_t = 30 \times (L/D_h)$, accounting for flow development, varying as a function of entrance length (L) and the hydraulic diameter (D_h). The three regimes described were based on differences in pressure drops due to inertial forces and viscous forces. Large length to hydraulic diameter ratios, greater than 70, give $\mathrm{Re}_t > 2300$, although since none of the microsystems operated in fully developed turbulent regimes ($\mathrm{Re} \approx 4000$) the value had little significance. Typically, as a system is scaled down the influences of inertial forces decreases, while viscous forces become more dominant. Thus, microflows are generally characterised as laminar, with transitions to turbulent flow ($\mathrm{Re} \geq 2300$) rarely developing (Brody *et al.*, 1996; Schulte *et al.*, 2002). Table 8.1 defines some other common dimensionless numbers used in describing Newtonian and non-Newtonian fluid characteristics in microfluidic systems (Ruzicka, 2008).

8.3.2 Properties of biofluids

The viscosity of a fluid is related to the fluid's resistance to motion and can be determined by relating shear force and velocity gradients in a flowing fluid as described by Newton's law of viscosity (Equation [8.14]), where shear stress (τ) is defined as force per unit area, $\dot{\gamma}$ is the shear rate ($= \mathrm{d}u/\mathrm{d}y$) and μ is the proportionality constant or viscosity.

$$\tau = -\mu \dot{\gamma} \quad [8.14]$$

Biological fluids are classified as non-Newtonian fluids (i.e., pseudoplastic) and their viscosity is dependent on the shear rate and shear stress ratio of the fluid. These are characterised by the power law (Equation [8.15]), where K is the consistency index and n is the flow behaviour index.

$$\tau = K\left(\dot{\gamma}\right)^{n} \quad [8.15]$$

The parameters characterise the rheology of power law fluids; when $n = 1$ the fluid type is Newtonian; $n > 1$ corresponds to dilatants; and $n < 1$ corresponds to pseudoplastics with an apparent viscosity (μ_a) that increases or decreases, respectively, with increasing shear rate. Fahraeus and Lindqvist (1931) first reported the dependence of haematocrit (~40% v/v) and relative apparent viscosity on tube radius. Subsequently, characterising the flow behaviour of RBCs in microcapillaries indicated that physical parameters such as velocity and thickness of suspending medium separating tube wall from the cell (dependent on pressure drop, capillary diameter and RBC volume fraction) all influence the RBC's shape deformation in flow (Zharov *et al.*, 2006).

Media solutions bathing cells typically consist of ions, proteins, carbohydrates, gases, etc., making fluid viscosities and conductivities (σ_m = ~1.5 S m^{-1}) extremely high. Experiments conducted in microfluidic systems for cell manipulation tend to deviate away from the ideal suspension mixture in favour of less viscous, Newtonian solutions (i.e., aqueous solutions), ensuring (1) resistance to fluid flow and (2) saturation of technological limits are minimised. As microfluidic networks and on-chip mixing/dilutions of fluids become more complex, and deviations in hydrodynamic resistance as a result of viscosity changes manifest (Pipe and McKinley, 2009), considerations of microfluidic geometries, interfaces and integrated components need to be factored into the design process from the outset.

8.3.3 Flow dynamics in microchannels

Common methods for flow actuation within microsystems are pressure or electrokinetically driven (Stroock and Whitesides, 2003; Trietsch *et al.*, 2011). For an incompressible fluid, the equivalent of Newton's second law ($F = ma$), can be represented by the Navier–Stokes equation (Equation [8.16]) where u is the velocity field (m s^{-1}), P is pressure (Pa) and F_b represents

external body forces acting on the bulk fluid, per unit volume (e.g., ρg, magnetic, electric potential, etc.).

$$-\nabla P + \mu\nabla^2 u + F_b = \underbrace{\rho\frac{\partial u}{\partial t}}_{\text{local}} + \underbrace{\rho u \bullet \nabla u}_{\text{convective}} \qquad [8.16]$$

Microflows predominantly fall within the laminar region (Re < 1), so the non-linear convective term in Equation [8.16] can be neglected, along with the body forces, leaving the Stokes equation for predictable linear flow in a channel (White, 1994).

$$\rho\frac{\partial u}{\partial t} = -\nabla P + \mu\nabla^2 u \qquad [8.17]$$

Applying the mass continuity equation for incompressible fluid flow, i.e., $\nabla \bullet u = 0$, we get a linear equation in which flow is determined by pressure at low Re, with variation in pressure in the X-direction of the channel only (Brody *et al.*, 1996).

$$\mu\nabla^2 u = \frac{\mathrm{d}P}{\mathrm{d}X} \qquad [8.18]$$

Steady-state flow away from the microchannel entrance, where height (h) << width (w) and length (l), is axial across the channel height (Fig. 8.1). Applying no-slip boundary conditions (i.e., $u = 0$), flow under pressure is described by Equation [8.19]. Known as Poiseuille profile flow, it has a constant negative curvature and a maximum velocity ($u_{\max}$) at $y = 0$.

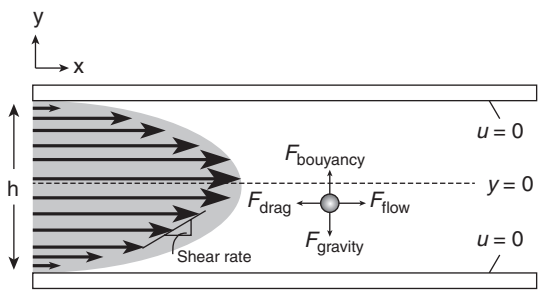

8.1 Parabolic flow profile within a microfluidic channel, where $h << w$. The gradient of the profile shows the shear rate, proportional to the fluid's viscosity influencing the general forces acting on a spherical particle within the flow field.

$$u = -\frac{\mathrm{d}P}{\mathrm{d}x}\frac{h^2}{2\mu}\left(1-\frac{y^2}{h^2}\right) \quad [8.19]$$

For circular channels, the average velocity, $\bar{u} = Q/A$, where Q is volumetric flow rate ($m^3\ s^{-1}$) and A is cross-sectional area of the channel (m^2), is often taken. Assuming no-slip conditions at the tube wall, i.e., $r = 0$ and $u = 0$, for fully developed laminar parabolic flow with a maximum velocity found at the centre, the volumetric flow rate is,

$$Q = \frac{1}{2}u_{\max}\pi R^2 = \frac{\pi R^4}{8\mu}\left[-\frac{\mathrm{d}}{\mathrm{d}X}(P+\rho gz)\right] \quad [8.20]$$

Equation [8.20] describes Hagen–Poiseuille flow, allowing for a fluid's resistance (R_H) to flow to be described in terms of pressure drop (ΔP) for circular channels, assuming $z = 0$, i.e., horizontal channel.

$$\Delta P = \frac{8\mu L\mathrm{Q}}{\pi R^4} = \mathrm{Q}R_H \quad [8.21]$$

Rectangular microchannels with aspect ratios ($\alpha = w/h$) where the channel width is larger than the height (i.e., $w > h$), have flows characterised as Hele–Shaw flow (Equation [8.22]). The flow profile remains parabolic along h, but as α increases, the average velocity over the channel width becomes increasingly plug-like.

$$\Delta P = \frac{12\mu LQ}{wh^3} = QR_H \quad [8.22]$$

For microchannels where $w < h$, Equation [8.22] is modified to Equation [8.23], which gives a less than 0.3% error for $\alpha < 1$ and Re < 1000 (Cornish, 1928; Beebe *et al.*, 2002; Fuerstman *et al.*, 2007).

$$\Delta P = \frac{12\mu L\mathrm{Q}}{wh^3}\times\left[1-\frac{0.63h}{w}\tanh\left(\frac{\pi \mathrm{w}}{2h}\right)\right]^{-1} \quad [8.23]$$

If α is unity, for a given cross-sectional area the maximum flow for a given pressure difference will exist and can be approximated to:

$$\Delta P = \frac{32\mu LQ}{h^4} \quad [8.24]$$

From Equations [8.21]–[8.24] we can see that pressure drops in microfluidic systems are influenced by (i) the volumetric flow rate, and (ii) the fluid's resistance to flow, quantities influenced by the geometry of the microchannel.

8.3.4 System design and operation

Computer aided simulation of physical phenomena is a useful tool in design optimisation of microfluidic devices, though experimental evaluation is still performed using test particles such as commercially available nano- or micropolystyrene beads. Rapid prototyping for inexpensive microfluidic systems through techniques such as soft lithography (Zhao *et al*., 1997; Whitesides *et al*., 2001), multilayer soft lithography (Quake and Scherer, 2000; Unger *et al*., 2000), cofabrication of multicomponent microsystems (Siegel *et al*., 2009) and maskless writing (Do *et al*., 2011) have had a significant impact in fabricating complex but cheap microfluidic systems, integrated with various elements required to manipulate particles.

Complex microfluidic networks

In pressure-driven laminar flow, the hydraulic-electric circuit analogy concept has been reported as a useful method for analysing and designing complex microfluidic network systems (i.e., multiple combining or branching microchannels at a node), based solely on channel dimensions and geometry (Kim *et al*., 2006; Oh *et al*., 2012). The relationship between voltage, current, resistance and conductor length in electrical circuits can be easily translated to microfluidic circuits between pressure, flow, hydraulic resistance and channel length, respectively. In systems where fluid mixing is relatively slow and the Pe number is quite large, a boundary between the streams will develop. Figure 8.2a shows a flow fraction-dependent microfluidic network, where the flow ratio of two incoming streams (Q_1 and Q_2) can be used to predict the boundary width (w) of a fully developed laminar flow a distance ($I \approx w \times \mathrm{Re}$) away from the channel node, possessing a parabolic velocity flow profile. The fractional areas (S_1, S_2) of the parabolic profile are proportional to the volumetric flow rate of each incoming stream. In high aspect ratio microchannels the pressure-driven flow velocity is independent of the position across the channel width, with an approximation to the boundary width realised from analysis of the ratio of incoming or outgoing volumetric flow rates (Equation [8.25]) as depicted in Fig. 8.2b. Figure 8.2c shows the equivalent electric circuit of Fig. 8.2a.

$$\frac{w_1}{w_2} = \frac{Q_1}{Q_2} \quad \text{or} \quad \frac{w_3}{w_4} = \frac{Q_3}{Q_4} \qquad [8.25]$$

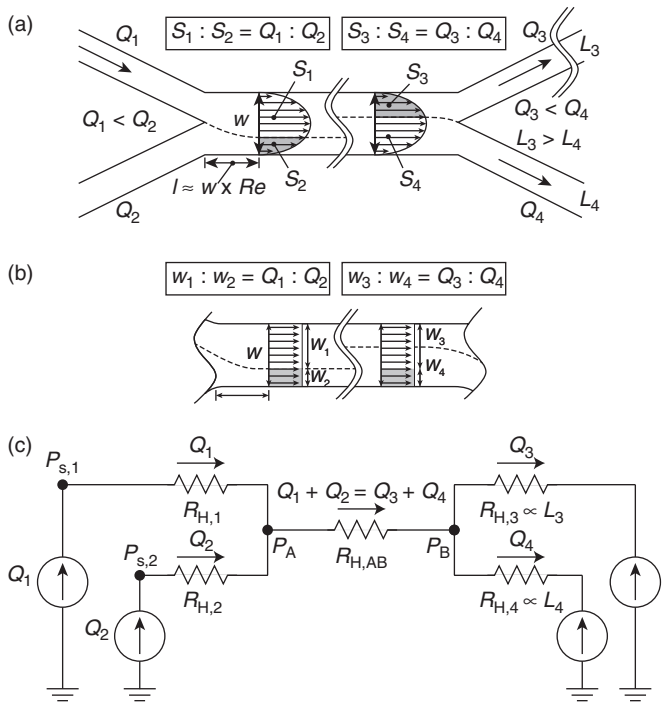

8.2 Schematic of a typical flow fraction-dependent microfluidic network when $Q_1 > Q_2$ and $Q_3 < Q_4$. There exists a boundary (dotted lines) between the two incoming streams or the two outgoing streams. (a) 2D model (e.g., parabolic flow profile) to estimate the boundary width. The partial areas of the parabola (S_1 and S_2, or S_3 and S_4) are proportional to the volumetric flow rates of each stream (Q_1 and Q_2, or Q_3 and Q_4). (b) 1D model (e.g., flat flow profile) to estimate the boundary width. With this rough approximation, the ratio of the boundary widths of the two incoming streams (w_1:w_2) or that of the two outgoing streams (w_3:w_4) can be estimated with the volumetric flow rate ratio of the input streams (Q_1:Q_2) or that of the output streams (Q_3:Q_4), respectively. (c) Equivalent electric circuit. (*Source*: Reproduced from Oh *et al.*, 2012, with permission of The Royal Society of Chemistry.)

This strategy is ideally suited to aqueous solutions where tuneable concentration gradients of chemical and biochemical stimuli can be generated for cell-based studies (Sun *et al.*, 2008). As fluid viscosity increases, hydraulic resistance of a microchannel is affected and stream combinations at a node of differing viscosity fluids result in unpredictable flow rates and concentration profiles. Design complexity and geometric dimensions of microfluidic networks for on-chip sample preparation or cell transportation are limited and dependent on process, cell size and cell concentration to

minimise clogging. For instance, hydrodynamic filtration setups with multiple branching microchannels of variable sizes were designed to separate highly dilute concentrations (0.3% v/v) of RBCs and leukocytes (Takagi *et al*., 2005; Yamada and Seki, 2005; Matsuda *et al*., 2011). Hydrodynamic focusing of particles and cells has been shown using parallel flow from two inlet buffer streams sandwiching a central stream of particles, island structures in channels to split flows, and by recombining split flows to main channels for sheath flow (Di Carlo *et al*., 2007; Aoki *et al*., 2009; Lee *et al*., 2009). Furthermore, PDMS (polydimethylsiloxane) a commonly used material for microfluidic channels, has a low elastic modulus and large increases in ΔP along a microfluidic channel has resulted in channel deformations making flow rates in complex networks unpredictable (Gervais *et al*., 2006; Sollier *et al*., 2011).

Bubble extraction

Gas bubble formation in microfluidic devices is regularly encountered and can cause unequal flow distribution or even inhibit flow through blockage. It arises from various sources including the device interfacing with the other modules, from the surface chemistry of the device itself, or from dead volumes upstream of fluidic channels. Elevated wall shear stresses occurring at the interfaces of bubbles and cells significantly affect the biological function of cells, causing detachment or cell membrane rupture. To enable normal device operation, strategies for eliminating gas progression have been devised, and include active bubble trap and debubbler on a two-layer PDMS substrate (Skelley and Voldman, 2008) and long-term stable integrated bubble traps (IBT) for use in 10 day mammalian culturing (Zheng *et al*., 2010). Lochovsky *et al*. recently described an in-plane bubble trap, compatible with soft lithography fabrication, where gas removal rates for nitrogen at $\Delta P = 94.6$ kPa was 0.144 μL/min and when multiple traps are operated in parallel achieved a rate of 0.6 μL/min, significantly faster and more reliable than previously reported strategies (Lochovsky *et al*., 2012).

8.4 Manipulation technologies

Biological cells are dielectric materials with variations in electrophysiological, biophysical and optical properties. Technologies utilising these properties can achieve high accuracy and precision in controlling and selecting particles, while in some cases competing against hydrodynamic forces. Manipulation processes include characterisation, sorting,

separation, trapping, patterning, concentrating or focusing cells in continuous flow or batch operations. As most of the technologies to be discussed have a form of 'heritage' and some similarities based on field flow fractionation operation, it is worthwhile considering this technique in a class of its own.

8.4.1 Field flow fractionation

First proposed in the 1960s, field flow fractionation (FFF) is a class of 'soft impact' elution techniques employed mainly to separate heterogeneous mixtures of supramolecules, proteins and bioparticles (<100 μm dia.) within laminar microfluidic flows (Giddings, 1968; Caldwell *et al.*, 1984). The basic principle is based on differential flow displacement along the axis of flow due to an external force field, $|F|$, applied perpendicular to the parabolic flow as in Fig. 8.3 (Giddings, 1993). Based on differences in particle mobility (i.e., physical characteristics), the field controls the equilibrium position of the particle into localised bands of laminar streamlines, varying in velocity as a function of channel height. Hence, particles positioned closest to the channel wall (the accumulation wall) are eluted slowest ($u_{\text{wall}} = 0$), while particles at the centre of the channel are eluted fastest ($u_{\text{centre}} = u_{\text{max}}$), resulting in different retention times. The rates at which particles move through a microchannel are governed by the retention equation, applicable to all FFF systems:

$$R = 6\lambda\left[\coth\left(\frac{1}{2\lambda}\right) - 2\lambda\right] \qquad [8.26]$$

where R is the retention ratio, which for small values of λ reduces to $R = 6\lambda$. The non-dimensional parameter λ is determined by the physical properties of the retained particle (Equation [8.27]), where U is the field induced velocity, D is the diffusion coefficient of the sub micron particle, T is absolute temperature, k is the Boltzmann constant, and h is the channel height (Giddings, 1993).

$$\lambda = \frac{D}{Uh} = \frac{kT}{|F|h} \qquad [8.27]$$

Influences of diffusion in FFF separation mechanisms are negligible when cells or microorganisms are the object of manipulation, with retention times influenced by size, shape, density, rigidity and surface

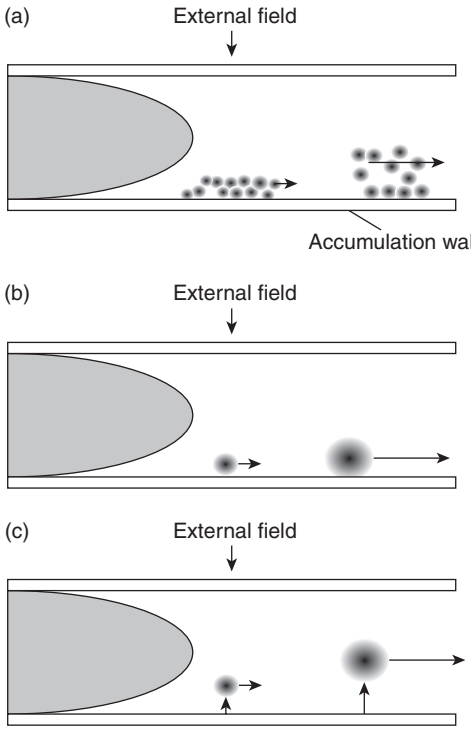

8.3 Elution modes of field flow fractionation (FFF) in a microfluidic channel with an external field acting perpendicular to the parabolic flow. (a) Normal (Brownian) FFF mode operation in which clouds of sub micron particles different distances away from the accumulation wall in the parabolic flow experience different velocities. (b) Steric FFF mode separation of particles. (c) Hyperlayer FFF mode separation.

features leading to larger bioparticles being eluted faster than smaller ones (Roda *et al*., 2009). Commonly referred to as 'steric' and 'hyperlayer' (Fig. 8.3b and 8.3c) elution modes (Giddings and Myers, 1978; Chianea *et al*., 2000), FFF mechanisms typically applied to cell manipulation include, in their broadest form, centrifugal sedimentation FFF (SdFFF) or gravitational FFF (GrFFF), flow FFF (FIFFF or F4) and electrical FFF (EIFFF) (Giddings, 1993; Kowalkowski *et al*., 2006). Modification of the retention ratio in Equation [8.26] takes into consideration steric exclusion of particles of radius r, where $\alpha = r/w$ from the accumulation wall, in which a reversal of the retention order of particles becomes apparent due to large particles protruding out into the flow streams (Myers and Giddings, 1982).

$$R = 6\gamma(\alpha - \alpha^2) + 6\lambda(1-2\alpha)\left[\coth\frac{1-2\alpha}{2\lambda} - \frac{2\lambda}{1-2\alpha}\right] \quad [8.28]$$

For spherical particles in steric FFF mode, the factor γ accounts for particle migration issues such as hydrodynamic lift forces which increase with shear rate and increased particle diameter. Equation [8.28] has been further simplified due to the small values of λ and α normally presented, giving a sterically controlled retention ratio of (Giddings *et al.*, 1987).

$$R = 6\gamma\alpha \quad [8.29]$$

The main driving forces and subtypes applicable to FFF cell manipulation are found in Table 8.2.

8.4.2 Hydrodynamic mechanisms

Deterministic physical interactions

Deterministic lateral displacement (DLD) uses periodic arrays of asymmetric microposts of different geometries to reduce multipath zone broadening of varying sized particles (Huang *et al.*, 2004). Processes such as separation, steering, refracting and focusing have been demonstrated (Morton *et al.*, 2008; Loutherback *et al.*, 2010). Each row of the micropost array is shifted horizontally with respect to the previous row by a distance (d), which can be a fraction of the centre-to-centre distance (λ) of the micropost as in Fig. 8.4. As laminar fluid flows through the gap of adjacent microposts it bifurcates around the micropost it meets in the next row. The gap is typically larger than the particles to avoid clogging, and based on the critical hydrodynamic diameter (D_c) of the particle all similar sized particles follow equivalent migration paths characterised by either the zigzag mode or displacement mode. Similar to the way light rays can be re-directed at the interfaces of differing materials (Fig. 8.5a), differences in the DLD of cells exists when compared to photons. In the zigzag mode particles flow in a cyclic procession, exiting and entering streamline lanes such as the bottom stream in Fig. 8.5e, while in displacement mode (top stream of Fig. 8.5e) particles with sizes greater than D_c move at an angle determined by the ratio of micropost offset to the row-to-row spacing ($\varepsilon = d/\lambda$) (Inglis *et al.*, 2006). As this separation technology relies on a deterministic process, faster flow rates improve the performance of the device limiting sporadic processes such as diffusional mixing. Two dimensionless numbers used to analyse fluid and particle motion in these microsystems are the Péclet number (Pe) of the particle, where $\varepsilon\lambda$ is the local characteristic length of the post where diffusion

Table 8.2 Broad categorisation of field flow fractionation (FFF) subtypes associated with cell manipulation

External force	FFF Subtypes	References
Cross flow (Fl)	Flow FFF (FlFFF), Hollow Fibre FlFFF, Symmetrical FlFFF (SF4), Asymmetric FlFFF (AF4)	Saenton *et al.*, 2000; Reschiglian *et al.*, 2002a, 2002b
Sedimentation (Sd)	Sedimentation FFF (SdFFF), Centrifugal SdFFF, Gravitational (GrFFF)	Chianea *et al.*, 1999 Urbankova *et al.*, 1992; Andreux *et al.*, 1993; Bernard *et al.*, 1995; Metreau *et al.*, 1997; Roda *et al.*, 2009a
Electrical (El)	Electrical FFF (ElFFF), Cyclic ElFFF, Dielectrophoretic (DEP-FFF)	Caldwell *et al.*, 1972; Kesner *et al.*, 1976; Caldwell and Gao, 1993; Markx *et al.*, 1997; Rousselet *et al.*, 1998; Tri *et al.*, 2000; Yang *et al.*, 2000; Gale *et al.*, 2001; Gale and Srinivas, 2005; Kantak *et al.*, 2006; Vykoukal *et al.*, 2008

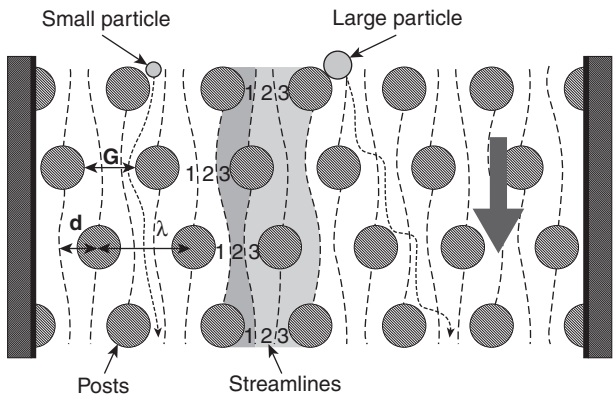

8.4 Schematic illustrating the separation by deterministic lateral displacement in an array of microposts, with an example row shift fraction of one-third. This shift creates three equal flux streamlines. The dashed lines are the boundaries between the streamlines, which are assigned an index in the gaps between the posts. Paths of particles both smaller and larger than the critical threshold are depicted with by their associated line paths. Small particles stay within a flow stream and large particles are displaced at each obstacle. *G* is the clear spacing between the gap, λ is the centre-to-centre post separation, and *d* is the relative shift of the post centres in adjacent rows. (*Source*: Reproduced from Davis *et al.*, 2006. Copyright 2006 National Academy of Sciences, USA.)

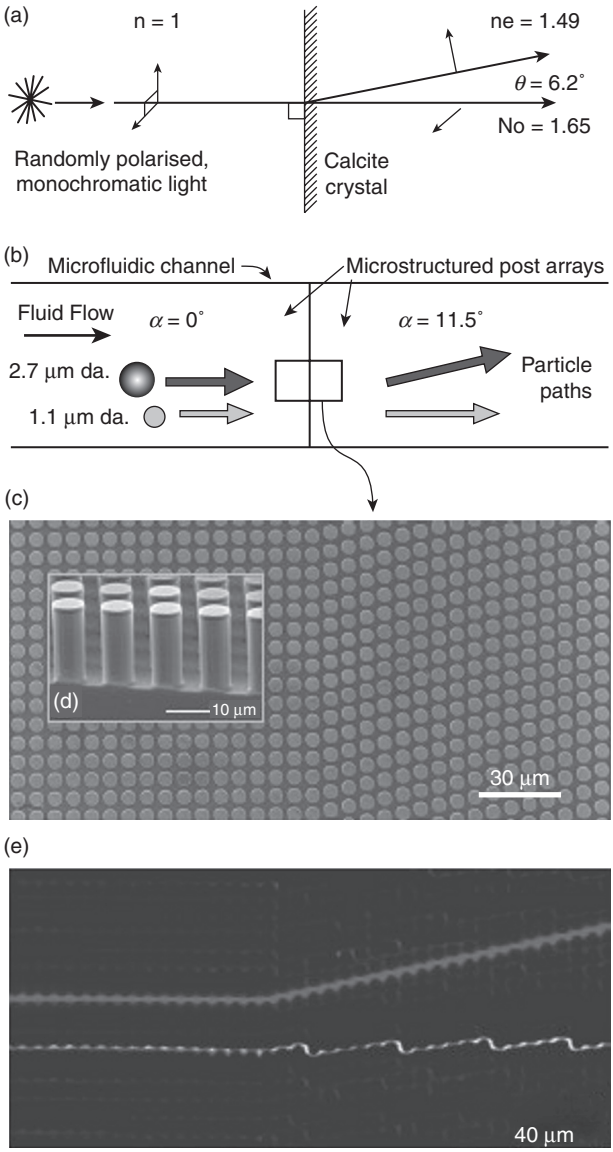

8.5 Optical and microfluidic birefringent interfaces. (a) Optical birefringence in a calcite crystal: normally incident, randomly polarised light, incident on the anisotropic crystal splits into two polarisation dependent paths. Remarkably, the extraordinary ray, whose polarisation is parallel to the calcite optical axis, is deflected away from the normal. (b) Schematic of particle trajectories at the interface between a neutral region and a microfluidic metamaterial element. Particles larger than a critical size follow the array asymmetry, whereas

(*Continued*)

competes with fluid transport (i.e., advection), and the Reynolds number, where the traditional cross-sectional length is replaced with a characteristic length over which the fluid changes its direction. If Pe > 1, the diffusion rate is less than the advection rate at the local scale, indicating smaller particles follow the stream line path created by the posts and larger particles experience a deterministic lateral migration. Design parameters such as gap size and shift fraction ε, influence D_c and when varied in successive regions of arrays ('chirped' or 'cascaded'), the dynamic range of the device is increased (Davis *et al.*, 2006; Inglis *et al.*, 2008).

Inertial migration

The phenomena of particle migration in Poiseuille flow macroscale and microscale systems have been observed and described (Segre and Silberberg, 1961, 1962; Kim and Yoo, 2008; Choi *et al.*, 2011). Characteristics such as particle distribution and equilibrium position have been reported to be influenced by parameters such as the channel diameter (D_h) to particle diameter (d_p) ratio, the particle volume fraction, particle density and flow velocity (Kim and Yoo, 2012).

Particles in fluid flow are subjected to shear forces (i.e., drag) and normal forces (i.e., lift) from bound fluidic elements. Dominant inertial lift forces direct particles laterally across streamlines to equilibrium positions within microchannels, particularly when microfluidic Re is in the range of 1–100 and particle Re (Re_p) is of the order of 1, as in Equation [8.30], where is the maximum fluid velocity and assuming $d_p / D_h << 1$.

$$\mathrm{Re}_p = \frac{\rho u_{\max} d_p}{\mu D_h} = \mathrm{Re}\left(\frac{d_p}{D_h}\right)^2 \qquad [8.30]$$

8.5 Continued

smaller particle follow the fluid flow. (c) The simplest metamaterial element is an asymmetric array of posts tilted at an angle __relative to the channel walls and bulk fluid flow. Shown is a top-view scanning electron micrograph (SEM) of the interface between a neutral array (α = 0°) and an array with array angle α = 11.3° (the gap G = 4 μm and post pitch λ = 11 μm are the same for both sides). (d) Cross-sectional SEM image showing the microfabricated post array. (e) Equivalent microfluidic birefringence based on particle size showing the time-trace of a 2.7-μm red fluorescent (top stream) transiting the interface and being deflected from the normal. Smaller, 1.1-μm beads (bottom) stream are not deflected at the interface. (*Source*: Reproduced from Morton *et al.*, 2008. Copyright 2008 National Academy of Sciences, USA.)

Microchannel cross-sectional position influences particle migration, with randomly distributed particles seen to concentrate into narrow bands, so called Segre and Silberberg annulus, within circular pipes (Fig. 8.6a). In square microchannels particles laterally focus to equilibrium positions and subsequently accumulate near the centre of each channel wall face (Fig. 8.6b) in a pseudo Segre and Silberberg annulus (Bhagat *et al.*, 2008b; Di Carlo, 2009). Lift forces (F_L) exerted on particles in flow, scales with the intrinsic properties of the fluid, Re_p squared and the dimensionless lift coefficient f_L which is a function of the channel Re and particle position within the channel, such that at equilibrium $f_L = 0$ (Ho and Leal, 1974; Schonberg and Hinch, 1989; Asmolov, 1999).

$$F_L = \frac{f_L \rho U_m^2 d_p^4}{D_h^2} \qquad [8.31]$$

Equilibrium positions or focusing reached by dilute suspensions of radially migrating spherical particles in microflows were attributed to the balancing of two major lateral forces: (1) inertial lift forces induced by shear-gradient fluid flow directs particles at the centre region towards the channel wall, and (2) wall repulsion forces at the channel wall region pushes particles towards the centreline of the fluid flow (Ho and Leal, 1974). Using Stokes' law ($F_{\mathrm{drag}} = 3\pi\mu d_p u_p$), an expression for the particle migration velocity (u_p) from the centreline due to lift can be approximated, where $f_L = 0.5$:

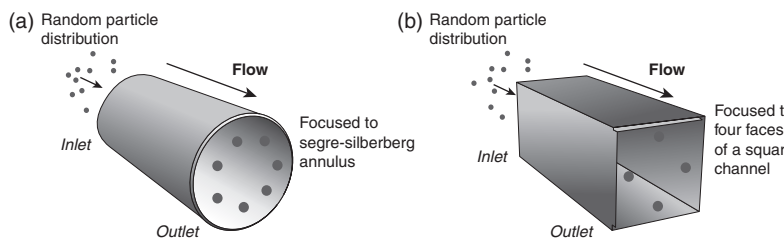

8.6 (a) In a cylindrical pipe, at moderate Reynolds numbers, randomly distributed particles are known to focus to an annulus located between the centre and wall of the pipe. (b) In square channels, following the symmetry of the system, particles instead focus to four equilibrium regions centred at the faces of the channels for dilute suspensions of particles flowing at moderate Reynolds numbers. (*Source*: Reproduced from Di Carlo, 2009, with permission of The Royal Society of Chemistry.)

$$u_p = \frac{F_L}{F_{\text{drag}}} = \frac{4\rho u_{\max}^2 d_p^3}{3\pi\mu D_h^2} f_L \qquad [8.32]$$

The microchannel length (L) required for a particle to completely migrate to its equilibrium position can be calculated from Equation [8.33], where L_p is the maximum required migration distance.

$$L = \frac{u_{\max} L_p}{U_p} = \frac{3\pi\mu D_h^2 L_p}{2\rho u_{\max} d_p^3 f_L} \qquad [8.33]$$

Curved channels

Curved microchannels have been shown to have a secondary inertial effect on fluids which in turn influences particle equilibrium positions and focusing capabilities (Fig. 8.7a–8.7d). The high momentum fluid at the channel centre displaces the lower momentum fluid at the wall surface, causing counter-rotating vortices perpendicular to primary flow and additional drag forces on the particle from this secondary flow. The flow is characterised by two dimensionless numbers, namely Dean number and the curvature ratio, $\delta = D_h/2r$ (Bhagat *et al.*, 2008a). Particle focusing based on curved geometries is independent of particle density, though the ratio of Dean drag and inertial lift is a key parameter in describing how particles behave in separation and concentration processes (Di Carlo *et al.*, 2007; Gossett and Di Carlo, 2009).

Hydrodynamic filtering and microfluidic networks

Hydrodynamic filtration (HDF) uses multiple side channels branching off a main microfluidic channel to concentrate and classify heterogeneously sized particles introduced at the system inlet (Yamada and Seki, 2005). As a particle's centre cannot be present near the channel sidewall at a length equivalent to the particle radius (r_p), flow rates distributed into the side channels at a sufficiently low rate will never let particles greater than a specific diameter into the these side channels, even when the cross-sectional size of the side channel is greater than the particle or the particle is flowing very close to the side wall as depicted in Fig. 8.8a. As fractions of pure fluid flow into upstream side channels, the concentration of particles increases downstream of the main channel, resulting in particle alignment along the side walls (Fig. 8.8d). By increasing the relative flow rates in the downstream side channels, aligned particles are collected according to size in a stepwise fashion.

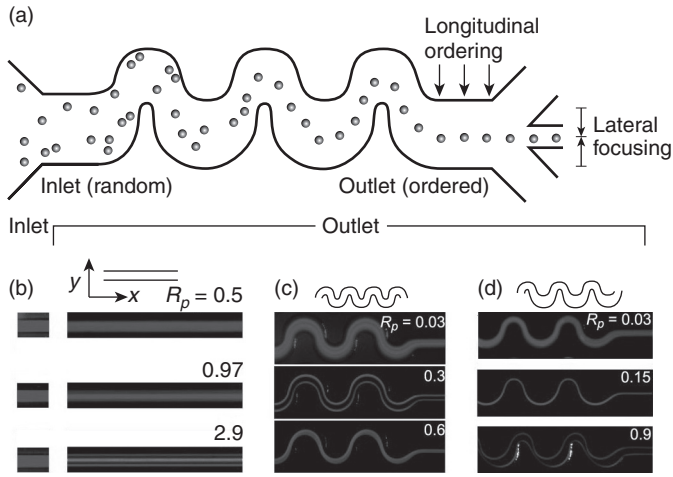

8.7 Inertial self-ordering. (a) Schematic drawing of the inertial ordering process. After flowing through a channel of a particular symmetry, precise ordering of initially scattered particles is observed both longitudinally along the direction of flow and laterally across the channel. (b) Top-down views of fluorescent streak images of flowing 9-μm-diameter particles in a square channel (50 μm) filled with water (density ρ = 1.00 g/mL and dynamic viscosity $\mu = 10^{-3}$ Pa·s). Flow is from left to right. The inlet region is shown at the left, where the particles are initially uniformly distributed within the fluid. Longer images show the outlet 3 cm downstream for the channel Reynolds number R_c = 15, 30, or 90 (particle Reynolds number R_p = 0.48, 0.97, or 2.9). Focusing of particles into four single streamlines is observed. From above this appears as three lines with double the intensity in the middle streak–line. (c) For a symmetric curving channel the symmetry of the system reduces focusing to two streams. Above a critical Dean number (De) focusing is perturbed. (d) For an asymmetric curving system, focusing down to a single stream is favoured. Focusing is again more complex as De increases. (*Source*: Reproduced from Di Carlo *et al.*, 2007. Copyright 2008 National Academy of Sciences, USA.)

The principle of pinch flow fractionation (PFF) is closely related to HDF (Nakashima *et al.*, 2004; Yamada *et al.*, 2004). Two fluidic inlet streams, one with particles and one without, at differing flow rates, meet at a 'pinch segment' (Fig. 8.9a) at which point the particle-rich fluid is focused onto one sidewall aligning particles in its stream, similar to flow FFF. Different sized particles assume characteristic positions away from the sidewall in the pinch segment, with smaller particles closest to the wall. Downstream of the pinch segment a broadening of the microchannel (broad segment) occurs and the slight differences in positions are amplified in the spreading flow profile. The ratio of inlet flow rates and microchannel geometries affects separation efficiencies. Takagi *et al.* (2005) introduced asymmetric pinched flow

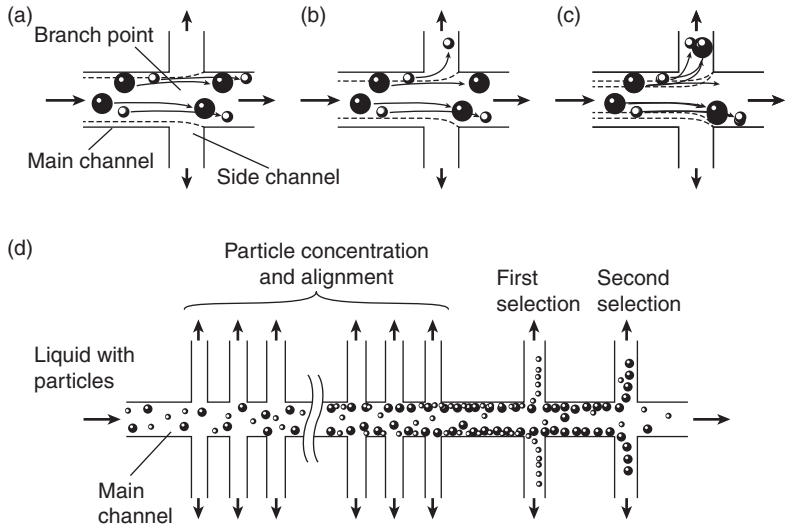

8.8 Principle of hydrodynamic filtration (a)–(c) Schematic diagrams showing particle behaviour at a branch point; (a) the relative flow rates distributed into side channels are low, (b) medium, and (c) high. Broken lines show the virtual boundaries of the flows distributed into side and main channels. (d) Schematic diagram showing particle concentration and alignment in a microchannel having multiple branch points and side channels. (*Source*: Reproduced from Yamada *et al.*, 2005, with permission of The Royal Society of Chemistry.)

fractionation (AsPFF) as an improvement to PFF in which multiple branching channels downstream of the pinch segment were (Fig. 8.9b). This offered the advantage of reduced system clogging and enhanced separation of particles through controlled flow resistance into the branched channels, achieved by adjusting channel dimensions.

Biomimetics

Naturally occurring hemodynamic phenomena found in microcirculatory systems, such as Zweifach-Fung (bifurcation law), margination and plasma skimming, has been mimicked for designing microfluidic devices for blood cell separation and enrichment (Kersaudy-Kerhoas *et al.*, 2010). RBCs tend to concentrate at the centre of a blood vessel under flow, which has two consequences: (1) plasma skimming between two asymmetrical daughter vessels reduces RBC fraction in one vessel, and (2) leukocyte margination to the vessel sidewalls as a result of RBC and leukocyte collisions. This biomimetic approach of margination was demonstrated in a microfluidic

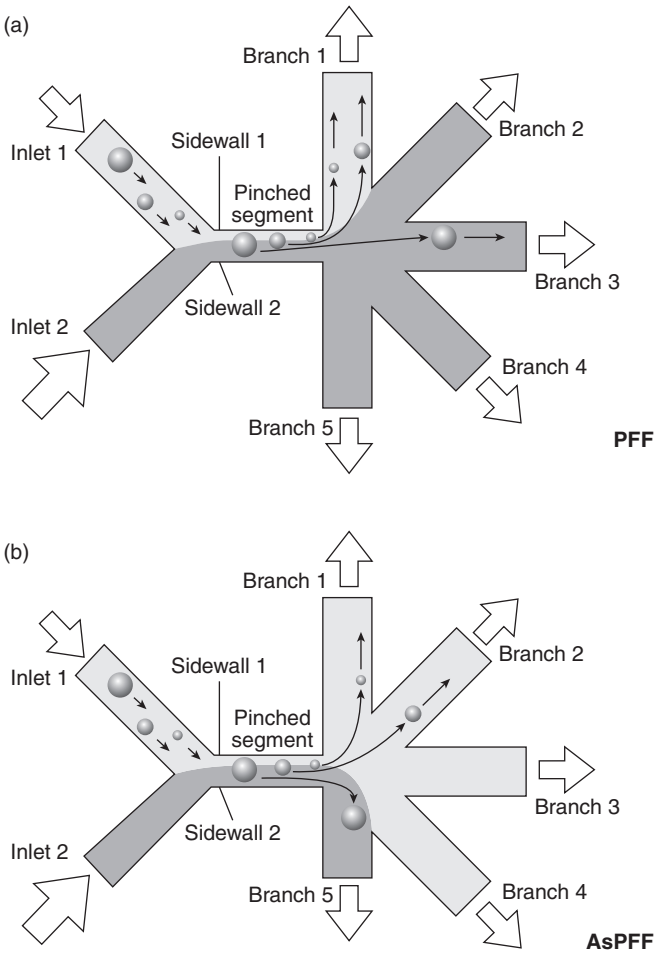

8.9 Schematic diagrams of particle separation: (a) is PFF, and (b) is AsPFF. Liquid containing particles is light-coloured, and liquid without particles is dark-coloured. The size of an arrow represents the flow rate. In PFF, identical branch channels are arranged, and liquid flow in the pinched segment is uniformly distributed. Therefore, Branch 4 and Branch 5 are never used, and the difference in effluent positions of particles is small. In AsPFF, one branch channel (drain channel) is designed to be short and/or broad, and liquid flow is asymmetrically distributed. So all the branch channels are effectively used, and the difference in effluent positions becomes large compared with PFF. (*Source*: Reproduced from Tagaki *et al.*, 2005, with permission of The Royal Society of Chemistry.)

system for leukocyte enrichment from blood, resulting in a 34-fold enrichment (Shevkoplyas *et al.*, 2005), while the use of multiple triangular expansions upstream (Fig. 8.10) mimicking postcapillary venules for nucleated cell margination from RBC gave a 45.75-fold enrichment (Jain and Munn, 2011). A recent demonstration of this technique was based on the blood condition sepsis where *E. coli* and *S. cerevisiae*, along with inflammatory cellular components, were removed from blood in a two stage single pass device at ~1 mL/h per channel, with realistic potential for multiplexing or parallelisation for higher throughput (Hou *et al.*, 2012).

Hydrophoresis and microstructure inclusions

Hydrophoresis is a technique whereby particles in a suspension are transported under the influence of a microstructure-induced pressure field, as

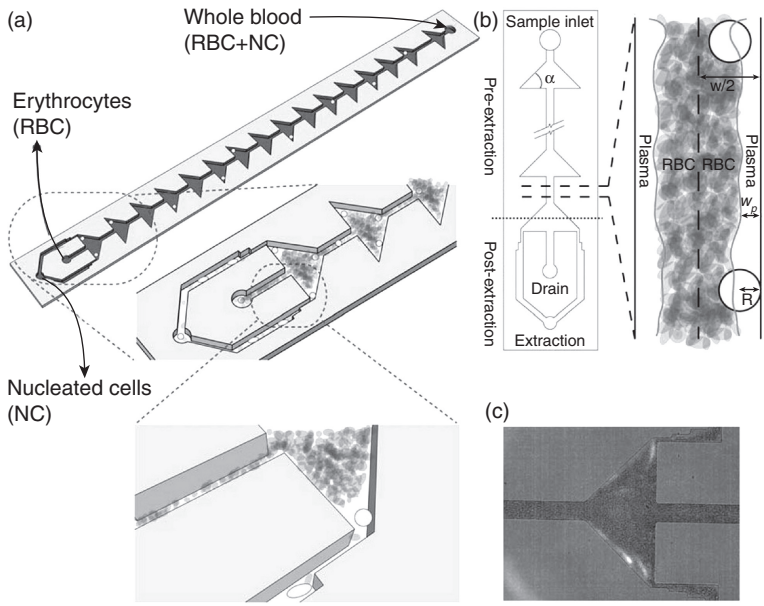

8.10 Design of nucleated cell separation unit. (a) Schematic of the separation device. The device is made using PDMS soft lithography. (b) Illustration of working principle. Whole blood enters the device at the inlet port. Nucleated cell margination is encouraged in the pre-extraction stage of the device. With the NCs segregated near the wall, they can then be collected into the extraction channels. Pure RBCs are also collected through the central drain channel. (c) A snapshot of the extraction region of the device. Labelled NCs can be seen entering the extraction channels at top and bottom. (*Source*: Reproduced from Jain and Munn, 2011, with permission of The Royal Society of Chemistry.)

illustrated in Fig. 8.11 (Choi and Park, 2007; Choi *et al*., 2007). Stroock *et al*. (2002) analytically quantified the anisotropic effect oblique grooved patterns within a microchannel wall had on pressure-driven flows resulting in the movement of fluid near the structure surface in the groove direction. Fluid transverses the microchannel, interacting with opposing transverse pressure gradients creating a recirculating flow component in the cross-section in addition to the principal Poiseuille flow component, with a net effect of generating helical streamlines (Stroock and Whitesides, 2003). Although this was exploited for fluid mixing, slanted obstacles on the top and bottom of a microfluidic channel were used to create transverse flows perpendicular to the main flow for size-based separation of microbeads, RBC and microbead sheathless focusing (Choi and Park, 2007; Choi *et al*., 2008).

Hydrodynamic devices

Inertial focusing and lift hydrodynamics within asymmetric microchannels have been used to filter platelets from dilute blood cells (Di Carlo *et al*., 2008; Geislinger *et al*., 2012) and isolate bacteria from human RBC at 10^8 cells/ml with >99% purity with an upper limit flow rate of 18 μL/min (Wu *et al*., 2009). Kuntaegowdanahalli *et al*. (2009) used a five-loop

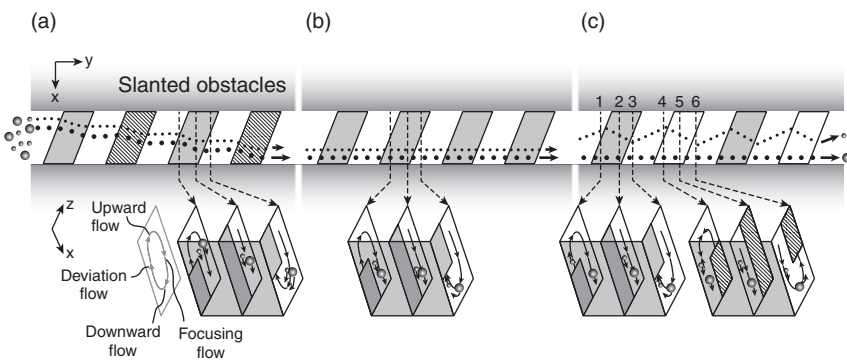

8.11 Hydrophoretic separation principle. Shaded- and lined-areas denote lower and upper slanted obstacles, respectively. A flow direction is along the *y*-axis. (a–c) Top-viewing and cross-sectional schematic diagrams of the slanted obstacles. (a) The slanted obstacles drive lateral flows across the *x*-axis by which particles are pushed to a sidewall. (b) The focused particles flow clockwise following the rotating flows generated by the bottom-side obstacles and move to the bottom of a channel. (c) The large particle is located in the area where there is no lateral pressure gradients and stays in the focused position. On the other hand, the small particle is exposed to lateral pressure gradients along the *x*-axis and deviates from its focused position. (*Source*: Reproduced from Choi and Park, 2007, with permission of The Royal Society of Chemistry.)

spiral microchannel device, as in Fig. 8.12, combining the effects of inertial and Dean drag forces to focus and separate size varying polystyrene beads into separate outlet channels and subsequently neuroblastomas from glioma cells at a throughput of 1×10^6 cells/min with 80% efficiency and >90% viability. This was further adapted for sorting (~15×10^6 cells/h) of asynchronous mammalian cell lines and human mesenchymal stem cells (hMSC) based on their phase in their cell cycle with a >95% viability (Lee *et al.*, 2011).

HDF has been shown to generate a 29-fold enrichment of leukocytes from human blood at a flow rate of 20 μL/min using a two-step process.

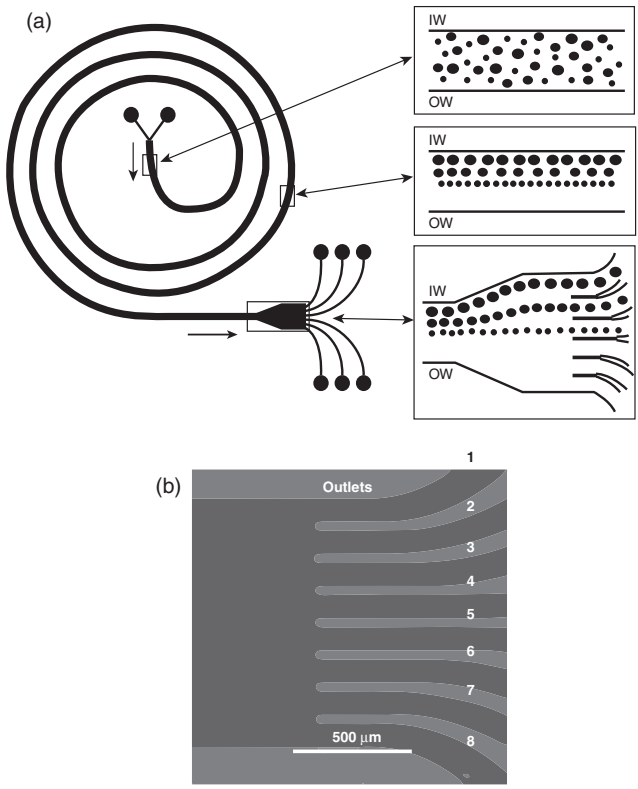

8.12 (a) Schematic of the spiral microparticle separator. The randomly dispersed particles equilibrate at different equilibrium positions along the inner wall (IW) of the spiral microchannel under the influence of lift and drag. Separation between individual particle streams is enhanced by opening the spiral channel into a wider straight channel before extracting the individual streams using a multiple outlet design. (b) The eight outlet channels of the PMMA-based microfluidic spiral device. (*Source*: Adapted from Kuntaegowdanahalli *et al.*, 2009, with permission from The Royal Society of Chemistry.)

An improvement on the original design was described by Yamada and Seki in which flow splitting and recombination with the main channel achieved perfect alignment of target particles along the sidewall for a more efficient separation process (Yamada and Seki, 2006) and at the centre of the main channel for particle focusing (Aoki *et al*., 2009). Size-based separation of erythrocytes from leukocytes, with up to 100 side channels, was shown to attain high levels of efficiency (Matsuda *et al*., 2011). Investigators recently observed the rotational behaviour of spherical particles and non-spherical Janus particles at branch points and applied their findings to HDF separation based on shape (Sugaya *et al*., 2011), while tuning viscoelastic polymer media was demonstrated in the hydrodynamic spreading of neural and glial cells with >90% viability (Wu *et al*., 2008).

A multistage-multiorifice flow fractionation (MS-MOFF) (Fig. 8.13) was introduced by Jung's group, in which the combined effects of inertial lift forces with turbulent secondary Dean flow were used to separate particles based on size, through multiple series of Re constant contraction and expansion microchannels, with high purity and recovery rates demonstrated with microspheres (Park and Jung, 2009; Park *et al*., 2009; Sim *et al*., 2011).

A tuneable hydrophoretic separation device fabricated from PDMS for elastic deformation was placed between two acrylic substrates (Choi and Park, 2009). Compressive forces applied to the substrates enabled cross-sectional tuning, allowing a range of particle diameters (2.5–7 μm), a separation criterion, to be employed without constant rebuilding of devices.

8.4.3 Electrokinetic mechanisms

H.A. Pohl described the phenomenon of dielectrophoresis (DEP) as the translational motion of a neutral particle resulting from polarisation effects produced by an inhomogeneous electric field (Pohl, 1951, 1958). It was not until the late 1960s/early 1970s that experimental and theoretical reports of DEP on biological cells in suspensions began to appear (Pohl and Hawk, 1966; Crane and Pohl, 1968, 1972; Pohl and Crane, 1971). AC electrokinetic theory, and the forces generated within these microsystems, are covered in depth by (Pohl, 1978; Pethig, 1979; Jones, 1995; Ramos *et al*., 1998; Castellanos *et al*., 2003; Hughes, 2003; Pethig, 2010).

Dielectrophoresis

A homogenous spherical dielectric particle of radius, r, placed in a uniform electric field (E) becomes polarised due to the field's interaction, inducing a dipole moment (p) in the sphere,

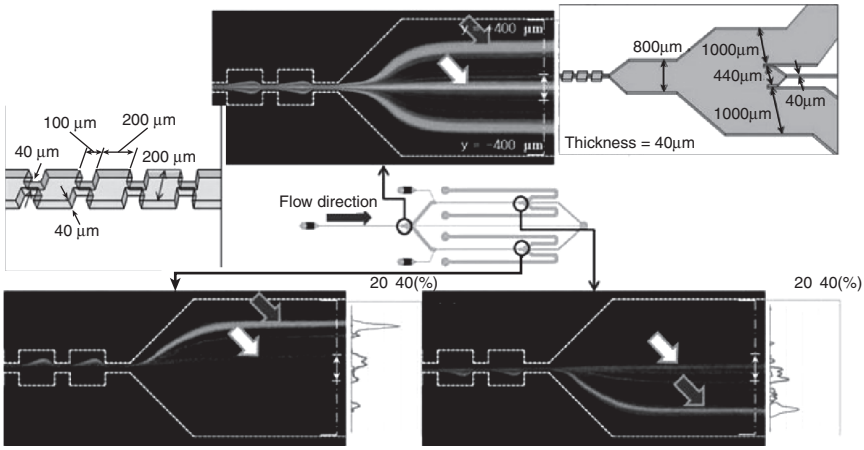

8.13 Photographs of simultaneous experiments using a mixture of the two polystyrene microspheres at Re = 85. Schematic view of MS-MOFF and position of image captured. The top photo represents the end of 1st multi-orifice segment. The photos represent the end of the 2nd two multi-orifice segments. Dark arrows indicate the 7 μm particles and white arrows indicate the 15 μm particles, respectively. Dimensions of the orifice and flow broadening sections are also shown. (*Source*: Adapted from Sim *et al.*, 2011, with permission from The Royal Society of Chemistry.)

$$p = 4\pi\varepsilon_m r^2 \left(\frac{\varepsilon_p - \varepsilon_m}{\varepsilon_p + \varepsilon_m} \right) E \qquad [8.34]$$

where $\varepsilon_{p,m} (= \varepsilon_0 \varepsilon_r)$ is the absolute permittivity of the suspending medium/particle, ε_r is the relative permittivity of the medium/particle, and ε_0 is the permittivity of free space ($\approx 8.8541878 \times 10^{-12}\,\mathrm{F\,m^{-1}}$). The time average DEP force acting on a polarisable particle placed in a non-uniform alternating current (ac) electrical field can be expressed in the form (Wang *et al.*, 1995),

$$\left\langle \overline{F}_{\mathrm{DEP}} \right\rangle = 2\pi\varepsilon_m r^3 \left\{ \mathrm{Re}\left(f_{\mathrm{CM}}(\omega) \right) \nabla E_{\mathrm{RMS}}^2 + \mathrm{Im}\left(f_{\mathrm{CM}}(\omega) \right) \left(E_x^2 \nabla \phi_x + E_y^2 \nabla \phi_y + E_z^2 \nabla \phi_z \right) \right\} \qquad [8.35]$$

where E_{RMS} and ϕ are the root mean square magnitude and phase of the applied electric field in Cartesian axis (x, y, z), respectively. The polarisability (or Clausius-Mossotti) factor $\left(f_{\mathrm{CM}}(\omega) \right)$, describes the frequency-dependent dielectric characteristics of the particle and suspending medium, where

the complex permittivity (ε_k^*) for the medium ($k = m$) and particle ($k = p$) is described by

$$\varepsilon_k^* = \varepsilon_k \varepsilon_0 - j\frac{\sigma_k}{\omega}, \quad j = \sqrt{-1} \qquad [8.36]$$

or by a complex conductivity (σ_k^*),

$$\sigma_k^* = \sigma_k + j\omega\varepsilon_0\varepsilon_k \qquad [8.37]$$

A homogeneous particle's conductivity is $\sigma_p = \sigma_b + (2K_s/r)$, where K_s is the surface conductance, σ_b is particle bulk conductivity, and ω is the angular frequency of the applied field. Thus, the complex Clausius–Mossotti factor can be expressed in terms of complex conductivities or the more common complex permittivities (Equation [8.38]).

$$f_{\mathrm{CM}}(\omega) = \left(\frac{\varepsilon_p^* - \varepsilon_m^*}{\varepsilon_p^* + 2\varepsilon_m^*}\right) \qquad [8.38]$$

In the absence of a spatially varying phased electric field, as found in travelling wave DEP (twDEP) (Masuda *et al*., 1988; Talary *et al*., 1996), the imaginary component (Im) of the Clausius–Mossotti factor in Equation [8.35] equals zero, leaving the typical anti-phase dielectrophoretic force, $\overline{F}_{\mathrm{DEP}}$, originally described by Pohl (1978).

$$\left\langle \overline{F}_{\mathrm{DEP}} \right\rangle = 2\pi\varepsilon_m r^3 \,\mathrm{Re}\left(f_{\mathrm{CM}}(\omega)\right)\nabla E_{\mathrm{RMS}}^2 \qquad [8.39]$$

DEP vector response to an applied field is dictated by $\mathrm{Re}\left(f_{\mathrm{CM}}(\omega)\right)$, with $-0.5 < \mathrm{Re}\left(f_{\mathrm{CM}}(\omega)\right) < 0$ indicating net particle movement to low intensity electrical fields (negative DEP) and $0 < \mathrm{Re}\left(f_{\mathrm{CM}}(\omega)\right) < +1$ indicating movement to high intensity electrical fields (positive DEP). A null response, $\mathrm{Re}\left(f_{\mathrm{CM}}(\omega)\right) = 0$, is referred to as the particle's crossover frequency, a parameter which has been used in DEP-based separation strategies (Gascoyne *et al*., 1992; Markx *et al*., 1994; Gascoyne and Vykoukal, 2004; Fatoyinbo *et al*., 2007b). Heterogeneity in cellular structures, along with variations in size and shape (e.g., discoid, ellipsoidal, oblate) have been captured in the Clausius–Mossotti factor using the 'multishell' model (Fricke, 1924; van Beek, 1960; Irimajiri *et al*., 1979). Using a 'smeared-out' approach, relative complex permittivities of the membrane ($\varepsilon_{\mathrm{mem}}^*$) and cytoplasm ($\varepsilon_{\mathrm{cyt}}^*$) for a cell

of radius (r) and plasma membrane thickness (d) are evaluated and combined to obtain a particle's effective complex permittivity ($\varepsilon^*_{p,\text{eff}}$), equivalent to a homogeneous particle, which can then replace ε^*_p in Equation [8.38] (Huang *et al*., 1992).

$$\varepsilon^*_{p,\text{eff}} = \varepsilon^*_{\text{mem}} \left\{ \frac{(r/r-d)^3 + 2\left(\left(\varepsilon^*_{\text{cyt}} - \varepsilon^*_{\text{mem}}\right)/\left(\varepsilon^*_{\text{cyt}} + 2\varepsilon^*_{\text{mem}}\right)\right)}{(r/r-d)^3 - 2\left(\left(\varepsilon^*_{\text{cyt}} - \varepsilon^*_{\text{mem}}\right)/\left(\varepsilon^*_{\text{cyt}} + 2\varepsilon^*_{\text{mem}}\right)\right)} \right\} \quad [8.40]$$

Equation [8.40] is useful in extracting electrophysiological properties from a cell's DEP spectrum (frequency-dependent manipulation), such as morphological changes, membrane capacitance and conductivity, revealing ion permeability and influences of drug exposure in microfluidic cell-based assays and capturing modes within flow regimes (Coley *et al*., 2007; Pethig and Talary, 2007; Sanchis *et al*., 2007; Hoettges, 2010; Fatoyinbo *et al*., 2011; Hawkins *et al*., 2011; Labeed *et al*., 2011; Mulhall *et al*., 2011; Wu *et al*., 2012; Unni *et al*., 2012).

AC electro-osmosis

In certain microelectrode configurations (e.g., coplanar electrodes), the application of an ac voltage generates fluid pumping with the direction and velocity dependent on the amplitude and frequency (~0.1–100 kHz) of the signal (Garcia-Sanchez *et al*., 2006). The flow occurs due to oscillating induced charges in the double layer, present at the electrode–electrolyte interface. It is driven by the tangential component of the electric field (E_t), which produces a slip velocity (u_{slip}) characterised by the voltage drop across the double layer ($\Delta\phi_{\text{DL}}$) and the tangential electric field outside the double layer (Yeh *et al*., 1997; Ramos *et al*., 1999).

$$u_{\text{slip}} = \frac{1}{2}\frac{\varepsilon_m}{u}\Lambda\,\text{Re}\left[\left(\Delta\phi_{\text{DL}}\right)E_t\right] \quad [8.41]$$

The parameter Λis given by the ratio of the Stern layer capacitance per unit area and the capacitances per unit area of both the Stern and diffuse layers (Castellanos *et al*., 2003). This non-linear electrokinetic flow of the fluid has been applied to asymmetrical electrode geometries for microfluidic pumping of fluids (Stroock and Whitesides, 2003), while others have demonstrated this technique in manipulating cells out of bulk flow and on to the electrode surfaces to enhance detection, concentration and patterning processes (Fatoyinbo *et al*., 2007a; Melvin *et al*., 2011). A more general

term describing the fluid flow, induced by electrical charges, around both metallic and dielectric surfaces in the presence of DC and low AC fields is induced-charge electro-osmosis (ICEO) coined by Bazant and Squires (2004, 2010).

Electrokinetic devices

Electrokinetics is a versatile technology that has benefited from advances in microelectrode fabrication technologies such as photolithography, thus an extremely large body of literature and variant technologies (based on operating strategy or electrode design) of the above principles exists. The dielectrophoretic force imparted on a cell varies with cell polarisability and volume. Applied fields can be either direct current (dc) or alternating current (ac), thus the range of electrokinetic based devices which have been designed is large and variably multifaceted or modular (Muller *et al*., 1999; Dalton and Kaler, 2007; Burgarella *et al*., 2010). The magnitude of the electric field gradient generated by 2D planar (e.g., spiral (Fig. 8.14h), interdigitated (Fig. 8.14b), interdigitated castellated (Fig. 8.14a)) or 3D microelectrode geometries (e.g., 3-D wells (Fig. 8.12j), DEP-dots (Fig. 8.14i)), decays exponentially away from the microelectrode edge (Wang *et al*., 1997; Morgan *et al*., 2001; Green *et al*., 2002; Hoettges *et al*., 2003; Tsukahara and Watarai, 2003; Fatoyinbo *et al*., 2008). Thus, microelectrode arrangements in DEP systems are important in generating varying morphological field gradients

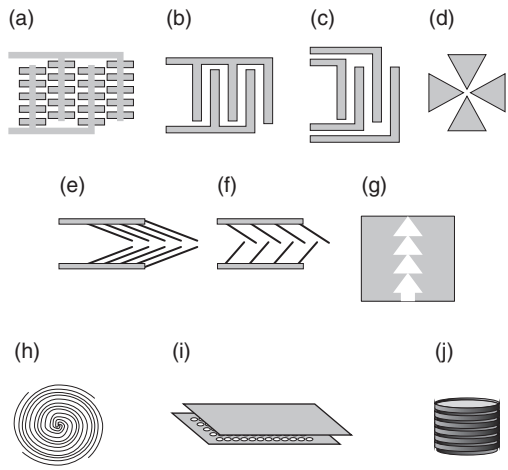

8.14 Some common microelectrode configurations for particle manipulation in electric fields. (a) Interdigitated castellated, (b) interdigitated, (c) linear quadrupole or twDEP config, (d) quadrapolar for electrorotation, (e) focusing, (f) deflectors, (g) ratchet, (h) spiral, (i) dots, and (j) wells.

required to induce motion, though consideration of the DEP force magnitude and other forces arising within the system, including, gravity, viscous drag, buoyancy and hydrodynamic flow must be optimised accordingly for flow through operations (Hughes, 2002).

Travelling wave DEP (twDEP) occurs when three or more consecutively energised microelectrodes, out of phase by X degrees and summing up to 360° (Fig. 8.14c), transport cells parallel to the substrate in a forward or backward direction depending on the sign of$\mathrm{Im}\left(f_{\mathrm{CM}}(\omega)\right)$, thus imposing variable rates of motion and retention times for different particles (Masuda *et al*., 1988; Huang *et al*., 1993; Hughes *et al*., 1995; Wang *et al*., 1997; Green *et al*., 2002; Cheng *et al*., 2009). When a quadrupolar microelectrode's (out of phase by 90° as in Fig. 8.14d) tips are focused towards each other and pointed at a specific region, particles undergo a rotational torque (electrorotation (ROT)) with a velocity that is a function of the field frequency (Gimsa, 1997; Holzel, 1998; Cen *et al*., 2004). ROT is useful in probing the electrophysiology of single cells, but lacks throughput and the set-up is more complex (e.g., particle drift) in comparison to DEP techniques (Wang *et al*., 1991, 1992; Hughes, 1998; Hoettges *et al*., 2008).

Dielectrophoretic field flow fractionation (DEP-FFF) uses dielectric and density properties to discriminate between cells. By balancing multiple forces in hydrodynamic flow, including hydrodynamic lift, cells of different electrophysiology and density attain an equilibrium height in a microchannel through nDEP and are eluted at different rates (Markx and Pethig, 1995; Markx *et al*., 1997; Wang *et al*., 2000; Gascoyne, 2009; Liao *et al*., 2012). Microelectrodes positioned at an angle to the main flow have been used to deflect (Fig. 8.14f) and focus (Fig. 8.14e) cells to regions of a channel cross-section, or into side channels, in sorting and separation processes (Doh and Cho, 2005; Kim *et al*., 2008). As a cell approaches an angled electrode the nDEP force can exceed drag forces, resulting in the cell travelling parallel to the electrode until the drag forces exceed the DEP force, enabling the cell to flow past the electrode in a path line specific to a cells' DEP mobility. Kim *et al*. (2011) described a fluorescence-activated sorting system in which fluorescent microbeads were hydrodynamically focused using a sheath flow for laser excitation which was simultaneously detected by a photomultiplier tube (Fig. 8.15). Depending on the level of intensity, the beads were focused into one of three outlet channels by angled electrodes, indicating DEP's ability to sort multiple particle mixtures effectively.

Insulator-based dielectrophoresis (iDEP) relies on the electric field non-uniformity being created by insulating structures/obstacles within a microfluidic channel, with a dc signal applied across these structures via two electrodes situated at either end of the channel (Cummings and Singh, 2000; Chou *et al*., 2002; Cummings and Singh, 2003). The reduction in fabrication costs arising from complex metallisation processes, a simple fluid and particle

transportation mechanism through electroosmotic flow from dc signals and the reduced fouling capabilities, has made this technology an increasingly popular approach for particle trapping and concentration (Lapizco-Encinas *et al.*, 2004, 2005). An extension of iDEP is contactless DEP (cDEP) in which fluid electrodes are used to generate the field non-uniformities (Demierre *et al.*, 2007; Shafiee *et al.*, 2009). The fluid electrode channels containing a highly conductive solution are separated from the sample channel where insulating structures reside by thin insulating membranes, eliminating

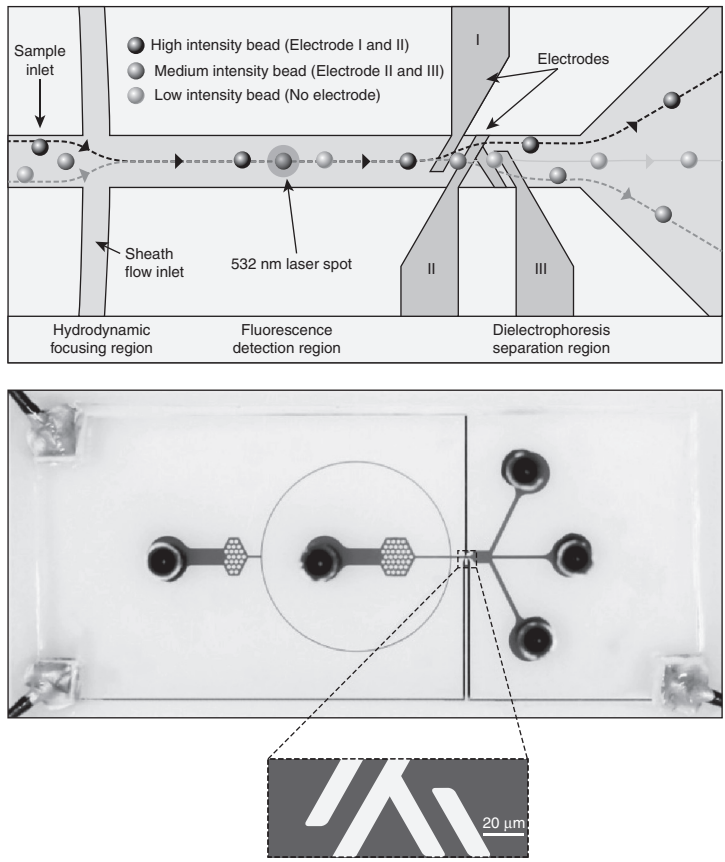

8.15 Beads were focused to the centre of the channel using sheath flow in the hydrodynamic focusing region, fluorescent tags were detected in the fluorescence detection region, and beads were separated using dielectrophoretic forces in the separation region. Photographic image of the microfabricated chip; the channel has an inlet to outlet length of 21 mm, a height of 30 μm and a width 100 μm. Electrodes have a gap length of 20 μm and a width of 20 μm. (*Source*: Adapted from Kim *et al.*, 2011, with permission from Elsevier.)

electrode–cell contact and minimising sample contamination, joule heating, bubble formation and electrochemical effects during cell manipulation (Henslee *et al.*, 2011; Sano *et al.*, 2012).

8.4.4 Acoustic mechanisms

Ultrasonic standing waves (USW) technology for fluid and particle manipulation, also referred to as acoustofluidics, is a rapidly evolving technology. Based on differences in acoustophysical properties (size, density and compressibility), particles can be manipulated effectively using acoustic radiation forces. The most common acoustic resonator microsystem designs include (1) layered, (2) transversal, and (3) surface acoustic wave (SAW) resonators as in Figs 8.16 and 8.17 (Lenshof *et al.*, 2012). The motion of microparticles and cells in acoustic fields is aptly termed acoustophoresis (Hagsater *et al.*, 2007; Bruus, 2012a, 2012b).

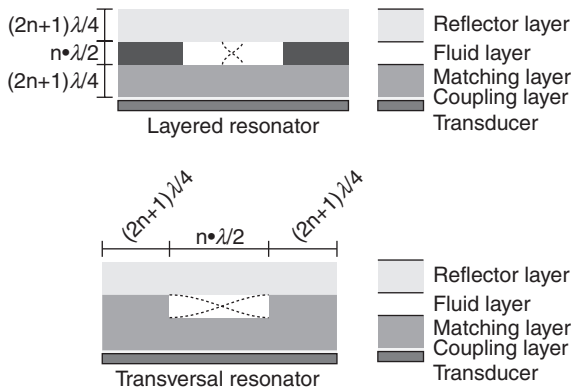

8.16 Acoustophoretic device classifications: transversal and layered resonators; the choice of material depends on what type of resonator is to be designed. The layered resonator requires carefully matched reflection and matching layers with regards to the wavelength in order to achieve a system with high Q-value. Although, as it is the system Q-value that is important here, it is possible to use materials which themselves are not acoustically optimal, such as polymers, and some losses could be acceptable as long as the system is well matched. Transversal resonators on the other hand rely more on materials with high characteristic acoustic impedance and are less sensitive to matched layers as the whole system resonates as one body. They are thus easier to design, but are limited to the choice of materials which can be utilised. (*Source*: Adapted from Lenshof *et al.*, 2012, with permission from The Royal Society of Chemistry.)

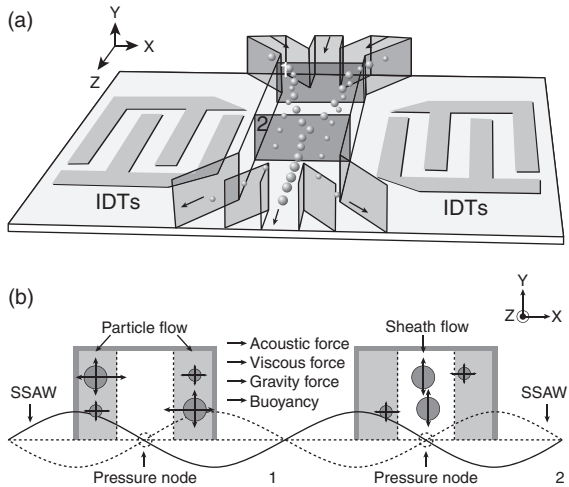

8.17 The resonance in SAW devices rely on waves propagating into a fluidic compartment via a wave guiding substrate. In order not to create interfering resonances, the material enclosing the fluid should be of similar characteristic acoustic impedance as the fluid, making polymers suitable. The surface waves are generated by one or more interdigitated (IDT) electrode transducers positioned outside of the channel, and constructive interference of two opposite SAWs results in a SSAW in the area where the microchannel is bonded. (a) Schematic of the separation mechanism showing particles beginning to translate from the sidewall to the centre of the channel due to axial acoustic forces applied to the particles when they enter the working region of the SSAW (site 1). The differing acoustic forces cause differing displacements, repositioning larger particles closer to the channel centre and smaller particles farther from the centre (site 2). (b) Comparison of forces (normally in pN range) acting on particles at Site 1 and Site 2, respectively. (*Source*: Adapted from Shi *et al.*, 2009, with permission from The Royal Society of Chemistry.)

Acoustic radiation force

The general acoustic radiation force, F_{rad}, for a spherical particle of radius r, immersed in a fluid in the presence of an acoustic field is given by Manneberg *et al*. (2009),

$$F_{\text{acoustic}} = -\left(\frac{4}{3}\pi r^3\right)\nabla\left(\gamma_1 \frac{\langle p^2\rangle}{2\rho_m c_m^2} - \frac{3}{2}\rho_m \gamma_2 \frac{\langle u^2\rangle}{2}\right) \quad [8.42]$$

where,

$$\gamma_1 = 1 - \frac{\rho_m c_m^2}{\rho_p c_p^2} \quad \text{and} \quad \gamma_2 = 2\frac{(\rho_p - \rho_m)}{2\rho_p + \rho_m} \qquad [8.43]$$

The pressure (p) and velocity (u) fields are time averaging, ρ and c are the density and speed of sound, for subscripts: medium (m) and particle (p). For a one dimensional plane acoustic standing wave, Equation [8.42] reduces to

$$F_{\text{acoustic}}(x) = 4\pi r^3 E_{\text{ac}} k \sin(2kx)\Phi \qquad [8.44]$$

where E_{ac} is the acoustic energy density of wavelength λ, wavenumber $k = 2\pi/\lambda = \omega/c_m$, and the acoustophoretic contrast factor, Φ, is defined as,

$$\Phi = \gamma_1 + \frac{3}{2}\gamma_2 = \frac{5\rho_\rho - 2\rho_m}{2\rho_\rho + \rho_m} - \tilde{k} \qquad [8.45]$$

From Equation [8.45], Φ is dependent on the relative densities of the medium and particle, the relative compressibility of both materials (i.e., $\tilde{k} = k_p / k_m$), and recently included, a fluid viscosity parameter for smaller-sized particles (Settnes and Bruus, 2012). It determines the direction the acoustic force is acting on the particle in a microchannel and for the case of the simple standing half-wavelength, particles are directed towards pressure nodes for $\Phi > 0$ (central plane) or towards the anti-node for $\Phi < 0$ (wall region) (Petersson *et al.*, 2005).

Acoustophoretic devices

Acoustophoresis is not limited by high conductive fluids, surface charges or pH, though complexities in device design, material choice and fabrication pose challenges owing to the high quality factor (Q-value) needed for the resonator and the minimisation of resonance attenuation when interfaced with channel wall forming substrates. As an alternative to the more expensive silicon substrate, isotropically wet-etched glass chips were shown to have superior performance in microfluidic acoustic cell washing and focusing also enabling visualisation of cell streams (Evander *et al.*, 2008). Acoustophoretic devices exploit half-wavelength resonators for separation, sorting, trapping and alignment of particles (Laurell *et al.*, 2007). Continuous separation of polystyrene beads on a silicon chip into multiple side channels was actuated by

a 2 MHz piezoceramic plate in the first harmonic mode ($2 * \lambda/2$). Separation efficiencies was found to be dependent on side channel angles branching off the main channels with a 45° branch more effective than a 90° branch (Nilsson *et al.*, 2004). This system was modified for the separation of 2.5% concentration of RBCs from 1% concentration of triglyceride emulsions (Petersson *et al.*, 2004). Reducing the cross-sectional dimensions of the microchannel to a half-wavelength ($\lambda/2$) standing wave increased the acoustic force at the channel centre focusing a band of RBC exiting via a central outlet channel (>70%) while lipid emulsions exited via the sides (>80%). Separation of whole blood cells from plasma in an elongated separation channel through a sequential stepwise removal of concentrated blood cells enabled subsequent plasma protein analysis (Lenshof *et al.*, 2009). The orthogonal acoustic redistribution of particles/cells based on size in a dual-inlet laminar flow system is known as free-flow acoustophoresis (FFA) fractionation (Kumar *et al.*, 2005; Petersson *et al.*, 2007). It can be seen from Equation [8.46] that the particle's velocity $v_p(x)$ due to the acoustic force is proportional to the square of the particle's radius. An acoustophoretic device operating in transversal mode with multiple outlet channels and a trifurcated inlet is driven under laminar flow with buffer media injected in the central inlet and sample media from the two side inlets. As the streams flow parallel upstream in the separation channel, under the influence of an applied acoustic force, balanced by Stokes drag, large particles transverse the channel at different speeds according to size, exiting at spatially positioned outlet channels.

$$v_p(x) = \frac{2\Phi k r^2 E_{ac}}{3\mu} \sin(2kx) \qquad [8.46]$$

Standing surface acoustic waves (SSAW), where parallel interdigitated transducers (IDT) generate lateral acoustic radiation forces on particles within the microchannel has also recently been used to separate and focus particles in continuous flows (Fig. 8.18) (Shi *et al.*, 2009b, 2011; Nam *et al.*, 2011a, 2011b). Acoustic tweezers in which RBCs and *E. coli* were patterned into grid-like arrays used SSAW technology as in Fig. 8.19, with the IDTs positioned orthogonally to each other (Shi *et al.*, 2009a). Although in its infancy, SSAW-based designs demonstrate versatility and lower power consumption over traditional bulk acoustic wave designs, with the potential of seamless integration of acoustic-based manipulation technologies in microfluidic systems.

8.4.5 Optical mechanisms

In the last decade the relatively new research field of optofluidics has seen a multitude of developments for LOC systems, mainly regarding miniaturised

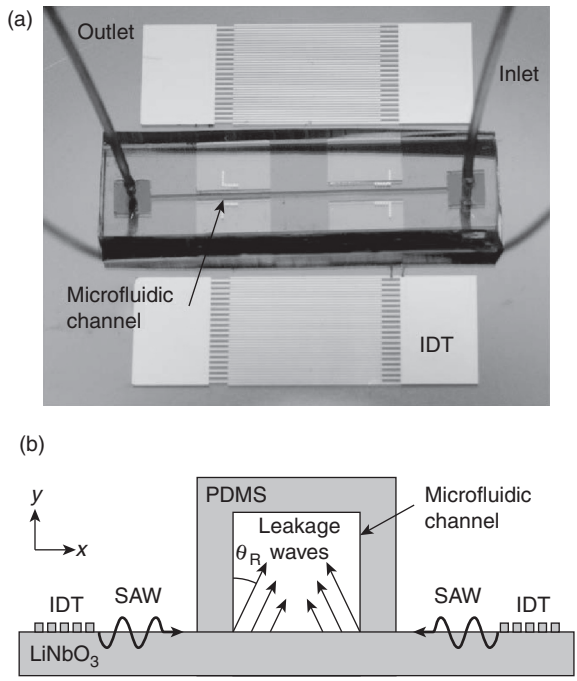

8.18 (a) A photograph a PDMS microchannel in between a pair of parallel IDTs used for particle focusing. (b) A cross-section schematic of the microchannel and IDTs used to generate two SAWs travelling in the opposite direction. The leakage waves are radiated into the liquid phase under the Rayleigh angle. (*Source*: Reproduced in part from Shi *et al.*, 2011, with permission from The Royal Society of Chemistry.)

detection systems (Mogensen and Kutter, 2009; Cho *et al.*, 2010b). Optofluidics can be considered as the merging of optics with microfluidic technology, i.e., the interaction of light with matter in microfluidic flow, whereas the term photophoresis has been used to describe the movement of micron-sized particles subjected to beams of light (Zhao *et al.*, 2006). The term optofluidics has been applied in a variety of ways and it can be justifiably argued that some well-established techniques and devices (e.g., optical tweezers, SPR) have quietly been included into this technological classification (Psaltis *et al.*, 2006; Horowitz *et al.*, 2008). The basic physics of light interactions with biological materials is well understood (Svoboda and Block, 1994). Platforms for cell sorting, trapping and manipulation in microfluidic systems, based on particle size and refractive index or fluorescence labelling, are becoming more widespread.

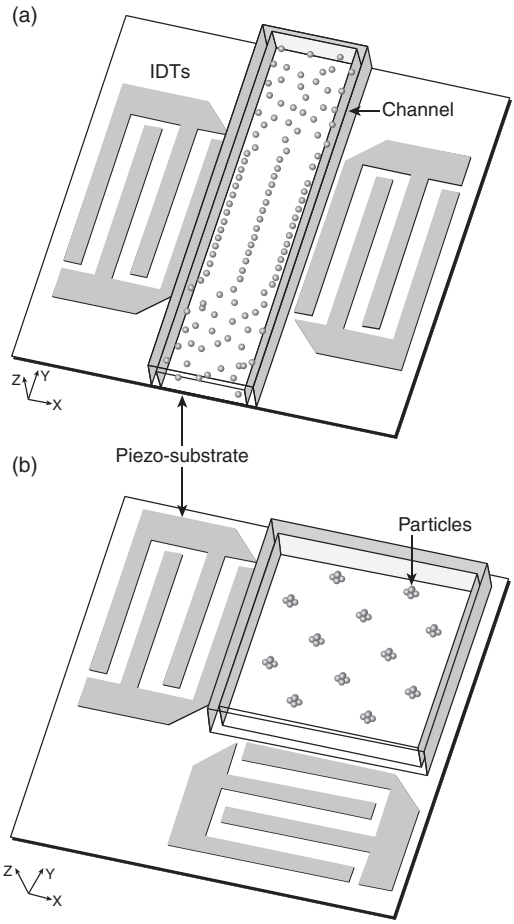

8.19 Schematic of the SSAW-based patterning devices. (a) 1D patterning using two parallel IDTs. (b) 2D patterning using two orthogonal IDTs (the angle between the IDTs can be changed to achieve different patterns). (*Source*: Reproduced from Shi *et al.*, 2009, with permission from The Royal Society of Chemistry.)

Optical devices

Cell manipulation using optical tweezers (also known as optical traps) was first demonstrated by Bell Laboratories using visible argon laser light and infrared (IR) light (Ashkin and Dziedzic, 1987; Ashkin *et al.*, 1987). Movement of a micron-sized dielectric particle is induced by the direct transfer of photon momentum to a non-absorbing particle during

refraction and reflection, i.e., the radiation pressure. The radiation pressure (optical force) from a high intensity, focused Gaussian profile laser has scattering and gradient force components, which gives a point of stable equilibrium near the beam focus. Particles are trapped transversely by the gradient force (~pN), while the axial motion of the particle is controlled by the scattering forces (Ashkin, 1997). For cells greater than the wavelength of light ($d_p >> \lambda$), ray optics has been used to derive the radiation force from scattering of the incident light momentum (Ashkin, 1992; Svoboda and Block, 1994).

Single beam and multiple beam configurations have been used to manipulate and trap cells in microfluidic systems with high precision and little or no damage to the cell integrity. Eriksson *et al*. (2010) assessed the impact of glucose level changes through reversible microfluidic flow on single cell *S. cerevisiae* by individually selecting and positioning them in a 5×5 array (1.28 mm^2) using optical tweezers. With a power density of 240 mW from the lasers, continuous cell budding indicated the cells were not adversely affected. Figure 8.20 shows a cell sorting system using multiple microfluidic streams, optical tweezers, and an image processing methodology for recognising fluorescence and size (Wang *et al*., 2011). This system uses multiple laser traps to dynamically trap and transport cells to a desired location for sorting purposes, achieving high purity factors with low sample populations. Optoelectronic tweezers (OET) were introduced by Choi *et al*. (2005) where light passing through a digital micromirror display image patterned that image onto a photoconductive layer to produce virtual electrodes. When the system was energised with an ac signal, cells moved into negative or positive energy traps due to electric field gradients originating from the illuminated area. This optical platform has low power consumption and mass parallelisation of single cell motion based on the combined technologies of optical tweezers and the principle of DEP manipulation. Further developments of OET technology have included integration with electrowetting on dielectric (EWOD) in which HeLa cells were either trapped or transported in microfluidic droplets via lateral droplet motion (LOET) (Shah *et al*., 2009). Recently polymer-based optically induced DEP (ODEP) devices have been developed to manipulate particles using dynamically changing virtual electrodes controlled by computer as in Fig. 8.21, or the concave curvature and flexibility of a device substrate (Wang *et al*., 2010; Lin *et al*., 2012). Continuous separation of targeted single cells through optical transportation perpendicular to the flow streams, using single or multiple laser traps, have extremely low throughput, which is a significant drawback at ~10 cells/s compared to ~10^5 cells/s for fluorescence activated cell sorting (FACS) technique (Murata *et al*., 2009).

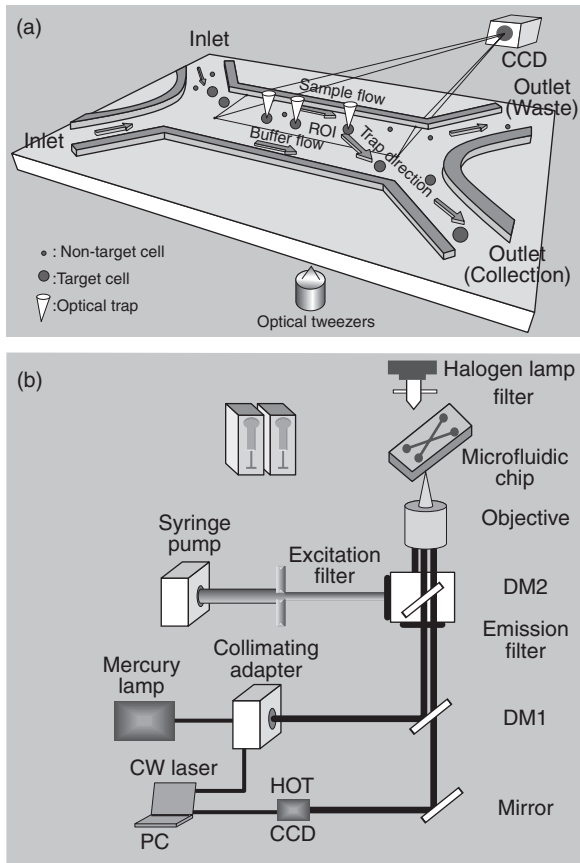

8.20 (a) Cell sorting procedure using multiple microfluidic inlet and outlet streams, optical tweezers and an image processing methodology for recognising fluorescence and size. (b) Cell sorter set-up combined with optical tweezers and a microfluidic chip. (*Source*: Reproduced from Wang *et al.*, 2011, with permission from the Royal Society of Chemistry.)

8.4.6 Magnetic mechanisms

Erythrocytes possess the protein haemoglobin, containing four iron atoms in a ferrous state for oxygen binding. Oxyhaemoglobin and deoxyhaemoglobin are diamagnetic and paramagnetic materials, respectively. The metalloprotein methaemoglobin ($Fe^{3}+$) is also present in erythrocytes, but in larger quantities for diseased cells, has a greater paramagnetic susceptibility than its ferrous state counterpart, and malaria infected erythrocytes (Hackett *et al.*, 2009). The first successful separation of erythrocytes from whole blood using magnetic field gradients was reported by Melville *et al.*

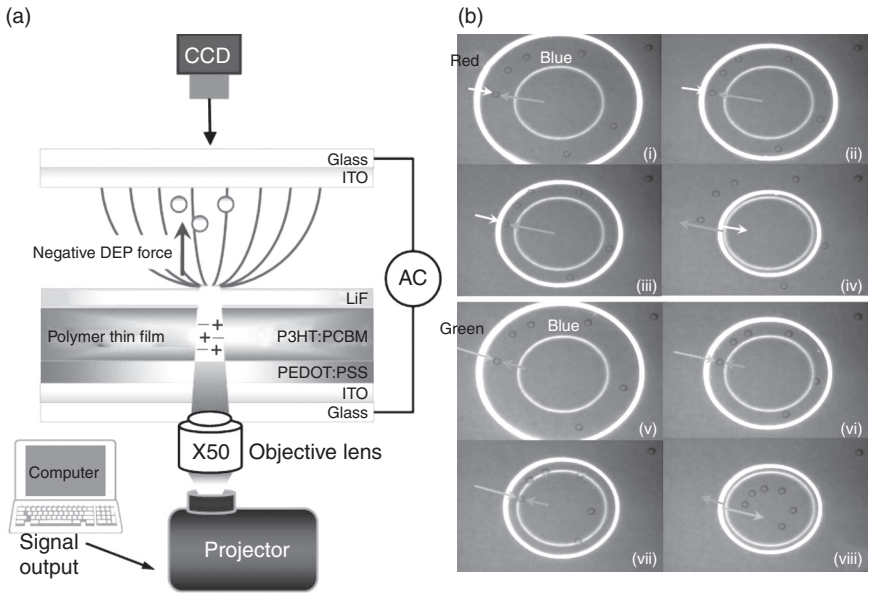

8.21 (a) Schematic illustration of polymer-based ODEP platform for selective manipulation of particles. (b) Series of photographs taken under an optical microscope, demonstrating the selective manipulation of polystyrene particles with a diameter of 20 μm. (i–iv) All polymer particles between the outer – and inner rings are excluded as the diameter of the outer ring shrinks. (v–viii) All the polymer particles between the new outer- and previous inner rings can be collected inside the inner ring as the diameter of the outer ring shrinks. (*Source*: Reproduced from Wang *et al.*, 2010, with permission from the American Institute of Physics.)

(1975a, 1975b). The use of magnetic susceptibility as a separation parameter for magnetophoresis in laminar flow has been successfully applied directly to biological cells (Paul *et al.*, 1981; Takayasu *et al.*, 2000; Zborowski *et al.*, 2003). Manipulating non-magnetic cells in a high gradient magnetic field coupled with microfluidics and applications of magnetic nanoparticles in medicine and biotechnology has previously been described (Pankhurst *et al.*, 2003; Pamme, 2006; Liu *et al.*, 2009).

Magnetic force

A magnetic material placed in a magnetic field (H) has a magnetic induction (B), measured in teslas (T), expressed by Equation [8.44], where μ_0 is the permeability of free space ($4\pi\times10^{-7}\,\mathrm{Tm\,A^{-1}}$) and the magnetisation, ($M = m/V$), is the magnetic moment (m) per unit volume (V) of the material (Oberteuf, 1974).

$$B = \mu_0 (H + M) \quad [8.47]$$

Magnetic susceptibility (χ) is a dimensionless number relating to the degree of magnetisation (A m^{-1}) of a material in response to a magnetic field.

$$M = \chi H \quad [8.48]$$

Materials classified according to their magnetic susceptibility are diamagnetic ($\chi < 0$), paramagnetic ($\chi > 0$) or ferromagnetic ($\chi >> 0$) (Fig. 8.22). Ferromagnets, also known as permanent magnets (e.g., iron and nickel) are strongly attracted to magnetic fields. Materials such as platinum and oxygen are considered paramagnetic and are weakly attracted and aligned in magnetic field maxima, while biological materials such as proteins, DNA and cells are weakly diamagnetic and are repelled to magnetic field minima. Due to such factors as intrinsic structural impurities or anisotropic lattice arrangements, ferromagnetic materials on the micron scale often exhibit irreversible magnetisation processes known as M-H hysteresis loops (magnetic remnant ≠ 0), while magnetic nanoparticles display antihysteresis, a quality related to superparamagnetism – the thermally activated flipping of the net moment (Pankhurst *et al.*, 2003). In the presence of a magnetic field superparamagnetic (SPM) particles become magnetised and upon removal of the magnetic field the magnetic remnant is zero, allowing particles to disperse freely within suspending media. In medical applications, SPM beads typically consist of a magnetic iron oxide core (e.g., magnetite or maghaemite) surrounded by a biomaterial of interest for preferential functionalisation, with size variations up to the micron scale.

The magnetic force (F_{magnetic}) on a magnetic particle in a magnetic field gradient is dependent on the particle volume (V_p) and the magnetic susceptibility difference ($\Delta\chi = \chi_p - \chi_m$) between particle and surrounding medium (Zborowski *et al.*, 1999; Gijs, 2004; Moore *et al.*, 2004).

$$F_{\text{magnetic}} = \frac{V_p \Delta\chi}{\mu_0} (B \bullet \nabla) B \quad [8.49]$$

Non-zero initial magnetisation (M_0) of SPM beads, observed in magnetisation curves of commercial suppliers, prompted Shevkoplyas *et al.* (2007) to modify the conventional expression for the magnetisation force. A comparison of Equations [8.49] and [8.50] against experimental results of the manufacturer showed better agreement with the modified equation, enabling better prediction of bead manipulation in microfluidic systems of weaker magnetic field strengths (up to ~10 mT).

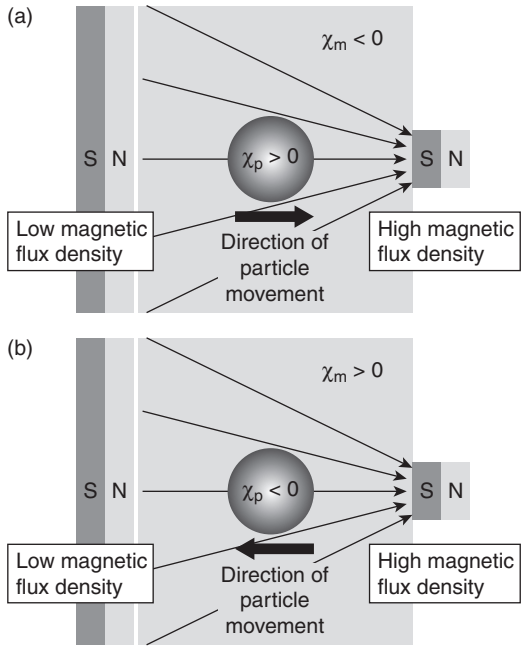

8.22 (a) Principle of magnetic attraction: a magnetic particle ($\chi_p > 0$) is suspended in a diamagnetic medium ($\chi_m < 0$), giving a Dc value greater than zero and resulting in attraction of the particle towards the magnetic field. (b) Principle of diamagnetic repulsion: a diamagnetic particle ($\chi_p < 0$) is suspended in a paramagnetic medium ($\chi_m > 0$), giving a Dc value less than zero and resulting in repulsion of the particle from the magnetic field. (*Source*: Reproduced from Rodríguez-Villarreal *et al.*, 2011, with permission from The Royal Society of Chemistry.)

$$F_{\text{magnetic}} = \left(m_p \bullet \nabla\right) B = \rho V_p \left(M_0 \bullet \nabla\right) B + \frac{V_p \chi_p}{\mu_0} \left(B \bullet \nabla\right) B \qquad [8.50]$$

Magnetophoretic devices

The most common approach to facilitate cell manipulation (excluding RBCs and magnetotactic bacteria (MTB)) in magnetic fields is through surface-labelling with functionalised SPM particles, commercially termed magnet-activated cell sorting (MACS) by Miltenyi Biotec. However other methods, such as endocytotic uptake of magnetic nanoparticles by inflammatory cells and separation based on their uptake capacity, have been reported (Robert *et al.*, 2011). McCloskey *et al.* (2003) identified four parameters which

significantly influenced the magnetophoretic mobility (m_{magnetic}) of immunomagnetically labelled cells as (1) antibody binding capacity, (2) secondary antibody amplification, (3) interaction parameter of particle-magnetic field, and (4) cell diameter. The magnetophoretic mobility arises when Stokes drag is set to equal the magnetic force on the particle and solved for the magnetic-induced migration velocity (V_{p}) in a magnetic force field strength (S_{magnetic}), and can be used as a separation parameter between magnetically tagged and untagged cells.

$$m_{\text{magnetic}} = \frac{V_{\text{p}}}{S_{\text{magnetic}}} \qquad [8.51]$$

This parameter was further explored by Moore *et al*. (2004), in which the medium was modified with gadolinium making it paramagnetic, thus minimising the crossover of non-specific (i.e., untagged) particles and RBCs (repulsive-mode magnetophoresis) into the adjacent outlet stream. These studies were predominantly based around large magnets driving the high gradient magnetic fields within millimetre-sized channels. The arrangement of magnets, either permanent magnets (e.g., NdFeB) or electromagnets, varied according to channel geometry and operation; for instance, quadrupole magnet sorter (QMS) arrangements have been described for continuous separation and sorting of cells (Zborowski *et al*., 1999; Moore *et al*., 2004), and perpendicular dipole arrangements to the flow channel for fractionation, magnetophoretic mobility studies, diamagnetic repulsion flow focusing and on-chip free-flow magnetophoretic separation and sorting as shown in Fig. 8.23 (Pamme and Manz, 2004; Pamme and Wilhelm, 2006; Schneider *et al*., 2006; Jin *et al*., 2008; Rodriguez-Villarreal *et al*., 2010). More complex microfabricated magnet arrangements, integrated with microsystems, have also been developed enabling localised field gradient generation for more accurate particle control and manipulation, with the aim of better integration of magnetophoretic devices into lab on a chip systems. A comprehensive overview of microelectromagnetic traps (MET), the geometries fabricated to produce magnetic field gradients which is proportional to current density and electromagnet size and their various applications from cell manipulation and ferrofluid actuation in microchannels to biosensors was recently discussed (Basore and Baker, 2012). Using soft lithography, micromagnetic systems (Fig. 8.24a–8.24c) employing current carrying circuits were used to transport 4.5 μm microbeads along the B-field maxima (Deng *et al*., 2001). Two serpentine wires, shifted linearly in phase by $\pi/3$, allowed the magnetic fields to become superimposed when current flowed, trapping magnetic beads. Upon changing the input current through the wires, the field maxima changed with the

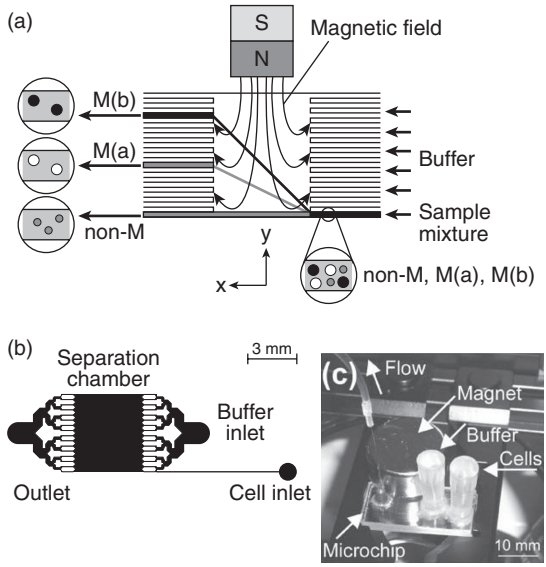

8.23 (a) Principle of free-flow magnetophoresis: laminar flow is applied in *x*-direction over a separation chamber, a magnetic field is applied in *y*-direction. Non-magnetic material follows the direction of laminar flow, whereas magnetic particles/cells are deflected from the direction of laminar flow. (b) The microfluidic design featuring the separation chamber, one cell inlet channel and 16 buffer inlet channels. On the opposite side there were 16 outlet channels. The structure was 30 mm deep. (c) Photograph of the microfluidic chip with cell and buffer inlet reservoirs, connection to syringe pump and NdFeB magnet. (*Source*: Reproduced from Pamme and Wilhelm, 2006, with permission from The Royal Society of Chemistry.)

microbead moving position in a zigzag path as in Fig. 8.24d–8.24h. Semi-encapsulated planar spiral electromagnets on a glass wafer generated a magnetic field in a microchannel from a 300 mA dc current applied to the inductor enabling magnetic microbead separation (Choi *et al.*, 2001). Continuous immunomagnetic separation of leukocytes from whole blood in a microfluidic system was achieved by inducing lateral forces from microfabricated magnetic diagonal parallel stripe arrays, which trapped and altered tagged particles' flow directions (Inglis *et al.*, 2004). Numerical models for the lateral magnetophoretic displacement of superparamagnetic beads and immunomagnetically labelled cells deflected in a microfluidic systems have recently been reported for a range of configurations (bead type, magnet type and orientation, binding capacity), flow rates and channel geometries to accurately predict magnetophoretic deflection or capture (Forbes and Forry, 2012).

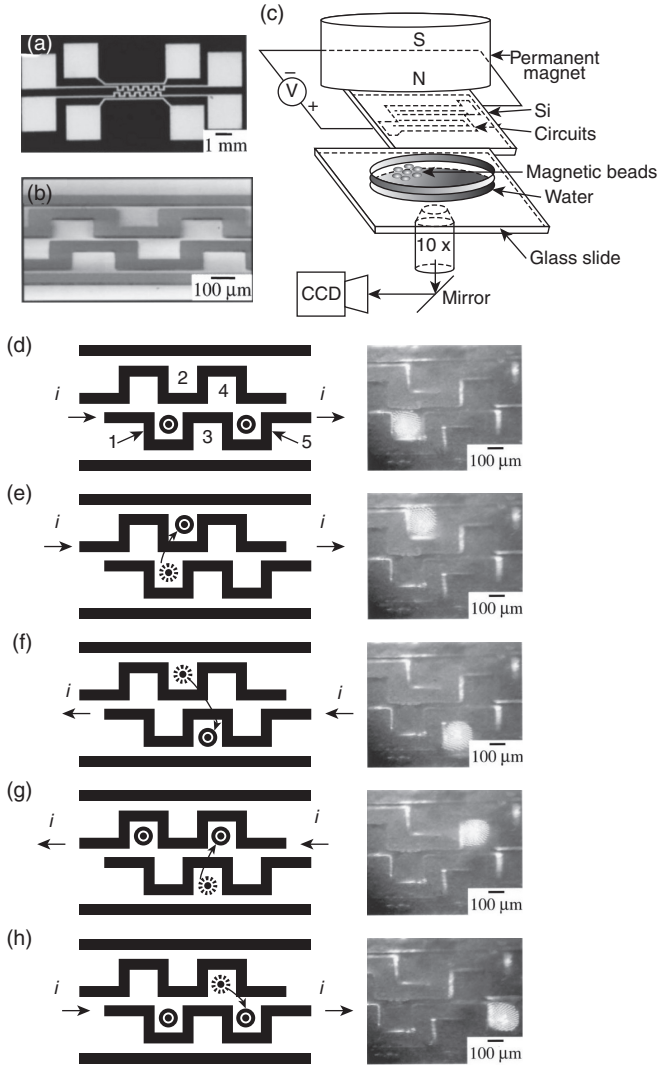

8.24 (a) Optical micrograph of micromagnetic system. The wires were ~100 μm wide and 10 μm high. The turns of the serpentine wires had an inner dimension of 200 μm × 200 μm. The closest vertical spacing between the two serpentine wires is ~50 μm. The closest horizontal distance between two turns of different wires was ~100 μm. The contact pads were 1 mm × 1 mm. (b) Magnified view of the fabricated system by SEM. (c) Set-up for the manipulation of superparamagnetic microbeads using the micromagnetic system. The distance between the circuits and the air–water interface was ~50–400 μm, and the permanent magnet was 2–4 cm away from the circuits during the experiment. (d)–(h) Manipulation of magnetic microbeads in the micromagnetic system. (*Source*: Reproduced from Deng *et al.*, 2001, with permission from the American Institute of Physics.)

8.5 Manipulation of cancer cells in microfluidic systems

Microfluidics in cell biology has been applied in the manipulation and analysis of rare cells – e.g., stem, foetal and cancer cells. The reduction in system dimensions, coupled with precise manipulation technologies, represents a positive shift towards accurate, low cost cellular bioprocesses with low sample volumes and parallelisation capabilities. Of particular interest are the potential offerings these technologies can provide in advancing our knowledge and understanding in cancer biology, from the molecular mechanisms of resistance to anti-cancer drugs and drug discovery, through to label-less on-chip flow cytometry and micro-sorting operations. Although challenges are still present, microfluidic systems are fast becoming key components in many labs undertaking cancer research.

8.5.1 Deformability and migration studies

Cancerous cells are able to change their migration mechanisms more robustly than non-cancerous cells in response to changes in external stimuli. This has led to therapeutic approaches for immobilising cancer cells via inhibition of signal transduction pathways to investigate migration mechanisms. Variations in speed and mode of migration have been identified amongst different cancer cell lines, with extracellular matrix-filled PDMS-microchannels designed to have predefined cell migration paths for visual quantification. Three modes of cancer migration identified include (1) mesenchymal, (2) amoeboid, and (3) collective cell migration, distinguishable by their morphology and migration characteristics in response to soluble chemokines, ECM, and surface cues (Huang *et al*., 2011). An underlying cause of a cancer cell's ability to migrate through confined 3D spaces is due to its high deformability afforded by cytoskeleton compliance (Suresh, 2007). Hou *et al*. (2009) described the use of microfluidics to probe the deformation of benign and tumour breast cancer cells through microchannel constrictions, indicating channel entry time was faster for metastatic cells and could be used as a label-free biomarker to differentiate between healthy and non-healthy cells. Employing inertial focusing and deformability-induced migration, Hur *et al*. (2011) were able to demonstrate a passive high-throughput cell classification system, based solely on size and deformation characteristics, for targeting and enriching MCF-7 cells spiked in peripheral blood. Furthermore, cells immobilised via adhesion molecules (e.g., cadherins) coated on the surfaces of channel walls or micropillars within the channels and subjected to fluid hydrodynamic flow, applied electric fields, and different chemoattractants in gradient or diffusion based flows have been used to investigate the influences of hydrodynamic loading, chemotaxis and

electrotaxis on mechanical interactions of the substrate and the migrating cell (Walker *et al*., 2005; Cheung *et al*., 2009; Li and Lin, 2011).

8.5.2 Microfluidic separation and sorting

Tanaka *et al*. (2012) investigated the relationship between haematocrit and circulating tumour cancer (CTC) cell-inertial migration for designing microfluidic separators, finding cancer cell equilibrium could only be achieved at up to 10% haematocrit volume with appropriate channel lengths. This enabled a separation strategy to be developed without the need of surface cell markers, such as epithelial cell adhesion molecules (EpCAM). Human liver cancer cells (HepG2) and fibroblasts (NIH/3T3) were separated based on their respective cell cycle phases indicating HDF's potential as a powerful damage-free separation technology in cellular genetics (Migita *et al*., 2010). Also, hydrophoretic sorting of an asynchronous human leukemic monocyte lymphoma population into G_o/G_1 and G_2/M cell cycle phases with 95.5% and 85.2% efficiencies, respectively, was achieved by Choi *et al*. (2009). Thévoz *et al*. (2010) demonstrated acoustophoretic cell synchronisation (ACS) of mammalian cells as in Fig. 8.25. An asynchronous sample of MDA-MB-231 human breast carcinoma cells was separated according to their size dependent phase within the cell cycle, with larger G_2/M and S-phases cells moving more rapidly to the central stream (outlet A) than the smaller G_1 phase cells (outlet B). G_1 phase synchrony at ~84% was achieved.

Magnetophoretic microfluidic devices have gained momentum in testing clinical samples to isolate, separate and analyse CTCs, haemopoietic stem cells (HSC) or endothelial progenitor cells (EPC) (Zborowski and Chamers, 2011; Plouffe *et al*., 2012). Iterative microsystem optimisation through either CD133+ or MCF-7 carcinoma cell separation from human blood was performed in a disposable microfluidic chip, with applied currents of up to 1 A, producing high purity and a >96% separation efficiency. An automated cell sorting microdevice consisting of nickel pillars, magnetised externally, fabricated on PDMS and microvalves, was used to separate A549 cancer cells (Liu *et al*., 2007). SPM beads were efficiently trapped between magnetised pillars arrays while *in situ* biofunctionalisation with a glycoprotein and washing of the beads took place in the vicinity of the pillars. Introduced A549 cells captured in the array, then released to the outlet, were enriched by a factor of 133, based on an original mixture ratio of 1:10 cancer to RBCs. A variation to Liu *et al*.'s (2007) technique was described by Saliba *et al*. (2010) in which biofunctionalised SPM beads self-assembled into microarray columns when magnetic traps, prepared by microcontact printing, were magnetised (Fig. 8.26). Using flow activated cell and SPM bead interaction, Jurkat and Raji cells were captured with a >94% efficiency, with successful *in situ* on-cell

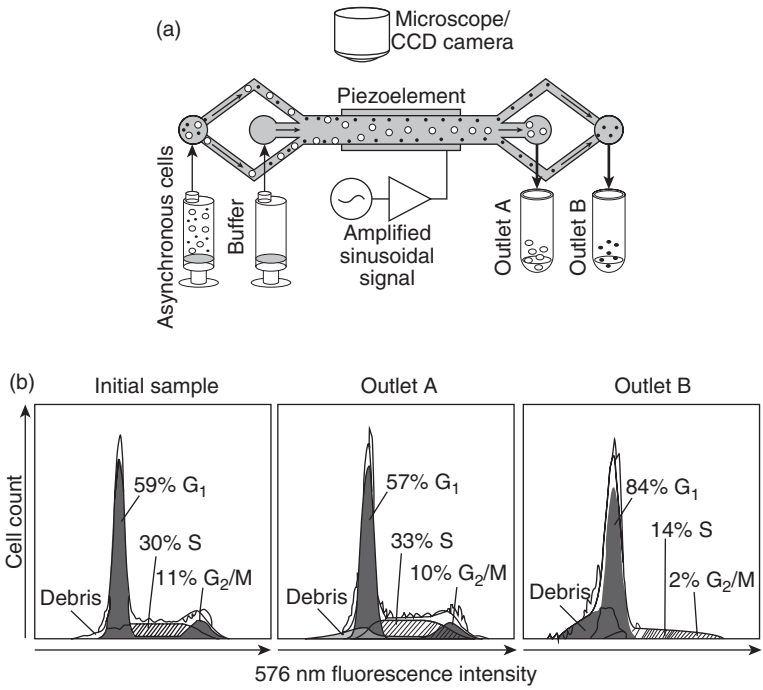

8.25 (a) Acoustophoretic cell synchronisation (ACS) device and experimental set-up. Asynchronous mixture of cells and buffer volumetrically pumped into the ACS device. Synchronisation is achieved by fractionating the cells according to size such that larger cells (*e*.g., G_2) elute through outlet A whereas smaller cells (e.g., G_1) elute through outlet B. (b) Flow cytometry histograms showing cell cycle distributions before and after synchronisation, based on measurements of red fluorescence centred at 576 nm, after staining the cellular DNA with propidium iodide. The populations in each phase of the cell cycle were determined by fitting cell cycle models to the histograms. The synchronised cell population at outlet B shows 84% of all cells in the G_1 phase, with 14% in the S phase and 2% in G_2/M phase. (*Source*: Reproduced in part from Thévoz *et al.*, 2010, with permission from American Chemical Society.)

culturing carried out immediately after sorting. These systems in which biofunctionalised SPM beads were used as an immobilised bed to capture untagged cells represented a new paradigm to the freely suspended multi-targeted immunomagnetic activation approach traditionally and still employed prior to sample injection in to the microchannel (Adams *et al.*, 2008).

Recently a tuneable magnetophoretic separation device was used to separate label-free cells in a flow focused paramagnetic ionic solution (Shen

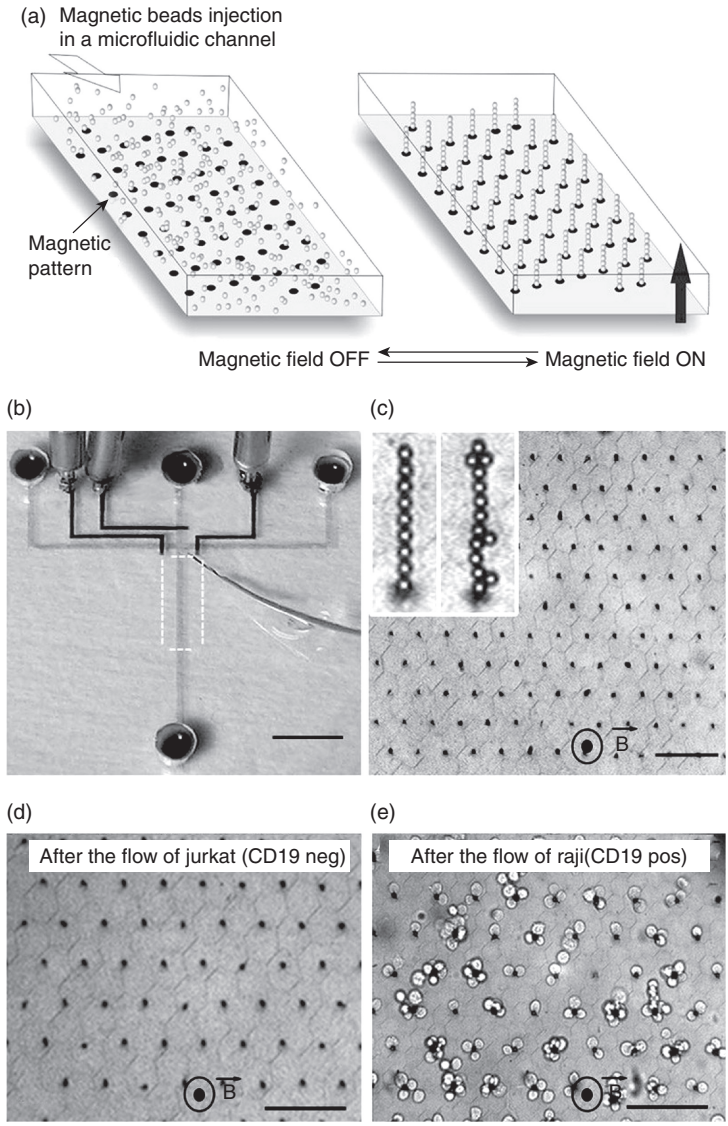

8.26 Principle and practical implementation of the Ephesia system. (a) Principle of magnetic self-assembly. A hexagonal array of magnetic ink is patterned at the bottom of a microfluidic channel. Beads coated with an antibody are injected in the channel. Beads are submitted to Brownian motion. The application of an external vertical magnetic field induces the formation of a regular array of bead columns localised on top of the ink dots. (b) Two level PDMS integrated microchip. Delivery and separation channels for the cells appear in the lighter shade channels. Inlets ports appear as the four

(Continued)

et al., 2012). Although at low throughput, human lymphoma monocytes (U937) and RBCs suspended in varying concentrations of paramagnetic solution gadolinium diethylenetriamine pentaacetic acid (Gd-DTPA), were separated through repulsion forces which drove the diamagnetic particles away from the magnet at varying magnetophoretic mobility rates based on size and magnetic susceptibility properties.

8.5.3 Current challenges in sorting and detection

High-throughput microfluidic flow cytometry devices in some combination, focus, count, detect or sort cells on a single chip and rival the more complex, costly and bulkier FACS flow cytometers (e.g., BD Biosciences). Since Fu *et al*. (1999) introduced μFACS, an assortment of activated cell sorting microdevices relying on DEP (DACS), synthetic tags for altering complex permittivities of multi-target cells (MT-DACS), Raman spectroscopy (RACS), hydrodynamics and magnetic susceptibilities (MACS) have been described, with some achieving throughputs as high as 10000 cells per second, or efficiencies >85% for cancerous and non-cancerous separation (Hu *et al*., 2005; Inglis *et al*., 2008; Kim *et al*., 2008; Lau *et al*., 2008; An *et al*., 2009; Kim and Soh, 2009; Cho *et al*., 2010a). These new microflow cytometers have been demonstrated on cancerous cells and, except for FACS and MACS, they do not require pre-labelling, relying only on the intrinsic properties (size, dielectric, deformability, refractive index) of the cells for sorting. Importantly, if any of the new microsystems is to be a serious challenger to the sheath-based, high speed quantification and sorting of FACS, issues regarding throughput, increased sensitivity and integration of actuating mechanisms need to be fully addressed and validated before uptake in a clinical setting can be endorsed.

8.26 Continued

dark circular reservoirs. The separation channel is the longer vertical branch. The area bearing magnetic posts is marked by the dotted white box. Channels in the upper PDMS layer, controlling the opening and closing of the inlet channels, appear as the darker shade channels. A thermocouple for in situ control of the temperature in the system is located at the top of the dotted white boundary. (Scale bar: 0.5 cm.) (c) Magnetically assembled array of columns of 4.5 μm beads coated with anti-CD19 mAb (specifically retaining Raji B-Lymphocytes). Typical column shapes are shown in the insets. (Scale bar: 80 μm.) (d) Optical micrograph of the columns after the passage of 1000 Jurkat cells, no cells seen. (e) After the passage of 400 Raji cells, numerous cells are captured and rosetted on the columns. (Scale bar: 80 μm.). (*Source*: Reproduced from Saliba *et al*., 2010, Copyright 2010 National Academy of Sciences, USA.)

8.6 Conclusion and future trends

To begin handling clinically relevant samples, a concerted effort in combining multiple manipulation technologies is needed. It could be argued that Giddings laid down this foundation, but nowadays the rapid advances in technology has had a profound impact on engineering design and optimisation of microfluidic devices for general purpose use. For example, when dealing with blood samples (~40% (v/v) haematocrit), if on-chip sample preparation units are to be incorporated for a fully automated LOC system, electrokinetic technologies with simple channel geometries would simply not cope with the high medium conductivities. Coupling of hydrodynamic technologies (e.g., hydrodynamic filtration), through flow splitting and recombining with low ionic solutions could improve downstream electrokinetic processing operations. This approach to multi-technology coupling (MTC) integration has recently begun to become more prominent, for instance the use of complex microfluidic networks to generate conductivity gradients in DEP separation (Vahey and Voldman, 2008); the serial combination of multi-orifice flow fractionation (MOFF) and DEP at high flow rates (126 μL/min) for continuous CTC separation from blood samples (Moon *et al*., 2011); combining acoustophoresis with DEP for focusing and preconcentration (Ravula *et al*., 2008); integrating acoustophoresis and magnetophoresis for multiparameter particle separation (Adams *et al*., 2009); or the apparent combination of PFF with DEP in an ApoStream™ flow cell for the continuous separation of CTCs from blood (Gupta *et al*., 2012).

8.7 Sources of further information and advice

Sources of information are predominantly in journal publications in which innovative applications of the technologies presented are used in microfluidic devices for a range of biomedical and biotechnological operations. These high impact journals include: Lab on a chip; Analytical Chemistry; Biomedical Microdevices; Biomicrofluidics; Proceedings of the National Academy of Sciences; Science; Nature Biotechnology and Electrophoresis.

Some commercial enterprises offering fabrication services of microfluidic devices for biological applications include: Fluidigm Corp (www.fluidgim.com); Dolomite Microfluidics (www.dolomite-microfluidics.com); Micralyne (www.micralyne.com) and Epigem Ltd (www.epigem.co.uk). Companies recently established to exploit different cell micromanipulation technologies for characterisation, separation, sorting, etc., include, Optofluidics, DEPtech, Apocell, CytonomeST with many more being created and larger biotech

and pharmaceutical firms also becoming involved. Lastly, established international conferences highlighting developments in this area include μTAS, Lab on a Chip World Congress, Biodetection Technologies and Sample Prep by the Knowledge Foundation.

8.8 References

Adams, J. D., Kim, U. and Soh, H. T. (2008). Multitarget magnetic activated cell sorter. *Proceedings of the National Academy of Sciences of the United States of America*, **105**, 18165–18170.

Adams, J. D., Thevoz, P., Bruus, H. and Soh, H. T. (2009). Integrated acoustic and magnetic separation in microfluidic channels. *Applied Physics Letters*, **95**, 254103–1.

Alberts, B., Bray, D., Lewis, J., Raff, M., Roberts, K. and Watson, J. D. (1994). *Molecular Biology of the Cell* New York, Garland Publishing.

An, J., Lee, J., Lee, S. H., Park, J. and Kim, B. (2009). Separation of malignant human breast cancer epithelial cells from healthy epithelial cells using an advanced dielectrophoresis-activated cell sorter (DACS). *Analytical and Bioanalytical Chemistry*, **394**, 801–809.

Aoki, R., Yamada, M., Yasuda, M. and Seki, M. (2009). In-channel focusing of flowing microparticles utilizing hydrodynamic filtration. *Microfluidics and Nanofluidics*, **6**, 571–576.

Ashkin, A. (1992). Forces of a single-beam gradient laser trap on a dielectric sphere in the ray optics regime. *Biophysical Journal*, **61**, 569–582.

Ashkin, A. (1997). Optical trapping and manipulation of neutral particles using lasers. *Proceedings of the National Academy of Sciences of the United States of America*, **94**, 4853–4860.

Ashkin, A. and Dziedzic, J. M. (1987). Optical trapping and manipulation of viruses and bacteria. *Science*, **235**, 1517–1520.

Ashkin, A., Dziedzic, J. M. and Yamane, T. (1987). Optical trapping and manipulation of single cells using infrared-laser beams. *Nature*, **330**, 769–771.

Asmolov, E. S. (1999). The inertial lift on a spherical particle in a plane Poiseuille flow at large channel Reynolds number. *Journal of Fluid Mechanics*, **381**, 63–87.

Barshtein, G., Ben-Ami, R. and Yedgar, S. (2007). Role of red blood cell flow behavior in hemodynamics and hemostasis. *Expert Review of Cardiovascular Therapy*, **5**, 743–52.

Basore, J. R. and Baker, L. A. (2012). Applications of microelectromagnetic traps. *Analytical and Bioanalytical Chemistry*, **403**, 2077–2088.

Bazant, M. Z. and Squires, T. M. (2004). Induced-charge electrokinetic phenomena: Theory and microfluidic applications. *Physical Review Letters*, **92**, 066101.

Bazant, M. Z. and Squires, T. M. (2010). Induced-charge electrokinetic phenomena. *Current Opinion in Colloid & Interface Science*, **15**, 203–213.

Beebe, D. J., Mensing, G. A. and Walker, G. M. (2002). Physics and applications of microfluidics in biology. *Annual Review of Biomedical Engineering*, **4**, 261–286.

Berthier, E., Warrick, J., Y, H. and Beebe, D. J. (2008). Managing evaporation for more robust microscale assays – Part 1. Volume loss in high throughput assays. *Lab on a Chip*, **8**, 852–859.

Bhagat, A. A. S., Kuntaegowdanahalli, S. S. and Papautsky, I. (2008a). Continuous particle separation in spiral microchannels using dean flows and differential migration. *Lab on a Chip*, **8**, 1906–1914.

Bhagat, A. A. S., Kuntaegowdanahalli, S. S. and Papautsky, I. (2008b). Enhanced particle filtration in straight microchannels using shear-modulated inertial migration. *Physics of Fluids*, **20**, 101702.

Brody, J. P., Yager, P., Goldstein, R. E. and Austin, R. H. (1996). Biotechnology at low Reynolds numbers. *Biophysical Journal*, **71**, 3430–3441.

Bruus, H. (2012a). Acoustofluidics 7: The acoustic radiation force on small particles. *Lab on a Chip*, **12**, 1014–1021.

Bruus, H. (2012b). Acoustofluidics 10: Scaling laws in acoustophoresis. *Lab on a Chip*, **12**, 1578–1586.

Burgarella, S., Merlo, S., Dell'Anna, B., Zarola, G. and Bianchessi, M. (2010). A modular micro-fluidic platform for cells handling by dielectrophoresis. *Microelectronic Engineering*, **87**, 2124–2133.

Caldwell, K. D., Cheng, Z. Q., Hradecky, P. and Giddings, J. C. (1984). Separation of human and animal-cells by steric field-flow fractionation. *Cell Biophysics*, **6**, 233–251.

Castellanos, A., Ramos, A., Gonzalez, A., Green, N. G. and Morgan, H. (2003). Electrohydrodynamics and dielectrophoresis in microsystems: Scaling laws. *Journal of Physics D-Applied Physics*, **36**, 2584–2597.

Cen, E. G., Dalton, C., Li, Y., Adamia, S., Pilarski, L. M. and Kaler, K. V. I. S. (2004). A combined dielectrophoresis, traveling wave dielectrophoresis and electrorotation microchip for the manipulation and characterization of human malignant cells. *Journal of Microbiological Methods*, **58**, 387–401.

Cheng, I. F., Froude, V. E., Zhu, Y. X., Chang, H. C. and Chang, H. C. (2009). A continuous high-throughput bioparticle sorter based on 3D traveling-wave dielectrophoresis. *Lab on a Chip*, **9**, 3193–3201.

Cheung, L. S. L., Zheng, X. G., Stopa, A., Baygents, J. C., Guzman, R., Schroeder, J. A., Heimark, R. L. and Zohar, Y. (2009). Detachment of captured cancer cells under flow acceleration in a bio-functionalized microchannel. *Lab on a Chip*, **9**, 1721–1731.

Chianea, T., Assidjo, N. E. and Cardot, P. J. P. (2000). Sedimentation field-flow-fractionation: emergence of a new cell separation methodology. *Talanta*, **51**, 835–847.

Chiou, P. Y., Ohta, A. T. and Wu, M. C. (2005). Massively parallel manipulation of single cells and microparticles using optical images. *Nature*, **436**, 370–372.

Cho, S. H., Chen, C. H., Tsai, F. S., Godin, J. M. and Lo, Y. H. (2010a). Human mammalian cell sorting using a highly integrated micro-fabricated fluorescence-activated cell sorter (mu FACS). *Lab on a Chip*, **10**, 1567–1573.

Cho, S. H., Godin, J. M., Chen, C. H., Qiao, W., Lee, H. and Lo, Y. H. (2010b). Review article: Recent advancements in optofluidic flow cytometer. *Biomicrofluidics*, **4**, 043001.

Choi, J.-W., Liakopoulos, T. M. and Ahn, C. H. (2001). An on-chip magnetic bead separator using spiral electromagnets with semi-encapsulated permalloy. *Biosensors and Bioelectronics*, **16**, 409–416.

Choi, S. and Park, J. K. (2007). Continuous hydrophoretic separation and sizing of microparticles using slanted obstacles in a microchannel. *Lab on a Chip*, **7**, 890–897.

Choi, S. and Park, J. K. (2009). Tuneable hydrophoretic separation using elastic deformation of poly(dimethylsiloxane). *Lab on a Chip*, **9**, 1962–1965.

Choi, S., Song, S., Choi, C. and Park, J. K. (2007). Continuous blood cell separation by hydrophoretic filtration. *Lab on a Chip*, **7**, 1532–1538.

Choi, S., Song, S., Choi, C. and Park, J. K. (2008). Sheathless focusing of microbeads and blood cells based on hydrophoresis. *Small*, **4**, 634–641.

Choi, S., Song, S., Choi, C. and Park, J. K. (2009). Microfluidic self-sorting of mammalian cells to achieve cell cycle synchrony by hydrophoresis. *Analytical Chemistry*, **81**, 1964–1968.

Choi, Y.-S., Seo, K.-W. and Lee, S.-J. (2011). Lateral and cross-lateral focusing of spherical particles in a square microchannel. *Lab on a Chip*, **11**, 460–465.

Chou, C.-F., Tegenfeldt, J. O., Bakajin, O., Chan, S. S., Cox, E. C., Darnton, N., Duke, T. and Austin, R. H. (2002). Electrodeless dielectrophoresis of single- and double-stranded DNA. *Biophysical Journal*, **83**, 2170–2179.

Coley, H. M., Labeed, F. H., Thomas, H. and Hughes, M. P. (2007). Biophysical characterization of MDR breast cancer cell lines reveals the cytoplasm is critical in determining drug sensitivity. *Biochimica Et Biophysica Acta-General Subjects*, **1770**, 601–608.

Cornish, R. J. (1928). Flow in a pipe of rectangular cross-section. *Proceedings of the Royal Society of London. Series A, Containing Papers of a Mathematical and Physical Character*, **120**, 691–700.

Crane, J. S. and Pohl, H. A. (1968). A study of living and dead yeast cells using dielectrophoresis. *Journal of the Electrochemical Society*, **115**, 584.

Crane, J. S. and Pohl, H. A. (1972). Theoretical models of cellular dielectrophoresis. *Journal of Theoretical Biology*, **37**, 15–41.

Cummings, E. B. and Singh, A. K. (2000). Dielectrophoretic trapping without embedded electrodes. *In:* Mastrangelo, C. H. and Becker, H. (eds.) *Microfluidic Devices and Systems Iii*. Bellingham: Spie-Int Soc Optical Engineering.

Cummings, E. B. and Singh, A. K. (2003). Dielectrophoresis in microchips containing arrays of insulating posts: Theoretical and experimental results. *Analytical Chemistry*, **75**, 4724–4731.

Dalton, C. and Kaler, K. V. I. S. (2007). A cost effective, re-configurable electrokinetic microfluidic chip platform. *Sensors and Actuators B: Chemical*, **123**, 628–635.

Davis, J. A., Inglis, D. W., Morton, K. J., Lawrence, D. A., Huang, L. R., Chou, S. Y., Sturm, J. C. and Austin, R. H. (2006). Deterministic hydrodynamics: Taking blood apart. *Proceedings of the National Academy of Sciences of the United States of America*, **103**, 14779–14784.

Demierre, N., Braschler, T., Linderholm, P., Seger, U., van Lintel, H. and Renaud, P. (2007). Characterization and optimization of liquid electrodes for lateral dielectrophoresis. *Lab on a Chip*, **7**, 355–365.

Deng, T., Whitesides, G. M., Radhakrishnan, M., Zabow, G. and Prentiss, M. (2001). Manipulation of magnetic microbeads in suspension using micromagnetic systems fabricated with soft lithography. *Applied Physics Letters*, **78**, 1775–1777.

Di Carlo, D. (2009). Inertial microfluidics. *Lab on a Chip*, 9, 3038–3046.

Di Carlo, D., Edd, J. F., Irimia, D., Tompkins, R. G. and Toner, M. (2008). Equilibrium separation and filtration of particles using differential inertial focusing. *Analytical Chemistry*, **80**, 2204–2211.

Di Carlo, D., Irimia, D., Tompkins, R. G. and Toner, M. (2007). Continuous inertial focusing, ordering, and separation of particles in microchannels. *Proceedings of the National Academy of Sciences of the United States of America*, **104**, 18892–18897.

Do, J., Zhang, J. Y. and Klapperich, C. M. (2011). Maskless writing of microfluidics: Rapid prototyping of 3D microfluidics using scratch on a polymer substrate. *Robotics and Computer-Integrated Manufacturing*, **27**, 245–248.

Doh, I. and Cho, Y.-H. (2005). A continuous cell separation chip using hydrodynamic dielectrophoresis (DEP) process. *Sensors and Actuators A: Physical*, **121**, 59–65.

Eriksson, E., Sott, K., Lundqvist, F., Sveningsson, M., Scrimgeour, J., Hanstorp, D., Goksor, M. and Graneli, A. (2010). A microfluidic device for reversible environmental changes around single cells using optical tweezers for cell selection and positioning. *Lab on a Chip*, **10**, 617–625.

Evander, M., Lenshof, A., Laurell, T. and Nilsson, J. (2008). Acoustophoresis in wet-etched glass chips. *Analytical Chemistry*, **80**, 5178–5185.

Fahraeus, R. and Lindqvist, T. (1931). The viscosity of the blood in narrow capillary tubes. *American Journal of Physiology*, **96**, 562–568.

Fatoyinbo, H. O., Hoeftges, K. F. and Hughes, M. P. (2008). Rapid-on-chip determination of dielectric properties of biological cells using imaging techniques in a dielectrophoresis dot microsystem. *Electrophoresis*, **29**, 3–10.

Fatoyinbo, H. O., Hoettges, K. F., Reddy, S. M. and Hughes, M. P. (2007a). An integrated dielectrophoretic quartz crystal microbalance (DEP-QCM) device for rapid biosensing applications. *Biosensors and Bioelectronics*, **23**, 225–232.

Fatoyinbo, H. O., Hughes, M. P., Martin, S. P., Pashby, P. and Labeed, F. H. (2007b). Dielectrophoretic separation of Bacillus subtilis spores from environmental diesel particles. *Journal of Environmental Monitoring*, **9**, 87–90.

Fatoyinbo, H. O., Kadri, N. A., Gould, D. H., Hoettges, K. F. and Labeed, F. H. (2011). Real-time cell electrophysiology using a multi-channel dielectrophoretic-dot microelectrode array. *Electrophoresis*, **32**, 2541–2549.

Forbes, T. P. and Forry, S. P. (2012). Microfluidic magnetophoretic separations of immunomagnetically labeled rare mammalian cells. *Lab on a Chip*, **12**, 1471–1479.

Fricke, H. (1924). A mathematical treatment of the electrical conductivity of colloids and cell suspensions. *Journal of General Physiology*, **6**, 375–384.

Fu, A. Y., Spence, C., Scherer, A., Arnold, F. H. and Quake, S. R. (1999). A microfabricated fluorescence-activated cell sorter. *Nature Biotechnology*, **17**, 1109–1111.

Fuerstman, M. J., Lai, A., Thurlow, M. E., Shevkoplyas, S. S., Stone, H. A. and Whitesides, G. M. (2007). The pressure drop along rectangular microchannels containing bubbles. *Lab on a Chip*, **7**, 1479–1489.

Gad-el-Hak, M. (2001). Flow physics in MEMS. *Mecanique and Industries*, **2**, 313–341.

Garcia-Sanchez, P., Ramos, A., Green, N. G. and Morgan, H. (2006). Experiments on AC electrokinetic pumping of liquids using arrays of microelectrodes. *IEEE Transactions on Dielectrics and Electrical Insulation*, **13**, 670–677.

Gascoyne, P. R. C. (2009). Dielectrophoretic-field flow fractionation analysis of dielectric, density, and deformability characteristics of cells and particles. *Analytical Chemistry*, **81**, 8878–8885.

Gascoyne, P. R. C., Huang, Y., Pethig, R., Vykoukal, J. and Becker, F. F. (1992). Dielectrophoretic separation of mammalian-cells studied by computerized image-analysis. *Measurement Science and Technology*, **3**, 439–445.

Gascoyne, P. R. C. and Vykoukal, J. V. (2004). Dielectrophoresis-based sample handling in general-purpose programmable diagnostic instruments. *Proceedings of the IEEE*, **92**, 22–42.

Geislinger, T. M., Eggart, B., Ler, S. B., Schmid, L. and Franke, T. (2012). Separation of blood cells using hydrodynamic lift. *Applied Physics Letters*, **100**, 4.

Gervais, T., El-Ali, J., Gunther, A. and Jensen, K. F. (2006). Flow-induced deformation of shallow microfluidic channels. *Lab on a Chip*, **6**, 500–507.

Giddings, J. C. (1968). Nonequilibrium theory of field-flow fractionation. *Journal of Chemical Physics*, **49**, 81.

Giddings, J. C. (1993). Field-flow fractionation – analysis of macromolecular, colloidal, and particulate materials. *Science*, **260**, 1456–1465.

Giddings, J. C., Chen, X., Wahlund, K. G. and Myers, M. N. (1987). Fast particle separation by flow/steric field-flow fractionation. *Analytical Chemistry*, **59**, 1957–1962.

Giddings, J. C. and Myers, M. N. (1978). Steric field-flow fractionation – new method for separating 1-μm to 100-μm particles. *Separation Science and Technology*, **13**, 637–645.

Gijs, M. A. M. (2004). Magnetic bead handling on-chip: New opportunities for analytical applications. *Microfluidics and Nanofluidics*, **1**, 22–40.

Gimsa, J. (1997). Particle characterization by AC-electrokinetic phenomena: 1. A short introduction to dielectrophoresis (DP) and electrorotation (ER). *In:* Exerowa, D. and Platikanov, D. (eds.) *Surface and Colloid Science*, July 1997. Sofia. Elsevier, 451–460.

Gossett, D. R. and Di Carlo, D. (2009). Particle focusing mechanisms in curving confined flows. *Analytical Chemistry*, **81**, 8459–8465.

Gravesen, P., Branebjerg, J. and Jensen, O. S. (1993). Microfluidics – a review. *Journal of Micromechanics and Microengineering*, **3**, 168–182.

Green, N. G., Ramos, A. and Morgan, H. (2002). Numerical solution of the dielectrophoretic and travelling wave forces for interdigitated electrode arrays using the finite element method. *Journal of Electrostatics*, **56**, 235–254.

Guido, S. and Tomaiuolo, G. (2009). Microconfined flow behavior of red blood cells in vitro. *Comptes Rendus Physique*, **10**, 751–763.

Gupta, V., Jafferji, I., Garza, M., Melnikova, V. O., Hasegawa, D. K., Pethig, R. and Davis, D. W. (2012). ApoStream (TM), a new dielectrophoretic device for antibody independent isolation and recovery of viable cancer cells from blood. *Biomicrofluidics*, **6**, 024133.

Hackett, S., Hamzah, J., Davis, T. M. E. and St Pierre, T. G. (2009). Magnetic susceptibility of iron in malaria-infected red blood cells. *Biochimica Et Biophysica Acta-Molecular Basis of Disease*, **1792**, 93–99.

Hagsater, S. M., Jensen, T. G., Bruus, H. and Kutter, J. P. (2007). Acoustic resonances in microfluidic chips: full-image micro-PIV experiments and numerical simulations. *Lab on a Chip*, **7**, 1336–1344.

Hawkins, B. G., Huang, C., Arasanipalai, S. and Kirby, B. J. (2011). Automated dielectrophoretic characterization of Mycobacterium smegmatis. *Analytical Chemistry*, **83**, 3507–3515.

Henslee, E. A., Sano, M. B., Rojas, A. D., Schmelz, E. M. and Davalos, R. V. (2011). Selective concentration of human cancer cells using contactless dielectrophoresis. *Electrophoresis*, **32**, 2523–2529.

Heo, Y. S., Cabrera, L. M., Song, J. W., Futai, N., Tung, Y.-C., Smith, G. D. and Takayama, S. (2006). Characterization and resolution of evaporation-mediated osmolality

shifts that constrain microfluidic cell culture in poly(dimethylsiloxane) devices. *Analytical Chemistry*, **79**, 1126–1134.

Ho, B. P. and Leal, L. G. (1974). Inertial migration of rigid spheres in 2-dimensional unidirectional flows. *Journal of Fluid Mechanics*, **65**, 365–400.

Hoettges, K. F. (2010). Dielectrophoresis as a cell characterisation tool. *In:* Hughes, M. P. and Hoettges, K. F. (eds.) *Microengineering in Biotechnology*. Totowa: Humana Press Inc.

Hoettges, K. F., Hubner, Y., Broche, L. M., Ogin, S. L., Kass, G. E. N. and Hughes, M. P. (2008). Dielectrophoresis-activated multiwell plate for label-free high-throughput drug assessment. *Analytical Chemistry*, **80**, 2063–2068.

Hoettges, K. F., McDonnell, M. B. and Hughes, M. P. (2003). Use of combined dielectrophoretic/electrohydrodynamic forces for biosensor enhancement. *Journal of Physics D-Applied Physics*, **36**, L101–L104.

Holzel, R. (1998). Nystatin-induced changes in yeast monitored by time resolved automated single cell electrorotation. *Biochimica Et Biophysica Acta*, **1425**, 311–318.

Horowitz, V. R., Awschalom, D. D. and Pennathur, S. (2008). Optofluidics: field or technique? *Lab on a Chip*, **8**, 1856–1863.

Hou, H. W., Gan, H. Y., Bhagat, A. A. S., Li, L. D., Lim, C. T. and Han, J. (2012). A microfluidics approach towards high-throughput pathogen removal from blood using margination. *Biomicrofluidics*, **6**, 024115.

Hou, H. W., Li, Q. S., Lee, G. Y. H., Kumar, A. P., Ong, C. N. and Lim, C. T. (2009). Deformability study of breast cancer cells using microfluidics. *Biomedical Microdevices*, **11**, 557–564.

Hu, X. Y., Bessette, P. H., Qian, J. R., Meinhart, C. D., Daugherty, P. S. and Soh, H. T. (2005). Marker-specific sorting of rare cells using dielectrophoresis. *Proceedings of the National Academy of Sciences of the United States of America*, **102**, 15757–15761.

Huang, L. R., Cox, E. C., Austin, R. H. and Sturm, J. C. (2004). Continuous particle separation through deterministic lateral displacement. *Science*, **304**, 987–990.

Huang, Y., Agrawal, B., Sun, D. D., Kuo, J. S. and Williams, J. C. (2011). Microfluidics-based devices: New tools for studying cancer and cancer stem cell migration. *Biomicrofluidics*, **5**, 013412.

Huang, Y., Holzel, R., Pethig, R. and Wang, X. B. (1992). Differences in the AC electrodynamics of viable and non-viable yeast cells determined through combined dielectrophoresis and electrorotation studies. *Physics in Medicine and Biology*, **37**, 1499–1517.

Huang, Y., Wang, X. B., Tame, J. A. and Pethig, R. (1993). Electrokinetic behavior of colloidal particles in traveling electric-fields – studies using yeast-cells. *Journal of Physics D-Applied Physics*, **26**, 1528–1535.

Hughes, M. P. (1998). Computer aided analysis of conditons for optimizing practical electrorotation. *Physics in Medicine And Biology*, **43**, 3639–3648.

Hughes, M. P. (2002). Strategies for dielectrophoretic separation in laboratory-on-a-chip systems. *Electrophoresis*, **23**, 2569–2582.

Hughes, M. P. (2003). *Nanoelectromechanics in Engineering and Biology*, Boca Raton, CRC Press.

Hughes, M. P., Pethig, R. and Wang, X.-B. (1995). Dielectrophoretic forces on particles in travelling electric fields. *Journal of Physics D: Applied Physics*, **29**, 474–482.

Hur, S. C., Henderson-Maclennan, N. K., McCabe, E. R. B. and Di Carlo, D. (2011). Deformability-based cell classification and enrichment using inertial microfluidics. *Lab on a Chip*, **11**, 912–920.

Inglis, D. W., Davis, J. A., Austin, R. H. and Sturm, J. C. (2006). Critical particle size for fractionation by deterministic lateral displacement. *Lab on a Chip*, **6**, 655–658.

Inglis, D. W., Davis, J. A., Zieziulewicz, T. J., Lawrence, D. A., Austin, R. H. and Sturm, J. C. (2008). Determining blood cell size using microfluidic hydrodynamics. *Journal of Immunological Methods*, **329**, 151–156.

Inglis, D. W., Riehn, R., Austin, R. H. and Sturm, J. C. (2004). Continuous microfluidic immunomagnetic cell separation. *Applied Physics Letters*, **85**, 5093–5095.

Irimajiri, A., Hanai, T. and Inouye, A. (1979). Dielectric theory of multi-stratified shell-model with its application to a lymphoma cell. *Journal of Theoretical Biology*, **78**, 251–269.

Jackson, M. B. (2006). *Molecular and Cellular Biophysics*, Cambridge, Cambridge University Press.

Jain, A. and Munn, L. L. (2011). Biomimetic postcapillary expansions for enhancing rare blood cell separation on a microfluidic chip. *Lab on a Chip*, **11**, 2941–2947.

Jendretzki, A., Wittland, J., Wilk, S., Straede, A. and Heinisch, J. J. (2011). How do I begin? Sensing extracellular stress to maintain yeast cell wall integrity. *European Journal of Cell Biology*, **90**, 740–744.

Jin, X., Zhao, Y., Richardson, A., Moore, L., Williams, P. S., Zborowski, M. and Chalmers, J. J. (2008). Differences in magnetically induced motion of diamagnetic, paramagnetic, and superparamagnetic microparticles detected by cell tracking velocimetry. *Analyst*, **133**, 1767–1775.

Jones, T. B. (1995). *Electromechanics of Particles*, Cambridge, Cambridge University Press.

Kersaudy-Kerhoas, M., Dhariwal, R., Desmulliez, M. P. Y. and Jouvet, L. (2010). Hydrodynamic blood plasma separation in microfluidic channels. *Microfluidics and Nanofluidics*, **8**, 105–114.

Kim, D., Chesler, N. C. and Beebe, D. J. (2006). A method for dynamic system characterization using hydraulic series resistance. *Lab on a Chip*, **6**, 639–644.

Kim, E. K. and Choi, E.-J. (2010). Pathological roles of MAPK signaling pathways in human diseases. *Biochimica et Biophysica Acta (BBA) – Molecular Basis of Disease*, **1802**, 396–405.

Kim, H. J., Moon, H. S., Kwak, B. S. and Jung, H. I. (2011). Microfluidic device to separate micro-beads with various fluorescence intensities. *Sensors and Actuators B-Chemical*, **160**, 1536–1543.

Kim, U., Qian, J., Kenrick, S. A., Daugherty, P. S. and Soh, H. T. (2008). Multitarget dielectrophoresis activated cell sorter. *Analytical Chemistry*, **80**, 8656–8661.

Kim, U. and Soh, H. T. (2009). Simultaneous sorting of multiple bacterial targets using integrated dielectrophoretic-magnetic activated cell sorter. *Lab on a Chip*, **9**, 2313–2318.

Kim, Y. W. and Yoo, J. Y. (2008). The lateral migration of neutrally-buoyant spheres transported through square microchannels. *Journal of Micromechanics and Microengineering*, **18**, 065015.

Kim, Y. W. and Yoo, J. Y. (2012). Transport of solid particles in microfluidic channels. *Optics and Lasers in Engineering*, **50**, 87–98.

Klis, F. M., Boorsma, A. and De Groot, P. W. J. (2006). Cell wall construction in *Saccharomyces cerevisiae*. *Yeast*, **23**, 185–202.

Kowalkowski, T., Buszewski, B., Cantado, C. and Dondi, F. (2006). Field-flow fractionation: Theory, techniques, applications and the challenges. *Critical Reviews in Analytical Chemistry*, **36**, 129–135.

Kultz, D. and Chakravarty, D. (2001). Maintenance of genomic integrity in mammalian kidney cells exposed to hyperosmotic stress. *Comparative Biochemistry and Physiology A-Molecular and Integrative Physiology*, **130**, 421–428.

Kumar, M., Feke, D. L. and Belovich, J. M. (2005). Fractionation of cell mixtures using acoustic and laminar flow fields. *Biotechnology and Bioengineering*, **89**, 129–137.

Kuntaegowdanahalli, S. S., Bhagat, A. A. S., Kumar, G. and Papautsky, I. (2009). Inertial microfluidics for continuous particle separation in spiral microchannels. *Lab on a Chip*, **9**, 2973–2980.

Labeed, F. H., Lu, J., Mulhall, H. J., Marchenko, S. A., Hoettges, K. F., Estrada, L. C., Lee, A. P., Hughes, M. P. and Flanagan, L. A. (2011). Biophysical characteristics reveal neural stem cell differentiation potential. *Plos One*, **6**, e25458.

Lapizco-Encinas, B. H., Davalos, R. V., Simmons, B. A., Cummings, E. B. and Fintschenko, Y. (2005). An insulator-based (electrodeless) dielectrophoretic concentrator for microbes in water. *Journal of Microbiological Methods*, **62**, 317–326.

Lapizco-Encinas, B. H., Simmons, B. A., Cummings, E. B. and Fintschenko, Y. (2004). Dielectrophoretic concentration and separation of live and dead bacteria in an array of insulators. *Analytical Chemistry*, **76**, 1571–1579.

Lau, A. Y., Lee, L. P. and Chan, J. W. (2008). An integrated optofluidic platform for Raman-activated cell sorting. *Lab on a Chip*, **8**, 1116–1120.

Laurell, T., Petersson, F. and Nilsson, A. (2007). Chip integrated strategies for acoustic separation and manipulation of cells and particles. *Chemical Society Reviews*, **36**, 492–506.

Lee, K., Kim, C., Ahn, B., Kang, J. Y. and Oh, K. W. (2009). Hydrodynamically focused particle filtration using an island structure. *Biochip Journal*, **3**, 275–280.

Lee, W. C., Bhagat, A. A. S., Huang, S., van Vliet, K. J., Han, J. and Lim, C. T. (2011). High-throughput cell cycle synchronization using inertial forces in spiral microchannels. *Lab on a Chip*, **11**, 1359–1367.

Lenshof, A., Ahmad-Tajudin, A., Jaras, K., Sward-Nilsson, A. M., Aberg, L., Marko-Varga, G., Malm, J., Lilja, H. and Laurell, T. (2009). Acoustic whole blood plasmapheresis chip for prostate specific antigen microarray diagnostics. *Analytical Chemistry*, **81**, 6030–6037.

Lenshof, A., Evander, M., Laurell, T. and Nilsson, J. (2012). Acoustofluidics 5: Building microfluidic acoustic resonators. *Lab on a Chip*, **12**, 684–695.

Li, J. and Lin, F. (2011). Microfluidic devices for studying chemotaxis and electrotaxis. *Trends in Cell Biology*, **21**, 489–497.

Liao, S. H., Cheng, I. F. and Chang, H. C. (2012). Precisely sized separation of multiple particles based on the dielectrophoresis gradient in the z-direction. *Microfluidics and Nanofluidics*, **12**, 201–211.

Lin, S. J., Hung, S. H., Jeng, J. Y., Guo, T. F. and Lee, G. B. (2012). Manipulation of micro-particles by flexible polymer-based optically-induced dielectrophoretic devices. *Optics Express*, **20**, 583–592.

Liu, C. X., Stakenborg, T., Peeters, S. and Lagae, L. (2009). Cell manipulation with magnetic particles toward microfluidic cytometry. *Journal of Applied Physics*, **105**, 102014.

Liu, Y. J., Guo, S. S., Zhang, Z. L., Huang, W. H., Baigl, D., Xie, M., Chen, Y. and Pang, D. W. (2007). A micropillar-integrated smart microfluidic device for specific capture and sorting of cells. *Electrophoresis*, **28**, 4713–4722.

Lochovsky, C., Yasotharan, S. and Gunther, A. (2012). Bubbles no more: In-plane trapping and removal of bubbles in microfluidic devices. *Lab on a Chip*, **12**, 595–601.

Loutherback, K., Chou, K. S., Newman, J., Puchalla, J., Austin, R. H. and Sturm, J. C. (2010). Improved performance of deterministic lateral displacement arrays with triangular posts. *Microfluidics and Nanofluidics*, **9**, 1143–1149.

Manneberg, O., Hagsater, S. M., Svennebring, J., Hertz, H. M., Kutter, J. P., Bruus, H. and Wiklund, M. (2009). Spatial confinement of ultrasonic force fields in microfluidic channels. *Ultrasonics*, **49**, 112–119.

Manz, A., Graber, N. and Widmer, H. M. (1990). Miniaturized total chemical analysis systems: A novel concept for chemical sensing. *Sensors and Actuators B: Chemical*, **1**, 244–248.

Markx, G. H., Huang, Y., Zhou, X. F. and Pethig, R. (1994). Dielectrophoretic characterization and separation of microorganisms. *Microbiology-UK*, **140**, 585–591.

Markx, G. H. and Pethig, R. (1995). Dielectrophoretic separation of cells: Continuous separation. *Biotechnology and Bioengineering*, **45**, 337–343.

Markx, G. H., Rousselet, J. and Pethig, R. (1997). DEP-FFF: Field-flow fractionation using non-uniform electric fields. *Journal of Liquid Chromatography and Related Technologies*, **20**, 2857–2872.

Masuda, S., Washizu, M. and Kawabata, I. (1988). Movement of blood cells in liquid by nonuniform traveling field. *Industry Applications, IEEE Transactions on*, **24**, 217–222.

Matsuda, M., Yamada, M. and Seki, M. (2011). Blood cell classification utilizing hydrodynamic filtration. *Electronics and Communications in Japan*, **94**, 1–6.

McCloskey, K. E., Chalmers, J. J. and Zborowski, M. (2003). Magnetic cell separation: Characterization of magnetophoretic mobility. *Analytical Chemistry*, **75**, 6868–6874.

Melville, D., Paul, F. and Roath, S. (1975a). Direct magnetic separation of red-cells from whole-blood. *Nature*, **255**, 706–706.

Melville, D., Paul, F. and Roath, S. (1975b). High gradient magnetic separation of red-cells from whole-blood. *IEEE Transactions on Magnetics*, **11**, 1701–1704.

Melvin, E. M., Moore, B. R., Gilchrist, K. H., Grego, S. and Velev, O. D. (2011). On-chip collection of particles and cells by AC electroosmotic pumping and dielectrophoresis using asymmetric microelectrodes. *Biomicrofluidics*, **5**, 034113.

Migita, S., Funakoshi, K., Tsuya, D., Yamazaki, T., Taniguchi, A., Sugimoto, Y., Hanagata, N. and Ikoma, T. (2010). Cell cycle and size sorting of mammalian cells using a microfluidic device. *Analytical Methods*, **2**, 657–660.

Mogensen, K. B. and Kutter, J. P. (2009). Optical detection in microfluidic systems. *Electrophoresis*, **30**, S92–S100.

Moon, H. S., Kwon, K., Kim, S. I., Han, H., Sohn, J., Lee, S. and Jung, H. I. (2011). Continuous separation of breast cancer cells from blood samples using multi-orifice flow fractionation (MOFF) and dielectrophoresis (DEP). *Lab on a Chip*, **11**, 1118–1125.

Moore, L. R., Milliron, S., Williams, P. S., Chalmers, J. J., Margel, S. and Zborowski, M. (2004). Control of magnetophoretic mobility by susceptibility-modified solutions as evaluated by cell tracking velocimetry and continuous magnetic sorting. *Analytical Chemistry*, **76**, 3899–3907.

Morgan, H., Izquierdo, A. G., Bakewell, D., Green, N. G. and Ramos, A. (2001). The dielectrophoretic and travelling wave forces generated by interdigitated electrode arrays: analytical solution using Fourier series. *Journal of Physics D-Applied Physics*, **34**, 1553–1561.

Morton, K. J., Loutherback, K., Inglis, D. W., Tsui, O. K., Sturm, J. C., Chou, S. Y. and Austin, R. H. (2008). Hydrodynamic metamaterials: Microfabricated arrays to steer, refract, and focus streams of biomaterials. *Proceedings of the National Academy of Sciences of the United States of America*, **105**, 7434–7438.

Mulhall, H. J., Labeed, F. H., Kazmi, B., Costea, D. E., Hughes, M. P. and Lewis, M. P. (2011). Cancer, pre-cancer and normal oral cells distinguished by dielectrophoresis. *Analytical and Bioanalytical Chemistry*, **401**, 2455–2463.

Muller, T., Gradl, G., Howitz, S., Shirley, S., Schnelle, T. and Fuhr, G. (1999). A 3-D microelectrode system for handling and caging single cells and particles. *Biosensors and Bioelectronics*, **14**, 247–256.

Murata, M., Okamoto, Y., Park, Y. S., Kaji, N., Tokeshi, M. and Baba, Y. (2009). Cell separation by the combination of microfluidics and optical trapping force on a microchip. *Analytical and Bioanalytical Chemistry*, **394**, 277–283.

Myers, M. N. and Giddings, J. C. (1982). Properties of the transition from normal to steric field-flow fractionation. *Analytical Chemistry*, **54**, 2284–2289.

Nakashima, M., Yamada, M. and Seki, M. (2004). Pinched flow fractionation (PFF) for continuous particle separation in a microfluidic device. *MEMS 2004: 17th IEEE International Conference on Micro Electro Mechanical Systems, Technical Digest*. New York: IEEE.

Nam, J., Lee, Y. and Shin, S. (2011a). Size-dependent microparticles separation through standing surface acoustic waves. *Microfluidics and Nanofluidics*, **11**, 317–326.

Nam, J., Lim, H., Kim, D. and Shin, S. (2011b). Separation of platelets from whole blood using standing surface acoustic waves in a microchannel. *Lab on a Chip*, **11**, 3361–3364.

Nilsson, A., Petersson, F., Jonsson, H. and Laurell, T. (2004). Acoustic control of suspended particles in micro fluidic chips. *Lab on a Chip*, **4**, 131–135.

Oberteuf, J. A. (1974). Magnetic separation – Review of principles, devices, and applications. *IEEE Transactions on Magnetics*, **MA10**, 223–238.

Oh, K. W., Lee, K., Ahn, B. and Furlani, E. P. (2012). Design of pressure-driven microfluidic networks using electric circuit analogy. *Lab on a Chip*, **12**, 515–545.

Pamme, N. (2006). Magnetism and microfluidics. *Lab on a Chip*, **6**, 24–38.

Pamme, N. and Manz, A. (2004). On-chip free-flow magnetophoresis: Continuous flow separation of magnetic particles and agglomerates. *Analytical Chemistry*, **76**, 7250–7256.

Pamme, N. and Wilhelm, C. (2006). Continuous sorting of magnetic cells via on-chip free-flow magnetophoresis. *Lab on a Chip*, **6**, 974–980.

Pankhurst, Q. A., Connolly, J., Jones, S. K. and Dobson, J. (2003). Applications of magnetic nanoparticles in biomedicine. *Journal of Physics D-Applied Physics*, **36**, R167–R181.

Park, J. S. and Jung, H. I. (2009). Multiorifice flow fractionation: Continuous size-based separation of microspheres using a series of contraction/expansion microchannels. *Analytical Chemistry*, **81**, 8280–8288.

Park, J. S., Song, S. H. and Jung, H. I. (2009). Continuous focusing of microparticles using inertial lift force and vorticity via multi-orifice microfluidic channels. *Lab on a Chip*, **9**, 939–948.

Paul, F., Melville, D., Roath, S. and Warhurst, D. C. (1981). A bench top magnetic separator for malarial parasite concentration. *IEEE Transactions on Magnetics*, **17**, 2822–2824.

Petersson, F., Aberg, L., Sward-Nilsson, A. M. and Laurell, T. (2007). Free flow acoustophoresis: Microfluidic-based mode of particle and cell separation. *Analytical Chemistry*, **79**, 5117–5123.

Petersson, F., Nilsson, A., Holm, C., Jonsson, H. and Laurell, T. (2004). Separation of lipids from blood utilizing ultrasonic standing waves in microfluidic channels. *Analyst*, **129**, 938–943.

Petersson, F., Nilsson, A., Jonsson, H. and Laurell, T. (2005). Carrier medium exchange through ultrasonic particle switching in microfluidic channels. *Analytical Chemistry*, **77**, 1216–1221.

Pethig, R. (1979). *Dielectric and Electronic Properties of Biological Materials*, Chichester, John Wiley & Sons.

Pethig, R. (2010). Review article-dielectrophoresis: Status of the theory, technology, and applications. *Biomicrofluidics*, **4**, 35.

Pethig, R. and Talary, M. S. (2007). Dielectrophoretic detection of membrane morphology changes in Jurkat T-cells undergoing etoposide-induced apoptosis. *IET Nanobiotechnology*, **1**, 2–9.

Pipe, C. J. and McKinley, G. H. (2009). Microfluidic rheometry. *Mechanics Research Communications*, **36**, 110–120.

Plouffe, B. D., Mahalanabis, M., Lewis, L. H., Klapperich, C. M. and Murthy, S. K. (2012). Clinically relevant microfluidic magnetophoretic isolation of rare-cell populations for diagnostic and therapeutic monitoring applications. *Analytical Chemistry*, **84**, 1336–1344.

Pohl, H. A. (1951). The motion and precipitation of suspensoids in divergent electric fields. *Journal of Applied Physics*, **22**, 869–871.

Pohl, H. A. (1958). Some effects of nonuniform fields on dielectrics. *Journal of Applied Physics*, **29**, 1182–1188.

Pohl, H. A. (1978). *Dielectrophoresis*, Cambridge, UK, Cambridge Unviersity Press.

Pohl, H. A. and Crane, J. S. (1971). Dielectrophoresis of cells. *Biophysical Journal*, **11**, 711–727.

Pohl, H. A. and Hawk, I. (1966). Separation of living and dead cells by dielectrophoresis. *Science*, **152**, 647.

Psaltis, D., Quake, S. R. and Yang, C. H. (2006). Developing optofluidic technology through the fusion of microfluidics and optics. *Nature*, **442**, 381–386.

Quake, S. R. and Scherer, A. (2000). From micro- to nanofabrication with soft materials. *Science*, **290**, 1536–1540.

Ramos, A., Morgan, H., Green, N. G. and Castellanos, A. (1998). Ac electrokinetics: A review of forces in microelectrode structures. *Journal of Physics D-Applied Physics*, **31**, 2338–2353.

Ramos, A., Morgan, H., Green, N. G. and Castellanos, A. (1999). AC electric-field-induced fluid flow in microelectrodes. *Journal of Colloid and Interface Science*, **217**, 420–422.

Ravula, S. K., Branch, D. W., James, C. D., Townsend, R. J., Hill, M., Kaduchak, G., Ward, M. and Brener, I. (2008). A microfluidic system combining acoustic and dielectrophoretic particle preconcentration and focusing. *Sensors and Actuators B-Chemical*, **130**, 645–652.

Reyes, D. R., Iossifidis, D., Auroux, P. A. and Manz, A. (2002). Micro total analysis systems. 1. Introduction, theory, and technology. *Analytical Chemistry*, **74**, 2623–2636.

Reynolds, O. (1883). An experimental investigation of the circumstances which determine whether the motion of water shall be direct or sinuous, and the law of resistance in parallel channels. *Philosophical Transactions Royal Society London*, **174**, 935–982.

Robert, D., Pamme, N., Conjeaud, H., Gazeau, F., Iles, A. and Wilhelm, C. (2011). Cell sorting by endocytotic capacity in a microfluidic magnetophoresis device. *Lab on a Chip*, **11**, 1902–1910.

Roda, B., Zattoni, A., Reschiglian, P., Moon, M. H., Mirasoli, M., Michelini, E. and Roda, A. (2009). Field-flow fractionation in bioanalysis: A review of recent trends. *Analytica Chimica Acta*, **635**, 132–143.

Rodriguez-Villarreal, A. I., Tarn, M. D., Madden, L. A., Lutz, J. B., Greenman, J., Samitier, J. and Pamme, N. (2010). Flow focussing of particles and cells based on their intrinsic properties using a simple diamagnetic repulsion setup. *Lab on a Chip*, **11**, 1240–1248.

Ruzicka, M. C. (2008). On dimensionless numbers. *Chemical Engineering Research and Design*, **86**, 835–868.

Saliba, A. E., Saias, L., Psychari, E., Minc, N., Simon, D., Bidard, F. C., Mathiot, C., Pierga, J. Y., Fraisier, V., Salamero, J., Saada, V., Farace, F., Vielh, P., Malaquin, L. and Viovy, J. L. (2010). Microfluidic sorting and multimodal typing of cancer cells in self-assembled magnetic arrays. *Proceedings of the National Academy of Sciences of the United States of America*, **107**, 14524–14529.

Sanchis, A., Brown, A. P., Sancho, M., Martinez, G., Sebastian, J. L., Munoz, S. and Miranda, J. M. (2007). Dielectric characterization of bacterial cells using dielectrophoresis. *Bioelectromagnetics*, **28**, 393–401.

Sano, M. B., Salmanzadeh, A. and Davalos, R. V. (2012). Multilayer contactless dielectrophoresis: Theoretical considerations. *Electrophoresis*, **33**, 1938–1946.

Schneider, T., Moore, L. R., Jing, Y., Haam, S., Williams, P. S., Fleischman, A. J., Roy, S., Chalmers, J. J. and Zborowski, M. (2006). Continuous flow magnetic cell fractionation based on antigen expression level. *Journal of Biochemical and Biophysical Methods*, **68**, 1–21.

Schonberg, J. A. and Hinch, E. J. (1989). Inertial migration of a sphere in poiseuille flow. *Journal of Fluid Mechanics*, **203**, 517–524.

Schulte, T. H., Bardell, R. L. and Weigl, B. H. (2002). Microfluidic technologies in clinical diagnostics. *Clinica Chimica Acta*, **321**, 1–10.

Segre, G. and Silberberg, A. (1961). Radial particle displacements in poiseuille flow of suspensions. *Nature*, **189**, 209.

Segre, G. and Silberberg, A. (1962). Behaviour of macroscopic rigid spheres in poiseuille flow. 2. Experimental results and interpretation. *Journal of Fluid Mechanics*, **14**, 136–157.

Settnes, M. and Bruus, H. (2012). Forces acting on a small particle in an acoustical field in a viscous fluid. *Physical Review E*, **85**, 12.

Shafiee, H., Caldwell, J. L., Sano, M. B. and Davalos, R. V. (2009). Contactless dielectrophoresis: a new technique for cell manipulation. *Biomedical Microdevices*, **11**, 997–1006.

Shah, G. J., Ohta, A. T., Chiou, E. P. Y., Wu, M. C. and Kim, C. J. (2009). EWOD-driven droplet microfluidic device integrated with optoelectronic tweezers as an automated platform for cellular isolation and analysis. *Lab on a Chip*, **9**, 1732–1739.

Shen, F., Hwang, H., Hahn, Y. K. and Park, J. K. (2012). Label-free cell separation using a tunable magnetophoretic repulsion force. *Analytical Chemistry*, **84**, 3075–3081.

Shevkoplyas, S. S., Siegel, A. C., Westervelt, R. M., Prentiss, M. G. and Whitesides, G. M. (2007). The force acting on a superparamagnetic bead due to an applied magnetic field. *Lab on a Chip*, **7**, 1294–1302.

Shevkoplyas, S. S., Yoshida, T., Munn, L. L. and Bitensky, M. W. (2005). Biomimetic autoseparation of leukocytes from whole blood in a microfluidic device. *Analytical Chemistry*, **77**, 933–937.

Shi, J. J., Ahmed, D., Mao, X., Lin, S. C. S., Lawit, A. and Huang, T. J. (2009a). Acoustic tweezers: Patterning cells and microparticles using standing surface acoustic waves (SSAW). *Lab on a Chip*, **9**, 2890–2895.

Shi, J. J., Huang, H., Stratton, Z., Huang, Y. P. and Huang, T. J. (2009b). Continuous particle separation in a microfluidic channel via standing surface acoustic waves (SSAW). *Lab on a Chip*, **9**, 3354–3359.

Shi, J. J., Yazdi, S., Lin, S. C. S., Ding, X. Y., Chiang, I. K., Sharp, K. and Huang, T. J. (2011). Three-dimensional continuous particle focusing in a microfluidic channel via standing surface acoustic waves (SSAW). *Lab on a Chip*, **11**, 2319–2324.

Siegel, A. C., Tang, S. K. Y., Nijhuis, C. A., Hashimoto, M., Phillips, S. T., Dickey, M. D. and Whitesides, G. M. (2009). Cofabrication: A strategy for building multicomponent microsystems. *Accounts of Chemical Research*, **43**, 518–528.

Sim, T. S., Kwon, K., Park, J. C., Lee, J. G. and Jung, H. I. (2011). Multistage-multiorifice flow fractionation (MS-MOFF): continuous size-based separation of microspheres using multiple series of contraction/expansion microchannels. *Lab on a Chip*, **11**, 93–99.

Skelley, A. M. and Voldman, J. (2008). An active bubble trap and debubbler for microfluidic systems. *Lab on a Chip*, **8**, 1733–1737.

Sollier, E., Murray, C., Maoddi, P. and Di Carlo, D. (2011). Rapid prototyping polymers for microfluidic devices and high pressure injections. *Lab on a Chip*, **11**, 3752–3765.

Squires, T. M. and Quake, S. R. (2005). Microfluidics: Fluid physics at the nanoliter scale. *Reviews of Modern Physics*, **77**, 977–1026.

Stone, H. A., Stroock, A. D. and Ajdari, A. (2004). Engineering flows in small devices: Microfluidics toward a lab-on-a-chip. *Annual Review of Fluid Mechanics*, **36**, 381–411.

Stroock, A. D., Dertinger, S. K., Whitesides, G. M. and Ajdari, A. (2002). Patterning flows using grooved surfaces. *Analytical Chemistry*, **74**, 5306–5312.

Stroock, A. D. and Whitesides, G. M. (2003). Controlling flows in microchannels with patterned surface charge and topography. *Accounts of Chemical Research*, **36**, 597–604.

Sugaya, S., Yamada, M. and Seki, M. (2011). Observation of nonspherical particle behaviors for continuous shape-based separation using hydrodynamic filtration. *Biomicrofluidics*, **5**, 13.

Sun, K., Wang, Z. X. and Jiang, X. Y. (2008). Modular microfluidics for gradient generation. *Lab on a Chip*, **8**, 1536–1543.

Suresh, S. (2007). Biomechanics and biophysics of cancer cells. *Acta Biomaterialia*, **3**, 413–438.

Svoboda, K. and Block, S. M. (1994). Biological applications of optical forces. *Annual Review of Biophysics and Biomolecular Structure*, **23**, 247–285.

Takagi, J., Yamada, M., Yasuda, M. and Seki, M. (2005). Continuous particle separation in a microchannel having asymmetrically arranged multiple branches. *Lab on a Chip*, **5**, 778–784.

Takayasu, M., Kelland, D. R. and Minervini, J. V. (2000). Continuous magnetic separation of blood components from whole blood. *IEEE Transactions on Applied Superconductivity*, **10**, 927–930.

Talary, M. S., Burt, J. P. H., Tame, J. A. and Pethig, R. (1996). Electromanipulation and separation of cells using travelling electric fields. *Journal of Physics D-Applied Physics*, **29**, 2198–2203.

Tanaka, T., Ishikawa, T., Numayama-Tsuruta, K., Imai, Y., Ueno, H., Yoshimoto, T., Matsuki, N. and Yamaguchi, T. (2012). Inertial migration of cancer cells in blood flow in microchannels. *Biomedical Microdevices*, **14**, 25–33.

Terry, S. C., Jerman, J. H. and Angell, J. B. (1979). A gas chromatographic air analyzer fabricated on a silicon wafer. *Electron Devices, IEEE Transactions on*, **26**, 1880–1886.

Thevoz, P., Adams, J. D., Shea, H., Bruus, H. and Soh, H. T. (2010). Acoustophoretic synchronization of mammalian cells in microchannels. *Analytical Chemistry*, **82**, 3094–3098.

Trietsch, S. J., Hankemeier, T. and van der Linden, H. J. (2011). Lab-on-a-chip technologies for massive parallel data generation in the life sciences: A review. *Chemometrics and Intelligent Laboratory Systems*, **108**, 64–75.

Tsukahara, S. and Watarai, H. (2003). Dielectrophoresis of microbioparticles in water with planar and capillary quadrupole electrodes. *IEE Proceedings Nanobiotechnology*, **150**, 59–65.

Unger, M. A., Chou, H. P., Thorsen, T., Scherer, A. and Quake, S. R. (2000). Monolithic microfabricated valves and pumps by multilayer soft lithography. *Science*, **288**, 113–116.

Unni, H. N., Hartono, D., Yung, L. Y. L., Ng, M. M. L., Lee, H. P., Khoo, B. C. and Lim, K. M. (2012). Characterization and separation of Cryptosporidium and Giardia cells using on-chip dielectrophoresis. *Biomicrofluidics*, **6**, 012805.

Vahey, M. D. and Voldman, J. (2008). An equilibrium method for continuous-flow cell sorting using dielectrophoresis. *Analytical Chemistry*, **80**, 3135–3143.

van Beek, L. K. H. (1960). Dielectric behaviour of heterogeneous systems. *Progress in Dielectrics*, **7**, 69–114.

Walker, G. M., Sai, J. Q., Richmond, A., Stremler, M., Chung, C. Y. and Wikswo, J. P. (2005). Effects of flow and diffusion on chemotaxis studies in a microfabricated gradient generator. *Lab on a Chip*, **5**, 611–618.

Wang, W., Lin, Y. H., Wen, T. C., Guo, T. F. and Lee, G. B. (2010). Selective manipulation of microparticles using polymer-based optically induced dielectrophoretic devices. *Applied Physics Letters*, **96**, 113302.

Wang, X.-B., Huang, Y., Holzel, R., Burt, J. P. and Pethig, R. (1992). Theoretical and experimental investigations of the interdependence of the dielectric, dielectrophoretic and electrorotational behaviour of colloidal particles. *Journal of Physics D: Applied Physics*, **26**, 312–322.

Wang, X.-B., Pethig, R. and Jones, T. B. (1991). Relationship of dielectrophoretic and electro-rotational behaviour exhibited by polarized particles. *Journal of Physics D: Applied Physics*, **25**, 905–912.

Wang, X. B., Huang, Y., Wang, X., Becker, F. F. and Gascoyne, P. R. (1997). Dielectrophoretic manipulation of cells with spiral electrodes. *Biophysical Journal*, **72**, 1887–1899.

Wang, X. B., Hughes, M. P., Huang, Y., Becker, F. F. and Gascoyne, P. R. C. (1995). Non-uniform spatial distributions of both the magnitude and phase of AC electric fields determine dielectrophoretic forces. *Biochimica et Biophysica Acta (BBA) – General Subjects*, **1243**, 185–194.

Wang, X. B., Yang, J., Huang, Y., Vykoukal, J., Becker, F. F. and Gascoyne, P. R. C. (2000). Cell separation by dielectrophoretic field-flow-fractionation. *Analytical Chemistry*, **72**, 832–839.

Wang, X. L., Chen, S. X., Kong, M., Wang, Z. K., Costa, K. D., Li, R. A. and Sun, D. (2011). Enhanced cell sorting and manipulation with combined optical tweezer and microfluidic chip technologies. *Lab on a Chip*, **11**, 3656–3662.

White, F. M. (1994). *Fluid Mechanics*, New York, McGraw-Hill Inc.

Whitesides, G. M., Ostuni, E., Takayama, S., Jiang, X. Y. and Ingber, D. E. (2001). Soft lithography in biology and biochemistry. *Annual Review of Biomedical Engineering*, **3**, 335–373.

Wu, L. Q., Yung, L. Y. L. and Lim, K. M. (2012). Dielectrophoretic capture voltage spectrum for measurement of dielectric properties and separation of cancer cells. *Biomicrofluidics*, **6**, 014113.

Wu, Z. G., Hjort, K., Wicher, G. and Svenningsen, A. F. (2008). Microfluidic high viability neural cell separation using viscoelastically tuned hydrodynamic spreading. *Biomedical Microdevices*, **10**, 631–638.

Wu, Z. G., Willing, B., Bjerketorp, J., Jansson, J. K. and Hjort, K. (2009). Soft inertial microfluidics for high throughput separation of bacteria from human blood cells. *Lab on a Chip*, **9**, 1193–1199.

Yamada, M., Nakashima, M. and Seki, M. (2004). Pinched flow fractionation: Continuous size separation of particles utilizing a laminar flow profile in a pinched microchannel. *Analytical Chemistry*, **76**, 5465–5471.

Yamada, M. and Seki, M. (2005). Hydrodynamic filtration for on-chip particle concentration and classification utilizing microfluidics. *Lab on a Chip*, **5**, 1233–1239.

Yamada, M. and Seki, M. (2006). Microfluidic particle sorter employing flow splitting and recombining. *Analytical Chemistry*, **78**, 1357–1362.

Yeh, S. R., Seul, M. and Shraiman, B. I. (1997). Assembly of ordered colloidal aggregates by electric-field-induced fluid flow. *Nature*, **386**, 57–59.

Zborowski, M. and Chamers, J. J. (2011). Rare cell separation and analysis by magnetic sorting. *Analytical Chemistry*, **83**, 8050–8056.

Zborowski, M., Ostera, G. R., Moore, L. R., Milliron, S., Chalmers, J. J. and Schechter, A. N. (2003). Red blood cell magnetophoresis. *Biophysical Journal*, **84**, 2638–2645.

Zborowski, M., Sun, L. P., Moore, L. R., Williams, P. S. and Chalmers, J. J. (1999). Continuous cell separation using novel magnetic quadrupole flow sorter. *Journal of Magnetism and Magnetic Materials*, **194**, 224–230.

Zhao, B. S., Koo, Y. M. and Chung, D. S. (2006). Separations based on the mechanical forces of light. *Analytica Chimica Acta*, **556**, 97–103.

Zhao, X. M., Xia, Y. N. and Whitesides, G. M. (1997). Soft lithographic methods for nano-fabrication. *Journal of Materials Chemistry*, **7**, 1069–1074.

Zharov, V. P., Galanzha, E. I., Menyaev, Y. and Tuchin, V. V. (2006). In vivo high-speed imaging of individual cells in fast blood flow. *Journal of Biomedical Optics*, **11**, 4.

Zheng, W., Wang, Z., Zhang, W. and Jiang, X. (2010). A simple PDMS-based microfluidic channel design that removes bubbles for long-term on-chip culture of mammalian cells. *Lab on a Chip*, **10**, 2906–2910.

9

Microfluidic devices for single-cell trapping and automated micro-robotic injection

X. Y. LIU, McGill University, Canada and Y. SUN, University of Toronto, Canada,

DOI: 10.1533/9780857097040.3.351

Abstract: This chapter presents the design and microfabrication of a glass-based microfluidic device for trapping and immobilization of single mouse embryos. The use of the device is demonstrated in automated robotic microinjection of mouse embryos for large-scale biomolecule testing. The working principle of the device is based on the hydrodynamic trapping effect generated when a vacuum (e.g., negative pressure) is applied to micrometer-sized through-holes on a glass substrate. A novel microfabrication process is developed for device construction, which includes two-sided glass wet etching and polydimethylsiloxane (PDMS)-glass oxygen plasma bonding. Experimental results of single embryo trapping and microinjection demonstrate that the device is capable of trapping and immobilizing 25 mouse embryos within 31 s, and that the hydrodynamic immobilization does not produce negative effects on embryonic development after microinjection.

Key words: single-cell trapping, microfluidics, microfabrication, robotic microinjection, cell manipulation, mouse embryos.

9.1 Introduction

Trapping/immobilization of single biological cells into a regular pattern is an important cell manipulation procedure and has applications in many single-cell-based studies, such as molecule/drug screening (Castel *et al*., 2006), fate/function studies (Chen and Davis, 2006), cell pairing/fusion (Skelley *et al*., 2009), and DNA damage analysis (Wood *et al*., 2010). With the advances of microfluidic technology, researchers have developed a variety of techniques for single-cell trapping, which are based on such different mechanisms as surface chemistry (Chen *et al*., 1997), dielectrophoresis (Voldman *et al*., 2002), optical tweezers (Jordan *et al*., 2005), ultrasonic trapping (Haake *et al*., 2005; Wiklund and Onfelt, 2012), magnetic trapping (Ino *et al*., 2008), and mechanical confinements (Rettig and Folch, 2005; Carlo *et al*., 2006; Deutsch *et al*., 2006; Carlborg *et al*., 2007; Suzuki *et al*., 2007; Tan and Takeuchi, 2007).

Besides the aforementioned applications, single-cell trapping and immobilization also promise a more efficient sample preparation approach for mechanical microinjection, which is a popular approach for introducing materials into cells for molecule screening, genetics, and reproductive studies. Microinjection utilizes a glass micropipette to deliver foreign materials into a target cell, during which the cell needs to be fixed for micropipette penetration. Conventionally, microinjection is performed by highly-skilled human operators, and is tedious and time-consuming. In manual microinjection, an operator controls a holding micropipette to randomly locate dispersed cells and fix one cell at a time. Although robotics promises automated microinjection at a high speed with high reproducibility, the use of a holding micropipette for cell immobilization is a serious bottleneck that makes the robotic control challenging, and limits the system throughput. The development of a microfluidic device that is capable of rapidly immobilizing many cells into a regular pattern can facilitate both manual and robotic microinjection of cells.

Among existing techniques for single-call trapping, only mechanical confinements are capable of providing sufficient immobilization forces required by microinjection. These mechanical confinement structures include microwells (Rettig and Folch, 2005), hydrodynamic traps (Carlo *et al*., 2006; Tan and Takeuchi, 2007), and vacuum-based confinements (Carlborg *et al*., 2007; Suzuki *et al*., 2007). Cells trapped in microwells (Rettig and Folch, 2005) can slightly move inside the microwells, which does not provide secured immobilization during cell penetration. The hydrodynamic traps (Carlo *et al*., 2006; Tan and Takeuchi, 2007) are built in closed microchannels, preventing an injection micropipette from accessing cells. The vacuum-based confinements employ an array of micrometer-sized through-holes connected to a vacuum chamber for immobilizing individual cells. In vacuum-based confinements, the construction of through-holes (e.g., 2–50 μm) on the immobilization devices is a critical procedure in the microfabrication process. Such through-holes have been formed on different materials such as silicon, PDMS, and photoresist (Matthews and Judy, 2006; Carlborg *et al*., 2007; Tan and Takeuchi, 2007).

Since differential interference contrast (DIC) microscopy is most commonly used in microinjection for cell imaging, glass should be chosen as the material for the construction of cell immobilization devices for microinjection applications (Murphy, 2001). However, forming through-holes with a diameter ≤50 μm on glass substrates remains a challenge. Although laser micromachining can be used to drill high-aspect-ratio through-holes on glass substrates (Gattass and Mazur, 2008), laser micromachined through-holes have rough surfaces along vertical walls, and minute amounts of debris can cause shadows around through-holes in imaging.

This paper presents the design and microfabrication of a glass-based cell holding device with ≤40 μm through-holes, formed on a standard cover slip (≤180 μm thick) for rapid immobilization of mouse embryos in microinjection. Two-sided glass wet etching was used to form the devices. PDMS-glass

bonding was used to form a vacuum chamber. Many trials of rapid immobilization and automated microinjection of mouse zygotes were conducted to determine possible negative effects of cell immobilization on post-injection embryonic development.

9.2 Device design and microfabrication

A vacuum-based device was designed to include an array of micrometer-sized through-holes that are connected to a vacuum inlet. Upon the application of a low vacuum (small negative pressure), each through-hole can trap a single cell, thus forming a cell array for micro-robotic injection. The device was fabricated using glass wet etching and PDMS-glass bonding, and the microfabrication process was experimentally characterized to determine the appropriate fabrication parameters.

9.2.1 Device design

As illustrated in Fig. 9.1, the cell holding device consists of a top glass layer with an array of through-holes, a bottom glass layer, and a PDMS spacer for forming a vacuum chamber. Considering the size of mouse oocytes/embryos

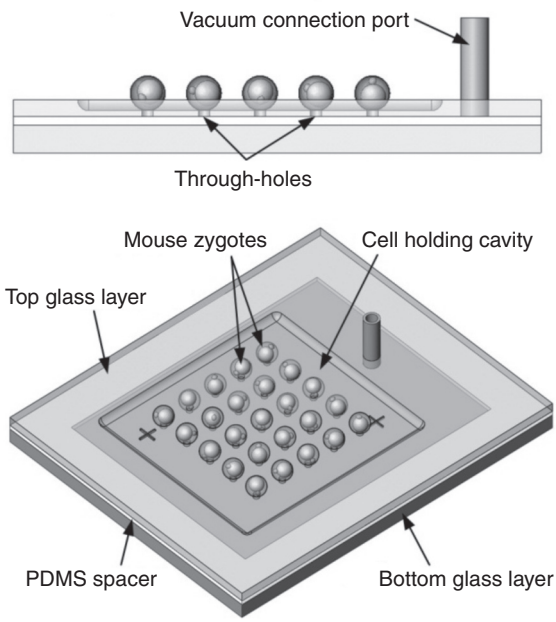

9.1 Schematic of the vacuum-based cell holding device. (*Source*: Adapted with permission from Springer.)

(~100 μm), the size of the through-holes was designed to be 35–40 μm. The use of glass in the microscopy light path meets the requirement of DIC imaging. Standard cover slips (size: 22 mm × 60 mm, thickness: ~100 μm, Fisher Scientific) were used as the top glass layer because they are low cost and their thickness (~180 μm) is suitable for minimizing the microfabrication time while maintaining sufficient mechanical stiffness. Microscope slides (size: 76 mm × 26 mm, thickness: 1 mm, Fisher Scientific) are used as the bottom glass layer.

9.2.2 Microfabrication

The fabrication process is summarized in Plate II (see colour section between pages 328 and 329). Hydrofluoric acid (HF)-based wet etching was selected for fabricating 35–40 μm through-holes on a cover slip since it remains the most common method and can produce through-holes with debris-free edges. Due to the isotropic nature of HF wet etching, it is necessary to first etch the ~180 μm cover slip and form a much thinner substrate for subsequent through-hole etching. Thus, a ~155 μm deep cell holding cavity was first etched into one side of the cover slip, leaving a ~25 μm thin layer of glass (Plate IIc). In cell trapping process, the cavity is able to first collect the cells close to the through-holes, making the trapping much easier. Evaporated metal layers of Cr/Au (30 nm/800 nm) plus hard-baked positive photoresist (S1818, Shipley) were used as etch masks (Iliescu *et al*., 2007). The S1818 layers are capable of preventing penetration of HF solution through defects of the Cr/Au layers.

Etching rates of cover slips as a function of HF concentration were experimentally determined, as shown in Plate III (see colour section). No agitation was used during glass wet etching. High concentrations of HF cause rough bottom surfaces (inlet pictures in Plate IIIa) of the cell holding cavities. The resultant poor optical clarity is also not acceptable for cell imaging. It was found that concentrations below 15% produced surfaces visually smooth under a 400× microscope objective. The surface roughness was measured to be ≤100 nm. A concentration of 14.3% was used in the final device fabrication, and the corresponding etching rate is 0.9 μm/min (Plate IIIa in colour section). Bottom flatness of the cell holding cavity was measured to be ≤0.8 μm using a Wyko optical profilometer (Veeco Instruments). Plate IIIb illustrates a 3D plot of the bottom surface (1200 μm × 900 μm) of the cell holding cavity from the profilometer measurements.

After the formation of the cell holding cavity, S1818 on both sides is removed with acetone. The Cr/Au layers on the bottom side of the cover slip are then patterned using photolithography. A second time wet etching from both the top and bottom sides is conducted to form through-holes (Plate IIb). In the meanwhile, a 1.7 mm through-hole is also formed on the cover slip to construct a connection port for applying vacuum (Fig. 9.2). Diameters of the etched micrometer-sized through-holes on each device are highly

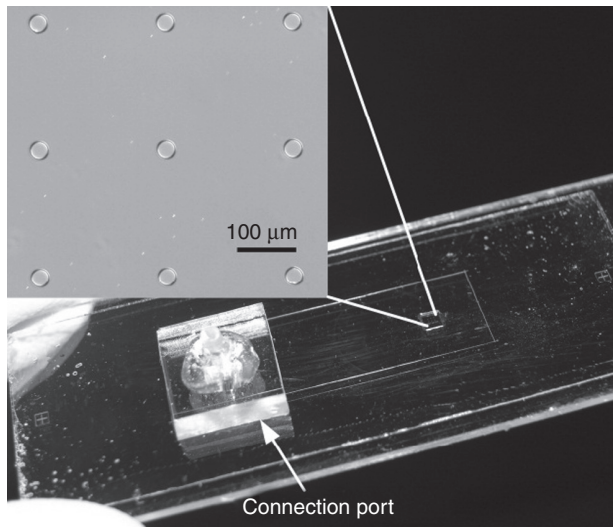

9.2 A completed device. *Inlet picture* shows zoomed-in through-holes. (*Source*: Reproduced with permission from Springer.)

uniform with a standard deviation less than 0.5 μm. The thickness of the thin portion of the cover slip after through-hole formation is 10–12 μm. Finally, S1818 and Cr/Au layers were removed, and the cover slip was cleaned in piranha solution (98% H_2SO_4 and 30% H_2O_2 with a volume ratio of 3:1).

The last fabrication step is PDMS-glass bonding to form a vacuum chamber. PDMS prepolymer (mixing weight ratio of 10:1, Dow Corning) is spin-coated on a 1 mm thick glass slide at 500 rpm, and is then completely cured to form a spacer layer of ~100 μm in thickness. The PDMS spacer layer is carefully cut with a scalpel, oxygen plasma treated, and bonded with the patterned cover slip. Figure 9.2 shows a ready-to-use cell holding device with the inlet showing the zoomed-in view of through-holes.

9.3 Experimental results and discussion

The glass devices were tested for immobilization of single-cell-stage mouse embryos (zygotes; 98 ± 2 μm) into a regular pattern, after which automated robotic microinjection was performed to validate the effectiveness of the devices. Postinjection embryo culture demonstrated that the cell holding devices do not pose obvious negative effect on development of the injected embryos.

9.3.1 Mouse zygote immobilization

Devices with arrays of 3 × 3 and 5 × 5 through-holes were used for immobilizing single-cell-stage mouse embryos (zygotes; 98 ± 2 μm). The average

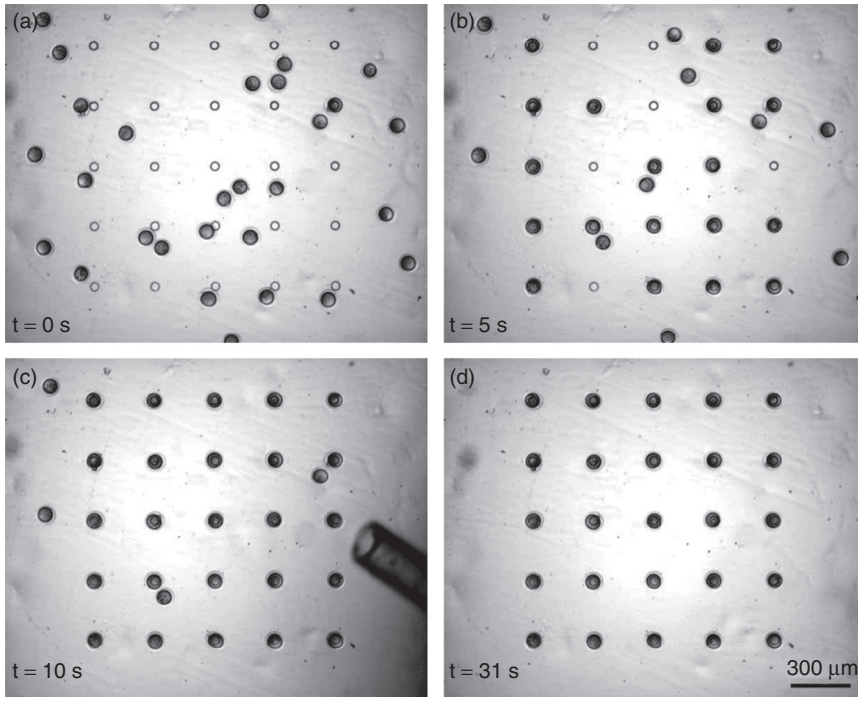

9.3 Immobilization on a 5 × 5 array of mouse zygotes. (a) Thirty mouse zygotes are transferred to the cell holding cavity. (b) With the application of a low sucking pressure (1.8 kPa), through-holes trap individual cells. Nineteen cells are immobilized within 5 s. (c) Twenty-five cells are immobilized within 10 s. A transfer pipette is used to remove extra untrapped zygotes. (d) The immobilized 5 × 5 array of mouse zygotes. The complete process including removal of extra untrapped cells typically takes 31 s. (*Source*: Reproduced with permission from Springer.)

diameter of the through-holes on the employed devices was 37 ± 0.5 μm. Low pressures of 1.6–2.2 kPa were experimentally determined to be effective for holding the cells in place with sufficient forces during micropipette penetration.

For devices with 5 × 5 through-holes, a batch of mouse zygotes, greater than the number of through-holes (e.g., 30–35), were first transferred to the cell holding cavity (Fig. 9.3a). With the application of a negative pressure, each through-hole trapped a single cell. The immobilization process took approximately 10 s. Extra untrapped cells were removed using a transfer pipette (Fig. 9.3c). The complete process including the removal of extra cells typically takes 31 s for devices with an array of 5 × 5 through-holes.

When a small number of zygotes need to be injected, devices with a lower number of through-holes (e.g., 3 × 3) were used. In this case, exactly the

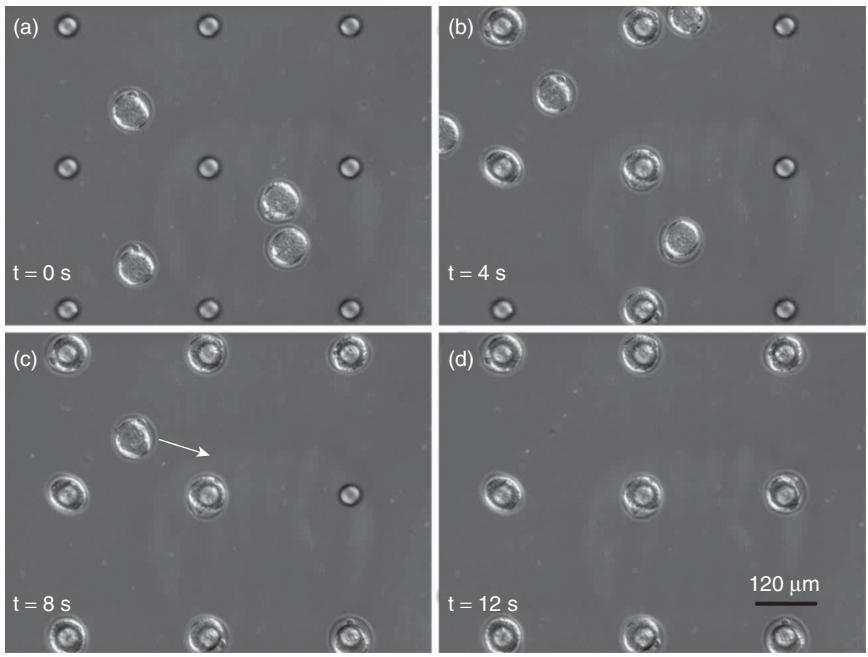

9.4 Immobilization on a 3 × 3 array of mouse zygotes. (a) Nine zygotes are delivered into the cell holding cavity. Five of them are out of field-of-view. (b) A 2 kPa sucking pressure initiates cell immobilization. (c) The last untrapped zygote is moving toward the final open through-hole. (d) The immobilized 3 × 3 array of mouse zygotes. The complete process typically takes 12 s. (*Source*: Reproduced with permission from Springer.)

same number of cells was transferred to the cell holding cavity. In Fig. 9.4a, only four cells of the nine delivered cells are within the field-of-view. Due to the small number of through-holes and the smaller cell holding cavity, the nine through-holes were capable of rapidly immobilizing nine cells without requiring the delivery of extra cells. Therefore, the step of removing extra untrapped zygote was not needed. The complete process for immobilizing nine cells into a 3 × 3 array took approximately 12 s.

9.3.2 Robotic mouse embryo microinjection

Immobilizing mouse zygotes into a regular pattern makes cell search and immobilization easier and is an important enabling factor for reliable automated microinjection. In order to quantify the possible negative effect of the cell holding device on post-injection embryonic development, the immobilized zygotes were injected by a robotic injection system (Liu and Sun, 2009). As shown in Fig. 9.5, the system consists of an inverted microscope

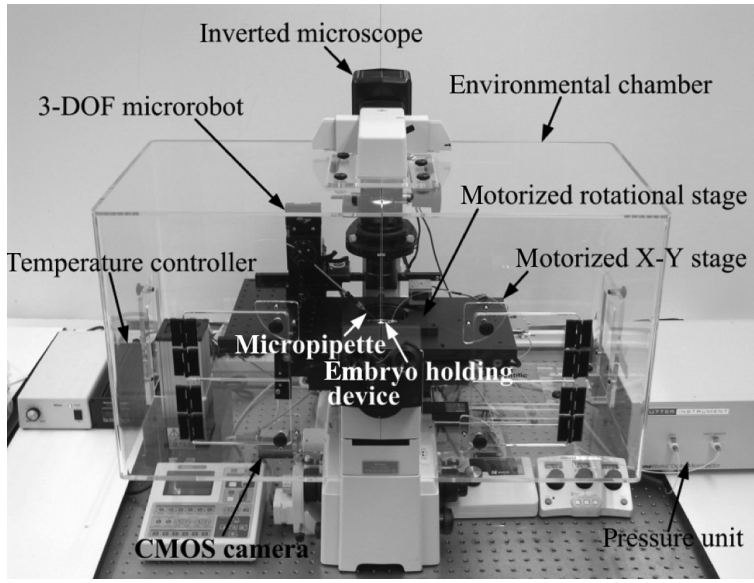

9.5 A robotic system for automated mouse zygote microinjection. (*Source*: Reproduced with permission from Springer.)

(Nikon TE-2000, DIC imaging), a CMOS camera (Basler A601f), the cell holding device, an in-house developed motorized rotational stage placed on a motorized X-Y translational stage (Prior ProScan II) for cell positioning and orientation control, an injection micropipette connected to a computer-controlled pressure unit (Sutter XenoWorks) for material deposition, a three-degree-of-freedom microrobot (Sutter MP-285) for controlling the injection pipette to inject cells, an environmental chamber to maintain cells at 37°, and a host computer (Pentium 4, 3.0 GHz CPU, 1 GB RAM) with a motion control board (NI PCI-6259). The system also integrates motion control and image processing algorithms for automatic microinjection (Liu and Sun, 2009). An injection micropipette is controlled by the microrobot to diagonally penetrate the immobilized zygote and deliver materials into the cytoplasm center, as schematically shown in Fig. 9.6.

In experiments, PBS buffer was used as the injection material. Figure 9.7a shows a zygote penetrated with the micropipette tip at the cytoplasm center. An injection speed of 200 μm/s and a retraction speed of 500 μm/s were used in the experiments, which have proven to be optimal in terms of minimizing injection-induced cell lysis. The robotic system injected a total of 240 mouse zygotes (imprinting control region strain, ICR strain) at a speed of 12 cells/min (as compared to two zygotes/min in manual injection by proficient injection technicians with over 12 years of experience). Based on visual inspection right after injection, the robotic system achieved a low cell lysis rate of

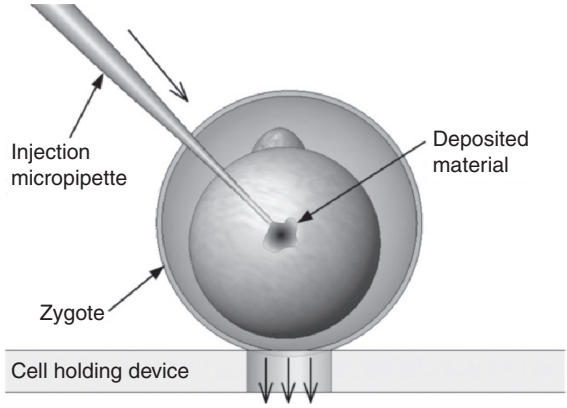

9.6 Schematic of mouse zygote microinjection. (*Source*: Reproduced with permission from Springer.)

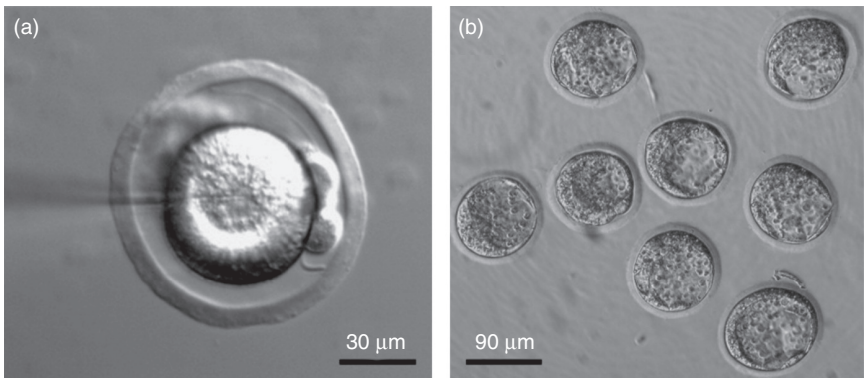

9.7 Photographs of robotically injected mouse zygotes. (a) A mouse zygote penetrated by a micropipette before material deposition. The micropipette injects a cell in a diagonal direction. (b) Robotically injected mouse zygotes developing into blastocysts. (*Source*: Reproduced with permission from Springer.)

1.1%. The injected zygotes were thereafter cultured in potassium simplex optimization medium (KSOM; Specialty Media) for 96 h (37°C, 5% CO_2) to allow the zygotes to develop into blastocysts. Figure 9.7b shows robotically injected zygotes that successfully developed to the blastocyst stage.

We define the cell survival rate as the ratio of the number of injected zygotes developing into the blastocyst stage to the total number of injected zygotes, quantitating the combined impact of vacuum-based cell immobilization and robotic microinjection. Control groups of non-injected zygotes

were cultured under the same conditions (KSOM, 37°C with 5% CO_2) to eliminate zygote quality differences across cell batches. Based on the 240 injected mouse zygotes, the cell holding device and the robotic injection system produced a survival rate of 89 ± 1.3%, higher than the best survival rate (~80%) achieved by proficient injection technicians using a holding micropipette and an injection micropipette. The result demonstrates that, compared to conventional manual microinjection, the cell holding devices do not produce additional negative impact on embryonic development.

9.3.3 Discussion

In this study, rapid cell trapping and immobilization were demonstrated using microfabricated glass devices with an array (e.g., 3 × 3 and 5 × 5) of through-holes connected to a vacuum source. Vacuum-based cell trapping was selected because of its capability of providing sufficient immobilization force during mechanical microinjection. The wet-etching-based microfabrication process only employs two masks, and allows one to fabricate a single through-hole or hundreds of through-holes (e.g., 25 × 25 = 625) for large-scale trapping, immobilization, and injection of mouse embryos. By tuning the microfabrication parameters, one can possibly build through-holes with diameters down to 5 μm on a standard cover slip, for example, for immobilizing smaller suspended cells (15–20 μm) for other single-cell studies that require the use of DIC optics and thus, glass microdevices.

Using the cell holding devices developed in this research, we have performed high-throughput microinjection of mouse embryos, in which >1000 embryos were injected, for large-scale biomolecule testing (Liu *et al*., 2011). A variety of assays (e.g., blastocyst cell-number quantification, reactive oxygen species measurement, and mitochondrial activity analysis) were conducted for monitoring the development of embryos injected by our robotic system and an injection technician. The experimental results revealed that robotically injected embryos have equivalent development competence to the manually injected ones, which proves that the cell holding devices impose negligible biological effect on the trapped embryos.

9.4 Conclusion

This chapter presented a glass-based, microfabricated cell holding device for single-cell immobilization via the application of a low vacuum. A cell holding cavity and an array of through-holes were formed on a cover slip using isotropic two-sided glass wet etching. To form a device assembly, a microscope slide and a patterned thin layer of PDMS were used to bond to the etched cover slip. The device assembly is compatible with DIC

imaging. Rapid immobilization of mouse zygotes was demonstrated using the cell holding devices. Automated injection of the immobilized mouse zygotes was conducted using a robotic injection system. The post-injection embryo culturing results demonstrated that the vacuum-based cell immobilization devices do not produce additional negative effects on embryonic development.

9.5 Acknowledgements

This work was supported by the Natural Sciences and Engineering Research Council of Canada, the Ontario Ministry of Research and Innovation, and the Ontario Centers of Excellence. We also acknowledge the financial support from the Canada Research Chairs Program to YS, and from the McGill University to XYL.

9.6 References

Carlborg, C. F., Haraldsson, T., Stemme, G. and Wijngaart, W. V. D. (2007). Reliable batch manufacturing of miniaturized vertical vias in soft polymer replica molding. *Proceedings of International Conference on Miniaturized Systems for Chemistry and Life Sciences (MicroTAS)*, Paris, France, October 7–11, 2007.

Carlo, D. D., Wu, L. Y. and Lee, L. P. (2006). Dynamic single cell culture array. *Lab on a Chip*, **6**, 1445–1449.

Castel, D., Pitaval, A., Debily, M. A. and Gidrol, X. (2006). Cell microarrays in drug discovery. *Drug Discovery Today*, **11**, 616–622.

Chen, C. S., Mrksich, M., Huang, S., Whitesides, G. M. and Ingber, D. E. (1997). Geometric control of cell life and death. *Science*, **276**, 1425–1428.

Chen, D. S. and Davis, M. M. (2006). Molecular and functional analysis using live cell microarrays. *Current Opinion in Chemical Biology*, **10**, 28–34.

Deutsch, M., Deutsch, A., Shirihai, O., Hurevich, I., Afrimzon, E., Shafran, Y. and Zurgil, N. (2006). A novel miniature cell retainer for correlative high-content analysis of individual untethered non-adherent cells. *Lab on a Chip*, **6**, 995–1000.

Gattass, R. R. and Mazur, E. (2008). Femtosecond laser micromachining in transparent materials. *Nature Photonics*, **2**, 219–225.

Haake, A., Neild, A., Kim, D.-H., Ihm, J.-E., Sun, Y., Dual, J. and Ju, B.-K. (2005). Manipulation of cells using an ultrasonic pressure field. *Ultrasound in Medicine and Biology*, **31**, 857–864.

Iliescu, C., Tay, F. E. H. and Miao, J. (2007). Strategies in deep wet etching of Pyrex glass. *Sensors and Actuators A: Physical*, **133**, 395–400.

Ino, K., Okochi, M., Konishi, N., Nakatochi, M., Imai, R., Shikida, M., Ito, A. and Honda, H. (2008). Cell culture arrays using magnetic force-based cell patterning for dynamic single cell analysis. *Lab on a Chip*, **8**, 134–142.

Jordan, P., Leach, J., Padgett, M., Blackburn, P., Isaacs, N., Goksor, M., Hanstorp, D., Wright, A., Girkin, J. and Cooper, J. (2005). Creating permanent 3D arrangements of isolated cells using holographic optical tweezers. *Lab on a Chip*, **5**, 1224–1228.

Liu, X., Fernandes, R., Gertsenstein, M., Perumalsamy, A., Lai, I., Chi, M., Moley, K. H., Greenblatt, E., Jurisica, I., Casper, R. F., Sun, Y. and Jurisicova, A. (2011). Automated microinjection of recombinant BCL-X into mouse zygotes enhances embryo development. *PLoS ONE*, **6**, e21687.

Liu, X. and Sun, Y. (2009). Automated mouse embryo injection moves toward practical use. *Proceedings of the 2009 IEEE International Conference on Robotics and Automation*. Kobe, Japan, May 12–17, 2009.

Matthews, B. and Judy, J. W. (2006). Design and fabrication of a micromachined planar patch-clamp substrate with integrated microfluidics for single-cell measurements. *Journal of Microelectromechanical Systems*, **15**, 214–222.

Murphy, D. (2001). *Fundamentals of Light Microscopy and Digital Imaging*, New York, Wiley-Liss.

Rettig, J. R. and Folch, A. (2005). Large-scale single-cell trapping and imaging using microwell arrays. *Analytical Chemistry*, **77**, 5628–5634.

Skelley, A. M., Kirak, O., Suh, H., Jaenisch, R. and Voldman, J. (2009). Microfluidic control of cell pairing and fusion. *Nature Methods*, **6**, 147–152.

Suzuki, T., Yamamoto, H., Ohoka, M., Kanno, I., Washizu, M. and Kotera, H. (2007). A low-damage cell trapping array fabricated by single mask multidirectional pho- tolithography with equivalent circuit analysis. *Proceedings of International Conference on Miniaturized Systems for Chemistry and Life Sciences (MicroTAS)*, Paris, France, October 7–11, 2007.

Tan, W.-H. and Takeuchi, S. (2007). A trap-and-release integrated microfluidic system for dynamic microarray applications. *Proceedings of the National Academy of Sciences*, **104**, 1146–1151.

Voldman, J., Gray, M. L., Toner, M. and Schmidt, M. A. (2002). A microfabrication-based dynamic array cytometer. *Analytical Chemistry*, **74**, 3984–3990.

Wiklund, M. and Onfelt, B. (2012). Ultrasonic manipulation of single cells. *Methods in Molecular Biology*, **853**, 177–196.

Wood, D. K., Weingeist, D. M., Bhatia, S. N. and Engelward, B. P. (2010). Single cell trapping and DNA damage analysis using microwell arrays. *Proceedings of the National Academy of Sciences of the United States of America*, **107**, 10008–10013.

10

Microfluidic devices for developing tissue scaffolds

L. T. CHAU, J. E. FRITH, R. J. MILLS, D. J. MENZIES, D. M. TITMARSH and J. J. COOPER-WHITE,
The University of Queensland, Australia

DOI: 10.1533/9780857097040.3.363

Abstract: This chapter begins by outlining the key hurdles that currently exist in terms of achieving directed tissue genesis, *in vitro* and *in vivo*, from available mature, progenitor and stem cell sources. The chapter then proceeds to describe how microfluidic device platforms can provide the required insights to overcome these hurdles to clinical translation, including the optimization of soluble factor provision to enhance cell expansion and differentiation outcomes, the impacts of pore architecture and surface engineering on scaffold colonization, and the biophysical needs of cells when creating three dimensional artificial vascular pedicles for improved scaffold vascularization post-implantation.

Key words: tissue engineering, scaffolds, microdevices, tissue genesis, stem cells.

10.1 Introduction

In vivo tissue repair and regeneration are substantially facilitated by recruited stem cells from peripheral blood, or from those resident in most, if not all, tissues (Sakamoto *et al.*, 2006). Their depletion within an organ system may lead to full or partial loss of function (Palsson and Bhatia, 2004), indicating their critical role in tissue repair and replacement. Cells within tissues are surrounded by a three dimensional (3D) microenvironment of three (principle) 'support' systems: vasculature, other cells (including stem cells), and cell-secreted extracellular matrix (ECM). Constitutionally, tissues vary from being cell-dense (1×10^9 cells/cm^3), vascularized and extracellular matrix-poor structures, in the case of, for example muscle and fat tissue, through to cell-poor (1×10^6 cells/cm^3), avascular and extracellular matrix-rich structures, in the case of cartilage.

The field of tissue engineering aims to bring together key design principles of engineering and our understanding of cell biology and tissue genesis to invoke local repair or regeneration of damaged or diseased tissue.

Researchers utilize a variety of cell sources, depending on their tissue end point or target, including mature (fully differentiated), progenitor and stem cells. Through their combination with biomaterials and *in vitro* culture environments, cells are encouraged to generate functional tissues. However, the significant regenerative potential and clinical translation of tissue engineering practices, especially those using stem cells or progenitor cells, remains largely untapped. This is due largely to deficiencies in our knowledge of what microenvironments must be provided to the chosen cell types to facilitate the development of tissues that are not only composed of the appropriate cell types and phenotypes but that also are functionally equivalent to the lost or damaged tissue. This chapter discusses the current status of microfluidic device-based research attempting to address and overcome these deficiencies, with the aim of ultimately enabling clinical translation of cell-based tissue engineering therapies.

10.2 Key issues and technical challenges for successful tissue engineering

While there are many alternative paths or approaches being taken by researchers to achieve what are intrinsically complex outcomes in order to produce a functional, engineered tissue, there remain a number of key challenges or hurdles to achieving such directed tissue genesis, both *in vitro* and *in vivo*, from available cell sources. They are: (1) obtaining clinically relevant numbers, through *ex vivo* expansion and/or differentiation (e.g. from pluripotent or multipotent stem cells to fully differentiated end points) of the targeted cell types for implantation with the chosen scaffold; (2) encouraging effective and efficient cell seeding and scaffold colonization within both *in vitro* (for extended culture prior to implantation) and *in vivo* (involving active recruitment of endogenous cells) contexts; and (3) rapid vascularization of the cell-laden scaffold post-implantation to avoid necrosis and encourage further tissue growth and maturation. We will now explore each of these challenges in more detail.

10.2.1 Clinically relevant cell numbers: from stem cells through to mature, fully differentiated cells

It is estimated that in a myocardial infarction, approximately 1 billion cardiomyocytes (the functional 'beating' cells in heart tissue) can be lost. Unfortunately, mature human cardiomyocytes are non-proliferative and hence, in order to invoke functional repair of damaged heart tissue through cardiomyocyte repopulation, the human body needs assistance. One of the current approaches which has significant potential is the implantation of

human cardiomyocytes into this damaged site that have been generated *in vitro* from human pluripotent stem cell (hPSC) sources (human embryonic stem cells (hESC) and induced pluripotent stem cells (iPSC)). However, the progression of a stem cell from a pluripotent, multipotent or early progenitor stage into a range of terminally differentiated, mature cells that form adult tissues involves differentiation through quite a number of intermediate populations. For example, in specifying contractile cardiomyocytes from hPSCs, cells must pass from the pluripotent phenotype through a primitive streak-like population, to pre-cardiac mesoderm, to cardiac progenitors, to cardiomyocytes, then to functional, mature cardiomyocytes, as a minimum set of developmental stages (there may be more undiscovered complexity within those stages). Current protocols for deriving cardiomyocytes from hPSCs quote 1–1.5 cardiomyocytes per input hPSC; therefore, ~1×10^9 hPSCs would be required as a starting point, requiring ~20×10^3 cm^2 of starting culture area (as an estimate based on some monolayer protocols). It is clear, then, that the problem of arriving at a clinical dose of functional cells is a significant challenge.

This is particularly true for therapies involving adult stem cells, which are typically rare cell populations and have a more limited potential for expansion than their pluripotent counterparts. For example, mesenchymal stem cells (MSC) make up between just 0.01–0.001% of mononuclear cells in the bone marrow and therefore require significant expansion in order to generate clinically relevant numbers (Pittenger *et al.*, 1999). However, comparisons of MSCs shortly after isolation to those that have undergone several passages, show a dramatic increase in population doubling time and a diminished ability to differentiate along the osteo-, adipo- and chondro-genic lineages (Banfi *et al.*, 2000). As a result, there is a significant drive to develop methods for expansion that retain the beneficial properties of the cells in a manner that is reproducible, fully-defined, and amenable to the scale-up that will be required for translation to the clinic.

An alternative strategy to using stem cells is to 'transdifferentiate' a resident cell in the damaged tissue site (or periphery) that is non-functional into a functional cell type, for example, in the case of cardiac tissue, transdifferentiation of cardiac fibroblasts (non-functional in terms of beating) into functional cardiomyocytes, has been proven to be possible (both *in vitro* and *in vivo*) (Kou *et al.*, 2011). However, for transdifferentiation (also known as direct reprogramming) approaches, the reprogramming method or process is itself a long and inefficient process (some can take place over a few weeks), with poor understanding of the molecular events and cellular changes that occur before arriving at the reprogrammed cell type, usually with a low efficiency. Producing enough cells for functional tissue recovery is thus still a significant challenge.

Ensuring that significant cell numbers of the target phenotype are present at the output of any bioprocess is thus essential for their successful use in the intended tissue engineering endpoint application. This can be achieved in several ways:

- Increasing the number of starting point cells (e.g. stem cells);
- Increasing efficiency of differentiation to intermediate and target phenotypes;
- Increasing the efficiency of direct reprogramming/transdifferentiation; or
- Selection processes (sorting, density gradient centrifugation, antibiotic selection, subculturing).

10.2.2 Effective cell seeding and scaffold colonization

One of the major challenges still confronting the application of tissue-engineered scaffolds in the clinic is inadequate cell colonization. Previous strategies have generally suffered from high cell colonization at the periphery and little to none within the centre of the constructs. To achieve sufficient cell colonization, an effective cell seeding methodology that allows homogenous cell seeding needs to be employed and the seeded cells need sufficient nutrients and oxygen in order to survive, proliferate and regenerate the required tissue.

Cell colonization of a biomaterial scaffold is influenced by its physical, spatial and biochemical properties (Fig. 10.1). Physical cues, including

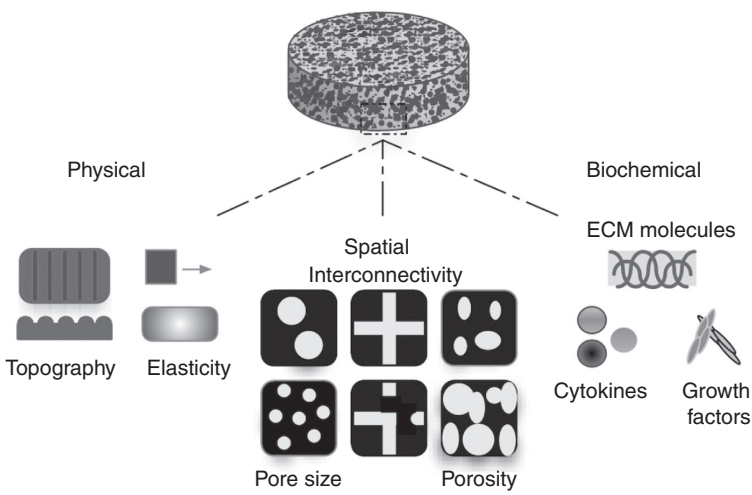

10.1 Physical, spatial and biochemical properties that influence cell colonization.

stiffness and topography, can have a profound effect on cell adhesion and migration (Diehl *et al*., 2005; Doyle *et al*., 2009; Isenberg *et al*., 2009; Kaiser *et al*., 2006; Lo *et al*., 2000; Pelham and Wang, 1997), while pore size (Cao *et al*., 2006; Chu *et al*., 2002; Malda *et al*., 2005; O'Brien *et al*., 2005; Oh *et al*., 2007; Tsuruga *et al*., 1997; van Tienen *et al*., 2002; Zmora *et al*., 2002), porosity (Baker *et al*., 2008; Karageorgiou and Kaplan, 2005; Silva *et al*., 2006; Spiteri *et al*., 2006), and interconnectivity (Griffon *et al*., 2006; Melchels *et al*., 2010) are examples of important spatial parameters that can similarly have substantial impacts. The material that the scaffold is made from will also affect colonization by altering the specific cell-material interactions (for example those mediated by integrins) with subsequent effects on cell adhesion and migration (Lawrence and Madihally, 2008). More recently there has been a wider appreciation of the variation in modes of cell migration and scaffold colonization observed in two dimensional (2D) and 3D environments, where the degradation rate of the material is a relevant parameter in determining the movement of cells into and within the scaffold. All of these factors must be taken into account during scaffold design in order to promote optimal cell colonization.

Traditionally, three seeding methodologies have been used:

- static,
- dynamic, and
- perfusion bioreactor cultures.

Of these, static seeding methods are the simplest, but perhaps the least effective. Using such methods, a high-density suspension of cells is added to the surface of the scaffold, where it is hoped they will adhere and migrate through to the centre. This may be aided by seeding several sides of the construct. Dynamic seeding methodologies can take many forms; however, one common example is the use of a spinner flask, which encourages movement of culture medium laden with cells through the pores of the scaffold. Such methods have been used to seed MSCs into calcium phosphate scaffolds for bone tissue engineering, resulting in an enhanced proportion of the cells adhering to the material and improved penetration throughout the construct (Griffon *et al*., 2011). Under perfusion, culture medium is passed through scaffolds from one direction to the other. This may occur with constant provision of fresh culture medium, or may exist in a closed loop with the medium passing across the construct multiple times. As with dynamic cell seeding strategies, the movement of the medium through the scaffold has been shown to aid both the efficiency of seeding and has also been shown to promote uniform tissue development across the construct (Zhao and Ma, 2005). For both dynamic and perfusion cultures, the rate of media flow through the scaffold is crucial, as it is necessary to balance the rate

of provision of nutrients and removal of waste products while at the same time minimizing the shear forces applied to cells to maximize viability and allow their initial adhesion to the presented biomaterial surface. Additional strategies, such as those involving growth factor incorporation, may be used to promote migration into the centre of the scaffold. Growth factors, such as vascular endothelial growth factor (VEGF), may also be used to promote vascularization, which in turn will bring cells into the scaffold, as well as providing an environment in which nutrients such as oxygen and glucose are available and where waste products are readily removed.

Effective cell seeding and colonization of scaffolds remains a significant challenge and limitations in our knowledge and understanding of the relevant parameter space mean that seeding strategies must currently be optimized for each individual situation. It is particularly difficult to separate out the effects of each individual factor on the final result, and more information is required in order enable the rational design guidelines for effective colonization of any given biomaterial construct.

10.2.3 Vascularization

Vascularization is the process of growing blood vessels into a tissue to improve oxygen and nutrient supply. It remains an overriding limiting factor in tissue engineering large 3D constructs, either during *in vitro* preculture or *in vivo* post-implantation. In the absence of a vascular network, metabolite supply and cell viability in a scaffold is compromised when diffusion distances are greater than 150–200 μm (Folkman and Hochberg, 1973) (Fig. 10.2). As a result, tissue engineering has been largely limited to thin or avascular tissues such as skin (Kremer *et al.*, 2000) or cartilage (Vacanti and Upton, 1994). Engineering a large complex tissue thus necessitates growing a physiologically relevant vasculature that promotes cell survival, tissue organization and rapid vascularization following implantation. The incorporation of a functional microcirculatory network into the scaffold prior to implantation is therefore essential. In addition, in order for the large 3D construct to remain viable, the microcirculatory network is required to mimic natural vasculature and carry out angiogenesis, a process where new capillaries are formed from pre-existing blood vessels (Patan, 2000).

Many methods have been developed to fabricate microvasculature for pre-vascularization of scaffolds. Early studies often involved fibres, synthetic or natural, as 'sacrificial' or temporary microvessel templates (Chrobak *et al.*, 2006; Ko and Iwata, 2001; Neumann *et al.*, 2003; Migliore *et al.*, 2008; Takei *et al.*, 2006). However, these approaches either resulted in a multichannelled microvascular construct without a common inlet and outlet (Ko and Iwata, 2001), or multiple single micron-scale vessels (Chrobak *et al.*,

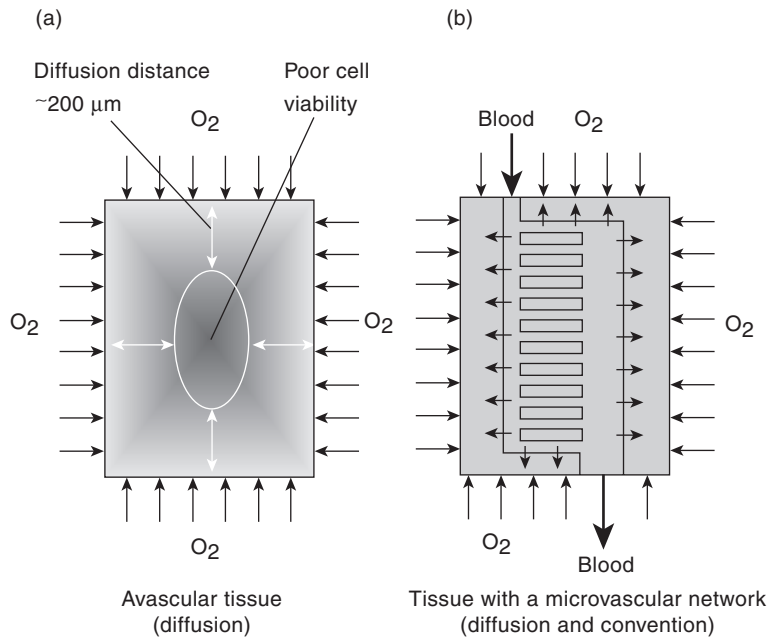

10.2 Distribution of oxygen and nutrients in an avascular tissue and a tissue with a microvascular network. (a) In an avascular tissue, diffusion alone can only supply metabolite sufficiently within the first 200 μm. This is assuming that the surface of the tissue is exposed to fresh blood supply via the flanking capillary network. As a result, cells which are at a distance of greater than 200 μm from this supply will be compromised. (b) In a tissue with a microvascular network, metabolite supply is both by convection and diffusion. Therefore, cells can be nourished and sustained throughout the tissue construct.

2006; Migliore *et al.*, 2008; Neumann *et al.*, 2003; Takei *et al.*, 2006), making them impractical and technically challenging for surgical implantation.

Researchers later fabricated larger complex 3D microvascular networks. These involved sacrificial 'cotton candy' sugar structures in polymeric (polydimethylsiloxane (PDMS), epoxy, or polycarbonate) matrices (Bellan *et al.*, 2009), and random assemblies of discrete, micron-scale gelatin components to form a large modular tissue-engineered construct (McGuigan and Sefton, 2007a, 2007b). However, while these methods are novel, there is limited control over the hydrodynamics of the random networks formed. Control over hydrodynamics in a microvascular network construct is important to ensure adequate delivery of nutrients to all cells, along with appropriate levels of shear stress for normal cell function.

Microfabrication is another method that has been commonly used in the development of artificial microvasculature. The main advantages of microfabrication technology over other methods include being able to achieve

resolutions of 10 μm, which are on the same lengthscale as capillaries (Borenstein *et al*., 2002; Kaihara *et al*., 2000), and the ability to invoke structural uniformity in such microvascular networks. Several investigators have recently used microfabrication to establish and optimize microvascular network designs and create microcirculatory networks with varying levels of success.

We will now highlight some of the past and present approaches utilizing microfluidic technology to overcoming the above listed hurdles to translation and clinical uptake of tissue-engineered products.

10.3 Microfluidic device platforms

Recent advances in microfluidic technology offer unprecedented control over fluid (both single phase and multiphase) flow, interface dynamics, droplet and particle size and size distribution, heat transfer and reaction conditions. This control results largely from the imposition of laminar flow and the domination of surface forces in the inherently small lengthscales within these devices. Microfluidic technologies are also ideally suited for parallelization or scale-up. It is for these reasons that researchers have turned to microfabrication and microfabricated *in vitro* environs to probe cellular behaviours that are otherwise difficult to investigate within standard cell culture methods. Further, such platforms permit the investigation, and real time read-out in some cases, of the impacts of varying microenvironmental conditions, including both biochemical factors (such as media exchange, oxygen concentration, pH, factor and ligand concentration) and biophysical factors (such as substrate mechanics, scaffold geometry, pore size and connectivity), on cell fate choices, such as morphology, migration, proliferation, differentiation and apoptosis. Ultimately, these choices determine the success or failure of our attempts at directed tissue genesis from any cell type, whether terminally differentiated or pluripotent. We now provide a review of some of the more recent examples of microdevices that have been designed to probe such complex parameter space in order to provide the necessary insight required to ensure successful tissue engineering outcomes.

10.3.1 Microdevices for optimization of microenvironments for cell/stem cell expansion and differentiation

Stem cells and their differentiated sub-lineages are important components in tissue-engineered constructs, either from the perspective of incorporation within the construct, or design of the construct in order to recruit and support native cells. Control of cell phenotype through isolation, expansion of

a stem cell population, and specification and maintenance of differentiated lineages of interest is therefore essential in ensuring the quality and efficacy of cells incorporated or targeted in tissue-engineered constructs.

Fortunately, microscale technologies are expanding the repertoire of assay platforms in investigating features of stem cell and stem cell-derived populations, including their expansion and differentiation (Salieb-Beugelaar *et al*., 2010). Because of several advantageous capabilities, including high parallelization, continuous fluid flow, and reduced culture dimensions, microscale (and particularly microfluidic) systems can provide opportunities for high-fidelity screening of stem cell culture processes under well-controlled microenvironmental conditions. Stem cells can sense and respond to a variety of stimuli, such as soluble factors, extracellular matrix proteins, cell–cell contacts, mechanical forces and properties (shear, strain, elastic and viscous moduli) and electrical stimulation, and further can be manipulated by introduction of genetic material and pharmacological agents, etc. Microtechnologies such as biomolecule spotting, surface micropatterning, and microfluidic systems are ideal platforms for screening these stimuli, as has been recently reviewed (Titmarsh *et al*., 2012a). While biomolecule spotting platforms have been applied more thoroughly for investigating combinations of ECM proteins for stem cells, microfluidic technologies in particular have made inroads into examining the physical, soluble factor, paracrine factor, and co-culture cues that drive stem cell expansion and differentiation, which we will now summarize.

Medium flow rate in continuous flow microfluidic systems affects biochemical and biophysical parameters (medium turnover, shear stress, etc.). Microbioreactor arrays have been developed to supply a logarithmic range of flow rates and assess mESC growth, which improved with increasing flow rate (Kim *et al*., 2006). For hESCs, a device with a much narrower, linear range of flow rates showed they were more sensitive, as they expanded best in a small window of flow rates, and were limited outside this window (Titmarsh *et al*., 2011). Fluidic resistance allowed control of fluid flow in these microfluidic systems. Instead of continuous flow, other systems have used programmed medium exchange to investigate temporal stimulation of mESCs (Ellison *et al*., 2009) and HSCs (Lecault *et al*., 2011) with various factors.

Microfluidic systems are also ideal for controlled introduction of soluble factors and screening their effects on the expansion or differentiation of stem cell populations. Moreover, this can be done in a semi-high-throughput manner due to the parallelization that can be achieved with microfabrication. For example, a multiplexed microbioreactor array platform recently enabled full factorial screening of exogenous and paracrine factors in hESC differentiation to a primitive streak-like population (Titmarsh *et al*., 2012b).

A fully-automated microfluidic system based on pneumatic valve control was developed to screen 96 discrete, individually-addressable microbioreactor chambers, which could be fed with arbitrary mixtures of up to 16 medium components or soluble factors. This system has been utilized for automated screening of culture environments for MSC growth and differentiation (Gómez-Sjöberg *et al.*, 2007). Importantly, the application of continuous medium perfusion in closed microfluidic stem cell culture systems has identified autocrine/paracrine effects as critical regulators of stem cell populations (Blagovic *et al.*, 2011; Moledina *et al.*, 2012). A recent review highlighted the way microfluidic technologies are providing new avenues to assess and manipulate paracrine effects (Przybyla and Voldman, 2012).

10.3.2 Microdevices for studying the effects of substrate and ligand type, pore geometry and scaffold architecture on cell migration, scaffold colonization and tissue development

Investigating the numerous parameters that influence scaffold colonization and tissue development within a 3D biomaterial is difficult. This is predominantly due to the inability to systematically investigate, and independently change, scaffold properties, and the ever-present immune response when performing *in vivo* studies. As such, microdevices have recently been used to introduce a high degree of control over the cellular microenvironment. The development of these devices has allowed the methodical evaluation of various scaffold parameters, including the substrate or ligand type, pore geometry and architecture on scaffold development.

Studying cell migration not only provides an insight into the fundamentals of cell biology, but it is also useful in assessing the suitability of various substrates and materials as a tissue engineering construct. Numerous microdevices have been developed to overcome the deficiencies associated with traditional methodologies, and have allowed investigation into the cell motility in response to chemokines (Lin and Butcher, 2006; Saadi *et al.*, 2006), ligands (Doran *et al.*, 2009), co-culture (Chung *et al.*, 2009) mechanical constraints (Irimia and Toner, 2009) and pore architecture (Mills *et al.*, 2011). These devices not only allow precise microenvironmental control, but can also elucidate results that are indiscernible using conventional assays or techniques.

A traditional assay to assess cell migration in response to a substrate is the wound healing or scrape assay. This involves creating a 'wound' within a confluent cell monolayer (generally by scraping the cell with a pipette tip), and observing the closure of the 'wound' edges to quantify cell migration rates. While this method is relatively straightforward, the outcomes are

confounded by a number of factors, including the ambiguity of the substrate, as a result of the wound generation removing the desired surface or fouling due to cellular secretions, and the damage to cells at the wound edge, which impacts cell migration.

A number of different microdevices have been developed to overcome the problems associated with techniques such as the wound healing assay and allow a more systematic investigation into cell migration. One of the earliest of these microdevices, developed by (Nie *et al*., 2007) uses a laminar flow of trypsin to generate a well-defined 'wound' edge. While this method elicits only minor damage to cells on the wound edge, the surface onto which the cells will migrate remains ambiguous. Poujade *et al*. also developed an eloquent PDMS-based stencil tool, in which a PDMS stencil is applied to a surface prior to cell seeding. The stencil is then peeled off, allowing cell migration to begin (Poujade *et al*., 2007). Although this approach overcomes many of the problems associated with the classical wound healing assay, even this solution potentially compromises surface composition, as the PDMS stencil must be fixed on top of the virgin surface until the cell monolayer is established.

More recently, a microdevice developed by Doran *et al*. has allowed the maintenance of a defined surface with no cellular damage during the initiation of cell migration (Doran *et al*., 2009). This device consists of a main inoculation chamber with perpendicular protruding migration channels (Fig. 10.3). In operation, cells are seeded into the main chamber, but the cell suspension does not enter the migration channels due to the presence of a fluid meniscus at each channel entrance, a result of the channel dimensions (100s of microns) and high (relative) fluid surface tension. This allows a confluent monolayer to be established within the central chamber with a 'cell edge' at the interface between this chamber and the migration channel. Cell migration is then initiated via backfilling the migration channels, to effectively 'break' the fluid meniscus and allow cells to access the channel. This microdevice thus allows the assessment of cell migration without the confounding issues of cellular damage or surface ambiguity, providing a rapid and robust tool to assess the influence of substrate biochemistry on cell migration, and thus cell colonization of space.

The flexibility of this device also allows the presentation of 2D geometrical challenges to mimic the architectural aspects and characteristics of 3D porous scaffolds. This adaption allows for the assessment of cell migration in response to geometrical challenges that mimic the architectural aspects and characteristics of 3D porous scaffolds in a 2D arrangement. This device has been utilized to investigate the influence of varying channel widths, degrees of channel tortuosity, the presence of contractions or expansions, and channel junctions on the migration of NIH 3T3

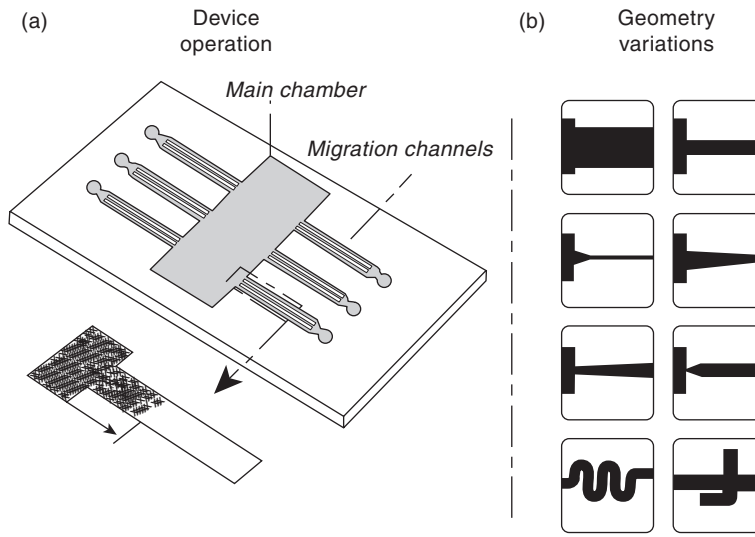

10.3 Schematic of microdevice operation and geometric constraint variations. (a) Once a cell monolayer is established within the main chamber, migration is initiated via backfilling of the migration channels. Migration can then be quantified by measuring cell progression into the channel. (b) This format can be used to study the effect of various substrates, or by incorporating geometry variations (as shown) along the length of the migration channels, can be used to determine how different cell types interpret architectural aspects of a tissue engineered scaffold. These parameters include various pore sizes, contractions, expansions, junctions and tortuosity.

mouse fibroblasts and human bone marrow-derived mesenchymal stromal cell (hMSC) (Mills *et al*., 2011). Data gained from this device showed that these two cell types have vastly different migration characteristics; 3T3 fibroblasts migrate as a collective cell front, whereas hMSCs migrate as single cells. This resulted in 3T3 fibroblasts displaying significant differences in migration depending on the type of geometrical constraint, while hMSCs were only influenced by channel width when it approached that of the length scale of a single cell, characteristics that would have a significant influence on the scaffold colonization by these two different cell populations. This clearly demonstrates the use of a microdevice to provide the necessary insight into how certain cell types, as a result of their migration characteristics, encounter and deal with different geometric constraints that may exist within biomaterial constructs, thereby highlighting the utility of microdevices to provide biological insights, relevant to tissue engineering, which could not be obtained using traditional techniques.

10.3.3 Microdevices for studying cell mechanics and impacts of shear stress on endothelial and smooth muscle cell function

Shear stress is known to influence the morphology, and even the fate, of many cell types (Gosgnach *et al*., 2000; Lu *et al*., 2004; Gutierrez *et al*., 2008; Kou *et al*., 2011; Qazi *et al*., 2011; Shi and Tarbell, 2011), including endothelial and smooth muscle cells (Song *et al*., 2005; Sakamoto *et al*., 2006; Plouffe *et al*., 2007; Chau *et al*., 2009; Tkachenko *et al*., 2009; Wang *et al*., 2010). As blood flows through a vessel, shear stress is generated and directly sensed by endothelial cells lining the vascular wall. Endothelial cells may act as a mediator between flow conditions and smooth muscle cell functions. Physiologically, smooth muscle cells exist below the endothelial cell lining and are protected from the shear stress. However, in pathological conditions involving endothelial injury, smooth muscle cells can become exposed to shear stress (Palumbo *et al*., 2000; Shi *et al*., 2010; Shi and Tarbell, 2011). Therefore, understanding cell mechanics and impacts of shear stress on endothelial and smooth muscle cell function is important in vascular studies and tissue engineering.

Many shear microdevices have been developed. In general, they were fabricated using conventional microfabrication techniques and their designs involved an inlet channel branching into multiple channels of varying dimensions, which allowed multiple shear forces to be studied simultaneously (Song *et al*., 2005; Gutierrez *et al*., 2008; Chau *et al*., 2009; Tkachenko *et al*., 2009; Kou *et al*., 2011; Li *et al*., 2012a). These microdevices have been used to study shear-dependent platelet aggregation (Li *et al*., 2012a) and adhesion to various extracellular matrix proteins (Gutierrez *et al*., 2008), and effects of shear stress on osteoblasts (Kou *et al*., 2011), fibroblasts (Lu *et al*., 2004), and endothelial cells (Song *et al*., 2005; Chau *et al*., 2009; Tkachenko *et al*., 2009).

A number of microdevices have been used for studying cell mechanics and shear stress on endothelial cell function. These include a multishear microfluidic device that allowed the simultaneous evaluation of ten shear stresses covering physiological shear range (0.7–130 dyn/cm^2, 0.07–13 Pa) (Chau *et al*., 2009) (Fig. 10.4), a shear culture system composed of microfluidic channels interfaced with computer-controlled piezoelectric pins on a Braille display that can generate pulsatile flow and shear stresses up to 12 dyn/cm^2 (1.2 Pa) (Song *et al*., 2005), and a microfluidic perfusion device with a magnetic clamp to secure an unsealed PDMS microfluidic chip against cover glasses with endothelial monolayers tested at a shear range of 0.07–9 dyn/cm^2 (0.007–0.9 Pa) (Tkachenko *et al*., 2009). All three studies confirmed cell elongation and alignment in the direction of shear over time.

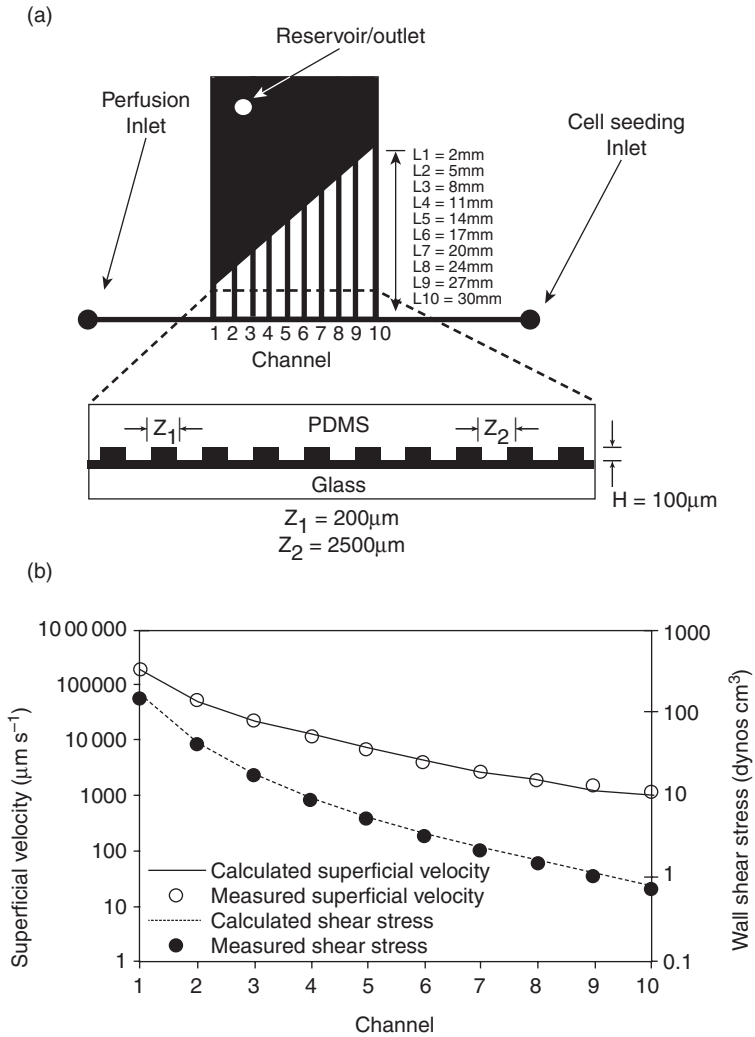

10.4 A multishear microdevice for the study of cell mechanics. The device delivers multiple physiologically relevant shear stresses, spanning over two orders of magnitude for any one flow rate. (a) Schematic of the device. (b) Measured and calculated superficial velocities and shear stresses for the multishear device at an inlet flow rate of 20 mL/h. (*Source*: Reproduced from Chau *et al.*, 2009 with permission from The Royal Society of Chemistry.)

Impacts of direct shear stress on smooth muscle cells have not been studied as extensively as on endothelial cells. This is likely due to smooth muscle cells not normally (at least in healthy tissue) being exposed to shear stress *in vivo*. However, after endothelial damage, shear stress can be sensed directly

by smooth muscle cells, triggering many complex mechanotransduction pathways and influencing cell properties and functions (Palumbo *et al*., 2000; Shi *et al*., 2010; Shi and Tarbell, 2011). Shear studies for smooth muscle cells have been conducted with endothelial cells in a parallel-plate flow chamber (Gosgnach *et al*., 2000; Chiu *et al*., 2003; Sakamoto *et al*., 2006; Ekstrand *et al*., 2010; Wang *et al*., 2010), a cone-and-plate apparatus (Palumbo *et al*., 2000), a rotating shear rod (Shi *et al*., 2010), and a microfluidic device (Plouffe *et al*., 2007). Murthy and colleagues (Plouffe *et al*., 2007) used a tapered channel microfluidic design to induce varying shear forces (1.9, 2.9 and 3.9 dyn/cm^2, 0.19, 0.29 and 0.39 Pa) and showed peptide-mediated selective adhesion of smooth muscle, endothelial cells and fibroblast cells under shear flow. All in all, the impacts of shear stress on smooth muscle and endothelial cells, and the interactions between these cells under fluid flow are highly complex and further investigations are required.

10.3.4 Microdevices for the creation of microcirculatory networks

Microcirculatory network formation is a significant and challenging goal in the engineering of large 3D artificial structures. As mentioned in Section 10.2.3, microfabrication has been commonly used to fabricate microdevices for creating microcirculatory networks. It provides both the required resolution and ability to control uniformity of microvascular network structures. In general, these microdevices can be used *in vitro* as platforms for vascular studies or *in vivo* as tissue-engineered microvascular constructs.

A well-designed vascular network is essential in microdevices for microcirculatory network formation. Over the past decade, several investigators have attempted to establish and optimize microvascular network designs (Borenstein *et al*., 2002; Shin *et al*., 2004; Weinberg *et al*., 2004; Fidkowski *et al*., 2005; Wang and Hsu, 2006; Chau *et al*., 2011). In general, they recognized the need for the network design to mimic natural vasculature dimensions and fluid dynamics, with a single inlet and outlet (Borenstein *et al*., 2002; Shin *et al*., 2004; Weinberg *et al*., 2004; Fidkowski *et al*., 2005; Wang and Hsu, 2006; Chau *et al*., 2011). Furthermore, each of the branches in the microvascular network design needs to have similar velocity profiles in order for oxygen and nutrients to be uniformly transported to all cells in the network, and allow uniform cell seeding, more rapid achievement of confluent coatings, and better control over cell behaviour for *in vitro* and *in vivo* studies (Chau *et al*., 2011; Wang and Hsu, 2006).

It is important that a well-designed vascular network also needs to be coupled with suitable flow and shear profiles required by the cells (Chau *et al*., 2011). Cells from diverse tissues and different parts of the vascular tree are

heterogeneous with respect to their surface phenotype and protein expression, such that they can express different markers and generate different responses to the same stimulus (McCarthy *et al*., 1991; Augustin *et al*., 1994; Jackson and Nguyen, 1997). Mismatches between flows and cells will lead to problems with endothelization, which seemed to be the case for some early microdevices (Shin *et al*., 2004; Fidkowski *et al*., 2005). Recognizing this, Chau *et al*. (2011) incorporated suitable flows for culturing human umbilical vein endothelial cells (HUVEC) in microchannels, previously elucidated in a 'multishear' device (Chau *et al*., 2009), into a 'ladder-like' microvascular

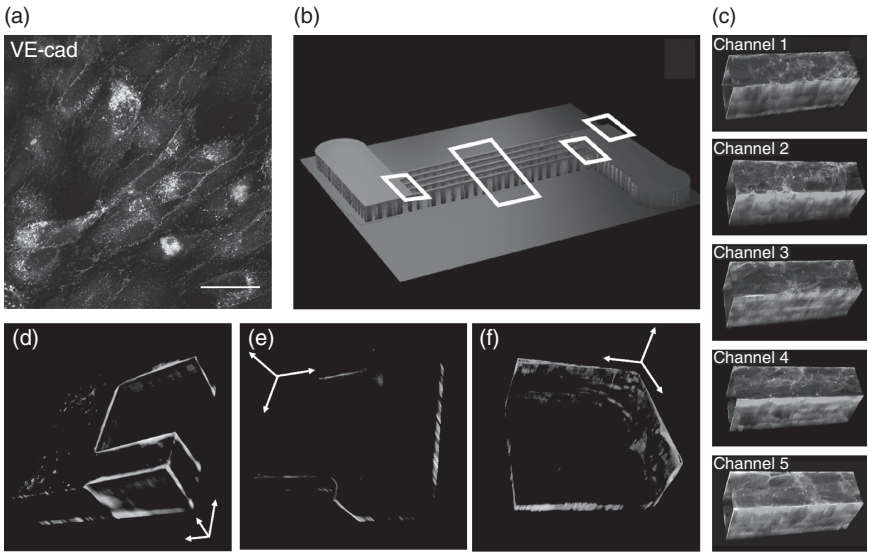

10.5 Endothelial cells fully lining the walls and corners of an artificial microvascular network after 24 h of culture. (a) The endothelial cells formed a monolayer with stable cell-cell adhesions, with the presence of VE-cadherin (the major adherens junction protein in endothelial cells) throughout the network after immunostaining. (b) A schematic of the microvascular network to show areas where 3D images were obtained. (c) Tilted 3D images of endothelial cells in microchannels with a height of 200 μm and width of 100 μm. The cells were immunostained for von Willebrand factor, actin stress fibres, and nuclei and found to form a confluent monolayer on all walls and corners of all channels of the network. Confocal Z-stacks: 40 slices, 5 μm spacing. (d, e, f) Tilted 3D images of endothelial cells at sections of the microvascular network. The cells were immunostained for von Willebrand factor, actin stress fibres and nuclei. Scale bars are shown as white arrows in x, y, and z axes. Scale bars are only an estimation: (d) 100 μm, (e) 50 μm, and (f) 50 μm. Confocal Z-stacks: (d) 40 slices, 5 μm spacing, (e) 30 slices, 2 μm spacing, and (f) 30 slices, 3.5 μm spacing. (*Source*: Reprinted with permission from *Biomicrofluidics*, **5**, 034115 (2011). Copyright 2011 American Institute of Physics.)

network design and showed the development, in less than 28 h, of a fully patent, microcirculatory network, composed of a contiguous monolayer of HUVECs (Fig. 10.5).

Similar to a number of other studies (Borenstein *et al*., 2002; Shin *et al*., 2004; Wang and Hsu, 2006), this microvascular network structure (Chau *et al*., 2011) was generated from a commonly used material in microfabrication, PDMS. However, while PDMS is ubiquitous and inexpensive, it is not biodegradable and has limited biocompatibility. Furthermore, the high stiffness of PDMS (580 kPa) (Galan *et al*., 2007) compared to natural solid tissues (~0.1–100 kPa) (Engler *et al*., 2006) may impede vascular sprouting or angiogenesis, the formation of new capillaries from pre-existing blood vessels (Patan, 2000). Therefore, these microdevices are limited as tissue-engineered constructs for implantation.

Problems of biocompatibility with synthetic materials eventually led researchers to explore the use of native extracellular matrix proteins and hydrogels in microfabrication. For examples, Golden and Tien (2007) fabricated a microfluidic system comprised of collagen Type I or fibrin, and Paguirigan and Beebe (2006, 2007) crosslinked gelatin with the naturally occurring enzyme transglutaminase to produce microfluidic devices. The vascular network design of Chau *et al*. (2011) has also been report to be moved from PDMS into a gelatin system and they observed HUVECs self-assembling after 24 h of perfusion and sprouting after 5 days of perfusion (Chau, 2010). Stroock and his team also developed a hydrogel microfluidic system using alginate (Cabodi *et al*., 2005; Choi *et al*., 2007) and recently moved onto collagen Type 1 (Zheng *et al*., 2012) to show the establishment of an artificial microcirculatory network.

10.4 Conclusion and future trends

As evidenced from the discussion above, there have been substantial developments in the past decade utilizing microbioreactors and microfluidic devices to probe cell behaviours in synthetic culture environments. These device platforms have been designed to: optimize culture outcomes in readiness for scaffold seeding and colonization; study parameters relevant to common scaffold characteristics (including surface chemistry or composition, pore size, connectivity, mechanical property); create ‘tissue-like’ environments that mimic diffusion and convective lengthscales in tissues, the magnitudes of shear stress and perfusion rates ‘seen’ by cells in tissues, the extracellular matrix composition of tissues, and the geometric challenges presented to cells when they ‘invade’ a synthetic microenvironment; and develop functional, microvascular tissue constructs that may one day be surgically integrated into the host environment to provide immediate support for a cell-laden scaffold. These device platforms and their associated

outcomes will continue to contribute to an ever-evolving set of design guidelines that will ultimately assist tissue engineers in achieving one of the major goals for the field: directed tissue genesis.

To date, much of the work related to the investigation of (stem) cell behaviour and optimization of the cells' microenvironment (for example, the stem cell niche) within microfluidic devices has in essence been performed with cells interacting with 2D substrates or surfaces, even though they may be enclosed within a 3D fluidic environment. However, all cells (including stem cells) are known to behave vastly differently in their native 3D environment, and in the future we are likely to see a significant trend away from 2D substrates. Bulk hydrogel scaffold systems, often thought to be a closer mimic of the native ECM, are currently being used to investigate the impact of a 3D microenvironment on a host of cell behaviours, such as migration, growth and differentiation. Microfluidic devices have only recently been utilized to move these bulk hydrogel systems into cell-laden microgel particles, with the significant advantages of uniform size, controlled physical and chemical properties, degradation rate, and encapsulated cell density. Some examples of materials used to generate hydrogel-based microparticles in microfluidic devices include alginate (Sugiura *et al.*, 2005; Hong *et al.*, 2007; Tan and Takeuchi, 2007) and collagen (Bruzewicz *et al.*, 2008; Hong *et al.*, 2012), agarose (Kumachev *et al.*, 2011) and poly(ethylene glycol) (Tumarkin *et al.*, 2012), which were crosslinked via chemical, thermal and photo stimuli, respectively. The use of microfluidic devices to encapsulate cells in hydrogel particles, or to otherwise provide 3D microenvironments (for a recent review see Li *et al.*, 2012b) has, however, only just begun, as this methodology provides to researchers a high throughput means to investigate a number of environmental variables on cell viability, proliferation and differentiation capabilities, such as mechanical properties, porosity, chemistry, the presentation of specific proteins and biochemical cues, encapsulated cell density and rate of degradation of the encapsulating material.

Cells within tissues respond to changes in their local (3D) microenvironment through actively remodelling extracellular matrix (ECM), the secretion of soluble factors, and through cell-cell mediated interactions. With the continual, rapid advancement in our capabilities to fabricate microdevices from a multitude of material systems, with high resolution and fidelity, inclusive of advanced measurement, sensing and control, we will in the near future have the capacity to develop *in vitro* device platforms or systems that mimic *simultaneously* many aspects of the *in vivo* extracellular (and intracellular) environment. In a highly controlled and tunable manner, with such device platforms, we will be able to decipher, manipulate and ultimately invoke control over critical contributors to tissue repair and remodelling that have previously been elusive to tissue engineers, bioengineers and

biologists, such as cell-cell communication, paracrine-autocrine signalling and tissue patterning.

10.5 References

Augustin, H. G., Kozian, D. H. and Johnson, R. C. (1994). Differentiation of endothelial cells: analysis of the constitutive and activated endothelial cell phenotypes. *Bioessays*, **16**, 901–6.

Baker, B. M., Gee, A. O., Metter, R. B., Nathan, A. S., Marklein, R. A., Burdick, J. A. and Mauck, R. L. (2008). The potential to improve cell infiltration in composite fiber-aligned electrospun scaffolds by the selective removal of sacrificial fibers. *Biomaterials*, **29**, 2348–58.

Banfi, A., Muraglia, A., Dozin, B., Mastrogiacomo, M., Cancedda, R. and Quarto, R. (2000). Proliferation kinetics and differentiation potential of ex vivo expanded human bone marrow stromal cells: Implications for their use in cell therapy. *Experimental Hematology*, **28**, 707–15.

Bellan, L. M., Singh, S. P., Henderson, P. W., Porri, T. J., Craighead, H. G. and Spector, J. A. (2009). Fabrication of an artificial 3-dimensional vascular network using sacrificial sugar structures. *Soft Matter*, **5**, 1297–540.

Blagovic, K., Kim, L. Y. and Voldman, J. (2011). Microfluidic perfusion for regulating diffusible signaling in stem cells. *PLoS ONE*, **6**, e22892.

Borenstein, J. T., Terai, H., King, K. R., Weinberg, E. J., Kaazempur-Mofrad, M. R. and Vacanti, J. P. (2002). Microfabrication technology for vascularized tissue-engineering. *Biomedical Microdevices*, **4**, 167–75.

Bruzewicz, D. A., McGuigan, A. P. and Whitesides, G. M. (2008). Fabrication of a modular tissue construct in a microfluidic chip. *Lab on a Chip*, **8**, 663–71.

Cabodi, M., Choi, N. W., Gleghorn, J. P., Lee, C. S., Bonassar, L. J. and Stroock, A. D. (2005). A microfluidic biomaterial. *Journal of American Chemical Society*, **127**, 13788–9.

Cao, Y., Mitchell, G., Messina, A., Price, L., Thompson, E., Penington, A., Morrison, W., O'Connor, A., Stevens, G. and Cooper-White, J. (2006). The influence of architecture on degradation and tissue ingrowth into three-dimensional poly(lactic-co-glycolic acid) scaffolds in vitro and in vivo. *Biomaterials*, **27**, 2854–64.

Chau L. T., Rolfe B. E., Cooper-White J. J., A microdevice for the creation of patent, three-dimensional endothelial cell-based microcirculatory networks. Biomicrofluidics (2011) **5**(3) 034115-1-034115-14.

Chau, L. (2010). *Ex Vivo Tissue Vascularisation*. Doctor of Philosophy PhD Thesis, The University of Queensland.

Chau, L., Doran, M. and Cooper-White, J. (2009). A novel multishear microdevice for studying cell mechanics. *Lab Chip*, **9**, 1897–902.

Chau, L. T., Rolfe, B. E. and Cooper-White, J. J. (2011). A microdevice for the creation of patent, three-dimensional endothelial cell-based microcirculatory networks. *Biomicrofluidics*, **5**, 034115-1–034115-14.

Chiu, J. J., Chen, L. J., Lee, P. L., Lee, C. I., Lo, L. W., Usami, S. and Chien, S. (2003). Shear stress inhibits adhesion molecule expression in vascular endothelial cells induced by coculture with smooth muscle cells. *Blood*, **101**, 2667–74.

Choi, N. W., Cabodi, M., Held, B., Gleghorn, J. P., Bonassar, L. J. and Stroock, A. D. (2007). Microfluidic scaffolds for tissue engineering. *Nature Materials*, **6**, 908–15.

Chrobak, K. M., Potter, D. R. and Tien, J. (2006). Formation of perfused, functional microvascular tubes in vitro. *Microvascular Research*, **71**, 185–96.

Chu, T. M. G., Orton, D. G., Hollister, S. J., Feinberg, S. E. and Halloran, J. W. (2002). Mechanical and in vivo performance of hydroxyapatite implants with controlled architectures. *Biomaterials*, **23**, 1283–93.

Chung, S., Sudo, R., Mack, P. J., Wan, C.-R., Vickerman, V. and Kamm, R. D. (2009). Cell migration into scaffolds under co-culture conditions in a microfluidic platform. *Lab on a Chip*, **9**, 269–75.

Diehl, K. A., Foley, J. D., Nealey, P. F. and Murphy, C. J. (2005). Nanoscale topography modulates corneal epithelial cell migration. *Journal of Biomedical Materials Research Part A*, **75A**, 603–11.

Doran, M. R., Mills, R. J., Parker, A. J., Landman, K. A. and Cooper-White, J. J. (2009). A cell migration device that maintains a defined surface with no cellular damage during wound edge generation. *Lab on a Chip*, **9**, 2364–9.

Doyle, A. D., Wang, F. W., Matsumoto, K. and Yamada, K. M. (2009). One-dimensional topography underlies three-dimensional fibrillar cell migration. *The Journal of Cell Biology*, **184**, 481–90.

Ekstrand, J., Razuvaev, A., Folkersen, L., Roy, J. and Hedin, U. (2010). Tissue factor pathway inhibitor-2 is induced by fluid shear stress in vascular smooth muscle cells and affects cell proliferation and survival. *Journal of Vascular Surgery*, **52**, 167–75.

Ellison, D., Munden, A. and Levchenko, A. (2009). Computational model and microfluidic platform for the investigation of paracrine and autocrine signaling in mouse embryonic stem cells. *Molecular BioSystems*, **5**, 1004–12.

Engler, A. J., Sen, S., Sweeny, H. L. and Discher, D. E. (2006). Matrix elasticity directs stem cell lineage specification. *Cell*, **126**, 677–89.

Fidkowski, C., Kaazempur-Mofrad, M. R., Borenstein, J., Vacanti, J. P., Langer, R. and Wang, Y. (2005). Endothelialized microvasculature based on a biodegradable elastomer. *Tissue Engineering*, **11**, 302–9.

Folkman, J. and Hochberg, M. (1973). Self-regulation of growth in three dimensions. *Journal of Experimental Medicine*, **138**, 745–53.

Galan, I., Deleon, J. A., Diaz, L., Hong, J. S., Khalek, N., Munoz-Fernandez, M. A. and Santolaya-Forgas, J. (2007). Effect of a bone marrow microenvironment on the ex-vivo expansion of umbilical cord blood progenitor cells. *International Journal of Laboratory Hematology*, **29**, 58–63.

Golden, A. P. and Tien, J. (2007). Fabrication of microfluidic hydrogels using molded gelatin as a sacrificial element. *Lab on a Chip*, **7**, 720–5.

Gómez-Sjöberg, R., Leyrat, A. A., Pirone, D. M., Chen, C. S. and Quake, S. R. (2007). Versatile, fully automated, microfluidic cell culture system. *Analytical Chemistry*, **79**, 8557–63.

Gosgnach, W., Challah, M., Coulet, F., Michel, J. B. and Battle, T. (2000). Shear stress induces angiotensin converting enzyme expression in cultured smooth muscle cells: possible involvement of bFGF. *Cardiovascular Research*, **45**, 486–92.

Griffon, D. J., Abulencia, J. P., Ragetly, G. R., Fredericks, L. P. and Chaieb, S. (2011). A comparative study of seeding techniques and three-dimensional matrices for mesenchymal cell attachment. *Journal of Tissue Engineering and Regenerative Medicine*, **5**, 169–79.

Griffon, D. J., Sedighi, M. R., Schaeffer, D. V., Eurell, J. A. and Johnson, A. L. (2006). Chitosan scaffolds: Interconnective pore size and cartilage engineering. *Acta Biomaterialia*, **2**, 313–20.

Gutierrez, E., Petrich, B. G., Shattil, S. J., Ginsberg, M. H., Groisman, A. and Kasirer-Friede, A. (2008). Microfluidic devices for studies of shear-dependent platelet adhesion. *Lab on a Chip*, **8**, 1486–95.

Hong, J. S., Shin, S. J., Lee, S., Wong, E. and Cooper-White, J. (2007). Spherical and cylindrical microencapsulation of living cells using microfluidic devices. *Korea-Australia Rheology Journal*, **19**(3), 157–64.

Hong, S., Hsu, H.-J., Kaunas, R. and Kameoka, J. (2012). Collagen microsphere production on a chip. *Lab on a Chip*, **12**, 3277–80.

Irimia, D. and Toner, M. (2009). Spontaneous migration of cancer cells under conditions of mechanical confinement. *Integrative Biology*, **1**, 506–12.

Isenberg, B. C., Dimilla, P. A., Walker, M., Kim, S. and Wong, J. Y. (2009). Vascular smooth muscle cell durotaxis depends on substrate stiffness gradient strength. *Biophysical Journal*, **97**, 1313–22.

Jackson, C. J. and Nguyen, M. (1997). Human microvascular endothelial cells differ from macrovascular endothelial cells in their expression of matrix metalloproteinases. *International Journal of Biochemistry & Cell Biology*, **29**, 1167–77.

Kaihara, S., Borenstein, J., Koka, R., Lalan, S., Ochoa, E. R., Ravens, M., Pien, H., Cunningham, B. and Vacanti, J. P. (2000). Silicon micromachining to tissue engineer branched vascular channels for liver fabrication. *Tissue Engineering*, **6**, 105–17.

Kaiser, J.-P., Reinmann, A. and Bruinink, A. (2006). The effect of topographic characteristics on cell migration velocity. *Biomaterials*, **27**, 5230–41.

Karageorgiou, V. and Kaplan, D. (2005). Porosity of 3D biomaterial scaffolds and osteogenesis. *Biomaterials*, **26**, 5474–91.

Kim, L., Vahey, M. D., Hsu-Yi, L. and Voldman, J. (2006). Microfluidic arrays for logarithmically perfused embryonic stem cell culture. *Lab on a Chip*, **6**, 394–406.

Ko, I. K. and Iwata, H. (2001). An approach to constructing three-dimensional tissue. *Annals of the New York Academy of Sciences*, **944**, 443–55.

Kou, S., Pan, L., Noort, D., Meng, G., Wu, X., Sun, H., Xu, J. and Lee, I. (2011). A multi-shear microfluidic device for quantitative analysis of calcium dynamics in osteoblasts. *Biochemical and Biophysical Research Communications*, **408**, 350–5.

Kremer, M., Lang, E. and Berger, A. C. (2000). Evaluation of dermal-epidermal skin equivalents ('composite-skin') of human keratinocytes in a collagen-glycosaminoglycan matrix(Integra artificial skin). *British Journal of Plastic Surgery*, **53**, 459–65.

Kumachev, A., Greener, J., Tumarkin, E., Eiser, E., Zandstra, P. W. and Kumacheva, E. (2011). High-throughput generation of hydrogel microbeads with varying elasticity for cell encapsulation. *Biomaterials*, **32**, 1477–83.

Lawrence, B. J. and Madihally, S. V. (2008). Cell colonization in degradable 3D porous matrices. *Cell Adhesion & Migration*, **2**, 9–16.

Lecault, V., Vaninsberghe, M., Sekulovic, S., Knapp, D., Wohrer, S., Bowden, W., Viel, F., McLaughlin, T., Jarandehei, A., Miller, M., Falconnet, D., White, A. K., Kent, D. G., Copley, M. R., Taghipour, F., Eaves, C. J., Humphries, R. K., Piret, J. M. and Hansen, C. L. (2011). High-throughput analysis of single hematopoietic stem cell proliferation in microfluidic cell culture arrays. *Nature Methods*, **8**, 581–586.

Li, M., Ku, D. and Forest, C. (2012a). Microfluidic system for simultaneous optical measurement of platelet aggregation at multiple shear rates in whole blood. *Lab on a Chip*, **12**, 1355–62.

Li, X-J., Valadez, A.V., Zuo, P. and Nie, Z. (2012b). Microfluidic 3D cell culture: potential application for tissue-based bioassays. *Bioanalysis*, **4**(12), 1509–25.

Lin, F. and Butcher, E. C. (2006). T cell chemotaxis in a simple microfluidic device. *Lab on a Chip*, **6**, 1462–9.

Lo, C.-M., Wang, H.-B., Dembo, M. and Wang, Y.-L. (2000). Cell movement is guided by the rigidity of the substrate. *Biophysical Journal*, **79**, 144–52.

Lu, H., Koo, L. Y., Wang, W. M., Lauffenburger, D. A., Griffith, L. G. and Jensen, K. F. (2004). Microfluidic shear devices for quantitative analysis of cell adhesion. *Analytical Chemistry*, **76**, 5257–64.

Malda, J., Woodfield, T. B. F., van der Vloodt, F., Wilson, C., Martens, D. E., Tramper, J., van Blitterswijk, C. A. and Riesle, J. (2005). The effect of PEGT/PBT scaffold architecture on the composition of tissue engineered cartilage. *Biomaterials*, **26**, 63–72.

McCarthy, S. A., Kuzu, I., Gatter, K. C. and Bicknell, R. (1991). Heterogeneity of the endothelial cell and its role in organ preference of tumour metastasis. *Trends in Pharmacological Sciences*, **12**, 462–7.

McGuigan, A. P. and Sefton, M. V. (2007a). Design criteria for a modular tissue-engineered construct. *Tissue Engineering*, **13**, 1079–89.

McGuigan, A. P. and Sefton, M. V. (2007b). Modular tissue engineering: fabrication of a gelatin-based construct. *Journal of Tissue Engineering and Regenerative Medicine*, **1**, 136–45.

Melchels, F. P. W., Barradas, A. M. C., van Blitterswijk, C. A., de Boer, J., Feijen, J. and Grijpma, D. W. (2010). Effects of the architecture of tissue engineering scaffolds on cell seeding and culturing. *Acta Biomaterialia*, **6**, 4208–17.

Migliore, A., Vozzi, F., Vozzi, G. and Ahluwalia, A. (2008). Controlled in vitro growth of cell microtubes: towards the realisation of artificial microvessels. *Biomedical Microdevices*, **10**, 81–8.

Mills, R. J., Frith, J. E., Hudson, J. E. and Cooper-White, J. J. (2011). Effect of geometric challenges on cell migration. *Tissue Engineering Part C Methods*, **17**, 999–1010.

Moledina, F., Clarke, G., Oskooei, A., Onishi, K., Gunther, A. and Zandstra, P. W. (2012). Predictive microfluidic control of regulatory ligand trajectories in individual pluripotent cells. *Proceedings of the National Academy of Sciences*, **109**, 3264–9.

Neumann, T., Nicholson, B. S. and Sanders, J. E. (2003). Tissue engineering of perfused microvessels. *Microvascular Research*, **66**, 59–67.

Nie, F. Q., Yamada, M., Kobayashi, J., Yamato, M., Kikuchi, A. and Okano, T. (2007). On-chip cell migration assay using microfluidic channels. *Biomaterials*, **28**, 4017–22.

O'Brien, F. J., Harley, B. A., Yannas, I. V. and Gibson, L. J. (2005). The effect of pore size on cell adhesion in collagen-GAG scaffolds. *Biomaterials*, **26**, 433–41.

Oh, S. H., Park, I. K., Kim, J. M. and Lee, J. H. (2007). In vitro and in vivo characteristics of PCL scaffolds with pore size gradient fabricated by a centrifugation method. *Biomaterials*, **28**, 1664–71.

Paguirigan, A. and Beebe, D. J. (2006). Gelatin based microfluidic devices for cell culture. *Lab on a Chip*, **6**, 407–13.

Paguirigan, A. L. and Beebe, D. J. (2007). Protocol for the fabrication of enzymatically crosslinked gelatin microchannels for microfluidic cell culture. *Nature Protocols*, **2**, 1782–8.

Palsson, B. and Bhatia, S. (2004). *Tissue Engineering*, New Jersey, Pearson Prentice Hall.

Palumbo, R., Gaetano, C., Melillo, G., Toschi, E., Remuzzi, A. and Capogrossi, M. C. (2000). Shear stress downregulation of platelet-derived growth factor receptor-beta and matrix metalloprotease-2 is associated with inhibition of smooth muscle cell invasion and migration. *Circulation*, **102**, 225–30.

Patan, S. (2000). Vasculogenesis and angiogenesis as mechanisms of vascular network formation, growth and remodeling. *Journal of Neurooncology*, **50**, 1–15.

Pelham, R. J. and Wang, Y.-L. (1997). Cell locomotion and focal adhesions are regulated by substrate flexibility. *Proceedings of the National Academy of Sciences*, **94**, 13661–5.

Pittenger, M. F., Mackay, A. M., Beck, S. C., Jaiswal, R. K., Douglas, R., Mosca, J. D., Moorman, M. A., Simonetti, D. W., Craig, S. and Marshak, D. R. (1999). Multilineage potential of adult human mesenchymal stem cells. *Science*, **284**, 143–7.

Plouffe, B. D., Njoka, D. N., Harris, J., Liao, J., Horick, N. K., Radisic, M. and Murthy, S. K. (2007). Peptide-mediated selective adhesion of smooth muscle and endothelial cells in microfluidic shear flow. *Langmuir*, **23**, 5050–5.

Poujade, M., Grasland-Mongrain, E., Hertzog, A., Jouanneau, J., Chavrier, P., Ladoux, B., Buguin, A. and Silberzan, P. (2007). Collective migration of an epithelial monolayer in response to a model wound. *Proceedings of the National Academy of Sciences of the United States of America*, **104**, 15988–93.

Przybyla, L. and Voldman, J. (2012). Probing embryonic stem cell autocrine and paracrine signaling using microfluidics. *Annual Review of Analytical Chemistry*, **5**, 293–315.

Qazi, H., Shi, Z. D. and Tarbell, J. M. (2011). Fluid shear stress regulates the invasive potential of glioma cells via modulation of migratory activity and matrix metalloproteinase expression. *PLoS One*, **6**, e20348.

Saadi, W., Wang, S.-J., Lin, F. and Jeon, N. (2006). A parallel-gradient microfluidic chamber for quantitative analysis of breast cancer cell chemotaxis. *Biomedical Microdevices*, **8**, 109–18.

Sakamoto, N., Ohashi, T. and Sato, M. (2006). Effect of fluid shear stress on migration of vascular smooth muscle cells in cocultured model. *Annals of Biomedical Engineering*, **34**, 408–15.

Salieb-Beugelaar, G. B., Simone, G., Arora, A., Philippi, A. and Manz, A. (2010). Latest developments in microfluidic cell biology and analysis systems. *Analytical Chemistry*, **82**, 4848–64.

Shi, Z. D., Abraham, G. and Tarbell, J. M. (2010). Shear stress modulation of smooth muscle cell marker genes in 2-D and 3-D depends on mechanotransduction by heparan sulfate proteoglycans and ERK1/2. *PLoS One*, **5**, e12196.

Shi, Z. D. and Tarbell, J. M. (2011). Fluid flow mechanotransduction in vascular smooth muscle cells and fibroblasts. *Annals of Biomedical Engineering*, **39**, 1608–19.

Shin, M., Matsuda, K., Ishii, O., Terai, H., Kaazempur-Mofrad, M., Borenstein, J., Detmar, M. and Vacanti, J. P. (2004). Endothelialized networks with a vascular geometry in microfabricated poly(dimethyl siloxane). *Biomedical Microdevices*, **6**, 269–78.

Silva, M. M. C. G., Cyster, L. A., Barry, J. J. A., Yang, X. B., Oreffo, R. O. C., Grant, D. M., Scotchford, C. A., Howdle, S. M., Shakesheff, K. M. and Rose, F. R. A. J. (2006). The effect of anisotropic architecture on cell and tissue infiltration into tissue engineering scaffolds. *Biomaterials*, **27**, 5909–17.

Song, J. W., Gu, W., Futai, N., Warner, K. A., Nor, J. E. and Takayama, S. (2005). Computer-controlled microcirculatory support system for endothelial cell culture and shearing. *Analytical Chemistry*, **77**, 3993–9.

Spiteri, C. G., Pilliar, R. M. and Kandel, R. A. (2006). Substrate porosity enhances chondrocyte attachment, spreading, and cartilage tissue formation in vitro. *Journal of Biomedical Materials Research*, **78A**, 676–83.

Sugiura, S., Oda, T., Izumida, Y., Aoyagi, Y., Satake, M., Ochiai, A., Ohkohchi, N. and Nakajima, M. (2005). Size control of calcium alginate beads containing living cells using micro-nozzle array. *Biomaterials*, **26**, 3327–31.

Takei, T., Sakai, S., Ono, T., Ijima, H. and Kawakami, K. (2006). Fabrication of endothelialized tube in collagen gel as starting point for self-developing capillary-like network to construct three-dimensional organs in vitro. *Biotechnology and Bioengineering*, **95**, 1–7.

Tan, W. H. and Takeuchi, S. (2007). Monodisperse alginate hydrogel microbeads for cell encapsulation. *Advanced Materials*, **19**, 2696–701.

Titmarsh, D., Hidalgo, A., Turner, J., Wolvetang, E. and Cooper-White, J. (2011). Optimization of flowrate for expansion of human embryonic stem cells in perfusion microbioreactors. *Biotechnology and Bioengineering*, **108**, 2894–904.

Titmarsh, D. M., Chen, H., Wolvetang, E. J. and Cooper-White, J. J. (2012a). Arrayed cellular environments for stem cells and regenerative medicine. *Biotechnology Journal*, **8**(2), 167–179. DOI: 10.1002/biot.201200149.

Titmarsh D.M., Hudson J.E., Hidalgo A., Elefanty A.G., Stanley E.G., Wolvetang, E. J. and Cooper-White, J. J. (2012b). Microbioreactor arrays for full factorial screening of exogenous and paracrine factors in human embryonic stem cell differentiation. *PLoS ONE*, **7**(12), e52405.

Tkachenko, E., Gutierrez, E., Ginsberg, M. H. and Groisman, A. (2009). An easy to assemble microfluidic perfusion device with a magnetic clamp. *Lab on a Chip*, **9**, 1085–95.

Tsuruga, E., Takita, H., Itoh, H., Wakisaka, Y. and Kuboki, Y. (1997). Pore size of porous hydroxyapatite as the cell-substratum controls BMP-induced osteogenesis. *Journal of Biochemistry*, **121**, 317–24.

Tumarkin, E., Tzadu, L., Csaszar, E., Seo, M., Zhang, H., Lee, A., Peerani, R., Purpura, K., Zandstra, P. W. and Kumacheva, E. (2012). High-throughput combinatorial cell co-culture using microfluidics. *Integrative Biology*, **3**, 653–62.

Vacanti, C. A. and Upton, J. (1994). Tissue-engineered morphogenesis of cartilage and bone by means of cell transplantation using synthetic biodegradable polymer matrices. *Clinics in Plastic Surgery*, **21**, 445–62.

van Tienen, T. G., Heijkants, R. G. J. C., Buma, P., de Groot, J. H., Pennings, A. J. and Veth, R. P. H. (2002). Tissue ingrowth and degradation of two biodegradable porous polymers with different porosities and pore sizes. *Biomaterials*, **23**, 1731–8.

Wang, G. J. and Hsu, Y. F. (2006). Structure optimization of microvascular scaffolds. *Biomedical Microdevices*, **8**, 51–8.

Wang, Y. H., Yan, Z. Q., Qi, Y. X., Cheng, B. B., Wang, X. D., Zhao, D., Shen, B. R. and Jiang, Z. L. (2010). Normal shear stress and vascular smooth muscle cells modulate migration of endothelial cells through histone deacetylase 6 activation and tubulin acetylation. *Annals of Biomedical Engineering*, **38**, 729–37.

Weinberg, E. J., Borenstein, J. T., Kaazempur-Mofrad, M. R., Orrick, B. and Vacanti, J. P. (2004). Design and fabrication of a constant shear microfluidic network

for tissue engineering. *Materials Research Society Proceedings*, **820**, O5.4.1/W9.4.1-O5.4.6/W9.4.6.

Zhao, F. and Ma, T. (2005). Perfusion bioreactor system for human mesenchymal stem cell tissue engineering: dynamic cell seeding and construct development. *Biotechnology and Bioengineering*, **91**, 482–93.

Zheng, Y., Chen, J., Craven, M., Choi, N. W., Totorica, S., Diaz-Santana, A., Kermani, P., Hempstead, B., Fischbach-Teschl, C., Lopez, J. A. and Stroock, A. D. (2012). In vitro microvessels for the study of angiogenesis and thrombosis. *Proceedings of the National Academy of Sciences of the United States of America*, **109**, 9342–7.

Zmora, S., Glicklis, R. and Cohen, S. (2002). Tailoring the pore architecture in 3-D alginate scaffolds by controlling the freezing regime during fabrication. *Biomaterials*, **23**, 4087–94.

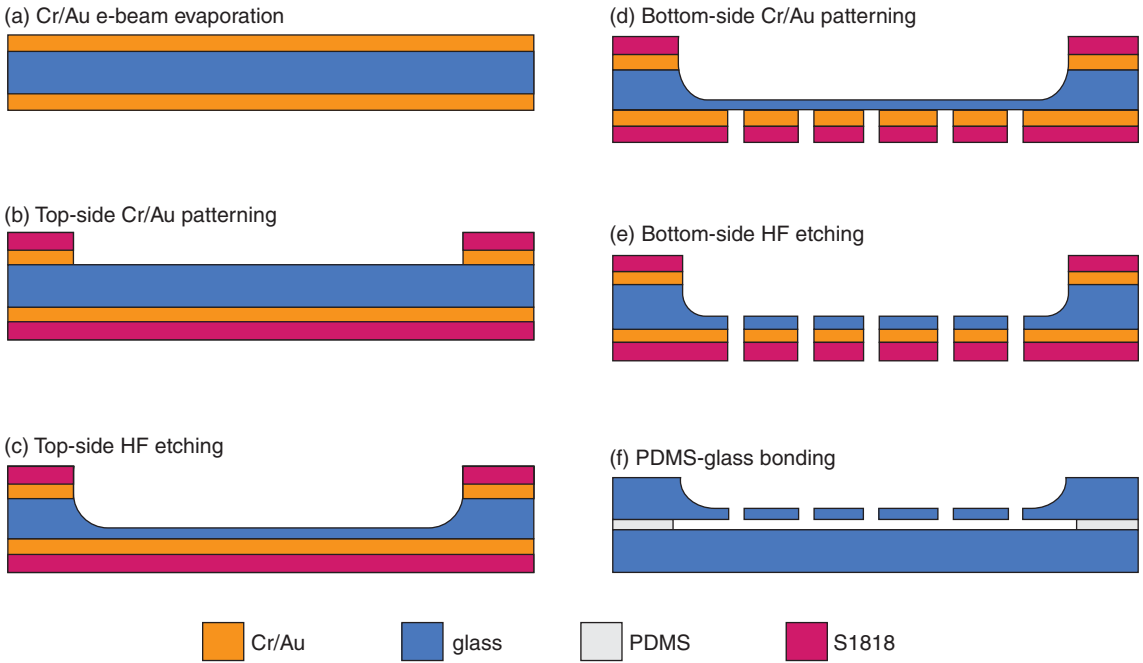

Plate II (Chapter 9) Microfabrication process. (a) E-beam evaporation of Cr/Au layers (30 nm/800 nm) on both sides of a glass cover slip. (b) Patterning of Cr/Au layers on the top side of the glass slide using photolithography and wet etching. (c) HF etching of the cell holding cavity. (d) Patterning of Cr/Au layers on the bottom side of the glass side. (e) HF etching of through-holes from both sides of the glass slide. (f) Removal of the photoresist and Cr/Au layers and PDMS-glass oxygen plasma bonding.

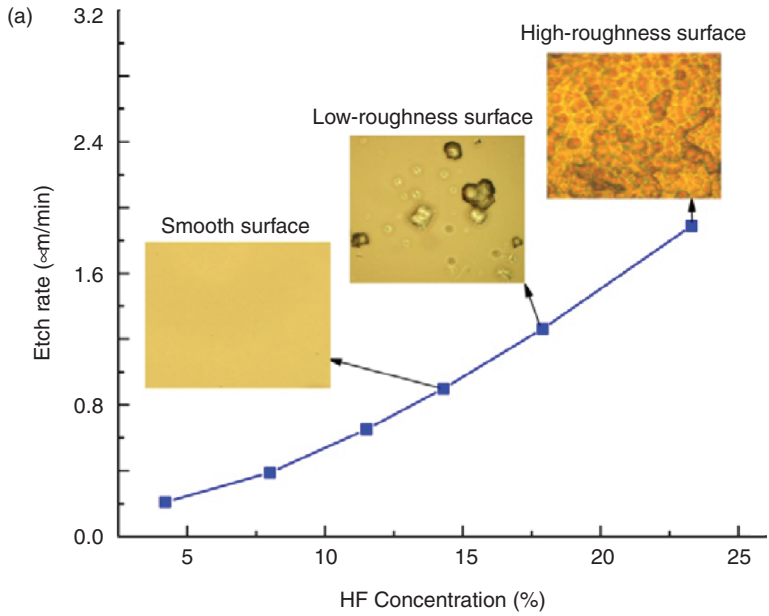

Plate III (Chapter 9) (a) Cover slip etching rates as a function of HF concentrations. (b) 3D plot of the bottom surface (1200 μm × 900 μm) of the cell holding cavity, measured by an optical profilometer. (Source: (a) Reproduced with permission from Springer.)

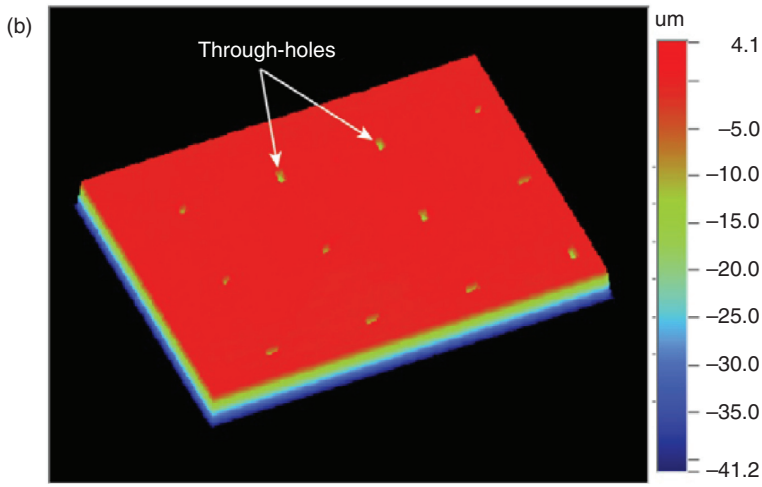

Plate III Continued

10

Microfluidic devices for developing tissue scaffolds

L. T. CHAU, J. E. FRITH, R. J. MILLS, D. J. MENZIES, D. M. TITMARSH and J. J. COOPER-WHITE,
The University of Queensland, Australia

DOI: 10.1533/9780857097040.3.363

Abstract: This chapter begins by outlining the key hurdles that currently exist in terms of achieving directed tissue genesis, *in vitro* and *in vivo*, from available mature, progenitor and stem cell sources. The chapter then proceeds to describe how microfluidic device platforms can provide the required insights to overcome these hurdles to clinical translation, including the optimization of soluble factor provision to enhance cell expansion and differentiation outcomes, the impacts of pore architecture and surface engineering on scaffold colonization, and the biophysical needs of cells when creating three dimensional artificial vascular pedicles for improved scaffold vascularization post-implantation.

Key words: tissue engineering, scaffolds, microdevices, tissue genesis, stem cells.

10.1 Introduction

In vivo tissue repair and regeneration are substantially facilitated by recruited stem cells from peripheral blood, or from those resident in most, if not all, tissues (Sakamoto *et al.*, 2006). Their depletion within an organ system may lead to full or partial loss of function (Palsson and Bhatia, 2004), indicating their critical role in tissue repair and replacement. Cells within tissues are surrounded by a three dimensional (3D) microenvironment of three (principle) 'support' systems: vasculature, other cells (including stem cells), and cell-secreted extracellular matrix (ECM). Constitutionally, tissues vary from being cell-dense (1×10^9 cells/cm^3), vascularized and extracellular matrix-poor structures, in the case of, for example muscle and fat tissue, through to cell-poor (1×10^6 cells/cm^3), avascular and extracellular matrix-rich structures, in the case of cartilage.

The field of tissue engineering aims to bring together key design principles of engineering and our understanding of cell biology and tissue genesis to invoke local repair or regeneration of damaged or diseased tissue.

Researchers utilize a variety of cell sources, depending on their tissue end point or target, including mature (fully differentiated), progenitor and stem cells. Through their combination with biomaterials and *in vitro* culture environments, cells are encouraged to generate functional tissues. However, the significant regenerative potential and clinical translation of tissue engineering practices, especially those using stem cells or progenitor cells, remains largely untapped. This is due largely to deficiencies in our knowledge of what microenvironments must be provided to the chosen cell types to facilitate the development of tissues that are not only composed of the appropriate cell types and phenotypes but that also are functionally equivalent to the lost or damaged tissue. This chapter discusses the current status of microfluidic device-based research attempting to address and overcome these deficiencies, with the aim of ultimately enabling clinical translation of cell-based tissue engineering therapies.

10.2 Key issues and technical challenges for successful tissue engineering

While there are many alternative paths or approaches being taken by researchers to achieve what are intrinsically complex outcomes in order to produce a functional, engineered tissue, there remain a number of key challenges or hurdles to achieving such directed tissue genesis, both *in vitro* and *in vivo*, from available cell sources. They are: (1) obtaining clinically relevant numbers, through *ex vivo* expansion and/or differentiation (e.g. from pluripotent or multipotent stem cells to fully differentiated end points) of the targeted cell types for implantation with the chosen scaffold; (2) encouraging effective and efficient cell seeding and scaffold colonization within both *in vitro* (for extended culture prior to implantation) and *in vivo* (involving active recruitment of endogenous cells) contexts; and (3) rapid vascularization of the cell-laden scaffold post-implantation to avoid necrosis and encourage further tissue growth and maturation. We will now explore each of these challenges in more detail.

10.2.1 Clinically relevant cell numbers: from stem cells through to mature, fully differentiated cells

It is estimated that in a myocardial infarction, approximately 1 billion cardiomyocytes (the functional 'beating' cells in heart tissue) can be lost. Unfortunately, mature human cardiomyocytes are non-proliferative and hence, in order to invoke functional repair of damaged heart tissue through cardiomyocyte repopulation, the human body needs assistance. One of the current approaches which has significant potential is the implantation of

human cardiomyocytes into this damaged site that have been generated *in vitro* from human pluripotent stem cell (hPSC) sources (human embryonic stem cells (hESC) and induced pluripotent stem cells (iPSC)). However, the progression of a stem cell from a pluripotent, multipotent or early progenitor stage into a range of terminally differentiated, mature cells that form adult tissues involves differentiation through quite a number of intermediate populations. For example, in specifying contractile cardiomyocytes from hPSCs, cells must pass from the pluripotent phenotype through a primitive streak-like population, to pre-cardiac mesoderm, to cardiac progenitors, to cardiomyocytes, then to functional, mature cardiomyocytes, as a minimum set of developmental stages (there may be more undiscovered complexity within those stages). Current protocols for deriving cardiomyocytes from hPSCs quote 1–1.5 cardiomyocytes per input hPSC; therefore, ~1×10^9 hPSCs would be required as a starting point, requiring ~20×10^3 cm^2 of starting culture area (as an estimate based on some monolayer protocols). It is clear, then, that the problem of arriving at a clinical dose of functional cells is a significant challenge.

This is particularly true for therapies involving adult stem cells, which are typically rare cell populations and have a more limited potential for expansion than their pluripotent counterparts. For example, mesenchymal stem cells (MSC) make up between just 0.01–0.001% of mononuclear cells in the bone marrow and therefore require significant expansion in order to generate clinically relevant numbers (Pittenger *et al.*, 1999). However, comparisons of MSCs shortly after isolation to those that have undergone several passages, show a dramatic increase in population doubling time and a diminished ability to differentiate along the osteo-, adipo- and chondro-genic lineages (Banfi *et al.*, 2000). As a result, there is a significant drive to develop methods for expansion that retain the beneficial properties of the cells in a manner that is reproducible, fully-defined, and amenable to the scale-up that will be required for translation to the clinic.

An alternative strategy to using stem cells is to 'transdifferentiate' a resident cell in the damaged tissue site (or periphery) that is non-functional into a functional cell type, for example, in the case of cardiac tissue, transdifferentiation of cardiac fibroblasts (non-functional in terms of beating) into functional cardiomyocytes, has been proven to be possible (both *in vitro* and *in vivo*) (Kou *et al.*, 2011). However, for transdifferentiation (also known as direct reprogramming) approaches, the reprogramming method or process is itself a long and inefficient process (some can take place over a few weeks), with poor understanding of the molecular events and cellular changes that occur before arriving at the reprogrammed cell type, usually with a low efficiency. Producing enough cells for functional tissue recovery is thus still a significant challenge.

Ensuring that significant cell numbers of the target phenotype are present at the output of any bioprocess is thus essential for their successful use in the intended tissue engineering endpoint application. This can be achieved in several ways:

- Increasing the number of starting point cells (e.g. stem cells);
- Increasing efficiency of differentiation to intermediate and target phenotypes;
- Increasing the efficiency of direct reprogramming/transdifferentiation; or
- Selection processes (sorting, density gradient centrifugation, antibiotic selection, subculturing).

10.2.2 Effective cell seeding and scaffold colonization

One of the major challenges still confronting the application of tissue-engineered scaffolds in the clinic is inadequate cell colonization. Previous strategies have generally suffered from high cell colonization at the periphery and little to none within the centre of the constructs. To achieve sufficient cell colonization, an effective cell seeding methodology that allows homogenous cell seeding needs to be employed and the seeded cells need sufficient nutrients and oxygen in order to survive, proliferate and regenerate the required tissue.

Cell colonization of a biomaterial scaffold is influenced by its physical, spatial and biochemical properties (Fig. 10.1). Physical cues, including

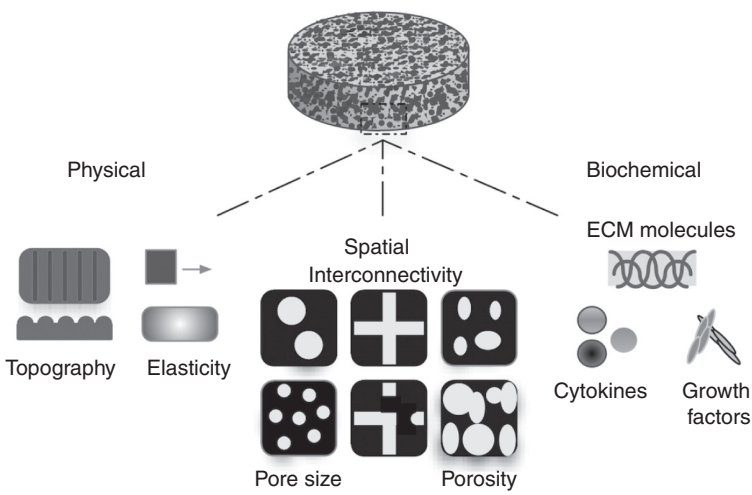

10.1 Physical, spatial and biochemical properties that influence cell colonization.

stiffness and topography, can have a profound effect on cell adhesion and migration (Diehl *et al*., 2005; Doyle *et al*., 2009; Isenberg *et al*., 2009; Kaiser *et al*., 2006; Lo *et al*., 2000; Pelham and Wang, 1997), while pore size (Cao *et al*., 2006; Chu *et al*., 2002; Malda *et al*., 2005; O'Brien *et al*., 2005; Oh *et al*., 2007; Tsuruga *et al*., 1997; van Tienen *et al*., 2002; Zmora *et al*., 2002), porosity (Baker *et al*., 2008; Karageorgiou and Kaplan, 2005; Silva *et al*., 2006; Spiteri *et al*., 2006), and interconnectivity (Griffon *et al*., 2006; Melchels *et al*., 2010) are examples of important spatial parameters that can similarly have substantial impacts. The material that the scaffold is made from will also affect colonization by altering the specific cell-material interactions (for example those mediated by integrins) with subsequent effects on cell adhesion and migration (Lawrence and Madihally, 2008). More recently there has been a wider appreciation of the variation in modes of cell migration and scaffold colonization observed in two dimensional (2D) and 3D environments, where the degradation rate of the material is a relevant parameter in determining the movement of cells into and within the scaffold. All of these factors must be taken into account during scaffold design in order to promote optimal cell colonization.

Traditionally, three seeding methodologies have been used:

- static,
- dynamic, and
- perfusion bioreactor cultures.

Of these, static seeding methods are the simplest, but perhaps the least effective. Using such methods, a high-density suspension of cells is added to the surface of the scaffold, where it is hoped they will adhere and migrate through to the centre. This may be aided by seeding several sides of the construct. Dynamic seeding methodologies can take many forms; however, one common example is the use of a spinner flask, which encourages movement of culture medium laden with cells through the pores of the scaffold. Such methods have been used to seed MSCs into calcium phosphate scaffolds for bone tissue engineering, resulting in an enhanced proportion of the cells adhering to the material and improved penetration throughout the construct (Griffon *et al*., 2011). Under perfusion, culture medium is passed through scaffolds from one direction to the other. This may occur with constant provision of fresh culture medium, or may exist in a closed loop with the medium passing across the construct multiple times. As with dynamic cell seeding strategies, the movement of the medium through the scaffold has been shown to aid both the efficiency of seeding and has also been shown to promote uniform tissue development across the construct (Zhao and Ma, 2005). For both dynamic and perfusion cultures, the rate of media flow through the scaffold is crucial, as it is necessary to balance the rate

of provision of nutrients and removal of waste products while at the same time minimizing the shear forces applied to cells to maximize viability and allow their initial adhesion to the presented biomaterial surface. Additional strategies, such as those involving growth factor incorporation, may be used to promote migration into the centre of the scaffold. Growth factors, such as vascular endothelial growth factor (VEGF), may also be used to promote vascularization, which in turn will bring cells into the scaffold, as well as providing an environment in which nutrients such as oxygen and glucose are available and where waste products are readily removed.

Effective cell seeding and colonization of scaffolds remains a significant challenge and limitations in our knowledge and understanding of the relevant parameter space mean that seeding strategies must currently be optimized for each individual situation. It is particularly difficult to separate out the effects of each individual factor on the final result, and more information is required in order enable the rational design guidelines for effective colonization of any given biomaterial construct.

10.2.3 Vascularization

Vascularization is the process of growing blood vessels into a tissue to improve oxygen and nutrient supply. It remains an overriding limiting factor in tissue engineering large 3D constructs, either during *in vitro* preculture or *in vivo* post-implantation. In the absence of a vascular network, metabolite supply and cell viability in a scaffold is compromised when diffusion distances are greater than 150–200 μm (Folkman and Hochberg, 1973) (Fig. 10.2). As a result, tissue engineering has been largely limited to thin or avascular tissues such as skin (Kremer *et al.*, 2000) or cartilage (Vacanti and Upton, 1994). Engineering a large complex tissue thus necessitates growing a physiologically relevant vasculature that promotes cell survival, tissue organization and rapid vascularization following implantation. The incorporation of a functional microcirculatory network into the scaffold prior to implantation is therefore essential. In addition, in order for the large 3D construct to remain viable, the microcirculatory network is required to mimic natural vasculature and carry out angiogenesis, a process where new capillaries are formed from pre-existing blood vessels (Patan, 2000).

Many methods have been developed to fabricate microvasculature for pre-vascularization of scaffolds. Early studies often involved fibres, synthetic or natural, as 'sacrificial' or temporary microvessel templates (Chrobak *et al.*, 2006; Ko and Iwata, 2001; Neumann *et al.*, 2003; Migliore *et al.*, 2008; Takei *et al.*, 2006). However, these approaches either resulted in a multichannelled microvascular construct without a common inlet and outlet (Ko and Iwata, 2001), or multiple single micron-scale vessels (Chrobak *et al.*,

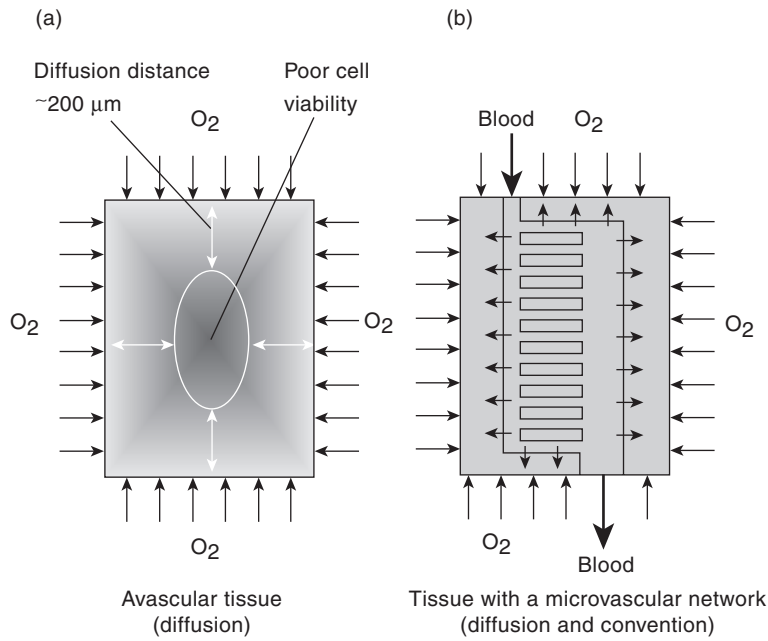

10.2 Distribution of oxygen and nutrients in an avascular tissue and a tissue with a microvascular network. (a) In an avascular tissue, diffusion alone can only supply metabolite sufficiently within the first 200 μm. This is assuming that the surface of the tissue is exposed to fresh blood supply via the flanking capillary network. As a result, cells which are at a distance of greater than 200 μm from this supply will be compromised. (b) In a tissue with a microvascular network, metabolite supply is both by convection and diffusion. Therefore, cells can be nourished and sustained throughout the tissue construct.

2006; Migliore *et al.*, 2008; Neumann *et al.*, 2003; Takei *et al.*, 2006), making them impractical and technically challenging for surgical implantation.

Researchers later fabricated larger complex 3D microvascular networks. These involved sacrificial 'cotton candy' sugar structures in polymeric (polydimethylsiloxane (PDMS), epoxy, or polycarbonate) matrices (Bellan *et al.*, 2009), and random assemblies of discrete, micron-scale gelatin components to form a large modular tissue-engineered construct (McGuigan and Sefton, 2007a, 2007b). However, while these methods are novel, there is limited control over the hydrodynamics of the random networks formed. Control over hydrodynamics in a microvascular network construct is important to ensure adequate delivery of nutrients to all cells, along with appropriate levels of shear stress for normal cell function.

Microfabrication is another method that has been commonly used in the development of artificial microvasculature. The main advantages of microfabrication technology over other methods include being able to achieve

resolutions of 10 μm, which are on the same lengthscale as capillaries (Borenstein *et al*., 2002; Kaihara *et al*., 2000), and the ability to invoke structural uniformity in such microvascular networks. Several investigators have recently used microfabrication to establish and optimize microvascular network designs and create microcirculatory networks with varying levels of success.

We will now highlight some of the past and present approaches utilizing microfluidic technology to overcoming the above listed hurdles to translation and clinical uptake of tissue-engineered products.

10.3 Microfluidic device platforms

Recent advances in microfluidic technology offer unprecedented control over fluid (both single phase and multiphase) flow, interface dynamics, droplet and particle size and size distribution, heat transfer and reaction conditions. This control results largely from the imposition of laminar flow and the domination of surface forces in the inherently small lengthscales within these devices. Microfluidic technologies are also ideally suited for parallelization or scale-up. It is for these reasons that researchers have turned to microfabrication and microfabricated *in vitro* environs to probe cellular behaviours that are otherwise difficult to investigate within standard cell culture methods. Further, such platforms permit the investigation, and real time read-out in some cases, of the impacts of varying microenvironmental conditions, including both biochemical factors (such as media exchange, oxygen concentration, pH, factor and ligand concentration) and biophysical factors (such as substrate mechanics, scaffold geometry, pore size and connectivity), on cell fate choices, such as morphology, migration, proliferation, differentiation and apoptosis. Ultimately, these choices determine the success or failure of our attempts at directed tissue genesis from any cell type, whether terminally differentiated or pluripotent. We now provide a review of some of the more recent examples of microdevices that have been designed to probe such complex parameter space in order to provide the necessary insight required to ensure successful tissue engineering outcomes.

10.3.1 Microdevices for optimization of microenvironments for cell/stem cell expansion and differentiation

Stem cells and their differentiated sub-lineages are important components in tissue-engineered constructs, either from the perspective of incorporation within the construct, or design of the construct in order to recruit and support native cells. Control of cell phenotype through isolation, expansion of

a stem cell population, and specification and maintenance of differentiated lineages of interest is therefore essential in ensuring the quality and efficacy of cells incorporated or targeted in tissue-engineered constructs.

Fortunately, microscale technologies are expanding the repertoire of assay platforms in investigating features of stem cell and stem cell-derived populations, including their expansion and differentiation (Salieb-Beugelaar *et al*., 2010). Because of several advantageous capabilities, including high parallelization, continuous fluid flow, and reduced culture dimensions, microscale (and particularly microfluidic) systems can provide opportunities for high-fidelity screening of stem cell culture processes under well-controlled microenvironmental conditions. Stem cells can sense and respond to a variety of stimuli, such as soluble factors, extracellular matrix proteins, cell–cell contacts, mechanical forces and properties (shear, strain, elastic and viscous moduli) and electrical stimulation, and further can be manipulated by introduction of genetic material and pharmacological agents, etc. Microtechnologies such as biomolecule spotting, surface micropatterning, and microfluidic systems are ideal platforms for screening these stimuli, as has been recently reviewed (Titmarsh *et al*., 2012a). While biomolecule spotting platforms have been applied more thoroughly for investigating combinations of ECM proteins for stem cells, microfluidic technologies in particular have made inroads into examining the physical, soluble factor, paracrine factor, and co-culture cues that drive stem cell expansion and differentiation, which we will now summarize.

Medium flow rate in continuous flow microfluidic systems affects biochemical and biophysical parameters (medium turnover, shear stress, etc.). Microbioreactor arrays have been developed to supply a logarithmic range of flow rates and assess mESC growth, which improved with increasing flow rate (Kim *et al*., 2006). For hESCs, a device with a much narrower, linear range of flow rates showed they were more sensitive, as they expanded best in a small window of flow rates, and were limited outside this window (Titmarsh *et al*., 2011). Fluidic resistance allowed control of fluid flow in these microfluidic systems. Instead of continuous flow, other systems have used programmed medium exchange to investigate temporal stimulation of mESCs (Ellison *et al*., 2009) and HSCs (Lecault *et al*., 2011) with various factors.

Microfluidic systems are also ideal for controlled introduction of soluble factors and screening their effects on the expansion or differentiation of stem cell populations. Moreover, this can be done in a semi-high-throughput manner due to the parallelization that can be achieved with microfabrication. For example, a multiplexed microbioreactor array platform recently enabled full factorial screening of exogenous and paracrine factors in hESC differentiation to a primitive streak-like population (Titmarsh *et al*., 2012b).

A fully-automated microfluidic system based on pneumatic valve control was developed to screen 96 discrete, individually-addressable microbioreactor chambers, which could be fed with arbitrary mixtures of up to 16 medium components or soluble factors. This system has been utilized for automated screening of culture environments for MSC growth and differentiation (Gómez-Sjöberg *et al.*, 2007). Importantly, the application of continuous medium perfusion in closed microfluidic stem cell culture systems has identified autocrine/paracrine effects as critical regulators of stem cell populations (Blagovic *et al.*, 2011; Moledina *et al.*, 2012). A recent review highlighted the way microfluidic technologies are providing new avenues to assess and manipulate paracrine effects (Przybyla and Voldman, 2012).

10.3.2 Microdevices for studying the effects of substrate and ligand type, pore geometry and scaffold architecture on cell migration, scaffold colonization and tissue development

Investigating the numerous parameters that influence scaffold colonization and tissue development within a 3D biomaterial is difficult. This is predominantly due to the inability to systematically investigate, and independently change, scaffold properties, and the ever-present immune response when performing *in vivo* studies. As such, microdevices have recently been used to introduce a high degree of control over the cellular microenvironment. The development of these devices has allowed the methodical evaluation of various scaffold parameters, including the substrate or ligand type, pore geometry and architecture on scaffold development.

Studying cell migration not only provides an insight into the fundamentals of cell biology, but it is also useful in assessing the suitability of various substrates and materials as a tissue engineering construct. Numerous microdevices have been developed to overcome the deficiencies associated with traditional methodologies, and have allowed investigation into the cell motility in response to chemokines (Lin and Butcher, 2006; Saadi *et al.*, 2006), ligands (Doran *et al.*, 2009), co-culture (Chung *et al.*, 2009) mechanical constraints (Irimia and Toner, 2009) and pore architecture (Mills *et al.*, 2011). These devices not only allow precise microenvironmental control, but can also elucidate results that are indiscernible using conventional assays or techniques.

A traditional assay to assess cell migration in response to a substrate is the wound healing or scrape assay. This involves creating a 'wound' within a confluent cell monolayer (generally by scraping the cell with a pipette tip), and observing the closure of the 'wound' edges to quantify cell migration rates. While this method is relatively straightforward, the outcomes are

confounded by a number of factors, including the ambiguity of the substrate, as a result of the wound generation removing the desired surface or fouling due to cellular secretions, and the damage to cells at the wound edge, which impacts cell migration.

A number of different microdevices have been developed to overcome the problems associated with techniques such as the wound healing assay and allow a more systematic investigation into cell migration. One of the earliest of these microdevices, developed by (Nie *et al*., 2007) uses a laminar flow of trypsin to generate a well-defined 'wound' edge. While this method elicits only minor damage to cells on the wound edge, the surface onto which the cells will migrate remains ambiguous. Poujade *et al*. also developed an eloquent PDMS-based stencil tool, in which a PDMS stencil is applied to a surface prior to cell seeding. The stencil is then peeled off, allowing cell migration to begin (Poujade *et al*., 2007). Although this approach overcomes many of the problems associated with the classical wound healing assay, even this solution potentially compromises surface composition, as the PDMS stencil must be fixed on top of the virgin surface until the cell monolayer is established.

More recently, a microdevice developed by Doran *et al*. has allowed the maintenance of a defined surface with no cellular damage during the initiation of cell migration (Doran *et al*., 2009). This device consists of a main inoculation chamber with perpendicular protruding migration channels (Fig. 10.3). In operation, cells are seeded into the main chamber, but the cell suspension does not enter the migration channels due to the presence of a fluid meniscus at each channel entrance, a result of the channel dimensions (100s of microns) and high (relative) fluid surface tension. This allows a confluent monolayer to be established within the central chamber with a 'cell edge' at the interface between this chamber and the migration channel. Cell migration is then initiated via backfilling the migration channels, to effectively 'break' the fluid meniscus and allow cells to access the channel. This microdevice thus allows the assessment of cell migration without the confounding issues of cellular damage or surface ambiguity, providing a rapid and robust tool to assess the influence of substrate biochemistry on cell migration, and thus cell colonization of space.

The flexibility of this device also allows the presentation of 2D geometrical challenges to mimic the architectural aspects and characteristics of 3D porous scaffolds. This adaption allows for the assessment of cell migration in response to geometrical challenges that mimic the architectural aspects and characteristics of 3D porous scaffolds in a 2D arrangement. This device has been utilized to investigate the influence of varying channel widths, degrees of channel tortuosity, the presence of contractions or expansions, and channel junctions on the migration of NIH 3T3

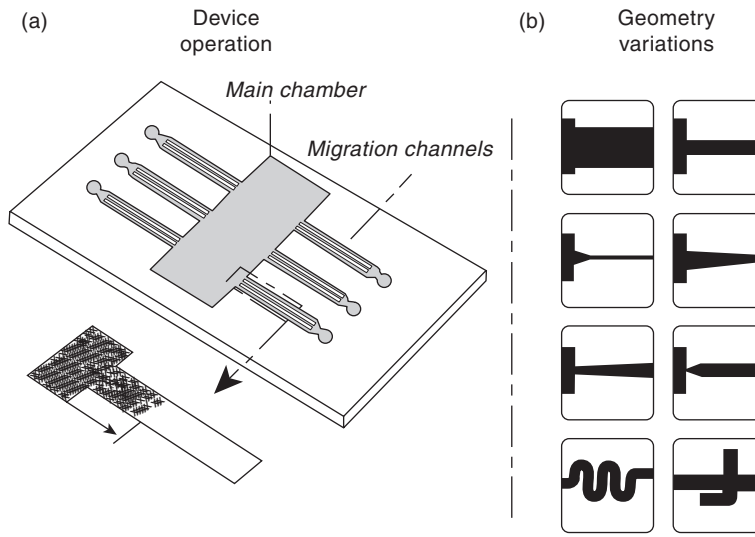

10.3 Schematic of microdevice operation and geometric constraint variations. (a) Once a cell monolayer is established within the main chamber, migration is initiated via backfilling of the migration channels. Migration can then be quantified by measuring cell progression into the channel. (b) This format can be used to study the effect of various substrates, or by incorporating geometry variations (as shown) along the length of the migration channels, can be used to determine how different cell types interpret architectural aspects of a tissue engineered scaffold. These parameters include various pore sizes, contractions, expansions, junctions and tortuosity.

mouse fibroblasts and human bone marrow-derived mesenchymal stromal cell (hMSC) (Mills *et al*., 2011). Data gained from this device showed that these two cell types have vastly different migration characteristics; 3T3 fibroblasts migrate as a collective cell front, whereas hMSCs migrate as single cells. This resulted in 3T3 fibroblasts displaying significant differences in migration depending on the type of geometrical constraint, while hMSCs were only influenced by channel width when it approached that of the length scale of a single cell, characteristics that would have a significant influence on the scaffold colonization by these two different cell populations. This clearly demonstrates the use of a microdevice to provide the necessary insight into how certain cell types, as a result of their migration characteristics, encounter and deal with different geometric constraints that may exist within biomaterial constructs, thereby highlighting the utility of microdevices to provide biological insights, relevant to tissue engineering, which could not be obtained using traditional techniques.

10.3.3 Microdevices for studying cell mechanics and impacts of shear stress on endothelial and smooth muscle cell function

Shear stress is known to influence the morphology, and even the fate, of many cell types (Gosgnach *et al*., 2000; Lu *et al*., 2004; Gutierrez *et al*., 2008; Kou *et al*., 2011; Qazi *et al*., 2011; Shi and Tarbell, 2011), including endothelial and smooth muscle cells (Song *et al*., 2005; Sakamoto *et al*., 2006; Plouffe *et al*., 2007; Chau *et al*., 2009; Tkachenko *et al*., 2009; Wang *et al*., 2010). As blood flows through a vessel, shear stress is generated and directly sensed by endothelial cells lining the vascular wall. Endothelial cells may act as a mediator between flow conditions and smooth muscle cell functions. Physiologically, smooth muscle cells exist below the endothelial cell lining and are protected from the shear stress. However, in pathological conditions involving endothelial injury, smooth muscle cells can become exposed to shear stress (Palumbo *et al*., 2000; Shi *et al*., 2010; Shi and Tarbell, 2011). Therefore, understanding cell mechanics and impacts of shear stress on endothelial and smooth muscle cell function is important in vascular studies and tissue engineering.

Many shear microdevices have been developed. In general, they were fabricated using conventional microfabrication techniques and their designs involved an inlet channel branching into multiple channels of varying dimensions, which allowed multiple shear forces to be studied simultaneously (Song *et al*., 2005; Gutierrez *et al*., 2008; Chau *et al*., 2009; Tkachenko *et al*., 2009; Kou *et al*., 2011; Li *et al*., 2012a). These microdevices have been used to study shear-dependent platelet aggregation (Li *et al*., 2012a) and adhesion to various extracellular matrix proteins (Gutierrez *et al*., 2008), and effects of shear stress on osteoblasts (Kou *et al*., 2011), fibroblasts (Lu *et al*., 2004), and endothelial cells (Song *et al*., 2005; Chau *et al*., 2009; Tkachenko *et al*., 2009).

A number of microdevices have been used for studying cell mechanics and shear stress on endothelial cell function. These include a multishear microfluidic device that allowed the simultaneous evaluation of ten shear stresses covering physiological shear range (0.7–130 dyn/cm^2, 0.07–13 Pa) (Chau *et al*., 2009) (Fig. 10.4), a shear culture system composed of microfluidic channels interfaced with computer-controlled piezoelectric pins on a Braille display that can generate pulsatile flow and shear stresses up to 12 dyn/cm^2 (1.2 Pa) (Song *et al*., 2005), and a microfluidic perfusion device with a magnetic clamp to secure an unsealed PDMS microfluidic chip against cover glasses with endothelial monolayers tested at a shear range of 0.07–9 dyn/cm^2 (0.007–0.9 Pa) (Tkachenko *et al*., 2009). All three studies confirmed cell elongation and alignment in the direction of shear over time.

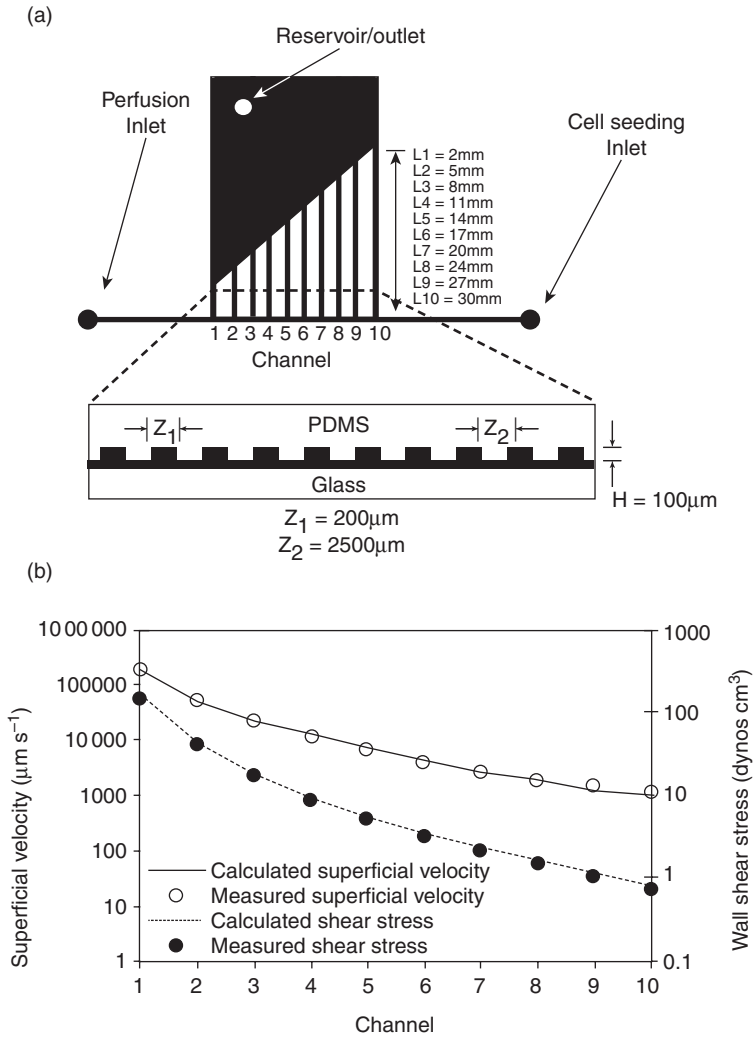

10.4 A multishear microdevice for the study of cell mechanics. The device delivers multiple physiologically relevant shear stresses, spanning over two orders of magnitude for any one flow rate. (a) Schematic of the device. (b) Measured and calculated superficial velocities and shear stresses for the multishear device at an inlet flow rate of 20 mL/h. (*Source*: Reproduced from Chau *et al.*, 2009 with permission from The Royal Society of Chemistry.)

Impacts of direct shear stress on smooth muscle cells have not been studied as extensively as on endothelial cells. This is likely due to smooth muscle cells not normally (at least in healthy tissue) being exposed to shear stress *in vivo*. However, after endothelial damage, shear stress can be sensed directly

by smooth muscle cells, triggering many complex mechanotransduction pathways and influencing cell properties and functions (Palumbo *et al*., 2000; Shi *et al*., 2010; Shi and Tarbell, 2011). Shear studies for smooth muscle cells have been conducted with endothelial cells in a parallel-plate flow chamber (Gosgnach *et al*., 2000; Chiu *et al*., 2003; Sakamoto *et al*., 2006; Ekstrand *et al*., 2010; Wang *et al*., 2010), a cone-and-plate apparatus (Palumbo *et al*., 2000), a rotating shear rod (Shi *et al*., 2010), and a microfluidic device (Plouffe *et al*., 2007). Murthy and colleagues (Plouffe *et al*., 2007) used a tapered channel microfluidic design to induce varying shear forces (1.9, 2.9 and 3.9 dyn/cm^2, 0.19, 0.29 and 0.39 Pa) and showed peptide-mediated selective adhesion of smooth muscle, endothelial cells and fibroblast cells under shear flow. All in all, the impacts of shear stress on smooth muscle and endothelial cells, and the interactions between these cells under fluid flow are highly complex and further investigations are required.

10.3.4 Microdevices for the creation of microcirculatory networks

Microcirculatory network formation is a significant and challenging goal in the engineering of large 3D artificial structures. As mentioned in Section 10.2.3, microfabrication has been commonly used to fabricate microdevices for creating microcirculatory networks. It provides both the required resolution and ability to control uniformity of microvascular network structures. In general, these microdevices can be used *in vitro* as platforms for vascular studies or *in vivo* as tissue-engineered microvascular constructs.

A well-designed vascular network is essential in microdevices for microcirculatory network formation. Over the past decade, several investigators have attempted to establish and optimize microvascular network designs (Borenstein *et al*., 2002; Shin *et al*., 2004; Weinberg *et al*., 2004; Fidkowski *et al*., 2005; Wang and Hsu, 2006; Chau *et al*., 2011). In general, they recognized the need for the network design to mimic natural vasculature dimensions and fluid dynamics, with a single inlet and outlet (Borenstein *et al*., 2002; Shin *et al*., 2004; Weinberg *et al*., 2004; Fidkowski *et al*., 2005; Wang and Hsu, 2006; Chau *et al*., 2011). Furthermore, each of the branches in the microvascular network design needs to have similar velocity profiles in order for oxygen and nutrients to be uniformly transported to all cells in the network, and allow uniform cell seeding, more rapid achievement of confluent coatings, and better control over cell behaviour for *in vitro* and *in vivo* studies (Chau *et al*., 2011; Wang and Hsu, 2006).

It is important that a well-designed vascular network also needs to be coupled with suitable flow and shear profiles required by the cells (Chau *et al*., 2011). Cells from diverse tissues and different parts of the vascular tree are

heterogeneous with respect to their surface phenotype and protein expression, such that they can express different markers and generate different responses to the same stimulus (McCarthy *et al*., 1991; Augustin *et al*., 1994; Jackson and Nguyen, 1997). Mismatches between flows and cells will lead to problems with endothelization, which seemed to be the case for some early microdevices (Shin *et al*., 2004; Fidkowski *et al*., 2005). Recognizing this, Chau *et al*. (2011) incorporated suitable flows for culturing human umbilical vein endothelial cells (HUVEC) in microchannels, previously elucidated in a 'multishear' device (Chau *et al*., 2009), into a 'ladder-like' microvascular

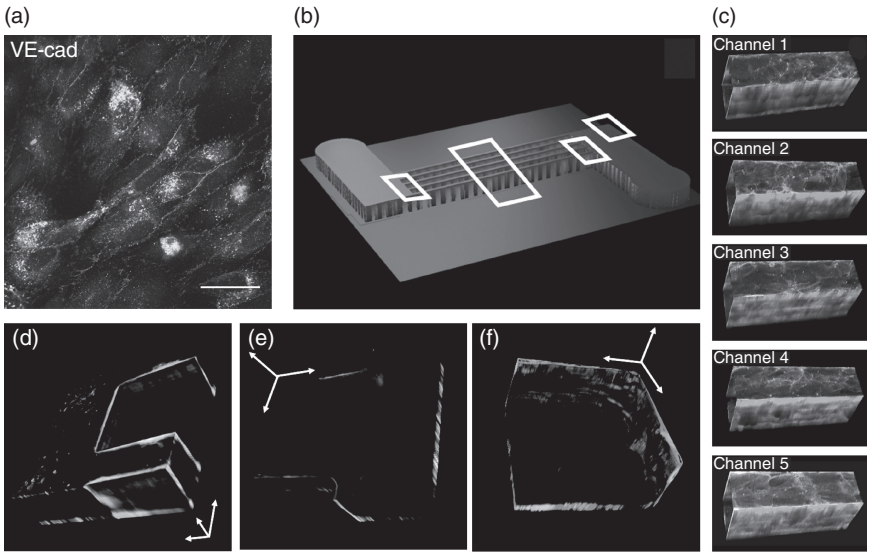

10.5 Endothelial cells fully lining the walls and corners of an artificial microvascular network after 24 h of culture. (a) The endothelial cells formed a monolayer with stable cell-cell adhesions, with the presence of VE-cadherin (the major adherens junction protein in endothelial cells) throughout the network after immunostaining. (b) A schematic of the microvascular network to show areas where 3D images were obtained. (c) Tilted 3D images of endothelial cells in microchannels with a height of 200 μm and width of 100 μm. The cells were immunostained for von Willebrand factor, actin stress fibres, and nuclei and found to form a confluent monolayer on all walls and corners of all channels of the network. Confocal Z-stacks: 40 slices, 5 μm spacing. (d, e, f) Tilted 3D images of endothelial cells at sections of the microvascular network. The cells were immunostained for von Willebrand factor, actin stress fibres and nuclei. Scale bars are shown as white arrows in x, y, and z axes. Scale bars are only an estimation: (d) 100 μm, (e) 50 μm, and (f) 50 μm. Confocal Z-stacks: (d) 40 slices, 5 μm spacing, (e) 30 slices, 2 μm spacing, and (f) 30 slices, 3.5 μm spacing. (*Source*: Reprinted with permission from *Biomicrofluidics*, **5**, 034115 (2011). Copyright 2011 American Institute of Physics.)

network design and showed the development, in less than 28 h, of a fully patent, microcirculatory network, composed of a contiguous monolayer of HUVECs (Fig. 10.5).

Similar to a number of other studies (Borenstein *et al*., 2002; Shin *et al*., 2004; Wang and Hsu, 2006), this microvascular network structure (Chau *et al*., 2011) was generated from a commonly used material in microfabrication, PDMS. However, while PDMS is ubiquitous and inexpensive, it is not biodegradable and has limited biocompatibility. Furthermore, the high stiffness of PDMS (580 kPa) (Galan *et al*., 2007) compared to natural solid tissues (~0.1–100 kPa) (Engler *et al*., 2006) may impede vascular sprouting or angiogenesis, the formation of new capillaries from pre-existing blood vessels (Patan, 2000). Therefore, these microdevices are limited as tissue-engineered constructs for implantation.

Problems of biocompatibility with synthetic materials eventually led researchers to explore the use of native extracellular matrix proteins and hydrogels in microfabrication. For examples, Golden and Tien (2007) fabricated a microfluidic system comprised of collagen Type I or fibrin, and Paguirigan and Beebe (2006, 2007) crosslinked gelatin with the naturally occurring enzyme transglutaminase to produce microfluidic devices. The vascular network design of Chau *et al*. (2011) has also been report to be moved from PDMS into a gelatin system and they observed HUVECs self-assembling after 24 h of perfusion and sprouting after 5 days of perfusion (Chau, 2010). Stroock and his team also developed a hydrogel microfluidic system using alginate (Cabodi *et al*., 2005; Choi *et al*., 2007) and recently moved onto collagen Type 1 (Zheng *et al*., 2012) to show the establishment of an artificial microcirculatory network.

10.4 Conclusion and future trends

As evidenced from the discussion above, there have been substantial developments in the past decade utilizing microbioreactors and microfluidic devices to probe cell behaviours in synthetic culture environments. These device platforms have been designed to: optimize culture outcomes in readiness for scaffold seeding and colonization; study parameters relevant to common scaffold characteristics (including surface chemistry or composition, pore size, connectivity, mechanical property); create ‘tissue-like’ environments that mimic diffusion and convective lengthscales in tissues, the magnitudes of shear stress and perfusion rates ‘seen’ by cells in tissues, the extracellular matrix composition of tissues, and the geometric challenges presented to cells when they ‘invade’ a synthetic microenvironment; and develop functional, microvascular tissue constructs that may one day be surgically integrated into the host environment to provide immediate support for a cell-laden scaffold. These device platforms and their associated

outcomes will continue to contribute to an ever-evolving set of design guidelines that will ultimately assist tissue engineers in achieving one of the major goals for the field: directed tissue genesis.

To date, much of the work related to the investigation of (stem) cell behaviour and optimization of the cells' microenvironment (for example, the stem cell niche) within microfluidic devices has in essence been performed with cells interacting with 2D substrates or surfaces, even though they may be enclosed within a 3D fluidic environment. However, all cells (including stem cells) are known to behave vastly differently in their native 3D environment, and in the future we are likely to see a significant trend away from 2D substrates. Bulk hydrogel scaffold systems, often thought to be a closer mimic of the native ECM, are currently being used to investigate the impact of a 3D microenvironment on a host of cell behaviours, such as migration, growth and differentiation. Microfluidic devices have only recently been utilized to move these bulk hydrogel systems into cell-laden microgel particles, with the significant advantages of uniform size, controlled physical and chemical properties, degradation rate, and encapsulated cell density. Some examples of materials used to generate hydrogel-based microparticles in microfluidic devices include alginate (Sugiura *et al.*, 2005; Hong *et al.*, 2007; Tan and Takeuchi, 2007) and collagen (Bruzewicz *et al.*, 2008; Hong *et al.*, 2012), agarose (Kumachev *et al.*, 2011) and poly(ethylene glycol) (Tumarkin *et al.*, 2012), which were crosslinked via chemical, thermal and photo stimuli, respectively. The use of microfluidic devices to encapsulate cells in hydrogel particles, or to otherwise provide 3D microenvironments (for a recent review see Li *et al.*, 2012b) has, however, only just begun, as this methodology provides to researchers a high throughput means to investigate a number of environmental variables on cell viability, proliferation and differentiation capabilities, such as mechanical properties, porosity, chemistry, the presentation of specific proteins and biochemical cues, encapsulated cell density and rate of degradation of the encapsulating material.

Cells within tissues respond to changes in their local (3D) microenvironment through actively remodelling extracellular matrix (ECM), the secretion of soluble factors, and through cell-cell mediated interactions. With the continual, rapid advancement in our capabilities to fabricate microdevices from a multitude of material systems, with high resolution and fidelity, inclusive of advanced measurement, sensing and control, we will in the near future have the capacity to develop *in vitro* device platforms or systems that mimic *simultaneously* many aspects of the *in vivo* extracellular (and intracellular) environment. In a highly controlled and tunable manner, with such device platforms, we will be able to decipher, manipulate and ultimately invoke control over critical contributors to tissue repair and remodelling that have previously been elusive to tissue engineers, bioengineers and

biologists, such as cell-cell communication, paracrine-autocrine signalling and tissue patterning.

10.5 References

Augustin, H. G., Kozian, D. H. and Johnson, R. C. (1994). Differentiation of endothelial cells: analysis of the constitutive and activated endothelial cell phenotypes. *Bioessays*, **16**, 901–6.

Baker, B. M., Gee, A. O., Metter, R. B., Nathan, A. S., Marklein, R. A., Burdick, J. A. and Mauck, R. L. (2008). The potential to improve cell infiltration in composite fiber-aligned electrospun scaffolds by the selective removal of sacrificial fibers. *Biomaterials*, **29**, 2348–58.

Banfi, A., Muraglia, A., Dozin, B., Mastrogiacomo, M., Cancedda, R. and Quarto, R. (2000). Proliferation kinetics and differentiation potential of ex vivo expanded human bone marrow stromal cells: Implications for their use in cell therapy. *Experimental Hematology*, **28**, 707–15.

Bellan, L. M., Singh, S. P., Henderson, P. W., Porri, T. J., Craighead, H. G. and Spector, J. A. (2009). Fabrication of an artificial 3-dimensional vascular network using sacrificial sugar structures. *Soft Matter*, **5**, 1297–540.

Blagovic, K., Kim, L. Y. and Voldman, J. (2011). Microfluidic perfusion for regulating diffusible signaling in stem cells. *PLoS ONE*, **6**, e22892.

Borenstein, J. T., Terai, H., King, K. R., Weinberg, E. J., Kaazempur-Mofrad, M. R. and Vacanti, J. P. (2002). Microfabrication technology for vascularized tissue-engineering. *Biomedical Microdevices*, **4**, 167–75.

Bruzewicz, D. A., McGuigan, A. P. and Whitesides, G. M. (2008). Fabrication of a modular tissue construct in a microfluidic chip. *Lab on a Chip*, **8**, 663–71.

Cabodi, M., Choi, N. W., Gleghorn, J. P., Lee, C. S., Bonassar, L. J. and Stroock, A. D. (2005). A microfluidic biomaterial. *Journal of American Chemical Society*, **127**, 13788–9.

Cao, Y., Mitchell, G., Messina, A., Price, L., Thompson, E., Penington, A., Morrison, W., O'Connor, A., Stevens, G. and Cooper-White, J. (2006). The influence of architecture on degradation and tissue ingrowth into three-dimensional poly(lactic-co-glycolic acid) scaffolds in vitro and in vivo. *Biomaterials*, **27**, 2854–64.

Chau L. T., Rolfe B. E., Cooper-White J. J., A microdevice for the creation of patent, three-dimensional endothelial cell-based microcirculatory networks. Biomicrofluidics (2011) **5**(3) 034115-1-034115-14.

Chau, L. (2010). *Ex Vivo Tissue Vascularisation*. Doctor of Philosophy PhD Thesis, The University of Queensland.

Chau, L., Doran, M. and Cooper-White, J. (2009). A novel multishear microdevice for studying cell mechanics. *Lab Chip*, **9**, 1897–902.

Chau, L. T., Rolfe, B. E. and Cooper-White, J. J. (2011). A microdevice for the creation of patent, three-dimensional endothelial cell-based microcirculatory networks. *Biomicrofluidics*, **5**, 034115-1–034115-14.

Chiu, J. J., Chen, L. J., Lee, P. L., Lee, C. I., Lo, L. W., Usami, S. and Chien, S. (2003). Shear stress inhibits adhesion molecule expression in vascular endothelial cells induced by coculture with smooth muscle cells. *Blood*, **101**, 2667–74.

Choi, N. W., Cabodi, M., Held, B., Gleghorn, J. P., Bonassar, L. J. and Stroock, A. D. (2007). Microfluidic scaffolds for tissue engineering. *Nature Materials*, **6**, 908–15.

Chrobak, K. M., Potter, D. R. and Tien, J. (2006). Formation of perfused, functional microvascular tubes in vitro. *Microvascular Research*, **71**, 185–96.

Chu, T. M. G., Orton, D. G., Hollister, S. J., Feinberg, S. E. and Halloran, J. W. (2002). Mechanical and in vivo performance of hydroxyapatite implants with controlled architectures. *Biomaterials*, **23**, 1283–93.

Chung, S., Sudo, R., Mack, P. J., Wan, C.-R., Vickerman, V. and Kamm, R. D. (2009). Cell migration into scaffolds under co-culture conditions in a microfluidic platform. *Lab on a Chip*, **9**, 269–75.

Diehl, K. A., Foley, J. D., Nealey, P. F. and Murphy, C. J. (2005). Nanoscale topography modulates corneal epithelial cell migration. *Journal of Biomedical Materials Research Part A*, **75A**, 603–11.

Doran, M. R., Mills, R. J., Parker, A. J., Landman, K. A. and Cooper-White, J. J. (2009). A cell migration device that maintains a defined surface with no cellular damage during wound edge generation. *Lab on a Chip*, **9**, 2364–9.

Doyle, A. D., Wang, F. W., Matsumoto, K. and Yamada, K. M. (2009). One-dimensional topography underlies three-dimensional fibrillar cell migration. *The Journal of Cell Biology*, **184**, 481–90.

Ekstrand, J., Razuvaev, A., Folkersen, L., Roy, J. and Hedin, U. (2010). Tissue factor pathway inhibitor-2 is induced by fluid shear stress in vascular smooth muscle cells and affects cell proliferation and survival. *Journal of Vascular Surgery*, **52**, 167–75.

Ellison, D., Munden, A. and Levchenko, A. (2009). Computational model and microfluidic platform for the investigation of paracrine and autocrine signaling in mouse embryonic stem cells. *Molecular BioSystems*, **5**, 1004–12.

Engler, A. J., Sen, S., Sweeny, H. L. and Discher, D. E. (2006). Matrix elasticity directs stem cell lineage specification. *Cell*, **126**, 677–89.

Fidkowski, C., Kaazempur-Mofrad, M. R., Borenstein, J., Vacanti, J. P., Langer, R. and Wang, Y. (2005). Endothelialized microvasculature based on a biodegradable elastomer. *Tissue Engineering*, **11**, 302–9.

Folkman, J. and Hochberg, M. (1973). Self-regulation of growth in three dimensions. *Journal of Experimental Medicine*, **138**, 745–53.

Galan, I., Deleon, J. A., Diaz, L., Hong, J. S., Khalek, N., Munoz-Fernandez, M. A. and Santolaya-Forgas, J. (2007). Effect of a bone marrow microenvironment on the ex-vivo expansion of umbilical cord blood progenitor cells. *International Journal of Laboratory Hematology*, **29**, 58–63.

Golden, A. P. and Tien, J. (2007). Fabrication of microfluidic hydrogels using molded gelatin as a sacrificial element. *Lab on a Chip*, **7**, 720–5.

Gómez-Sjöberg, R., Leyrat, A. A., Pirone, D. M., Chen, C. S. and Quake, S. R. (2007). Versatile, fully automated, microfluidic cell culture system. *Analytical Chemistry*, **79**, 8557–63.

Gosgnach, W., Challah, M., Coulet, F., Michel, J. B. and Battle, T. (2000). Shear stress induces angiotensin converting enzyme expression in cultured smooth muscle cells: possible involvement of bFGF. *Cardiovascular Research*, **45**, 486–92.

Griffon, D. J., Abulencia, J. P., Ragetly, G. R., Fredericks, L. P. and Chaieb, S. (2011). A comparative study of seeding techniques and three-dimensional matrices for mesenchymal cell attachment. *Journal of Tissue Engineering and Regenerative Medicine*, **5**, 169–79.

Griffon, D. J., Sedighi, M. R., Schaeffer, D. V., Eurell, J. A. and Johnson, A. L. (2006). Chitosan scaffolds: Interconnective pore size and cartilage engineering. *Acta Biomaterialia*, **2**, 313–20.

Gutierrez, E., Petrich, B. G., Shattil, S. J., Ginsberg, M. H., Groisman, A. and Kasirer-Friede, A. (2008). Microfluidic devices for studies of shear-dependent platelet adhesion. *Lab on a Chip*, **8**, 1486–95.

Hong, J. S., Shin, S. J., Lee, S., Wong, E. and Cooper-White, J. (2007). Spherical and cylindrical microencapsulation of living cells using microfluidic devices. *Korea-Australia Rheology Journal*, **19**(3), 157–64.

Hong, S., Hsu, H.-J., Kaunas, R. and Kameoka, J. (2012). Collagen microsphere production on a chip. *Lab on a Chip*, **12**, 3277–80.

Irimia, D. and Toner, M. (2009). Spontaneous migration of cancer cells under conditions of mechanical confinement. *Integrative Biology*, **1**, 506–12.

Isenberg, B. C., Dimilla, P. A., Walker, M., Kim, S. and Wong, J. Y. (2009). Vascular smooth muscle cell durotaxis depends on substrate stiffness gradient strength. *Biophysical Journal*, **97**, 1313–22.

Jackson, C. J. and Nguyen, M. (1997). Human microvascular endothelial cells differ from macrovascular endothelial cells in their expression of matrix metalloproteinases. *International Journal of Biochemistry & Cell Biology*, **29**, 1167–77.

Kaihara, S., Borenstein, J., Koka, R., Lalan, S., Ochoa, E. R., Ravens, M., Pien, H., Cunningham, B. and Vacanti, J. P. (2000). Silicon micromachining to tissue engineer branched vascular channels for liver fabrication. *Tissue Engineering*, **6**, 105–17.

Kaiser, J.-P., Reinmann, A. and Bruinink, A. (2006). The effect of topographic characteristics on cell migration velocity. *Biomaterials*, **27**, 5230–41.

Karageorgiou, V. and Kaplan, D. (2005). Porosity of 3D biomaterial scaffolds and osteogenesis. *Biomaterials*, **26**, 5474–91.

Kim, L., Vahey, M. D., Hsu-Yi, L. and Voldman, J. (2006). Microfluidic arrays for logarithmically perfused embryonic stem cell culture. *Lab on a Chip*, **6**, 394–406.

Ko, I. K. and Iwata, H. (2001). An approach to constructing three-dimensional tissue. *Annals of the New York Academy of Sciences*, **944**, 443–55.

Kou, S., Pan, L., Noort, D., Meng, G., Wu, X., Sun, H., Xu, J. and Lee, I. (2011). A multi-shear microfluidic device for quantitative analysis of calcium dynamics in osteoblasts. *Biochemical and Biophysical Research Communications*, **408**, 350–5.

Kremer, M., Lang, E. and Berger, A. C. (2000). Evaluation of dermal-epidermal skin equivalents ('composite-skin') of human keratinocytes in a collagen-glycosaminoglycan matrix(Integra artificial skin). *British Journal of Plastic Surgery*, **53**, 459–65.

Kumachev, A., Greener, J., Tumarkin, E., Eiser, E., Zandstra, P. W. and Kumacheva, E. (2011). High-throughput generation of hydrogel microbeads with varying elasticity for cell encapsulation. *Biomaterials*, **32**, 1477–83.

Lawrence, B. J. and Madihally, S. V. (2008). Cell colonization in degradable 3D porous matrices. *Cell Adhesion & Migration*, **2**, 9–16.

Lecault, V., Vaninsberghe, M., Sekulovic, S., Knapp, D., Wohrer, S., Bowden, W., Viel, F., McLaughlin, T., Jarandehei, A., Miller, M., Falconnet, D., White, A. K., Kent, D. G., Copley, M. R., Taghipour, F., Eaves, C. J., Humphries, R. K., Piret, J. M. and Hansen, C. L. (2011). High-throughput analysis of single hematopoietic stem cell proliferation in microfluidic cell culture arrays. *Nature Methods*, **8**, 581–586.

Li, M., Ku, D. and Forest, C. (2012a). Microfluidic system for simultaneous optical measurement of platelet aggregation at multiple shear rates in whole blood. *Lab on a Chip*, **12**, 1355–62.

Li, X-J., Valadez, A.V., Zuo, P. and Nie, Z. (2012b). Microfluidic 3D cell culture: potential application for tissue-based bioassays. *Bioanalysis*, **4**(12), 1509–25.

Lin, F. and Butcher, E. C. (2006). T cell chemotaxis in a simple microfluidic device. *Lab on a Chip*, **6**, 1462–9.

Lo, C.-M., Wang, H.-B., Dembo, M. and Wang, Y.-L. (2000). Cell movement is guided by the rigidity of the substrate. *Biophysical Journal*, **79**, 144–52.

Lu, H., Koo, L. Y., Wang, W. M., Lauffenburger, D. A., Griffith, L. G. and Jensen, K. F. (2004). Microfluidic shear devices for quantitative analysis of cell adhesion. *Analytical Chemistry*, **76**, 5257–64.

Malda, J., Woodfield, T. B. F., van der Vloodt, F., Wilson, C., Martens, D. E., Tramper, J., van Blitterswijk, C. A. and Riesle, J. (2005). The effect of PEGT/PBT scaffold architecture on the composition of tissue engineered cartilage. *Biomaterials*, **26**, 63–72.

McCarthy, S. A., Kuzu, I., Gatter, K. C. and Bicknell, R. (1991). Heterogeneity of the endothelial cell and its role in organ preference of tumour metastasis. *Trends in Pharmacological Sciences*, **12**, 462–7.

McGuigan, A. P. and Sefton, M. V. (2007a). Design criteria for a modular tissue-engineered construct. *Tissue Engineering*, **13**, 1079–89.

McGuigan, A. P. and Sefton, M. V. (2007b). Modular tissue engineering: fabrication of a gelatin-based construct. *Journal of Tissue Engineering and Regenerative Medicine*, **1**, 136–45.

Melchels, F. P. W., Barradas, A. M. C., van Blitterswijk, C. A., de Boer, J., Feijen, J. and Grijpma, D. W. (2010). Effects of the architecture of tissue engineering scaffolds on cell seeding and culturing. *Acta Biomaterialia*, **6**, 4208–17.

Migliore, A., Vozzi, F., Vozzi, G. and Ahluwalia, A. (2008). Controlled in vitro growth of cell microtubes: towards the realisation of artificial microvessels. *Biomedical Microdevices*, **10**, 81–8.

Mills, R. J., Frith, J. E., Hudson, J. E. and Cooper-White, J. J. (2011). Effect of geometric challenges on cell migration. *Tissue Engineering Part C Methods*, **17**, 999–1010.

Moledina, F., Clarke, G., Oskooei, A., Onishi, K., Gunther, A. and Zandstra, P. W. (2012). Predictive microfluidic control of regulatory ligand trajectories in individual pluripotent cells. *Proceedings of the National Academy of Sciences*, **109**, 3264–9.

Neumann, T., Nicholson, B. S. and Sanders, J. E. (2003). Tissue engineering of perfused microvessels. *Microvascular Research*, **66**, 59–67.

Nie, F. Q., Yamada, M., Kobayashi, J., Yamato, M., Kikuchi, A. and Okano, T. (2007). On-chip cell migration assay using microfluidic channels. *Biomaterials*, **28**, 4017–22.

O'Brien, F. J., Harley, B. A., Yannas, I. V. and Gibson, L. J. (2005). The effect of pore size on cell adhesion in collagen-GAG scaffolds. *Biomaterials*, **26**, 433–41.

Oh, S. H., Park, I. K., Kim, J. M. and Lee, J. H. (2007). In vitro and in vivo characteristics of PCL scaffolds with pore size gradient fabricated by a centrifugation method. *Biomaterials*, **28**, 1664–71.

Paguirigan, A. and Beebe, D. J. (2006). Gelatin based microfluidic devices for cell culture. *Lab on a Chip*, **6**, 407–13.

Paguirigan, A. L. and Beebe, D. J. (2007). Protocol for the fabrication of enzymatically crosslinked gelatin microchannels for microfluidic cell culture. *Nature Protocols*, **2**, 1782–8.

Palsson, B. and Bhatia, S. (2004). *Tissue Engineering*, New Jersey, Pearson Prentice Hall.

Palumbo, R., Gaetano, C., Melillo, G., Toschi, E., Remuzzi, A. and Capogrossi, M. C. (2000). Shear stress downregulation of platelet-derived growth factor receptor-beta and matrix metalloprotease-2 is associated with inhibition of smooth muscle cell invasion and migration. *Circulation*, **102**, 225–30.

Patan, S. (2000). Vasculogenesis and angiogenesis as mechanisms of vascular network formation, growth and remodeling. *Journal of Neurooncology*, **50**, 1–15.

Pelham, R. J. and Wang, Y.-L. (1997). Cell locomotion and focal adhesions are regulated by substrate flexibility. *Proceedings of the National Academy of Sciences*, **94**, 13661–5.

Pittenger, M. F., Mackay, A. M., Beck, S. C., Jaiswal, R. K., Douglas, R., Mosca, J. D., Moorman, M. A., Simonetti, D. W., Craig, S. and Marshak, D. R. (1999). Multilineage potential of adult human mesenchymal stem cells. *Science*, **284**, 143–7.

Plouffe, B. D., Njoka, D. N., Harris, J., Liao, J., Horick, N. K., Radisic, M. and Murthy, S. K. (2007). Peptide-mediated selective adhesion of smooth muscle and endothelial cells in microfluidic shear flow. *Langmuir*, **23**, 5050–5.

Poujade, M., Grasland-Mongrain, E., Hertzog, A., Jouanneau, J., Chavrier, P., Ladoux, B., Buguin, A. and Silberzan, P. (2007). Collective migration of an epithelial monolayer in response to a model wound. *Proceedings of the National Academy of Sciences of the United States of America*, **104**, 15988–93.

Przybyla, L. and Voldman, J. (2012). Probing embryonic stem cell autocrine and paracrine signaling using microfluidics. *Annual Review of Analytical Chemistry*, **5**, 293–315.

Qazi, H., Shi, Z. D. and Tarbell, J. M. (2011). Fluid shear stress regulates the invasive potential of glioma cells via modulation of migratory activity and matrix metalloproteinase expression. *PLoS One*, **6**, e20348.

Saadi, W., Wang, S.-J., Lin, F. and Jeon, N. (2006). A parallel-gradient microfluidic chamber for quantitative analysis of breast cancer cell chemotaxis. *Biomedical Microdevices*, **8**, 109–18.

Sakamoto, N., Ohashi, T. and Sato, M. (2006). Effect of fluid shear stress on migration of vascular smooth muscle cells in cocultured model. *Annals of Biomedical Engineering*, **34**, 408–15.

Salieb-Beugelaar, G. B., Simone, G., Arora, A., Philippi, A. and Manz, A. (2010). Latest developments in microfluidic cell biology and analysis systems. *Analytical Chemistry*, **82**, 4848–64.

Shi, Z. D., Abraham, G. and Tarbell, J. M. (2010). Shear stress modulation of smooth muscle cell marker genes in 2-D and 3-D depends on mechanotransduction by heparan sulfate proteoglycans and ERK1/2. *PLoS One*, **5**, e12196.

Shi, Z. D. and Tarbell, J. M. (2011). Fluid flow mechanotransduction in vascular smooth muscle cells and fibroblasts. *Annals of Biomedical Engineering*, **39**, 1608–19.

Shin, M., Matsuda, K., Ishii, O., Terai, H., Kaazempur-Mofrad, M., Borenstein, J., Detmar, M. and Vacanti, J. P. (2004). Endothelialized networks with a vascular geometry in microfabricated poly(dimethyl siloxane). *Biomedical Microdevices*, **6**, 269–78.

Silva, M. M. C. G., Cyster, L. A., Barry, J. J. A., Yang, X. B., Oreffo, R. O. C., Grant, D. M., Scotchford, C. A., Howdle, S. M., Shakesheff, K. M. and Rose, F. R. A. J. (2006). The effect of anisotropic architecture on cell and tissue infiltration into tissue engineering scaffolds. *Biomaterials*, **27**, 5909–17.

Song, J. W., Gu, W., Futai, N., Warner, K. A., Nor, J. E. and Takayama, S. (2005). Computer-controlled microcirculatory support system for endothelial cell culture and shearing. *Analytical Chemistry*, **77**, 3993–9.

Spiteri, C. G., Pilliar, R. M. and Kandel, R. A. (2006). Substrate porosity enhances chondrocyte attachment, spreading, and cartilage tissue formation in vitro. *Journal of Biomedical Materials Research*, **78A**, 676–83.

Sugiura, S., Oda, T., Izumida, Y., Aoyagi, Y., Satake, M., Ochiai, A., Ohkohchi, N. and Nakajima, M. (2005). Size control of calcium alginate beads containing living cells using micro-nozzle array. *Biomaterials*, **26**, 3327–31.

Takei, T., Sakai, S., Ono, T., Ijima, H. and Kawakami, K. (2006). Fabrication of endothelialized tube in collagen gel as starting point for self-developing capillary-like network to construct three-dimensional organs in vitro. *Biotechnology and Bioengineering*, **95**, 1–7.

Tan, W. H. and Takeuchi, S. (2007). Monodisperse alginate hydrogel microbeads for cell encapsulation. *Advanced Materials*, **19**, 2696–701.

Titmarsh, D., Hidalgo, A., Turner, J., Wolvetang, E. and Cooper-White, J. (2011). Optimization of flowrate for expansion of human embryonic stem cells in perfusion microbioreactors. *Biotechnology and Bioengineering*, **108**, 2894–904.

Titmarsh, D. M., Chen, H., Wolvetang, E. J. and Cooper-White, J. J. (2012a). Arrayed cellular environments for stem cells and regenerative medicine. *Biotechnology Journal*, **8**(2), 167–179. DOI: 10.1002/biot.201200149.

Titmarsh D.M., Hudson J.E., Hidalgo A., Elefanty A.G., Stanley E.G., Wolvetang, E. J. and Cooper-White, J. J. (2012b). Microbioreactor arrays for full factorial screening of exogenous and paracrine factors in human embryonic stem cell differentiation. *PLoS ONE*, **7**(12), e52405.

Tkachenko, E., Gutierrez, E., Ginsberg, M. H. and Groisman, A. (2009). An easy to assemble microfluidic perfusion device with a magnetic clamp. *Lab on a Chip*, **9**, 1085–95.

Tsuruga, E., Takita, H., Itoh, H., Wakisaka, Y. and Kuboki, Y. (1997). Pore size of porous hydroxyapatite as the cell-substratum controls BMP-induced osteogenesis. *Journal of Biochemistry*, **121**, 317–24.

Tumarkin, E., Tzadu, L., Csaszar, E., Seo, M., Zhang, H., Lee, A., Peerani, R., Purpura, K., Zandstra, P. W. and Kumacheva, E. (2012). High-throughput combinatorial cell co-culture using microfluidics. *Integrative Biology*, **3**, 653–62.

Vacanti, C. A. and Upton, J. (1994). Tissue-engineered morphogenesis of cartilage and bone by means of cell transplantation using synthetic biodegradable polymer matrices. *Clinics in Plastic Surgery*, **21**, 445–62.

van Tienen, T. G., Heijkants, R. G. J. C., Buma, P., de Groot, J. H., Pennings, A. J. and Veth, R. P. H. (2002). Tissue ingrowth and degradation of two biodegradable porous polymers with different porosities and pore sizes. *Biomaterials*, **23**, 1731–8.

Wang, G. J. and Hsu, Y. F. (2006). Structure optimization of microvascular scaffolds. *Biomedical Microdevices*, **8**, 51–8.

Wang, Y. H., Yan, Z. Q., Qi, Y. X., Cheng, B. B., Wang, X. D., Zhao, D., Shen, B. R. and Jiang, Z. L. (2010). Normal shear stress and vascular smooth muscle cells modulate migration of endothelial cells through histone deacetylase 6 activation and tubulin acetylation. *Annals of Biomedical Engineering*, **38**, 729–37.

Weinberg, E. J., Borenstein, J. T., Kaazempur-Mofrad, M. R., Orrick, B. and Vacanti, J. P. (2004). Design and fabrication of a constant shear microfluidic network

for tissue engineering. *Materials Research Society Proceedings*, **820**, O5.4.1/W9.4.1-O5.4.6/W9.4.6.

Zhao, F. and Ma, T. (2005). Perfusion bioreactor system for human mesenchymal stem cell tissue engineering: dynamic cell seeding and construct development. *Biotechnology and Bioengineering*, **91**, 482–93.

Zheng, Y., Chen, J., Craven, M., Choi, N. W., Totorica, S., Diaz-Santana, A., Kermani, P., Hempstead, B., Fischbach-Teschl, C., Lopez, J. A. and Stroock, A. D. (2012). In vitro microvessels for the study of angiogenesis and thrombosis. *Proceedings of the National Academy of Sciences of the United States of America*, **109**, 9342–7.

Zmora, S., Glicklis, R. and Cohen, S. (2002). Tailoring the pore architecture in 3-D alginate scaffolds by controlling the freezing regime during fabrication. *Biomaterials*, **23**, 4087–94.

11

Microfluidic devices for stem cell analysis

D.-K. KANG, J. LU, W. ZHANG, E. CHANG, M. A. ECKERT, M. M. ALI and W. ZHAO,
University of California, Irvine, USA

DOI: 10.1533/9780857097040.3.388

Abstract: Stem cells are the basic building blocks of the human body; they can be differentiated into almost any type of cell found in our body. However, because of their unique properties, including heterogeneity and sensitivity to their niche environment, stem cells and their mechanisms are not completely understood. Traditional technologies have provided a limited understanding of stem cell biology and their differentiation mechanisms. To overcome the limitations of current approaches to stem cell research, microfluidic technologies have emerged as powerful tools for stem cell analysis. In this chapter, we will briefly introduce several microfluidic technologies for stem cell analysis and its future trends. We believe that this chapter will stimulate new directions for future development and use of micro-fabricated devices for stem cell analysis and stem cell-based regenerative medicine.

Key words: microfluidics, microfabrication, cell analysis, stem cell, stem cell analysis.

11.1 Introduction

Over the past decades, stem cells have demonstrated great potential to treat diseases ranging from paralysis to heart failure to liver disease. Recently, the relatively new field of microfluidics has provided tools to study stem biology in novel, previously impossible ways that promise to hasten the translation of stem cells from the bench to the bedside.

11.1.1 Stem cells: the current status

Stem cells are defined as cells that can unlimitedly regenerate while maintaining the ability to become one or more specialized cell types through the process called differentiation. There are two kinds of stem cells that have been isolated from mammals: (1) embryonic stem cells (ESC) that are derived from the inner cell mass of blastocysts, an early stage embryo (Thomson *et al*., 1998) and (2) adult stem cells that are found in various tissues and

D.-K. Kang and J. Lu contributed equally.

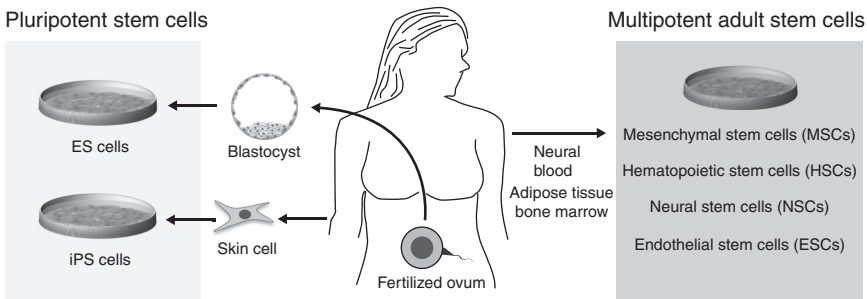

11.1 Derivation and differentiation of human stem cells for cell-based therapies. ESCs are usually derived from the inner cell mass of a blastocyst. iPS cells are produced by *in vitro* reprogramming of adult cells so that they enter an ESC–like state. Both ES and iPS cells are pluripotent – they can be differentiated into a wide range of specialized cell types via multipotent intermediate cells. Adult stem cells can be collected from a variety of sources, including bone marrow, peripheral blood, adipose tissue, and neural tissue. They are generally believed to be multipotent, with the ability to differentiate into specialized cell types belonging to the organ from which they were derived.

bone marrow. The primary difference between ESCs and adult stem cells is their differentiation potencies *in vivo*. ESCs are categorized as pluripotent stem cells that can differentiate into almost any cell lineage within the three germ layers (endoderm, mesoderm, and ectoderm). In contrast, adult stem cells include lineage-restricted stem cells such as hematopoietic stem cells (HSC) (Muller-Sieburg *et al*., 2002), mesenchymal stem cells (MSC) (Jiang *et al*., 2002), endothelial stem cells (Gehling *et al*., 2000), neural stem cells (NSC) (Altman and Das, 1965; Alvarez-Buylla *et al*., 2002), mammary stem cells (Liu *et al*., 2005), intestinal stem cells (van der Flier and Clevers, 2009), olfactory adult stem cells (Roisen *et al*., 2001), and neural crest stem cells (Fig. 11.1) (Clewes *et al*., 2011; Dupin and Coelho-Aguiar, 2012). On the other hand, adult stem cells are classified as multipotent stem cells that can only differentiate into their closely related progeny. For instance, NSCs can only differentiate into neurons, astrocytes, and oligodendrocytes while HSCs can only repopulate cells existing in blood, such as T-lymphocytes, B-lymphocytes, natural killer cells, monocytes, macrophages, granulocytes, platelets, and erythrocytes. Despite the differences in their fate potencies as well as their origins, both ESCs and adult stem cells possess great potential to impact human health. Currently induced pluripotent stem cells (iPSC), derived from adult skin, liver, and stomach cells, have the capability to differentiate into all of the cells of the adult body (Takahashi and Yamanaka, 2006).

With their extraordinary abilities to repopulate specific cells of therapeutic interest, stem cells have attracted attention as potential therapeutic agents in regenerative medicine, a process of replacing or regenerating damaged cells,

tissues, or organs to restore or establish normal function (Mason and Dunnill, 2008). In the past decade, substantial progress has been made in the fields of adult stem cells and ESCs. For instance, HSCs have been used to improve the treatment of autoimmune diseases (Burt *et al.*, 2008; Sykes and Nikolic, 2005), and MSCs have been used in regeneration or treatment of damaged heart tissues, neurological disorders, vascular disease, kidney disease, diabetes, lung injury, osteogenesis imperfecta, cartilage injury, bone injury, spinal cord injury, autoimmune diseases, and others (Phinney and Prockop, 2007). Recently in Canada, MSCs have been approved for the treatment of children who suffer from graft-versus-host disease, a potentially deadly complication of bone marrow transplantation. Additionally, a recent study led by Notta and colleagues demonstrated that isolated HSCs are capable of long-term multi-lineage engraftment (Notta *et al.*, 2011), which indicates the potential of using HSCs as an *in vitro* source of red blood cells for transfusion (Migliaccio *et al.*, 2012). NSC-based transplantation studies have been reported for brain injury (Nakatomi *et al.*, 2002) and various untreatable central nervous system (CNS) disorders such as stroke, Parkinson's disease, Huntington's disease, multiple sclerosis, and spinal cord injury (SCI) (Martino and Pluchino, 2006). ESCs have been shown to benefit patients who suffer from intractable epilepsy (Noebels *et al.*, 2012), and aid the process of cardiac regeneration (Boheler, 2010; Shiba *et al.*, 2012). With all the promising scientific progress in the stem cell field, several adult and ESC-based treatments are in clinical trials to prove their safety and efficacy.

11.1.2 Stem cells culture and analysis: conventional approaches

The most valuable trait of stem cells is their potency, the ability to turn into specific tissues in addition to those from which they were derived. Although this unique property could potentially transform current medicine and shape the future of regenerative medicine, it is also a problem that impedes the development of stem cell therapeutics. While stem cell scientists continually work on the discovery and development of new approaches to analyze and derive cells for therapeutic applications, the major challenge in developing these therapeutics is controlling the fate of the cells when scaling up the stem cell culture techniques for clinical usage (Sharma *et al.*, 2011; Serra *et al.*, 2012). Insufficient understanding of stem cell biology is the major bottleneck. Thus, developing not only a new cell culture platform, but also new technologies for stem cell analysis is essential for furthering our understanding of stem cell biology.

To overcome this hurdle, it is important to recognize the problems associated with conventional approaches that are used for stem cell culture and analysis. *In vivo*, stem cells reside in a three-dimensional (3D) dynamic microenvironment, where they interact with the surrounding cells and extracellular matrix and are exposed to low oxygen content and growth

factor gradients. The crosstalk between stem cells and their environmental cellular niche provides signals that modulate the cellular response, such as self-renewal, differentiation, and apoptosis. Each cellular response of stem cells *in vivo* pertains to a unique environmental signal. For example, the environmental signal to each stem cell is spatially and dynamically different. In addition, there are physiological factors in *in vivo* systems that a culture dish or an incubator cannot fully mimic. In conventional *in vitro* approaches, such as two-dimensional (2D) adhesion cultures, stem cells are grown on Petri dishes or flasks in humidity, temperature, and CO_2 controlled incubators, which are not the exact mimic of the natural physiological environment. Furthermore, physiological fluid flow (Csete, 2010) and shear stresses (Csete, 2010) are impossible to introduce to a culture dish. Without a precisely controlled microenvironment in the *in vitro* culture, it is impossible to decipher the biological mechanism that modulates stem cell plasticity *in vitro*. Moreover, failure to maintain these key niche factors may trigger unexpected differentiation and cell death and may lead to inaccurate results. A detailed understanding of the variant micro-environmental interactions and signaling pathways of stem cells *in vivo* will allow many stem cell-based therapeutic approaches to become possible.

11.1.3 Emerging technologies for cell research: microfluidics

Over the past decade, miniaturized devices known as 'micro total analysis systems' (μTAS) or 'lab on a chip' devices have been continuously developed for cell manipulation and analysis. Soft lithography introduced in the late 1990s has become the most common method for fabrication of miniaturized devices, due to its advantages, which include low cost, fast fabrication time, and physical characteristics of the materials. Specific advantages in microdevice-based cell research include: (1) single-cell manipulation, (2) high throughput, (3) reduction of reagent consumption and the number of cells required, (4) tight control of signal gradients and flow in space and time, (5) tight control of physical and chemical factors, and (6) automation. Miniaturized devices present enormous opportunities to analyze, characterize, and manipulate cells.

In this chapter, we will first describe several microfluidic technologies that have advanced the molecular and cellular analysis of cells, including cell culture platforms, novel biosensor development, and microtechnologies that have potential to enable stem cell analysis. Then, we will discuss state-of-the-art micro-fabricated devices that have revealed new insights in stem cell biology. Finally, we will discuss micro-fabricated devices that have potential to impact the stem cell field and its future trends. We believe that this chapter will stimulate new directions for future development and use of micro-fabricated devices for stem cell analysis and regenerative medicine.

11.2 Technologies used in stem cell analysis

'Lab on a chip' is a miniaturized multi-function apparatus; various microdevices have been developed, such as microchannels, gradient generators, microdroplet generators, dilution chambers, cell capture devices, microwells, microvalves, mixers, and microelectrodes. Recently, various applications have been developed that possess substantial potential to advance analytical assays on cells. Examples include 'micro-fabricated cell culture platforms' for deciphering the niche environment to cellular responses (Fig. 11.2), concentration generating microfluidics devices to regulate biochemical/biological components (Fig. 11.3), 'single-cell and high-throughput PCR' to identify gene expression (Fig. 11.4), micro-fabricated cell sorters (Fig. 11.5), cell separator (Figs 11.6 and 11.7), and novel biosensor development.

11.2.1 Miniaturized devices for cell culture

In vitro mammalian cell culture has played a fundamental role in facilitating the development of biotechnology and accelerating our understanding of cell biology. However, the microenvironment, and the role it plays in homeostasis, is still poorly understood because it comprises a complex array of biochemical and physical cues localized both temporally and

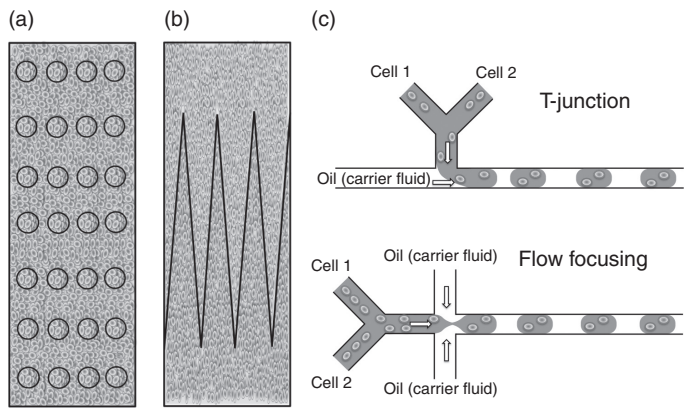

11.2 Emerging microfluidic platforms for advancing cell analysis. Microfluidics cell culture platform. (a) Microwell chip for cell culture (Khademhosseini *et al.,* 2006a). (b) Silicon comb structured microdevice for studying the dynamics of intercellular communication between hepatocytes and supportive stromal cells in co-culture (Hui and Bhatia, 2007). (c) Droplet microfluidics device for cell analysis. The compartmentalizing of cells can be accomplished with microfluidics using T-junctions (top) or Flow-focusing (bottom).

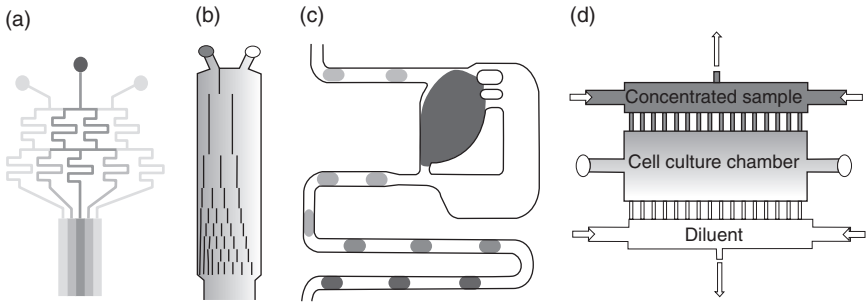

11.3 Microfluidics concentration gradient generators. (a) 'Christmas tree' structured concentration gradient generator (Jeon *et al.*, 2000). (b) Universal microfluidic gradient generator (Irimia *et al.*, 2006). (c) Microdroplet dilutor (Niu *et al.*, 2011). (d) Sink/source chamber (Shamloo *et al.*, 2008). Showing positions of source and sink (reagent) channels and cell culture chamber.

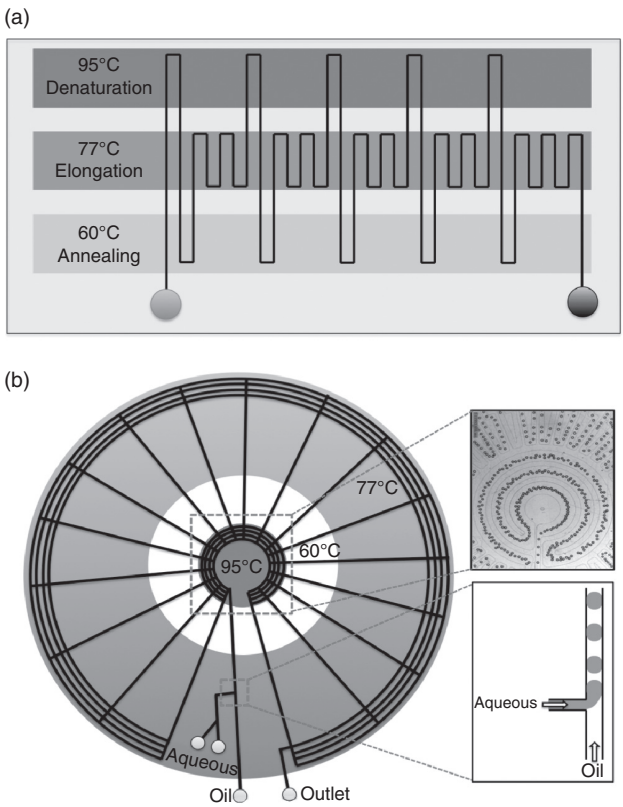

11.4 Microfluidics-based PCR (Kopp *et al.*, 1998). (a) Continuous microfluidics PCR. (b) Droplet microfluidics PCR. (*Source*: Reprinted and reproduced by permission of Schaerli *et al.*, 2009).

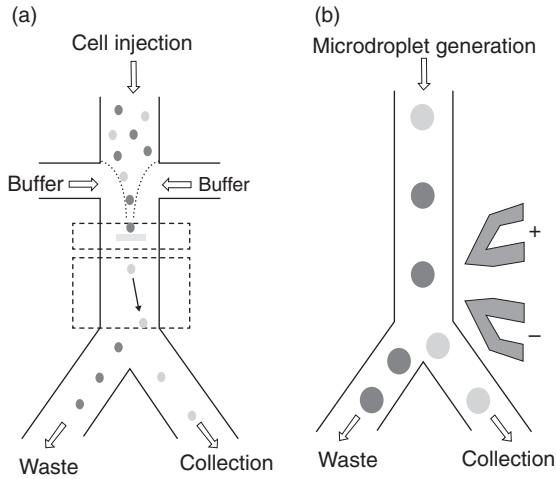

11.5 Fluorescence-activated sorting. (a) Optical switching sorter (Wang *et al.*, 2005). (b) Microelectrode-based sorter (Baret *et al.*, 2009).

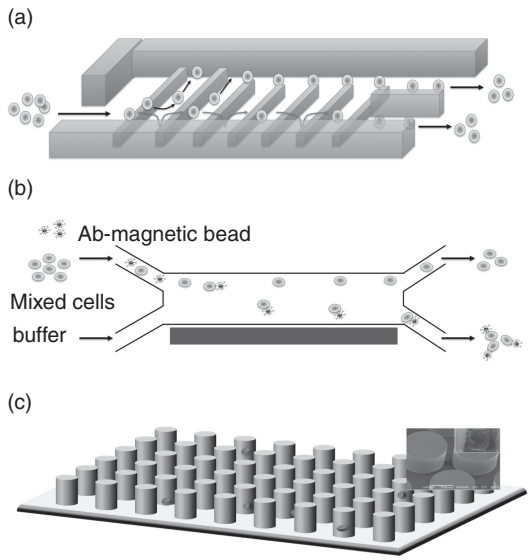

11.6 Cell surface marker targeting cell sorter. (a) Scalable parallel sorting device (Choi *et al.*, 2012). Deterministic cell rolling based cell sorting (cell surface marker targeting). (b) Micro-magnetic microfluidics cell sorter (Yung *et al.*, 2009). Based on magnetic isolation, target cells or pathogens can be isolated from complex mixtures or whole blood. (c) Micropost cell sorter. (*Source*: Reprinted and reproduced by permission of Nagrath *et al.*, 2007.) Microposts coated with antibodies against target cells such as circulating cancer cells (CTC).

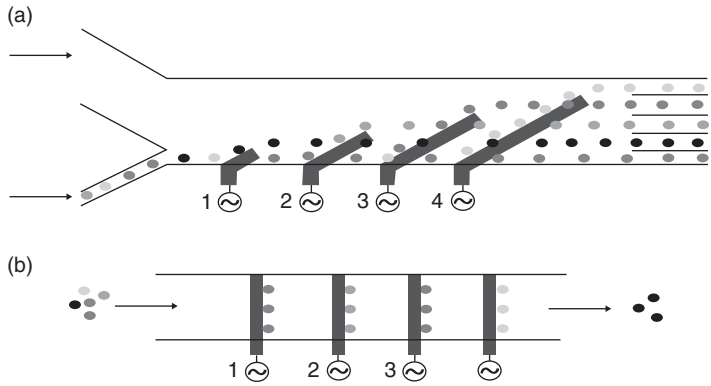

11.7 Dielectrophoresis (DEP) based cell sorter. At a particular frequency, cells move either away from the electrode (negative DEP) (Hu *et al.*, 2005) (a) or toward the electrode (positive DEP) (b) (Flanagan *et al.*, 2008).

spatially that alters the behavior of cells (Davenport, 2005). To effectively improve cell analysis, decoupling the interaction between the microenvironment and cellular response is critical. Microfluidic cell culture systems create new opportunities for the spatial and temporal control of cell growth and stimuli by combining surfaces that mimic the complex biochemistries and geometries of the extracellular matrix (ECM) within microfluidic channels with the ability to transport of fluids and soluble factors (El-Ali *et al.*, 2006; Meyvantsson and Beebe, 2008) in controlled manner. These systems not only provide more accurate control over environmental cues, including cell–cell interaction, precise soluble factor control, and cell–ECM interaction (Csete, 2010); but they can also be used to manipulate physiological stresses (Csete, 2010) and *in vivo* micro-environmental factors in a precise way. Several recently developed miniaturized cell culture devices have the ability to mimic precise niche environments and serve as tools to further improve cell analysis, including control over cell–cell (Hui and Bhatia, 2007), cell–soluble (Dahan *et al.*, 2008; Chen *et al.*, 2012; Kim *et al.*, 2010), and cell–ECM(Roach *et al.*, 2010) cues in both 2D and 3D microenvironments and the manipulation of mechanical characteristics of the cell niche (Fig. 11.9) (Vanapalli *et al.*, 2009). Stem cell fate and function is regulated by a combination of intrinsic programs and signals from the microenvironment. Intrinsic determinants can consist of both genetic and epigenetic components. In addition, the importance of environmental signals in stem cell function has been highlighted by the identification of distinct stem cell niches in a wide range of organ systems. Overall, high-throughput analysis of stem cells, utilizing both controlled cellular microenvironments and perturbations of intrinsic elements, can provide substantial insight into the factors governing stem cell biology.

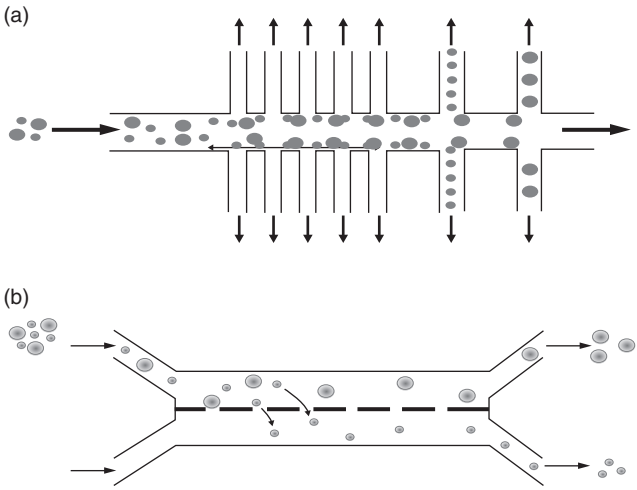

11.8 Size-based cell sorting. (a) Hydrodynamic filtration based cell sorter (Yamada and Seki, 2005). (b) Microfiltration based cell sorter (Wei *et al.*, 2011). Porous membrane integrated microfluidics device can be used to separate different sized particles or cells.

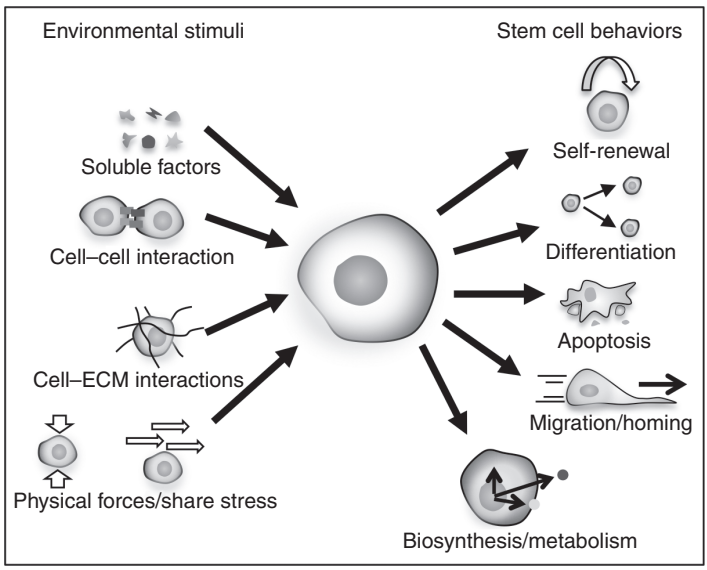

11.9 Microfluidics-based stem cell culture platform to mimic the *in vivo* culture condition *in vitro.* Combination of various factors involved in controlling stem cell fate and behavior in the stem cell niche. (*Source*: Reproduced by permission from Underhill and Bhatia, 2007).

Biophysical regulation

For capturing and growing cells within microfluidic channels, Khademhosseini and his colleagues introduced microwell integrated microfluidic devices (Fig. 11.2a) (Khademhosseini *et al*., 2004). Poly(ethylene glycol) (PEG)-based microwells were fabricated by the PDMS stamping method, and NIH3T3 fibroblasts were adhered and cultured on the microwell in the microfluidics device. After the introduction of microwell-based microfluidics, there have been developments to control the fabrication of cell aggregates of uniform shape from differentiated cell lines (Fukuda *et al*., 2006) to control the interaction of ESCs with other cells (Khademhosseini *et al*., 2006) and to control size, shape, and homogeneity of embryoid bodies (EB) (Karp *et al*., 2007). In addition, it is increasingly recognized that cells behave very differently when surrounded by a 3D extracellular matrix (ECM) compared to anchored 2D substrate. Modeling the *in vivo* microenvironment typically involves placing cells in a 3D ECM in a physiologically relevant context with respect to other cells. Microfluidic perfusion co-culture devices for 3D microenvironments act as systems for investigating cell–cell and cell–ECM interactions (Huang *et al*., 2009). Huang and colleagues utilized this system to construct a multicellular 3D culture for investigating the behaviors of metastatic breast cancer cells and tumor-derived macrophages in spatially, well-defined geometries. They demonstrated the versatility and potential of this new microfluidic platform to engineer 3D microscale architectures. Furthermore, tremendous progress has been made in the context of organ on a chip systems, including lung-on-a-chip (Huh *et al*., 2010), blood-vessel-on-a-chip (Bellan *et al*., 2009; Song *et al*., 2009), and liver-on-a-chip (Van Midwoud *et al*., 2011). Nevertheless, microfluidic cell culture systems provide a great opportunity to decipher cellular responses to the niche microenvironment.

Cell–cell interaction

To study cell–cell interactions in a microsystem and control cell–cell crosstalk in 2D, micro-fabricated devices with silicon comb structures were developed (Hui and Bhatia, 2007). Hui and Bhatia developed a microdevice consisting of two silicon combs that could be separated and brought into close contact with each other for precise cellular positioning to study the dynamics of intercellular communication between hepatocytes and supportive stromal cells in co-culture (Fig. 11.2b). Using this micro-fabricated device, they demonstrated, with micrometer-scale precision, the dynamic regulation of cell–cell interactions via direct manipulation of adherent cells. As a proof-of-concept study, they utilized this tool in deconstructing the dynamics of intercellular communication between hepatocytes and supportive stromal cells in co-culture. They concluded that preservation of hepatocyte viability

and liver-specific functions in co-culture depends on an initial contact-mediated signal followed by a sustained short-range soluble signal from fibroblasts to hepatocytes. This platform enables the investigation of dynamic cell–cell interaction in a multitude of applications and shows the potential in deciphering part of the stem cell niche.

Hydrogel, a type of material widely used as synthetic extracellular matrix, has been integrated in microfluidic devices to investigate cell–cell interactions (Lanza *et al*., 1996). Various hydrogel materials are available for cell encapsulation such as collagen, gelatin, fibrin, alginate, and agarose (Wan, 2012). With precise manipulation, droplet microfluidics technologies are able to encapsulate the cells into the picoliter-sized droplets for growing and analyzing them (Fig. 11.2c and 11.2d). Due to their ability to control the size, shape, and morphology, microfluidics have become one of the most promising approaches for cell encapsulation. For instance, Tumarkin and colleagues developed a microfluidic platform for the high-throughput generation of hydrogel microbeads for cell co-culture (Tumarkin *et al*., 2011). The platform was used to co-encapsulate factor-dependent and responsive blood progenitor cell lines (MBA2 and M07e cells, respectively) at varying ratios and demonstrated that in-bead paracrine secretion can modulate the viability of the factor-dependent cells. Microgel encapsulation platforms are tools that help to determine how different cell types communicate with each other while minimizing the barriers of complex paracrine interactions that are seen in conventional cell culture techniques.

Biochemical regulation

To mimic the biochemical microenvironment *in vivo,* Jeon and colleagues introduced the first microfluidics gradient generator based on a 'Christmas Tree structure' to dilute chemical/biological samples for a concentration dependent experiment (Fig. 11.3a) (Jeon *et al*., 2000). *In vivo*, a wide range of biological processes, including proliferation, migration, differentiation, wound healing, cancer metastasis, inflammation, and stem cell development, are governed by a gradient of specific molecular cues. Thus, generating concentration differences in both growth factors and transcription factors *in vitro* plays a critical role in reconstituting the niche environments. The microfluidics device was composed of a network of channels consisting of horizontal channels, vertical channels (serpentine), and a branching point. At the branching point, highly concentrated samples met with buffer and moved to the serpentine channel where they can be mixed. After mixing in the serpentine channel, the fluid splits into two side horizontal channels and the split fluid meets other fluids of both higher concentration and lower concentration. After several generations of branched systems, each fluid stream may achieve different concentration gradients. Because of the importance of concentration gradients for cell

biological analysis, various microfluidic-based gradient generators have been developed after the introduction of the 'Christmas Tree' structured device for both 2D and 3D cell culture. In particular, microjet devices (Keenan *et al*., 2006), universal gradient generators (Fig. 11.3b) (Irimia *et al*., 2006), source/sink gradient generators (Abhyankar *et al*., 2006), osmotic pump gradient generators (Park *et al*., 2007), and microdroplet dilutors (Fig. 11.3c) (Niu *et al*., 2011) have been developed and used in cell signaling assays (Abhyankar *et al*., 2006), cell migration assays (Lin *et al*., 2005), differentiation studies (Chung *et al*., 2005, 2007; Park *et al*., 2007, 2009b), chemotaxis assays (Lin *et al*., 2005), and drug toxicity tests (Toh *et al*., 2009).

11.2.2 Miniaturized conventional technologies for cell analysis

The critical advantage of microfluidic technology over traditional assays is its high sensitivity in the micrometer scale. Several miniaturized technologies have been developed to perform accurate analytical gene/protein assays, such as microfluidic PCR. Additionally, microfluidic technologies, such as the miniaturized cell sorters, have been developed to enhance the performance of existing technologies.

Microfluidic PCR technologies are great examples of improved analytical assays using microtechnology. In the early 1990s, micro-fabricated PCR devices were first introduced by Northrup and colleagues (Northrup *et al*., 1993). Manz and colleagues then introduced a continuous-flow microfluidics-based PCR system in which a channel (40 m deep, and 90 m wide) was fabricated in glass with a total length of 2.2 m for 20 cycles (Kopp *et al*., 1998) (Fig. 11.4a). The temperature was controlled with heated copper blocks (60°C, 77°C, 95°C) that were integrated under the microfluidics channels for denaturation, annealing, and extension. This pioneering work has since inspired the development of a broad range of chip-based microfluidic PCR devices (Bu *et al*., 2003; Crews *et al*., 2008; Schneegass *et al*., 2001; Sun *et al*., 2002). In 2009, Hollfelder and colleagues developed a droplet-based microfluidics PCR (microdroplet PCR) device in which an oil inlet joined two aqueous inlet channels to form a droplet at a T-junction (Fig. 11.4b). Generated droplets passed through the inner circles of the hot zone to denature the template. Then, as the droplets travel through the device, annealing and template extension occurs until the droplets finally exit the device after 34 cycles (Schaerli *et al*., 2009). This microdroplet PCR device allows efficient amplification from a single molecule of DNA per droplet. Since then, microdroplet-based PCR devices have been rapidly developing (Markey *et al*., 2010; Schaerli *et al*., 2009; Taly *et al*., 2007; Tewhey *et al*., 2009). (See Chapter 13 for more information about PCR techniques.)

Miniaturized cell sorters are another great example of existing technologies that were redesigned to perform on the micrometer scale (Fu *et al.*, 1999). The first miniaturized cell sorter was the fluorescence-activated cell sorter (FACS), the gold standard in conventional cell isolation processes. Basing their technology on targeting cell surface markers, Fu and colleagues introduced micro-fabricated FACS (ìFACS), which was fabricated by soft lithography. Cells expressing green fluorescent protein were sorted out using ìFACS (Fig. 11.5a and 11.5b). Moreover, miniaturized magnetic-activated cell sorters (MACS) have also been developed (Fig. 11.6b). These cell sorters are advantageous because they have a short operating time, are user-friendly, can be fabricated a low cost, are less labor-intensive, and have reduced sample/reagent consumption. Ingber and colleagues introduced micro-fabricated high-gradient magnetic field concentrator (HGMC; micro-needle) integrated microfluidic devices to remove bacteria from blood. HGMCs generate a stronger magnetic field gradient across the microchannel in which bacteria could be isolated by anti *E. coli* antibody coated paramagnetic micro-particles within the magnetic field (Xia *et al.*, 2006) (Fig. 11.6b). Taking advantage of the higher surface to volume ratio present at micro-scales, micropost microfluidics device was developed to isolate circulating tumor cells (CTC) from the blood stream based on specific surface protein (Nagrath *et al.*, 2007). CTC-targeting antibodies (Anti-EpCAM) were coated onto microposts in microfluidic channels and CTCs were captured from the peripheral blood of cancer patients (Fig. 11.6c). Cell rolling properties were also utilized to isolate the cells using microfluidics. Karnik and his colleagues introduced a cell rolling microfluidics device in which the microfluidic channels were coated with P-selectin to guide the target cells into an isolating chamber (Fig. 11.6a) (Choi *et al.*, 2012; Lee *et al.*, 2011). In addition to the surface protein targeting strategy, Huang and colleagues introduced microfluidic size-based particle separation (Huang *et al.*, 2004). Size differences between the particles have become one of the most important parameters that are used to isolate the particles using microfluidics (Fig. 11.28a). For instance, various devices have been developed to isolate CTCs from blood based on size differences between blood components and CTCs (RBC: ~8 ìm, WBC: 10~15 m and CTC:16~20 m) (Fig. 11.28b) (Hosokawa *et al.*, 2010; Hur *et al.*, 2011; Mach *et al.*, 2011; Mohamed *et al.*, 2009; Tan *et al.*, 2009; Zheng *et al.*, 2007). Additionally, there are reports of microfluidic devices that continuously monitor a patient's inflammatory response during cardiac surgery involving cardiopulmonary bypass (CPB) procedures (Aran *et al.*, 2011) and remove bacteria from human blood (Aran *et al.*, 2011; Mach and Di Carlo, 2010; Wu *et al.*, 2009b). The development of novel, microscale cell sorting strategies, such as microfluidics-based cell sorters, have paved the way to a better understanding of cell biology.

11.2.3 Emerging microfluidics technologies

We have demonstrated that we can mimic *in vivo* environments of cellular niches and enhance the sensitivity of existing technologies through microfluidic devices. In the following section, we will discuss the development of emerging technologies that investigate transport phenomena in microscale cell analysis.

The concept of droplet microfluidics was first introduced by Song and colleagues (Song *et al*., 2003) to address issues in cross-contamination, Taylor dispersion, solute surface interactions, and the need for substantial volumes of reagents and relatively long channel lengths for continuous flow in microfluidics. Since then, various droplet-based microfluidic devices have been developed. By combining two immiscible phases (typically water and oil) in microfluidic channels (two main channel geometries are T-junction and flow focusing), picoliter-sized droplets can be generated and serve as compartments for reactions (Fig. 11.2c and 11.2d). The rate of droplet formation in microfluidic channels can reach up to millions per second, and the concentration of encapsulated molecules can also be precisely controlled by manipulating the concentration of ingredients and speed of the fluid injections. With high accuracy and high-throughput potential, droplet microfluidics permits multiple reactions to be performed by varying the reaction conditions (Song *et al*., 2006). Various chemical and biological samples including DNA/RNA, protein, mammalian cells, bacteria, and worms have been manipulated and analyzed using droplet microfluidics. Furthermore, gene/protein expression, enzyme kinetics, cell proliferation, cell differentiation, cell signaling, protein crystallization, cytotoxicity assays, and organic synthesis have been achieved in droplet microfluidics. It has been shown that droplet microfluidics could satisfy demands that are not met by continuous-microfluidic devices (deMello, 2006; Solvas and deMello, 2011).

The integration of electrokinetics in microfluidics has also created systems with the potential to reveal important cellular traits (Markx and Davey, 1999; Pethig *et al*., 2004). Electrical analyses of biological cells that detect dielectric properties represent a powerful tool for label-free analysis, characterization, and manipulation of biological cells (Fuhr *et al*., 1994;Gagnon, 2011; Pethig, 1996). To measure the dielectric characteristic of cells, two different techniques have been used: impedance spectroscopy and dielectrophoresis (DEP) (Fig. 11.7a and 11.7b). So far, the electrokinetic analysis of cells using microfluidics has revealed significant cellular behaviors, including cell cycle (Kim *et al*., 2007), proliferation (Lu *et al*., 2012), differentiation (Bagnaninchi and Drummond, 2011; Park *et al*., 2011; Reitinger *et al*., 2012), and apoptosis induced by both chemical and physical impact (Patela and Markxb, 2008). By realizing that cells have distinct behaviors under exposure to an electric field, Becker and colleagues introduced DEP-based

cancer cell isolation from blood (Becker *et al*., 1995). Additionally, Fiedler and colleagues first introduced a DEP-based cell sorter in microfluidics (Fiedler *et al*., 1998). Moreover, isolation of pathogens (such as bacteria) (Hu *et al*., 2005) and CTCs (Moon *et al*., 2011) from human blood has been achieved using DEP-based microfluidics. Based on the examples provided here, it is evident that electrokinetics-based microfluidics will contribute to the advancement of stem cell analysis.

11.3 Examples of microfluidic platform for stem cell analysis: stem cell culture platform – mimicking *in vivo* culture conditions *in vitro*

In the above sections, we introduced various platform technologies in microfluidics, including miniaturized cell culture systems, miniaturized analytical tools, and cell separators/sorters. Furthermore, we introduced microfluidic devices with specific functions, such as microelectrophoresis, single-cell analysis, and gene expression profiling. Recently, microdevices have also been used as tools for understanding stem cell behavior and have shown great potential in analysis of stem cells (Blagovic *et al*., 2011), such as stem cell culture, stem cell purification, labeling detection, cell separation, gene discrimination, and cell identification. Additionally, integration of microchannels with nano-electrospray emitters allows for sample preparation for mass spectrometry in high-throughput and proteomics analysis.

Stem cell behavior is extremely sensitive to environmental stimuli, as depicted in Fig. 11.9; the stimuli are difficult to manipulate, demonstrate, and quantify with traditional methods. Schofield first proposed the 'niche' hypothesis, to describe the physiologically limited microenvironment which supports stem cells (Schofield, 1978). The stem cell niche is a reservoir of multipotent stem cells that can maintain normal, injured, or aged organs and tissues, in response to signals that regulate whether they should remain quiescent, undergo self-renewal, or differentiate (Vazin and Schaffer, 2010). Recently, engineers have been able to create microfluidic microenvironments that can qualitatively and quantitatively emulate several key properties of the stem cell niche *in vitro*, thus enabling reductionist studies of their influences on stem cell behavior, including both biochemical and biophysical regulation. Previously, Toh *et al*. and Gupta *et al*. have summarized the engineered miniaturized cell culture platforms and microfluidics-based approaches that can be translated to address particular issues in stem cell research (Gupta *et al*., 2010; Toh *et al*., 2010). Wu and colleagues have provided a comprehensive review of papers published in recent years studying stem cells using microtechnologies (Wu *et al*., 2011). Here, we will emphasize the state-of-the-art miniaturized stem cell culture platforms that have contributed to understanding the relationship between micro-environmental

cues and stem cell behavior *in vivo,* with an emphasis on biochemical regulation, cell–cell interactions, and biophysical regulation.

11.3.1 Biochemical regulation

In vivo, cells frequently respond to spatially distinct profiles of a variety of morphogens, growth factors, and other biochemical cues. In order to study the biochemical regulation of environmental cues, mimicking those biochemical profiles *in vivo* is critical. Distinct approaches have been developed in microfluidics to help identify the biochemical regulators that affect stem cell behavior, including external molecular gradients, paracrine and autocrine signaling, and spatially distinct microenvironments for stem cell manipulation.

Spatially distributed gradient generation

The molecular gradients generated by microfluidic devices are precise and comparable to *in vivo* systems (Csete, 2010). Gradient characteristics such as slope and concentrations can be quantified and correlated. With an increased *in vivo*-like chemotactic gradient in the microchannels, migration of stem cells can be studied on a single-cell basis instead of in mass cultures using Boyden chambers. An interesting study led by Chung and his colleagues investigated neural stem/progenitor cells (NSPC) differentiation in response to a combinational gradient consisting of fibroblast growth factor 2 (FGF2), platelet derived growth factor (PDGF), and epidermal growth factor (EGF). They demonstrated that human NSPCs (hNSPC) can be grown in microfluidic devices and can be induced to differentiate into other cells depending on the specific growth factor concentration gradients (Fig. 11.10a) (Chung *et al*., 2005). Similarly, Park and colleagues cultured an enriched population of neural progenitors derived from human ESCs in a microfluidic chamber for 8 days with continuous cytokine gradients (sonic hedgehog, fibroblast growth factor 8, and bone morphogenetic protein 4) (Park *et al*., 2009a). They found that the average numbers of both neuronal cell body clusters and neurite bundles were directly proportional to sonic hedgehog concentrations in the gradient chip. Both studies showed that gradient-generating microfluidic devices are useful systems for both basic and translational research, with straightforward mechanisms and operational schemes.

Spatially distinct biochemical profile exposure

As we discussed previously, microfluidic technologies enable the possibility of precisely manipulating spatially distinct molecular profiles and dynamic fluidic environments. Fung and colleagues developed a Y-channel device with two inlets for two different culture media (Fung *et al*., 2009). An EB, a transient state of ESC to multipotent stem cells, was immobilized between

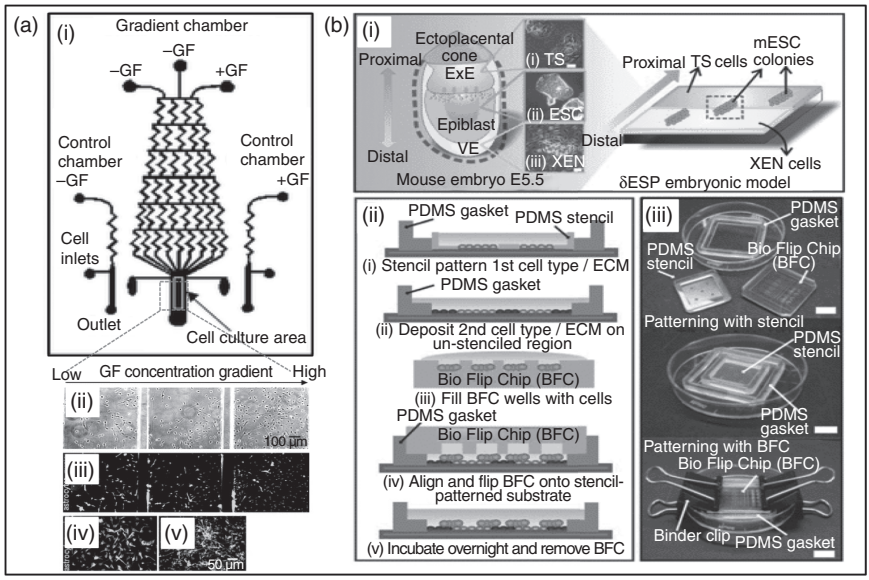

11.10 Microfluidics-based biochemical regulation (a) 'Christmas tree' structured concentration gradient generator. (*Source*: Reprinted by permission from Chung *et al.*, 2005.) (i) Schematic design of the microfluidic device showing the gradient chamber and two control chambers. Cells are loaded into the chambers via inlet ports (top of panel). Human NSCs cultured in the gradient chamber (ii, iii) for 7 days differentiated into astrocytes (stained with antibody against GFAP). Phase contrast images (ii) and fluorescence micrographs (iii, iv, v) showing stained nuclei (Hoechst) to identify all cells in the field. Astrocytic differentiation occurred more readily in the low GF compartment (iii). (b) Reconstituting proximal-distal (PD) epiblast patterning *in vitro* with Differential Environmental Spatial Patterning (δESP). (*Source*: Reprinted by permission from Toh *et al.*, 2011.) (i) Conceptual design. (ii) Operation of δESP. (iii) Components and assembly of δESP; middle and bottom panels show the assembly of components during the stenciling and flipping steps of δESP respectively. Scale bar = 1 cm.

the two streams. They demonstrated that by independently cultivating the two halves of an EB in two separate media, from laminar co-flow in a microchannel, cell differentiation could be induced in half of the EB while retaining the other half of the EB in an un-induced stage.

Adhesive ligands (extracellular matrix) regulation

Signals that promote the anchoring or localization of stem cells to their proper niches are critical for maintaining their ability to self-renew and differentiate (Guilak *et al.*, 2009; Scadden, 2006). Contrary to the combinatorial

nature of extracellular matrix *in vivo*, it is difficult to investigate the influence of adhesive ligands on stem cell phenotypes. Anderson and colleagues introduced a polymer array synthesis approach for rapid, nanoliter-scale synthesis of biomaterials and characterization of their interactions with cells (Anderson *et al*., 2004). As a proof-of-principle experiment, over 1700 human ESC (hESC)–material interactions were investigated. They identified various levels of hESC attachment and spreading, cell-type specific growth, growth factor-specific proliferation, and differentiation into cytokeratin-positive cells. This microarray approach offers new levels of control over hESC behavior.

The introduction of micro-printing technologies in microfluidics represents another approach that has enabled our understanding of the role of ECM components on stem cell phenotypes in a high-throughput and combinatorial manner. Flaim and colleagues first developed an ECM microarray platform for the culture of patterned cells atop a combinatorial matrix mixture (Flaim *et al*., 2005). This platform is used to investigate stem cell differentiation in response to a multitude of adhesive ligands in parallel. They observed mouse ESCs (mESC) on multiple unique combinations of multiple ECMs, which indicated that differentiation towards the hepatic fate is influenced in a combinatorial and complex dose-dependent manner. They further extended the platform to study human neural precursors in which they demonstrated how ECM components affect self-renewal and differentiation into neurons and glia (Flaim *et al*., 2008). This platform facilitates the study of almost any insoluble ligand in a combinatorial fashion. Though we have only discussed a few examples, there are several microfluidic devices that have been developed to cultivate stem cells and to investigate the relationship between adhesive ligands and stem cell regulation (Chin *et al*., 2004; Lanfer *et al*., 2009; Solanki *et al*., 2010).

In addition to the development of microfluidics as a tool for understanding the interactions between adhesive molecules and stem cells, Toh and colleagues introduced a spatially organized stem cell developmental model to interrogate the role of space in fate specification (Toh *et al*., 2011) using micropatterning (Fig. 11.10b). They introduced 'spatially organized stem cell developmental models' to interrogate the role of space in fate specification. Specifically, they developed differential environmental spatial patterning (dESP) to organize different microenvironments around single ESC colonies via sequential micropatterning. This study demonstrates the potential of using microfluidic devices to mimic the developmental progression of stem cell *in vivo*.

11.3.2 Cell–cell interaction

Cell–cell signaling via membrane protein contact or paracrine/autocrine signaling is crucial for maintaining stem cell homeostasis. For example, ESCs

must be cultured in clumps in order for them to survive *in vitro*. To understand the influence of cell–cell interactions on stem cell homeostasis, three different approaches have been adapted in microfluidics, including controlling paracrine/autocrine signals and the development of cell co-culture systems.

Paracrine and autocrine signaling control

Autocrine and paracrine signaling mechanisms are traditionally difficult to investigate due to limited technology and the sub-micromolar concentrations that are involved. Ellison and colleagues developed a computational model and a microfluidic cell culture platform that could control the removal of molecular factors secreted by cells into the surrounding media. With this system, they investigated the influence of paracrine and autocrine signaling in mESCs (Ellison *et al*., 2009). They proved that the existence of soluble autocrine/paracrine factors, secreted by mESCs, contributes to their viability in *in vitro* culture conditions. Moreover, Blagovic and colleagues utilized the microfluidic perfusion system to investigate the biological role of autocrine and paracrine signals (Blagovic *et al*., 2011) (Fig. 11.11a). They developed a multiplex microfluidic platform to continuously remove cell-secreted (autocrine\paracrine) factors to downregulate diffusible signaling. By comparing cell growth and differentiation in side-by-side chambers with or without added cell-secreted factors, they isolated the effects of diffusible signaling from artifacts such as shear, nutrient depletion, and microsystem effects, and found that cell-secreted growth factor(s) are required during neuroectodermal specification. Then they induced FGF4 signaling in minimal chemically defined medium (N2B27) and inhibited FGF signaling in fully supplemented differentiation medium with cell-secreted factors to determine that the non-FGF cell-secreted factors are required to promote growth of differentiating mESCs. From this study, they found that autocrine/paracrine signaling drives neuroectodermal commitment of mESCs through both FGF4-dependent and -independent pathways, and demonstrated that microfluidic perfusion systems are able to alter diffusible signaling of mESCs.

Controlling cell shape: EB formation and size control

Currently, there are two major approaches for culturing hESCs. The first method, also the most traditional way, is to co-culture hESCs with a feeder layer consisting of mitotically inactivated murine embryonic fibroblasts (MEF). MEFs supply a microenvironment for hESCs by maintaining the growth and health conditions necessary to maintain the undifferentiated status of hESCs. The second approach is to culture hESCs under feeder-free conditions such as Matrigel. Nevertheless, the common problem in both of these approaches is that they generate variable sized aggregates

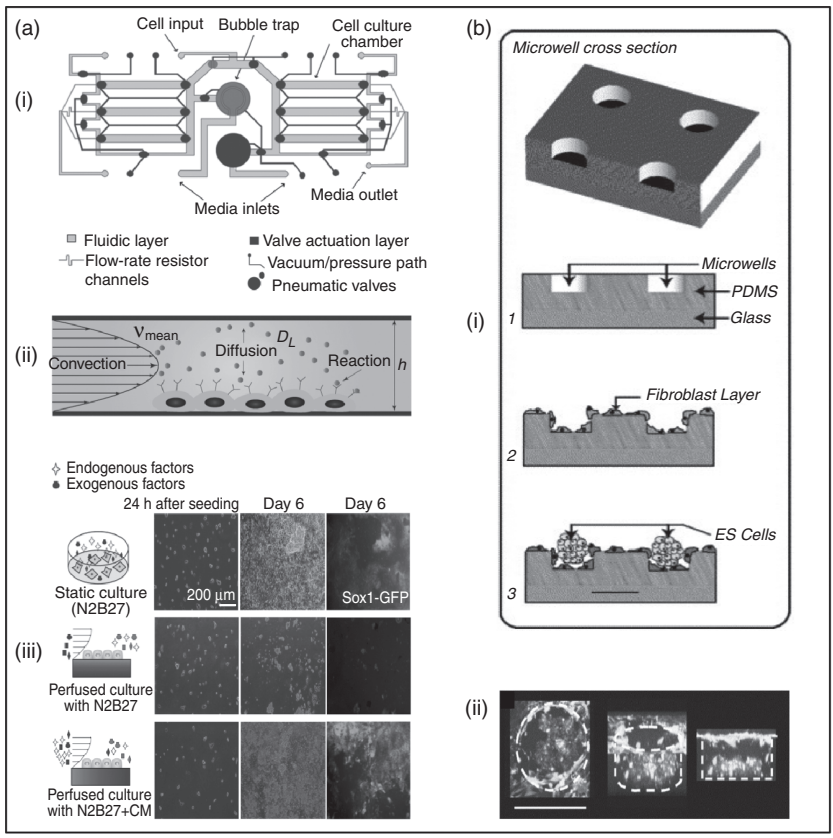

11.11 Microfluidics-based cell–cell interaction study. (a) Paracrine and autocrine signaling control. (*Source*: Reprinted by permission from Blagovic *et al.*, 2011.) (i) Schematic of the perfusion device. Gray and black outlines represent fluidic and control layers, respectively. (ii) Microfluidic perfusion systems use flow to fine-tune the relative significance of convection, diffusion, and reaction. (iii) Monoculture neuroectodermal differentiation and comparison of differentiation makers in static and perfusion systems (upper, middle, bottom). (b) Microwell chip-based EB formation and EB size controlling. (*Source*: Reprinted by permission from Khademhosseini *et al.*, 2006.) (i) Schematic representation of the co-culture system formed by hES and MEF cells. PDMS was cured on a silicon master to produce microwell-patterned surfaces. Surfaces were treated with fibronectin and seeded with MEFs to create a monolayer for ES culture. (ii) 3D confocal reconstruction of hES–MEF co-cultures within a microwell on day 1 rotated at 45°C intervals. In all figures, scale bars correspond to 200 µm.

of cells. Large cell clusters tend to differentiate at the borders and small clusters of cells hinder proliferation and recovery of hESCs in culture. In addition, different sizes of EBs might lead to different cell lineage differentiation. For example, it has been reported that sufficient blood formation

in EBs requires from 500 to 1000 cells. EBs with higher cell numbers were not able to form erythroid lineages (Ng, 2005). Therefore, controlling the size of cell aggregates is important for controlling the homogeneity of the cultures.

Recently, microfabrication based approaches have become powerful tools for controlling the cellular microenvironment as well as the size of cell aggregates. Immobilizing cells on micropatterned surfaces in a microfluidic device allows cell shape and differentiation to be controlled. It has been reported that if hESCs/MEFs are co-cultured in a microwell system, and the hESC aggregates are removed afterwards, then 26% of the EBs had an area between 10 000 and 21 000 μm^2. These results show that it is possible to generate EBs with controllable sizes (Khademhosseini *et al.*, 2006). In comparison, EBs that were prepared from hESC aggregates without the microwell system had variable sizes and less homogeneity than those prepared with the microwell system (Fig. 11.11b).

11.3.3 Biophysical regulation

In addition to biochemical factors, the stem cell niche environment also has unique mechanical properties that play an important role in regulating stem cell differentiation (Reilly and Engler, 2010). Microfluidic devices have been engineered to study the mechanical interactions between stem cells and their microenvironment. These devices facilitate our understanding of how mechanical signals (the mechanical interaction between the cell and its matrix) regulate stem cell behavior. Recently developed microfluidic devices have the ability to control microscale biophysical factors such as stiffness of the ECM, the geometry and shape of the cells, and the external shear stress experienced by the cells.

Controlling environmental mechanical influence

The stiffness of the ECM has been recognized as an influential component in stem cell differentiation. A landmark study led by Engler *et al.* has shown that the elasticity of the ECM can direct MSC's lineage specification (Engler *et al.*, 2006). Alexander and his colleagues introduced stem cell encapsulation in hydrogel microbeads (agarose gel) to study the effects of variable cellular microenvironment elasticity on stem cell fate (Fig. 11.13) (Kumachev *et al.*, 2011). The mESCs were encapsulated within the agarose microgels and different elastic moduli were obtained by injecting, into a microfluidic droplet generator, two streams of agarose solutions, one with a high concentration of agarose and the other with a low concentration of agarose, at varying relative volumetric flow rates.

Not only does the stiffness of the ECM affect stem cell differentiation, but also the geometry and the shape of the cells also exert a force on cells, which regulates stem cell behavior. To address the relationship between cell shape and stem cell behaviors, Yim and colleagues utilized a nanoimprinting technique to create nanostructures to further our understanding of the role of topography on stem cell phenotypes (Fig. 11.12a) (Yim *et al*., 2007). They found that the combination of nanotopography and biochemical cues, such as retinoic acid, further enhances the up-regulation of neuronal marker expression. However, nanotopography showed a stronger effect, compared to retinoic acid alone, on an unpatterned surface. This study demonstrated the significance of nanotopography in understanding the differentiation mechanisms of adult stem cells.

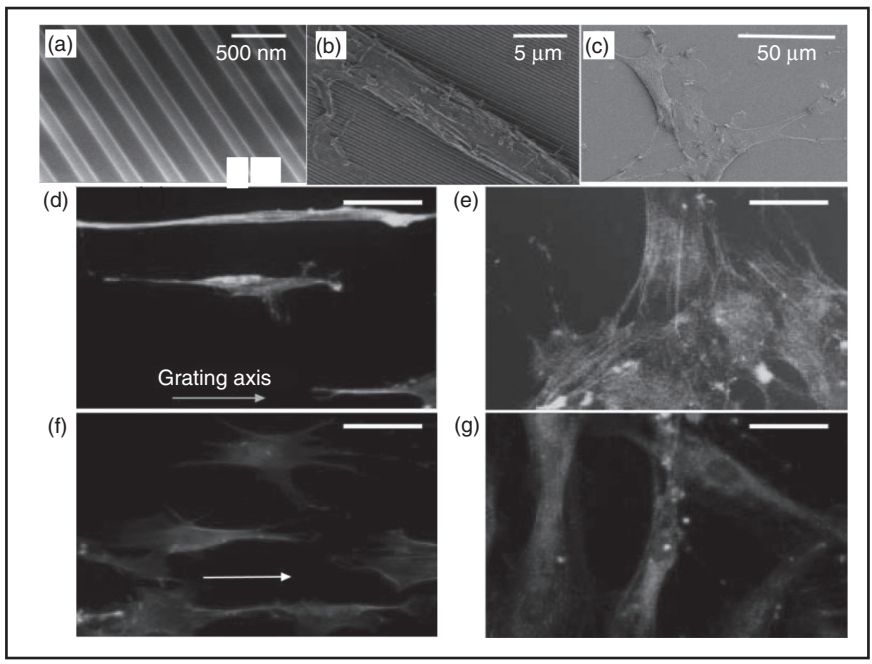

11.12 Control of biophysical factors at the microscale. Changes in morphology and proliferation of human mesenchymal stem cells (hMSC) cultured on nano-gratings. (*Source*: Reprinted by permission from Yim *et al*., 2007.) Scanning electron micrographs of (a) PDMS nano-patterned by replica molding; hMSCs cultured on (b) nano-patterned PDMS and (c) unpatterned PDMS. Confocal micrographs of F-actin-stained hMSCs on (d) nano-patterned PDMS and (e) unpatterned PDMS in hMSC proliferation medium; (f) nano-patterned PDMS and (g) unpatterned PDMS cultured in presence of 1 μM of retinoic acid (RA). Bar = 500 nm for (i), 5 μm for B, 50 μm for C-G.

Controlling external shear stress

Evidence of mechanically-induced stem cell differentiation has been reported using several types of mechanical forces including stretch, strain, compression, and shear stress (Stolberg and McCloskey, 2009). Even though the mechanism on how cells sense and translate mechanical signals into a biological response remains poorly characterized, recently developed microfluidic cell culture devices have been used as tools to study the influence of shear stress on stem cell behavior. Toh and colleagues designed a multiplex logarithmic microfluidics array to directly screen perfusion effects across a wide range of flow rates, corresponding to 1000 times variation in applied shear stress in a single device (Toh and Voldman, 2011). They found flow-induced shear stress specifically up-regulates the epiblast marker Fgf5. Epiblast-state transition in mESCs involves heparin sulfate proteoglycans, which have also been shown to transduce shear stress in endothelial cells. This study demonstrates that self-renewing mESCs possess the molecular machinery to sense shear stress.

11.4 Examples of microfluidic platform for stem cell analysis: single stem cell analysis

The fundamental goal of cell biology is to understand how cells operate, communicate with each other, and regulate their behaviors. Traditionally, 10^3~10^6 cells are used for cell biology experiments such as cell signaling, proliferation, migration, and invasion assays. However, cell behavior is dictated by their microenvironment, including soluble factors, ECM, and other cells. Specifically, stem cells and their fates are controlled by various niche factors, such as other cells within the niche, with stem cell behavior and differentiation dependent on the microenvironment (Moore and Lemischka, 2006). In addition, fundamental misunderstandings of the heterogeneity of stem cells have hindered development of clinically effective cell-based therapies; heterogeneity in cell populations poses a major obstacle in understanding complex biological processes (Lecault *et al.*, 2011). As a result, high-throughput, single stem cell analysis is essential to expand our understanding of the heterogeneity within complex cell populations. Based on phenotype (protein expression) and genotype (gene expression), various microfluidic-based single-cell analytical methods have been developed recently (Guo *et al.*, 2012; Zare and Kim, 2010).

11.4.1 Single-cell culture platform

Single cells can be cultured or controlled in micro-fabricated devices such as microdroplet- (Fig. 11.13) or microwell-based devices. Lecault *et al.* introduced microfluidics-based platforms for analysis of single HSC proliferation (Fig. 11.14) (Lecault *et al.*, 2011). They fabricated PDMS-based microfluidic

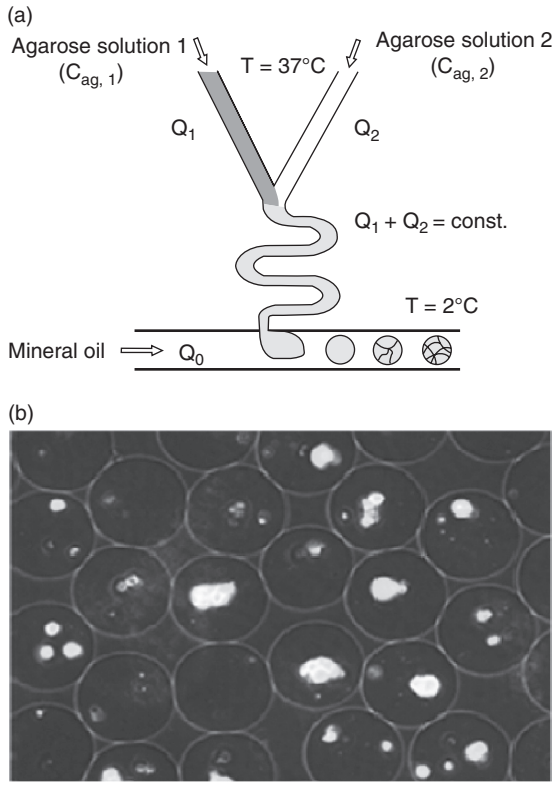

11.13 Microfluidics-based single stem cell analysis. Fluorescence optical microscopy images of agarose microgels encapsulating R1 mES cells in HBSS buffer. (*Source*: Reprinted by permission from Kumachev *et al.,* 2011.)

devices featuring 1600 cell culture chambers, each with a volume of 4.1 nL, and integrated microvalves for automated control and exchange of cell culture media. The effect of steel factor (SF) concentrations on survival and proliferation of HSCs, at a single-cell level, was defined and the growth rates of all clones (single cells) could be monitored and compared in real-time.

11.4.2 Cell cycle analysis

Recently, Kobel and colleagues introduced a single-cell cytometric microfluidics device (Kobel *et al.*, 2012). The microfluidic device consisted of 2048 arrayed single-cell traps and was utilized to quantify the spatial distribution of single cell for automatic tracking of dividing HSCs at single-cell level (Fig. 11.15). By using the 'Fluorescence Ubiquitination Cell Cycle Indicator' (FUCCI) system, HSCs were transfected to regenerate red fluorescence (in

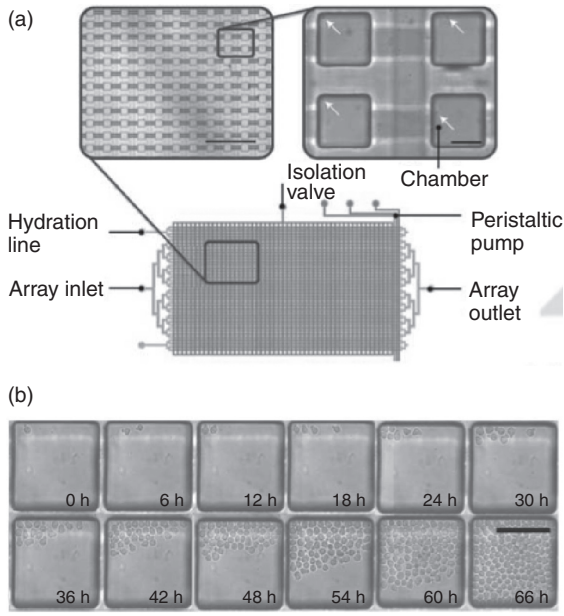

11.14 High-throughput analysis of single HSC proliferation in microfluidic. (*Source*: Reprinted by permission from Lecault *et al.*, 2011.) (a) Schematic of the device with micrographs as insets. The cell culture layer contains 1600 chambers connected by flow channels (gray). Arrows indicate single cells. Scale bars, 1 mm (left) and 100 μm (right). (b) Time-lapse automated imaging of clonal ND13 cell expression in a chamber. Scale bar, 100 μm.

G1 or G0 phase) or green fluorescence signal (in S/G2-M phase). Transfected cells were introduced and trapped in an image-based cytometry chip on a single-cell level. Then the microfluidics chip was imaged using an automated microscope to analyze cell cycle phase. This approach should allow on-chip cytometry of diverse single-cell behaviors in long-term microfluidics culture.

11.4.3 Gene expression profiling

To characterize the heterogeneity within stem cells, microfluidics-based single-cell analysis has been employed on a variety of stem cell populations, including HSCs and ESCs. Glotzbach and colleagues developed a microfluidic RT-PCR platform to investigate the heterogeneity of HSCs (Fig. 11.16) (Glotzbach *et al.*, 2011). Murine HSCs were sorted by FACS into each well of a 96-well plate with RT-PCR reagents preloaded in each well. To create cDNA for each gene target within each individual cell, low-cycle RT-PCR was performed. Single-cell cDNA was then loaded into a microfluidic

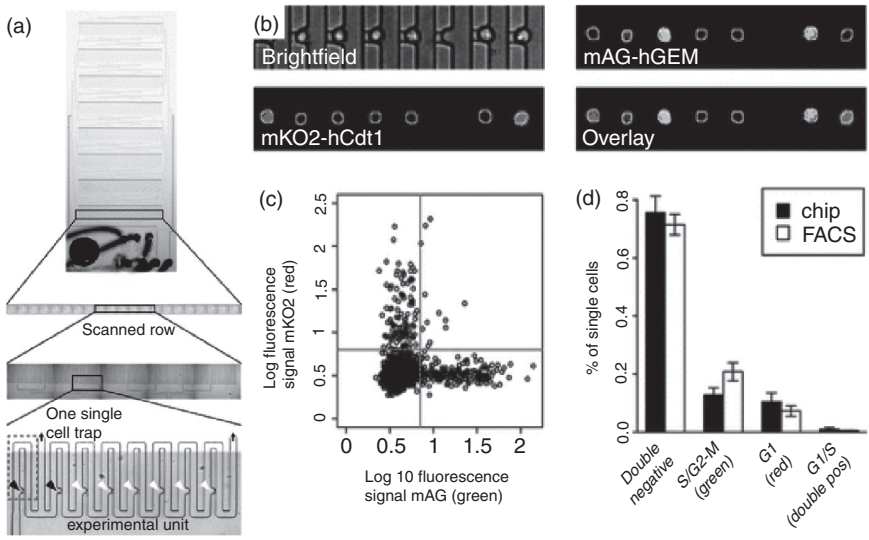

11.15 Cell cycle analysis of single stem cells with microfluidics. (*Source*: Reprinted by permission from Kobel *et al.*, 2012.) (a) Image-based cytometry on a microfluidic chip. (b) Micrographs of trapped HSCs. S/G2-M (marked in gray, left bottom panel) and G1 (marked in white, right top panel). (c) The populations of S/G2-M and G1 phase HSCs (marked in gray and white) on the microfluidic chip. (d) Comparison of microfluidic chip and flow cytometry for the analysis of the cell cycle phases.

device, along with the primer-probe sets for each gene target, and qPCR was performed for each cell across all 48 gene targets in parallel by using the BioMark instrument (Glotzbach *et al.*, 2011). This resulted in 2304 data points for each chip run. Using this microfluidics-based approach, 43 gene expressions (known to be highly relevant to hematopoiesis) were successfully measured from 300 individual HSCs. In addition, Zhong and colleagues developed microfluidic processors to profile single hESC expression through extraction of single-cell mRNA; synthesis of the cDNA was accomplished using the same device (Zhong *et al.*, 2007). The group concluded that whole population gene expression does not represent the gene expression present in individual cells. Using the unique advantages of microfluidics, it is possible to profile the gene expression of individual cells in the same niche that is otherwise considered heterogeneous using conventional gene expression methods.

Increasing numbers of miniaturized technologies have been developed to investigate the single-cell gene profile. Yet, none of these technologies has been applied to the stem cell field (Cai *et al.*, 2006; Dhof *et al.*, 2011; White *et al.*, 2011). Especially, White and his colleagues developed RT-qPCR, which can measure gene expression from hundreds of single cells (Fig. 11.17). This

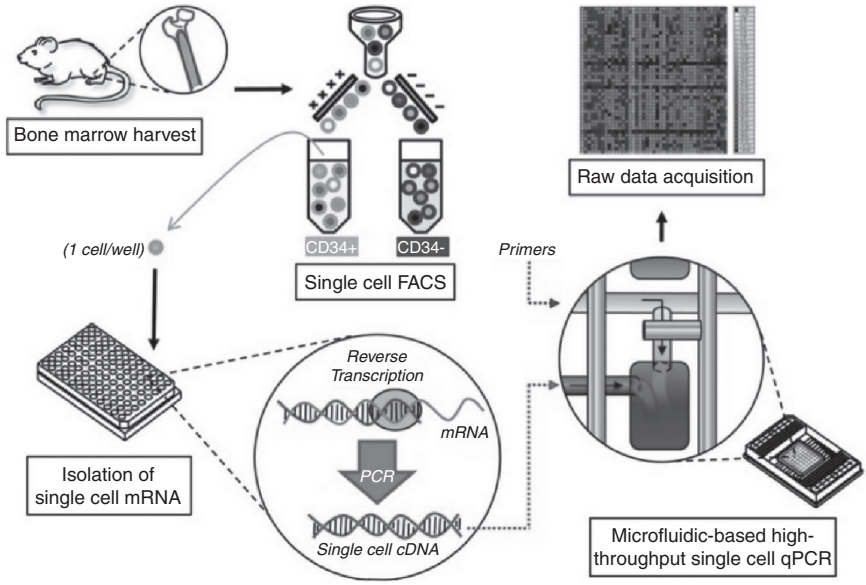

11.16 Single-cell gene expression analysis demonstrates transcriptional variation in murine LT-HSCs. (*Source*: Reprinted by permission from Glotzbach *et al.*, 2011.) Schematic of high-throughput microfluidic chip-based single-cell transcriptional analysis. A single-cell is sorted by FACS into each well of a 96-well plate preloaded with RT-PCR reagents. A low-cycle RT-PCR pre-amplification step creates cDNA for each gene target within each individual cell. Single-cell cDNA and primer-probe sets for each target gene are then loaded onto the microfluidics chip. The BioMark machine performs qPCR for each cell across all 48 gene targets in parallel, resulting in 2304 data points for each chip run.

technology was applied to 3300 single-cell measurements of (i) miRNA expression in K562 cells, (ii) coregulation of a miRNA and one of its target transcripts during differentiation in ESCs, and (iii) single nucleotide variant detection in primary lobular breast cancer cells. However, it is expected that these miniaturized technologies will pave the way to fully understanding stem cell heterogeneity in gene/protein expression levels and will help realize the potential of stem cells in regenerative medicine in the near future.

11.5 Microdevices for label-free and non-invasive monitoring of stem cell differentiation

Because the interest in utilizing stem cells for therapeutic purposes is increasing, it becomes even more critical to develop technologies that track the cellular status of cells *in vitro* without the need for cell labeling. Intrinsic dielectric properties of cells have been proven as a new label-free

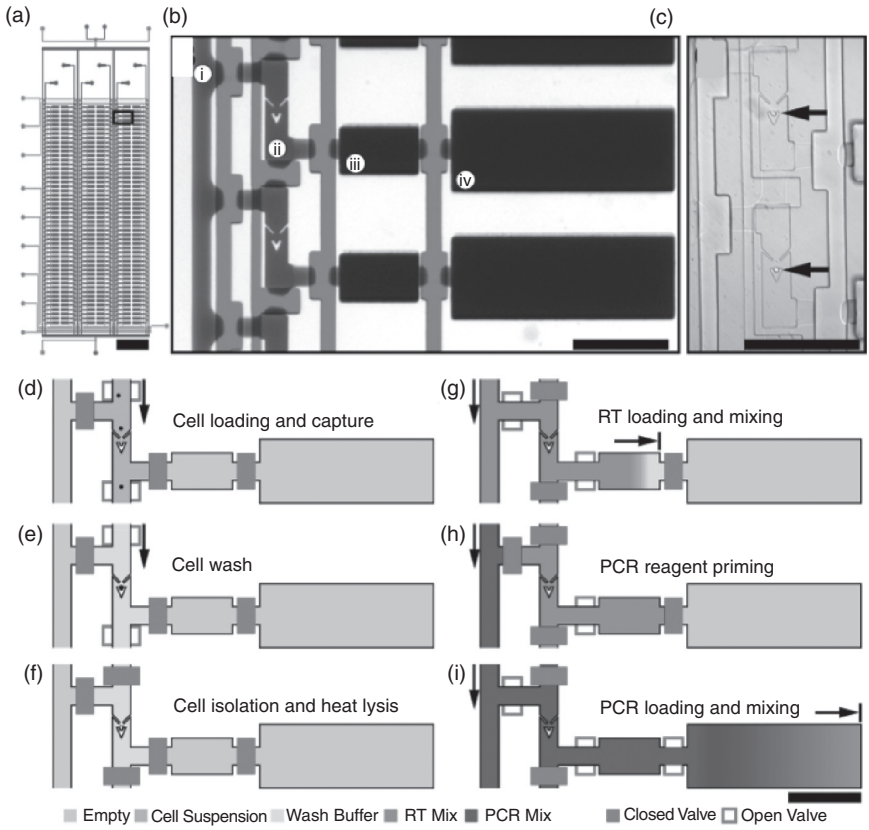

11.17 Design and operation of the microfluidic device for single-cell gene expression analysis. (*Source*: Reprinted by permission from White *et al.*, 2011.) (a) Schematic of microfluidic device. Scale bar: 4 mm. The device features six sample input channels, each divided into 50 compound reaction chambers for a total of 300 RT-qPCR reactions using approximately 20 μL of reagents. The rectangular box indicates the region depicted in (b). (b) Optical micro-graph of array unit. For visualization, the fluid paths and control channels are loaded with blue (marked in dark gray) and red (marked in gray) dyes, respectively. Each unit consists of (i) a reagent injection line, (ii) a 0.6 nL cell capture chamber with integrated cell traps, (iii) a 10 nL reverse transcription (RT) chamber, and (iv) a 50 nL PCR chamber. Scale bar: 400 μm. (c) Optical micro- graph of two cell capture chambers with trapped single cells indicated by black arrows. Each trap includes upstream deflectors to direct cells into the capture region. Scale bar: 400 μm. (d–i) Device operation. (d) A single-cell suspension is injected into the device. (e) Cell traps isolate single cells from the fluid stream and permit washing of cells to remove extracellular RNA. (f) Actuation of pneumatic valves results in single-cell isolation prior to heat lysis. (g) Injection of reagent (gray) for RT reaction (10 nL). (i) Reagent injection line is flushed (dark gray) for PCR. (ii) Reagent for qPCR (black) is combined with RT product in 50 nL qPCR chamber. Scale bar for (d–i): 400 μm.

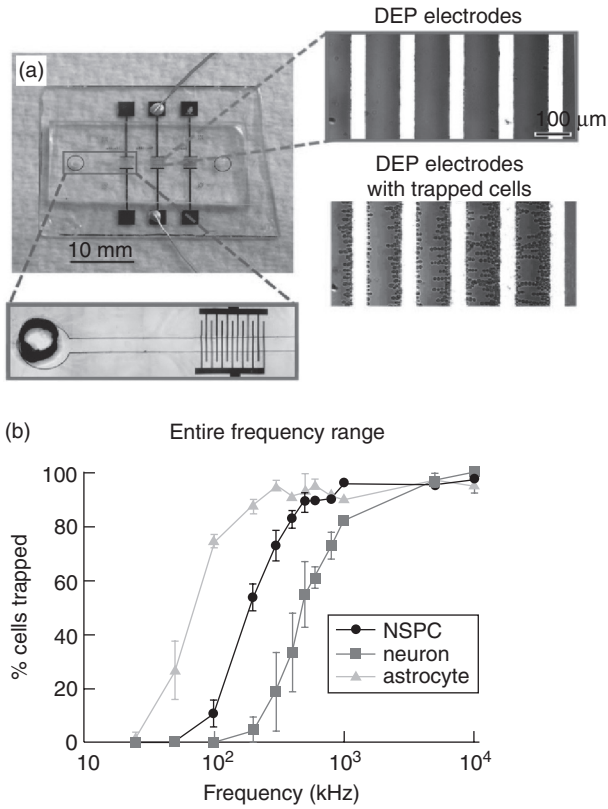

11.18 Microdevices for label-free and non-invasive monitoring of stem cell differentiation. DEP microfluidics device based stem cell isolation by using distinct dielectric properties of stem cells. (*Source*: Reprinted by permission from Flanagan *et al.*, 2008.) (a) Image of the DEP device. The top right panel is enlarged to show a higher-magnification view of the electrodes in the channel and the bottom right panel shows a higher-magnification view of the electrodes when the DEP force is applied and cells are trapped. (b) Dielectrophoresis trapping efficiency curves distinguish embryonic day 12.5 mouse NSPCs, neurons, and astrocytes. NSPCs, neurons, and astrocytes showed distinct trapping efficiency curves.

approach in characterizing and monitoring stem cells (Pethig, 2010). The cell's dielectric characteristics can be attributed to the plasma membrane and the cytoplasm. The dielectric characteristics are defined by two parameters, capacitance and conductance. The majority of microfluidic studies have focused on the dielectric properties of the plasma membrane because of technical limitations (Bagnaninchi and Drummond, 2011; Fatoyinbo *et al.*, 2008). Specific membrane capacitance (Cspec) is the measurement of a membrane's capacity to hold charges, which reveals the level of membrane folding

and composition. Specific membrane conductance (Gspec), in contrast, is the membrane's ability to deliver charges, which reflects the expressions of ion channels. Several groups have successfully integrated electrokinetics in microtechnologies and have developed platforms to either track stem cell differentiation without the need for cell surface markers using dielectrophoresis (DEP) (Fatoyinbo *et al.*, 2008; Hoettges *et al.*, 2008; Patela and Markxb, 2008), or to distinguish subpopulations of stem cell progeny using single-cell impedance cytometry (Figs 11.18–11.21).

Among the studies utilizing DEP to reveal the distinct dielectric signatures existing among stem cell populations, Flanagan and Lu *et al.* first identified that the dielectric response of NSPC to a non-uniform electric field is different from the response from differentiated mouse astrocytes and mouse neurons in a single DEP trapping device (Fig. 11.18) (Flanagan *et al.*, 2008). They also observed distinct dielectric responses existing between NSPCs isolated from different embryonic stages (E12, E16 for day 12 and day 16, respectively) with similar cell surface protein expression patterns (Nestin

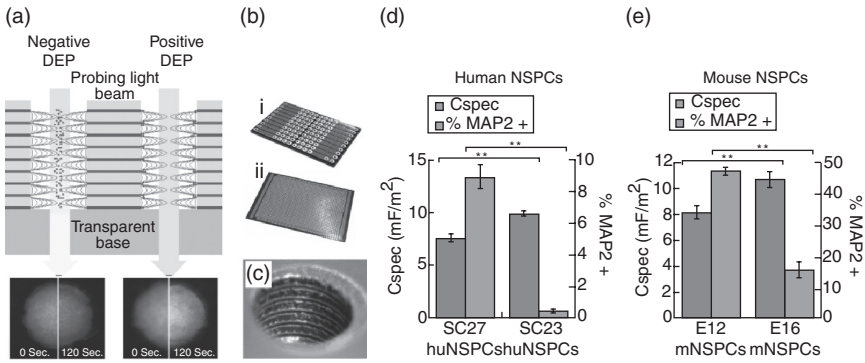

11.19 DEP-well system used to measure cellular dielectric properties by correlating the cellular dielectric response to light transmission through a microwell system. (*Source*: Reprinted by permission from Hoettges *et al.*, 2008; Labeed *et al.*, 2011.) (a) The electrodes are energized at a range of frequencies, eliciting the response of particles contained within the well of either positive or negative DEP. The intensity of light passing through the well indicates the magnitude and sign of the force. (b) The DEP-well formats devised are (i) the smaller spectra-chip (size 37 × 23.5 mm^2), which can be energized by up to 19 parallel frequencies on four wells each, and (ii) the larger 1536-well plate (size 127 × 86 mm^2) on a standard well-plate template. (c) Close inspection of the inside of a 1.2 mm diameter well reveals the gold-plated conducting electrode 'stripes' that surround the inside of each well. (d) The specific membrane capacitance (Cspec, mF = milliFarad) of SC27 and SC23 human NSPCs (huNSPC). (e) The specific membrane capacitance of E12 and E16 mouse NSPCs (mNSPC) (**$p < 0.01$, $n = 3$ or more separate experiments with different sets of cells).

and GFAP protein expression). They further identified that the intrinsic dielectric characterization could be used to reveal the heterogeneity of NSPCs within the culture. Labeed and Lu *et al*. exploited another DEP-well system to further verify if the difference in NSPCs isolated from distinct embryonic stages is attributed to the dielectric properties of the membrane components or cytoplasmic components (Fig. 11.19) (Labeed *et al*., 2011). By measuring the dielectric properties of both the cell membrane and the cytoplasm, they identified the specific membrane capacitance (Cspec) as a novel biophysical marker to reflect the neuronal fate potential of NSPCs. They confirmed these findings by measuring Cspec of NSPCs with a distinct neuronal fate (human NSPCs isolated from distinct regions of brain with similar developmental stage and mouse NSPCs isolated from cortical brain regions from distinct developmental stage). Furthermore, the Cspec of cells dynamically changes as NSPCs lose their neuronal fate potential by passaging the cells *in vitro* over 20 times. In addition, DEP has also been applied to other adult stem cell fields. Vykoukal and colleagues utilized a simple approach method, called the conductivity method, to extract the dielectric properties of subpopulations of HSCs (Fig. 11.20) (Vykoukal *et al*., 2009). They used cell size verse Cspec plots as a way to discriminate the complete mononuclear and polymorphonuclear blood cell subpopulations from each other. These studies provide evidence that the dielectric signature of the cell membrane can be used as a label-free marker in reflecting the fate potential and differentiation progression of stem cells.

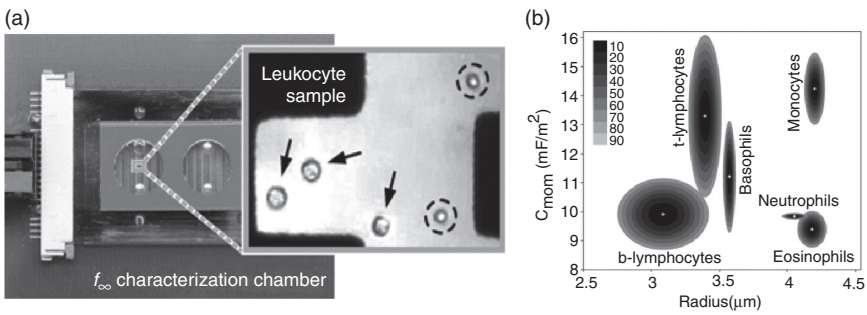

11.20 Dielectric characterization of complete mononuclear and polymorphonuclear blood cell subpopulations by label-free discrimination. (*Source*: Reprinted by permission from Vykoukal *et al*., 2009). (a) Photograph of cell characterization device with DEP microelectrode, fluidic reservoirs, electrical interconnect, and signal input. (insert) Eosinophil preparation on castellated electrode; eosinophils are indicated by arrows while erythrocytes are circled. (b) Scattergram of leukocyte subpopulation properties as determined during DEP crossover frequency analysis.

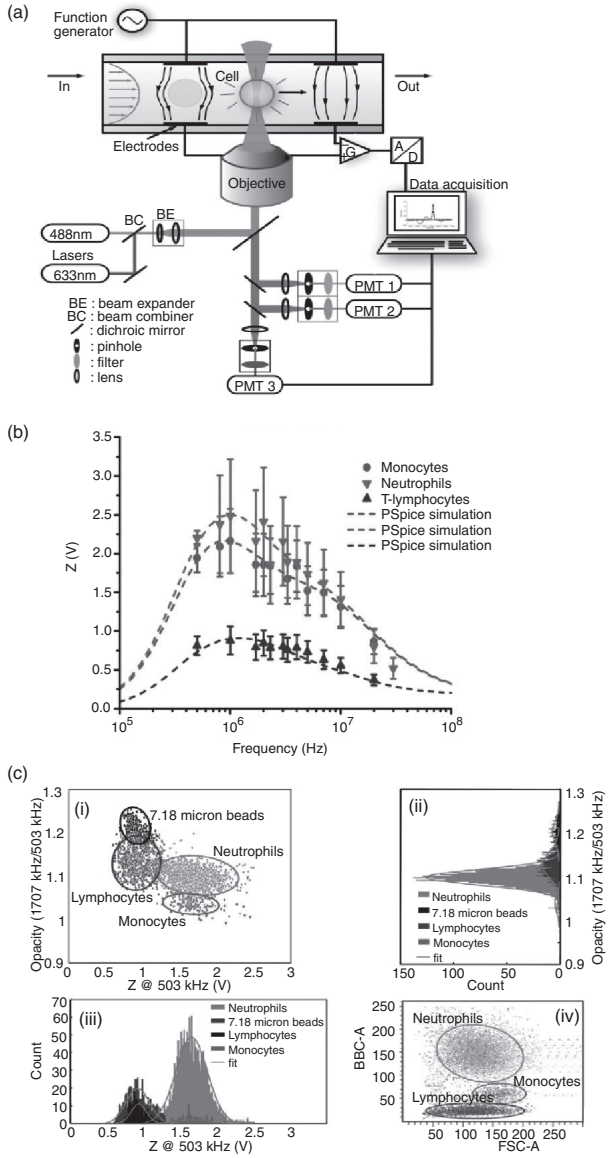

11.21 Microfluidic impedance cytometry to measure the impedance of single cells at two frequencies. (*Source*: Reprinted by permission from Holmes *et al.*, 2009.) (a) Schematic diagram of the micro impedance cytometer system, including the confocal-optical detection setup. Dual laser excitation and three color detection are implemented along with dual frequency impedance measurement. The cell flows through the microchannel and passes between two pairs of electrodes and the optical detection region. The fluorescence properties and impedance of the cell are measured simultaneously, allowing comparison of the electrical and optical properties of single cells. (b) MACS purified populations of T-lymphocytes, monocytes, and neutrophils.

In addition to monitoring Cspec of cells using DEP, impedance spectroscopy has recently been developed to monitor the differentiation of stem cells in real-time (Bagnaninchi and Drummond, 2011; Park *et al*., 2011; Reitinger *et al*., 2012). For instance, Bagnaninchi *et al*. identified that the differentiation of adipose-derived stem cells along osteogenic and adipogenic lineages can be monitored based on their Cspec measurements (Bagnaninchi and Drummond, 2011). Park *et al.* found that neural differentiation of MSCs can be monitored using impedance sensing (Park *et al*., 2011). Although those studies were not using microfluidics-based-approaches, it extended the applicability of using dielectric signatures of cells as markers for MSCs. Recently, single-cell impedance cytometry represents an alternative approach to measuring cell dielectric characteristics (Sun and Morgan, 2010) on a micrometer scale. Holmes and colleagues developed a microfluidic impedance cytometry device to measure the impedance of a single cell at two frequencies (Fig. 11.21) (Holmes *et al*., 2009). They found that the low frequency (503 kHz) impedance magnitude, a measure of cell size, enables discrimination of the T-lymphocyte population from the larger cells that make up the monocyte and neutrophil populations. Dual frequency measurements enabled discrimination of the cells according to both membrane capacitance and size and allowed them to distinguish monocytes, neutrophils, and lymphocytes from each other at the same time. These studies indicate that single-cell impedance cytometry devices have potential to track stem cell differentiation without the need for cell labeling or genetic manipulation, which is beneficial for the development of stem cell-based regenerative medicine.

One of the concerns in integrating electrokinetics in microtechnologies for stem cell research is the potential adverse effect that electric field exposures can have on stem cell plasticity or differentiation potential. To address this issue, Lu and colleagues completed a comprehensive study investigating the impact of AC electric field exposures on stem cells that are required for DEP and impedance measurements (Lu *et al*., 2012). No adverse impact on cell viability, proliferation, or fate potential of NSPCs was noticed for the time that was required for the dielectric property measurements. This study indicated that monitoring stem cell differentiation using DEP and impedance spectroscopy *in vitro* is non-invasive and has the potential to advance stem cell research.

11.6 Microfluidics stem cell separation technology

The detection, isolation, and sorting of specific subpopulations of stem cells are important in both fundamental research and clinical applications of stem cell-based therapeutics. Advances in microfluidic cell sorting devices have enabled scientists to attain improved separation with comparative

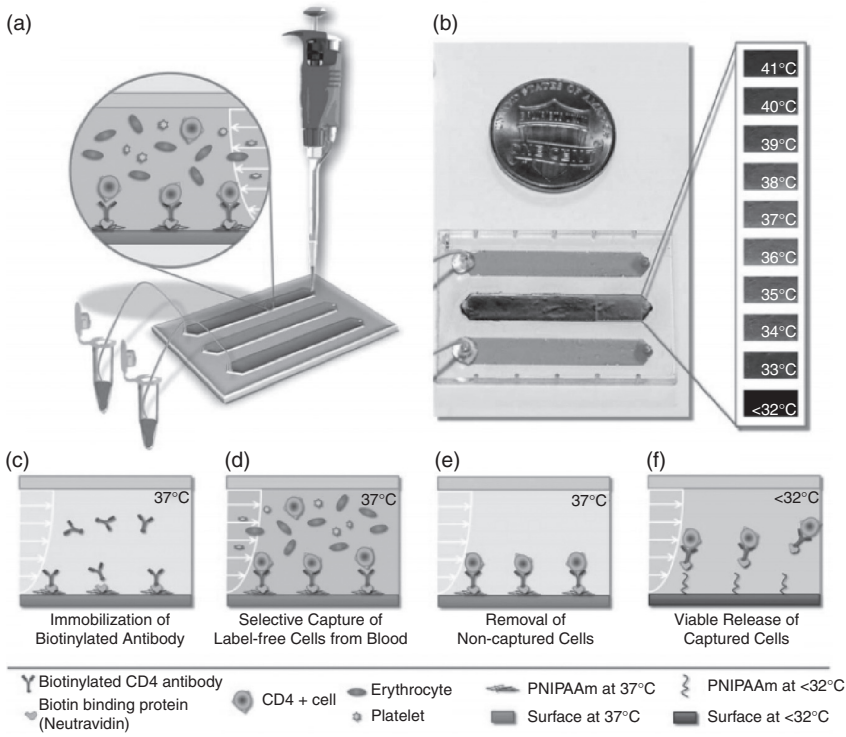

11.22 Microfluidic cell sorting devices based on marker-dependent or label-free approaches. Thermo-responsive microfluidic chip developed for releasing selectively captured cells from blood. (*Source*: Reprinted by permission from Gurkan *et al.*, 2011.) (a) The microfluidic chip is composed of three parallel channels (4 mm × 22 mm × 80 mm), one of which (middle channel) is used as the temperature indicator channel. Blood is introduced into the top and bottom release channels with manual pipetting. (b) The middle channel is coated with temperature sensitive liquid crystal dye, which is responsive to temperatures between 35°C and 40°C. The target temperature is maintained in the middle channel. (c–f) Schematic of the working principle of label-free selective capture from whole blood and controlled release of cells in thermo-responsive microfluidic channels.

ease and considerable timesaving (Baret *et al.*, 2009; Kiermer, 2005). Based on the detection method utilized, microfluidic cell sorting devices can be classified as either marker-dependent or label-free (Figs 11.22–11.26). The marker-dependent approach relies on the identification of specific cell surface protein expression levels. For example, thermo-responsive microfluidics has been used to selectively release captured cells from blood (Fig. 11.22) (Gurkan *et al.*, 2011). In this case, the authors used anti-CD4 and anti-CD34 antibodies immobilized in a microfluidic device to capture CD4+ and CD34+

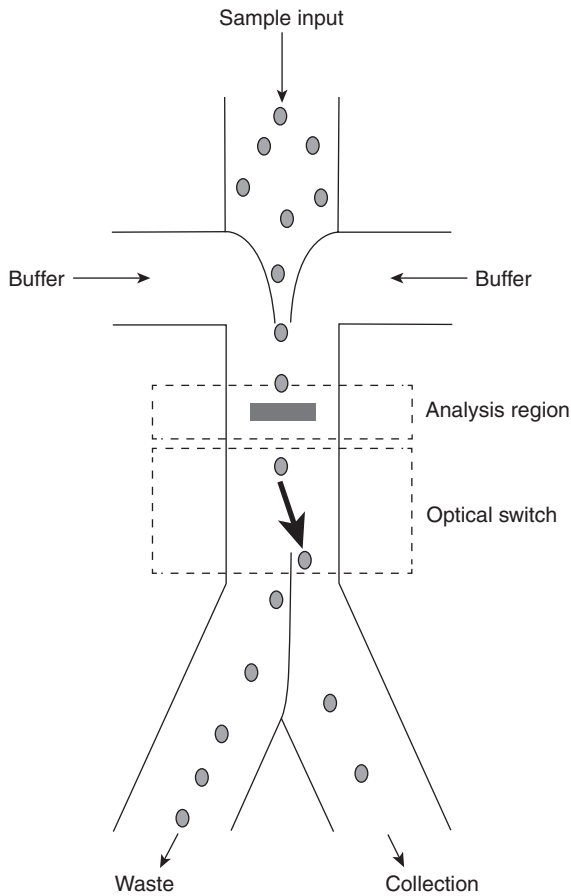

11.23 Layout of a microfluidic based cell sorting system showing the sorting junction and optical switch. (*Source*: Reprinted by permission from Wang *et al.*, 2005.) Cells in the sample are aligned to the center of the channel by flow focusing. Fluorescently labeled target cells are analyzed and detected by turning on the optical switch. Target cells are directed by the laser to the collection output while all other cells flow to the waste output.

cells from blood. Cooling the microchip below 32°C led to release of the collected cells. 195 CD4+ cells and 19 CD34+ cells per million blood cells were successfully quantified without labeling using this affinity microfluidics device. Optical switching based fluorescence-activated microfluidic cell sorters have been also developed to isolate green fluorescent protein (GFP) expressing cells (Fig. 11.23) (Wang *et al.*, 2004). When GFP expressing cells are detected and determined to be a target cell, the optical switch is activated

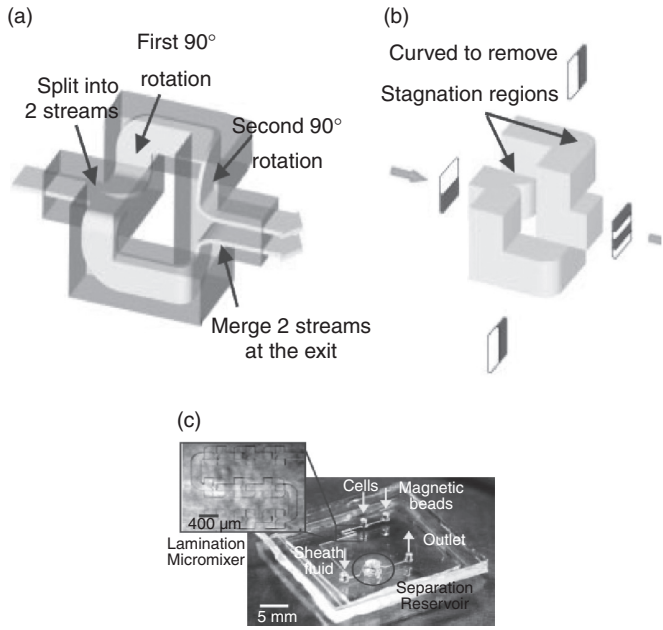

11.24 Micro-magnetic separators for stem cell sorting. (*Source*: Reprinted by permission from Tan *et al.*, 2005.) (a) Lamination micro-mixer with 180° rotation. (b) Geometry of a single mixer unit. (c) Prototype μ-IMCS.

and a focused laser spot deflects the cell to the target output channel. The laser spot is translated at a speed matched to the flow velocity and at a small angle relative to the axis of the flow to maximize the interaction time between the laser and the cell. The resulting lateral displacement of the cell across the flow stream is sufficient to ensure that it will be directed toward the target output channel. In addition, MACS has been achieved in microfluidics for stem cell extraction (Fig. 11.24) (Tan *et al.*, 2005). Anti-CD31 (PECAM1) monoclonal antibody-conjugated magnetic beads were introduced into the microfluidics device to remove human umbilical cord vein endothelial cells (HUVEC) from a mixture of HUVEC and hMSC cells introduced into the device at the same time through the other channel. The two streams are completely mixed in the micro-mixer and the cell–bead complexes separated into the buffer fluid by an external magnetic field. For the label-free approach, unique biophysical characterizations, such as size and electrophysiological properties of the membrane, are required to enable the label-free cell separation in microfluidic devices. Various microfluidics-based cell sorters that are used to isolate stem cells are summarized in Table 11.1.

Table 11.1 Microfluidics devices for stem cell isolation/separation

Isolation method	Details of isolation	Targeted cells	Carrier medium and control cells	% recovery	% Purity/fold increase	Marker-dependent	Label-free	References
Cell affinity	Anti-EPCs marker antibody immobilized microfluidics channel (CD23, VEGFR-2, CD31 and CD146)	EPCs	MSCs, VSMCs, VECs	N/A	N/A	Yes	Yes	Plouffe *et al.*, 2009; Gurkan *et al.*, 2011b
Cell affinity	CD34 antibody immobilized PNIPAAm microfluidics channel	EPCs	Whole blood	N/A	19 cells/10^6 blood cells (EPCs/WBCs + RBCs)	Yes	Yes	Liu *et al.*, 2005
Magnetic microbead	CD31 antibody-conjugated magnetic bead	CD31-hMSCs (hMSCs)	HUVEC	90.2	N/A	Yes	Yes	Miwa *et al.*, 2005a
Magnetic microbead	Anti-SSEA1 antibody-conjugated magnetic bead.	SSEA-1+ mESCs	Heterogeneous mESCs (SSEA-1+ mESCs and SSEA-1- mESCs)	N/A	95~99.5	Yes	Yes	Sousa *et al.*, 2011
DEP-based microfluidics	N/A	Hematopoietic CD34+ stem cells	Bone marrow and peripheral blood stem cell harvests	N/A	5-fold enrichment	Yes	Yes	Talary *et al.*, 1995; Stephens *et al.*, 1996
DEP-based microfluidics	N/A	NG2+ cells AND Nestin+ cells (putative progenitor cells)	Nucleated cell fraction isolated from adipose tissue and the bulk of the erythrocytes	N/A	(1.9% ⊠ 28%) /14-fold increase	Yes	Yes	Vykoukal *et al.*, 2008b
DEP-based microfluidics	N/A	Neurons	Neurons and NSPCs,	N/A	1.4-fold enrichment to neuron culture	Yes	Yes	Prieto *et al.*, 2012
Size	Louver-array structure	AFMSCs	Endothelial cells in amniotic fluid	97.1 %	N/A	No	Yes	Wu *et al.*, 2009a
Size	Porous membrane integrated microfluidics	HSCs	Bone marrow	98%	N/A	No	Yes	Schirhagl *et al.*, 2011

11.6.1 Marker-dependent approach

Fluorescence-activated stem cell sorting

FACS, the golden standard for conventional stem cell separation, has also been developed in microfluidics to isolate rare cells. Although developing a practical technology for microfluidic-based FACS has proved challenging, Wang *et al.* took a unique approach to developing this technology by first integrating an optical switching system for the rapid (2–4 ms), active control of cell routing on a microfluidics chips (Fig. 11.23) (Wang *et al.*, 2004). Using all-optical switching, a fluorescence-activated microfluidic cell sorter has been implemented and evaluated. This study suggests the possibility of integrating FACS on a microfluidic chip to allow more precise analysis of stem cells in real-time.

Magnetic-activated stem cell sorting

MACS, one of the most popular conventional cell isolation methods, has recently been developed in microfluidics to isolate rare cells. Tan and colleagues first introduced micro-magnetic separators for stem cell sorting (Fig. 11.24) (Tan *et al.*, 2005). A 3D mixer was integrated in a microfluidic channel to achieve lamination with 180-degree rotations and rapid mixing between cells and magnetic beads. To isolate the target cell from the mixture, magnetic beads conjugated with CD31 antibodies were used to remove CD31+ endothelial cells with an external magnetic field. Up to 90.2% of hMSCs were isolated and recovered. In addition, Souse and colleagues introduced a two-inlet/two-outlet microfluidics device to isolate mouse mESCs using super-paramagnetic particles. To isolate specific embryonic antigen 1 positive (SSEA-1+) mESCs from a heterogeneous population of mESCs, anti-SSEA-1 antibodies were conjugated onto super-paramagnetic beads and mixed with the cell mixture. Once the mixture was injected into the microfluidics channel and the magnetic field was applied, SSEA-1+ mESCs were deviated from the direction of laminar flow according to their magnetic susceptibility and were thus separated from SSEA-1$^-$ mESCs.

Cell affinity-based stem cell isolation

Affinity chromatography is one of the most popular methods for separation, isolation, and purification of target biomolecules from whole mixtures based on highly sensitive and specific interactions between antigen and antibody, or receptor and ligand. Brian and colleagues developed microfluidics-based cell affinity devices that have the capability of capturing circulating endothelial progenitor cells (EPC) (Plouffe *et al.*, 2009), suggesting its

potential application for MSC isolation. Gurkan and colleagues developed a thermo-responsive microfluidics device for selectively releasing captured cells from blood (Fig. 11.22) (Gurkan *et al.*, 2011). Anti-human CD34+ antibodies were immobilized in a PNIPAAm microfluidics channel at 37°C; when blood containing CD34+ stem cells was injected into the channel (e.g. to capture CD34+ EPCs) the CD34+ cells were successfully captured from the whole blood. To release the captured cells, the microfluidics device was then cooled down below 32°C. The released cells displayed greater than 90% viability by a live/dead assay.

11.6.2 Label-free approach

Electrophysiological properties

Isolating specific progenies and progenitor cells based on their distinct behavior under the exposure of an AC electric field represents a new approach in the stem cell field. Contrary to conventional techniques, which rely on the presence of specific cell surface markers, DEP separates cells based on cells' intrinsic dielectric characteristics without the need of labeling. Talary and colleagues first demonstrated the potential usage of DEP in a HSC sorter (Talary *et al.*, 1995). By applying a sinusoidal AC electric field (6 V peak–peak at 5 kHz), they found a 5.9-fold enrichment of CD34+ cells (0.84–4.97%) trapped in the integrated castellated electrode. Similarly, Stephens and colleagues utilized the same platform to isolate CD34+ cells directly from the diluted peripheral blood stem cell harvests. They demonstrated a nearly five fold increase in the frequency of the CD34+ cells populations in the fractions collected within the 50–10 kHz range. They further confirmed that the isolated CD34+ cells were capable of forming colonies using a colony formation assay. These two studies demonstrate the possibility of exploiting DEP as a non-invasive and label-free sorting approach in the stem cell field.

Recently, Prieto and colleagues developed a dielectrophoretic assisted cell sorting (DACS) array, which consists of a DEP electrode array with three multiplexed trapping regions that can be independently activated at different frequencies. This device was used to separate a mixture of NSPCs and differentiated neurons (Fig. 11.25) (Prieto *et al.*, 2012). They reported the first statistically significant neural cell sorting using DACS to enrich neurons from a heterogeneous population of mouse derived NSPCs and differentiated neurons. A 1.4-fold neuronal enrichment was achieved. In addition, Vykoukal and co-workers developed a dielectrophoretic field-flow fractionation separator (DEP-FFF) using a novel microfluidics–microelectronic hybrid flex-circuit fabrication approach. They applied DEP-FFF to separation putative stem cells (NG2+) from adipose tissue (Vykoukal *et al.*, 2008).

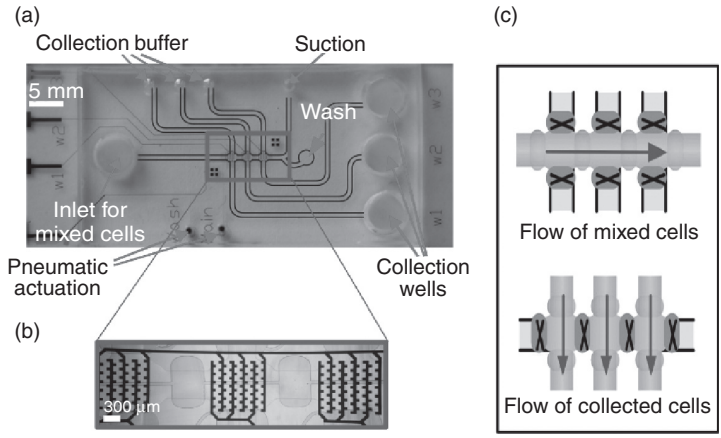

11.25 DEP-based microfluidics cell sorter. (*Source*: Reprinted by permission from Prieto *et al.*, 2012.) (a) PDMS-glass microfluidic device for DEP trapping. (b) The device has three trapping sites with castellated electrodes that can be independently addressed. The initial mixture of cells flows through all three trapping sites. (c) The collection is done with three perpendicular flows after isolating each trapping zone by closing adjacent pneumatic valves.

In this study, a nucleated cell fraction from cell debris and the bulk of the erythrocyte population was first isolated from adipose tissue. By introducing the cell fraction into the DEP-FFF, they found a 14-fold enrichment in the NG2+ cell population (2–28% purity). They further identified that NG2+ cell enrichment is coincident with Nestin+ cell enrichment, indicating that the isolation of the cells occurred in the early developmental stage. These studies imply that the intrinsic dielectric characteristic of cells could be used as a label-free approach for stem cell isolation for transplantation.

Size differences

Size difference between distinct cell types and between subpopulations of HSCs has been well recognized and could be used as a parameter for stem cell sorting. For example, the presence of MSCs in amniotic fluid (AF) is an attractive cell source, as MSCs do not have the same ethical issues that surround ESCs. A variety of cells are present in the AF, including stem cells, amniotic cells, and many dead epithelial cells with diameters of 4–6 µm, 15–20 µm, and 40–60 µm, respectively. Taking this into consideration, Wu and colleagues developed a microfluidic device to isolate MSCs from amniotic fluid using a combination of a T-junction focusing structure and a louver-like structure to isolate amniotic fluid MSCs (AFMSCs) (Fig. 11.26) (Wu *et al.*, 2009a). Another example of size-based stem cell isolation was introduced recently by Schirhagl and colleagues (Schirhagl *et al.*, 2011). Their layered

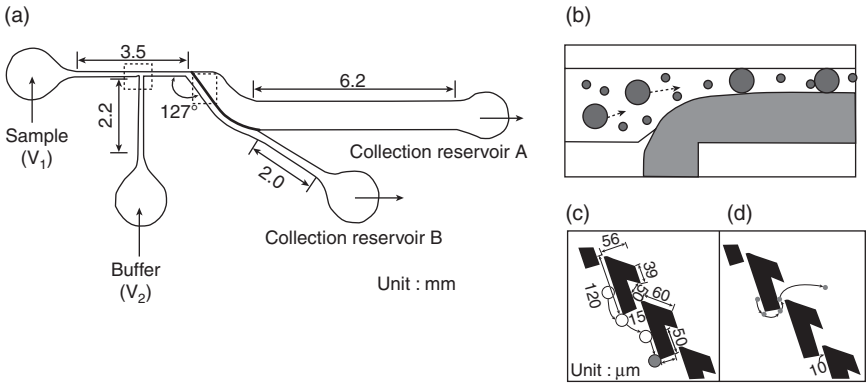

11.26 Microfluidic device for separation of AF MSCs utilizing louver-array structures. (*Source*: Reprinted by permission from Wu *et al.*, 2009.) (a) Schematic illustration of the cell separation chip. (b) Detailed view showing that beads or cells can be focused to form a narrow stream. (c) and (d) Detailed dimensions of the chip and cell separation mechanism. (c) The larger beads or cells are separated by the louver-like structures. (d) The smaller beads or cells flow through the gap between the louver-like structures.

microfluidics device was fabricated to generate a sorter that could simultaneously valve and filter. The top and bottom layers contained channels and pressure-valves, while the middle layer was a PDMS porous membrane (pore size: 10, 15, or 20 μm). The porous membrane was fabricated using soft lithography and it was integrated between the microfluidics layers. Because HSCs are larger in size than other cells present in bone marrow, with the exception of monocytes, HSCs were successfully isolated from human bone marrow samples without any sample pre-treatment. At smaller pore sizes (≤15 μm), stem cell isolation efficiency was significantly increased.

11.7 Conclusion and future trends

For practical therapeutic purposes, ESCs hold greater therapeutic potential compared to adult stem cells due to their multipotency *in vivo*, as they are an unlimited source of any kind of adult stem cells. However, the ethical implications surrounding the way in which ESCs are obtained prevent ESC-based therapeutics reaching their full potential as a viable option for clinical applications. To circumvent this issue, Takahashi and Yamanaka discovered a process in 2006, called de-differentiation, to reprogram differentiated adult fibroblasts back to an embryonic-like state by introducing four transcriptional factors, Oct3/4, Sox2, c-Myc, and Klf4, under ES cell culture conditions (Takahashi and Yamanaka, 2006). These derived stem cells were designated as induced pluripotent stem cells (iPS cells) – adult stem cells that not only exhibit the

morphology and growth properties of ESCs, but also express ES cell marker genes. Because of the similarities between ESCs and iPS cells in differentiation potential and the absence of ethical issues that surround human ES research, iPS cells have great clinical potential in regenerative medicine. Microfluidics will certainly play a role in the development of the iPS field in the future. In particular, microfluidics offers unique opportunities to assess the viability, differentiation potential, and heterogeneity of these cells in a high-throughput manner. In addition, the fine control of chemical and physical gradients allowed with microfluidic techniques also offer great utility in regulating the differentiation and understanding the biology of iPS cells.

Ethical issues are not the only concerns surrounding stem cell research. Because stem cell biology is not completely understood, their use in clinical applications remains uncertain. Stem cell migration and homing are mechanisms that are continually investigated, as the exact mechanisms of stem cell recruitment and migration is vastly unknown. Nevertheless, microfluidic devices have enabled new discoveries in identifying some of the key mechanisms involved in stem cell recruitment and migration. In response to injury or inflammation, stem cells may be mobilized into the circulatory system; to migrate to these areas, they must interact with the local endothelium and extravasate into the surrounding tissue. Recently, vascular microenvironments were mimicked in microfluidic devices by cultivating endothelial cells in the microfluidic channels. The microenvironment of a blood vessel, including shear stress, cellular interactions between multiple co-cultured cells, and microstructures, could be incorporated into the device. Based on microfluidic artificial blood vessels (MABV), various cell migration and cell invasion assays were developed. Kamm and colleagues developed a co-cultivating microfluidics device in which cancer and endothelial cells were co-cultured. After co-culturing both cells for four days, endothelial cells migrated toward MTLn3 cells, a highly invasive breast adenocarcinoma cell line (Chung *et al.*, 2009). Similar co-culture microfluidic devices were also constructed to investigate hepatocyte-induced blood vessel formation (angiogenesis) in microfluidics (Chung *et al.*, 2009). Unfortunately, we do not yet have an example of stem cell migration research using MABVs, although these devices hold great potential to yield tremendous opportunities in understanding stem cell migration and homing mechanisms.

Specifically, through microfluidics-based vasculature research, critical roles of endothelial selectins (P and E) and vascular cell adhesion molecule-1 (VCAM-1) have been identified in hematopoietic progenitor cells (HPCs) homing to the BM (Frenette *et al.*, 1998; Mazo *et al.*, 1998). Recently microfluidics-based cell rolling has been achieved with by coating the device with a molecule, P-selectin, which stimulates cell rolling (Choi *et al.*, 2012). The P-selectin coated microfluidic channels have repetitive slant ridges with

trenches in between. The target cells roll through the slant ridges via interaction between the P-selectin on slant ridges and the ligand on the cell surface. The cells eventually roll through the trenches and flow into a collecting chamber. In the future, we anticipate that similar devices will be used to both understand the normal interactions of other stem cells with endothelial adhesion ligands as well as engineer therapies that maximize these interactions for therapeutic interventions.

During injury and inflammation, adult stem cells are mobilized to the circulatory system (Roufosse *et al.*, 2004). Specifically, multiple groups have observed an increase in MSC populations in the vasculature following injury. Although the functional role of these circulating MSCs remains poorly understood, similar processes may underlie MSC recruitment to tumors and inflamed tissues (Karnoub *et al.*, 2007). Unfortunately, current techniques make studying the individual steps underlying this phenomenon difficult. In particular, current intravital microscopy techniques are difficult to apply to the processes of intravasation into the bloodstream and extravasation into distant organs. Understanding the fundamental biology of stem cell recruitment and homing has major implications for influencing therapeutic applications of these cells as they become more widely used in diverse clinical settings (Karp and Teol, 2009).

In recent years, the concept of the cancer stem cell (CSC) has become a new paradigm for understanding cancer initiation, progression, and response to therapies (Visvader and Lindeman, 2012). The fundamental hypothesis is that a cellular subpopulation of the tumor possesses both self-renewal abilities and the capacity to give rise to other, differentiated cells in the tumor. Recent observations have suggested that CSCs themselves are responsible for the spread of cancer cells to other organs in the process of metastasis (Baccelli and Trumpp, 2012). As metastasis involves intravasation into the blood stream, tropism to cancer-specific secondary organs, and eventual extravasation into those organs, microfluidics offers numerous opportunities to reveal the biology underlying CSC-driven metastasis (Valastyan and Weinberg, 2011). The central role of CSCs in sustaining tumor growth and progression suggests that therapies specifically targeting the CSC or its associated niche could more effectively treat cancer. Microfluidics again offers opportunities to accelerate the identification of novel pathways and targets through novel drug screening platforms. In addition, microfluidics has a clear role to play in the isolation of CSCs from the heterogeneous cell population of primary tumors. As current markers for CSCs vary widely between cancers types, the label-free technologies described above, including DEP, will be interesting to apply to the detection and isolation of CSCs.

Additionally, future trends in microfluidic-based stem cell research will be focused on developing technologies to effectively screen drug candidates, investigate stem cell differentiation, and test the efficacy of engineered stem

cells in an *in vitro* model that closely mimics human biology. Microfluidics could be used to assess potential drugs for pregnant women as drugs can be harmful to the fetus in the womb, microfluidics can be a useful tool to safely screen side effects of the drug candidates on ESCs. Furthermore, drug companies could use this platform to further enhance their stringency tests during drug development. Alternatively, microfluidics can be used to differentiate, analyze, and sort stem cells for the purposes of cell therapy. Ultimately, through investigating stem cells with microfluidic devices, it may be possible to control stem cell differentiation to develop artificial organs/tissues and to repair damaged internal body systems. In the future, integration of multiple 'organs on a chip' to generate microfluidic systems that mimic the full range of physiology of humans may be useful for understanding normal biology, disease processes, and the role of stem cells in these processes. For these reasons, companies such as Aldagen (http://www.aldagen.com) and Innovative Micro Technology (IMT, http://www.imtmems.com/) focus on the development of microfluidic devices dealing with stem cells. In the near future, microfluidic-based systems will become a powerful platform not only for fundamental stem cell research, but also for stem cell-based clinical applications.

11.8 Sources of further information and advice

Sun, Y. B., Weng, S. and Fu, J. P. (2012). Microengineered synthetic cellular microenvironment for stem cells. Wiley Interdisciplinary Reviews-*Nanomedicine and Nanobiotechnology*, **4**, 414–27.

Lutolf, M. P. and Blau, H. M. (2009). Artificial stem cell niches. *Adv Mater*, **21**, 3255–68.

Ashton, R. S., Keung, A. J., Peltier, J. and Schaffer, D. V. (2011). Progress and prospects for stem cell engineering. *Annu Rev Chem Biomol Eng*, **2**, 479–502.

Gossett, D. R., Weaver, W. M., Mach, A. J., Hur, S. C., Tse, H. T., Lee, W., Amini, H. and di Carlo, D. (2010). Label-free cell separation and sorting in microfluidic systems. *Anal Bioanal Chem*, **397**, 3249–67.

Squires, T. M. and Quake, S. R. (2005). Microfluidics: Fluid physics at the nanoliter scale. *Rev Modern Phys*, **77**, 977–1026.

Beebe, D. J., Mensing, G. A. and Walker, G. M. (2002). Physics and applications of microfluidics in biology. *Annu Rev Biomed Eng*, **4**, 261–86.

11.9 References

Abhyankar, V. V., Lokuta, M. A., Huttenlocher, A. and Beebe, D. J. (2006). Characterization of a membrane-based gradient generator for use in cell-signaling studies. *Lab Chip,* **6**, 389–93.

Altman, J. and Das, G. D. (1965). Autoradiographic and histological evidence of postnatal hippocampal neurogenesis in rats. *J Comp Neurol,* **124**, 319–35.

Alvarez-Buylla, A., Seri, B. and Doetsch, F. (2002). Identification of neural stem cells in the adult vertebrate brain. *Brain Res Bull,* **57**, 751–8.

Anderson, D. G., Levenberg, S. and Langer, R. (2004). Nanoliter-scale synthesis of arrayed biomaterials and application to human embryonic stem cells. *Nat Biotechnol,* **22**, 863–6.

Aran, K., Fok, A., Sasso, L. A., Kamdar, N., Guan, Y. L., Sun, Q., Undar, A. and Zahn, J. D. (2011). Microfiltration platform for continuous blood plasma protein extraction from whole blood during cardiac surgery. *Lab Chip,* **11**, 2858–68.

Baccelli, I. and Trumpp, A. (2012). The evolving concept of cancer and metastasis stem cells. *J Cell Biol,* **198**, 281–93.

Bagnaninchi, P. O. and Drummond, N. (2011). Real-time label-free monitoring of adipose-derived stem cell differentiation with electric cell-substrate impedance sensing. *Proc Natl Acad Sci USA,* **108**, 6462–7.

Baret, J.-C., Miller, O. J., Taly, V., Ryckelynck, M., El-Harrak, A., Frenz, L., Rick, C., Samuels, M. L., Hutchison, J. B., Agresti, J. J., Link, D. R., Weitz, D. A. and Griffiths, A. D. (2009). Fluorescence-activated droplet sorting (FADS): efficient microfluidic cell sorting based on enzymatic activity. *Lab Chip,* **9**, 1850–8.

Becker, F. F., Wang, X. B., Huang, Y., Pethig, R., Vykoukal, J. and Gascoyne, P. R. C. (1995). Separation of human breast-cancer cells from blood by differential dielectric affinity. *Proc Natl Acad Sci U S A,* **92**, 860–4.

Bellan, L. M., Singh, S. P., Henderson, P. W., Porri, T. J., Craighead, H. G. and Spector, J. A. (2009). Fabrication of an artificial 3-dimensional vascular network using sacrificial sugar structures. *Soft Matter,* **5**, 1354.

Blagovic, K., Kim, L. Y. and Voldman, J. (2011). Microfluidic perfusion for regulating diffusible signaling in stem cells. *PLoS One,* **6**, e22892.

Boheler, K. R. (2010). Pluripotency of human embryonic and induced pluripotent stem cells for cardiac and vascular regeneration. *Thromb Haemost,* **104**, 23–9.

Bu, M. Q., Melvin, T., Ensell, G., Wilkinson, J. S. and Evans, A. G. R. (2003). Design and theoretical evaluation of a novel microfluidic device to be used for PCR. *J Micromech Microeng,* **13**, S125–30.

Burt, R. K., Testori, A., Craig, R., Cohen, B., Suffit, R. and Barr, W. (2008). Hematopoietic stem cell transplantation for autoimmune diseases: What have we learned? *J Autoimmun,* **30**, 116–20.

Cai, L., Friedman, N. and Xie, X. S. (2006). Stochastic protein expression in individual cells at the single molecule level. *Nat Cell Biol,* **440**, 358–62.

Chen, C. Y., Wo, A. M. and Jong, D. S. (2012). A microfluidic concentration generator for dose-response assays on ion channel pharmacology. *Lab Chip,* **12**, 794–801.

Chin, V. I., Taupin, P., Sanga, S., Scheel, J., Gage, F. H. and Bhatia, S. N. (2004). Microfabricated platform for studying stem cell fates. *Biotechnol Bioeng,* **88**, 399–415.

Choi, S., Karp, J. M. and Karnik, R. (2012). Cell sorting by deterministic cell rolling. *Lab Chip,* **12**, 1427–30.

Chung, B. G., flanagan, L. A., Rhee, S. W., Schwartz, P. H., Lee, A. P., Monuki, E. S. and Jeon, N. L. (2005). Human neural stem cell growth and differentiation in a gradient-generating microfluidic device. *Lab Chip,* **5**, 401–6.

Chung, B. G., Park, J. W., Hu, J. S., Huang, C., Monuki, E. S. and Jeon, N. L. (2007). A hybrid microfluidic-vacuum device for direct interfacing with conventional cell culture methods. *BMC Biotechnol,* **7**, 60.

Chung, S., Sudo, R., Mack, P. J., Wan, C. R., Vickerman, V. and Kamm, R. D. (2009). Cell migration into scaffolds under co-culture conditions in a microfluidic platform. *Lab Chip,* **9**, 269–75.

Clewes, O., Narytnyk, A., Gillinder, K. R., Loughney, A. D., Murdoch, A. P. and Sieber-Blum, M. (2011). Human epidermal neural crest stem cells (hEPI-NCSC) – characterization and directed differentiation into osteocytes and melanocytes. *Stem Cell Rev,* **7**, 799–814.

Crews, N., Wittwer, C. and Gale, B. (2008). Continuous-flow thermal gradient PCR. *Biomed Microdevices,* **10**, 187–95.

Csete, M. (2010). Q&A: What can microfluidics do for stem-cell research? *J Biol,* **9**, 1.

Dahan, E., Bize, V., Lehnert, T., Horisberger, J. D. and Gijs, M. A. M. (2008). Rapid fluidic exchange microsystem for recording of fast ion channel kinetics in Xenopus oocytes. *Lab Chip,* **8**, 1809–18.

Davenport, R. J. (2005). What controls organ regeneration. *Science,* **309**, 84.

Demello, A. J. (2006). Control and detection of chemical reactions in microfluidic systems. *Nature,* **442**, 394–402.

Dhof, T. C. S. U., Wernig, M., Citri, A., Pang, Z. P. and Malenka, R. C. (2011). Comprehensive qPCR profiling of gene expression in single neuronal cells. *Nat Protoc,* **7**, 1–10.

Dupin, E. and Coelho-Aguiar, J. M. (2012). Isolation and differentiation properties of neural crest stem cells. *Cytometry A*, **83**, 38–47.

El-Ali, J., Sorger, P. K. and Jensen, K. F. (2006). Cells on chips. *Nature,* **442**, 403–11.

Ellison, D., Munden, A. and Levchenko, A. (2009). Computational model and microfluidic platform for the investigation of paracrine and autocrine signaling in mouse embryonic stem cells. *Mol BioSyst,* **5**, 1004.

Engler, A. J., Sen, S., Sweeney, H. L. and Discher, D. E. (2006). Matrix elasticity directs stem cell lineage specification. *Cell,* **126**, 677–89.

Fatoyinbo, H. O., Hoettges, K. F. and Hughes, M. P. (2008). Rapid-on-chip determination of dielectric properties of biological cells using imaging techniques in a dielectrophoresis dot microsystem. *Electrophoresis,* **29**, 3–10.

Fiedler, S., Shirley, S. G., Schnelle, T. and Fuhr, G. (1998). Dielectrophoretic sorting of particles and cells in a microsystem. *Anal Chem,* **70**, 1909–15.

Flaim, C. J., Chien, S. and Bhatia, S. N. (2005). An extracellular matrix microarray for probing cellular differentiation. *Nat Methods,* **2**, 119–25.

Flaim, C. J., Teng, D., Chien, S. and Bhatia, S. N. (2008). Combinatorial signaling microenvironments for studying stem cell fate. *Stem Cells Dev,* **17**, 29–40.

Flanagan, L. A., Lu, J., Wang, L., Marchenko, S. A., Jeon, N. L., Lee, A. P. and Monuki, E. S. (2008). Unique dielectric properties distinguish stem cells and their differentiated progeny. *Stem Cells,* **26**, 656–65.

Frenette, P. S., Subbarao, S., Mazo, I. B., von Andrian, U. H. and Wagner, D. D. (1998). Endothelial selectins and vascular cell adhesion molecule-1 promote hematopoietic progenitor homing to bone marrow. *Proc Natl Acad Sci U S A,* **95**, 14423–8.

Fu, A. Y., Spence, C., Scherer, A., Arnold, F. H. and Quake, S. R. (1999). A microfabricated fluorescence-activated cell sorter. *Nat Biotechnol,* **17**, 1109–11.

Fuhr, G., Müller, T., Schnelle, T., Hagedorn, R., Voigt, A., Fiedler, S., Arnold, W. M., Zimmermann, U., Wagner, B. and Heuberger, A. (1994). Radio-frequency microtools for particle and liver cell manipulation. *Die Naturwissenschaften,* **81**, 528–35.

Fukuda, J., Khademhosseini, A., Yeo, Y., Yang, X. Y., Yeh, J., Eng, G., Blumling, J., Wang, C. F., Kohane, D. S. and Langer, R. (2006). Micromolding of photo-

crosslinkable chitosan hydrogel for spheroid microarray and co-cultures. *Biomaterials,* **27**, 5259–67.

Fung, W.-T., Beyzavi, A., Abgrall, P., Nguyen, N.-T. and Li, H.-Y. (2009). Microfluidic platform for controlling the differentiation of embryoid bodies. *Lab Chip,* **9**, 2591.

Gagnon, Z. R. (2011). Cellular dielectrophoresis: applications to the characterization, manipulation, separation and patterning of cells. *Electrophoresis,* **32**, 2466–87.

Gehling, U. M., Ergun, S., Schumacher, U., Wagener, C., Pantel, K., OTTE, M., Schuch, G., Schafhausen, P., Mende, T., Kilic, N., Kluge, K., Schafer, B., Hossfeld, D. K. and Fiedler, W. (2000). In vitro differentiation of endothelial cells from AC133-positive progenitor cells. *Blood,* **95**, 3106–12.

Glotzbach, J. P., Januszyk, M., Vial, I. N., Wong, V. W., Gelbard, A., Kalisky, T., Thangarajah, H., Longaker, M. T., Quake, S. R., Chu, G. and Gurtner, G. C. (2011). An information theoretic, microfluidic-based single cell analysis permits identification of subpopulations among putatively homogeneous stem cells. *Plos One,* **6**, e21211.

Guilak, F., Cohen, D. M., Estes, B. T., Gimble, J. M., Liedtke, W. and Chen, C. S. (2009). Control of stem cell fate by physical interactions with the extracellular matrix. *Stem Cell,* **5**, 17–26.

Guo, M. T., Rotem, A., Heyman, J. A. and Weitz, D. A. (2012). Droplet microfluidics for high-throughput biological assays. *Lab Chip,* **12**, 2146.

Gupta, K., Kim, D.-H., Ellison, D., Smith, C., Kundu, A., Tuan, J., Suh, K. Y. and Levchenko, A. (2010). Lab-on-a-chip devices as an emerging platform for stem cell biology. *Lab Chip,* **10**, 2019.

Gurkan, U. A., Anand, T., Tas, H., Elkan, D., Akay, A., Keles, H. O. and Demirci, U. (2011). Controlled viable release of selectively captured label-free cells in microchannels. *Lab Chip,* **11**, 3979–89.

Hoettges, K. F., Hübner, Y., Broche, L. M., Ogin, S. L., Kass, G. E. N. and Hughes, M. P. (2008). Dielectrophoresis-activated multiwell plate for label-free high-throughput drug assessment. *Anal Chem,* **80**, 2063–8.

Holmes, D., Pettigrew, D., Reccius, C. H., Gwyer, J. D., van Berkel, C., Holloway, J., Davies, D. E. and Morgan, H. (2009). Leukocyte analysis and differentiation using high speed microfluidic single cell impedance cytometry. *Lab Chip,* **9**, 2881–9.

Hosokawa, M., Hayata, T., Fukuda, Y., Arakaki, A., Yoshino, T., Tanaka, T. and Matsunaga, T. (2010). Size-selective microcavity array for rapid and efficient detection of circulating tumor cells. *Anal Chem,* **82**, 6629–35.

Hu, X. Y., Bessette, P. H., Qian, J. R., Meinhart, C. D., Daugherty, P. S. and Soh, H. T. (2005). Marker-specific sorting of rare cells using dielectrophoresis. *Proc Natl Acad Sci U S A,* **102**, 15757–61.

Huang, C. P., Lu, J., Seon, H., Lee, A. P., Flanagan, L. A., Kim, H.-Y., Putnam, A. J. and Jeon, N. L. (2009). Engineering microscale cellular niches for three-dimensional multicellular co-cultures. *Lab Chip,* **9**, 1740–8.

Huang, L. R., Cox, E. C., Austin, R. H. and Sturm, J. C. (2004). Continuous particle separation through deterministic lateral displacement. *Science,* **304**, 987–90.

Huh, D., Matthews, B. D., Mammoto, A., Montoya-Zavala, M., Hsin, H. Y. and Ingber, D. E. (2010). Reconstituting organ-level lung functions on a chip. *Science,* **328**, 1662–8.

Hui, E. E. and Bhatia, S. N. (2007). Micromechanical control of cell-cell interactions. *Proc Natl Acad Sci U S A,* **104**, 5722–6.

Hur, S. C., Henderson-MacLennan, N. K., McCabe, E. R. B. and di Carlo, D. (2011). Deformability-based cell classification and enrichment using inertial microfluidics. *Lab Chip,* **11**, 912–20.

Irimia, D., Geba, D. A. and Toner, M. (2006). Universal microfluidic gradient generator. *Anal Chem,* **78**, 3472–7.

Jeon, N. L., Dertinger, S. K. W., Chiu, D. T., Choi, I. S., Stroock, A. D. and Whitesides, G. M. (2000). Generation of solution and surface gradients using microfluidic systems. *Langmuir,* **16,** 8311–16.

Jiang, Y., Jahagirdar, B. N., Reinhardt, R. L., Schwartz, R. E., Keene, C. D., Ortiz-Gonzalez, X. R., Reyes, M., Lenvik, T., Lund, T., Blackstad, M., Du, J., Aldrich, S., Lisberg, A., Low, W. C., Largaespada, D. A. and Verfaillie, C. M. (2002). Pluripotency of mesenchymal stem cells derived from adult marrow. *Nature,* **418**, 41–9.

Karnoub, A. E., Dash, A. B., Vo, A. P., Sullivan, A., Brooks, M. W., Bell, G. W., Richardson, A. L., Polyak, K., Tubo, R. and Weinberg, R. A. (2007). Mesenchymal stem cells within tumour stroma promote breast cancer metastasis. *Nature,* **449**, 557-U4.

Karp, J. M. and Teol, G. S. L. (2009). Mesenchymal stem cell homing: The devil is in the details. *Cell Stem Cell,* **4**, 206–16.

Karp, J. M., Yeh, J., Eng, G., Fukuda, J., Blumling, J., Suh, K. Y., Cheng, J., Mahdavi, A., Borenstein, J., Langer, R. and Khademhosseini, A. (2007). Controlling size, shape and homogeneity of embryoid bodies using poly(ethylene glycol) microwells. *Lab Chip,* **7**, 786–94.

Keenan, T. M., Hsu, C. H. and Folch, A. (2006). Microfluidic 'jets' for generating steady-state gradients of soluble molecules on open surfaces. *Appl Phys Lett,* **89**, 114103.

Khademhosseini, A., Ferreira, L., Blumling, J., 3rd, Yeh, J., Karp, J. M., Fukuda, J. and Langer, R. (2006). Co-culture of human embryonic stem cells with murine embryonic fibroblasts on microwell-patterned substrates. *Biomaterials,* **27**, 5968–77.

Khademhosseini, A., Yeh, J., Jon, S., Eng, G., Suh, K. Y., Burdick, J. A. and Langer, R. (2004). Molded polyethylene glycol microstructures for capturing cells within microfluidic channels. *Lab Chip,* **4**, 425–30.

Kiermer, V. (2005). FACS-on-a-chip. *Nat Methods,* **2**, 91.

Kim, S., Kim, H. J. and Jeon, N. L. (2010). Biological applications of microfluidic gradient devices. *Integr Biol,* **2**, 584–603.

Kim, U., Shu, C. W., Dane, K. Y., Daugherty, P. S., Wang, J. Y. J. and Soh, H. T. (2007). Selection of mammalian cells based on their cell-cycle phase using dielectrophoresis. *Proc Natl Acad Sci U S A,* **104**, 20708–12.

Kobel, S. A., Burri, O., Griffa, A., Girotra, M., Seitz, A. and Lutolf, M. P. (2012). Automated analysis of single stem cells in microfluidic traps. *Lab Chip,* **12**, 2843–9.

Kopp, M. U., de Mello, A. J. and Manz, A. (1998). Chemical amplification: Continuous-flow PCR on a chip. *Science,* **280**, 1046–8.

Kumachev, A., Greener, J., Tumarkin, E., Eiser, E., Zandstra, P. W. and Kumacheva, E. (2011). High-throughput generation of hydrogel microbeads with varying elasticity for cell encapsulation. *Biomaterials,* **32**, 1477–83.

Labeed, F., LU, J., Mulhall, H., Marchenko, S., Hoettges, K., Estrada, L., Lee, A., Hughes, M. and Flanagan, L. (2011). Biophysical characteristics reveal neural stem cell differentiation potential. *PLoS one,* **6**, e25458.

Lanfer, B., Seib, F. P., Freudenberg, U., Stamov, D., Bley, T., Bornhäuser, M. and Werner, C. (2009). The growth and differentiation of mesenchymal stem and progenitor cells cultured on aligned collagen matrices. *Biomaterials,* **30**, 5950–8.

Lanza, R. P., Hayes, J. L. and Chick, W. L. (1996). Encapsulated cell technology. *Nat Biotechnol,* **14**, 1107–11.

Lecault, V., Vaninsberghe, M., Sekulovic, S., Knapp, D. J., Wohrer, S., Bowden, W., Viel, F., McLaughlin, T., Jarandehei, A., Miller, M., Falconnet, D., White, A. K., Kent, D. G., Copley, M. R., Taghipour, F., Eaves, C. J., Humphries, R. K., Piret, J. M. and Hansen, C. L. (2011). High-throughput analysis of single hematopoietic stem cell proliferation in microfluidic cell culture arrays. *Nat Methods,* **8**, 581–6.

Lee, C. H., Bose, S., van Vliet, K. J., Karp, J. M. and Karnik, R. (2011). Examining the lateral displacement of hl60 cells rolling on asymmetric p-selectin patterns. *Langmuir,* **27**, 240–9.

Lin, F., Nguyen, C. M. C., Wang, S. J., Saadi, W., Gross, S. P. and Jeon, N. L. (2005). Neutrophil migration in opposing chemoattractant gradients using microfluidic chemotaxis devices. *Ann Biomed Eng,* **33**, 475–82.

Liu, S., Dontu, G. and wicha, M. S. (2005). Mammary stem cells, self-renewal pathways, and carcinogenesis. *Breast Cancer Res,* **7**, 86–95.

Lu, J., Barrios, C. A., Dickson, A. R., Nourse, J. L., Lee, A. P. and Flanagan, L. A. (2012). Advancing practical usage of microtechnology: a study of the functional consequences of dielectrophoresis on neural stem cells. *Integr Biol,* **4**, 1223–6.

Mach, A. J. and di Carlo, D. (2010). Continuous scalable blood filtration device using inertial microfluidics. *Biotechnol Bioeng,* **107**, 302–11.

Mach, A. J., Kim, J. H., Arshi, A., Hur, S. C. and di Carlo, D. (2011). Automated cellular sample preparation using a centrifuge-on-a-chip. *Lab Chip,* **11**, 2827–34.

Markey, A. L., Mohr, S. and Day, P. J. R. (2010). High-throughput droplet PCR. *Methods,* **50**, 277–81.

Markx, G. and Davey, C. (1999). The dielectric properties of biological cells at radiofrequencies: Applications in biotechnology. *Enz Microbial Tech,* **25**, 161–71.

Martino, G. and Pluchino, S. (2006). The therapeutic potential of neural stem cells. *Nat Rev Neurosci,* **7**, 395–406.

Mason, C. and Dunnill, P. (2008). A brief definition of regenerative medicine. *Regener Med,* **3**, 1–5.

Mazo, I. B., Gutierrez-Ramos, J. C., Frenette, P. S., Hynes, R. O., Wagner, D. D. and von Andrian, U. H. (1998). Hematopoietic progenitor cell rolling in bone marrow microvessels: Parallel contributions by endothelial selectins and vascular cell adhesion molecule 1. *J Exp Med,* **188**, 465–74.

Meyvantsson, I. and Beebe, D. J. (2008). Cell culture models in microfluidic systems. *Annu Rev Anal Chem,* **1**, 423–49.

Migliaccio, A. R., Whitsett, C., Papayannopoulou, T. and Sadelain, M. (2012). The potential of stem cells as an in vitro source of red blood cells for transfusion. *Cell Stem Cell,* **10**, 115–19.

Mohamed, H., Murray, M., Turner, J. N. and Caggana, M. (2009). Isolation of tumor cells using size and deformation. *J Chromatogr,* **1216**, 8289–95.

Moon, H. S., Kwon, K., Kim, S. I., Han, H., Sohn, J., Lee, S. and Jung, H. I. (2011). Continuous separation of breast cancer cells from blood samples using multi-orifice flow fractionation (MOFF) and dielectrophoresis (DEP). *Lab Chip,* **11**, 1118–25.

Moore, K. A. and Lemischka, I. R. (2006). Stem cells and their niches. *Science,* **311**, 1880–5.

Muller-Sieburg, C. E., Cho, R. H., Thoman, M., Adkins, B. and Sieburg, H. B. (2002). Deterministic regulation of hematopoietic stem cell self-renewal and differentiation. *Blood,* **100**, 1302–9.

Nagrath, S., Sequist, L. V., Maheswaran, S., Bell, D. W., Irimia, D., Ulkus, L., Smith, M. R., Kwak, E. L., Digumarthy, S., Muzikansky, A., Ryan, P., Balis, U. J., Tompkins, R. G., Haber, D. A. and Toner, M. (2007). Isolation of rare circulating tumour cells in cancer patients by microchip technology. *Nature,* **450**, 1235–9.

Nakatomi, H., Kuriu, T., Okabe, S., Yamamoto, S., Hatano, O., Kawahara, N., Tamura, A., Kirino, T. and Nakafuku, M. (2002). Regeneration of hippocampal pyramidal neurons after ischemic brain injury by recruitment of endogenous neural progenitors. *Cell,* **110**, 429–41.

Ng ES, D. R., Azzola, L., Stanley, E. G. and Elefanty, A. G. (2005). Forced aggregation of defined numbers of human embryonic stem cells into embryoid bodies fosters robust, reproducible hematopoietic differentiation, *Blood*, **106**, 1601–3.

Niu, X. Z., Gielen, F., Edel, J. B. and Demello, A. J. (2011). A microdroplet dilutor for high-throughput screening. *Nat Chem,* **3**, 437–42.

Noebels, J. L., Avoli, M., Rogawski, M. A., Olsen, R. W., Delgado-Escueta, A. V., Naegele, J. R., Vemuri, M. C. and Studer, L. (2012). *Embryonic Stem Cell Therapy for Intractable Epilepsy,* Bethesda (MD), National Center for Biotechnology Information (US).

Northrup, M.A., Ching, R.M. and Watson, A. R. T. (1993). DNA amplification with a microfabricated reaction chamber. Proceedings of the 7th International Conference on Solid State Sensors and Actuators, 1993 Yokohama, Japan, 924–6.

Notta, F., Doulatov, S., Laurenti, E., Poeppl, A., Jurisica, I. and Dick, J. E. (2011). Isolation of single human hematopoietic stem cells capable of long-term multilineage engraftment. *Science,* **333**, 218–21.

Park, H. E., Kim, D., Koh, H. S., Cho, S., Sung, J.-S. and Kim, J. Y. (2011). Real-time monitoring of neural differentiation of human mesenchymal stem cells by electric cell-substrate impedance sensing. *J Biomed Biotechnol,* **2011**, 1–8.

Park, J. Y., Hwang, C. M., Lee, S. H. and Lee, S. H. (2007). Gradient generation by an osmotic pump and the behavior of human mesenchymal stem cells under the fetal bovine serum concentration gradient. *Lab Chip,* **7**, 1673–80.

Park, J. Y., Kim, S.-K., Woo, D.-H., Lee, E.-J., Kim, J.-H. and Lee, S.-H. (2009a). Differentiation of neural progenitor cells in a microfluidic chip-generated cytokine gradient. *Stem Cells,* **27**, 2646–54.

Park, J. Y., Kim, S. K., Woo, D. H., Lee, E. J., Kim, J. H. and Lee, S. H. (2009b). Differentiation of neural progenitor cells in a microfluidic chip-generated cytokine gradient. *Stem Cells,* **27**, 2646–54.

Patela, P. and Markxb, G. H. (2008). Dielectric measurement of cell death. *Enzyme Microb Technol,* **43**, 463–70.

Pethig, R. (1996). Dielectrophoresis: Using inhomogeneous AC electrical fields to separate and manipulate cells. *Crit Rev Biotechnol,* **16**, 331–48.

Pethig, R. (2010). Dielectrophoresis: Status of the theory, technology, and applications. *Biomicrofluidics,* **4**, 022811.

Pethig, R., Lee, R. and Talary, M. (2004). Cell physiometry tools based on dielectrophoresis. *JALA,* **9**, 324–30.

Phinney, D. G. and Prockop, D. J. (2007). Concise review: mesenchymal stem/multipotent stromal cells: The state of transdifferentiation and modes of tissue repair – current views. *Stem Cells,* **25**, 2896–902.

Plouffe, B. D., Kniazeva, T., Mayer, J. E., Murthy, S. K. and Sales, V. L. (2009). Development of microfluidics as endothelial progenitor cell capture technology for cardiovascular tissue engineering and diagnostic medicine. *FASEB J,* **23**, 3309–14.

Prieto, J. L., Lu, J., Nourse, J. L., Flanagan, L. A. and Lee, A. P. (2012). Frequency discretization in dielectrophoretic assisted cell sorting arrays to isolate neural cells. *Lab Chip*, **12**, 2182–9.

Reilly, G. C. and Engler, A. J. (2010). Intrinsic extracellular matrix properties regulate stem cell differentiation. *J Biomech,* **43**, 55–62.

Reitinger, S., Wissenwasser, J., Kapferer, W., Heer, R. and Lepperdinger, G. (2012). Electric impedance sensing in cell-substrates for rapid and selective multipotential differentiation capacity monitoring of human mesenchymal stem cells. *Biosensors Bioelectron,* **34**, 63–9.

Roach, P., Parker, T., Gadegaard, N. and Alexander, M. R. (2010). Surface strategies for control of neuronal cell adhesion: A review. *Surf Sci Rep,* **65**, 145–73.

Roisen, F. J., Klueber, K. M., Lu, C. L., Hatcher, L. M., Dozier, A., Shields, C. B. and Maguire, S. (2001). Adult human olfactory stem cells. *Brain Res,* **890**, 11–22.

Roufosse, C. A., Direkze, N. C., Otto, W. R. and Wright, N. A. (2004). Circulating mesenchymal stem cells. *Int J Biochem Cell Biol,* **36**, 585–97.

Scadden, D. T. (2006). The stem-cell niche as an entity of action. *Nature,* **441**, 1075–9.

Schaerli, Y., Wootton, R. C., Robinson, T., Stein, V., Dunsby, C., Neil, M. A. A., French, P. M. W., Demello, A. J., Abell, C. and Hollfelder, F. (2009). Continuous-flow polymerase chain reaction of single-copy DNA in microfluidic microdroplets. *Anal Chem,* **81**, 302–6.

Schirhagl, R., Fuereder, I., Hall, E. W., Medeiros, B. C. and Zare, R. N. (2011). Microfluidic purification and analysis of hematopoietic stem cells from bone marrow. *Lab Chip,* **11**, 3130–5.

Schneegass, I., Brautigam, R. and Kohler, J. M. (2001). Miniaturized flow-through PCR with different template types in a silicon chip thermocycler. *Lab Chip,* **1**, 42–9.

Schofield, R. (1978). The relationship between the spleen colony-forming cell and the haemopoietic stem cell. *Blood Cells,* **4**, 7–25.

Serra, M., Brito, C., Correia, C. and Alves, P. M. (2012). Process engineering of human pluripotent stem cells for clinical application. *Trends Biotechnol,* **30**, 350–9.

Shamloo, A., Ma, N., Poo, M. M., Sohn, L. L. and Heilshorn, S. C. (2008). Endothelial cell polarization and chemotaxis in a microfluidic device. *Lab Chip,* **8**, 1292–9.

Sharma, S., Raju, R., Sui, S. and Hu, W.-S. (2011). Stem cell culture engineering – process scale up and beyond. *Biotechnology J,* **6**, 1317–29.

Shiba, Y., Fernandes, S., Zhu, W.-Z., Filice, D., Muskheli, V., Kim, J., Palpant, N. J., Gantz, J., Moyes, K. W., Reinecke, H., van Biber, B., Dardas, T., Mignone, J. L., Izawa, A., Hanna, R., Viswanathan, M., Gold, J. D., Kotlikoff, M. I., Sarvazyan, N., Kay, M. W., Murry, C. E. and Laflamme, M. A. (2012). Human ES-cell-derived cardiomyocytes electrically couple and suppress arrhythmias in injured hearts. *Nature*, **489**, 322–5.

Solanki, A., Shah, S., Memoli, K. A., Park, S. Y., Hong, S. and Lee, K.-B. (2010). Controlling differentiation of neural stem cells using extracellular matrix protein patterns. *Small,* **6**, 2509–13.

Solvas, X. C. I. and Demello, A. (2011). Droplet microfluidics: Recent developments and future applications. *Chem Commun,* **47**, 1936–42.

Song, H., Chen, D. L. and Ismagilov, R. F. (2006). Reactions in droplets in microfluidic channels. *Angew Chemie-Int Ed,* **45**, 7336–56.

Song, H., Tice, J. D. and Ismagilov, R. F. (2003). A microfluidic system for controlling reaction networks in time. *Angew Chemie-Int Ed,* **42**, 768–72.

Song, J. W., Cavnar, S. P., Walker, A. C., Luker, K. E., Gupta, M., Tung, Y.-C., Luker, G. D. and Takayama, S. (2009). Microfluidic endothelium for studying the intravascular adhesion of metastatic breast cancer cells. *PLoS One,* **4**, e5756.

Stolberg, S. and McCloskey, K. E. (2009). Can shear stress direct stem cell fate? *Biotechnol Progr,* **25**, 10–19.

Sun, K., Yamaguchi, A., Ishida, Y., Matsuo, S. and Misawa, H. (2002). A heater-integrated transparent microchannel chip for continuous-flow PCR. *Sens Actuators B,* **84**, 283–9.

Sun, T. and Morgan, H. (2010). Single-cell microfluidic impedance cytometry: A review. *Microfluid Nanofluid*, **8**, 423–43.

Sykes, M. and Nikolic, B. (2005). Treatment of severe autoimmune disease by stem-cell transplantation. *Nature,* **435**, 620–7.

Takahashi, K. and Yamanaka, S. (2006). Induction of pluripotent stem cells from mouse embryonic and adult fibroblast cultures by defined factors. *Cell,* **126**, 663–76.

Talary, M. S., Mills, K. I., Hoy, T., Burnett, A. K. and Pethig, R. (1995). Dielectrophoretic separation and enrichment of Cd34+ cell subpopulation from bone-marrow and peripheral-blood stem-cells. *Med Biol Eng Comput,* **33**, 235–7.

Taly, V., Kelly, B. T. and Griffiths, A. D. (2007). Droplets as microreactors for high-throughput biology. *Chembiochem,* **8**, 263–72.

Tan, S. J., Yobas, L., Lee, G. Y. H., Ong, C. N. and Lim, C. T. (2009). Microdevice for the isolation and enumeration of cancer cells from blood. *Biomed Microdevices,* **11**, 883–92.

Tan, W. H., Suzuki, Y., Kasagi, N., Shikazono, N., Furukawa, K. and Ushida, T. (2005). A lamination micro mixer for mu-immunomagnetic cell sorter. *JSME Int J Ser C,* **48**, 425–35.

Tewhey, R., Warner, J. B., Nakano, M., Libby, B., Medkova, M., David, P. H., Kotsopoulos, S. K., Samuels, M. L., Hutchison, J. B., Larson, J. W., Topol, E. J., Weiner, M. P., Harismendy, O., Olson, J., Link, D. R. and Frazer, K. A. (2009). Microdroplet-based PCR enrichment for large-scale targeted sequencing. *Nat Biotechnol,* **27**, 1025-U94.

Thomson, J. A., Itskovitz-ELDOR, J., Shapiro, S. S., Waknitz, M. A., Swiergiel, J. J., Marshall, V. S. and Jones, J. M. (1998). Embryonic stem cell lines derived from human blastocysts. *Science,* **282**, 1145–7.

Toh, Y.-C., Blagović, K. and Voldman, J. (2010). Advancing stem cell research with microtechnologies: Opportunities and challenges. *Integr Biol,* **2**, 305–25.
Toh, Y.-C., Blagovic, K., Yu, H. and Voldman, J. (2011). Spatially organized in vitro models instruct asymmetric stem cell differentiation. *Integr Biol,* **3**, 1179–87.
Toh, Y.-C. and Voldman, J. (2011). Fluid shear stress primes mouse embryonic stem cells for differentiation in a self-renewing environment via heparan sulfate proteoglycans transduction. *FASEB J,* **25**, 1208–17.
Toh, Y. C., Lim, T. C., Tai, D., Xiao, G. F., van Noort, D. and Yu, H. R. (2009). A microfluidic 3D hepatocyte chip for drug toxicity testing. *Lab Chip,* **9**, 2026–35.
Tumarkin, E., Tzadu, L., Csaszar, E., Seo, M., Zhang, H., Lee, A., Peerani, R., Purpura, K., Zandstra, P. W. and Kumacheva, E. (2011). High-throughput combinatorial cell co-culture using microfluidics. *Integr Biol,* **3**, 653–62.
Underhill, G. H. and Bhatia, S. N. (2007). High-throughput analysis of signals regulating stem cell fate and function. *Curr Opin Chem Biol,* **11**, 357–66.
Valastyan, S. and Weinberg, R. A. (2011). Tumor metastasis: Molecular insights and evolving paradigms. *Cell,* **147**, 275–92.
van der Flier, L. G. and Clevers, H. (2009). Stem cells, self-renewal, and differentiation in the intestinal epithelium. *Annu Rev Physiol,* **71**, 241–60.
van Midwoud, P. M., Verpoorte, E. and Groothuis, G. M. M. (2011). Microfluidic devices for in vitro studies on liver drug metabolism and toxicity. *Integr Biol,* **3**, 509–21.
Vanapalli, S. A., Duits, M. H. G. and Mugele, F. (2009). Microfluidics as a functional tool for cell mechanics. *Biomicrofluidics,* **3**, 12006.
Vazin, T. and Schaffer, D. V. (2010). Engineering strategies to emulate the stem cell niche. *Trends Biotechnol,* **28**, 117–24.
Visvader, J. E. and Lindeman, G. J. (2012). Cancer stem cells: Current status and evolving complexities. *Cell Stem Cell,* **10**, 717–28.
Vykoukal, D. M., Gascoyne, P. R. C. and Vykoukal, J. (2009). Dielectric characterization of complete mononuclear and polymorphonuclear blood cell subpopulations for label-free discrimination. *Integr Biol,* **1**, 477–84.
Vykoukal, J., Vykoukal, D. M., Freyberg, S., Alt, E. U. and Gascoyne, P. R. C. (2008). Enrichment of putative stem cells from adipose tissue using dielectrophoretic field-flow fractionation. *Lab Chip,* **8**, 1386–93.
Wan, J. (2012). Microfluidic-based synthesis of hydrogel particles for cell microencapsulation and cell-based drug delivery. *Polymers*, **4**, 1084–108.
Wang, M. M., TU, E., Raymond, D. E., Yang, J. M., Zhang, H., Hagen, N., Dees, B., Mercer, E. M., Forster, A. H., Kariv, I., Marchand, P. J. and Butler, W. F. (2004). Microfluidic sorting of mammalian cells by optical force switching. *Nat Biotechnol,* **23**, 83–7.
Wei, H. B., Chueh, B. H., Wu, H. L., Hall, E. W., Li, C. W., Schirhagl, R., Lin, J. M. and Zare, R. N. (2011). Particle sorting using a porous membrane in a microfluidic device. *Lab Chip,* **11**, 238–45.
White, A. K., Vaninsberghe, M., Petriv, I., Hamidi, M., Sikorski, D., Marra, M. A., Piret, J., Aparicio, S. and Hansen, C. L. (2011). High-throughput microfluidic single-cell RT-qPCR. *Proc Natl Acad Sci U S A,* **108**, 13999–4004.
Wu, H.-W., Lin, C.-C. and Lee, G.-B. (2011). Stem cells in microfluidics. *Biomicrofluidics,* **5**, 013401.
Wu, H. W., Lin, X. Z., Hwang, S. M. and Lee, G. B. (2009a). A microfluidic device for separation of amniotic fluid mesenchymal stem cells utilizing louver-array structures. *Biomed Microdevices,* **11**, 1297–307.

Wu, Z. G., Willing, B., Bjerketorp, J., Jansson, J. K. and Hjort, K. (2009b). Soft inertial microfluidics for high throughput separation of bacteria from human blood cells. *Lab Chip,* **9**, 1193–9.

Xia, N., Hunt, T. P., Mayers, B. T., Alsberg, E., Whitesides, G. M., Westervelt, R. M. and Ingber, D. E. (2006). Combined microfluidic-micromagnetic separation of living cells in continuous flow. *Biomed Microdevices,* **8**, 299–308.

Yamada, M. and Seki, M. (2005). Hydrodynamic filtration for on-chip particle concentration and classification utilizing microfluidics. *Lab Chip,* **5**, 1233–9.

Yim, E. K. F., Pang, S. W. and Leong, K. W. (2007). Synthetic nanostructures inducing differentiation of human mesenchymal stem cells into neuronal lineage. *Exp Cell Res,* **313**, 1820–9.

Yung, C. W., Fiering, J., Mueller, A. J. and Ingber, D. E. (2009). Micromagnetic-microfluidic blood cleansing device. *Lab Chip,* **9**, 1171–7.

Zare, R. N. and Kim, S. (2010). Microfluidic platforms for single-cell analysis. *Annu Rev Biomed Eng,* **12**, 187–201.

Zheng, S., Lin, H., Liu, J. Q., Balic, M., Datar, R., Cote, R. J. and Tai, Y. C. (2007). Membrane microfilter device for selective capture, electrolysis and genomic analysis of human circulating tumor cells. *J Chromatogr,* **1162**, 154–61.

Zhong, J. F., Chen, Y., Marcus, J. S., Scherer, A., Quake, S. R., Taylor, C. R. and Weiner, L. P. (2007). A microfluidic processor for gene expression profiling of single human embryonic stem cells. *Lab Chip,* **8**, 68–74.

12

Development of immunoassays for protein analysis on nanobioarray chips

J. LEE and P. C. H. LI, Simon Fraser University, Canada

DOI: 10.1533/9780857097040.4.445

Abstract: Immunoassays have been utilized as a method to detect secreted proteins such as antibodies or cytokines. These soluble proteins in blood or serum allow for clinical diagnostics of diseases ranging from hepatitis, autoimmune disorders, and Alzheimer's to cancer. Immunoassays can be homogeneous or heterogeneous, with heterogeneous immunoassay (e.g. enzyme-linked immunosorbent assay (ELISA)) being much more common because the unbound proteins are easily washed away from the solid substrate. The need for sample volumes in excess of 10 μL in ELISA poses a restriction to the detection of antibodies and cytokines, usually found in low concentrations and low volumes in clinical samples. This necessitates the development of nanoliter-volume liquid handling, and high detection sensitivity of low-volume and low-concentration samples. The recent development of the nanobioarray chip technology will address these needs.

Key words: heterogeneous immunoassay, enzyme-linked immunosorbent assay, antibody, cytokine, mosaic array, covalent immobilization, fluorescence, chemiluminescence.

12.1 Introduction

Immunoassays have been utilized as a method of protein detection for biological samples. This method uses the immune reaction that takes place between an antibody and an antigen. Antibodies are proteins secreted in the body in order to identify and neutralize foreign objects in the body. Antigens are markers on these objects that antibodies bind to in order to recognize them. The introduction of immunoassays represented a significant leap in the ability to detect proteins, such as antibodies and cytokines secreted by the body. Antibodies are utilized for the detection of diseases such as hepatitis and autoimmune disorders. Cytokines are involved in the studies of diseases such as Alzheimer's and cancer, due to the gene regulation ability of the cytokines. As such, immunoassays have played an important role in protein detection and clinical diagnostics (see Table 12.1). Immunoassays can be classified as homogeneous or

Table 12.1 Comparison of different commercial bioarray methods

Indication	Target	Vendor	Platform	FDA cleared
Allergies	Antibodies	VBC-Gcnomics (www.vbc-gcnomics.at)	Planar array	–
Allergies, celiac disease	Antibodies	1NOVA Diagnostics (wwvv. inovadx.com)	Luminex	–
Allergies, common	Antibodies	ImmuneTech (www. immunetech.com)	Luminex	i
Allergies, indoor allergens	Antibodies	INDOOR Biotechnologies (www.inbio.coin)	Luminex	–
Autoimmune	Antibodies	BioArray Solutions (www. bioarrays.com)	Bead array	–
Autoimmune	Antibodies	Biomedical Diagnostics (www.bmd-nel.com)	Luminex	+
Autoimmune	Antibodies	INOVA Diagnostics (www. inovadx.com)	Luminex	–
Autoimmune	Antibodies	Zeus Scientific (www. zcusscicntiiic.com)	Luminex	–
Autoimmune	Antibodies	Bio-Rad Laboratories (www.bio-rad.com)	Luminex	+
Autoimmune	Antibodies	Whatman (wwwAvhatman. com)	Planar array	–
Cancer	Proteins	RBM (www. rulesbasedmcdicmcxom)	Luminex	–
Cardiac, heart failure	Proteins	Biomcricux (www. biomcricux-dlagnostics. com)	VIDAS	–
Cardiac, myocardial infarction	Proteins	Biosite (www.biosite.com)	Triage system	–
Cardiac, shortness of breath	Proteins	Biositc (www.biositc.eom)	Triage system	–
Infectious disease	Antibodies	Bio-Rad Laboratories (www.bio-rad.com)	Luminex	–
Infectious disease, Epstein-Barr	Antibodies	Zeus Scientific (www. zeusscientific.com)	Luminex	–
Infectious disease, FSME, Borrclia	Antibodies	Multimctrix (www. multimctrix.eom)	Luminex	–
Infectious disease, Herpes virus	Antibodies	Focus Diagnostics (www. focusdx.com)	Luminex	–
Multiple immunoassays	ProLeins	Randox (www.randox.com)	Evidence	+
Neurologic, Alzheimer's disease	Proteins	Innogenetics (www. innogenetics.com)	Luminex	–
Typing, IILA	Antibodies	Tepnei (www.lepnel.com)	Luminex	i

Source: From Hartmann *et al.*, 2009. With permission from Springer Science.

heterogeneous assays. In homogeneous assays, the probes and the samples will be mixed in liquid phase; this method requires a separation step to detect the presence of the reaction products. In heterogeneous assays the samples in the liquid phase interact with the probes immobilized on a solid phase. While both of these assays are in practical use, heterogeneous assays are much more common due to the ease of washing away unbound particles from the solid substrate. Heterogeneous immunoassays usually take the form of the ELISA. The need for sample volumes in excess of 10 μL in ELISA poses a restriction to the detection of antibodies and cytokines. These proteins are found in low concentrations and low volumes in clinical samples. This makes the development of nanoliter-volume liquid handling, and high detection sensitivity of low-volume and low-concentration samples particularly important (Chu *et al.*, 1997). The miniaturization of the immunoassay technology came to light during the 1990s when development of DNA and protein microarrays began (Ekins *et al.*, 1998; Silzel, 1998). Furthermore, the need for simultaneous detection of a large number of analytes led to the development of multianalyte binding assays. Nanofluidics conducted in micron-sized channels provided a system in which minimal liquid could be utilized while maintaining or even improving the sensitivity of the protein detection in these materials. The development of such technologies as nanobioarray chips, which can perform multianalyte detection in nanoliter-volume of samples, will be described in detail in subsequent sections.

12.2 Technologies

Two major technologies are currently used in producing bioarrays, namely, the microspot array and mosaic array.

12.2.1 Microspot arrays

The most commonly developed immunoassay method is the spot array. It is a simple method whereby many probe spots are printed onto a chip substrate. Since the minimum volume of materials required for ELISA kits is >10 μL, microspots that utilize liquid handling of nanoliters in micro-sized channels help to remove this limitation. Typically, the probe spot density is several thousand spots, and they are printed as a rectangular array within a single 1 cm × 1 cm square chip. This bioarray is then tested against a single sample, which is flowed on top of the array. With this method, a large amount of data can be obtained from using a single sample.

There are three common methods utilized in microspotting the substrate: photolithography, mechanical microspotting, and ink-jet printing (see Fig. 12.1). These printing methods provide the ability to print multiple individualized spots on a single chip substrate.

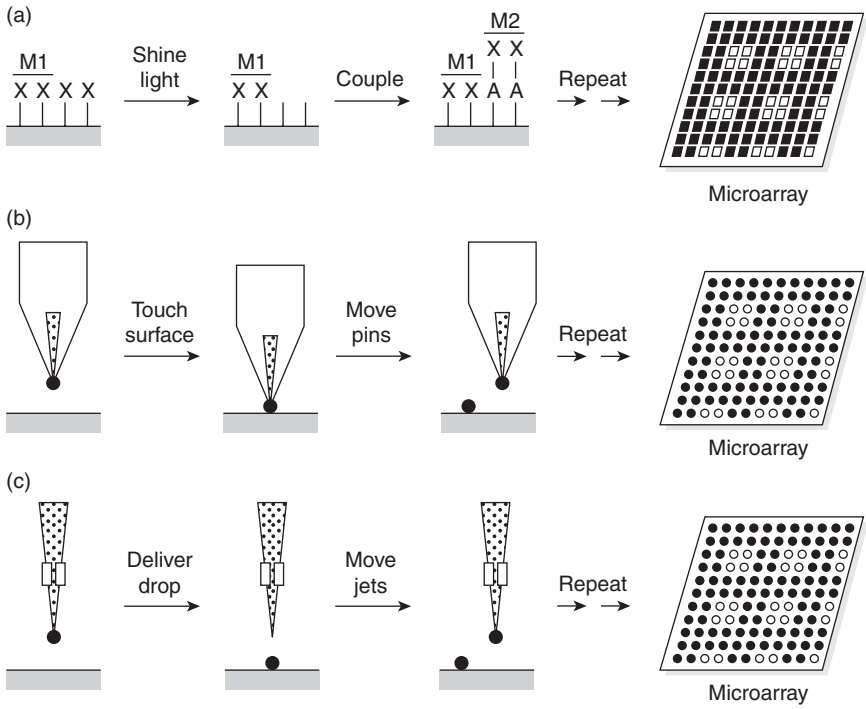

12.1 Microspot array fabrication. (a) Photolithography: A substrate modified with photo labile protecting groups (X) can be selected for activation by using a photo mask (M1). The chip is then covered with a photo protected protein (A-X), which will be immobilized onto the surface, generating defined regions on the surface. A second mask (M2) is then applied to deprotect another set of defined regions for protein coupling. Repeated deprotection and coupling will allow for a high density protein microarray. (b) Mechanical Microspotting: This method requires the loading of the protein into a spotting pin via capillary action. The pin is then placed into direct contact with the surface of the substrate where a small volume of the protein is delivered. Once this is completed, the pins are washed and then loaded with the second sample, which is spotted on an adjacent location. This method can be automated using robotic control systems and multiplexed printheads. (c) Ink-jet printing utilizes piezoelectric fittings (rectangles) and an electrical current to dispense a precise quantity of a loaded sample in the nozzle. Once this step is completed, the nozzle is washed and loaded with the second sample, and then deposited on the adjacent spot. By utilizing multiple jets, microarrays can be printed rapidly. (*Source*: From Schena *et al.* 1998. With permission from Elsevier.)

Photolithography is used to pattern many spots accurately on the surface. This method is highly reproducible, with little variations in the microspot locations (Kim *et al.*, 2010). This method does require a photomask for fabrication, which can be costly as compared to other methods. This fabrication

process is also time-consuming, as each photomask must be designed and built before the chip fabrication can occur.

Mechanical microspotting utilizes a liquid droplet delivery mechanism with direct contact of spotting tips against the substrate to print the liquid from spot to spot. This method is simple and can be implemented in rapid prototyping. In addition, the microspotting procedure can be easily automated. Unlike the photolithography method, mechanical microspotting is not as precise, and so the high spot density achieved using photolithography cannot be obtained. Nevertheless, this method remains a simple method for use in research labs.

Ink-jet printing is a droplet delivery system using nozzles to transfer substances onto the substrate. This method allows for a spot density comparable to mechanical microspotting, while reducing the chip fabrication time as the ink-jet liquid delivery method is contactless. The downside of this method is the robustness of the system. The delivery of the liquids is not always reliable and reproducible, due to clogging of the nozzle, which limits the use of this method.

12.2.2 Mosaic arrays

The mosaic array is an immunoassay method that allows for multiple probes to react with multiple samples. Rather than having a single sample react with multiple probes, this method has several samples tested against multiple probes simultaneously.

In the mosaic array, the liquid is flowed through PDMS channels placed on top of the substrate (see Fig. 12.2). This method is simple to use and it utilizes micron-sized channels to define precisely and accurately the regions of the probes utilizing nanoliters of reagents. This method requires the removal of the first chip and the assembly of a second chip before detection can occur. In other words, the channels in the chips must be intersecting in order to conduct the multiple-probe, multiple-sample test.

In the methods of both microspot and micromosaic arrays, a high spot density can be obtained. In the mosaic bioarray, the multiple probes will not only detect proteins in one sample, but also detect multiple samples; whereas the microspot array will not (Murphy *et al.*, 2008). However, the microspot array can be fabricated to generate isolated detection regions. In this case, only one probe will detect each sample in each region. The microspot method requires that each spot must have an individual probe and sample solution, whereas the micromosaic does not have this limitation. Recent advances show that a microspot array can be modified to alleviate this limitation by performing homogeneous-like immunoassays assays in which the probes are fixed on beads and remain in solutions for binding with samples in the same solution. This type of assay is commonly utilized in assays where a microwell is used to isolate the detection of samples at individual spots.

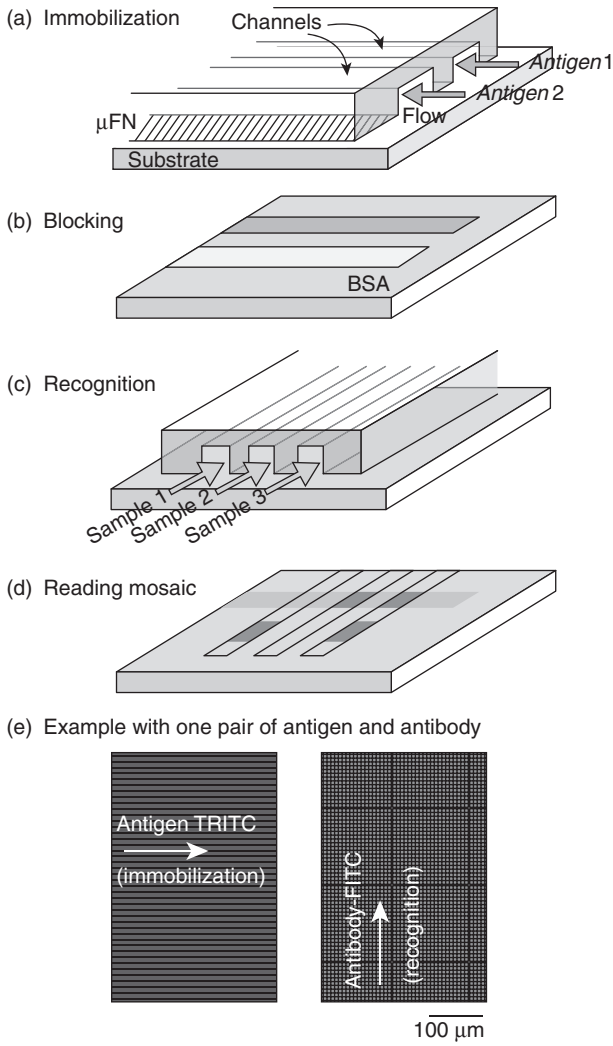

12.2 Steps to perform a micromosaic immunoassay: (a) Different antigens are patterned on the substrate in single lines using a microfluidic chip network. (b) Any areas not patterned in Step (a) are blocked with BSA to prevent any non-specific binding. (c) The first microfluidic network is replaced with another chip and antibodies are flowed through to bind to the patterned antigens. (d) The mosaic generated will allow for the detection and quantification of antibodies on the surface. (e) In this method, a 200 μg/mL rabbit IgG labeled with TRITC is immobilized on the surface using the microfluidic network. The substrate was then blocked with BSA, and then the second chip was positioned across the printed antigen lines and a FITC-labeled anti-rabbit-IgG solution was applied to allow for immunobinding. (*Source*: From Bernard *et al.*, 2001. With permission from American Chemical Society.)

12.3 Immobilization chemistry

In heterogeneous immunoassays, there are various methods of immobilizing the probes onto the surface. Covalent attachment, adsorption, and bioaffinity attachment are the most common methods used (see Fig. 12.3).

Adsorption is a simple method in which physisorption is commonly used to immobilize proteins onto a surface. This method can be achieved by adding proteins with high affinity to a particular substrate that is able to adsorb materials well. The drawback of this method is the occurrence of nonspecific binding. In addition, the weak binding force of physisorption means that desorption can easily occur through changes in reaction conditions, such as temperature, pH, and solvent composition (Kusnezow *et al.*, 2003). These drawbacks make this method rather limited in application. While adsorption is a viable method in microspot arrays, it is not ideal in micromosaic arrays.

In bioaffinity attachment, the most common method is through the use of biotinylated groups coupled to probes, which will attach to immobilized avidin analogs bound on a solid substrate. The high binding affinity of biotin to avidin groups and the ease of biotinylation of various probes make this a simple method for anchoring probes on solid substrates (Peluso *et al.*, 2003; Ramachandran *et al.*, 2004). In addition, the biotin–avidin link is very robust and is able to withstand many extreme conditions that may be encountered in a reaction (Moy *et al.*, 1994). In order to avoid steric hindrance due to biotin on the active group of the probe, a carbon-chain linker is usually used between

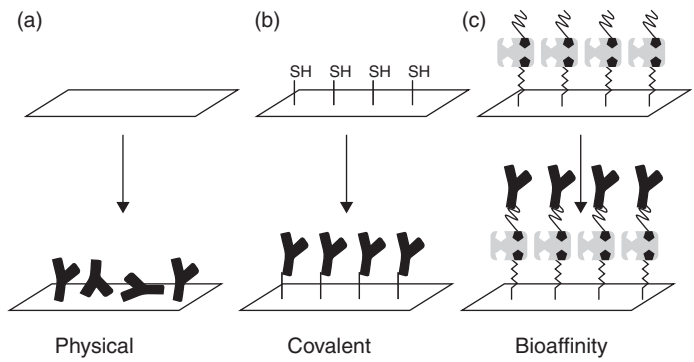

12.3 Diagram of various immobilization techniques. (a) Physical immobilization occurs by the directly exposing the sample onto the surface through physisorption. (b) Covalent attachment requires for surface functionalization of the surface before exposing the sample for immobilization. (c) Bioaffinity utilizes an immobilized biomolecule to create a bond of the sample through another biomolecule onto the substrate. (*Source*: From Rusmini *et al.,* 2007. With permission from American Chemical Society.)

Table 12.2 Comparison of immobilization techniques

Side groups	Amino	Acids surfaces
$-NH_2$	Lys, hydroxyl-Lys	Carboxylic acid active ester (NHS) epoxy aldehyde
-SH	Cys	Maleimide pyridyil disulfide vinyl sulfone
-COOH	Asp. Glu	Amine
-OH	Ser. Thr	Epoxy

Source: From Rusmini *et al.*, 2007. With permission from American Chemical Society.

the biotin moiety and the probe. The drawback is that the probes must be biotinylated prior to being used, which requires an additional purification step.

Covalent attachment requires surface functionalization in order to attach the probes. Depending on the amino acids present in the protein or peptide probes (see Table 12.2), there are several methods of surface functionalization. Rusmini *et al*. (2007) lists two of these methods as (1) N-hydroxysuccinimide (NHS) with 1-ethyl-3-(3-dimethylaminopropyl) carbodiimide) (EDC) chemistry to couple with amino groups in proteins, and (2) aldehyde chemistry to couple with amino groups in proteins. The EDC is used with NHS in various applications to create an amine-reactive NHS ester, which is easily attached to proteins through forming a stable amide bond. In the aldehyde method, glutaraldehyde may be used for the modification of the surface. Then, the aldehyde will interact with an amino group on the proteins. It is possible to modify the linker length to avoid steric hindrance and to improve the binding efficiency. However, the drawback of both methods is the requirement for a free primary amino group to be present in the protein molecules.

12.4 Detection methods

The common detection methods for immunoarrays are based on tags that produce chemiluminescence, fluorescence, colorimetry, electrochemistry, and radioactivity (Pollard *et al.*, 2007).

Chemiluminescent detection can be obtained with a horseradish peroxidase (HRP) tag, which is an enzyme that catalyzes chemiluminescent reaction of chemical substrates such as luminol. The HRP can be tagged onto the detection antibody which will be applied to the system. This method allows for a two orders of magnitude increase in detection ability as compared to the use of a fluorescent tag. The drawback of this method is longevity of the chemiluminescent reaction. The detection must be completed rapidly upon

the introduction of the substrate. In other words, this method of detection will be inaccurate if the substrate is not introduced to all detection regions or wells simultaneously (Yakovleva *et al.*, 2002). This method is excellent for high throughput detection, but light shielding from other wells (usually white) is required in order to prevent any residual light from bleeding into other wells, causing false positives (Lee *et al.*, 2010).

Fluorescence offers a solution to the issues of the chemiluminescence by removing the need to introduce the HRP substrates as well as the need for reagent localization. In fluorescent detection, the tag is localized on the detection antibody and no substrate is required for signal generation. In terms of fluorescence, there is a variety of methods for the detection. The most direct method is attaching the fluorescent tag to the detection antibody (Ghafari *et al.*, 2009). This method is the simplest and requires the least amount of time to detect. However, this method does not generate light as bright as chemiluminescence, which has chemical amplification and hence does not have as low a detection limit as chemiluminescence. Nevertheless, fluorescent detection can be enhanced in many ways. One way is to multiply the number of fluorescent tags by adding a chain reaction or using a multiple tag antibody. Another way is by utilizing fluorescent beads for detection, and it is possible to increase the detection by two orders of magnitude. Fluorescence is a versatile method that can be utilized in a high throughput design, but light shielding from other wells (usually black) is required so that the light does not bleed from one spot to the next, thus causing false positives (Ressine *et al.*, 2003).

The third approach is colorimetric detection, which can be achieved by a variety of methods. The simplest method is the introduction of a colorimetric substrate such as 3,3',5,5'-tetramethylbenzidine that can be catalyzed by HRP to produce a colored compound. Another method for the colorimetric detection is immunogold silver staining (IGSS), which uses silver nanoparticles to aggregate against the gold-tagged detection antibody (Holgate *et al.*, 1983; Hayat, 1995; Lackie, 1996). This method has a detection ability that is visible to the naked eye even at concentrations of 0.005 nM. While normal colorimetric methods are not as sensitive as chemiluminescence or fluorescence, silver staining enhances the detection ability to a comparable level. In addition, the ease of detection allows them to be viable for low cost detection equipment such as scanners, when large and bulky instruments are unavailable.

Electrochemical detection utilizes the reduction and oxidation abilities of the materials for detection. The method requires electrodes (usually the working electrode) to be fabricated directly onto the device. This method is more sensitive than colorimetric detection, and it does not require transparent material. However, it is dependent on flow conditions within the channels, and the electrodes must be treated to prevent inaccurate results due to biofouling.

Radioactivity is another method that can be used for immunoassay detection. The requirement for a transparent material for the nanofluidic system can be bypassed, as this method does not depend on optical detection methods. In addition, this method requires the radiolabelling of the protein, which allows tracing of the protein in the nanofluidic system. However, it requires specialized equipment that reduces the compactness of this method. In addition, radioactive hazard is a concern that requires specialized safety training.

12.5 Applications

There are many applications that benefit from using the bioarray chip. These include detection of antibodies and cytokines, both of which have clinical importance.

12.5.1 Antibody detections

Antibody detection has been utilized in a wide variety of applications. For instance, immunoassays have been applied in water analysis to detect pathogenic bacteria, such as *Escherichia coli* (*E. coli*) (Noguera *et al.*, 2011). Conventional methods for detection of this bacterial material require 18–24 h to complete due to the required bacterial cultivation time. However, with the introduction of a stopped flow immunoassay system reported by Langer *et al.* (2011), the time required was reduced to 67 min (see Fig. 12.4). This method utilized the immobilization of polyclonal goat antibodies against *E. coli* cells utilizing 2000-Da diaminopolyethyleneglycol (DAPEG) to trap the cells. The detection was completed by the introduction of polyclonal antibodies conjugated with biotin, which would be coupled to streptavidin labeled with HRP. This will then react with chemiluminescent substrates to produce a signal. The detection limit obtained from this method, i.e. 4×10^5 cells/mL, is two orders of magnitude lower than a comparable conventional ELISA. In the stopped flow method, the standard microspot array has been modified for a solution to be introduced into system and allowed to react. The signal is enhanced when the flow rate of sample introduction is reduced (see Fig. 12.5). The benefit of this stop flow method is the ability to significantly enhance the signal, compared to other methods which run a sample continuously.

By using the immunoassay for detection of antibodies, we can specifically look for pathogenic cells, such as *E. coli* or *Staphylococcus aureus* (*S. aureus*) without killing them, as this will interfere with the ability to study these cells. In serum diagnostics, a multitude of proteins such as albumins, immunoglobulins (IgG) and regulatory proteins may be evaluated. In specific cases, the detection of a protein may just require a positive or negative result. IGSS is an excellent way to produce a rapid detection method that does not require expensive and bulky instruments and does generate

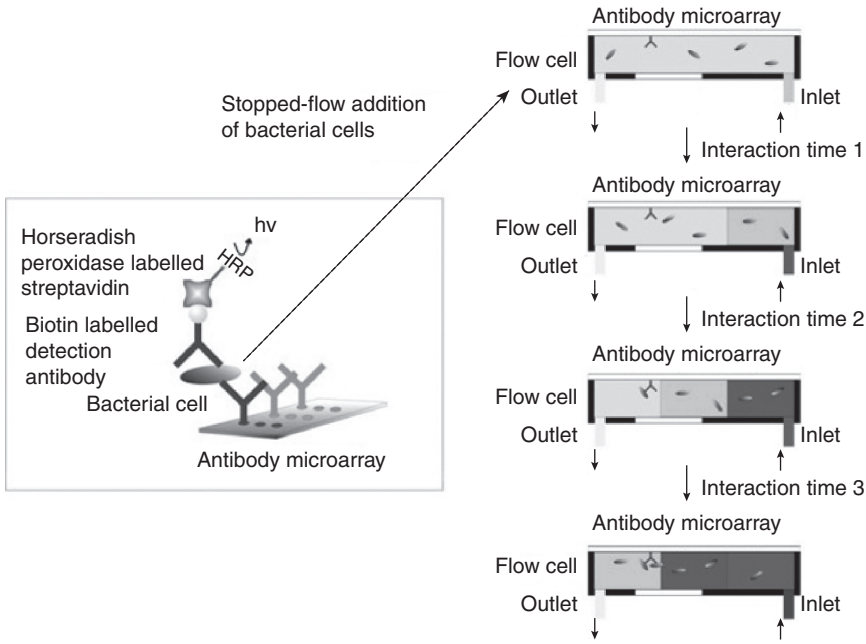

12.4 Application 1 Detection of *E. coli* using chemiluminescence. A standard sandwich immunoassay is performed using the stop flow method. First, biotin-conjugated polyclonal antibodies. These will be coupled to the HRP labeled streptavidin. HRP will then react with the chemiluminescent substrates. The various colored sections indicate the reagent volumes used in the various incubation steps. The results are shown in Fig. 12.5. (*Source*: From Langer *et al.*, 2011. With permission from Springer-Verlag.)

fast results. This method was shown by Yeh *et al*. (2009) to detect protein A obtained from *S. aureus*, and IgGs obtained from humans or goats (see Fig. 12.6). Over time, the signals gradually increase, resulting in the detection of positive or negative result (see Fig. 12.7). In countries where expensive equipment is not readily available, these colorimetric immunoassays are economically viable.

In the paper by Yang *et al*. (2007), they demonstrated a microarray based on multiple wells to detect antiepileptic drugs (AED), namely carbamazepine(CBZ), phenytoin(PHT), and valproic acid(VPA), simultaneously and quantitatively (see Fig. 12.8). The results of this competitive homogeneous immunoassay have a variation in results of less than 10%, as compared to values obtained from intra- and inter-assays, allowing for the method to be clinically viable (see Fig. 12.9). In this method, the bioarray was constructed on wells (2.50 mm in diameter) cut out of a vinyl film that was then supported by a glass cover slip. After the enzyme and bioluminogenic

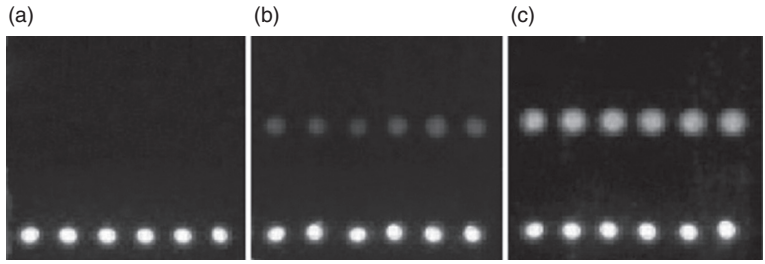

12.5 Chemiluminescent signals obtained from (a) 20 μL/s, (b) 0.5 μL/s, and (c) stopped flow system for measurement of *E. coli* cells. In each image, the top row represent six spot replicates of pAb anti-*E. coli, the middle of* negative control and the bottom of positive control. The signals obtained from continuous flow are weaker than that using the stopped flow system The positive control was polyclonal antibody anti-peroxidase and the negative control was spotting buffer. In each row, the interspot distance was 1100 μm. (*Source*: From Langer *et al.*, 2011. With permission from Springer-Verlag.)

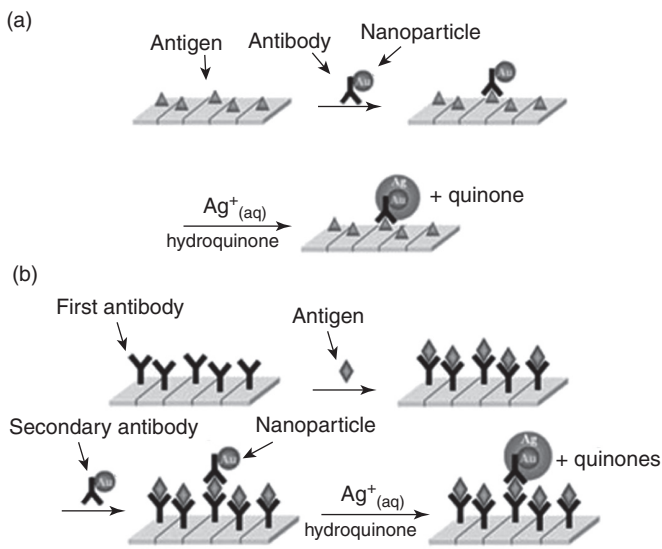

12.6 Schematic of the sandwich immunoassay using immunogold silver stain detection on a microspot bioarray. (a) The test used to evaluate the precipitation effects of the silver. (b) The actual method used to perform the ELISA-type immunoassay. The results are shown in Fig. 12.7. (*Source*: From Yeh *et al.*, 2009. With permission from Springer Berlin/Heidelberg.)

substrate (6-O-β-galactopyranosyl-luciferin) were dispensed into the wells on the bioarray surface, these reagents were frozen or lyophilized using dry ice placed below the chip. When used, the reagents were reconstituted when the serum-containing AED solutions were added. The detection method

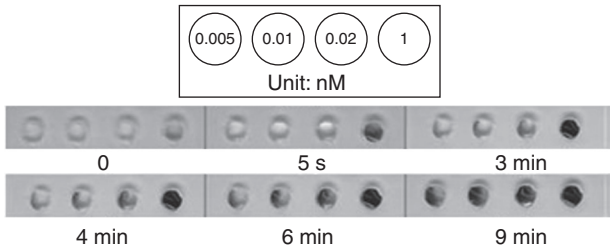

12.7 Images obtained from immunogold silver staining (IGSS) results on a microspot array. Colorimetric changes were obtained from the IgG-AuNPs conjugates once immersed in the silver enhancer solution from 0 s to 9 min. This demonstrated the IgG-AuNPs catalyzing the reduction of the silver ion solution to silver metal. (*Source*: From Yeh *et al.*, 2009. With permission from Springer Berlin/Heidelberg.)

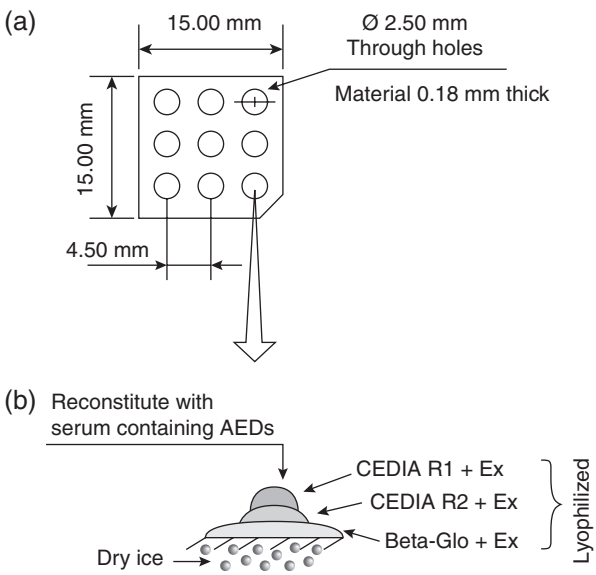

12.8 ImmunoChip design and dispensing of the assay reagents. (a) The setup and dimensions of a 3 × 3 multiwell ImmunoChip. The reagents specific to the three antiepileptic drugs (AEDs) were dispensed in individual rows (VPA, PHT, and CBZ) in triplicate. (b) Dry ice was placed under the platform (XYZ stage), supporting a number of ImmunoChips, to achieve freezing or lyophilization of the assay reagents as soon as they were dispensed. In each well, the assay's reagents were dispensed in the following order (from bottom to top): (i) Beta-Glo solution with excipients (Ex) (500 nL); (ii) R2, an AED–ED conjugate and Ex (188 nL); and (iii) R1, an anti-AED antibody and Enzyme Acceptor (EA) and Ex (250 nL). Enzyme Donor (ED) and EA are two genetically engineered fragments of β-galactosidase. (*Source*: From Yang *et al.*, 2007. With permission from Elsevier.)

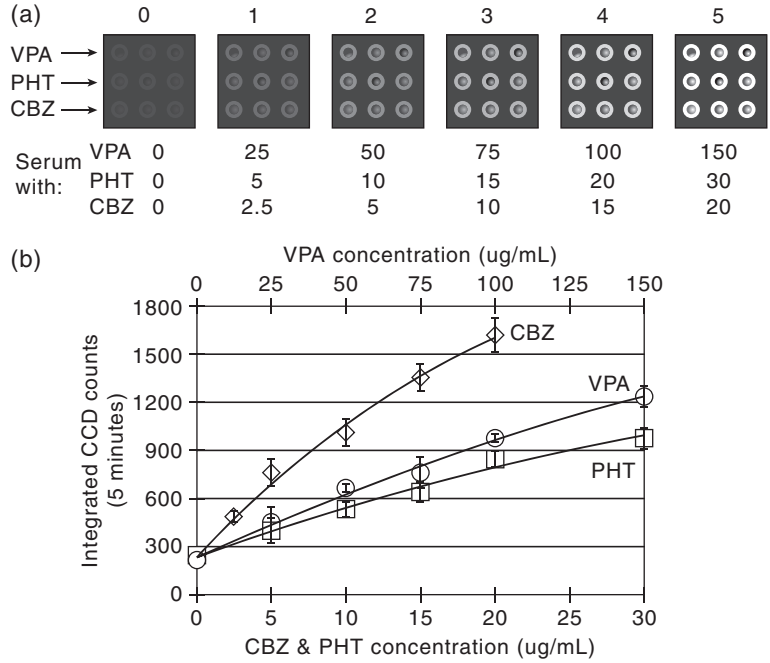

12.9 Homogeneous assay results on microfluidic array ImmunoChip. Simultaneous detection of three antiepileptic drugs (AEDs). (a) CCD images for the serum samples. Various concentrations of the AEDs were added in each well displaying the luminescent signals. (b) Calibration curves are from the CCD counts from 5 min exposures. CBZ and PHT utilize the lower concentration axis, whereas VPA uses the higher concentration axis. (*Source*: From Yang *et al.*, 2007. With permission from Elsevier.)

utilizes a β-galactosidase to produce bioluminescent luciferin, which allows for detection of AEDs in a single-step process.

Another system developed by Lee *et al.* (2012) for the detection of antibodies involves the NBA chip method. This system is similar to the micromosaic approach, but utilizes a spiral/radial chip configuration (see Fig. 12.10) rather than the horizontal/vertical chip configuration. This system utilizes the spiral channels to increase the residence time of the antibody–antigen reaction, thereby increasing the sensitivity of detection. This system utilizes a secondary antibody for fluorescent detection. The linear channel bioarray proposed by Bernard *et al.* (2001) was able to detect the antibodies down to levels of 0.5 nM. Utilizing the spiral NBA chip to detect monoclonal 17/9 antibodies, which bind to hemagglutinin A of the influenza virus A, 0.1 nM of the 17/9 Abs were detectable.

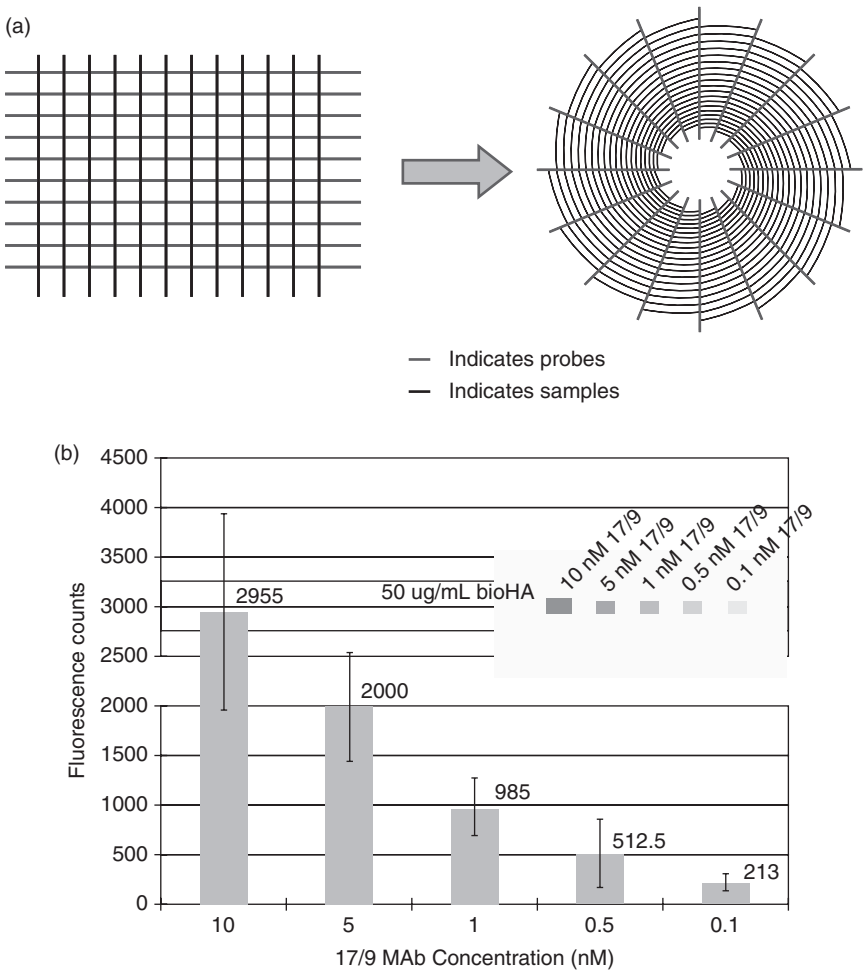

12.10 (a) The NBA chip (radial/spiral) as compared to the micromosaic chip (vertical/horizontal). (b) Results displaying the detection of monoclonal 17/9 antibodies dispensed into adjacent spiral channels intersecting with bioHA antigens immobilized along radial lines. Results were detected using a flat bed confocal fluorescence scanner. (*Source*: With permission from the International Society for Optics and Photonics or SPIE.)

12.5.2 Cytokine detection

Cytokines, e.g. interleukins, have been an area of interest as they are important proteins secreted by cells in diseases such as cancer and Alzheimer's, as well as during transplant rejections. An immunoassay proposed by Zhou *et al.* (2010) utilizes a system that is designed for materials that are difficult to detect or that do not have a sandwich test kit for ELISA (see Fig. 12.11).

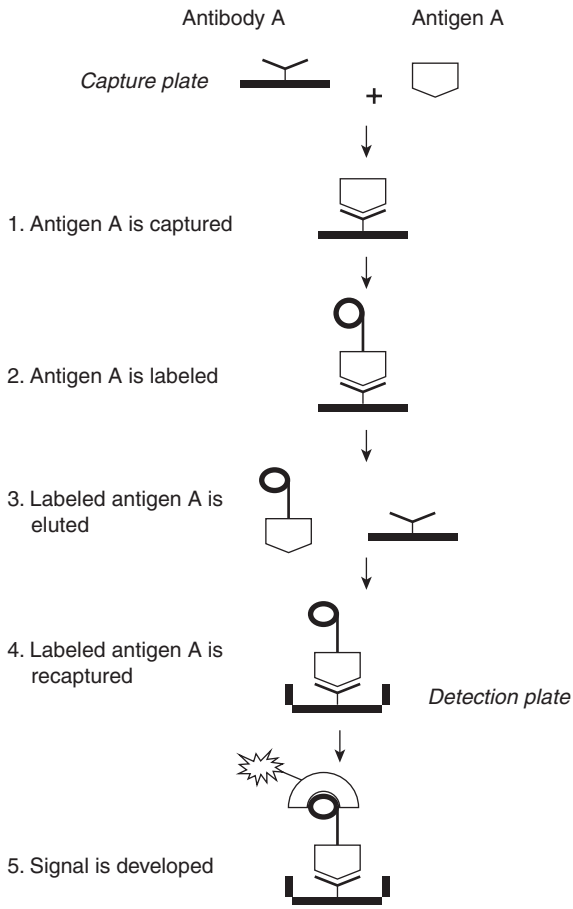

12.11 Cytokine Assay using Single Antibody. 1. Antigen A is captured on the surface utilizing an immobilized antibody A. 2. The captured antigen is then biotin labeled. 3. The labeled antigen is then eluted. 4. The eluted antigen is reintroduced into the system for recapture. 5. Streptavidin-HRP is introduced to bind to the biotinylated antigen to develop a signal. (*Source*: From Zhou *et al.,* 2010. With permission from Elsevier.)

The method proposed is called the specific analyte labeling and recapture assay. First, the antigen is bound to the capture antibody. Second, the bound antigen is labeled. Third, the labeled antigen is eluted. Fourth, the antigen is then recaptured utilizing the same capture antibody. This method allows for the use of a single detection antibody, rather than two antibodies-one for capture and one for detection. Moreover, the high specificity allows the same antigen to be recaptured. In this method, they trapped and detected the

various cytokines that are detected, the majority of which are interleukins (IL) such as IL-1β, IL-4, IL-8, and IL-10, using their corresponding capture antibodies. Once the cytokines are trapped, they are then labeled with biotin. Finally, the antigens are released from the antibodies, and they are then recaptured using the same antibody. Poly-HRP streptavidin is then added for the detection of the antigens using the colorimetric substrate 2,2'-azinobis [3-ethylbenzothiazoline-6-sulfonic acid]-diammonium salt (ABTS). This system allows for multiple antigens to be detected from one sample. The sensitivity of this method allowed for a detection of samples containing 0.01 ng/mL of cytokines.

In the study of Blicharz *et al*. (2009), IL-6, IL-8 as well as other cytokines found in saliva of patients with pulmonary inflammatory diseases are detected. The cytokines in saliva have been detected through the use of microspheres in a homogeneous assay (see Fig. 12.12). The microspheres are surface-modified using aldehyde chemistry for immobilization of the corresponding monoclonal capture antibodies, such as anti-IL-8, on the surface. This method uses the sandwich detection method, in which once the antigen has been captured; a biotinylated detection antibody is incubated. Then, fluorescently labeled streptavidin is applied for detection. By utilizing fiber optics, each of these beads can be identified by their colors and intensities, allowing for a quantitative method for cytokine detection. This proof-

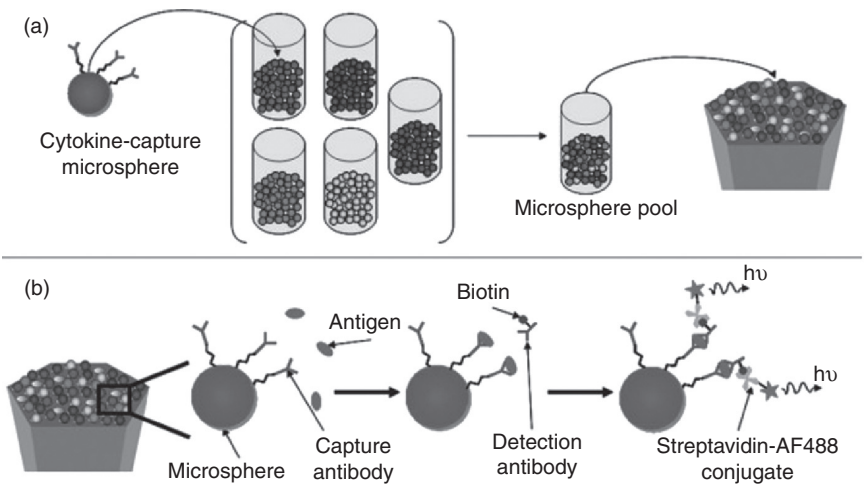

12.12 Microspheres for Cytokine Capture: (a) Capture antibodies are attached to the fluorescently encoded, amine functionalized microspheres. A mixture of various microspheres is loaded onto the fiber optic array. (b) The loaded microspheres are then incubated with the cytokines and then incubated with biotinylated antibodies. (*Source*: From Blicharz *et al.*, 2009. With permission from American Chemical Society.)

of-concept experiment utilizes the saliva samples obtained from patients to study the relationship between cytokines and pulmonary inflammatory diseases.

12.6 Conclusion and future trends

In terms of technology advances, there will be a need to improve the immunoassay systems for ease of automation. This will lead to much higher throughput and more reproducible results. While most of the instruments have automated operations, dispensing of the materials does not, which can lead to variations in detected signals. Another area that needs to be improved is the sensitivity of the instruments. It has been shown that the use of fluorescent detection results in lower detection limits in micro- or nano-fluidic devices than in conventional methods such as ELISA. To compete with chemiluminescence, which offers better signal enhancement, in order to obtain better fluorescent signal a variety of methods such as fluorescent beads may be utilized. However, the ultimate goal is to improve upon this so that single molecule detection is possible. To achieve this goal it will require system optimization as well as the development of novel detection methods involving the use of nanostructured materials.

Current applications are focused on samples that have ELISA kits developed. However, there are a wide variety of antibodies and cytokines that are not so easily captured. In addition to proteins that are difficult to analyze, many samples need to be purified before they can be analyzed. Furthermore, there will be a need for a high throughput system that will be able to analyze a large number of samples in a short amount of time. In addition, only a single aspect of these samples is currently analyzed. If instruments are able to completely characterize a sample, it will provide significantly more information. This will vastly improve our ability to understand the role of the antibodies and cytokines in a variety of physiological environments.

12.7 References

Bernard, A., Michel, B. and Delamarche, E. (2001). Micromosaic immunoassays. *Analytical Chemistry*, **73**, 8–12. DOI: 10.1021/ac0008845

Blicharz, T. M., Siqueira, W. L., Helmerhorst, E. J., Oppenheim, F. G., Wexler, P. J., Little, F. F. and Walt, D. R. (2009). Fiber-optic microsphere-based antibody array for the analysis of inflammatory cytokines in saliva. *Analytical Chemistry*, **81**, 2106–2114. DOI: 10.1021/ac802181

Chu, F. W., Edwards, P. R., Ekins, R. P., Berger, H., Finckh, P. and Krause, F. (1997). Microarray-based immunoassays. *Immunochemical Technology for Environmental Applications*, **657**, 170–184.

Ekins, R. P. (1998). Ligand assays: From electrophoresis to miniaturized microarrays. *Clinical Chemistry*, **44**, 2015–2030. DOI: 10.1016/S0167–7799(99)01329–3

Ghafari, H., Zhou, Y. Z., Ali, S. and Hanley, Q. S. (2009). Confocal detection of planar homogeneous and heterogeneous immunosorbent assays. *Journal of Biomedical Optics*, **14**, 10. DOI: 10.1117/1.3268772

Hartmann, M., Roeraade, J., Stoll, D., Templin, M. and Joos, T. (2009). Protein microarrays for diagnostic assays. *Analytical and Bioanalytical Chemistry*, **393**, 1407–1416. DOI: 10.1007/s00216–008–2379-z

Hayat, M. A. (1993). Immunogold-silver staining overview. *Journal of Histotechnology*, **16**, 197–199.

Holgate, C. S., Jackson, P., Cowen, P. N. and Bird, C. C. (1983). Immunogold silver staining – new method of immunostaining with enhanced sensitivity. *Journal of Histochemistry and Cytochemistry*, **31**, 938–944.

Kim, M., Choi, J. C., Jung, H. R., Katz, J. S., Kim, M. G. and Doh, J. (2010). Addressable micropatterning of multiple proteins and cells by microscope projection photolithography based on a protein friendly photoresist. *Langmuir*, **26**, 12112–12118. DOI: 10.1021/la1014253

Kusnezow, W., Jacob, A., Walijew, A., Diehl, F. and Hoheisel, J. D. (2003). Antibody microarrays: An evaluation of production parameters. *Proteomics*, **3**, 254–264. DOI: 10.1002/pmic.200390038

Lackie, P. M. (1996). Immunogold silver staining for light microscopy. *Histochemistry and Cell Biology*, **106**, 9–17. DOI: 10.1007/BF02473198

Langer, V., Niessner, R. and Seidel, M. (2011). Stopped-flow microarray immunoassay for detection of viable E. coli by use of chemiluminescence flow-through microarrays. *Analytical and Bioanalytical Chemistry*, **399**, 1041–1050. DOI: 10.1007/s00216–010–4414–0

Lee, B., Tajima, A., Kim, J., Yamagata, Y. and Nagamune, T. (2010). Fabrication of protein microarrays using the electrospray deposition (ESD) method: Application of microfluidic chips in immunoassay. *Biotechnology and Bioprocess Engineering*, **15**, 145–151. DOI: 10.1007/s12257–009–3033–0

Lee, J., Gulzar, N., Scott, J.K., Li, P.C.H. (2012). A nanofluidic bioarray chip for fast and high-throughput detection of antibodies in biological fluids. SPIE 2012 Global Congress on NanoMedicine, Incheon, South Korea, 10–13 September 2012, 1–7.

Moy, V. T., Florin, E. L. and Gaub, H. E. (1994). Intermolecular forces and energies between ligands and receptors. *Science*, **266**, 257–259. DOI: 10.1126/science.7939660

Murphy, B. M., He, X. Y., Dandy, D. and Henry, C. S. (2008). Competitive immunoassays for simultaneous detection of metabolites and proteins using micromosaic patterning. *Analytical Chemistry*, **80**, 444–450. DOI: 10.1021/ac7019046

Noguera, P. S., Posthuma-Trumpie, G. A., van Tuil, M., van der Wal, F. J., de Boer, A., Moers, A. and van Amerongen, A. (2011). Carbon nanoparticles as detection labels in antibody microarrays. Detection of genes encoding virulence factors in shiga toxin-producing *Escherichia coli*. *Analytical Chemistry*, **83**, 8531–8536. DOI: 10.1021/ac201823v

Peluso, P., Wilson, D. S., Do, D., Tran, H., Venkatasubbaiah, M., Quincy, D., Heidecker, B., Poindexter, K., Tolani, N., Phelan, M., Witte, K., Jung, L. S., Wagner, P. and Nock, S. (2003). Optimizing antibody immobilization strategies for the con-

struction of protein microarrays. *Analytical Biochemistry*, **312**, 113–124. DOI: 10.1016/S0003–2697(02)00442–6

Pollard, H. B., Srivastava, M., Eidelman, O., Jozwik, C., Rothwell, S. W., Mueller, G. R., Jacobowitz, D. M., Darling, T., Guggino, W. B., Wright, J., Zeitlin, P. L. and Paweletz, C. P. (2007). Protein microarray platforms for clinical proteomics. *Proteomics Clinical Applications*, **1**, 934–952. DOI: 10.1002/prca.200700154

Ramachandran, N., Hainsworth, E., Bhullar, B., Eisenstein, S., Rosen, B., Lau, A. Y., Walter, J. C. and Labaer, J. (2004). Self-assembling protein microarrays. *Science*, **305**, 86–90. DOI: 10.1126/science.1097639

Ressine, A., Ekstrom, S., Marko-Varga, G. and Laurell, T. (2003). Macro-/nanoporous silicon as a support for high-performance protein microarrays. *Analytical Chemistry*, **75**, 6968–6974. DOI: 10.1021/ac034425q

Rusmini, F., Zhong, Z. Y. and Feijen, J. (2007). Protein immobilization strategies for protein biochips. *Biomacromolecules*, **8**, 1775–1789. DOI: 10.1021/bm061197b

Schena, M., Heller, R. A., Theriault, T. P., Konrad, K., Lachenmeier, E. and Davis, R. W. (1998). Microarrays: Biotechnology's discovery platform for functional genomics. *Trends in Biotechnology*, **16**, 301–306. DOI: 10.1016/S0167–7799(98)01219–0

Silzel, J. W., Cercek, B., Dodson, C., Tsay, T. and Obremski, R. J. (1998). Mass-sensing, multianalyte microarray immunoassay with imaging detection. *Clinical Chemistry*, **44**, 2036–2043.

Yakovleva, J., Davidsson, R., Lobanova, A., Bengtsson, M., Eremin, S., Laurell, T. and Emneus, J. (2002). Microfluidic enzyme immunoassay using silicon microchip with immobilized antibodies and chemiluminescence detection. *Analytical Chemistry*, **74**, 2994–3004. DOI: 10.1021/ac015645b

Yang, X., Janatova, J., Juenke, J. M., McMillin, G. A. and Andrade, J. D. (2007). An ImmunoChip prototype for simultaneous detection of antiepileptic drugs using an enhanced one-step homogeneous immunoassay. *Analytical Biochemistry*, **365**, 222–229. DOI: 10.1016/j.ab.2007.03.019

Yeh, C. H., Hung, C. Y., Chang, T. C., Lin, H. P. and Lin, Y. C. (2009). An immunoassay using antibody-gold nanoparticle conjugate, silver enhancement and flatbed scanner. *Microfluidics and Nanofluidics*, **6**, 85–91. DOI: 10.1007/s10404–008–0298–0

Zhou, S. L., Lu, X. J., Chen, C. F. and Sun, D. X. (2010). An immunoassay method for quantitative detection of proteins using single antibodies. *Analytical Biochemistry*, **400**, 213–218. DOI: 10.1016/j.ab.2010.01.038

13

Integrated microfluidic systems for genetic analysis

B. ZHUANG, W. GAN and P. LIU, Tsinghua University, China

DOI: 10.1533/9780857097040.4.465

Abstract: Driven by the ambitious goals proposed in various genome-related studies, microfluidic systems fully integrated by microfabrication technology have been developed rapidly and are poised to advance the field of genetic analysis substantially. To produce a high-performing microsystem, several key microchip elements must be strategically considered, including the selection of device materials, accurate temperature control, precise microfluidic control, and efficient sample/product transport during the process. We review several significant examples achieved recently in DNA sequencing: gene expression analysis, pathogen / infectious disease detection, and forensic short tandem repeat (STR) typing. With the advantages of high speed, increased sensitivity, and enhanced reliability, these fully integrated microsystems provide researchers with leverage to explore a variety of challenging research topics, such as automated DNA sequencing, single-cell gene expression characterisation, decentralised pathogen detection and forensic human identification.

Key words: microfabrication, DNA sequencing, genetic analysis, pathogen detection, short tandem repeat analysis.

13.1 Introduction

The completion of the human genome project (HGP) announced the start of the post-genome era (Lander *et al.*, 2001; Venter *et al.*, 2001). With the reference human genome sequence and ever-growing individual sequences established (Levy *et al.*, 2007; Wang *et al.*, 2008; Wheeler *et al.*, 2008), researchers' attentions have been directed towards investigating the effects of DNA variations among individuals and their implications for diseases (Calvo *et al.*, 2006; Beckmann *et al.*, 2007; Fanciulli *et al.*, 2007; Buchanan and Scherer, 2008), to discover genetic clues and evidence for understanding cellular behaviours (Blais and Dynlacht, 2005), and to develop more powerful genetic tools for application in forensics (Jobling and Gill, 2004; Butler, 2006), health care (Guttmacher *et al.*, 2007), food

safety (Abee *et al*., 2004), and so on. These research interests have posed further challenges to current genetic analytical techniques. For example, to fully understand gene functions and the importance of genome structural variations (block substitutions, insertions, deletions, inversions, and duplications) to speciation, evolution, and diseases (Zhao *et al*., 2004; Check, 2005; Ellegren, 2008), numerous large-scale genomes need to be sequenced to obtain comparative information. A high-throughput and low-cost sequencing technology, which can generate accurate long-range read lengths, is therefore of particular importance for many studies, such as the Cancer Genome Project. It is also known that subtle changes in gene expression are central for an organism to survive and these changes can vary substantially among some type of cells under identical conditions (Acar *et al*., 2008; Choi *et al.*, 2008). In addition, many biological processes, such as embryo development, and diseases such as cancer (Quintana *et al.*, 2008), originate from a single cell. Therefore, a genetic and gene expression analysis platform, which can manipulate single cells efficiently and provide single-molecule sensitivity, will be greatly appreciated by researchers. Genetic analysis is poised to emerge from research laboratories and play an important role in our daily lives, such as in forensics and clinical diagnosis. Ideally, these applications require compact instruments that are fast, low cost, easy to operate, and even portable for decentralised or point-of-care analysis. Undoubtedly, all these challenges suggest that future genetic analytical techniques must require less cost and time, have high sensitivity and high throughput, and provide flexible platforms to meet various applicable situations.

Although genetic analytical methods have advanced significantly through the application of robotics, there are several intrinsic limiting drawbacks.

(i) Sample loading. As the analytical targets are changing to single cells, the conventional serial dilution method for cell loading becomes ineffectual. Because the number of cells in each reaction follows the Poisson distribution, the variation of starting materials inevitably leads to irreproducible results.

(ii) Sample dilution. The liquid handling limitations of conventional analytical techniques are usually 5–10 μL, which not only consumes more expensive reagents, but also causes inevitable sample dilution. For example, to analyse a single gene (one DNA strand) in a cell, we conventionally put it into a working volume of 10 μL, which causes extreme dilution of this single template down to $<10^{-18}$ M. The most sensitive systems for DNA detection require concentrations in the femtomolar-picomolar range, which is already close to the maximum concentration of polymerase chain reaction (PCR) products practically generated from a single template in a 10 μL reaction.

(iii) Inefficient sample/product transport. During conventional genetic analysis, samples are transferred from one instrument to another several times, which can cause significant sample dilution and loss. For instance, in DNA capillary electrophoresis (CE) analysis, a sample of 1–2 μL is usually taken from 10 μL PCR products and later only ~2 nL of that sample is injected into the capillary for separation and detection (Butler *et al*., 2004). This inefficient sample transfer compromises the sensitivity and quantitative capability of current analytical methods.

(iv) Contamination. Contamination issues become prominent when dealing with low-copy-number samples, since the contaminants can overwhelm real target signals. Current analytical processes that have multiple open sample transfer steps make contamination inevitable (Gill *et al*., 2000). Nevertheless, the precipitous gap between the vast requirements of genetic analyses and the limited capabilities provided by current techniques will spur the improvement of existing tools and the innovation of new technologies.

13.2 Integrated microfluidic systems

Micro-total analysis systems (μTAS), or the so-called 'lab-on-a-chip', have attracted increasing attention because of their ability to integrate multiple biochemical processes at pL/nL-scale in a single device using microfabrication technology. The advantages of miniaturising and integrating genetic analysis include high speed, less reagent consumption, and a reduction in size of instruments (Manz *et al*., 1990, 1992; Harrison *et al*., 1993). Moreover, microfabrication technology has the potential to overcome the hurdles associated with conventional techniques. Since the intrinsic length (μm) and volume scales (pL-nL) of microstructures in a device are close to those of single cells, efficient manipulation and loading of individual cells in a high-throughput manner becomes possible (Sims and Allbritton, 2007). The limited diffusion distances and concentrated reagents realised by performing assays in nanolitre-scale reactors could also substantially increase the sensitivity and speed of biochemical reactions (Jensen, 1998). By integrating the analytical process on a single device, efficient connections between each functional unit can be achieved, so that the loss and dilution of samples is minimised. Additionally, microfluidic automations can also eliminate the risks of sample mix-up and contamination, which are critical for high-sensitivity genetic analyses. Given all these inherent advantages, fully integrated microfluidic systems are a promising technology.

The development of integrated microdevices for genetic analyses has advanced rapidly. The early development of microfabricated genetic analysis

devices focused on translating individual analytical steps into chip formats, such as DNA extraction, PCR, and microchannel CE, to replace their counterparts in conventional genetic analyses. Current research work has centred on the development of fully integrated microsystems to provide complete solutions with enhanced performances to specific applications. Many review articles have been published in recent years, covering various aspects of microfluidic devices, including microfabrication, materials, device interface, fluidic control, and a wide range of applications (Fredrickson and Fan, 2004; Lagally and Mathies, 2004; Roman and Kennedy, 2007; West *et al.*, 2008). Therefore, this chapter focuses on the development of integrated genetic analyses that have significant impacts on DNA sequencing, gene expression analysis, pathogen/infectious disease detection, and forensic STR typing.

13.3 Development of integrated microdevices

To develop fully integrated microsystems for gene expression and genetic analysis, several necessary chip elements must be strategically chosen, including device material, heaters and temperature sensors for thermal cycling of reactions, microvalves for fluidic control, and sample/product transport between analytical steps. We will briefly discuss these aspects as they closely relate to genetic analysis, but it is advisable to refer to other dedicated chapters on these aspects for more detailed information.

13.3.1 Device material

The choice of device material is important for the development of integrated microsystems, because the design, fabrication and operation of the device are heavily dependent on the properties of the substrates used to manufacture them. Glass remains by far the most extensively used substrate for implementing integrated microfluidic devices for genetic analysis due to its extraordinary advantages, including optical transparency for detection, and mature surface chemistry manipulation (Waters *et al.*, 1998; Lagally *et al.*, 2001; Ferrance *et al.*, 2003; Blazej *et al.*, 2006). The disadvantage of glass is its high cost in terms of material and fabrication. Plastic and elastomers, such as poly(methylmethacrylate) (PMMA) and poly(dimethylsiloxane) (PDMS), have also been successfully utilised in microsystems and thus have become increasingly popular (Quake and Scherer, 2000; Wang *et al.*, 2002; Fiorini and Chiu, 2005). In contrast to glass, their simple fabrication and low cost make plastic and elastomers the best choice for disposable devices. However, these materials are limited due to their incompatibility with metal microfabrication, uneasy surface modification techniques, and native fluorescence background. However, as material science continues to develop, new materials with excellent properties for microfluidics will be introduced in the near future.

13.3.2 Temperature control

Gene expression and genetic analyses usually include DNA or RNA amplification steps, which require rapid and accurate temperature control for thermally cycling reagents loaded in microreactors. To prevent the heat from affecting other chip elements and to reduce the thermal mass for rapid heating and cooling, the heating space should be precisely localised and minimised. Many temperature control methods, including contact and non-contact heating, have been successfully demonstrated on microdevices. Contact heating methods include external heaters attached to the chip surface, such as Peltier heaters (Kopp *et al*., 1998), and microfabricated thin film heaters made of Ti/Pt (Lagally *et al*., 2001), aluminium, (Burns *et al*., 1996), or indium tin oxide (ITO) (Fukuba *et al*., 2004). Non-contact heating can be realised by the infrared (IR) method (Huhmer and Landers, 2000). While these heating systems demonstrate similar performances in the laboratory setting, contact heating is most suitable for point-of-care applications due to its inherently smaller size.

13.3.3 Microfluidic control

Microvalves are essential parts for moving samples and products and preventing interference between each analytical step in a fully integrated microsystem (Oh and Ahn, 2006). Microvalves can be categorised into four different groups: actively mechanical, actively non-mechanical, passively mechanical, and passively non-mechanical. Table 13.1 lists several examples in each category that have been integrated into microdevices (Unger *et al*., 2000; Yobas *et al*., 2001; Oh *et al*., 2002; Feng *et al*., 2003; Grover *et al*., 2003; Koh *et al*., 2003; Feng and Kim, 2004; Li *et al*., 2004, Richter *et al.*, 2004). The following requirements should be taken into consideration when selecting microvalves: whether they are normally close or open mode, dead volume, power consumption, pressure resistance, and insensitivity to particle contamination. Generally speaking, actively mechanical microvalves have the best performance and are the most commonly used in microsystems considering their flow stability and automation. In addition, a micropump can be easily formed by connecting three valves in serial on a microchip (Quake and Scherer, 2000; Grover *et al.*, 2003). However, in a given application other simple passive valves may be more suitable. For example, in an integrated PCR-CE microdevice, the interface between the viscous separation matrix and the PCR solution can act as a passive valve to restrain the PCR solution in the reactor during thermal cycling (Lagally *et al.*, 2001). This passively mechanical valve is incontrollable, non-resistant to high pressure, but reliable for this situation.

Table 13.1 Microvalves for fluidic control on integrated devices

Categories	Mechanism	References
Actively mechanical	Electromagnetic	Oh *et al.*, 2002
	Electrostatic	Yobas *et al.*, 2001
	Piezoelectric	Li *et al.*, 2004
	Pneumatic	Unger *et al.*, 2000; Grover *et al.*, 2003
Actively non-mechanical	Phase change materials (Sol-gel, paraffin, etc.)	Richter *et al.*, 2004
Passively mechanical	Check valves (flap, membrane, etc.)	Feng and Kim, 2004
Passively non-mechanical	Hydrophobic valves	Feng *et al.*, 2003
	Gel valves	Koh *et al.*, 2003

13.3.4 Sample/product transport

The integration of the whole analytical process on a single device is more complex than simply combining several microfabricated units. Efficient and reproducible transport of the sample/product between function units is the key to a seamlessly integrated system and to fully demonstrate the advantages of sensitivity, reproducibility and reliability. Methods available to transport samples within a device include: (1) sample moved by timing-controlled pumps (Easley *et al.*, 2006), (2) sample driven by timing-controlled electric field (Liu *et al.*, 2006a), (3) sample carried by transport vehicles, such as DNA captured and transported using magnetic beads (Ueberfeld *et al.*, 2006; Beyor *et al.*, 2008), and (4) sample captured at the destination, such as filters (Khandurina *et al.*, 1999), capture gel (Blazej *et al.*, 2007), and solid phase extraction column (Long *et al.*, 2007). The pump and electric field methods are simple but require delicate timing. In particular, when there is a large volume mismatch between two structures, precious samples will be wasted or diluted. In contrast, the carrying and capture methods are more efficient and reliable, especially when volume mismatch exists in microdevices.

13.4 Applications of fully integrated systems in genetic analysis

13.4.1 DNA sequencing

As the demand for large-scale DNA sequencing grows, the National Institute of Health (NIH) in the USA continues to fund the development of new technologies to reduce the total cost of DNA sequencing from approximately $10m to $1000 per genome (Blow, 2008), which will eventually make

DNA sequencing a reliable and routine analytical procedure for biological researchers to explore complex biological processes, or even for physicians to tailor a personal treatment according to patients' genetic variations. To meet future expanding demands of DNA sequencing, extensive studies have been conducted to develop new technologies and to improve the current Sanger sequencing method. Next-generation DNA sequencing (NGS) technologies are evolving rapidly, and have been commercialised into many successful products providing massively high throughput with low cost (Mardis, 2008; Shendure and Ji, 2008). Recently published reviews provide a comprehensive introduction and analysis of their potential applications in the future, which will not be covered here (Shendure and Ji, 2008; Metzker, 2010). Although the NGS is replacing the conventional Sanger sequencing method in most whole-genome areas, Sanger sequencing remains by far the best choice for low-scale applications because of its long read lengths, flexibility in scale, and ease of operation.

Significant advances have been achieved towards developing microfabricated devices on which the conventional Sanger sequencing process can be carried out. The first four-colour electrophoretic separation of Sanger sequencing products on a microfabricated glass CE chip was demonstrated by Woolley and Mathies in 1995 (Woolley and Mathies, 1995). Since then, numerous studies have been conducted to improve the data quality and read-length of chip-based DNA sequencing separations. By optimising channel length and injector geometry (Liu *et al*., 1999), employing energy-transfer (ET) fluorescent reagents for fragment labelling (Ju *et al*., 1996; Kheterpal *et al.*, 1998; Berti *et al*., 2001), and utilising novel separation matrixes and coating polymers (Doherty *et al*., 2004; Chiesl *et al*., 2006), DNA sequencings with >500 bp read-length and ~99% accuracy have been repeatedly demonstrated by many research groups (Schmalzing *et al.*, 1998; Liu *et al.*, 1999; Backhouse *et al*., 2000). More recently, Barron *et al.* developed a pDMA (Poly(*N,N*-dimethylacrylamide)) separation matrix and pHEA (poly(*N*-hydroxyethylacrylamide)) dynamic coating to achieve an ultrafast separation of 600 bases in just 6.5 min by microchip electrophoresis (Fredlake *et al*., 2008). To improve the sequencing throughput, a 768-lane DNA sequencing system, which alternatively runs two 394-lane plates, was also demonstrated by Aborn *et al.* (2005). Although these chip-based CE systems demonstrate impressive performances, considering the rapid development of NGS technologies and the extensive use of the conventional Sanger sequencing method, the future of these Sanger sequencing microdevices is still yet to be seen.

The future of the Sanger sequencing microdevice relies on the true power of the microfabricated platform: the capability of integrating sample preparations with electrophoresis to achieve rapid and low-cost DNA sequencings. In 2006, Mathies *et al.* demonstrated a nanolitre-scale microfabricated

bioprocessor, which integrates all three Sanger sequencing steps – thermal cycling, sample purification, and CE – into a four-inch hybrid glass-polydimethylsiloxane (PDMS) wafer (Blazej *et al*., 2006). This fully integrated system, as shown in Plate IV (see colour section between pages 328 and 329). (Panel a), contains a 250-nL reactor with microfabricated four-point resistance temperature sensors and an external thin film heater for rapid thermal cycling (Panel b), PDMS micropumps and valves for efficient sample transport (Panel c) from the reactor to the capture chamber, via a hole for transporting the samples from the top-layer to the bottom-layer channels (Panel d). It has an affinity-capture chamber (Panel e) where Sanger sequencing fragments are captured by complementary oligos for purification and concentration, and a 30-cm folded channel with taper turns for CE separation with a long-range single-base resolution (Panel f). As shown in Plate IV (Panel g,) a complete DNA sequencing from 1 fmole of DNA template can be finished in under 30 min with a 556-base read-length and 99% accuracy, equivalent to those used in the initial human genome sequencing (Lander *et al*., 2001). To further improve the sensitivity, enhanced sample/product transport between thermal cycling and electrophoresis is of great importance. The concept of on-line sample preconcentration and injection for electrophoresis has been explored extensively (Breadmore, 2007; Sueyoshi *et al.*, 2008). For chip-based sequencing separation, Ueberfeld *et al.* developed a method for low-quantity DNA sample loading (Ueberfeld *et al.*, 2006). DNA was reversibly captured onto paramagnetic microspheres, injected into a channel using a magnetised wire, and then released for separation. Although ten-fold signal improvement was achieved, this method is not readily incorporated into an integrated microchip system. Recently, a gel-based affinity DNA capture, concentration, and inline-injection method integrated with on-chip CE was developed by Blazej *et al*. (2007). By replacing the conventional cross-injector with the new efficient, time-independent inline injector, 30 nL of sequencing sample produced from only 100 amol of human mitochondrial HVII template was near 100% immobilised in a capture gel and inline injected into a separation channel for electrophoresis. The successful development of these microfluidic systems provides excellent platforms on which automated DNA sequencing in a low scale can be performed quickly. This may suggest that the Sanger sequencing microsystem could be extensively used in clinical diagnosis, where a patient's short gene fragment can be quickly sequenced to aid diagnosis or personal treatments.

13.4.2 Gene expression analysis

A cell can be treated as a well-organised tiny machine, or as an electric circuit, which is full of certainty, so that cell behaviours can be precisely predicted based on environmental conditions and cell histories. However, more

and more studies indicate that even genetically identical cells with seemingly identical cell histories and conditions can have significant differences (Cai *et al*., 2006; Raj *et al*., 2006; Choi *et al*., 2008). Although gene expression is highly regulated for precise coordination within living organisms and is predicable on a general varying trend, the very low copy numbers of genes can cause random fluctuations of mRNA production in individual cells due to the thermal dynamic nature of biochemical reactions of only a few molecules, which cannot be averaged out by statistics of large numbers of reactants and lead to detectable differences in mRNA, protein, and eventually phenotype levels. The traditional analytical methods usually target cell contents extracted from 10^3 to 10^6 cells, the variations of which cannot be completely eliminated by careful experimental design and control of cell conditions (Di Carlo and Lee, 2006). Therefore, the information obtained is the average response from a population of cells, which disguises the behaviours of individual cells and even gives misleading information. Due to the difficulties of manipulating large numbers of tiny cells and detecting minute changes of low concentrations, conventional single-cell probing approaches usually suffer from intense manual operation, susceptibility to contamination, and extremely high cost. By combining microfabrication technology with these methods or translating the analyses into chip formats, significant improvements can be achieved due to the intrinsic small size and volume of microdevices, which are valuable for cell manipulation, sensitivity improvement, and system scale-up for high-throughput operation. Here we will illustrate several different microfabricated platforms for gene expression analysis by highlighting some impressive research results.

Fluorescence *in situ* hybridisation (FISH) is a powerful and widely-used technique that allows researchers to quantitatively probe single-copy mRNA in individual living cells (Levsky *et al*., 2002; Raj *et al.*, 2006). The analytical process includes the incubation of fluorescence-labelled oligonucleotide probes with target cells followed by the excess washing and visualisation of cells using confocal fluorescence microscopy. The major hurdle of this method is the cell manipulation step, which can be dramatically improved by microfabrication technology. Matsunaga *et al.* developed a highly-efficient single-cell entrapment system consisting of a microfabricated poly(ethylene terephthalate) micromesh and PDMS microfluidic channels (Matsunaga *et al*., 2008). By applying negative pressure on the micromesh, 70–80% of the introduced Raji Burkitt's lymphoma cells can be trapped and uniformly arranged in the microdevice. On-chip FISH assays including membrane permeabilisation, hybridisation, washing, and imaging were successfully performed to analyse β-actin mRNA expression in individual cells in a high-throughput manner. The development of such large-scale cell manipulation structures compatible with the following analytical operations would dramatically improve the data productivity of single-cell analysis.

Reverse-transcription PCR (RT-PCR) plays a central role in gene expression analysis. Many efforts have been made to improve RT-PCR in terms of sensitivity, automation, and throughput by miniaturising and integrating the whole process on a microdevice. Additionally, since enclosed microsystems can effectively prevent mRNA from exposure to RNases, this reliability can be significantly improved. Quake *et al.* constructed a multilayer PDMS microsystem using the soft photolithography method, which is capable of performing single-cell lysis, affinity mRNA purification, and cDNA synthesis (Marcus *et al.*, 2006a). Two key components implemented in this microsystem assured the success of on-chip quantitative mRNA analysis: enhanced reaction efficiency provided by nL-scale reactors, and 100% sample transfer within the microdevice achieved using oligo(dT)-modified paramagnetic beads for mRNA capture. Meanwhile, the same authors also developed a microfluidic reactor-array chip consisting of 8×9 (total 72) 450-pL reactors for RT-PCR. TaqMan hydrolysis probe chemistry was employed to detect RNA templates with a limit of 34 copies, which is close to mRNA amounts usually obtained from single cells (Marcus *et al.*, 2006b). Therefore, it is possible to develop a fully integrated system for gene expression analysis by combining the techniques described above. By using a similar device, Zhong *et al.* constructed an improved system for extracting total mRNAs from single human embryonic stem cells and synthesising cDNA directly (Zhong *et al.*, 2008). Bontoux *et al.* successfully integrated the single-cell trapping, total mRNA extraction, and RT-PCR into a microdevice using similar rotary reactors and PDMS microvalves developed by Quake *et al.* (Bontoux *et al.*, 2008). Both studies showed increased efficiency in extractions and reactions due to smaller volumes and integrated analytical processes. However, their dependence on off-chip amplification and detection limits their throughput and sensitivity.

Integrated PCR-CE microdevices developed for DNA amplification and separation should be an excellent platform for gene expression analysis from single cells, due to their excellent sensitivity, integrated operation, and the potential for high throughput. However, until recently no such microsystem was reported due to the lack of efficient sample/product transfer between each step for sensitive and quantitative analysis. Toriello *et al.* recently made a giant step forward and reported a fully integrated microsystem (Fig. 13.1a) with a single-cell sensitivity (Toriello *et al.*, 2008). In this microdevice, single cells surface-modified with oligos can be captured via DNA hybridisation by a size-limited gold pad modified with complementary oligos and located in a RT-PCR reactor. Following cell lysis using dry ice, on-step RT-PCR was performed in this 200-nL reactor with a microfabricated RTD and a heater for 25 min. After amplification, a three-valve PDMS micropump was employed to move amplicons from the reactor to an oligo-modified capture gel matrix, where amplicons were captured, purified and concentrated. By heating the

chip over the DNA melting temperature, amplicons were released into a CE separation channel for a size-based separation. Single Jurkat cell analyses targeting GAPDH and 18S rRNA genes were successfully performed on the microdevice with a total analytical time of <75 min, and clearly revealed gene expression variations of GAPDH between eight individual cells compared

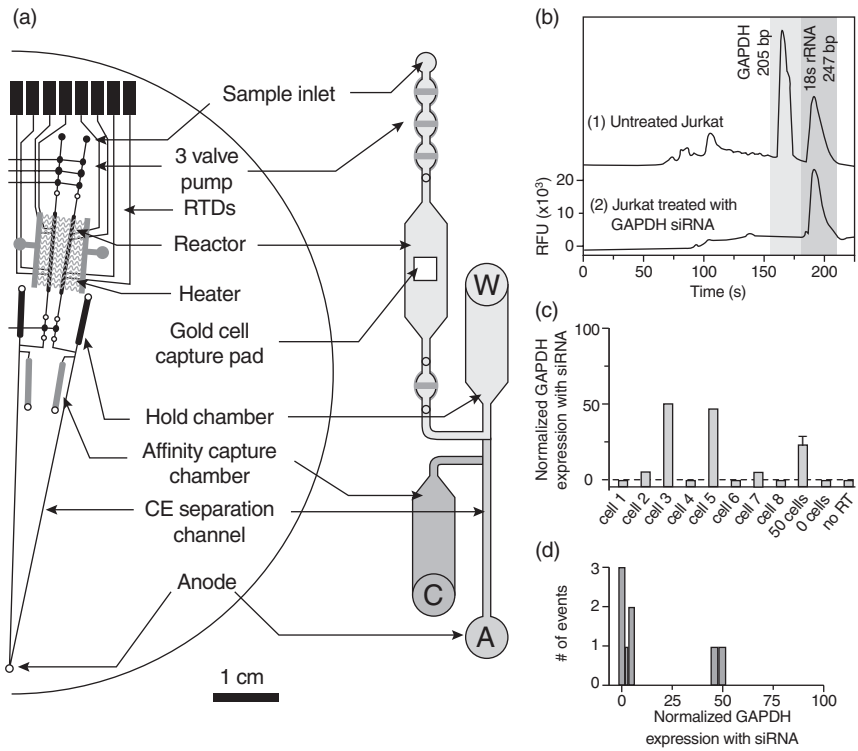

13.1 An integrated microdevice for gene expression analysis of single cells. (a) Schematic of the chip layout. This four-layer PDMS-glass hybrid device has four independent systems, each of which contains a three-valve pump, a size-limited gold pad, a 200-nL reactor with RTDs and a heater, a hold chamber and an affinity-capture chamber and inline injection, and a CE separation channel. (b) Gene expression and silencing experiments at the single-cell level. An untreated Jurkat cell shows a 200-bp (GAPDH) and a 247-bp (18S rRNA) peak in the electropherogram, while a cell treated with siRNA shows only a single peak for 18S rRNA. (c) Gene expression of GAPDH from eight individual Jurkat cells show GAPDH mRNA levels at 0%, 5%, 50%, 1%, 48%, 0%, 5%, and 0%. However, GAPDH expression measured from 50 cells shows an average of 21% ± 4%. (d) Histogram of the number of events for siRNA treated cells shows that there are two distinct populations of cells whose expression levels are very distinct from the population average. (*Source*: Adapted with permission from Toriello *et al.*, 2008.)

with bulk measurement from 50 cells (Fig. 13.1b–13.1d). This microsystem establishes the feasibility of performing single-cell gene expression analysis on an integrated device, and provides a powerful tool for scientists to explore the stochastic nature of gene expression.

Another promising method to facilitate massively high-throughput single-cell mRNA analysis on a microsystem is the use of microemulsions. Single cells can be efficiently encapsulated into droplets that contain the necessary reagents for enzymatic amplifications (He *et al.*, 2005; Edd *et al.*, 2008; Kumaresan *et al.*, 2008). He *et al.* demonstrated that single cells can be selectively isolated into pL- or fL-volume aqueous droplets in an immiscible phase (He *et al.*, 2005). Cells in these stable compartments were laser-induced lysed, and their contents were detected through enzymatic reactions. As described previously, the research by Mathies *et al.* showed that single-cell PCR can be performed within droplets (Kumaresan *et al.*, 2008). Recently, single-copy real-time reverse-transcription PCR was successfully demonstrated in isolated picolitre droplets (Beer *et al.*, 2007, 2008). Based on these results, it is predicted that single-cell real-time RT-PCR in droplets will be achieved in the near future for extremely high-throughput gene expression analysis.

13.4.3 Pathogen/infectious disease detection

Another application where microchip technology can play an important role is in pathogen or infectious disease detection, where point-of-care analysis is highly desirable (Ivnitski *et al.*, 2003; Yeung *et al.*, 2006b). In particular, the threat of biological warfare agents, including bacterial spores, vegetative bacteria, viruses, as well as protein and non-protein based toxins, is no longer a hypothetical concern for military and civilian populations (Haffer *et al.*, 2002). Routine standards for pathogen detection rely on culture plating and microscopy technologies, which are slow and sometimes even not applicable since culture methods may be unknown. To replace the bacterial culture process, PCR-based detection technology has found the greatest use for pathogen detection due to its speed (less than an hour), sensitivity (down to a single copy), as well as its capability of detecting minute amounts of targets from a huge non-pathogenic background. Many integrated microfluidic systems that utilise the PCR-based method have been constructed, demonstrating the capability of rapid, decentralised detection of various pathogens.

Real-time PCR is a prevalent method for rapidly detecting pathogens on a chip format because its combination of DNA amplification and detection on a single structure simplifies the system design and operation. The first handheld real-time thermal cycler for bacterial detection was demonstrated

by Higgins *et al.* in 2003 (Higgins *et al.,* 2003). This 1 kg handheld advanced nucleic acid analyser (HANAA) can perform up to four real-time PCRs in about 30 min using a 12V battery pack. Later, the integration of real-time PCR with sample preparation on a single device was also explored (Cady *et al.*, 2005). A silicon microdevice, consisting of a serpentine microchannel filled with silica pillars for DNA purification and a chamber for real-time PCR amplification and detection, was packed with all the necessary electronics and optics into a suitcase-sized instrument for purposes of on-site analysis. As low as 10^4 *L. monocytogenes* cells could be detected in about 45 min using this system. The disadvantages of real-time PCR-based pathogen detection are susceptibility to nonspecific PCR amplification and limited multiplexing due to the spectral overlap of fluorescent dyes.

A microarray-based system can provide much higher multiplexing than real-time PCR. Liu *et al.* demonstrated a fully integrated system capable of rapidly identifying influenza A hemagglutinin and neuraminidase subtypes and sequence portions of both genes (Liu *et al*., 2006b). This 12 000-spot DNA microarray chip, integrated with microfluidic control structures, demonstrated a great potential to detect numerous types of bacteria simultaneously. However, the need for fluorescent image scanning of the microarray limits the portability of this system. To simplify detection systems, electrochemical sequence-specific detection using oligo probes and silver-enhanced gold nanoparticles was developed for detecting *E. coli* and *Bacillus subtilis* cells (Yeung *et al*., 2006b). Although effective and simple, the detection limit of this system is about 100 cells, which may not be enough to detect some pathogens, such as *E. coli* O157, as few as ten cells of which can result in infections.

Chip-based CE following DNA amplification can provide not only high sensitivity, but also superb capability of detecting multiple targets since additional information regarding amplicon sizes can be obtained through DNA separation. A portable system consisting of an integrated PCR-CE microdevice and a compact instrument for electrical control and laser-induced fluorescence detection has been developed by Lagally *et al.* (2004). The limit of detection of this system was determined as two to three bacterial cells using *E. coli* K12, and a complete run can be completed in 20 min. Analysis of both methicillin-sensitive and methicillin-resistant *S. aureus* directly from intact cells was also successfully performed on the microsystem. This integrated genetic analyser established the feasibility of on-site pathogen detection using electrophoresis as the final detection method. Using a similar chip design, Kaigala *et al.* constructed a microfluidic PCR-CE system capable of detecting BK viruses directly from human urine samples with a detection limit of one to two viral copies (Kaigala *et al*., 2006). Prakash *et al*. integrated nine independent PCR chambers with one CE separation channel on a single chip for simultaneous amplification and sequential detection

of respiratory pathogen *Bordetella pertussis* (Prakash *et al.*, 2008). Pal *et al.* have developed a more complicated microfluidic device, integrating two nL-scale reactors for sequential PCR and restriction fragment length polymorphism (RFLP) reactions, valves and mixers for microfluidic control, and a separation channel for miniaturised gel electrophoresis (Pal *et al.*, 2005). Influenza viral strain subtyping by distinguishing the polymorphism in the hemagglutinin coding region was successfully performed on the microdevice with a total analysis time of around 40 minutes. Due to the compact size and the use of mass production technologies, the low fabrication cost of this device (~$7) makes a single use feasible. Nevertheless, one critical drawback of the integrated PCR-CE systems discussed above is that they may suffer from low or even no PCR amplifications when processing crude samples with PCR inhibitors due to the lack of integrated cell isolation and DNA purification steps prior to PCR.

To achieve the sample-in-answer-out capability of identifying bacteria from various samples with complex chemical or biological backgrounds, Landers *et al.* developed an integrated microfluidic genetic analysis system (Plates Va–Vc (see colour section between pages 328 and 329)), which can perform three major DNA processing steps: DNA extraction, PCR amplification, and electrophoretic separation (Easley *et al.*, 2006). The entire analysis timeline, as shown in Plate Vd, is <24 min, which is about ten times less than conventional methods. Briefly, DNA extraction from whole blood or nasal aspirate was performed in a microchannel packed with silica beads in under 10 min. The purified DNA samples together with a PCR mix were moved into a 550-nL PCR chamber, where rapid thermal cycling was conducted using a non-contact infrared (IR) heating system in under 11 min. After that, PCR products and a sizing standard were pressure-injected into a separation channel for electrophoresis using an on-chip diaphragm pump. Although the detection limits of this system were not thoroughly investigated, the successful analyses of *Bacillus anthracis* (anthrax) in 750 nL of whole blood and of *Bordetella pertussis* in 1 μL of nasal aspirate from a patient clearly indicate the wide application of this integrated system for rapid and large-scale screening of disease outbreaks. With further simplification and optimisation of the off-chip components for chip operations, this integrated genetic analyser could provide the capability required for point-of-care analysis.

Magnetic beads are an excellent sample transfer medium in an integrated microsystem because they can be precisely manipulated using an external magnet. Beyor *et al.* developed a cell concentration and isolation microdevice using immunomagnetic beads (Beyor *et al.*, 2008). *E. coli* cells are driven through a fluidised bead bed immobilised in microchannels using an integrated on-chip pump. 70% capture efficiency and 2 cfu/μL detection limit were obtained. More recently, they integrated this cell capture structure into

a PCR-CE microdevice to achieve cell preconcentration, purification, PCR, and capillary electrophoretic analysis on a single device (Beyor *et al.*, 2009). Since the magnetic beads can efficiently capture and concentrate target cells in the microchannels, and the cell-bead conjugates were precisely transported and located into the PCR chamber using on-chip pumps and external magnets without delicate timing issues, an impressive sensitivity of 0.2 cfu/μL *E. coli* O157 cells in a 50 μL input volume was obtained on this integrated system. O157 cells can also be selectively detected in a high commensal background of *E. coli K12* at a ratio of 1:1000. This cell capture PCR-CE microsystem represents a significant advancement in the development of rapid, sensitive and specific lab-on-a-chip devices for pathogen detection.

13.4.4 Short tandem repeat analysis

STR assays have become an indispensable and routine technique in forensic investigations due to their ability to produce highly distinctive profiles from minute amounts of DNA (Andersen *et al.*, 1996; Chakraborty *et al.*, 1999; Jobling and Gill, 2004; Butler, 2006). The current STR typing process includes DNA extraction from collected evidences, DNA quantitation for sample characterisation, multiplex PCR amplification using a STR typing kit, and amplicon separation and detection using a slab gel or CE. Although the automation of the STR analytical process is underway using robotics (Butler *et al.*, 2004; Montpetit *et al.*, 2005; Greenspoon *et al.*, 2006), a mere displacement of manual operations with automated instruments can only provide a limited degree of improvement, as this process is still performed in μL-scale volume on several bulky instruments. The limited genotyping technologies and the rising number of DNA samples submitted for DNA testing have resulted in an escalating backlog of crime scene evidence pending examination in forensic laboratories around the world. In addition to the huge demands for STR typing, forensic investigators are facing a unique challenge, in that forensic casework samples usually have lower amplification efficiency due to DNA degradation by exposure to environmental elements or natural contaminants, or low-copy-number DNA extracted from 'touch evidence' (Gill *et al.*, 2000; Whitaker *et al.*, 2001; Wickenheiser, 2002; Butler *et al.*, 2003). Mixture samples from several contributors are also often encountered in forensic investigations (Clayton *et al.*, 1998; Gill *et al.*, 1998).

Microfabrication technology could also substantially improve STR typing in the near future. Some impressive progress has been achieved and the translation of casework sample typing to microchip-based instruments is underway. Ehrlich *et al.* demonstrated baseline resolved separations of single-locus STR samples in 30 s using a microfabricated CE microchip with a 2.6-cm-long separation channel (Schmalzing *et al.*, 1997). Analyses of PCR samples containing four loci (CSF1PO, TPOX, THO1, and vWA)

were completed in less than two minutes. More impressive work demonstrated by Mathies *et al.* consisted of a 96-channel microfabricated capillary array electrophoresis (μCAE) device coupled with a four-colour confocal fluorescence scanner for high-throughput STR typing (Yeung *et al.*, 2006a). A prototype of the Berkeley μCAE device was successfully installed at the Virginia Department of Forensic Science for testing of routine forensic STR analyses (Greenspoon *et al.*, 2008). The successful transfer of this technology from an academic environment to a forensic laboratory indicates that chip-based CE technology is poised for application in forensic laboratories.

As mentioned in the previous section on DNA sequencing, sample preparation steps, such as PCR and post-PCR clean-up, are also being integrated into CE microdevices to achieve further improvements in STR typing. Not only does such an integrated analytical process expedite the analysis and lower the cost, but also prevent contaminations and sample mix-up, an outcome extremely valuable in forensic investigations. Liu *et al.* constructed an integrated PCR-CE microdevice for forensic STR analysis, as well as a portable analysis instrument containing all the electronics and optics for chip operation and four-colour fluorescence detection (Liu *et al.*, 2007). Multiplex amplification of amelogenin and three Y STR loci (DYS390, DYS393, DYS439) with 35 PCR cycles and CE separation were completed in 1.5 h with a detection limit of 20 copies of genomic DNA. To further explore the concept of performing rapid STR analyses in a setting outside a forensic laboratory, they conducted real-time DNA analyses at a mock crime scene (Liu *et al.*, 2008). The crime scene was investigated following standard procedures, and three blood stain samples were extracted, amplified and correctly typed at the scene. A DNA profile search against a mock CODIS database with a 'convicted offender' sample was successfully conducted within six hours of arrival at the crime scene. The successful demonstration of on-site STR typing at a crime scene validates the feasibility of real-time human identification for crime scene investigation, as well as mass disaster and security checkpoint applications.

To improve the sensitivity of the conventional STR analysis, post-PCR sample purification prior to CE has been employed (Smith and Ballantyne, 2007). Yeung *et al.* have developed an integrated STR sample clean-up and separation microdevice and method that employ a streptavidin capture gel chemistry coupled to a simple direct-injection geometry (Yeung *et al.*, 2009). Compared to microchip CE experiments performed using a cross-injector under similar conditions, the fluorescence intensity can be improved by 10–50 times for monoplex samples, and 14–19-fold for nine-plex STR products. The analyses of two artificial degraded DNA samples on the inline-injection CE microchip provided ~33% and ~71% more allelic markers respectively than those on the cross-injection chip. This enhanced sensitivity is highly valuable for low-copy-number and degraded DNA typing. Furthermore,

the capture structure incorporated into the high-throughput μCAE has also been reported (Liu *et al.*, 2011b). The near 100% amplicon product transfer between processing steps provided by the capture, concentration and inline-injection method should significantly advance the STR typing on the sensitivity, robustness and data quality for a variety of applications.

The miniaturisation of other 'upstream' STR steps is also under investigation towards fully integrated microfluidic systems for automated STR analysis. For example, Bienvenue *et al*. developed a single-channel extraction device and method for on-chip sperm cell lysis and DNA purification, which has direct implications on forensic STR analysis (Bienvenue *et al*., 2006). The purity and concentration of the DNA samples obtained from on-chip extraction were verified using conventional STR amplification and separation. Later, they reported another glass microdevice that integrated a silica

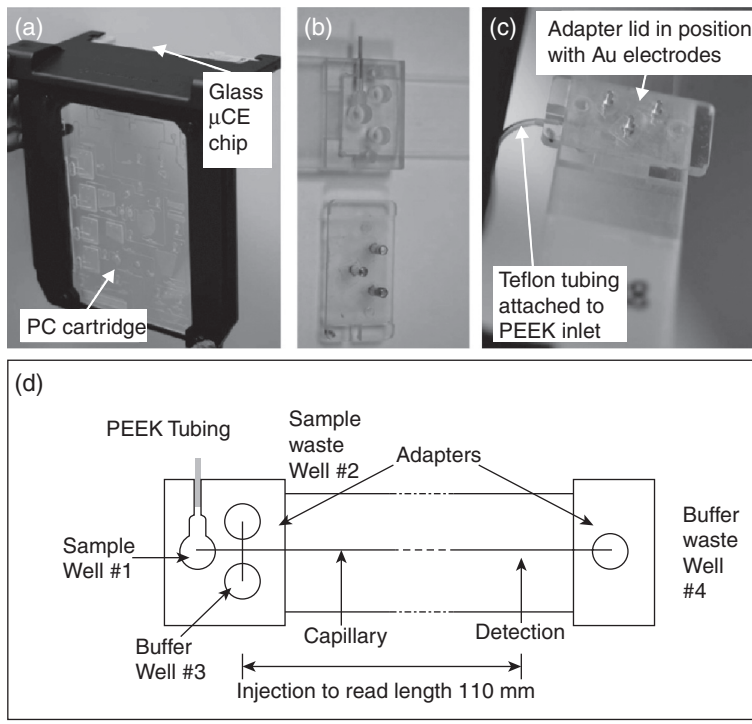

13.2 Assembly of the polycarbonate sample preparation cartridge and the glass CE microchip. (a) The PC cartridge is positioned in a vertical plane, the glass CE chip in the horizontal plane. (b) Image of the adapter with wells for the electrodes. A PEEK tubing was employed to load the sample processed in the PC cartridge to the CE chip. (c) The adapter lid in position. (d) Schematic of the layout of the CE microchip. (*Source*: Adapted with permission from Hopwood *et al.*, 2010.)

bead column and a PCR chamber together for fast DNA extraction and STR amplification from whole blood samples (Bienvenue *et al*., 2010). Recently, several true sample-in-answer-out microsystems were finally published. As shown in Fig. 13.2, Hopwood *et al.* successfully developed an integrated microfluidic system that consists of a DNA extraction and amplification cartridge coupled with a CE microchip for rapid STR analysis from reference buccal samples (Hopwood *et al.*, 2010). An aliquot of 150 μL of the sample lysate was introduced into the extraction and amplification cartridge. Using several electrochemical pumps and wax valves, the lysate was first mixed with ChargeSwitch magnetic beads for DNA extraction. Then the purified DNA was loaded into a 10-μL PCR chamber where PowerPlex ESI 16 PCR mix was pre-packaged. After amplification, amplicons along with preloaded sizing standards were injected into a separated CE chip via tubing for separation. During the overall analytical process, no manual operation was needed. Liu *et al.* developed a fully integrated micro-total analysis system that includes sequence-specific DNA template purification, PCR, post-PCR clean-up and capture inline injection, and CE (Liu *et al*., 2011a). While these systems demonstrated impressive performances, complicated operations need to be overcome before they can be practically applied in real forensic cases.

13.5 Conclusion and future trends

Over the past two decades, microfluidic devices for genetic analysis have advanced rapidly. Most of the analytical steps have been successfully translated into chip formats, demonstrating at least ten times better performances in speed and sample consumption over their conventional counterparts. Although quite a few companies have invested in developing and commercialising this new technology, the majority of the research society is not fully embracing microfluidic solutions. This is because most microfluidic products can only function as one single conventional step in the overall multi-step process and they still heavily rely on support from other off-chip instruments. Therefore, the additional capital investments caused by adopting microfluidic techniques, as well as the time and cost to train laboratory personnel, still outweigh the advantages.

We believe fully integrated microfluidic systems, which contain all the necessary analytical steps and provide a complete solution to users, are the inevitable direction in which to look to find a 'killer app' for microfluidics, because these integrated systems provide many extraordinary advantages that are not seen in discrete microdevices with single functions. Reduced reaction volume expedites the assay and enhances the sensitivity; precise fluidic control coupled with efficient sample transport prevents sample loss or dilution and increases assay efficiency; and automated operation saves labour and eliminates the risks of contamination. Therefore, unlike the

application of robotics, the introduction of microfluidic devices to society will skip the phase of replacing single steps in the conventional analytical process. Rather, fully integrated microsystems with high performances and the desired sample-in-answer-out capability will be introduced as complete solutions in the near future.

13.6 References

Abee, T., van Schaik, W. and Siezen, R. J. (2004). Impact of genomics on microbial food safety. *Trends in Biotechnology,* **22,** 653–660.

Aborn, J. H., El-Difrawy, S. A., Novotny, M., Gismondi, E. A., Lam, R., Matsudaira, P., McKenna, B. K., O'Neil, T., Streechon, P. and Ehrlich, D. J. (2005). A 768-lane microfabricated system for high-throughput DNA sequencing. *Lab on a Chip,* **5,** 669–674.

Acar, M., Mettetal, J. T. and van Oudenaarden, A. (2008). Stochastic switching as a survival strategy in fluctuating environments. *Nature Genetics,* **40,** 471–475.

Andersen, J. F., Greenhalgh, M. J., Butler, H. R., Kilpatrick, S. R., Piercy, R. C., Way, K. A., Myhill, H. S., Wright, J. C., Hallett, R. and Parkin, B. H. (1996). Further validation of a multiplex STR system for use in routine forensic identity testing. *Forensic Science International,* **78,** 47–64.

Backhouse, C., Caamano, M., Oaks, F., Nordman, E., Carrillo, A., Johnson, B. and Bay, S. (2000). DNA sequencing in a monolithic microchannel device. *Electrophoresis,* **21,** 150–156.

Beckmann, J. S., Estivill, X. and Antonarakis, S. E. (2007). Copy number variants and genetic traits: closer to the resolution of phenotypic to genotypic variability. *Nature Reviews Genetics,* **8,** 639–646.

Beer, N. R., Hindson, B. J., Wheeler, E. K., Hall, S. B., Rose, K. A., Kennedy, I. M. and Colston, B. W. (2007). On-chip, real-time, single-copy polymerase chain reaction in picoliter droplets. *Analytical Chemistry,* **79,** 8471–8475.

Beer, N. R., Wheeler, E. K., Lee-Houghton, L., Watkins, N., Nasarabadi, S., Hebert, N., Leung, P., Arnold, D. W., Bailey, C. G. and Colston, B. W. (2008). On-chip single-copy real-time reverse-transcription PCR in isolated picoliter droplets. *Analytical Chemistry,* **80,** 1854–1858.

Berti, L., Medintz, I. L., Tom, J. and Mathies, R. A. (2001). Energy-transfer cassette labeling for capillary array electrophoresis short tandem repeat DNA fragment sizing. *Bioconjugate Chemistry,* **12,** 493–500.

Beyor, N., Seo, T. S., Liu, P. and Mathies, R. A. (2008). Immunomagnetic bead-based cell concentration microdevice for dilute pathogen detection. *Biomedical Microdevices,* **10,** 909–917.

Beyor, N., Yi, L., Seo, T. S. and Mathies, R. A. (2009). Integrated capture, concentration, PCR, and capillary electrophoretic analysis of pathogens on a chip. *Analytical Chemistry,* **81,** 3523–3528.

Bienvenue, J. M., Duncalf, N., Marchiarullo, D., Ferrance, J. P. and Landers, J. P. (2006). Microchip-based cell lysis and DNA extraction from sperm cells for application to forensic analysis. *Journal of Forensic Sciences,* **51,** 266–273.

Bienvenue, J. M., Legendre, L. A., Ferrance, J. P. and Landers, J. P. (2010). An integrated microfluidic device for DNA purification and PCR amplification of STR fragments. *Forensic Science International: Genetics,* **4,** 178–186.

Blais, A. and Dynlacht, B. D. (2005). Constructing transcriptional regulatory networks. *Genes & Development,* **19,** 1499–1511.

Blazej, R. G., Kumaresan, P., Cronier, S. A., Mathies, R. A. and Jk (2007). Inline injection microdevice for attomole-scale sanger DNA sequencing. *Analytical Chemistry,* **79,** 4499–4506.

Blazej, R. G., Kumaresan, P. and Mathies, R. A. (2006). Microfabricated bioprocessor for integrated nanoliter-scale Sanger DNA sequencing. *Proceedings of the National Academy of Sciences of the United States of America,* **103,** 7240–7245.

Blow, N. (2008). DNA sequencing: generation next-next. *Nature Methods,* **5,** 267–274.

Bontoux, N., Dauphinot, L., Vitalis, T., Studer, V., Chen, Y., Rossier, J. and Potier, M. C. (2008). Integrating whole transcriptome assays on a lab-on-a-chip for single cell gene profiling. *Lab on a Chip,* **8,** 443–450.

Breadmore, M. C. (2007). Recent advances in enhancing the sensitivity of electrophoresis and electrochromatography in capillaries and microchips. *Electrophoresis,* **28,** 254–281.

Buchanan, J. A. and Scherer, S. W. (2008). Contemplating effects of genomic structural variation. *Genetics in Medicine,* **10,** 639–647.

Burns, M. A., Mastrangelo, C. H., Sammarco, T. S., Man, F. P., Webster, J. R., Johnson, B. N., Foerster, B., Jones, D., Fields, Y., Kaiser, A. R. and Burke, D. T. (1996). Microfabricated structures for integrated DNA analysis. *Proceedings of the National Academy of Sciences of the United States of America,* **93,** 5556–5561.

Butler, J. M. (2006). Genetics and genomics of core short tandem repeat loci used in human identity testing. *Journal of Forensic Sciences,* **51,** 253–265.

Butler, J. M., Buel, E., Crivellente, F. and McCord, B. R. (2004). Forensic DNA typing by capillary electrophoresis using the ABI Prism 310 and 3100 genetic analyzers for STR analysis. *Electrophoresis,* **25,** 1397–1412.

Butler, J. M., Shen, Y. and McCord, B. R. (2003). The development of reduced size STR amplicons as tools for analysis of degraded DNA. *Journal of Forensic Sciences,* **48,** 1054–1064.

Cady, N. C., Stelick, S., Kunnavakkam, M. V. and Batt, C. A. (2005). Real-time PCR detection of Listeria monocytogenes using an integrated microfluidics platform. *Sensors and Actuators B-Chemical,* **107,** 332–341.

Cai, L., Friedman, N. and Xie, X. S. (2006). Stochastic protein expression in individual cells at the single molecule level. *Nature,* **440,** 358–362.

Calvo, S., Jain, M., Xie, X. H., Sheth, S. A., Chang, B., Goldberger, O. A., Spinazzola, A., Zeviani, M., Carr, S. A. and Mootha, V. K. (2006). Systematic identification of human mitochondrial disease genes through integrative genomics. *Nature Genetics,* **38,** 576–582.

Chakraborty, R., Stivers, D. N., Su, B., Zhong, Y. X., Budowle, B. and Dp (1999). The utility of short tandem repeat loci beyond human identification: implications for development of new DNA typing systems. *Electrophoresis,* **20,** 1682–1696.

Check, E. (2005). Human genome: patchwork people. *Nature,* **437,** 1084–1086.

Chiesl, T. N., Putz, K. W., Babu, M., Mathias, P., Shaikh, K. A., Goluch, E. D., Liu, C. and Barron, A. E. (2006). Self-associating block copolymer networks for microchip electrophoresis provide enhanced DNA separation via 'inchworm' chain dynamics. *Analytical Chemistry,* **78,** 4409–4415.

Choi, P. J., Cai, L., Frieda, K. and Xie, S. (2008). A stochastic single-molecule event triggers phenotype switching of a bacterial cell. *Science,* **322,** 442–446.

Clayton, T. M., Whitaker, J. P., Sparkes, R. and Gill, P. (1998). Analysis and interpretation of mixed forensic stains using DNA STR profiling. *Forensic Science International,* **91,** 55–70.

di Carlo, D. and Lee, L. P. (2006). Dynamic single-cell analysis for quantitative biology. *Analytical Chemistry,* **78,** 7918–7925.

Doherty, E. A. S., Kan, C. W., Paegel, B. M., Yeung, S. H. I., Cao, S. T., Mathies, R. A. and Barron, A. E. (2004). Sparsely cross-linked 'nanogel' matrixes as fluid, mechanically stabilized polymer networks for high-throughput microchannel DNA sequencing. *Analytical Chemistry,* **76,** 5249–5256.

Easley, C. J., Karlinsey, J. M., Bienvenue, J. M., Legendre, L. A., Roper, M. G., Feldman, S. H., Hughes, M. A., Hewlett, E. L., Merkel, T. J., Ferrance, J. P. and Landers, J. P. (2006). A fully integrated microfluidic genetic analysis system with sample-in-answer-out capability. *Proceedings of the National Academy of Sciences of the United States of America,* **103,** 19272–19277.

Edd, J. F., di Carlo, D., Humphry, K. J., Koster, S., Irimia, D., Weitz, D. A. and Toner, M. (2008). Controlled encapsulation of single-cells into monodisperse picolitre drops. *Lab on a Chip,* **8,** 1262–1264.

Ellegren, H. (2008). Comparative genomics and the study of evolution by natural selection. *Molecular Ecology,* **17,** 4586–4596.

Fanciulli, M., Norsworthy, P. J., Petretto, E., Dong, R., Harper, L., Kamesh, L., Heward, J. M., Gough, S. C. L., de Smith, A., Blakemore, A. I. F., Owen, C. J., Pearce, S. H. S., Teixeira, L., Guillevin, L., Graham, D. S. C., Pusey, C. D., Cook, H. T., Vyse, T. J. and Aitman, T. J. (2007). FCGR3B copy number variation is associated with susceptibility to systemic, but not organ-specific, autoimmunity. *Nature Genetics,* **39,** 721–723.

Feng, G. H. and Kim, E. S. (2004). Micropump based on PZT unimorph and one-way parylene valves. *Journal of Micromechanics and Microengineering,* **14,** 429–435.

Feng, Y. Y., Zhou, Z. Y., Ye, X. Y. and Xiong, H. J. (2003). Passive valves based on hydrophobic microfluidics. *Sensors and Actuators A-Physical,* **108,** 138–143.

Ferrance, J. P., Wu, Q. R., Giordano, B., Hernandez, C., Kwok, Y., Snow, K., Thibodeau, S. and Landers, J. P. (2003). Developments toward a complete micro-total analysis system for Duchenne muscular dystrophy diagnosis. *Analytica Chimica Acta,* 500, 223–236.

Fiorini, G. S. and Chiu, D. T. (2005). Disposable microfluidic devices: fabrication, function, and application. *Biotechniques,* **38,** 429–446.

Fredlake, C. P., Hert, D. G., Kan, C. W., Chiesl, T. N., Root, B. E., Forster, R. E. and Barron, A. E. (2008). Ultrafast DNA sequencing on a microchip by a hybrid separation mechanism that gives 600 bases in 6.5 minutes. *Proceedings of the National Academy of Sciences of the United States of America,* **105,** 476–481.

Fredrickson, C. K. and Fan, Z. H. (2004). Macro-to-micro interfaces for microfluidic devices. *Lab on a Chip,* **4,** 526–533.

Fukuba, T., Yamamoto, T., Naganuma, T. and Fujii, T. (2004). Microfabricated flow-through device for DNA amplification – towards in situ gene analysis. *Chemical Engineering Journal,* **101,** 151–156.

Gill, P., Sparkes, R., Pinchin, R., Clayton, T., Whitaker, J. and Buckleton, J. (1998). Interpreting simple STR mixtures using allele peak areas. *Forensic Science International,* **91,** 41–53.

Gill, P., Whitaker, J., Flaxman, C., Brown, N. and Buckleton, J. (2000). An investigation of the rigor of interpretation rules for STRs derived from less than 100 pg of DNA. *Forensic Science International,* **112,** 17–40.

Greenspoon, S. A., Sykes, K. L. V., Ban, J. D., Pollard, A., Baisden, M., Farr, M., Graham, N., Collins, B. L., Green, M. M. and Christenson, C. C. (2006). Automated PCR setup for forensic casework samples using the Normalization Wizard and PCR Setup robotic methods. *Forensic Science International,* **164,** 240–248.

Greenspoon, S. A., Yeung, S. H. I., Johnson, K. R., Chu, W. K., Rhee, H. N., McGuckian, A. B., Crouse, C. A., Chiesl, T. N., Barron, A. E., Scherer, J. R., Ban, J. D. and Mathies, R. A. (2008). A forensic laboratory tests the Berkeley microfabricated capillary array electrophoresis device. *Journal of Forensic Sciences,* **53,** 828–837.

Grover, W. H., Skelley, A. M., Liu, C. N., Lagally, E. T. and Mathies, R. A. (2003). Monolithic membrane valves and diaphragm pumps for practical large-scale integration into glass microfluidic devices. *Sensors and Actuators B-Chemical,* **89,** 315–323.

Guttmacher, A. E., Porteous, M. E. and McInerney, J. D. (2007). Educating healthcare professionals about genetics and genomics. *Nature Reviews Genetics,* **8,** 151-U6.

Haffer, A. S. T., Rogers, J. R., Montello, M. J., Frank, E. C. and Ostroff, C. (2002). 2001 anthrax crisis in Washington, DC: clinic for persons exposed to contaminated mail. *American Journal of Health-System Pharmacy,* **59,** 1189–1192.

Harrison, D. J., Fluri, K., Seiler, K., Fan, Z. H., Effenhauser, C. S. and Manz, A. (1993). Micromachining a miniaturized capillary electrophoresis-based chemical-analysis system on a chip. *Science,* **261,** 895–897.

He, M. Y., Edgar, J. S., Jeffries, G. D. M., Lorenz, R. M., Shelby, J. P. and Chiu, D. T. (2005). Selective encapsulation of single cells and subcellular organelles into picoliter- and femtoliter-volume droplets. *Analytical Chemistry,* **77,** 1539–1544.

Higgins, J. A., Nasarabadi, S., Karns, J. S., Shelton, D. R., Cooper, M., Gbakima, A. and Koopman, R. P. (2003). A handheld real time thermal cycler for bacterial pathogen detection. *Biosensors and Bioelectronics,* **18,** 1115–1123.

Hopwood, A. J., Hurth, C., Yang, J., Cai, Z., Moran, N., Lee-Edghill, J. G., Nordquist, A., Lenigk, R., Estes, M. D., Haley, J. P., Mcalister, C. R., Chen, X., Brooks, C., Smith, S., Elliott, K., Koumi, P., Zenhausern, F. and Tully, G. (2010). Integrated microfluidic system for rapid forensic DNA analysis: sample collection to DNA profile. *Analytical Chemistry,* **82,** 6991–6999.

Huhmer, A. F. R. and Landers, J. P. (2000). Noncontact infrared-mediated thermocycling for effective polymerase chain reaction amplification of DNA in nanoliter volumes. *Analytical Chemistry,* **72,** 5507–5512.

Ivnitski, D., O'Neil, D. J., Gattuso, A., Schlicht, R., Calidonna, M. and Fisher, R. (2003). Nucleic acid approaches for detection and identification of biological warfare and infectious disease agents. *Biotechniques,* **35,** 862–869.

Jensen, K. (1998). Chemical kinetics – smaller, faster chemistry. *Nature,* **393,** 735–736.

Jobling, M. A. and Gill, P. (2004). Encoded evidence: DNA in forensic analysis. *Nature Reviews Genetics,* **5,** 739–751.

Ju, J. Y., Glazer, A. N. and Mathies, R. A. (1996). Energy transfer primers: a new fluorescence labeling paradigm for DNA sequencing and analysis. *Nature Medicine,* **2,** 246–249.

Kaigala, G. V., Huskins, R. J., Preiksaitis, J., Pang, X. L., Pilarski, L. M. and Backhouse, C. J. (2006). Automated screening using microfluidic chip-based PCR and product detection to assess risk of BK virus-associated nephropathy in renal transplant recipients. *Electrophoresis,* **27,** 3753–3763.

Khandurina, J., Jacobson, S. C., Waters, L. C., Foote, R. S. and Ramsey, J. M. (1999). Microfabricated porous membrane structure for sample concentration and electrophoretic analysis. *Analytical Chemistry,* **71,** 1815–1819.

Kheterpal, I., Li, L., Speed, T. P. and Mathies, R. A. (1998). A three-wavelength labeling approach for DNA sequencing using energy transfer primers and capillary electrophoresis. *Electrophoresis,* **19,** 1403–1414.

Koh, C. G., Tan, W., Zhao, M. Q., Ricco, A. J. and Fan, Z. H. (2003). Integrating polymerase chain reaction, valving, and electrophoresis in a plastic device for bacterial detection. *Analytical Chemistry,* **75,** 4591–4598.

Kopp, M. U., de Mello, A. J. and Manz, A. (1998). Chemical amplification: continuous-flow PCR on a chip. *Science,* **280,** 1046–1048.

Kumaresan, P., Yang, C. J., Cronier, S. A., Blazei, R. G. and Mathies, R. A. (2008). High-throughput single copy DNA amplification and cell analysis in engineered nanoliter droplets. *Analytical Chemistry,* 80, 3522–3529.

Lagally, E. T., Emrich, C. A. and Mathies, R. A. (2001). Fully integrated PCR-capillary electrophoresis microsystem for DNA analysis. *Lab on a Chip,* **1,** 102–107.

Lagally, E. T. and Mathies, R. A. (2004). Integrated genetic analysis microsystems. *Journal of Physics D-Applied Physics,* **37,** R245–R261.

Lagally, E. T., Scherer, J. R., Blazej, R. G., Toriello, N. M., Diep, B. A., Ramchandani, M., Sensabaugh, G. F., Riley, L. W. and Mathies, R. A. (2004). Integrated portable genetic analysis microsystem for pathogen/infectious disease detection. *Analytical Chemistry,* **76,** 3162–3170.

Lander, E. S., Linton, L. M., Birren, B., Nusbaum, C., Zody, M. C., Baldwin, J., Devon, K., Dewar, K., Doyle, M., Fitzhugh, W., Funke, R., Gage, D., Harris, K., Heaford, A., Howland, J., Kann, L., Lehoczky, J., Levine, R., McEwan, P., McKernan, K., Meldrim, J., Mesirov, J. P., Miranda, C., Morris, W., Naylor, J., Raymond, C., Rosetti, M., Santos, R., Sheridan, A., Sougnez, C., Stange-Thomann, N., Stojanovic, N., Subramanian, A., Wyman, D., Rogers, J., Sulston, J., Ainscough, R., Beck, S., Bentley, D., Burton, J., Clee, C., Carter, N., Coulson, A., Deadman, R., Deloukas, P., Dunham, A., Dunham, I., Durbin, R., French, L., Grafham, D., Gregory, S., Hubbard, T., Humphray, S., Hunt, A., Jones, M., Lloyd, C., McMurray, A., Matthews, L., Mercer, S., Milne, S., Mullikin, J. C., Mungall, A., Plumb, R., Ross, M., Shownkeen, R., Sims, S., Waterston, R. H., Wilson, R. K., Hillier, L. W., McPherson, J. D., Marra, M. A., Mardis, E. R., Fulton, L. A., Chinwalla, A. T., Pepin, K. H., Gish, W. R., Chissoe, S. L., Wendl, M. C., Delehaunty, K. D., Miner, T. L., Delehaunty, A., Kramer, J. B., Cook, L. L., Fulton, R. S., Johnson, D. L., Minx, P. J., Clifton, S. W., Hawkins, T., Branscomb, E., Predki, P., Richardson, P., Wenning, S., Slezak, T., Doggett, N., Cheng, J. F., Olsen, A., Lucas, S., Elkin, C., Uberbacher, E., Frazier, M., *et al.* (2001). Initial sequencing and analysis of the human genome. *Nature,* **409,** 860–921.

Levsky, J. M., Shenoy, S. M., Pezo, R. C. and Singer, R. H. (2002). Single-cell gene expression profiling. *Science,* **297,** 836–840.

Levy, S., Sutton, G., Ng, P. C., Feuk, L., Halpern, A. L., Walenz, B. P., Axelrod, N., Huang, J., Kirkness, E. F., Denisov, G., Lin, Y., MacDonald, J. R., Pang, A. W. C., Shago, M., Stockwell, T. B., Tsiamouri, A., Bafna, V., Bansal, V., Kravitz, S. A.,

Busam, D. A., Beeson, K. Y., McLntosh, T. C., Remington, K. A., Abril, J. F., Gill, J., Borman, J., Rogers, Y. H., Frazier, M. E., Scherer, S. W., Strausberg, R. L. and Venter, J. C. (2007). The diploid genome sequence of an individual human. *Plos Biology,* **5,** 2113–2144.

Li, H. Q., Roberts, D. C., Steyn, J. L., Turner, K. T., Yaglioglu, O., Hagood, N. W., Spearing, S. M. and Schmidt, M. A. (2004). Fabrication of a high frequency piezoelectric microvalve. *Sensors and Actuators a-Physical,* **111,** 51–56.

Liu, C. N., Toriello, N. M. and Mathies, R. A. (2006a). Multichannel PCR-CE microdevice for genetic analysis. *Analytical Chemistry,* **78,** 5474–5479.

Liu, P., LI, X., Greenspoon, S. A., Scherer, J. R. and Mathies, R. A. (2011a). Integrated DNA purification, PCR, sample cleanup, and capillary electrophoresis microchip for forensic human identification. *Lab on a Chip,* **11,** 1041–1048.

Liu, P., Scherer, J. R., Greenspoon, S. A., Chiesl, T. N. and Mathies, R. A. (2011b). Integrated sample cleanup and capillary array electrophoresis microchip for forensic short tandem repeat analysis. *Forensic Science International: Genetics,* **5,** 484–92.

Liu, P., Seo, T. S., Beyor, N., Shin, K. J., Scherer, J. R. and Mathies, R. A. (2007). Integrated portable polymerase chain reaction-capillary electrophoresis microsystem for rapid forensic short tandem repeat typing. *Analytical Chemistry,* **79,** 1881–1889.

Liu, P., Yeung, S. H. I., Crenshaw, K. A., Crouse, C. A., Scherer, J. R. and Mathies, R. A. (2008). Real-time forensic DNA analysis at a crime scene using a portable microchip analyzer. *Forensic Science International: Genetics*, **2,** 301–309.

Liu, R. H., Lodes, M. J., Nguyen, T., Siuda, T., Slota, M., Fuji, H. S. and McShea, A. (2006b). Validation of a fully integrated microfluidic array device for influenza A subtype identification and sequencing. *Analytical Chemistry,* **78,** 4184–4193.

Liu, S. R., Shi, Y. N., Ja, W. W. and Mathies, R. A. (1999). Optimization of high-speed DNA sequencing on microfabricated capillary electrophoresis channels. *Analytical Chemistry,* **71,** 566–573.

Long, Z. C., Shen, Z., Wu, D. P., Qin, J. H. and Lin, B. C. (2007). Integrated multilayer microfluidic device with a nanoporous membrane interconnect for online coupling of solid-phase extraction to microchip electrophoresis. *Lab on a Chip,* **7,** 1819–1824.

Manz, A., Graber, N. and Widmer, H. M. (1990). Miniaturized total chemical-analysis systems – a novel concept for chemical sensing. *Sensors and Actuators B-Chemical,* **1,** 244–248.

Manz, A., Harrison, D. J., Verpoorte, E. M. J., Fettinger, J. C., Paulus, A., Ludi, H. and Widmer, H. M. (1992). Planar chips technology for miniaturization and integration of separation techniques into monitoring systems – capillary electrophoresis on a chip. *J. Chromatogr.,* **593,** 253–258.

Marcus, J. S., Anderson, W. F. and Quake, S. R. (2006a). Microfluidic single-cell mRNA isolation and analysis. *Analytical Chemistry,* **78,** 3084–3089.

Marcus, J. S., Anderson, W. F. and Quake, S. R. (2006b). Parallel picoliter RT-PCR assays using microfluidics. *Analytical Chemistry,* **78,** 956–958.

Mardis, E. R. (2008). Next-generation DNA sequencing methods. *Annual Review of Genomics and Human Genetics,* **9,** 387–402.

Matsunaga, T., Hosokawa, M., Arakaki, A., Taguchi, T., Mori, T., Tanaka, T. and Takeyama, H. (2008). High-efficiency single-cell entrapment and fluorescence in situ hybridization analysis using a poly(dimethylsiloxane) microfluidic device

integrated with a black poly(ethylene terephthalate) micromesh. *Analytical Chemistry,* **80,** 5139–5145.

Metzker, M. L. (2010). Applications of next-generation sequencing sequencing technologies – the next generation. *Nature Reviews Genetics,* **11,** 31–46.

Montpetit, S. A., Fitch, I. T. and O'Donnell, P. T. (2005). A simple automated instrument for DNA extraction in forensic casework. *Journal of Forensic Sciences,* **50,** 555–563.

National Cancer Institute. The Cancer Genome Atlas. http://cancergenome.nih.gov/.

NIH News Release. New Grants Bolster Efforts to Generate Faster and Cheaper Tools for DNA Sequencing. http://www.genome.gov/25522229.

Oh, K. W. and Ahn, C. H. (2006). A review of microvalves. *Journal of Micromechanics and Microengineering,* **16,** R13.

Oh, K. W., Han, A., Bhansali, S. and Ahn, C. H. (2002). A low-temperature bonding technique using spin-on fluorocarbon polymers to assemble microsystems. *Journal of Micromechanics and Microengineering,* **12,** 187–191.

Pal, R., Yang, M., Lin, R., Johnson, B. N., Srivastava, N., Razzacki, S. Z., Chomistek, K. J., Heldsinger, D. C., Haque, R. M., Ugaz, V. M., Thwar, P. K., Chen, Z., Alfano, K., Yim, M. B., Krishnan, M., Fuller, A. O., Larson, R. G., Burke, D. T. and Burns, M. A. (2005). An integrated microfluidic device for influenza and other genetic analyses. *Lab on a Chip,* **5,** 1024–1032.

Prakash, A. R., de la Rosa, C., Fox, J. D. and Kaler, K. V. I. S. (2008). Identification of respiratory pathogen Bordetella Pertussis using integrated microfluidic chip technology. *Microfluidics and Nanofluidics,* **4,** 451–456.

Quake, S. R. and Scherer, A. (2000). From micro- to nanofabrication with soft materials. *Science,* **290,** 1536–1540.

Quintana, E., Shackleton, M., Sabel, M. S., Fullen, D. R., Johnson, T. M. and Morrison, S. J. (2008). Efficient tumour formation by single human melanoma cells. *Nature,* **456,** 593-U33.

Raj, A., Peskin, C. S., Tranchina, D., Vargas, D. Y. and Tyagi, S. (2006). Stochastic mRNA synthesis in mammalian cells. *Plos Biology,* **4,** 1707–1719.

Richter, A., Howitz, S., Kuckling, D., Kretschmer, K. and Arndt, K. F. (2004). Automatically and electronically controllable hydrogel based valves and microvalves – design and operating performance. *Macromolecular Symposia,* **210,** 447–456.

Roman, G. T. and Kennedy, R. T. (2007). Fully integrated microfluidic separations systems for biochemical analysis. *Journal of Chromatography A,* **1168,** 170–188.

Schmalzing, D., Adourian, A., Koutny, L., Ziaugra, L., Matsudaira, P. and Ehrlich, D. (1998). DNA sequencing on microfabricated electrophoretic devices. *Analytical Chemistry,* **70,** 2303–2310.

Schmalzing, D., Koutny, L., Adourian, A., Belgrader, P., Matsudaira, P. and Ehrlich, D.(1997). DNA typing in thirty seconds with a microfabricated device. *Proceedings of the National Academy of Sciences of the United States of America,* **94,** 10273–10278.

Shendure, J. and Ji, H. L. (2008). Next-generation DNA sequencing. *Nature Biotechnology,* **26,** 1135–1145.

Sims, C. E. and Allbritton, N. L. (2007). Analysis of single mammalian cells on-chip. *Lab on a Chip,* **7,** 423–440.

Smith, P. J. and Ballantyne, J. (2007). Simplified low-copy-number DNA analysis by Post-PCR purification. *Journal of Forensic Sciences,* **52,** 820–829.

Sueyoshi, K., Kitagawa, F. and Otsuka, K. (2008). Recent progress of online sample preconcentration techniques in microchip electrophoresis. *Journal of Separation Science,* **31,** 2650–2666.

Toriello, N. M., Douglas, E. S., Thaitrong, N., Hsiao, S. C., Francis, M. B., Bertozzi, C. R. and Mathies, R. A. (2008). Integrated Microfluidic Bioprocessor for Single-Cell Gene Expression Analysis. *Proceedings of the National Academy of Sciences of the United States of America,* **105,** 20173–20178.

Ueberfeld, J., El-Difrawy, S. A., Ramdhanie, K. and Ehrlich, D. J. (2006). Solid-support sample loading for DNA sequencing. *Analytical Chemistry,* **78,** 3632–3637.

Unger, M. A., Chou, H. P., Thorsen, T., Scherer, A. and Quake, S. R. (2000). Monolithic microfabricated valves and pumps by multilayer soft lithography. *Science,* **288,** 113–116.

Venter, J. C., Adams, M. D., Myers, E. W., Li, P. W., Mural, R. J., Sutton, G. G., Smith, H. O., Yandell, M., Evans, C. A., Holt, R. A., Gocayne, J. D., Amanatides, P., Ballew, R. M., Huson, D. H., Wortman, J. R., Zhang, Q., Kodira, C. D., Zheng, X. Q. H., Chen, L., Skupski, M., Subramanian, G., Thomas, P. D., Zhang, J. H., Miklos, G. L. G., Nelson, C., Broder, S., Clark, A. G., Nadeau, C., McKusick, V. A., Zinder, N., Levine, A. J., Roberts, R. J., Simon, M., Slayman, C., Hunkapiller, M., Bolanos, R., Delcher, A., Dew, I., Fasulo, D., Flanigan, M., Florea, L., Halpern, A., Hannenhalli, S., Kravitz, S., Levy, S., Mobarry, C., Reinert, K., Remington, K., Abu-Threideh, J., Beasley, E., Biddick, K., Bonazzi, V., Brandon, R., Cargill, M., Chandramouliswaran, I., Charlab, R., Chaturvedi, K., Deng, Z. M., di Francesco, V., Dunn, P., Eilbeck, K., Evangelista, C., Gabrielian, A. E., Gan, W., Ge, W. M., Gong, F. C., Gu, Z. P., Guan, P., Heiman, T. J., Higgins, M. E., Ji, R. R., Ke, Z. X., Ketchum, K. A., Lai, Z. W., Lei, Y. D., Li, Z. Y., Li, J. Y., Liang, Y., Lin, X. Y., Lu, F., Merkulov, G. V., Milshina, N., Moore, H. M., Naik, A. K., Narayan, V. A., Neelam, B., Nusskern, D., Rusch, D. B., Salzberg, S., Shao, W., Shue, B. X., Sun, J. T., Wang, Z. Y., Wang, A. H., Wang, X., Wang, J., Wei, M. H., Wides, R., Xiao, C. L., Yan, C. H., *et al*. (2001). The sequence of the human genome. *Science,* **291,** 1304–1351.

Wang, J., Pumera, M., Chatrathi, M. P., Escarpa, A., Konrad, R., Griebel, A., Dorner, W. and Lowe, H. (2002). Towards disposable lab-on-a-chip: poly(methylmethacrylate) microchip electrophoresis device with electrochemical detection. *Electrophoresis,* **23,** 596–601.

Wang, J., Wang, W., Li, R. Q., Li, Y. R., Tian, G., Goodman, L., Fan, W., Zhang, J. Q., Li, J., Zhang, J. B., Guo, Y. R., Feng, B. X., Li, H., Lu, Y., Fang, X. D., Liang, H. Q., Du, Z. L., Li, D., Zhao, Y. Q., Hu, Y. J., Yang, Z. Z., Zheng, H. C., Hellmann, I., Inouye, M., Pool, J., Yi, X., Zhao, J., Duan, J. J., Zhou, Y., Qin, J. J., Ma, L. J., Li, G. Q., Yang, Z. T., Zhang, G. J., Yang, B., Yu, C., Liang, F., Li, W. J., Li, S. C., Li, D. W., Ni, P. X., Ruan, J., Li, Q. B., Zhu, H. M., Liu, D. Y., Lu, Z. K., Li, N., Guo, G. W., Zhang, J. G., Ye, J., Fang, L., Hao, Q., Chen, Q., Liang, Y., Su, Y. Y., San, A., Ping, C., Yang, S., Chen, F., Li, L., Zhou, K., Zheng, H. K., Ren, Y. Y., Yang, L., Gao, Y., Yang, G. H., Li, Z., Feng, X. L., Kristiansen, K., Wong, G. K. S., Nielsen, R., Durbin, R., Bolund, L., Zhang, X. Q., Li, S. G., Yang, H. M. and Wang, J. (2008). The diploid genome sequence of an Asian individual. *Nature,* **456,** 60–66.

Waters, L. C., Jacobson, S. C., Kroutchinina, N., Khandurina, J., Foote, R. S., Ramsey, J. M. and Ty (1998). Multiple sample PCR amplification and electrophoretic analysis on a microchip. *Analytical Chemistry,* **70,** 5172–5176.

West, J., Becker, M., Tombrink, S. and Manz, A. (2008). Micro total analysis systems: Latest achievements. *Analytical Chemistry,* **80,** 4403–4419.

Wheeler, D. A., Srinivasan, M., Egholm, M., Shen, Y., Chen, L., McGuire, A., He, W., Chen, Y. J., Makhijani, V., Roth, G. T., Gomes, X., Tartaro, K., Niazi, F., Turcotte, C. L., Irzyk, G. P., Lupski, J. R., Chinault, C., Song, X. Z., Liu, Y., Yuan, Y., Nazareth, L., Qin, X., Muzny, D. M., Margulies, M., Weinstock, G. M., Gibbs, R. A. and Rothberg, J. M. (2008). The complete genome of an individual by massively parallel DNA sequencing. *Nature,* **452,** 872–877.

Whitaker, J. P., Cotton, E. A. and Gill, P. (2001). A comparison of the characteristics of profiles produced with the AMPFlSTR SGM Plus multiplex system for both standard and low copy number (LCN) STR DNA analysis. *Forensic Science International,* **123,** 215–23.

Wickenheiser, R. A. (2002). Trace DNA: a review, discussion of theory, and application of the transfer of trace quantities of DNA through skin contact. *Journal of Forensic Sciences,* **47,** 442–450.

Woolley, A. T. and Mathies, R. A. (1995). Ultra-high-speed dna-sequencing using capillary electrophoresis chips. *Analytical Chemistry,* **67,** 3676–3680.

Yeung, S. H. I., Greenspoon, S. A., McGuckian, A., Crouse, C. A., Emrich, C. A., Ban, J. and Mathies, R. A. (2006a). Rapid and high-throughput forensic short tandem repeat typing using a 96-lane microfabricated capillary array electrophoresis microdevice. *Journal of Forensic Sciences,* **51,** 740–747.

Yeung, S. H. I., Liu, P., del Bueno, N., Greenspoon, S. A. and Mathies, R. A. (2009). Integrated sample cleanup-capillary electrophoresis microchip for high-performance short tandem repeat genetic analysis. *Analytical Chemistry,* **81,** 210–217.

Yeung, S. W., Lee, T. M. H., Cai, H. and Hsing, I. M. (2006b). A DNA biochip for on-the-spot multiplexed pathogen identification. *Nucleic Acids Research,* **34**.

Yobas, L., Huff, M. A., Lisy, F. J. and Durand, D. M. (2001). A novel bulk-micromachined electrostatic microvalve with a curved-compliant structure applicable for a pneumatic tactile display. *Journal of Microelectromechanical Systems,* **10,** 187–196.

Zhao, S. Y., Shetty, J., Hou, L. H., Delcher, A., Zhu, B. L., Osoegawa, K., de Jong, P., Nierman, W. C., Strausberg, R. L. and Fraser, C. M. (2004). Human, mouse, and rat genome large-scale rearrangements: stability versus speciation. *Genome Research,* **14,** 1851–1860.

Zhong, J. F., Chen, Y., Marcus, J. S., Scherer, A., Quake, S. R., Taylor, C. R. and Weiner, L. P. (2008). A microfluidic processor for gene expression profiling of single human embryonic stem cells. *Lab on a Chip,* **8,** 68–74.

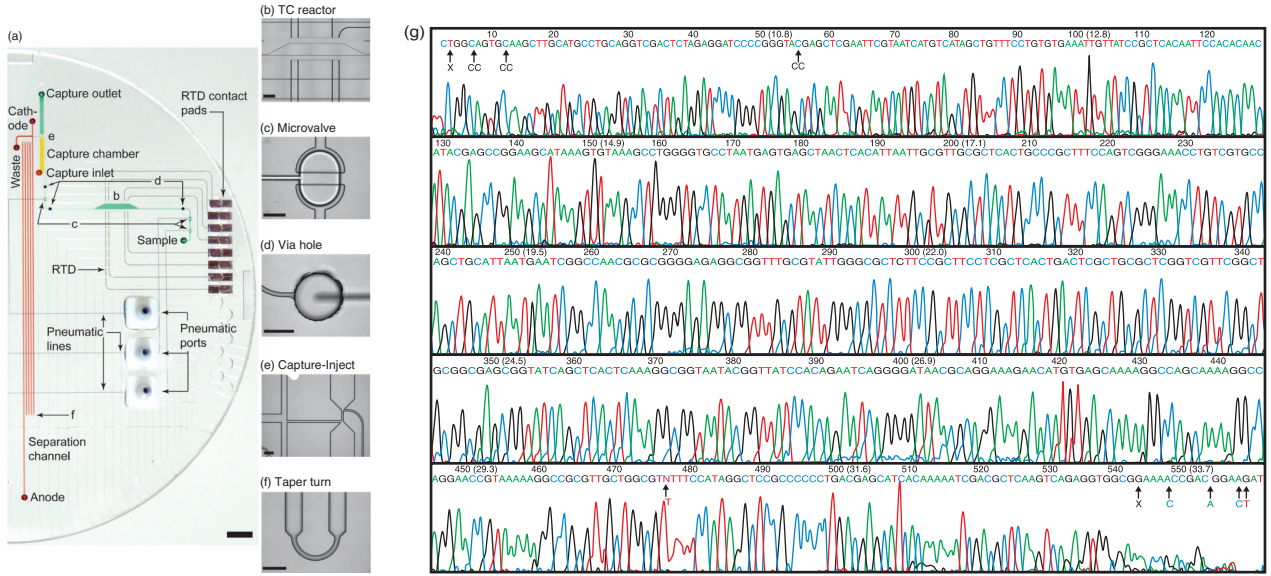

Plate IV (Chapter 13) Sanger sequencing bioprocessor. (a) Photograph of the microdevice (one of two complete nucleic acid processing systems). Colours indicate the location of sequencing reagent (green), capture gel (yellow), separation gel (red), and pneumatic channels (blue). (b) A 250-nL thermal cycling reactor with microfabricated RTDs. (c) A 5-nL displacement volume microvalve for reagent movement. (d) A 500-μm-diameter via hole. (e) Capture chamber for sample purification and cross injector. (f) A 65-μm-wide tapered turn. All the structures are etched to a depth of 30 μm on a glass wafer. (*Source*: Adapted with permission from Blazej *et al.*, 2006.)

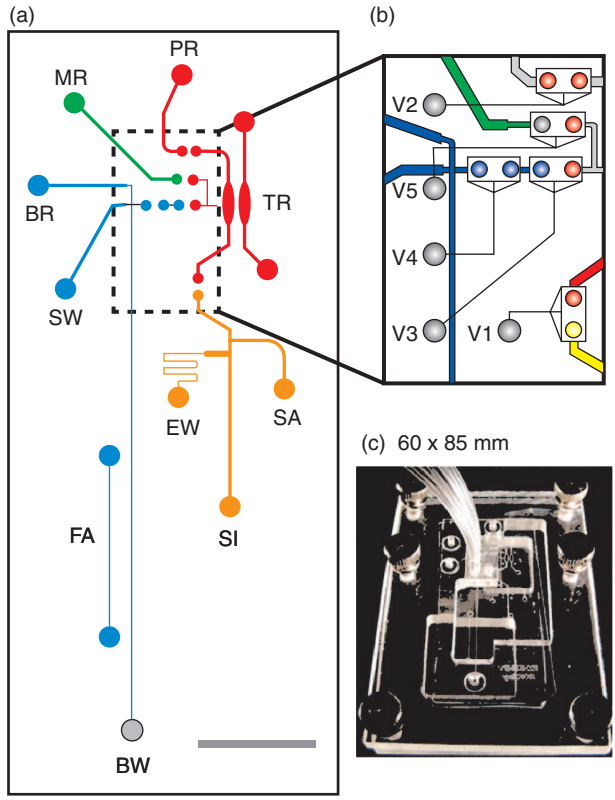

Plate V (Continued)

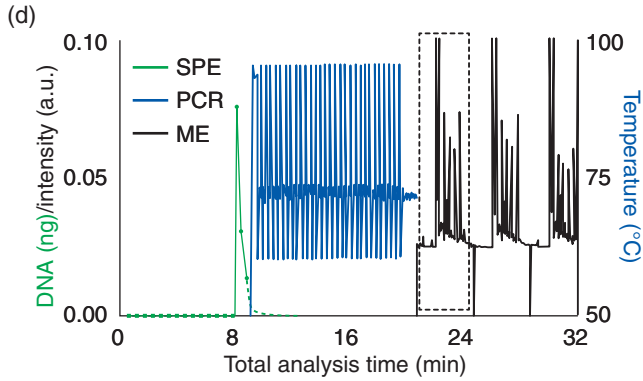

Plate V (Chapter 13) A fully integrated microfluidic genetic analysis system for pathogen detection. (a) Schematic of the microdevice. This device contains three domains for DNA extraction (yellow), PCR amplification (red), and CE separation (blue). All the reservoirs and structures are labelled as: sample inlet (SI), sidearm (SA), and extraction waste (EW) for DNA extraction; PCR reservoir (PR), marker reservoir (MR), sample waste (SW), and temperature reference (TR) chamber for PCR; buffer reservoir (BR), buffer waste (BW), and fluorescence alignment (FA) channel for electrophoresis. (b) Expanded view of the PDMS microvalves integrated on the chip for microfluidic control. V1 for the separation of PCR and DNA extraction domains. V2-V3-V4 forming a pump for sample pressure injection. V5-V3-V4 forming a pump for sizing ladder pressure injection. (c) A photograph of the chip assembly. (d) The timeline of the entire analysis performed on the microdevice. The green line is the DNA concentrations released from the solid-phase DNA extraction column as a function of time. The blue line is the temperature cycling profile for PCR. The black line is the three sequential separation traces. (*Source*: Adapted with permission from Easley *et al.*, 2006.).

14

Low-cost assays in paper-based microfluidic biomedical devices

M. BENHABIB, San Francisco, USA and X.J. LI, University of Texas at El Paso, USA

DOI: 10.1533/9780857097040.4.492

Abstract: Low-cost easy-to-use paper testing devices such as strips for pH, pregnancy, or diabetes testing have been commercially available for years. Recently, using advances from microfluidics, researchers have enhanced these tools and developed microfluidic paper-based analytical devices (μPAD). These 'lab-on-paper' devices are capable of achieving complex and precise qualitative and quantitative measurements of a wider array of biochemicals inexpensively. This chapter explores the current methods for low-cost assays in paper-based microfluidic devices. It summarizes device fabrication, performance, and reliability, as well as the techniques and progress achieved in detection with examples of applications to explain how they represent a promising platform for biochemical sensing. Finally, it presents the current limitations and a few perspectival trends.

Key words: paper-based microfluidics, lab-on-paper, point-of-care testing, environmental testing.

14.1 Introduction

Silicon/glass-based devices can provide the sensitivity, specificity, robustness, and rapidity needed for biomedical diagnostics. However, their cost and the skilled labor necessary to operate them make them difficult to access in resource-poor settings. To provide a low-cost, easy-to-use analytical tool, the Whitesides group introduced microfluidic paper-based analytical devices (μPADs) (Martinez *et al.*, 2007). Paper is a cellulose fiber web with a high surface area, abundant, inexpensive, and compatible with biological samples, which has been extensively used since the early twentieth century as a substrate for analytical and clinical chemistry (Feigle, 1939; Clegg, 1950; Helfferich *et al.*, 1965). Nowadays, paper and paper like materials are some of the most prevalent substrates for point-of-care diagnostics (Von Lode, 2005). Immunochromatographic strips (ICS), are widely used as quantitative or semi-quantitative tests in non-laboratory settings (Abe *et al.*, 2010). Additionally, paper is an ideal substrate for a disposable equipment-free

testing solution, because cellulose is biodegradable and can transport fluids by capillary effect. The objective of μPADs is to be a simple, portable and mass-producible solution that combines all the benefits of microfluidics and paper. μPADs are an appealing diagnostic tool in home settings, for less-industrialized countries, in remote or resource-poor locations, or during bioemergencies and first response accidents. They also can be of great use for environmental and food safety monitoring.

To circulate the fluids, μPADs rely on capillary action. It naturally occurs in the micro-scale channels, which are well-defined hydrophilic areas patterned on the hydrophobized sheet of paper (Li *et al.*, 2010b). When patterned with microstructures, paper becomes a platform where sample preparations and purifications, as well as multiple bioreactions, can occur simultaneously without cross-contamination.

This chapter first discusses the technologies for fabricating μPADs, presents the detection methods currently used on that platform, and then provides examples of applications. Finally, this chapter will discuss the limitations and the research perspective for this new analytical tool.

14.2 Fabrication techniques for paper-based microfluidic devices

There are two principal patterning strategies: a one-step selective hydrophobization of certain areas of the device that leaves untouched, thus hydrophilic, the fluidic paths, and a two-step entire hydrophobization of the device, then selective dehydrophobization of certain areas for fluidic flow. The dehydrophobization is achieved by etching away or dissolving the previously deposited hydrophobic agent to expose the underlying original hydrophilic paper. The straight forward, one-step method preserves the fluidic channels and detection zones, leaving their physicochemical proprieties unaltered (e.g. original paper color, no residues). μPADs are fabricated with hydrophobizing reagents that can be classified in three categories depending on their function: physical filling of pores in papers, deposition of hydrophobizing agent, and chemical modification of the paper-fiber to make it hydrophobic. This study will explore the different fabrication strategies in functioning of the category of hydrophobization reagent and patterning strategy. Before, let us start by reviewing the types of paper that are suitable as building material for microfluidic devices.

14.2.1 The different paper substrates

A large variety of paper materials can be used as substrate for μPADs. The selection of the appropriate one depends on the field of application and the method of fabrication. Most researchers use cellulose paper, which is affordable, naturally hydrophilic, and allows fast liquid penetration. Among

the different kinds of cellulosic paper, Whatman® filters are the most popular (Fenton *et al.*, 2008; Martinez *et al.*, 2009; Apilux *et al.*, 2010; Li *et al.*, 2010a). They are categorized by function in terms of their porosity, particle retention, and flow rate. Whatman® filter No. 1 is their standard grade filter, which allows medium retention and flow rate. Although widely adopted, due to its compatibility with many of the patterning techniques (Fenton *et al.*, 2008; Martinez *et al.*, 2008a, 2009, 2010; Ellerbee *et al.*, 2009; Hossain *et al.*, 2009b; Apilux *et al.*, 2010; Carvalhal *et al.*, 2010; Songjaroen *et al.*, 2011, Yu *et al.*, 2011a), Whatman® No. 1 is not ideal for all fabrication techniques. For instance, because their fabrication technique, etch printing, requires a solvent that swells the cellulose fibers and restricts the pore size, Li *et al*. needed a filter paper with larger pores and used a Whatman® No 4 (Li *et al.*, 2010a). Another example includes the electrochemical detection-based device by Nie *et al*., which required a chromatography paper. They have a more uniform structure that avoids the deformation of the screen-printed electrodes when wetted by fluids (Nie *et al.*, 2010b). Chromatography paper has also the advantage of lacking additives that would otherwise interfere with the electrochemical reaction (Wang *et al.*, 2012a). Other groups reported using chemically modified cellulosic substrate usually blended with an inorganic filler, such as polyester. They are available commercially as ion-exchange paper. They are non-degradable and present a smoother surface better suited for surface chemical modification or deposition (Arena *et al.*, 2010; Nie *et al.*, 2010b). Another important type of paper substrate is the hydrophobic nitrocellulose membranes, which are smooth and with reasonably uniform pore size (0.45 μm) that allows for a more stable and reproducible liquid flow. They have been used for a long time for antigen immobilization (Hawkes *et al.*, 1982) in, for instance, dot-immunobinding assays (Cheng *et al.*, 2010), because they manifest a high degree of nonspecific binding towards biomolecules, making them suitable for immobilization of enzymes (Martinez *et al.*, 2008a; Lu *et al.*, 2009a, 2009b), proteins (Fenton *et al.*, 2008), DNA (Cretich *et al.*, 2010), and cells (Li *et al.*, 2013). Besides, pores in nitrocellulose can perform purification based on size by filtering impurities of larger diameter than the analyte, which can mitigate interferences during the assay (Abe *et al.*, 2010).

14.2.2 Techniques based on physical filling of pores with a hydrophobic polymer

Photolithography

The original method to pattern fluidics on paper was a two-step method derived from silicon lithographic techniques and applied to chromatography paper substrate. This fabrication technique, named fast lithographic

activation of sheets (FLASH) and developed by Martinez *et al.* (2007, 2008b, 2008c), is capable of creating features as small as 100 μm wide, and hydrophobic barriers to direct the flow as small as 200 μm wide. It requires an inkjet printer or copier machine, a UV light, and a hot plate. The patterning technique of the device, which takes less than 30 min, is described in Fig. 14.1. First, the sheet is impregnated with a hydrophobic polymer, photoresist (e.g. SU8); second, its front side is covered with a transparent film and its back side with a black construction paper. Third, the microfluidic pattern is printed on the transparent film and the three-component structure is exposed to UV. Finally, the backing and transparent films are removed, the sheet is baked, and the excess photoresist is removed during the development step with a mixture of isopropyl alcohol and acetone. The first device fabricated combined glucose and protein tests (Martinez *et al.*, 2007), with the reagents spotted in each detection region and allowed to air-dry. The major cost driver of these devices is the photoresist used, SU8,

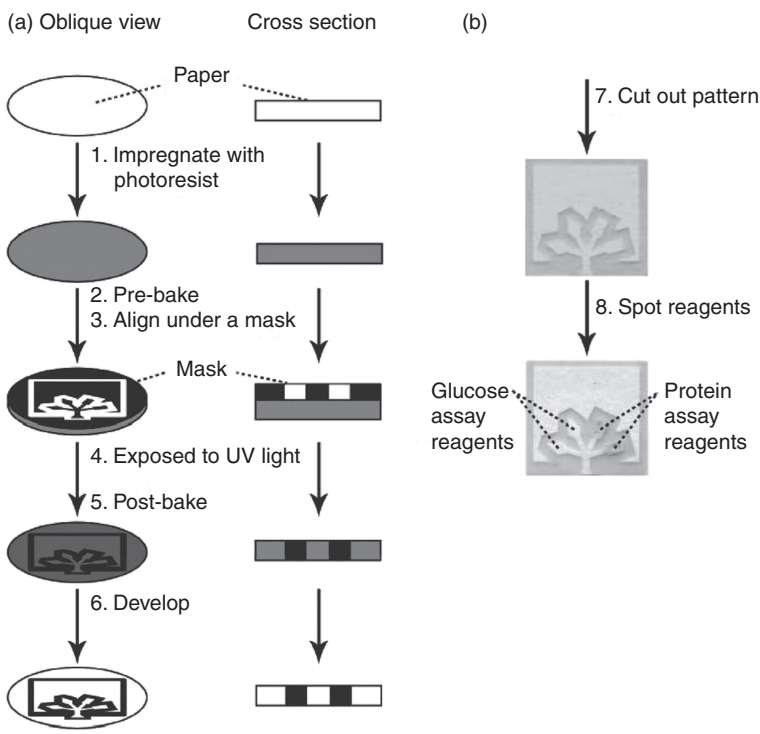

14.1 Schematic of the FLASH method for fabricating paper-based microfluidic devices. (a) Procedure for patterning paper with hydrophobic photoresist. (b) Derivatization of the device for assays. (*Source*: Adapted with permission from Martinez *et al.,* 2008a. Copyright © 2008 American Chemical Society.)

estimated at \$0.93/m^2 of paper. Additionally, SU8 requires over 20 min to cure, and a plasma oxidation treatment to ensure full recovery of hydrophilicity. One can use less expensive alternative photoactive polymers but most of them are very opaque, rendering UV exposure through the full paper depth difficult (Klasner *et al.*, 2010). Then, it becomes necessary to align and expose the back side of the device as well, adding more complexity to the process (Carrilho *et al.*, 2009b). Some novel polymer, such as Klasner's blend of polymers, can be used to make devices in less than 3 min, without plasma oxidation and give similar minimum feature size. He reported features at 90 μm and barriers at 250 μm (Klasner *et al.*, 2010). This method requires organic solvents, which can damage the flexibility of the paper and uses expensive brittle hydrophobic polymers (SU8 and PMMA cost 1\$/g and \$0.15/g respectively, (Bruzewicz *et al.*, 2008)) that make the devices susceptible to folding and bending (Li *et al.*, 2010b), (Dungchai *et al.*, 2011), and (Songjaroen *et al.*, 2011). The fabrication process requires cleanrooms, sophisticated equipment (masks, UV lamps, and proprietary software), and skilled labor, which are not available in every part of the world. It involves many complicated, laborious and time consuming steps. However, this method creates small barriers and yields sharp resolution between hydrophobic and hydrophilic areas.

Plotting with analog plotter

A more direct way to define hydrophobic patterns on paper, compared to the multistep lithographic process, is printing the hydrophobic polymer. Printing uses lower volumes of readily available and less expensive polymers. It was first investigated by Bruzewicz *et al.*, when they modified a plotter to print onto filter paper hydrophobic barriers made of a hexane solution of PDMS (polydimethylsiloxane), an inexpensive, non-toxic, and readily available polymer (Bruzewicz *et al.*, 2008). They created their own PDMS dispensing pens for the x,y-plotter using PDMS and polyurethane, and optimized their ink to ensure its rapid flow and its entire penetration through the sheet's thickness. It takes 1 h at 70°C for the elastomer to cure, during which time PDMS spreads laterally, reducing the printing resolution. Even though the smallest feature and barrier were reported to be 1 mm, in practice 2–4 mm-wide channels were needed because patterned lines are hardly straight. Indeed, paper, a non-uniform porous substrate, does not permit a controllable penetration of PDMS (Li *et al.*, 2008). As opposed to FLASH devices, PDMS devices are flexible and bendable, making foldable devices (3D) devices (that can be folded without destruction of the channel) possible. The cost of material was calculated to be 50 times less than with FAST, \$0.02/m^2. Other elastomers, such as Teflon, polystyrene, polypropylene, and polyisobutylene, can be used as 'ink' with a plotter, but PDMS is cheaper and

more common in microfluidics. Although this method does not damage the flexibility of the paper, it is time consuming and requires modification of a hard-to-find plotter, and the special preparation of the elastomer diluted in hexane (Songjaroen *et al.*, 2011).

14.2.3 Techniques based on soaking the paper with a hydrophobic chemical

Inkjet etching

Inspired by the FAST method, Abe *et al.* used a two-step approach: impregnation of the paper with a polymer to fill the paper matrix with a hydrophobic layer, then patterning the microfluidic channels by finely disolving the polymer with a solvant using a microdrop dispenser (such as an inkjet printer). Inkjet has been used in the plastic electronic and the manufacture of polymer light emitting diodes. It is simpler and less expensive than the multistep photolithography. First, the filter paper is soaked in a 1.0 wt% solution of polystyrene in toluene for 2 h for complete hydrophobicity. Then, after letting it dry for 15 min at room temperature, the modified-paper is patterned by inkjet printing of toluene to locally dissolve the polymer and precisely reexpose hydrophilic areas that will constitute fluidic paths (Abe *et al.*, 2008). A 550 μm wide flow channel with a sensing area of 1.5 mm × 1.5 mm was printed on filter paper by inkjet etching for simultaneous determination of pH, total protein, and glucose (Abe *et al.*, 2008). A single apparatus (the inkjet printer) was used to dissolve the hydrophobic coating (patterning) and print the biochemical indicator inks (reagent deposition). Compared to a plotting system with an inkjet printer, the position and the amount of liquid dispensed is reproducible and can be precisely controlled, which allows this technology to not only create hydrophilic/hydrophobic contrasts but also to deposit the exact quantity of sensing reagents required, which makes this technique more cost effective and less time consuming (Abe *et al.*, 2010). Even antibody immobilization on cellulosic surfaces by printing them as an ink was demonstrated (Abe *et al.*, 2010). In addition, as opposed to lithography, ink jet printing is flexible (easy to change the design of the fluidic pattern), lower cost, and adapted to mass manufacturing. However, with polystyrene, only hydrophobic fluids can be transported (surface tension has to be higher than 35 mN/m) (Olkkonen *et al.*, 2010). Whereas fluidic channel made of photoresist can guide extremely low surface tension fluids without any leaks. Another disadvantage of poly(styrene) is that it is time consuming to coat the paper with it, about 2 h. Also, multiple printing runs are necessary to remove the coat; Abe *et al.* used 10–30 printing cycles for best results. This method also requires a customized, potentially expensive, inkjet printer (Dungchai *et al.*, 2011).

Flexographic printing

Olkkonen used flexographic printing to pattern polystyrene boundaries onto chromatographic paper (Olkkonen *et al.*, 2010). Although this technology can be used with many different hydrophobizing agents (such as Alkyl ketene dimer (AKD), polymethylmethacrylate, or cross-linked polyvinyl alcohol), polystyrene was favored because it does not require heat treatment and it is biocompatible. With a 5% polystyrene ink and a single impression cycle, patterns of polystyrene are formed on the front side of the device and partially penetrate the paper thickness. To complete the waterproofing though all the paper thickness, a uniformed polystyrene layer is printed on the back side. This approach leads to devices that have shallow channels (about 50 μm), and thus requiring less sample volume. The minimum barrier and channel size made in that way is 400 μm. This flexographic method is compatible with roll-to-roll mass production of fluidic devices using existing tools already present in printing houses. Figure 14.2 shows a schematic of the process. The ink is first pipetted into an ink reservoir, and then transferred to the anilox

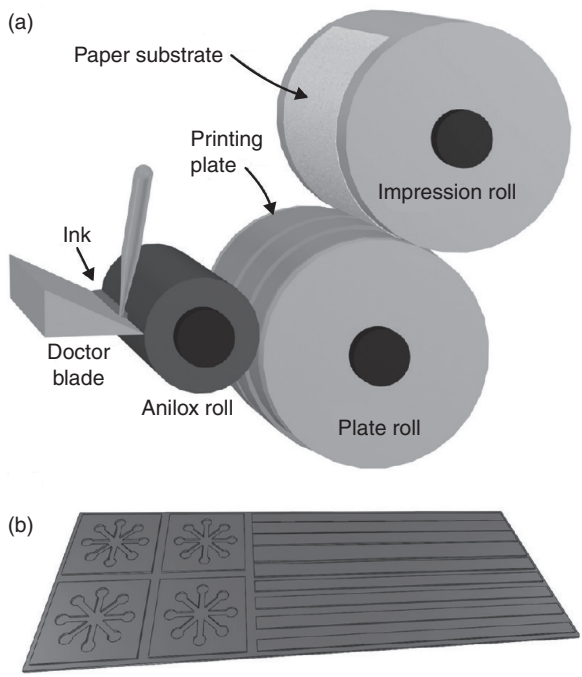

14.2 (a) Schematic illustration of the flexography unit used in the study. (b) Relief patterns in the printing plate define the hydrophobic regions to be formed into paper. (*Source*: Adapted with permission from Olkkonen *et al.*, 2010. Copyright © 2010 American Chemical Society.)

roll, which is covered with thousands of small volume cells. Each anilox cell transfers its ink content onto the printing plate, which contains the pattern. When printing, the anilox rotates four times to transfer the ink to the printing plate, which in turn transfers it into the paper by pressing the paper against the impression roll as it rotates at 60 m/min. The ink penetration is promoted by pressure between the printing plate and the paper substrate. He reports 500 μm wide channels with 30 μm boundary roughness, in reproducible manner, and with negligible lateral ink spreading.

Wax printing

Wax is another hydrophobic reagent that inspired two groups, Whitesides and Lin, to use it as material for fluidic barrier on paper (Carrilho *et al.*, 2009a; Lu *et al.*, 2009a). It is malleable at ambient temperature, insoluble in water, easy to obtain anywhere in the world, inexpensive, sustainable, non-toxic, biodegradable, and with a relatively low viscosity when melted. In wax printing, first, a pattern of wax is deposited on a sheet of paper using a commercially available solid-ink printer, in the case of large volume productions, or a wax pen when doing only manual prototyping. The paper is then heated to melt the wax so that it diffuses through the entire thickness of the paper. The method is simple to learn, rapid (~5 min) and only requires two pieces of equipment – a solid-ink printer and a hot plate or oven. Compared to the previous fabrication methods, it relies on cheaper consumables and is more environmentally friendly. However, melted wax in paper spreads by capillarity in all directions, with the lateral component of that flow allowing the wax feature to change shape and size. This undesirable effect is amplified by the anisotropic character of paper fibers, being more horizontally than vertically aligned, and renders the patterns ill-defined and wider. Despite this lack of resolution, and because molten wax in paper behaves as a fluid in porous media, a simple relationship can predict the final width of the hydrophobic barrier and is used to take into account this phenomenon in the design. In fact, the spreading distance is constant for a given heating time and temperature. The features fabricated with this method are not as sharp as those generated by photolithography. By heating at 150°C for 120 s, Carrilho measured a spreading distance of 300 μm with a root-mean-square roughness of 57 μm. They produced a minimum barrier and channel widths of 850 and 560 μm, respectively (Carrilho *et al.*, 2009a). Nevertheless, with this procedure, they showed they could fabricate a 96-zone paper plate with sample distribution channels and a 384-zone microliter paper plate. To improve resolution, vacuum could be applied to drive the flow of molten wax into the paper thickness and minimize lateral spreading. Also, the wax pattern could be printed on both sides, reducing by a factor of two the required spreading distance. Additionally, the use of nitrocellulose membranes as substrate led to more controlled and precise wax

patterns since their pores were more uniform and smaller (Lu *et al.*, 2009b). On nitrocellulose as thin as 300 μm channels and 60 μm barriers have been reported (Lu *et al.*, 2009b). On the one hand, wax has the advantage of not needing to use solvents in the fabrication process. On the other hand, wax-printed channels are not compatible with organic solvents, since they react with it. That can be an advantage: one can remove interferences in a sample by washing them away with organic solvents (Leung *et al.*, 2010).

Screen printing

Wax printing is a method that combines high-speed, simplicity, versatility, adaptability, and low-cost and can accommodate large batch productions (Wang *et al.*, 2012b). However, for most developing countries, wax-printers are not a standard, readily available tool and are expensive (Dungchai *et al.*, 2011). To overcome this limitation, Dungchai *et al.* modified this method and introduced screen printing for wax (Dungchai *et al.*, 2011). The technique consists in rubbing solid wax onto a paper filter through an ink-blocking stencil supported by a mesh. This mesh, made of porous fabric finely woven stretched over a frame, can transfer through material pressed against it, such as ink or wax. The loading of the wax is controlled by the size of the mesh, and is fully blocked in the areas where the mesh has an impermeable coating. Then, similarly to wax printing, the device is put on a hot plate and the wax is melted to form a hydrophobic barrier throughout the entire paper thickness. The wax penetration can be controlled by adjusting the temperature and the time of heating (the ideal conditions were found to be 100°C for 60 s). A direct linear relationship exists between the width of the hydrophobic barrier deposited and the width of its design on the mask. The minimum designable channel and barrier widths are, on a Whatman #1, 0.65 mm and 1.3 mm, respectively (Dungchai *et al.*, 2011). Compared to using a wax printer, this technique is simpler and adequate for remote places where such complex equipment is unavailable. As opposed to manually depositing wax with a pen, this technique is scalable and reproducible, as long as the force applied to the solid wax can be controlled.

Wax dipping

Because it is difficult to control the pressure on the wax with precision, screen printing suffers from poor reproducibility between batches which lead Songjaroen *et al.* to develop another wax-based fabrication method: wax dipping. This technique uses a mold that is pressed against the sheet of paper before the two are dipped for 1 s into melted wax at 120°C. After cooling, the sheet is peeled off and only has the areas protected by the mold remain without wax, as shown in Fig. 14.3 (Songjaroen *et al.*, 2011). This one-minute method creates good resolution channels in a single dipping step. The

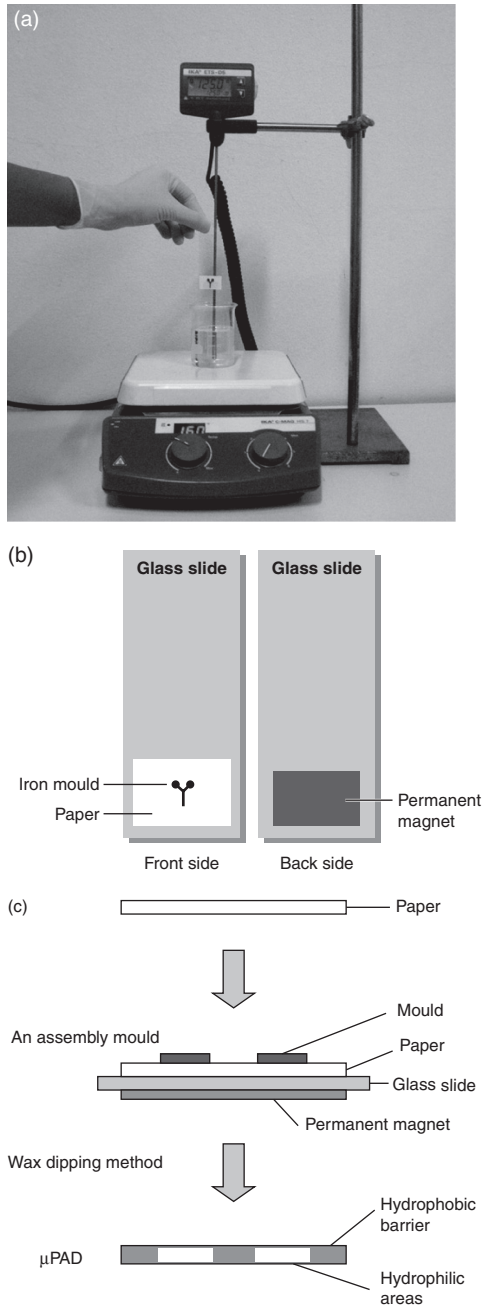

14.3 Fabrication process of the PAD using the wax-dipping method: (a) simple wax-dipping set-up system and (b) procedure for patterning paper by wax dipping in top view (b) and lateral view (c). (*Source*: Adapted with permission from Songjaroen *et al.*, 2011. Copyright © 2011 Elsevier B.V.)

relationship between the mask dimensions and the final hydrophilic dimensions is simple to derive. The smallest channel size rendered is 639 μm, similar to that obtained with wax printing or wax screen printing, but the reproducibility is better than the latter (%CV between 2% and 7%) when the temperature and the length of the dip in the bath of wax is perfectly controlled. The estimated total cost of a μPAD made by wax dipping is less than 5 cents.

14.2.4 Techniques based on chemical modification of the paper surface

Certain reagents can change the wetting properties of the cellulose pulp and can be used to create hydrophilic–hydrophobic contrasts, which is a simpler and more affordable approach than pore filling or deposition. AKD, and alkenyl succinic acid anhydrate (ASA), are commonly used for that purpose in paper sizing. They are very low-cost patterning agents that impart hydrophobicity by esterification of the hydroxy group of the cellulose (Li *et al.*, 2010b). Flexography, ink jet and gravure are expected to be the most suitable techniques to print sizing agents. AKD and ASA require curing, typically in an oven at 100°C for 5 min, so heating stations are added between processes. An important advantage of this method is that the paper treated retains its original flexibility and bendability (as opposed to, for instance, photoresist-coated devices), which makes packaging and handling easier. Moreover, the hydrophobic areas of the device show no visible mark or change of color, which is a critical characteristic for colorimetric-based assays.

Plasma oxidation etching

Li *et al.* are the first to have developed a two-step process using a paper sizing reagent (Li *et al.*, 2008, 2010a, 2010b). First, the paper is sized in AKD heptane solution and cured for 45 min at 100°C, making the treated paper strongly hydrophobic with contact angles greater than 110°. Then, sandwiched between two metal masks, the paper undergoes a plasma treatment that patterns the hydrophilic area following the mask design. However, with plasma processes over-etching is common: the long mean free path of the energized electron causes bigger hydrophilic patterns than the mask. However, once the treatment duration and intensity are optimized, this process leads to very reproducible hydrophilic areas. This patterning technique has the drawbacks of requiring long curing times and a plasma oxidation tool, which is not everywhere readily available (Klasner *et al.*, 2010). Similarly to inkjet etching, this process creates a hydrophilic area that is exposed to solvents and polymers, which can be undesirable for certain assays (Songjaroen *et al.*, 2011).

Inkjet printing

Inkjet printing relies on a digital inkjet printer to accurately deposit an AKD–heptane solution where the paper needs to be hydrophobic (Li *et al.*, 2010a). After printing, the device is heated to allow curing and, in a second step, the same printer can be used to deposit bio-indicators in the sensing zones. This hydrophobic deposition requires only a single side print to deposit the agent, which then freely penetrates through the thickness of the sheet (and laterally). The use of heptane, a very volatile solvent, allows for the few picoliters of printed solution to evaporate quickly and minimize lateral spread of the agent. This printing method is adapted to low-cost high-volume manufacturing. This process combines the advantage of PDMS printing (affordable devices that can withstand folding and bending) with the advanced patterning definition of photolithography. Finer wettable channels than 300 μm on Whatman paper (No. 4) have been reported. The estimated cost of a device with this method is a thousand times lower than barrier-based PDMS devices. Digital inkjet printing is an easy and rapid fabrication process, with the pattern design solely requiring software changes to be modified. It is suitable for high-speed production of a large number of devices, with multiple devices printable on a single piece of paper in 10 min with a single print-heat cycle (Li *et al.*, 2010c). In addition, among all deposition processes, inkjet has the benefit of being a non-contact liquid deposition, which is highly desirable for printing of biomolecules because that minimizes cross-sample contamination and risk of substrate damage (Gauvreau and Laroche, 2005; Nagler, 2008; Li *et al.*, 2010b).

An important limitation to the use of AKD and ASA is their non-resistance to the penetration of oil or low surface tension aqueous solution (typically solution with surface tension < 35 mN/m). If that is the case, a fluorocarbon-based sizing agent should be used instead. Other alternatives, such as the thread-based device, that do not rely on hydrophobic barriers have been successfully used to transport oil (Li *et al.*, 2010b).

14.2.5 Other techniques

Laser printing and treatment

Laser printing is a one-step patterning method that starts with a hydrophobic paper substrate such as parchment, wax, or palette paper, and uses CO_2 laser to pattern hydrophilic areas (Chitnis *et al.*, 2011). The surfaces treated become more fibrous and oxidized hydrophilic groups are formed. They can then trap chemicals but do not allow lateral diffusion of liquid. To achieve fluidic circulation, an additional coating of silica microparticles is needed. Therefore, after laser printing, a water suspension of these particles is poured on top of the patterned paper and, after water evaporation and

heavy shaking, they only remain in the hydrophilic areas. The high resolution and speed of this technique are its main advantages. By controlling the laser power and the scanning speed it is possible to design features with little roughness and as small as 62 ± 1 μm.

Paper cutting and paper taping

The simplest method to fabricate paper-based devices is by cutting and taping. Fluidic flow in these kinds of devices is not bound in channels by hydrophobic barrier, but by air instead. Cutting is rapid and only requires a cutting instrument, such as a pair of scissors or, for more complex patterns, a laser cutter or die cutter (Wang *et al.*, 2012a). With this method, tape is necessary to support any free-standing structures, which leads to an extra step in the fabrication.

Fenton *et al.* fabricated a nitrocellulose lateral flow device that was shaped in two dimensions by a computer-controlled knife on an xy-plotter (Fenton *et al.*, 2008). Afterwards, the resulting cut device was sandwiched between a vinyl and a polyester film to minimize evaporation, dehydration, and protect against external contamination. This technique is simple, direct, rapid, and suitable for mass manufacturing as well as for prototyping, and can work with any type of cellulosic substrate. The smallest feasible dimensions are 1 mm for an arm and 0.7 mm diameter for a hole. With this technique, interpretational errors can be minimized by carving labels describing analytes directly next to the test strip. The cost of the cutting tool is about US $5000.

Fabrication of 3D paper-based devices has been demonstrated using double-sided adhesive, as depicted on Plate VI (see in color section between pages 328 and 329) (Martinez *et al.*, 2008b). Regular μPADs rely on 1D lateral flow wicking. 3D devices combine lateral and vertical wicking for an increased microfluidic capability, which opens the door to array-based analytical strategies commonly used in the pharmaceutical and drug discovery industries. Martinez *et al.* used water-impermeable double-sided carpet tape, and SU-8 photolithography patterning. Each individual layer of paper and tape was fabricated then stacked, alternating patterned paper and tape with via holes (60 μm thick and 800 μm in diameter). Via holes were punched through the tape and filled with a cellulose paste to create a vertical fluidic path. Finally, the reagents were spotted before device assembly. As an example of the application they demonstrated a glucose test with control; four samples were tested for four analytes. The 3D device showed reliable and reproducible distribution of the sample in 1 min to multiple detection zones, making it easy to produce calibration curves. The estimated cost for a 3D device is US $30 for 1 m^2. Figure 14.4 shows another technique to bond multiple layers to form a 3D chip utilizing wax as an adhesive (Gong *et al.*, 2010). Patterns that will form fluidic channels were cut out from the substrate,

then the substrate was soaked in melted wax and sandwiched between glass or polymer sheets. Then, using vacuum, the wax was pumped out from the channel. This bonding process was durable, biocompatible with cell culture, reversible, and provided a good seal. Additionally, as shown on Plate VII (see in color section between pages 328 and 329), origami methods have also been used for 3D building of paper-based devices (Liu and Crooks, 2011).

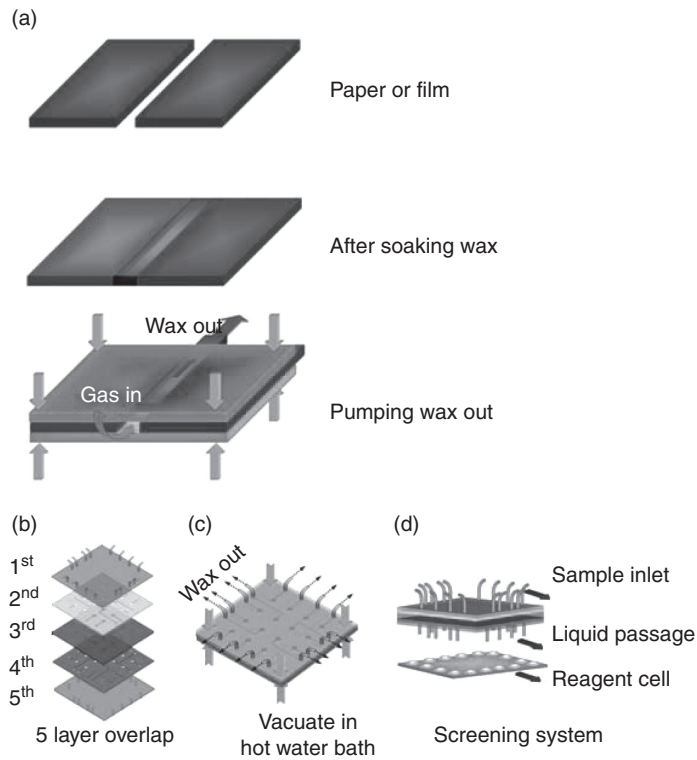

14.4 (a) After laser or scalpel cutting, the paper or film absorbed wax at the wax's melting point. After cooling, the film or paper was sandwiched between two glass slides and immersed in a hot-water bath. The gas was introduced from the inlet to the outlet through which the wax in the channel was pushed. (b) Five layers were overlapped and aligned. All of the layers were wetted by melt wax before being overlapped. (c) Layers were pressed together by four clamps at four corners. (d) Structure of bacterial screening system comprised of an upper screening chamber and a lower reagent cell. The liquid passage was a glass capillary which allowed the movement of liquid by capillary action. (*Source*: Adapted with permission from Gong *et al.*, 2010. Copyright © 2010 Royal Society of Chemistry.)

14.3 Detection and read-out technologies

In order to obtain a complete analytical instrument using the fabrication methods described above, an adequate transduction strategy needs to be adopted. These sensing and read-out technologies are chosen in accordance with the type and the concentration of the analyte to be detected, as well as on the desired accuracy. These strategies also need to comply with the overall goal of paper-based devices – to be simple, mass-manufacturable and low-cost. Optical and electrochemical based-methods are the most simple, compact, low power, and low-cost analytical techniques. They are, therefore, the best suited for paper-based assays. To this date, the major analytical assays reported are based on colorimetry (Martinez *et al.*, 2007, 2008a, 2009; Abe *et al.*, 2008; Bruzewicz *et al.*, 2008; Fenton *et al.*, 2008; Klasner *et al.*, 2010; Wang *et al.*, 2010; Ratnarathorn *et al.*, 2012), electrochemistry (Dungchai *et al.*, 2009, 2011; Nie *et al.*, 2010a, 2010b; Liu and Crooks, 2011, Lankelma *et al.*, 2012; Shiroma *et al.*, 2012), conductivity (Steffens *et al.*, 2009; Arena *et al.*, 2010), chemiluminescence, and electrochemiluminescence (Delaney *et al.*, 2011; Yu *et al.*, 2011a; Ge *et al.*, 2012).

14.3.1 Colorimetric detection

Colorimetric assays are reactions that lead to a change of color due to an enzymatic or chemical interaction between spotted reagents and the analyte. μPADs are well-suited for colorimetric biochemical assays; already most commercially available paper strip tests use color change to qualitatively detect analytes (Dungchai *et al.*, 2010). Colorimetric assays are ideal for simple, semi-quantitative answers, or when a yes/no answer is needed. When μPADs were first introduced they were successfully applied to the colorimetric detection of glucose and protein, at levels that are clinically relevant (Martinez *et al.*, 2007). The testing of glucose was done by reacting the sample with potassium iodine mixed with horseradish peroxidase and glucose oxidase, which led to the detection zone changing color from clear to brown proportionally to the glucose concentration. The testing of protein concentration was done using citrate buffer with tetrabromophenol blue and the change of color observed was from yellow to blue. These are well known colorimetric assays commonly used in urine analysis. The different chemicals and enzymes were spotted at the last step of the device fabrication and left to dry in the detection zones. Similar glucose and protein tests were tried on devices patterned with different methods: PDMS plotting (Bruzewicz *et al.*, 2008), wax printing (Lu *et al.*, 2009a), wax dipping (Songjaroen *et al.*, 2011), and inkjet printing of the device as well as the reagents (Abe *et al.*, 2008). Other colorimetric tests published include: glucose using glucose oxidase with phenol red (Olkkonen *et al.*, 2010) or bromocresol green (Songjaroen *et al.*, 2011) as

colored indicators; pH with bromothymol blue (Abe *et al.*, 2008; Bruzewicz *et al.*, 2008); nitrite test based on the Griess reaction principle (Klasner *et al.*, 2010; Li *et al.*, 2010a); uric acid test based on a bicinchoninate chelate method (Dungchai *et al.*, 2010); protein test (Wang *et al.*, 2010); lactate test (Dungchai *et al.*, 2010); ketones test using the first spatially-separated online double chemical derivatization (Klasner *et al.*, 2010); total iron test ion using 1,10-phenanthroline (Dungchai *et al.*, 2011); and IgG immunosensing, which opens the doors to pathogen detection (Abe *et al.*, 2010). For these assays, a linear response over the range of interest is generally observed. The dynamic range is limited by the amount of reagents and samples present, with most reactions stopping when the sample has completely evaporated and the channels dried out. Therefore, colorimetric reactions need to be faster than the rate of evaporation. Keeping the device incubated in a humidity chamber reduces evaporation and improves the dynamic range (Klasner *et al.*, 2010).

Visually comparing the color intensity of a reaction spot by naked eye is challenging. It represents a major hindrance to making this technology quantitative. Many factors including visual perception of color, lighting, and difference of color between a dry printed color on a label and the color on the reacted wetted paper can influence the reading (Dungchai *et al.*, 2009). In an attempt to quantify results more accurately, multiple researchers have digitalized the resulting color. They used a hand-held optical colorimeter that measured the transmission of light through paper (Ellerbee *et al.*, 2009), cellphone cameras (Martinez *et al.*, 2008a), and scanners (Apilux *et al.*, 2010; Klasner *et al.*, 2010). With a scanner the device picture was converted to CMYK format and using image processing software the change in intensity of the color was quantified and related to the concentration in analyte more accurately then by eye (Klasner *et al.*, 2010). In addition, Whitesides and co-worker have envisioned the use of a camera phone to send the digitalized result to be interpreted at an off-site location by an expert immediately after the on-site testing has been achieved (Martinez *et al.*, 2008a). The widespread existing cell phone communication infrastructures and the omnipresence of phone equipped with camera makes this digital exchange affordable. It allows for the monitoring to be collected more effectively by less valuable personnel for a better deployment of resources. However, experimental conditions such as lighting, sensitivity of the color measurement device, and background color of the paper substrate, which can change with time and in between batches, remain sources of interpretation errors. These reading mistakes can be minimized if, as Li *et al.* proposed, an internal calibration standard is run in parallel to the sample using the same device under the same conditions (Li *et al.*, 2010c). They used inkjet printing of AKD to pattern a six-branch device to analyze for nitrite ion and uric acid, and a low-cost desktop scanner for the image digitalization. They spotted the unknown solution in one of the detection zones, and five dilutions from

a standard in the rest, then introduced the indicator reagents in the central inlet zone, as described in Fig. 14.5. They obtained an increase in reliability and an accuracy approaching that of conventional UV-Vis spectrophotometry. Similarly, Wang *et al.* developed a tree-shape design, represented in Fig. 14.6, that is convenient for multiplexed assays and can self-calibrate to eliminate systematic errors (Wang *et al.*, 2010). The paper-based device allows uniform flow of water from its stem to the multiple branches, where each single analysis takes place. After the assay is completed, the operator can easily compare the color of the unknown with the benchmark. Another strategy to improve accuracy and help visual reading can be using multiple indicators for the same analyte, which will generate different colors and react at different concentrations of the analyte. (Dungchai *et al.*, 2010). This approach, developed by Dungchai *et al.*, can be accomplished by spotting an oxidase enzyme that produces hydrogen peroxide proportionally to the concentration in analyte, and spotting indicators that react at different levels of concentration of hydrogen peroxidase. This method was used to develop a nine-branch device for simultaneous analytical measurement of

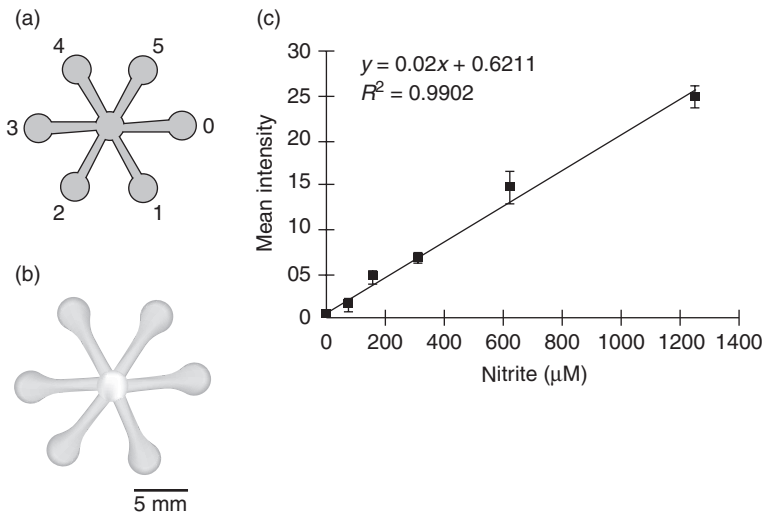

14.5 Quantitative biological/chemical assay using paper-based microfluidic devices. (a) The assay design: NO_2 – standard solutions (0.5 IL) with different concentration from 0 to 1250 Imol/L were deposited into detection zone 0 to zone 5 in sequence; (b) NO_2 – indicator solution was added into the device from central inlet zone and caused different color changes in different detection zones; (c) calibration curve created by color density measurement using Adobe Photoshop of the scanned images of the tests. Error bars were obtained from six repeated measurements. (*Source*: Adapted with permission from Li *et al.,* 2010. Copyright © Springer Science+Business Media B.V. 2010.)

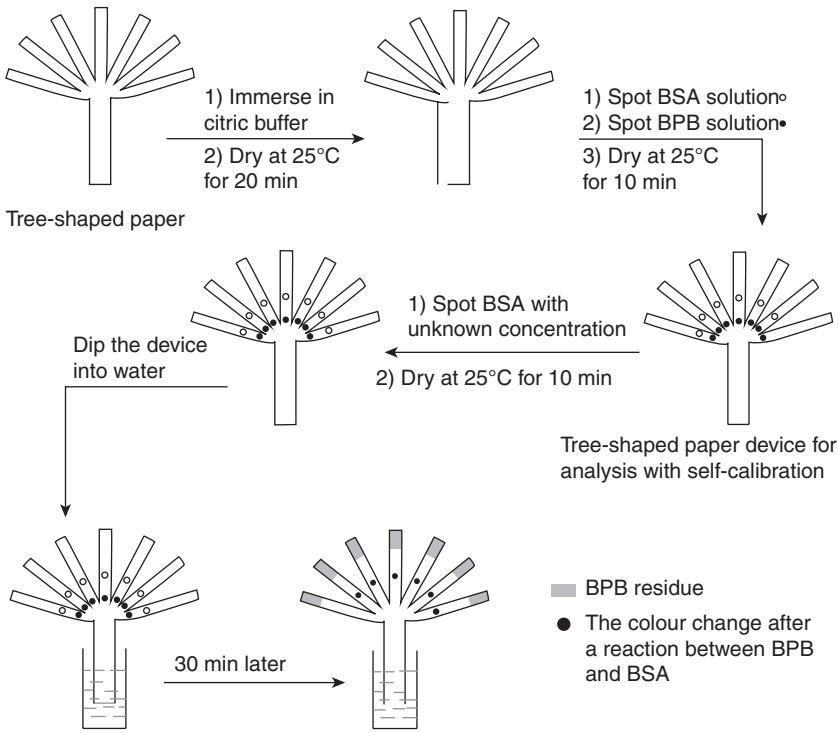

14.6 Diagram of the procedure for tree-shaped device with self-calibration for detection. (*Source*: Adapted with permission from Wang *et al.,* 2010. Copyright © 2010 Elsevier B.V.)

glucose, lactate, and uric acid in clinically relevant ranges and demonstrated a significant improvement in reading accuracy (Dungchai *et al.*, 2010).

With their high extinction coefficient, gold nanoparticles (AuNP) and silver nanoparticles (AgNP) represent very strong indicators. Because their colors strongly depend upon their size, their aggregation or dissociation leads a change of color. Zhao *et al.* demonstrated that DNA cross-linked gold nanoparticles (AuNPs) can be used on paper for biosensing and stored for weeks without loss of performance (Zhao *et al.*, 2008). Upon addition of a target solution, the aggregated AuNPs dissociated resulting in change of color. The paper substrate served as a protection from nonspecific stimuli making aggregated AuNPs stable. Sensitive detection of adenosine and endonuclease was performed, and with the use of DNA aptamers the assay can be generalized to many targets. Additionally, colorimetric assay based on the aggregation of NPs was also demonstrated. To produce a copper detector, AgNPs functionalized with homocysteine (Hcy) and dithiothreitol (DTT) were spotted on a paper-based device. AgNPs showed a change of color upon addition of copper, which induced their aggregation through carboxyl and amino binding

with Hcy and DTT (Ratnarathorn *et al.*, 2012). This sensitive assay exhibited a limit of detection as low as 7.8 nM.

14.3.2 Electrochemical detection (ECD)

Electrochemical detection, as opposed to colorimetric assays, is capable of precise quantification of the analyte's concentration. ECD is a redox based method that relies on a three electrode system: the working, the counter and the reference electrodes. On paper-based devices, these electrodes can be screen printed with a conductive ink at a low cost. Commonly, a carbon ink is used for the working and counter electrodes and a silver/silver chloride ink for the reference electrode and the pads (Dungchai *et al.*, 2009; Apilux *et al.*, 2010). Figure 14.7 shows screen-printed electrodes; they have the advantage of being disposable and easy to functionalize by chemical derivatization. Although ECD on paper requires external equipment, the latter remains minimal, consumes little power, and can be miniaturized (Dungchai *et al.*, 2009). The first microfluidic paper-based electrochemical device (μPED) was introduced by Dungchai *et al.* with the simultaneous quantification of glucose, lactate, and uric acid in biological samples (Dungchai *et al.*, 2009). After being printed, the electrodes were chemically modified with Prussian blue to improve their

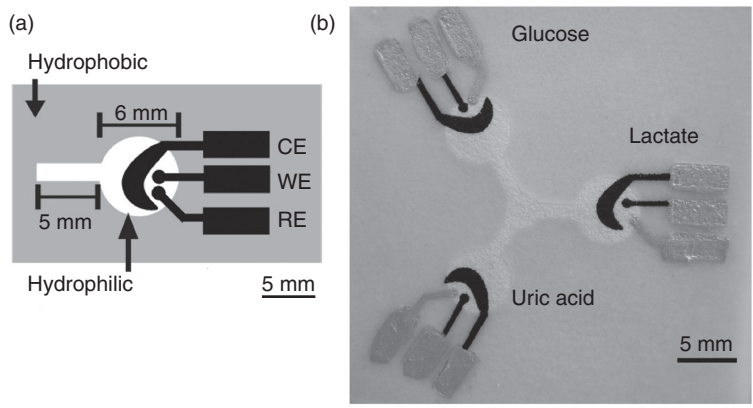

14.7 (a) Basic design of the electrochemical detection cell for paper-based microfluidic devices. WE, working electrode; RE, reference electrode; CE, counter electrode. (b) Picture of three electrode paper-based microfluidic devices. The hydrophilic area at the center of the device wicks sample into the three separate test zones where independent enzyme reactions occur. The silver electrodes and contact pads are made from Ag/AgCl paste with the black electrode portions being the Prussian blue modified carbon electrodes. The device size is 4 cm × 4 cm. (*Source*: Adapted with permission from Dungchai *et al.*, 2009. Copyright © 2009 American Chemical Society.)

selectivity toward hydrogen peroxide, then they were spotted with the appropriate oxidase enzymes, which catalyzed the oxidation of their substrate (the analyte) while reducing oxygen to hydrogen peroxide. When a sample drop is deposited at the center of the paper, it flows to the reaction sites where chronoamperometry is performed using the optimal potential for hydrogen peroxide production. Low detection limits within the range of clinical relevance were obtained with performances comparable to that of traditional diagnostic tools (Dungchai *et al.*, 2011). Nie *et al.* also demonstrated glucose testing using chronoamperometry and showed a limit detection five times lower than traditional glucometers and two times lower than colorimetric assays (Nie *et al.*, 2010b). They also fabricated a paper-based device with four electrodes to be used with commercial hand-held glucometer (Nie *et al.*, 2010a). Additionally, they demonstrated ECD's good selectivity by specifically quantifying Pb(II) at ppb-level concentrations in solutions containing Zn(II) and Pb(II) using anodic stripping voltammetry. ECD can be readily combined with a separation step for improved sensing. Carvalhal *et al.* separated via chromatography, then analyzed by chronoamperometry, a mixture of uric and ascorbic acid on a paper-based device (Carvalhal *et al.*, 2010). The separation, whose efficiency depends on the thickness, length, and quality of the paper, occurred during travel of the sample through the paper column.

A hurdle for the common methods used in ECD, amperometric or coulometric, is their need for external bulky electrochemical detectors. An alternative method, requiring only a simple reader, is the monitoring of streaming potentials, as described by Leung *et al.* Their group showed that these potentials are sensitive to the presence of charged polymers adsorbed on the surface of the paper. They proposed derivatizing the cellulosic channel to bind the target, and detecting the binding events by measuring the changes in streaming potential (Apilux *et al.*, 2010; Leung *et al.*, 2010). Electrical conductivity measurement is another technique that uses a simpler external instrument. But most of the research in that field has been limited to gas-phase applications, such as an ethanol (Arena *et al.*, 2010), or a nitrogen sensor (Steffens *et al.*, 2009). To overcome another hindrance from ECD, the inability to detect certain analytes and/or to prevent the overlapping response of contaminants with the analyte of interest, a strategy of dual electrochemical and colorimetric assays on a single device can be adopted. Apilux *et al.* used that option to simultaneously screen for Au(III) and Fe(III), which have reduction currents that overlap (Apilux *et al.*, 2010). They detected Au(III) using square wave voltammetry in aqua regia buffer, and Fe(III) using a phenanthroline-based colorimetric assay.

Microfluidic paper-based electrochemical devices (μPED) combine simplicity, moderate cost, portability, speed, accuracy, high sensitivity, and high selectivity by adequate pick of electrode material and/or detection potential (Dungchai *et al.*, 2009; Nie *et al.*, 2010b).

14.3.3 Chemiluminescent (CL) and electrochemiluminescent (ECL) detections

Chemiluminescence is simple, highly sensitive, and can be performed in the dark, therefore, independently of the ambient light. Yu *et al.* designed a μPAD for the simultaneous analysis of glucose and uric acid relying on the chemiluminescence reaction between rhodamine derivatives and hydrogen peroxide (Yu *et al.*, 2011a). The hydrogen was generated by the two oxidase enzymes immobilized on separate channels.

Electrochemiluminescent (ECL) detection corresponds to a CL reaction in which luminescence is established and controlled by the application of an electrical potential. This method inherits the advantages of CL, such as emission of light independently of the ambient light, with an improved selectivity and an increased dynamic range due to better control of the reaction through electrochemistry (Delaney *et al.*, 2011; Ge *et al.*, 2012; Yan *et al.*, 2012). ECL also possesses the advantages of EC detection, namely high sensitivity, and good control over timing and spatial location of the reaction (Delaney *et al.*, 2011). Figure 14.8 shows the first paper-based device with ECL detection by Delaney *et al.* (2011). They used screen-printed electrodes and chronoamperometry to induce ECL between a biological compound, nicotinamide adenine dinucleotide, and an ECL reagent, tris(bipyridine)ruthenium(II), which yields an orange luminescence. Using a camera phone as a photo sensor, they successfully obtained calibration curves with detection limits lower than colorimetric assays. Additionally, they showed that mass transport was unaffected by the fibrous substrate.

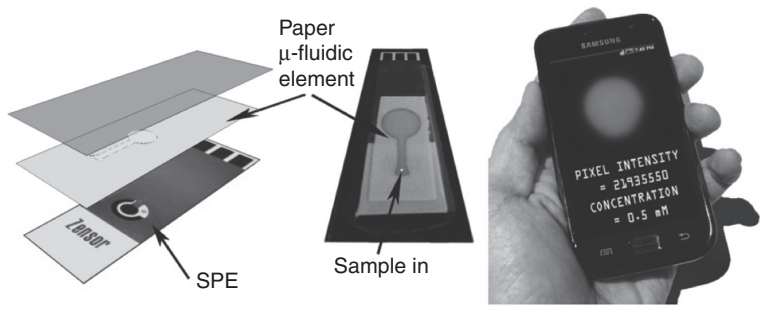

14.8 ECL detection of a sample solution (2-(dibutylamino)-ethanol (DBAE)). The device was filled with a 10 mM $Ru(bpy)_3^{2}$+ solution before drying, and was then aligned and fixed onto the face of the screen-printed electrode (SPE) by laminating with transparent plastic. A drop of sample was introduced through a small aperture in the plastic at the base of the channel. After the detection zone being fully wetted, a potential of 1.25 V was applied and the resulting emission was captured and analyzed. (*Source*: Adapted with permission from Delaney *et al.*, 2011. Copyright © 2011 American Chemical Society.)

14.4 Application of paper-based microfluidic devices

Made of readily available materials, small, lightweight, easy to stack, store and transport, paper-based microfluidics has the potential to be a privileged analytical platform for a wide range of applications in health diagnostics (Martinez *et al.*, 2007, 2008b, 2010; Abe *et al.*, 2008; Li *et al.*, 2008, 2010a, 2010b, 2010c, 2011; Dungchai *et al.*, 2009, 2010, 2011; Lu *et al.*, 2009a; Cheng *et al.*, 2010; Klasner *et al.*, 2010, Nie *et al.*, 2010a; Delaney *et al.*, 2011; Yu *et al.*, 2011a, 2011b), as well as in environmental monitoring (Wang *et al.*, 2009; Apilux *et al.*, 2010; Nie *et al.*, 2010b; Lankelma *et al.*, 2012), or food quality testing (Hossain *et al.*, 2009b; Nie *et al.*, 2010a; Lankelma *et al.*, 2012). Relying on the different detection techniques described earlier, it can provide qualitative and/or quantitative (sometimes semi-quantitative) results for the detection of a single or multiple analytes. μPADs exist in two major formats: the on-demand devices, which are empty generic platforms that require the user to introduce detection reagents into the device prior to testing; and the ready-to-use devices, which are complete devices with reactive sensing reagents already integrated in the detection zones.

14.4.1 On-demand μPADs

On-demand devices are general-purpose tools with only the desired microfluidic features for handling fluids. They are generic platforms that can be utilized for common biological or chemical assays, such as quantifying an analyte concentration, or creating a calibration curve. Li *et al.* presented an example of such devices, a star-shaped platform that allows a single drop of indicator react with six different concentrations of nitrate (Li *et al.*, 2010b). Another example is Bruzewicz's design, which has an inlet channel splitting into five equally sized channels leading to different test zones where the user can pipette different reagents for parallel testing. They used an open inlet channel with no border, which allowed a simple dipping of the inlet edge of the device to draw some sample in and start the assays (Bruzewicz *et al.*, 2008).

To perform more complex and reliable measurements with ease of use comparable to conventional lateral flow tests, on-demand devices need inexpensive paper-based processing capabilities. Two-dimensional fluidic networks on paper can enable these sophisticated capabilities and render multiple step assays possible. The Yager group, after doing quantitative studies on flow in fluidic networks, has demonstrated methods for controlling fluid transport (Fu *et al.*, 2010b, 2011; Kauffman *et al.*, 2010). By playing with the geometry of the fluidic network and introducing dissovable barriers, they enable automated sequential delivery of fluid, and sample pretreatment before analysis (Fu *et al.*, 2010a; Lutz *et al.*, 2011). The introduction of functional elements to actively control the movement of the fluid

as on standard lab-on-a-chip instruments is critical to the development of improved assay execution on paper. Li *et al*. developed a simple element, shown on Fig. 14.9, that functions as a switch (Li *et al.*, 2010b). A reactor can be made using two switches that control the access of two liquid reactants from their dosing sites (A1, A2) to the reactor site B (Li *et al.*, 2010a). Other circuit elements have been fabricated such as a fluidic timer based on paraffin wax (Noh and Phillips, 2010a, 2010b), an 'on' button for connecting and disconnecting the fluidic flow (Martinez *et al.*, 2010), or a filter that separates plasma from whole blood (Yang *et al.*, 2012). Additional work on adapting common microfluidic techniques to paper-based devices includes hydrodynamic focusing, sized-based extraction of molecules, micromixing, and dilution (Osborn *et al.*, 2010; Rezk *et al.*, 2012).

14.4.2 The ready-to-use μPADs

Devices that already incorporate the reagents needed in a particular detection chemistry meant for specific analytes are ready-to-use devices. They correspond to most of the published work, and are designed to respond to the needs of a given field. Table 14.1 presents a compilation of most of the reported analytes and the methods used for their detection, with respect to the field of application: health diagnostics, biochemical analysis, environmental monitoring, food quality control, and forensic.

In health diagnostics, μPADs find application as low-cost, disposable, and easy to fabricate testing devices that, if quantitative enough, can be used to directly establish a diagnostic. When only semi-quantitative or qualitative, they represent a fast and inexpensive initial screening tool that can indicate if a more expensive and labor-intensive examination is required. To be of clinical use, μPADs (such as those reported in Table 14.1) have to be capable of analyzing samples from body fluid such as urine, saliva, sputum, or blood. Additionally, to be the most representative of the patient's health condition, they are usually designed for simultaneous detection of multiple analytes using a single sample drop. Examples include the simultaneous detection in urine of glucose and protein (Martinez *et al.*, 2007, 2008a), or in saliva of nitrite and uric acid, which are potential biomarkers for monitoring hemodialysis (Li *et al.*, 2010b).

Besides, nowadays a large range of commercially available health testing tools are based on immunorecognition assays. Some examples include the urine test for pregnancy, and the blood test for hepatitis C. Usually, with these immuno-test strips the analyte flows by capillary effect to spotted antibodies and is subsequently bound to them, leading to a color appearance at the test line (Dungchai *et al.*, 2010). They are extremely sensitive, reliable and fast. By using these existing immune-based assays and the powerful platform that is microfluidics, paper-based devices open up new possibilities for clinical testing (Fenton

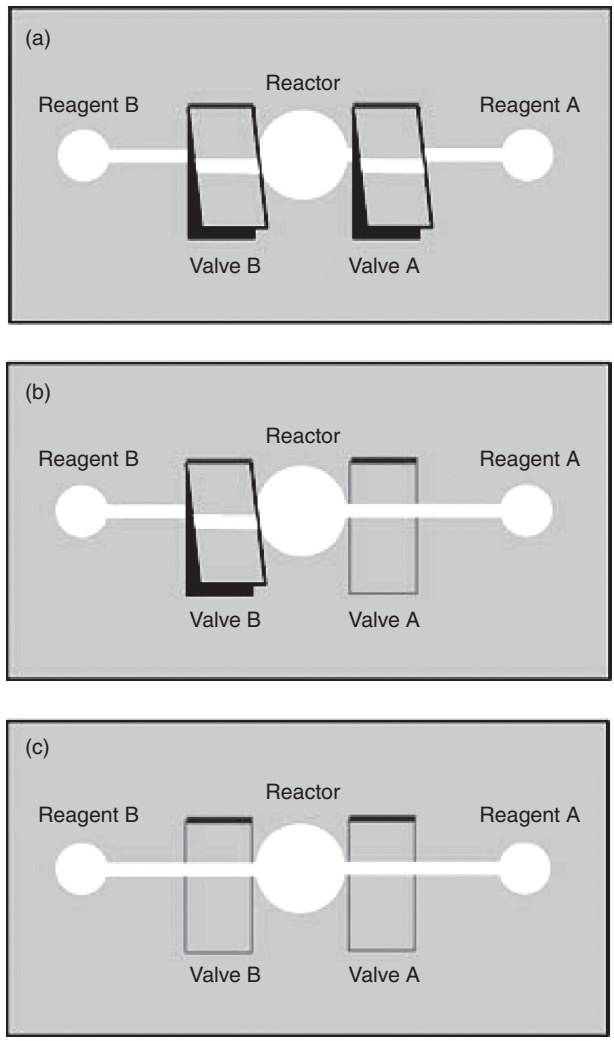

14.9 (a)–(c) A design of a simple paper-based microfluidic reactor consisting of two sample dosing sites, two valves, and one central reaction site; (d)–(f) a paper-based microfluidic reactor based on this design was tested using acid–base neutralization reaction ((d) Phenolphthalein indicator solution was deposited onto the central reaction zone. NaOH and HCl solutions were added into reagent zones A and B, respectively; (e) NaOH solution was introduced into the reaction zone to trigger color change; (f) HCl solution was introduced later into the reaction zone via valve B to neutralize NaOH in the reaction zone). (*Source*: Adapted with permission from Li *et al.*, 2010. Copyright © Springer Science+Business Media B.V. 2010.)

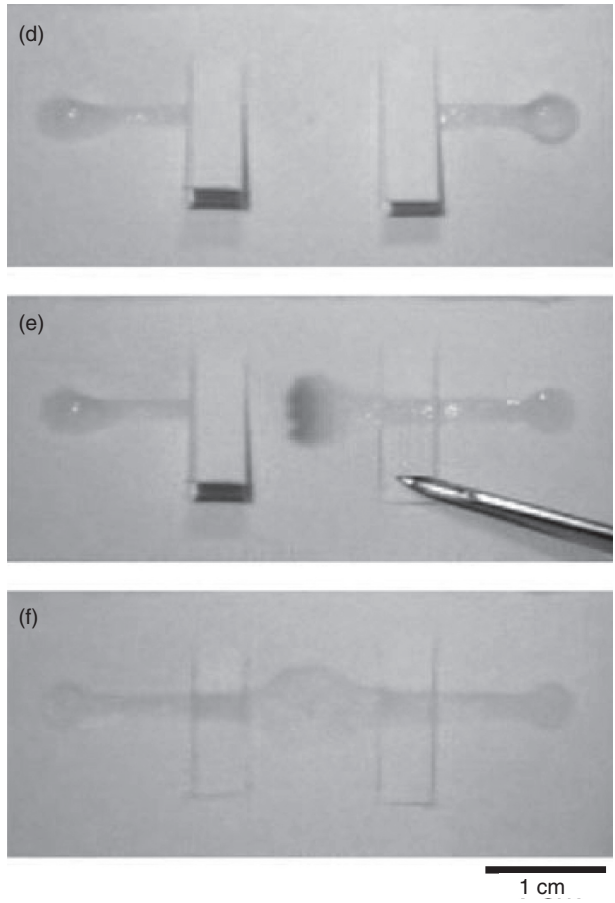

14.9 Continued

et al., 2008). For instance, Khan demonstrated a paper-based device for blood typing using a three-armed prototype, where each arm was treated with a different solution of antibody (A, B, and O) (Khan *et al.*, 2010). After a drop of whole blood was spotted at the center of the device, it flowed to the different arms, and when the red cells carried with the blood encountered their specific antibodies they agglutinated, causing a visible chromatographic mark on that arm. This paper-based diagnostics, at a cost of only a few cents, can promote health in the developing world by rapidly providing the blood test result necessary to many chirurgical procedures. Other work relying on antigenic binding include the electroluminescent detection based method for diagnostic of carcinoembryonic antigen from real serum sample (Yan *et al.*, 2012), and the chemiluminescence detection of four cancer biomarkers (Ge *et al.*, 2012). Another major immunological test adapted to paper-fluidics is the enzyme-linked immunosorbent

Table 14.1 Summary of the main fields of application for paper-based microfluidic devices, with examples of analytes reported detected and the method used

Application	Analyte	Detection method	Quantitative/ qualitative?	Reference
Health diagnostic	Glucose	Colorimetric	Semi-quantitative	Dungchai *et al.*, 2010
		Colorimetric	Quantitative	Dungchai *et al.*, 2010; Martinez *et al.*, 2007, 2008b., 2010; Noh and Phillips, 2010a; Klasner *et al.*, 2010; Abe *et al.*, 2008; Lu *et al.*, 2009a; Bruzewicz *et al.*, 2008; Fenton *et al.*, 2008; Olkkonen *et al.*, 2010; Songjaroen *et al.*, 2011
		Electrochemical Detection	Quantitative	Dungchai *et al.*, 2009, 2011; Nie *et al.*, 2010a, 2010b; Lankelma *et al.*, 2012
		Chemiluminescence, Electrochemiluminescence	Quantitative	Yu *et al.*, 2011b
	Uric acid	Colorimetric	Semi-quantitative	Li *et al.*, 2010b; Dungchai *et al.*, 2010
		Colorimetric	Quantitative	Li *et al.*, 2010c; Dungchai *et al.*, 2010
		Electrochemical	Quantitative	Dungchai *et al.*, 2009; Carvalhal *et al.*, 2010b
	Protein (e.g. bovine serum albumin)	Colorimetric	Semi-quantitative	Martinez *et al.*, 2007, 2008a; Bruzewicz *et al.*, 2008; Abe *et al.*, 2008; Fenton *et al.*, 2008; Wang *et al.*, 2010; Lu *et al.*, 2009a; Martinez *et al.*, 2010; Ellerbee *et al.*, 2009; Songjaroen *et al.*, 2011
	Nitrate/nitrite	Colorimetric	Quantitative	Klasner *et al.*, 2010; Ellerbee *et al.*, 2009
		Colorimetric	Semi-quantitative	Li *et al.*, 2010a, 2010b

(*Continued*)

Table 14.1 Continued

Application	Analyte	Detection method	Quantitative/ qualitative?	Reference
	ketones	Colorimetric	Quantitative	Klasner *et al.*, 2010; Ellerbee *et al.*, 2009
	Lactate	Colorimetric	Semi-quantitative	Dungchai *et al.*, 2010
	pH	Colorimetric	Semi-quantitative	Abe *et al.*, 2008, 2010
	Human IgG	Colorimetric	Semi-quantitative	Abe *et al.*, 2008
	Total iron	Electrochemical	Quantitative	Dungchai *et al.*, 2011
	Pathogenic bacteria	Colorimetric	Semi-quantitative	Li *et al.*, 2011
	ABO antigens	Colorimetric	Non-quantitative	Khan *et al.*, 2010
	Nucleic acid	Colorimetric	Semi-quantitative	Allen *et al.*, 2012
	Cholesterol	Electrochemical	Quantitative	Nie *et al.*, 2010a
Biochemical Analysis and Forensic	HIV-1 antigen	Colorimetric	Semi-quantitative	Cheng *et al.*, 2010
	Nicotinamide adenine dinucleotide (NADH)	Electrochemiluminescence	Quantitative	Delaney *et al.*, 2011
	Alkaline Phosphatase	Colorimetric	Quantitative	Li *et al.*, 2008, 2010a
Environmental Monitoring	Pb(II)	Electrochemical	Quantitative	Nie *et al.*, 2010b
	Au(III)	Electrochemical	Quantitative	Apilux *et al.*, 2010
	Fe(III)	Colorimetric	Quantitative	Apilux *et al.*, 2010
	Toxin (microcystin-LR)	Electrochemical	Quantitative	Wang *et al.*, 2009
Food quality control	Ethanol	Electrochemical	Quantitative	Nie *et al.*, 2010a
	Pesticides	Colorimetric	Quantitative	Hossain *et al.*, 2009b
Forensic	Iron in Hemoglobin	Chemiluminescence	Quantitative	Chitnis *et al.*, 2011

assay (ELISA), which combines antibodies and enzymes to provide specificity and sensitivity (Wang *et al.*, 2009; Abe *et al.*, 2010; Cheng *et al.*, 2010; Martinez, 2011; Wang *et al.*, 2012b). Figure 14.10 from Abe *et al.* shows the fabrication process of a paper-based device using immunosensing inks and gold-labeled antibodies. They demonstrate that the antibodies are successfully adsorbed on the cellulose and are released from their immobilization site only upon sample application. Likewise, Wang *et al.* wax printed a device combining the specific ELISA method with the sensitive chemiluminescence detection and showed quantitative clinical testing of three tumor markers (Wang *et al.*, 2012b). In parallel, to satisfy the need for high throughput, low-cost, and low-volume

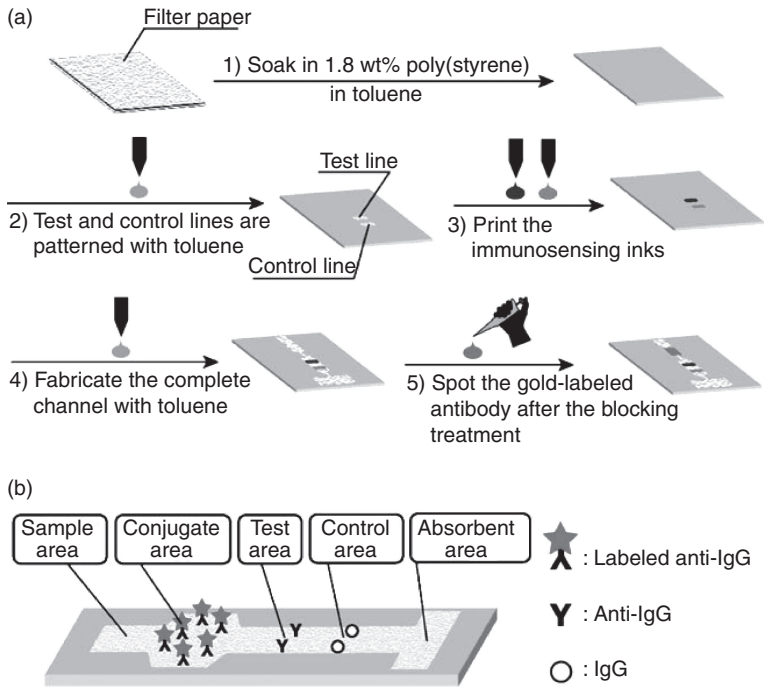

14.10 (a) Fabrication process of the inkjet-printed microfluidic immunosensing strip. Patterning of the test/control lines (step 2), dispensing of the immunosensing inks onto the test/control lines (step 3), and patterning of the entire channel and remaining areas (step 4) are performed on the same inkjet printing apparatus (the pen symbol indicates the use of the inkjet printer). A gold-labeled antibody is spotted onto the conjugate area by a micropipette. (b): Schematic representation of the finalized strip featuring a microfluidic channel consisting of a sample inlet area, a conjugate area, a sensing area containing a test line and a control line, and an absorbent area. (*Source*: Adapted with permission from Abe *et al.*, 2010. Copyright © Springer Science+Business Media B.V. 2010.)

ELISA assays, Cheng *et al.* printed paper-based microarray plates (Cheng *et al.*, 2010). They represented an affordable device equivalent to the conventional 96-microzone plate onto which researchers demonstrated quantitative detection of HIV-1. All these testing devices, used in conjunction with the modern communication tools such as camera phones, are powerful telemedicine and general health monitoring tools.

μPADs have the potential to be useful in food quality control, where inspections from production to packaging are required, and where monitoring the lifetime of products once on the shelves is critical. As an example, Nie *et al.* developed electrochemical μPADs that used a commercial glucometer to measure on-site the concentration of ethanol in food products (Nie *et al.*, 2010a). Another example is the work done by Hossain *et al.* on the detection of acetylcholinesterase (AChE) inhibitors, including organophosphate pesticides in food and beverages (Hossain *et al.*, 2009a). Their colorimetric assay relied on a printed sol-gel silica ink that entrapped acetylcholinesterase and a chromogenic substrate on the paper-based device. They reported excellent detection limits and successful detections in milk and apple juice, demonstrating its applicability for in-field rapid trace testing.

Lastly, a major field of testing is environmental and water monitoring, where extremely low-cost, real-time and on-site detection is one of the most pressing demands from many communities. The major categories of contaminants are heavy metals, chemical and agricultural pollutants, as well as toxins and pathogens. For ionic metals, a good example of μPAD is one from Apilux *et al.* on the monitoring of gold refining waste. They designed a dual electrochemical/colorimetric μPAD for detecting both Au(III) and Fe(III) on the same device (Apilux *et al.*, 2010). Iron needed to be measured colorimetrically since it interferes with the electrochemical detection of gold. Additional harmful ions comprise lead and zinc, for which Nie *et al.* designed a rapid and cost-effective μPAD based on anodic stripping voltammetry (Nie *et al.*, 2010b). Agricultural runoffs carrying pesticides and insecticide constitute, as well, a threat to human health and the environment. Hossain *et al.* tested bioactive paper sensors sensitive to organophosphates, which are a class of chemicals widely used in agriculture (Hossain *et al.*, 2009b). Regarding the probing of biohazards, and toxins in particular, Wang *et al.* developed a simple but high-performance fibrous-based biosensor faster than traditional ELISA. They impregnated a paper-based device with antibody-coated single walled carbon-nanotubes, which electrical conductivity depended on the concentration in toxins the antibodies are sensitive to (Wang *et al.*, 2009). They demonstrated the effectiveness of their platform by detecting, at levels lower than the World Health Organization standard, microcystin, a lethal toxin that travels to the liver, binds covalently to protein phosphatases and disrupts cellular control processes.

14.5 Conclusion and future trends

Microfluidic paper devices have the potential to be widely adopted analytical tools with attractive features such as low cost, portability, disposability, limited waste, simplicity, speed, lower consumption of reagents and sample, and ease of fabrication and use (Auroux *et al.*, 2002; Reyes *et al.*, 2002; Coltro *et al.*, 2010; Li *et al.*, 2013; Liana *et al.*, 2012). Their downsized reaction zones compared to dipstick tests make them attractive when working with scarce or hard-to-get samples (Abe *et al.*, 2008). However, they will have to overcome multiple limitations to match the performance of conventional analytical techniques. Some are impediments related to the substrate's nature, others originate from fabrication and detection hurdles. These limitations have to be overcome for μPADs to be as compelling as traditional analytical instruments.

A large volume of the sample gets lost during transport across a μPAD. In fact, at least half of it is retained within the paper matrix or evaporates in the air before reaching the detection zones, resulting in less concentrated, thus harder to detect, analytes (Li *et al.*, 2013). Losses are particularly undesirable when quantities of samples are limited. To improve sample delivery, a group proposed a technique to fully enclose devices, avoiding evaporation (Schilling *et al.*, 2012). In addition, fully enclosing a device protects the channels from outside contamination, improves storage of the reagents, and eases its handling and transport. Prior to Schilling *et al.*, others reported using double-sided tape to enclose 3D devices, but the adhesion of the protective tape becomes poor when the device gets wet and diffusion of adhesive in paper over time has been noticed. Back side protection was proposed as well, using polyester-backed nitrocellulose (Fenton *et al.*, 2008) or flexographic printing of a polyester-layer (Olkkonen *et al.*, 2010). Moreover, performing the separation in a closed system, to control the vapor pressure of the eluent, would decrease separation time and improve its efficiency (Carvalhal *et al.*, 2010). To mitigate sample retention, other groups have suggested using non-porous V-groove channels on polymer instead of cellulose (Tian *et al.*, 2010), or a thread-based microfluidic system, where sewed threads through a supporting substrate such as a polymer film are used to channel fluids (Li *et al.*, 2010d; Reches *et al.*, 2010). These threaded devices have higher wet strength than the paper-based ones.

To make lab-on-paper a low-cost diagnostic tool its fabrication needs to be compatible with high-speed, high-volume manufacturing without compromising quality. It is critical to ensure that the channel extends through the full thickness of the paper and holds the fluid properly. Because paper fibers are intertwined in a planar fashion and layered on top of each other, which makes hydrophobic wicking anisotropic, it is challenging for single-

step fabrication processes to pattern thin and well-defined channels (Li *et al.*, 2010a). As for the two-steps methods, a common issue is the interference of the sample with some residues of hydrophobic reagent that have not been completely removed from the channel (Dungchai *et al.*, 2011). Furthermore, not all patterning strategies relying on hydrophobic agents can build hydrophobic barriers strong enough to withstand samples of low surface tension, such as biological samples with surfactant. To have an effective transport of all kinds of liquids, it is better to pattern by blocking cellulosic pores which, unfortunately, uses extensive amounts of material. Other challenges that can be solved with novel fabrication designs concern the difficulty in multiplex analysis, and high integration of multiple analytical procedures on a single device (Wang *et al.*, 2012b). 3D structures described previously are a tentative to achieve this goal necessary for quantitative analysis. The future will see more of these intricate devices and novel techniques to route fluids, separate analytes, and wash, all the while avoiding fluidic cross-talks.

μPADs need to detect very low concentrations of biomarkers and contaminants to be relevant. Commonly, food and drinking water levels of contamination are in the ppb to ppt range, and currently typical colorimetric-based devices are limited to ppm. Research to enhance sensitivity and selectivity has already started with the development of gold nanoparticle-based detection and biorecognition on paper (Zhao *et al.*, 2008a, 2008b). In addition, any detection strategy needs to be compatible with transport and room temperature long-term storage. Understanding biomolecule immobilization and their stability is complex, and comprehensive optimizations still need to be conducted. Finally, to stay appealing, any detection strategy on μPADs needs to preserve their portability and their low power consumption. An innovation by Thom *et al.*, consisting in galvanic cells patterned within the paper device, represent an attractive approach toward self-powered analytical assays (Thom *et al.*, 2012).

Although paper is starting to be recognized as a substrate material for sensing devices, paper-based microfluidics is still at an early stage. Any success in the diagnostic market will depend on μPADs being mass producible at a low-cost, capable of reliable and easy to interpret results, and compatible with telemedicine. The lower the need for complicated external equipment, the easier will be the adoption. Solutions requiring complicated tools to interpret results may only be valuable for laboratory use.

14.6 References

Abe, K., Kotera, K., Suzuki, K. and Citterio, D. (2010). Inkjet-printed paperfluidic immuno-chemical sensing device. *Anal Bioanal Chem,* **398,** 885–893.

Abe, K., Suzuki, K. and Citterio, D. (2008). Inkjet-printed microfluidic multianalyte chemical sensing paper. *Anal Chem,* **80,** 6928–6934.

Apilux, A., Dungchai, W., Siangproh, W., Praphairaksit, N., Henry, C. S. and Chailapakul, O. (2010). Lab-on-paper with dual electrochemical/colorimetric detection for simultaneous determination of gold and iron. *Anal Chem,* **82,** 1727–1732.

Arena, A., Donato, N., Saitta, G., Bonavita, A., Rizzo, G. and Neri, G. (2010). Flexible ethanol sensors on glossy paper substrates operating at room temperature. *Sens Actuators B,* **145,** 488–494.

Bruzewicz, D. A., Reches, M. and Whitesides, G. M. (2008). Low-cost printing of poly(dimethylsiloxane) barriers to define microchannels in paper. *Anal Chem,* **80,** 3387–3392.

Carrilho, E., Martinez, A. W. and Whitesides, G. M. (2009a). Understanding wax printing: a simple micropatterning process for paper-based microfluidics. *Anal Chem,* **81,** 7091–7095.

Carrilho, E., Phillips, S. T., Vella, S. J., Martinez, A. W. and Whitesides, G. M. (2009b). Paper microzone plates. *Anal Chem,* **81,** 5990–5998.

Carvalhal, R. F., Kfouri, M. S., Piazetta, M. H., Gobbi, A. L. and Kubota, L. T. (2010). Electrochemical detection in a paper-based separation device. *Anal Chem,* **82,** 1162–1165.

Cheng, C. M., Martinez, A. W., Gong, J., Mace, C. R., Phillips, S. T., Carrilho, E., Mirica, K. A. and Whitesides, G. M. (2010). Paper-based ELISA. *Angew Chem Int Ed,* **49,** 4771–4774.

Chitnis, G., Ding, Z., Chang, C. L., Savran, C. A. and Ziaie, B. (2011). Laser-treated hydrophobic paper: an inexpensive microfluidic platform. *Lab Chip,* **11,** 1161–1165.

Cretich, M., Sedini, V., Damin, F., Pelliccia, M., Sola, L. and Chiari, M. (2010). Coating of nitrocellulose for colorimetric DNA microarrays. *Anal Biochem,* **397,** 84–88.

Delaney, J. L., Hogan, C. F., Tian, J. and Shen, W. (2011). Electrogenerated chemiluminescence detection in paper-based microfluidic sensors. *Anal Chem,* **83,** 1300–1306.

Dungchai, W., Chailapakul, O. and Henry, C. S. (2009). Electrochemical detection for paper-based microfluidics. *Anal Chem,* **81,** 5821–5826.

Dungchai, W., Chailapakul, O. and Henry, C. S. (2010). Use of multiple colorimetric indicators for paper-based microfluidic devices. *Anal Chim Acta,* **674,** 227–233.

Dungchai, W., Chailapakul, O. and Henry, C. S. (2011). A low-cost, simple, and rapid fabrication method for paper-based microfluidics using wax screen-printing. *Analyst,* **136,** 77–82.

Ellerbee, A. K., Phillips, S. T., Siegel, A. C., Mirica, K. A., Martinez, A. W., Striehl, P., Jain, N., Prentiss, M. and Whitesides, G. M. (2009). Quantifying colorimetric assays in paper-based microfluidic devices by measuring the transmission of light through paper. *Anal Chem,* **81,** 8447–8452.

Fenton, E. M., Mascarenas, M. R., López, G. P. and Sibbett, S. S. (2008). Multiplex lateral-flow test strips fabricated by two-dimensional shaping. *ACS Appl Mater Interfaces,* **1,** 124–129.

Fu, E., Kauffman, P., Lutz, B. and Yager, P. (2010a). Chemical signal amplification in two-dimensional paper networks. *Sens Actuators B,* **149,** 325–328.

Fu, E., Lutz, B., Kauffman, P. and Yager, P. (2010b). Controlled reagent transport in disposable 2D paper networks. *Lab Chip,* **10,** 918–920.

Fu, E., Ramsey, S. A., Kauffman, P., Lutz, B. and Yager, P. (2011). Transport in two-dimensional paper networks. *Microfluid Nanofluid,* **10,** 29–35.

Gauvreau, V. and Laroche, G. (2005). Micropattern printing of adhesion, spreading, and migration peptides on poly (tetrafluoroethylene) films to promote endothelialization. *Bioconjugate Chem,* **16,** 1088–1097.

Ge, L., Yan, J., Song, X., Yan, M., Ge, S. and Yu, J. (2012). Three-dimensional paper-based electrochemiluminescence immunodevice for multiplexed measurement of biomarkers and point-of-care testing. *Biomaterials,* **33,** 1024–1031.

Gong, X., Yi, X., Xiao, K., Li, S., Kodzius, R., Qin, J. and Wen, W. (2010). Wax-bonding 3D microfluidic chips. *Lab Chip,* **10,** 2622–2627.

Hawkes, R., Niday, E. and Gordon, J. (1982). A dot-immunobinding assay for monoclonal and other antibodies. *Anal Biochem,* **119,** 142–147.

Hossain, S. M. Z., Luckham, R. E., McFadden, M. J. and Brennan, J. D. (2009a). Reagentless bidirectional lateral flow bioactive paper sensors for detection of pesticides in beverage and food samples. *Anal Chem,* **81,** 9055–9064.

Hossain, S. M. Z., Luckham, R. E., Smith, A. M., Lebert, J. M., Davies, L. M., Pelton, R. H., Filipe, C. D. M. and Brennan, J. D. (2009b). Development of a bioactive paper sensor for detection of neurotoxins using piezoelectric inkjet printing of sol–gel-derived bioinks. *Anal Chem,* **81,** 5474–5483.

Kauffman, P., Fu, E., Lutz, B. and Yager, P. (2010). Visualization and measurement of flow in two-dimensional paper networks. *Lab Chip,* **10,** 2614–2617.

Khan, M. S., Thouas, G., Shen, W., Whyte, G. and Garnier, G. (2010). Paper diagnostic for instantaneous blood typing. *Anal Chem,* **82,** 4158–4164.

Klasner, S. A., Price, A. K., Hoeman, K. W., Wilson, R. S., Bell, K. J. and Culbertson, C. T. (2010). Paper-based microfluidic devices for analysis of clinically relevant analytes present in urine and saliva. *Anal Bioanal Chem,* **397,** 1821–1829.

Lankelma, J., Nie, Z., Carrilho, E. and Whitesides, G. M. (2012). Paper-based analytical device for electrochemical flow-injection analysis of glucose in urine. *Anal Chem,* **84,** 4147–4152.

Leung, V., Shehata, A. A. M., Filipe, C. D. M. and Pelton, R. (2010). Streaming potential sensing in paper-based microfluidic channels. *Colloids Surf A,* **364,** 16–18.

Li, A., Wang, Y., Deng, L., Zhao, X., Yan, Q., Cai, Y., Lin, J., Bai, Y., Liu, S. and Zhang, Y. (2013). Use of nitrocellulose membranes as a scaffold in cell culture. *Cytotechnology*, **65**(1), 71-81.

Li, C., Vandenberg, K., Prabhulkar, S., Zhu, X., Schneper, L., Methee, K., Rosser, C. J. and Almeide, E. (2011). Paper based point-of-care testing disc for multiplex whole cell bacteria analysis. *Biosens Bioelectron,* **26,** 4342–4348.

Li, X., Tian, J., Garnier, G. and Shen, W. (2010a). Fabrication of paper-based microfluidic sensors by printing. *Colloids Surf B Biointerfaces,* **76,** 564–570.

Li, X., Tian, J., Nguyen, T. and Shen, W. (2008). Paper-based microfluidic devices by plasma treatment. *Anal Chem,* **80,** 9131–9134.

Li, X., Tian, J. and Shen, W. (2010b). Progress in patterned paper sizing for fabrication of paper-based microfluidic sensors. *Cellulose,* **17,** 649–659.

Li, X., Tian, J. and Shen, W. (2010c). Quantitative biomarker assay with microfluidic paper-based analytical devices. *Anal Bioanal Chem,* **396,** 495–501.

Liu, H. and Crooks, R. M. (2011). Three-dimensional paper microfluidic devices assembled using the principles of origami. *J Am Chem Soc,* **133,** 17564–17566.

Lu, Y., Shi, W., Jiang, L., Qin, J. and Lin, B. (2009a). Rapid prototyping of paper-based microfluidics with wax for low-cost, portable bioassay. *Electrophoresis,* **30,** 1497–1500.

Lu, Y., Shi, W., Qin, J. and Lin, B. (2009b). Fabrication and characterization of paper-based microfluidics prepared in nitrocellulose membrane by wax printing. *Anal Chem,* **82,** 329–335.

Lutz, B. R., Trinh, P., Ball, C., Fu, E. and Yager, P. (2011). Two-dimensional paper networks: programmable fluidic disconnects for multi-step processes in shaped paper. *Lab Chip,* **11,** 4274–4278.

Martinez, A. W. (2011). Microfluidic paper-based analytical devices: from POCKET to paper-based ELISA. *Bioanalysis,* **3,** 2589–2592.

Martinez, A. W., Phillips, S. T., Butte, M. J. and Whitesides, G. M. (2007). Patterned paper as a platform for inexpensive, low-volume, portable bioassays. *Angew Chem Int Ed,* **46,** 1318–1320.

Martinez, A. W., Phillips, S. T., Carrilho, E., Thomas, S. W., 3rd, Sindi, H. and Whitesides, G. M. (2008a). Simple telemedicine for developing regions: camera phones and paper-based microfluidic devices for real-time, off-site diagnosis. *Anal Chem,* **80,** 3699–3707.

Martinez, A. W., Phillips, S. T., Nie, Z., Cheng, C. M., Carrilho, E., Wiley, B. J. and Whitesides, G. M. (2010). Programmable diagnostic devices made from paper and tape. *Lab Chip,* **10,** 2499–2504.

Martinez, A. W., Phillips, S. T. and Whitesides, G. M. (2008b). Three-dimensional microfluidic devices fabricated in layered paper and tape. *Proc Natl Acad Sci U S A,* **105,** 19606–19611.

Martinez, A. W., Phillips, S. T., Whitesides, G. M. and Carrilho, E. (2009). Diagnostics for the developing world: microfluidic paper-based analytical devices. *Anal Chem,* **82,** 3–10.

Martinez, A. W., Phillips, S. T., Wiley, B. J., Gupta, M. and Whitesides, G. M. (2008c). FLASH: a rapid method for prototyping paper-based microfluidic devices. *Lab Chip,* **8,** 2146–2150.

Nagler, R. M. (2008). Saliva analysis for monitoring dialysis and renal function. *Clin Chem,* **54,** 1415–1417.

Nie, Z., Deiss, F., Liu, X., Akbulut, O. and Whitesides, G. M. (2010a). Integration of paper-based microfluidic devices with commercial electrochemical readers. *Lab Chip,* **10,** 3163–3169.

Nie, Z., Nijhuis, C. A., Gong, J., Chen, X., Kumachev, A., Martinez, A. W., Narovlyansky, M. and Whitesides, G. M. (2010b). Electrochemical sensing in paper-based microfluidic devices. *Lab Chip,* **10,** 477–483.

Noh, H. and Phillips, S. T. (2010a). Fluidic timers for time-dependent, point-of-care assays on paper. *Anal Chem,* **82,** 8071–8078.

Noh, H. and Phillips, S. T. (2010b). Metering the capillary-driven flow of fluids in paper-based microfluidic devices. *Anal Chem,* **82,** 4181–4187.

Olkkonen, J., Lehtinen, K. and Erho, T. (2010). Flexographically printed fluidic structures in paper. *Anal Chem,* **82,** 10246–10250.

Osborn, J. L., Lutz, B., Fu, E., Kauffman, P., Stevens, D. Y. and Yager, P. (2010). Microfluidics without pumps: reinventing the T-sensor and H-filter in paper networks. *Lab Chip,* **10,** 2659–2665.

Ratnarathorn, N., Chailapakul, O., Henry, C. S. and Dungchai, W. (2012). Simple silver nanoparticle colorimetric sensing for copper by paper-based devices. *Talanta*, **99**, 552–557.

Rezk, A. R., Qi, A., Friend, J. R., Li, W. H. and Yeo, L. Y. (2012). Uniform mixing in paper-based microfluidic systems using surface acoustic waves. *Lab Chip,* **12,** 773–779.

Shiroma, L. Y., Santhiago, M., Gobbi, A. L. and Kubota, L. T. (2012). Separation and electrochemical detection of paracetamol and 4-aminophenol in a paper-based microfluidic device. *Anal Chim Acta,* **725,** 44–50.

Songjaroen, T., Dungchai, W., Chailapakul, O. and Laiwattanapaisal, W. (2011). Novel, simple and low-cost alternative method for fabrication of paper-based microfluidics by wax dipping. *Talanta,* **85,** 2587–2593.

Steffens, C., Manzoli, A., Francheschi, E., Corazza, M., Corazza, F., Oliveira, J. V. and Herrmann, P. (2009). Low-cost sensors developed on paper by line patterning with graphite and polyaniline coating with supercritical CO2. *Synthetic Metals,* **159,** 2329–2332.

Wang, L., Chen, W., Xu, D., Shim, B. S., Zhu, Y., Sun, F., Liu, L., Peng, C., Jin, Z. and Xu, C. (2009). Simple, rapid, sensitive, and versatile SWNT – paper sensor for environmental toxin detection competitive with ELISA. *Nano Lett,* **9,** 4147–4152.

Wang, P., Ge, L., Yan, M., Song, X., Ge, S. and Yu, J. (2012a). Paper-based three-dimensional electrochemical immunodevice based on multi-walled carbon nanotubes functionalized paper for sensitive point-of-care testing. *Biosens Bioelectron,* **32,** 238–243.

Wang, S., Ge, L., Song, X., Yu, J., Ge, S., Huang, J. and Zeng, F. (2012b). Paper-based chemiluminescence ELISA: lab-on-paper based on chitosan modified paper device and wax-screen-printing. *Biosens Bioelectron,* **31,** 212–218.

Wang, W., Wu, W. Y. and Zhu, J. J. (2010). Tree-shaped paper strip for semiquantitative colorimetric detection of protein with self-calibration. *J Chromatogr A,* **1217,** 3896–3899.

Yan, J., Ge, L., Song, X., Yan, M., Ge, S. and Yu, J. (2012). Paper-based electrochemiluminescent 3D immunodevice for lab-on-paper, specific, and sensitive point-of-care testing. *Chemistry,* **18,** 4938–4945.

Yang, X., Forouzan, O., Brown, T. P. and Shevkoplyas, S. S. (2012). Integrated separation of blood plasma from whole blood for microfluidic paper-based analytical devices. *Lab Chip,* **12,** 274–280.

Yu, J., Ge, L., Huang, J., Wang, S. and Ge, S. (2011a). Microfluidic paper-based chemiluminescence biosensor for simultaneous determination of glucose and uric acid. *Lab Chip,* **11,** 1286–1291.

Yu, J., Wang, S., Ge, L. and Ge, S. (2011b). A novel chemiluminescence paper microfluidic biosensor based on enzymatic reaction for uric acid determination. *Biosens Bioelectron,* **26,** 3284–3289.

Zhao, W., Ali, M. M., Aguirre, S. D., Brook, M. A. and Li, Y. (2008). Paper-based bioassays using gold nanoparticle colorimetric probes. *Anal Chem,* **80,** 8431–8437.

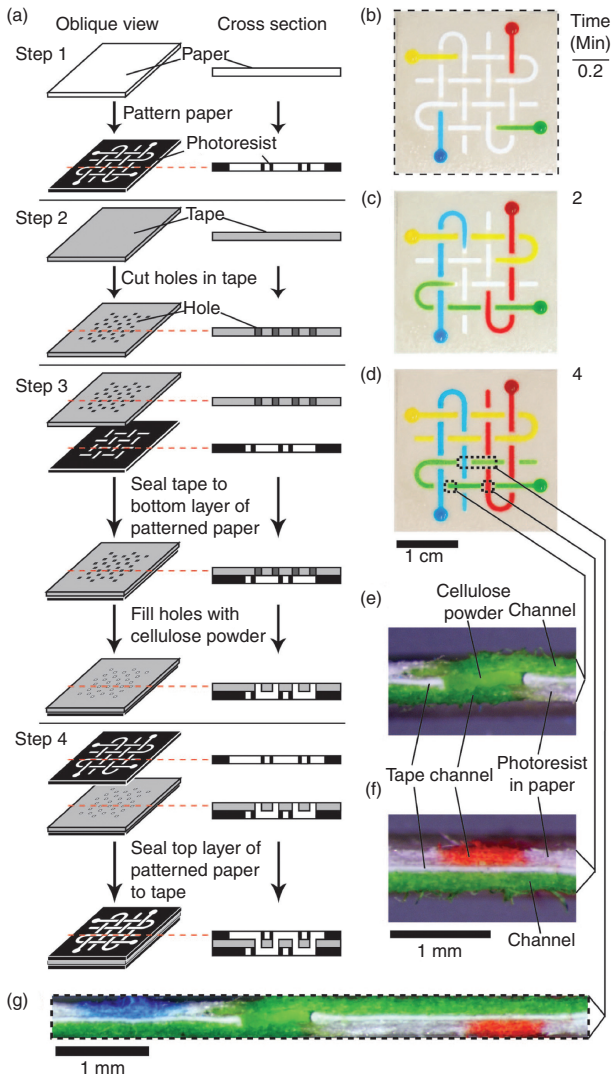

Plate VI (Chapter 14) Preparation and demonstration of a 3D PAD. (a) Fabrication. (b) Photograph of a basketweave system 10 s after adding red, yellow, green, and blue aqueous solutions of dyes to the sample reservoirs. The dotted lines indicate the edge of the device. (c and d) Photographs taken 2 min (c) and 4 min (d) after adding the dyes. The streams of fluids crossed each other multiple times in different planes without mixing. The dotted lines in (d) show the positions of the cross sections shown in (e), (f), and (g). (e) Cross section of the device showing a channel connecting the top and bottom layers of paper. (f) Cross section of the device showing the three layers of the device with orthogonal channels in the top and bottom layers of paper. (g) Cross section of the device showing the layers and the distribution of fluid (and colors) in each layer of the device shown in (d). The dotted lines indicate the edges of the cross section. (*Source*: Adapted with permission from Martinez *et al.*, 2008b. Copyright © 2008 National Academy of Sciences, USA.)

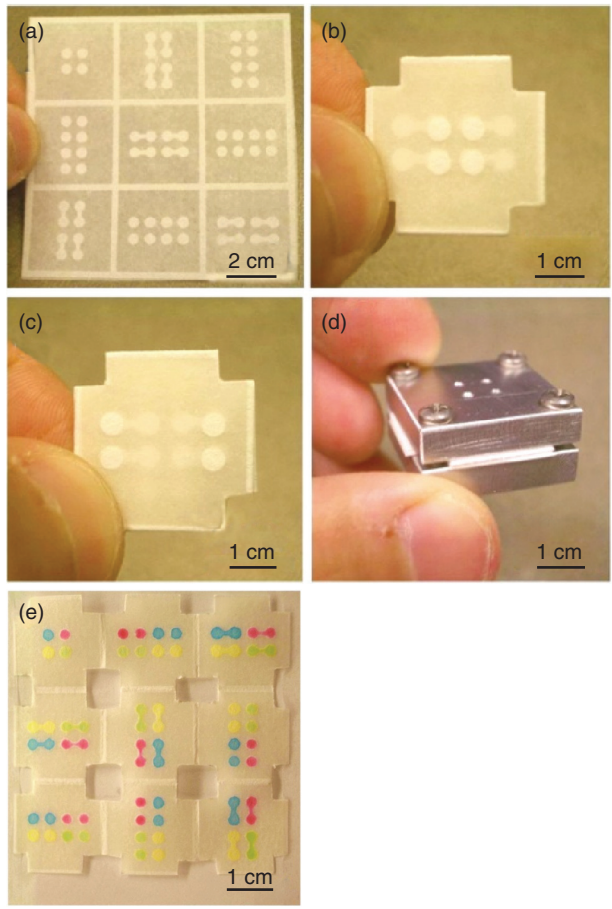

Plate VII (Chapter 14) (a) Chromatography paper (100 μm thick) having photolithographically patterned channels, reservoirs, and a folding frame. All channels were 900 μm wide, and the reservoirs were 2.5 mm in diameter. (b) Top layer of the folded paper revealing four inlet reservoirs in the center of the device. The four flanking circular features are present within the 3-D structure of the device but are visible due to the transparency of the paper. Four corners of the folded paper were cut so it could be clamped in the aluminum housing shown in (d). (c) Bottom layer of the folded paper. (d) The aluminum housing used to support the 3-D paper microfluidic system. The four holes drilled in the top of the housing are used for injecting solutions. (e) An unfolded, nine-layer paper microfluidic device after injecting four 1.0 mM, aqueous, colored solutions (rhodamine 6G, red; erioglaucine, blue; tatrazine, yellow; and a mixture of erioglaucine and tatrazine, 1:10, green) through the four injection ports in the aluminum clamp. The colored solutions passed through their designated channels and reservoirs without mixing. (*Source*: Adapted with permission from Liu and Crooks, 2011. Copyright © 2011 American Chemical Society.)

15

Microfluidic devices for viral detection

J. SUN and X. JIANG, National Center for Nanoscience Technology, China

DOI: 10.1533/9780857097040.4.527

Abstract: Microfluidic techniques are emerging as cost-efficient and disposable tools for rapid diagnosis of viral infection. This chapter reviews the conventional and microfluidic methods for viral detection and highlights the critical need for point-of-care (POC) and inexpensive diagnostics. This chapter includes several examples of microfluidic devices used for selective and sensitive viral detection based on immunoassays of virus-related antigens or antibodies, nucleic acid amplification, and flow cytometry. The chapter concludes with a discussion of future trends in detection, diagnosis, and assessment of viral infection by microfluidic tools.

Key words: microfluidics, viral infection, diagnostics, point-of-care.

15.1 Introduction

Infectious diseases result from pathogenic microorganisms, such as bacteria, viruses, parasites, and fungi (Ryan *et al*., 2004; Fauci and Morens, 2012). The outbreak of infectious diseases severely threatens public health and greatly increases the risk of morbidity and mortality, especially in developing countries (Yager *et al*., 2006; Pang and Peeling, 2007; Strauss and Strauss, 2008; Leke, 2010). Viral infectious diseases, including human immunodeficiency virus (HIV), hepatitis B, hepatitis C, malaria, and tuberculosis are the major causes of death in developing countries (Fig. 15.1) (Hauck *et al*., 2010). The World Health Organization (WHO) recently reported that HIV is the sixth leading cause of death worldwide (WHO, 2011). Rapid and effective diagnostic technologies are crucial for identifying viruses and pathogens, providing appropriate treatment, and preventing the outbreak of infection (Free, 2004; Malkin, 2007; Singer *et al*., 2007).

Gold-standard techniques for detection of viral infectious disease include tissue culture, enzyme-linked immunosorbent assay (ELISA), and polymerase chain reaction (PCR) (Mackay, 2004; Foudeh *et al*., 2012). Although these diagnostic approaches are commonly adopted in the developed world, they are still labor intensive, time consuming, and they typically are associated

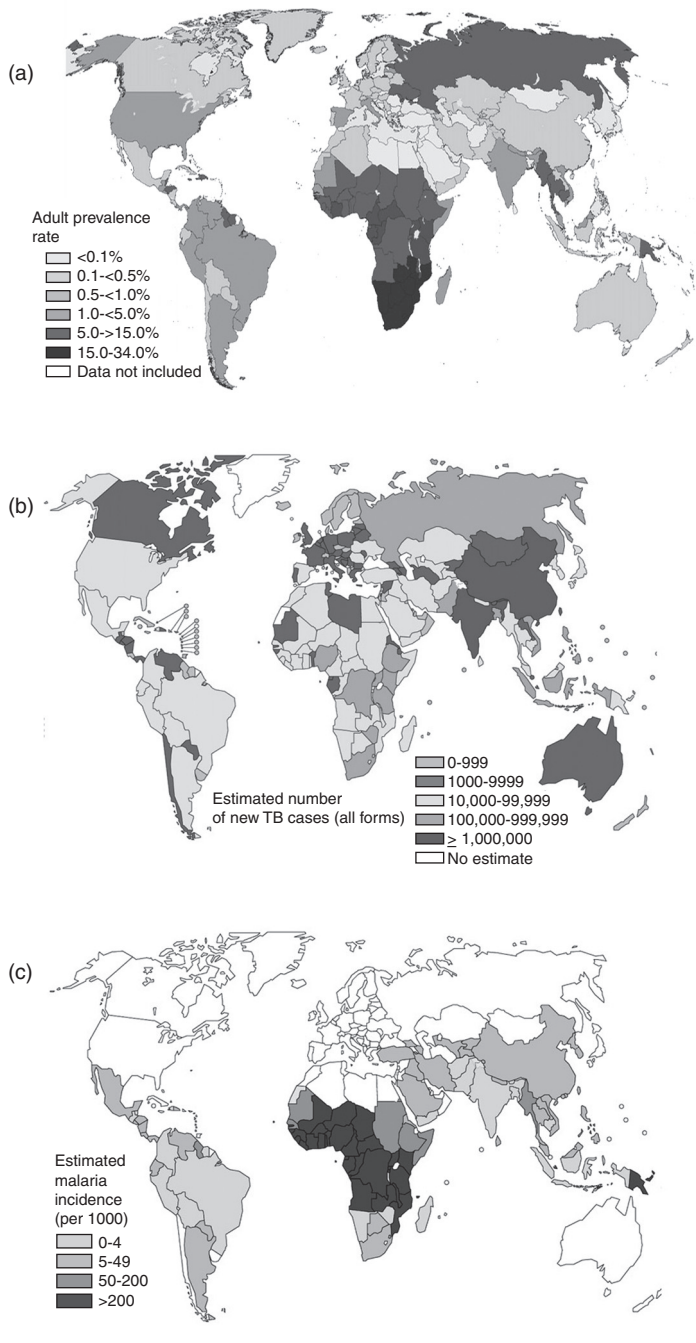

15.1 (a) A global view of HIV infection. There were around 39.5 million people with HIV infection in 2006. (b) Estimated number of tuberculosis sufferers worldwide in 2007. (c) Estimated incidence of malaria per 1000 population in 2006. (*Source*: Reprinted with permission from Hauck *et al*. (2010), copyright 2010 Elsevier.)

with high equipment and reagent expenses (Yang and Rothman, 2004). For example, diagnosis of HIV involves an enzyme immunoassay combined with a western blot (Schupbach, 2002; Branson, 2007). These tests are not suitable to perform outside the laboratory, or without trained personnel (Sturenburg and Junker, 2009). Malarial identification requires high-resolution microscopes as well as experienced staff for reading slides (McMorrow *et al.*, 2008). For detection of very low density infections, PCR remains the most effective tool, but is limited in low-resource settings because of their high cost, long analysis time, and the influence of contamination (Drakeley and Reyburn, 2009). Despite the fact that diagnostic methods are well established in the developed world, these approaches are generally not affordable or feasible in resource-poor settings where modern healthcare infrastructure is not available (Yager *et al.*, 2008). According to WHO guidelines, cost-effective, portable, disposable, and POC diagnostic approaches are needed in order to enhance the health-related quality of life in worldwide populations (Urdea *et al.*, 2006).

Microfluidic technologies, with increased sensitivity and decreased cost, offer great promise to develop effective diagnostic tools to overcome the hurdles imposed by conventional methods (Gervais *et al.*, 2011; Chin *et al.*, 2012; Govindarajan *et al.*, 2012; Sun *et al.*, 2012a). These technologies provide many benefits, including compactness, portability, disposability, and integration of multiple functions. The small dimension of microfluidic channels inherently reduces reagent consumption, decreases reaction time, and provides the ability to analyze low volume samples (Beebe *et al.*, 2002; Sia and Whitesides, 2003; Bange *et al.*, 2005). Microfluidic technologies can automate various steps of assays, including sample preparation, reaction, transportation, and analysis, inside a single chip (Melin and Quake, 2007; Sun *et al.*, 2010). This enclosed, integrated, and automated format of microfluidics significantly avoids cross-contamination and enables multiplexed detection of pathogens. In addition, mass production of disposable microfluidic devices for viral detection can be implemented by using low-cost plastic fabrication and screen-printing techniques (Dong *et al.*, 2007; Liu *et al.*, 2007). Currently, microfluidic systems are becoming essential and revolutionary tools for POC viral diagnostics (Kelly and Woolley, 2005; Zhang *et al.*, 2012; Sun *et al.*, 2012b).

15.2 Microfluidic technologies used for viral detection

This section introduces a variety of promising microfluidic technologies used for viral detection. These technologies hold great potential for addressing issues raised by conventional methods including immunological detection, nucleic acid amplification, and flow cytometry.

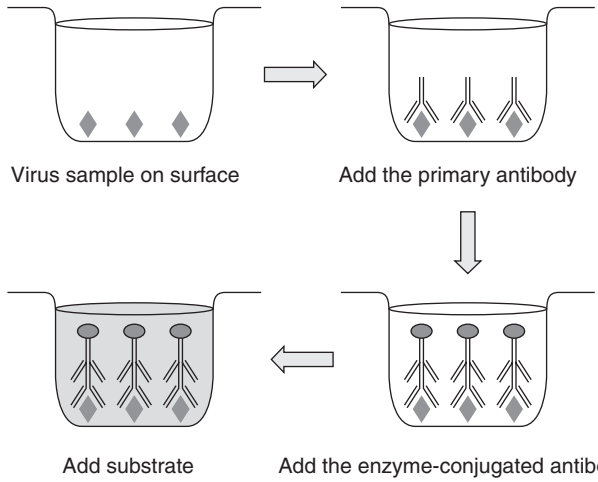

15.2 Schematic of ELISA. Briefly, the virus sample (pathogenic antigen) is immobilized on a solid substrate. The substrate is then incubated with the serum, which contains the corresponding antibody (the primary antibody). A second, enzyme-conjugated antibody is added to bind the primary antibody, followed by adding a substrate for this enzyme. The substrate changes color upon reaction with the enzyme.

15.2.1 Microfluidic immunoassay

Immunological detection is one of the most powerful clinical tools for viral diagnostics because of its relative simplicity (Wang *et al*., 2002; Jiang *et al*., 2003; Ansaldi *et al*., 2006). Immunoassays rely on the sensitive and specific affinities of the antibody–antigen interaction to test either the antigen or the antibody (Wu, 2006). Among a diverse set of immunoassays, ELISA is the most widely used one, involving enzyme-conjugated antibodies and the enzyme's substrate to detect antigens of interest indicated by a color change (Fig. 15.2) (Borkowsky *et al*., 1987; Liu *et al*., 2007). Because of the high sensitivity and selectivity of antigen–antibody binding, ELISA has been commonly adopted for diagnosis of such infectious diseases as HIV, hepatitis B, hepatitis C, and Chagas disease (Cordes and Ryan, 1995; Misiani *et al*., 1992; Ferreira *et al*., 1997). However, ELISA often requires labor-intensive procedures, long assay times, and expensive reagents, making this technology poorly suited for low-resource settings (Yang *et al*., 2008a; Qu *et al*., 2011). Another commonly used immunological method for viral detection is the western blot (protein immunoblot) that uses gel electrophoresis to separate proteins, followed by subsequent blotting to identify proteins. The western blot is a widely accepted HIV diagnostic assay, but also requires cumbersome manual protocols during assays (He and Herr, 2009; Liu *et al*., 2010; Pan *et al*., 2010; Song *et al*., 2012).

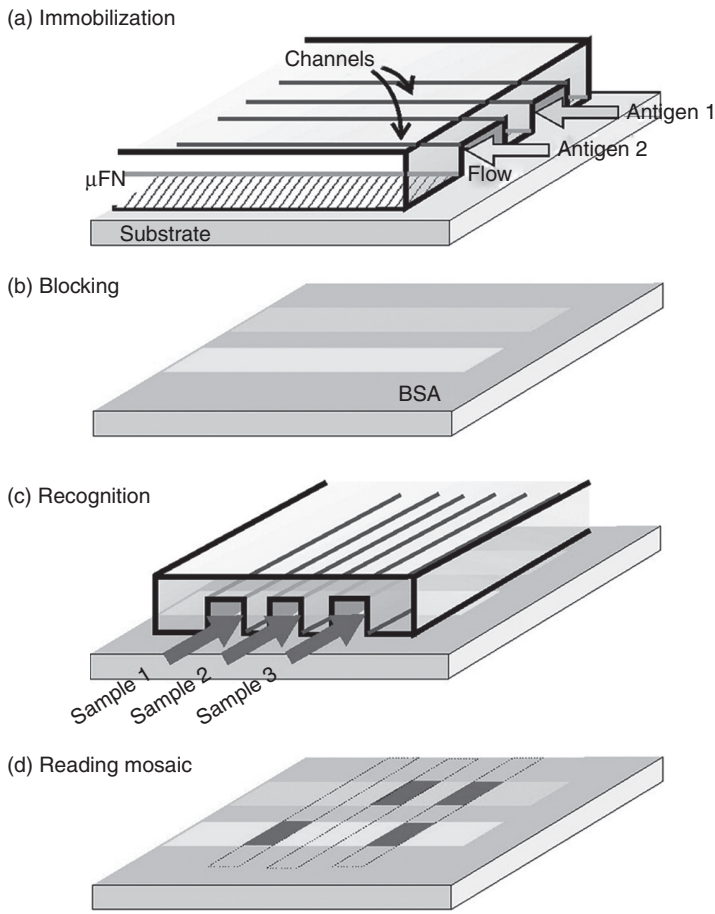

15.3 Schematic of microfluidic immunoassay. (a) A microfluidic network (μFN) to pattern different antigens on the substrate. (b) Block unpatterned area with BSA to prevent nonspecific binding of proteins. (c) Induce antibodies to bind with antigens using a second μFN. (d) Read the binding mosaic pattern. (*Source*: Reprinted with permission from Bernard *et al*. (2001), copyright 2001 American Chemical Society.)

Microfluidic immunoassay can address many of these issues raised by conventional immunological detection. To perform a microfluidic immunoassay, a microfluidic network (μFN) is designed to pattern different antigens on the substrate, followed by blocking the unpatterned area with bovine serum albumin (BSA) to prevent nonspecific binding of proteins. The next step is to induce a sample solution containing specific antibodies to bind with antigens using a second μFN. As the immunobinding occurs along micrometer-wide intersecting lines, a mosaic of signals from cross-reacted zones can be read using a fluorescence microscope (Fig. 15.3) (Bernard *et al*., 2001).

This miniaturized format of microfluidic assays only uses a small amount of reagents such as antibodies and enzymes that are often hundreds of dollars per milligram, thus dramatically reducing the cost of each test. Moreover, microfluidic techniques allow the integration and automation of immunoassay procedures such as sample preparation, reagent delivery, and multiple incubation and washing steps. Because of the rapid transportation inside the microchannels, the time required for each incubation step can be dramatically reduced from 1 h to 5 min (Rossier and Girault, 2001). In addition, microfluidic devices can be designed to perform parallel, quantitative assays of multiple viral samples in one test.

Yakovleva *et al*. reported a silicon microchip with immobilized antibodies for microfluidic enzyme immunoassays using chemiluminescence detection. They evaluated different immobilization protocols and buffer selection to reach the best assay stability and sensitivity (Yakovleva *et al*., 2002). Wang *et al*. designed a microfluidic diagnostic system consisting of several reaction wells, micro-pneumatic valves, peristaltic micro-pumps, and an automatic platform (Wang and Lee, 2005). The micro-pneumatic valves were used to separate analytes and reagents, while the spider-web peristaltic micropumps were employed to drive the fluids into the microchannels. After the analytes and reagents gradually entered the reaction/detection area, fluorescence signals caused by antibody–antigen interaction were detected by a fluorescent reader so as to detect the diseases. This integrated microfluidic system allowed fast diagnosis of hepatitis C virus and syphilis in an automated and efficient format (Fig. 15.4). Yang *et al*. applied electrospun nanofibrous membranes as the solid substrates to detect HIV-specific antibodies from human serum samples (Yang *et al*., 2008a). These nanofibers with large specific surface areas could increase the adsorption of proteins, thus improving the sensitivity and signal-to-noise ratio of microfluidic immunoassays (Fig. 15.5). Moreover, fabrication of these nanofibrous membranes was simple and cost effective, which could be easily incorporated with existing microchannel designs. This membrane-based microfluidic assay was well suited for resource-poor settings. Song *et al*. recently described a fluorescent microfluidic immunoassay for rapid, multiple HIV sample screening and confirmation through removing the blocking step (Song *et al*., 2012). This method could significantly improve the assay speed while keeping the limit of detection comparable to conventional ELISA, which made it an excellent candidate for a quick HIV test for both screening and confirmation.

Pan *et al*. developed a microfluidic Western blot by combining a microfluidic immunoassay with conventional protein blotting, which was termed as μWB (Pan *et al*., 2010). This μWB consisted of five steps: (1) using sodium dodecyl sulfate polyacrylamide gel electrophoresis (SDS-PAGE) to separate proteins in cell lysates according to their molecular weights; (2) transferring proteins from the polyacrylamide gel to a polyvinylidene fluoride (PVDF)

membrane by an electrotransfer system; (3) placing a microfluidic network on the blotted membrane with the channels perpendicular to the protein bands; (4) detecting multiple proteins simultaneously on the PVDF membrane by incubating different primary antibodies in parallel microfluidic channels; and (5) peeling off the microfluidic network and incubating the whole PVDF membrane in fluorescent dye-labeled secondary antibody solution. This microfluidic system could analyze multiple proteins simultaneously consuming only microliters of antibodies, and indicated a new avenue for POC diagnosis of viral infection. Following the concept of μWB, Hughes

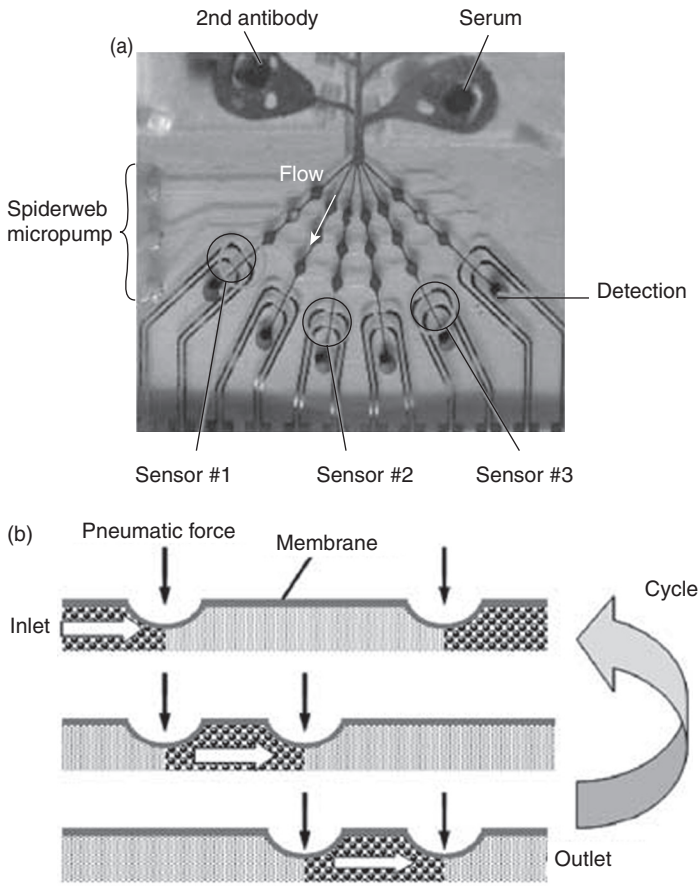

15.4 (a) An automated microfluidic system consisting of micro-pneumatic valves and peristaltic micro-pumps for fast immunoassays. (b) Schematic diagram of the working principle of peristaltic micro-pumps. Results of detecting hepatitis C virus (c) and syphilis (d) by using the microfluidic chip. (*Source*: Reprinted with permission from Wang and Lee (2005), copyright 2005 Elsevier.)

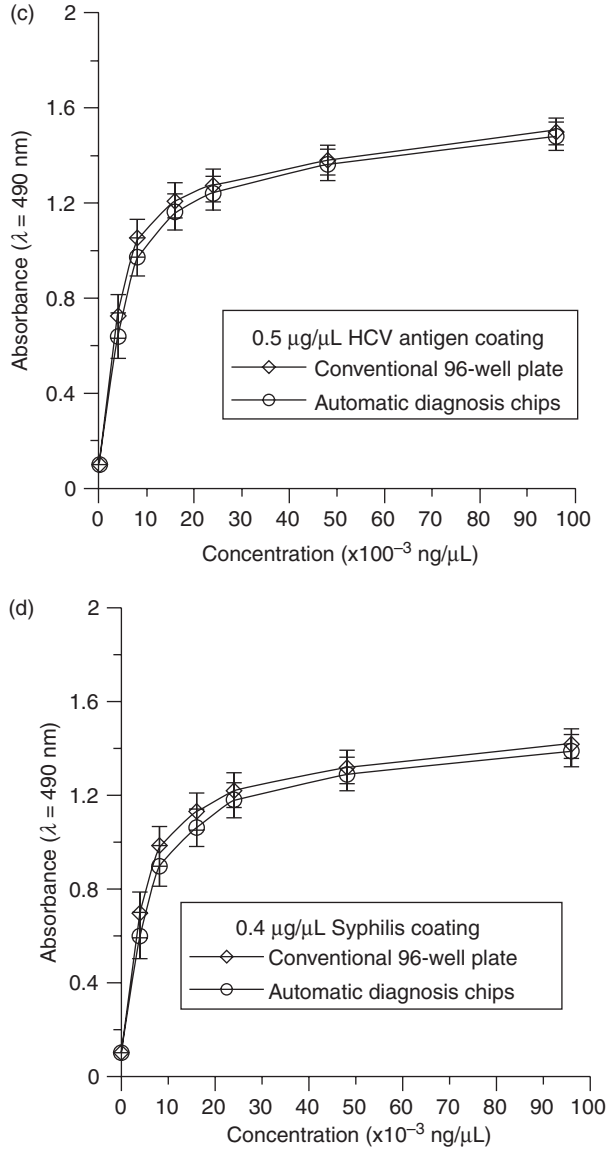

15.4 Continued

et al. applied an automated microfluidic Western blot to detect purified HIV proteins gp120 and p24 from human sera with the increased protein blotting efficiency and reduced reagent consumption (Hughes and Herr, 2012; Kim *et al*., 2012). This microfluidic system also decreased the overall assay duration to 10–60 min, enabled multiplexed analyte detection, lowered the detection limit to 50 pM, and realized quantitation over a wide dynamic range. These improvements were attributed to unique microscale conditions.

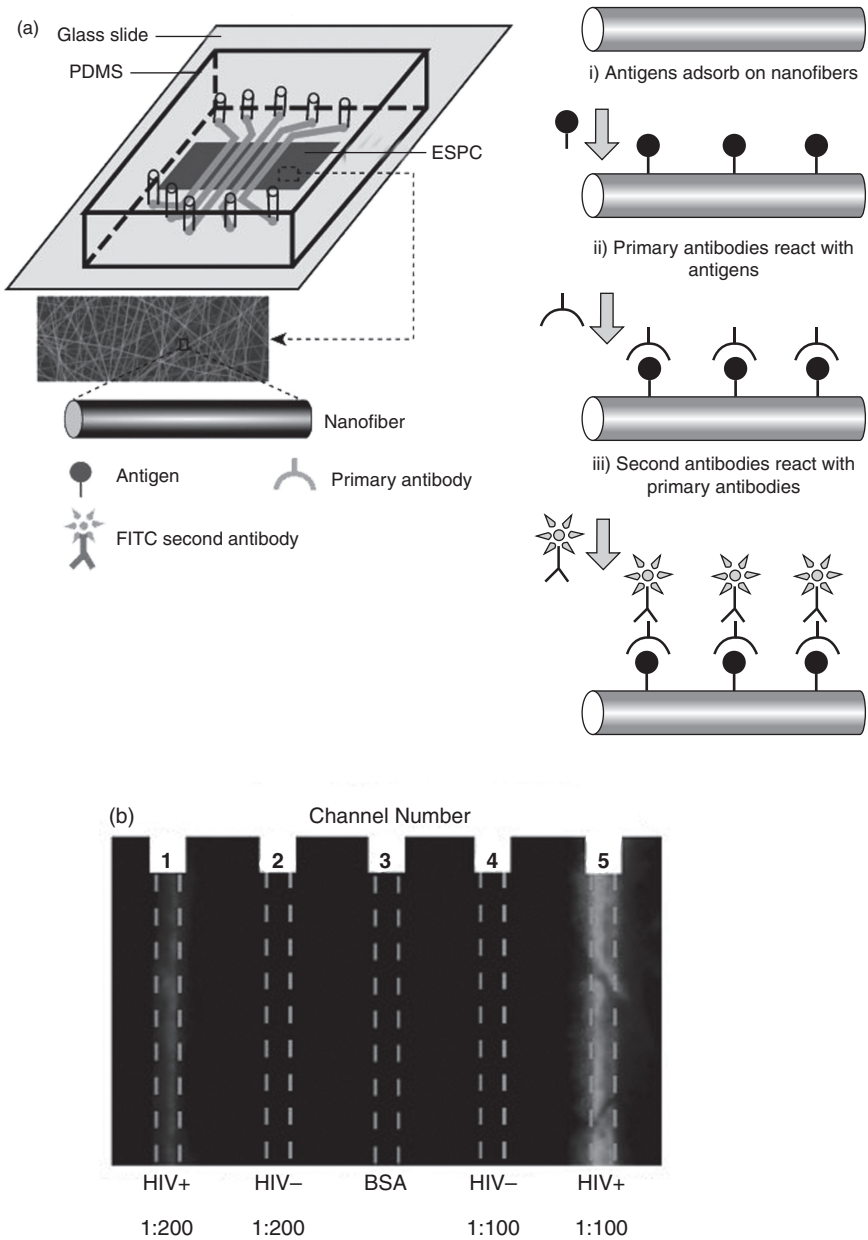

15.5 (a) A microfluidic device for HIV immunoassays with the electrospun polycarbonate fibrous membrane (ESPC) as the solid substrate. ESPC substrate with the large specific surface areas can increase antigen adsorption. (b) Results of the assays using different samples of patient serum to detect anti-gp41 at lower concentrations. (*Source*: Reprinted with permission from Yang *et al.* (2008a), copyright 2008 WILEY-VCH.)

15.2.2 Microfluidic nucleic acid amplification

Over the past decades, nucleic acid amplification methods have evolved as the cornerstone of clinical assessment and prevention of infectious diseases (Yager *et al*., 2008; Fang *et al*., 2010). Advantages of nucleic acid amplification-based diagnostic assays include the increased detection sensitivity that can theoretically amplify a single copy (at least 10^6 higher than lateral flow immunoassays), the improved specificity to differentiate pathogen strains, and the faster diagnostic time than tissue culture (Mackay, 2004). Strategies for nucleic acid amplification can be simply classified as non-isothermal amplification (PCR) and isothermal amplification (such as loop-mediated isothermal amplification (LAMP), nucleic acid sequence-based amplification (NASBA), and nicking enzyme amplification reaction (NEAR)) (McCalla and Tripathi, 2011). PCR relies on thermal cycling consisting of repeated temperature changes to realize deoxyribonucleic acid (DNA) denaturation, annealing, and extension. PCR testing can rapidly and accurately screen hepatitis C virus, hepatitis B virus, HIV-1, and HIV-2 in blood samples (Peeters *et al*., 1992; Roth *et al*., 1999). Isothermal amplification technologies use a constant temperature rather than thermal cycling, thus performing assays in a simple and effective manner (Notomi *et al*., 2000). Isothermal amplification assays have been developed for detecting circulating HIV-1 virus in blood, malaria, and tuberculosis (Kievits *et al*., 1991; Iwamoto *et al*., 2003; Poon *et al*., 2006). As microfluidic technology carries many advantages, such as disposable, low cost, reduced cross-contamination, and biohazard risks, on-chip nucleic acid amplification is expected to have great impact on viral diagnostics.

Gascoyne *et al*. proposed an integrated microfluidic system for detection of malarial parasites in blood samples (Gascoyne *et al*., 2004). This small, self-contained microfluidic device contained a dielectrophoretic field-flow-fractionation (DEP–FFF) front end for malarial specimen preparation, a cell lysis stage, and an on-chip real-time PCR system for gene amplification and detection (Fig. 15.6). The serpentine microfluidic channel in Fig. 15.6b traversed through different temperature zones and accomplished the continuous thermal cycling with the reduced sample volumes and reaction times. They believed this microfluidic diagnostic tool could address not only malaria but also a variety of other infectious diseases. Cho *et al*. developed a real-time microfluidic-based PCR system consisting of six individual thermal cycling modules (Cho *et al*., 2006). In comparison with conventional PCR machines, which require 25 μL of reaction mixtures and 2–3 h reaction time, the on-chip PCR systems consumes only 1 μL of reaction mixtures and amplifies DNA within 20 min (Fig. 15.7). They used this on-chip PCR system to conduct the large-scale clinical screening of the hepatitis B virus infection, the results of which showed a sensitivity of 94% and specificity of 93%.

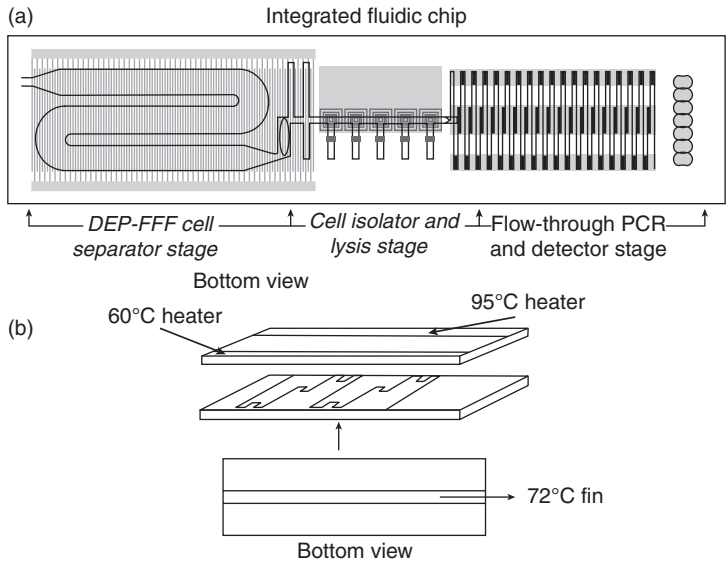

15.6 (a) Schematic of an integrated microfluidic system for detection of malaria. This microfluidic chip comprises an DEP–FFF front end, a cell lysis stage, and a real-time PCR system. (b) Design of a microfluidic PCR system consisting of a serpentine microfluidic channel in the first two temperature cycling stages. As the sample slowly flows through the channel with thermal cycling, nucleic acid amplification occurs. (*Source*: Reprinted with permission from Gascoyne *et al.* (2004), copyright 2004 Elsevier.)

Another popular format of microfluidic-based PCR for viral diagnostics is the droplet emulsion PCR system, which relies on the integration of microfluidic PCR and discrete water-in-oil droplets as the reaction chambers generated by flow focusing or electric field (Park *et al.*, 2011). Each of millions of aqueous droplet containing PCR mixtures is protected by immiscible oil, enabling the large-scale and high-throughput amplification and screening of the nucleic acid of viruses with decreased risk of cross containment. Zeng *et al.* reported the use of a droplet emulsion PCR system for pathogenic cell detection in a high background of normal cells with the detection limit of $1/10^5$ (Fig. 15.8) (Zeng *et al.*, 2010).

Compared with PCR systems, isothermal amplification strategies can eliminate the thermal cycling steps, thus simplifying both the chip design and the instrument configuration. Gulliksen *et al.* demonstrated a microfluidic real-time NASBA system for diagnosis of human papilloma virus (HPV) (Gulliksen *et al.*, 2004). NASBA is an isothermal, transcription-based amplification technique specifically designed for amplification of ribonucleic acid (RNA) that requires two primers and three enzymes to proceed (McCalla

15.7 (a) Photography of the rapid real-time microscale chip-based PCR system for screening of the hepatitis B virus infection. (b) The microfluidic PCR chip. (*Source*: Reprinted with permission from Cho *et al*. (2006), copyright 2006 Elsevier.)

and Tripathi, 2011). The microfluidic NASBA chip was made by bonding the etched silicon wafer with glass to form a 10- or 50-nL reaction chamber and fluid delivery channels. The reaction mixture was preheated at 65°C before loading into the chamber, which was placed above a heater at a temperature around 41°C. Real-time NASBA process inside the microfluidic chip was monitored by using fluorescent molecular beacon probes and an external optical detection system. This proof-of-concept system successfully amplified and detected HPV positive control (1 μM) and single stranded deoxyribonucleic acid (ssDNA) (0.1 μM) in nanoliter volumes. Dimov *et al*. developed a microfluidic device that integrated the functions of RNA purification and NASBA (Dimov *et al*., 2008). This integrated microfluidic device had two functional domains: a silica bead-bed chamber for RNA

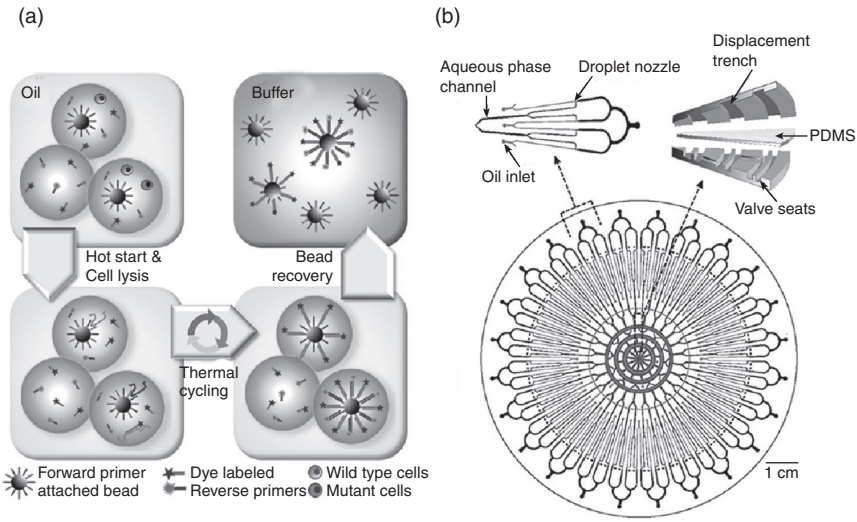

15.8 Schematic of the droplet emulsion PCR system. (a) Statistically dilute beads and templates are encapsulated into uniform nanoliter volume droplets for PCR amplification. (b) Layout of the integrated microfluidic chip composed of a single ring pump and 96 droplet generators for droplet-based PCR system. (*Source*: Reprinted with permission from Zeng *et al.* (2010), copyright 2010 American Chemical Society.)

purification, and a NASBA chamber for real-time amplification and detection (Fig. 15.9). Cell lysate samples first passed over the silicon beads that were used to capture and purify RNA. The genetic material was washed off the beads and delivered into the NASBA channel, followed by heating at 65°C before adding enzymes. An adjacent no-template negative control was included on the same chip for direct comparison. On-chip amplification was monitored in real-time using molecular beacon fluorescent probe technology. This microfluidic NASBA system enabled ten times faster (< 3 min) and ten times less volume (2 μL) than conventional reactions.

Another intensively developed isothermal amplification technology is LAMP, which bypasses thermal cycling by using a set of specially designed primers and a DNA polymerase for strand displacement (Notomi *et al.*, 2000). The microfluidic system (μLAMP) developed by Fang *et al.* had an octopus-like configuration containing ten microchambers, each of which was connected to the corresponding thin microchannel via a dimension gradient bridge (Fig. 15.10) (Fang *et al.*, 2011). The microchambers were precoated with specific LAMP probe sets, and the separate microchannels were used to forbid the cross-talk of probes among different microchambers. This microfluidic system was applied to simultaneously differentiate three types of human influenza in a single chip, with the detection limit of less

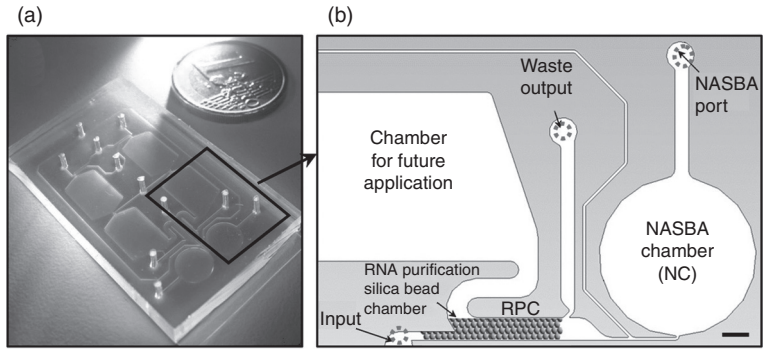

15.9 Schematic of microfluidic device for RNA purification and real-time NASBA of *E. coli* bacteria. (a) Photograph of microfluidic architecture that is mirrored to allow a NASBA reaction and a negative control in the same chip. (b) Layout of the single device incorporating RNA purification chamber and real-time NASBA chamber. (*Source*: Reprinted with permission from Dimov *et al*. (2008), copyright 2008The Royal Society of Chemistry.)

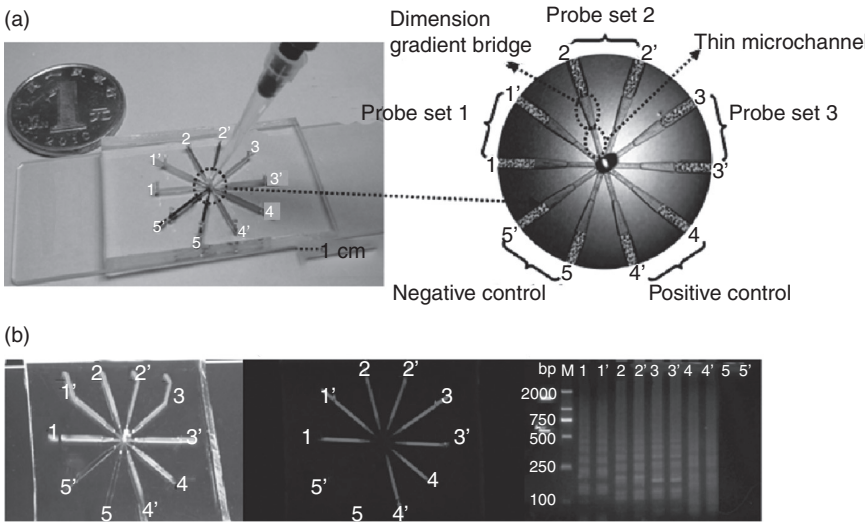

15.10 (a) Schematic of the octopus-like mμLAMP system in a PDMS-glass format. Microchambers were connected to the corresponding thin microchannel via dimension gradient bridges. Microchambers 1/1′, 2/2′, and 3/3′ were coated with seasonal H1N1-probes, flu A-probes, and pandemic H1N1-probes, respectively; the fourth microchamber set (4 and 4′) loaded with human β actin-probes was applied as a positive control while the chamber 5/5′ with no probes patterned worked as the negative control. (b) Determination of the assay result by naked eye, fluorescence and agarose gel electrophoresis. (*Source*: Reprinted with permission from Fang *et al*. (2011), copyright 2011 American Chemical Society.)

than ten copies/μL in 2 μL quantities of sample within 0.5 h. Identification of eight important swine viruses was also performed using the octopus-like mμLAMP system. Liu *et al*. designed a microfluidic LAMP cassette equipped with an integrated Flinders Technology Associates (FTA) membrane for on-chip HIV-1 detection (Liu *et al*., 2011). As the saliva sample flowed through the cassette, the nucleic acids were captured and concentrated by the FTA membrane, which were directly used as templates for real-time LAMP monitored by a fluorescent reader. The FTA-based LAMP device had a simple chip design with a detection limit of less than ten HIV particles. Ahmad *et al*. developed microfluidic-based real-time fluorescence LAMP assays using cyclic olefin polymer microchips and a monochromatic charge-coupled device (CCD) camera. This microfluidic LAMP assay was used to rapidly and sensitively detect waterborne pathogens within 20 min (Ahmad *et al*., 2011). These microfluidic nucleic acid amplification and detection systems hold great significance for rapid diagnosis of viral infections.

15.2.3 Microfluidic flow cytometry

Flow cytometry has been routinely used for rapidly counting and differentiating cells based on their biophysical properties, and plays significant roles in clinical estimation of viral infections such as HIV and hepatitis B virus (Stoop *et al*., 2005; Cheng *et al*., 2007). Over the last two decades, substantial improvements and refinements to this established technique have been made using microfluidic approaches. Microfluidic flow cytometry has competitive advantages including downscaling sizes, automated process, high-throughput, and accurate measurements, making the technology ideal for POC viral diagnostics such as influenza, baculovirus, and dengue virus (Ferris *et al*., 2002; Stoffel *et al*., 2005; Yang *et al*., 2008b).

There are several components for design and construction of the microfluidic flow cytometer: (1) a miniaturized fluidics system combined with hydrodynamic focusing, acoustophoresis, or dielectrophoresis to rapidly align biological samples inside the microfluidic channel; (2) an integrated optical, or/and electrical detection system to interrogate particles/cells based on their physicochemical characteristics when they flow through the detection zone of the microfluidic chip; and (3) an on-chip post-processing system to sort, differentiate, and recover samples. Ferris *et al*. constructed a microfluidic flow cytometer for rapid detection of single viruses (Ferris *et al*., 2002). They used an argon ion laser operating at 488-nm emission combined with a photomultiplier tube (PMT)-based optical system to produce a diffraction-limited spot size of ~ 0.5 μm and a probe volume of ~ 8 fL, and successfully detected and enumerated fluorescently stained viruses including adenovirus-5, respiratory syncytial virus, and influenza.

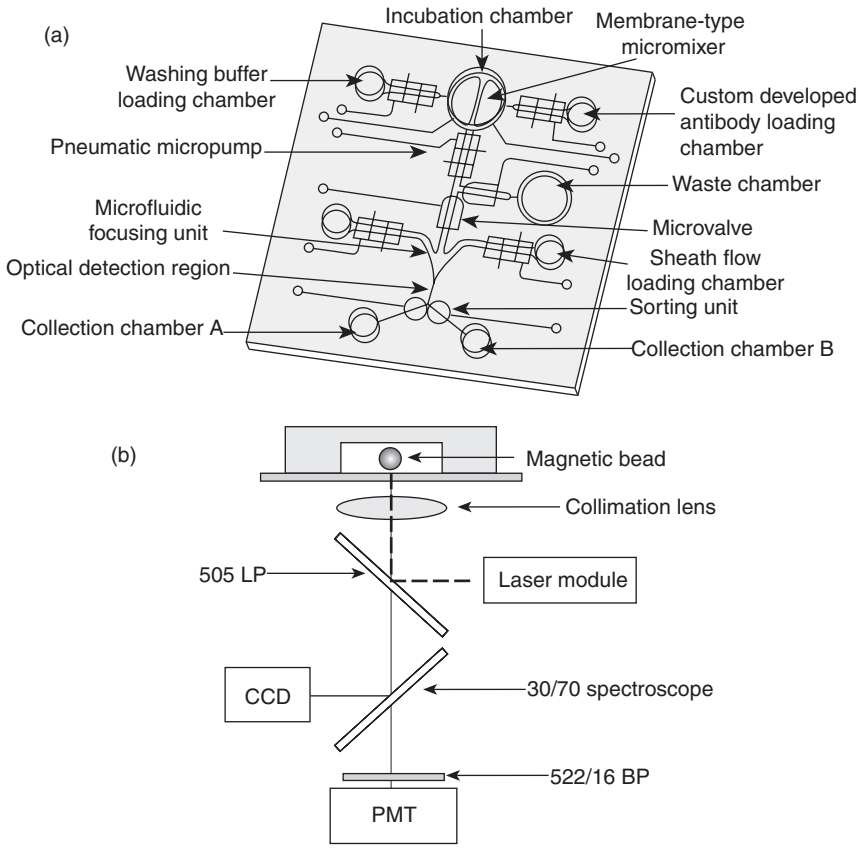

15.11 (a) Schematic of the magnetic-bead-based microfluidic flow cytometer for fast viral detection. This system integrated multiple modules into a single chip such as sample incubation, delivery, focusing, sorting and collecting. (b) Schematic of the optical detection system. (*Source*: Reprinted with permission from Yang *et al.* (2008b), copyright 2008 Elsevier.)

Stoffel *et al.* constructed a dual-channel microfluidic flow cytometer to detect unpurified baculovirus (BV) samples. They used a two-dye staining method, targeting both the protein capsid and genome of BV, and developed an algorithm to identify simultaneous events on the DNA and protein channels (Stoffel *et al.*, 2005).

Yang *et al.* reported a magnetic-bead-based microfluidic flow cytometer for fast viral detection (Yang *et al.*, 2008b). The antibody-conjugated magnetic beads were first used to capture target viruses, followed by using another dye-labeled anti-virus antibody to mark the bead-bound virus for the subsequent optical detection. This system integrated multiple modules into a single chip such as sample incubation, delivery, focusing, sorting, and collecting,

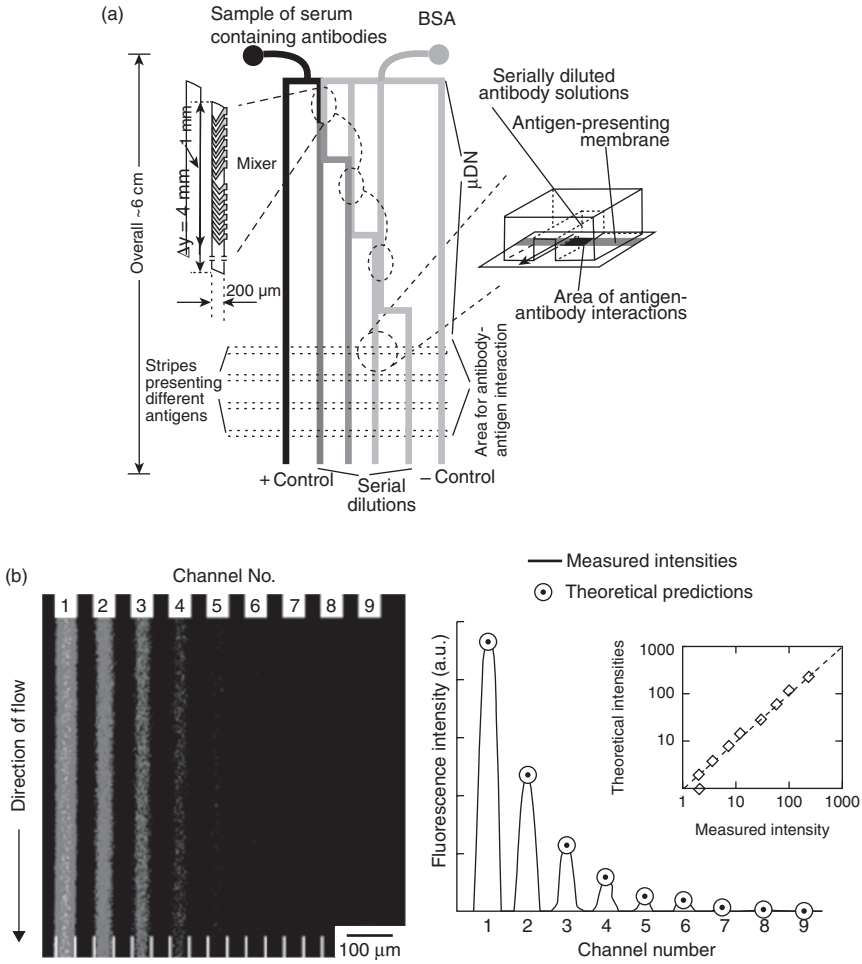

15.12 (a) Schematic of the microfluidic immunoassay device for detecting HIV infection. (b) A μDN that serially dilutes the serum sample through nine branched channels. (*Source*: Reprinted with permission from Jiang *et al*. (2003), copyright 2003 American Chemical Society.)

allowing automatic detection of the dengue virus with the detection limit of 10^3 PFU/mL (Fig. 15.11). Plaque forming units (PFU) are a measure of the quantity of viruses that are capable of lysing host cells and forming a plaque. Emaminejad *et al*. developed a microfluidic contactless impedance cytometer containing a disposable biochip. This chip can be inserted onto a printed circuit board (PCB) with reusable electrodes that can dramatically reduce the manufacturing costs of microfluidic cytometers. This microfluidic approach has potential for counting clusters of differentiation 4 (CD4) cells in blood samples from HIV patients in resource-poor settings (Emaminejad

et al., 2012). These stated microfluidic flow cytometers can overcome the size and cost constraints of conventional flow cytometry, providing a new way for rapid, automated, and cost-effective viral diagnosis.

15.3 Examples of applications

This section provides three examples of microfluidic technologies for viral detection. These tools may advance conventional diagnostic techniques in terms of high throughput, integration, and automation.

15.3.1 A microfluidic immunoassay device for HIV diagnosis

Immunoassay is an established and relatively simple technique for virus detection, particularly suited for flow-through microfluidics. The microfluidic immunoassay device developed by Jiang *et al*. consists of: (1) a microdilutor network (μDN) with herringbone patterns to dilute human serum serially and (2) an antigen-coated polycarbonate (PC) membrane located at the bottom of the device to interact with antibodies in human serum (Fig. 15.12) (Jiang *et al*., 2003). The μDN dilutes the serum sample by one half each time the sample flows through a branch. To induce local mixing inside each branch in which laminar flow is dominated at small Reynolds number, chaotic advective mixers are designed on the channel surface, each of which includes four cycles of herringbone patterns (Jiang *et al*., 2005; Sun *et al*., 2009). The performance of the μDN is first characterized using BSA conjugated to fluorescein (BSA-FITC) and phosphate buffer saline (PBS). The result shows that the μDN can generate an exponentially decreased concentration gradient, with a dynamic range of almost 10^3 (Fig. 15.12).

For diagnosis of HIV infection, an antigen-coated polycarbonate membrane is first made by sandwiching the membrane between two freshly oxidized polydimethylsiloxane (PDMS) layers. One layer has the embedded microfluidic channels for flowing through solutions of antigens, and the other layer is flat to seal the membrane. After incubating the antigen solutions inside the channels for 30 min, the sealed PDMS/membrane/PDMS slab is cut with a razor blade to release the antigen-coated membrane. This membrane is treated by washing and incubating in 5% BSA in PBS, followed by quick drying in vacuum. Finally, the antigen-coated membrane is placed between the μDN and a flat PDMS (Fig. 15.12).

In the experiments, the sample of serum containing anti-gp120 and anti-gp41 is introduced from the left inlet, and the buffer containing 5% BSA is injected from the right inlet. As the sample flows orthogonally across the

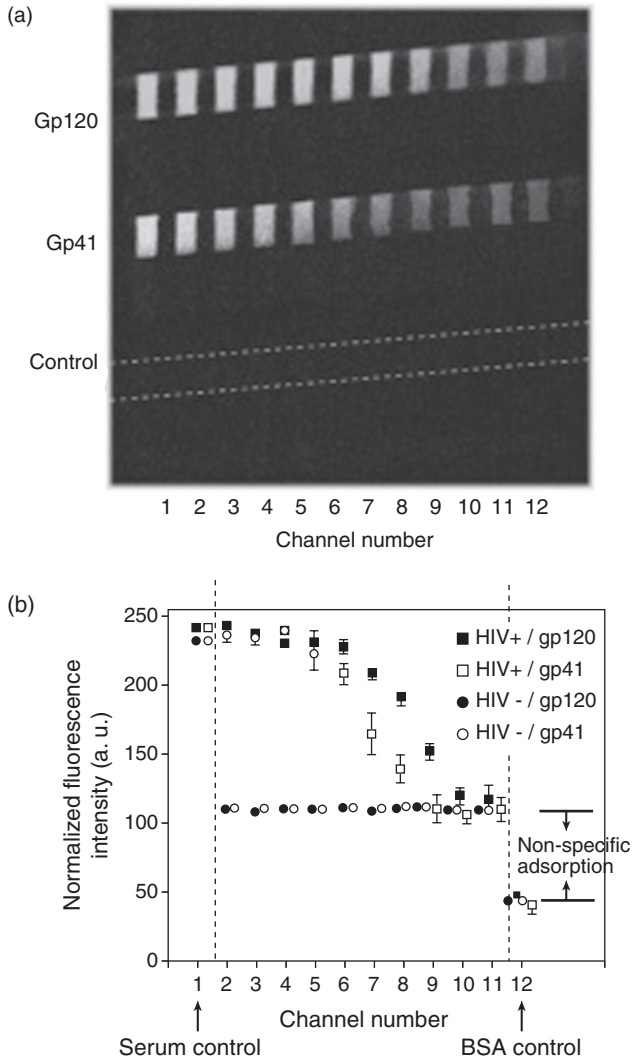

15.13 (a) Immunofluorescence image of anti-gp120 and anti-gp41 interaction with the membrane-bound antigens. (b) Plots of the normalized fluorescence intensity versus the channel number. (*Source*: Reprinted with permission from Jiang *et al.* (2003), copyright 2003 American Chemical Society.)

antigen-coated membrane, the antibodies in the serum bind to the immobilized antigens, observed as a fluorescent micromosaic pattern (Fig. 15.13). To generate a calibration curve for quantification of analytes, the solution of human immunoglobulin Gs (IgGs) with known concentrations is

flowed through the μDN, followed by plotting the fluorescent intensities of micromosaic versus the channel number. Based on this calibration curve, the absolute concentrations of anti-gp120 and anti-gp41 in serum can be determined. A unique advantage of this microfluidic immunoassay device is to build the positive and negative controls inside the channels to increase the test reliability. In all experiments, Channel 1 is the positive control that the sample of serum flows through a distinct channel without dilution, while Channel 12 is the negative control where there is no serum. A similar design is adopted for quantitative analysis of multiple HIV samples simultaneously inside a single chip (Song *et al*., 2012). These microfluidic immunoassay devices are promising in the direction of sensitive and effective POC viral diagnostics.

15.3.2 Microfluidic loop-mediated isothermal amplification (μLAMP) for parallel detection of pathogens

LAMP is an isothermal nucleic acid amplification technique that is used extensively for routine pathogen screening. Combination of LAMP and microfluidic technology will miniaturize the LAMP detection system and realize rapid and parallel viral diagnostics in a simple and cost-effective way. Fang *et al*. demonstrated that LAMP can be integrated in a multichannel microfluidic system (μLAMP) for parallel detection of the pseudorabies virus (PRV) with high sensitivity and specificity (Fang *et al*., 2010). The μLAMP allows the direct analysis of a sample of 0.4 μL of interested DNA in less than 1 h with the detection limit of 10 fg/μL. The readout of μLAMP could be either by the naked eye or via absorbance measured by an optic sensor.

The PDMS-glass hybrid chip for μLAMP system contains eight 5 μL microchannels connected with conically shaped inlets/outlets without the complicated valve/pump configuration (Fang *et al*., 2010) (Fig. 15.14a). A sample containing 0.4 μL of nucleic acid first fills the channel through the inlet, followed by slowly introducing a reaction mixture for LAMP of 4.6 μL by capillary force. The same procedures are repeated eight times to load all the channels with analytes and reagents. The inlets and outlets are tightly sealed by uncured PDMS to form the closed microchambers. The LAMP reaction and readout are simultaneously performed inside the chambers by incubating the μLAMP chip at 63°C for 1 h using a water bath. LAMP produces a large amount of magnesium pyrophosphate precipitate as the byproduct of reaction, which can be analyzed directly by the naked eye or turbidity measurement. These results are further confirmed by agarose gel electrophoresis.

In the experiments for detecting PRV by μLAMP, the sensitivity of the system is first evaluated by using a series of PRV DNA dilutions (10^{-2} to 10^{-8}) as templates (original concentration of DNA sample is 10 ng/μL). Both

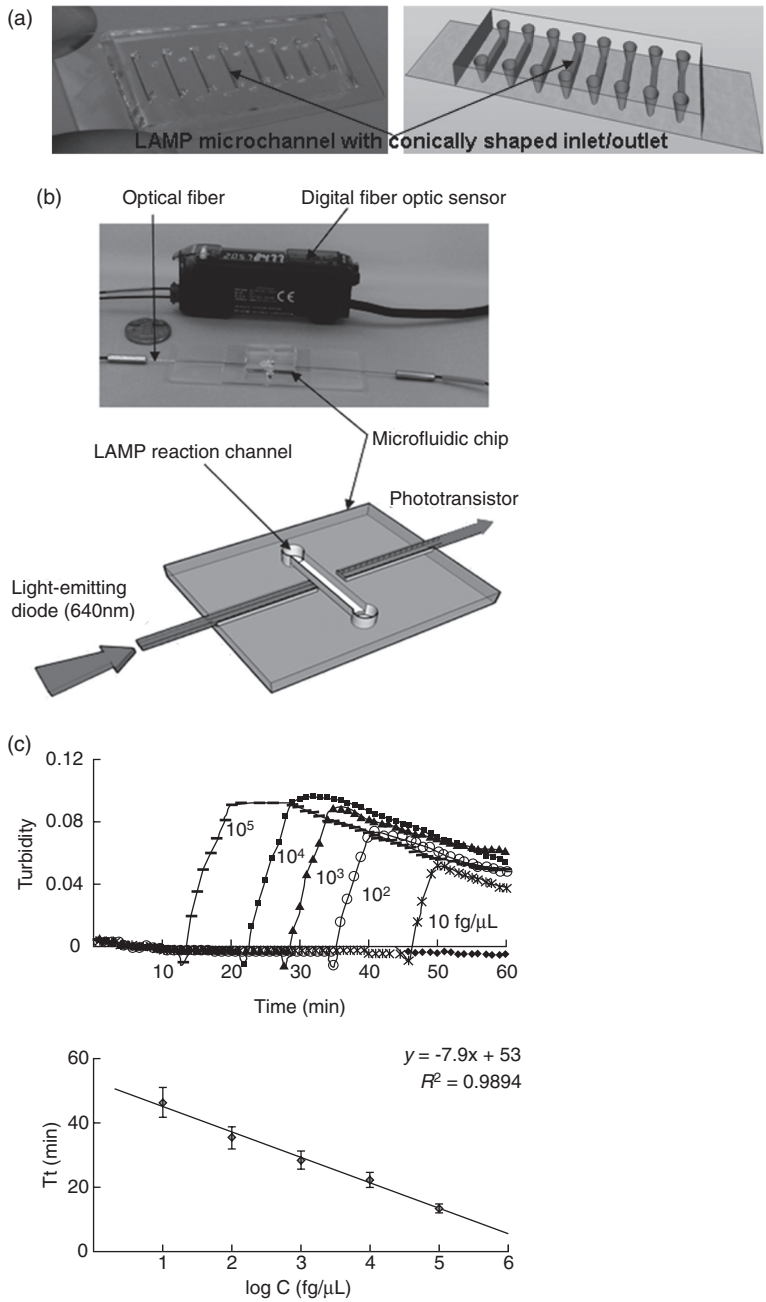

15.14 (a) Photograph and schematic of the eight-channel μLAMP chip for amplification and detection of PRV. (b) Photograph and schematic of the quantitative analysis unit. (c) Dynamic curves (upper) and standard curve (lower) of the real-time absorbance detection of μLAMP method. (*Source*: Reprinted with permission from Fang *et al*. (2010), copyright 2010 American Chemical Society.)

Table 15.1 Merits of μLAMP compared with other techniques

Methods	Sensitivity (fg/μL)	Specificity	Sample (μL)	Time (h)	Equipment
μLAMP	10	High	0.4	0.5–1	Water bath
PCR	10^3	High	2	1.5–2	Thermocycler
ELISA	~10^3	Low	2	2–3	ELISA reader
Neutralization	low	High	~50	72	Biosafety lab

Source: Reprinted with permission from Fang *et al.* (2010), copyright 2010 American Chemical Society.

the naked eye visual analysis and standard agarose gel electrophoresis show that the detection limit of the assay is 10 fg of DNA, 100-fold lower than the standard PCR for PRV detection. To validate the specificity of μLAMP for PRV, nontargeted viruses including foot-and-mouth disease virus (FMDV), transmissible gastroenteritis of swine virus (TGEV), and porcine parvovirus (PPV) are tested as control experiments. The result shows that μLAMP is highly specific and does not lead to cross-reaction from nontargeted viruses. These notable merits of the μLAMP are compared with other methods, including PCR, ELISA, and direct virus isolation assay, which are listed in Table 15.1.

Moreover, a single channel optical detection module is developed for the quantitative μLAMP via measuring the absorbance of the reaction mixture (Fig. 15.14b). A serial dilutions (10-fold) of DNA templates from 10^5 to 10 fg/μL are used to generate standard dynamic curves by the optical μLAMP chip. The log linear regression plot between template concentration and threshold time (Tt) indicates a correlation coefficient of 0.9894, making the fiber optical μLAMP chip useful for quantitative DNA analysis (Fig. 15.14c). The μLAMP system with a parallel, multiple, high-throughput, and integrated format has a huge potential to facilitate the realization of POC viral diagnostics.

15.3.3 Microfluidic flow cytometer for monitoring HIV infection

The important clinical parameters in managing HIV-infected subjects are the absolute number and percentage of CD4+ T lymphocytes (Hulgan *et al.*, 2007). The microfluidic flow cytometer developed by Wang *et al.* enables simultaneously counting the number and the percentage of CD4+ T lymphocytes based on resistive pulse sensing and fluorescence detection (Wang *et al.*, 2008). The microfluidic chip used for cell analysis consists of a three-terminal PDMS microfluidic circuit bonded to a glass substrate. The horizontal fluidic circuit is composed of two large

microchannels sandwiching a small sensing channel of 16 μm × 30 μm in cross-section and 150 μm in length. A vertical microchannel connects the sensing channel to the gate of a metal-oxide-semiconductor field-effect transistor (MOSFET), which amplifies the voltage pulses caused by the translocation of cells through the small sensing channel. Meanwhile, an optical fiber is arranged close to the sensing channel for detecting fluorescently labeled cells (Fig. 15.15).

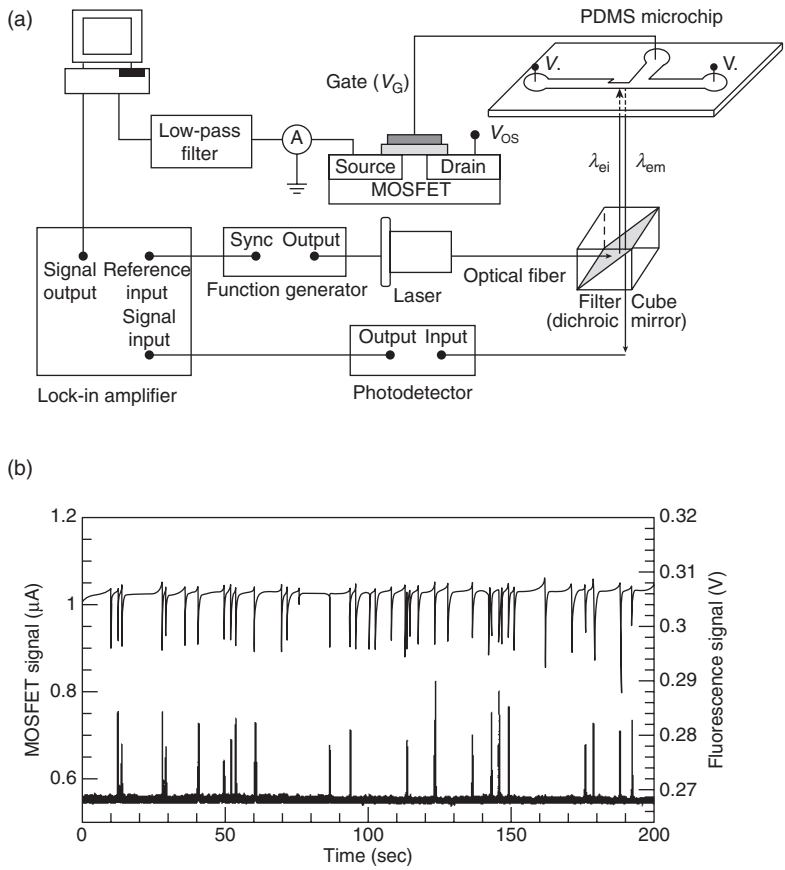

15.15 (a) Schematic of measurement setup of the microfluidic flow cytometer. This system consists of a microchip, a MOFET-based resistive pulse sensor, and a fluorescence detector. (b) Detection of a 50% stained cell suspension. The upper plot and left axis indicate the MOSFET signals indicating the total number of the cells passing through the sensing aperture; the lower plot and right axis indicate the fluorescent signals showing the translocation events of fluorescently labeled CD4+ T lymphocytes cells. (*Source*: Reprinted with permission from Wang *et al.* (2008), copyright 2008 The Royal Society of Chemistry.)

In the experiment, lymphocytes are obtained from healthy donors, in which CD4+ T cells are fluorescently labeled by immunostaining. The mixture of stained CD4+ T and other unstained lymphocytes is introduced into the microchannel by electroosmosis. When a cell passes through the sensing channel, it will displace a volume of electrolyte equivalent to its own volume, resulting in a transient resistance change. This resistance change is proportional to the cell size, which is amplified tens-fold by a MOSFET (Sun *et al.*, 2010). The so-called MOSFET-based resistive pulse sensing can count and size the cells passing through the aperture, whether the cells are fluorescently labeled or not. The characterization run shows that the diameter of lymphocytes ranges from 5.33 to 7.53 μm, consistent with the results from the commercial flow cytometer.

To determine the percentage of fluorescently labeled CD4+ T lymphocytes, an optical fluorescence system is integrated with the MOSFET-based resistive pulse sensing. When the stained cells pass through the sensing channel, the fluorescence signals are detected by the optical fiber, and converted to electrical signals. As a 50% stained cell suspension flows through the sensing channel, both MOSFET drain current and fluorescence signal are recorded (Fig. 15.15). MOSFET signals indicate the total number of the cells passing through the sensing aperture, whereas the fluorescence signals show the translocation events of fluorescently labeled cells. The measured percentage of the stained cells is 48.7%, indicating a comparable accuracy with the result of 46.1% from commercial flow cytometer. This microfluidic flow cytometer is small, cost effective, easy to operate, and comparably accurate and may eventually be used to monitor HIV progression in infected patients.

15.4 Conclusion and future trends

Low-cost, high-efficient, POC, and automated assays for viral diagnosis are the pressing need for global health improvement. Microfluidic technologies have shown great potential to advance conventional diagnostic techniques in terms of high throughput, integration, and automation. This chapter reviews microfluidic methods for viral detection including microfluidic immunoassay, microfluidic nucleic acid amplification, and microfluidic flow cytometry. Several samples of microfluidic devices used for selective and sensitive viral detection are presented.

Despite the promising success of microfluidics for the detection of viral infection, most devices are proof-of-concept prototypes. One challenge of commercializing microfluidic-based viral detection tools is batch fabrication of multifunctional microchips. The multi-layer chips containing on-chip pumps, valves, mixers or heaters for biological assays are usually assembled one by one by trained personnel. Another challenge is the design and construction of miniaturized and an automated fluid-control

system equipped with microfluidic devices. The control system, which can precisely manipulate micro- to nano-liter volumes of fluid, is necessary to ensure the stability and performance of microfluidic assays. Integration of an optical detection system for signal readout and measurement is also a challenge, because the detection area of a microchip is relatively small. Further efforts in developing microfluidic viral diagnostic tools also include user-friendly software for data acquisition and analysis, and remote data collection with the ultimate goal of publically available assays.

15.5 Acknowledgements

J. S. and X. J. acknowledge financial support from MOST (2011CB933201, 2009CB930001), NSFC (51105086, 21025520, 90813032), and CAS (KJCX2-YW-M15). J. S. and X. J. gratefully acknowledge Elsevier, American Chemical Society, The Royal Society of Chemistry, and Wiley-VCH for their permission to reprint materials from publications.

15.6 References

Ahmad, F., Seyrig, G., Tourlousse, D. M., Stedtfeld, R. D., Tiedje, J. M. and Hashsham, S. A. (2011). A CCD-based fluorescence imaging system for real-time loop-mediated isothermal amplification-based rapid and sensitive detection of waterborne pathogens on microchips. *Biomedical Microdevices,* **13**, 929–937.

Ansaldi, F., Bruzzone, B., Testino, G., Bassetti, M., Gasparini, R., Crovari, P. and Icardi, G. (2006). Combination hepatitis C virus antigen and antibody immunoassay as a new tool for early diagnosis of infection. *Journal of Viral Hepatitis,* **13**, 5–10.

Bange, A., Halsall, H. B. and Heineman, W. R. (2005). Microfluidic immunosensor systems. *Biosensors & Bioelectronics,* **20**, 2488–2503.

Beebe, D. J., Mensing, G. A. and Walker, G. M. (2002). Physics and applications of microfluidics in biology. *Annual Review of Biomedical Engineering,* **4**, 261–286.

Bernard, A., Michel, B. and Delamarche, E. (2001). Micromosaic immunoassays. *Analytical Chemistry,* **73**, 8–12.

Borkowsky, W., Krasinski, K., Paul, D., Moore, T., Bebenroth, D. and Chandwani, S. (1987). Human-immunodeficiency-virus infections in infants negative for anti-HIV by enzyme-linked immunoassay. *Lancet,* **1**, 1168–1171.

Branson, B. M. (2007). State of the art for diagnosis of HIV infection. *Clinical Infectious Diseases,* **45** Suppl 4, S221–S225.

Cheng, X. H., Irimia, D., Dixon, M., Sekine, K., Demirci, U., Zamir, L., Tompkins, R. G., Rodriguez, W. and Toner, M. (2007). A microfluidic device for practical label-free CD4+T cell counting of HIV-infected subjects. *Lab on a Chip,* **7**, 170–178.

Chin, C. D., Linder, V. and Sia, S. K. (2012). Commercialization of microfluidic point-of-care diagnostic devices. *Lab on a Chip,* **12**, 2118–2134.

Cho, Y. K., Kim, J., Lee, Y., Kim, Y. A., Namkoong, K., Lim, H., Oh, K. W., Kim, S., Han, J., Park, C., Pak, Y. E., Ki, C. S., Choi, J. R., Myeong, H. K. and Ko, C. (2006). Clinical evaluation of micro-scale chip-based PCR system for rapid detection of hepatitis B virus. *Biosensors & Bioelectronics,* **21**, 2161–2169.

Cordes, R. J. and Ryan, M. E. (1995). Pitfalls in HIV testing. Application and limitations of current tests. *Postgraduate Medicine,* **98**, 177–180, 185–186, 189.

Dimov, I. K., Garcia-Cordero, J. L., O'Grady, J., Poulsen, C. R., Viguier, C., Kent, L., Daly, P., Lincoln, B., Maher, M., O'Kennedy, R., Smith, T. J., Ricco, A. J. and Lee, L. P. (2008). Integrated microfluidic tmRNA purification and real-time NASBA device for molecular diagnostics. *Lab on a Chip,* **8**, 2071–2078.

Dong, H., Li, C. M., Zhang, Y. F., Cao, X. D. and Gan, Y. (2007). Screen-printed microfluidic device for electrochemical immunoassay. *Lab on a Chip,* **7**, 1752–1758.

Drakeley, C. and Reyburn, H. (2009). Out with the old, in with the new: the utility of rapid diagnostic tests for malaria diagnosis in Africa. *Transactions of the Royal Society of Tropical Medicine and Hygiene,* **103**, 333–337.

Emaminejad, S., Javanmard, M., Dutton, R. W. and Davis, R. W. (2012). Microfluidic diagnostic tool for the developing world: contactless impedance flow cytometry. *Lab on a Chip,* **12**, 4499–4507.

Fang, X. E., Chen, H., Yu, S. N., Jiang, X. Y. and Kong, J. L. (2011). Predicting viruses accurately by a multiplex microfluidic loop-mediated isothermal amplification chip. *Analytical Chemistry,* **83**, 690–695.

Fang, X. E., LIU, Y. Y., Kong, J. L. and Jiang, X. Y. (2010). Loop-mediated isothermal amplification integrated on microfluidic chips for point-of-care quantitative detection of pathogens. *Analytical Chemistry,* **82**, 3002–3006.

Fauci, A. S. and Morens, D. M. (2012). 200 NEJM Anniversary Article the perpetual challenge of infectious diseases. *New England Journal of Medicine,* **366**, 454–461.

Ferreira, M. S., Nishioka SDE, A., Silvestre, M. T., Borges, A. S., Nunes-Araujo, F. R. and Rocha, A. (1997). Reactivation of Chagas' disease in patients with AIDS: Report of three new cases and review of the literature. *Clinical Infectious Diseases,* **25**, 1397–1400.

Ferris, M. M., McCabe, M. O., Doan, L. G. and Rowlen, K. L. (2002). Rapid enumeration of respiratory viruses. *Analytical Chemistry,* **74**, 1849–1856.

Foudeh, A. M., Didar, T. F., Veres, T. and Tabrizian, M. (2012). Microfluidic designs and techniques using lab-on-a-chip devices for pathogen detection for point-of-care diagnostics. *Lab on a Chip,* **12**, 3249–3266.

Free, M. J. (2004). Achieving appropriate design and widespread use of health care technologies in the developing world. Overcoming obstacles that impede the adaptation and diffusion of priority technologies for primary health care. *International Journal of Gynecology & Obstetrics,* **85**, S3–S13.

Gascoyne, P., Satayavivad, J. and Ruchirawat, M. (2004). Microfluidic approaches to malaria detection. *Acta Tropica,* **89**, 357–369.

Gervais, L., de Rooij, N. and Delamarche, E. (2011). Microfluidic chips for point-of-care immunodiagnostics. *Advanced Materials,* **23**, H151–H176.

Govindarajan, A. V., Ramachandran, S., Vigil, G. D., Yager, P. and Bohringer, K. F. (2012). A low cost point-of-care viscous sample preparation device for molecular diagnosis in the developing world; an example of microfluidic origami. *Lab on a Chip,* **12**, 174–181.

Gulliksen, A., Solli, L., Karlsen, F., Rogne, H., Hovig, E., Nordstrom, T. and Sirevag, R. (2004). Real-time nucleic acid sequence-based amplification in nanoliter volumes. *Analytical Chemistry,* **76**, 9–14.

Hauck, T. S., Giri, S., Gao, Y. L. and Chan, W. C. W. (2010). Nanotechnology diagnostics for infectious diseases prevalent in developing countries. *Advanced Drug Delivery Reviews,* **62**, 438–448.

He, M. and Herr, A. E. (2009). Microfluidic polyacrylamide gel electrophoresis with in situ immunoblotting for native protein analysis. *Analytical Chemistry,* **81**, 8177–8184.

Hughes, A. J. and Herr, A. E. (2012). Microfluidic Western blotting. *Proceedings of the National Academy of Sciences of the United States of America*, **109**, 21450–21455.

Hulgan, T., Shepherd, B. E., Raffanti, S. P., Fusco, J. S., Beckerman, R., Barkanic, G. and Sterling, T. R. (2007). Absolute count and percentage of CD4(+) lymphocytes are independent predictors of disease progression in HIV-infected persons initiating highly active antiretroviral therapy. *Journal of Infectious Diseases,* **195**, 425–431.

Iwamoto, T., Sonobe, T. and Hayashi, K. (2003). Loop-mediated isothermal amplification for direct detection of *Mycobacterium tuberculosis* complex, *M. avium*, and *M. intracellulare* in sputum samples. *Journal of Clinical Microbiology,* **41**, 2616–2622.

Jiang, X. Y., Ng, J. M. K., Stroock, A. D., Dertinger, S. K. W. and Whitesides, G. M. (2003). A miniaturized, parallel, serially diluted immunoassay for analyzing multiple antigens. *Journal of the American Chemical Society,* **125**, 5294–5295.

Jiang, X. Y., Xu, Q. B., Dertinger, S. K. W., Stroock, A. D., Fu, T. M. and Whitesides, G. M. (2005). A general method for patterning gradients of biomolecules on surfaces using microfluidic networks. *Analytical Chemistry,* **77**, 2338–2347.

Kelly, R. T. and Woolley, A. T. (2005). Microfluidic systems for integrated, high-throughput DNA analysis. *Analytical Chemistry,* **77**, 96a–102a.

Kievits, T., van Gemen, B., van Strijp, D., Schukkink, R., Dircks, M., Adriaanse, H., Malek, L., Sooknanan, R. and Lens, P. (1991). NASBA isothermal enzymatic in vitro nucleic acid amplification optimized for the diagnosis of HIV-1 infection. *Journal of Virological Methods,* **35**, 273–286.

Kim, D., Karns, K., Tia, S. Q., He, M. and Herr, A. E. (2012). Electrostatic protein immobilization using charged polyacrylamide gels and cationic detergent microfluidic Western blotting. *Analytical Chemistry,* **84**, 2533–2540.

Leke, R. G. F. (2010). Global health governance-the response to infectious diseases. *Lancet,* **376**, 1200–1201.

Liu, C. C., Geva, E., Mauk, M., Qiu, X. B., Abrams, W. R., Malamud, D., Curtis, K., Owen, S. M. and Bau, H. H. (2011). An isothermal amplification reactor with an integrated isolation membrane for point-of-care detection of infectious diseases. *Analyst,* **136**, 2069–2076.

Liu, Y. X., Cady, N. C. and Batt, C. A. (2007). A plastic microchip for nucleic acid purification. *Biomedical Microdevices,* **9**, 769–776.

Liu, Y. Y., Sun, Y., Sun, K., Song, L. S. and Jiang, X. Y. (2010). Recent developments employing new materials for readout in lab-on-a-chip. *Journal of Materials Chemistry,* **20**, 7305–7311.

Mackay, I. M. (2004). Real-time PCR in the microbiology laboratory. *Clinical Microbiology and Infection,* **10**, 190–212.

Malkin, R. A. (2007). Design of health care technologies for the developing world. *Annual Review of Biomedical Engineering,* **9**, 567–587.

McCalla, S. E. and Tripathi, A. (2011). Microfluidic Reactors for Diagnostics Applications. *Annual Review of Biomedical Engineering*, **13**, 321–343.

McMorrow, M. L., Masanja, M. I., Abdulla, S. M. K., Kahigwa, E. and Kachur, S. P. (2008). Challenges in routine implementation and quality control of rapid diagnostic tests for malaria-Rufiji district, Tanzania. *American Journal of Tropical Medicine and Hygiene,* **79**, 385–390.

Melin, J. and Quake, S. R. (2007). Microfluidic large-scale integration: The evolution of design rules for biological automation. *Annual Review of Biophysics and Biomolecular Structure,* **36**, 213–231.

Misiani, R., Bellavita, P., Fenili, D., Borelli, G., Marchesi, D., Massazza, M., Vendramin, G., Comotti, B., Tanzi, E., Scudeller, G. and Zanetti A. (1992). Hepatitis C virus infection in patients with essential mixed cryoglobulinemia. *Annals of Internal Medicine,* **117**, 573–577.

Notomi, T., Okayama, H., Masubuchi, H., Yonekawa, T., Watanabe, K., Amino, N. and Hase, T. (2000). Loop-mediated isothermal amplification of DNA. *Nucleic Acids Research,* **28**, E63.

Pan, W. Y., Chen, W. and Jiang, X. Y. (2010). Microfluidic Western blot. *Analytical Chemistry,* **82**, 3974–3976.

Pang, T. and Peeling, R. W. (2007). Diagnostic tests for infectious diseases in the developing world: two sides of the coin. *Transactions of the Royal Society of Tropical Medicine and Hygiene,* **101**, 856–857.

Park, S., Zhang, Y., Lin, S., Wang, T. H. and Yang, S. (2011). Advances in microfluidic PCR for point-of-care infectious disease diagnostics. *Biotechnology Advances,* **29**, 830–839.

Peeters, M., Gershy-Damet, G. M., Fransen, K., Koffi, K., Coulibaly, M., Delaporte, E., Piot, P. and van der Groen, G. (1992). Virological and polymerase chain reaction studies of HIV-1/HIV-2 dual infection in Cote d'Ivoire. *Lancet,* **340**, 339–340.

Poon, L. L., Wong, B. W., Ma, E. H., Chan, K. H., Chow, L. M., Abeyewickreme, W., Tangpukdee, N., Yuen, K. Y., Guan, Y., Looareesuwan, S. and Peiris, J. S. (2006). Sensitive and inexpensive molecular test for falciparum malaria: detecting *Plasmodium falciparum* DNA directly from heat-treated blood by loop-mediated isothermal amplification. *Clinical Chemistry,* **52**, 303–306.

Qu, W., Liu, Y., Liu, D., Wang, Z. and Jiang, X. (2011). Copper-mediated amplification allows readout of immunoassays by the naked eye. *Angewandte Chemie International Edition England,* **50**, 3442–3445.

Rossier, J. S. and Girault, H. H. (2001). Enzyme linked immunosorbent assay on a microchip with electrochemical detection. *Lab on a Chip,* **1**, 153–157.

Roth, W. K., Weber, M. and Seifried, E. (1999). Feasibility and efficacy of routine PCR screening of blood donations for hepatitis C virus, hepatitis B virus, and HIV-1 in a blood-bank setting. *Lancet,* **353**, 359–363.

Ryan, K. J., Ray, C. G. and Sherris, J. C. (2004). *Sherris Medical Microbiology: An Introduction to Infectious Diseases,* New York, McGraw-Hill.

Schupbach, J. (2002). Measurement of HIV-1 p24 antigen by signal-amplification-boosted ELISA of heat-denatured plasma is a simple and inexpensive alternative to tests for viral RNA. *AIDS Review,* **4**, 83–92.

Sia, S. K. and Whitesides, G. M. (2003). Microfluidic devices fabricated in poly(dimethylsiloxane) for biological studies. *Electrophoresis,* **24**, 3563–3576.

Singer, P. A., Taylor, A. D., Daar, A. S., Upshur, R. E. G., Singh, J. A. and Lavery, J. V. (2007). Grand challenges in global health: The ethical, social and cultural program. *Plos Medicine,* **4**, 1440–1444.

Song, L. S., Zhang, Y., Wang, W. J., Ma, L. Y., Liu, Y., Hao, Y. L., Shao, Y. M., Zhang, W. and Jiang, X. Y. (2012). Microfluidic assay without blocking for rapid HIV screening and confirmation. *Biomedical Microdevices,* **14**, 631–640.

Stoffel, C. L., Kathy, R. F. and Rowlen, K. L. (2005). Design and characterization of a compact dual channel virus counter. *Cytometry Part A,* **65A**, 140–147.

Stoop, J. N., van der Molen, R. G., Baan, C. C., van der Laan, L. J. W., Kuipers, E. J., Kusters, J. G. and Janssen, H. L. A. (2005). Regulatory T cells contribute to the impaired immune response in patients with chronic hepatitis B virus infection. *Hepatology,* **41**, 771–778.

Strauss, J. H. and Strauss, E. G. (2008). *Viruses and Human Disease,* Amsterdam; Boston, Elsevier/Academic Press.

Sturenburg, E. and Junker, R. (2009). Point-of-care testing in microbiology: the advantages and disadvantages of immunochromatographic test strips. *Deutsches Aerzteblatt International,* **106**, 48–54.

Sun, J., Gao, Y., Isaacs, R. J., Boelte, K. C., Lin, C. P., Boczko, E. M. and Li, D. (2012a). Simultaneous on-chip dc dielectrophoretic cell separation and quantitative separation performance characterization. *Analytical Chemistry,* **84**, 2017–2024.

Sun, J., Li, M., Liu, C., Zhang, Y., Liu, D., Liu, W., Hu, G. and Jiang, X. (2012b). Double spiral microchannel for label-free tumor cell separation and enrichment. *Lab on a Chip,* **12**, 3952–3960.

Sun, J., Stowers, C. C., Boczko, E. M. and Li, D. (2010). Measurement of the volume growth rate of single budding yeast with the MOSFET-based microfluidic Coulter counter. *Lab on a Chip,* **10**, 2986–2993.

Sun, Y., Liu, Y. Y., Qu, W. S. and Jiang, X. Y. (2009). Combining nanosurface chemistry and microfluidics for molecular analysis and cell biology. *Analytica Chimica Acta,* **650**, 98–105.

Urdea, M., Penny, L. A., Olmsted, S. S., Giovanni, M. Y., Kaspar, P., Shepherd, A., Wilson, P., Dahl, C. A., Buchsbaum, S., Moeller, G. and Hay Burgess, D. C. (2006). Requirements for high impact diagnostics in the developing world. *Nature,* **444** Suppl 1, 73–79.

Wang, C. H. and Lee, G. B. (2005). Automatic bio-sampling chips integrated with micro-pumps and micro-valves for disease detection. *Biosensors and Bioelectronics,* **21**, 419–425.

Wang, D., Coscoy, L., Zylberberg, M., Avila, P. C., Boushey, H. A., Ganem, D. and Derisi, J. L. (2002). Microarray-based detection and genotyping of viral pathogens. *Proceedings of the National Academy of Sciences of the United States of America,* **99**, 15687–15692.

Wang, Y. N., Kang, Y. J., Xu, D. Y., Chon, C. H., Barnett, L., Kalams, S. A., Li, D. Y. and Li, D. Q. (2008). On-chip counting the number and the percentage of CD4+T lymphocytes. *Lab on a Chip,* **8**, 309–315.

WHO (2011). The top 10 causes of death. http://who.int/mediacentre/factsheets/fs310/en/.

Wu, A. H. (2006). A selected history and future of immunoassay development and applications in clinical chemistry. *Clinica Chimica Acta,* **369**, 119–124.

Yager, P., Domingo, G. J. and Gerdes, J. (2008). Point-of-care diagnostics for global health. *Annual Review of Biomedical Engineering,* **10**, 107–144.

Yager, P., Edwards, T., Fu, E., Helton, K., Nelson, K., Tam, M. R. and Weigl, B. H. (2006). Microfluidic diagnostic technologies for global public health. *Nature,* **442**, 412–418.

Yakovleva, J., Davidsson, R., Lobanova, A., Bengtsson, M., Eremin, S., Laurell, T. and Emneus, J. (2002). Microfluidic enzyme immunoassay using silicon microchip with immobilized antibodies and chemiluminescence detection. *Analytical Chemistry,* **74**, 2994–3004.

Yang, D. Y., Niu, X., Liu, Y. Y., Wang, Y., Gu, X., Song, L. S., Zhao, R., Ma, L. Y., Shao, Y. M. and Jiang, X. Y. (2008a). Electrospun nanofibrous membranes: A novel solid substrate for microfluidic immunoassays for HIV. *Advanced Materials,* **20**, 4770.

Yang, S. and Rothman, R. E. (2004). PCR-based diagnostics for infectious diseases: Uses, limitations, and future applications in acute-care settings. *Lancet Infectious Diseases,* **4**, 337–348.

Yang, S. Y., Lien, K. Y., Huang, K. J., Lei, H. Y. and Lee, G. B. (2008b). Micro flow cytometry utilizing a magnetic bead-based immunoassay for rapid virus detection. *Biosensors & Bioelectronics,* **24**, 855–862.

Zeng, Y., Novak, R., Shuga, J., Smith, M. T. and Mathies, R. A. (2010). High-performance single cell genetic analysis using microfluidic emulsion generator arrays. *Analytical Chemistry,* **82**, 3183–3190.

Zhang, Y., Tang, Y. F., Hsieh, Y. H., Hsu, C. Y., Xi, J. Z., Lin, K. J. and Jiang, X. Y. (2012). Towards a high-throughput label-free detection system combining localized-surface plasmon resonance and microfluidics. *Lab on a Chip,* **12**, 3012–3015.

16

Microfluidics for monitoring and imaging pancreatic islet and β-cells for human transplant

Y. WANG and J. E. MENDOZA-ELIAS, University of Illinois at Chicago, USA and J. F. LO, University of Michigan at Dearborn, USA and T. A. HARVAT, F. FENG, Z. LI, Q. WANG, M.NOURMOHAMMADZADEH, D. GUTIERREZ, M. QI, D. T. EDDINGTON and J. OBERHOLZER, University of Illinois at Chicago, USA

DOI: 10.1533/9780857097040.4.557

Abstract: This chapter discusses various microfluidic technologies that have been developed to study islets and β-cells. The chapter first introduces key issues in the field of pancreatic islet transplantation as a clinical therapy for Type I diabetes. It then reviews microfluidic technologies that have been developed for the study of pancreatic islet and β-cell physiology and disease pathophysiology. The chapter then describes the design, fabrication, and application of UIC's microfluidic-based multimodal islet perifusion and live-cell imaging system. Protocols are available at the end of the chapter.

Key words: microfluidics, pancreatic islet of langerhans, islet perifusion, islet physiology, human islet transplantation.

16.1 Introduction

Since the introduction of the Edmonton Protocol in 2000, islet transplantation has been emerging as promising therapy for Type I diabetes mellitus (T1DM) and currently is the only therapy that can achieve glycemic control without the need for exogenous insulin (Alejandro *et al*., 2008; Gangemi *et al*., 2008; Ryan *et al*., 2005; Shapiro *et al*., 2000). Transplanting islet cells has several advantages over transplanting a whole pancreas, in that it involves only a minor surgical procedure with low morbidity and mortality, and a significantly lower cost. Although insulin replacement therapy via injection or pump has been proven as an effective therapy for controlling blood glucose levels and minimizing hypoglycemic episodes, the risk of hypoglycemia

Y. Wang and J.E. Mendoza-Elias contributed equally.

remains, as well as diabetes-related complications such as metabolic syndrome, cardiovascular renal disease, and retinopathy. The potential advantage of islet transplantation over insulin therapy is that the transplanted islets can maintain normal blood glucose levels under a wide range of physiological conditions without producing excess insulin that might result in hypoglycemic episodes.

To date, islet transplantation has shown variable success in demonstrating both short- and long-term insulin independence (Alejandro *et al*., 2008; Bellin *et al*., 2008; Gangemi *et al*., 2008; Ryan *et al*., 2005), and much of this variability is associated with factors relating to both organ donor and recipient. As a cell therapy, islet transplantation is a multistep process involving pancreas organ procurement and preservation, tissue digestion and dissociation, islet purification, cell culture, islet transplantation via the hepatic portal vein, and graft maintenance by non-steroidal immunosuppressant regimens. Successful islet transplantation is dictated by the cumulative success of each aforementioned step.

16.1.1 Obstacles toward Food Drug Administration (FDA) approval of the islet product for clinical use

The U.S. Food and Drug Administration (FDA) defines the islet product as a biological drug; therefore, isolated human islets for transplant need to be prepared under FDA-approved guidance before islet transplant can be approved as a clinical therapy. Despite application and standardization of current good manufacturing practices (cGMP) in the islet isolation process, lot-to-lot variability still cannot be avoided. To reduce the risk of transplanting low-quality islets, appropriate product release tests are needed. While tests for identity, sterility, and purity are well established, so far no reliable assessment of islet potency is available prior to transplant. This continues to be one of the key hurdles associated with variable clinical outcomes.

16.1.2 Standard assays currently used to determine islet potency

The existing standard assays for islet function and viability include static glucose-stimulated insulin secretion (GSIS) for potency, and inclusive and exclusive dyes to stain membrane integrity for viability. Both of these assays have no predictive values and do not correlate well with clinical transplant outcomes (Armann *et al*., 2007; Papas *et al*., 2007, 2009; Street *et al*., 2004; Sweet *et al*., 2008). Therefore, clinicians are more dependent on morphology and islet cell mass, IEq (Islet Equivalent, a volumetric quantification of islet mass), to determine the suitability of a given islet preparation. The static GSIS only measures

'bulk' insulin release from an islet product under extreme conditions (exposure to 16.7 mM glucose for 60 min) and fails to observe and quantify the dynamic nature of β-cell insulin secretory kinetics. In addition, insulin secretion data alone does not provide any useful information on the key stimulus-coupling factors that control and regulate insulin secretion, and therefore may be a source of false positives and false negatives in islet function and viability tests. For example, mild stress during islet isolation process can lead to temporary insulin degranulation and leakage caused by cell membrane damage, even though the islets are still viable. Therefore, a low GSIS may not indicate irreversible loss of function, as temporarily impaired islet cells may recover once transplanted into a recipient. Likewise, a high GSIS result may be caused by insulin degranulation stemming from membrane damage.

In addition, islet size may also play a role in the variable GSIS outcomes. In contrast to *in vivo* perfusion-limited diffusion, the isolated islet's sensing of ambient glucose changes, as well as nutrient/waste exchange, is totally dependent on the passive diffusion (Dionne *et al*., 1993; Papas *et al*., 2007). In clinical practice, IEq is often used as a determining factor in deciding the suitability of a given islet preparation when human islet potency is less defined or difficult to quantify. In the transplant field, it is a general consensus that in order to reverse diabetes in T1DM islet recipients, at least 5000 IEqs per kilogram of recipient body weight are needed per transplant. Since smaller islets have a larger surface area to volume ratio, they are expected to have better GSIS (Lehmann *et al*., 2007; Nam *et al*., 2010). Paradoxically, larger islets contribute to a higher IEq, yet have been demonstrated to release less insulin in response to stimulus, which provides another likely explanation of why islet graft success does not correlate strongly with transplanted islet mass.

In contrast to both GSIS and IEq assessments, an *in vivo* potency assay conducted by transplanting human islets into the kidney capsule of immunodeficient nude mice correlates extremely well with clinical transplant outcomes and is currently the 'gold standard' for evaluating islet potency. However, this *in vivo* analysis takes several weeks to complete and, therefore, only provides a retrospective indication of islet function, which renders this assay impractical as a pre-transplant assessment in the time critical clinical setting (Bertuzzi *et al*., 2007; London *et al*., 1991; Ricordi *et al*., 1988, 2001).

16.1.3 Benefits and obstacles: emerging techniques for islet potency

To address this problem, a variety of *in vitro* tests have been investigated in order to assess islet potency and viability prior to islet release for transplant, including: the measurement of the oxygen consumption rate (OCR) (Papas *et al*., 2007; Sweet *et al*., 2006, 2008; Wang *et al*., 2005); the quantification of

reactive oxygen species (ROS) (Armann *et al*., 2007); and ADP/ATP ratios (Goto *et al*., 2006; Kim *et al*., 2009). Apart from providing less predictive data and being of a more retrospective usefulness, these assays have also multiple limitations. Most OCR and ROS assays are conducted in a static manner under a single static parameter. Additionally, OCR and ROS assays lack β-cell specificity, as an islet is composed of at least five different cell types, with β-cells contributing only 65–80% of a human islet cell mass. Even with a weighted analysis of OCR and ROS for each individual cell group, this information may be confounded and artifactual. Recently, new research evidences chemical and ion communication among β-cells, or between β-cells and α-cells, being important for regulation of insulin secretion (Spigelman *et al*., 2010). In addition, gap junctional complexes between adjacent islet cells are also needed to facilitate intra-islet cell–cell communications and in coordinating hormonal output (Carvalho *et al*., 2012). Therefore, the ADP/ATP assay is often challenged for its accuracy since islet dissociation is involved.

16.2 Insulin secretory pathway: how glucose sensing and metabolic coupling translates to insulin kinetics

As seen in Plate VIII (see in color section between pages 328 and 329), β-cell insulin secretion is governed by cellular electrical activity, metabolic events, and ion signaling, which display complex biphasic and pulsatile kinetic profiles (Luciani *et al*., 2006; Porksen *et al*., 2002). The first phase of the biphasic profile corresponds to a prompt, marked increase in the insulin secretory rate that is transient (4–8 min). In the absence of glucose, this profile decreases back to baseline. With continuous glucose stimulation, a secondary phase consisting of a gradual increase is observed (Henquin *et al*., 2006; Komjati *et al*., 1986). Glucose-induced insulin secretion is a dynamic process that is tightly regulated. In short, glucose enters β-cells via GLUT2 facilitated transport; subsequent glycolysis generates pyruvate, entering the tricarboxylic acid cycle (TCA cycle) in the mitochondria. Newly produced NADH then enters the electron transport chain (ETC) to undergo oxidative phosphorylation, generating an electrical potential gradient across the mitochondrial membrane. Mitochondrial hyperpolarization subsequently leads to ATP generation and closure of ATP-sensitive K+ (K_{ATP}) channels. This initiates plasma membrane depolarization and an increase in intracellular calcium concentration ($[Ca^{2}+]_{i}$), through a rapid influx of calcium ions via voltage-dependent calcium channels (VDCC). In this way, glucose induces an increase in $[Ca^{2}+]_{i}$, which triggers the fusion of insulin granules to the cell plasma membrane resulting in the exocytosis of insulin, C-peptide, and proinsulin (Babenko *et al*., 1998; Henquin *et al*., 1985; Roe *et al*., 1996; Warnotte *et al*., 1994). Alternate pathways of GSIS, independent of either

K_{ATP} channels or $[Ca^{2}+]_i$, have been described (Gembal *et al.*, 1992; Straub *et al.*, 2002), but play a smaller role in insulin secretion. Some evidence demonstrates that glucose-induced $[Ca^{2}+]_i$ is associated with calcium concentration inside the mitochondria (Kennedy *et al.*, 1996; Maechler *et al.*, 1998). The rise in intra-mitochondrial calcium, together with the aforementioned coupling messengers/factors, evokes insulin secretion independent from K_{ATP} channels, or amplifies the K_{ATP}–dependent pathway (Kennedy *et al.*, 1998; Maechler *et al.*, 1998). However, it has been confirmed that the K_{ATP} and $[Ca^{2}+]_i$-mediated pathway remains the primary mechanism of GSIS.

In addition to the mitochondria's well-established role in the insulin secretory pathway, mitochondrial energetics and calcium signaling are also essential for β-cell viability. Mitochondria actively mediate and regulate a variety of effector mechanisms involving cell life and death. Intracellular calcium acts as a secondary messenger in a variety of cells, and tightly regulates many cellular functions within sub-cellular microdomains. In addition, the level and pattern of $[Ca^{2}+]_i$ modulates cell viability and influences both apoptotic and necrotic pathways (Duchen *et al.*, 2000). In the search for a more reliable and β-cell-specific potency assay, several approaches to measuring mitochondrial integrity and calcium influx have been tested as an alternative assay, in the form of a single parameter or combined with other parameters for islet viability and potency.

For example, the static measurement of mitochondrial membrane potentials for islet viability using tetramethylrhodamine ethyl ester (TMRE) has been investigated in conjunction with either Newport Green (NP) (Ichii *et al.*, 2005) or FluoZin-3 (Jayaraman *et al.*, 2008), suggesting that β-cell mitochondrial integrity is critically important and has predictive value for transplant outcomes when compared against the gold standard immunodeficient nude mouse model; this has been confirmed by others (Iglesias *et al.*, 2008). While these results are promising, the aforementioned assessments of mitochondrial integrity measure a static value of β-cell energetic status with only retrospective values, since these assays may take days to conduct and cannot predict islet graft function at the time of transplant. In addition, as the enzymatic dissociation of the islets is involved, the assays' methodology is often questioned for introduction of artifacts, such as selective damage and loss of the β-cell population. Furthermore, most of these assays require more sophisticated laboratory setups, such as FACS, confocal microscope, and laser scanning cytometry.

Although individual assays that quantify either mitochondrial energetics or $[Ca^{2}+]_i$ have been used extensively to study β-cell stimulus-secretion coupling, they have never been combined with islet perifusion for human islet potency and viability studies. In this chapter, we will discuss a microfluidic-based islet perifusion apparatus with the integration of multichannel fluorescence imaging for changes in mitochondrial electrical potentials ($\Delta\Psi_M$) and $[Ca^{2}+]_i$ and off-chip insulin analysis for human islet function assessment.

16.3 Technologies: the emergence of microfluidics applied to islet and β-cell study

Under normal *in vivo* conditions, islets experience a dynamically changing microenvironment where insulin is secreted in a biphasic oscillatory pattern in response to blood glucose levels which is oscillatory. Therefore, an imperative emerges to have a perfusion setup that can better mimic the native microenvironment islets are exposed to through the precise control of physiologically relevant parameters. In order to better understand β-cell physiology and pathophysiology, in the past four decades a series of perifusion devices have been developed with the capability to regulate perifusate temperature, pH, and with the ability to switch between various streams of stimuli (Hoshi *et al*., 1973; Lacy *et al*., 1972, 1976; Weaver *et al*., 1978). However, these devices have several limitations including: difficult operation, limited flow control, inadequate mimicking of the *in vivo* microenvironment, and a lack of integration with conventional analysis techniques.

In recent years, microfluidic technology has emerged as a valuable tool for studying pancreatic islets mainly due to its higher efficiency and configurable versatility. Microfluidic devices allow for the minimal consumption of reagents and analytes, as well as the leveraging of microscale phenomena, such as laminar flow, capillary flow, electro-osmotically driven flow, electrokinetically driven flow, microdroplet formation, (Liu *et al*., 2008; Mosadegh *et al*., 2007; Taylor *et al*., 2006), and rapid diffusion (Oppegard *et al*., 2009). Microfluidics allows the development and application of new experimental modalities and techniques currently not possible with conventional macroscale tools. Additionally, multiple tasks and/or analytical tools can be integrated to improve experimental throughput (Craighead *et al*., 2006; El-Ali *et al*., 2006). In regard to microfluidic devices for islet and β-cell study, several advantages of the microscale are utilized such as: (i) islet immobilization; (ii) creation, maintenance, and optimization of culture microenvironments; (iii) continuous live-cell imaging of β-cell physiological function with the ability to resolve the rapid secretory and metabolic waveforms intrinsic to β-cells; and (iv) integration with single or multiple analytical tools.

16.3.1 Islet immobilization: design considerations and strategies

One of the greatest technical challenges in applying microfluidics to islets is the immobilization of islets, owing to their unique cellular composition and 3-D cytoarchitecture, which must be preserved. An islet is a cluster of 1000–2000 cells, which can range in size between 50 and 500 μm in diameter; and although only composing 1–2% of pancreas mass, islets receive 2–10% of pancreatic blood perfusion (Svensson *et al*., 1994). Islets are composed of at

least five different cell types: α-cells, secreting glucagon; β-cells, producing insulin and amylin; δ-cells secreting somatostatin; PP cells secreting pancreatic polypeptide; and ε-cells secreting ghrelin. In diabetes research, we are primarily concerned with β-cells as they secrete insulin and compose 65–80% of human islet mass.

One approach to immobilizing islets uses a PDMS plug or wall in order to position an islet into a microchannel (Dishinger *et al*., 2009; Rocheleau *et al*., 2004, 2008). In this method, the advantage lies in being able to predictably place and locate islets; however, a potential disadvantage is introduction of mechanical stresses, which can cause islet damage and insulin leakage. As an alternative islet trapping method, others have designed an array of circular microwells (pockets) (Adewola *et al*., 2010; Mohammed *et al*., 2009). The bottom layer of the device achieves this immobilization with an array of circular wells (500 μm in diameter and 150 μm in depth), which allows the islets to fall, and then passively sit and react to medium, without undue mechanical stress and shear forces. More than one islet can be analyzed simultaneously, which increases analytical throughput. However, this device pools the secreted products together, which can be either an advantage or a disadvantage, depending on the intended application. Another approach is an open-channel device, in which islets are first cultured on a glass-bottom dish or coverslip, and then the microfluidic apparatus is placed over the islets.

16.3.2 Fluid control: creation, maintenance, and optimization of culture microenvironments

A stable and flexible fluid control system is necessary for β-cell applications in microfluidics. Flow driven by pressure, in either a continuous or stepwise manner is the standard method that has been proven adequate for many islet applications (Adewola *et al*., 2010; Chen *et al*., 2008; Dishinger *et al*., 2009). However, one potential obstacle is pressure oscillations at low flow rates, and when starting or stopping as observed in syringe pumps. In response to this problem, reciprocating and continuous flow micropumps have been pursued (Zhang *et al*., 2009). Electroosmotic flow also plays an important role in the manipulation of liquid flow in microfluidic applications since electroosmotic velocities can be independent of channel size, which is beneficial when applied to small microchannels. Additionally, droplets have also been used in β-cell study using syringe or vacuum (Chen *et al*., 2008; Zhang *et al*., 2009). As demonstrated by the Piston group using vacuum driven flow, they were able to generate a passive method for microfluidic droplet sampling method that was used to quantify β-cell zinc secretion (zinc and insulin are co-secreted) with significantly improved spatiotemporal resolution

(average droplet volume was 470 ± 9 pL under a flow rate of 0.100 μL/min) (Easley *et al*., 2009).

Another microfluidic device employing droplet-based fluid flow was the chemistrode developed by the Ismagilov group (Chen *et al*., 2008). In contrast to traditional path clamp electrode setups, which can be used to directly measure β-cell electrical activity, this method's strength lies in its ability to manipulate and record molecular signals with high spatial and temporal resolution requiring 50 ms for stimuli pulse and 1.5 s for secreted insulin sampling. This system has a maximum temporal resolution of 50 ns, with the ability to measure insulin secretion from a single islet at a frequency of 0.67 Hz. This high level of resolution is achieved by droplets that are continuously encapsulated and separated from an islet.

The generation of chemical gradients into microfluidic setups is needed to generate dynamically changing microenvironments that will help elucidate the mechanisms underlying β-cell secretory kinetics. In order to generate these gradients, the Roper group has integrated two diaphragm pumps with off-chip valves that generate chemical gradient in sine and triangle waveforms (Zhang *et al*., 2009). In another solution to this problem, our group currently employs an integrated on-chip inlet staggered herringbone chaotic mixer with computer controlled syringes to generate preprogrammed glucose stimulation profiles (Adewola *et al*., 2010; Lee *et al*., 2011; Mohammed *et al*., 2009).

16.3.3 Detection: live-cell imaging of islets and β-cells

Highly coordinated spatiotemporal changes in $[Ca^{2}+]_i$ regulate many β-cell cellular processes including GSIS and therefore require real-time detection of electrical, biochemical, and ion signaling activities. Therefore, $[Ca^{2}+]_i$ may be a direct indicator of insulin secretory kinetics. One of the most critical limiting factors for studying calcium signaling using microfluidics is spatiotemporal resolution. In terms of spatial resolution, the use of fluorescent calcium indicator dyes such as Fura-2 AM or Fluo-4 AM (family of EGTA analogs) have been well-characterized to have high selectivity and sensitivity in conventional and microfluidic imaging applications. In contrast, temporal resolution of calcium signaling remains a function of each microfluidic device's flow dynamics and can also be controlled by medium delivery methods, valves, and device geometry.

Another method that may be used as an assay for insulin secretion is the detection of zinc ions. In β-cells, zinc is complexed with insulin to form a 2-Zn-hexameric crystal. When insulin is secreted, along with c-peptide, zinc is also co-secreted into plasma. The Piston group has exploited this feature of β-cells and has developed a droplet-based device with a sampling

drop volume of approximately 0.47 nL (Easley *et al.*, 2009). Their single islet studies demonstrated a high temporal resolution that allowed the detection of two zinc oscillatory frequencies: fast (~20–40 s) and slow (~5–10 m). Concurrently, zinc oscillatory waveforms were shown to closely coincide with intra-islet calcium oscillations and secreted insulin patterns. Insulin quantification was determined off-chip using either enzyme-linked immunosorbent assay (ELISA) or radioimmunoassay (RIA). In a similar concept, the Kennedy group developed a 15-channel microfluidic device capable of perifusing individual islets and then mixing perifusate with FITC-insulin and anti-insulin-antibody to perform a competitive immunoassay (Dishinger *et al.*, 2009). Performed in real-time, this system is capable of detecting insulin secretion at a resolution of 10 s. The ability to rapidly quantify temporally-resolved insulin secretion at the single islet level will have significant applications in islet research.

In the pursuit of developing a reliable islet potency test to address a clinical need and overcome the limitations of current tests, we have been developing and characterizing a three-layer microfluidic network (Adewola *et al.*, 2010; Mohammed *et al.*, 2009) that combines the measurement of mitochondrial potential changes ($\Delta\Psi_{Mito}$), calcium influx ($[Ca^{2}+]_{i}$), and dynamic insulin kinetics into a single and real-time assay.

16.4 Design and fabrication of the University of Illinois at Chicago (UIC) microfluidic device

Microfluidic-based tissue culture techniques begin with the design, fabrication, and application of a specific device for the manipulation of fluids at the microscale level. Typically, *micro* means one of the following features: small volume (often in the scale of nl, pl, and fl), small size (sub-millimeter), low energy consumption, or the use of some physical phenomenon within the *micro* domain, such as surface area to volume ratio, laminar flow, or diffusion dominant transport. Several materials can be used for fabrication, including silicon, metal, glass, and polymers. Since all studies discussed in this chapter use microfluidic devices composed of either polydimethylsiloxane (PDMS) (sometimes combined with glass components), only the fabrication of these devices will be briefly described.

16.4.1 Polydimethylsiloxane (PDMS) devices

Due to the ease of prototyping, stiffness, and high aspect ratio, SU8 photoresist has become the standard method for PDMS micromolding in microfluidic fabrication (Weibel *et al.*, 2007). The basic steps of soft photolithography have been described previously. Currently, soft photolithography

manufacture is carried out in a clean room facility to prevent contamination with dust; however, given the application, they may be carried out in a conventional chemical hood. For this device, the PDMS fabrication workflow begins with the design of a photomask using transparency printing, SU-8 master-mold fabrication, followed by PDMS curing, and ends with PDMS-glass bonding.

Mask design

Masks are designed using CAD programs that can generate vector-based graphic files and convert them into raster formats such as encapsulated PostScript (EPS) files. Photomasks then are printed at a resolution higher than that of the minimum feature size. In designing a photomask, at least three alignment markers should be included to facilitate photomask alignment during SU-8 master-mold fabrication (Fig. 16.1).

SU-8 master-mold fabrication

Master-mold fabrication begins by sequential cleaning of a 3-inch silicon wafer with acetone, methanol, and isopropanol, followed by DI water. The wafer is then dried by spraying with a stream of compressed nitrogen gas and dehydration baked on a hotplate at 120°C. Further organic residues can be oxidized by subsequent treatment with oxygen plasma at 100 W for 30 s (Plasma Preen). The silicon wafer is spin-coated with SU-8 photoresist to achieve a thickness of 500 μm. Protocols vary depending on SU-8 thicknesses and are available from the SU-8 manufacturer (Microchem, www.microchem.com). Once coated, the wafers undergo pre-exposure baking at: 65°C for 5 min, 95°C for 2 h, and 65°C for 1 min.

Finally, the high-resolution photomask (Fig. 16.2a–16.2e) is placed in contact with the resist covered wafer and a flat glass plate placed on the top of the photomask. Weights are placed over the edges to ensure contact between the photomask and resist. The wafer is irradiated with 365 nm filtered UV light at an energy of 600 mJ cm^{-2} to initiate crosslinking. The irradiated wafer is further crosslinked on a hotplate at 95°C for 1 h and then allowed to cool to room temperature. The wafer is then placed in 200 mL of developer solution where unpolymerized SU-8 is dissolved. The completed master is then cleaned by isopropyl alcohol and water, dried with compressed N_2 gas and dehydration baked.

PDMS micromolding

After completing the master, PDMS is prepared for the molding, or soft-lithography. PDMS precursor (usually Sylgard 184) and a crosslinking agent is added to a weighting boat at a 10:1 ratio by mass and thoroughly mixed.

A vacuum chamber is then used to extract bubbles and the PDMS mixture is then poured over the SU8 master. After overnight curing at room temperature, or 2 h on an 85°C hotplate, the PDMS is completely cured, retaining the channel structures from the master. After cutting the bulk PDMS into separate devices, circular access ports are punched and the device is cleaned by a piece of scotch tape to remove any dust or debris from the surface. Then the device and a cleaned piece of glass are plasma treated to create hydroxyl radicals, which, when in contact, allow permanent chemical bonding between the PDMS and the glass.

16.4.2 Design features associated with this chip

The device described here is composed of three layers: the top layer, 500 μm in height, comprising inlet and outlet channels 2 mm wide (5 mm at fanned-ends); the middle layer composing a spacer layer; the bottom layer, 150 μm in height, containing microwells for islet immobilization. The microwells are 500 μm in diameter and 100 μm apart. Once the photomask drafts are complete they are printed onto a photomask at a resolution of 16 000 dpi.

Immobilization of multiple islets

Immobilizing large islet populations is one of the biggest challenges associated with developing a successful islet potency assay. We have designed an array of small circular wells (pockets), located at the bottom of a perifusion chamber that allow the islets to passively sit and react to medium mimicking perfusion-limited exchange. The prevention of bubbles and dead space formation is accomplished through a pre-treatment process explained in Section 16.6.5 (Protocol Step 37–39). Using a P200 micropipette, islets are introduced into the perifusion chamber via an islet loading port by dialing down pipette. Given islets are denser than the perifusing media ($\rho_{islet} > \rho_{Kreb's\ Ringer\ Buffer}$), islets fall into microwells by gravity. Islets are then maintained in position by gravity and selection of a flow rate that does not dislodge islets from microwells. In addition to avoiding unnecessary mechanical stress and shear force, this method is simple to use, and multiple islets can be analyzed simultaneously, which significantly increases analytical throughput.

Simple design geometry

The design of the device allows for efficient mixing and uniform distribution of rapidly alternating solutions, providing the capability of measuring moment-to-moment secretory and metabolic waveforms intrinsic to β-cells. The simplicity of the device is beneficial for future standardization and integration of the device in a routine clinical islet isolation protocol.

Easy flow control and manipulation

This microfluidic device is capable of generating and maintaining various chemical gradients with a high level of complexity and consistency. As shown in Plate IXa (see in color section between pages 328 and 329), a CFD-GEOM computer simulation demonstrates uniform flow distribution in the perifusion system with most of the flow reaching bottom of the device where islets are trapped in microwells without significant fluid shunting. Additionally, *in vitro* FITC microscope intensity measuring experiments verify fluid dynamics at three different regions in the perifusion chamber and at three different flow rates: 250, 500, and 1000 μL (Plate IXb).

Resolved spatiotemporal resolution

High spatiotemporal resolution is critical for real-time sensing and monitoring of whole islet endocrine function and metabolic parameters. The flow characteristics of this device allow for the accurate characterization of insulin secretion kinetics with high spatiotemporal resolution. In addition, high signal-to-noise ratios of released insulin and fluorescence have been demonstrated, even with a relatively large chamber volume.

Easy integration and multiplexing

We have demonstrated the successful integration of a fluorescence-based analytical approach (either single or multiple probes) in accordance with islet perifusion concepts. This has significantly increased its analytical power for characterizing islet potency and viability. Additionally, a multiple-perifusion system has been integrated to simultaneously monitor a larger islet population.

User-friendly operation

Fluorescent microscopy-based measurement of biological activities using fluorescence probes is a common laboratory practice. When designing the UIC-MS (UIC Microfluidic System), thought was given to establishing a balance between complexity and practicality. The microscale nature and easy flow control greatly enhances the applicability of UIC-MS for studying β-cell kinetics. The simple design geometry, on a microscale level, and portability allow the UIC-MS to be easily adopted by others without the need for extensive training.

True real-time analysis

Since the system does not require islet fixation or dissociation, islet perifusion and concurrent fluorescence imaging can be performed 3–5 h

post-isolation, allowing the UIC-MS to be considered as a real-time pre-transplant assay.

In order to develop a clinically useful islet functional assay, a path from identification and optimization of a testing protocol must inform prototype development. Proof-of-principle studies need to be performed to evaluate feasibility, followed by further evaluation and trials to obtain data for regulatory submission and approval. In the proof-of-principle test, the following criteria must be explored: (i) the device performance, including test sensitivity and specificity, as well as the positive and negative predictive values; (ii) the ease of use, including explicitly determining the number of process steps, extent of training, and supervision required; (iii) the conditions of use, such as physical and environmental requirements; (iv) the conditions of storage; and (v) the shelf life. These criteria for proof-of-principle will be discussed in later sections.

16.5 Protocol: materials

The following section outlines all the materials and equipment used in experiments with the UIC-MS. Section 16.5.1 covers microfluidic device fabrication. Section 16.5.2 covers islet isolation and culture. Section 16.5.3 covers simultaneous islet perifusion and flourescence imaging.

16.5.1 Microfluidic device fabrication

Reagents and tools

- Photomask (CAD/Art service)
- Polydimethyl siloxane (PDMS) (Dow Corning, cat. no. Sylgard 184)
- Photoresist SU-8–2150 (Microchem, cat no. Y111077)
- SU-8 photoresist developer (Microchem, Y020100)
- Silicon Wafer (Silicon Sense, 3” dummy wafers)
- Acetone (Sigma-Aldrich, cat. no. 650501)
- Methanol (Sigma-Aldrich, cat. no. 34860)
- Isopropanol (Sigma-Aldrich, cat. no. I9030)
- N_2 compressed gas (AirGas, UN1066)
- Mixing Spatula (Sigma-Aldrich, cat. no. Z283274)
- Tweezers (TDI Switzerland, 4WFG-SA)
- Weighing boats (Sigma-Aldrich, cat. no. W2876)
- 3M scotch tape (Office Deport, cat no. 489461)
- Razor blade/Scalpel (Office Depot, cat. no. 550476)
- Gauge no. 11 stainless Luer needles as hole-punch (Grainger, cat. no. 5FTW5)
- Gauge no. 0 Hole puncher (Cole-Parmer, cat. no. EW-06298–93)
- Circular 3” 2.0 kg weights (custom machined).

Equipment

- Digital Balance (Mettler Toledo Inc., PL602–5)
- Spinner (Laurell Technologies, WS-400B 6NPP/LITE)
- 3 Hot plates (PMC Dataplate, 730) (for curing PDMS, replaceable with oven)
- UV-Lamp (EXFO-Omnicure, S1000)
- Digital profiler (Starrett, F2730–0) (for confirming photoresist thickness)
- Vacuum desiccator for degassing PDMS (Cole-Parmer, cat. no. EW-06514–30)
- Plasma Torch (Electro-Technic Products, Inc. BD-20)
- HEPA filtered custom cleanroom or standard biosafety hood.

16.5.2 Islet isolation and culture

Reagents

- Collagenase P (Roche, cat. no. 1 249 000)
- RPMI 1640 (Mediatech, cat. no. 10–041-CV) (see REAGENT SETUP)
- Fetal bovine serum (FBS) (Clontech, cat. no. 631106)
- Streptomycin/Penicillin (Gibco, cat. no. 15140)
- 1.018 kg m^{-3} Ficoll (Mediatech, cat. no. 99–692-CIS)
- 1.096 kg m^{-3} Ficoll (Mediatech, cat. no. 99–691-CIS)
- 1.069 kg m^{-3} Ficoll (Mediatech, cat. no. 99–815-CIS)
- 1.037 kg m^{-3} Ficoll (Mediatech, cat. no. 99–690-CIS)
- 1× HBSS (Mediatech, cat. no. 99–597-CM)
- Isoflurane (Baxter, cat. no. 10019–773–40).

Equipment and materials

- C57/B6 mice (Jackson Laboratory)
- Biosafety hood (NUAIR, model NU-425–600)
- Water-bath with temperature control (Precision, 180 series)
- Centrifuge (Beckman, J6-MI, maximum RPM 6000)
- Incubator (Thermo Electron, Thermo Series II)
- Inverted microscope (Leica, S6F)
- 35 × 10 mm Petri dish (Becton-Dickson, cat.no. 35–1008)
- Surgical tools (Straight and curved forceps, 4 ½" iris scissors, 3 ½" hemostat clamp)
- 5 mL Syringe (Becton-Dickinson, REF. 309603)
- 30g ½" needle (Becton-Dickinson, Reorder. 305128)
- Isoflurane vaporizer (Viking Medical, model: ISOV-2).

Cell culture media

RPMI 1640 culture medium: supplemented with: 10% of FBS (vol/vol) and 100 unit mL^{-1} of penicillin and 100 μg mL^{-1} of streptomycin.

16.5.3 Simultaneous islet perifusion and fluorescence imaging

Reagents

- Krebs-Ringer bicarbonate buffer (KRB) (see REAGENT SETUP)
- Sodium chloride, NaCl (Sigma-Aldrich, cat.no. S3014)
- Sodium bicarbonate, $NaHCO_3$ (Sigma-Aldrich, cat.no. S5761)
- Potassium chloride, KCl (Sigma-Aldrich, cat.no. P5405)
- Monopotassium phosphate, KH_2PO_4 (Sigma-Aldrich, cat.no. P5655)
- Calcium chloride dihydrate, $CaCl_2 \bullet 2H_2O$ (Sigma-Aldrich, cat.no. C7902)
- Magnesium sulfate heptahydrate, $MgSO_4 \bullet 7H_2O$ (Sigma-Aldrich, cat. no. 63138)
- HEPES (Mediatech, cat. no. 25–066-CI)
- Insulin ELISA kit (Mercodia, cat. no.11–1113–10)
- D-Glucose (Sigma-Aldrich, cat. no. G7528)
- Fura-2 AM (Invitrogen, cat. no. F1221. 20 × 50 μg) (see REAGENT SETUP)
- Rhodamin 123 (Rh 123) (Sigma-Aldrich, cat. no. R8004) (see REAGENT SETUP)
- Dimethyl sulfoxide (DMSO) (Fisher, cat. no. D128)
- Bovine serum albumin (BSA) (Sigma-Aldrich, cat. no.A-7906)
- Ethanol (Decon laboratories, cat. no.8416)
- 0.22 μm Vacuum Filter (Millipore, cat. no. SCGPU5RE).

Cell culture media

KRB (mM): NaCl (129), $NaHCO_3$ (5.0), KCl (4.7), KH_2PO_4 (1.2), $CaCl_2 \bullet 2H_2O$ (1.0), $MgSO_4 \bullet H_2O$ (1.2), HEPES (10), pH 7.35–7.40.

▲**CRITICAL** Sterilize the working solution by filtration with a 0.22 μm vacuum filter. Adjust the buffer pH with KOH to prevent potential precipitation and store for no more than 1 week at 4°C.

KRB stock solutions should be stored for no more than one month at 4°C.

Preparation of Fura-2 AM stock solution: add 100 μL DMSO to each tube (50 μg) so that final concentration is 2 mM. Store at –20°C in the dark.

Preparation of Rh 123 stock solution: Dissolve Rh123 in 100% ethanol (vol/vol) at concentration of 1 mg mL^{-1}. Store at –20°C in the dark.

Equipment and materials

- Microfluidic device (see PROCEDURE)
- Syringe pumps (Harvard Apparatus, Model 22)
- Digital Hotplates (Dataplate, PMC 720 series)
- Thermometer (Omega Engineering, Inc, model HH-25TC)
- 60 mL Luer Lock syringes (Becton-Dickinson, cat.no.R07945–28)
- Fraction collector (Gibson, FC-203B)
- Epifluorescence microscopy setup (see Equipment setup)
- Leica DMI 4000B fluorescence microscope (see Equipment setup)
- Xenon light source
- Excitation and emission filter wheels (Chroma Technology)
- Lambda DG-4 wavelength switcher (Ludl Electronic Ltd)
- Fura-2/FITC Polychroic beamsplitter and double band emission filter (Chroma Technology. Part number: 73.100bs)
- High-speed and high-resolution charge coupled device (CCD, Retiga-SRV, Fast 1394, QImaging)
- Imaging acquisition and analysis (SimplePCI, Hamamatsu Corp)
- LabVIEW 8.0 (National Instruments)
- 30” Silicone tubings (Cole Palmer 1/16 × 1/8”)
- 1.5 mL Eppendorf tube (Fisher Scientific)
- Y-connectors (1/16” and 4 mm) (Cole Palmer, cat. no. WU-30703–90)
- Syringe connectors (female Luer plug 1/16”) (Cole Palmer, cat. no. ED-45502–00)
- Straight connectors (1/16”) (Cole Palmer, cat. no. ED-30622–23)
- Elbow connector (1/16”) (Cole Palmer, cat. no. ED-06365–17)
- In-line bubble trap (Alltech Association, cat. no. 01–0221).

Equipment and experimental setup (Fig. 16.3 – see page 579)

The setup consists of a Leica DMI 4000B fluorescence microscope equipped with 10× and 20× objectives and a 1.4-megapixel CCD camera (12-bit digital output and IEEE 1394 USB interface). Dual wavelength Fura-2 is excited at 340 and 380 nm, and the increases in $[Ca^{2}+]_{i}$ are expressed as a ratio of F340/F380 (%). Rh123 is a lipophilic cation that partitions selectively into the negatively charged mitochondrial membrane. Mitochondrial energization causes hyperpolarization of the mitochondrial membrane resulting in the uptake of Rh123 into the mitochondria and fluorescence quenching expressed as F/F0 (%). Rh123 is excited at 495 nm. Excitation wavelengths are controlled by means of corresponding excitation filters (Chroma Technology) mounted in a Lambda DG-4 wavelength switcher. Emission

of Fura-2 (510 nm ± 10) and Rh123 fluorescence (530 nm ± 10) is filtered using a Fura-2/FITC Polychroic beamsplitter and a double band emission filter (Chroma Technology. Part number: 73.100bs). SimplePCI software (Hamamatsu Corp.) is used for image acquisition.

16.6 Protocol: procedures

The following section provides three protocols used with the UIC-MS system. Steps 1-20 cover device fabrication. Steps 21-36 cover mouse islet isolation. Steps 37-45 cover microfluidic device preconditioning and islet loading. Steps 46-55 cover flourescence imaging.

16.6.1 Design of the photomask for the SU-8-negative master

1| Use CAD software to design photomask patterns (Fig. 16.1). Make sure the photomask is printed at a resolution of 16 000 dpi or higher. The microfluidic device used in this work involves a three-layer device with two layers requiring microfabrication, and one layer of spacer with reservoir wells. Include alignment markers to help with manual alignment of multilayered devices (typically within 100 μm). See Table 16.1 for information on the different layers of the device.

Fabrication of the SU-8-negative master: timing 4 h

The following describes the fabrication of an SU-8 master with a 500 μm height using SU-8–2150 as an example. For other thicknesses, the parameters such as spin speed and exposure time can be found from the MicroChem manufacturer's references. Fabrication should be done in a HEPA filtered environment; this could be a cleanroom or in a biosafety hood to minimize particle contaminants. All manufacturing steps are intended for room temperature (25°C) unless otherwise indicated by hotplate temperatures. See Fig. 16.2 for diagram of a typical PDMS workflow.

- 1| **Critical step** Ensure that all working surfaces/tables are level, as tilted hotplates can cause flow of the photoresist and alter the heights of the microchannels.
- 2| Substrate pre-treatment: Rinse a 3" (75 mm) Si wafer sequentially for 30 s with acetone, methanol, and isopropanol, followed by DI water. Dry with a stream of compressed N_2 gas. Perform dehydration bake of the cleaned wafer on the hotplate at 120°C for 10 min to improve adhesion of the photoresist to the wafer.

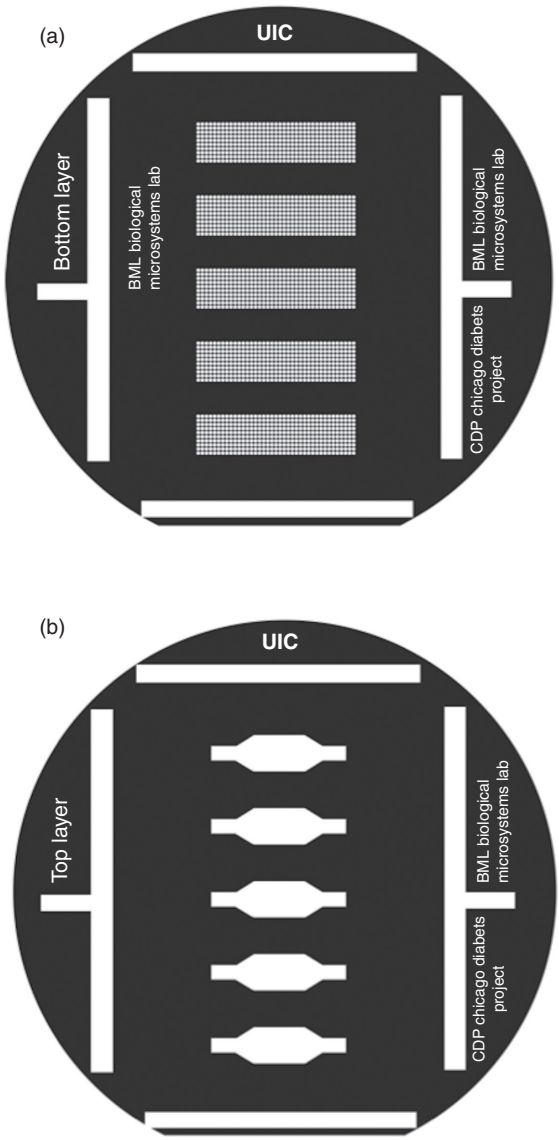

16.1 Photomask design for three-layer UIC-MS microfluidic device. (a) Bottom layer containing microwells with diameter of 500 μm gridded in 100 μm array. (b) Top layer containing inlet and outlet channels to perifusion chamber 2 mm wide (5 mm at fanned edges). Light areas correspond to SU-8 regions areas that are polymerized under UV-irradiation. Dark areas will be dissolved by SU-8 developer solution. Photomasks are printed at a resolution of 16 000 dpi.

Table 16.1 Device PDMS layers and description

Layers (top to bottom)	SU-8 Thickness	Features	PDMS Thickness	Punches
Microfluidic channel	500 μm	2 mm wide channels (5 mm at fanned-end)	5 mm	gauge 11/~2 mm
Chamber Layer	N/A	7 mm wide chamber	3 mm	gauge 0/~7 mm
Microwell Layer	150 μm	500 μm microwells	2 mm	N/A

- 3| Expose the wafer to oxygen plasma for 30 s at a power of 100 Watts (Terra Universal) to oxidize any remaining organic residue.
- 4| Spin coat: Warm-up spinner before use by testing spin program to ensure correct spin speeds. Spinner Program for SU-8–2150: 500 rpm. spread for 10 s and 1000 rpm. for 30 s to yield a thickness of 500 μm. Cover 25% of Si wafer surface with SU-8 photoresist and execute spin program.
- **Caution** If temperature in the clean room is ± 2°C of room temperature, then adjust spin speed by 150 rpm. ± 2°C inversely as resist viscosity decreases with increase in temperature.
- 5| Soft bake (pre-exposure bake): After spinning is complete, keeping the coated wafer level, transfer it to hot plates in the following sequence: (i) 65°C for 10 min; (ii) 95°C for 120 min; 65°C for 1 min.
- **Critical step** After these steps, turn off the hot plate and allow the coated wafer to cool down to room temperature.
- 6| Mask exposure: Take the high-resolution transparent mask (containing microfeatures and alignment markings) and overlay it on top of the SU-8 coated wafer. Expose the wafer to UV light (365 nm filtered Omnicure S1000) with an energy of 600 mJ cm^{-2}. If delamination occurs later in the development step increase UW irradiation dosage.
- **Caution** Make sure to use UV safety goggles when lamp shutter is open.
- 7| Post-exposure bake: After exposing the SU-8, transfer the wafer back to the hotplate for further baking in the following sequence: (i) 65°C for 5 min; (ii) 95°C for 30 min; (iii) 65°C for 1 min.
- **Critical step** After these steps, turn off the hot plate and allow the coated wafer to cool down to room temperature.
- 8| Develop master: Working under a hood, pour 200 mL of MicroChem SU-8 developer into a 500 mL flat beaker. Transfer the wafer into the developer and bathe for 30 min. Agitate the wafers throughout this duration to ensure adequate development of high aspect ratio features.
- **Caution** SU-8 developer is a toxic volatile chemical. Work under hood and well-ventilated area with appropriate protective gear.
- 9| Rinse wafer with isopropanol to confirm development completion.

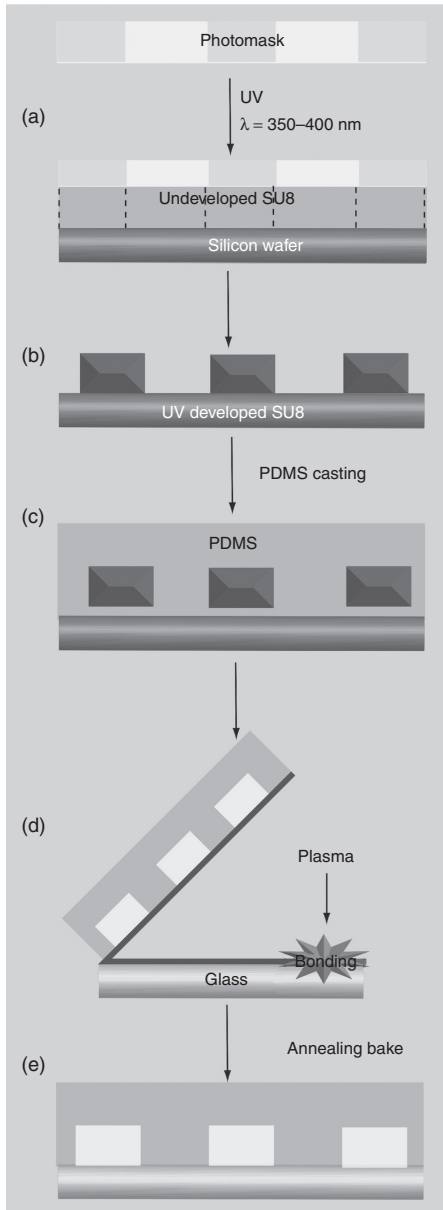

16.2 PDMS-based microfluidic device fabrication workflow. (a) Photomask microfeatures are transferred onto a silicon wafer spin-coated with SU-8 photoresist. (b) Developer solution washes away unexposed (unpolymerized) regions of SU-8 and forms a SU8 master-mold with the desired microfeatures. (c) Premixed, degassed PDMS is then pour over the master and cured on the hotplate. (d) Two layers are exposed to oxygen plasma, sealed and chemically bonded. (e) Device is annealed baked to strengthen chemical bonding. (*Source*: Reprinted with permission from Future Science Ltd.)

- **Critical step** If the wafer is milky-white, then the SU-8 is not completely developed; return to developer for an additional 20 s.
- 10| When development is complete, rinse thoroughly with isopropanol to wash away unexposed SU-8. Then rinse with DI water and blow dry with compressed N_2 gas. Use a digital profiler to confirm design specifications of microfeature heights.

PAUSE POINT Developed master molds can be stored in a Petri dish sealed with parafilm (to prevent the entry of dust).

16.6.2 PDMS casting: timing 3 h

The device is comprised of three molded PDMS layers: two SU-8 masters and one blank or spacer layer.

- 11| Mixing PDMS: For a 3" wafer, weigh out 35 g of PDMS elastomer base and curing agent (Sylgard 184) at a 10:1 ratio, into a weighing boat and mix thoroughly for 5 min.
- **Critical step** If PDMS is NOT mixed thoroughly, or the catalyst is inadequate, the PDMS will not cure completely and the master-mold will be unusable.
- 12| Place the master-mold into a Petri dish, then slowly pour the mixed PDMS over the master-mold.
- 13| Degassing PDMS: Place the Petri dish that holds the master-mold into a dedicated PDMS-only vacuum desiccator. Seal and engage the desiccator for 30 min. Bubbles will be seen to move to the surface. Periodically vent the chamber (e.g., bleeder valve) to release the chamber pressure. After removal from chamber, use a pipette bulb to expel remaining bubbles. At this point, also make PDMS plugs by filling some 1/16" straight connectors with PDMS and curing (step 14).
- 14| PDMS curing: Place the Petri dish on an 85°C hot plate for 2 h. When fully cured, the PDMS will become solid.
- **PAUSE POINT** Casted PDMS molds can be stored in a Petri dish sealed with parafilm (to prevent the entry of dust).
- 15| PDMS mold release: Cut out the casted PDMS molds, using a scalpel or razor blade. Use tweezers to carefully and slowly peel PDMS away from the mold. Place the PDMS mold on a sheet of transparency film (microchannels facing downward) for preparation of bonding or storage.
- **PAUSE POINT** Multiple PDMS molds can be made and stored at this point.
- **Critical step** When cutting out cured PDMS, make sure to avoid touching the photoresist pattern or breaking the silicon wafer. If not, the master will become unusable a new one must be produced.

16.6.3 Bonding of multilayer microfluidic device: timing 3 h

After molding and cutting of the three PDMS layers, assemble the device by chemical bonding using plasma treated surface activation, in the following procedures (Fig. 16.4).

- 16| Prepare the top layer microchanneled PDMS by using a gauge 11 (~2 mm diameter) needle punch to carefully punch three holes for each perifusion network: 1 inlet, 1 outlet, 1 loading port. Make sure to remove the punch cores with a tweezers before bonding.
- 17| Prepare the middle layer PDMS spacer by using a gauge 0 (~7 mm diameter) hole-punch to carefully punch one hole to make the perifusion chamber. Remove the cores.
- 18| Using Scotch Tape, clean and remove any dust and debris from the area to be bonded. Then, activate the bonding surfaces with the oxygen plasma torch. Alternating between the two surfaces, treat each bonding surface with plasma for 30 s for a total of three times on each bonding surface.
- **Critical step** Do not touch or bend the activated surface as this can prevent the device from bonding completely.
- 19| Then align the bonding surfaces and apply pressure to bonding area. Make sure to remove any air bubbles. Place bonded device on an 85°C hot plate pressed with a 2.0 kg weights for 2 h.
- **Critical step** The bonding process is irreversible. Make sure that the alignment is correct and that there is no debris or bubbles, as this will introduce leaks into the device and encourage delamination.
- 20| To make sure the device is bonded and sealed correctly, pump DI water with a 1 mL syringe to check for leaks. Alternatively, air can be pumped with a pipette with the device submerged in DI water.

16.6.4 Preparation of mouse pancreatic islets: timing 1 h and 15 min

- 21| Enzyme preparation: Prepare Collagenase P solution at concentration of a 0.375 mg mL^{-1} in HBSS for 5 mL per mouse pancreas and keep on ice.
- **Caution** Optimal collagenase concentration is different for each strain of mouse.
- **Critical step** Keep the collagenase enzyme on ice to prevent enzyme degradation.
- 22| Euthanize mice with compressed CO_2 and 3% isoflurane followed by cervical dislocation to ensure no discomfort to the animals. Disinfect the mouse by spraying it with 70% ethanol (vol/vol).
- **Caution** Follow national and institutional guidelines for animal handling.

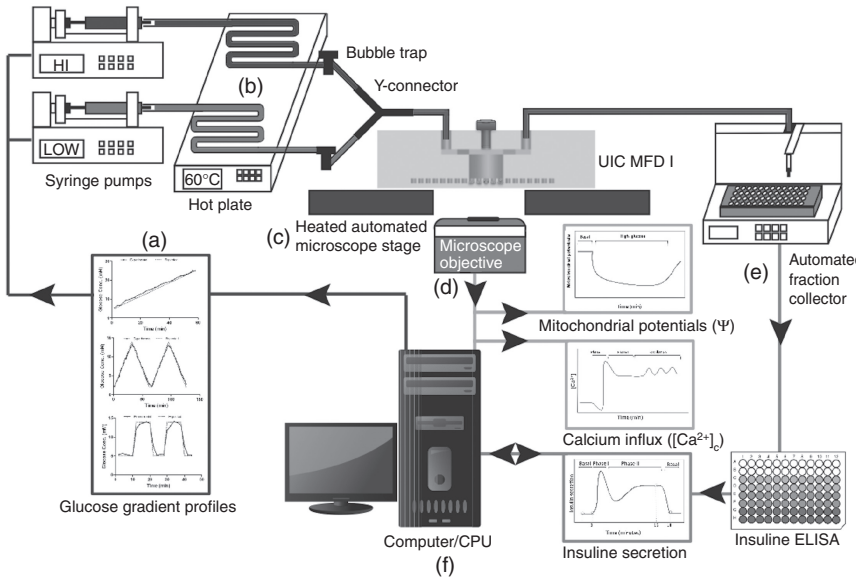

16.3 Microfluidic-based multimodal islet perifusion system and experimental setup. (a) A computer governs a syringe system and generates a preprogrammed temporal glucose gradient while maintaining constant total flow. (b) The incoming media is heated on a hotplate to be brought up to near physiological temperatures (37°C ± 3°C) and then pass through a bubble trap and Y-connector. (c) As the perifusing media enters the microdevice, the perifusion chamber temperature is maintained by a heating stage. (d) $[Ca^{2}+]_{i}$ and $\Delta\Psi_{Mito}$ are recorded. (e) Perifusate leaving the device outlet is collected by a fraction collector and quantified off-chip by ELISA (f) All physiological responsive data of $[Ca^{2}+]_{i}$, $\Delta\Psi_{Mito,}$ and insulin are compiled.

- 23| Make a V-incision starting at the genital area and move the bowel to left side of the open mouse and clearly expose common bile duct.
- 24| Clamp the ampulla on the surface of the duodenum using a hemostat.
- 25| Pancreas distension: Distend (inflate) the pancreas through the bile duct with a 30-gauge needle and 5 mL syringe containing 2 mL of cold collagenase solution, starting at the gall bladder.
- 26| Digestion: Remove the distended pancreas and place in a 15 mL tube containing 2 mL of the collagenase solution.
- 27| Place in 37°C water-bath and incubate for 12 min.
- 28| Shake for 5 s and add then 10 mL of cold HBSS to stop digestion when 80% of pancreas falls apart.
- **Critical step** Do not shake too much. Otherwise the islets will be over-digested and fragment.
- 29| Centrifuge the digested tissue at 284 *g* (1000 rpm. in a Beckman J6-MI) for 30 s at 4°C and discard supernatant.

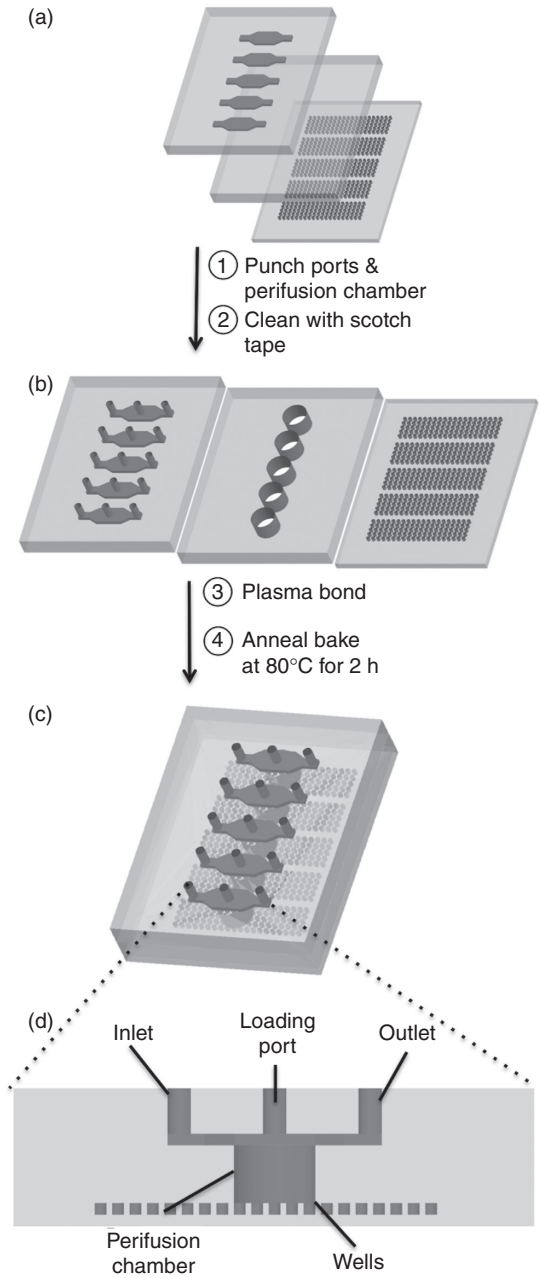

16.4 Microfluidic device final assembly. (a) 3-layers are microfabricated using soft photolithography, as shown in Fig. 16.1, and prepared by punching appropriate ports and chambers. (b) Bonding surfaces are cleaned with scotch tape. (c) Bonding surfaces are plasma treated,

(*Continued*)

- 30| Resuspend the pellet with 14 mL of cold HBSS and centrifuge with the previous setting and discard supernatant as completely as possible.
- **Critical step** Remaining HBSS might cause a change of the Ficoll density (steps 31–33).
- 31| Discontinuous gradient purification: Add 5 mL of 1.108 kg m^{-3} Ficoll and vortex vigorously.
- 32| Layer 2 mL of Ficoll solutions in descending density gradients: 1.096, 1.069, and 1.037 kg m^{-3}.
- **Critical step** Work quickly. Long-term exposure of Ficoll to islets is toxic.
- 33| Centrifuge at 640 *g* (1800 rpm. in a Beckman J6-MI) for 15 min at 4°C, with brake off.
- 34| Pick islets from the interface between density layers 1.069 and 1.096 using a plastic transfer pipette and place in a 50 mL conical tube containing 25 mL of cold HBSS.
- 35| Wash: Wash two times with cold HBSS (repeating step 29).
- 36| Culture: Resuspend the islet pellet in 10 mL RPMI-1640 containing 10% FBS (vol/vol), 100 IU/mL penicillin, 100 μg/mL streptomycin, and 20 mM HEPES and transfer into a Petri dish and place in a humidified incubator (37°C, 5% CO_2).

16.6.5 Device preconditioning: timing 20–65 min

- 37| Debubbling and vacuum loading of microfluidic device. PDMS is a hydrophobic material which makes it difficult for aqueous solutions to coat the device and also is a source of bubbles. Therefore, we recommend this five-step process: (i) immerse the microfluidic device in a vessel and flush with 100% EtOH for 10 min; (ii) place ethanol treated device in vacuum desiccator (Fisher Scientific, PA) connected to a standard laboratory wall vacuum system for 30 min at a pressure of ~110–120 kPa; (iii) exchange 100% ethanol with distilled (DI) water; (iv) and vacuum treated for an additional 30 min; (v) Optional sterilization step: the device can now be wrapped in aluminum foil and autoclaved at 125°C for 30 min (Fig. 16.5).

16.4 Continued

bonded, and then followed by pressured contact on a hotplate while anneal baking. Each completed device is composed of five perifusion systems used in parallel with an automated stage, or individually. (d) Cross-sectional view of a perifusion system. The completed device and device components shown here are proportional to the original device. For clarity, channels are indicated in red. Microwells in the bottom layer not bounded by the perifusion chamber, are not connected to perifusion network. This microwell array is maintained for simplicity for the novice fabricator. (*Source*: Reprinted with permission from Springer.)

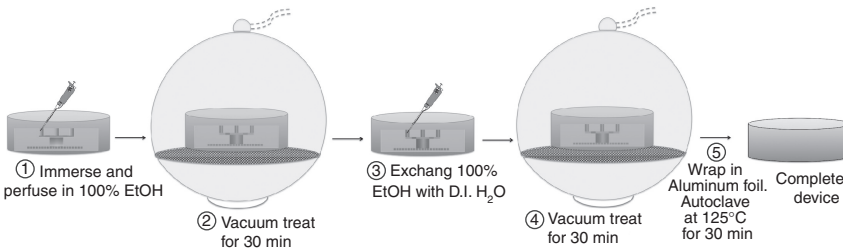

16.5 Device debubbling and vacuum loading. Five-step protocol of PDMS surface treatment and vacuum filling protocol for bubble formation prevention. (*Source*: Reprinted with permission from Springer.)

- 38| Connect a 10 mL syringe filled with 70% ethanol (vol/vol) to the inlet port with Tygon tubing, flow the ethanol for 10 min through the device channels to sterilize and prevent the introduction of bubbles. Then, rinse with DI water for 5 min (Fig. 16.6a and 16.6b).
- **Critical step** Pumping ethanol is important to minimize the introduction of bubbles. If bubbles cannot be completely removed, use a pipette to force DI water with repeated injection and withdrawal.
- 39| Rinse tubings and device with KRB containing 0.3% BSA (wt/vol) for 5 min. Then rinse with KRB containing 2 mM glucose for 5 min (Fig. 16.6c).
- **Critical step** BSA coating prevents non-specific absorption of released hormones to interior surfaces of tubings and microchannel walls, thus ensuring accuracy when later measuring bioanalyte or insulin secretion levels.
- **Critical step** Whenever disconnecting or reconnecting tubing, care needs to be taken to minimize the introduction of bubbles into the microfluidic network. This can be accomplished by merging the fluid medial meniscus of the tubing with that of the inlet or outlet port prior to inserting the tubing (Fig. 16.6e and 16.6f).

16.6.6 Islet cells preparation and loading: timing 40 min

- 40| Fluorescence labeling: Under the microscope, hand-pick 25 mouse islets and place in a Petri dish with 2 mL of KRB containing 2 mM glucose. In the Petri dish, an ellipsoid swirling motion is used to aggregate in a cluster for easier handling in subsequent steps. Add Fura-2 AM at a final concentration of 5 μM and Rh 123 at final concentration of 2.5 μM.
- 41| Place the dish into the humidified incubator (37°C and 5% CO_2) for 30 min.

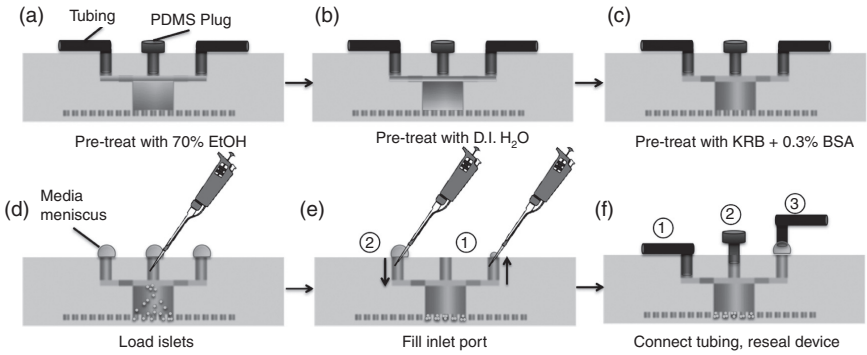

16.6 Microfluidic device preconditioning and islet loading. (a) EtOH Pre-treatment: Preconditioning begins by perifusing tubings and microfluidic devices with 70% ethanol (vol/vol) to apply a hydrophilic coating. (b) DI H_2O rinse: DI water is perifused to rinse out excess ethanol. (c) BSA Rinse: 0.3% BSA in Krebs-Ringer Buffer (wt/vol) is then applied to prevent insulin and other organic species from being trapped in tubing and microfluidic device. (d) Islet Loading: Tubing is disconnected and inlet ports are filled and overflowed with perifusate to create a meniscus. Islets are then loaded with 20 µL pipette which is dialed down until empty. (e) Inlet Preparation: Medium from outlet (1) and inlet (2) is overflowed. (f) Final Connections: Inlet tubing is reconnected (1). Media at islet loading port and outlet port overflow. Loading port is sealed (2). Finally, outlet tubing is reconnected to outlet port (3). (*Source*: Reprinted with permission from Springer.)

- 42| Islet loading: Disconnect the device from syringe pumps and place device on a flat surface. Making sure that a media meniscus bead of buffer overflows each unconnected port.
- 43| After 30 min incubation, pick up the islets using a 20 µL pipette, insert into the loading port, and gently load the islets by dialing down the pipette (Fig. 16.6d).
- 44| Aspirate another 20 µL KRB from the outlet and inject into the inlet port, dispensing the loaded islets into the bottom of perifusion chamber (Fig. 16.6e).
- 45| Place the preconditioned device with the loaded islets on the 37°C heated microscope stage and connect the inlet to syringe pumps containing 2 and 25 mM glucose solutions via the Y-connector with the Tygon tubing. Connect the outlet of the microfluidic device to fraction collector (Fig. 16.6f).
- **Critical step** GSIS is sensitive to temperature changes, maintain a temperature range of 37 ± 3°C in the perifusion chamber and confirm with a temperature probe. To further avoid temperature change, place a hot plate set between 45°C and 60°C upstream of the device inlet to heat the incoming perifusing media (Fig. 16.3b).

- **Critical step** In order to prevent sudden pressure changes and bubble formation in the perifusion chamber, islet loading is best done on a flat surface and when all the tubings are disconnected from the device. Rapid changes in pressure can cause islets to become dislodged and exit the perifusion chamber through the outlet.
- **Critical step** Make sure syringes, tubing, microfluidic device, and outlet are all on the same level surface or height. Different heights will cause different pressures and fluid flow which may eject islets. If perifusion is stopped, make sure to clamp outlet to prevent fluid flow which may eject islets.

16.6.7 Simultaneous islet perifusion and fluorescence imaging: timing 40 min

- 46| Start the syringe pump containing 2 mM glucose KRB solution to wash the excess dye from the perifusion chamber and islets at a speed of 250 μL/min for 10 min.
- **Critical step** To maximize signal-to-noise ratio, make sure that there is enough time for hydrolysis and washing of excess fluorescent indicator dyes.
- 47| During the washing period, start searching the areas of interest (ROIs) using transmitted light illumination.
- **Critical step** Start this step as soon as possible without waiting until the completion of the washing.
- 48| Open Simple PCI imaging software and LabVIEW.
- 49| Use the ROI tool of the imaging software to define the islets and islet regions to be imaged and also circle a non-islet area for later background subtraction.
- 50| Designate the excitation and emission filter sets for simultaneous imaging of Fura-2 for intracellular calcium changes and Rh 123 for mitochondrial potential changes. Fura-2 excitation occurs at 340 and 380 nm and detected at 510 nm ± 10. The Fura-2 excitation ratio (F380/ F340) is obtained using Simple PCI. Rh 123 is excited at 490 nm and detected at 530 nm ± 10.
- 51| Initialize LabVIEW to create a defined linear glucose gradient (2–25 mM) (Plate Xa (see in color section between pages 328 and 329)) and set the fraction collector at 1-minute intervals.
- **Caution** When programming LabVIEW, you can confirm the creation of the desired glucose gradient profile by sampling the perifusate and using a glucometer to measure glucose levels before experimentation.
- **Critical step** Adjust fluorescence intensity gains at each wavelength to prevent artifacts.

- 52| Start acquiring a time series of Fura-2 and Rh 123 fluorescence at the ROIs at 15-second capture interval.
- 53| Turn off the syringe pump containing 25 mM glucose after the completion of glucose gradient. Let the low glucose pump continue to wash out the effect of the high glucose for 10 min.
- 54| Following the perifusion, export the data to excel for analysis. The amount of insulin secreted into the perifusate is determined by ELISA according to manufacturer protocol (Plate Xb and Xc).
- 55| Flush out islets and cellular debris with 1 mL pipette and commence flushing the perifusion. Then flush chambers with 70% ethanol (vol/vol) for 10 min and DI H_2O for 10 min. Cleaning is variable and dependent on media used.

Troubleshooting advice can be found in Table 16.2.

16.7 Anticipated results

As an example of expected results, below, we briefly present published data from experiments that followed this protocol and where the simultaneous islet perifusion and fluorescence imaging are conducted in mouse pancreatic islets. The glucose-stimulated β-cell insulin secretory pathway is a complex process involving glycolysis, mitochondrial ATP production, followed by ATP-sensitive K+ (K_{ATP}) channel closure, subsequent plasma membrane depolarization, and the resulting rapid influx of calcium ions through VDCCs. Finally, the increase in $[Ca^2+]_i$ triggers the fusion of the insulin granules with the plasma membrane resulting in the exocytosis of proinsulin, C-peptide, and insulin (Henquin *et al*., 2006; Keizer *et al*., 1989). Alternate pathways, independent of K_{ATP} and $[Ca^2+]_i$, have been described. However, the K_{ATP} and $[Ca^2+]_i$-mediated pathway remains the primary mechanism of insulin secretion (Henquin *et al*., 2000).

Using this protocol, we apply Fura-2 and Rh123 fluorescence probes for the simultaneous measurement of intracellular calcium and mitochondrial potentials during controlled islet perifusion in response to various insulin secretagogues. As shown in Plate Xb, islets initially exhibit the canonical hyperpolarization of mitochondrial membrane potentials and subsequent biphasic calcium signaling pattern with a primary initial maximal influx pulse and a secondary lower and sustained pulse period with slow calcium oscillation. Insulin release exhibits a typical biphasic profile. In contrast, islets stimulated with tolbutamide exhibit both monophasic calcium signaling and insulin secretory patterns, without significant decrease in mitochondrial membrane hyperpolarization proceeding recorded changes in $[Ca^2+]_i$ (Plate Xc). Unlike glucose-induced calcium influx, tolbutamide directly closes K_{ATP} channels, causing membrane depolarization and VDCC activation.

Table 16.2 Troubleshooting table

Step	Problem	Possible reason	Solution
4	SU8 too thin	Spinning parameter	Adjust spin speed according to temperature
6, 8, 9	SU8 residue	Resist adhesion	Dehydration bake, increase UV exposure, cool slowly after bake steps
9	SU8 residue	Poor development	Add new developer, increase UV, agitate solution
14	PDMS not curing	Mixing, contamination	Mix well, avoid vacuum desiccator contamination, alternative degassing using centrifuge, etc.
19	Poor or no bonding, leaking	Poor surface	Plasma not strong, add pressure, dirty surface, PDMS not cured
25	Stomach or duodenum distended during enzyme injection	Wrong clamp site	Recheck the ampulla that is a white spot on the surface of the duodenum and reclamp it
27, 28	Over-digestion/ fragmentation	Digestion condition	Adjust enzyme concentration, digestion time, and the degree of hand shack
38	Bubbles in chamber	Chamber conditioning	Precondition with ethanol
39	Precipitates in chamber	Chamber conditioning	Wash thoroughly with DI water after ethanol
43	Poor islet loading with bubbles	Bad loading order	Fill ports with buffer and observe order of loading
52	Low fluorescence intensity	Bad illumination	Change microscope fluorescence source or increase signal gain
52	Poor islet calcium response	Bad perifusion control	Check temperature, KRB pH, and fluorescent dye expiration
52	Bubble introduced in chamber	Bad connection, chamber conditioning	Check tube connections, change to clean tubing, check bubble trap, clean and redo preconditioning. Ensure syringes, device, tubing, and fraction collector are leveled
54	Poor or insulin levels	Chamber conditioning	Make sure to precondition device with 0.3% BSA (wt/vol)
	Poor result due to dirty device	Chamber conditioning	Sonicate with ethanol in chamber, one perifusion chamber has lifetime of ~10 uses. Device has lifetime of 50 uses, as there are five chambers for each device.

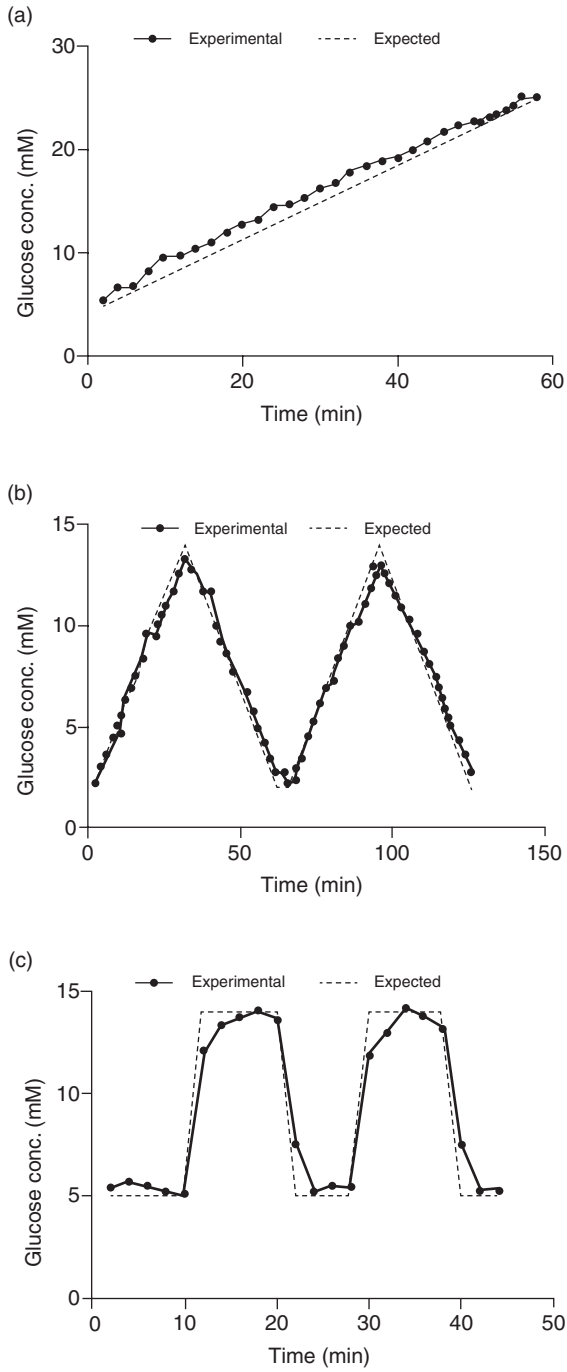

16.7 The creation of various glucose temporal gradients in the microfluidic network vs. expected values. (a) Symmetric-bell shape at range of 2–14 mM. (b) Square-shape of 5–14 mM glucose. (c) Linear 5–25 mM glucose.

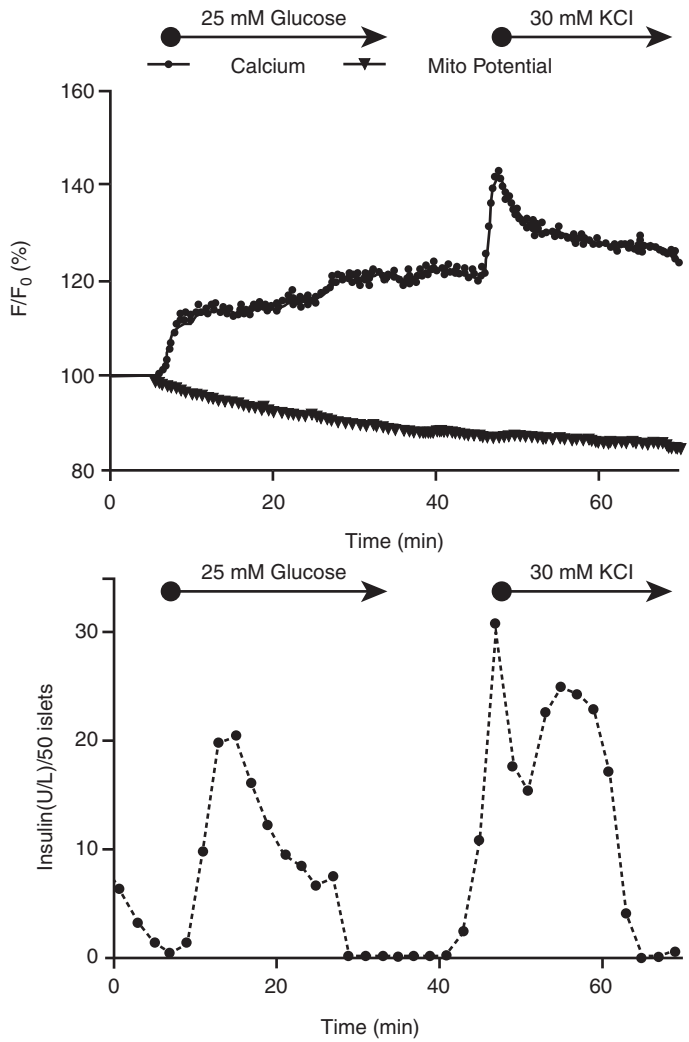

16.8 Human islet response to glucose and high potassium stimulation (a) A representative of tracing of calcium influx and mitochondrial potential changes of human islets in response to 25 mM glucose and 30 mM potassium chloride. (b) A representative of trace of insulin secretion profile of 50 human islets in response to 25 mM glucose and 30 mM potassium chloride.

A high signal-to-noise ratio is required in order to have valid real-time fluorescence detection from active monitoring of β-cell metabolic and ion signaling events. In the demonstrated results, both fluorescence signals show a good signal-to-noise ratio in more than 20% changes. The insulin secretion profiles from 25 islets in response to glucose and tolbutamide

demonstrate that the system has sufficient sensitivity and temporal resolution to detect either biphasic or monophasic insulin secretion. In addition, various user-defined temporal glucose gradients can be created and maintained stably in the perifusion chamber (Fig. 16.7a–16.7c).

As aforementioned, the microfluidic device and its accessories were originally designed for functional human islet evaluation prior to transplant. Islet transplantation is a promising therapy for Type 1 diabetes, but shows variable success rates. It is thought that inconsistent outcomes are mostly related to the variable quality of human islet preparations. While tests for sterility, identity, and purity are well established, no reliable method for assessing islet potency is available. The results of human islet function using static glucose incubation do not correlate with clinical outcomes such as islet graft function and insulin independence. With the approach in this protocol, a β-cell specific and glucose-stimulated multimodal assay will be established for human islet evaluation, with the ultimate goal being validated as an islet potency test that meet FDA standards. At this moment, we are still in the process of evaluating this device and testing different stimulation protocols for human islet potency and viability study as shown in Fig. 16.8.

16.8 Acknowledgements

This study was supported Chicago Diabetes Project (CDP) and National Institutes of Health (NIH) [R01 DK091526 (J.O)]. Joshua E. Mendoza-Elias is supported by: the University of Illinois at Chicago Hispanic Center of Excellence (HCOE) *Medical Summer Research Fellowship*; the American Diabetes Association *Clinical Scientist Training Program Grant* (Grant Reference No.: 7–12-CST-03); the American Society of Transplant Surgeons (ASTS) *Presidential Student Mentor Grant*; academic support from the University of Illinois at Chicago Urban Health Program (UHP). We would also like to pay a thank you to Gerardo Mauleon for his technical support for figures.

16.9 References

Adewola AF, Lee D, Harvat T, Mohammed J, Eddington DT, Oberholzer J, Wang Y (2010). Microfluidic perifusion and imaging device for multi-parametric islet function assessment. *Biomed Microdevices*;**12**(3):409–417.

Alejandro R, Barton FB, Hering BJ, Wease S (2008). 2008 Update from the collaborative islet transplant registry. *Transplantation*;**86**(12):1783–1788.

Armann B, Hanson MS, Hatch E, Steffen A, Fernandez LA (2007). Quantification of basal and stimulated ROS levels as predictors of islet potency and function. *Am J Transplant*;**7**(1):38–47.

Babenko AP, Aguilar-Bryan L, Bryan J (1998). A view of sur/KIR6.X, KATP channels. *Annu Rev Physiol*;**60**:667–687.

Bellin MD, Kandaswamy R, Parkey J, Zhang HJ, Liu B, Ihm SH, Ansite JD, Witson J, Bansal-Pakala P, Balamurugan AN, Papas KK, Sutherland DE, Moran A, Hering BJ (2008). Prolonged insulin independence after islet allotransplants in recipients with type 1 diabetes. *Am J Transplant*;**8**(11):2463–2470.

Bertuzzi F, Ricordi C (2007). Prediction of clinical outcome in islet allotransplantation. *Diabetes Care*;**30**(2):410–417.

Carvalho CP, Oliveira RB, Britan A, Santos-Silva JC, Boschero AC, Meda P, Collares-Buzato CB (2012). Impaired beta-cell-beta-cell coupling mediated by Cx36 gap junctions in prediabetic mice. *Am J Physiol Endocrinol Metab*;**303**(1):E144–E151.

Chen D, Du W, Liu Y, Liu W, Kuznetsov A, Mendez FE, Philipson LH, Ismagilov RF (2008). The chemistrode: a droplet-based microfluidic device for stimulation and recording with high temporal, spatial, and chemical resolution. *Proc Natl Acad Sci U S A*;**105**(44):16843–16848.

Craighead H (2006). Future lab-on-a-chip technologies for interrogating individual molecules. *Nature*;**442**(7101):387–393.

Dionne KE, Colton CK, Yarmush ML (1993). Effect of hypoxia on insulin secretion by isolated rat and canine islets of Langerhans. *Diabetes*;**42**(1):12–21.

Dishinger JF, Reid KR, Kennedy RT (2009). Quantitative monitoring of insulin secretion from single islets of Langerhans in parallel on a microfluidic chip. *Anal Chem*;**81**(8):3119–3127.

Duchen MR (2000). Mitochondria and Ca(2+)in cell physiology and pathophysiology. *Cell Calcium*;**28**(5–6):339–348.

Easley CJ, Rocheleau JV, Head WS, Piston DW (2009). Quantitative measurement of zinc secretion from pancreatic islets with high temporal resolution using droplet-based microfluidics. *Anal Chem*;**81**(21):9086–9095.

El-Ali J, Sorger PK, Jensen KF (2006). Cells on chips. *Nature*;**442**(7101):403–411.

Gangemi A, Salehi P, Hatipoglu B, Martellotto J, Barbaro B, Kuechle JB, Qi M, Wang Y, Pallan P, Owens C, Bui J, West D, Kaplan B, Benedetti E, Oberholzer J (2008). Islet transplantation for brittle type 1 diabetes: the UIC protocol. *Am J Transplant*;**8**(6):1250–1261.

Gembal M, Gilon P, Henquin JC (1992). Evidence that glucose can control insulin release independently from its action on ATP-sensitive K+ channels in mouse B cells. *J Clin Invest*;**89**(4):1288–1295.

Goto M, Holgersson J, Kumagai-Braesch M, Korsgren O (2006). The ADP/ATP ratio: A novel predictive assay for quality assessment of isolated pancreatic islets. *Am J Transplant*;**6**(10):2483–2487.

Henquin JC (2000). Triggering and amplifying pathways of regulation of insulin secretion by glucose. *Diabetes*;**49**(11):1751–1760.

Henquin JC, Nenquin M, Stiernet P, Ahren B (2006). In vivo and in vitro glucose-induced biphasic insulin secretion in the mouse: pattern and role of cytoplasmic Ca2+ and amplification signals in beta-cells. *Diabetes*;**55**(2):441–451.

Henquin JC, Schmeer W, Nenquin M, Meissner HP (1985). Effects of a calcium channel agonist on the electrical, ionic and secretory events in mouse pancreatic B-cells. *Biochem Biophys Res Commun*;**131**(2):980–986.

Hoshi M, Shreeve WW (1973). Release and production of insulin by isolated, perifused rat pancreatic islets. Control by glucose. *Diabetes*;**22**(1):16–24.

Ichii H, Inverardi L, Pileggi A, Molano RD, Cabrera O, Caicedo A, Messinger S, Kuroda Y, Berggren PO, Ricordi C (2005). A novel method for the assessment of cellular composition and beta-cell viability in human islet preparations. *Am J Transplant*;**5**(7):1635–1645.

Iglesias I, Bentsi-Barnes K, Umeadi C, Brown L, Kandeel F, Al-Abdullah IH (2008). Comprehensive analysis of human pancreatic islets using flow and laser scanning cytometry. *Transplant Proc*;**40**(2):351–354.

Jayaraman S (2011). Assessment of beta cell viability. *Curr Protoc Cytom*;Chapter **6**:Unit 6 27.

Jayaraman S (2008). A novel method for the detection of viable human pancreatic beta cells by flow cytometry using fluorophores that selectively detect labile zinc, mitochondrial membrane potential and protein thiols. *Cytometry A*;**73**(7):615–625.

Keizer J, Magnus G (1989). ATP-sensitive potassium channel and bursting in the pancreatic beta cell. A theoretical study. *Biophys J*;**56**(2):229–242.

Kennedy ED, Rizzuto R, Theler JM, Pralong WF, Bastianutto C, Pozzan T, Wollheim CB. Glucose-stimulated insulin secretion correlates with changes in mitochondrial and cytosolic Ca2+ in aequorin-expressing INS-1 cells. *J Clin Invest*;**98**(11):2524–2538.

Kennedy ED, Wollheim CB (1998). Role of mitochondrial calcium in metabolism-secretion coupling in nutrient-stimulated insulin release. *Diabetes Metab*;**24**(1):15–24.

Kim JH, Park SG, Lee HN, Lee YY, Park HS, Kim HI, Yu JE, Kim SH, Park CG, Ha J, Kim SJ, Park KS (2009). ATP measurement predicts porcine islet transplantation outcome in nude mice. *Transplantation*;**87**(2):166–169.

Komjati M, Bratusch-Marrain P, Waldhausl W (1986). Superior efficacy of pulsatile versus continuous hormone exposure on hepatic glucose production in vitro. *Endocrinology*;**118**(1):312–319.

Lacy LR, Knudson MM, Williams JJ, Richards JS, Midgley AR, Jr. (1976). Progesterone metabolism by the ovary of the pregnant rat: discrepancies in the catabolic regulation model. *Endocrinology*;**99**(4):929–934.

Lacy PE, Walker MM, Fink CJ (1972). Perifusion of isolated rat islets in vitro. Participation of the microtubular system in the biphasic release of insulin. *Diabetes*; **21**(10):987–998.

Lee D, Wang Y, Mendoza-Elias JE, Adewola AF, Harvat TA, Kinzer K, Gutierrez D, Qi M, Eddington DT, Oberholzer J (2011). Dual microfluidic perifusion networks for concurrent islet perifusion and optical imaging. *Biomed Microdevices*; **14**(1):7–16.

Lehmann R, Zuellig RA, Kugelmeier P, Baenninger PB, Moritz W, Perren A, Clavien PA, Weber M, Spinas GA (2007). Superiority of small islets in human islet transplantation. *Diabetes*;**56**(3):594–603.

Liu WW, Goodhouse J, Jeon NL, Enquist LW (2008). A microfluidic chamber for analysis of neuron-to-cell spread and axonal transport of an alpha-herpesvirus. *PLoS One*;**3**(6):e2382.

London NJ, Thirdborough SM, Swift SM, Bell PR, James RF (1991). The diabetic "human reconstituted" severe combined immunodeficient (SCID-hu) mouse: a model for isogeneic, allogeneic, and xenogeneic human islet transplantation. *Transplant Proc*;**23**(1 Pt 1):749.

Luciani DS, Misler S, Polonsky KS (2006). Ca2+ controls slow NAD(P)H oscillations in glucose-stimulated mouse pancreatic islets. *J Physiol*;**572**(Pt 2):379–392.

Maechler P, Kennedy ED, Wang H, Wollheim CB (1998). Desensitization of mitochondrial Ca2+ and insulin secretion responses in the beta cell. *J Biol Chem*;**273**(33):20770–20778.

Mohammed JS, Wang Y, Harvat TA, Oberholzer J, Eddington DT (2009). Microfluidic device for multimodal characterization of pancreatic islets. *Lab Chip*;**9**(1):97–106.

Mosadegh B, Huang C, Park JW, Shin HS, Chung BG, Hwang SK, Lee KH, Kim HJ, Brody J, Jeon NL (2007). Generation of stable complex gradients across two-dimensional surfaces and three-dimensional gels. *Langmuir*;**23**(22):10910–10912.

Nam KH, Yong W, Harvat T, Adewola A, Wang S, Oberholzer J, Eddington DT (2010). Size-based separation and collection of mouse pancreatic islets for functional analysis. *Biomed Microdevices*;**12**(5):865–874.

Oppegard SC, Nam KH, Carr JR, Skaalure SC, Eddington DT (2009). Modulating temporal and spatial oxygenation over adherent cellular cultures. *PLoS One*;**4**(9):e6891.

Papas KK, Colton CK, Nelson RA, Rozak PR, Avgoustiniatos ES, Scott WE, 3rd, Wildey GM, Pisania A, Weir GC, Hering BJ (2007). Human islet oxygen consumption rate and DNA measurements predict diabetes reversal in nude mice. *Am J Transplant*;**7**(3):707–713.

Papas KK, Pisania A, Wu H, Weir GC, Colton CK (2007). A stirred microchamber for oxygen consumption rate measurements with pancreatic islets. *Biotechnol Bioeng*;**98**(5):1071–1082.

Papas KK, Suszynski TM, Colton CK (2009). Islet assessment for transplantation. *Curr Opin Organ Transplant*;**14**(6):674–682.

Porksen N, Hollingdal M, Juhl C, Butler P, Veldhuis JD, Schmitz O (2002). Pulsatile insulin secretion: detection, regulation, and role in diabetes. *Diabetes*;**51** Suppl 1:S245–S254.

Ricordi C, Lakey JR, Hering BJ (2001). Challenges toward standardization of islet isolation technology. *Transplant Proc*;**33**(1–2):1709.

Ricordi C, Scharp DW, Lacy PE (1988). Reversal of diabetes in nude mice after transplantation of fresh and 7-day-cultured (24 degrees C) human pancreatic islets. *Transplantation*;**45**(5):994–996.

Rocheleau JV, Piston DW (2008). Chapter 4: Combining microfluidics and quantitative fluorescence microscopy to examine pancreatic islet molecular physiology. *Methods Cell Biol*;**89**:71–92.

Rocheleau JV, Walker GM, Head WS, McGuinness OP, Piston DW (2004). Microfluidic glucose stimulation reveals limited coordination of intracellular Ca2+ activity oscillations in pancreatic islets. *Proc Natl Acad Sci USA*;**101**(35):12899–12903.

Roe MW, Worley JF, 3rd, Tokuyama Y, Philipson LH, Sturis J, Tang J, Dukes ID, Bell GI, Polonsky KS (1996). NIDDM is associated with loss of pancreatic beta-cell L-type Ca2+ channel activity. *Am J Physiol*;**270**(1 Pt 1):E133–E140.

Ryan EA, Paty BW, Senior PA, Bigam D, Alfadhli E, Kneteman NM, Lakey JR, Shapiro AM (2005). Five-year follow-up after clinical islet transplantation. *Diabetes*;**54**(7):2060–2069.

Shapiro J, Lakey J, Ryan E, Korbutt G, Toth E, al e (2000). Islet transplantation in seven patients with type 1 diabetes mellitus using a glucocorticoid-free immunosuppressive regimen. *N Engl J Med*;**343**(4):230–238.

Spigelman AF, Dai X, MacDonald PE (2010). Voltage-dependent K(+) channels are positive regulators of alpha cell action potential generation and glucagon secretion in mice and humans. *Diabetologia*;**53**(9):1917–1926.

Straub SG, Sharp GW (2002). Glucose-stimulated signaling pathways in biphasic insulin secretion. *Diabetes Metab Res Rev*;**18**(6):451–463.

Street CN, Lakey JR, Shapiro AM, Imes S, Rajotte RV, Ryan EA, Lyon JG, Kin T, Avila J, Tsujimura T, Korbutt GS (2004). Islet graft assessment in the Edmonton Protocol: implications for predicting long-term clinical outcome. *Diabetes*;**53**(12):3107–3114.

Svensson AM, Sandler S, Jansson L (1994). Pancreatic islet blood flow in the rat after administration of islet amyloid polypeptide or calcitonin gene-related peptide. *Diabetes*;**43**(3):454–458.

Sweet IR, Gilbert M (2006). Contribution of calcium influx in mediating glucose-stimulated oxygen consumption in pancreatic islets. *Diabetes*;**55**(12):3509–3519.

Sweet IR, Gilbert M, Scott S, Todorov I, Jensen R, Nair I, Al-Abdullah I, Rawson J, Kandeel F, Ferreri K (2008). Glucose-stimulated increment in oxygen consumption rate as a standardized test of human islet quality. *Am J Transplant*;**8**(1):183–192.

Taylor AM, Rhee SW, Jeon NL (2006). Microfluidic chambers for cell migration and neuroscience research. *Methods Mol Biol*;**321**:167–177.

Wang W, Upshaw L, Strong DM, Robertson RP, Reems J (2005). Increased oxygen consumption rates in response to high glucose detected by a novel oxygen biosensor system in non-human primate and human islets. *J Endocrinol*;**185**(3):445–455.

Warnotte C, Gilon P, Nenquin M, Henquin JC (1994). Mechanisms of the stimulation of insulin release by saturated fatty acids. A study of palmitate effects in mouse beta-cells. *Diabetes*;**43**(5):703–711.

Weaver DC, McDaniel ML, Naber SP, Barry CD, Lacy PE (1978). Alloxan stimulation and inhibition of insulin release from isolated rat islets of Langerhans. *Diabetes*;**27**(12):1205–1214.

Weibel DB, Diluzio WR, Whitesides GM (2007). Microfabrication meets microbiology. *Nat Rev Microbiol*;**5**(3):209–218.

Zhang X, Roper MG (2009). Microfluidic perfusion system for automated delivery of temporal gradients to islets of Langerhans. *Anal Chem*;**81**(3):1162–1168.

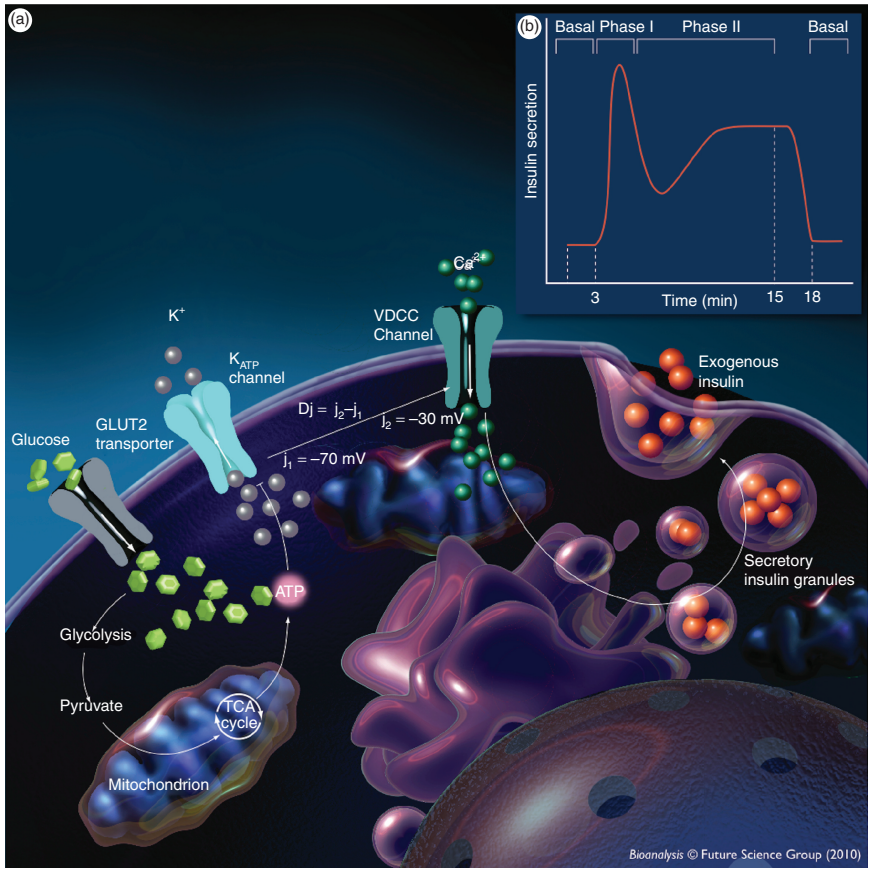

Plate VIII (Chapter 16) Insulin secretory pathway and kinetic profile. (a) Ionic control of secretion. (b) Biphasic insulin secretory kinetics. (*Source*: Reprinted with permission from Future Science Ltd.)

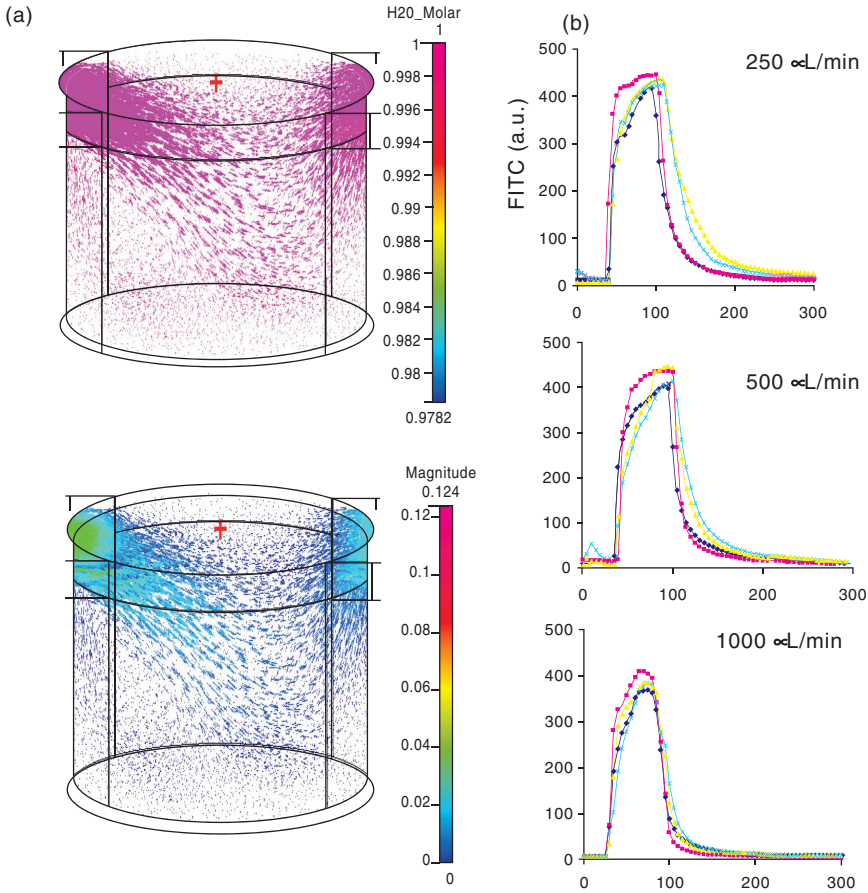

Plate IX (Chapter 16) Characterization of perifusion chamber fluid dynamics. The device was modeled using CFD-GEOM software. CFD-ACE software was use to simulate exchange of solution at an inlet flow rate of 1 mL/min. Channel was set with initial condition of 0 M dye followed by flow with 1 M dye. Simulation results were processed using CFD-View software. Simulations were performed at steady-state. (a) Computer Simulation of Fluid Dynamics: Molar Concentration superimposed with vector field flow and velocity superimposed with vector field flow. (b) *In vitro* verification of fluid dynamics: FITC mixing plots vs. time across different regions at three different flow rates. (Blue: inlet-well bottom, Red: center-well bottom, Yellow: outlet-well bottom, Green side-well bottom). (*Source*: Reprinted with permission from Springer.)

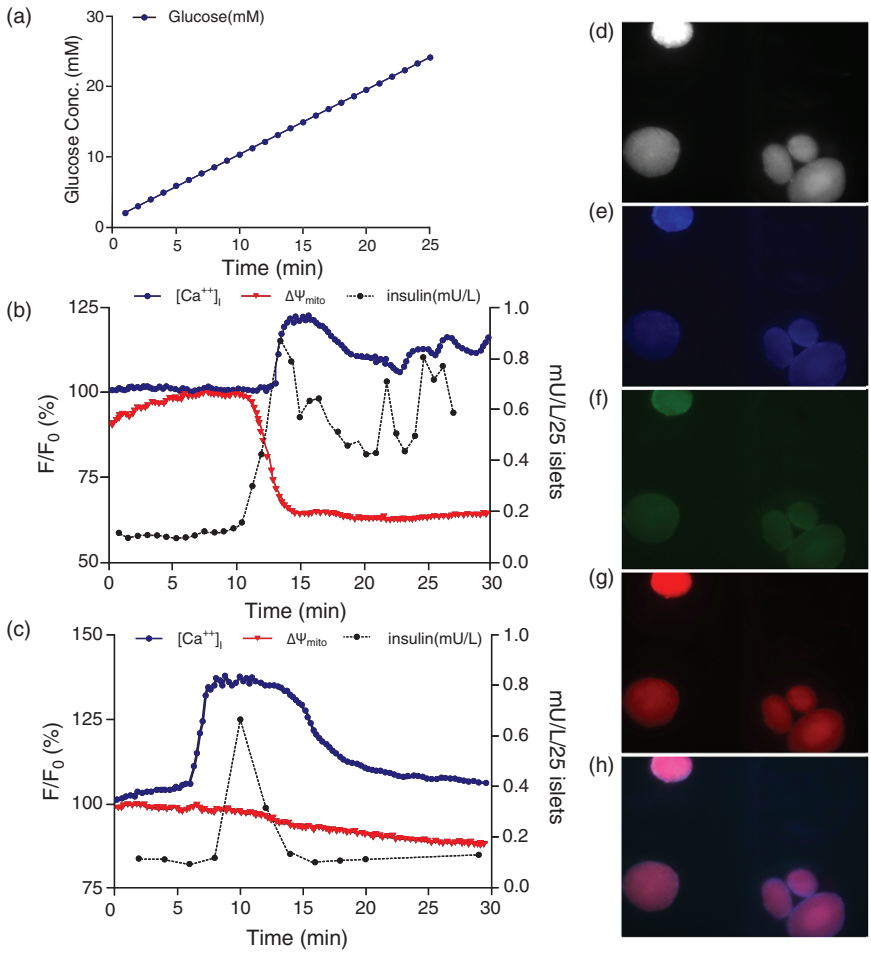

Plate X (Chapter 16) Simultaneous islet perifusion and fluorescence imaging of mouse isolated islets. (a) A preprogrammed 2–25 mM glucose ramp. (b) Δ_{Mito}, $[Ca^2+]_i$, and dynamic insulin release (mU/L/25 islets) and profiles in response to the glucose stimulation. (c) Δ_{Mito}, $[Ca^2+]_i$, and dynamic insulin release (mU/L/25 islets) profiles in response to the 250 μM tolbutamide stimulation.(d) The transmitted islet image. (e-f). The Fura-2 islet images. (g) The Rh 123 islet image. (h) The merged image of Fura-2 and Rh 123.

17

Microfluidic devices for radio chemical synthesis

A. Y. LEBEDEV, University of California, Los Angeles, USA

DOI: 10.1533/9780857097040.4.594

Abstract: Microfluidic devices feature several properties potentially beneficial for radiochemical synthesis. High surface-to-volume ratio of the reactor allows for improved process control and heat transfer; low amount of the reagent simplifies the purification procedure; high concentration of the radioactive reagent potentially increases the reaction rate. A number of successful experimental devices have been reported, but wide adoption of the technology is hindered by limited choice of materials, scarce feedback, and underdeveloped means of coupling with macro-devices. This chapter discusses the reported applications of microfluidics for radiochemical synthesis, the areas in need of improvement, and potentially relevant recent developments.

Key words: positron emission tomography, radiolabeling, microfluidic reactor, radiochemistry automation, nuclear medicine.

17.1 Introduction

The first patent applications for the use of microfluidic devices in radiochemical synthesis were filed in early 2000s,[1] and since then almost a hundred publications have appeared. Early publications were quickly followed by reviews optimistically discussing prospects of the emerging technology.[2,3] The explosive growth of the publication count illustrates enthusiasm of the radiochemical community to the new technology. Nevertheless, the installed base of microfluidic radiochemistry modules does not exceed several dozens, but only a small fraction of the number of conventional modules. The slow acceptance of the technology is an alerting sign, indicating that the technology lacks some key features to be expected in successful radiochemistry equipment. This review summarizes the advantages microfluidic technology can offer but, more importantly, discusses the drawbacks impeding its wider acceptance.

A number of experimental apparatuses having some traits of microfluidic machines have been reported; not all of them, though, exhibit the titular

feature of microfluidic: low volume. Devices with reactors as large as 0.5 mL have been presented as microfluidic in the literature[4] because one of the reactor dimensions was on the scale of hundreds of microns. This broad interpretation of microfluidic devices[5] covers some other types of devices, such as 'captive-solvent' machines dating as far back as 1986.[6] Since this chapter is devoted to practical application of the technology, it includes all publications related to performing radiochemistry in miniature devices.

17.2 Medical applications of microfluidic radiochemistry: positron emission tomography (PET) and single photon emission computed tomography (SPECT)

The majority of publications reporting uses of microfluidic devices in radiochemical synthesis are related to production of tracers for positron emission tomography (PET) or to a similar technique, single photon emission computed tomography (SPECT). PET is a relatively new medical imaging modality, used for the quantification of biochemical processes in live organisms, with medicine being its major application.

In a typical PET imaging study, a molecule labeled with a positron emitting radionuclide is injected into patient's bloodstream and, after a predefined time, the patient is placed in the PET scanner. The scanner and the processing software reconstruct a 3D spatial distribution of injected radionuclide in patient's body. Since the effects of biochemical processes on the biodistribution of this labeled molecule are well studied, imaging specialists can draw conclusions about biochemical processes in the patient's body. [^{18}F]-2-deoxy-2-fluoro-D-glucose (FDG), is the only PET agent currently reimbursed by insurance companies in the US, and therefore is the most widely used in routine studies. This molecule is known to accumulate in metabolically active tissues, most notably in actively growing tumors. This property made FDG-PET an invaluable tool in oncological imaging with approximately 5 millions scans performed yearly worldwide. SPECT operates under similar principles, but relies on isotopes emitting γ-photons, rather than positrons emitting nuclides.

17.2.1 Typical workflow of an imaging study: reliability

A PET imaging study is a costly, concerted process involving many people and often several organizations. The first step is production of labeling radionuclide on biomedical cyclotrons, equipment usually installed only at major production facilities. In the second step, the radioisotope is incorporated into an organic molecule and a final tracer is produced. The incorporation

process and other steps of the chemical synthesis, are performed on an automated module. Making this step more efficient is the point in the imaging workflow where microfluidic technology might be applied. Once the radiotracer is produced, it undergoes a complex quality control procedure, normally performed by the team that produced the tracer. On the third step, the tracer is transferred to the imaging team at the hospital. The patient is injected with a dose of the tracer and an image is acquired at the predefined time after injection. The scanner and its infrastructure are the second biggest investment in the imaging equipment (after the cyclotron facility); small clinics can rarely afford this equipment. In the final step, a qualified radiologist analyzes the image and communicates the interpretation to a treating physician.

Due to the complexity of the workflow, the reliability of tracer production is a critical parameter. It is important to emphasize that the whole chain of events is highly organized and a flaw in any of the links will cause a failure of the entire effort and considerable financial loss; currently, the cost of one scan varies from $2000 to $6000. This puts significant pressure onto each team, which increases toward the beginning of the chain: *a failed cyclotron run or radiochemical synthesis will result in cancelation of nearly a hundred of studies, while untimely scan interpretation only delays one patient's treatment.* It is also important to note that the cyclotron only produces radioactivity in batches, taking normally 2–4 h to produce the amount of radioactivity needed for the production facility to meet a daily demand. Therefore, once the radioactive nuclei are produced, the downstream steps have to be executed flawlessly, since there will be virtually no chance to correct any problems. The key factor determining the entire workflow of the PET study is the lifetime of the radionuclide used. Most commonly employed ^{18}F has a half-life of 109.7 min; and ^{11}C – a less widespread, but sought after isotope – has a half-life of 22 min. This invariable physical constant imposes very strict time constraints on each step of the imaging study. ^{18}F allows no more than 10 h between the end of cyclotron production and the start of the scan, while use of ^{11}C-labeled tracer shortens this time to about an hour.

In this situation, the equipment suitable for modern PET probe production would have to meet certain criteria:

(a) Tracer production should occur with minimal loss of radioactivity, meaning high chemical yield and short process time.
(b) The instrument reliability should be predictable, preventive maintenance operations should be established, and a sufficient set of pre-production self-checks should be implemented.
(c) Instrument automation should eliminate routine manual procedures, up to production of final injectable formulation.
(d) The instrument software should comply with GMP guidelines.

Less important requirements include production of a range of tracers, self-shielding, and the option to operate the instrument at the imaging facility and not the center where radionuclide is produced.

17.3 Advantages and disadvantages of microfluidic devices

Microfluidic systems feature a set of unique properties determined by their size and geometry. This chapter discusses some of these features from a radiochemist's perspective.

17.3.1 Beneficial properties of microfluidics

Microfluidic devices exhibit a set of properties that can improve production of radiotracers. Mainly, potential benefits stem from the titular feature of microfluidic – small volume of the reactor. Other improvements are not directly related to the volume of the reactor, but can be more easily realized in microfluidic setting.

High surface/volume ratio

As the radius of a sphere decreases, its volume decreases as its cube, but its surface area only decreases as its square. Therefore, smaller reactors have more surface area per unit of volume. This basic property of microreactors has several important implications for chemical processes. Thermal exchange with a temperature controlling media is defined by the area of contact between the reactor and heat-transferring material; therefore, it becomes much more efficient in the case of the microfluidic device. This starts a cascade of interrelated improvements. Increased thermal exchange leads to more uniform temperature distribution inside the reactor volume; it also leads to increased rate of temperature change, allowing for very rapid and even heating and cooling. In terms of chemical processes, that means that the reaction conditions can be tightly controlled, and there is no need to overheat part of the reaction mixture in order to increase the temperature of the whole reaction volume.

Low volume of the reactor can be a benefit in itself, as it might decrease the rate of radiolysis. Radiolysis is a degradation of a target molecule caused by the energy of the radioactive decay that occurred in the adjacent molecule. Obviously, once radionuclide incorporated into a molecule disintegrates, this molecule ceases to exist. The energy of this disintegration though is so large that it also breaks chemical bonds in the neighboring molecules, whose radionuclide has not yet disintegrated. This is a highly undesirable process, responsible for the formation of radioactive impurities in the final product.

The mechanism of radiolysis is poorly studied. Presumably it is mediated by free radicals formed at the disintegration event. It is noteworthy that the positrons formed upon disintegration of positron emitting isotopes scatter kinetic energy within several millimeters from the origin. The exact diffusion distance depends on the initial positron energy and varies between ~0.6 mm for ^{18}F to ~4 mm for ^{124}I.[7] That is, positron energy emitted by ^{18}F nuclei is distributed along a path of approximately 0.6 mm. In theory, if a significant portion of this energy is scattered outside of the reactor volume, the rate of radiolysis should be diminished. Therefore, if the reactor dimension is smaller than the positron diffusion path, it is logical to expect a diminished radiolysis rate.

Another important consequence of high surface/volume ratio is greater mechanical strength. It is easier to withstand high pressure within a small cavity than in a conventional vessel.

High reagent concentration

The key distinction of radiochemistry from conventional chemistry is the trace amounts of radioactive reagents. Concentrations of the radioactive molecules in the mixture are often lower than concentrations of the impurities introduced with solvent and other reagents. The lack of control over the nanomolar level of radioactive materials causes notorious fluctuation in radiosynthesis efficiency. Not only does low concentration of the key reagent make all processes kinetically unfavorable, but the presence of the impurities, not significant enough to be controlled in macroscopic synthesis, become significant in the radiochemical setting.

Assuming that the same number of radioactive atoms is used, lower volume reactor will provide higher concentration of radionuclide. To realize this opportunity, an efficient system for the radioactivity concentration has to be developed as well.

Low amount of reagents used

To maintain the prescribed concentration of reagents, smaller amounts of these reagents are needed in a smaller reactor. Aside from the obvious economic benefits, this feature has a major impact on the purification process. At the end of the chemical synthesis, the reaction mixture always contains overwhelming amount of impurities, often chemically similar to the target product. Purification is usually performed by semi-preparative high performance liquid chromatography (HPLC). Use of a lower amount of starting material decreases the amount of the mixture to purify, thus reducing the size of the column needed for the purification. Smaller columns are normally more efficient, due to better packing of sorbent, which makes the purification process more reliable.

Additionally, smaller columns operate at lower absolute flow rates, thus increasing concentration of the purified product. This is a desirable property

in a number of cases. The strength of the final dose can be important in the case of ethanol-based eluent, when the eluent is used directly for injection and the amount of injected ethanol limits the injectable volume. It is also important if other organic solvents are used in eluent. A process called 'reformulation' or 'reconstitution, is then performed to replace toxic organic solvent for less toxic ethanol. A large volume of the solution to be reformulated has a detrimental effect on the efficiency of this process. Finally, in case of preclinical applications, the maximum volume allowed for injection can be as small as 200 μL in the case of a mouse.

Therefore, due to cost savings, increased purification efficiency, and increased concentration of the final product, an opportunity to reduce the amount of the starting material is greatly desirable.

High automation

Any microfluidic device developed past the stage of a crude prototype is a highly automated system controlled by computer software. Remote operation of this device thus becomes natural, allowing for easy installation inside radiation shields – important requirements for production of radioactive compounds. Additionally, the exclusion of an operator reduces human error in production, and increases overall reliability.

17.3.2 Problematic properties of microfluidic devices

Despite its advantageous characteristics, microfluidic production of radiotracers has yet to become a commonly accepted technique. Several problematic features impede its wider acceptance in the radiochemistry community.

Macro to micro interface

A microfluidic reactor provides the option of performing the reaction in very concentrated solution, but an efficient concentration system is needed for quick conversion of radioactivity from 2 mL of target water supplied by cyclotron to several microliters of solution. For the initial proof-of-concept devices, this was of less concern and these experimental devices used small portions of the target water without any concentration. In the production environment, it is important to use all radioactivity produced by the cyclotron, while avoiding transfer losses.

Purification of the reaction mixture requires transfer of the microreactor content back to the macro-scale. Lossless transfer is of particular importance in this case, because a little volume left in the reactor can contain a significant portion of the product. Typically, this problem is resolved by using a vast excess of diluting solvent to carry the radioactivity to the purification

system. This solution though undermines the purification benefits microfluidic systems can potentially provide. Milliliter-scale solutions require semi-preparative setups for purification and the carrier solvent might be incompatible with the purification eluent.

Gathering feedback

Control of every process occurring in the chemistry module and a set of pre-run checks is prerequisite for reliable performance of a radiochemical module. Conventional radiochemical modules are equipped with a set of sensors reporting process parameters and system status. Parameters such as temperature, pressure in the reactor, as well as gas flow at the critical points in the plumbing system, are constantly monitored. Radioactivity detectors are normally installed in several critical locations in the instrument, providing real-time information on the radioactivity transfers. Additionally, cameras are often used to observe those parts of the instrument obstructed by lead shields.

Control of these parameters in the microfluidic device is an engineering problem in itself. No radiochemical devices have been reported so far that report temperature or pressure inside a microreactor. Gas flows through the reactor are easier to control, and some systems do provide this functionality. Accurate measurements of radioactivity in the integrated microfluidic chip, where distances between components do not exceed millimeters, is challenging at the current level of technology.

In this situation, the microfluidic radiochemistry modules operate under a set of unverified assumptions. Because of the lack of real-time information the operator cannot intervene and salvage a run even if that were possible, so that preventive maintenance and troubleshooting of the equipment become very inefficient. As a result, microfluidic devices installed in radiochemistry labs become ongoing projects, rather than reliable tools helping radio chemists.

Sensitivity to particulate matter

Advion NanoTek, the only commercial microfluidic device for radiochemistry, relies on a reactor with internal diameter of only 100 μm.[5] Solutions passing through tubing of this diameter have to be free of particulates, which is difficult to ensure due to the possible formation of the solids during reaction. Organic reactions often produce solid byproducts that can occlude the reactor. This becomes of practical concern in the absence of efficient fluid transfer control and pre-run diagnostics.

Specialized device manufacturing methods

Methods commonly utilized in the production of microfluidic devices require setups not widely available in radiochemistry labs. As a result, integrated

devices have to be built specifically for a particular radiochemical process, and can hardly be customized after. Systems coupling microfluidic reactors with conventional equipment, such as the NanoTek device, avoid this inflexibility at the expense of reagent and radioactivity losses occurring at each micro-to-macro interface.

Manufacturing of microfluidic devices is readily adaptable for mass production, but development of any particular device normally requires specialized equipment and only becomes commercially viable if mass scale application is anticipated.

17.4 Realization of promises: the superiority of microfluidic systems

The previous section presented a list of properties generally attributable to microfluidic devices, focusing on those relevant to radiochemical synthesis. These properties by themselves do not automatically confer any advantages to microfluidic systems. This section will review reports of the microfluidic systems surpassing conventional systems in at least some aspects.

17.4.1 Main microfluidic device types reported

Reactor classification adopted in classical chemical engineering is well applicable to the microfluidic radiochemistry platforms. There are two conceivable types of reactors: flow-through and batch. Combinations of these also exist.

The flow-through reactor in its typical form is a long channel (or a vessel with a mixer) kept at a predefined conditions. Reagents are continuously infused into the reactor and then the mixture of products is continuously collected at the outlet. This type of reactor is widely used in the chemical industry where it allows for uninterrupted production of product dependent only on the continuous supply of the reagents. Early examples of the microfluidic devices applied for radiochemical synthesis followed this principle.

The first example of such a device was disclosed in 2003 in the form of patent applications by Brady *et al*.[1] The patent introduced a series of novel ideas. First, this was the earliest publication that focused on microfabricated devices for radiochemical synthesis. Second, the patent application described a device integrating all aspects of radiopharmaceutical production, from processing of the cyclotron output to the quality control of the final dose. Third, the apparatus described in the published examples was designed to perform radiolabeling with a wide range of radioisotopes: ^{18}F, ^{11}C, and ^{124}I. Fourth, an important innovation with this patent was the sequential connection of two identical chips for a two-step synthesis. This concept was implemented

in a form of a T-mixer, followed by a long reaction channel etched on a glass substrate and covered by another layer of glass. The reagents were infused using syringe pumps, the temperature of the chip being controlled with an external heater. In the reported examples, all processes, aside from mixing and reaction, were performed in a conventional manner and decay corrected radiochemical yield (RCY) of FDG was 24%, unacceptably low by modern production standarts.[8] A series of more sophisticated and automated devices based on this platform was later reported by the same group of authors, but the RCY of FDG remained unimpressive.[9–11] Substantial reduction on process time was also reported by the same group.[12]

Another group reported a microfabricated device for radiochemical synthesis almost at the same time.[13] The device featured a very similar architecture: a T-shaped channel (220 μm (W) × 60 μm (D) × 14 mm (L); and total volume 0.2 μL) located at the interface of two bonded borosilicate glass layers. Two entry ports were connected to precision syringe pumps, and one exit port led to a collection reservoir (Fig. 17.1). The apparatus was used for alkylation of a carboxylic acid with [^{11}C]-MeI and [^{18}F]-FCH_2CH_2OTos. Yield as high as 88% was reported for the former reaction, while RCY for the later one did not exceed 10%. This early prototype already demonstrated a high degree of the control microfluidic technology can provide for radio chemists. Just by changing the infusion rate, authors could modulate the reaction time with high precision and reproducibility. Soon after, another continuous flow design based on the simplest flow-through vial was published.[11] In this design, the volume of the reactor was made up of a coin-shaped disk with inlets and outlet. The feasibility of very fast FDG synthesis was demonstrated using this design: 50% of radioactivity was converted to protected FDG in just 4 s. The design of a continuous flow reactor combining a series of flow-through cavities connected with capillaries was later investigated by others.[14]

Flow-through reactors proved particularly useful for the labeling procedures involving gaseous radioactive precursors. The high liquid–gas surface achievable in a microfluidic reactor was used for carbonylation reactions involving gaseous [^{11}C]-CO.[4,15]

The high degree of reaction control, and the ability to sample process conditions in fine steps, encouraged commercialization of the flow-through microfluidic reactors. Advion currently offers a configurable microfluidic system under the 'NanoTek' brand (Fig. 17.2).[16] The central part of the machine is a reactor manufactured from fused silica and housed in a thermostated brass cartridge. One cartridge houses two-meter long 100 μm diameter tubing with total volume 15.7 μL; the cartridges can be linked together to increase the length and volume of the reactor. The key feature of the system is its ability to perform a series of experiments sampling just one parameter at a time. That is normally done even with the same batch of the ^{18}F-K_{222} complex and the same batch of the precursor solution that eliminates variability

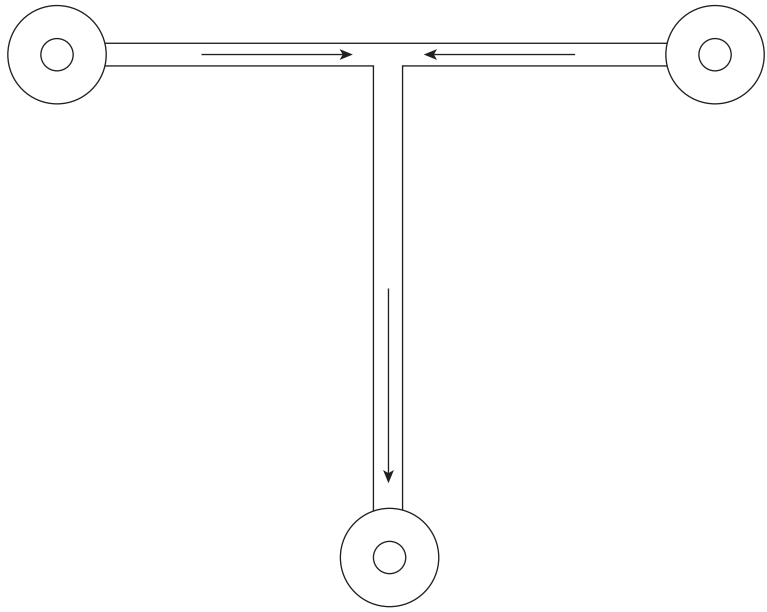

17.1 The simple T-shaped microfluidic reactor reported by Lu *et al*. Reagents enter from the two ports and the product is collected at the outlet. (*Source*: Reproduced with permission from Lu, S. *et al.*, *Lab on a Chip* 2004, **4**, 523–5.[13])

associated with trace impurities (e.g. moisture). Commercial availability of a microfluidic system stimulated a series of reports on detailed optimization of reaction conditions of several important radiochemical transformations. The system was used for labeling with both ^{18}F[5] and ^{11}C.[17] More than 30 compounds have been radiolabeled using this device, some of them involving complex synthetic procedures.[18] In order to enable sequential transformations, a simple T-mixer can be installed downstream from the reactor. The mixer combines the output from the first reactor with a stream of reagent needed for the next step, and feeds the mixture into the second reactor.[19] Nevertheless, it has been a trend that after careful study of the reaction with the microfluidic apparatus, authors opted for conventional synthetic modules for large scale production, and Section 17.5 will be discussing this in more detail.

As opposed to the flow reactor, the batch reactor in its classic form is a vessel that is loaded with reagents and then the product mixture is unloaded after the content has been treated under certain conditions for a predefined time.

In fact, a series of machines built upon the so-called captive-solvent method can be considered the first generation of microfluidic devices with mixed batch-flow architecture. The devices were used for preparation of

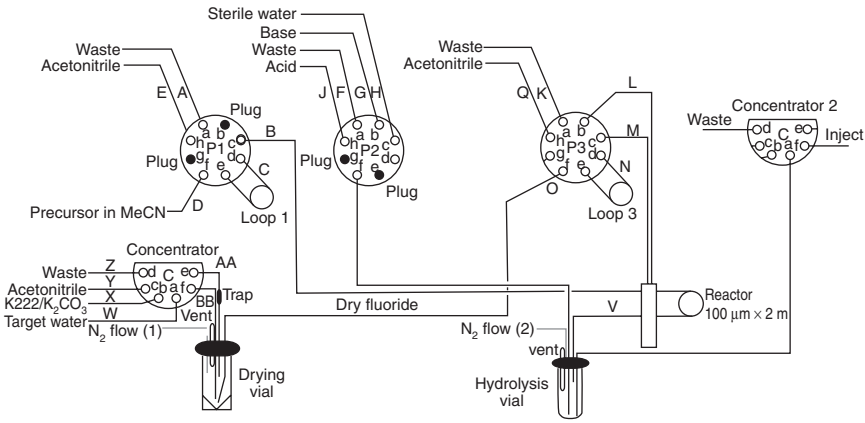

17.2 Principal schematic of one of the configurations of Advion 'NanoTek' system. The system is built in the form of several independent blocks, which can be plumbed and reconfigured according to specific needs of each synthesis. Note dedicated vial for fluoride drying. (*Source*: Reproduced with permission from Ravert, H. T., Holt, D. P. & Dannals, R. F. *Radiochemical Synthesis* 2012, 139–154.[16])

[^{11}C]-labeled radiopharmaceuticals as early as 1985.[6,20,21] The central feature of these machines was a reactor in a form of a long tube. In some cases, the long tube was packed with an inert porous material. The inner surface of the tube was covered with a concentrated solution of the labeling precursor. Gaseous radioactive precursor was then passed through the reactor and the radioactivity was trapped in the tube due to the labeling process. A typical example[22] of the captive-solvent apparatus is illustrated in Fig. 17.3.

The volume of the reactor in these devices ranged from 125 to 500 µL. However, the real reaction volume was most likely considerably smaller, because the reagent captured in the reactor was only spread over a thin layer. In terms of the hardware the devices were more similar to the Advion setup, than to the later generation microfluidic batch reactors; however, the captive-solvent process is a clearly batch method, as it involves sequential loading of the reagents and only a finite amount of the product produced in one run. This early research revealed long before the 2003 Bradley patent application that radiosynthesis in a small volume benefits from low precursor consumption, easy purification due to low mass of impurities, and high labeling yield.[20]

There are two critical advantages of the batch reactors as compared to flow-through reactors. First, production of the radiopharmaceuticals is inherently batch process: the cyclotron produces radioactivity in batches, and the flow reactor will operate out of its optimum mode in this situation. Second, performing a multistep synthesis in a flow-through reactor is

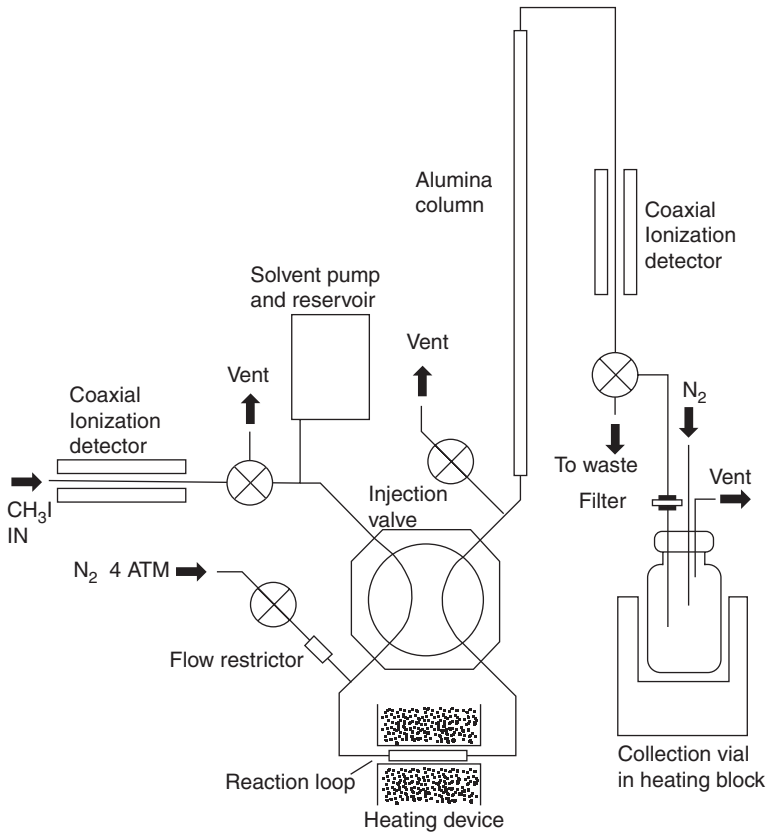

17.3 Schematic of a captive-solvent apparatus for ^{11}C-methylation. The reactor is coated with concentrated solution of precursor prior to the reaction, the original design of the heating device allowing for rapid changes in temperature. Reactor volume is 124 μL, and reactor volume is further decreased and surface increased by filling with acrylic yarn. (*Source*: Reproduced with permission from Watkins *et al., Applied Radiation and Isotopes* 1988, **39**, 441.[22])

inherently difficult, due to cross-contamination between reagent streams and technical difficulties of switching from the solvent of the first reaction to a solvent suitable for the second one. Due to these considerations, batch microfluidic devices received early attention.

A fully integrated microfluidic device, performing on one chip all the synthetic operations needed for production of FDG (Fig. 17.4), was in fact one of the first reported devices.[23] A complex pattern of channels and valves enabled all necessary processes: fluoride concentration, drying, radioactivity incorporation, hydrolysis, and evaporation. In just 14 min this circuit produced enough FDG for a mouse image. The main drawback of the device

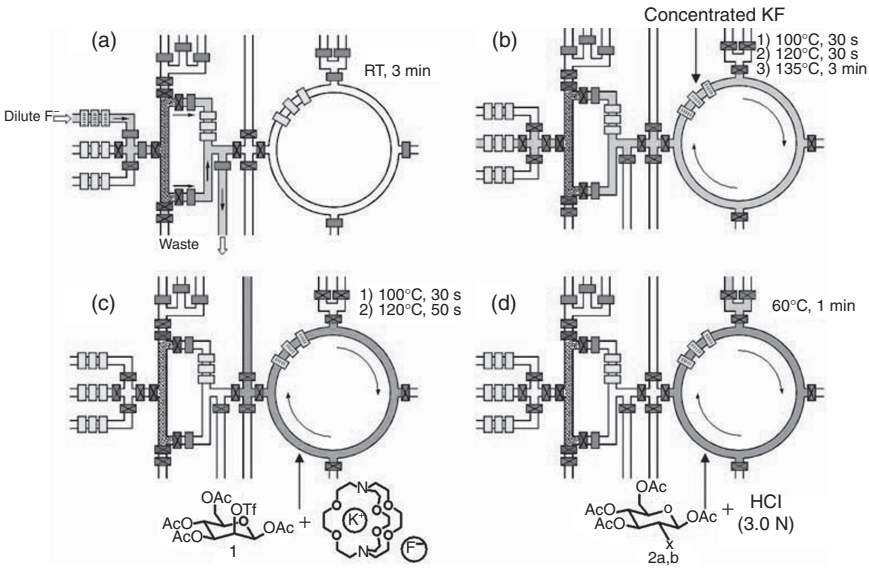

17.4 Schematic diagrams showing main steps of FDG production in an early batch reactor (a) Concentration of dilute fluoride ion. (b) Evaporation of water from the concentrated KF solution. (c) Fluorination reaction. (d) Hydrolysis reaction. The entire device is made out of PDMS; valves are hydraulically actuated (see original publication for further explanation). (*Source*: Reproduced with permission from Lee C.-C. *et al. Science* 2005, **310**, 1793–6.[23])

was a very low overall yield (26%), the result of interaction of free fluoride with polydimethylsiloxane PDMS, the polymer used for the device fabrication.[23] Microfabrication technology allowed bringing together components that normally constitute separate hardware blocks, such as valves, pumps, and ion exchange column. Integration of all components on one device was the first step toward the production of cheap integrated circuits for use in the radiochemical processes. Use of an elastomer for fabrication of this complex structure was critical, as all valves in the device relied on the elastic properties of the material. A recent 'digital' batch microfluidic device, reported for optimization of protein labeling,[24] also relies on PDMS for its operation.

The latest development in batch microfluidic radiochemistry is an application of electro-wetting-on-dielectric (EWOD) method for control of liquid movement. In the previous example, segregation of the chip into distinct process zones is achieved with the mechanical valves. The EWOD device (Fig. 17.5) uses an electromagnetic field to control movement of independent droplets, and thus different zones of the reactor are separated not by valves, but by gas surrounding droplets. The first EWOD synthesis of radiopharmaceutical was reported as part of a conference presentation[25] and

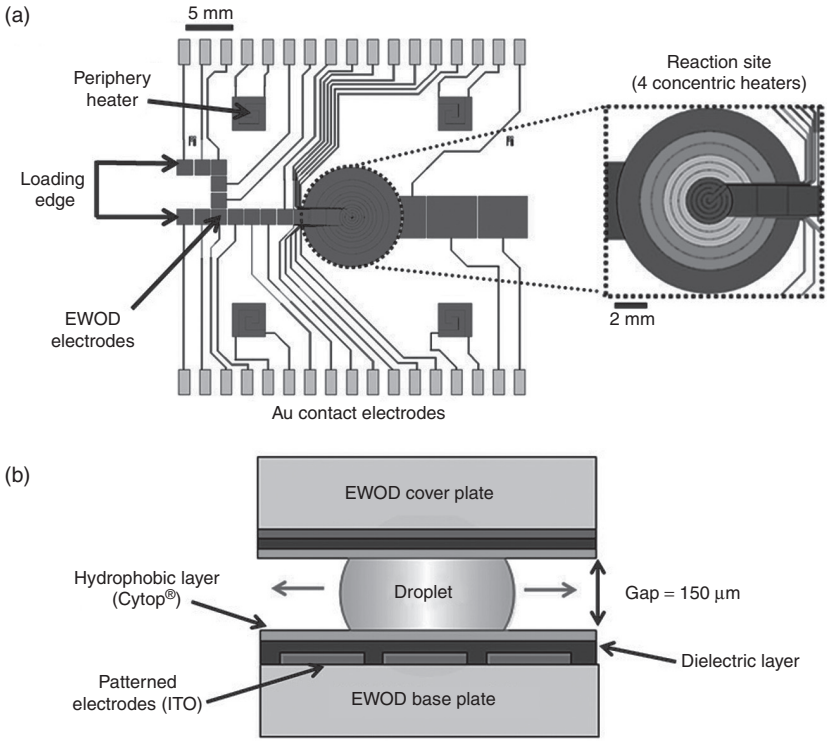

17.5 (a) EWOD microchip with four concentric heaters (dashed circle) with a maximum volume of 17 μL. Inset shows the magnified area of the heater with four concentric individually controlled resistive heating rings. (b) Schematic side view of the EWOD chip sandwiching a reaction droplet between two plates coated with ITO electrodes, a dielectric layer, and a hydrophobic layer. (*Source*: Reproduced with permission from Keng, P.Y. *et al*. *PNAS* 2012, **109**, 690–5.[26])

recently disclosed with full details.[26] Several reported advances include, but are not limited to, use of the same electrodes to change the temperature and receive feedback, absence of mechanical parts, and use of a Cherenkov camera to monitor radioactivity.

Use of microfluidic reactors recently brought microfluidic technology to an important milestone: the first clinical PET image obtained with microfluidically produced radiopharmaceutical. The synthesis of the tracer was performed with P-IV machine, a late stage prototype developed by Siemens Molecular Imaging (Fig. 17.6).[27] This fully integrated system includes all necessary parts for successful clinical production of a radiopharmaceutical, starting from concentration of fluoride and up to the optional reformulation of the final product. The machine is based around a 50 μL reactor,

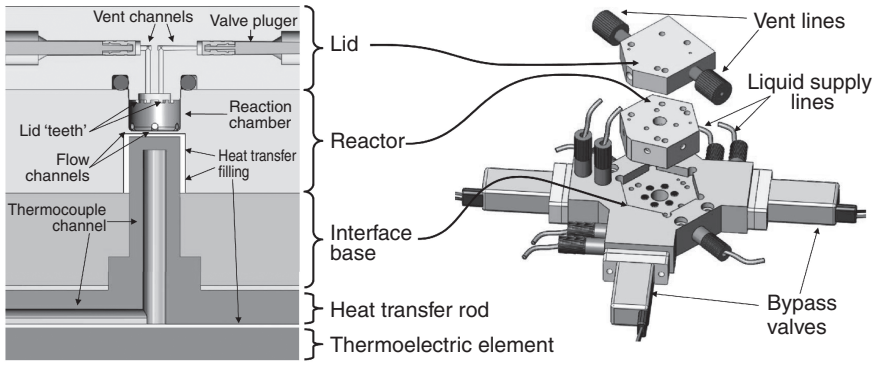

17.6 Main parts of the reactor assembly used in clinical production of ^{18}F-Fallypride. Left: Schematic cross-section of the reactor cavity, lid, and heater; Right: 3D rendering of the same parts.[27]

made up of a PEEK chip and transparent polydicyclopentadiene (PDCPD) lid. The reactor utilizes on-chip pneumatically actuated valves for liquid control. Demonstration of clinical capabilities is admittedly simplistic: [^{18}F]-Fallypride production performed in one step, followed by a specially designed purification procedure eliminating reformulation. The capability of the system to perform multistep complex reactions was demonstrated separately.[28]

17.4.2 Superior reaction control and low variability

The extreme conditions needed for efficient radiolabeling also promote unwanted processes, including decomposition of the final product and side reactions. Successful radiolabeling is therefore a product of fine balance between reaction time and temperature favoring labeling and not decomposition. Another challenge for reaction control arises from the fact that the radiolabeling reactions always occur at very low concentrations of the radioactive atoms. Concentration of the impurities coming from the reagents and solvents is often much higher than the concentration of radionuclide. Hence, relative rates of the desire labeling reaction and competing reaction with impurity vary unpredictably. Therefore small variations in the reaction conditions can dramatically affect the net outcome of the labeling process.

Conventional reactors are based on 1–10 mL reaction vessels coupled to various supporting parts with tubing and valves. Accurate monitoring and precise control of the actual reaction parameters is complicated by several factors. First, heat transfer from the heating element occurs at a finite rate thus creating a temperature gradient inside the reactor and complicating temperature control. Precise time control is also difficult, for heating and

cooling of the reaction mixture consume significant time. For example, in a typical heating profile observed on a Siemens Explora GN module, heating of the reaction mixture to 140°C can take as long as 3 min, which is comparable to the duration of most radiochemical reactions. Second, the headspace in the reactor does not have the same conditions as the main batch of the reaction mixture, which further complicates control of the reaction conditions. As a result, the temperature profile in a conventional reactor is rarely known and predictable.

Microfluidic reactors, particularly those based on the flow-through principle, can effectively address these problems. It is assumed that due to the low absolute heat capacity of the reaction mixture, its temperature is equal to the temperature of the heating media, and the reaction time is defined by residence time in the reactor. Additionally, variability introduced by human error is reduced in microfluidic reactors due to the high degree of automation. Several researchers employed these advantages to elucidate the relationship between the reaction parameters and efficiency of radionuclide incorporation.

Superior process control in microfluidic reactors was first demonstrated in its simplest form in the captive-solvent apparatus developed for ^{11}C-acetate production. The amount of radioactive byproducts arising from sequential reactions of the initially formed radioactive adduct was minimized by easy control of the carboxylation time.[21] Using a custom-built flow-through reactor, a group of authors from Seoul University studied the kinetic parameters in a series of nucleophilic radiofluorination reactions.[29] The microfluidic setup allowed for tight control over the reaction conditions, thus reducing variability in the labeling reaction outcome. Consequently, temperature dependence of the radiolabeling efficiency was elucidated with a high degree of certainty (Fig. 17.7). In the pioneering paper by Lu *et al.*[13] the high degree of control provided by the microfluidic setup was also employed to study alkylation of carboxylic acids by various radiolabeled alkylating agents, including [^{11}C]-methyliodide. A practically important example of this reaction is a synthesis of ^{11}C-labeled benzodiazepine receptor ligand. The authors suggested that the rate of radiolabeling was primarily determined by the mixing of the reagents, and that a more optimized reactor configuration could have allowed for even better mixing. Study of another diffusion limited reaction, synthesis of deuterium-labeled amides, performed with a nearly identical device, also yielded similar residence time-conversion curves.[30]

Commercial availability of a flow-through microfluidic apparatus encouraged a series of publications detailing the efficiency–conditions correlation with previously unattainable precision. Optimization of the reaction time and the process temperature using NanoTek technology was done for many radiofluorination reactions.[18,31–33]

A particularly illustrative example is a study of reaction of [^{18}F]-fluoride with *ortho*-substituted diaryliodonium salts, where NanoTek machine was

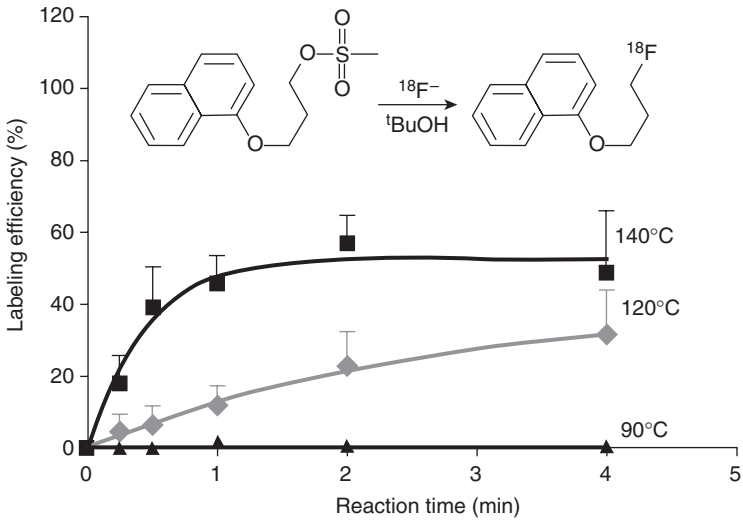

17.7 Correlation between the residence time, temperature, and the radiochemical yield was elucidated with simple flow-through microfluidic reactor. High degree of control provided by microfluidic apparatus provided for low variability, thus increasing experimental accuracy. (*Source*: Reproduced with permission from Yang, B.Y. *et al*. *Tetrahedron* 2011, **67**, 2427–33.[29])

employed to control reaction time with accuracy on the scale of seconds, and a rigorous investigation was performed to determine the reaction efficiency and selectivity at various temperatures (Fig. 17.8).[34] It is important that the machine provided for the use of multiple small portions of the fluoride solution drawn from the same batch. This way water concentration, an important player in the reactions of fluoride anion, was kept constant while other parameters were probed. More than ten consecutive experiments could be performed with the same batch of fluoride. The tight control allowed the investigators to determine the rarely reported activation energies for the reactions of radioactive fluoride. The NanoTek apparatus was later used by the same group to investigate fluorination of meta-substituted analogs.[35] The knowledge obtained from these model reactions enabled the authors to develop a synthesis of a series of radioligands for brain mGluR5 protein. The synthetic procedure was again optimized using the NanoTek apparatus.[36] Large scale production, however, was performed using conventional technology. The group continued to explore the synthesis of [^{18}F]-labeled ligand for imaging brain peripheral benzodiazepine receptors with the NanoTek apparatus.[37]

The NanoTek apparatus was used to probe an array of reaction parameters in the production of the hypoxia imaging agent [^{18}F]-FAZA.[38] It was

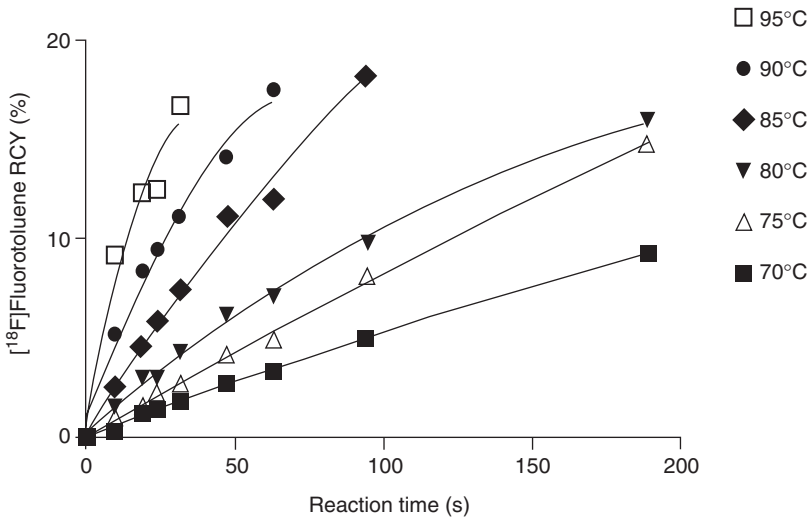

17.8 An example of the extensive sampling of the reaction parameters attainable with NanoTek apparatus. (*Source*: Reproduced with permission from J.-H. Chun, S. Lu, Y.-S. Lee, and V. W. Pike, *Journal of Organic Chemistry*, 2010, **75**, 3332.[34])

discovered that the optimal temperature for the reaction was 120°C. An extra 20°C led to degradation of product, while temperatures lower than optimal resulted in reduced fluoride conversion. The optimal reaction time was 5.3 min. The fluoride to precursor ratio was also optimized using NanoTek. Unfortunately, it is difficult to draw any conclusions of the production efficiency of the developed method because the overall efficiency of the process was only judged by the HPLC analysis of the reaction mixture.

Production of another important radiopharmaceutical, [^{18}F]-Fallypride was studied using NanoTek.[5] Figure 17.9 demonstrates the dependence of RCY on the reaction temperature. Several important conclusions can be drawn from these data. The most important is the fact that the decomposition does not affect the reaction, even at higher temperatures. What is even more interesting is that these two data curves were obtained at two different research centers. Considering the variability in the data published on the subject using conventional apparatus,[39] such reproducibility is definitely noteworthy. Two-step reactions were also studied using NanoTek as well. As has already been mentioned, two flow-through reactors can be linked sequentially to perform multistep processes. A synthesis of [^{18}F]-fluorocholine derivatives, comprising synthesis of fluoroalkylating agent followed by alkylation of choline, was studied using a microfluidic device.[40] Fine control over the parameters of the second step allowed the authors to establish the optimal concentration with a high degree of certainty.

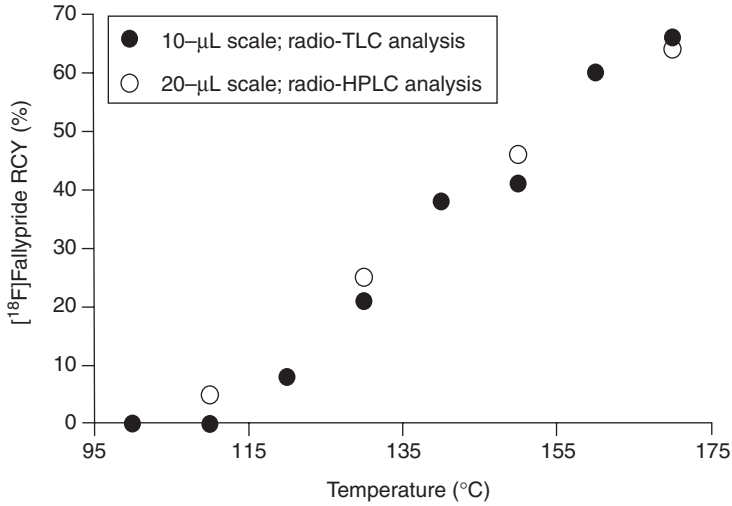

17.9 Example of high stability of the observations made with a microfluidic apparatus. Effects of reaction temperature on the RCY of ^{18}F-Fallypride determined in two different laboratories. (*Source*: Reproduced with permission from S. Lu, A. M. Giamis, and V. W. Pike, *Current Radiopharmaceuticals*, 2009, **2**, 49.[5])

Radiolabeling with ^{11}C can also be successfully performed with NanoTek if the radioactive precursor is dissolved in an appropriate solvent.[41] Palladium-catalyzed incorporation of [^{11}C]-CO into the amide molecule was studied using the apparatus when the monoxide molecule was bound in a form of copper complex. The critical problem associated with the synthesis is an incorporation of [^{11}C]-CO into a urea by-product. The issue was alleviated after a careful study of the reaction selectivity at various temperatures. ^{11}C methylation reaction was also studied with the NanoTek apparatus.[42]

A comparison of NanoTek with a conventionally sized microwave-heated reactor illustrated the degree of control a microfluidic apparatus can provide.[43] Authors noted for a ^{99m}Tc-labeling procedure that a microwave apparatus takes 1.5 min to reach the set temperature, followed by overheating by 5°C. Subsequent cooling to the set temperature also takes at least 1.5 min. These delays were eliminated in the flow-through microfluidic device.

Aside from the precise control over the time and temperature, microfluidic devices allow rapid changes in temperature due to the low absolute heat capacity of the reactor and its content. This was demonstrated in the 'captive-solvent' apparatus for ^{11}C-methylation. Reactor temperature could be changed in the range from –50°C to 60°C in a matter of a few seconds. This feature was used to capture methyl iodide gas at low temperature and then to perform the reaction at higher temperature, all within minutes.[22]

The ability to perform reactions at elevated pressure with only a small amount of radioactive gas is required for radiolabeling involving many ^{11}C precursors. High pressure reactors are also desirable for performing reactions in overheated volatile solvents. Microfluidic reactors are well suited for this purpose because total force exerted on capillary walls is less than the force a large reactor experiences under the same pressure. This advantage was first demonstrated using a 500 μL stainless steel capillary reactor for carbonylation reactions with [^{11}C]-CO. The reaction was carried out at 5000 psi pressure created with an HPLC pump, conditions unattainable with most conventional radiochemical modules.[44] Micro-autoclaves were also developed around this feature of microreactors. A patent application form 2002 describes carbonylation process in a 200 μL microplug in which concentrated carbon monoxide is compressed to occupy only 10% of the reactor volume.[45]

A vivid demonstration of this advantageous feature was presented in a recent paper describing palladium-catalyzed synthesis of amides from amine, aryl halide, and [^{11}C]-CO.[15] For this reaction, the authors developed a custom reactor etched in a borosilicate glass. The reactor was built similarly to the T-shaped flow-through reactors discussed above, and featured a 5 m long channel downstream of the mixing junction. A stream of [^{11}C]-CO in a carrier helium gas and toluene solution of the precursors and catalysts was infused through the mixer. The ability to keep minute amounts of gas at a certain pressure allowed the reactor to operate at annular flow regime and ensured efficient contact between gas and liquid. The high pressure rating of the NanoTek reactor was critical to the success of a similar carbonylation reaction utilizing a solution of complexed [^{11}C]-CO.[41] Preliminary studies revealed that the optimal temperature for reaction selectivity was 200°C, which is much higher than the boiling point of MeCN (82°C) used as co-solvent. Although it is technically challenging to construct a conventional reactor suitable for these conditions, the NanoTek capillary reactor allowed for fluorination at this temperature with no loss of radioactivity.

A digital microfluidic device reported recently had demonstrated a high level of reaction control in terms of the ability to precisely change the reagent ratio in a series of automated experiments.[24] The device forming droplets of reagent mixture separated by gas gaps were manufactured out of PDMS elastomer. Liquid transport was controlled with hydraulically actuated valves. Droplets were generated in a long channel, connected to storage containers. To achieve control over the droplet composition, valves were used to subdivide the mixing channel into multiple subvolumes. The composition of the droplet generated in the channel could be regulated by independent filling of the subvolumes. For example, there were five subvolumes available for mixing of the precursor solution with the buffer solution. Filling one of them with the precursor solution, and four with buffer, produced droplets with 4:1 ratio of diluted protein. The total volume of the

droplets was maintained constant. Thus, the composition of each droplet could be independently controlled. To increase the number of the reagents available for the study, the inlets into the mixing channel could be coupled to a reagent distribution chip. This way, different reagents (for instance, various buffers) could be used in the same automated process. This setup allowed for rapid and repetitive sampling of multiple parameters appropriate for protein labeling.

17.4.3 Improved product yields and reaction kinetics

Radiochemical reactions involve trace amounts of radioactive isotopes, and the actual concentration is on the scale of nanomoles even at high levels of radioactivity. Utilization of a microreactor enables a higher radiolabeling rate by concentrating a radioactive precursor and more efficient competition with side processes. Additionally, reaction conditions are easier to optimize in a microfluidic apparatus (*vide supra*). In the repetitive production less deviation from the established conditions occurs. Combined, these factors often improve the product yield. Although nearly all reports on microfluidic processes claim improved reaction yields, only a few are suitable for direct comparison with conventional modules. This is presumably due to the fact that the reaction conditions found optimal for microfluidic reactors do not match optimal conditions for the respective conventional reactor process.[37]

Enhanced kinetics in a capillary reactor was recognized in 2000 for the reaction of ^{11}C-MeI and amines at room temperature in captive-solvent reactor.[20] Previous reports conducted the same reaction in a conventional setup at 90°C.

Very fast reaction kinetics was established at the onset of the microfluidic radiochemistry. Conversion of [^{18}F]-fluoride reached 25% within 6 s in a reaction with mannose triflate.[46] The same reaction was reported to occur quantitatively in a microfluidic coin-shaped reactor, although overall performance of the device was hindered by the use of PDMS material.[47] Likewise, a batch microfluidic device was claimed to demonstrate exceptional performance in the production of [^{18}F]-FLT (85% yield after HPLC) in a patent application.[48]

As the technology matured, real production benefits were shown as well. Preparation of FDG was accelerated in a custom-built capillary reactor. Reaction of mannose triflate with ^{18}F fluoride required only 40 s for 88% conversion at 105°C. Subsequent quantitative hydrolysis of the intermediate by 0.3 M NaOH for 1 min at 40°C afforded pure FDG with 88% RCY in less than 7 min.[49] This is an impressive improvement if compared with the conventional 50–60% over 40–50 min.[50] The NanoTek microfluidic apparatus showed a yield improvement in production of hypoxia tracer [^{18}F]-FAZA.[38] Starting from less than 0.5 GBq of fluoride, the decay corrected radiochemical

yield was reported to be 63% after HPLC purification. Initial radioactivity of 2.1 GBq gave only 40% yield, which is still significantly higher than the 20.7% ± 3.5% efficiency reported for conventional modules.[51] Similarly, NanoTek compared favorably to a conventional system in the production of [^{18}F]FE@SUPPY and [^{18}F]FE@SUPPY:2 adenosine A3-receptor tracers. A statistically significant increase of 6.7% (from 88.2% to 94.1%, p-value < 0.0001, n = 11) for [^{18}F]FE@SUPPY, and of 102% (from 42.5% to 95.5%, p-value < 0.0001, n = 5) for [^{18}F]FE@SUPPY:2, were observed. Overall, synthesis time was reduced for the microfluidic preparation by 52–65 min.[31]

The kinetic benefits of a microreactor were highlighted in a study comparing click reaction between peptide bearing carbon–carbon triple bond and [^{18}F]-β-fluoroazidoethane in a custom-built microfluidic reactor and conventional macro-scale reactor.[52] Authors took a unique approach, using the walls of the reactor as a catalyst for the labeling step. The microfluidic reactor was formed by a 1.0-m long copper capillary with 0.56 mm internal diameter. The reagents were premixed and infused into the reactor, kept at 80°C. The first pass afforded 85% conversion by HPLC analysis, and the second pass through the reactor completed the reaction. This could not be achieved in a vial reactor with copper powder, even with increased peptide concentration.

Production of [^{18}F]-FSB, an important prosthetic labeling group, was considerably improved using Siemens P-IV microfluidic batch reactor. Original publication describing one-step synthesis of this compound cited 44% decay corrected yield in 60 min.[53] Optimization of reaction conditions revealed that temperatures unavailable in a conventional reactor due to the solvent boiling are, in fact, beneficial for the synthesis. Combining this finding with higher fluoride concentration, the authors developed a method yielding 64% of the target material in 25 min production.[54]

An illustrative example was recently reported that directly compared a microfluidic NanoTek apparatus, a microwave reactor, and a conventional module.[43] A group of authors from McMaster University, Canada, compared all three technologies in a model reaction of ^{99m}Tc carbonyl complex with a popular ^{99m}Tc chelate dithiazole valeric acid (Fig. 17.10). They discovered that the conventional module required chelate concentration of no less than 1 mg/mL and 30 min of heating at 80°C to furnish a complete conversion of the radioactive precursor. If the chelate concentration was lowered to 0.1 mg/mL, the conventional apparatus only demonstrated moderate conversion, while the reaction in the microfluidic setup was completed in less than 8 min. A microfluidic platform outperformed the microwave apparatus at 0.01 mg/mL of the chelate, despite incomplete conversion. Markedly increased performance was surprising considering that the concentrations of all reagents including ^{99m}Tc precursor were the same in these experiments. Notably, not only radiochemical yield, but radiochemical purity was

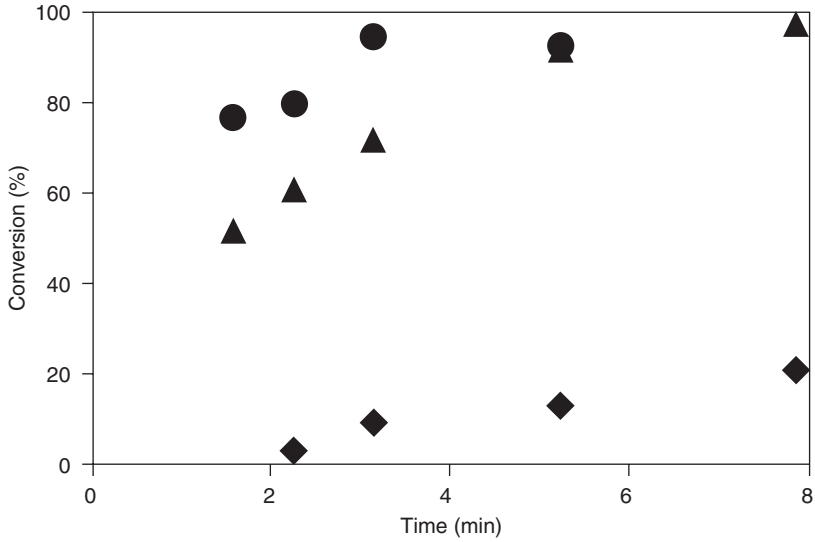

17.10 Conversion vs time plots for the $[^{99m}Tc(CO)_3(H_2O)_3]$+labeling of 0.1 mg/ml of dithiazole valeric acid at 80°C. (▲) microfluidic reactor; (•) microwave reactor; (♦) conventional reactor. (*Source*: Reproduced with permission from Simms, R. W. *et al. Journal of Labelled Compounds and Radiopharmaceuticals* 2012, **55**, 18–22.[43])

improved as well. This is a clear sign that the reaction kinetic parameters were affected, and the rate of product formation relative to formation of impurities was increased.[43]

Another example of direct comparison between a microfluidic reactor and a conventional setup is reported with copper labeling of DOTA-RGDfK conjugate.[14] A custom flow-through reactor with interim storage volumes was evaluated. Reagents were injected into the reactor through the areas of passive mixing. The content of the reactor was thermostated for a certain time after filling the storage volume. The mixture was then purged out with buffer solution. Figure 17.11 clearly demonstrates the advantage of the microfluidic reactor over the conventional vial. The authors explain this improvement with enhanced heat and mass transfer in the microfluidic reactor. Interestingly, a smaller volume of the reaction mixture does not bring the vial reaction closer to microfluidic results.

Two important points need to be made with respect to the reported improvements of the yield. First, it is common to report yield averaged over ten or more production runs in the literature on radiochemistry. In the light of yield instability, discussed above, a yield averaged over two or three runs bears low validity. This issue is increasingly recognized by the developers of the microfluidic devices.[26] Second, the ratio of radioactivity in the injectable

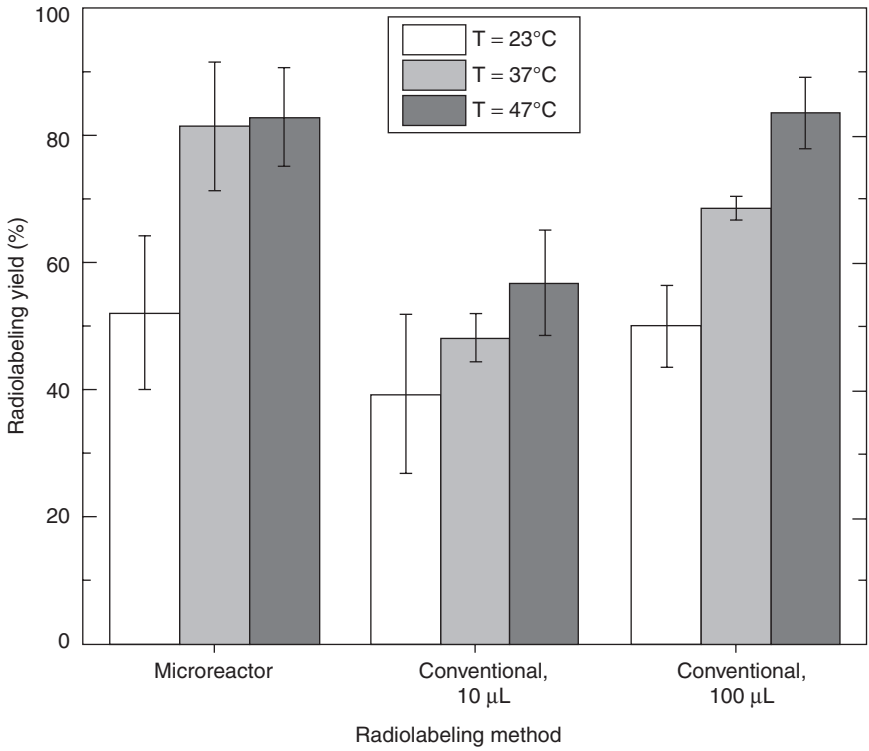

17.11 Direct comparison of microfluidic and conventional vial synthesis. Incorporation of ^{64}Cu into a DOTA moiety attached to an RGD peptide was studied in a conventional non-automated vial reactor and in an in-house made flow-through microfluidic device. (*Source*: Reproduced with permission from T. D. Wheeler, D. Zeng, A. V Desai, B. Önal, D. E. Reichert, and P. J. A. Kenis, *Lab on a Chip*, 2010, **10**, 3387.[14])

form to the radioactivity delivered by cyclotron, total production yield, needs to be reported in order to gauge the value of a technology presented in a particular publication. Many publications cited above only report the radiolabeling efficiency that is the fraction of the product in the mixture of radioactive species obtained from the reactor. The latter does not take into account losses associated with the radioactivity preparation (concentration, drying, complexation, etc.), product purification and transfer.

17.4.4 Simplified integration with downstream processes

Nearly all radiotracers produced for clinical or preclinical use have to be purified after radiolabeling. Semi-preparative HPLC is the most common method for purification of radiopharmaceuticals. In a typical purification

procedure, reaction mixture is purified on a 10 × 250 mm reversed phase column with acetonitrile/aqueous buffer mixture as a mobile phase at a flow rate of 5–10 mL/min. These conditions are usually sufficient to separate tens of milligrams of organic matter formed in the labeling reaction.

When radiotracer is produced in a microfluidic apparatus, the overall purification process can be simplified by enrichment of the reaction mixture with the target compound. This fact arises from a simple consideration that the amount of the produced radiotracer solely depends on the amount of a radioactive material, and not on the non-radioactive precursor. In contrast, the amounts of the contaminants accompanying the product in the reaction mixture increases proportionally to the amount of the cold reagents loaded into the reactor. Microfluidic devices normally produce around 1 mg of mixture, making possible use of smaller chromatographic columns. Several groups have reported purification of the microfluidically produced tracers on analytical columns, typically 4.6 × 250 mm, at 1–2 mL/min flow rate. Smaller columns usually have higher resolution, which improves chances of successful purification of the product.

This advantage was noted in an early paper on the synthesis of ^{11}C-palmitic acid via the captive-solvent method.[6] Later the concept was exploited in the synthesis of [^{11}C]-flumazenil.[55] An exact volume for the reactor reported in that publication is difficult to estimate, as it was made in a form of a tube packed with stainless steel powder. The amount of precursor did not exceed 0.04 mg, thus permitting analytical (d = 4.6 mm) column for purification. Later, the concept was applied in the [^{18}F]-Fallypride synthesis with a NanoTek device.[5] The low amount of precursor allowed purification on the analytical scale column (4.6 x 250 mm).

In extreme cases, HPLC purification can be omitted completely. Well-optimized reactions form minute impurities, which are similar in chemical properties to the final product. A typical example is a product of elimination reaction that competes with fluorination in the nucleophilic synthesis of ^{18}F-labeled compounds.[56] This by-product can have similar polarity and solubility to the target compound and therefore high-resolution HPLC is required to purify the product. The high selectivity attainable with microfluidic reactors suppresses by-product formation enough for successful purification by low resolution chromatography or even solid-phase extraction (SPE). For instance, ^{18}F-labeled ligand for benzodiazepine receptors obtained from the NanoTek apparatus was only purified with SPE in the preclinical production.[37] Utilization of a fluorinated intermediate produced microfluidically omits the purifications steps in the synthesis of [^{18}F]-FIAU.[18]

A reduced amount of a precursor is a particularly important advantage for labeling of biological macromolecules, because radiolabeled product often cannot be separated from the precursor. In this situation, a small amount of the precursor used for the reaction translates into a high effective specific

activity (SA). SA is the ratio of molecules bearing radionuclide to the same molecules with the stable isotope. It is an important parameter in defining the suitability of a tracer for imaging of low abundance targets: molecules carrying a stable isotope will occupy all binding sites, resulting in poor target-to-background ratio in the image. The chemical difference between the precursor and the labeled tracer is negligible for a large biomolecule. Since both compete for the scarce binding sites, ratio of labeled biomolecules to all biomolecules of this sort (effective SA) is an important metric. Reduction of the precursor used in the labeling procedure becomes a major concern in the tracer production. Several examples demonstrated use of microfluidic technology to increase effective SA of the radiolabeled tracer.

The high efficiency of custom-built microreactor determined a complete conversion in radiolabeling of DOTA-Peptide conjugate by ^{64}Cu. The stability of the peptide under labeling conditions eliminated any need for purification of the final product. The practical applicability of these results needs to be further investigated, as radioactive copper was doped with stable isotope for these experiments.[14] In a similar study the radiochemical labeling yield of insulin labeled with ^{94m}Tc was improved from 21% in the conventional vial procedure to 40% in microfluidic apparatus, which translated into a nearly two-fold improvement of SA.[43]

Improvements in SA of a microfluidically produced product were also reported for small molecule labeling. In the case of synthesis of [^{18}F]-FMISO, a popular hypoxia tracer, the SA of the product obtained with Siemens P-IV prototype was three- to four-fold greater than that of the product produced in a conventional manner.[28] Presumably, smaller surfaces of fluorinated materials employed in the prototype instrument led to the improvement. In a very specific case of production of [^{18}F]-XeF_2 via fluorine exchange efficient radiolabeling also translated into increased SA because the labeling product was chemically identical to the precursor.[19]

Reduction of the amount of solvent used for the reaction opened additional opportunities. The microfluidic processes use negligible amounts of solvents relative to the flow of chromatographic eluents in HPLC purifications and are capable of withstanding a high pressure. These factors are crucial in the integration of a reactor with a purification system. In this type of devices, the loading loop of chromatograph is replaced with a reactor. This purely engineering improvement eliminates losses associated with transfer of the mixture from the synthetic module to a purification unit, and also eliminates the tricky process of loading the HPLC loop. Several reported examples[20,22,44,57] were in the field of ^{11}C radiolabeling, in which a short run time and a minimal number of operations was particularly important due to the 20 min half-life of ^{11}C.

The benefits of microfluidic technology integration into radionuclide production were briefly discussed in the context of low cyclotron capacity.[58] Indeed, if the entire amount of radioactivity produced by a cyclotron is on

the scale of a few patient doses, high concentration of the radionuclide is particularly desirable. Unfortunately, the patent does not provide any relevant experimental data.

17.4.5 Additional benefits

Smaller footprint and improved safety

Safety is a major concern in radiopharmacy. The levels of radioactivity involved in the routine radiopharmaceutical production are prohibitively high for any manual operation. All processes from radionuclide production to final doses dispensing are performed behind bulky and heavy shields, mostly in semi-automatic mode. Often radioactive shields take up much more space that the machinery they shield. A typical chemistry module is of a size comparable to carry-on luggage, but placed in an adequate shield will occupy the space of a fume hood. Smaller instruments will require less lead and concrete to achieve the same or greater level of personnel protection. Lower shielding requirements due to miniaturization of the synthesis unit have already been discussed in the pioneering publications.[6] Indeed, a smaller reactor implies smaller overall dimensions of the instrument. However, the bulk of an automated chemical module is made up of the auxiliary devices, such as the control unit, vacuum pump, various detectors, etc. As a result, mere reduction of the reactor size does not ensure reduction of the instrument size. Nevertheless, some simplifications associated with microfluidic technology allowed for smaller components. For instance, less powerful Peltier heaters have been employed[28] instead of the traditional resistive modules. A combination of technical improvements not directly associated with the reactor allowed for development of self-shielding devices comparable in size to a conventional module. The new device was rated for processing up to 500 mCi of ^{18}F, which is relevant to commercial production of radiotracers.[54] Similar improvements led to the construction of a device with only some of the components shielded.[14]

Cost reduction

There are several compelling reasons to believe that the cost per dose of final tracers might be significantly reduced once microfluidic machines become widely adopted by radiopharmaceutical production. One obvious reason for the lower cost is reduced use of a precursor and other reagents. Reactive precursors for radiopharmaceuticals are fine chemicals often produced to order and undergoing strict quality control. Thus, the cost of a precursor needed for one run can be on the scale of several hundred dollars. This idea is supported by reports of 10- to 100-fold reduction in precursor use.[24,31,32,49,59] Another reason for lower cost is economy of scale. Successful application of

microfabrication techniques, in theory, should yield very cheap mass-produced reactors. This, in turn, might facilitate production of reaction cartridges pre-manufactured and supplied to radiopharmacies. Although the commercially available NanoTek platform does not rely on such technology, there are multiple examples of experimental devices produced with lithographic techniques.[14,15,23,24] One example of mass production of radiochemical reactors is a batch reactor of the Siemens P-IV machine, mass manufactured via an injection molding process. It is important to note, though, that this advantage can only be fully realized if not only the reactor but also a significant portion of the wetted path is integrated in the disposable chip.

17.4.6 Applications impossible with conventional reactors

Apart from improvements over the existing technology, the microfluidic approach in radiosynthesis sometimes offers opportunities impossible with conventional reactors. The unique properties of capillary structures in performing radiochemical reactions had first been reported in the context of ^{32}P labeling of live cells. As early as 1984, a group of authors from Australia noted that the radiation damage inflicted on the cells during biosynthetic radiolabeling depended on the vessel geometry. In thin capillaries (<1 mm diameter), radiation dose to the cells can be reduced to as low as one tenth of the dose absorbed by the cells in Petri dishes.[60] This observation correlates remarkably well with the recent report on the correlation between the FDG radiolysis rate and the container geometry.[61] It was discovered that if PEEK tubing 0.25 mm ID was used as container, radiolysis could be suppressed by 86% as compared to bulk vial. The effect was rationalized in terms of energy positron deposits in the media (Fig. 17.12). Theoretical modeling predicted a steep increase for energy deposited as a function of the distance from the decay event. The same logic can be applied to the electrons emitted by ^{32}P. Another manifestation of this phenomenon is a lack of expected radiolysis during high activity production of FMISO in microfluidic reactor.[28]

A unique opportunity specific to microfluidic reactors is the use of reactors prefilled with the reactant.[6] This is hardly possible with conventional reactors, which are tightly integrated with the rest of the module. However, it becomes an attractive option if the reactor is easily replaceable or even disposable. An extreme example of this approach is the patent publication claiming copper capillary reactor acting as a catalyst.[52]

17.5 Current problems for microfluidic technology

Microfluidic devices were first proposed for use in radiochemistry more than 10 years ago, but so far none have been installed for commercial production of clinical tracers. Intrinsic inertia in the radiopharmaceutical community is

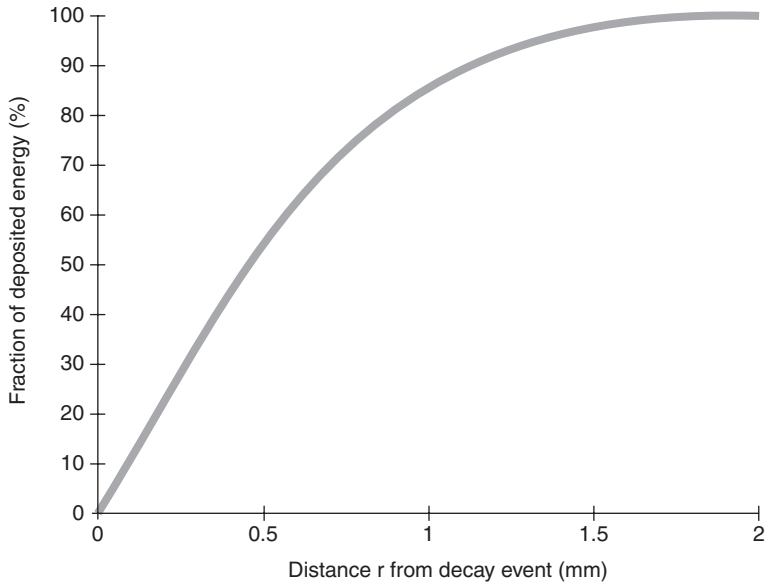

17.12 Fraction of energy deposited by a positron as a function of distance. The curve is plotted for positron originating from ^{18}F decay. Note that at 0.125 mm, typical radius of a microfluidic flow-through reactor; positrons originating from the center of the reactor and traveling perpendicularly to the wall deposits only 15% of energy in the reactor. (*Source*: Reproduced with permission from Rensch C. *et al. Applied Radiation and Isotopes* 2010, **70**, 1691.[61])

partially to blame for the delay, but also the technology has yet to mature to the level, at which field practitioners see a compelling reason to invest in purchasing a new instrument. Several technical issues will have to be addressed before microfluidic technology is accepted as a reliable tool of modern radiopharmacy.

17.5.1 Micro/macro interface

Reagents and materials supplied to a microfluidic device most often come in macro-form: cyclotron produces ^{18}F-fluoride in the form of 1–2-mL batches, ^{11}C gases are diluted with carrier gas, precursors come in multi-milligram quantities, and solvents are never supplied by microliters. This raises two problems.

The first is in the concentration of radioactive material produced by a cyclotron. So far, no commercial and just a few experimental devices have successfully addressed concentration of fluoride. Activated radioactive precursor (^{18}F-K_{222} complex[46]; [^{18}F]-SFB[24]; [^{11}C]-MeI, etc.) is often prepared

in a conventional manner before it is used in a microfluidic reaction. As a result, microfluidic process utilizes only a fraction of available radioactivity, and only in a dilute form. The commercial NanoTek system includes a dedicated module for fluoride processing. However, the dry fluoride solution prepared by the module has a volume on the scale of 0.5 mL; this forced NanoTek users to revert to conventional modules for production of even modest doses of radioactivity.[19,36,37] Another consequence of the low concentration of radioactivity is prolonged time of production. Without efficient concentration system, production scale up can only be done with a proportional increase of a production time.[32] Other devices are plagued with the same problem. Attempts to improve ^{124}I labeling of annexin in a microfluidic device failed because of the low radioisotope concentration, despite some encouraging results with fluorination reactions in the same device.[62] In fact, concentration of radioactive precursor into a very small volume is a complex technical issue that is likely to require an individual solution for each precursor. There is a vigorous research in the field of fluoride concentration (*vide infra*) but concentration of exotic isotopes and pre-labeled molecules will unlikely receive similar attention. For instance, there have yet to be developed methods for production of high concentration ^{18}F-SFB. As a result, conditions for labeling of diabody with this prosthetic group were worked out in a microfluidic setting, but production of imaging doses was done in a conventional beaker.[24] Similarly, pre-concentration of [^{11}C]-CO_2 is cited as a prerequisite for using this precursor in a microfluidic setting.[6]

The second problem is related to use of a small portion of a bulk of precious material. A common approach implies preparation of diluted solutions and using of only a fraction of it.[23,24,26] In case of flow-through reactors the problem is aggravated by the need to prime the feeding lines and syringe pumps. All lines leading to the reactor and often the reactor itself need to be filled with the reagent prior the start of the synthesis; syringe pumps must be filled with the solution free of gas bubbles. This is normally achieved by pushing a portion of the solution into the waste. While this procedure is acceptable for cheap reagents such as buffer solution, it is impractical in the case of valuable reagents. The problem was recognized already in the publications of the early proof-of-principle devices.[62] It became particularly evident in the detailed descriptions of operation of devices that were designed for production of radiopharmaceuticals. For instance, in case of in-capillary production of FDG, the reactor is primed with mannose triflate solution.[49] In a report describing use of the NanoTek device for ^{11}C radiolabeling, it was mentioned that out of 700 μL of radioactive precursor solution prepared, only 400 μL were actually used.[41] It is therefore an important practical concern that needs to be resolved before microfluidic machines can become admitted into production practice. In summary, a way of using 1 mg out of 50 mg and leaving the remaining 49 mg intact needs to be found.

Oddly enough, translation from micro-scale back to macro-world might present a considerable problem as well. It is especially true for batch reactors that are designed to hold the reaction mixture inside. This trait of batch reactors makes quick and efficient extraction a technical challenge. In the Siemens P-IV device, for example, a copious amount of extraction solution pushes the reaction mixture out of the reactor.[28] Theoretical modeling of the process has elucidated some of the underlying trends, but the practical applicability of these findings was limited.[63] The problem is even more severe in the case of an EWOD chip that has to be taken apart to access the product after the reaction is finished.[26]

17.5.2 Limited choices of materials

A suboptimal choice of the reactor material can hamper the labeling efficiency in many ways. Leaching of impurities into the reaction mixture, or unwanted interactions with the reaction components, are major concerns. Stability of mechanical properties in the relevant range of temperatures is another prerequisite. An interesting discussion of the suitability of several materials for the reactions with XeF_2 was published in connection with microfluidic radiolabeling.[19] Acidity of the surface and/or presence of moisture adsorbed on the reactor walls were major concerns for this application. The authors discussed common materials such as glass, Teflon, and glossy carbon, and found glass to be most suitable, probably due to the catalytic properties of its surface.

Methods of micromanufacturing also impose a set of restrictions on the material used for the reactor. Although basic patterns can be etched on a wide variety of materials, complex liquid routing requires valves and other moving parts. Construction of these essential components of the reactor often requires use of elastomers, with PDMS being the most frequent choice. This elastomer is known for poor chemical stability, especially toward organic solvents.[64] Reactivity of PDMS toward fluoride has been a severe limitation for the development of integrated microfluidics.[23,47] Similar problems arose with the development of PDMS reactor for copper radiolabeling.[14] It was found to absorb copper ions, and had to be pretreated with cold copper to ensure an efficient reaction. Another widespread material for micromanufacturing, SU-8 resin, used for bonding of polycarbonate layers, was found to be incompatible with MeCN, a common solvent in the radiochemical synthesis.[62] The fused silica used in the commercial NanoTek reactor absorbs large amounts of reactive fluoride.[31,38] Although 85% of radioactivity was recovered from the reactor in some cases,[5,34] occasionally as much as 50% of fluoride was irreversibly absorbed on the reactor walls.[35]

Fluoropolymers are commonly used in applications requiring high chemical stability. However, this is a questionable approach for radiochemical applications: many fluorinated polymers are known to degrade in a high radiation

field. Furthermore, a fluoride anion is one of the degradation products, and SA of ^{18}F-tracers was shown to suffer from this interference.[65] The relatively low chemical reactivity of the ^{11}C precursors alleviates this problem in the case of ^{11}C labeling. Reactors made out of glass,[15] stainless steel,[20] and fluoropolymers[4] have been successfully used. However, the adsorptive properties of the material were noted to affect radio methylation yield in a microreactor.[66]

17.5.3 Scarce feedback: poor control and consequent poor reliability

On-line experimental evaluation of the reaction parameters is critically important for process development and control. In conventional chemical reactors numerous methods are available for precise measurement of temperature, pressure, light absorption, and other parameters. Applications of most of these techniques to very small volumes and miniature reactors are impossible. As a result, the important parameters of the process in microfluidic device are often assumed rather than measured. For instance, so far no microfluidic radiochemical unit has a temperature sensor in the reaction area. It is only assumed the temperature inside the reactor is equal to the temperature of the heating element, due to the low absolute heat capacity of the reaction mixture and efficient heat exchange. Likewise, simple visual control is taken for granted in conventional vial synthesis but is rarely possible in microfluidic reactors, except for relatively large batch devices[26,54] with digital microscopic cameras. In flow-through devices made out of non-transparent material such as stainless steel or PEEK, this is impossible. As a result, mixing efficiency in the flow-through devices remains a subject of speculation. Several reports have questioned the assumption that in narrow passages diffusive mixing should eliminate any heterogeneity. Researchers studying ^{11}C-methylation reactions in NanoTek apparatus found that premixing of reagents improved the yield and explained this fact by a lag time necessary for mixing of co-infused reagents.[42] Another group found for [^{18}F]-FET production that the higher rate of infusion improves the yield of the product if the controlled residence time is adjusted by the reactor length. This result is a clear indication that a turbulent flow is responsible for the reagent mixing rather than diffusion.[32] Visual control of the reactor would resolve these concerns but its implementation is technically challenging.

17.5.4 Complex and unreliable liquid routing

Many operational problems with microfluidic reactors are determined by the geometry of the reactors. Highly specialized geometry is what differentiates microfluidic reactors from their conventional counterparts. Hence, it is

expected to see a set of specific issues associate with the layout of the reactor. The most obvious limitation of performing synthesis in the reactor with very narrow passages is clogging. It is possible to diminish this problem by installing in-line filters for all solutions injected into the reactor, but formation of solid byproducts is an almost inescapable problem. This issue was emphasized in a recent application of NanoTek apparatus.[40] Another limitation is associated with operation of complex mechanisms for measuring and routing of microscopic amounts of liquid. In the conventional systems, the synthetic module is normally loaded with liquids premeasured by some conventional methods. Control of liquid transfer is a challenging engineering problem in the microfluidic reactor. Connection of syringe pumps via stream selectors to the storage vials and the reactor often solves the problem. Correct operation of this subsystem of the synthetic module requires special preparation and priming procedures. This was cited as a major source of radioactivity losses in a recent study of [^{18}F]FE@SUPPY synthesis.[31]

Batch microfluidic devices have their own set of limitations revolving around reactor filling. Surface tension of the liquid is a significant force at the scale of the microfluidic reactor. As a result, gas bubbles formed in the liquid have characteristic dimensions comparable with the reactor size, and tend to push the reactor content out of the reactor. Evaporation of the liquid in this setting requires elaborate manipulations specific for each reactor architecture.[26,47] Furthermore, adding liquid to a partially filled reactor becomes an unreliable procedure, and researchers tend to avoid it.[28]

17.6 Recent developments with potential impact

Radiochemical applications of microfluidic technology can benefit from many general developments in the microfluidic field. However, several areas of research are specific to radiochemistry.

17.6.1 New materials

Mismatch between the materials desirable for radiochemical applications and the materials typical for micromanufacturing is a long-standing concern. Recent reports on the chemically inert materials for micromanufacturing mostly revolve around fluoropolymer-based elastomers.[67,68] This is an expected choice, given the chemical inertness of this type of polymers. Applications of this material for [^{18}F] radiochemistry, though, are highly questionable. Teflon is a known source of ^{19}F impurities and SA of tracers produced using fluorinated plastics will likely be diminished. From this perspective, recent reports on a chemically resistant polyurethane microfluidic device might be the direction for future development.[69]

17.6.2 New means of gathering feedback

Methods for controlling common process parameters such as temperature[70] and pressure[71] in microfluidic systems are constantly being developed and will eventually be applied to microfluidic radiochemical platforms. One specialized technique of particular relevance for radiochemistry is high-resolution imaging of radioactivity concentration. Current state of-the-art radioactivity detectors designed for detection of positron emitting isotopes have a spatial resolution on the scale of millimeters and are prohibitively costly.[72] Several recent publications have attempted to sidestep this limitation by leveraging the 2D nature of the microfluidic devices and using longer exposure time. Positron Sensitive Avalanche photo detectors were shown to achieve 0.5 mm spatial resolution while maintaining sensitivity of 56 pls/min for 14 pCi/mm^2.[73] Plastic scintillator coupled to CCD devices were proposed as well.[74,75] A recent approach is based around detection of Cherenkov radiation associated with the positron rather than capturing γ-photons produced in an annihilation event.[76] A broad-spectrum emission was detected with CCD camera, on the image of a 0.2 mm channel was filled with 107 mCi/mL ^{18}F full width of the signal at half of the maximum intensity was as low as 0.35 mm (5 min exposure). The method was later applied to monitor processes in an EWOD chip described earlier. This technology provides much the sought ability to detect radioactivity in microfluidic chips, although is limited to transparent chip materials.

Regular cameras have used to visually observe the processes in the chips and provided valuable feedback for an experienced operator.[54] Use of computer vision software would be the next logical step in development of this approach.

17.6.3 Means of micro-macro coupling

As stated above, transition of reagents from macro-world to micro-scale has been a major challenge in radiochemical applications of a microfluidic technology. The problem of concentration of fluoride anion is the most relevant to practical applications, and has been recently actively investigated. Three main methods of fluoride concentration have been published. The most straightforward is evaporation of the MeCN/Water mixture containing fluoride. This approach has been implemented in the NanoTek apparatus.[77] The inherent drawback of the approach is evaporation in conventional vials. A significant portion of radioactivity remains in the vial, due to its relatively large surface area.[31] Evaporation of fluoride solution directly from a microfluidic channel through gas-permeable PDMS membrane was also considered.[78,79]

Two alternatives have been proposed. The first one relies on an electrochemical cell to reach a desired concentration. The general idea behind electrochemical concentration is to use an electromagnetic field to extract fluoride anion from the passing flow of water and then reverse voltage to release fluoride into anhydrous solution. First attempts to perform this procedure were made right at the onset of microfluidic radiochemistry.[80] Glossy carbon electrodes were utilized for this application with ~80% efficiency.[81] Platinum electrodes allowed for some improvements over glossy carbon, but the overall efficiency of the process was still far from production standards.[82] A disposable microfluidic cell providing for very high concentration has been reported.[83] The device releases fluoride solution in portions as little as 60 μL, but the overall efficiency of the process is again less than 60%. However, the fluoride solution produced in this setup was active in fluorination processes, and allowed for 98% of fluoride incorporation in synthesis of [^{18}F]FDG, 80% [^{18}F]FMISO, 20% for [^{18}F]-flumazenil, and 60% for [^{18}F]fluoromethyl.[84] It appears that irreversible binding of reactivate fluoride anion to the electrode material hampers this otherwise attractive method.

A more traditional approach relies on ion exchange resin to trap fluoride and then release it in a smaller volume of release solution. This approach is used in conventional scale modules for solvent exchange, but not for concentration. In microfluidic devices, a miniature 5 μL ion exchange column for concentration of fluoride anion was already integrated in the radiochemical circuit.[23] The efficiency of the proposed device was difficult to estimate, due to the confounding issue of fluoride absorption on PDMS. The method matured into an off-chip column,[47] and was subsequently established as a reliable procedure.[28,54] A miniature cartridge packed with 7 μL of an anion exchange resin trapped up to 7 Ci of ^{18}F with >95% efficiency followed by release of >95% of trapped activity in 45 μL of release solution. A similar methodology improved efficiency of NanoTek apparatus. 95% trap/release efficiency was achieved albeit with 0.5 mL of the release solution. The latter drawback is most likely related to the fact that, in general, the NanoTek machine is not capable of processing low volumes of stock solutions.[85,86] A method of producing microfluidic chips packed with an ion exchange resin was recently disclosed in a patent application.[87] The achieved efficiency, however, is not clear for the devices produced according to this methodology.

An attractive idea has emerged from the ion exchange approach. If the composition of release solution/ion exchange resin is optimized, a water amount might be low enough to eliminate the need for the azeotropic drying that usually follows the concentration step. The approach has been discussed in application to conventional radiochemical units[88] and was later applied to flow-through reactors.[29]

17.7 Conclusion

The examples of the reactors discussed in this chapter and the variety of the processes studied in these reactors clearly demonstrate that the concept of microfluidic radiochemistry is proven. Major advantages are improved yields, short reaction time, short overall production time, reduced use of precursor, and high degree of control. These advantages stem from the fundamental properties of microfluidic devices, such as low volume, low absolute heat capacity, and high surface-to-volume ratio. Additionally, inevitable automation helps in reducing human error.

These advantages, though, are not yet sufficient to adopt the microfluidic technology in the everyday practice of radiopharmaceutical production. Efficient systems for transition of reagents from macro-world to micro-scale and back need to be developed. Materials meeting the criteria of both radiochemistry and micromanufacturing need to be found. Above all, the reliability of the new instruments should be experimentally proven with hundreds of test runs before the sensitive matter of human doses production will be entrusted to the new technology. Research applications of the microfluidics will likely follow. Preclinical research on its own, however, is not sufficient to create an attractive market for instrument manufacturers.

Microfluidic chips are often compared to the integrated microelectronic circuits. Adopting this analogy one might say that chemistry automation is still in 1930s. Current radiochemical devices can only perform functions foreseen at the design stage, as opposed to modern computer that can be used for applications not even thought of by its manufacturer. The hardware of the radiochemical module often has to be reconfigured to accommodate a new process. The flexibility of modern computers is largely determined by the fact that data and instructions are treated in a similar fashion, both being streams of numbers stored in computer memory. In radiochemical modules, on the other hand, the reagents (data) and the liquid manipulating devices such as valves and tubes (instruction) are viewed as two distinctly different classes of objects. In that regard, the technology closest to the microelectronic is EWOD chips, which use the reagent as a material to create the reactor as the droplet. However, even in these devices, electrical leads need to be reconfigured to alter the liquid routing. It is likely that a true ability to change the processes without changing hardware would open a pathway for a rapid improvement of existing processes as well as developing new methods.

17.8 References

1. Brady, F.; Luthra, S. K.; Gillies, J. M.; Jeffery, N. T. Use of microfabricated devices for radiosynthesis of radiotracers for positron emission tomography. *International Patent Application* 2003.

2. Lu, S.; Pike, V. W. In *PET Chemistry, The Driving Force in Molecular Imaging*; Schubiger, P. A.; Lehman, L.; Friebe, M., Eds.; Springer: Berlin, 2007; pp. 271–87.
3. Audrain, H. *Angewandte Chemie (International ed. in English)* 2007, **46**, 1772–5.
4. Miller, P. W.; Long, N. J.; De Mello, A. J.; Vilar, R.; Audrain, H.; Bender, D.; Passchier, J.; Gee, A. D. *Angewandte Chemie (International ed. in English)* 2007, **46**, 2875–8.
5. Lu, S.; Giamis, A. M.; Pike, V. W. *Current Radiopharmaceuticals* 2009, **2**, 49–55.
6. Jewett, D. M.; Ehrenkaufer, R. L.; Ram, S. *International Journal of Radiation and Isotopes* 1985, **36**, 672–4.
7. Bailey, D. L.; Karp, J. S.; Sutri, S. In *Positron Emission Tomography*; Valk, P. E.; Bailey, D. L.; Townsend, D. W.; Maisey, M. N., Eds.; Springer, 2003; pp. 41–67.
8. Richards, M. L.; Scott, P. J. H. In *Radiochemical Syntheses, vol.* 1; Scott, P. J. H.; Hockley, B. G., Eds.; Wiley, 2012; pp. 3–13.
9. Liow, E.; O'Brien, A. T.; Luthra, S. K.; Brady, F.; Steel, C. *Journal of Labelled Compounds and Radiopharmaceuticals* 2005, **48**, S28.
10. Gillies, J. M.; Prenant, C.; Zweit, J. *Journal of Labelled Compounds and Radiopharmaceuticals* 2005, **48**, S29.
11. Gillies, J. M.; Prenant, C.; Chimon, G. N.; Smethurst, G. J.; Dekker, B. A.; Zweit, J. *Applied Radiation and Isotopes* 2006, **64**, 333–6.
12. Brady, F.; Luthra, S. K.; Gillies, J. M.; Jeffery, N. T. Use of microfabricated devices. *US Patent Application* 2005.
13. Lu, S.; Watts, P.; Chin, F. T.; Hong, J.; Musachio, J. L.; Briard, E.; Pike, V. W. *Lab on a Chip* 2004, **4**, 523–5.
14. Wheeler, T. D.; Zeng, D.; Desai, A. V; Önal, B.; Reichert, D. E.; Kenis, P. J. A. *Lab on a Chip* 2010, **10**, 3387–96.
15. Miller, P. W.; Audrain, H.; Bender, D.; De Mello, A. J.; Gee, A. D.; Long, N. J.; Vilar, R. *Chemistry: A European Journal* 2011, **17**, 460–3.
16. Ravert, H. T.; Holt, D. P.; Dannals, R. F. In *Radiochemical Synthesis*; Scott, P. J. H.; Hockley, B. G., Eds.; Wiley, 2012; pp. 139–54.
17. Brichard, L.; Aigbirhio, F. I. *Journal of Labelled Compounds and Radiopharmaceuticals* 2009, **52**, S497.
18. Anderson, H.; Pillarsetty, N.; Cantorias, M.; Lewis, J. S. *Nuclear Medicine and Biology* 2010, **37**, 439–42.
19. Lu, S.; Pike, V. W. *Journal of Fluorine Chemistry* 2010, **131**, 1032–8.
20. Wilson, A. A.; Garcia, A.; Jin, L.; Houle, S. *Nuclear Medicine and Biology* 2000, **27**, 529–32.
21. Davenport, R. J.; Dowset, K.; Pike, V. W. *Applied Radiation and Isotopes* 1997, **48**, 1117–20.
22. Watkins, G. L.; Jewett, D. M.; Kilbourn, M. R.; Toorongian, S. A. *Applied Radiation and Isotopes* 1988, **39**, 441–4.
23. Lee, C.-C.; Sui, G.; Elizarov, A. M.; Shu, C. J.; Shin, Y.-S.; Dooley, A. N.; Huang, J.; Daridon, A.; Wyatt, P.; Stout, D.; Kolb, H. C.; Witte, O. N.; Satyamurthy, N.; Heath, J. R.; Phelps, M. E.; Quake, S. R.; Tseng, H.-R. *Science* 2005, **310**, 1793–6.
24. Liu, K.; Lepin, E. J.; Wang, M.-W.; Guo, F.; Lin, W.-Y.; Chen, Y.-C.; Sirk, S. J.; Olma, S.; Phelps, M. E.; Zhao, X.-Z.; Tseng, H.-R.; Van Dam, R. M.; Wu, A. M.; Shen, C. K.-F. *Molecular Imaging* 2011, **10**, 168–76, 1–7.

25. Satyamurthy, N.; Kim, C.-J.; Dam, R. M. Van; Keng, P. Y.; Chen, S.; Ding, H.-J.; Sadeghi, S.; Phelps, M. E.; Van Dam, R. M. In *14th International Conference on Miniaturized Systems for Chemistry and Life Sciences*; 2010; pp. 668–70.
26. Keng, P. Y.; Chen, S.; Ding, H.; Sadeghi, S.; Shah, G. J.; Dooraghi, A.; Phelps, M. E.; Satyamurthy, N.; Chatziioannou, A. F.; Kim, C.-J.; Van Dam, R. M. *Proceedings of the National Academy of Sciences of the United States of America* 2012, **109**, 690–5.
27. Lebedev, A.; Miraghaie, R.; Kotta, K.; Ball, C. E.; Zhang, J.; Buchsbaum, M. S.; Kolb, H. C.; Elizarov, A. M. *Lab on a Chip* 2013, **13**, 136–45.
28. Yokell, D. L.; Leece, A. K.; Lebedev, A.; Miraghaie, R.; Ball, C. E.; Zhang, J.; Kolb, H. C.; Elizarov, A. M.; Mahmood, U. *Applied Radiation and Isotopes* 2012, **70**, 2313–16.
29. Yang, B. Y.; Jeong, J. M.; Lee, Y.-S.; Lee, D. S.; Chung, J.-K.; Lee, M. C. *Tetrahedron* 2011, **67**, 2427–33.
30. Hooper, J.; Watts, P. *Journal of Labelled Compounds and Radiopharmaceuticals* 2007, **50**, 189–96.
31. Ungersboeck, J.; Philippe, C.; Mien, L.-K.; Haeusler, D.; Shanab, K.; Lanzenberger, R.; Spreitzer, H.; Keppler, B. K.; Dudczak, R.; Kletter, K.; Mitterhauser, M.; Wadsak, W. *Nuclear Medicine and Biology* 2011, **38**, 427–34.
32. Bouvet, V. R.; Wuest, M.; Tam, P.-H.; Wang, M.; Wuest, F. *Bioorganic & Medicinal Chemistry Letters* 2012, **22**, 2291–5.
33. Pascali, G.; Mazzone, G.; Saccomanni, G.; Manera, C.; Salvadori, P. A. *Nuclear medicine and biology* 2010, **37**, 547–55.
34. Chun, J.-H.; Lu, S.; Lee, Y.-S.; Pike, V. W. *Journal of Organic Chemistry* 2010, **75**, 3332–8.
35. Chun, J.-H.; Lu, S.; Pike, V. W. *European Journal of Organic Chemistry* 2011, **2011**, 4439–4447.
36. Telu, S.; Chun, J.-H.; Siméon, F. G.; Lu, S.; Pike, V. W. *Organic & Biomolecular Chemistry* 2011, **9**, 6629–38.
37. Briard, E.; Zoghbi, S. S.; Siméon, F. G.; Imaizumi, M.; Gourley, J. P.; Shetty, H. U.; Lu, S.; Fujita, M.; Innis, R. B.; Pike, V. W. *Journal of Medicinal Chemistry* 2009, **52**, 688–99.
38. Bouvet, V. R.; Wuest, M.; Wiebe, L. I.; Wuest, F. *Nuclear Medicine and Biology* 2011, **38**, 235–45.
39. Gao, M.; Wang, M.; Mock, B. H.; Glick-Wilson, B. E.; Yoder, K. K.; Hutchins, G. D.; Zheng, Q.-H. *Applied Radiation and Isotopes* 2010, **68**, 1079–86.
40. Pascali, G.; Nannavecchia, G.; Pitzianti, S.; Salvadori, P. A. *Nuclear Medicine and Biology* 2011, **38**, 637–44.
41. Kealey, S.; Plisson, C.; Collier, T. L.; Long, N. J.; Husbands, S. M.; Martarello, L.; Gee, A. D. *Organic & Biomolecular Chemistry* 2011, **9**, 3313–9.
42. Kealey, S.; Plisson, C.; Martarello, L.; Long, N. J.; Gee, A. D. *Journal of Labelled Compounds and Radiopharmaceuticals* 2009, **52**, S498.
43. Simms, R. W.; Causey, P. W.; Weaver, D. M.; Sundararajan, C.; Stephenson, K. a.; Valliant, J. F. *Journal of Labelled Compounds and Radiopharmaceuticals* 2012, **55**, 18–22.
44. Hostetler, E. D.; Burns, H. D. *Nuclear Medicine and Biology* 2002, **29**, 845–848.
45. Kihlberg, T.; Langstrom, B. Method and apparatus for production and use of [11C] carbon monoxide inlabeling synthesis. *International Patent Application* 2002.

46. Steel, C. J.; O'Brien, A. T.; Luthra, S. K.; Brady, F. *Journal of Labelled Compounds and Radiopharmaceuticals* 2007, **50**, 308–11.
47. Elizarov, A. M.; Van Dam, R. M.; Shin, Y.-S.; Kolb, H. C.; Padgett, H. C.; Stout, D.; Shu, J.; Huang, J.; Daridon, A.; Heath, J. R. *Journal of Nuclear Medicine* 2010, **51**, 282–7.
48. Elizarov, A. M.; Ball, C. E.; Zhang, J.; Kolb, H. C.; Van Dam, R. M.; Diener, L. T.; Ford, S.; Miraghaie, R. Microfluidic radiosynthesis system for positron emission tomography biomarkers. *US Patent Application* 2009.
49. Wester, H.-J.; Schoultz, B. W.; Hultsch, C.; Henriksen, G. *European Journal of Nuclear Medicine and Molecular Imaging* 2009, **36**, 653–8.
50. Yu, S. *Biomedical Imaging and Intervention Journal* 2006, **2**, e57.
51. Reischl, G.; Ehrlichmann, W.; Bieg, C.; Solbach, C.; Kumar, P.; Wiebe, L. I.; Machulla, H.-J. *Applied Radiation and Isotopes: Including Data, Instrumentation and Methods for Use in Agriculture, Industry and Medicine* 2005, **62**, 897–901.
52. Arstad, E.; Steel, C. Chemical method and apparatus. *International Patent Application* 2007.
53. Tang, G.; Zeng, W.; Yu, M.; Kabalka, G. *Journal of Labelled Compounds and Radiopharmaceuticals* 2008, **51**, 68–71.
54. Bejot, R.; Elizarov, A. M.; Ball, C. E.; Zhang, J.; Miraghaie, R.; Kolb, H. C.; Gouverneur, V. *Journal of Labelled Compounds and Radiopharmaceuticals* 2011, **54**, 117–22.
55. Cleij, M. C.; Clark, J. C.; Baron, J.-C.; Aigbirhio, F. I. *Journal of Labelled Compounds and Radiopharmaceuticals* 2007, **50**, 19–24.
56. Roeda, D.; Dolle, F. *Current Radiopharmaceuticals* 2010, **3**, 81–108.
57. Moran, M. D.; Wilson, A. a.; Stableford, W. T.; Wong, M.; Garcia, A.; Houle, S.; Vasdev, N. *Journal of Labelled Compounds and Radiopharmaceuticals* 2011, **54**, 168–70.
58. Nutt, R. Biomarker generator system. *US Patent* 2009.
59. Iwata, R.; Pascali, C.; Bogni, A.; Yanai, K.; Kato, M.; Ido, T.; Ishiwata, K. *Journal of Labelled Compounds and Radiopharmaceuticals* 2002, **45**, 271–80.
60. Cooper, P. C.; Burgess, A. W. *Analytical Biochemistry* 1985, **144**, 329–35.
61. Rensch, C.; Waengler, B.; Yaroshenko, A.; Samper, V.; Baller, M.; Heumesser, N.; Ulin, J.; Riese, S.; Reischl, G. *Applied Radiation and Isotopes* 2012, **70**, 1691.
62. Gillies, J. M.; Prenant, C.; Chimon, G. N.; Smethurst, G. J.; Perrie, W.; Hamblett, I.; Dekker, B. A.; Zweit, J. *Applied Radiation and Isotopes* 2006, **64**, 325–32.
63. Elizarov, A. M.; Meinhart, C.; Miraghaie, R.; Van Dam, R. M.; Huang, J.; Daridon, A.; Heath, J. R.; Kolb, H. C. *Biomedical Microdevices* 2011, **13**, 231–42.
64. McDonald, J. C.; Whitesides, G. M. *Accounts of Chemical Research* 2002, **35**, 491–9.
65. Berridge, M. S.; Apana, S. M.; Hersh, J. M. *Journal of Labelled Compounds and Radiopharmaceuticals* 2009, **52**, 543–8.
66. Studenov, A. R.; Jivan, S.; Adam, M. J.; Ruth, T. J.; Buckley, K. R. *Applied Radiation and Isotopes* 2004, **61**, 1195–201.
67. Rolland, J. P.; Elizarov, A. M.; Brewster, J.; Heath, J. R.; DeSimone, J. M. In *Technical Proceedings of the 2006 NSTI Nanotechnology Conference and Trade Show, Vol. 2*; Nano Science and Technology Institute: Boston, MA, 2006; pp. 645–6.

68. Huang, Y.; Castrataro, P.; Lee, C.-C.; Quake, S. R. *Lab on a Chip* 2007, **7**, 24–6.
69. Stoyanov, I.; Tewes, M.; Koch, M.; Löhndorf, M. *Microelectronic Engineering* 2006, **83**, 1681–3.
70. Ross, D.; Gaitan, M.; Locascio, L. E. *Analytical Chemistry* 2001, **73**, 4117–23.
71. Chung, K.; Lee, H.; Lu, H. *Lab on a Chip* 2009, **9**, 3345–53.
72. Joung, J.; Miyaoka, R. S.; Lewellen, T. K. *Nuclear Instruments and Methods in Physics Research Section A: Accelerators, Spectrometers, Detectors and Associated Equipment* 2002, **489**, 584–98.
73. Vu, N. T.; Chung, Y. H.; Yu, Z. T. F.; Silverman, R. W.; Taschereau, R.; Farrell, R.; Shah, K. S.; Tseng, H.-R.; Chatziioannou, A. F. In *2006 IEEE Nuclear Science Symposium Conference Record*; IEEE, 2006; pp. 3536–9.
74. Cho, J. S.; Vu, N. T.; Chung, Y. H.; Yu, Z. T.; Silverman, R. W.; Taschereau, R.; Tseng, H.-R.; Chatziioannou, A. F. In *2006 IEEE Nuclear Science Symposium Conference Record*; IEEE, 2006; pp. 1977–81.
75. Mikecz, P.; Miklovicz, T.; Galuska, L.; Tron, L. *Journal of Labelled Compounds and Radiopharmaceuticals* 2009, **52**, S504.
76. Cho, J. S.; Taschereau, R.; Olma, S.; Liu, K.; Chen, Y.-C.; Shen, C. K.-F. K.-F.; Van Dam, R. M.; Chatziioannou, A. F. *Physics in Medicine and Biology* 2009, **54**, 6757–71.
77. Matteo, J. C. Evaporator and concentrator in reactor and loading system 2011.
78. Tseng, W. Y.; Cho, J. S.; Ma, X.; Kunihiro, A.; Chatziioannou, A. F.; Van Dam, R. M. In *NSTI-Nanotech 2010*; 2010; Vol. 2, pp. 472–5.
79. Tseng, W. Y.; Cho, J. S.; Ma, X.; Mahal, K.; Chatziioannou, A. F.; Van Dam, R. M. In *14th International Conference on Miniaturized Systems for Chemistry and Life Sciences*; Groningen, The Netherlands, 2010; pp. 1010–12.
80. Lu, S.; Clements, J. T.; Gilde, M. J.; Prak, A.; Watts, P.; Pike, V. W. *Journal of Labelled Compounds and Radiopharmaceuticals* 2007, **50**, 597–9.
81. Rensch, C.; Boeld, C.; Bachmann, B.; Riese, S.; Reischl, G.; Ehrlichmann, W.; Heumesser, N.; Baller, M.; Samper, V. *Journal of Labelled Compounds and Radiopharmaceuticals* 2009, **52**, S8.
82. Sadeghi, S.; Ly, J.; Deng, Y.; Van Dam, R. M. In *14th International Conference on Miniaturized Systems for Chemistry and Life Sciences*; Groningen, The Netherlands, 2010; pp. 318–20.
83. Saiki, H.; Iwata, R.; Nakanishi, H.; Wong, R.; Ishikawa, Y.; Furumoto, S.; Yamahara, R.; Sakamoto, K.; Ozeki, E. *Applied Radiation and Isotopes* 2010, **68**, 1703–8.
84. Wong, R.; Iwata, R.; Saiki, H.; Furumoto, S.; Ishikawa, Y.; Ozeki, E. *Applied Radiation and Isotopes* 2012, **70**, 193.
85. De Leonardis, F.; Pascali, G.; Salvadori, P. A.; Watts, P.; Pamme, N. In *14th International Conference on Miniaturized Systems for Chemistry and Life Sciences*; Groningen, The Netherlands, 2010; pp. 1604–6.
86. De Leonardis, F.; Pascali, G.; Salvadori, P. A.; Watts, P.; Pamme, N. *Journal of Chromatography A* 2011, **1218**, 4714–19.
87. Steel, C.; Fortt, R.; Liow, E.; Riese, S. Nucleophilic radiofluorination using microfabricated devices. *US Patent Application* 2009.
88. Lemaire, C. F.; Aerts, J. J.; Voccia, S.; Libert, L. C.; Mercier, F.; Goblet, D.; Plenevaux, A. R.; Luxen, A. J. *Angewandte Chemie (International ed. in English)* 2010, **49**, 3161–4.

Index